CRANFIELD UNIVERSITY

MARK G. HUDSON

WELDING OF X100 LINEPIPE

SCHOOL OF INDUSTRIAL AND MANUFACTURING SCIENCE

PhD THESIS

CRANFIELD UNIVERSITY

SCHOOL OF INDUSTRIAL AND MANUFACTURING SCIENCE

PhD THESIS

Academic Year 2003-2004

Mark G. Hudson

Welding of X100 Linepipe

Supervisor S.A.Blackman

March 2004

Abstract

The benefits of high strength steels in terms of reduced material volume due to enhanced mechanical performance have been known for some time. Large diameter transmission linepipe steels of minimum 690MPa ('X100') yield strength have been developed throughout the previous decade, and have recently become commercially available. Before these steels are used in linepipe construction projects, fundamental work regarding their ability to be field welded required undertaking. This thesis presents data arising from girth welding experiments involving a variety of X100 linepipe steels, welding consumables and welding processes.

Target girth weld mechanical properties thought suitable for a strain-based X100 pipeline design were proposed at the outset of the research. Optimisation of pulsed gas metal arc welding waveforms for the single and tandem wire processes, alongside the establishment of the base material properties formed an early part of the research. An extensive programme of solid wire welding consumable evaluation was then undertaken for single, tandem and dual torch narrow gap welding processes. The majority of equipment and procedures used throughout the work were as close to current field practice as possible, to minimise the time required to transfer the technology to the field situation. Work then focussed on the optimised alloy levels and welding procedure requirements for the production of full girth welds, using a variety of industry pipeline welding standards and supplemental techniques to assess the joint integrity.

It has been demonstrated that, subject to careful selection of welding consumable and fairly precise control of welding process variables and parameters, there are no major problems in obtaining weld metal strength levels of at least 120 MPa above the 690 MPa specified minimum yield strength (SMYS) of the parent pipe. This objective has been achieved in welds made using all three mechanised process variants examined. The desired target properties of strength and toughness were achieved with a variety of consumables and pipe materials of different composition.

Tie-in and repair procedures were also developed during the course of the research, with particular attention focussed on the application of high strength rutile flux cored wires. These wires attained strength levels overmatching the pipe specified minimum yield strength (690MPa), but would not reach the guaranteed overmatch level of 810MPa.

An examination of the thermocycles associated with four mechanised narrow gap welding techniques (single, tandem, dual and dual tandem) was undertaken. The experimental technique developed allowed the solidifying weld bead to be monitored, as well as the cumulative temperature cycles experienced by the underlying layers. Succesful determination of the cooling rates, times and transformation temperatures allowed a comparative evaluation of the four processes, using an optimum weld metal composition suitable for single wire welding of X100. This led to an understanding of the metallurgical history, and its consequent effect on the associated mechanical and microstructural properties. A similar series of experiments was undertaken to examine these effects using variations in preheat with a single wire process. In most cases considerable property variations were attained for the same weld metal chemistry, joint geometry and arc energy, highlighting the sensitivity of the process and procedure in achieving the required properties.

The high cooling rates determined from the thermocycle experiments explained the microstructural and mechanical properties attainable from lean alloying levels. A series of metal cored wires, based around the same alloy as for the thermocycle experiments, was consequently manufactured to examine small changes in weld metal chemistry. The individual wires involved changes in carbon, nickel, molybdenum and chromium to examine potential property variations arising from a highly controlled narrow gap welding procedure. The results again highlighted the sensitivity of the narrow gap welding technique in generating considerable property variation within the weld metal. Tolerance ranges for specific alloying additions to attain the proposed strength levels with a single and tandem wire process were derived from the data.

Acknowledgments

I would like to thank Mr S. Blackman for allowing me the opportunity to pursue this course of study and for providing the extensive laboratory facilities required during the experimental programme.

Thanks are due to the many technical staff and colleagues at Cranfield who have contributed in many ways. I particularly wish to thank Mr J. Savill, welding facilities manager extraordinaire, without whose help and encouragement this work would not have been completed. Mr R. Newman and Mr V. DiCarlo helped with many of the practical aspects of this work, Mr G. Lopes provided invaluable help with electronic data manipulation and Dr T. Lauenroth contributed to many fruitful discussions and practical help with all things associated with data acquisition and thermocouples. Dr J. Spurrier and Mr D.Yapp also contributed to many noteworthy discussions surrounding the research.

I also wish to acknowledge the financial support of the Pipelines Research Council International, TransCanada and BP Exploration in funding this research, in particular Dr D. Dorling (TCPL) and Mr J. Hammond (BP), both of whom provided constructive discussion and encouragement throughout the research project.

Several welding consumable manufacturers provided significant support to the project through the provision of materials and testing facilities. Considerable thanks are due to Dr D. Widgery and Mrs R. Tongue of ESAB Group UK, Dr C. Thornton and Mr B. Cowe of Oerlikon UK Ltd., Dr S. Nagarajan and Mr J. Bundy of Hobart Brothers, and Dr C. Jochum of Bohler Thyssen.

Finally, I wish to thank my wife Claire, without whose patience, support and consistent encouragement this work would not have been possible, let alone completed. This thesis is as much for her as it is for me.

Contents

List of Figures

List of Tables

Nomenclature

α	Allotriomorphic or idiomorphic ferrite which forms by reconstructive transformation
δ	Delta-ferrite
δm	value of CTOD at the first attainment of a maximum force plateau for fully plastic behaviour
δu	critical CTOD at the onset of brittle crack extension or pop-in when the event is preceded by Δa equal to or greater than 0.2mm
δc	critical CTOD at the onset of brittle crack extension or pop-in when Δa is less than 0.2mm
γ	Austenite
σ_y	Yield Stress
A	Elongation
Ac_3	Temperature at which a sample becomes fully austenitic during heating
Ae_3	Temperature separating the $\alpha+\gamma$ and γ phase fields for a specific alloy
Ar_3	Temperature at which an austenitic sample begins to transform to ferrite during cooling
Ac_1	Temperature at which ferrite, bainite, martensite and other room temperature steel phases begin to transform to austenite during heating
Bs	Bainite start temperature
$C_v$trans	Charpy impact toughness transition temperature
HV	Vickers hardness
Ms	Martensite start temperature
$R_{p0.2}$	0.2% proof stress
$R_{t0.5}$	0.5% tensile elongation stress
R_m	Ultimate tensile stress
Ts	Transformation start temperature
Tf	Transformation finish temperature
t_{85}	Cooling time from 800°C to 500°C
Y/T	Yield to Tensile ratio
z	Reduction of area

Abbreviations

ACC	Accelerated Cooling
AF	Acicular Ferrite
API	American Petroleum Institute
ASME	American Society of Mechanical Engineers
AUT	Automatic Ultrasonic Testing
AWS	American Welding Society
bpm	beats per minute
BS	British Standard
BCC	Body Centred Cubic
BCT	Body Centred Tetragonal
CCT	Continuous Cooling Transformation diagram
CE	Carbon Equivalent
CET	Carbon Equivalent (BS EN 1011-2)
CLR	Crack Length Ratio
CTOD	Crack Tip Opening Displacement
CTWD	Contact Tip to Workpiece Distance
Cv	Charpy V-Notch
CWP	Curved Wide Plate
DAQ	Data Acquisition
FCAW	Flux Cored Arc Welding
HAZ	Heat Affected Zone
HI	Heat Input
HICC	Hydrogen Induced Cold Cracking
ID	Internal Diameter
IIW	International Institute for Welding
IWM	Internal Welding Machine
LBZ	Local Brittle Zone
MCAW	Metal Cored Arc Welding
MMA	Manual Metal Arc
NACE	National Association of Corrosion Engineers
NDT	Non-Destructive Testing
NGW	Narrow Gap Welding

OD	Outside Diameter
OE	Optical Emission Spectroscopy
ppm	Parts per million by weight
Pcm	Parameter Crack Measurement
PGMAW	Pulsed Gas Metal Arc Welding
PWHT	Post Weld Heat Treatment
Q and T	Quench and Tempered
ROW	Right Of Way
SAW	Submerged Arc Welding
SEM	Scanning Electron Microscope
SMAW	Shielded Metal Arc Welding
SMYS	Specified Minimum Yield Strength
SMTS	Specified Minimum Tensile Strength
SSCC	Sulphide Stress Corrosion Cracking
TEM	Transmission Electron Microscope
TIG	Tungsten Inert Gas Welding
TMCP	Thermomechanical Controlled Processing
TTT	Time-Temperature-Transformation diagram
ULCB	Ultra Low Carbon Bainitic
UOE	U-pressed, O-pressed, Expanded
UTS	Ultimate Tensile Strength
WERC	Welding Engineering Research Centre, Cranfield University
WFS	Wire Feed Speed
WPS	Welding Procedure Specification
WPAR	Welding Procedure Approval Record
WT	Wall Thickness
YS	Yield Strength

1 INTRODUCTION

A trend towards consideration of the use of higher strength linepipe is steadily evolving as a result of moves towards higher allowable operating pressures and reducing material/installation costs of major pipelines. Traditional high strength steels (i.e. those produced by a quench and tempered (Q and T) processing route) gave rise to the commonly held belief of many engineers that high strength came at a high cost, high alloy content and were difficult to fabricate. The significant technological advances made in steel manufacture, particularly during the last fifteen years, have dispelled many of the factors previously limiting the uptake of high strength steels. Excellent combinations of strength and toughness, whilst still maintaining good weldability, are now readily achievable[1-10]. In the last few years several major steel suppliers have developed higher strength linepipe having a 689 MPa minimum yield ($R_{p0.2}$ or $R_{t0.5}$) strength (equivalent to an API 5L X100 grade if it were to exist)[5,7-10]. Although only limited quantities of this pipe have been manufactured to date, most items supplied to oil/gas companies and/or their contractors have been full size pre-production pipes manufactured under typical production conditions in the suppliers' pipe mills.

Significant cost savings are possible with the use of high strength steels, notably in terms of handling/carriage (reduced material volume) and welding (reduced weldment volume, welding time and welding consumables). The sophisticated alloying and processing routes allow the use of lean alloy compositions, in comparison to Q and T steels. This in turn offers savings in fabrication through an increase of the allowable welding parameters to provide a greater tolerance to higher heat input levels, resulting in greater productivity. Lean alloying/low carbon equivalent values also promote the reduction or elimination of expensive preheat and post weld heat treatment procedures, further enhancing the material cost effectiveness. It is consequently important that cost comparisons of modern high strength steels with their lower strength counterparts go beyond the initial material costs, with full account taken of the cumulative advantages that accrue from design, selection, fabrication and operation using these materials.

To date, only a limited amount of welding research has been performed on X100 linepipe, with the emphasis placed on the longitudinal seam weld properties. At the outset of the research programme no information existed on the properties required of girth, repair or tie-in welds for this material. As a precursor to considering such new materials for a major capital project or before pipeline operators can be fully confident in the use of X100 linepipe, it is necessary to undertake a detailed study of the welding technology relevant to field construction of the material. This is necessary to confirm that satisfactory welds can be made and to determine the data for a reliability-based design with appropriate weld-defect acceptance criteria. Acceptance of the material and its ability to be fabricated is also required by regulatory bodies in many countries, most of whom require that the material is present in standards and codes of practice prior to sanctioning any construction project. A wide body of data is usually a prerequisite for inclusion of a material within a standard or code, and in this respect it is important to increase and promote the knowledge base via research with respect to X100 and its fabrication. The natural conservatism within the industry towards new materials can only be overcome through effective communication of research findings and construction trials. In this respect communication between all parties involved in the integration of new developments (for instance Universities, transmission line

owner/operators, construction contractors, equipment suppliers) is of paramount importance in the timely acceptance of new technology.

The metallurgical properties of X100 linepipe and potential weld metals are such that consumable selection, welding procedure development and production welding controls require comprehensive evaluation to ascertain their feasibility in the field. Such testing and qualification of procedures by contractors is needed to ensure that the procedures, and any variation thereof, are technically sound and will produce welds of the required quality and properties. The incremental change in technology between Grade 550 (X80) and Grade 690 (X100) is significantly more complex than it was between Grade 485 (X70) and Grade 550, with markedly different microstructures present in both linepipe and the weld metals that are potential candidates for pipeline welding.

Since the early 1970's pipeline constructors have gained significant cost savings and quality improvements through the development and implementation of gas metal arc welding (GMAW) processes for mainline welding. Mechanised, high productivity welding with minimum intervention by the welder also offers distinct advantages in the harsh conditions and short construction seasons anticipated for some possible areas of linepipe routing, particularly in Arctic regions such as Alaska, Canada or Siberia. The advent of higher productivity mechanised narrow gap welding processes, such as the dual torch, tandem wire or dual tandem torch GMAW variants of the process, further increases the potential for economic savings during pipeline construction.

The novelty within the current work is aimed at the examination of various aspects relevant to the field welding construction of X100 linepipe. The welding equipment and procedures were kept as close as possible to those currently used in the field, such that transfer of successful research outcomes from the programme to a field situation should be minimised, both in terms of time and equipment modification. A range of wall thickness and diameter variants of pre-production pipe sections were received from several pipe manufacturers for the purposes of girth welding procedure development and associated research. Prior to the current research programme no girth welding trials, let alone systematic studies, had been reported using X100 linepipe. The programme of work included single, dual and tandem torch narrow gap mechanised welds to simulate pipelay main line welding, alongside manual/semi-automatic repair and tie-in procedures. Pulsed gas metal arc (PGMAW), conventional short-circuit gas metal arc (GMAW), shielded metal arc (SMAW) and flux-cored arc welding (FCAW) were used selectively, as appropriate to each application. The development of a tandem torch pipeline welding system at Cranfield just prior to the start of the current research programme[11,12,13] enabled the first full welding procedure development and qualification of the technology during this research. This process is unique amongst modern mechanised fixed position pipeline welding techniques in using two wires to feed a single weldpool, thereby allowing high travel speeds but still maintaining weldpool control. A further novelty involved the use of the process with X100 pipeline steels. Proposed mechanical property requirements of the weld metal relevant to strain based design using X100 pipe were established at the research programme outset, from which a variety of consumable electrodes were used to initially determine potential weld metal chemistry levels. This was followed by full weld procedure testing of selective chemistries with conformance to the requirements of existing European and American transmission pipeline welding standards, wherever possible. Analysis of the data

resulted in an optimal weld metal chemistry, from which a further series of experiments were designed to examine various procedural and chemical permutations.

The variety of mechanised GMAW systems on offer for pipeline construction in today's market provided the impetus for a comparative process study; single wire, tandem wire, dual torch and dual tandem torch welding techniques were examined by minimising all variables between the processes. A novel technique for multiple weld metal thermocycle measurement from an initially molten weldpool was developed, particularly with a view to capturing data from multi-layer deposition processes such as dual torch and dual tandem torch. The resultant data provided a valuable insight into the weld metal cooling variations possible throughout the thickness of a multi pass narrow gap weldment, with the data compared with various mechanical property measurements. In a similar fashion, several variants of preheat and interpass temperature changes using the conventional single wire mechanised GMAW technique were also examined.

The high cooling rates determined through the various experimental procedures were shown to be the cause of the significant strength increases when compared with the results of the same alloy in a more convential cooling rate regime. These results prompted the final research area undertaken, namely the examination of alloying effects in a typical narrow groove associated with mechanised pipewelding. Specific alloy chemistries were manufactured to gain an understanding of the property variations possible when all other variables were minimised. From this information an idea of the tolerance box associated with a nominally 'optimal' chemistry could be determined in order to maintain the required target properties using typical mechanised welding practices.

It is proposed that this work, in combination with other research projects and programmes worldwide will help to bridge some of the gaps in knowledge associated with high strength steel linepipe welding practices, and generally promote a more positive view of these material types. It is also anticipated that research of this type will help instigate end user development and confidence with the various procedures and technologies discussed, which in turn will promote the more timely inclusion of these materials in standards and codes of practice.

2 LITERATURE REVIEW

2.1 THE REQUIREMENT FOR TRANSMISSION PIPELINES

It is estimated that the world currently consumes 402 thousand tonnes of oil/hour and 290 million cubic metres of gas/hour[14]. A forecast for future world energy usage is expected to show an increase by 60% to 2020, with fossil fuels continuing to dominate up to 2050[15]. At the end of 2002 the world proven reserves of gas were nearly 156 trillion cubic meters and that of oil nearly 143 billion tonnes (cf. total proven coal reserves of 984 billion tonnes)[14]. The ratio of natural gas in total primary energy sources consumed will increase in the first half of the present century[15] such that it will have an estimated market share of nearly 80% in 2025 (doubling the current volume consumed[16]). In Europe gas consumption will increase rapidly, and by 2020, 70% will be imported. Ten countries contain 80% of proven gas reserves, 30% of which are in the Russian Federation and 36% in the Middle East. The Russian Federation is the second largest consumer of gas (15%), although the USA and West Europe collectively consume a larger amount even though they possess only 11% of proven reserves[17]. Over 65% of proven recoverable oil reserves are in the Middle East (25% in Saudi Arabia)[14], with the major oil producers being Saudi Arabia, the Russian Federation and the USA (descending order of magnitude). Oil demand is greatest in the Atlantic basin and Asia pacific, highlighting the net surplus production of the Middle East in providing the world 'energy balance'[18]. As can be seen, the supply and demand for fuels occur in differing locations, such that politics will be an integral component of our energy future.

The exploration and production of fuels to meet the increasing demands posed throughout the world have seen a consequent requirement for a transmission infrastructure. Two of the primary energy sources, oil and gas, are ideally suited to distribution via pipelines on- and offshore due to their fluid constitution and high volume requirement. The function of pipelines is the transport of the specified medium in large quantities, safely and in the most economic fashion; it is these criteria which pose great material technological challenges, particularly in the case of gas transmission. The desire to locate and extract from new oil and gas fields that will be both economically attractive and less liable to political pressures and changes have resulted in considerable assessment of areas such as the North Slope development of Alaska[19], and the Tarim desert region of northwest China[4]. Both of these examples will involve the construction of very long distance (>2000 miles) gas pipelines through hostile environments to bring the fuel to the desired locations. This in turn places greater demands on the system in the form of mechanical properties and material integrity, with the best possible compromise on safety levels.

2.2 THE CASE FOR HIGHER STRENGTH STEELS

Conventionally, high pressure gas transmission is at approximately 10 MPa (1450 psi) for which API 5L Grade X80[20] is adequate, but it is proposed to increase this to 15 MPa (2175 psi) in the near future. The increase in operating pressure will offer a distinct advantage by allowing a greater volume of gas to be transported in a given time period or for longer lengths. This has generated the drive for higher strength steel development, enabling a reduction in wall thickness and diameter for a given pressure. Additional

advantages are the decreased construction costs and steel volumes. Long distance gas pipelines require expensive compressor stations at specified intervals; increasing the gas pressure requires less stations and therefore has a significant impact on the project economics. Petroleum and gas fields have been surveyed in areas which were once considered uneconomical to exploit due to geographical location and/or environment e.g. Arctic or areas of seismic activity, but with the advent of new materials the situation becomes more favourable. Reduced linepipe weight significantly decreases the costs of transportation of the pipe sections prior to construction in the field, whilst reduced wall thickness decreases construction time due to the lower volume of weld metal required. As a result the prospect of high strength steels are widely recognised as the future of bulk gas transportation. The strength level being investigated by several major producers of high quality/technology line pipe is designed to meet a specified minimum 0.5% tensile elongation ($R_{t0.5}$) strength of 689 MPa (100 ksi) i.e. equivalent to an API 5L X100 if the latter were to exist. The material properties for this strength of linepipe have currently only been specified in the Canadian standard for linepipe[21], but it is undoubtedly the intention of further specification bodies to include pipes at these strength levels in the near future. An example of the cost reduction possible from changing the pipe strength from X70 to X100 has been shown to be just less than 20%, even when the increased premium for the material is taken into account[22]. The corresponding reduction in weight approaches 30% for identical volume/time transportation.

Research and development of even higher strength linepipe of specified minimum yield strength (SMYS) 827 MPa (120 ksi) is also under-way[23] to further increase the economic benefits. The challenge to the manufacturers is the provision of consistent strength levels coupled with the highest possible toughness and weldability. The higher the strength, the greater this challenge becomes in maintaining the correct balance of properties for both the base material and weld metal.

2.3 DEVELOPMENT OF PIPELINE STEELS

2.3.1 HISTORICAL DEVELOPMENT

Pipelines have been employed for thousands of years as a means of making mankind's lifestyle more amenable. Early water transportation systems used bamboo in the far eastern civilizations, with the Romans famed for their lead piping infrastructure. With the increasing variation of materials requiring transport over the last few centuries, such as sewage, oil, refined products, gas, chemicals and slurries, the number of material variants used to transport them has increased. Vitrified clay, asbestos-cement, concrete, ductile iron, carbon steel, alloy steel, plastic and composites are typical examples[24]. The location of pipelines has also moved from solely onshore locations to offshore, with increases in water depth occurring all the time (pipelines in over 2000m water depth have been laid[25]).

There has been continual progress in the demands made on steel linepipe since the first major milestone in, what was then, high strength/long distance oil transportation for the Trans Alaska Pipeline System (TAPS) in 1968. 500,000 tons of API 5L Grade X65 of 48 in. outside diameter were manufactured by three Japanese steel companies for the project. This development stimulated the demand for higher transportation efficiency,

field welding efficiency and safety through pipes with greater strength and low temperature toughness. Strength levels have increased through projects such as the Trans Siberian pipeline (X70)[1] and the Ruhrgas pipeline (X80)[2], with toughness levels increased to cope with the greater wall thickness and colder environments. Resistance to hydrogen induced cracking (HIC) and sulphide stress corrosion cracking (SSCC) is now an important aspect of pipe design due to the development of sweet or sour resources containing various amounts of H_2S, Cl and CO_2. Where levels permit the use of conventional steels as opposed to corrosion resistant alloys (eg modified 13Cr, duplex, super duplex), HIC test methods of increasing severity (eg NACE TM 01-77[26] or NACE TM 02-84[27]) have been developed to provide a basis for material suitability.

The rationale behind high strength linepipe development is shown diagramatically in Figure 2-1. A summary of linepipe changes from the mid 1960's to the early 1990's is shown in Figure 2-2, with the following paragraphs highlighting the major differences between the grades:

- API 5L X52 linepipe was one of the first high strength low alloy (HSLA) steels to be used for the transmission of oil and gas. The microstructure essentially consisted of ferrite and pearlite, the former involving a matrix of polygonal ferrite with varying amounts of interspersed pearlite.
- API 5L X70 linepipe is generally classed as a ferrite and pearlite microstructure[28]. X70 was introduced to satisfy higher strength and toughness requirements. Improvements in mechanical properties were produced by a combination of strengthening mechanisms, microalloying and TMCP technology. The latter allowed higher accelerated cooling rates of 10-15°C/s together with a leaner base metal chemistry to produce greater homogeneity within the microstructures[29].
- API 5L X80 linepipe. Whereas X70 linepipe was characterised as predominantly a ferrite and pearlite microstructure, X80 linepipes are said to comprise of a bainitic-ferritic and bainitic microstructure[10], or tempered bainite and tempered martensite[30]. The chemical composition of X80 steel is based on a low carbon and high manganese content with microalloying combinations typically involving niobium and titanium or niobium and vanadium. Additional elements such as copper, chromium, nickel, molybdenum and boron are sometimes also present.

The technological challenges can be broken down into four major, often related, areas of development; increased strength, increased low temperature toughness, ease of field weldability and reduction of HIC/SSCC.

2.3.1.1 STRENGTH INCREASES

Classical alloying techniques for increasing the strength of steel involve high carbon levels (>0.3%) with possible additions including manganese, chromium, vanadium, molybdenum, nickel and copper. However, these elemental additions reduce the ease of fabrication due to high hardenability levels experienced throughout the heat affected zone of a welded joint. Hardenability is a measurement of a materials ability to generate a martensitic structure, and it has been found that the resulting martensite hardness is directly related to the amount of carbon present in the steel. Increased hardenability can be achieved by higher alloying (except cobalt or aluminium) or increased cooling rates,

both of which modify the materials microstructure by suppressing the transformation temperature or increasing the driving force for lower transformation temperature products such as martensite or bainite. The expensive application of preheat to lower the cooling rate may reduce or eliminate the chances of problems associated with high hardenability, such as heat affected zone cracking, but with the emphasis on speed and ease of fabrication in industry, the elimination or reduction of preheating by alloy design is of major importance.

The incentive of reducing expensive alloying additions to generate higher strength steels prompted research into the fundamental principles governing steel properties. Pioneering work undertaken by Hall, Petch, Cracknell and Cottrell[31,32,33,34] found that a reduction in the ferrite grain size raised the yield stress (σ_y) and lowered the impact transition temperature ($C_v$trans) simultaneously. Through this knowledge, the advent of controlled rolling within the steel plate production process allowed fine grained ferrite-pearlite steels to gain widespread acceptance as a means of manufacturing high specification steel with lower levels of major alloying elements from the late 1960's. Similar advances were made using microalloying technology (typically involving additions of Nb, V, Ti and B) to further control the austenite (γ) and ferrite (α) grain sizes throughout the reheating, rolling and cooling processes, coupled with precipitation hardening effects. A further benefit was found in the use of accelerated cooling after final rolling to increase strength via transformation hardening without a loss in the low temperature toughness. The technology derived from these studies resulted in the modern day thermomechanical controlled processing (TMCP) of steel production employed by linepipe manufacturers. Compared to the traditional Q and T high strength steels which rely predominantly on transformation strengthening to generate their properties, the lower carbon equivalent (CE_{IIW}[35] or P_{cm}[36]) attainable through TMCP for a given plate thickness appreciably enhances the field weldability via a reduction in heat affected zone (HAZ) hardness (comparing identical welding conditions). The absence of a tempering stage also enhances the productivity and economy; essential attributes for the mass production of linepipe.

2.3.1.2 TOUGHNESS INCREASES

Pipelines are required to resist fracture initiation and propagation in the event of severe integrity compromisation in order to avoid large scale catastrophes. An example causing such compromisation could be a defect greater than the allowable critical size due to corrosion. The exploration and recovery of oil and gas resources are moving to more remote and hostile environments, where the arrest of fracture requires high toughness levels at low temperatures for both the base material and weld metal. Fractures occurring in oil pipelines observe rapid decompression at the crack tip with the result that fracture is arrested over a short distance. Gas pipelines, on the other hand, involve slow decompression due to the high stored energy, with a consequent possibility of propagation over long distances (running fractures). As described earlier, the future requirements of gas transportation will involve even higher pressures, so arrest of brittle and unstable ductile fracture is of prime importance.

Brittle fracture arrestability can be judged empirically by the Battelle drop weight tear test (BDWTT) (a supplementary requirement in API 5L[20]). The resulting percentage shear area is recorded, and if found to be above 40% with the test conducted at the

design temperature, the propagation speed of brittle fracture (typical maximum value 300-400m/sec[37]) is regarded as being lower than the decompression rate (typically 450m/min), with the result that brittle fracture is arrested[38]. Due to the distribution of results from various heats from which pipes of varying diameter/wall thickness will be manufactured (API 5L states >80% of the heats should exhibit shear areas >40%), it is generally specified for gas pipeline material to give a shear area of 80 to 85% at the design temperature to ensure fracture arrest. BDWTT temperatures have continually reduced over the last few decades due to the environments encountered; what was formerly 0°C to –20°C can now be as low as –50°C to –60°C. Through full scale burst testing and corresponding small scale testing various companies and institutes have established a correlation between BDWTT and Charpy V notch (Cv) impact toughness with the design stress for arresting unstable ductile fracture in pipelines at the design temperature. As an example, work by the high strength linepipe committee of the Japanese Iron and Steel Institute [39], resulted in the following equation:

$$Cv = 2.498 \times 10^{-6} \cdot \sigma_H^{2.33} D^{0.30} \cdot t^{0.47}$$

where σ_H = Hoop stress (MPa), D = diameter (mm), t = wall thickness (mm), Cv = 2/3 subsize Charpy specimen energy (J). A pipeline of 1219mm (48 in.) OD, 18.3mm WT carrying a single phase gas would require approximately 49J Cv (6.67 x 10mm specimen) or 3 kJ standard BDWTT for an X60 grade (300 MPa design stress), compared with approximately 95J Cv or 4.5 kJ BDWTT for an X80 grade (400 MPa design stress). Extrapolating this for X100 (550 MPa design stress) results in a Cv minimum value of 200J or 7.5kJ BDWTT; this value however needs confirmation through reliability testing for ductile fracture arrestability, as the background data have yet to be substantially generated for X100 grade steels. The main conclusion from the research is a recognition that, with increasing pipe OD, WT and operating pressure, increased values of Cv or BDWTT are required.

Full-scale burst tests are becoming more frequently used in determining pipeline fracture behaviour, typically using gas of a specified composition comparable with that of the project pipeline gas. The results can be used to define the material toughness requirements for arresting a fast propagating ductile fracture (providing that the material in the test produces a self-arrest), as well as verifying the applicability of using Cv impact or BDWTT levels for characterising the fracture resistance of the particular material. The mechanical properties (YS, UTS, Cv, BDWTT) of each pipe in the string to be tested are assessed, such that their expected toughness usually increases either side of the crack initiation point. Predictive arrest Cv values for a particular pipe can be calculated using either the Battelle simplified equation[40] or Battelle two curve approach[41], with the latter favoured for high pressure values[37]. An explosive charge is used to initiate the crack, with typical instrumentation involving pressure transducers for measuring both the test pressure and pressure decay, and timing wires for crack speed measurement during crack propagation. Comparison of the actual pipe toughness versus the predicted Battelle toughness has shown a discrepancy for recent X100 tests [37], such that a correction factor should be applied to the equation for future arrest predictions.

Another test used to assess fracture propagation toughness is the Battelle West Jefferson test. This involves pressurising a pipe section with water, air or fuel gas at a specified temperature to the desired percentage of the pipe SMYS. Crack initiation is again initiated by an explosive charge. Crack arrestors are sometimes incorporated within the

projected fracture area to assess their suitability, with the resulting shear area of the fracture surface calculated for comparison with Cv or BDWTT results.

Brittle fracture is initiated mostly in weld metal and rarely in the base material of pipelines, hence the necessity for 'robust' weld metal designs. Charpy values for both the weld metal and HAZ are consequently specified, their level depending upon the service conditions and permissible flaw size in non-destructive testing. Another test developed to characterise a materials fracture initiation resistance is the fatigue-notch crack tip opening displacement (CTOD) or J-Integral, the results of which are often correlated with Cv values. Typical values for pipelines and their welds up to X80 grade are 30 to 60J Cv and 0.1 to 0.25mm CTOD at the operating temperature. Ring expansion testing with intentional defects at specific locations (e.g. HAZ of seam weld) and curved wide plate testing are further tests used to assess fracture initiation toughness. The latter is often used to determine girth weld fracture initiation resistance, defect size tolerance and axial strain capacity[23].

2.3.1.3 INCREASED WELDABILITY

The ease of welding a given material has traditionally been of great concern for all branches of steel fabrication. A major objective of steel manufacturers is to provide a material which allows the largest possible range of heat input due to the welding thermocycle(s) over which the desired base metal properties can be maintained. Numerous formulae have been developed by various researchers[42], often applicable within certain boundary conditions. The original hardenability equation developed by Dearden and O'Neill [35] and adopted by the International Institute of Welding (IIW) in terms of a carbon equivalent value was derived from the hardenability of the HAZ due to the presence of certain elements:

$$CE_{IIW} = C + \frac{Mn}{6} + \frac{(Ni + Cu)}{15} + \frac{(Cr + Mo + V)}{5}$$

It has been found that good agreement using the formula exists between the resulting hardness (and the consequent susceptibility to cold cracking) when C levels are >0.18%, or the time for the base material to cool from 800°C to 500°C ($t_{8/5}$) due to the heat cycle is longer than approximately 12 seconds [43]. Pipeline steels, however, have traditionally used leaner alloying coupled with advanced processing routes. The Ito and Bessyo[36] Parameter crack measurement (P_{cm}) formula, derived from cold cracking tests in a Y groove (test method JIS Z 3158), has become the benchmark value for assessing pipeline weldability. It is particularly applicable for welding processes giving $t_{8/5}$ times of less than 6 seconds and C levels well below 0.22%[43]:

$$P_{cm} = C + \frac{Si}{30} + \frac{(Mn + Cu + Cr)}{20} + \frac{Ni}{60} + \frac{Mo}{15} + \frac{V}{10} + 5B$$

A further carbon equivalent (CE) formula that has been developed with a variety of normalized, Q and T and TMCP ferritic steels in mind is the CET formula specified in the latest BS EN recommendations for the arc welding of ferritic steels[44]. Part 2, Annex C.3 of this standard provides guidance on the avoidance of hydrogen cracking in non-alloyed, fine grained and low alloy steels (groups 1 to 4 of CR ISO 15608[45]) using the CET value in the calculation. The formula is applicable for carbon contents in the

range of 0.05 to 0.32 weight %, and also specifies maximum limits for all the major and micro-alloying elements:

$$CET = C + \frac{(Mn + Mo)}{10} + \frac{Cr + Cu}{20} + \frac{Ni}{40}$$

The use of CE values in providing a measure of hardenability in the material has promoted the use of maximum allowable hardness values in weld metal and the HAZ. These are typically set at a maximum of 325-350 HV10 for pipes not experiencing a sour medium, and less than 250-275 HV10 for those that do in order to prevent stress corrosion cracking[46]. As seen from the above equations, carbon exerts a strong influence on the calculated CE value, resulting in a major drive by the linepipe manufacturers to reduce carbon levels to increasingly lower levels[47] (see Figure 2-3), thereby reducing the hardness and cold cracking susceptibility. There is obviously a balance to be attained between the required strength level and the resulting weldability due to the required alloying. It should be noted also that the above three equations exclude factors such as additional elements (e.g. Nb), the variation of cooling rates and diffusible hydrogen contents of weld metals, all of which can significantly affect the outcome. Further studies incorporating these variants have therefore been pursued (for example the Yurioka CEN formula[48]), but widely applicable solutions to a broad band of material compositions and thermal histories have not been found with any great degree of confidence. This has resulted in the continued need for weld procedure qualification following the development of new steels or welding techniques.

2.3.1.4 REDUCTION IN SUSCEPTIBILITY TO HYDROGEN INDUCED CRACKING AND STRESS CORROSION CRACKING

Pipelines used to transport sour oil and gas have been in existence for over three decades. An accident involving leakage of oil from a pipeline in the Persian Gulf in 1972 however prompted research[1] into what became known as hydrogen induced cracking (HIC). HIC is classified as cracking in the absence of an external applied stress, contrary to stress corrosion cracking (SCC) which occurs under the influence of an external stress system, and is observed usually with steels of yield strengths above 550MPa. The mechanism of HIC can be explained by the following steps:

1/ Hydrogen evolution as a product of corrosion processes on the steel surface, or introduction via the welding consumable, followed by its diffusion into the steel.

2/ Atomic hydrogen combination at precipitation sites such as elongated non-metallic inclusions and coarse precipitates to form molecular hydrogen. Internal pressure caused by the molecular hydrogen may initiate cracks, and the steel surface may show a blistering effect.

3/ Propagation of the cracks occurs along adjacent non-metallic inclusions and susceptible (hard) microstructures such as those found along the centre segregated zone of a plate.

The avoidance of elongated non-metallic inclusions can be achieved through the addition of elements which influence their morphology. An example is calcium; this element combines with sulphides, reducing their aspect ratio and thereby their tendency to promote crack propagation. Clean steel production (low levels of sulphur,

phosphorus, oxygen and nitrogen) reduces the volume of non- metallic inclusions and subsequent sites for atomic hydrogen combination.

Studies on centreline segregation have imposed limits on its width to prevent crack propagation. The segregation of manganese and phosphorus, as measured by electron probe microanalysis (EPMA) in the vicinity of HIC after testing in NACE solution has shown crack arrestability for combinations of manganese and phosphorus resulting in hardness levels below 250 HV0.025[49]. Figure 2-4 summarises the propagation/composition boundary; increasing manganese is required for higher strength levels and low (<0.02%) phosphorus should ensure HIC arrest.

HIC resistance is measured in terms of a crack length, thickness or sensitivity ratio[26] calculated after immersion in a specific solution (e.g. BP test solution: H_2S saturated artificial seawater with a pH of 4.8 to 5.4 or NACE test solution: H_2S saturated solution of 5% NaCl and 0.5% CH_3COOH with a pH of 2.7 to 4.0) for a given time (e.g. 96 hours). Current requirements for sour service pipe in the North Sea are less than 10% crack length ratio (CLR) (see Figure 2-5) after immersion in the more severe NACE solution.

As per the recommendation for avoiding HIC, hardness levels below 248 HV10 have been specified in the NACE material requirement MR-01-75[50] for both parent plate and welds for avoidance of SSCC. A requirement of less than 1% nickel in both steel and weld metal is also specified due to increased susceptibility of SSCC above this value. Microstructural homogenization is considered an important attribute in reducing SSCC, alongside the previously mentioned material characteristics for lowering HIC susceptibility. SSCC has been observed in the softened HAZ of pipe welds with HV10 values below 248 [51], leading to the term stress-oriented HIC (SOHIC).

2.3.2 DEVELOPMENT OF HIGH STRENGTH STEEL PIPELINES

The replacement of carbon with manganese, coupled with microalloying additions and controlled rolling to attain the required strength and toughness, has occurred since the 1960's. Early generation microalloying was undertaken using additions of niobium and vanadium coupled with controlled rolling to produce steels with ferrite/pearlite microstructures. The early steel compositions for projects such as TAPS were 0.11-0.14% carbon, 1.2-1.4% manganese with niobium and vanadium additions. Niobium (typically 0.01% to 0.05%) provides the steelmaker with two important characteristics:

1/ At typical slab/bloom reheating temperatures of 1250°C, substantial amounts of niobium are taken into solution. On cooling to the specified rolling temperature, the recrystallisation of austenite below 900°C[29] is delayed due to the strain induced precipitation of Nb(CN) within the austenite matrix. Combined with a short period between finish rolling passes occurring below this temperature, the progressively deformed austenite grains release only a minor part of their stored energy due to recovery. The consequent highly elongated grains with a high level of stored energy result in a fine ferrite grain size (<8μm) on transformation of the deformed austenite. The latter occurs principally due to the higher nucleation rate per grain surface area of the deformed austenite (higher grain boundary energy), alongside the greater number of intragranular nucleation sites. This results from the presence of deformation bands and annealing twins[52]. The two previous effects vary as a function of strain and

transformation temperature, thereby emphasising the correct selection of controlled rolling schedules.

2/ Precipitation hardening by Nb(CN) occurs within the ferrite matrix after transformation; the coherent precipitates pose formidable obstacles to dislocation motion thereby increasing the hardness with tempering time.

Higher levels of niobium were investigated (0.1%) with lower carbon levels, in which the precipitation hardening and grain refinement effects were enhanced[53], but the strength levels failed to break through that of the ferrite/pearlite steels, with field weldability being rather poor.

Vanadium, like niobium, has a strong affinity for carbon and nitrogen, and amounts typically in the range of 0.04% to 0.15% are added to form V_4C_3 and VN. Complete solution of V_4C_3 occurs at typical normalizing temperatures of 920°C (cf. Nb(CN) where very small amounts will be dissolved) resulting in high levels of precipitation on transformation to ferrite, with consequent high levels of precipitation strengthening (up to 150 MPa per 0.1% V[54]). VN goes into solution at slightly higher temperatures (~1050°C) than V_4C_3, although in aluminium killed steels (as was typical practice), Al is the more powerful nitride former resulting in mainly V_4C_3 precipitation. When high levels of vanadium (0.45%) are combined with high nitrogen levels (0.01%) and lower carbon levels VN forms, causing the retardation of austenite recrystallisation (as per Nb(CN)) during rolling alongside the generation of precipitation hardening[55]. The strength level achieved, however, is again only up to around 590 MPa (ferrite/pearlite steel limit) with limits placed on the attainable wall thickness and poor field weldability.

A further microalloying element employed to increase the strength level is titanium. Additions of 0.03% - 0.07% have been utilised[29,56] for the formation of TiC, which retards austenite recrystallisation and promotes precipitation hardening. TiN is stable above normal slab reheating temperatures and does not therefore contribute to hardening through strain induced precipitation. The effects, however, are again limited to strengths similar to those of ferrite/pearlite steels. Figure 2-6 shows the relative effect of Nb, Ti, Al and V on the static recrystallisation stop temperature (dynamic recrystallisation is hard to achieve with controlled rolling); Nb is the most effective in raising the recrystallisation stop temperature, with Ti, Al and V following in order of reduced effectiveness[57].

Further investigations using low carbon coupled with various additions of nickel, chromium and copper totalling 0.5%, so as not to impair weldability were performed[58]. Results demonstrated that the strength/toughness relationship was improved due to enhanced grain refinement caused by controlled rolling in conjunction with a drop in the Ar_3 temperature, alongside solid solution strengthening. The microstructure, however, remained as ferrite/pearlite with a consequent limit on the maximum attainable strength level.

Work undertaken by Pickering[59] provided the key to increasing steel strengths without using medium to high carbon levels. Figure 2-7 shows the relationship between 50% transformation temperature (usually the maximum rate of transformation) and tensile strength for a variety of normalised steel compositions (0.05 – 0.2% C). As the transformation temperature falls, the microstructure changes from ferrite/pearlite to acicular ferrite, to upper then lower bainite and finally martensite. Strength levels correspondingly increase; the large variation observed with bainitic microstructures was

found to be in good agreement of their particular 50% transformation temperature. It was observed that the variety of alloying levels resulting in a given transformation temperature could be achieved in numerous ways, pointing to a certain independence of microstructure and chemistry.

In the early 1970's acicular ferrite steels were developed for linepipe use comprising low carbon (0.04-0.06%), high manganese (1.8-2.0%), molybdenum (0.4%) and niobium (0.04%)[60]; carbide precipitation was avoided with transformation strengthening the predominant mechanism. The resulting microstructure exhibited improved low temperature toughness with higher strength levels and the ability to manufacture thicker plate sections. The downside was an increased CE_{IIW}/P_{cm} due to the high manganese and molybdenum levels employed, with a consequent reduction in field weldability. Steels with reduced manganese and molybdenum levels followed to improve the weldability, with the strength maintained by vanadium additions coupled with titanium to aid grain refinement (thereby increasing toughness) via the formation of TiN[61]. The TiN particles significantly reduce austenite grain growth during slab reheating due to their high melting point (>1450°C)[62], resulting in a fine grained microstructure classified as one involving a mix of ferrite/pearlite and acicular ferrite.

Developments to further increase strength were aimed at generating bainitic microstructures with very low carbon levels, leading to the terminology of ultra low carbon bainitic (ULCB) steels. One method utilises the strong effect of boron as an extremely efficient strengthening agent when used in combination with elements such as aluminium, titanium and niobium. Boron has a strong affinity for oxygen and nitrogen, but this is reduced when aluminium and titanium are present, with the result that soluble boron is present to fill interstitial sites in a similar fashion to carbon and provide solid solution strengthening. The level of carbon in combination with boron is consequently very important; the lower the carbon level the more potent a given amount of soluble boron (this is recognised in the P_{cm}[36] hardenability formula). The addition of niobium to steels with boron additions suppresses the formation of $Fe_{23}(CB)_6$ through the development of niobium carbides, with a consequent lowering of the austenite to ferrite transformation temperature. Boron levels of 7 to 20 parts per million (ppm) in conjunction with niobium and molybdenum have been investigated, with the result that yield strength levels in excess of 700 MPa with reasonable levels of toughness (>100J at –20°C) are attainable[5].

To improve the low C-B-Nb-TiN system, additions of copper[6] for strength (precipitation hardening) and nickel[63] for higher toughness (refinement in grain size due to the suppression of the A_{r3}, with a relatively small increase in hardenability) were investigated.

The previous strengthening mechanisms were developed in conjunction with controlled rolling (thermo-mechanical rolling) of steel plates. This process allows rolling to be performed using a predefined amount of reduction in specific temperature regions to generate optimum microstructures. The advent of accelerated cooling (ACC) after final rolling enhanced the effects learnt through the previous alloy and microalloy additions, such that lower overall alloying levels were required with consequently even lower P_{cm} and CE_{IIW} values, thereby enhancing the material weldability.

2.3.3 *THERMO-MECHANICAL CONTROLLED PROCESSING FOR HIGH STRENGTH PIPELINE PLATE MATERIAL*

Thermo-mechanical controlled processing (TMCP) of steel incorporates the thermo-mechanical rolling (TMR) of steel plates coupled with ACC. TMR is illustrated in Figure 2-8; the repeated action of rolling, recovery and recrystallisation refines γ grains coarsened by slab reheating, but at high rolling temperatures rapid grain growth follows the recrystallisation thereby negating the refinement; hence the requirement of effective pinning agents such as titanium and niobium precipitates. Further rolling in the non-recrystallisation and intercritical (two-phase) regions, however, greatly refines the structure due to the increase in austenite grain-boundary area, alongside an increased ferrite nucleation rate at the austenite grain boundaries. The presence of deformation bands and annealing twins created by rolling at these lower temperatures also increases the ferrite nucleation sites. The transformed ferrite grains also work harden due to the resultant substructures, following in further refinement of the grain size. The TMCP of steel can be divided into two main types[66]: direct quenching and tempering, and accelerated cooling (Figure 2-9). The former (often referred to as Type I) involves the water cooling of plates close to room temperature via a high cooling rate; tempering is usually required after the initial processing to obtain the appropriate ductility and toughness. The latter method (often referred to as Type II) involves water cooling at a moderate rate in the transformation region only; air cooling can then be employed, resulting in a self-tempering effect which provides excellent toughness and ductility without the need for a separate, time consuming and expensive tempering stage. It is this method that is employed in the production of pipeline steels in view of the balance between mechanical properties and productivity.

The main stages for TMCP can be divided into three major areas, each of which have their specific control parameters[64]:

Stage	**Main Control Parameters**
Slab reheating	Reheating temperature Holding time
Rolling	Cumulative reduction in the recrystallisation region of γ (down to ~950°C) Cumulative reduction in the non-recrystallisation region of γ Cumulative reduction in the intercritical region (i.e. between Ar_3 and Ar_1) Finish rolling temperature
Accelerated cooling	Start temperature Stop temperature Cooling rate

The numerous variables highlighted above generate a highly complex situation for property generation when taking into account the chemistry variations possible, alongside the desired plate thickness. Linepipe manufacturers have experimented with various development routes, some of which are examined below in the generation of TMCP 690 MPa minimum yield strength pipe steels.

2.3.3.1 690 MPA (X100) YIELD STRENGTH LINEPIPE

By the mid 1980's the development of an X100 grade material had been extensively researched on a laboratory scale[7], and in the early 1990's a number of oil and gas companies started project design studies based on this grade of material. As strength levels rise it becomes increasingly difficult to attain the required low temperature toughness. X100 steels are produced using a combination of closely controlled alloying elements together with optimised TMCP technology. Both upper and lower bainite microstructures have been reported as the major constituent in X100 research work, as a result of the particular alloy and TMCP technology employed[5,7,8,9,10,64,68]. The cooling start temperature and subsequent cooling cycle play an extremely important part in the microstructural development as shown in Figure 2-10[9].

The way forward now comprised large scale mill trials, the like of which were taken up by high quality pipe manufacturers in Western Europe and Japan. Typical stress strain curves for low to high strength steels are shown in Figure 2-11 highlighting the increase in yield to tensile ratio and reduction in overall elongation as the strength level is raised[8]. Table 2-1 gives an overview of the chemistries, manufacturing routes and resultant properties from four companies involved in the development of TMCP 690 grade steels. Although the chemistries and processing routes differ considerably, the microstructures generated all exhibited a high proportion of bainite, with one manufacturer[64] proposing a preference for upper bainite in conjunction with high toughness. The latter is not normally associated with upper bainite (Figure 2-12) due to the larger effective grain boundary (Figure 2-13), so the key to higher toughness development lies in the refinement of the prior austenite grain size. Various researchers have recognised the benefits of bainite in the microstructure of X100 grade linepipe. Their description of the microstructure however varies from a ferrite-bainite structure[7] or a bainitic ferrite with small amounts of second phase[10] to bainite with finely dispersed martensite[9]. A bainitic microstructure gives rise to high strength with very little sacrifice in toughness, and has a superior strength/toughness balance to that of the ferrite-bainite or polygonal ferrite-martensite types.

The traditional technique employed to produce lower bainite or martensite requires considerable amounts of alloying elements, which consequently result in a large deterioration of field weldability. Improvements in low temperature toughness are therefore centred on efforts involving grain refinement (microalloying with e.g. Nb, Ti, Al, Mg, V, B) together with optimised TMCP. This produces a reduction in martensite-retained austenite (M-A) constituents (i.e. hard phases) by reducing overall carbon levels and P_{cm}/CE_{IIW}. Lowering levels of phosphorus and sulphur and/or modifying their morphology (eg. Ca treatment) reduces the possibility of centreline segregation effects in continually cast slabs[9]. Specific improvements to toughness in the HAZ have involved titanium oxide (Ti_2O_3) particles which are stable above 1350°C, and are therefore available to nucleate fine intragranular α on the transformation of γ to α. Above this temperature TiN particles dissolve, consequently losing their effectiveness in controlling the γ grain growth by boundary pinning. As the weld heating cycle will involve temperatures adjacent to the weld metal rising in excess of 1450°C, the presence of Ti_2O_3 particles enables the maintenance of high toughness HAZ's. Low carbon levels also show an improvement for HAZ toughness (Figure 2-14) due to a reduction of M-A constituents and a consequent decrease in embrittlement (Figure

2-15). The complex relationship between carbon content, carbon equivalent, accelerated cooling rate and stop temperature for the attainment of X100 strength levels allow varying routes to be taken, as illustrated in Figure 2-16.

2.3.4 MANUFACTURING PROCESSES FOR LARGE DIAMETER LINEPIPES

Large diameter (>24 in.) transmission pipelines are traditionally produced via three main methods:

1/ UOE longitudinally seam welded

2/ continuous spirally welded

3/ continuous high frequency resistance welded

High strength (i.e. >X80), large diameter steel pipes produced from TMCP steels are currently only made using the UOE process. The production route involves five main processes: preparation, forming, welding, expansion and inspection/testing.

Preparation starts with the edge planing and bevelling of the longitudinal plate edges with parallel planers into a double 'V' shape in readiness for welding, thereby generating the required plate width (i.e. pipe circumference) and bevel profile. The forming operation firstly involves crimping (upsetting) of the plates to ensure the best possible match during the O-pressing stage, then U-pressing and finally O-pressing (see Figure 2-17). This is a process carried out at room temperature, thereby avoiding heat treatment effects within the TMCP plate (except in the vicinity of the longitudinal seam weld). The cold forming (and subsequent cold expansion) however modifies the mechanical properties. The resultant work hardening and effect of the Bauschinger phenomenon[71] particularly influences the pipe yield strength. During cold forming of the pipe, the plate is subjected to bending in the transverse direction with the resultant outside diameter in tension and the inner diameter in compression (a neutral axis exists at plate mid thickness). The severity of the deformation is dependent on the ratio of the plate thickness to the pipe diameter formed. It has been reported that the plate shows a loss in yield strength after forming, with the magnitude of this loss dependent upon the plate microstructure[72]. Ferrite-pearlite microstructures (i.e. typical X65 pipe) have been observed to show a greater loss in yield strength than ferrite-bainite microstructures (i.e. typical X80 pipe).

After forming, the pipe is first tack welded together using GMAW, with run-on/off plates attached at either end of the seam line to ensure pipe wall thickness maintenance and minimise the chance of end defects. Multi-head SAW is then used to form the seam weld. A typical electrode current configuration would be DC/AC/AC/AC for a four wire system; this would allow a welding speed of 2m/min for a 25mm WT pipe[1]. The pipe internal diameter is usually welded first, using a column and boom system to support the welding head inside the pipe, followed by the external weld seam. The composition of the seam weld metal in conjunction with the resultant HAZ properties are an important aspect of the final pipe reliability due to the potential for defects and inferior mechanical properties (notably toughness and hardness) being located here. Consequently considerable research is undertaken in this area, especially in terms of maintaining optimum microstructures in the base material HAZ after the welding process[1,10,64].

The pipe is subsequently expanded to minimise out-of-roundness and out-of-straightness effects resulting from the forming and welding processes. The inner and outer diameters are subjected to various degrees of strain reversal, dependant on the o'clock position of the pipe within the U/O press. The expansion leads to a change in the yield strength; the degree of overall increase or decrease compared to the original plate material can be explained by the Bauschinger effect, which in turn is dependent on the plate microstructure and the rate of expansion (strain). Work carried out has revealed that ferrite-pearlite steels did not show a large increase in strength and the combination of forming and expansion resulted in an overall drop in yield strength[72]. Conversely, ferrite-bainite steels showed an overall increase in yield strength due to the increase from expansion being greater than the losses due to forming. It has subsequently been shown that a predominantly bainitic microstructure (i.e. X100) shows an even greater increase in yield strength than a ferrite-bainite or ferrite–pearlite microstructure.

The pipes are normally end-faced after expansion with a 30° bevel and 1.5-2.5mm landing, ready for manual/semi-automatic welding. Non-destructive testing (NDT) typically consists of hydrostatic testing, automatic ultrasonic testing of the longitudinal seam weld, radiographic examination of the weld area at each pipe end, ultrasonic inspection of the pipe ends and final visual inspection. Pipes are then marked to the customers specifications, typically using laser or robot stencilling machines[73].

2.4 FIELD WELDING PROCESSES FOR TRANSMISSION PIPELINES

The welding of transmission pipelines in the field involves three main groups:

1/ Mainline welding on the right of way (ROW)

2/ Tie-in welding for river/road/rail crossings, branch connections, pipe diameter reductions etc.

3/ Repair welding of NDT defects

Groups 1 and 3 occur both on and offshore, with the former comprising the bulk of the welding requirement for any pipeline construction. Group 2 may occur offshore, but is much more of a specialist operation than the onshore equivalent (the pipeline is either raised for welding above water, or the whole operation is performed hyperbarically). The significant cost of installing a pipeline requires that all construction operations are carried out as quickly as possible, in conjunction with the often limited construction season due to environmental considerations. Mainline welding consists of a large number of repetitive welds typically every 12 or 18 m, dependant on the individual pipe lengths. Welding is usually the limiting time factor during construction, as well as being one of the major cost elements; alignment, welding and NDT typically account for 20% of total laying costs; the remainder include ROW preparation, ditching, access and materials[74]. Consequently any improvement in welding speed (normally measured by the number of joints completed per day) can make for a significant cost saving on long distance pipelines. Of paramount importance is the compliance with the relevant construction specification in terms of joint mechanical properties. This normally takes the form of acceptance criteria to be reached through an initial (destructive) weld procedure test for the type of weld, coupled with monitoring of each field weld (non-destructive).

The primary method used to weld pipelines in the early 1920's involved the oxy-acetylene process, and it was not until the late 1920's that an electric arc in the form of manual metal arc electrodes was utilised for this purpose[75]. The covered electrode, originally developed in Sweden by Oscar Kjellberg in 1909[76], was the main method of welding pipelines until the late 1970's, typically involving a cellulose-based covering of the wire electrode. This coating breaks down in the arc to provide a shielding environment (hence shielded metal arc welding, SMAW). Short (i.e. <10 km) pipelines laid in the developed world customarily still use this process as the most economic method of construction. Less developed countries may still use this process for longer construction lengths due to the balance of mechanised equipment and labour costs.

The 1940's saw the development of the continuously fed electrode wire welding process, commonly known as metal inert gas (MIG) or gas metal arc welding (GMAW). Increased productivity for the majority of welding situations provided the incentive for its development. It was initially used for welding aluminium or other non-ferrous metals, and required the development of electrode wire with low carbon and a carefully balanced addition of deoxidising agents before it was acceptable for use with steels[76]. The welding power source technology required considerable advancement to improve the fusion characteristics of GMAW; power sources were originally relatively crude devices converting the high voltage, low current input from the mains to the low voltage, high current output suitable for welding. The discovery of dip-transfer (or short-circuit) GMAW dramatically improved the applicability of the process for steels, allowing positions other than those in the flat to be welded at low mean currents. Sufficient stored energy to fuse the short circuit and re-start the arc several times a second is essential, for which advances in the transformer-rectifier circuitry were required. Prevention of explosive wire rupture alongside developments in shielding gases improved the operating range of the process and mechanical integrity of the joint, such that by the early 1960's GMAW (or CO_2 welding as it was then known) was used in onshore gas pipeline construction[77]. Mechanised GMAW has followed its semi-automatic forerunner, and together with SMAW remain the most widely used processes for the girth welding of pipelines. FCAW, TIG, SAW and a number of so called one-shot or hybrid processes are also used, some of which will be discussed in later sections. These are dependent on the application, production requirement, economic viability and quality required.

2.4.1 GAS METAL ARC WELDING PROCESS AND POWER SOURCE CONSIDERATIONS

The conventional GMAW process and equipment are shown in Figure 2-18 and Figure 2-19. The process is characterised by an arc formed between the continuously consumed electrode and the workpiece. Due to the small diameter of the wire (usually less than 1.6 mm), the current density is high, resulting in a high burnoff rate (several metres per minute of wire are consumed). Traditional GMAW uses a constant voltage power source (flat characteristic) which allows the arc length to remain steady even in the hand of a manual operator, due to an electrical feature known as self-adjustment. If the arc length should change (giving a change in contact tip to workpiece distance (CTWD) and hence arc voltage) a corresponding change in arc current will occur such that the burnoff rate will alter to oppose the original arc length change. Consistency in operation is achieved due to the burnoff rate being considerably higher than the rate of change of CTWD. This advantage coupled with the ability of the small diameter wire to be pushed

(or pulled) through a flexible conduit makes the process ideally suited for mechanisation.

GMAW is virtually always carried out using a DC power source, with the consumable electrode polarity usually positive due to the improved arc stability. Some tubular wires have been developed to run DC-ve, which consequently benefit from the higher deposition rates allowable with this polarity[76]. Helium (in the USA) and Argon (in Europe) were initially used to provide the necessary shielding from the atmosphere, but the relatively high cost and poor performance of totally inert gases saw the introduction of carbon dioxide in the 1950's[78], with the resultant process termed metal active gas (MAG) or CO_2 welding. The weld quality improved further with combined mixtures of inert and active shielding gases, some of which will be reviewed in a later section.

The welding power source is a continually developing item and for DC welding the transformer-rectifiers exist with various forms of power regulation.

2.4.1.1 CONVENTIONAL REGULATION AND RECTIFICATION.

A transformer-rectifier consists of three basic components: the transformer (usually for a three phase supply), a regulator (current control device) and the rectifier[76]. The regulation is usually achieved by either a moving iron transformer, moving coil transformer, tapped reactance or magnetic amplifier[95]. Conventional diodes in the secondary circuit are used to rectify the current. The resultant output characteristics are fixed at the design stage, exhibit a slow response time and usually have no mains stabilisation. The costs are however low, with the equipment robust and reliable.

2.4.1.2 SILICON CONTROLLED RECTIFIER PHASE CONTROL

The transformer-rectifiers described above can employ silicon controlled rectifiers (SCR's) to regulate the voltage output. These devices may be regarded as switchable diodes; they only conduct in the forward direction when a signal is applied to the gate connection, and under normal circumstances the device cannot be turned off until this current falls to zero[95]. If a delay is introduced between the normal onset of conduction and the gate signal, the resultant voltage output can be regulated (e.g. long firing delay≡low output level). Limitations of the system are potentially high ripple and low response rate (3-10 ms), but offsetting this is the simplicity, robustness, reduced size and large amplification possible of the system allowing high output levels to be controlled by low-level electronic signals.

2.4.1.3 TRANSISTOR REGULATION

The equipment consists of that described above, but with an electronic current regulation device. A capacitor smoothing system is often employed to reduce voltage ripple, with current control performed via a feedback controlled transistor amplifier with its associated control electronics. The transistor power amplifier has two modes of operation to give current control, leading to the following terms describing the particular transformer-rectifier.

In series regulator mode the amplifier functions as a variable resistor whereby the output current is controlled by adjusting the small current flowing through its 'base' connection. Large amounts of power are dissipated in the transistor banks (typically 10 kW), consequently requiring a water cooling system to prevent overheating. Their inherent complexity makes them costly and bulky, but for smoothness of operation and accuracy of output they are considered excellent.

The amplifier can also be of a secondary switched transistor type. This is a much more energy efficient design (typically dissipating 1kW) due to the rapid switching of the transistors to regulate the output (c.f. a transistor series regulator where they are continuously operating). The mean output level is consequently a function of the on to off time ratio; this can be achieved with frequency modulation or pulse width control. Chopping frequencies of 1000 to 25000 Hz are commonly used; the higher the frequency the faster the response rate and the greater the arc stability. Advantages are the use of fan-assisted air cooling (rather than water cooling), simpler design and reduced cost when compared with a series regulator.

2.4.1.4 PRIMARY RECTIFIER-INVERTER

Up until the mid 1980's a conventional transformer (operating at the mains frequency) was used to achieve the required step down in voltage for welding purposes. If the operating frequency of the transformer is increased, however, its size can be significantly reduced. The sequence of events involve the primary AC supply first rectified to high voltage DC, and then converted to high frequency AC by the inverter. At this point the supply is transformed to a voltage suitable for welding and then rectified again. The frequency used within the transformer is typically 5 to 50 kHz, with output control achieved through chopping or phaseshifting the voltage waveform within the inverter. The high response rates attainable coupled with good electrical efficiency and cost effectiveness have made these the standard power supply design in the last five to ten years for the majority of pulsed GMAW, SMAW and TIG applications.

2.4.1.5 COMPUTER CONTROLLED POWER SUPPLIES

The very latest designs are totally digitised, microprocessor controlled inverter power sources, often incorporating interactive output management with a digital signal processor to control and regulate the entire welding process. Control algorithms have been developed to maintain a specified target status using high speed data gathering and machine response. This real-time adaption of the process to maintain optimum transfer stability can also be included either from preset levels within a data bank or customised by the operator. Waveform output can be designed by the operator, often via remote linked PC in real time, or stored synergic programs can be read from the machines permanent data bank/ROM. The internal logic of power supplies is now extremely complex and manufacturers apply their own philosophy for a particular welding situation. Consequently, if a comparison of power supplies is desired, a high speed/high resolution data gathering system for current and voltage is necessary to 'spot the differences'. The resultant flexibility of available output characteristics is however considerable, effectively allowing 'tailor-made' solutions for a given welding situation. The high number of available variables can also introduce considerable complexity to

waveform design, highlighting the need for a thorough understanding of pulsed waveforms and metal transfer in order to optimise the welding process.

2.4.2 *METAL TRANSFER IN GMAW*

Metal transfer forms an integral part of the welding process, and although it is not a key concern of this work, a short section is included to highlight the effects of the various modes on fixed position pipewelding. Heat and mass transfer in welding is an extensive subject for which considerable detail is available in other works concentrating on the subject[88,89,90,91,92].

In 1976 the IIW proposed a classification system for the various metal transfer modes from the major consumable electrode welding processes[93] as shown (slightly modified) in Table 2-2. GMAW metal transfer can be divided into three major transfer groups (see Figure 2-20), with sub groups existing within these major groups. A generalised schematic of heat transport and flow phenomena in GMAW is shown in Figure 2-21. The consumable electrode wire is melted by the heat of the arc to form droplets at the wire tip, with the size of the droplets and their detachment from the electrode a function of electromagnetic, gravity and surface tension forces. The ability to control the melting rate of the wire is the key to providing stable and spatter free transfer. Traditional GMAW power supplies had limited control of droplet morphology such that arc length, arc shape and arc root position fluctuated considerably in time and space[96]. The development of modern day power sources coupled with high speed photography and electrical parameter data acquisition have dramatically improved the consistency and understanding of metal transfer, leading to improved weld quality.

Short-circuit or 'dip' transfer occurs at low mean voltages when the wirefeed rate is greater than the wire burnoff rate. The short circuit of the wire with the base material causes a rapid rise in current at this point, such that the wire acts like a fuse. The resistance heating melts a section of wire which is then pulled into the weldpool by surface tension effects. The resulting gap causes the arc to be re-ignited which effectively pre-heats the end of the wire prior to the next short-circuit. The process is shown schematically in Figure 2-22. A common problem with the process is the rapid rise in current during the short circuit causing explosive rupture and consequent ejection of molten material. The incorporation of secondary inductance within the power supply to control the rate of current rise helps to stabilise the transfer, but is often not included in the design on the grounds of cost and 'undue complexity'. The process however has been the dominant one used for mechanised pipewelding, due to the simplicity of the power sources and the consequent ability of the latter to cope with field conditions. A variant of the process which has been commercialised in the last five years is controlled dip transfer, marketed by one leading power source manufacturer as surface tension transfer (STT™)[87]. A common feature of the current control waveforms are a rapid current decrease prior to short circuit rupture, followed by a current increase on the re-establishment of the arc. After a preset time the arcing current is then lowered to a final level that offers the required heat input and fusion characteristics (see Figure 2-23). The approaches to control philosophy within the power supplies to achieve this transfer can differ considerably, with large variations in build cost dependent on the methodology taken[97]. The process has gained widespread use in the semi-automatic open root

welding of plates and pipes due to the accomplishment of controlled penetration and fusion.

Globular transfer normally occurs at low arc currents and fairly high arc voltages (see Figure 2-20) and is characterised by large droplets of random volume and low transfer rates. The droplets are larger than the electrode diameter and detach purely by virtue of their weight exceeding the surface tension holding them to the electrode. As gravity is the dominant detachment force, globular transfer can only be used in the flat position. The unstable transfer results in high spatter and low penetration characteristics, limiting any practical application.

Within a small current range a shift from globular to spray type transfer occurs. This point is known as the transition current and varies according to the wire type, diameter and shielding gas used (for a 1.0mm C-Mn steel wire with 80% Ar/20% CO_2 it is around 200A[95]). Spray transfer is characterised by small droplets of a diameter typically less than or equal to the wire diameter. Electromagnetic forces are dominant in detaching the droplets axially, with the transfer mode subdivided into two main regions: projected spray and streaming spray (with increasing current respectively).

Projected spray transfer involves droplet detachment before they reach a size greater than the electrode diameter. In this mode the electrode tip does not become tapered. Due to the relatively high currents, the heat input is high and the weldpool large making the process ideal for high-deposition-rate downhand welding but having a very limited capability for positional welding. As the current increases further, the droplet size reduces with increasing droplet transfer frequency, eventually leading to streaming transfer. In this mode a tapered molten tip forms on the electrode (with steel wires), and a significant increase in electromagnetic forces occurs, forcing the droplets axially through the arc. As per projected spray transfer, the heat input and weldpool size are large with potential weldpool turbulence and gas entrainment limiting the usefulness of this mode of transfer.

At current levels above that of streaming transfer a long molten filament of wire is formed on the tip of the solid wire, which then rotates due to very high electromagnetic forces, leading to the term rotating transfer. Droplets are expelled from the end of the filament in a streaming transfer, and although this mode is usually undesirable it has been used in surfacing applications[95].

The transition to projected spray from globular transfer occurs over a small current range (typically 20A), but within this region an important intermediate transfer mode can be identified. Ma[98] termed this 'drop-spray' transfer, which is characterised by the formation of a solid conic neck on the wire tip, with spherical droplets slightly larger than the wire diameter suspended from the tip before being detached. Efficient detachment and high droplet velocities with low spatter generation and particulate fume can be achieved with high quality electronic power sources, with reasonable positional welding capability. The main disadvantage is the very restricted operating range, although this can be extended by the use of pulsed transfer techniques.

2.4.3 PULSED CURRENT AND SYNERGIC GMAW

Pulsed arc welding using GMAW emerged in the 1960's[79,80,81] enabling the operation of a continuously open arc below the spray transition current for a range of mean

welding currents. Short-circuit or dip-transfer enables positional welding due to the low mean heat input, but can suffer from fusion defects if care is not taken. Pure spray transfer has the advantage of high heat input from a continuous open arc, but the resultant burn-off rate gives a large molten pool which cannot solidify fast enough in positional welding (using ferrous consumables). The advantage of pulsed welding is the positional capability with improved fusion characteristics.

The original pulsed current waveforms were sinusoidal and typically of 10 ms duration, whereby small droplets were detached from the electrode tip in a stable spray-like mode[78]. The main stumbling block in the early years of development was the inability to change the pulse frequency for stable wire burnoff of varying diameters and compositions. The basic mains supply frequency (50 Hz in the UK) or submultiples of this (e.g. 25, 33⅓, 66⅔, 100 Hz etc.) determined the pulse frequency and consequently made the process difficult to obtain the correct transfer and stability characteristics. The fixed pulse duration and frequency required careful setting of peak and background current levels in conjunction with the wire feed speed if a useable welding condition was to be achieved. For a given mean current this was not always possible.

Advances in power electronics in the 1970's removed the deficiencies mentioned above with the development of the transistor series regulator power supply. Virtually square wave pulses of any desired frequency, peak current values up to 500A and pulse durations of 1 ms or less could be obtained[82]. Mains voltage stabilisation also allowed the power sources to overcome the previously intractable problem of transferring the welding conditions established at one site to another situation (providing the same equipment type was used). The optimum transfer characteristics have long been regarded as one-drop-per-pulse (see Figure 2-24), with considerable research having been carried out using the above mentioned power supply type in determining these conditions for a variety of situations[83,84,85,86]. The continued development of welding current control has enabled extremely smooth, spatter free transfer characteristics for virtually any wire and gas combination. This has been achieved through the ability to specify the rise and fall rates, as well as multiple steps in current levels within a given waveform cycle (see Figure 2-25). Examples from two leading manufacturers of high specification GMAW power supplies highlighting the number of variables that are now used to create a particular welding condition are shown in Table 2-3. The high degree of flexibility can lead to complications in set-up if the operators are not experienced in pulse waveform development; and for this reason the manufacturer usually provides a library of standard welding programs to suit most materials and applications.

The main advantage of electronic power sources is the ability for an operator to change a single parameter, for example wire feed speed, such that all other associated parameters are automatically changed in line with this to a pre-determined optimum value. This has become known as 'one-knob' or synergic control of the power supply and was instrumental in promoting the use of pulsed welding due to the large number of variables in use. A synergic curve describes an operating range which has been developed from at least two preset and stored welding conditions. If available within the power source interpolation (usually linear) is carried out by the inbuilt processor from each point generated (see Figure 2-26), or alternatively a library of synergic curves are burnt to a ROM on lower end-user specification machines.

Tandem wire welding using two electrically isolated switched arcs to generate a single weldpool was demonstrated by Brown[99] in 1978. The technique minimised the effect of arc-blow (instability of the welding process due to the interaction of magnetic fields associated with two arcs in close proximity) by switching the current between each wire. This technique was refined by Lassaline and co-workers[100], who developed a synchronised PGMAW system, based on conventional PGMAW power supplies, using a time delay between the peak current values applied to each electrode. They demonstrated the suitability of the technique for narrow gap plate welding, and performed trials with HY-100 and HSLA-100 high strength steels. The heat inputs (2.1-2.6kJ/mm) and wire diameters (1.2mm) used in this research were not suitable for pipeline girth welding applications, but the power source principles developed laid down the foundations for the modern synchronised pulsed welding power supply technology used today. Several leading welding equipment manufacturers (e.g. Fronius, Cloos, Lincoln Electric) have developed and marketed their own versions of synchronised power supplies suitable for tandem welding, but applications to-date have centred on flat plate or horizontal/vertical robotic welding techniques.

The higher welding speeds and increased deposition rates using the tandem welding technique over conventional single wire welding are possible for several reasons. The combined current may well be higher using tandem wires, but the arc pressure is reduced due to its distribution across a larger weld pool area[101]. This allows higher total current levels than the equivalent single wire system for the avoidance of weld defects such as undercut or lack of fusion. The elongated weldpool increases the time that the joint sidewalls are exposed to high temperatures, thereby increasing the likelihood of complete sidewall fusion. The increased weldpool length also prolongs the time available for de-gassification[102] and separation of the deoxidation products, reducing the potential for pore formation and the percentage inclusion content.

2.4.4 MECHANISED GMAW EQUIPMENT FOR TRANSMISSION PIPELINES

The increased mechanisation of arc welding, particularly GMAW, has occurred at a steady rate in industry over the last two decades, predominantly due to the cost and/or shortage of suitable skilled welders alongside the inherently low duty cycle of the manual process. Mechanisation should not be confused with automation; the former terminology still requires manual input to the welding process even if this is restricted to e.g. remote guidance of the welding head, whereas the latter in its purest sense has no human intervention throughout the process. Early mechanisation concentrated on flat position welding where the tolerance level of suitable parameters is often large and the equipment relatively simple, for example a GMAW torch held on a tractor using guide rails for torch positioning. On moving to positional welding it is often necessary to introduce a weaving action to control the weldpool and fusion/bead characteristics, hence an oscillating system for the torch head is necessary, adding a further level of equipment complexity. The advantages of mechanisation, however, can produce considerable improvements in welding speed, metal deposition rate, duty cycle and reliability.

Oil and gas companies, along with their contractors, are always looking at ways to reduce costs in any pipeline construction project. Of all the activities that take place

along a pipeline route from stringing to cleaning up, manual welding is one of the most costly[103], hence it is not surprising that the industry was quick to investigate mechanisation. The first reported use of welding mechanisation on a pipeline ROW involved CO_2 GMAW of a square edged narrow groove pipe preparation in 0.219 in. WT, 6 in. OD X46 pipe[104]. The process was developed by Esso, Battelle and AIRCO in 1959, and was shortly followed by numerous developments in processes and equipment (see Table 2-4). A milestone in onshore pipeline construction productivity was achieved by CRC-Crose in 1969 with their development of internal and external welding equipment, coupled with pipe bevelling machines. Twenty five joints per hour were produced in 762mm OD, 7.9mm WT pipe[105]. The pipeline spread concept was introduced, whereby several welding stations were located close by and in sequence for the full completion of the joint. The stations typically consist of pipe end bevelling, internal welding or Cu back-up clamp, root and/or hot pass welding, fill passes and cap passes. The latter two weld pass types require enough stations for the given pipe wall thickness such that the production rate keeps pace with the root and hot pass weld stations. Figure 2-27 clarifies the typical joint geometry terminology used for narrow gap welding.

The internal welding machines (IWM) developed by CRC-Crose can be used for pipe diameters down to 24 in.[109], below which they are not practical to use (Cu back-up clamps have been used on pipes as small as 6 in. diameter). The larger the pipe diameter, the more welding heads per internal side are used simultaneously, such that the productivity rate is maximised (machines with up to 4 heads per half pipe diameter are in existence). The whole operation of the machine from the initial clamping of the pipe to its advancement to the next welding location is carried out remotely.

It was not long before several other companies in the USA and Europe developed similar systems, primarily for offshore laybarge use. H.C Price, after early setbacks with the practical application of mechanised CO_2 welding in the late 1950's, developed an all-external 4-head automatic welding machine used offshore in the North Sea in 1975[105,106]. A maximum of 254 joints per day were recorded in the construction of a 914mm OD, 19mm WT X65 pipe. Saipem developed an external mechanised welding system in 1977 (Passo) which was used successfully in both onshore and offshore pipeline projects[107], with Serimer Dasa following H.C.Price's lead with a 4-head automatic welding system (Saturne) used offshore on laybarges in 1979[108]. Serimer subsequently developed the Saturne system for smaller diameter pipes, such that each welding head comprised two torchés (Saturnax dual torch), used offshore from 1988 and onshore (as a bug and band system) from 1994. The Saturne system was also extended to use multiple dual torch welding heads (Saturne 8), used offshore from 1989. Although two weld beads are deposited in one weld run using the dual torch system, the deposition rate is not double that of a single torch using typical production procedures (1.4 times a single wire deposition rate has been quoted[109]). A common feature of the previously mentioned systems is the use of a pipe line-up clamp with a copper backing shoe. This allows all welding to be performed from the outside of the pipe, with the added bonus of a potentially larger root bead than an IWM, thereby possibly reducing the number of passes by one. The copper shoe conducts heat away from the joint and is therefore an integral component of the weld procedure/resultant mechanical properties, and should be considered with respect to preheat calculations[109] . IWM's are generally considered to be less sensitive to high-low due to the internal welding arc and resultant

fusion capability, and may not require a shelter as per the remaining joint passes (on land based pipelines.)

Several other companies have developed mechanised pipewelding equipment in the last decade, most notably RMS (MOW I/II) in Canada and Allseas/Vermaat Technics (Phoenix/Veraweld) in the Netherlands[103]. Both of these companies, alongside CRC-Evans (P600) and Saipem (Presto) have developed dual torch systems in competition with Serimer-Dasa's Saturne/Saturnax to enhance productivity levels. Manipulation technology through computer control plays an increasingly important part in improving the productivity and quality of pipeline welding equipment. Adaptive control of the process coupled with segmentisation of the pipe circumference (in the case of ASME IX 5G and continuous 2G welding) and seam tracking allow the optimum welding parameters and highest possible torch travel speeds to be utilised. Realtime monitoring and data logging create the ideal situation for quality assurance (QA)/quality control (QC) systems and enable on-the-spot comparisons with mechanised ultrasonic NDT results. A further advantage of computer control is the ability to remotely change and store numerous welding parameters such that a single external bug can be used for all passes of the weld joint. Basic mechanised welding machines (bugs) are often preset for a given weld pass and any changes require a degree of down-time.

An important distinction between the above mentioned external mechanised equipment designs is the position of the welding consumable. CRC (single wire) and Passo both carry the welding wire on the welding head, whereas Serimer Dasa, Vermaat, RMS (dual torch) and CRC (dual torch) use remote wire feed units and their associated umbilicals. The former provides for extremely consistent wire feeding and wire positioning due to the proximity of the consumable, but adds weight to the system. The latter allows larger reel sizes to be used, minimising down time, but the extended umbilicals can cause wire feeding, cast and helix problems as the bug circumnavigates the pipe. The torch holding mechanism position is also an important consideration, as this determines the operators viewing access of the arc/weldpool. Torches held at 90° to the joint line allow easy viewing of the arc at both 12 and 6 o'clock for ASME IX 5G welding, as is the case for all the above mentioned systems except the single wire CRC. Remote control of the bug via a pendant has become a common feature in the latest equipment due to the considerable number of variables that are required, particularly in the case of dual torch systems. An LCD screen is often used as the user interface, which due to the nature of the welding operation, should be a reasonable distance away from the arc. With this system, viewing of the arc by the operator is less restricted in terms of the control position. The welding and equipment power supplies are remote from the welding head in all cases. A typical internal/external mechanised pipeline welding setup is shown in Figure 2-28.

2.4.5 SOLID AND TUBULAR GMAW CONSUMABLES

Solid wires are traditionally the consumables used in GMAW (and SAW) due to their ease of production from hot drawn wire. The wire chemistry is determined at the ingot/slab casting stage with the exception of copper levels, the latter increasing if a coating is applied prior to final drawing to size. High purity solid wires invariably cost more than their less controlled counterparts, with the choice being a reflection of the criticality/application of the weld joint. Control of cast and helix, in combination with

the wire diameter, chemistry and copper coating thickness are the major quality control issues associated with GMAW wire production. High volumes of solid wire are used in today's fabrication environment due to the high productivity available from semi-automatic, mechanised and robotic application. The market for supply of solid wires is consequently highly competitive, ensuring prices are kept at low levels.

A major setback with solid wire, in novel weld metal chemistry terms, is the large production batch requirement (typically a 20 tonne cast) resulting in far more welding wire than is necessary for initial weld metal property evaluation. Tubular wires can be produced in relatively small batch quantities (experimentally in a single reel typically less than 15kg), with a tailored chemistry at very low cost in comparison to a solid wire. Slag systems can also be tailored for smooth/fine droplet weld metal transfer of high fusion capability allowing, for example, positional welding or welding over plate primers, using specific powdered constituents within the metal sheath (described in the following sections). The deposition rates are often higher than the equivalent solid wire due to the reduced area of metal carrying the current, resulting in more I^2R heating for the same CTWD. The increased burn-off rate therefore requires a higher wire feed speed leading to a greater deposition rate. The thinner the sheath wall thickness, the greater the resistance, and consequently the greater the deposition rate, however the energy balance between melting the wire versus melting the parent material can lead to reduced penetration if too much energy is expended in the former[110]. There are also cases when the electrical resistivity of the tubular wire is less than a solid wire of the same diameter if the former sheath material is a rimming, or at any rate very soft steel. Solid wires typically contain more than 1% Mn and 0.5% Si and therefore work harden at a faster rate during drawing, increasing their electrical resistance and explaining the often lower running voltages experienced with the more ductile sheath steel in metal cored wires[111].

Manufacturing routes of tubular wires vary from company to company, although the majority of production is via a 'form, fill and draw' route (see Figure 2-29). The equipment used to deposit tubular wire weld metal is the same as for conventional solid wire GMAW, although the transfer characteristics of the molten wire differ depending on the particular constituents within the metal sheath (see Figure 2-30). The main benefits of tubular wires over their solid counterpart have been summarised by Widgery[110] as increased productivity, ease of use and quality. For these reasons the use of cored wires has predominantly overtaken that of SMAW in most applications, one notable exception being traditional field pipewelding. Even in the latter case though, significant inroads are beginning to emerge as traditional pipeline welders and the SMAW process are being replaced by semi-automatic welding and mechanisation. Mechanisation of the process can reap further benefits in all three cases mentioned previously by Widgery, with the type of tubular wire used being dependent on the particular application. Four main varieties of tubular wire exist, for which a short description of each follows.

2.4.5.1 METAL CORED WIRES

The use of metal powders within the core of an electrode were initially manufactured to counter the unavailability of solid wires for the same composition[110]. It was only later that the advantages of higher deposition rates and improved penetration characteristics

were realised over those of solid wires. Formulations allowed the cheap development of exotic alloy combinations through the powdered metal core, with the addition of small amounts of non-metallic constituents further enhancing the transfer characteristics in a particular gas shielding environment. Wires can be formulated, for example, with low slag levels as the main criterion, for high toughness, or for best performance on millscale (black bar) or primed plate. Their ability to provide a spray transfer characteristic (due to the oxide film surrounding the molten droplet) and good dip transfer capability provides easy handling in all welding positions, with the modern generation wires also exhibiting low weld metal (wm) hydrogen levels (<10mls H_2/ 100g wm). Depending on the production route the wires tend to favour a particular electrode polarity; baked wires are often run electrode negative and unbaked positive, mainly due to the particular wire surface chemistry in evidence. Weld metal oxygen levels are typically twice that of solid wires due to the powdered constituents, and as a direct consequence the toughness levels are not as good. This can be varied, but a balance needs to be struck between transfer characteristic (i.e. arc smoothness) and the required toughness level desired.

2.4.5.2 BASIC WIRES

Early basic cored wire compositions mimicked those of their SMAW predecessors, being lime-fluorspar based. When these constituents are broken down in the arc they provide considerable atmospheric shielding due to the CO_2 formed, thereby reducing porosity to very low levels. An added benefit of this system was the ability of silica to form silicate ions in the presence of an excess of calcium ions derived from the CaO and CaF_2. The silicate ions have a much lower tendency to dissociate than silica, and as a consequence the weld metal oxygen content is reduced upon solidification (due to its low solubility in steel) via this effective cleaning action[110]. Metallic deoxidants (e.g. Mg) can also be added to decrease oxygen levels even further. The levels of oxygen are, however, still higher than those found in bulk steel production, due to the rapid weld metal solidification rates trapping the oxide inclusions before they can reach the surface. The basic slags also promote desulphurisation, resulting in a very 'clean' weld metal to allow designers the maximum control over optimum strength and toughness combinations. The level of hydrogen (water) pickup by the various powdered ingredients is also minimised by the use of limestone and fluorspar, and in combination with controlled raw materials and production methods, diffusible hydrogen levels of <5ml H_2/100g wm are typical for basic wires.

The main disadvantage of basic wires is their poor performance in the low current ranges required for positional welding in combination with their fluid slag systems; the resultant dip transfer mode involves large droplets and high levels of spatter with an associated risk of lack-of-fusion defects. Some improvement is observed in setting the wire polarity to DC-ve (the energy balance is directed to favour wire melting rather than the plate) or by using pulsed current power supplies, but in the majority of applications the advancement of rutile wire capabilities has reduced the need for basic wires[110]. Hence, for fixed pipewelding applications where high levels of strength and/or toughness are required, the user has a considerable challenge on his hands to generate sound weldments with basic wires.

2.4.5.3 RUTILE WIRES

The use of rutile (TiO_2) in flux cored wires arose in a similar fashion to that of the basic wires. SMAW electrodes initially used rutile to enable greater control over the viscosity and melting point range of the slag systems, and the compositions were consequently transferred to use in wires. Control over the slag system improves the operating range of wires, exemplified in their suitability for positional welding or high speed flat position welding. Titanium is also a good arc stabiliser[110], enabling a smoother arc characteristic, and for this reason is often added in either metallic or mineral form to improve basic flux systems. It also has a strong affinity for oxygen, thereby acting as a deoxidant as well as a nucleation site (in combination with oxygen) for desirable microstructure evolution (e.g. acicular ferrite). Siliceous or acid materials are often combined with rutile to achieve the optimum transfer characteristics (physical weldability) via a fine spray of molten metal. The acid component (principally silica) promotes some oxidation of the droplet surface, which consequently lowers its surface energy allowing smaller droplet creativity. This can be formulated to occur over a wide operating range as long as sufficient oxygen (typically > 650ppm) is present in the weld metal. Unfortunately there is a direct link between oxygen and toughness levels; the higher the oxygen, the lower the toughness, but considerable development over the last few decades has pushed up rutile based weld metal toughness levels. The wires are a classic case of the trade-offs required between mechanical properties and physical weldability; in most cases wire developers tend to favour the latter due to the bulk market requirements.

Rutile melts between 1700°C and 1800°C, so it is necessary to add a fluxing agent to reduce the freezing point to that required of a welding slag (~1200°C). Many minerals will form low melting point eutectics with rutile, but the main challenge is getting this to happen within the powdered core in the short time available from when the wire exits the end of the contact tube (where resistance heating of the sheath starts). A solution was found in the use of titanates (Na, K and Mn) which have lower melting points than that of the steel sheath. These compounds consequently transfer the heat in order to dissolve the rutile and other high melting point minerals. The melting point issue became much less of a problem when wire diameters reduced in the 1970's. An added benefit was the reduction in weld metal hydrogen levels (often <5ml H_2/100g wm) from the lower amounts of hygroscopic titanates subsequently required, in combination with improved production routes. Smaller wire diameters also improved the positional welding capability, and in conjunction with optimum slag systems for the particular welding application, these wires are now widely used in all branches of fabrication for weld metal yield strength levels typically up to 550MPa.

Rutile wires exhibit high deposition rates when used at high current levels (see Figure 2-31), the full benefit of which can be obtained by mechanisation or automation, and the fatigue of the operator can be reduced/avoided. Even in pipewelding where the operating range may be restricted due to the particular welding position, significant gains in productivity can be exploited for tie-ins, repairs etc. The ease of use for this wire type in positional applications has enabled traditional SMAW users to get to grips quickly with the new consumables and techniques, thereby quickly realising the economic benefits.

2.4.5.4 SELF SHIELDING WIRES

Gas shielding of the weldpool is necessary for avoidance of high levels of porosity (mainly from oxygen and nitrogen contamination) and for improved metallurgical features. This has traditionally been supplied via an external shielding gas typically of inert (Ar/He), active (CO_2) or combinations of both components. This is both expensive and cumbersome; avoiding its use enables welding on tall structures without the health and safety issues of heavy gas bottles, alongside the reduced chance of external gas shielding being blown away by potentially even light breezes. The challenge for the consumable developer is in providing enough shielding from the powdered ingredients within the core, without sacrificing physical weldability or metallurgical issues.

Two options are available to the formulist in designing wires to run without external shielding. In practice these are often combined for the best effect. Materials which dissociate or vaporise are used to form a physical barrier against atmospheric contamination. Alternatively materials which are strong deoxidants or nitride formers are added to combine with any oxygen or nitrogen within the weldpool. Calcium fluoride (fluorspar) easily dissociates within an arc and consequently provides a very effective vapour blanket, but unfortunately does not promote arc stability or smooth/consistent metal transfer. Considerable fume and condensates are also a feature of its use, but nevertheless it is still the main non-metallic ingredient of many self-shielding wires. Carbonates are not used in any significant amount due to the high levels of spatter often generated, and in extreme cases can peel open the tube due to the production of too much CO_2. Metals which form a vapour blanket due to their relatively low melting points are aluminium, magnesium and lithium, with the former two also powerful oxide and nitride formers. Titanium and zirconium are also added for their abilities to combine with nitrogen. The balance of these elements, however, must be very carefully controlled due to their metallurgical potency if the correct equilibrium of strength and toughness is to be achieved.

Barium compounds are extremely useful for the self-shielding wire developer for two main reasons. The resulting arc voltages produced are much lower than for wires not containing barium (due to the low work function of Ba compounds), and the higher decomposition temperature of $BaCO_3$ compared with $CaCO_3$ results in a more controlled (i.e. less explosive) arc characteristic. The lower arc voltages (reductions from 22V to 14V are typically observed) are beneficial in terms of reducing the arc energy for a given current/wire burn off rate. This allows easier control for positional welding, as well as diminishing the chances of oxygen/nitrogen pickup by the droplets due to the reduced arc length. Some controversy exists, however, around the toxicity of barium compounds. Although it is known that $BaCO_3$ is highly insoluble, the decomposition of the material during the welding process may yield products that are poisonous.

Rutile is also used in self-shielding wires, but only usually when low levels of ductility and toughness can be accommodated (e.g. on thin material). The strong deoxidants present reduce TiO_2 to metallic Ti, which subsequently produces fine carbide and nitride precipitates. These will strengthen and embrittle the weld metal. The process of TiO_2 reduction also yields TiO as an intermediate product, the latter having a lattice parameter very close to that of ferrite such that the resulting slag sticks undesirably efficiently to the weld metal.

The limited space available within the wire core in conjunction with all the requirements necessary of the powdered ingredients for self-shielding wires has resulted in the use of pre-fused materials to great effect. A price is paid for the versatility of the wires resulting in lower deposition efficiencies and greater procedure control required for high toughness weld metal. Their use in the field welding of pipes, offshore jackets and bridges has been commonplace, but the ever increasing demands of strength, toughness and production economics have invariable resulted in other consumable designs overtaking them.

2.4.6 SUBMERGED ARC WELDING

The origins of submerged arc welding (SAW) can be traced to the USA in 1935 when Kennedy, Jones and Rodermund patented a process involving an electric arc covered by a blanket of granulated welding flux[113]. During welding the heat of the arc melts the flux which forms a protective layer over the weld pool. Both unmelted flux and slag act as effective arc radiation shields, and with minimal fume given off the process has considerable health and safety advantages.

The process can be likened to that of SMAW, whereby a wire is surrounded by flux, but with the significant advantage of continuous wire feeding allowing much higher productivity levels (see Figure 2-32). The fact that the flux is added around or in front of the wire allows the user a considerable degree of flexibility in optimising the process for the required properties e.g. speed, mechanical properties, deposition rate. The flux composition influences the stability, temperature and heat distribution of the arc plasma. The molten slag influences the weld bead appearance, promotes slower cooling helping to avoid cracking and brittle microstructures, as well as continuing to provide protection from the atmosphere as the weld metal cools[318].

Submerged arc fluxes are classified in several ways[113]; by composition, chemical characteristic, method of manufacture or use. A convenient way of grading any given flux is via a basicity index (BI), which indicates the ratio of acid to alkali components within the flux. A formula frequently employed is that given by Tuliani, Boniszewski and Eaton[114]:

$$BI = \frac{CaO + CaF_2 + MgO + K_2O + Na_2O + Li_2O + BaO + SrO + \tfrac{1}{2}(MnO + FeO)}{SiO_2 + \tfrac{1}{2}(Al_2O_3 + TiO_2 + ZrO_2)}$$

When the BI is less than 1, the flux is categorised as an acid type and typically contains high oxygen levels with concomitant low levels of toughness. These fluxes, however, are very suitable for high speed welding with good bead shape and slag detachability. As the BI moves above 1, the flux type becomes progressively more basic, until an index of 2.5 or above would indicate a fully basic flux. Basic fluxes exhibit high toughness levels, but slag removal is more difficult and bead shape is not as smooth as acid fluxes.

The manufacture of fluxes can be split into four main types: mechanically mixed, bonded, agglomerated and fused[94]. The latter two are the most common production methods, and allow manufacture of all flux types except the highly basic fluxes; these are produced solely in agglomerated form due to the addition of metallic ingredients as deoxidisers (which would oxidise during melting in fused flux production). Fused

fluxes have an extremely low ability to pick up moisture, and hence the weld metals are usually low in diffusible hydrogen, although trapped hydroxyl ions in the silicate lattice can lead to some hydrogen evolution. Agglomerated fluxes are hygroscopic to various degrees, but careful control in their use reduces the chances of moisture pickup. Rebaking and holding these fluxes in heated hoppers provides for very low weld metal diffusible hydrogen levels.

Particle size control is very important in a flux; granules of a very fine nature tend to reduce the volume of flux melted and restrict the escape of gases from the melting flux and molten metal[115]. Agglomerated fluxes break down at a much faster rate than their fused counterpart, and as a direct consequence can only be recirculated a finite number of times.

A major restriction of SAW is the welding position; deposition can only take place in the downhand (1G/1F) or horizontal-vertical (2F) orientation due to the flux blanket. The use of positioning and rotating equipment, even for extremely large components (e.g. submarine hull sections), however enables the wider use of the process. The equipment is normally fully automatic or at least mechanised to a considerable degree, with power sources usually of the constant current variety for the larger wire diameters (>2.4mm). Multiple wires can be fed into the same weldpool, either using the same power supply (e.g. twin wire) or different power supplies with often different polarities (e.g. tandem wire). In the latter case it is normal to use DC+ve on the lead wire, followed by one to five AC wires. This reduces the electromagnetic influences of the individual wires on each other and helps to avoid arc blow. Wire polarity coupled with the feeding angle (i.e. pushing or pulling) has a significant influence on the penetration and bead profile. Tubular wires are being increasingly used in SAW (flux cored submerged arc welding; FCSAW), due to their higher deposition capabilities, coupled with the greater alloy possibilities of the system.

The use of SAW in the pipeline industry is in two major areas: seam welding during pipe manufacture, and double (or triple) jointing standard factory pipe lengths in the field. The former usually involves multiple head welding to produce a single internal and external weld bead along the pipe length to maximise production rates. Heat inputs are consequently considerable, and the challenge for high strength linepipe manufacture is often centred on obtaining adequate strength and toughness within the HAZ of the base material, alongside minimising the required alloying levels in the weld metal. Double or triple jointing is common practice on offshore laybarges, and is sometimes used onshore where the geography allows it. The pipe is placed on rollers, enabling both internal and external welding in a fixed position on the pipe circumference. All beads except the final internal sealing run are performed externally, using a joint preparation suitable for a single pass per layer. High weld metal deposition rates with consistent weld bead profiles and properties for most material grades and wall thicknesses are usually easily obtained due to the fixed welding position. The major disadvantage (particularly onshore) is the added complexity of pipe handling and transportation of the long (e.g. 24 or 36m) lengths from the double jointing station.

2.4.7 SHIELDED MANUAL METAL ARC WELDING

Shielded metal arc welding (SMAW; traditionally known in the UK as MMA or stick welding) has its origins dating back to the first decade of the 20th Century[76], when a

Swede (Oscar Kjellberg) patented his invention and formed a company (ESAB) to commercially produce the electrodes. The patent identified a valuable feature of covered electrodes in their ability to form a ceramic cup on the end of the rod if the flux melts at a slightly higher temperature than the core wire[110]. This attribute explains two of the major benefits of the welding process: the cone formed at the rod end directs the arc making out-of-flat positional welding possible in conjunction with a suitable slag system, as well as improving the atmospheric shielding for the transferring metal droplets.

The electrodes can be grouped into similar categories as per the tubular wires: flux coatings based on rutile, basic or cellulosic constituents are the three main varieties, although variants of these are also commonplace (e.g. acid rutile, iron powder rutile, rutile cellulosic)[116]. Silicates (water glasses) and alginates are added to the flux ingredients to act as binders and extrusion agents, and, depending on their base (e.g. Na, K, Li), they help stabilise the arc for a particular welding polarity. The electrodes are dried at a specific temperature and rate dependent on their coating type. Basic electrodes need high temperatures (~400-500°C) to drive off as much water as possible to reduce the potential weld metal diffusible hydrogen. Cellulosics benefit from a degree of moisture content (~4% of coating weight) to enhance the power of the arc. As for tubular wires, the ability to tailor the coating ingredients for the physical welding and mechanical properties has resulted in an extremely large range of electrode types. Small batches can also be produced, unlike solid wires, with small turnaround times possible for new alloy developments.

A major advantage of these consumables is the simplicity of the power sources coupled with their small size (especially if an inverter power source). The only other piece of site equipment possibly required would be a heated quiver if low hydrogen electrodes are being used, although vacuum-packed electrode packets have largely superseded the need for these. Disadvantages of the process are the relatively high level of welder skill required, particularly for out-of-flat welding, coupled with inherently low deposition rates due to the fixed electrode length (typically 350 or 450mm). Slag removal is an operation that is usually required, although well developed electrodes coupled with welder skill may avoid the majority of this process.

Pipeline welding has a long tradition of using SMAW, and it is still the predominant method of joining even large diameter pipes in some countries, particularly where the cost of labour dictates its use over mechanised equipment. Cellulosic electrodes are particularly suited for this application due the high productivity levels. These are achieved through the vertical down welding technique allowing high travel speeds. High penetration levels provide a degree of assurance in minimising fusion defects; cellulose boils at temperatures below 650°C and on entering the arc instantly becomes a gas, expanding and forming a high power jet action. The two main disadvantages of this consumable type are the relatively wide bevel preparation required, and the initially high hydrogen levels of the weld metal. The former is a requirement to enable the root and early fill runs to exhibit good fusion and lack of defects via adequate manipulation of the arc/weldpool, whilst the latter is a direct result of the breakdown of cellulose releasing (amongst other products) hydrogen. The inherently high weld metal hydrogen levels[118] require a second weld bead to be deposited as soon as possible after the root run to aid the hydrogen diffusion process, alongside increasing the overall bead size to minimise the chances of cracking. Welding procedures consequently stipulated the 'hot

pass' be completed within a few minutes of the root run. The increase in pipe strengths observed over the last 10-15 years have seen the demise of cellulosic SMAW due to the problems of fabrication associated with high strength and high hydrogen[117]. Mechanised GMAW, and latterly PGMAW, in narrow grooves have improved the productivity and quality levels, as well as the solid wire consumables used exhibiting very low diffusible hydrogen levels, typically less than 2mls H_2/100g wm (see Figure 2-33).

SMAW still has a place in high strength pipeline construction, particularly for tie-ins and repairs. Basic coated low hydrogen vertical down electrodes have been in existence for some years, and provide strength and toughness levels suitable for the guaranteed overmatching of X80/X90 pipe yield strengths[119]. Higher strength electrodes of a similar classification suitable for a guaranteed overmatching of X100 pipe are also in existence, although it is only very recently (after the end of the current experimental programme) that their physical weldability has improved to allow their effective use. Vertical-up high strength basic low hydrogen electrodes have been used for construction of cranes, submarine hulls, offshore jack-up legs and so on for many years, and their application to high strength pipelines poses no technical problems. The main issue involved is the low productivity, especially on thick walled pipes; compound bevels are employed to improve this situation, but if possible the use of a semi-automatic process is favoured.

SMAW is the ideal process for root welding of pipeline tie-in joints or full thickness repairs, where variations in fit-up would require complex feedback mechanisms for mechanised pipewelding. A backing system for conventional GMAW/FCAW in the root is usually not possible, although open root welding has been used in pipelines from the 1960's[77,120]. In these situations a skilled welder can compensate for variations in gap width and landing to ensure full fusion and penetration around the pipe circumference. The advent of modern power sources and specialist transfer processes such as STT have enlarged the tolerance box of usability with GMAW, but the SMAW process is still the favoured one in field welding of the root and hot pass (see Figure 2-27).

2.4.8 MECHANISED NARROW GAP GMAW

Welding within a narrow joint preparation first came into prominence in the USA in the 1930's, mainly for economic reasons[78]; the smaller weld metal volume required reduced the welding consumable costs as well as the fabrication time. One of the earliest references to narrow gap welding (NGW) as a distinct process terminology was in a paper by Meister and Martin in 1966[121]. A general definition of NGW describes welding within an essentially parallel sided joint (bevel angles of 2-10° are also often used) in thick material, i.e. typically 10 to 200mm. Open and closed butt root preparations have been used, both with and without backing bar systems. Numerous welding processes other than GMAW are applicable for NGW; electroslag, electrogas, SAW, TIG, FCAW and SMAW have all been applied in various situations[122], with the following advantages[123,124,125]:

- Reduction in welding time;
- Lower consumable costs;

- Reduced heat input leading to improved mechanical properties and less distortion;
- Reduction in slag removal time if applicable for the process;
- Reduction in preheating and post-weld heat treatment.

As can be seen, this joint design type has many benefits, providing several potential problem areas are overcome. The most often reported problem with NGW is attaining adequate sidewall fusion. Due to the small tolerances available for the welding torch/contact tip/electrode within the groove, the process is virtually always mechanised or automated, with increased assembly time and high operator skill often required. Careful control over welding parameters is necessary, with a smaller working range often resulting in comparison to more conventional joint preparations. A major consideration often overlooked is the difficulty in carrying out repairs, particularly with very thick section components.

A review of early NGW GMAW joint designs of the leading companies in mechanised pipeline construction show variations in philosophy, particularly with the root configuration[105]. Figure 2-34 shows the joint design, equipment and welding process requirements of these companies in their early days, with Figure 2-35 showing a couple of their modern day equivalents.

2.4.8.1 WELD BEAD CHARACTERISTICS

Arc and weldpool stability is a key factor in maintaining high quality narrow gap welded joints. This is particularly important when welding around a fixed pipe, where the effect of gravity changes the weldpool dynamics; consistent and stable weld metal transfer is a prerequisite for sound joint completion. Tight control over bead shape is essential, and in this respect an understanding of fusion characteristics and welding parameters is extremely important. Numerous investigations have been undertaken, often leading to mathematical expressions[84,85,86,127,128,129,130], but it should be remembered that these are based on laboratory conditions and may not be able to predict the required parameters for a given practical situation with sufficient accuracy.

The optimum weld bead shape for NGW is regarded as being slightly concave (except the cap), with beads having depth to width ratios in the range of 0.7 – 1.0[131], and a weldpool length twice that of its width[132]. This profile ensures ease of fusion at the toes of each preceding weld bead. Maintaining a concave, or at least flat profile around the entire pipe circumference is the major challenge in fixed position pipewelding to ensure complete fusion within the joint. Parameters which influence the resultant bead shape such as arc voltage, welding current/heat input/deposition rate, electrode oscillation, electrode polarity, joint gap width and wire diameter will be discussed in the following sections.

2.4.8.1.1 ARC VOLTAGE

Arc voltage is directly related to arc length i.e. the greater the arc length, the greater the voltage required to maintain that arc. The arc is a sustained electrical discharge across a gap between poles[94], and in simplistic terms its shape within GMAW/PGMAW can be

considered as a cone emanating from the end of the wire electrode to the workpiece. Within certain limits, the greater the arc length, the greater the arc diameter at the workpiece. This phenomenon provides a limitation on the usable arc voltage due to an 'undercutting' effect at the arc extremities, which in certain instances (notably too high a torch travel speed) is not filled by the molten weldpool. In narrow gap welding, the mean voltage (c.f. arc length) is critical in maintaining the correct fusion characteristics without undercutting the sidewalls and consequently providing slag traps or fusion problems for the subsequent passes. The arc will always find the path of least resistance, and in close proximity to joint sidewalls, can arc up the sides rather than the base or toes of the existing groove. For this reason a small (≤3mm) arc length is often desired in circumferential pipewelding where maintenance of arc directionality is of prime importance. Compared with a downhand narrow gap weld the use of high mean voltages and continuous spray transfer is not an option. Work in these situations[128] has shown that with a constant groove width, the resultant bead width is directly related to arc voltage.

The transfer characteristic traditionally used with mechanised pipewelding and solid GMAW involves the short circuiting of the wire, such that the average arc length is kept inherently short for optimum transfer. Inductance, amongst other electronic circuitry within the power supply, is used to change the rise and fall rates of current and voltage, thereby stabilising the transfer process as well as changing the arc shape. Soft (wide and 'fluffy'/reduced directionality) or hard (concentrated and stiff) arcs can thus be engineered to suit the material and joint configuration for optimum fusion. The same principles apply when using pulsed current waveforms, although in these cases the user has more control over the arc shape due to the high degree of output variability possible.

2.4.8.1.2 WELDING CURRENT, HEAT INPUT AND DEPOSITION RATE

The mean current in GMAW is a function of the wire feed speed, and has a direct bearing on the resultant heat input and deposition rate. High deposition rates and hence high current values can be utilised in downhand welding with spray transfer, combining good fusion characteristics and bead profiles to best effect, but this is not possible for fixed position pipewelding. The challenge in pipewelding is to maximise the deposition rate without compromising the bead shape, hence an upper and lower limit are imposed on the mean current for a given torch travel speed. Control over the weldpool must be maintained in all positions, and in this respect heat input is naturally limited to a narrow range when compared with the potential operating envelope of the process. Although studies[128,133,134] have been conducted using deposition rate/arc energy to determine bead shape variance in NGW, these have mostly been limited to constant downhand or horizontal-vertical situations. Figure 2-36 shows the results of high current GMAW trials in a narrow groove, illustrating the voltage and travel speed relationship required to avoid weld pool flooding, undercut or convex profiles[135]. The same effects will be observed in fixed pipe welds, although constant welding parameters can create multiple profile effects around the circumference due to the variation in weldpool flow.

2.4.8.1.3 ELECTRODE OSCILLATION

As previously mentioned, spray transfer GMAW and the associated high voltages allow the greatest chance of fusion in a narrow gap joint due to the high power, constant and wide arc if oscillation of the electrode was not employed. In relatively shallow (<30mm thick) downhand narrow gap joints coupled with highly accurate electrode positioning within the groove, this technique may be feasible, but for the majority of practical situations, thicker plates and all-positional welding capability (i.e. dip/pulse transfer) some form of electrode oscillation will be required to ensure sidewall fusion for the fill and cap passes.

The techniques employed are many and varied for downhand, horizontal-vertical (H-V), and vertical position high deposition welding (e.g. air weaver, flapper plate, twist arc, corrugated wire, Loop Nap, high speed rotating arc, AC-MIG etc.[122]), but the weight and complexity invariably preclude their use within pipewelding bugs. A simple torch oscillator is the most common method for weaving the electrode for use on a pipeline bug and band system, and due to the relatively thin material thickness (typically <30mm) a pendulum or fixed slide system can be employed without the risk of the contact tip touching the sidewall. Pendulum systems provide enhanced weld toe/sidewall fusion but are not usually as rigid as sliding systems. Although rigidity of the system is extremely important in narrow gap welding, the light weight of air cooled torches used in the majority of current commercial systems presents no problems for a pendulum action, particularly when the welding wire reel is on the bug (no wire liner adding weight and inertia).

Pneumatic or electric motor oscillators are used, and typically provide up to 200 beats per minute (BPM) for single or dual torch processes (1 beat represents a single sinusoidal waveform). Research into the optimum weave width, frequency, pattern and inclusion of sidewall dwell of fillet welds provided a good background source for optimising narrow gap fusion[136]. The general 'rule of thumb' for the required beats per minute/travel speed (inches) ratio is 10/1, but it is not unusual for the fill passes to be oscillated at slightly higher rates, particularly with pulsed GMAW[137]. As torch travel speeds increase, the required oscillation frequency will have to increase in order to avoid a 'saw blade' deposition and undercut effect, but at the same time a limit for weld pool stability must not be exceeded. It is also general practice (using dip transfer) to oscillate the wire to within one wire diameter of the sidewall (the increasing joint width towards the pipe OD necessitates greater oscillation for subsequent weld passes). The arc characteristics of pulsed GMAW should theoretically allow slightly less weave width than its dip transfer counterpart for the same degree of fusion, but increasing the fusion attained without a loss in weld profile is a highly desirably attribute of pulsed GMAW. Vertical-down welding is usually undertaken at travel speeds that do not require a dwell at the groove sidewalls to maintain a flat/concave profile, hence the mechanised welding bugs for the process do not normally incorporate this facility. Vertical-up welding, however, is much slower due to the weldpool dynamics, with the result that the wider the weave, the greater the dwell requirement at the joint sidewalls to maintain a flat profile. Hence, mechanised bugs for vertical-up welding are slightly more complex with the addition of sidewall dwell circuitry/mechanics.

2.4.8.1.4 ELECTRODE POLARITY

GMAW has traditionally employed direct current, with the consumable electrode set as the positive polarity. There are two major reasons for this: the stability of the arc is improved when it is 'rooted' on the base material rather than the electrode (electrons in the ionized plasma flow from the workpiece (cathode) to the electrode (anode))[76]; and the increased penetration attainable in the fusion zone as a result of the electron flow direction. Some tubular wires have been developed to run on DC-ve with the addition of arc stabilisers on the wire surface or within the filling[110]. These benefit from the increased deposition due to the heat balance favouring higher wire burn-off rates (see Figure 2-37). AC GMAW has been investigated, and although benefits such as improved current ranges, bead profiles and absence of arc-blow[138,139] have been reported, the arc stabilisation for solid wires traditionally requires a dangerously high open circuit voltage. This can be reduced in the power source design, but for everyday use the simplicity and costs of a DC GMAW power supply have generally precluded the use of AC. Recent advances in terms of output control with variable polarity power supplies have, however, re-instigated investigations into AC GMAW[92].

There are reports of DC electrode negative improving the bead shape within a narrow groove[128], possibly attributed to a change in the arc envelope and the resulting change in arc force[140]. It has been observed that smaller droplets are detached as the gap width reduces, with the sidewalls producing a 'pinching' effect associated with arc cooling[141]. A change in electrode polarity has also shown apparent changes in solidification behaviour according to one group of investigators[128]; DC+ve was reported to involve solidification from the sidewalls to the centre producing a higher incidence of solidification cracking, whereas DC-ve produced solidification from the bottom and back of the weldpool. Details regarding the determination of the previous phenomena have not been described. The advantages discussed above occur with high current values which are not applicable to a pipewelding situation, hence DC+ve is used exclusively with solid wires in these applications.

2.4.8.1.5 JOINT WIDTH

The geometry of the root preparation is designed to allow maximum penetration for complete root fusion, and as a result the welding parameters for this area are biased towards achieving this. Extensive studies have been undertaken into root welding, particularly for manual and semi-automatic pipeline applications[120,142] where joint geometry tolerance levels are relatively wide. Although the principles can be applied to mechanised joints in terms of correct bead shape, a distinct advantage of mechanisation is the ability to accurately direct the electrode coupled with maintaining torch travel speed consistency.

The 30° to 45° chamfer machined at the base of the main sidewall bevel angle (viewed from the pipe OD; see Figure 2-27) is designed to maximise the penetration effect whilst preventing excessive heating/melting in this area, which may lead to root suck-back on solidification. The torch travel speed is consequently high in comparison to fill and cap passes to ensure a low chance of over penetration (burn-through), as well as generating low depth to width ratios to avoid centreline cracking. The first externally deposited bead should ideally fuse up to the base of the main sidewall bevel angle (e.g.

5°), from which point wire feed and travel speed for the following layers are optimised for high deposition rates. The mechanised pipewelding GMAW bevel design is required to ensure consistent weld bead profile and fusion characteristics, whilst minimising the weld metal volume required. Different contractors apply differing philosophies for the major sidewall bevel angle. Some use a fixed angle and root chamfer offset (e.g. CRC-Evans) regardless of pipe wall thickness, whereas others change the angle to ensure a fixed cap gap width (e.g. Serimer-Dasa). The latter has considerable benefits for inclined-overhead/overhead welding in larger wall thickness pipes when filling out and capping. This is a direct result of the increased surface tension available to 'hold-up' the molten weld bead and avoid convex bead profiles, but care needs to be taken with contact tip tracking within the resultant groove.

Cooling rates are also likely to change with variances in joint geometry, with consequent changes in mechanical properties, especially with higher strength weld metals. It is therefore very important to ensure the weld procedures developed cover likely variances in joint preparation and welding parameters to be encountered in the field. The machining tolerance levels are very narrow (see Figure 2-35), but as feedback mechanisms at present mostly involve the operator rather than automation, consistency in joint preparation minimises any adjustments required during welding and allows the highest levels of bead consistency and repeatability to be achieved.

2.4.8.1.6 WIRE DIAMETER

Prior to the advent of pulsed power supplies, early work conducted with conventional constant voltage (flat) power supplies for semi-automatic pipewelding applications concluded that a 1.2 mm diameter wire appeared to offer the best compromise between control of penetration and deposition rate[142]. The experimental programme involved dip transfer, CO_2 shielding, various joint root preparations and included angles (40°, 50° and 60°), with wire diameters of 0.8, 1.2 and 1.6mm being evaluated. The introduction of mechanised girth welding by CRC-Crose in the late 1960's required high positional weldpool control and fusion characteristics, resulting in the adoption of 0.9mm wires[105]. The next standard size of wire specified in the US national standards[143,144] is 1.1 mm (0.045 in.), but weldpool control/fusion characteristics do not improve compared with the 0.9 mm wires. Other narrow gap pipewelding contractors in Europe have tended to favour 1.0 mm diameter wires due to the standard alternatives being 0.8 or 1.2 mm. The burn off characteristics will influence the arc shape and penetration for a given wire diameter (alongside alloy and shielding gas composition), but the choice of 0.9 mm or 1.0 mm should not drastically change the fusion capability/bead profile providing optimum welding parameters are defined. In practice, welding procedures for a given pipeline project however have used both wire diameters to optimize their characteristics; 0.9 mm in the root for penetration coupled with reduced arc pressure, and 1.0 mm in the hot pass, fill and cap for increased deposition[145].

Most of the early development work conducted on pulsed welding with solid wires utilised a 1.2 mm diameter wire[83,84,85], with the result that frequency/mean current (e.g 50 Hz/100 A) and one drop per pulse ($I_p^n T_p$=const) relationships were established[85,86,146]. Although melting rate and penetration characteristics have been determined for a variety of wire diameters[84], the compromise between deposition rates, bead profile and positional capability has again resulted in the use of 0.9 or 1.0 mm

wires for fixed position narrow gap pipewelding. The advancement in pulsed power supplies, particularly over the last decade, has enabled far greater control over droplet formation and transfer characteristics, and in theory the optimum transfer should be perfectly attainable for a given wire diameter and composition in the required welding situation.

2.4.8.1.7 CONTACT TIP TO WORKPIECE DISTANCE

The contact tip to workpiece distance has an influence on the current and voltage drawn, due to the change in resistance caused by varying the electrode extension lengths. If the CTWD changes during a weld run, particularly when any adaptive control is avoided or minimised and the classical 'self-adjustment' effect is not applicable, the arc length and pressure can significantly affect the resultant bead profile. In this respect most high-end GMAW power supplies utilise control algorithms to stabilise the metal transfer. A major disadvantage in terms of fundamental pulse parameter development with these power supply types is the unknown control logic with respect to applied current and voltage through the wire during transfer instabilities. In a laboratory environment it is possible to accurately set up and maintain a constant CTWD (unlike a traditional semi-automatic human welding operation), and to a certain degree this is possible with mechanised pipewelding. In these cases the development of optimum pulse conditions is maximised if the designed output (e.g. ramp up/down rates, peak current) is delivered at all times. Whilst it is important to maintain the most constant CTWD possible for process stability in any welding situation, small changes should not allow an undesirable bead profile to be generated, and in this respect a degree of 'self-adjustment' or feedback control is advantageous over the pre-determined pulse structure.

2.4.9 SHIELDING GASES

The original arc welding processes undertaken at the end of the nineteenth century did not incorporate any form of externally applied gas shielding, and as a direct result high levels of porosity and weld brittleness occurred. Although the deleterious effects of atmospheric contamination due to high levels of oxygen and nitrogen took several decades to fully comprehend, improvements were immediately apparent in the weld appearance and arc/droplet transfer characteristics when various coatings were added to the wire electrodes[76]. The coating breakdown effectively generated a shielding gas, reducing the chances of atmospheric contamination of the molten weldpool. Gas solubility differs considerably depending on the physical state of the metal. Liquid iron contains higher levels of oxygen and nitrogen, with the latter's solubility changing significantly depending on the crystallographic state of the solid (see Figure 2-38). The classification of shielding gases according to the EN standard for arc welding and cutting[148] has resulted in the following classification groups: reducing mixtures; inert gases and mixtures; oxidising mixtures containing O_2 and/or CO_2; highly oxidising gases and mixtures; and unreactive gases. It is the second and third groups which are of interest in C-Mn and low alloy steel GMAW.

From its inception, solid wire GMAW has required a shielding gas to enable stable arc and metal transfer, with the actual composition of gas used having a direct influence on

bead shape, fusion characteristics, welding speed, metallurgical/mechanical properties and cost. The original steel GMAW used CO_2 as the predominant shielding gas due to easy availability and low cost. The arc voltage is normally 1-2V higher than argon based mixtures for the same arc length/mean current[95], with the resultant increased heat input improving fusion. Unfortunately, the transfer characteristics and arc stability are not as good as other gas mixtures, particularly at high current levels, resulting in higher levels of spatter[149]. The dissociation of CO_2 within the arc into CO and O_2 results in an active gas component, which in turn reacts with elements having a high affinity for oxygen, such as Si, Mn and Ti, thereby reducing their recovery within the weld metal and/or increasing the inclusion volume. The term metal active gas (MAG) is consequently applicable for GMAW with this shielding gas and others containing a component of O_2 or CO_2. Mechanised girth welding often uses pure CO_2 for the fill (and sometimes cap) passes to enhance fusion, and when high toughness levels are not a major requirement[107,28,150,151]. The advent of new power sources allowing controlled metal transfer compared with a conventional dip transfer have reduced the spatter levels normally associated with CO_2, although bead appearance using solid wires is often inferior to other gas mixtures.

During the 1970's a large part of the European welding industry was owned by gas suppliers. They often promoted the use of argon based shielding, not least because of the significant tonnages of argon produced as a by product of oxygen distillation, large quantities of which were required due to the expansion of oxygen steelmaking[110]. Argon has a low ionization potential (15.75 eV)[95] and therefore facilitates easy arc striking. For steel GMAW pure argon is not desirable, resulting in an unstable arc and consequently irregular bead profile. It was found that small additions of oxygen and/or carbon dioxide resulted in improved arc stability, reduced spatter volume and better bead profile. In addition the operating range improved such that the power source settings were less critical in their ability to produce sound weldments. Oxygen improves the wetting ability of the weldpool, as well as promoting fine droplet volumes due to a reduction in the surface tension of the molten steel. True axial spray transfer develops in argon-based gases with the addition of 2% O_2 or 5%CO_2[94], which continues until around 30% CO_2 addition, from which point true axial spray transfer does not develop (the gas mixture then behaves in a similar fashion to pure CO_2). Numerous combinations of Ar plus CO_2 and/or O_2 have been marketed, with the major distinction in usage usually involving the transfer mode employed (PGMAW, dip or spray transfer GMAW) and bevel design/plate thickness to be joined. As a general rule, the greater the number of weld passes the larger the oxygen potential of the shielding gas required in order to improve the fusion characteristics. However, an increase in oxygen potential creates a deterioration in toughness levels, unless the consumable design has been tailored for a specified gas in terms of de-oxidation levels and microstructural development. This follows an initial increase in toughness with low levels of O_2/CO_2 addition as described in the later section on weld metal metallurgy. The commonly used Ar/CO_2 mix (typically 20-50% CO_2) for the root and cap runs of mechanised dip transfer GMAW improves arc and penetration control, coupled with smooth plate/bead toe transition enhancing the joint fatigue resistance[28,108,145,150,151]. Where optimum mechanical properties are required, the Ar/CO_2 mix is often used for all weld passes within the joint. Oxygen levels up to 2% are present in some proprietary gas mixtures e.g. BOC Argoshield Heavy; 78%Ar/20%CO_2/2%O_2. Compared with a mixture containing no oxygen, the arc/transfer characteristics and mechanical property

difference is marginal, and the gas production costs may be cheaper due to reduced processing (purity) required of the base argon.

Helium, like argon, is a totally inert gas that has been used in welding shielding applications, particularly in Canada, the USA and Russia where it is found naturally occurring in ground wells. The ionization potential of helium is much higher than argon (24.9 eV versus 15.7 eV[94]) and consequently requires a greater arc voltage to maintain identical conditions in terms of current and arc length. The heat input (power) to the base material will be higher, resulting in greater fusion, but the arc is more diffuse so depth to width ratios are less than with an argon arc. A summary of penetration profiles/transfer characteristics for a variety of gas mixtures and current types is shown in Figure 2-39. Helium costs in Europe are considerably higher than argon, but the increased heat input has benefits when welding high conductivity thick materials such as aluminium, where the increased travel speed attainable can reduce the overall production costs. Due to the reduced specific gravity of He, the corresponding flow rates are normally increased to make sure adequate gas coverage is achieved. The main benefit of helium as an additive gas in steel GMAW is the promotion of increased fusion whilst retaining the smooth arc and transfer characteristics of the more classical $Ar/CO_2/O_2$ mixtures. With the advent of pulsed GMAW and its application within mechanised narrow gap pipewelding, a programme of study into the optimum shielding gas was funded by a leading gas transmission company in conjunction with their government[152]. The results revealed that a trimix shielding gas of 82.5%Ar/12.5%CO_2/5%He gave a 60% increase in sidewall fusion for vertical down welding over a conventional Ar/CO_2 mix. Weld metal toughness properties were also improved due to the optimisation of the oxidation potential, resulting in weld metal oxygen contents of 200-250 ppm (400-500ppm were typical with the CO_2 and Ar/CO_2 mixes traditionally used). Due to the increased heat input of the helium-containing gas and the limitations of certain welding bugs in terms of torch movement (specifically no sidewall dwell), it has been found necessary in some cases to steer clear of helium additions for the cap pass in order to avoid undercut[145].

Many gas mixtures have been proposed as providing the optimum combination of arc/transfer characteristics, low fume/ozone levels and enhanced mechanical properties for a given material/joint configuration. A four component gas mix has gained popularity with the high deposition rate rotating arc metal transfer T.I.M.E. (transferred ionized molten energy) GMAW process. The gas, known as T.I.M.E. gas consists of 65%Ar/26.5%He/8%CO_2/0.5%O_2 and has been reported to produce welds with improved mechanical properties over standard Ar/CO_2 mixes, coupled with less spatter[153].

All the above gas mixtures have been incorporated to greater or lesser extents within Cranfield's recent pipeline GMAW process and material investigations[154,155,11,156,12]. The general conclusion in terms of shielding gas composition is that an Ar/20%CO_2(O_2) mix attains a good combination of welding and mechanical properties with dip transfer GMAW, whilst an Ar/12.5%CO_2/5%He mix exhibits promising attributes for pulsed GMAW.

2.5 FERRITIC STEEL WELD METAL METALLURGY

The ability of carbon and low-alloy steels to transform through several crystallographic structures on solidification from the melt provides metallurgists with the opportunity to engineer mechanical properties from a vast range of chemical, thermal and mechanical variations. Desirable mechanical treatment during the weld cooling process is virtually impossible for industrial and practical purposes, such that the cooling transformation from austenite plays the most important part in the final solidification structure via cooling rate, prior austenite grain size, total alloy content and non-metallic inclusion composition/size distribution considerations[158]. Although the general principles of steel solidification apply to weld metals, in comparison to bulk steel plate production the heating/cooling rates involved are usually much greater. The particular welding process used, in conjunction with the joint geometry and welding consumable(s), results in unique transformation products with their associated mechanical properties. Solid state transformations occur in both the weld metal and HAZ by heterogeneous nucleation at high energy sites such as grain corners (e.g. triple points), grain boundaries, dislocations and vacancy clusters[158]. Non-metallic inclusions of oxides, sulphides and nitrides also play an important part in the transformation kinetics, and considerable research has been conducted in this direction[158,159,160,161,162,163,164,165]. The various microstructural constituents that have been classified for C-Mn and low alloy steel weld metals are discussed in the following sections along with their metallurgical development.

2.5.1 STEEL MICROSTRUCTURE AND ITS DEVELOPMENT

The weld metal (WM) [or fusion zone for homogeneous welds], heat-affected zone (HAZ) and the unaffected base metal are the three main regions observed in a welded joint. The description of microstructural constituents within steels and weld metals has resulted in numerous investigators proposing various classification systems[167,168,169,170,171,172]. The highly non-isothermal conditions generated during the welding process generate multiple microstructural morphologies, often leading to confusion in descriptive terminology. The International Institute of Welding has consequently attempted to unify the process of identifying various microstructural constituents, and it is this scheme which will be used in describing the following steel transformation products[173] (the abbreviations used conform to this system).

On removal of the heat source, the molten metal in the weldpool solidifies as delta (δ) ferrite when the cooling rate is not too fast (see Figure 2-40). These delta-ferrite grains form via epitaxial growth from the fusion boundary, and subsequently follow the direction of maximum heat flow within the solidifying weldpool to produce an elongated (columnar) structure[174]. Decreasing temperature allows the delta-ferrite to transform to austenite, starting at the delta-ferrite grain boundaries. The columnar grain structure is maintained due to nucleation from the delta-ferrite grain boundaries, but the major growth direction is offset due to the temperature isotherms shifting on account of the moving heat source[175,176].

On further cooling (typically to around 900°C) the austenite to ferrite transformation progressively starts to take place (known as the Ar_3 temperature in the relevant equilibrium phase diagram). At slow cooling rates the first austenite to ferrite

transformation product is allotriomorphic[1] (blocky) ferrite (also known as primary ferrite, PF); this can nucleate heterogeneously at the austenite grain boundary and grow at a reducing rate into the austenite by diffusion (reconstructive thickening)[174], or intragranularly within the prior austenite grain boundary (PF(I)). The former can also form at slightly faster cooling rates where the ferrite still grows via a planar front, but the carbon redistribution is not as efficient, leading to veins rather than a polygonal structure. As a result the solute gradient into the austenite is steeper, and the growth front occurs behind an essentially incoherent (large-angle) phase boundary[177], compared with growth of the allotriomorphic ferrite behind both semi-coherent and incoherent boundaries. This form of ferrite is known as grain boundary ferrite (PF(G)) or proeutectoid ferrite.

At lower transformation temperatures (typically between 750 and 690°C) the primary ferrite formation subsides, and depending on composition and cooling rate, a morphology of ferrite with a second phase (FS) can develop from the prior austenite grain boundary or proeutectoid ferrite. Needle-like parallel ferrite plates result, which have been referred to as ferrite with an aligned second phase (FS(A)) or Widmanstätten side plates (FS(SP)). This is a direct result of carbon enrichment within the γ regions between the growing ferrite plates from which carbon is rejected. These later transform (below the Ar_1 temperature) to cementite (FeC_3) or pearlite (ferrite + FeC_3). The growing α plates have been shown to possess the Kurdjumov-Sachs orientation relationship with the parent γ[174,177].

At even lower temperatures of transformation (close to Ar_1) acicular ferrite (AF) can form (discussed in detail later). These are small non-aligned ferrite grains found within prior austenite grains, with a typical random section aspect ratio of 10:1. On completion of the AF formation there may be some areas of austenite between AF grains, enriched in carbon, which have still not transformed. These are generally small areas in the order of 1μm, which are retained either as austenite or transform to an aggregate of ferrite and carbides (FC) or martensite (M). These small areas are referred to as "microphases" because their volume fraction is generally very low, typically below 5%[174].

As the transformation temperature falls even lower (below Ar_1) the carbon does not have time to diffuse into the austenite as the grain boundary ferrite forms, resulting in massive ferrite or upper bainite formation (bainite will be discussed in detail later). Massive ferrite takes its name from a massive transformation which occurs by the movement of a high angle phase boundary. Short range diffusion of the atoms from parent to product lattice occurs, implying that carbon distribution in both phases is the same (massive ferrite is similar in morphological classification to allotriomorphic or idiomorphic ferrite[174]). Upper bainite formation, however, involves ferrite nucleation at the grain boundary followed by rapid growth of the ferrite into the grain behind a low energy semi-coherent interface. The ferrite grows as needles, precipitating cementite predominantly between the grains, and consequently resembles finely spaced Widmanstätten side plates, hence the microstructural description of upper bainite as ferrite with an aligned second phase (FS(A) or more specifically FS(UB)).

---

[1] Allotriomorph: a grain which does not possess the regular geometric shape corresponding to the atomic arrangement, due to non-uniform conditions of growth or contact with other grains.

At temperatures just above the martensite start (Ms) temperature, the formation of bainitic laths may occur with the resulting structure referred to as lower bainite. This phase requires the short range diffusion of sufficient carbon to form carbides having an orientation relationship within the ferrite grains. Due to the slow carbon diffusion at these temperatures, plate growth via cementite precipitation at the ferrite/austenite interface allows the advancement of the interface, resulting in a lath-like structure of ferrite containing finely dispersed carbide platelets, with small amounts of cementite between the laths[177]. In morphological terms the structure is regarded as ferrite with an aligned second phase (FS(A) or more specifically FS(LB)). Given that distinction between upper and lower bainite is not normally possible with optical microscopy, a general description for bainite is covered within the morphological classification as FS(B).

Martensite (M) can form in weld metals if the cooling rate is very fast and/or the alloy system involved increases the range over which martensite formation is enhanced over other transformation products. In low carbon steels the martensite exhibits a lath morphology, with very thin regions of retained austenite between the laths[177]. The laths exhibit a high aspect ratio and are typically about 0.5μm wide at carbon levels of less than 0.5wt%. The martensitic transformation occurs via shear of the face centred cubic austenite lattice to accommodate the higher carbon levels attainable within this structure, resulting in a body centred tetragonal form rather than the normal body centred cubic ferrite form[178]. Martensite, bainite, acicular ferrite and Widmanstätten ferrite are the result of displacive transformations involving the co-ordinated movement of atoms; such movements cannot be sustained across grain boundaries. As a result, it is normally possible to observe easily the prior austenite grain boundary, the overall grain size of which allows an indication of the weld metal thermal history[174].

As can be seen, a large variety of microstructures can develop on weld metal transformation from austenite, depending upon cooling rate and chemical composition of the weld metal. A schematic of a continuous cooling transformation (CCT) diagram applicable to a typical steel weld metal is shown in Figure 2-41, highlighting the various transformation products mentioned above. Photomicrographs of typical morphologies as identified in the IIW classification are shown in Figure 2-42.

In the higher yield strength weld metals, notably 690 MPa grade and upwards, the microstructures tend to consist of either a fine acicular ferrite matrix with some low carbon martensite, together with upper/lower bainite or granular bainite, as observed with research on ULCB weld metals[179]. Consequently, increased weld metal strength leads to relatively small morphological differences between the constituents that are increasingly difficult to quantify using optical metallography. The existing IIW C-Mn/ low alloy weld metal terminology[173] can be readily applied to welds with yield strength levels below ~700 MPa and conventional heat inputs (~1 - 4 kJ/mm), but it becomes increasingly difficult to accurately determine very high strength/low heat input weld optical microstructures. However, until a new terminology is proposed and accepted the existing standard will no doubt continue to be applied.

2.5.1.1 INFLUENCE OF THE PRIOR AUSTENITE GRAIN BOUNDARY

The austenite grain size plays an important role in determining the final weld metal microstructure. It has been demonstrated that in very small austenite grains, large grain boundary areas exist which contain a high density of favourable nucleation sites[180]. This results in a high proportion of grain boundary α nucleation and the likely formation of fine grained Widmanstätten ferrite/bainite. Larger austenite grains enhance intragranular acicular ferrite formation, provided nucleation of the latter is favourable over other products, due to the reduced density of grain boundary sites. Compared with bainite formation, the prior austenite grain boundaries are likely to exhibit a degree of allotriomorphic, proeutectoid or Widmanstätten ferrite. The effect on the difference in austenite grain size is illustrated in Figure 2-43. Further work has revealed that the prior austenite grain size is a function of the weld metal oxygen content[175]. Consequently, small changes in the prior austenite grain size produced by variations in oxygen content can strongly influence the formation of undesirable microstructures that may well prove detrimental to the mechanical properties of the weld metal.

2.5.1.2 ACICULAR FERRITE

Acicular ferrite is a typical α morphology formed in a temperature range where reconstructive transformations (e.g. allotriomorphic ferrite) give way to displacive ones (e.g. bainite, Widmanstätten ferrite or martensite), particularly with low-alloy steel weld deposits[174]. It possesses a microstructure that is superior in toughness and strength to most other transformation products due to its fine grained interlocking plates formed within the prior austenite grains. Acicular ferrite appears to have the morphology of thin, lenticular plates[159] in three dimensions, and is generally agreed to have a high dislocation density, fine grain size and high angle grain boundaries which act as effective crack arresters. Compared with other morphologies a cleavage crack is far more likely to be deflected or have a far more tortuous propagation route. Previous work[160] has revealed a dislocation density within a plate of 10^8 to10^{10} lines/cm^2. The fine grain size associated with acicular ferrite is due to the suppressed transformation temperature coupled with particular nucleation and growth mechanisms. In random planar sections the plates are typically in the range of 1μm wide and 10μm long. The true aspect ratio is therefore likely to be smaller than 0.1[174].

2.5.1.2.1 NUCLEATION AND GROWTH OF ACICULAR FERRITE

During the early stages of transformation non-metallic inclusions such as TiO, Ti_2O_3, TiO_2, Al_2O_3-MnO (galaxite), SiO_2, MnS, (Mn,Cu)S, TiN, TiO-MnO-SiO_2 and Al_2O_3-MnO-SiO_2 combinations have been shown to provide sites for the heterogeneous nucleation of AF within the large columnar austenite grains of weld deposits[160,161,181]. The inclusions are present through impurities or via deliberate alloying additions, but due to their complexity and the difficulty in conducting controlled experiments, their individual nucleation potency is not clearly understood[174]. Numerous mechanisms have been proposed over the years to explain inclusion-controlled acicular ferrite nucleation, with a popular explanation suggesting it results from a small lattice disregistry between the ferrite and the non-metallic inclusions[174]. Other mechanisms include increased stress-strain fields around the inclusions due to differences in thermal expansion

coefficients between the inclusions and γ matrix promoting AF nucleation, providing an inert surface which reduces the nucleation free energy barrier for the ferrite embryo, and localised chemical composition variations around the inclusion[181]. As mentioned earlier, the prior austenite grain size, inwhich inclusions also play an important role, has a direct influence on AF nucleation.

Larger inclusions are thought to be more effective in promoting AF nucleation due to the reduced curvature of the inclusion/ferrite nucleus interface reducing the activation energy. The larger the driving force for transformation, the smaller the activation energy required, resulting in the effective inclusion size varying with the particular transformation conditions in evidence.

Subsequent AF plates can be formed autocatalytically, such that it is not expected to find a direct correlation between the number of inclusions and the number of acicular ferrite plates[174].

There is strong evidence to suggest that acicular ferrite growth in the weld metal is diffussionless, with carbon partitioning into the austenite after the transformation event[161]. It appears that AF is an intragranularly nucleated bainite[174] and work carried out has revealed that as the oxygen concentration is increased, a microstructure containing bainite is replaced by one containing acicular ferrite[181]. The morphology of acicular ferrite, however, differs from that of conventional bainite; the former nucleates intragranularly at inclusions within the large austenite grains whereas bainite nucleates at austenite grain boundaries, as found in Widmanstätten ferrite, and growth produces a sheaf morphology[182].

In summary, it is generally agreed that high (i.e >70%) volumes of acicular ferrite in the weld metal microstructure give enhanced strength and toughness values[183]. The formation of acicular ferrite is dependent on many factors, for which the following are considered highly important: a large prior austenite grain size; a relatively specific weld metal oxygen content (typically 200ppm-400ppm for GMAW) coupled with judicious macro- and microalloying; an evenly distributed small non metallic inclusion size (typical mean diameter 0.4μm[174]) and volume fraction (typically 0.1-0.4%[164]); and controlled cooling rates (i.e. explicit heat input ranges).

2.5.1.3 Bainite

Bainite was first reported by Davenport and Bain in 1930[184] and refers to the microstructure resulting from the decomposition of austenite at temperatures above that at which martensite first forms, but below that at which pearlite is found[185]. The transformation temperature range between 250°C-550°C is generally thought to comprise the region in which a fine aggregate of ferrite plates (known as sheaves of bainitic ferrite) separated by cementite, martensite or untransformed austenite exist, commonly referred to as upper or lower bainite. The plates making up each sheaf are termed sub-units, and are connected to each other in three dimensions with the result that they share a common crystallographic orientation[182] (see Figure 2-44). It is also now well established that the nature of bainite changes from what is termed upper bainite to lower bainite as the transformation temperature is decreased, with corresponding changes in aspect ratio, dislocation density, subunit/sheaf width and number of sub units per sheaf (see Figure 2-45)[186]. Other forms of bainite exist such as

granular bainite, inverse bainite and grain boundary lower bainite, but these are not normally associated with the steels/weld metals under examination in the current work[182].

2.5.1.3.1 UPPER BAINITE

Upper bainite consists of fine plates of ferrite, each of which is typically 0.1-0.2μm thick[187] and 10μm long, and is considered to occur within a transformation temperature range between 400°C-550°C[185]. When viewed under optical microscopy upper bainite resembles a 'feathery' appearance.

Upper bainite is said to evolve in distinct stages beginning with the heterogeneous nucleation of bainitic ferrite sub-units at the austenite grain boundaries. The sub-units then lengthen until their growth is prevented by plastic deformation of the adjacent austenite, automatically limiting the maximum sub-unit size, at which point a new sub-unit nucleates at its tip. This process continues until a sheaf structure is produced (see Figure 2-46). Carbon is partitioned from the growing platelets into the residual austenite (a secondary event in comparison with the ferrite growth), and if the austenite is thermodynamically unstable with respect to carbide precipitation, the remaining austenite decomposes to cementite and more ferrite (see Figure 2-47). The amount and distribution of cementite is directly proportional to the alloy carbon concentration. These plates are often formed in clusters and within each sheaf the plates are separated by low angle grain boundaries of identical crystallographic orientation, each with a well defined crystallographic habit. The relationship between bainitic ferrite and γ can be explained in terms of the classical Kurdjumov-Sachs (KS) and Nishiyana-Wassermann (NW) crystallographic relationships.

2.5.1.3.2 LOWER BAINITE

Lower transformation temperatures (typically 250° to 400°C) result in the formation of lower bainite, consisting of heavily dislocated ferrite plates. The plates comprise a cluster of smaller sub-units/platelets as in upper bainite, but carbides are observed to precipitate either between the bainite platelets or as a fine dispersion within the bainite plates (see Figure 2-47). The plate-like carbides (not necessarily always cementite) precipitated within the ferrite platelets do so in a single crystallographic variant (at about 60° to the growth direction of the platelets), as opposed to the multi variant precipitation orientation within tempered martensite[182]. When viewed under an optical microscope lower bainite is observed to have an acicular appearance similar to that of tempered martensite. Nucleation of the plates is again stated as occurring from the prior austenite grain boundaries or from previously formed plates (see Figure 2-46), with the crystallographic orientation between the lower bainite plates and parent austenite similar to that of upper bainite (i.e. KS relationship).

2.5.1.3.3 TRANSITION FROM UPPER BAINITE TO LOWER BAINITE

Both upper and lower bainite consist of a non-lamellar mixture of ferrite and carbides and as a result the generalised transformation behaviour is very similar. The growth of each platelet is accompanied by an invariant-plane strain shape change comprising a

large shear component, although the shape strain of the sheaf tends to be less than the individual platelets due to the latter's separation by films of residual phases. Considerable differences in mechanical properties however highlight the need to differentiate between the two forms (c.f. the large variation in strength levels shown in Figure 2-7). When the initial bainitic ferrite forms, it is supersaturated with carbon as illustrated in Figure 2-47. At the temperatures associated with upper bainite, decarburisation by diffusion into austenite occurs so rapidly that there is no time for carbide precipitation within the ferrite, resulting in upper bainite. As the transformation temperature is reduced, the time available for decarburisation of the bainitic ferrite decreases, allowing some of the carbides the opportunity to precipitate within the ferrite. This leaves the remaining carbon to be partitioned into the residual austenite where it eventually precipitates as inter-plate carbides and results in the lower bainite microstructure. These inter-plate carbides are smaller in volume than those associated with upper bainite, due to the reduced carbon content available for precipitation. The reduced size/volume of inter-plate carbides explains why lower bainite is generally found to be much tougher than upper bainite, even though it has a higher strength due to the highly refined microstructure and increased dislocation density[182].

Differentiation between the two microstructural types via optical microscopy requires considerable expertise and magnification levels at the technological limits, but the use of transmission electron microscopy provides for relatively easy distinction[182].

2.5.1.4 TEMPERING AND RECRYSTALLISATION OF BAINITE AND ACICULAR FERRITE

Multi-pass weldments involve remelting some of the preceding weld bead and tempering others to varying degrees, depending on the distance of the particular bead from the fusion line of the weld pass in progress. Partial or complete reverse transformation to austenite will occur, with the carbon/alloy content of the ferrite playing an important part in the resulting properties. Unlike the tempering of low transformation start (T_s) temperature martensite, the redistribution of carbon from supersaturated ferrite and carbide precipitation has already happened to a large extent in bainite, such that autotempering is a naturally occurring feature of the transformation process. As a direct consequence bainite and acicular ferrite are far less sensitive to reheating effects below Ac_1 due to the low levels of carbon in solid solution. Minor changes in strength can be attributed to cementite particle coarsening and a general recovery of the dislocation substructure, with more pronounced effects occurring due to general microstructure coarsening and the onset of recrystallisation producing equiaxed α grains from the bainite sheafs.

Secondary hardening effects occur in steels containing strong carbide forming elements (e.g. Cr, Mo, V, Nb) which are held at elevated temperature for considerable amounts of time, such as those used in the power plant industry. Long range diffusion of substitutional atoms is required for the formation of these alloy carbides, and kinetically cementite precipitates first (at the expense of carbon) resulting in an initial drop in hardness. As the carbides form there is an increase in hardness due to dislocation hindrance, but as the carbides coarsen with time the hardness decreases, resulting in a secondary hardening peak[182]. These effects can occur for in-service weld metals held at elevated operating temperatures, but the reheating effects occurring during the welding process happen over very small timescales and distances, thereby limiting carbide

precipitation. The operating temperatures of transmission pipeline steels are well below that associated with causing significant microstructural changes.

Refinement of the microstructure via reheating above Ac_1 results in considerable benefits for the weld metal in terms of toughness improvements and reduction of residual stresses. The as-cast microstructure usually consists of various transformation products and a high dislocation density. Subsequent heat treatment of the as-cast microstructure results in various degrees of normalising taking place, and the volume fraction of dislocations reduce at the same time (temper annealing). If the weld metal is fairly low alloyed, there will be little resistance to hinder recrystallisation and grain growth, particularly if stable carbonitrides are absent. However, as the heat input to weld runs below the one being conducted is low, grain growth is restricted[177]. In the process of grain refinement, segregation effects such as columnar grain boundary carbides can be reduced or removed. This results in improved notch toughness. Theory for predicting the rates of reverse transformation to austenite and the consequent secondary microstructures do not exist in any useful form for weld metals[174], therefore predicting a TTT diagram for reaustenitisation (and also partial reaustenitisation) is currently impossible. This makes modelling austenite decomposition or changes in the tempered regions for any degree of confidence extremely hard.

2.5.1.5 The Role and Characteristics of Non-Metallic Inclusions

The formation of a high toughness C-Mn or low alloy weld metal microstructure is dependent on a number of factors. The role of non-metallic inclusions has been extensively investigated[162,163,164], with the conclusion that they exert an important influence on the weld microstructure formation. They are also responsible for the nucleation of voids during ductile fracture, or cleavage cracks during brittle failure[174]. Inclusions in the size range of 0.1μm to 0.5μm have a significant role in the nucleation of acicular ferrite, whilst inclusions <0.1μm are instrumental in pinning γ grain boundaries and preventing grain growth[165]. The inclusion diameter increases as welding heat input increases due to the time available for growth in the weld pool. Weld metal inclusions will be either exogenous or indigenous. Exogenous inclusions arise as a result of welding slags and surface scale, while indigenous inclusions are formed as a result of deoxidisation reactions (oxides) or solid state precipitation reactions (nitrides and carbides). The latter group are normally seen to be heterogeneous in nature with respect to chemistry, shape and crystallographic properties[158].

For many years it has been recognised that an increasing non-metallic inclusion content within C-Mn weld metals reduces the upper shelf toughness[188]. Cleavage resistance, however, is not at its maximum with a very low oxygen content, i.e., <50ppm, with a corresponding lower inclusion content, but typically requires 150 – 550ppm oxygen[189], and therefore, a higher inclusion content. A high proportion of 'tough' fine-grained intragranular acicular ferrite will nucleate if the level of alloying, weld cooling rate and inclusions of appropriate character are present[160,190]. A corresponding lack of nucleants caused by very low levels of oxygen and a sufficiently rapid cooling rate may result in ferrite with aligned second phases (upper/lower bainite) or even martensite, instead of acicular ferrite, with the resulting toughness often directly related to the microstructure types in evidence.

It is also known that larger non-metallic inclusions can reduce cleavage resistance by initiating cleavage fracture[191]. Inclusion formation is a result of deoxidation products e.g. Al_2O_3, SiO_2, TiO_2 becoming trapped in the solidifying weld metal. Some are formed before the steel solidifies, e.g., Al_2O_3 (melting point 2050°C) and these often crystallise as angular shapes; others solidify after the steel, and are often more spherical in nature[164]. Quantitative data on weld metal inclusions have been reported for numerous welding processes, giving inclusion contents from 0.10 to 2.1 volume %, mean diameters of 0.15 to 1.1μm and number densities of 2×10^7 to $16 \times 10^7 mm^{-3}$ with weld metal oxygen contents of 200 – 1200ppm[321,181,190,192]. Widgery [193] and Franklin [194] have estimated weld inclusion contents (volume %) as 5.5(wt%O + wt%S) and 5.0(wt%O) + 5.4 (wt%S - 0.003%) respectively from inclusion measurements in various weldments.

Inclusion composition is often reported as being inhomogenous [181], with the core generally consisting of oxide mixtures containing manganese, silicon and aluminium, unless minimal aluminium or substantial amounts of titanium are present. Sulphide shells have been reported around the oxide cores in numerous weld metals[163,181,195], and have been shown to inhibit the nucleation of acicular ferrite[196,197]. Conversely, the existence of TiO within inclusions is claimed to be an effective nucleant for ferrite due to the low lattice disregistry between TiO and ferrite[162]. Crystalline/polycrystalline patches containing titanium compounds (TiO, TiN, and TiC) have been identified towards the edges of inclusions[198], although the exact nature of the compound appears to be an amalgamation of the various constituents, exhibiting a face-centred cubic structure. Aluminium compounds on the surface of inclusions have also been detected [162] and their role is analogous to that of titanium. One compound, Galaxite ($MnO.Al_2O_3$), has a low planar disregistry with ferrite, accounting for its suitability as an effective ferrite nucleator. Inclusions with a similar proportion of Al_2O_3 can also be expected to be effective ferrite nucleants[164].

The ternary phase diagram consisting of MnO, SiO_2 and Al_2O_3 can be used to consider the bulk inclusion composition[198]; the majority lie close to the line joining rhodonite ($Mn.SiO_2$) to corundum (Al_2O_3), particularly where inclusions contain minimal titanium[164]. If the oxides of titanium are considered in the previous (ternary) phase diagram, these can be added to the oxides of silicon [199], thereby allowing inclusions containing aluminium, manganese, silicon and titanium to be represented. Inclusion composition measurements by Saggase et al.[199] noted weld microstructures containing greater than 2% titanium within the inclusions (i.e. approximately greater than 2.5% TiO) resulted in acicular ferrite contents greater than 80%, with such inclusions also often containing greater than 50% Al_2O_3. Devilliers et al.[163] have claimed that an inclusion composition of $2MnO\text{-}2Al_2O_3\text{-}5SiO_2$ is particularly effective in acting as a nucleation site for AF due to the large thermal expansion difference with respect to the γ, resulting in an increased stress-strain field around the inclusion.

As highlighted above, weld metal inclusions are primarily a mixture of oxides of manganese and silicon, and other stronger deoxidants (e.g. Al and Ti) when these are present in the weld. Their composition is important in influencing ferrite nucleation and the subsequent mechanical properties of the weld metal. High levels of AF are desirable due to the high toughness levels associated with this type of microstructural constituent, especially when grain refinement by subsequent passes is limited within the weldment. A sufficient inclusion content is required to provide an adequate number of nucleants,

but oxygen levels within the weld metal need to be optimised. The inclusions act as inert substrates with the ability to reduce the free energy barrier to nucleation. Their number and size distribution are latterly regarded as the dominant factor for AF nucleation (c.f. thermal stress-strain fields and lattice disregistry effects)[181].

2.5.2 SINGLE PASS HEAT AFFECTED ZONE MICROSTRUCTURE

The heat-affected zone adjacent to the weld metal/fusion zone is heated up to temperatures just below the base material's melting point, such that microstructural changes occur to varying degrees in the parent material around the fusion area (see Figure 2-48). This feature is a direct consequence of the need to heat the material to be welded above its melting point for adequate fusion to take place coupled with the sharp temperature profile generated between weld and base plate.

The type and volume fraction of transformation product are dependent on similar considerations as discussed for the weld metal i.e. cooling rate, alloying elements present (macro and micro) as well as the peak temperature reached and the original grain size. This results in numerous metallurgically different regions, which will be classified in the following sections and their typical attributes discussed.

2.5.2.1 COARSE GRAINED HEAT AFFECTED ZONE (CGHAZ)

The CGHAZ occurs at peak temperatures well above Ac_3 and up to the melting point of the parent material (typically above 1100°C, depending on the chemical composition of the steel). In this region complete retransformation to austenite allows the cementite and microalloy precipitates to coarsen and/or dissolve, resulting in grain growth coupled with the possible formation in the presence of high cooling rates/CE values of bainite and untempered martensite (hence the use of CE formulae to predict the propensity for high hardenability). Toughness within this zone is consequently often inferior, due to the reduced capability of the microstructure to prevent crack propagation. This can be offset to a degree by the limited time available (and hence narrow band) for grain growth to occur with low welding heat input values (such as for mechanised pipe girth welding). The drive for improved HAZ properties has resulted in steel development with lower carbon contents, which in turn can raise the Ms temperature, thereby allowing autotempering of the martensite formed[201]. Compared with bainite or Widmanstätten ferrite formation at lower cooling rates, tempered martensite has a very fine grain size leading to improved toughness. Further alloying (macro and micro) can complicate transformation temperatures and the resultant products, highlighting the need to examine an individual steel's HAZ.

2.5.2.2 FINE GRAINED HEAT AFFECTED ZONE (FGHAZ)

The FGHAZ occurs at temperatures above Ac_3 (typically between 900°C to 1100°C, depending on the chemical composition of the steel). Retransformation to austenite occurs, but its growth is considerably limited due to the lower temperatures experienced. On cooling, the smaller grained austenite, and hence large grain boundary area, is transformed to produce a fine equiaxed ferrite grain structure that is associated with high toughness. The width of this region can be enhanced with microalloyed steels

due to the precipitates (especially carbonitrides) pinning austenite grain boundaries and preventing growth.

2.5.2.3 INTERCRITICAL HEAT AFFECTED ZONE (ICHAZ)

At peak temperatures between Ac_1 and Ac_3 (i.e. between ~720°C and 900°C) partial retransformation to austenite occurs on heating; during cooling the carbon enriched austenite decomposes to various transformation products depending on the chemical composition of the steel and its cooling rate. It is possible to find phases which contain areas rich in carbon through partial dissolution of the cementite/pearlite; on transformation back to ferrite a mixture of martensite and retained austenite (MA constituent) can be created at fast cooling rates. These M-A constituents appear as small islands and can initiate brittle fracture[202].

At temperatures just above Ac_1 there exists little transformation of ferrite to austenite, whereas any cementite/pearlite, with its lower transformation temperature, can spheroidise. This typically occurs at grain boundaries and triple points, emphasising the function these areas have in providing high diffusivity channels for carbon at these low temperatures.

2.5.2.4 SUBCRITICAL HEAT AFFECTED ZONE (SCHAZ)

When the peak temperatures experienced are below Ac_1 (i.e. typically below 720°C) no phase changes occur, but partial spheroidisation of carbides can take place. At slightly lower temperatures up to ~650°C there is no obvious change in morphology (using a light microscope) but dynamic strain ageing can occur. The mobility of dislocations increases at these temperatures, during which time they are able to sweep up interstitial impurities such as carbon and nitrogen. At ambient temperature the solute enriched dislocations are effectively locked in position, thereby embrittling the material. Multi run welds enhance the possibility of this phenomenon.

2.5.3 MULTIPASS WELD METAL MICROSTRUCTURE

The construction of pipelines involves numerous weld passes in each joint, and as a result multiple thermal cycles reheat the lower weld beads to various temperatures. A change of microstructure, and therefore mechanical properties, can be observed in both the weld bead and HAZ of the previously deposited passes as shown in Figure 2-49. The high carbon MA islands found in the CGHAZ may remain unchanged after reheating, or alternatively may be tempered, depending on the peak temperatures achieved. The microstructural features found in the coarse grained reheated HAZ's are similar to those in the single pass CGHAZ, but grain growth up to three times the original may occur in the prior CGHAZ exposed to temperatures above Ac_3. Grain refinement that occurs on heating the CGHAZ into the fine grained reheated range generally improves the toughness of the prior CGHAZ[203].

At lower temperatures of reheating the CGHAZ, two further regions of note are the intercritically and subcrictically reheated coarse grained HAZ's (IRCGHAZ & SRCGHAZ). Both zones have been related to toughness deterioration in multipass weldments, particularly the IRCGHAZ. This is thought to be due to the formation of

small regions of limited ductility and cleavage resistance known as localised brittle zones (LBZ's), through the formation of martensite islands[203,204]. Embrittlement through precipitation of carbonitrides can also occur in the SRCGHAZ; during the original heating cycle the carbonitrides dissolve and are then precipitated again during the second thermal cycle. This can have a positive effect though in terms of 'mopping up' free nitrogen which can severely embrittle ferritic steels[201]. Spheroidisation of grain boundary cementite and carbide precipitation from martensitic islands can also occur during sub-critical reheating of the CGHAZ, both of which are beneficial for toughness.

2.5.4 EFFECT OF MICROSTRUCTURE ON TOUGHNESS

There are various microstructural constituents that may be present within a high strength weld metal. It is generally agreed that acicular ferrite is the optimum microstructure in terms of strength and toughness, however the maximum yield/proof strength level attainable with this microstructure (600-700 MPa[205]) is unlikely to satisfy the strength requirement of X100 girth welds on its own. Microstructural products which enhance strength are usually associated with a corresponding decrease in toughness. Martensitic and bainitic microstructures (ferrite with aligned or non-aligned second phase, Widmanstätten ferrite) together with grain boundary ferrite, retained austenite and ferrite-carbide aggregates are all considered detrimental to toughness, due to the structures providing preferential crack propagation paths to varying extents[206]. Martensitic and bainitic microstructures develop as a result of fast cooling rates or the involvement of alloy systems which suppress the transformation temperature to enhance the hardenability. Previous work[207] has reported that the presence of martensite in an acicular ferrite matrix can however produce excellent toughness (a weld metal oxygen content at 350ppm was considered important for this result). More importantly, the strength levels required of X100 linepipe will necessitate the use of a bainitic and/or martensitic constituent within the steel microstructure, coupled with high levels of toughness.

Although grain boundary ferrite can be considered as a soft and ductile phase, if it is associated with a significantly stronger phase, i.e. acicular ferrite, then the resultant strain concentration in the softer material can lead to the initiation of cleavage cracks. In work conducted on ULCB weld metals for HSLA-100 structural plate it was found that the factors affecting Charpy impact toughness were dependent upon the microstructural constituents together with the tensile strength, carbon content, and average size and volume of inclusions. Improved toughness occurred as a result of decreasing all the previous factors[208]. Of particular importance is the effect of oxygen on toughness, for which a more detailed evaluation will follow in a later section.

Irrespective of the manufacturing route of the linepipe (e.g. TMCP or Q and T), the major factor affecting the properties across the HAZ on production of a girth weld is the resultant variation in microstructure. This is largely dependent on the transformation temperature, which in turn is influenced by composition, austenite grain size and cooling rate. The range of temperatures experienced promote varying degrees of grain coarsening, redilution of alloying elements and the destabilisation of compounds which fix ageing or segregating elements. However, the reduction of impurity elements such as sulphur throughout the steel production route, combined with the judicious addition of

macro- and micro-alloying elements, have allowed great advances in the toughness levels experienced in the HAZ of TMCP steels. Provided the heat input of a given weld is maintained within the manufacturer's guidelines for the material in question (graphs defining the strength obtained with a given cooling rate are often available), the toughness, as well as the hardness, should remain within acceptable limits.

The general microstructure and inclusion characteristics are therefore considered as the two basic factors that determine fracture toughness in both the weld metal and HAZ. Segregated microphases, nitrogen and impurity elements also play an important role; their extent should be maintained at the lowest possible levels to ensure high toughness[201]. A small grain size in the weld metal reduces the number of coarse grains in which the cleavage cracks can nucleate, leading to a model of brittle fracture in weld metals being nucleation controlled via the inclusion content, rather than propogation controlled (the latter is more applicable for the base material).

A multi-pass weld metal and HAZ are easily arranged into three major regions: columnar (as-deposited) weld metal; reheated weld metal; and base material HAZ's. Consequently, the location of the Charpy/CTOD notch in relation to the macrostructure is an important factor to consider when evaluating toughness properties. Pipeline girth welding specifications generally require Charpy notch testing to be taken from the weld metal, fusion line, fusion line +2mm and fusion line +5mm. The main areas of concern appear to lie with the fusion line/fusion line + 2mm area, where the CGHAZ formed during the previous pass is reheated to temperatures within the intercritical and subcritical regions, thus creating the IRCGHAZ and SRCGHAZ mentioned previously.

2.6 WELD METAL COOLING RATES

Weld metal and HAZ cooling rates form an integral part of the microstructural development in a weldment. The phase transformations that occur in steel solidification are of major importance in determining the metallurgical and mechanical properties, and have been the subject of many investigations for both weld and parent metal in the quest for structure/property relationship understanding. The measurement of cooling rates coupled with microstructural classification allows a range of welding parameters to be generated for the desired mechanical properties[44].

The decomposition of austenite during the cooling cycle results in a crystallographic change of the bulk matrix from face centred cubic (fcc) lattice to body centred cubic (bcc) (or body centred tetragonal; bct) lattice. Whilst there is an increase in volume of the unit cell (~1%) from fcc to bcc, due to the increased efficiency of atomic packing in fcc (74% occupation) over bcc (68% occupation). However, the interstitial diameter available is higher in the fcc lattice (1.04Å vs 0.72Å for bcc) accounting for the higher solubility of interstitial solute atoms of carbon/nitrogen etc. in austenite[94]. Among the techniques for observing the austenite decomposition are thermal analysis, dilatometry or magnetic analysis[209], as well as by means of acoustic emission[210]. Thermal analysis and dilatometry are the most common techniques used, either via weld thermal simulation (analytical methods) or during the actual welding situation (in-situ or direct methods). Thermal analysis observes the heat liberated via the enthalpy difference of free energy reduction during the phase transformation, resulting in a slowing of the cooling rate through the transformation range. Measurement of the volume change, as described previously on heating or cooling can be recorded by dilatometric methods. A

schematic illustration of typical results from both measurement techniques for steel transformation is shown in Figure 2-50.

2.6.1 WELD THERMAL SIMULATION TECHNIQUES

Nippes and Savage[211] developed an analytical technique for reproducing HAZ microstructures in the late 1940's subjecting small scale specimens to heating/cooling rates similar to those experienced at a given point in the HAZ. A common thermal simulator used today in research and development laboratories around the world is the Gleeble™ equipment, which is capable of accurately reproducing controlled heating and cooling rates[212]. Specimen size is usually 11x11 mm cross section (allowing a standard 10x10 mm Cv specimen to be subsequently machined), with the sample resistance or induction heated. Temperature measurement of the sample via attached thermocouples, and possibly lateral expansion or contraction at specimen mid-length is recorded during the simulation. The technique has been applied to both weld metals and HAZ's[213,214,215,216,217], but small variations in the microstructural composition (and hence transformation temperatures) have been observed when compared to real welds of similar cooling profiles[214,218]. This has been attributed to a mismatch of austenite grain size in the coarse grained region of a simulated weld as compared with a real weld specimen, thought to result from steep temperature gradients in the real HAZ. Possible differences in heating rates[214] were also felt to have an influence, even with modern simulation equipment capable of heating at 10,000°C/s[212]; discrepancies in the results have been attributed to a general problem with the technique rather than the design of the simulator[214].

2.6.2 IN-SITU TEMPERATURE MEASUREMENT

Measurement of thermal cycles during welding has become a well established experimental technique, primarily by the use of thermocouples placed in and/or around the weldpool[219,220,221,222,223,224]. Infra-red temperature measurement with an optical pyrometer[225,226] and in-situ dilatometric analysis[209] have also been applied with varying degrees of success, but the specific placement possible with small diameter thermocouples provides for a high degree of confidence in the cooling curves and transformation temperatures observed. The advancement of data logging equipment over the last decade has enabled multiple channel thermocouple systems to be easily and cheaply customised for data acquisition. Data is now stored electronically, allowing easy manipulation in numerous software packages for analysis in real-time or at a later date. The problem of electromagnetic interference of the thermocouple voltage signals due to the welding process can also be minimised using custom designed signal filtering, either during or post data acquisition.

Several thermocouple techniques have been developed to acquire the temperature cycles in the HAZ. The implant method developed by Granjon[219,227] involves the insertion of a pre-drilled plug into a steel plate. One or two holes are drilled and thermocouples placed in them, such that the HAZ temperature profile at a specific distance from the fusion line is monitored (see Figure 2-51). When two thermocouples are used, the temperature difference between them can be used to highlight phase transformations; a rapid reduction in difference demonstrates the onset of transformation, whilst the finish

of transformation is considered as the resumption of the normal cooling rate after the transformation discontinuity[228]. The technique is useful when limited amounts of the material to be investigated are available, but the distortion of the plug in the plate during welding may cause a gap to develop, and as a result the heat flow through the plug will be considerably different[223]. The original experiments[227] were carried out at low heat inputs (≤2 kJ/mm; $t_{8/5}$ < 6s), where experiments with various fit-up tolerances and integral testpieces showed no observable differences, but later experiments at high heat inputs (≥2 kJ/mm) did show discrepancies[223].

Drilling holes directly into the material to be examined and inserting thermocouples has been practiced by numerous investigators[222,223,224,229,230]. The technique requires a knowledge of the penetration depth of the welding process, such that the hole is drilled from the reverse side of deposition to the correct place in the subsequent HAZ. This is determined using the same welding parameters, joint preparation, preheat etc. as for the thermal cycle measurement, and then sectioning the weld to measure the penetration. Due to the inherent nature of arc welding the penetration is likely to vary somewhat along the weld length, hence it is normal practice to vary the drilled depth in small increments (relative to the HAZ width) and place several thermocouples when trying to obtain data from a specific region in the HAZ. The hole itself will cause a disturbance in the heat flow, but experiments have shown that the smaller the hole the greater the reproducibility and the smaller the disturbance of the welding arc[223]. It has also been reported that heat flow disturbance is minimised by placing the thermocouple normal to the fusion line[221]. Thermocouples placed at the root of the weld bead have also been shown not to cause significant disturbance to the heat flow around the hole[230]. Hole diameters of between 1.7 and 4.0mm have typically been used[223]; diameters below this are usually not feasible due to the ceramic insulators required to separate the wires, and above this value the hole is likely to significantly affect heat flow. It has been suggested that coating the thermocouple wires with a refractory mixture may eliminate the requirement for ceramic insulators, but little evidence has been found of experimentation with this technique[221].

The above techniques have predominantly been applied to HAZ studies; measurement of the weld cooling cycle via a drilled hole was achieved unintentionally when the penetration allowed the thermocouple to enter the molten weldpool, and was not destroyed in the process. Weldpool cooling curves are commonly obtained by plunging (harpooning) a thermocouple into the solidifying bead behind the arc[220], with either manual or automated placement. The degree of precision required is directly related to the weldpool size behind the arc, hence submerged arc or high current GMAW is likely to be much easier than low current GMAW, SMAW or TIG.

2.6.3 THERMOCOUPLE EQUIPMENT

The choice of thermocouple composition is usually determined by the peak temperatures to be measured alongside the time spent at this temperature. The heat affected zone of a typical low-alloy steel will be subjected to temperatures at levels in excess of 1300°C, although the extremes occur for very short time periods (typically < 1 second). It is therefore common practice to use NiCr-Ni wires (Type K in accordance with IEC 584-1) which are defined (temperature limit in which the thermal voltage is covered by a standard specification) to 1370°C, although a maximum deviation of

reading is specified until 1200°C[231]. For higher temperatures, such as those experienced in a cooling weldpool or for greater confidence in the CGHAZ, Pt+13%Rh-Pt wires (Type R) are defined until 1760°C with a maximum deviation specified up to 1600°C. An added advantage of Pt based thermocouples is their reduced ageing drift over base metal thermocouples, along with the smaller tolerances attainable (at 1000°C a NiCr-Ni thermocouple gives ±7.5°C [class 2] or ±4°C [class 1], Pt+13%Rh-Pt gives ±2.5°C [class 2] or ±1°C [class 1])[231]. Disadvantages are the high cost and reduced thermal voltages (see Figure 2-52). Weldpool temperature measurements have also been made using W-W/26%Re wires which are capable of continuous exposure at 2300°C, and for short periods up to 2750°C[232]. Cost and electromotive force (emf) output are again limiting factors for the use of this wire type.

Due to the high cost of thermocouple wires (particularly the noble and refractory metals), they are usually only employed within the region of high temperature. It is also often desirable to locate the recording equipment away from the experimental area, particularly in the case of welding. In these situations it is normal practice to use compensating cables to transfer the signal to the reference junction box. These have the same thermoelectric properties as the thermocouple wire, but only within a limited temperature range (typically 0-100°C). For ease of identification they are normally colour coded: Type K compensating cable is typically Cu (green sheath, +ve) and Cu/Ni (white sheath, –ve) with the outer sheath green, Type R compensating cable is also typically Cu (orange sheath, +ve) and Cu/Ni (white sheath, –ve) with the outer sheath orange. It should be noted that the Cu/Ni alloy used for the negative wire in both cases is tailored for the given thermocouple wire and therefore not interchangeable[231].

Thermocouple wire diameter is an important consideration in terms of durability and cost. The larger the diameter the greater the long term stability of emf output, and the increased chance of survival for extremely high temperatures (i.e. within the arc for short periods of time). Conversely, smaller wires allow a reduced diameter ceramic insulating sheath, thereby lowering the chances of heat flow disruption. The noble metals are sold on a weight basis, such that significant savings can be made on using small wire diameters. A difficulty may arise with small wire diameters in welding the contact point between the two wire types (hot junction). The minimum volume of material (ideally just the wire diameter) is required at the point of contact so that the heating/cooling cycle is not artificially altered.

Shielding cables (twisted filament) or tubes (iron) are sometimes used to minimise the electromagnetic effects of the welding process disrupting the signals from the hot junction to the recording equipment. It is latterly more common to introduce some form of electronic filtering during or after data acquisition. Correct earthing of the acquisition junction box also helps reduce interference.

Ceramic sheaths are normally used in welding applications to isolate the wires from the junction of the compensating cable to the hot junction. These are usually circular or oval externally, and contain twin bores of a size suitable for the thermocouple wires. High purity (99.7%) sintered alumina is considered one of the most stable materials for high temperature applications. Platinum thermocouples are very sensitive to poisoning by foreign atoms, in particular Si, As, P, S and B. Of these SiO_2 reduced to SiO by iron contamination is very detrimental due to the formation of highly brittle Pt_5Si_2 silicides if left in contact with the platinum over long term exposure. Hence grease, oil (S) and

finger perspiration (NaCl, KCl, $CaCl_2$) should be thoroughly removed from the Pt wires. Aluminium oxides exhibit appreciable thermal conductivity above 1000°C, but in view of the short time periods, high temperature stability (up to 1900°C) and inertness with platinum at these levels, it is considered the optimum sheath material[231]. The stiffness of the sheath is also an important factor considering the physical handling of the thermocouples during temperature measurement. Care needs to be taken due to the brittleness of ceramic structures.

Soldering of the thermocouple wires to the relevant compensating cable is often considered the most suitable technique to avoid signal losses[223], but the situation may not allow this to be easily performed. Specialist push/pull connectors have consequently been developed and are suited to a particular thermocouple type.

2.6.4 RECORDING INSTRUMENTS

The e.m.f. generated at a particular temperature is dependent on the thermocouple type, the value of which needs to be recorded by some means. The main criterion for welding temperature measurement is the capability of the equipment to record the very steep temperature gradients experienced. Very early temperature measurement used oscillographs and photoelectric potentiometers, but calibration and resolution were limited[233]. Later techniques often employed electrically actuated chart recorders for producing a permanent record in analogue form. These have been classified into two main groups according to the principle of operation[232]: galvanometric; and potentiometric. Galvanometric instruments consist of a moving coil meter which measures the current produced by the thermoelectric e.m.f. A pointer attached to the meter can indicate the temperature on a precalibrated scale (typically in 5°C or 10°C increments), or in the case of a direct-writing moving-coil instrument a pen writes in sympathy with the coil movement on a chart (strip or circular records can be produced). The equipment is cheap, but due to the fine mechanical set-up is not very robust. It is also prone to deviate quickly from a calibrated value.

Potentiometric instruments operate by balancing the thermocouple e.m.f. against a known fraction of a reference voltage. High precision can be attained in properly maintained and calibrated instruments; resolution of 0.1μV and an accuracy of ±1μV are possible (c.f. thermocouple e.m.f.'s up to 80 mV). Use of this equipment in a chart recorder requires a servo-amplifier and associated motor. The bridge circuit is initially adjusted such that the two voltages are in balance and the motor therefore stationary. When the e.m.f. signal changes, the output of the amplifier causes the servo-motor to drive a balancing potentiometer, which in turn refers a feedback voltage to the amplifier input. The servo-motor will stop when the two signals are equal and opposite. A pen can consequently be attached to the motor-potentiometer mechanised drive, and at the point of balance the pen will show the proportional value of the input signal. Although in theory these instruments are capable of recording temperature changes of a fraction of a degree at 1000°C, in practice it is difficult to find a sufficiently stable balancing voltage to do this for more than a short period of time[224].

Before the onset of high frequency digital storage, ultraviolet chart recorders were used to monitor various high frequency signals. The equipment relies on a mirror attached to the moving coil of a galvanometer, which directs a light spot onto ultraviolet sensitive paper as it is fed through the recorder. Although considerable care has to be taken when

handling the equipment, it has been used successfully in weld thermocycle temperature measurement[222,223,230] For all the previous techniques mentioned, data analysis requires time consuming conversion to the correct time/temperature plot, especially when multiple thermocouple inputs are used.

It is now standard practice to employ electronic data acquisition systems to capture the e.m.f.'s produced by the thermocouples with respect to time, thereby allowing data analysis at a later date[224]. Analogue input data is fed into an electronic device where it is converted at a specified rate into digital code, and subsequently stored in the computer's memory. Due to the information being 'grabbed' in specified chunks there will be discontinuities compared with the continuous variation of an analogue signal, for which the latter exhibits no lower limit in terms of observable change. This leads to a limit in the conversion precision of the analogue signal, i.e. a resolution limit. The A/D converter produces a binary number which represents the magnitude of an analogue input signal, but the number assigned has a range for which it is valid. As a result there is inevitably a degree of uncertainty in the binary number, such that analogue values which lie within this range all give rise to the same binary number (i.e. they are not resolved as being different). Electronic advances over the last decade have significantly improved the resolution capability of A/D converters. The resolution is usually expressed in terms of bits, such that the higher the bits the greater the resolution (e.g. 12 bit = 2^{12} combinations i.e. 4095 values that can be assigned to the given voltage range, compared with 65536 for a 16 bit converter).

2.6.5 TRANSFORMATION TEMPERATURE DETERMINATION

As well as determining cooling times over specific ranges (e.g. 800°C to 500°C; $t_{8/5}$) or cooling rates at specific temperatures, cooling curve analysis can show the start, maximum rate and finish of various transformations providing the equipment is sensitive enough. This allows a correlation with the observed microstructures, and, if various cooling rates are employed, the generation of CCT diagrams for a given weld metal composition. Several methods have been applied and can be grouped according to the processing of the signal: temperature – time; direct rate; differential; and derived logarithmic[209].

The temperature – time (T-t) method simply involves analysing the cooling curve for deflections from the normal exponential decay. The start (T_s) and finish (T_f) temperature of transformation for various products can be observed due to the latent heat generated during the lattice change. The deflections, however, are often very small and a precise point of change is not necessarily easily distinguished. In order to exaggerate the point of change successive intervals of equal temperature drop are plotted against the actual temperature, resulting in a linear plot until a marked deviation at transformation is seen. This is known as the direct rate analysis of T-t curves. Another method of transformation temperature enhancement is differential thermal analysis (DTA). The cooling curve of the material in question is continuously compared with that of a reference specimen undergoing the same temperature profile; deviations due to the heat of transformation are easily distinguished in the resulting plot. Further precision is gained by applying the direct rate analysis to the differential curve, resulting in a method named derived DTA. The above methods can all be performed in real time during the experiment using relatively simple electrical circuitry[219]. When chart

recorders were the major method of data capture the results could be displayed with or without the conventional T-t graph. With the advent of electronic data analysis and storage, the above methods can still be employed, but do not necessarily need to be displayed in real time. First and second derivatives of the cooling curves are easily obtained using proprietary software packages, e.g. Matlab/Axum, which again enhance the transformation temperatures (see Figure 2-53).

Another method of transformation analysis reported to give good results is the derived logarithmic as described by Christensen and Simonsen[234]. The rate of heat loss from the sample is assumed to be proportional to the change in temperature:

$$\frac{-dQ}{dt} \sim \frac{dT}{dt} \sim T - T_0$$

where Q = Heat, T = sample temperature, T_0 = surrounding temperature and t = time

If cooling is considered from the high temperature region, i.e. above transformation, at a chosen level T_i, where the time is taken to be equal to zero, integrating the above expression to obtain the area under the curve gives:

$$T - T_0 = (T_i - T_0)\exp(-Bt) \qquad (1)$$

where B is a constant. If logarithms are taken of both sides in equation (1) to obtain a straight line in the constant cooling regime, and then differentiation is used to enhance the inflection points:

$$\ln(T - T_0) = \ln(T_i - T_0) - Bt \qquad (2)$$

$$\frac{d\ln(T - T_0)}{dt} = -B \qquad (3)$$

The resultant slope in the transformation region should show a pronounced deviation from linearity (see Figure 2-54). The start of transformation (e.g. B_s and M_s) can usually be fairly precisely determined with the above methods, but the finish of transformation is harder to detect due to the relatively low amounts of heat liberated. It has been reported[234] that both dilatometric and thermal analysis techniques gave good agreement for $t_{8/5}$ cooling times of between 5s and 30s, but for longer times than this transformations were best observed using dilatometric techniques.

2.7 THE EFFECTS OF ELEMENTS ON STEEL WELD METAL PROPERTIES

One of the most effective ways to maintain the required properties of a weld metal over the widest possible range of operational parameters (e.g. heat input, joint geometry, impurity control) is by the careful selection and use of alloying elements. These can be divided into several groups depending on their functions within the iron lattice, or their affinity for combination with other elements. The following two tables ascribe the common elements and compounds found, or used, in steels to the various groups[94,201]:

Nonmetallic inclusions	Gases	Impurities	Deoxidisers
Oxides	Nitrogen	Sulphur	Aluminium
Sulphides	Oxygen	Phosphorus	Titanium
Nitrides	Hydrogen	Tin	Manganese
Silicates		Arsenic	Silicon
		Antimony	Magnesium
		Calcium	Zirconium
		Zirconium	
		Rare earth elements	

Interstitial Elements	Substitutional Elements	Carbide Formers	Sulphide Shape Control Elements
Carbon	Manganese	Molybdenum	Calcium
Nitrogen	Silicon	Chromium	Cerium
Boron	Nickel	Vanadium	Lanthanum
	Copper	Titanium	
	Molybdenum	Niobium	
	Chromium	Tungsten	
	Aluminium		
	Vanadium		
	Titanium		
	Niobium		

The interstitial and substitutional elements can be regrouped in terms of macro (Mn, Si, Ni, Mo, Cr) and micro-alloying (B, Al, V, Ti, Nb), relative to the typical weight % added. A further classification is possible based on the effect the various elements have in restraining or promoting either the fcc or bcc phase [94]:

Austenite (fcc) stabilisers	Ferrite (bcc) stabilisers
Carbon	Chromium
Nickel	Aluminium
Manganese	Molybdenum
Nitogen	Silicon
Cobalt	Niobium
Copper (weak).	Tungsten
	Vanadium

It should be noted that combinations of the above elements balance out the respective ferrite or austenite forming capabilities depending on the relative amount added. The C curves in TTT diagrams can also be displaced to faster or, more commonly, slower times for transformation to occur, hence elements can control the rate of transformation as well as the temperature. For instance manganese and nickel both lower the

transformation start temperature and displace the C curves to longer times, thereby promoting martensitic or bainitic microstructures).

Numerous investigations have been conducted to ascertain the effect of alloying elements in weld metals in terms of their mechanical properties. The majority of work has used SMAW, SAW or FCAW due to the relative ease and low cost of adjusting compositions via the flux addition, but considerable work has also been performed with GMAW and TIG. The following sections highlight the pertinent effects of the common alloying elements. It should be noted that most of the conclusions drawn from alloying changes involved wide bevel (i.e. typical bevels as described in the relevant consumable classification test standards) rather than high cooling rate/low heat input narrow gap preparations.

2.7.1 CARBON

Pure iron is of extremely limited use in terms of engineering structure fabrication due to its low strength, but it was realised from an early date that small amounts of carbon (e.g. <0.1%) significantly increased the strength and hardness level. This is due to interstitial solid solution hardening alongside, metastable phases (e.g.Fe_3C) being formed above 0.008% carbon at room temperature. The true equilibrium diagram of iron-carbon alloys would result in an iron and graphite composite if diffusion were allowed to proceed to completion (which is quite possible at elevated temperatures), but the addition of further alloying elements is highly efficient in ensuring the carbon is more tightly bonded as a carbide. The effectiveness of carbon as a strengthening mechanism is compromised by the reduction in toughness as alloy levels increase; a greater percentage of brittle Fe_3C is formed, or in the case of the high cooling rates experienced within weld metals larger amounts of martensite may be formed. It is therefore common practice to improve the hardenability by the use of additional elements which promote better toughness, allowing very low levels of C (eg <0.05%) to be employed. The combination of carbon with additional elements significantly changes the eutectoid composition, as well as changing the Ae_1 (and hence Ae_3) boundary temperature. The transformation kinetics are thus considerably changed enabling many combinations of microstructure to be generated for varying cooling rates and alloying levels.

Work with a low strength C-Mn SMAW electrode (AWS E7018) resulted in optimum carbon levels between 0.07% and 0.09% in terms of strength and toughness[235]. Further investigations with high strength electrodes (AWS E10019/ E11018) corroborated these levels with an optimum carbon content in the region of 0.07%[236]. The potency of carbon limits its allowable variance when compared with many other additions, such that its usefulness as a mechanical property modifier is restricted in most welding applications.

Several alloying elements (see tables above) possess a strong tendency to form complex multi-metal carbides, sometimes with a greater affinity than iron, with the result that they can be more stable in the ferrite matrix and promote improved mechanical properties. The nature of the particles can affect the steel by changing the temperature and time required for their dissolution when heating to austenitise the steel. This changes the tempering temperature to generate a given hardness level, allowing the possibility of secondary hardening during heat treatment and changing the toughness of the material via the carbide size and dispersion.

2.7.2 *MANGANESE*

Manganese is the most common alloying element present in steels due to its relatively low cost, coupled with its ability to increase the steel hardenability by lowering the fcc to bcc transformation without a deterioration in toughness. Other benefits are its ability to combine with oxygen in the molten steel, thereby acting as a deoxidiser (limited with respect to other elements). It also ties up any sulphur, thereby reducing the chances of iron sulphide inclusions which promote hot cracking.

Investigations into increasing manganese contents of C-Mn SMAW electrodes have shown a decrease in grain boundary (pro-eutectoid) ferrite and a consequent increase in AF. The grain size of AF is also refined with higher manganese, explaining the improvement in toughness alongside strength[237]. Weld metal contents in high strength steels are typically between 1.6 and 2.0% for optimum as welded strength and toughness; slightly lower levels show improvements after stress-relief thermal cycles.

2.7.3 *SILICON*

In combination with carbon and manganese, silicon is a typical addition in steel alloying primarily due to its strong deoxidising capabilities. Silicon is a powerful ferrite strengthener in comparison to most other alloying elements (see Figure 2-55) and promotes considerable hardenability through solid solution[94]. At levels in excess of 0.5% a consequent reduction in toughness is observed due to the promotion of martensite/austenite microphases, but providing manganese levels are optimised, silicon levels up to 0.5% can be tolerated[238]. Typical weld metal silicon levels are maintained between 0.3% and 0.5% as a compromise between weldpool fluidity, deoxidation and toughness. The inclusion of oxide particles promotes the nucleation of acicular ferrite, but their total number and volume require a balance to prevent a reduction in toughness. A Mn/Si ratio has been proposed by certain investigators[239], but others[238] have seen a toughness peak for a fixed silicon content when the manganese is varied, pointing towards a microstructural explanation for optimum results.

2.7.4 *NICKEL*

Nickel promotes austenite stabilisation in steel and displays no inclination to form carbides or oxides due to iron having the greater affinity for oxygen and carbon. As a solid solution hardening element it promotes effective ferrite strengthening, and at the same time increases toughness. The latter is due to the suppression of the γ to α transformation throughout the weld metal cooling range (as per manganese additions), with the temperature of primary ferrite formation reduced below that of acicular ferrite/bainite or martensite morphologies, which consequently nucleate in preference (the final structure is dependent on the cooling rate, inclusion content and nickel level)[240]. Work by Taylor and Evans[241] has shown that the promotion of acicular ferrite structures is enhanced with optimum slag and deoxidation systems coupled with nickel. Levels of the latter between 0.8% and 1.5% offer a good compromise between cost, strength and toughness (>30J at -40°C are easily achieved in production welding situations) when combined with ~1.0 - 1.2% Mn (for both as-welded and stress relieved situations).

The level of nickel providing optimum strength and toughness is closely associated with a particular manganese content; the higher the Mn, the lower the Ni level required to avoid deleterious microstructures and vice-versa. Weight for weight, manganese additions have been demonstrated to show a greater influence in lowering transformation temperatures in all regions of the relevant CCT diagram compared with nickel[240]. One of the main advantages attributed to nickel additions is a 'flattening' of the Cv impact transition curve. Although the upper shelf toughness is not as high as an equivalent C-Mn electrode, lower shelf toughness is increased and the change from high to low shelf is spread over a greater temperature range[241]. Engineering structures are safer from a design point of view if any mechanical property transition does not occur at a sharp point, as freak conditions may have disastrous consequences.

2.7.5 MOLYBDENUM

Molybdenum is a strong α former and as little as 3 wt% will retain the bcc structure in iron at all temperatures. It possesses a great affinity for carbide formation and markedly increases hardenability through solid solution strengthening. Additions of <0.5% are typically used (often in combination with Cr and Ni) to produce high strength weld metals. Up to this level of Mo the proportion of acicular ferrite increases at the expense of primary and grain boundary ferrite[242]. Widmanstätten side plate ferrite is also reduced thereby enhancing the weld metal toughness[244]. Above 0.5% there is an increasingly significant drop in toughness due to the marked increase in hardenability. At levels below 0.25% Mo, Mn additions of up to 2% appear to have no influence on toughness levels, but above this Mo level Mn additions need to be carefully balanced[242].

2.7.6 CHROMIUM

Like molybdenum, chromium has a strong affinity for carbide formation as well as restricting the range over which the austenite phase is stable (>13% Cr in iron retains the bcc structure on heating or cooling through all temperatures). It is consequently highly efficient at promoting steel hardenability, with the carbides produced promoting elevated temperature property maintenance (it is often combined with Mo for enhanced effect e.g. 2¼Cr/½Mo). The rapid cooling rates normal to most welding situations restrict the alloy content in parent and weld metals if low preheat levels are to be maintained. Additions up to 1% in the weld metal have been shown to increase the content of acicular ferrite, mainly at the expense of grain boundary ferrite, but above this level the structure becomes predominantly bainitic thereby reducing the toughness[242,243].

2.7.7 COPPER

In pure molten iron, copper is completely soluble. However, small amounts of carbon (i.e. 0.1 wt %) prevent all the Cu remaining in solid solution. Within the delta ferrite and austenite phases about 10% Cu can be accommodated, but this falls to around 2-3% in ferrite on transformation, and with slow cooling to room temperature less than 1% Cu will be retained in solid solution. At fast cooling rates (i.e. quenching) much greater levels of Cu can be retained in solid solution, and are then able to precipitate out and

increase the steel's hardenability during tempering treatment. This system has been employed for high strength steel development (e.g. HSLA 100), allowing very low C and a consequently enhanced weldability. Although an addition of only 0.2% copper significantly refines the prior austenite grain size, acicular ferrite and coarse and fine grained reheated structures, there is no improvement in toughness (this property is significantly impaired above ~1.0%). Changes of Cu levels within 0 to 1.4% appear not to affect inclusion volume fraction, size distribution or chemistry[245]. The use of copper in weld metals has invariably been restricted to matching the composition of weathering steels, and not as a strengthening element due to its poor effect on promoting strength in solid solution when compared with other elements.

2.7.8 TITANIUM

Titanium is an efficient deoxidiser as well as having a strong affinity for carbon and nitrogen when added to steel. It is also a potent ferrite former with iron and steel, such that very small quantities (e.g. 0.001%) can promote significant metallurgical changes[246]. The ultimate distribution of the Ti depends on several factors, in-which the condition and handling of the molten steel prior to solidification and subsequent heating and cooling cycles play prominent roles.

Steel is normally deoxidised by silicon and then aluminium prior to any titanium addition, but the latter will still invariable bind to any oxygen left in the melt[94]. The resulting TiO/TiO_2 inclusions have been shown to have a positive effect on microstructural development, as mentioned in earlier sections, due to the promotion of acicular ferrite nucleation on titanium inclusions[180,181]. Titanium nitride and carbide have a mutual solubility, leading to carbonitrides of $Ti_x(C,N)_y$ composition (Nb, Ta, V and Zr form similar compounds). The carbides do not dissolve as readily as those of Mn above the Ac_3 temperature, such that hardenability is decreased if some carbon remains tied to the titanium. If sufficient prior deoxidation has occurred, the formation of TiN particles can occur. These are typically of a small diameter (~0.2μm) and form at high temperatures, resulting in stable particles which both promote strength increases and resist high temperature grain growth that can potentially occur in the HAZ and weld metal.

Weld metals with titanium additions of 30-300 ppm have been found to promote improved toughness whilst maintaining strength for a variety of welding processes[247]. The actual titanium level employed is very sensitive to other alloy levels, and in some cases (e.g. Nb) detrimental effects can occur with their combination[94]. Levels of 30ppm have been shown to significantly enhance acicular ferrite formation in C-Mn SMAW; levels above and below this produce inferior microstructure balances, until around 200ppm Ti are present[246]. If boron is present this effect is enhanced, with levels in excess of 200ppm showing a significant drop in toughness. Analysis of various weld metal properties by Abson[164] resulted in a proposal that acicular ferrite content (c.f. toughness) is maximised when the ratio of Ti to (O+S) is 1/15; typical basic SMAW weld metals contain ~300ppm O_2 and ~50ppm S thereby generating a calculated titanium content of 23 ppm. This level is close to the optimum titanium content of 30ppm discussed above. Yield strengths have been reported to increase as much as 150MPa with various titanium additions, highlighting the potent hardenability of the element[248]. Research conducted with ultra low carbon (<0.03%)

5.5%Ni/0.6%Mo/0.35%Cr GMAW wires with titanium additions from 30-450ppm, however showed very little change in mechanical properties (HI of 4.4 kJ/mm)[252].

2.7.9 ALUMINIUM

Aluminium performs several important functions when added to steel: it is a highly efficient deoxidiser and nitrogen fixator, as well as promoting grain refinement. Increasing aluminium content will consequently produce aluminium oxides as the predominant inclusion type[249], often at the expense of other oxygen gathers (e.g. Ti, Zr), hence it is common practice to balance aluminium with titanium for optimum microstructural development[250]. If the weld metal composition is maintained constant bar aluminium, increasing the aluminium from <5 to 600ppm has shown no change in inclusion diameter with a basic SMAW metal, even though the volume fraction increases. Over the same range of aluminium increase, the weld toughness exhibits an initial decrease in acicular ferrite to ~80ppm aluminium, followed by a small increase to ~400ppm aluminium from which point a significant decrease is noted[249]. This is in line with the volume fraction of acicular ferrite observed. The increasing amount of Widmanstätten ferrite occurring at higher aluminium concentrations can be explained in terms of the oxide inclusion transition from a mixed spinel oxide (Al_2O_3.MnO) to γ aluminium[251]. If the oxygen content is kept low (e.g. 150ppm) an aluminium level around 100ppm coupled with a low titanium content has been shown to promote galaxite (Al_2O_3.MnO), which in turn promotes acicular ferrite[201]. Results from high strength GMAW consumable development have verified the above findings in the observance of a decrease in impact toughness from 87J to 57J at -40°C when the aluminium was increased from 8ppm to 350ppm in the weld metal[252].

2.7.10 NIOBIUM

Niobium possesses a strong affinity for carbon, with considerably less affinity for nitrogen and oxygen. It has been added to steels in order to precipitate niobium carbide in the ferrite matrix, and in controlled amounts significantly improves the properties of steel when used in combination with TMCP. Its addition to weld metals however is detrimental; any addition shows a significant reduction in toughness, regardless of other alloying elements[253]. The low temperature reheated regions (i.e. <720°C) show a refinement in grain size, but tempering of these regions (i.e. during stress relief) precipitates harmful grain boundary carbides. The effect on toughness after stress relief exhibites a non-linear effect with increasing niobium and manganese, highlighting the complex effect of niobium. Levels are thus minimised during consumable manufacture, but due to its addition in many steels, dilution effects can result in niobium pick-up. This occurs predominantly in the root or joint sidewalls, especially when high heat inputs are employed.

2.7.11 VANADIUM

Vanadium, like niobium, is not a normal addition to weld metals, although it is a common microalloying element in high strength low alloy steels, hence it can appear in regions of high dilution. It also has a strong affinity for carbon, a reasonable tendency to combine with nitrogen, but a low affinity for oxygen[94]. Its influence in increasing

hardenability through substitutional solid solution and complex carbide formation is considerable. Vanadium nitrides have the added benefit of high temperature stability above Ac_3, thereby reducing austenite grain growth and promoting fine grained transformation products. Basic weld metals (with typical manganese contents of 1.2-1.6%) did not show significant microstructural changes (using an optical microscope) when vanadium levels were increased from 0-800ppm; acicular ferrite remained the major constituent[254]. Toughness levels did not suffer over this range, even with the strength increase. Stress relief however considerably deteriorates toughness levels with increasing vanadium due to carbide precipitation on the grain boundaries. Levels of up to 200ppm vanadium have been reported as retaining acceptable properties within the weld metal if stress relieving the structure is necessary. The rutile used in many flux systems often contains vanadium at levels which are harmful if weld stress relieving temperatures are employed. In this respect, careful design is required if the benefits of both mechanical properties and physical weldability are to be maintained.

The precipitation effects exhibited by the addition of niobium and vanadium can be countered by suppressing the austenite transformation temperature with manganese or molybdenum[255].

2.7.12 BORON

Boron is a very powerful promoter of hardenability in steel due to its ability to go into interstitial solid solution. The solubility limit is, however, extremely small, and levels above 100ppm are ineffective in increasing hardenability further. The combination of titanium and boron additions to weld metals has been extensively investigated due to the enhanced low temperature toughness properties attainable with this system. Mori et al.[196,256] have attributed the toughness increases due to a two fold mechanism. During terminal transient solidification of the weld metal boron is capable of reducing free nitrogen, whilst titanium protects the boron from oxygen. Any active boron remaining during the austenite to ferrite transformation segregates to the austenite grain boundaries where it retards the nucleation of grain boundary ferrite, allowing the TiO particles to promote the intragranular nucleation of acicular ferrite. SAW weld metal investigations found that boron levels of ~40 ppm, titanium ~280 ppm, oxygen ~200 ppm with low levels of nitrogen (< 50 ppm) and manganese ~ 1.5% gave extremely low impact toughness transition temperatures (typically -70°C), even at heat inputs of 4.5 kJ/mm[256]. It should be noted though that boron contents need to be carefully matched with the other microalloying and non-metallic elements. An excess of soluble boron will tend to combine with carbon to form brittle boron carbides, thereby reducing the material toughness. A major limitation of the system is the temper embrittlement that occurs during post weld (stress relief) heat treatment. This is due to the combined action of matrix hardening, impurity (phosphorus) segregation and intergranular borocarbide ($Fe_{23}(B,C)_6$) precipitation at 550-650°C, which facilitates brittle fracture development along the prior γ grain boundaries[257].

2.7.13 NITROGEN

Nitrogen, like carbon and boron, can fit interstitially within the steel lattice, and if high cooling rates are in evidence through the austenite to ferrite transformation, distortion of

the lattice into a bct structure can significantly enhance the steel's hardenability. The solid solubility of nitrogen behaves in a similar fashion to that of hydrogen i.e. it is higher in the fcc lattice than in bcc (see Figure 2-38). Dissolved (uncombined) nitrogen will attempt to precipitate out of solution at slow cooling rates, during room or elevated temperature or by cold straining of the metal. Carbon, silicon and oxygen all decrease nitrogen solubility in ferrite, whereas elements such as chromium, manganese, titanium, vanadium and zirconium all increase it[94].

Nitrogen is damaging in weld metals due to two important effects: it causes porosity when present above ~300ppm due to over-saturation effects[258]; and when present in the form of iron nitrides, it has a severely embrittling tendency. The latter is enhanced if any plastic deformation occurs, such as in the root pass of a V-butt weldment, leading to strain ageing. If nitride formers such as Si, V, Ti, Al and Zr are present, both 'quench ageing' and strain ageing are eliminated due to the precipitation of stable nitrides during cooling[259]. Increasing nitrogen (from 80 to 240 ppm) within the weld metal will increase yield, tensile and hardness levels, but cause a general deterioration in Cv and CTOD levels. The amount of grain boundary ferrite increases significantly at the same time, coupled with a general coarsening of the microstructure[260]. Nitrogen values reported in the literature are sometimes misleading as they do not often differentiate between combined nitrogen held as an intermetallic phase or compound (often relatively harmless), dissolved or free nitrogen, or total nitrogen. It is considered general best practice to minimise weld metal nitrogen contents either by consumable design, efficient atmospheric shielding or welding techniques (e.g. short arc length with SMAW electrodes).

2.7.14 OXYGEN

It has been understood for many years[193,259,261] that oxygen is an important factor in controlling the ductility and toughness of weld metal deposits at temperatures below that of room temperature (~20°C). Oxygen, like nitrogen, can enter the weld metal by various methods: atmospheric entrapment; the core wire of the electrode; the slag via the slag/metal reactions; the parent plate via dilution effects; as well as possible slag entrapment within the weld metal. It generally occurs in the form of various simple and complex oxides and oxysulphides[114], and, as stated earlier, optimised oxygen contents between 150ppm – 500ppm are required to generate high toughness microstructures with maximum cleavage resistance.

The oxygen content of the weld metal can be related to the volume fraction (Vf) of inclusions due to the majority of the oxygen being tied up in the form of oxides. This has been verified on work carried out using GMAW welding and ULCB weld metal, where it was found that increasing the oxygen content increased the average size and volume fraction of inclusions[208]. Consequently various authors[193,194,199] have shown that by converting the analytical oxygen and sulphur concentrations it is possible to estimate the volume fraction of inclusions in the weld metal. The following equation derived by Widgery is an example:

$$Vf\ (\%) = 5.5(\text{wt\% oxygen} + \text{wt\% sulphur})$$

The oxygen content in the weld metal greatly affects the microstructure, and research[262,263,264] has shown that there are three levels which differentiate the microstructure/toughness relationship:

- Low oxygen content (<~200ppm) will produce a microstructure consisting of grain boundary ferrite and ferrite with aligned second phases, which is detrimental to toughness. This is due to the low inclusion content which provides insufficient nucleation sites for acicular ferrite formation. When there are very few oxide inclusions the shape of sulphide and phosphide precipitates change from globular to film-like, decreasing the weld plasticity[263].

- Medium oxygen contents (~200ppm - ~500ppm) are often regarded as the optimum levels that produce sufficient inclusions to act as nucleation sites for acicular ferrite formation in a variety of welding processes. Previous work has revealed that 200ppm-300ppm of oxygen were the optimum levels required to produce SAW, GMAW and SMAW metals with good toughness[263,265,266].

- High oxygen contents (>~500ppm) result in a high inclusion content and greatly increase the formation of undesirable microstructures such as grain boundary ferrite and ferrite side plates, due to a reduction in the prior austenite grain size. Toughness is consequently reduced, with inclusions acting as sites for microvoidal coalescence[201] or as crack initiation sites due to the strain of dislocation pile-ups caused by them[267].

2.7.15 SULPHUR AND PHOSPHORUS

Sulphur and phosphorus are normally regarded as impurity elements in steel weld metals. Sulphur can form low melting point eutectics (FeS ~ Mp 1200°C) thereby enhancing the possibility of hot cracking within the steel. The iron sulphides formed are virtually insoluble in solidified steel and have a tendency to segregate, but it was found that manganese has a stronger affinity for sulphur than iron, with the bonus that manganese sulphide inclusions have a much higher melting temperature[94]. It should be noted that these can be detrimental in steel processing due to sulphide stringer formation. It has been best practice to reduce sulphur levels to the minimum possible in both parent and weld metals for some time, however the attainable levels were restricted by the economics of producing the clean steels. It is only in the last 10-15 years that very low levels (e.g. <0.002%) have been possible on a commercial basis, and combined with improvements in raw material impurity controls weld metals typically contain <0.010% sulpur. Evans[268] demonstrated the significant loss in toughness (combined with a slight reduction in strength) evident with every increase in sulphur from 0.007% – 0.046%. The as deposited microstructures changed from ~70% acicular ferrite to <50% acicular ferrite, the difference being taken up by increased ferrite with aligned martensite-austenite-carbides (MAC).

Phosphorus is one of the most potent alloying elements available to strengthen the ferrite matrix in steels by substitutional solid solution hardening (see Figure 2-55), but the amount that can be tolerated is severely restricted due to reasons of segregation and embrittlement (< 0.1% can be held in solid solution at room temperature). Like sulphur, phosporus segregates to grain boundaries and can also act to lower melting points in the interdendritic regions or by reducing intergranular cohesion causing hot cracking[147]. Impact toughness, strength levels and microstructural classification exhibited minor

changes when increasing phosphorus from levels of 0.007 to 0.040% in the as welded state, but a significant drop in strength and a slight increase in toughness (up to 0.03% phosphorous) were observed after a stress relief treatment[268]. Temper embrittlement by phosphorous segregation during post weld heat treatment (PWHT) can cause intergranular fracture, possibly attributed to one or more microalloying elements acting to remove soluble carbon and allowing the segregation of phosphorus to the prior austenite grain boundaries[270].

2.7.16 HYDROGEN

The minimisation of hydrogen levels within weld metals and HAZ's has long been realised as a requirement to reduce the chances of cracking. Embrittlement can occur either via the elevated temperature effect (hydrogen attack - where dissolved hydrogen reacts with carbides to form methane which precipitates at the grain boundaries) or through the more common low temperature embrittlement of the steel lattice (HICC)[147]. The latter occurs within a temperature range of -100°C to 200°C; the mobility of dissolved hydrogen to accumulate within the steel and cause embrittlement outside of this range is either too low or too high. The actual process of a crack developing requires the cumulative effect of stress (either applied or residual), a susceptible microstructure (i.e. the ability for crack propogation within the material), the correct temperature range and the presence of sufficient hydrogen. The actual mechanism of hydrogen embrittlement is the subject of numerous theories, but a popular explanation involves the decohesion of atoms in the metal lattice in proportion with increasing hydrogen levels, coupled with increased hydrogen solubility in the strained region of a crack tip[271]. Normally a period of incubation is necessary for the hydrogen atoms to manifest within the steel and cause cracking, hence the terminology of delayed cracking.

The presence of hydrogen within the weld metal is derived from the dissociation of hydrogenous compounds within the arc column. These compounds can be found in the fluxing ingredients of SAW, SMAW and FCAW, by contamination of the parent material or gas lines, from lubricants used during GMAW or FCAW wire manufacture and from water vapour drawn into the arc from the air. The most common source is from the fluxes; the higher the baking temperature used in their manufacture, the lower the potential weld metal diffusible hydrogen content. Hence basic coated SMAW electrodes are normally heated to 450-500°C, and basic SAW agglomerated fluxes to 800°C. Some consumable classification standards specify the maximum permissible moisture content in the flux (e.g. 0.2 wt%), whereas others designate a code following compliance with a standardised test to determine the hydrogen content of the weld metal. The latter is normally expressed in terms of number of mls diffusible H_2 per 100g deposited weld metal, determined from immersion in mercury (typically 30 days), or more latterly by hot extraction methods (typically 20 minutes). The lowest range specified in consumable classification standards is typically less than 4 or 5 mls, and this is normally specified for high strength steel welding.

Preheating is an efficient method to reduce the chances of hydrogen cracking by slowing the cooling rate and allowing more hydrogen to diffuse out of the weld and HAZ. Hydrogen has a high solubility but low diffusion rate in γ compared with α/martensite, and for these reasons the γ decomposition behaviour is important in terms

of hydrogen transport and distribution. Traditionally the HAZ of the base material would undergo transformation from γ after that of the weld metal due to the lower Ms temperature of the HAZ (higher CE). In this case hydrogen is effectively 'sucked out' of the weld metal and then locked in the HAZ due to the poor mobility in the fcc structure, leading to potential underbead cracking. The situation however reverses when the weld metal is overmatched (in alloying terms) with respect to the base metal, such that the weld metal Ms temperature is lower than that of the HAZ, leading to longer times of transformation. The hydrogen is then trapped within the weld metal leading to potential cracking within it[272,273]. Equations have been developed which predict Ms temperatures for both the weld metal and HAZ over a wide range of alloy compositions in an attempt to predict the likely area of cracking[274]. Recent work with tubular wires has centred on improving weld metal HICC resistance by modification of the microstructure, notably by optimising the volume percentage of certain morphologies (e.g. PF(G) and MAC) and non metallic inclusions to cope with a range of hydrogen levels up to 4.5mls[275]. The careful selection of raw materials for the manufacture of fluxes (e.g. low moisture absorption binding agents for SMAW coatings) as well as improved production techniques (e.g. roller die or seamless for tubular wire) have reduced the potential hydrogen dissolution in the weld metal and extended the safe working time outside of heated ovens/hoppers/vacuum packaging.

2.8 WELDING CONSUMABLE DEVELOPMENT FOR HIGH STRENGTH PIPELINES

As the strength of pipelines increase, the development of weld metals need to keep pace at a comparable rate. Whilst the base material can undergo complex thermo-mechanical and controlled cooling treatments to attain high strength and toughness with the minimum of alloying, weld metals do not have the same post solidification processing capability. In comparison to thick sectioned (i.e.> 25mm) high strength (i.e. $R_{p0.2}$ 450-650 MPa) structural steels, weld metal bulk alloying levels are normally lower. This is due to the high cooling rates experienced (normally less than 10s for $t_{8/5}$), in combination with carefully designed microstructural development generating the required strength without compromising hardness or toughness levels. Modern generation high strength pipeline steels are however comparatively lean, offering enhanced weldability when compared with conventional Q and T steels such as HSLA-100 or HY-100. The weak link in the weldment can consequently shift to the weld metal rather than the HAZ.This is due to the total alloying levels of the filler metals, and their diffusible hydrogen levels, compared with that of the base material, particularly when a guaranteed overmatch is required using conventional 60° joint preparations. As a direct consequence there has been considerable investigative work to try to reduce the alloying and hydrogen levels required in the weld metal, whilst at the same time trying to ensure the widest possible envelope (in terms of cooling rate) that will generate the required mechanical properties. The following sections summarise the current practice/development work recently undertaken for weld metal yield strength levels of 550MPa and 690MPa.

2.8.1 *550MPa (X80) WELD METAL YIELD STRENGTH DEVELOPMENT*

In order to develop possible procedures for the joining of X100 steels, an examination of typical practices and weld metal compositions with X80 pipelines was considered of paramount importance as a base-line study. Pipeline SMYS levels of 550MPa have been common practice in Canada for most of the last decade, and their use is gaining momentum in many other countries[28,150,151,276]. A conventional manually welded pipe preparation typically involves a 30° bevel (or a 30° + 10° compound bevel for thick walled pipe) coupled with the use of numerous welding consumable types. The type of consumables chosen depends on the contractors' preference and/or the mechanical property requirements. Vertical-down cellulosic electrodes of AWS 5.5 E9010 classification[277], vertical-up lime basic electrodes of AWS 5.5 E10018 or vertical-down low hydrogen electrodes (AWS 5.5 E9018)[28] are the preferred SMAW consumables. Rutile (AWS 5.29 E101T1)[279] vertical-up FCAW or self shielding (AWS 5.29 E91T8) vertical-down FCAW electrodes[280] have also been used to good effect. The actual degree of overmatch is dependent on the weld procedure and weld metal alloy content employed; the latter can vary considerably, but for the previously mentioned consumables, typical major alloy contents are in the ranges of 0.05-0.08%C, 1.0-1.8%Mn, 0.3-0.6%Si and 1.0-2.5%Ni (1.0% Al in self shielding wires). A recently conducted investigation[278] used a wide variety of alloying variants (Mn, Cr, V, Mo) in order to determine the optimum composition suitable for X80 welding using vertical-down cellulosic SMAW electrodes. The research concluded that molybdenum gave the best compromise for its weight percentage addition between increased strength, high toughness and low propensity for hydrogen cracking. The optimum composition appeared to be 0.2C-0.85Mn-0.2Si-0.75Ni-0.4Mo, but it should be noted that preheat/interpass levels of 160-175°C were used throughout, with heat inputs of a nominal 1.6 kJ/mm; much higher in both cases than would normally be used in mainline mechanized pipewelding.

The root and hot pass is normally accomplished with a much lower strength consumable, typically a cellulosic SMAW of AWS 5.5 E6010, E7010 or E8010 classification (C-Mn-Si or C-Mn-Si-Ni/Mo variants). This allows a greater degree of ductility and crack resistance during pipe moving operations (e.g. lowering in), as well as the greater likelihood of generating low root hardness levels (e.g. for sour service)[28,279]. If pipe fit-up or welder skill is not of a high degree, vertical-up SMAW electrodes of AWS 5.5 E10018 may be employed for X80[28].

The 60° joint type mentioned above is suitable for main-line and tie-in welds, but for high productivity the mechanised welding system is increasingly being employed for both main-line (narrow gap) and tie-in (conventional preparation) joints. To date, only the single wire GMAW, PGMAW or MCAW processes have been employed on narrow gap X80. As highlighted in an earlier section, the process is used almost exclusively in the vertical-down mode ensuring high travel speeds and low heat input. The narrow bevel geometry induces high cooling rates for all passes (particularly the root and hot pass), with the result that lean alloying can be employed to generate the 550MPa minimum yield strength. The most commonly referenced wire in X80 applications is either Thyssen K-Nova (C-Mn-Si-Ti), ESAB XTi (C-Mn-Si-Ti) both of which are classified as AWS 5.18 ER70S-6, or Thyssen NiMo80 classified as AWS 5.28 ER90S-G (C-Mn-Si-1.1Ni-0.4Mo, currently known as Thyssen Union MoNi)[28,150,151,281]. The

fill and cap passes normally use a 0.9 or 1.0mm diameter wire with Ar/CO_2 or pure CO_2 shielding gas for dip transfer, or more commonly for pulsed welding an $Ar/He/CO_2$ or Ar/CO_2 mixture. The latter is often used for the cap pass to avoid undercut with welding bugs without sidewall dwell capability[145]. The root pass normally involves either an internal (typically 0.9mm diameter wire) or external (0.9 or 1.0mm diameter wire) weld of C-Mn-Si-Ti (ER70S-6) composition with Ar/CO_2 shielding. Dip welding is virtually always used on the root pass due to the susceptibility of the pulsed GMAW process to any residual pipe magnetism[145]. Arc energy values of 0.4-1.0 kJ/mm are typical, with preheat levels of 50-150°C with a minimum interpass usually around 80°C[151]; the actual levels need to be determined via the pre-production qualification procedures, using the highest carbon equivalent values for the pipes to be welded. Yield strength distributions of the weld metals using the above consumables results in a typical spread from 610-670MPa[276] and CTOD levels at -5°C often >0.30mm[145].

Metal cored wires are also beginning to be used on X80 pipelines instead of solid wires due to several useful attributes of the consumable type. Productivity improvements of up to 20% appear to be possible due to the increased deposition rates. Enhanced arc characteristics and wetting capabilities over solid wires are also possible due to special additions in the powdered core. The improved arc characteristics come with a price; oxygen levels in the weld metal are higher than solid wires, and as a direct consequence the toughness is inferior. To counter this effect small nickel additions (e.g. 0.8%) are usually required to improve toughness to acceptable levels[279]. The economics of consumable cost and benefit also need to be assessed carefully.

Major advantages of using mechanised welding, other than high productivity, are the reduced heat affected zone width (and hence softening) in the base material; high quality and repeatability of weldment properties; and very low diffusible weld metal hydrogen levels from solid GMAW wires. It is from this standpoint that investigations into the welding of 690MPa minimum yield pipeline steels have taken root.

2.8.2 690MPA (X100) WELD METAL YIELD STRENGTH DEVELOPMENT

The welding of high strength low alloy steels involving weld metal yield (proof) levels greater than 690MPa has been practiced for many years, with applications involving the legs of offshore jack-up rigs, crane bodies and submarine hulls to name a few. The steels have predominantly been of the quench and tempered variety, with standard welding processes and joint preparations being used. The main problem has usually been associated with the heat affected zone hardenability, but improvements in consumable hydrogen control and parent material design have enabled sound weldments to be achieved providing the welding procedure control is adequate. Advances in parent material design and processing have led to steels such as HSLA-80 and HSLA-100, with a potential shift of the problem back to the weld metal in terms of propensity to crack. The use of traditional consumables designed for high strength steels also exhibit the potential for a wide range of mechanical properties to be obtained with small changes in cooling rate. This problem has been recognised for some time and numerous investigations have been conducted in conjunction with novel consumable development[179,207,208,216,217,248,252,282-287]. A major effort has been expended in attaining the lowest possible preheat temperatures, with research tending to be biased towards

solid GMAW wires due to the high joint production rates and inherently low weld metal hydrogen levels associated with the process.

Pickering conducted work in the 1960s[59] which demonstrated the beneficial effects of lowering carbon contents to expand the transformation range in which high strength bainitic microstructures can form. The consequent introduction of low carbon based weld metal alloy systems is reputed to enhance the tolerance box of acceptable cooling rates to generate a consistent microstructure type. These wire types have been termed ultra low carbon bainitic (ULCB). Figure 2-56 shows the proposed CCT diagram to enable consistent mechanical property generation compared with a more conventional (variable transformation product) weld metal design[252]. The latter has been shown by Lord[217] to exhibit considerable property variation with different cooling rates. The major alloying additions investigated have been carbon, manganese, nickel, molybdenum and chromium, with microalloying changes using aluminium, titanium, boron and zirconium. Conventional alloying involves stabilisation of the austenite to generate the desired transformation products (achieved with additions of Mn, Ni, Mo and Cr), whilst carbon levels are minimised to avoid high hardness levels.

Considerable controversy exists over the exact microstructural morphology that is best suited to generate high strength (i.e. $R_{p0.2}$ > 800MPa) weld metals. This controversy is illustrated in patents taken out by two leading consumable manufacturers[288,289]; to achieve the same improved toughness and HICC resistance one used a predominantly bainitic microstructure and the other martensistic. Regression analysis[290] of the data sets supplied in the patents however do not support these claims, as all results lie close to the regression line as shown in Figure 2-57. Assuming the classification of the microstructure types described in the patents is valid, the similarity of the results may be due to the ultra low carbon levels employed in both cases leading to little difference in the low carbon martensite or bainite. Further analysis of the data[291] for the major alloying elements present allows their relative effects to be assessed; vector diagrams provide for an easy interpretation of strength and toughness as shown in Figure 2-58. Manganese, nickel, molybdenum and chromuim were all shown (for 1% additions) to decrease toughness at the expense of strength, whereas carbon (0.01% additions) maintained the same toughness with increasing strength.

An interesting effect has been noted with respect to strength levels in combination with the specific joint geometry. Using the same alloy content obtained from conventional (60°) and narrow gap joints a convergence of proof strength values is clearly observed when a series of increasing strength levels are plotted against various consumable compositions (see Figure 2-59). This clearly demonstrates a reduction in the strength enhancement effect of increased alloying levels with the likely cooling rate increase in changing from a wide to narrow bevel. As a consequence, lower strength pipelines (i.e. X70/X80) benefit from a considerable degree of weld metal strength overmatch for a low alloying level (e.g. C-Mn-Ti). In contrast the differential in overmatch becomes less at higher pipe strengths using the associated higher weld metal alloying requirements.

Recent trials in Japan using solid wire GMAW with 80%Ar/20%CO_2 shielding gas and no preheat for X100 grade steels have shown the potential for a 0.06%C, 0.5%Si, 1.4%Mn, 2.7%Ni, 0.2%Cr and 0.5%Mo composition. Although the bevel design was not reported, heat inputs of less than 1.5 kJ/mm gave $R_{p0.2}$ values in excess of 750 MPa with ~75J Cv at -40°C[292]. It was also stated that development work was required for

suitable field welding procedures. Similar work conducted by Saipem/SNAM using their Presto dual torch GMAW narrow gap system in 16mm WT, 36 in. OD X100 pipe employed a 0.11%C, 1.1%Mn, 0.5%Si, 0.5%Ni, 0.2%Mo, 0.5%Cr solid wire (ESAB OK Autrod 13.13), resulting in a yield strength of ~720MPa, weld and HAZ hardness levels below 300 HV10, weld metal impact toughness of ~85J at -30°C and CTOD of ~0.20mm (all classified as δM) at -10°C. Details of the welding procedure/ preheat/interpass levels were not reported[293].

Lassaline and co-workers used a synchronized tandem wire welding process in a straight-sided narrow groove preparation (10mm root opening) using HY-100 and HSLA-100 plate[100]. Two 1.2mm Linde AWS 5.28 ER120S-1[144] wires were used at a combined heat input of 2.1-2.6 kJ/mm and preheat/interpass levels of 93/150°C (90% Ar/10% CO_2 shielding gas). The actual wire or weld metal composition was not stated, but the classification requires nickel and molybdenum, and possibly chromium, titanium, aluminium and zirconium, alongside the conventional alloying (C, Mn, Si). Weld metal impact toughness levels of approximately 40J at -46°C, and weld metal Vickers hardness levels of 250-280 reflect the high heat input levels used. These heat inputs and wire diameters are unlikely to be used in fixed position pipewelding applications, but indicate the minimum property levels achievable.

An important advantage of solid GMAW wires is their ability to produce very low (<200ppm) weld metal oxygen contents when used with small active shielding gas components, thereby reducing the amount of second phase particles within the microstructure. This is important in generating high toughness deposits due to the strong embrittling effects of oxide inclusions in high strength microstructures. Basic metal cored wires have been developed[290] which can mimic solid wire oxygen levels, but their practical use in pipewelding applications has not been reported. Arc energy values typically employed with conventional GMAW butt welds range from 1 to 4 kJ/mm, and consequently give slower cooling rates than can be expected from narrow gap fixed position pipeline welding if typical preheat levels of 100°C are employed. As a direct result of this, the actual alloying levels suitable for high strength (i.e. $R_{p0.2}$>700MPa) weld metals in narrow gap pipewelds are likely to be considerably different to conventional (wide) bevel situations.

The microstructures of high strength weld metals are typically extremely fine, and due to the low carbon levels often employed, characterisation of them by optical methods can prove extremely hard or impossible. Work conducted using an ULCB weld metal of unreported composition (other than C = 0.04%, with likely additions of Mn, Si, Ni, Mo, and Ti) but satisfying MIL-120S specification criteria involved a reclassification of the traditionally established steel microstructural description[294]. At $t_{8/5}$ times of 2.2s, the microstructure appeared to be martensitic, but at decreasing cooling rates (up to $t_{8/5}$ times of 28s) the microstructure contained increasing amounts of a morphology described as 'lath ferrite'. In medium or high carbon steels the nonlamellar eutectoid decomposition product is often referred to as upper or lower bainite, where sufficient carbon exists for carbides to be formed. Ultra low carbon weld metal often contains insufficient carbon to form carbides (other than in coarse autotempered martensite) resulting in the lath ferrite description for these structures. At intermediate cooling rates, for example $t_{8/5}$ of 5-20s which are typical of many GMAW situations, a mixture of martensite and ferrite results, which cannot be readily resolved in the optical microscope. At these cooling rates, even apparently conclusive optical microscopy

results can be misleading when trying to distinguish between lath martensite and lath ferrite. For these reasons it is normal to use transmission electron microscopy (TEM) to benefit from its high resolution capability.

At fast cooling rates (e.g. $t_{8/5}$ times of <2.2s) a combination of fine lath martensite and coarse autotempered martensite with a plate morphology were the majority phases observed using TEM in the ultra low carbon weld metal described above (the lath martensite is more prevalent at the slower cooling rate). The progressive appearance of long laths of ferrite at slower cooling rates and its distinction from fine lath martensite were confirmed by TEM using several distinctive features of the latter morphology. Lath martensite has different lath orientation variants within a packet, which often lead to significant crystallographic misorientations between adjacent laths (i.e. high angle boundaries). The interlath boundaries are often straight, with long thin sheets of retained austenite often appearing between them (showing up as dark lines in bright field TEM). It is also generally finer in nature than the lath ferrite. In contrast to lath martensite, the distinctive features of lath ferrite are their often parallel appearance, with low-angle interlath boundaries and similar crystallographic orientation. Retained austenite between the laths usually also has a blocky or truncated appearance. At even slower cooling rates ($t_{8/5}$ times > 14s) increasingly larger amounts of long isolated ferrite laths appear, coupled with the accumulation of parallel ferrite lath packets and decreasing amounts of martensite and retained austenite. Acicular ferrite, recognised by its classical basket weave appearance, can also appear. Under an optical microscope the structure appears to range from mostly ferritic to fully ferritic, with the martensite and ferrite packets between the long ferrite laths often unresolvable, leading to an underestimate of any high hardness phases. Microhardness measurements, dilatometry and electron energy loss spectroscopy (e.g. for local carbon content determination) can be used in combination with TEM/optical microscopy to help accurate determination of the final transformation structure balance that exists in the resultant weld metal.

Martensite transformation start temperatures are typically in the region of 400°C, with the various low temperature lath ferrite morphologies transforming at 460 - 480°C for the above mentioned alloy[294].

The use of low hydrogen welding processes is considered of paramount importance for the welding of high strength steels with the minimum possible preheat requirement. In this respect the use of rutile flux cored wires for main-line, tie-in and repair welds has traditionally been limited to lower strength levels. The advent of high strength low hydrogen (<5mls H_2/ 100 g wm) consumables have however provided an opportunity for their use in these applications. Basic low hydrogen vertical-down SMAW electrodes have been used on X80 pipelines for some time, and variants have been developed for potential use on X100 pipelines. The latter consumable types have potential hinderences in strength and impact levels, coupled with poor arc characteristics/physical weldability. The lower productivity basic low hydrogen vertical-up SMAW electrodes are well established at strength levels suitable for X100 but, as mentioned earlier, the potential for property variation with current electrode designs is considerable[217]. Their versatility in providing a tie-in root/hot pass, or for repair weldments, is not in question though.

As a final note on weld metal properties, the advent of an 'X120' grade pipe[23] developed by ExxonMobil, in conjunction with several Japanese pipe manufacturers,

has also instigated a development programme for the main-line girth weld chemistry using solid wire PGMAW in a narrow gap[295]. The typical weld metal compositions investigated involved changes in C (0.05-0.08%), Mn (1.5-1.9%), Si (0.25-0.6%), Ni (2.4-3.1%), Mo (0.55%), Cr (0-0.6%), Cu (0.15-0.5%), Zr (0-0.03%), V (0.004-0.036%), B (4-13ppm) and oxygen via the shielding gas (220-370ppm). Proof strength ($R_{p0.2}$) measurements in standard narrow gap pipewelds using 6.4mm round bar tensiles, with most tests employing 100-125°C preheat/interpass values, showed levels always in excess of 800MPa. Corresponding UTS values and $R_{p0.2}/R_m$ ratios were typically 950-1000MPa and 0.85-0.95 respectively. Charpy upper shelf energies were between 60 and 170J, with DBTT between -45 and -105°C. It was concluded that carbon, which was relatively constant throughout the series, played the most significant role in tensile strength via the amount of martensite or similar lath products. The proof strength was influenced by macro/microalloying and oxygen content, which gave considerable scatter when plotted against weld P_{cm}. Zirconium additions of ~0.02% in the wire (giving ~0.01% in the weld metal) were considered beneficial in improving toughness levels via an improved AF nucleation mechanism for many small and finely dispersed nuclei, in conjunction with low (200-260ppm) weld metal oxygen contents. The microstructures (classified using TEM) were described as comprising mainly acicular ferrite, lath martensite and degenerate upper bainite. The latter two were closely related such that the whole structure was termed acicular ferrite interspersed with martensite (AFIM). Typical levels of AF content observed in the pipewelds were between 5-15%, and whilst higher levels would improve toughness, well dispersed microstructural phases will promote toughness and still maintain high strength. Extracting data from the research paper[295] highlighted a weld metal chemistry composition of 0.065%C, 0.5%Si, 1.8%Mn, 2.7%Ni, 0.55%Mo, 0.2%Cr, 0.15%Cu, 0.008%Ti, 0.010%Zr, 0.010%V, 250ppm O_2 and trace levels of B and N_2 should generate a proof strength around 850-900 MPa and tensile strength of 950-1000 MPa. Cv impact toughness levels of 75J minimum at -50°C and CTOD of 0.13mm at -50°C should also result, with the weld procedure involving a standard (CRC-Evans) narrow gap bevel, Ar/CO_2/He shielding gas, PGMAW and preheat/interpass of 100/125°C. Depending on the weld metal versus parent metal proof strength philosophy employed, the above wire design may be a useful composition for X100.

2.9 X100 TARGET GIRTH WELD PROPERTIES

At the start of the current research programme, it was quickly identified that no standards existed for transmission pipelines in excess of 80 ksi (552 MPa) yield strength steels, let alone the girth, repair or tie-in weld metal/HAZ properties. During the course of this study the Canadian Standards Association (CSA) released CSA Z245.1-02[21] which includes a 690MPa minimum yield strength steel (designated Grade 690), whilst the European (BS ISO 3183-3[296]) and American (API 5L[20]) standards have yet to incorporate pipe at these strength levels. The joining of X100 steels requires careful consideration of the likely spread of mechanical properties to be obtained from production pipes. The design philosophy regarding weld metal strength in comparison to pipe strength is a subject of extensive research, especially considering that overmatching weld metal is harder to achieve consistently in X90+ steels[297]. The following sections examine the current standards and specifications with regard to linepipe, welding procedure and field construction, with a view to the proposal of

certain mechanical criteria for girth weld attainment. Brief reviews involving the relevant part of a linepipe specification are incorporated in the applicable subsection to act as a baseline comparison.

2.9.1 X100 LINEPIPE PROPERTIES

The yield strength is usually the main design criterion for pipelines. Its measurement has been a constant source of discussion between suppliers and purchasers, since the properties of the manufactured linepipe can differ greatly from those of the original plate, with the method of testing also influencing the results obtained. Differences between longitudinal and transverse tensile properties within the finished pipe are also likely to be evident as a result of cold expansion strains being prevalent in the transverse direction coupled with the higher alloy systems required of X100. Bainitic materials exhibit a higher strain hardening rate than ferrite-bainite materials, so planar anisotropy due to controlled rolling, pipe forming and expansion is expected to be greater. The DNV standard for submarine pipeline systems[298] specifies a maximum variation of 120 MPa between transverse and longitudinal SMYS, although this standard only covers steels up to a SMYS of 555MPa.

Traditionally the pipe yield strength is determined by the API 5L[20] method; this involves cutting a full thickness transverse and longitudinal specimen from the pipe and cold flattening, in the case of the transverse specimen, prior to testing. The flattening leads to a lower yield strength value than the linepipe is capable for the X80+ steels due to the Bauschinger effect[299,300]. The margin by which the flattening test underestimates the true yield strength of the pipe is dependent on the strength, diameter and cold expansion of the pipe. It has been observed that a difference in yield strength between specimens close to the surface and those close to the centre of the material can also take place. This particular variation was very pronounced for flattened specimens. Differences of up to 140MPa were measured between the flattened and non-flattened specimens, using samples which were taken from the outer surface of the pipe[72,301]. The true yield strength of the linepipe can be measured using the ring expansion test devised by British Gas, however it is expensive and time consuming, but is included in the API 5L and CSA Z245.1 specifications as an option.

Investigations into accurate yield strength measurement of high strength linepipe have concluded that the tensile properties should be determined by round bar specimens[7,304]. The transverse specimen, which should not be flattened prior to machining, will sample various areas through the pipe wall thickness and consequently may contain varying degrees of strain distribution, depending on the pipe diameter/wall thickness coupled with the sample cross sectional area (A_0) and length. Sample location around the pipe should also be stated (e.g. relative to the longitudinal seam weld being at 12 o'clock) to observe any trends in forming stress/strain variance around the circumference.

The Canadian linepipe specification[21] requires the transverse yield strength ($R_{t0.5}$) to be between 690 and 825MPa, determined using a flattened strip or round bar specimen. Round bar tensile testing is also an option within API 5L, and in both cases close control of the reporting needs to be undertaken with respect to the actual sample location within the pipe wall thickness.

CSA Z245.1 also states an ultimate tensile strength (R_m) range from 760MPa to 970MPa for the transverse (hoop) direction only. One of the reasons for specifying this parameter is the defining of a 'saftey margin' between yield and ultimate tensile stress (load controlled design), leading to the avoidance of unnecessary failure during field hydrotesting[305].

Conventional pipeline design (stress based) dictates that the safe operating maximum pressure is normally taken as a fraction of the specified minimum pipe yield strength. This is typically 0.72 and sometimes 0.8[304], with the intention that the operational stresses are confined to the elastic region of the stress-strain curve. Consequently there exists a margin of safety which comprises the elastic portion above the design stress and the stable region of plastic deformation between the material yielding and the onset of necking (ultimate tensile strength). However, as modern lean alloyed TMCP high strength steels exhibit a higher yield/tensile ratio (Y/T) than conventional steels, the yield strength is closer to the ultimate tensile strength which reduces the stable plastic region. The yield/tensile ratio is an important consideration when defects or discontinuities exist. This has been examined from a limit-state design approach with the conclusion that the strain hardening modulus was mainly dependent upon the differential between the tensile strength and yield strength (R_m-$R_{t0.5}$), rather than the yield ratio ($R_{t0.5}/R_m$). Hence for the same safety factor, the allowable yield ratio depends on the steel grade[315].

A maximum allowable yield ($R_{t0.5}$) to tensile ratio has been stated in the Canadian specification as 0.93, with minimum elongation levels dependant on the cross sectional area under test. For pipes with WT > 12.7mm and OD > 219.1mm, full thickness strip tensiles require elongation values > 17% over a 50mm gauge length. Both Y/T and elongation measurements are only required in the transverse direction using the Canadian specification. If lower strength steel specifications are extrapolated, similar levels are observed. Using the EEMUA 166[307] requirement of a 70 MPa differential between SMYS and SMTS results in an acceptable Y/T ratio of approximately 0.91 for X100 linepipe. DNV rules stipulate a maximum Y/T ratio of 0.92 (up to 555 MPa SMYS pipe), whilst API 5L states a maximum Y/T ratio of 0.93 (up to X80 pipe). Previous research indicates that a Y/T ratio of between 0.74-0.93 represents a minimum and maximum value expected for X100 grade linepipe[7]. These values must be treated with caution, as the orientation of the tensile specimen and whether flattening took place prior to testing have a significant role on influencing the Y/T ratio. It has been stated that a high yield ratio for X100 linepipe is quite natural and cannot be surpressed[7].

Toughness testing normally involves Charpy V impact testing and drop weight tear testing at the specified design temperature. The Canadian specification[21] requires only the transverse plate toughness for both tests, with minimum average Cv (3 samples) of 40J (Category III notch toughness requirements) and minimum drop weight shear area of 50% for any test (category II only) for pipes with OD > 457mm in both cases. The average of each drop weight tear test (2 samples) should exhibit greater than 60% shear area, and if more than 4 heats are used to fulfil the order, the all-heat average should not be less than 85% shear area. Some standards increase the absorbed energy requirements with respect to the steel SMYS, and/or reduce the testing temperature with respect to the design temperature[298]. The EEMUA 166[307] linepipe specification extrapolates to 70J average and 58J minimum (10 x 10mm) taken from both the seam weld and base material (at 10°C below the design temperature). However, work by various researchers

states that the seam weld criteria must exceed 50J or 54J respectively at -20°C[10,306]. API 5L states that X80 grade pipe (base material only) requires a minimum all-heat average for a given purchase order of 68J at 0°C for transverse full thickness specimens. Extrapolating the difference in energy values from X70 to X80 for X100 linepipe would result in a minimum average of 150J at 0°C. The Cv fracture surface requires a minimum shear area for X80 of 40% for each heat, and 70% for the all-heat average. Company pipe procument specifications often require considerably higher impact or drop weight tear shear areas than are specified in generic standards, particularly when toughness issues play an important part in the pipeline design (e.g. for fracture arrest). The first X100 pipeline installed in Canada during the course of this research by Transcanada Pipelines (2002) required pipe body transverse Cv impacts of a minimum 140J at -5°C from the average of 3 samples for each heat, and 210J for the average from all heats procured. Weld and HAZ toughness (longitudinal seam) was specified at 75J minimum average at -5°C. Drop weight shear areas at -5°C for a single heat and all heat average were specified at 85% minimum and 90% minimum respectively[304].

Minimum impact toughness levels can also be predicted by the use of deterministic models such as the Batelle two-curve model. Using a correction factor of 1.7 for a 48 in. OD X100 pipe operating at 15MPa and a usage factor of 0.72 with rich gas, a minimum absorbed Cv energy of 500J would be required to arrest a propagating ductile fracture[302]. This level is clearly unrealistic for pipe mills to produce, particularly at the temperatures envisaged for Arctic use. A more realistic approach is to develop criteria that recognises the inherent scatter of toughness values within both a single pipe as well as the pipes in a given string length. A toughness level can then be set to ensure a shear fracture will propagate no more than a specific number of pipe lengths to a given level of confidence[303]. The use of crack arrestors is another option should the toughness requirements be outside those economically attainable.

Hardness levels of the pipe material are often not specified, and this is the case within CSA Z245.1. The DNV submarine pipeline specification[298] quotes maximum permissible hardness levels of 300 HV10 for base metal, HAZ and weld metal (for SMYS 555 MPa), with EMUUA 166 stating the same but just for the longitudinal seam weld (for SMYS up to 485MPa). Other typical pipeline specifications studied only require maximum hardness levels for sour service pipe[46,296].

2.9.2 WELD METAL STRENGTH LEVELS

Increasing weld metal strength is mainly achieved by increased alloy content. This may reduce weld metal toughness and increase both the yield ratio, hardness and the tendency for weld metal cracking. Other factors, most notably weld microstructure, welding process and welding heat input may also contribute to altering weld metal strength.

Traditionally, optimisation of weld metal strength and toughness is generally achieved through the correct increase in alloy content coupled with a microstructure consisting of predominately acicular ferrite. The latter has been shown to provide the optimum morphology i.e. fine randomly oriented grains, and can be generated with a controlled heat input welding process depositing small thin beads to ensure a high degree of grain refinement. However, as linepipe strength levels increase, weld metal microstructures

will need to consist of mixed microstructures incoporating fine acicular ferrite, bainite and/or martensite in order to attain the required strength levels.

The philosophy of requiring the weld metal yield strength to overmatch the linepipe yield strength is now common practice, brought about to ensure failure occurs outside of the weld metal where defects in construction could cause stress localisation if yielding were to occur here prior to the pipe material[297,310]. However, this overmatching requirement, especially in high strength steels, is usually accompanied by a decrease in weld metal toughness and an increased propensity for weld metal cracking[285]. In the situation where the weld metal yield strength is higher than that of the linepipe, plastic straining occurs in the linepipe, whilst the weld remains elastically strained and therefore protected.

The degree of weld metal overmatching is not usually stated in typical pipeline welding specifications (e.g. API 1104[308], BS 4515-1[46], CSA Z662[309]); it simply specifies that the weld metal is to meet the minimum requirements of the base material, and that extensive overmatching is to be avoided. DNV OS-F101, however, does specify an overmatch of 80-250 MPa above the pipe SMYS[310]. Failure of a cross weld tensile test should occur in the base material, with any failure in the weld metal occuring above the SMTS of the base material. Previous work indicates that a value of between 15% and 20% be proposed as a minimum weld metal overmatching requirement[311] i.e. 793 or 828MPa SMYS.

Considerable work has taken place in recent years in terms of pipeline design, the results of which have implications for weld metal strength and toughness levels. A transition from elastic to plastic methods is steadily occurring, and for arctic regions a strain-based design has recently been applied within an overall limit-state design. The limit states are typically classified into several catagories e.g. operability, safety and serviceability; each state can then have its own design criteria applied in terms of the limiting factor for external loading or displacement conditions[304]. In these situations examples of displacement-controlled loads are considered to be thermal expansion, frost heave and thaw settlement, whilst load-controlled loads include the pipe self-weight, internal pressure and the constant (external) forces applied to the structure. The particular pipeline in question will therefore have applicable limit states based on potential and practical failure modes relevant to that structure. Currently there is little guidance available for the determination of weld/pipe strength mismatch, pipe Y/T ratio and uniform strain required for strain-based designs. A proposal has been put forward however for the selection of the most suitable weld and pipe metal combinations by the use of an index linking the respective yield strength, weld strength mismatch and uniform strain (YMU-index) to determine the composite attainable plastic straining capacity. The area between the weld and pipe engineering stress/strain curves up to the point of weld metal failure describes in general terms the overmatching effect; a pipe of lower weld metal yield strength overmatch can compensate for this by having a higher strain hardening capability[297]. The full stress/strain curve is required for both weld and pipe material coupled with the supporting results of curved wide plate tests on notched girth welds for the complete development of a YMU-criterion.

Discussions with various manufacturers of X100 linepipe coupled with tensile test results on latest generation X100 pipe have highlighted a considerable degree of spread. A range of 690 to 790 MPa yield strength would not be uncommon, and still require

careful quality control to achieve; hence the 825MPa maximum YS in CSA Z245.1, thereby necessitating a weld metal YS of at least 790MPa. A SMYS for the weld metal of 810MPa has consequently been proposed to ensure weld metal overmatching of the base material[312,313]. Taking into account the likely variation of weld metal yield results due to cooling rate variations at these high strengths, a target upper limit of 860 MPa for the yield has also been proposed in order to avoid too much overmatching.

It is also common practice in girth welding of the current higher strength linepipes (X70/X80) to use matching/undermatching weld metal for the root and hot passes. Reported data for the welding of X80 using GMAW revealed that the root pass was carried out using an AWS ER70S-6 filler wire due to its increased ductility, thereby reducing the possibility of weld metal cracking[117,145,150,314]. This is especially prevalent if movement occurs prior to completion of the joint, such as lowering into a trench or after the internal line-up clamp is removed. Problems may arise using X100 however with respect to toughness in the root area depending upon the welding process/preheat used and the amount of dilution with the linepipe.

2.9.3 YIELD TO TENSILE RATIO

Previous work[316] states that the weld metal yield ratio is considerably higher than that of the linepipe or plate and this only serves to decrease weld metal toughness and increase the probability of weld metal failure. It is important therefore that the weld metal yield ratio is as low as possible, however it is unlikely that Y/T ratios of <0.93 will be consistently achieved for the guaranteed overmatching criteria sought with X100; a more realistic maximum value is likely to be around 0.95. Using this ratio a SMTS of the weld metal would be 853MPa, based on a SMYS of 810MPa.

2.9.4 IMPACT TESTING

Design codes specify toughness levels which have traditionally been based on the prevention of structural failure by elastic strain. Comprehensive testing of curved wide plate (CWP) tests for a variety of pipeline steel strengths (X52 to X80) and wall thicknesses (6.6mm to 25.4mm) have been used to generate data in terms of remote failure strain versus the relative defective area in the weld or parent metal. If these results are correlated with the material Cv or CTOD properties, lower bound values of absorbed energy or CTOD can be specified[297]. It has been demonstrated that in the specific case of pipeline girth welds, failure by pipe metal yielding (0.5% pipe metal strain) is ensured if 1) the defective area is less than 7% in any 300mm length, and 2) the average impact properties of the weld metal exceed 40J average (30J minimum individual) at the design temperature[317].

For the case of girth welds subject to longitudinal plastic strains, knowledge is required for the minimum acceptable toughness ensuring remote pipe yielding. Work at the University of Ghent involving further CWP test analysis has concluded that the previously stated toughness levels are most probably still valid for the plastic range of loading[297].

Although some of the current pipeline welding specifications have incorporated the 30J minimum or 40J average impact toughness (e.g. BS 4515, EN 12732[317], AS 2885.2),

no specification covers the welding of pipe at X100 strength levels. However, through extrapolation of various specifications it has been possible to produce potential average and minimum Cv values (10 x 10mm specimens) for X100 girth welds. DNV rules for submarine pipeline systems[298] would indicate 69J minimum average and 52J minimum individual (this is based on R_e/10 for the minimum average, with the minimum individual at least 75% of the minimum average). The Statoil pipeline welding specification R-SF-260[318] also extrapolates to 69J average and 52J minimum individual for production tests (89J average and 67J minimum individual for procedure qualification). BS 4515-1 or EN 12732 does not allow an extrapolation due to a single impact energy requirement for all steel strengths (40J average, 30J minimum individual up to X65). API 1104 and CSA Z662 do not contain any impact toughness requirements. All of the above are relevant for Cv impact specimens taken from the weld metal and heat affected zone. No testing temperature has been indicated above, as this is dependent upon the minimum design temperature (often including a further lowering of test temperature for impact testing due to triaxiality effects) and the type of media flowing through the pipeline. If linear extrapolation is a valid methodology for weld and heat affected zone impact toughness, then a requirement of 69J minimum average and 52J minimum individual constitute applicable levels.

2.9.5 CTOD TESTING

CTOD values are usually required for use in the engineering critical assessment of a given structure with respect to allowable flaw sizes, and for this reason they are often included as a supplementary testing requirement in the various pipeline welding codes. Appendix A of API 1104 quotes a welding procedure qualification minimum CTOD value of 0.127mm, whereas no value is quoted in BS 7910[319] or CSA Z662-99 Appendix K. As per the Cv impact toughness requirements specified in EN 12732, CTOD values have been determined through correlation between CWP and CTOD test data resulting in values of 0.15mm (average) and 0.10mm (minimum individual) CTOD conducted at the design temperature for matching/overmatching pipeline welds. EN 12732 only covers steel grades up to X70 (483MPa YS). These levels have also been adopted by AS 2885.2. The Statoil specification R-SF-260 requires CTOD levels of 0.15mm minimum from each of 4 specimens (12, 3, 6, 9 o'clock) from production welds, and a minimum of 0.20mm from procedure qualification welds (the specification covers girth welds in pipe up to X70 strength levels and WT > 16mm).

A comparison between three CTOD values of 0.31mm, 0.20mm and 0.15mm was conducted in accordance with BS 7910 incorporating a 100mm long flaw (arbitary choice). This revealed that critical flaw depths of 4.5mm, 3.4mm and 2.75mm were ascertained for the 0.31mm, 0.20mm and 0.15mm CTOD values respectively[156]. Further discussion is required if a precise CTOD value is to be assigned for X100 girth welds. A fitness for purpose approach such as BS 7910 also needs to be assessed on its use as an appropriate document in conjunction with X100 linepipe, and consequently if the defect sizes calculated above represent inspectable flaw sizes. The test method for CTOD determination (BS 7448[320]) may provide an over-estimate of conservatism for pipeline use; alternative methods such as wide plate testing or single-edged notched tensiles may be better suited for the geometry in question.

The values quoted above suggest a minimum individual CTOD value applicable for X100 girth welds and HAZ's in the region of 0.10mm to 0.15mm at the design temperature.

2.9.6 HARDNESS

A review of pipeline welding specifications with respect to allowable hardness levels has shown some discrepancies between those investigated. BS 4515-1 states a maximum of 275 HV10 for the weld metal and 350 HV10 maximum for the HAZ, for non-sour service and any welding process other than manual welding with cellulosics. No hardness criterion is stated in API 1104 or CSA Z662-99. DNV OS-F101 quotes a maximum of 300 HV10 for weld metal, base metal and HAZ (non-sour service), which is in agreement with Statoil R-SF-260 for procedure qualification welds (325 HV10 for production welds). Assuming that X100 steels will not be used for sour service applications, research has indicated that 350 HV10 would be a more realistic maximum value for X100 weldments[7] given the direct correlation between strength and hardness.

2.9.7 NDT REQUIREMENTS

The non-destructive testing requirements for pipeline welds and their acceptance criteria form comprehensive sections within most of the pipeline welding specifications. It is not intended to discuss the numerous flaw types, locations and sizes, suffice to say that they form an integral part of both procedure qualification and production testing. Radiography via X-ray or isotope has been the traditional method of assessment, but the increasing use of automatic ultrasonic testing (AUT) equipment using phased arrays of probes provides a faster and more comprehensive picture of the completed weld characteristics than radiography. Careful calibration of the system is a prerequisite for accurate flaw determination; calibration blocks of the actual pipe in question are normally required. The very fine grained microstructures evident in X100 may also cause potential beam attenuation[321]. Digital data gathering has enabled AUT to provide a record suitable for archiving in the same fashion that the film from radiography allows. A possible concern for the use of AUT following closely behind the welding spread is the discovery of hydrogen cracks; as stated in a previous section, these normally require a delay prior to their appearance. It is therefore prudent to assess the hydrogen cracking propensity of the base and weld metal coupled with the ability of the AUT system to pick it up[321].

Table 2-1: 690 grade steel development

Manufacturer	Kawasaki Steel Corporation[10]	Nippon Steel Corporation[5]	Mannesmann/ Europipe[7]	Vanitech[69]
Material Dimensions	20mm thick plate	762mm OD, 19.05mm WT Pipe	762mm OD, 19.1mm WT Pipe	15mm thick plate
Material Chemistry				
C	0.06	0.06	0.06-0.08	0.08
Si	0.3	0.22	1.85-2.00	0.44
Mn	1.8	1.96	0.20-0.30	1.84
P	0.01	0.006	0.015 max	0.006
S	0.001	0.0026	0.0020 max	0.002-0.003
Ni		0.39	0.20-0.25	0.27
Mo		0.11	0.25-0.35	0.24
Cu		0.17	0.20-0.25	0.26
Al	0.03		0.020-0.040	0.027
Ti	0.015	0.013	0.015-0.020	0.01
Nb	0.06	0.045	0.045-0.055	0.05
B	not stated	not stated		
V			not stated	0.08
N	0.004		0.004 max	0.004
Pcm	0.19	0.19		0.23
Mechanical Properties				
YS (MPa)	718	710 (API 5L Transverse specimen)	739 ($R_{t0.5}$, round bar transverse)	690 ($R_{t0.5}$, round bar transverse)
UTS (MPa)	887	848 (API 5L Transverse specimen)	792 (R_m, round bar transverse)	820 (R_m, round bar transverse)
El (%)	27	30 (API 5L Transverse specimen)	18.4 (A_5)	19
YS/UTS (%)	81	84	93	84
Cv @ -40°C(Av. J)	224			
Cv @ -20°C(Av. J)		133 (transverse)	235	210
DWTT SA @ -30°C (%)	88			
DWTT 85%SA (°C)		-15	-15 (Cvtrans)	-27 (Cvtrans)

Table 2-1 (Cont.): 690 grade steel development

Manufacturer	Kawasaki Steel Corporation	Nippon Steel Corporation	Mannesmann/ Europipe	Vanitech
Longitudinal Seam Properties				
YS (MPa)			640 (OD), 700(ID), round bar	
UTS (MPa)		793 (API 5L X-Weld incl. reinf.)	750 (OD), 825 (ID), round bar	
Fracture Location		HAZ	x-weld UTS 800 (in base mat.)	
Weld CL Cv @ 0°C (Av. J)		144 (-10°C)	140-170 (OD)	
Weld CL Cv @ -40°C (Av. J)			50-140 (OD)	
HAZ Cv @ 0°C (Av. J)	225 (2mm sub OD)	130 (-10°C)	20-180	90
HAZ Cv @ -40°C (Av. J)	120 (2mm sub OD)		10-70	HAZ value from simulated HAZ; heat input simulated = 4KJ/mm i.e. SAW seam
50%HAZ/50% WM Cv @ 0°C (Av. J)	140 (2mm sub OD)	71 (-10°C)		
50%HAZ/50% WM Cv @ -40°C (Av. J)	50 (2mm sub OD)			
Metallurgical characteristics of plate/pipe	Majority bainitic ferrite with small amounts of finely dispersed martensite/austenite islands	upper bainite with TiN and TiO precipitates	Majority phase fine bainite, with even distribution of remaining phases	80-90% bainite, 10-20% ferrite, remainder martensite, with evidence of relatively coarse Ti and Nb-Ti rich precipitates
Production Conditions				
Slab reheating Temperature (°C)	1150	1150	1180	1150
Finish Rolling Temperature (°C)			730	800
% reduction in non-recrystallisation region	88	75	75	67
Accelerated cooling Rate (°C/s)	35	20 or 25	20	30
Finish Cooling Temperature (°C)	200	300	530	550
		NB above production conditions are best guesses based on previous trials from the paper		NB consideration of the 0.2% proof stress indicates that after UOE pipe forming, 690MPa YS should be obtained with 0.04-0.06V in conjunction with the above plate chemistry and a finish rolling temp. of 800°C, 25-30°C cooling rate and 550°C cooling stop temp.

Table 2-2: Classification of metal transfer modes (after ref. 78 and 95)

Transfer Group	Transfer Sub Group	Dominant Force or Mechanism	Example
Bridging	Short-circuiting	Surface tension and electromagnetic forces	Low Current GMAW
	Bridging transfer without interruption	Surface tension and (hot wire) electromagnetic forces	Welding with filler wire addition
Globular	Drop	Gravity and electromagnetic	Low current GMAW
	Repelled	Chemical reaction generating vapour	CO_2 shielded GMAW
Spray	Projected	Electromagnetic pinch instability	GMAW above spray transition
	Streaming	Electromagnetic	Medium to high current GMAW
	Rotating	Electromagnetic kink instability	High current, extended stick out GMAW
	Explosive	Chemical reaction to form a gas bubble	SMAW
Slag Protected	Flux-wall guided	Chemical and electromagnetic	SAW
	Other modes	Chemical and electromagnetic	SMAW, FCAW
Mixed-Mode	Drop-spray	Gravity and electromagnetic pinch instability	Pulsed GMAW
	Controlled short circuit	Surface tension and electromagnetic pinch forces	Surface tension transfer (STT) GMAW

Table 2-3: Examples of latest generation GMAW power supply variables

Lincoln Electric Powerwave 455	Fronius TPS 4000
Wire feed (m/min)	Wire feed, vD (m/min)
Ramp up rate (A/ms)	U r (V)
Tailout time (ms)	I r (A)
Peak amps (A)	Start volt, U pstart (V)
Stepoff amps (A)	U pinit (V)
Background amps (A)	I sigon (A)
Peak time (ms)	Background amps, I b (A)
Background time (ms)	Ramp up rate, d pup (A/ms)
Frequency (Hz)	Ramp up time, tau pup (ms)
Tailout speed	Peak amps, I p1 (A)
Ramp overshoot (%)	Peak time, t p1 (ms)
Peak voltage (V)	Ramp down rate, d pdo (A/ms)
Inductance (mH)	Second level peak amps, I p2 (A)
Short detect voltage (V)	Second level peak time, t p2 (ms)
Pinch current rise rate (A/ms)	Frequency, f puls (Hz)
Arc re-establish voltage (V)	Set voltage, U set (V)
End amp (A)	F Ib pureg pi (%)
End time (ms)	F Ip1 pureg pi (%)
Strike peak amps (A)	F f pureg pi (%)
Start volt (V)	F f pureg p (%)
Start time (ms)	I p1min (A)
Start amps (A)	F Uact int (%)
Adapt peak Amps	F pbal pureg (%)
Adapt peak time	F dldU pureg (%)
Adapt stepoff	F Ib alcorr (%)
Adapt background amp	F Ip1 alcorr (%)
Adapt frequency	

Table 2-4: History of pipeline welding methods and technologies (after ref. 105)

Date	Welding Method (Company, Country of Origin)
1930's	Stovepipe welding established using cellulosic electrodes with a downward welding technique.
1948	MIG welding process applied to pipelines (AIRCO, USA)
1953-1955	CO_2 arc welding process invented (Russia, Holland, USA, Japan)
1958-1961	Dip transfer welding method developed (USA, UK, Russia)
1959	Automatic CO_2 girth welding apparatus developed (Esso, Battelle, AIRCO, USA)
1959-1967	H.C.Price developed vertical down welding with CO_2 and torch weaving (USA)
1961	Ar-CO_2 mixed gas GMAW developed (Germany)
1963	Thomas Contracting Co. developed 4-head automatic welding system (USA)
1963	Narrow gap welding process developed (Battelle, USA)
1960-1964	Semi-automatic CO_2 GMAW applied to 24,200km of oil and gas pipelines (USA)
1969	CRC-Crose development of internal and external pipewelding machines with pipeline spread concept, (USA)
1975	H.C.Price development of 4-head external narrow gap automatic welding system, internal back-up clamp, for offshore use (USA)
1977	Saipem/ARCOS external mechanised welding system (Passo), internal back-up clamp (Italy)
1979	Serimer Dasa field use of 4-head external automatic welding system (Saturne), internal back-up clamp, for offshore use (France)
1980's	Off-line programming of welding parameters, on-line seam tracking, continuous circumferential welding [12-6-12 o'clock](Japan)
1988	Serimer Dasa field use of mechanised dual torch external welding system (Saturnax), internal Cu back-up clamp, for offshore use (France)
1989	Serimer Dasa field use of 4-head (8 torches) automatic welding system (Saturne 8), internal Cu back-up clamp, for offshore use (France)
1990's	Arc sensing, contact sensors, CCD weld monitoring, laser/magnetic sensors, adaptive control, inprocess monitoring
1994	Serimer Dasa field use of mechanised dual torch external welding system (Saturnax), internal Cu back-up clamp, for onshore use (France)
1999+	Saipem dual torch 'presto', CRC dual torch P600 and RMS dual torch MOW II systems developed. Cranfield tandem and dual tandem torch technique

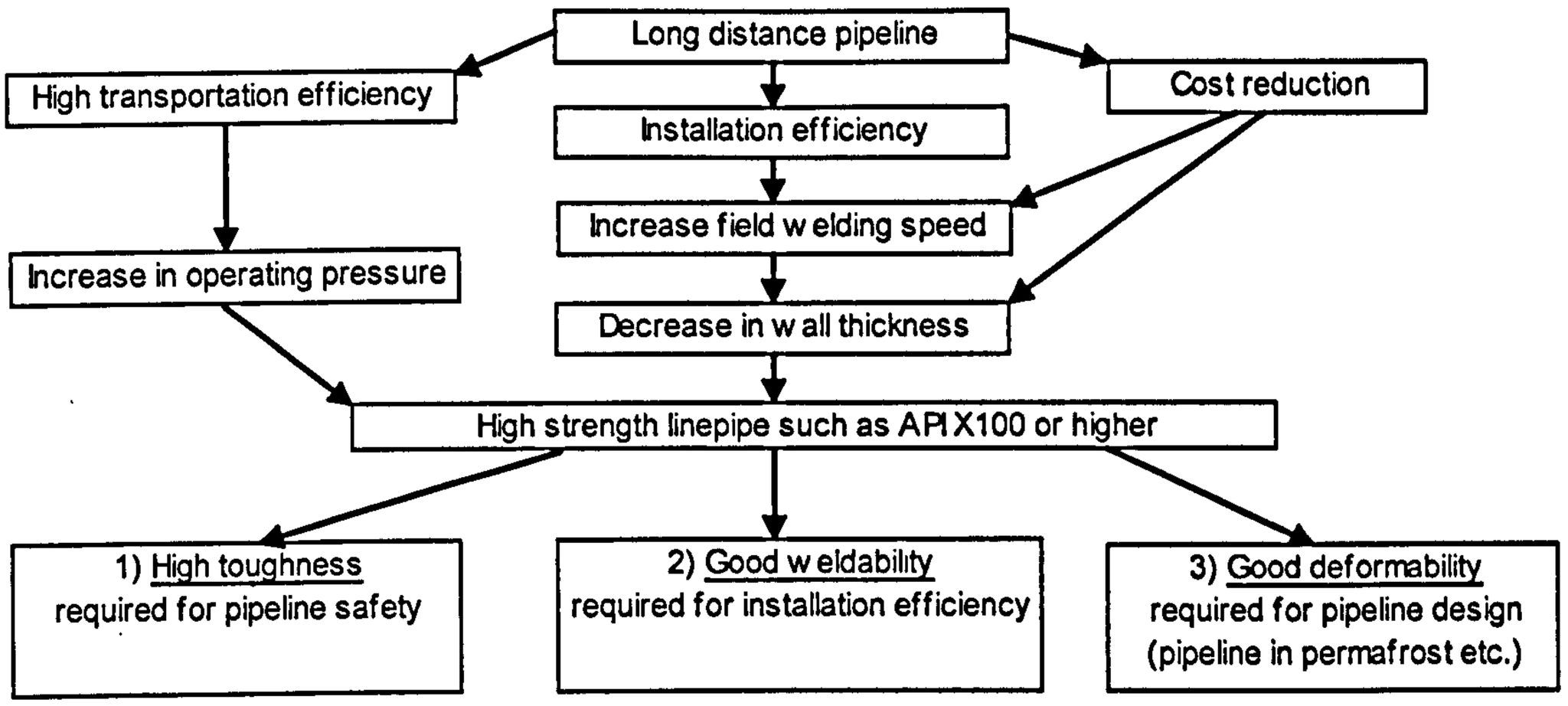

Figure 2-1: The rationale and requirements for high strength linepipe (after ref. 9)

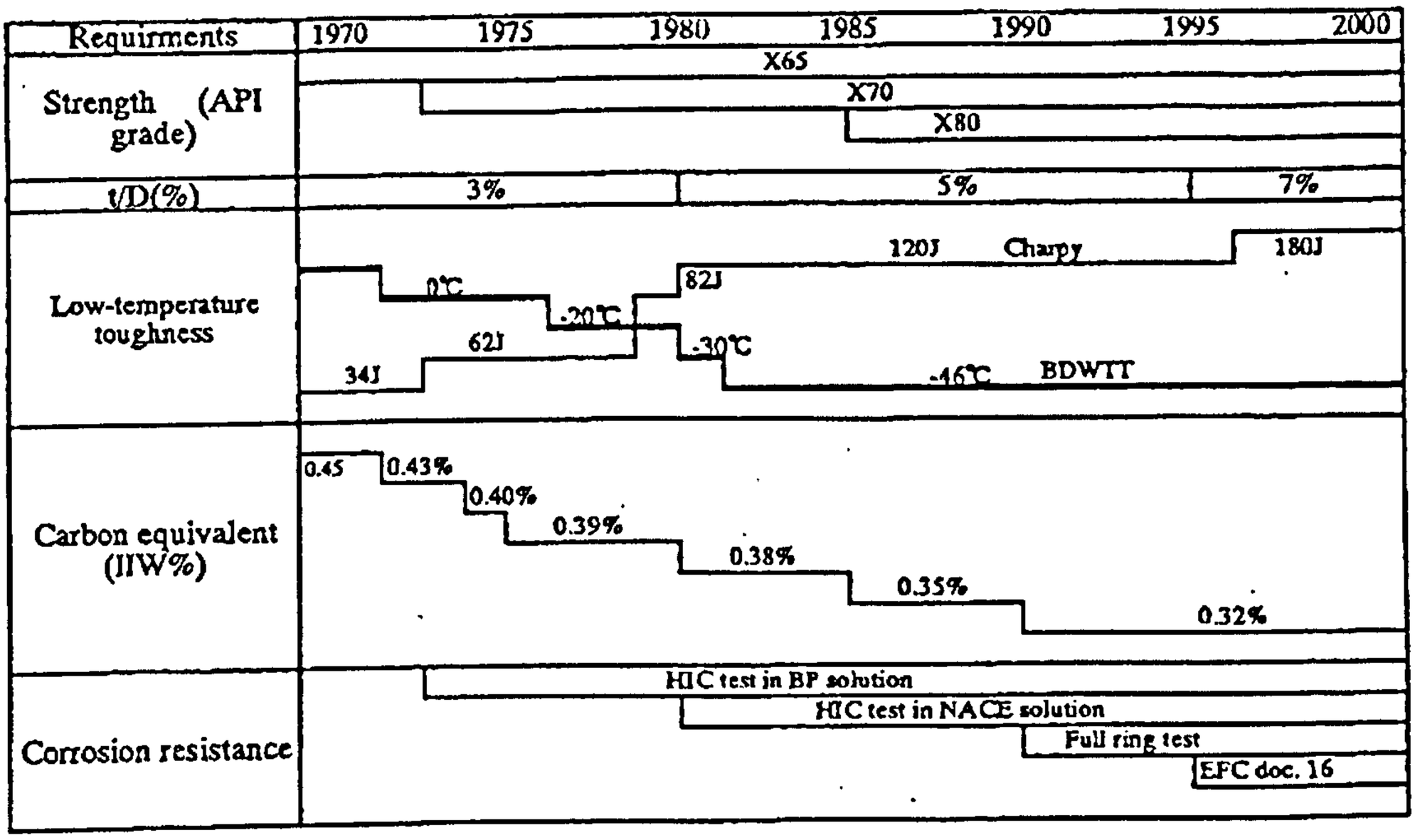

Figure 2-2 : Changes in line pipe property requirements (after ref. 1)

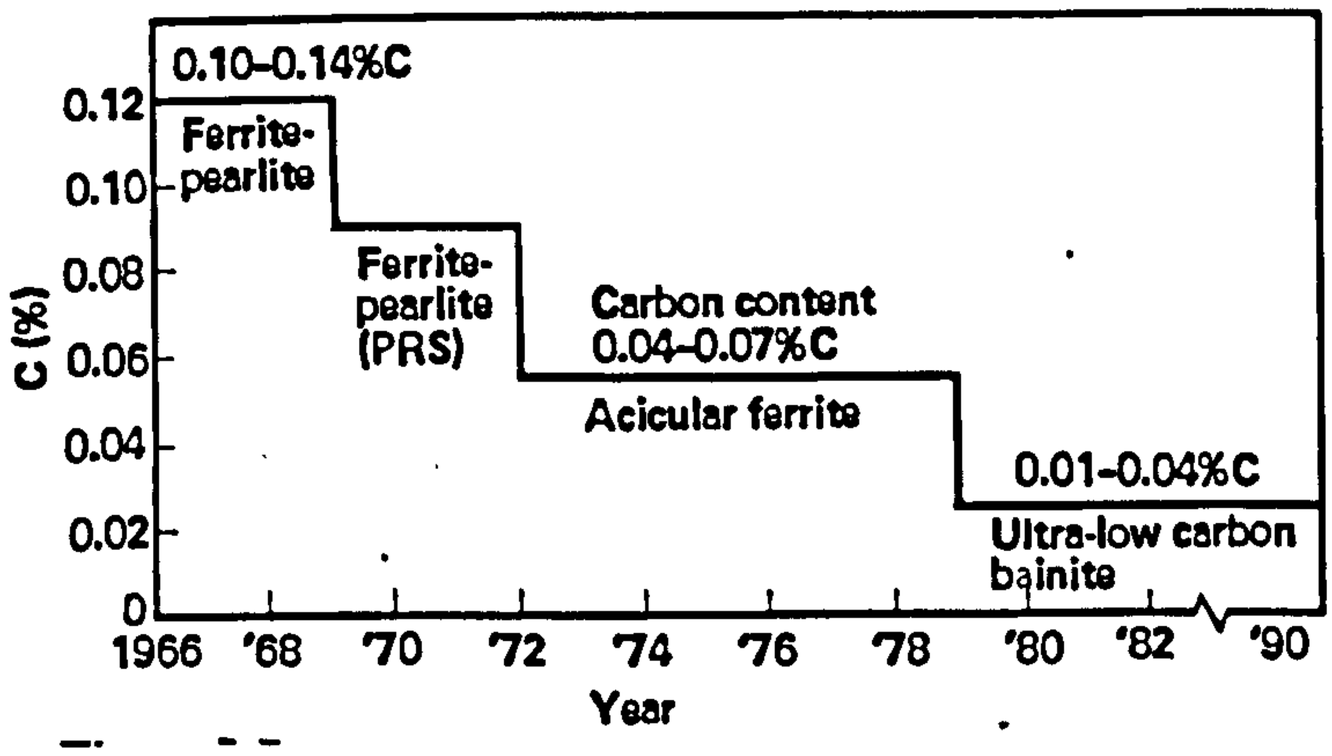

Figure 2-3: Changes in carbon content and microstructure of pipeline steels (after ref. 47)

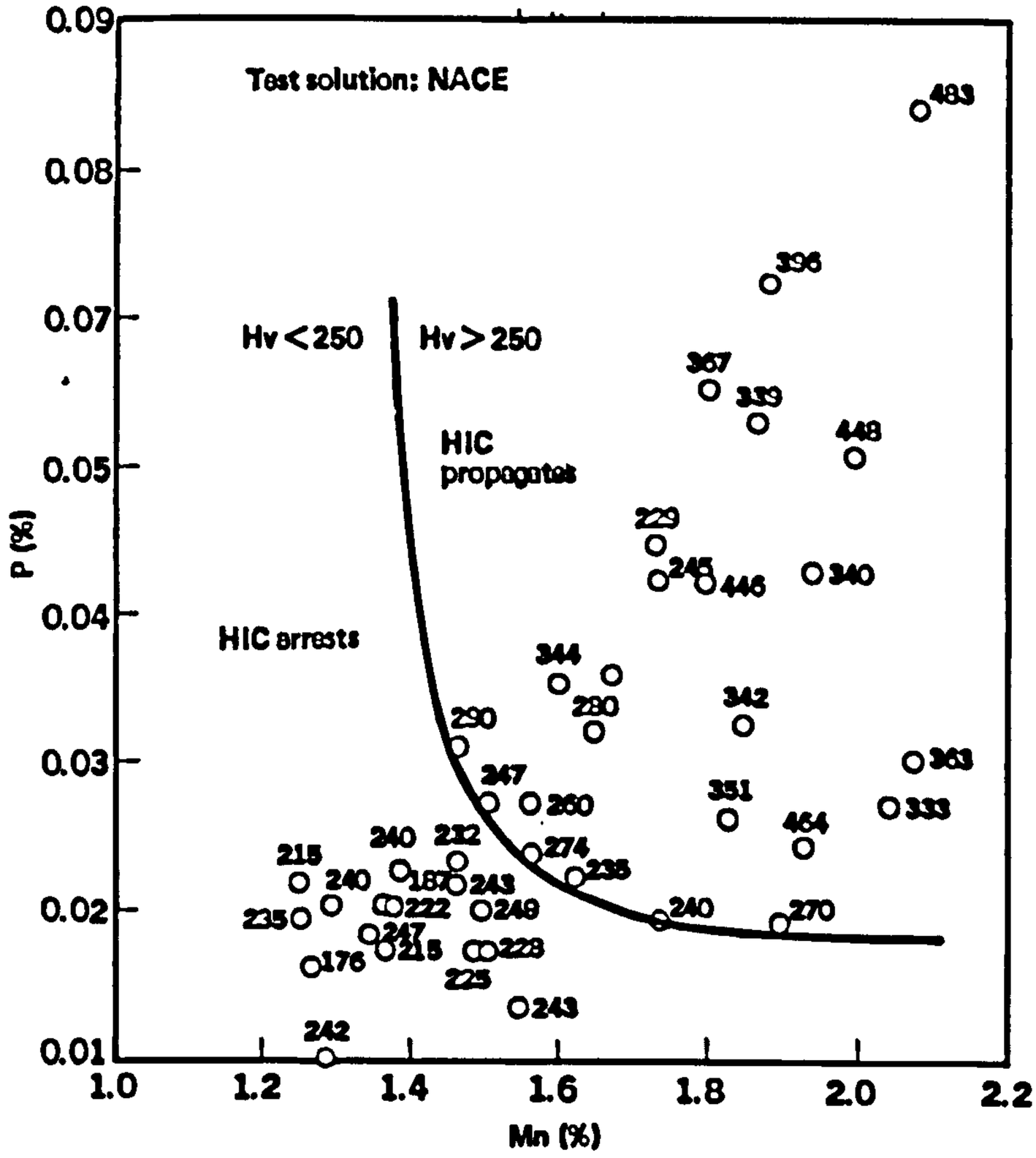

Figure 2-4: Criterion for preventing HIC in terms of Mn and P concentrations measured by EPMA and microhardness in the vicinity of HIC. Figures indicate HV0.025 (after ref. 49)

$$\text{Crack Sensitivity Ratio, CSR} = \frac{\Sigma (a \times b)}{W \times T} \times 100\ \%$$

$$\text{Crack Length Ratio, CLR} = \frac{\Sigma a}{W} \times 100\ \%$$

$$\text{Crack Thickness Ratio, CTR} = \frac{\Sigma b}{T} \times 100\ \%$$

Where : a = crack length
b = crack thickness
W = section width
T = specimen thickness

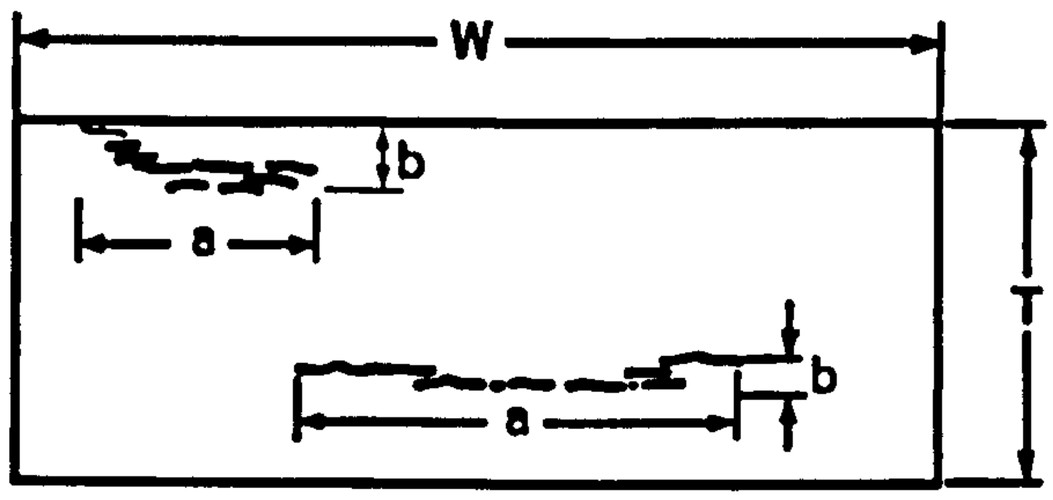

Figure 2-5: Evaluation methods of HIC test results (after ref. 26)

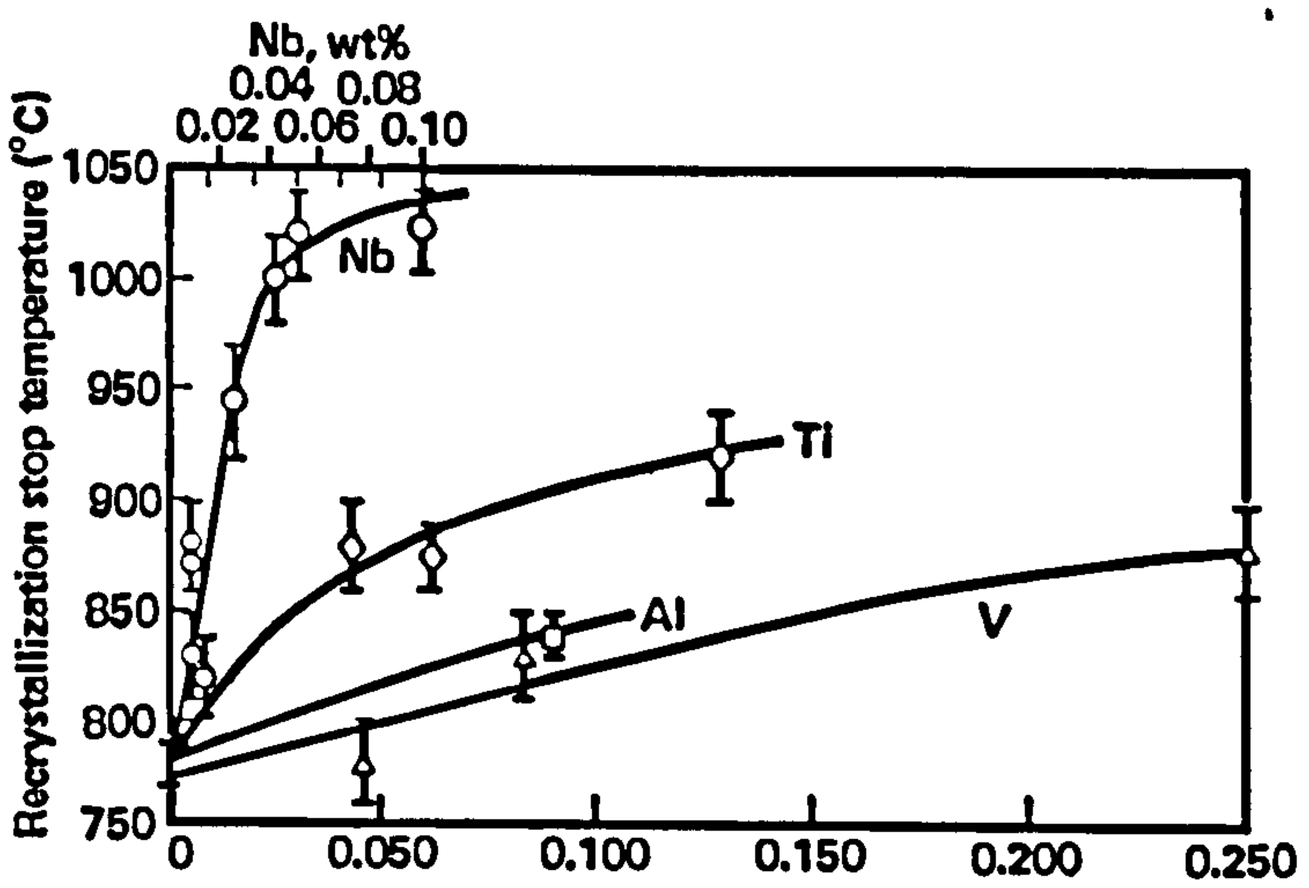

Figure 2-6: Change in recrystallisation stop temperature with microalloy content (base composition 0.07%C – 1.4%Mn)(after ref. 57)

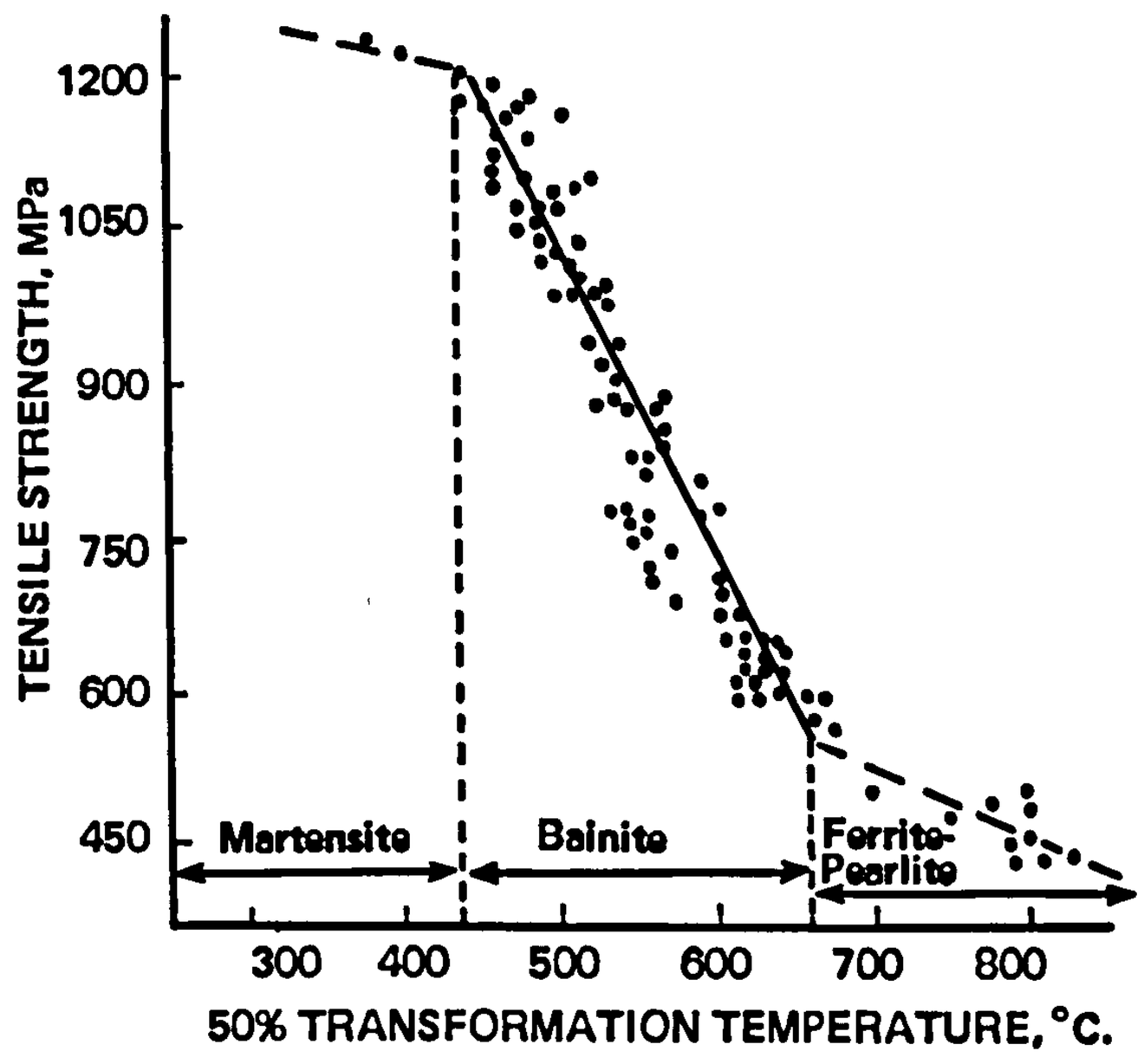

Figure 2-7: Relationship between 50% transformation temperature and tensile strength (after ref. 59)

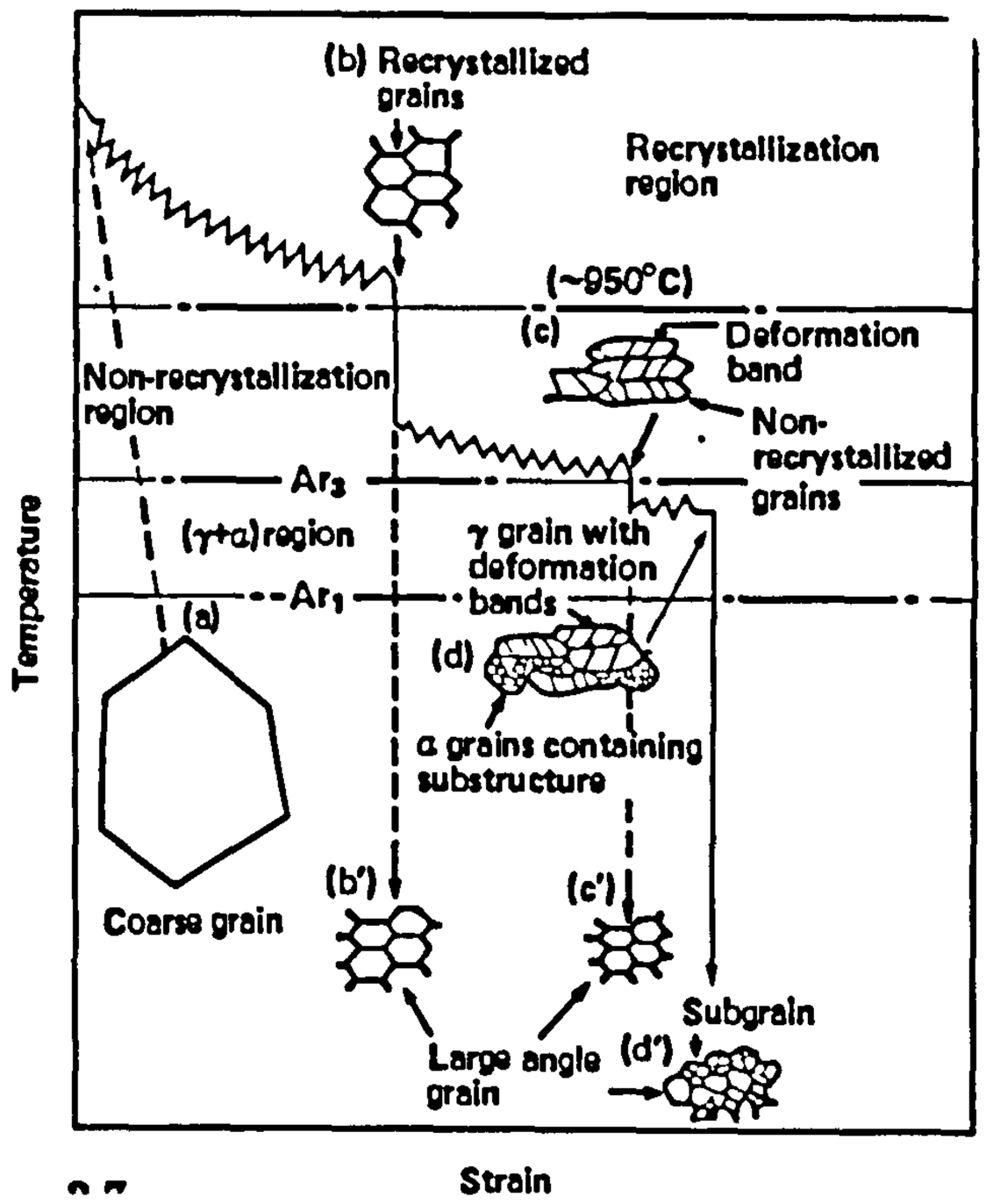

Figure 2-8: Schematic illustration of structural changes in controlled rolling (after ref. 65)

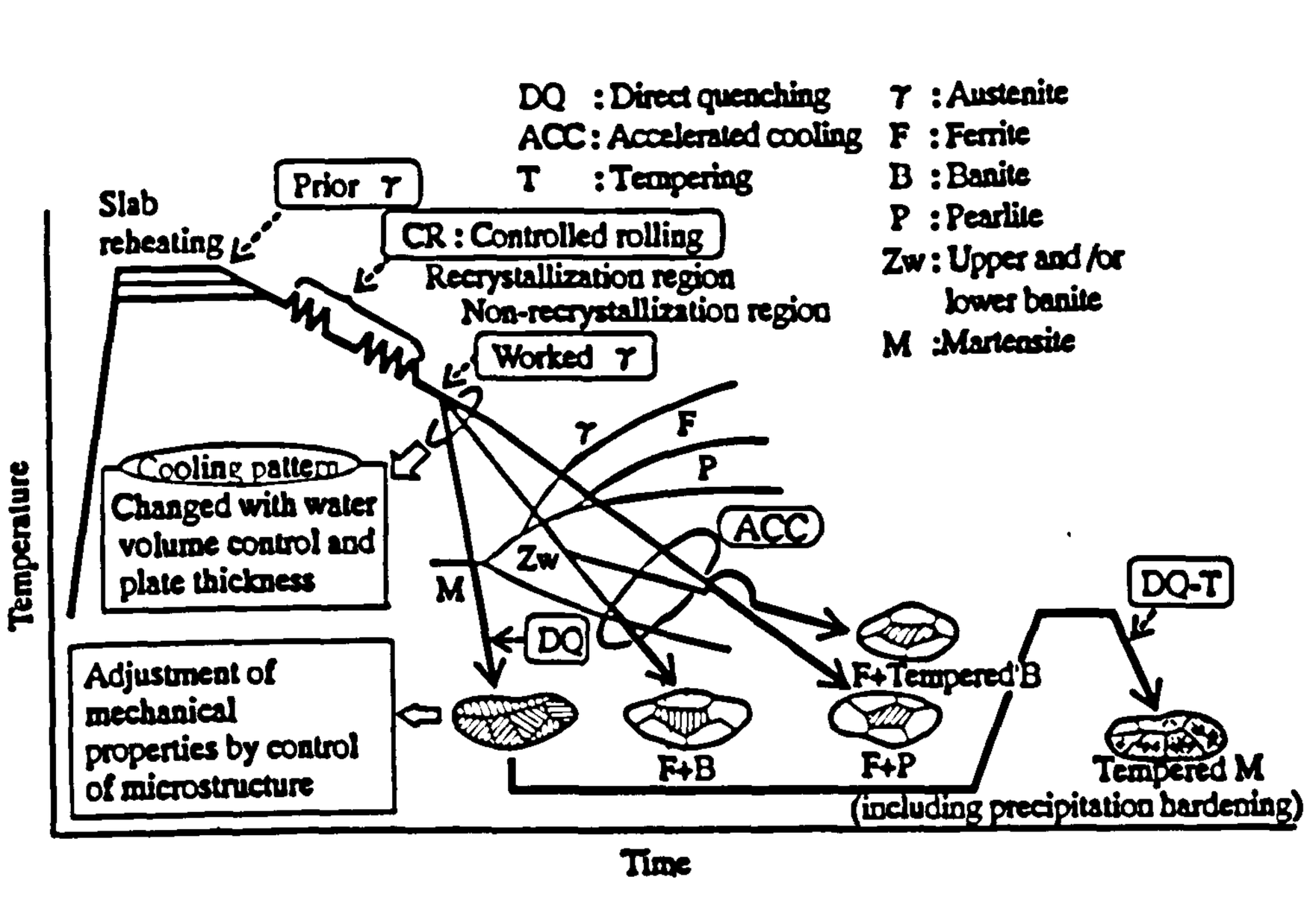

Figure 2-9 : Concept of microstructure control by TMCP (after ref. 66)

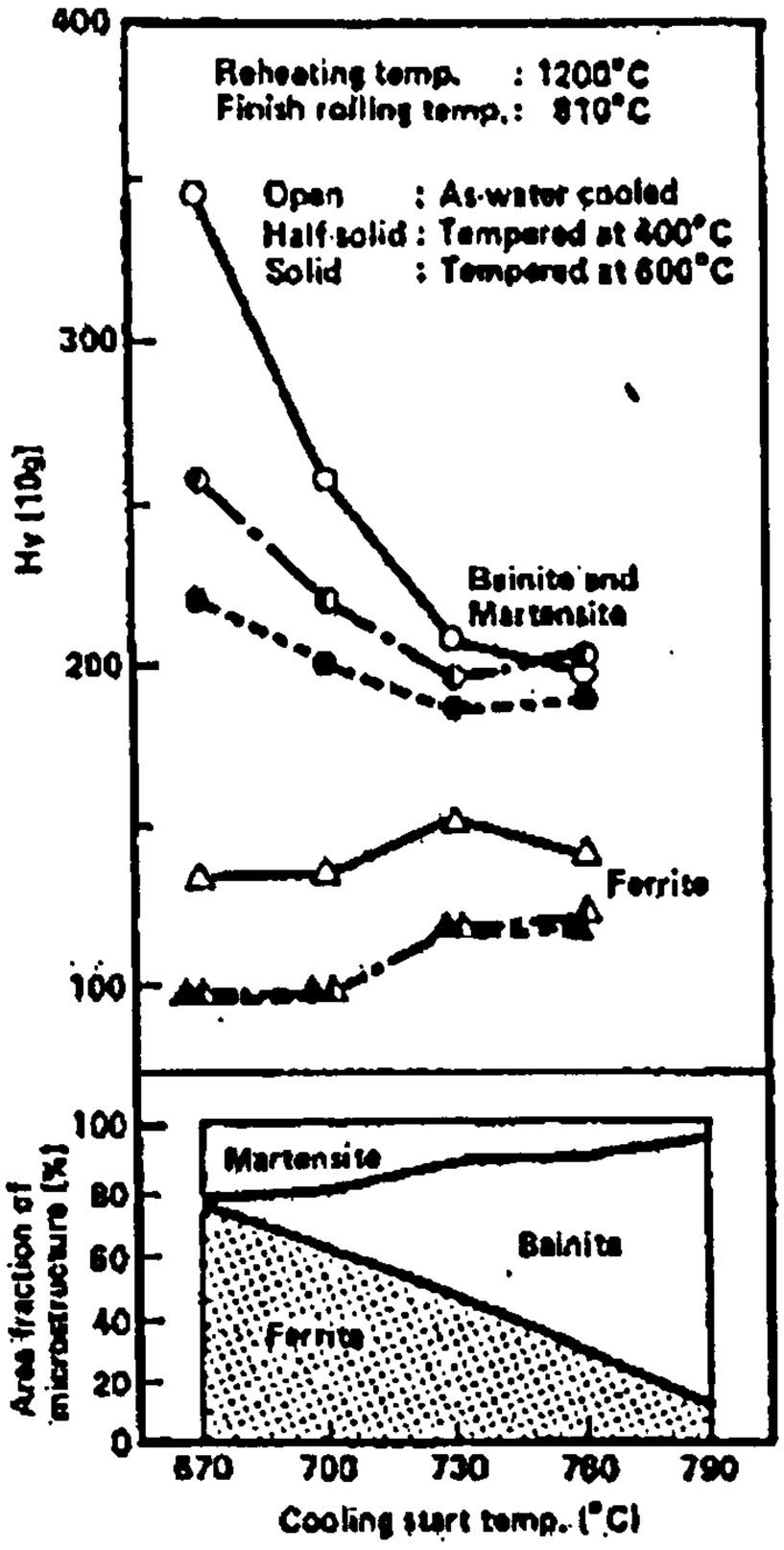

Figure 2-10: Effect of cooling start temperature on area fraction and hardness of microstructure (after ref. 9)

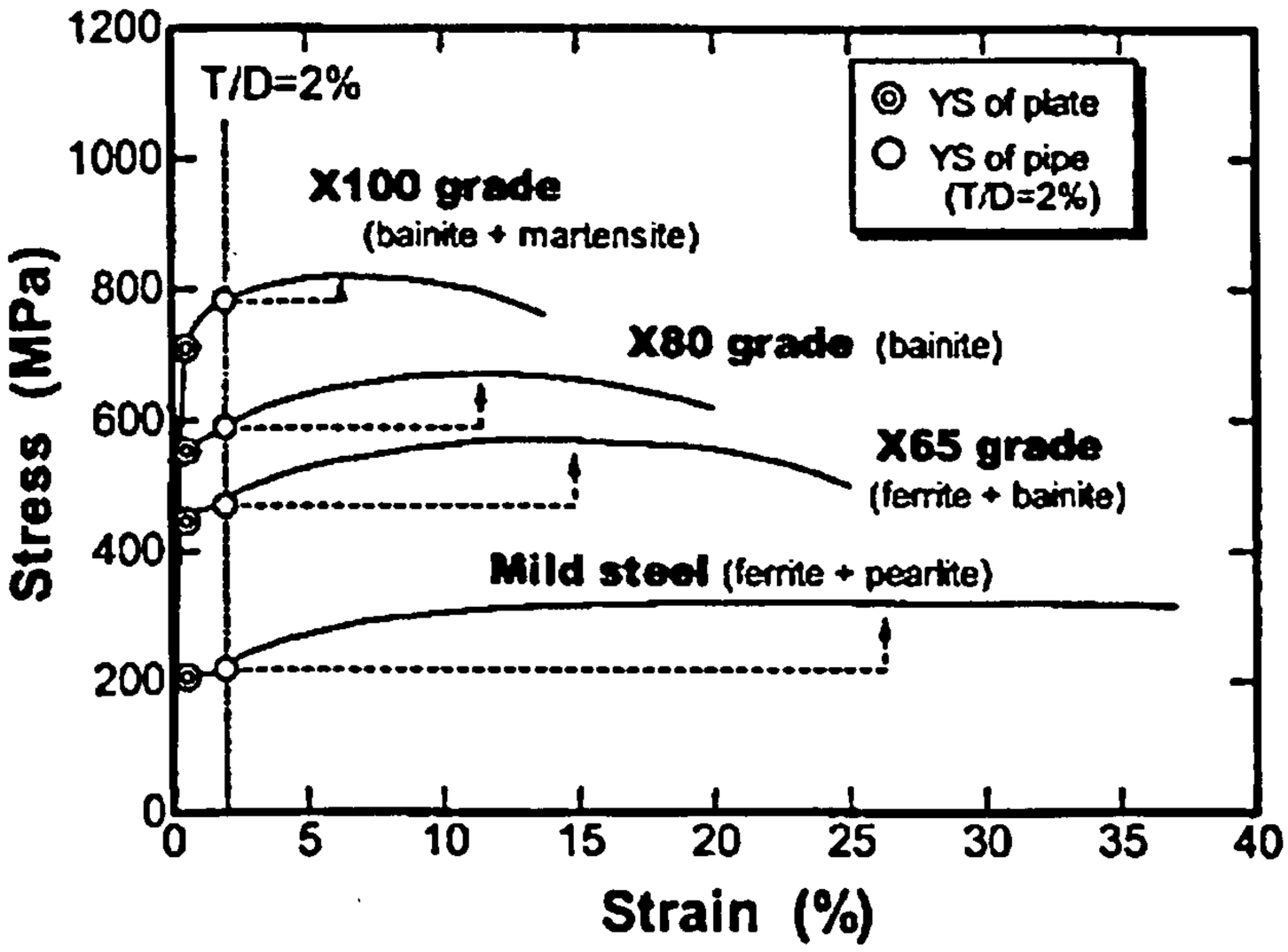

Figure 2-11: Typical stress strain curves for low to high strength steels (after ref. 8)

Figure 2-12: Effect of tensile strength on impact transition temperature of low carbon bainitic steels (after ref. 67)

Figure 2-13: Effective grain size (d_{eff}) measurement (after ref. 64)

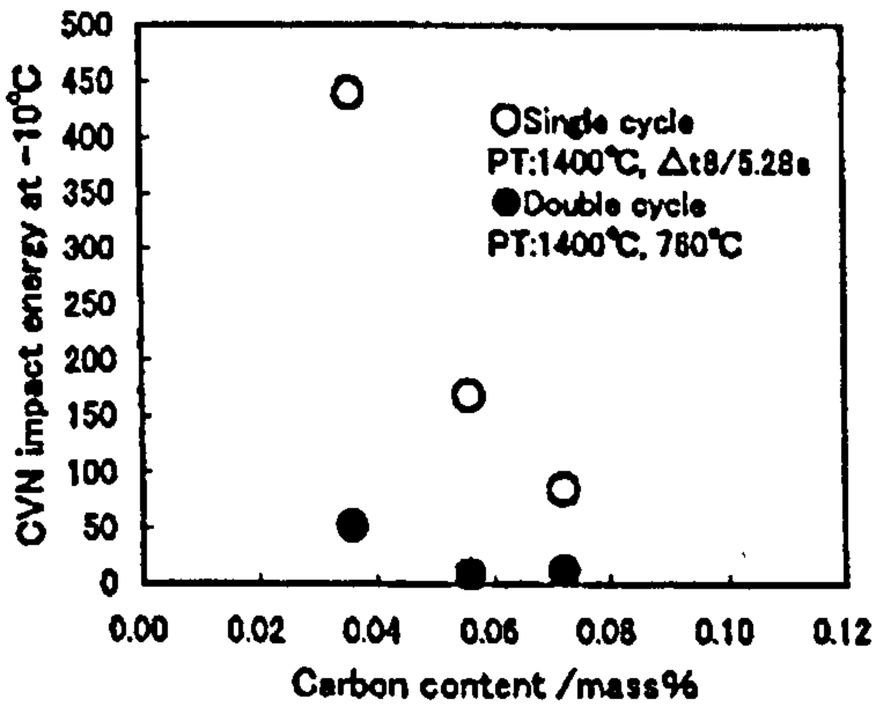

Figure 2-14: Effect of carbon content on simulated HAZ toughness of X100 linepipe steel (after ref. 9)

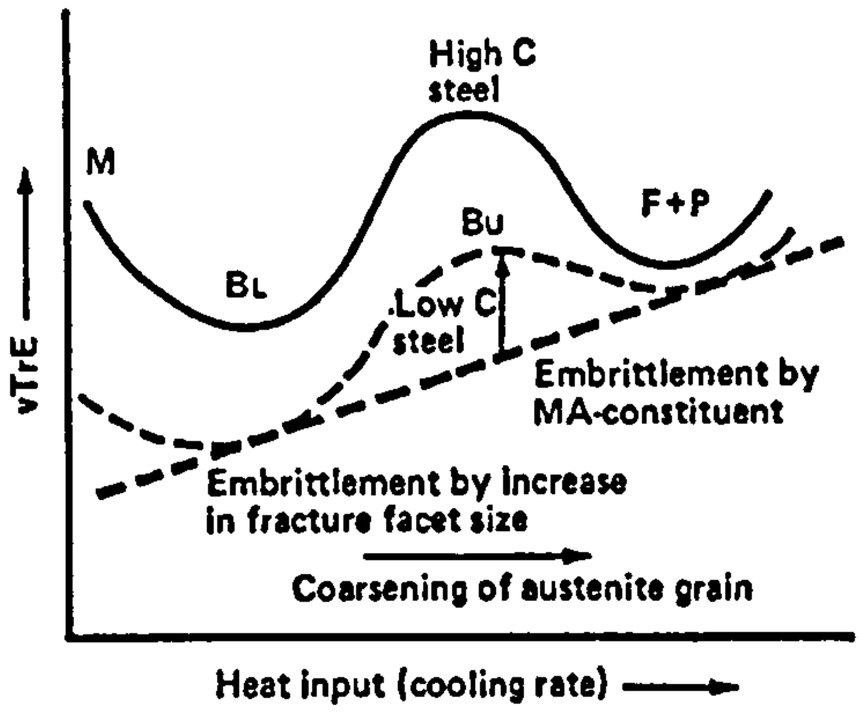

Figure 2-15: Schematic illustration of relationship between microstructure and HAZ toughness (after ref. 9)

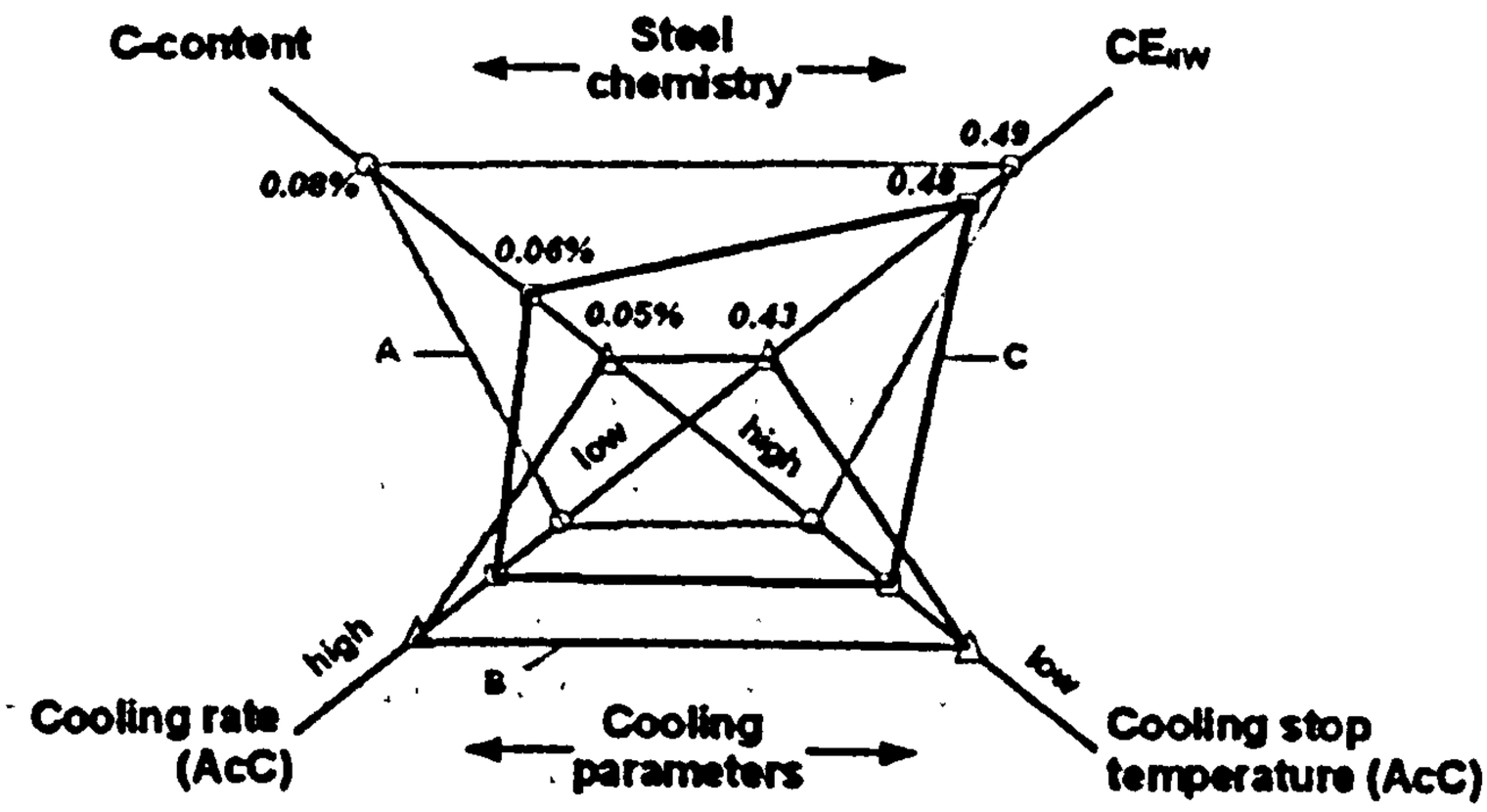

Figure 2-16: Interrelation between steel chemistry and cooling parameters to attain X100 strength levels (after ref. 68)

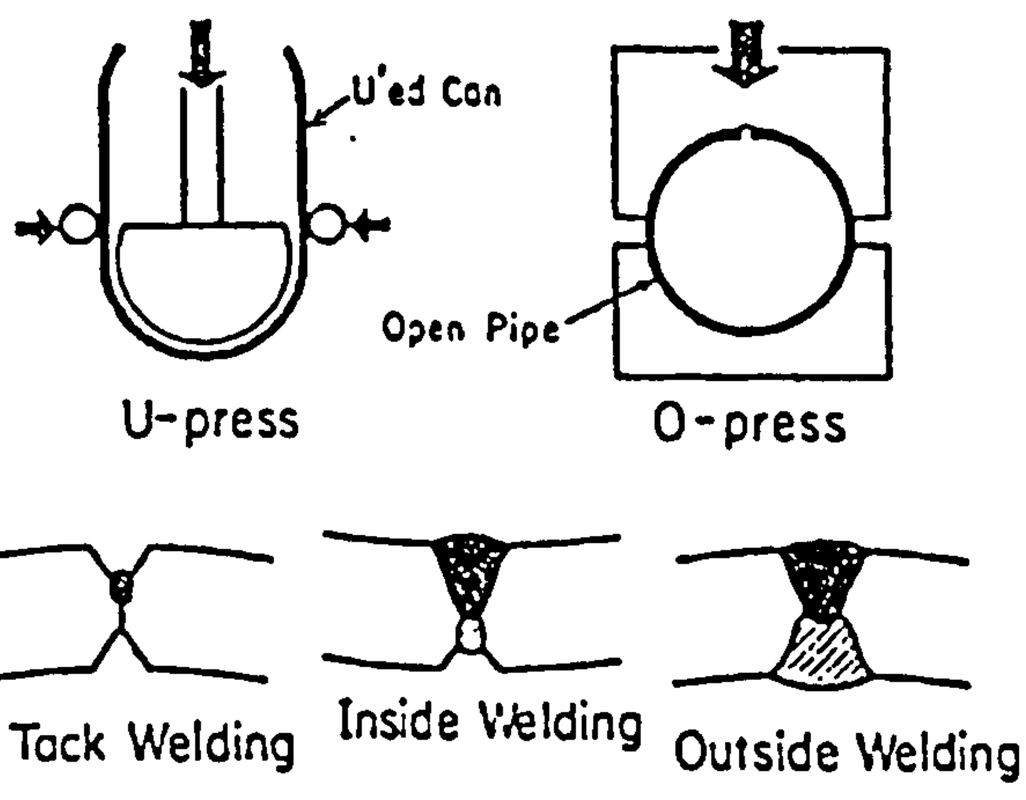

Figure 2-17: Forming and longitudinal seam welding of UOE pipe (after ref. 70)

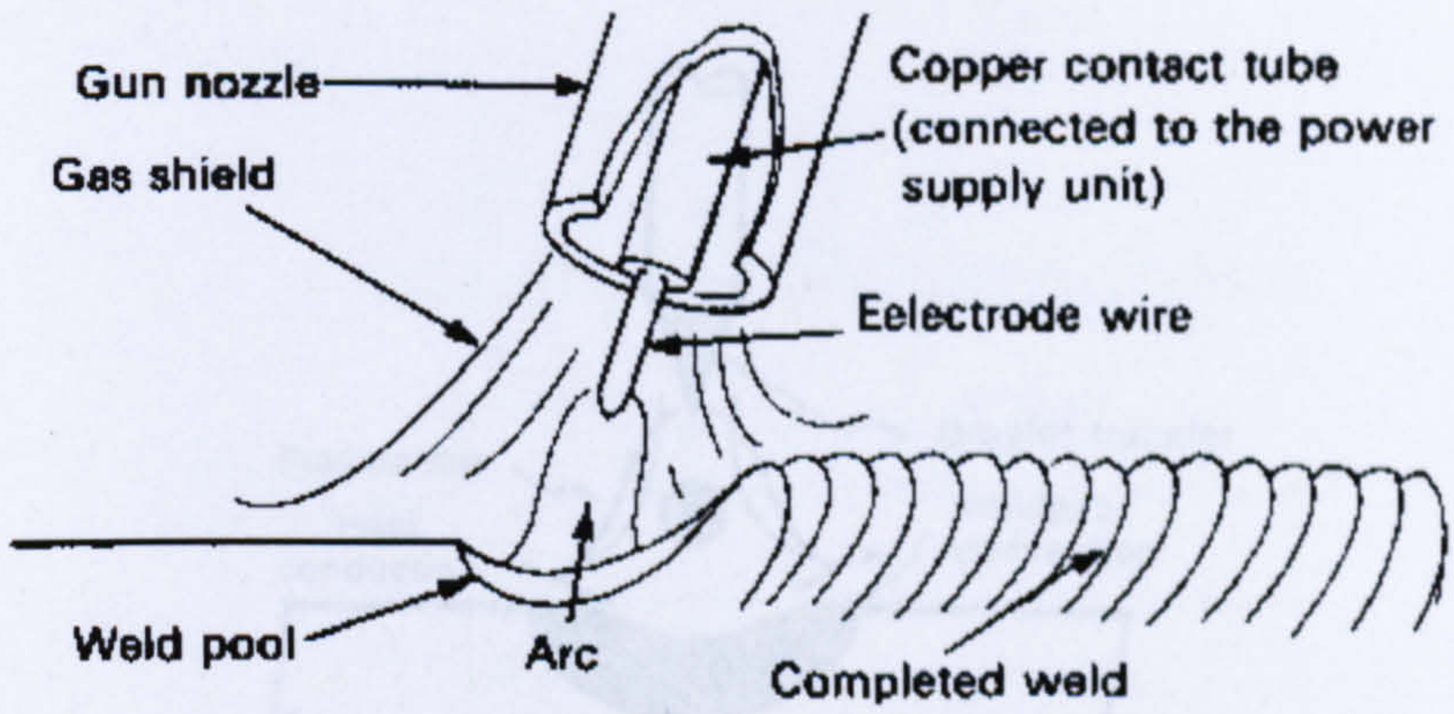

Figure 2-18: GMAW Process Schematic (after ref. 76)

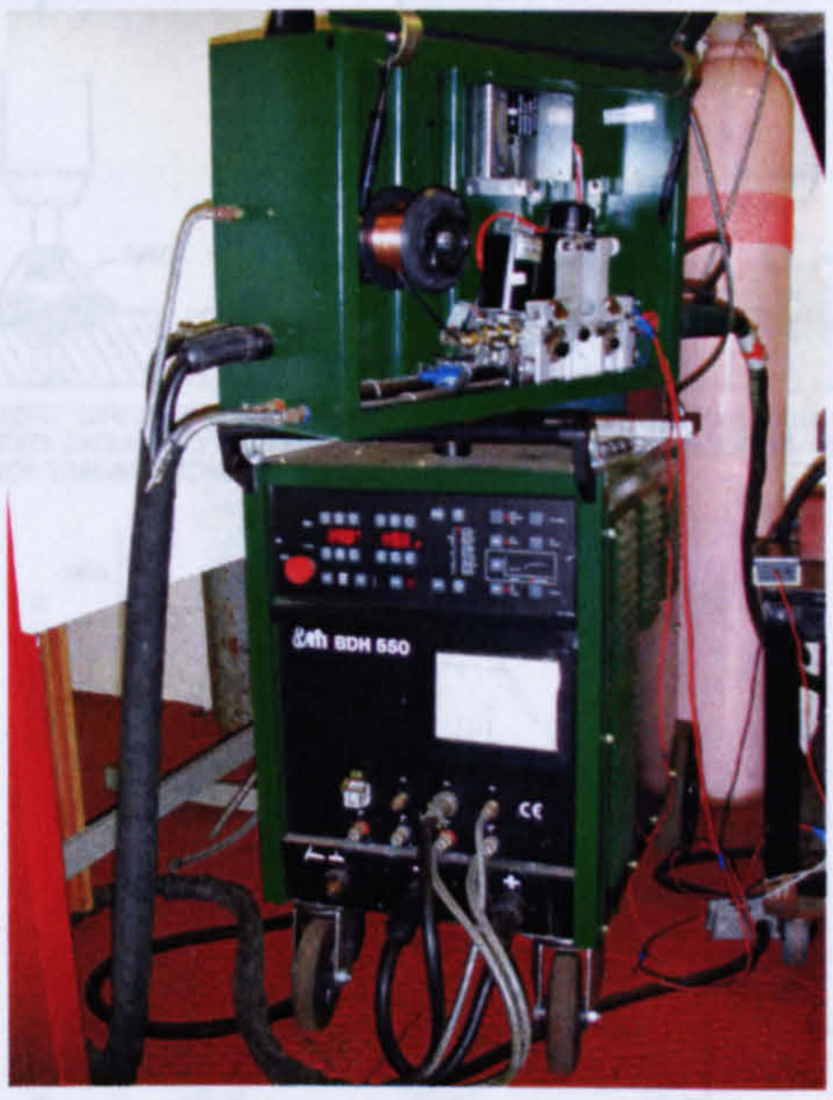

Figure 2-19: Typical GMAW Equipment

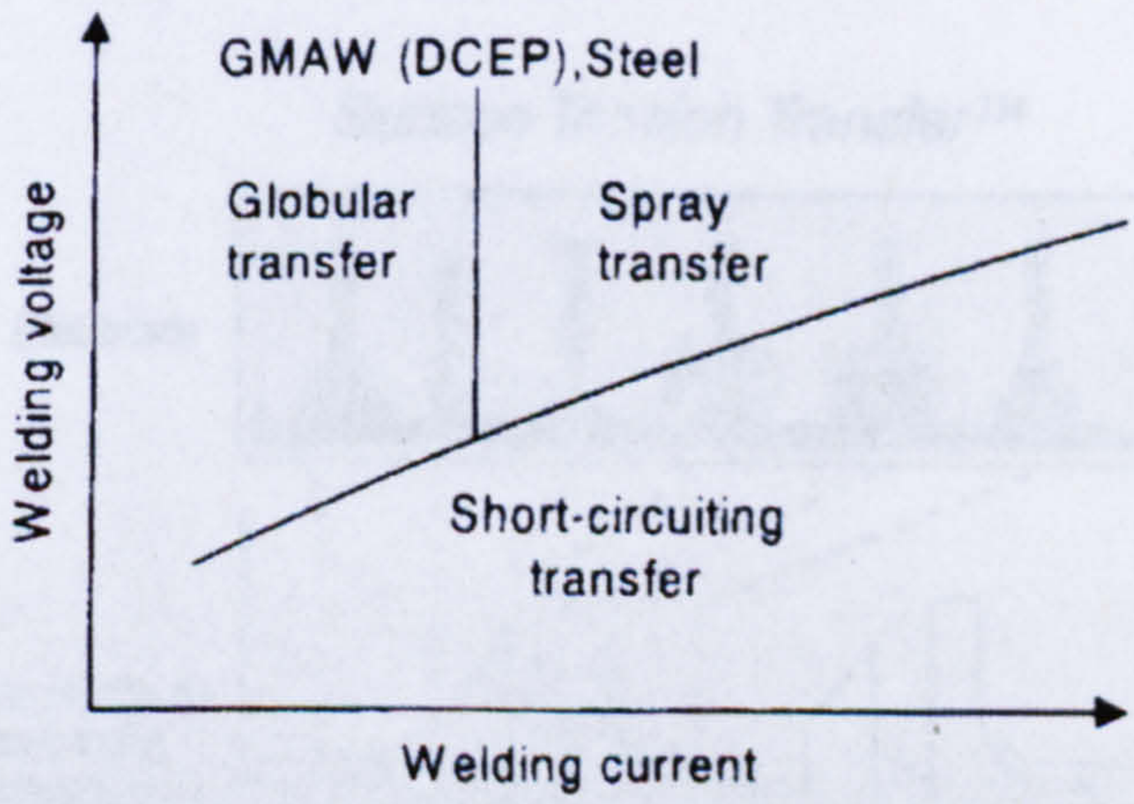

Figure 2-20: Relationship between current and voltage in GMAW (after ref. 96)

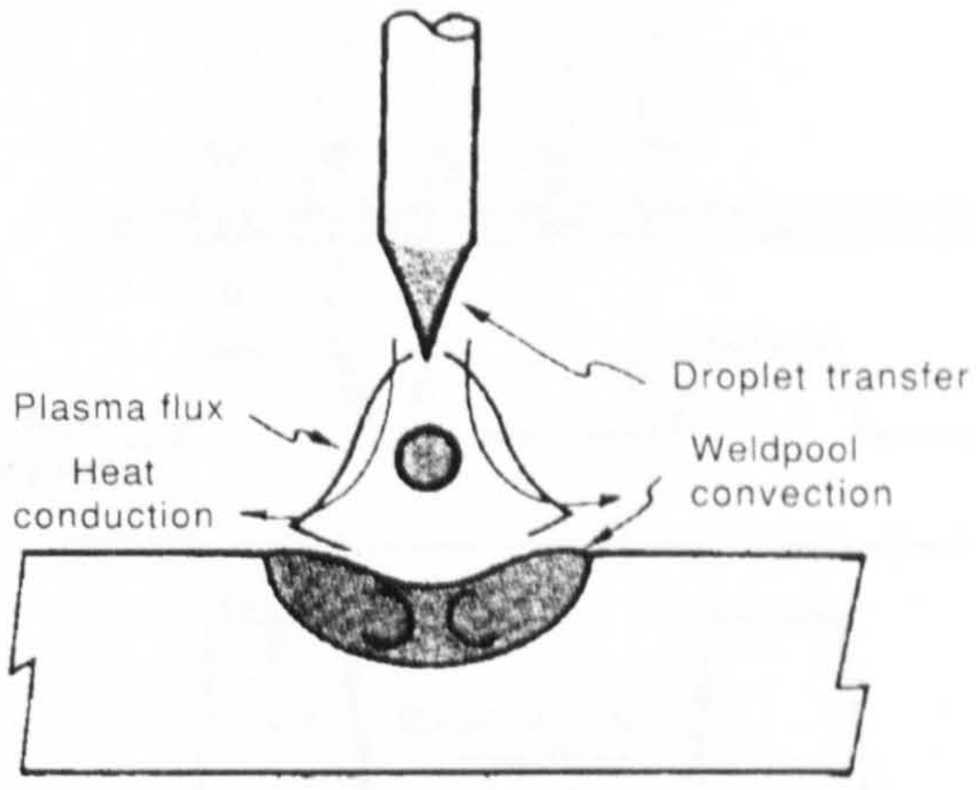

Figure 2-21: Heat transport and flow phenomena in arc welding (after ref. 96)

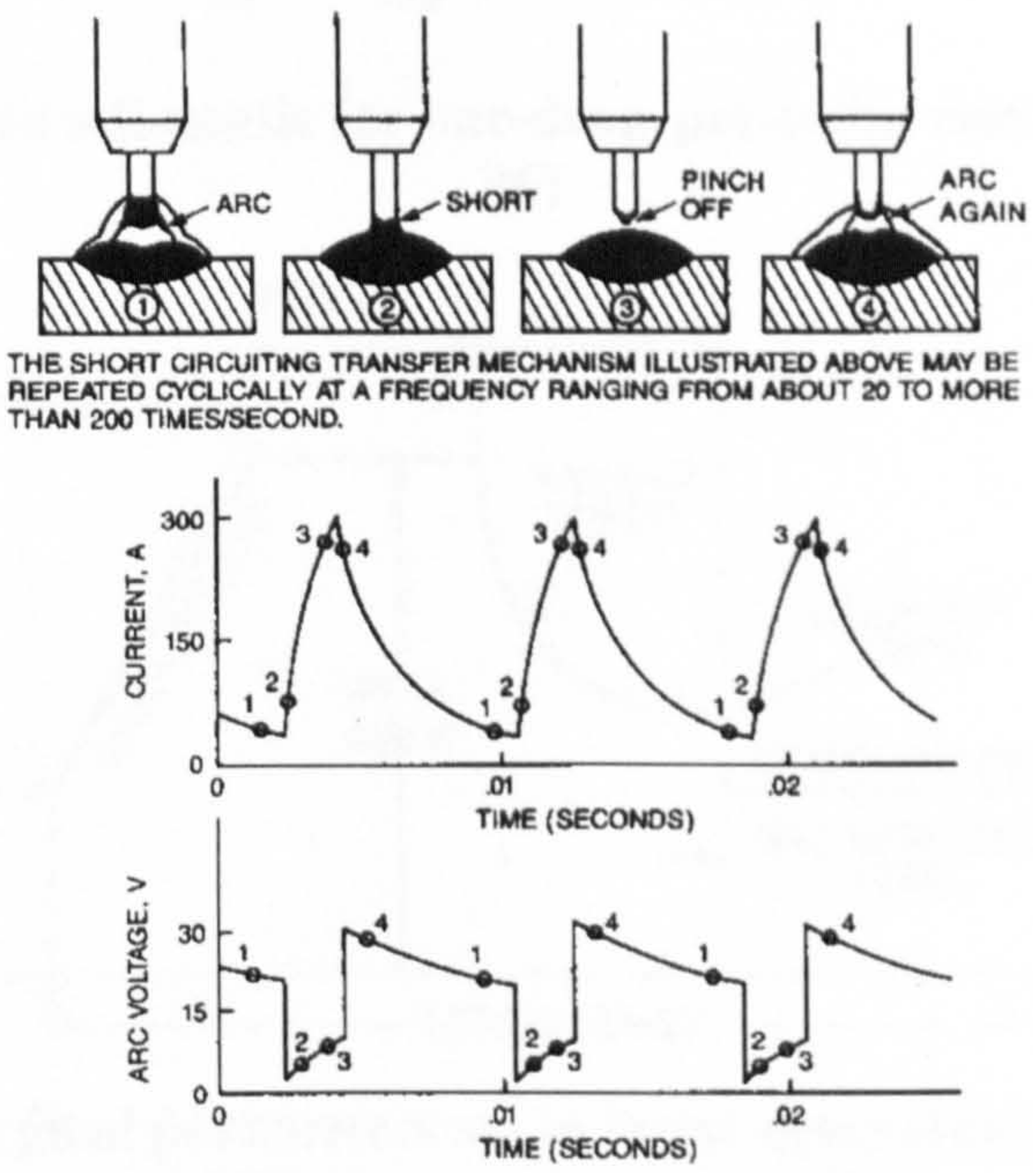

Figure 2-22: Schematic of short-circuit ('dip' transfer) GMAW (after ref. 94)

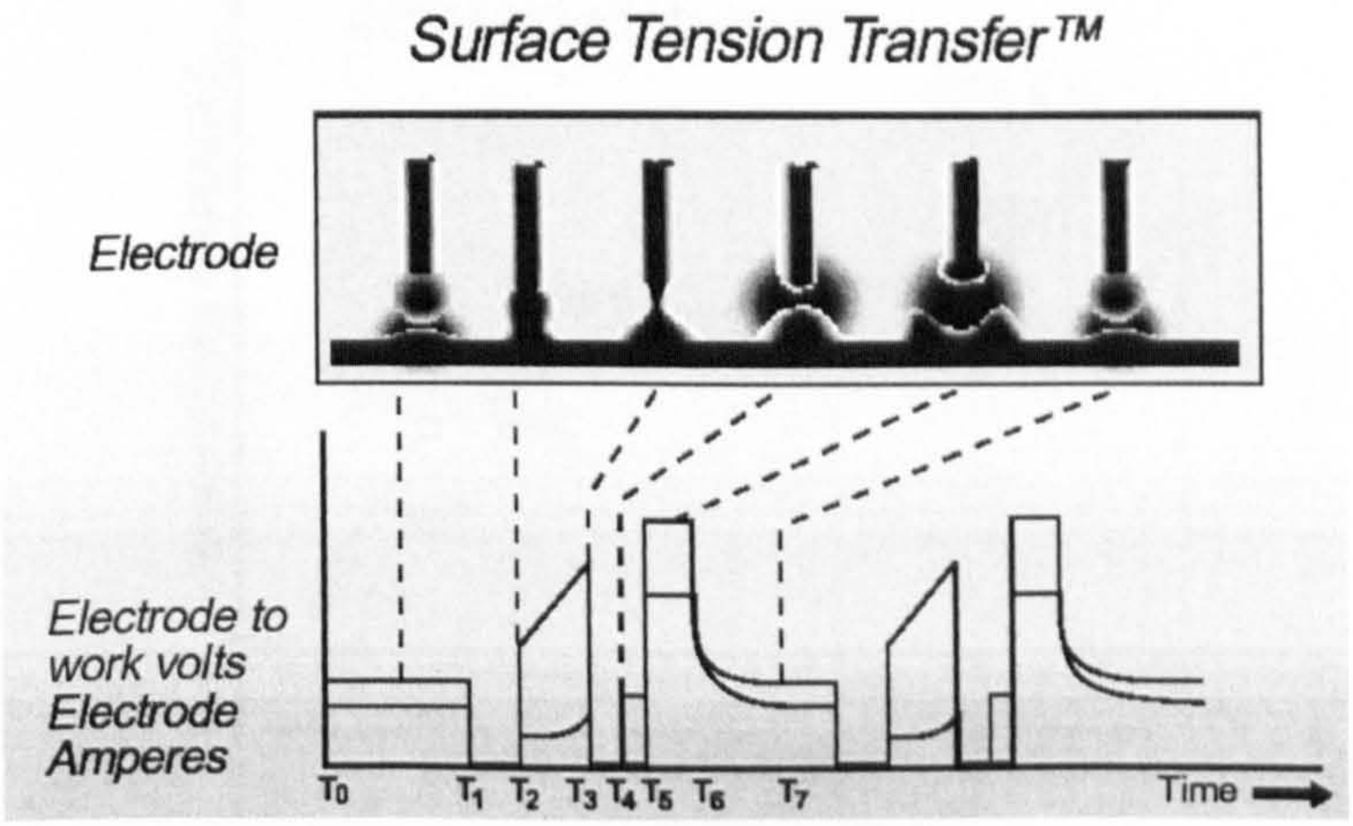

Figure 2-23: Controlled dip transfer (after ref. 87)

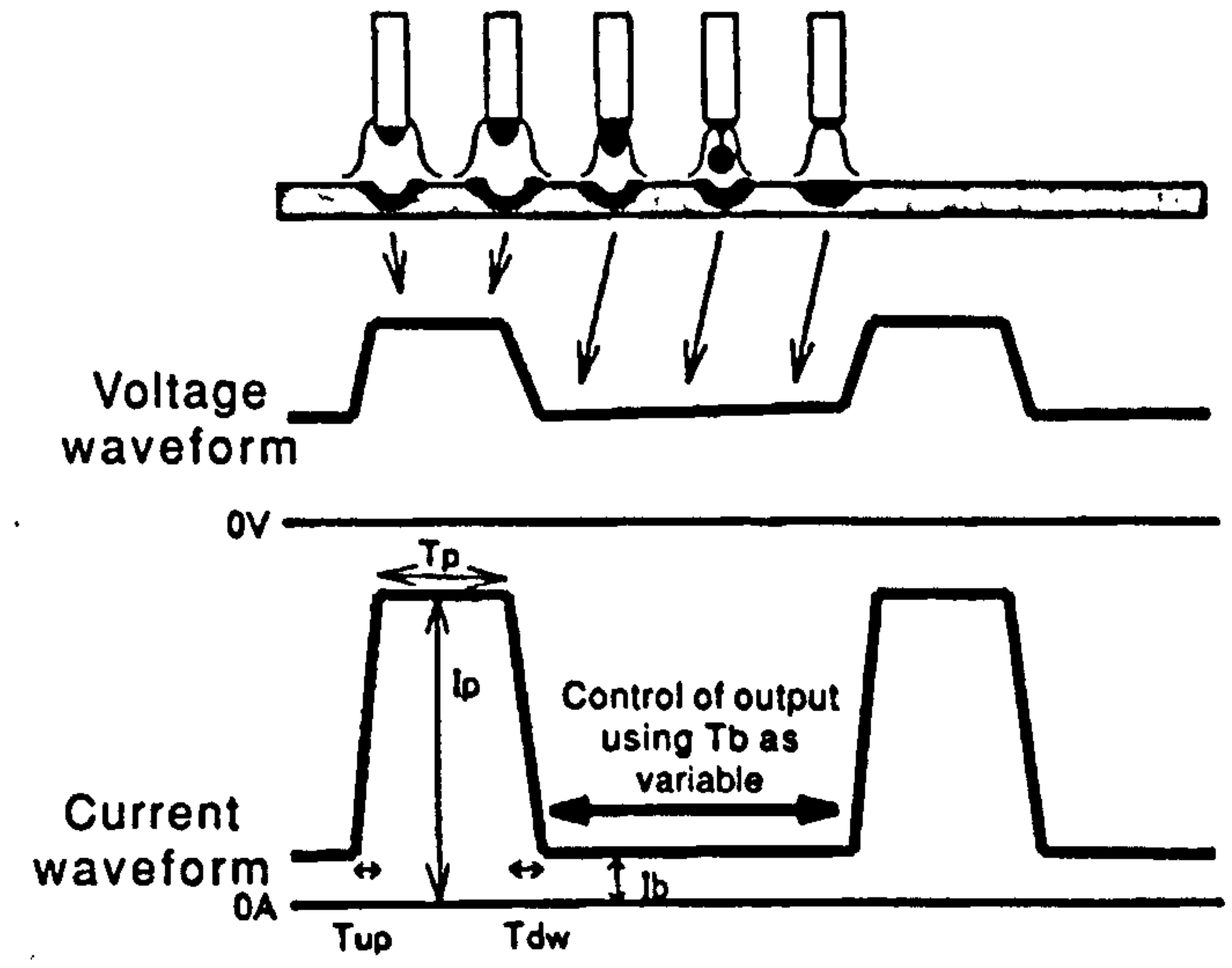

Figure 2-24: Idealised schematic for one-drop-per-pulse metal transfer (after ref. 96)

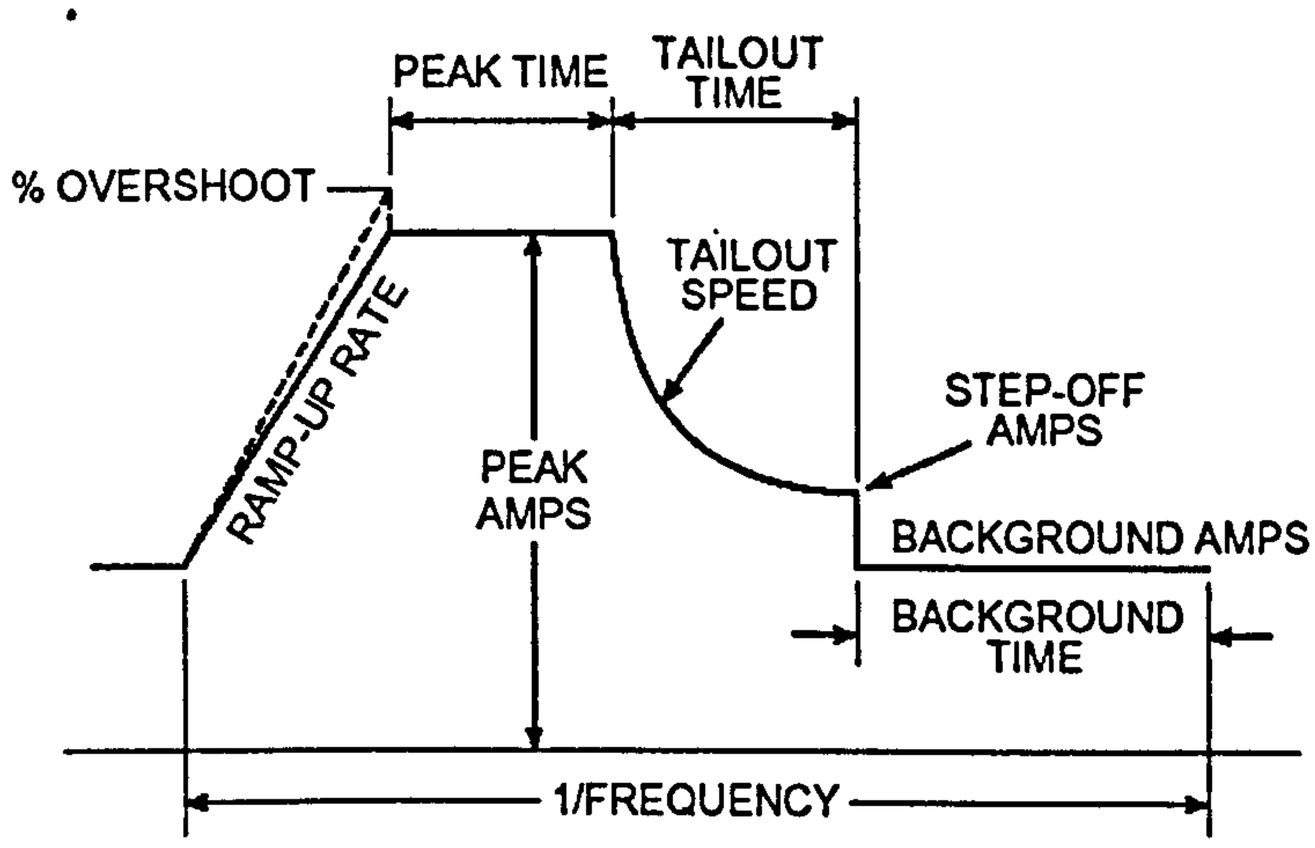

Figure 2-25: Typical parameters set in latest generation pulse waveform development (after ref. 87)

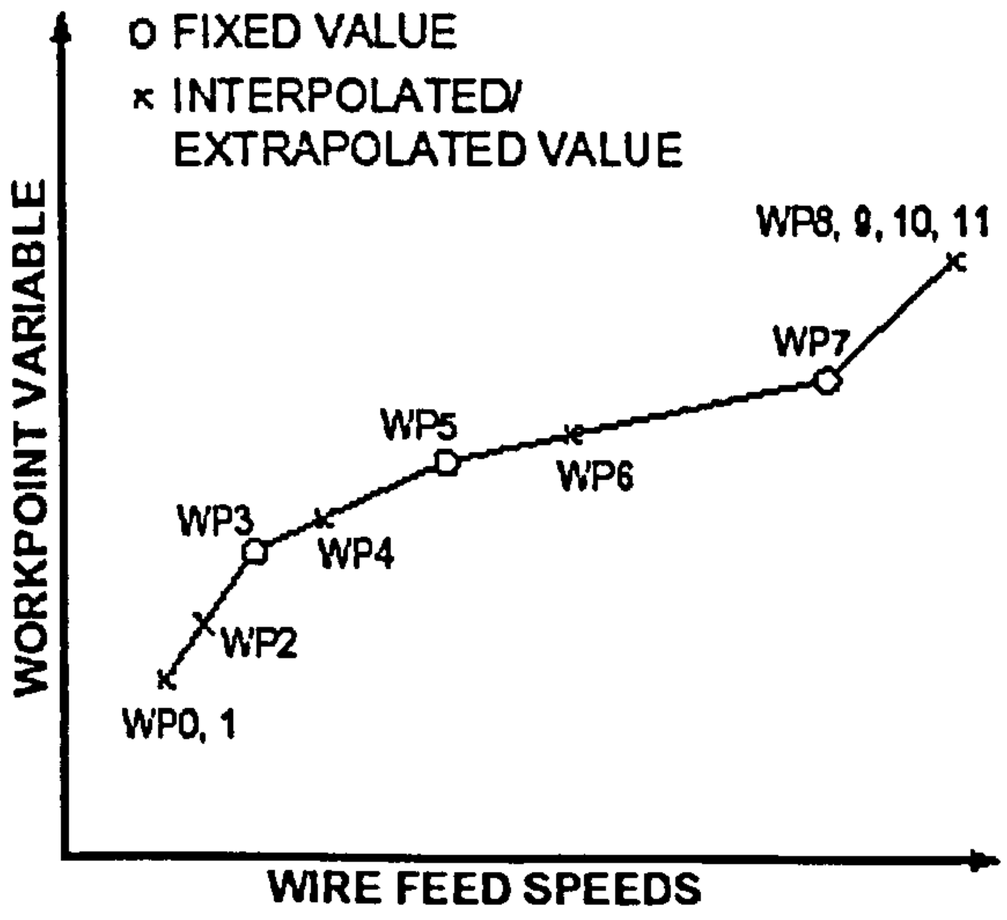

Figure 2-26: Example of synergic curve development (after ref. 87)

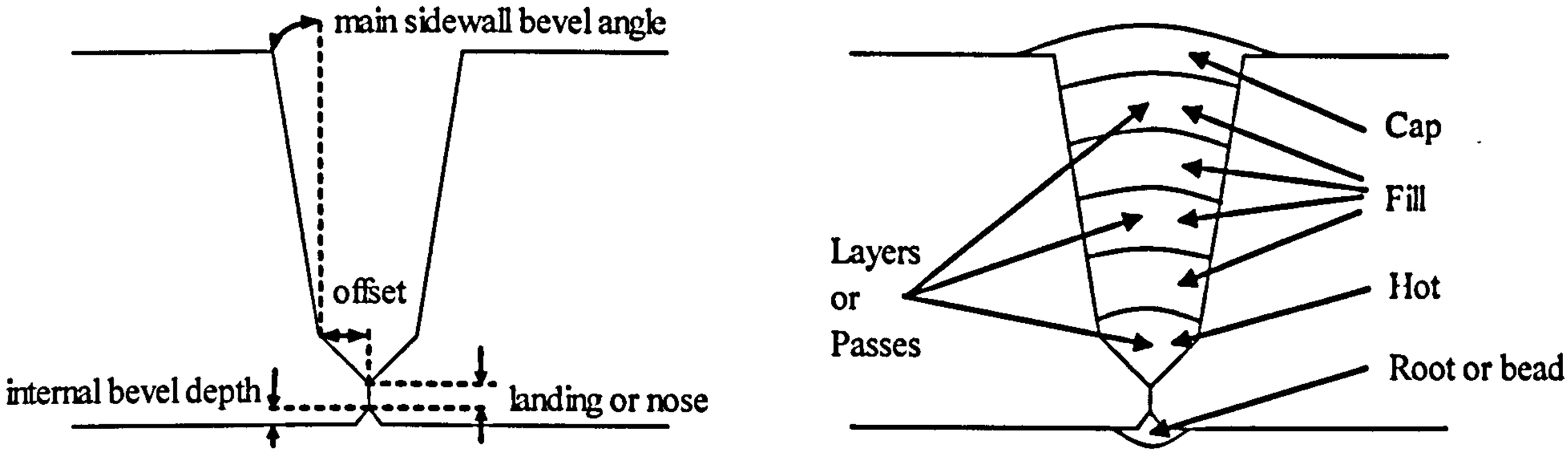

Figure 2-27: Typical joint geometry terminology

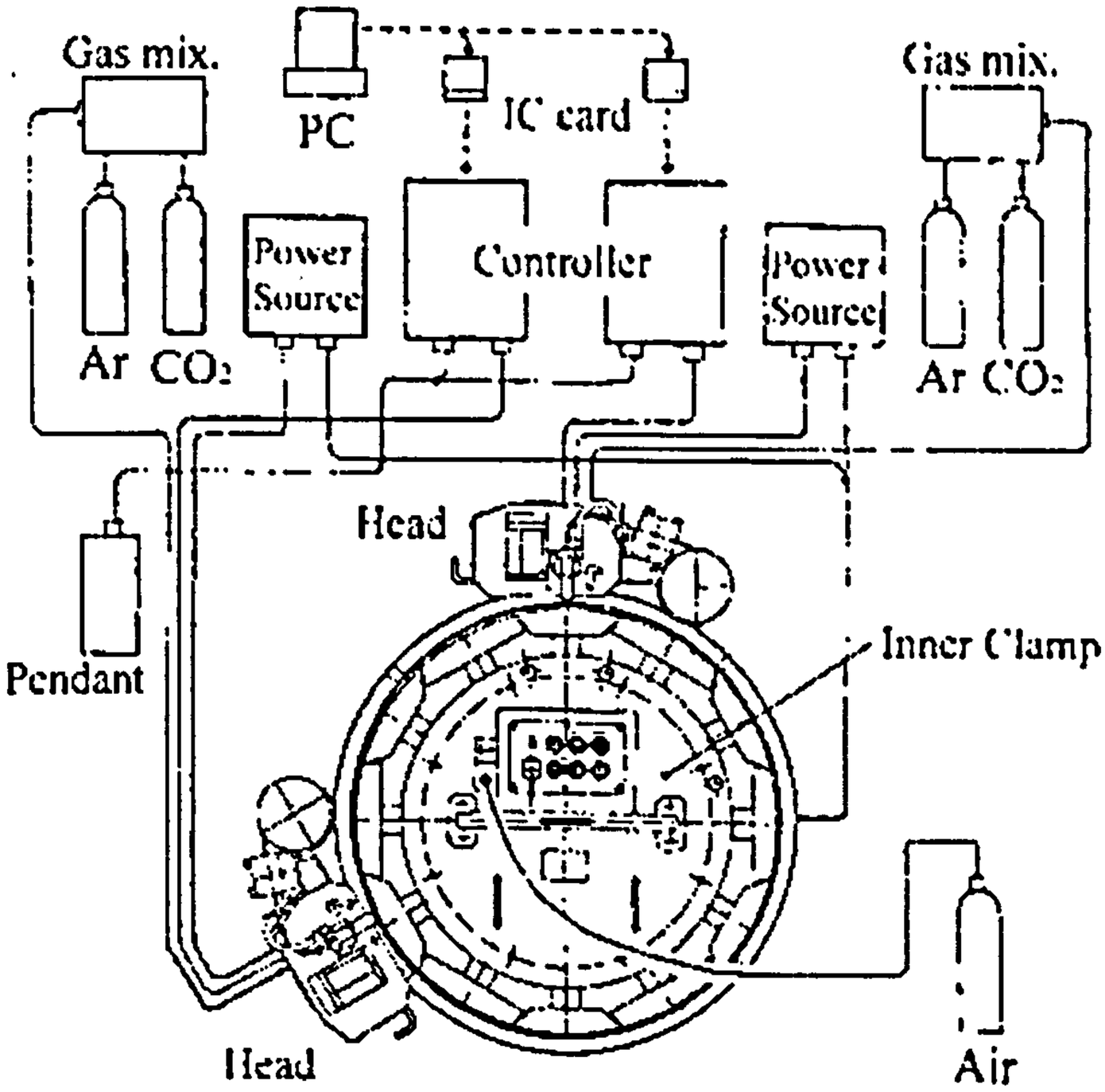

Figure 2-28: Typical mechanised main line pipewelding system showing an internal clamp and external welding bugs (after ref. 105)

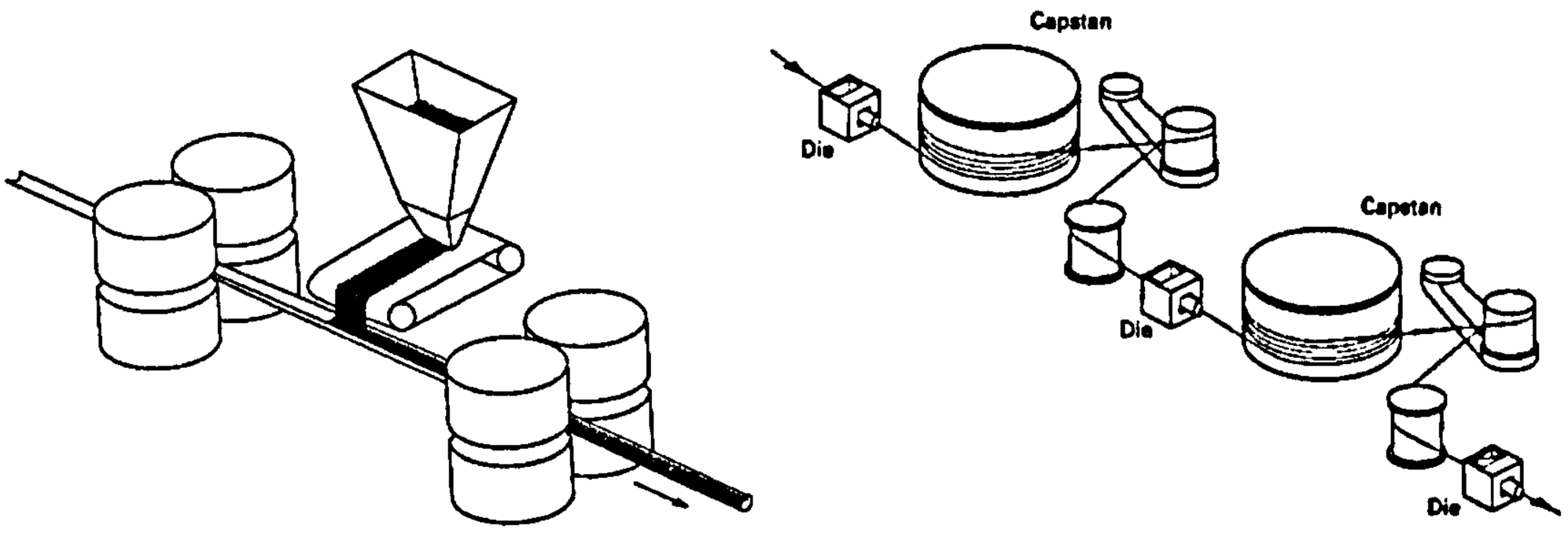

Figure 2-29: 'Form, fill and draw' route for tubular wire production (after ref. 110)

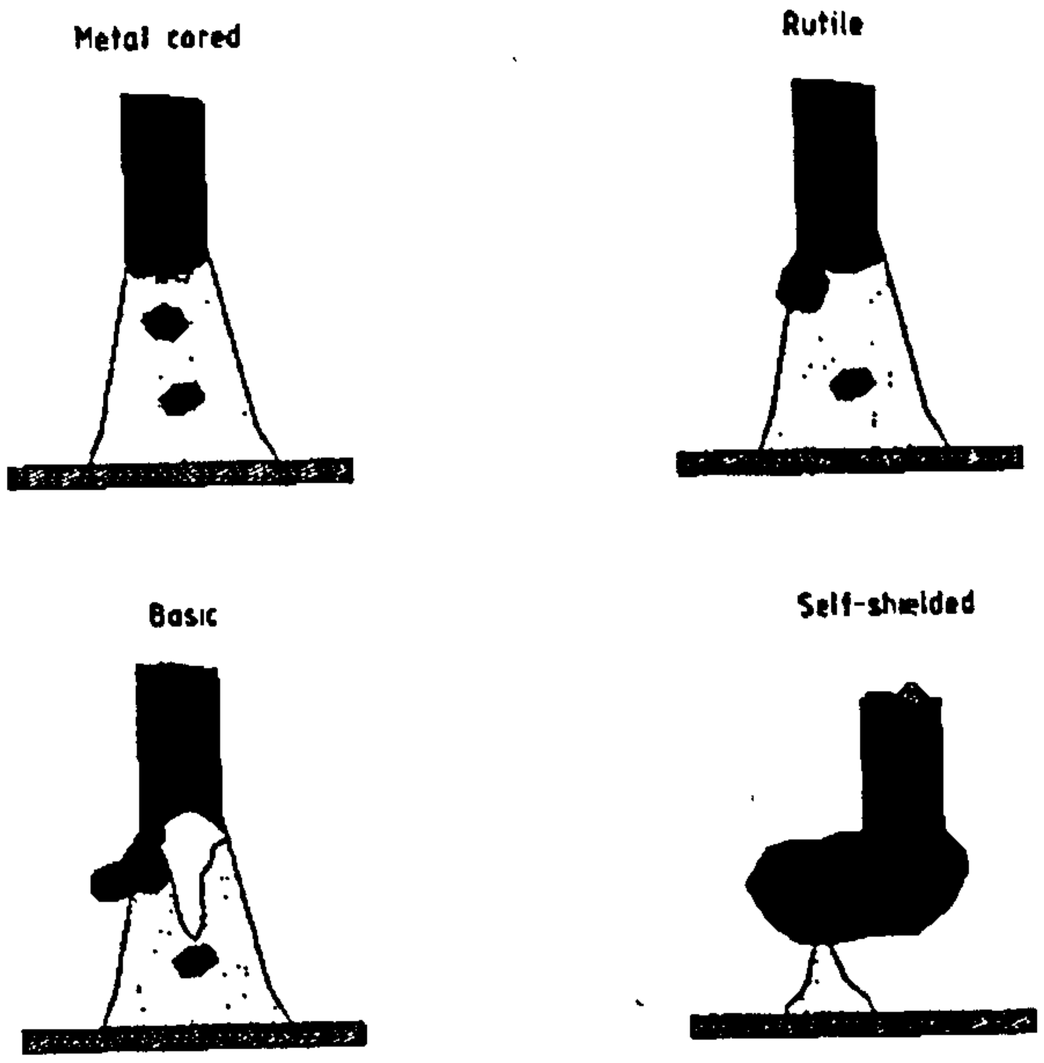

Figure 2-30: Transfer characteristics of various tubular wires (after ref. 95)

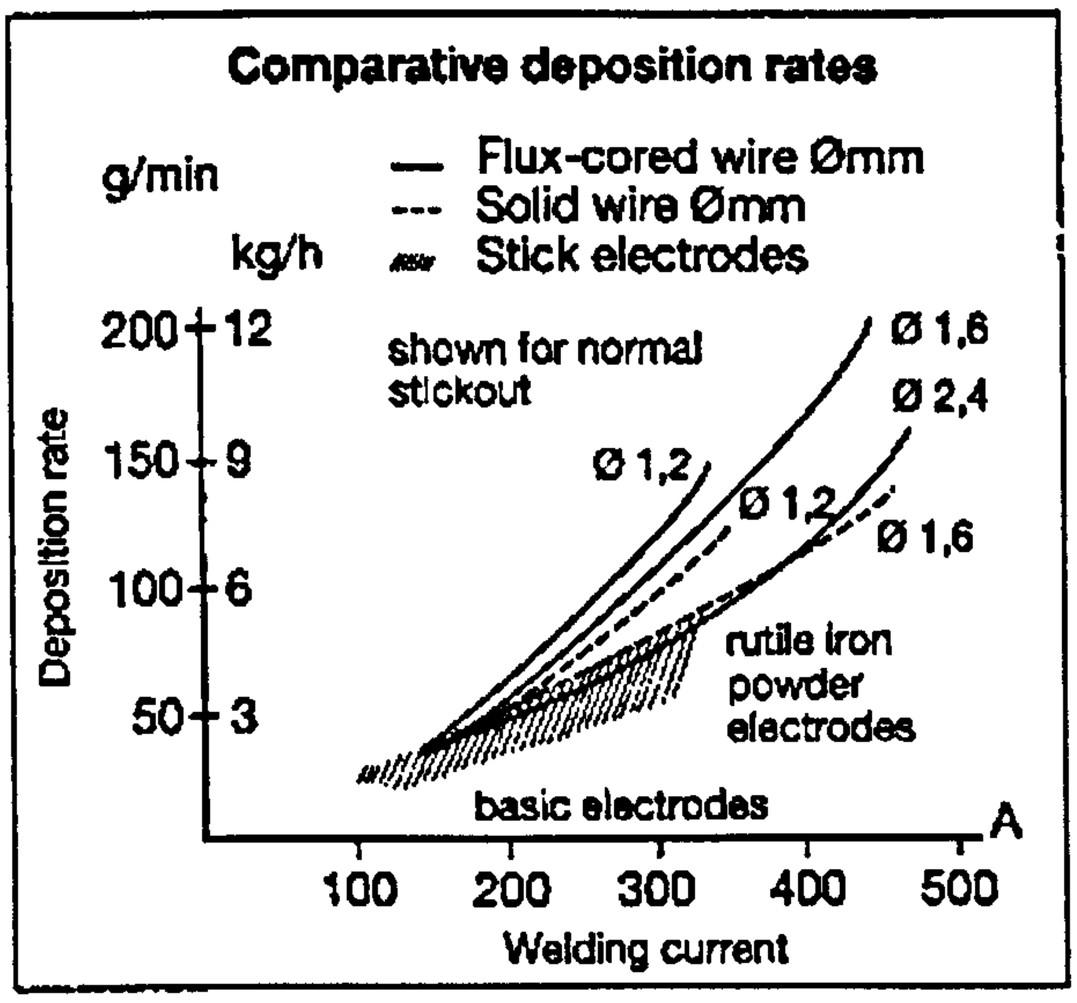

Figure 2-31: Deposition rate data comparison for solid versus tubular wires (after ref. 112)

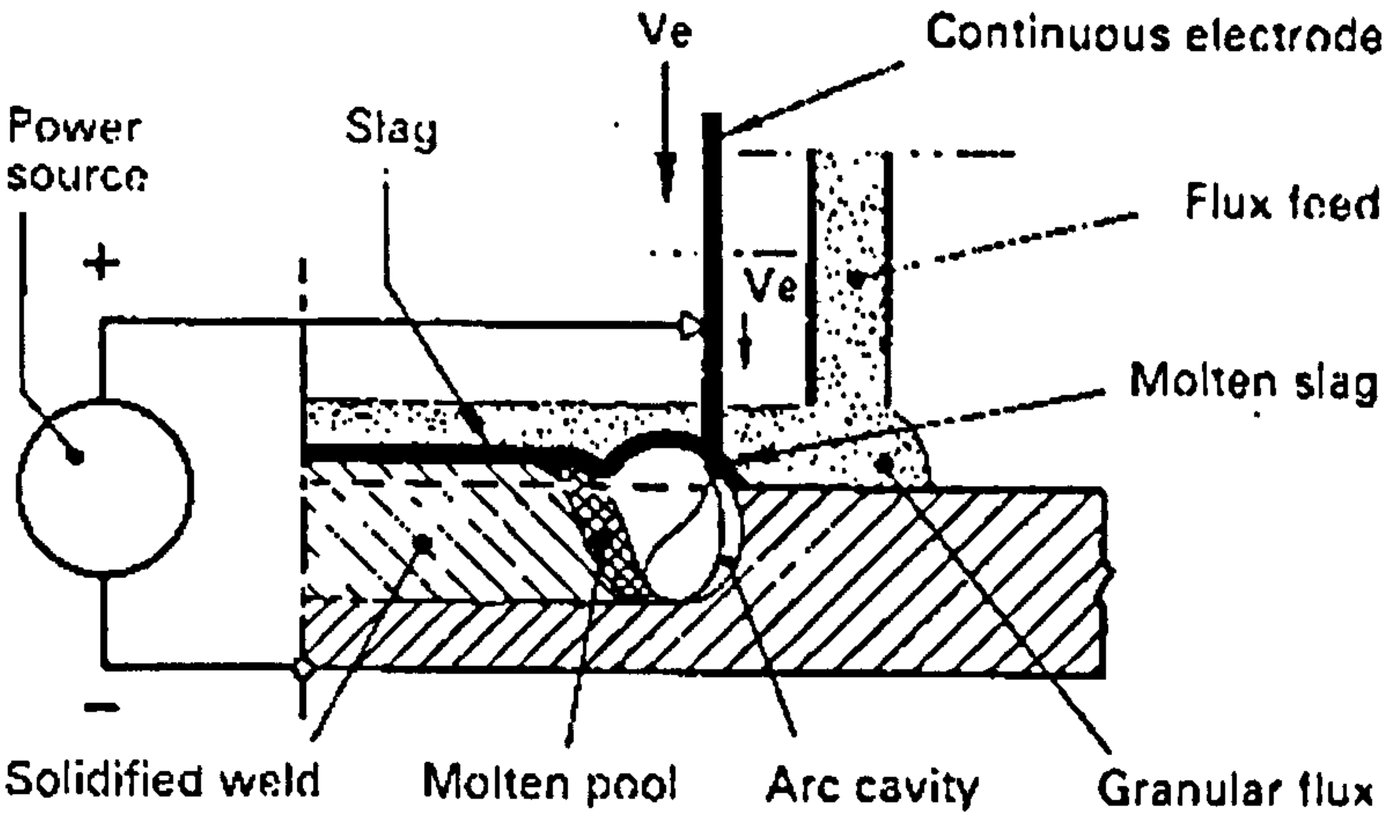

Figure 2-32: Submerged arc welding (after ref. 113)

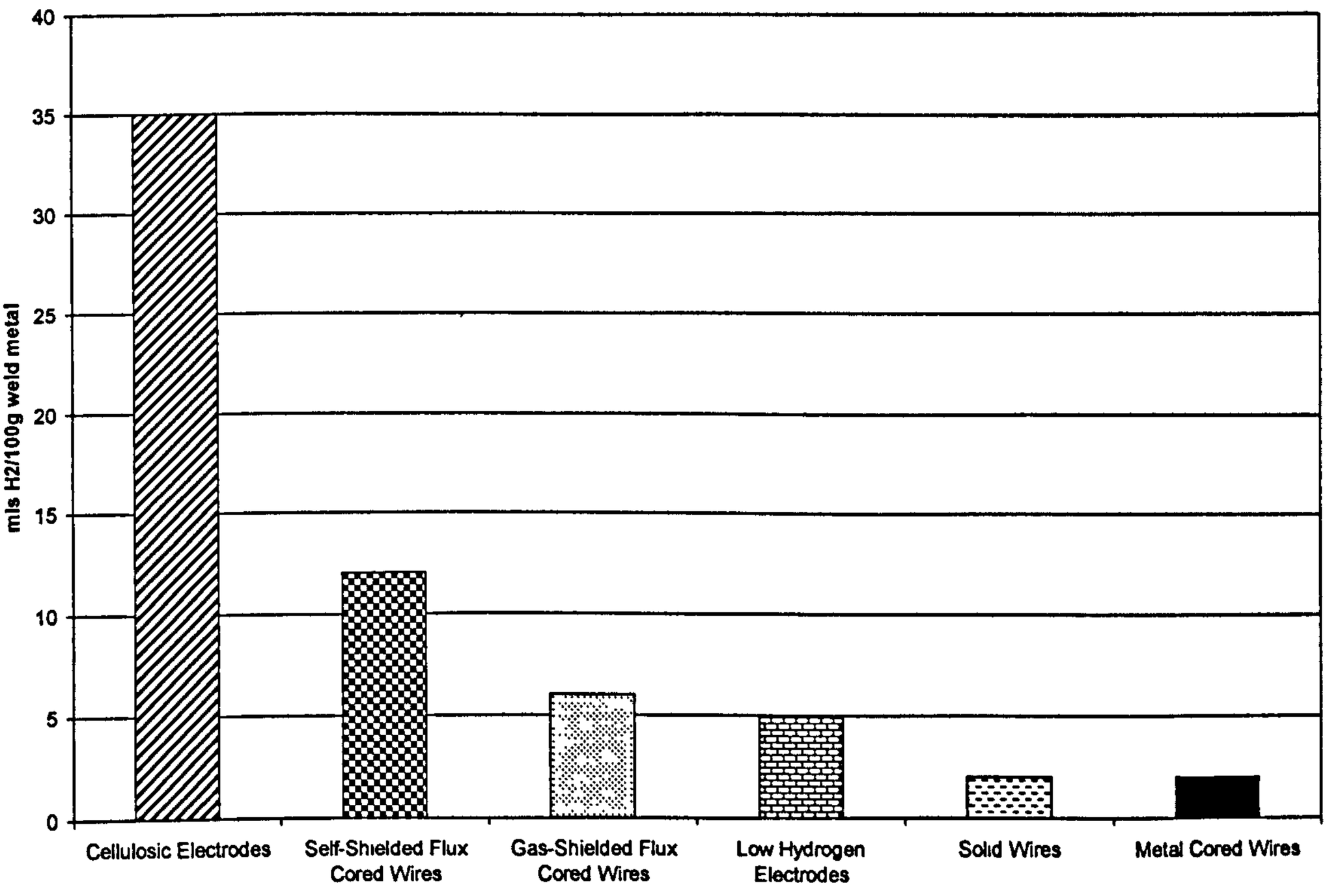

Figure 2-33: Typical diffusible weld metal hydrogen contents of different consumable types (after ref 118)

Contractor (System name)	CRC-Evance	H.C.Price McDermott	Serimer (Saturn)	Saipem (Passo)
Groove Shape	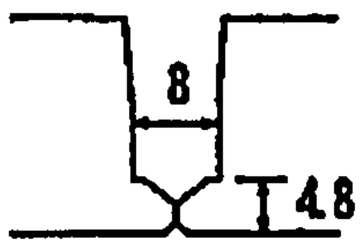	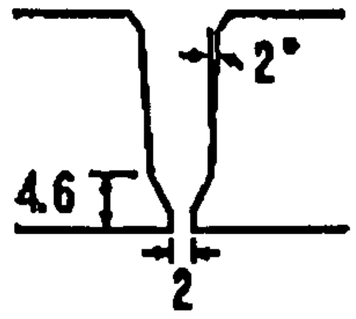	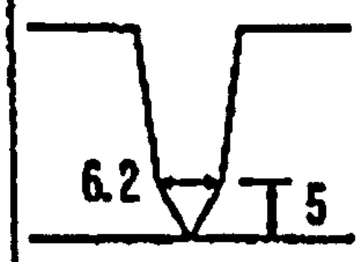	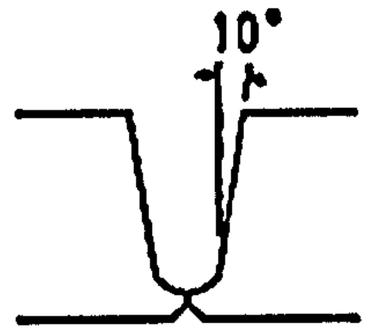
System Composition	1 External welding bugs (2sets) 2 4-6 torches Internal welding unit with a clamp 3 End facing machine	1 External 4-torch welding unit with 2 fixed frame 2 Internal clamp with a copper back up ring 3 same as left	1 same as left 2 same as left 3 same as left	1 External welding bugs (2sets) 2 same as left 3 same as left
Welding Process	1 Inside root pass welding 2 Outside narrow gap multi pass welding 3 Torch weaving (2-3Hz) 4 0.9mm wire 5 R : 75%Ar+25%CO_2 F&C : 100%CO_2	1 none 2 Outside narrow gap one side multi pass weld. 3 same as left 4 same as left 5 50%Ar+50%CO_2	1 none 2 same as left 3 same as left 4 1.0mm wire 5 same as left	1 none 2 same as left 3 same as left 4 same as left 5 100%CO_2 or Ar-CO_2 mixed. gas
Application	1969	1975	1980	1977

Figure 2-34: Comparison of early mechanised narrow gap GMAW joint designs (after ref. 105)

a)

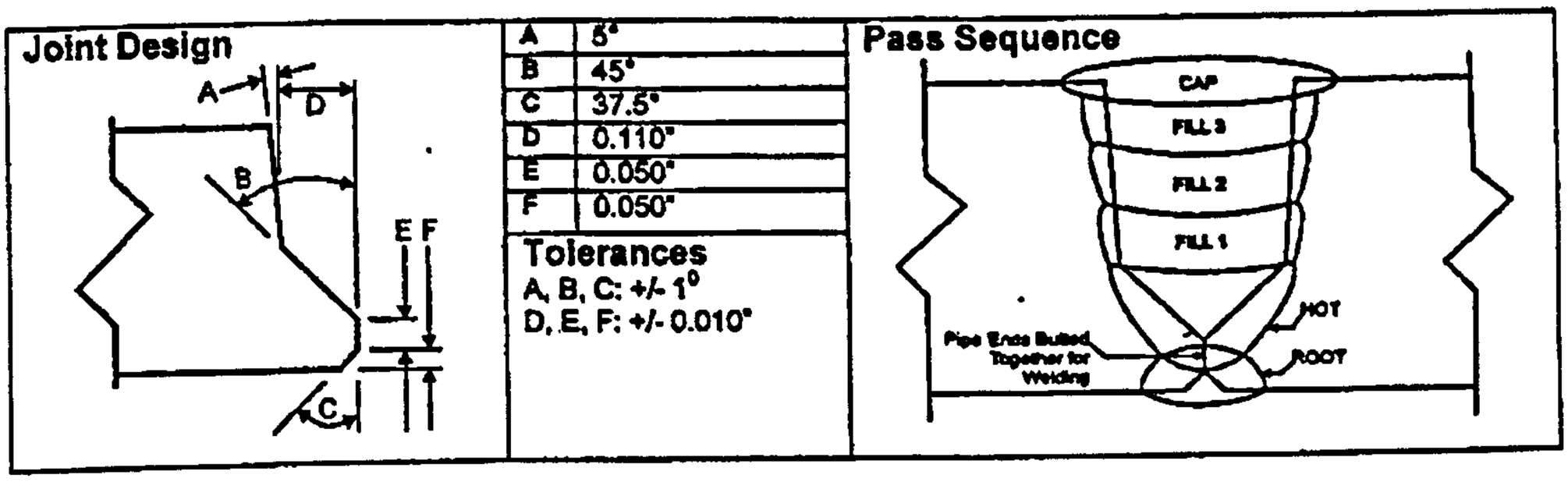

b)

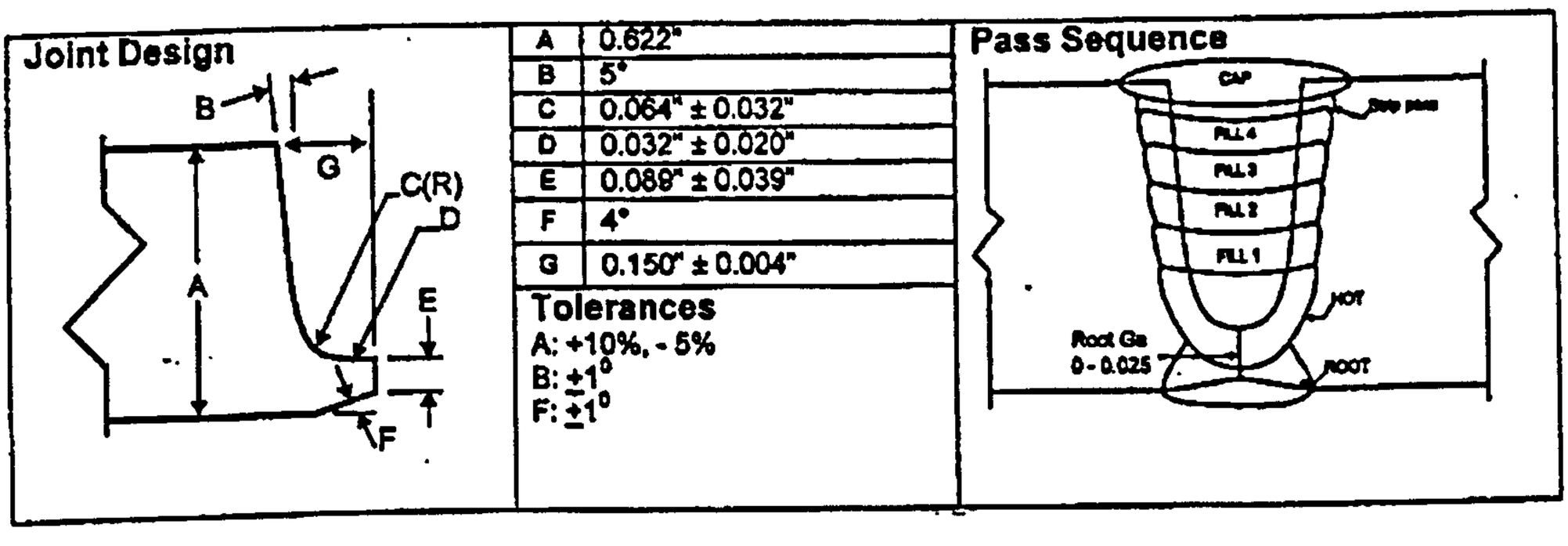

Figure 2-35: Current typical mechanised narrow gap GMAW joint designs a)CRC and RMS b) Serimer-Dasa (after ref. 126)

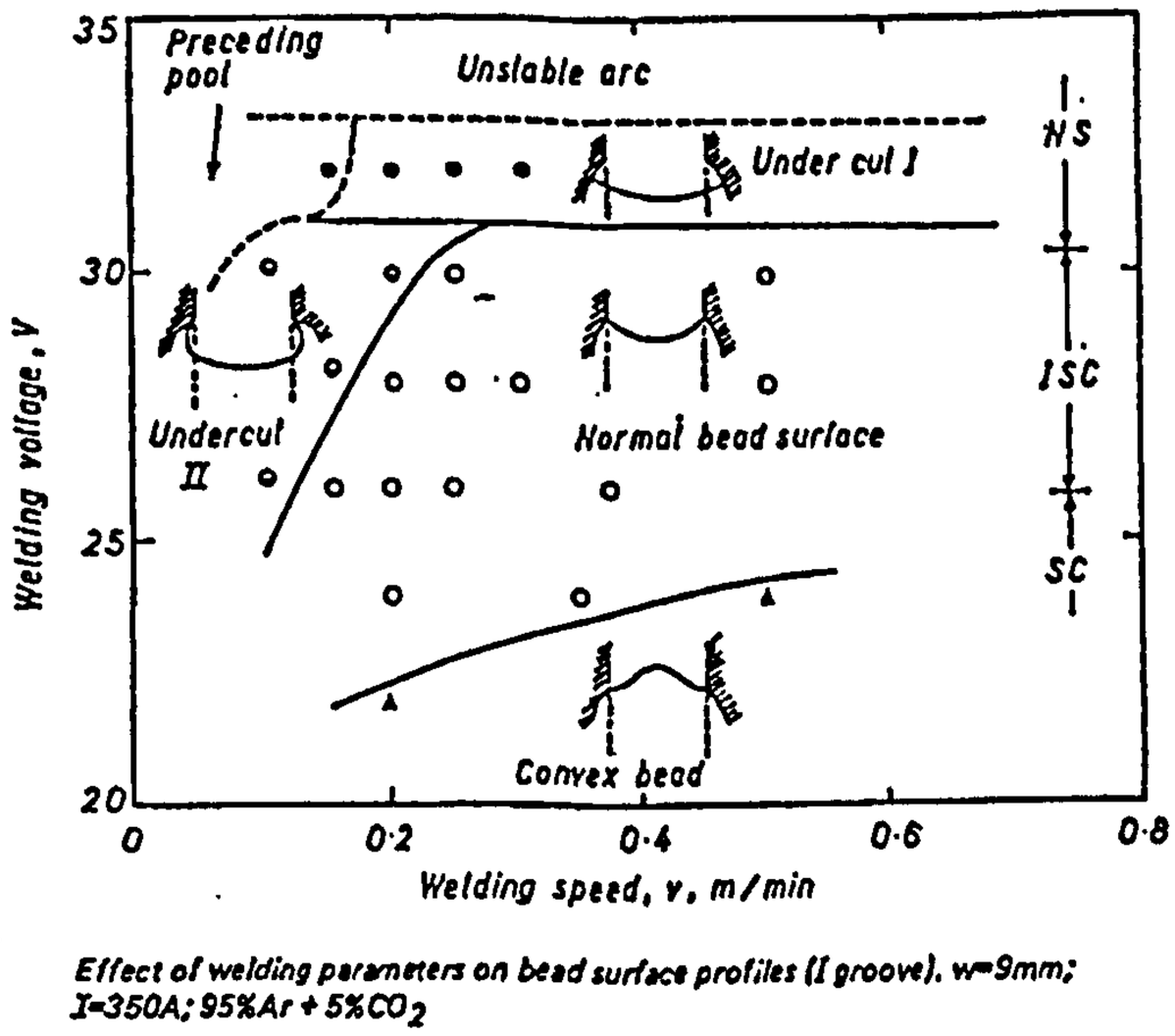

Effect of welding parameters on bead surface profiles (I groove). w=9mm; I=350A; 95%Ar + 5%CO_2

Figure 2-36: Effect of voltage and travel speed on a NGW bead profile (after ref. 135)

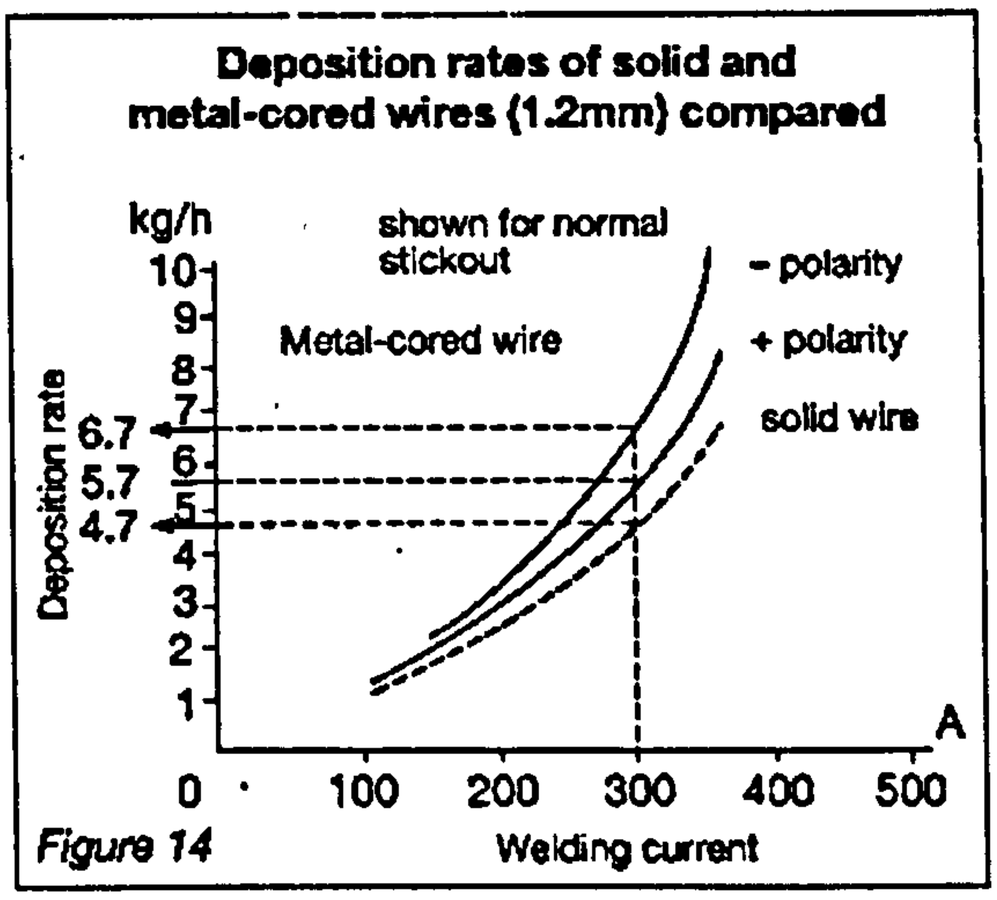

Figure 2-37: Comparison of deposition rates for 1.2mm dia. solid and metal cored wires (after ref. 112)

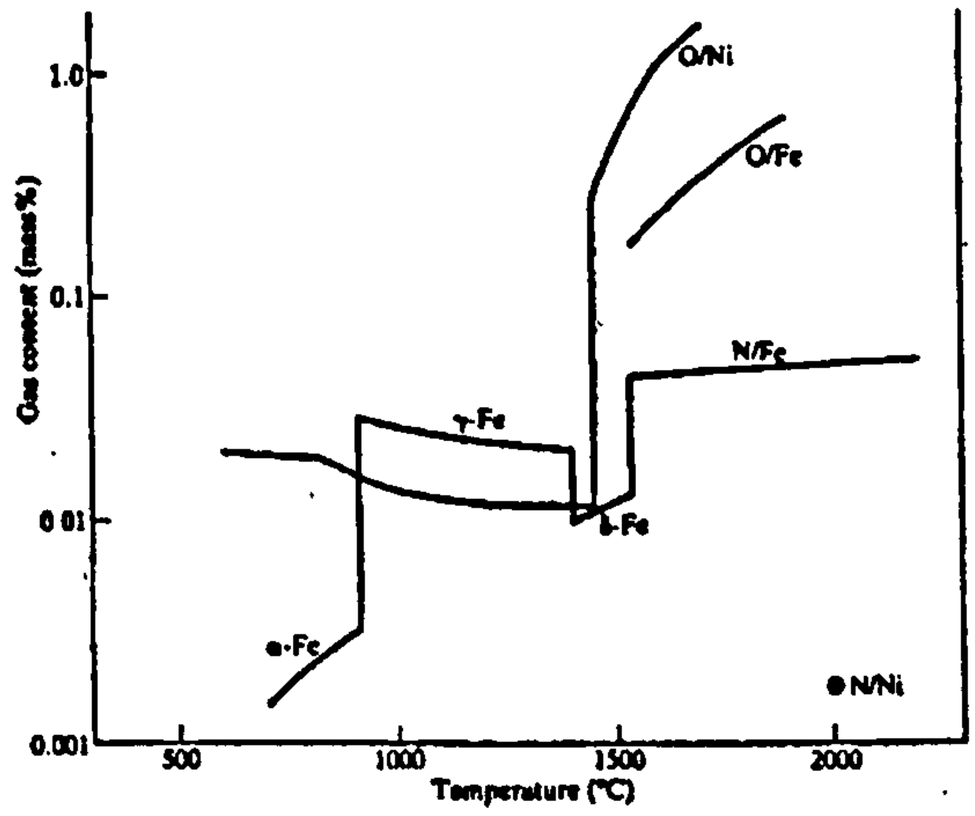

Figure 2-38: The equilibrium solubility of oxygen and nitrogen in iron and nickel at 1 atm pressure (after ref. 147)

SHIELDING GAS	KIND OF WELDING CURRENT		
	DIRECT CURRENT		ALTERNATING CURRENT
	ELECTRODE POSITIVE (DCEP)	ELECTRODE NEGATIVE (DCEN)	
100% ARGON	 ARC WANDERS, FINE SPRAY TRANSFER	 WILD ARC, POOR GLOBULAR TRANSFER	 ALTERNATING GLOBULAR AND SPRAY TRANSFER
98% ARGON 2% OXYGEN	 STIFF ARC, GOOD SPRAY TRANSFER	 FAIR SPRAY TRANSFER	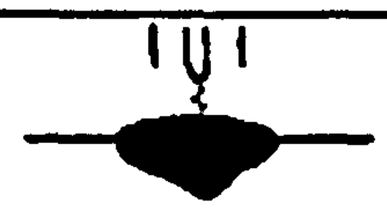 GOOD SPRAY TRANSFER IF ELECTRODE EMISSIVE COATED
100% HELIUM	 "HOT" ARC, GLOBULAR TRANSFER	 POOR GLOBULAR TRANSFER	
50% ARGON 50% HELIUM	 DEEP PENETRATION FAIR SPRAY TRANSFER	 GLOBULAR TRANSFER	
100% CARBON DIOXIDE	 GLOBULAR TRANSFER MUCH SPATTER		 SPRAY TRANSFER IF ELECTRODE EMISSIVE COATED
90% ARGON 10% CARBON DIOXIDE	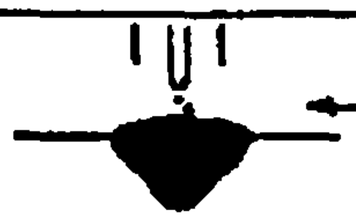 FINE GLOBULAR TRANSFER	← (SHORT-CIRCUITING TRANSFER CAN USE 75% Ar + 25% CO_2)	
100% CARBON DIOXIDE SHORT-CIRCUITING TRANSFER	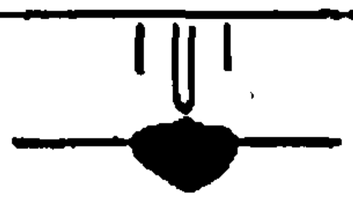 SEE FIG. 6.13		

Figure 2-39: Typical weld bead deposit shapes in GMAW for a variety of shielding gases and welding parameters (after ref. 94)

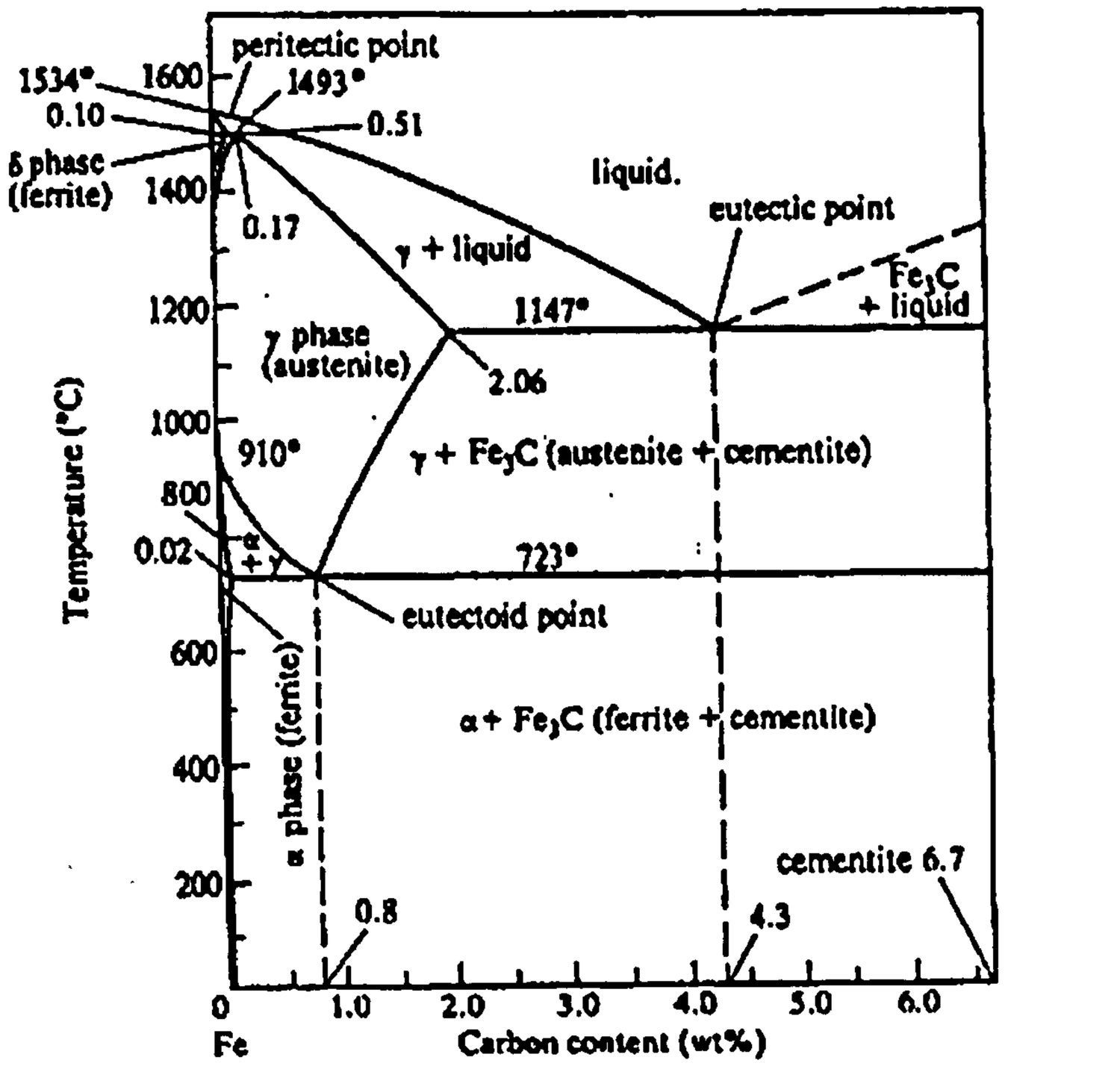

Figure 2-40: Iron/carbon phase transformation diagram (after ref. 166)

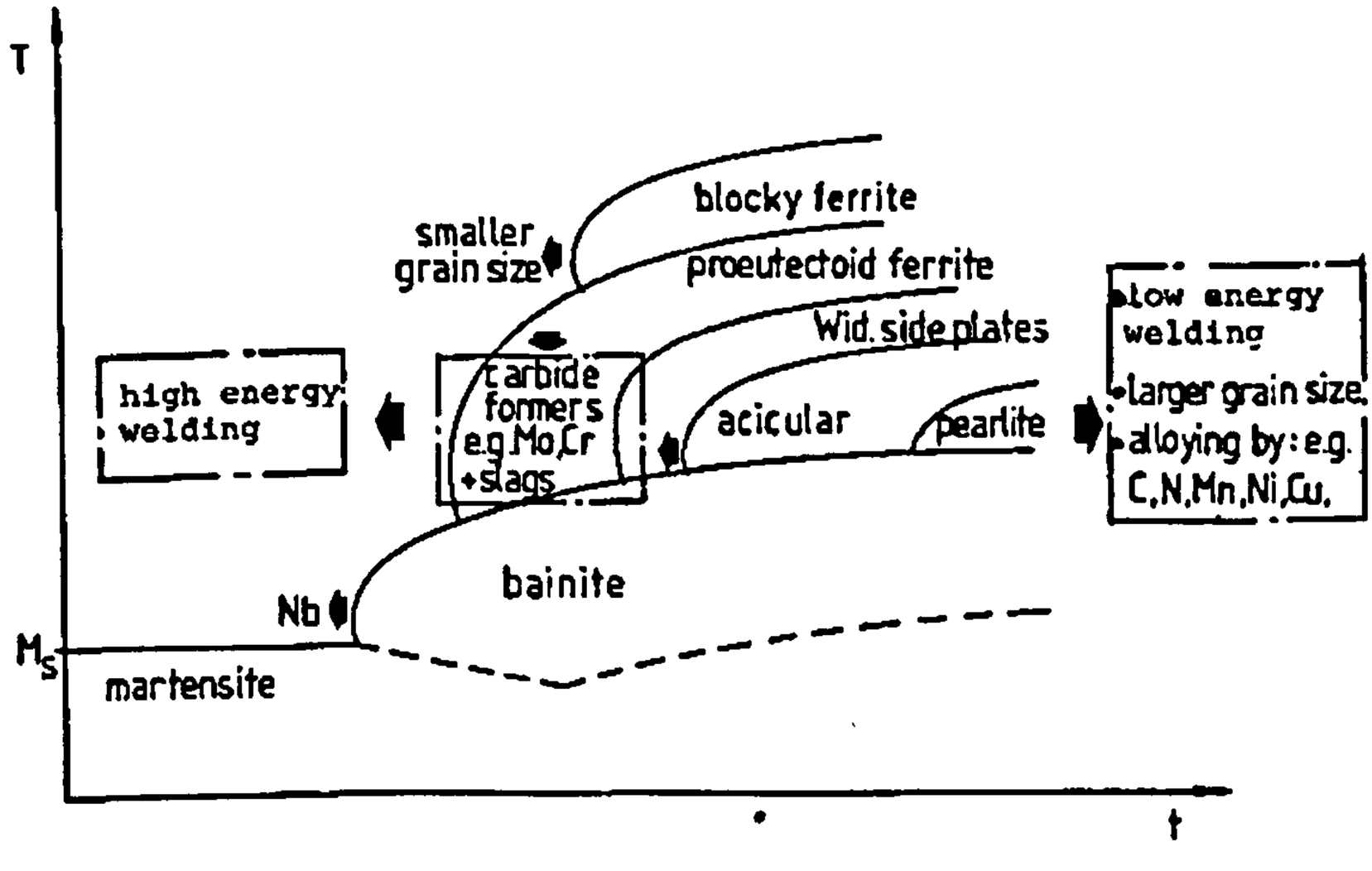

Figure 2-41: Schematic CCT diagram for steel weld metal (after ref. 177)

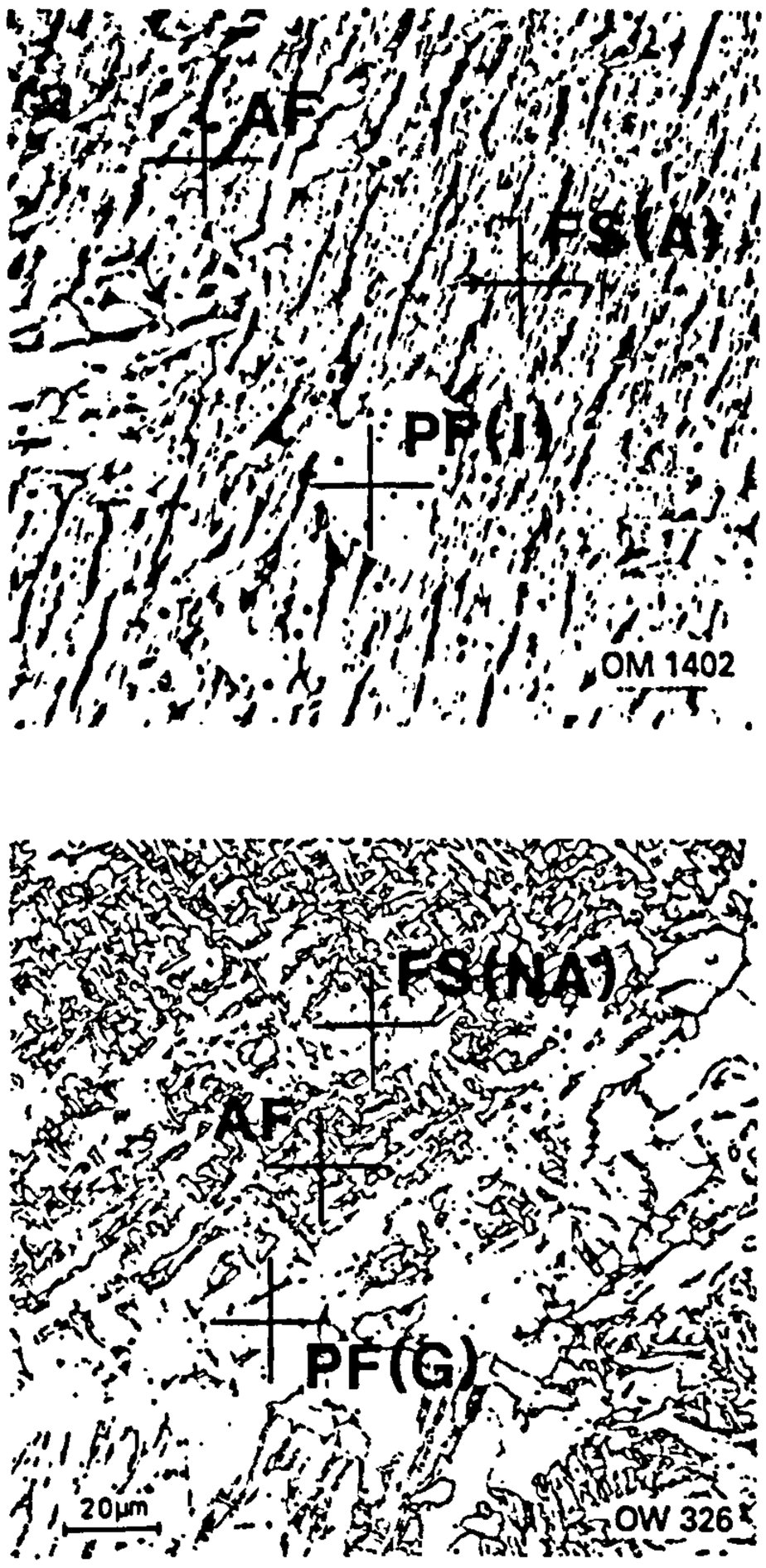

Figure 2-42: As deposited ferritic steel weld metal microstructures (after ref. 173)

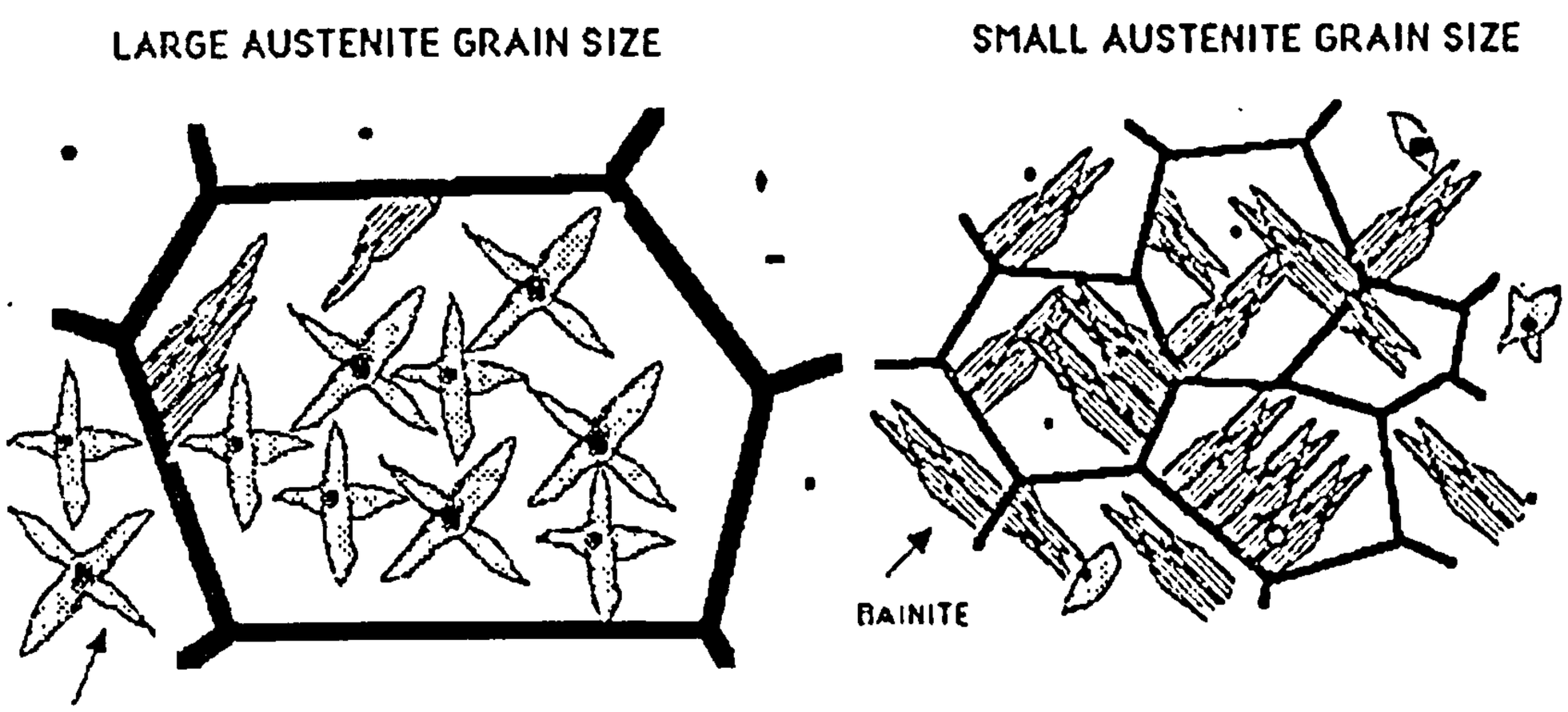

Figure 2-43: Effect of the austenite grain size on the production of an acicular ferrite or bainite microstructure(after ref. 174)

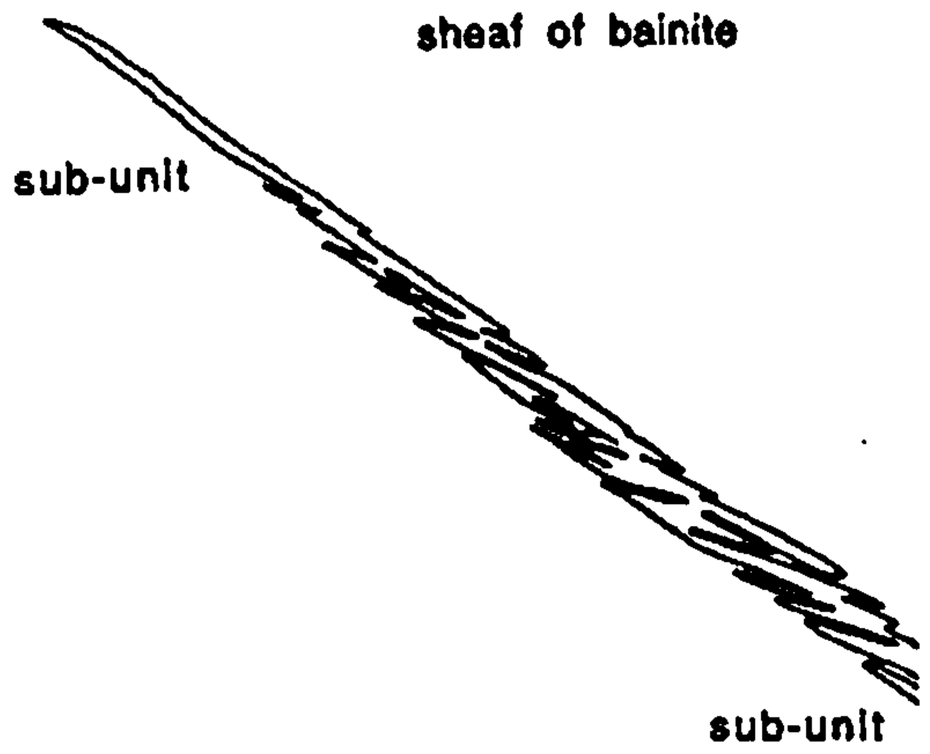

Figure 2-44: Schematic representation of a Bainite sheaf (after ref. 182)

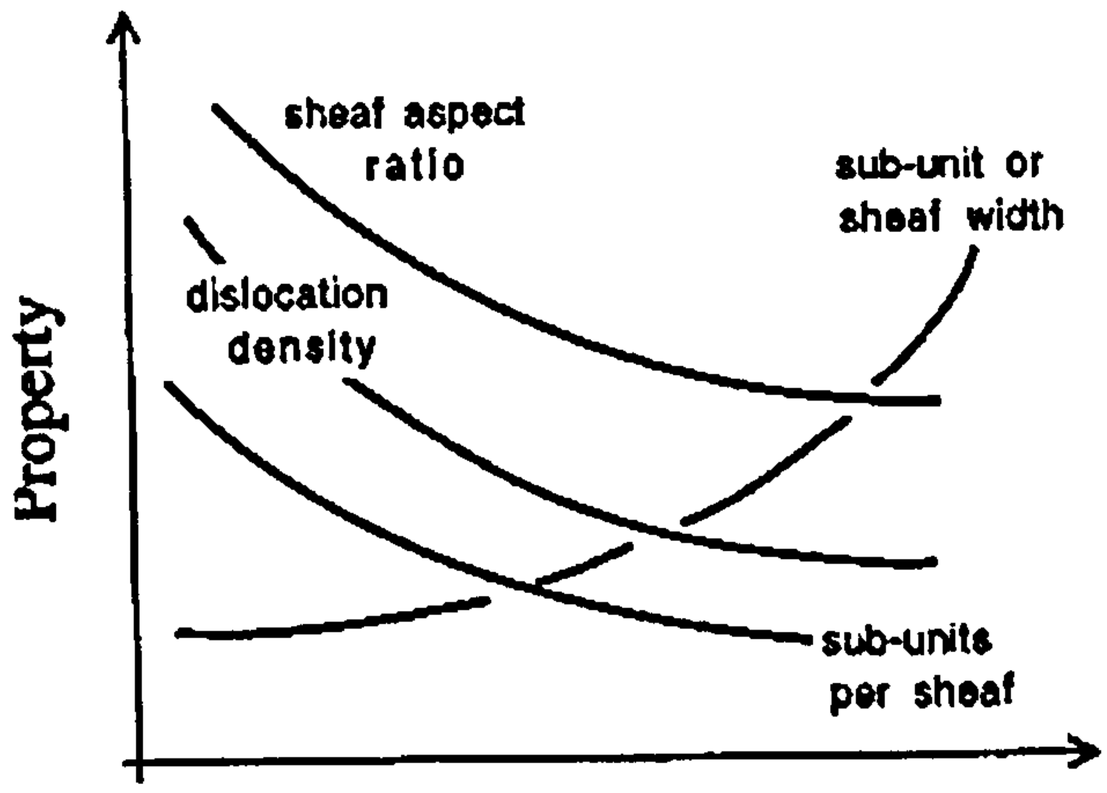

Figure 2-45: Qualitative trends in bainite microstructure as a function of transformation temperature (after ref. 186)

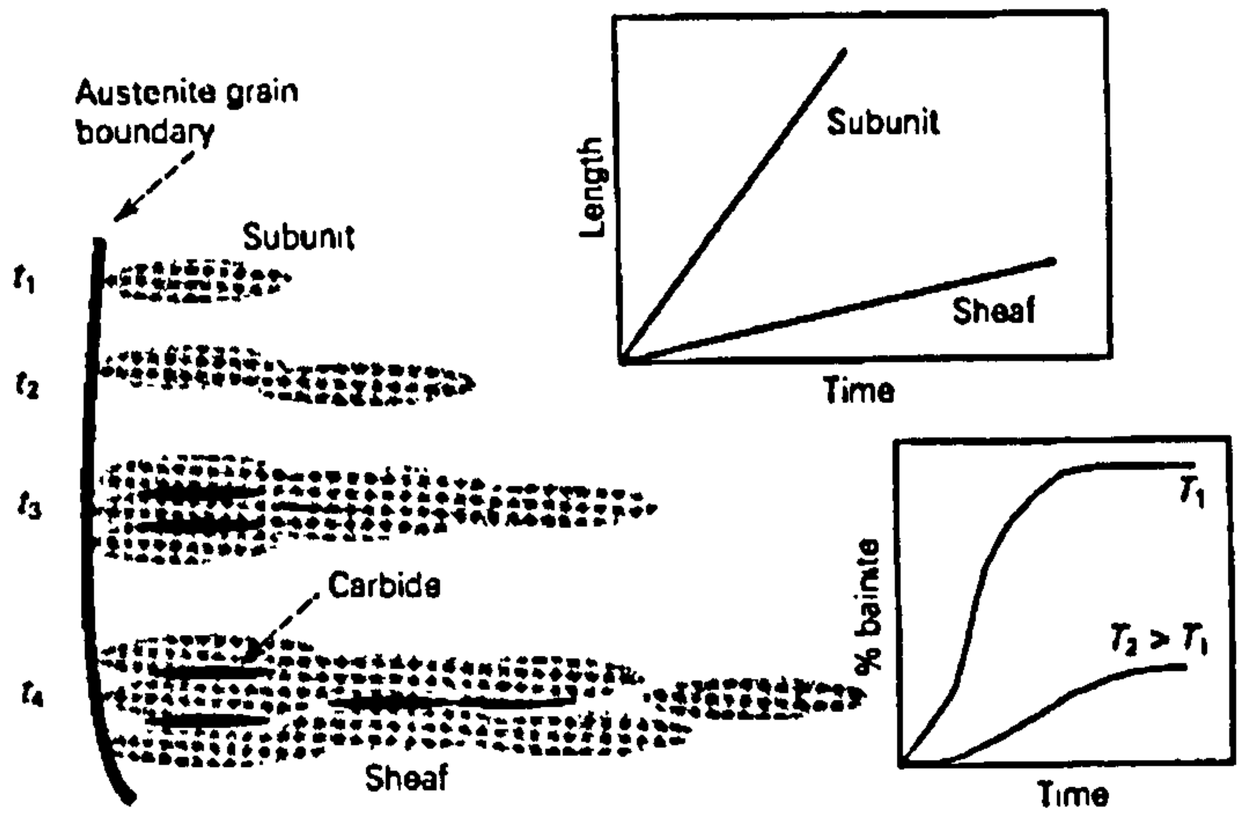

Figure 2-46: Schematic showing bainite growth mechanism (after ref. 185)

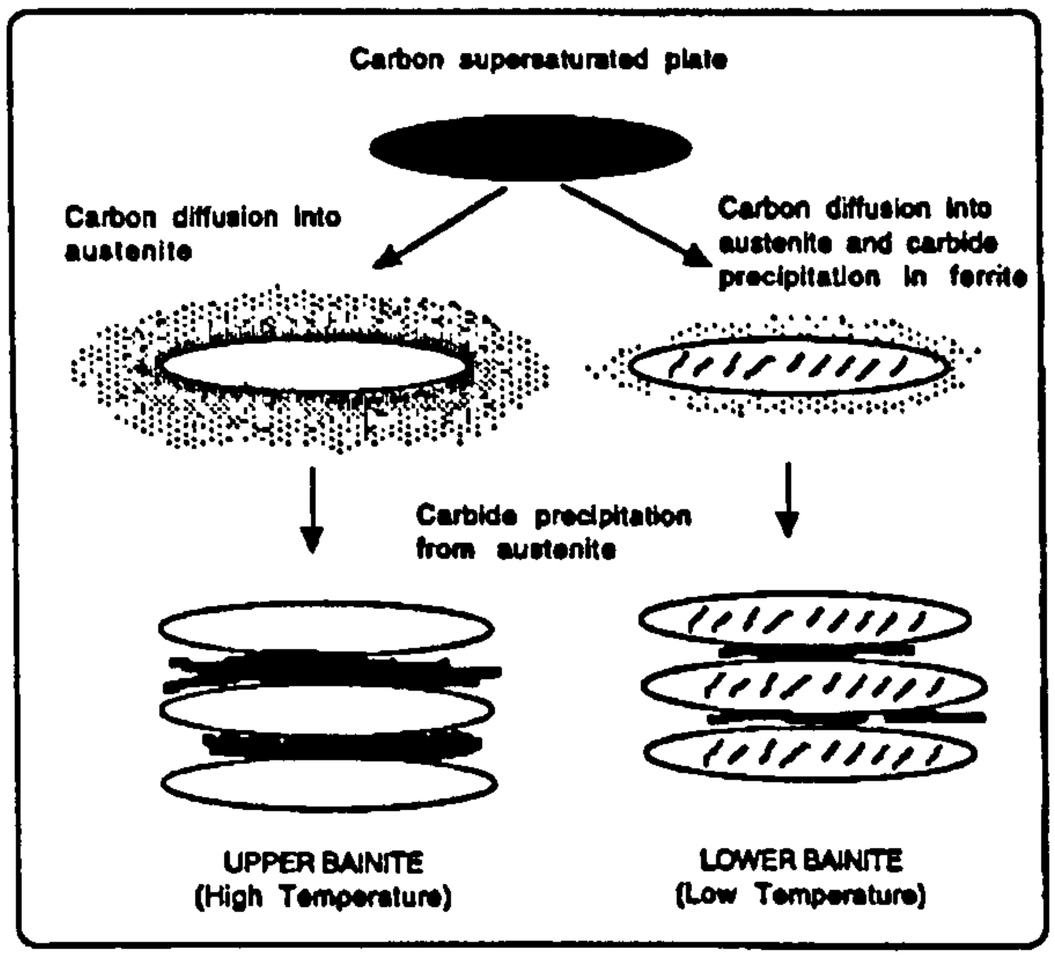

Figure 2-47: Formation of upper and lower bainite from austenite (after ref. 182)

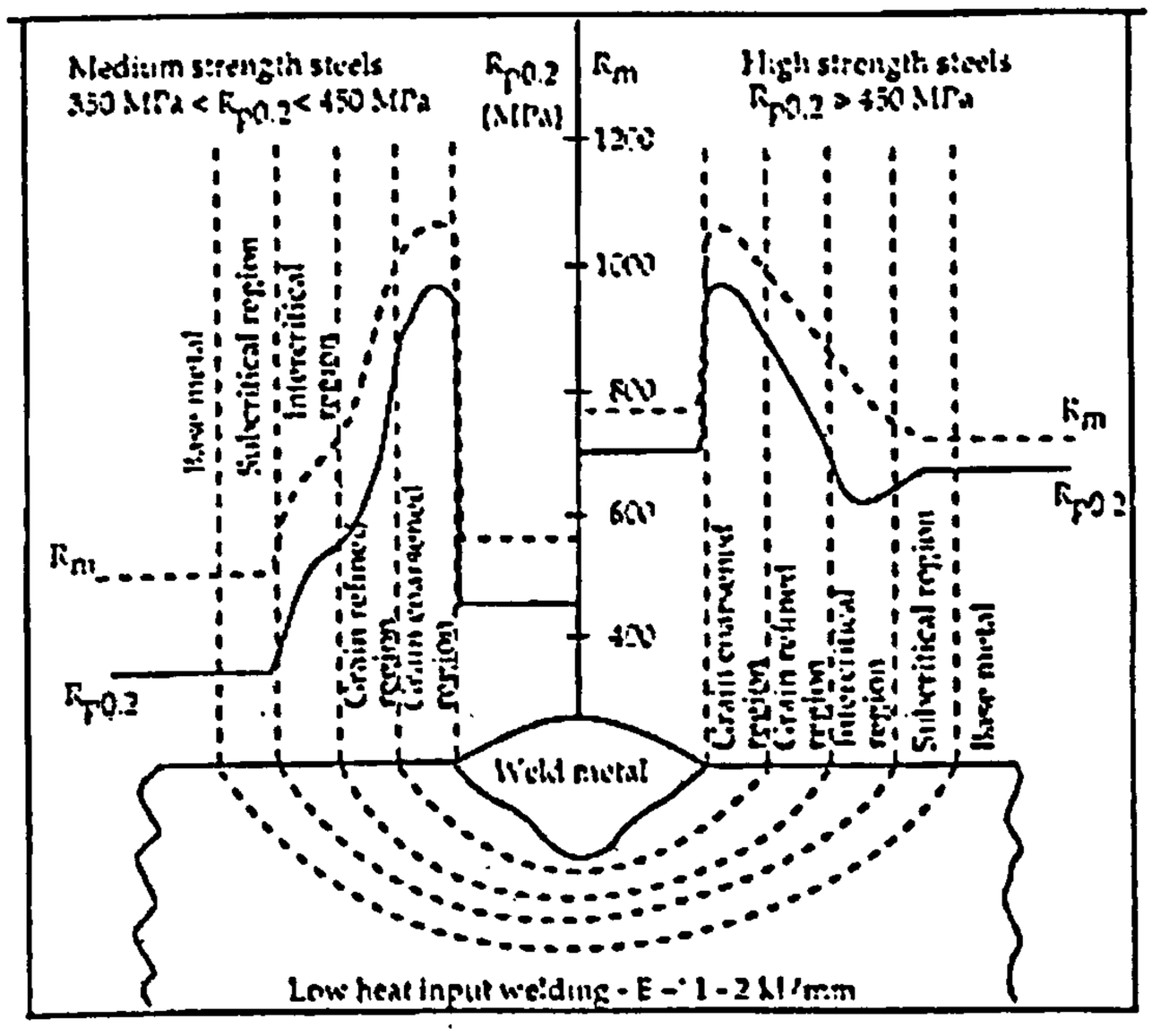

Figure 2-48: Typical HAZ microstructural classification (after ref. 200)

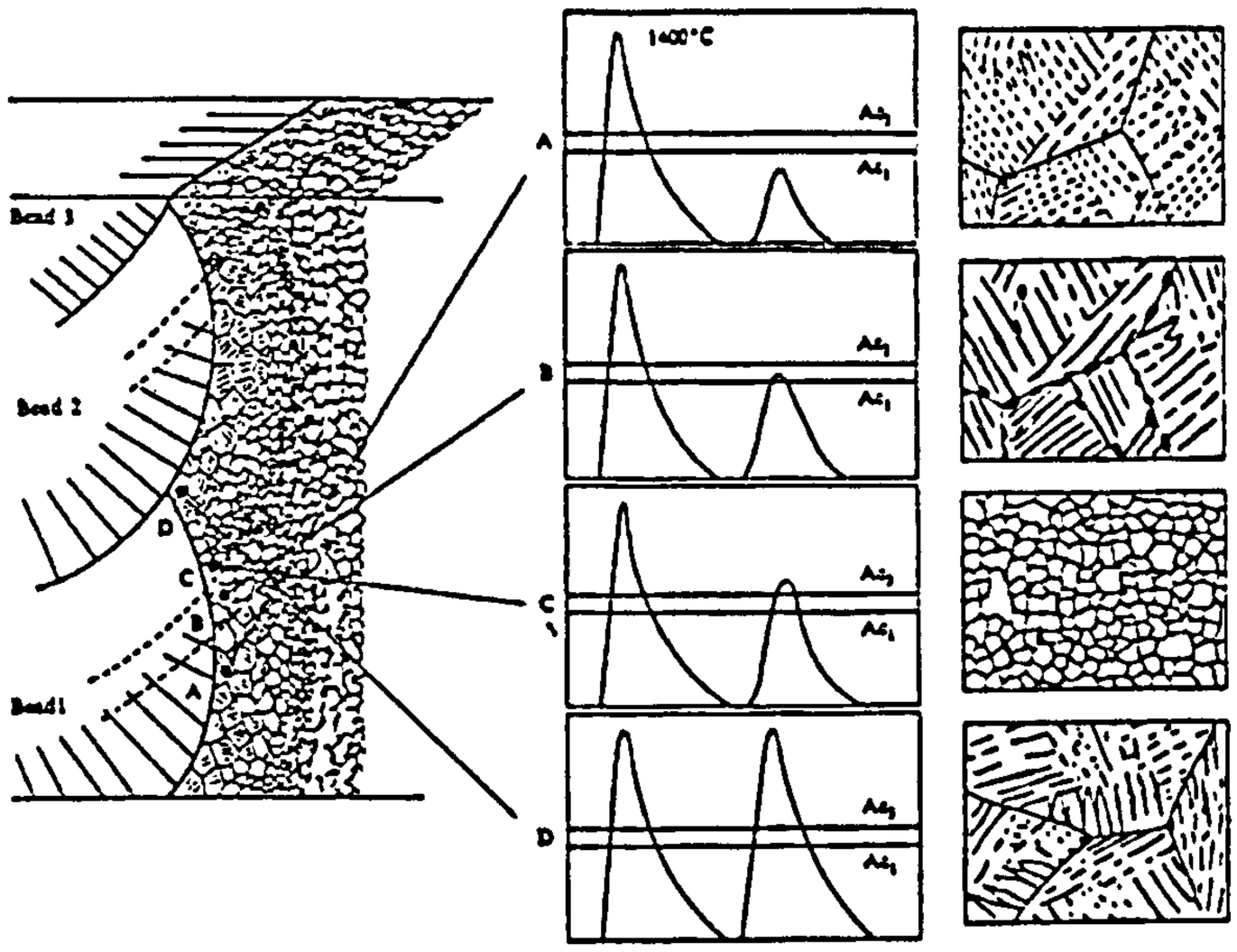

Figure 2-49: Schematic illustration of microstructures and thermal cycles of a welded joint (after ref. 43)

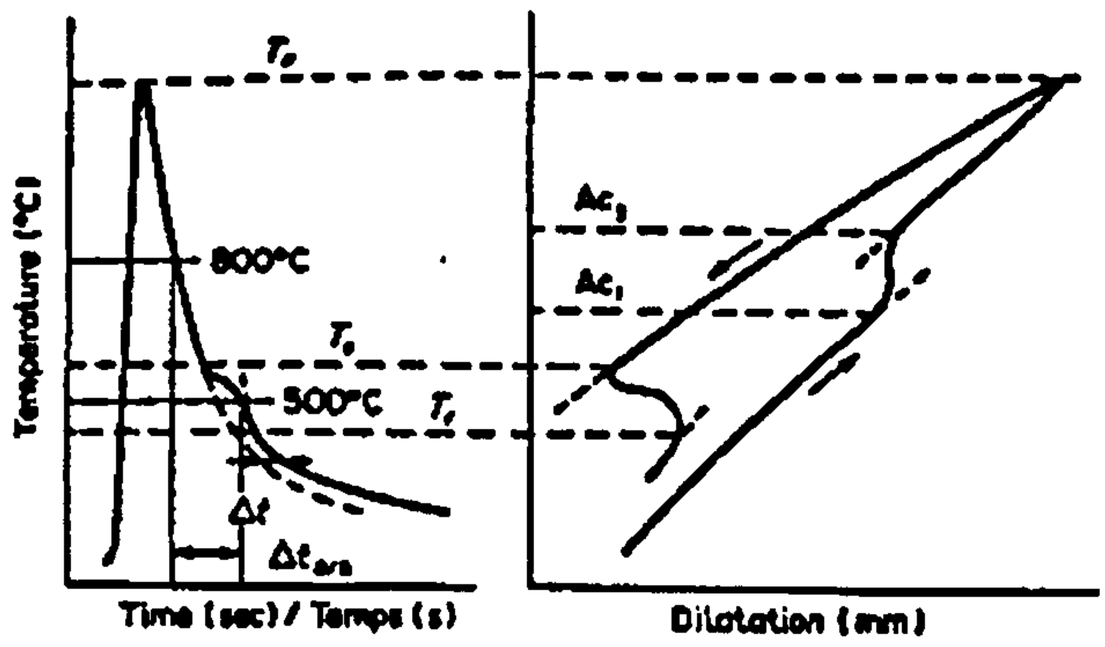

Figure 2-50: Schematic illustration of a cooling curve (left) with the corresponding dilation curve (right) (after ref. 209)

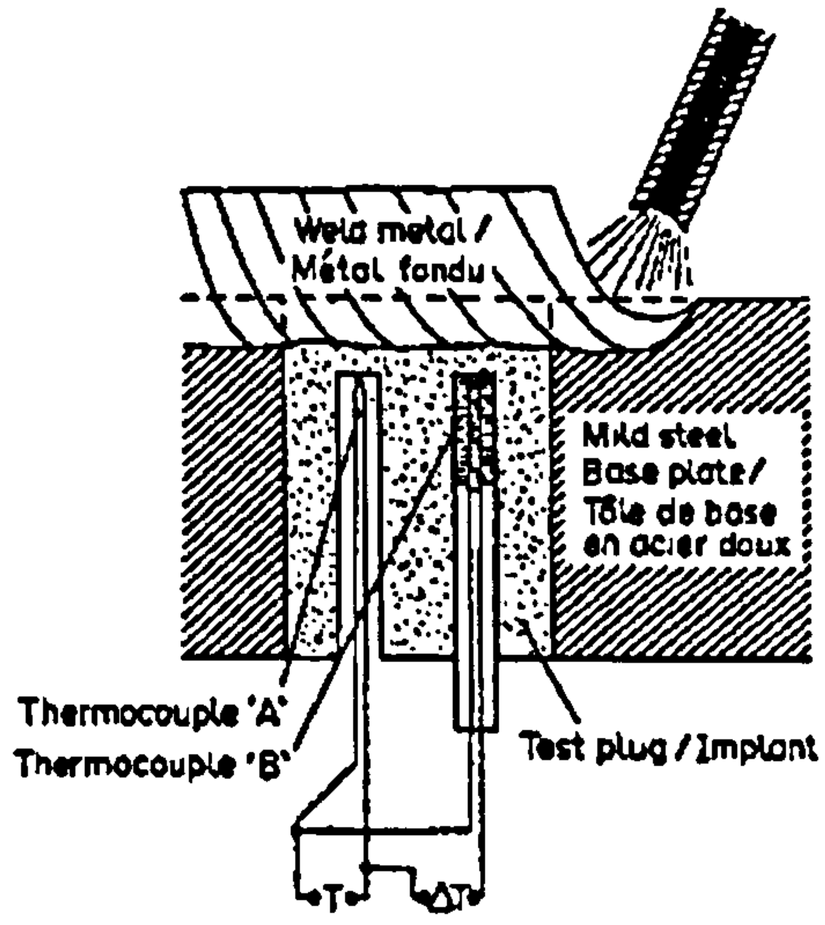

Figure 2-51: Implant technique for in-situ weld HAZ thermal cycle measurement (after ref. 228)

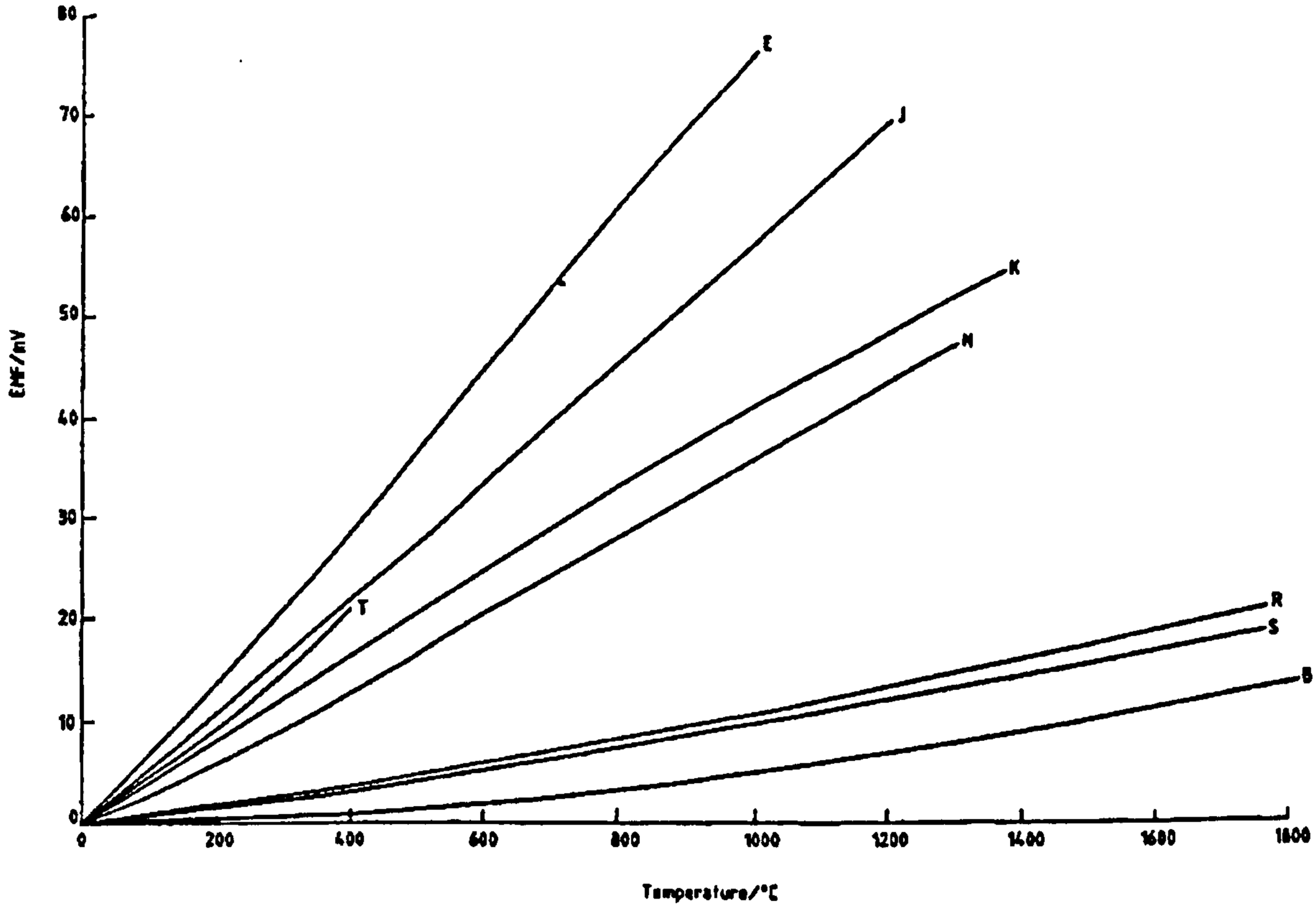

Figure 2-52: Comparison of standardised thermocouple electromotive force measurements (after ref. 232) (letters correspond to thermocouple type)

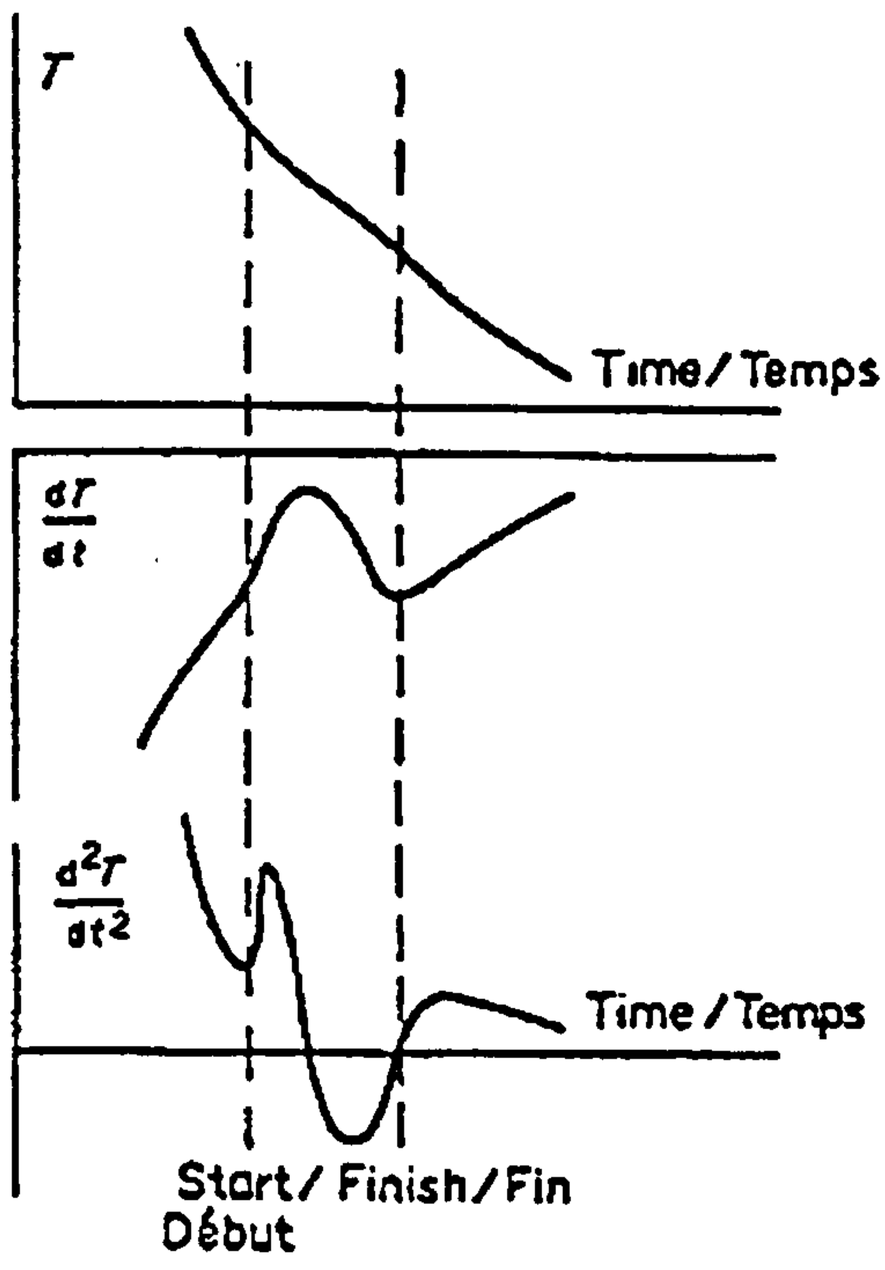

Figure 2-53: Thermal analysis of temperature-time cycle using 1st and 2nd derivatives (after ref. 209)

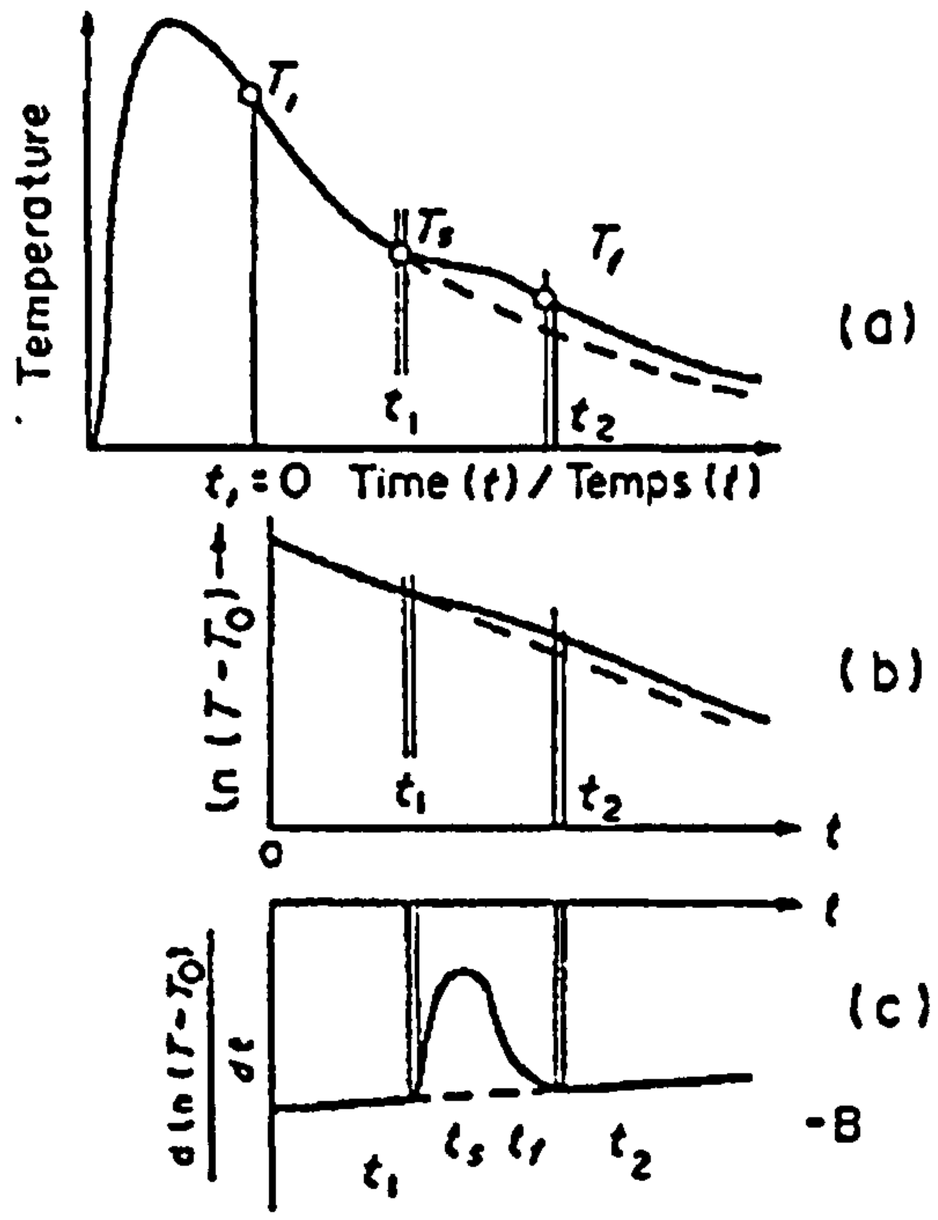

Figure 2-54: Transformation temperature determination using logarithmic differentiation of temperature-time curves (after ref. 234)

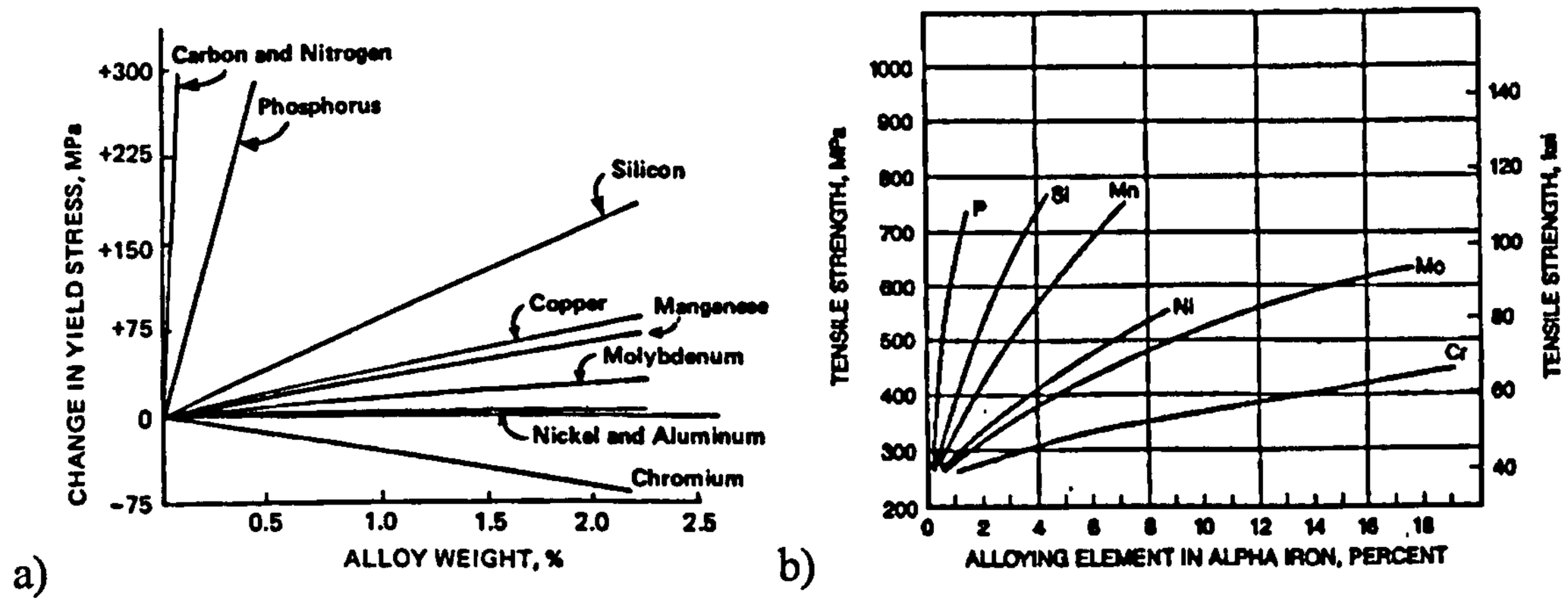

Figure 2-55: Relative effectiveness of common alloying elements in steels which strengthen a)yield (after ref. 269) and b)tensile (after ref. 94) properties of α ferrite

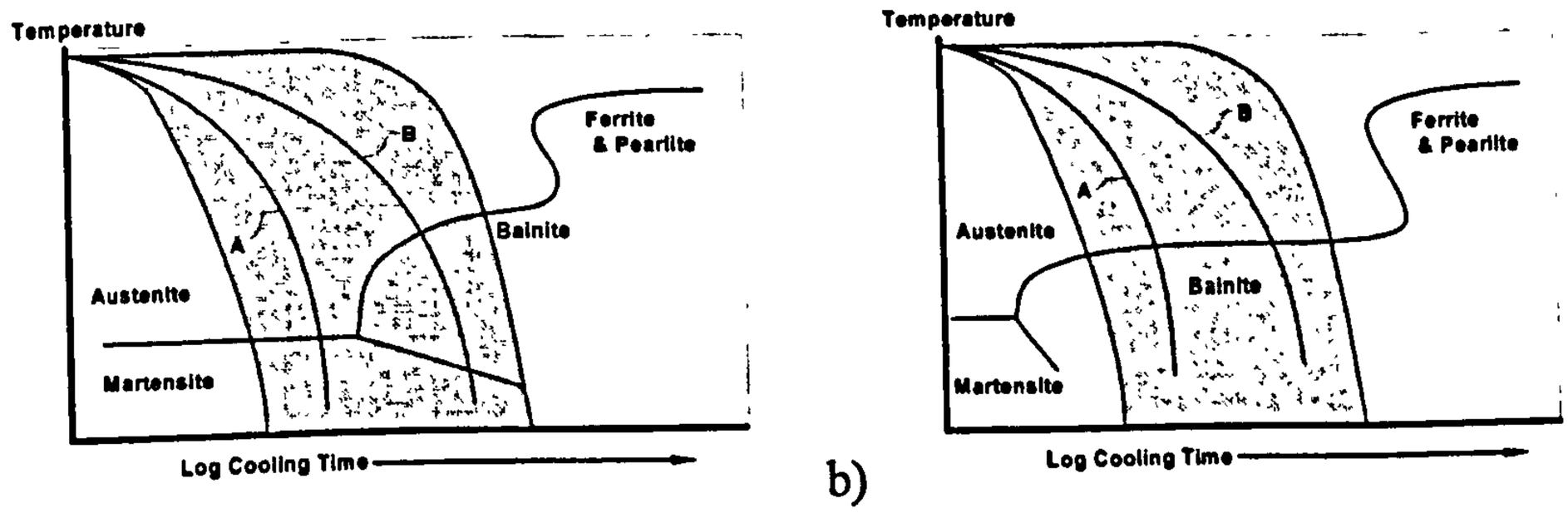

Figure 2-56: CCT diagrams for a) cooling rate sensitive and b) cooling rate insensitive microstructure design (after ref. 252)

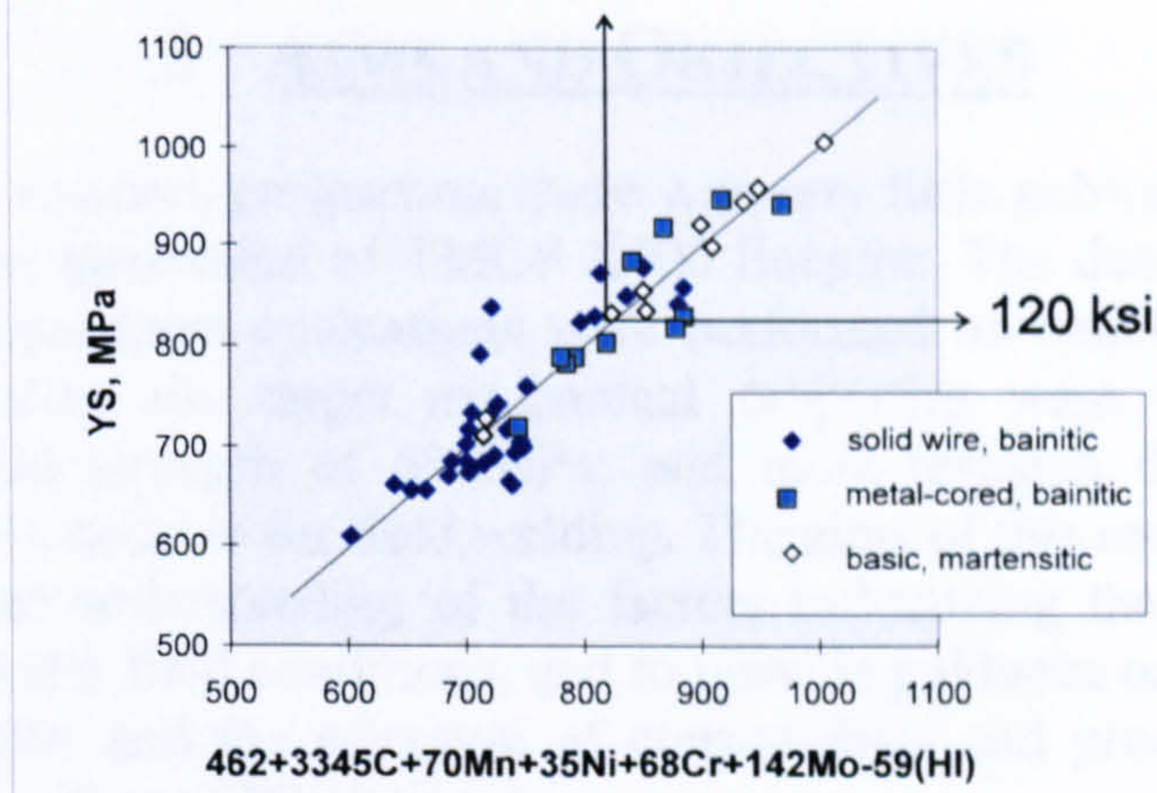

Figure 2-57: Regression analysis of various bainitic and martensitic HSLA weld metal patent data (after ref. 290)

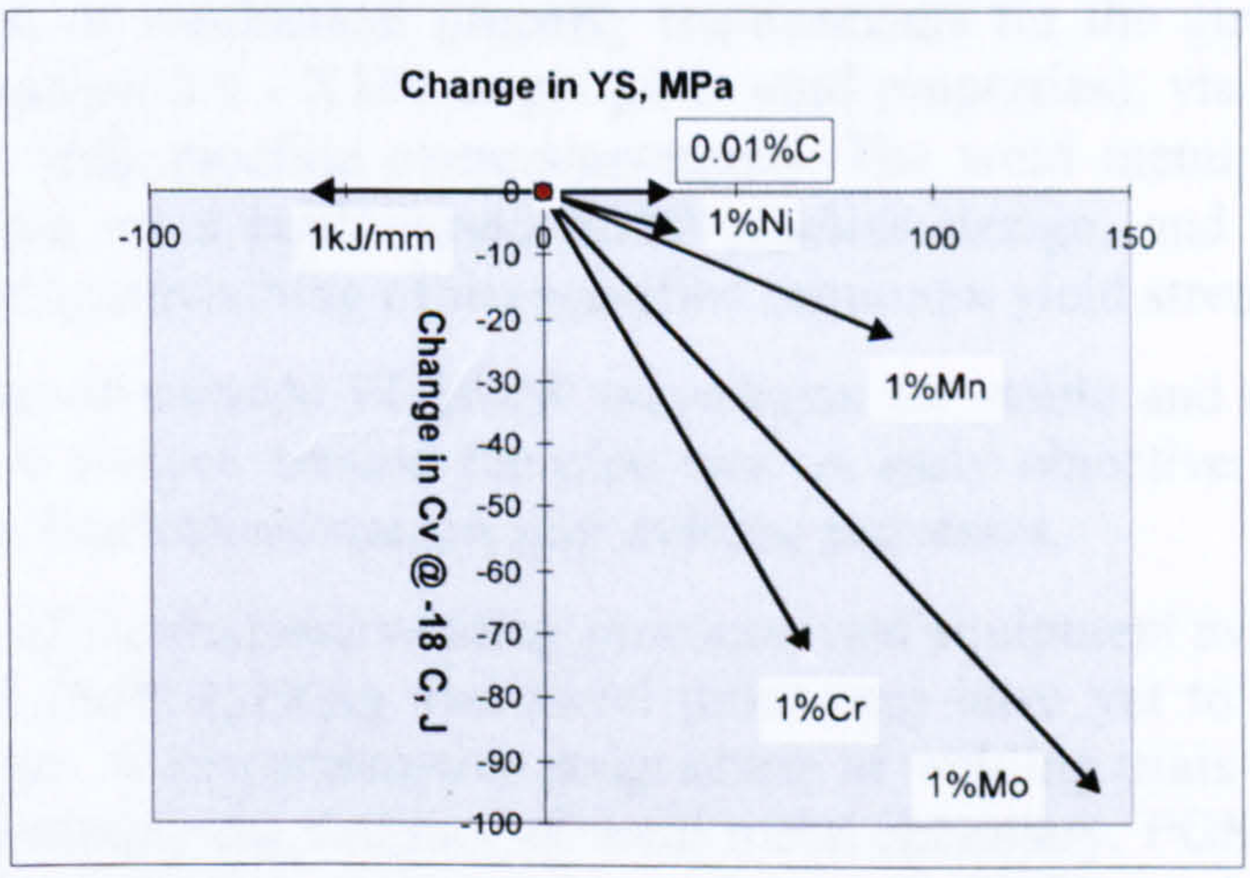

Figure 2-58: Vector diagram showing the effects of alloying and heat input on yield strength and toughness from various bainitic and martensitic HSLA weld metal patent data (after ref. 291)

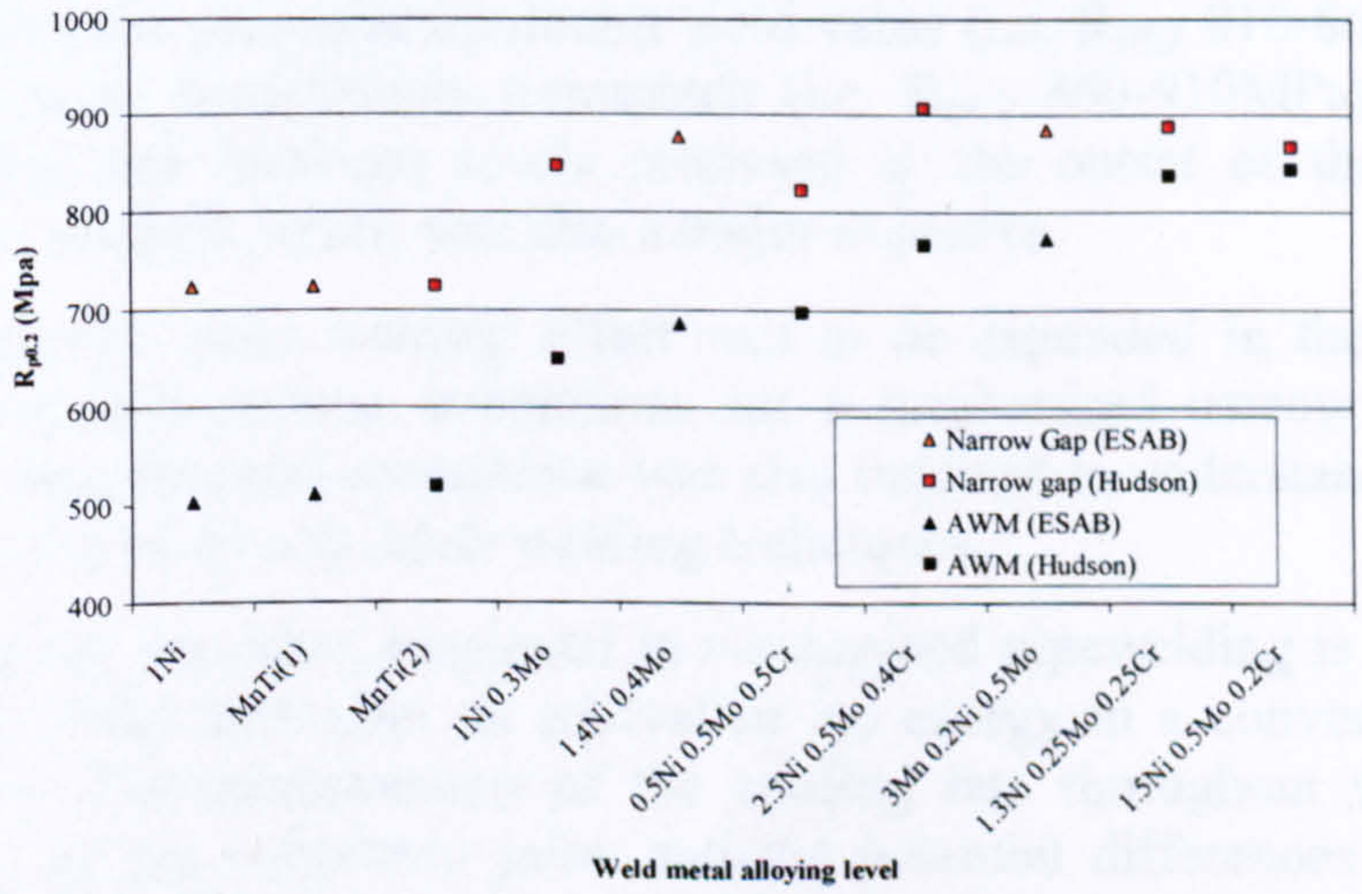

Figure 2-59: Proof strength comparison of narrow gap and conventional 60° joint (AWM) for the same alloy content (after ref. 345)

3 AIMS AND OBJECTIVES

At the outset of the research programme there was very little published data on the girth welding of the latest generation of TMCP X100 linepipe. The data that were available were limited in scope: most evaluations were performed on small test coupons rather than pipe girth welds; the target mechanical properties were solely the specified minimum pipe yield strength of 690MPa; and most research did not use welding processes/parameters suitable for field welding. The aims of this research were therefore to develop a greater understanding of the factors influencing the properties of X100 girth welds made under field conditions, and to provide guidance on the specification of mechanical properties and the selection of consumables and processes that could be used for the field-welding of X100 linepipe.

Specific objectives of the research included:

- The proposal of mechanical property requirements for the girth weld metal and HAZ (see section 2.9 - X100 target girth weld properties), via a literature survey and contact with pipeline owners/operators. The weld metal properties desired were focussed on a strain-based X100 pipeline design, and therefore required considerable overmatching of the specified minimum yield strength of the pipe.
- Development of suitable PGMAW waveforms for stable and consistent welding from 12 to 6 o'clock around the pipe was an early objective for the single and tandem wire mechanised narrow gap welding processes.
- The variety of mechanised welding processes and equipment available for pipeline construction (both existing and novel processes) have yet to be evaluated with X100 linepipe. A comprehensive programme of welding trials were consequently devised to examine the variance of weld metal chemistry, PGMAW/GMAW, and single, dual and tandem wire processes for use in X100 mechanised narrow gap pipewelding. The experimental programme was designed to allow two wires for each welding process variant to be chosen for extensive welding trials and mechanical testing after analysis of all the preliminary data. One wire was to just overmatch the proposed minimum yield value (i.e. $R_{p0.2}$ 810-860MPa), whilst the other was to considerably overmatch (i.e. $R_{p0.2}$ 860-910MPa). Maintaining the toughness and hardness levels proposed at the outset of the research, at the required strength levels, was also a major objective.
- Although the main welding effort was to be expended in the understanding of chemistry and process interactions for a mechanised narrow gap procedure, a similar experimental programme was also required to understand the requirements for suitable tie-in and repair welding techniques.
- The narrow gap bevel employed in mechanised pipewelding is presumed to incur faster cooling rates than an equivalent arc energy in a conventional wide bevel situation. The measurement of the cooling rate throughout the various passes making up the completed joint, and the potential differences associated with a given welding process (single, dual, tandem and dual tandem torch) for a given alloy were considered important in defining the attainable properties from the particular process. A similar exercise was undertaken for the single wire process using variations of preheat, with the results of both sets of experiments used to

correlate with the resultant mechanical properties, thereby allowing the definition of likely alloy/welding process/welding procedure combinations.

- With the establishment of an optimum commercially available weld metal chemistry, joint bevel design, and cooling rate, the effect of minor changes in several alloying elements on the resultant mechanical properties arising from a narrow gap weldment were sought. The alloying levels available from commercial wires occur in relatively large steps, such that the effect of minor changes, e.g. batch to batch variation, or from one manufacturer's version to another's of the same generic type, would not be observed. A matrix of carefully controlled weld metal chemistries was considered a suitable system to examine the mechanical properties with a view to defining the alloy tolerance range. Single wire mechanised welding with metal cored wires, optimised arc energy and bevel geometry were judged the most favourable method to examine the effect of alloying levels.

- The use of X100 linepipe within a gas transmission system was a possibility at the outset of the research. An objective would be the inclusion of the chosen optimum alloy chemistry and weld procedure details developed from various aspects of the research within the weld procedure specifications for the first TMCP X100 construction project.

- Personal objectives desired from the research include the understanding and development of techniques for a structured research methodology, scientific report writing and conference paper presentations. Pipeline welding is a specific area of welded construction and brings with it many specialised techniques and terminologies. It is hoped that being involved at all stages of the processes required for welded pipeline construction during the experimental work, in conjunction with discussions involving numerous individuals around the world who are concerned with pipe manufacture and field construction on a day-to-day basis, will enable a thorough understanding of the processes and challenges typically encountered.

4 EQUIPMENT, MATERIALS AND EXPERIMENTAL TECHNIQUES

4.1 INTRODUCTION

A flow diagram of the research programme undertaken during this work is shown in Figure 4-1, highlighting the major experimental phases. Previous work at Cranfield[154-156] involved a considerable number of solid wire GMAW/PGMAW all-weld metal conventional wide bevel (60° included angle) flat plate tests. These were designed to gain an understanding of potential welding consumable chemistries suitable for high strength steel fabrication. Whilst these were generated using preheat and arc energy levels typical of single wire mechanised pipeline welding practice thought to be relevant for X100 type steels, no work was performed involving a narrow groove bevel preparation. Preliminary work at Cranfield conducted just prior to the research reported in this thesis examined several promising weld metal chemistries in a narrow groove preparation. This work is included in a PRCI report[157], although at the time the investigations were carried out account had not been taken of certain attributes such as the effect of small differences in arc energy and joint geometry, or transference from a plate to pipe welding situation. At the outset of the current research programme initial PGMAW single wire waveform development was performed in a flat plate narrow groove situation, but transferred as soon as possible to a pipe. This avoided any potential problems associated with cooling rate differences, the examination of which formed part of the current investigations.

The main body of work within this thesis addressed single wire mechanised narrow gap fixed position pipewelding, with special attention paid to the weld metal chemistry requirements to generate properties suitable for an X100 pipeline using a strain-based design. This requires a guaranteed overmatching of the actual pipe yield strength as discussed in section 2.9.2. Similar work was conducted using the tandem wire and dual torch mechanised welding processes; test and qualification welds of the latter process being generated by a specialist welding contractor due to equipment and time restraints. Several proprietary welding bug and band systems, alongside standard pipe bevel preparation equipment, were used to assess the applicability of current commercial pipeline apparatus for X100 construction. The practical pipeline welding techniques used throughout the research were based as far as possible on current typical practices. Any improvements or modifications to a given system were duly noted in the relevant sections of this chapter.

Mechanised welding provides for high quality, high repeatability and high production rates when the geography of the pipeline route allows the use of straight or minimal bend angle joints. At some point in the pipeline construction however, a requirement will exist for large angle bends, fittings, river/road/rail crossing sections etc. to be joined to the main-line. These tie-in sections are usually manually or semi-automatically welded with SMAW or FCAW and therefore form part of the necessary welding technology required for X100 construction. Likewise, repair procedures are equally important to rectify any defects identified from the NDT. As a consequence, both of these welding requirements for X100 have been examined in the course of this research.

The considerable number of mechanised pipewelding experiments provided for correlation attempts of all the data to ascertain any trends relating to chemistry and property relationships.

Analysis of the single wire mechanised weld procedure data highlighted a weld metal chemistry suitable for use as a base line design for the thermocycle and alloy variation experiments. An optimum welding procedure was selected, with the various pipe and plate welds manufactured under highly repeatable conditions. The thermocycle welds were designed to examine the effects of four mechanised welding processes suitable for pipeline applications on the cooling rates/transformation temperatures of individual weld layers and the associated joint mechanical properties. A further series of thermocycle experiments were undertaken using the single wire process but with various levels of preheat.

The alloy variation experiments were designed to examine changes in chemistry using specific levels which were generally larger than batch-to-batch variations of a nominal composition, but smaller than the commercially available steps offered from manufacturers.

Combining the results of the previously listed series of experiments should enable some understanding of the tolerance box applicable for the welding of X100 linepipe steels.

4.2 PIPELINE MATERIALS

The pipeline materials comprised a nominal $R_{t0.5}$ 690MPa, i.e. X100 strength level, with some of the manufacturers also providing plate of the same composition prior to pipe forming. Table 4-1 identifies the materials received; in the interests of confidentiality an alphanumeric code was applied to each pipe manufacturer. Pipes were received typically in 3 metre lengths and individually identified via heat, pipe and piece number. Three WT variants were received; 14.9, 16.3 and 19.05 mm. Pipe ODs were 30 in. (762 mm) and 36 in. (914 mm).

The pipes were produced from TMCP and accelerated cooled plate, and formed into pipe via the UOE process described in chapter 2. Detailed conditions of manufacture were not available to the WERC as this is usually regarded as proprietary information. Longitudinal SAW seams comprised a single pass internal weld and a similar external weld, both being deposited by multi-head SAW equipment.

4.3 WELDING CONSUMABLES

The solid wires were of nominal 1.0 mm diameter (except the ESAB Spoolarc 120 which was 0.9 mm diameter), with the wire type and analyses as shown in Table 4-2 and Table 4-3. As can be seen in the tables, the main alloying elements examined were nickel, molybdenum and chromium, often in combination, to maintain toughness (Ni) whilst increasing the strength (Mo and Cr). Some of the wires incorporated titanium and vanadium micro-alloying additions for improved deoxidation or strength. Carbon, manganese and silicon levels were similar for most of the wires, although their relative amounts were taken into account when analysing the chemistry/mechanical property balance.

The consumables used for the tie-in and repair welds are also shown in these tables. Two high strength rutile FCAW wires and a low hydrogen basic SMAW electrode were selected for trials, based on their alloying levels and manufacturers recommendations. A GMAW wire (0.5Ni 0.5Cr 0.5Mo) used in various narrow gap procedure welds was also included for semi-automatic repair trials.

A series of metal cored wires was manufactured to test particular variations of chemistry based around a control level of 0.9Ni 0.3Mo. The control chemistry was selected after successful weld procedure testing of numerous girth welds. Although analyses of the unwelded wires were not undertaken, the target chemistries are shown in Table 4-4. The chemistries chosen were predominantly to examine the effect of C, Ni, Mo and Cr in isolation from each other, although a few wires were manufactured with several alloy changes in the given wire after correlation attempts with all the preceding girth weld data.

4.4 SHIELDING GASES

Procedures at the WERC utilised a trimix gas for all the mechanised welds (both solid and metal cored wires) following work performed on metal transfer stability and the resultant mechanical properties[152]:

82.5% Ar/12.5% CO_2/5% He

A standard BOC gas (Argoshield Heavy) was used for the GMAW/FCAW repairs and tie-in procedures, alongside the mechanised internal root run dip transfer welding. This resulted from the extensive industry background with this gas type, alongside recent research carried out at Cranfield[156]:

78% Ar/20% CO_2/2% O_2

All of the dual torch procedure welds and some of the single torch welds were produced by Serimer-Dasa, a pipewelding contractor situated close to Paris, France. Three gas mixtures were used in producing the mechanised welds at Serimer-Dasa:

A 50% Ar/50% CO_2 mix for dip transfer welding

An 80% Ar/20% CO_2 mix for dip transfer welding

A 90% Ar/10% CO_2 mix for pulsed welding

The company are world leaders in dual torch narrow gap welding technology; coupled with sponsor requirements of technology transfer together with a limited timescale for the current programme it was decided at the outset of the work that co-operation between the WERC and Serimer-Dasa would result in optimal data generation for X100 field joining technology. All mechanical and metallurgical investigations on the weld procedure test pup pieces were undertaken as part of this research.

4.5 WELDING POWER PLANT

Several types of welding equipment were used throughout the programme of work, with selection based on the particular application. Single wire welding used a Lincoln Powerwave, with tandem welding using synchronised Fronius power supplies. Both are high performance GMAW/PGMAW equipment from manufacturers at the leading edge

of welding power source technology. The dual torch procedure trials conducted at Serimer-Dasa's development facility used a Kempii 3500 MIG power source operated in dip transfer mode. The welds produced using PGMAW utilised a Miller Invision 456P power source with their 564M controller. The tie-in and repair welds involved several types of welding equipment as discussed in the relevant subsection.

4.5.1 SINGLE WIRE NARROW GAP POWER SUPPLY

Single wire narrow gap welding utilised a Lincoln Powerwave 455 STT (designed to give 400A at 100% duty cycle of 10 minutes) in conjunction with their Wavedesigner Pro® on-line control software (Figure 4-2). The power plant is of the inverter type with external wire feed drives placed on top of the power source. Dip/spray, pulsed or STT waveforms for GMAW are accessed through the software, with their manipulation made extremely easy via the relevant screens. Previous research[150,156] showed a marked improvement in mechanical properties using pulsed metal transfer, such that this was the only transfer mode examined for the single wire narrow gap application. Although the power source had the capability to water cool the welding torch, this facility was not used; an air cooled torch was attached to the welding bug as per common field practice for mechanised narrow gap pipewelding. This power supply was also used for the metal cored wire plate trials, with a pulsed waveform developed for the narrow groove preparation. A standard water cooled hand held MIG torch was adapted for use on a welding bug with all the plate welds.

4.5.2 TANDEM WIRE NARROW GAP POWER SUPPLIES

Tandem torch welding development began at the WERC with Fronius T.I.M.E.-Twin TransPuls Synergic 450 power sources (Figure 4-3(a)) [11,12,13,324] coupled with a WERC-designed tandem torch. The 100% duty cycle of this machine is 450A for 10 minutes. The main feature of the power supply is the ability to specify numerous points on a given welding waveform, generating a synergic curve as well as synchronising the two power supplies. Synergic control of a power source allows multiple welding settings (usually based on deposition levels) with stable metal transfer throughout the operating range. The possibility exists in these power sources to change the phasing between them, but the initial work focussed on always producing the second wire pulse at the end of the first (effectively 180° out of phase). Pulsing the waveform alternately was deemed essential to avoid the electric/magnetic interactions of two closely spaced arcs, thereby promoting a stable metal transfer. In theory one drop per pulse is thought to provide the most stable and efficient transfer for positional solid wire PGMAW. Considerable effort was expended in developing suitable waveforms for narrow gap PGMAW with wire of a given diameter[11,12].

During the course of the work, new versions of the Fronius power supplies (TransPuls Synergic 4000) were introduced (Figure 4-3(b)), and these were consequently used for the remaining procedure trials and process comparison evaluation. These machines offer a 100% duty cycle of 320A for 10 minutes. Although digital in make-up, at the time of the research the power supplies were not as flexible as the original, in that only minor variation from a pre-programmed arc characteristic was possible. The original WERC-developed synergic curves for tandem welding were slightly modified before being

uploaded into the machines' welding data bank at the factory. The welding characteristics of the resultant synergic curves are noticeably 'crisper' than the previous generation and provide for smooth, very low spatter metal transfer. The wire feeder and control pendant for each power source are remote from the power supply, allowing greater flexibility in equipment set-up, especially considering the relatively small space available inside pipeline welding 'shacks'. One important feature added to the power supply is the ability to set inductance and resistance levels appropriate to the length/diameter of welding cables (power and work return) used. Given that cable lengths of 25 m are not uncommon in pipeline welding applications, the resultant voltage drop (resistance) and current rise/fall rates (inductance) can have a significant effect on the resultant pulse shape. Appropriate waveform modifications are consequently automatically set by the power source once a datum has been established on initial equipment set-up. Cable lengths of 25 m were used with the digital Fronius power sources.

4.5.3 TIE-IN AND REPAIR POWER SUPPLIES

The tie-in and repair procedure trials used the ESAB Aristo 2000 (power source LUD 450W, dual drive wire feeder MEK 44C) multi-process welding power source (Figure 4-4), consisting of an inverter based power supply capable of 360A at a 100% duty cycle of 10 minutes. With this power source GMAW, PGMAW, SMAW and GTAW are all possible for DC welding. The standard synergic curves preset in the machine were used for both the rutile flux cored wires and the solid wires, operating in DC electrode +ve mode. Roughly halfway through the programme of work it was decided to produce internal GMAW roots via rotated pipe rather than with a conventional internal pipewelding machine for reasons described later. The Aristo 2000 was consequently set with dip welding conditions identical to those for the internal welder, with the torch placed on a SAW column and boom for easy access/control within the pipe. For SMAW the polarity and current type were set appropriate to the electrode and its application within the joint sequence.

Certain repairs necessitated arc-air gouging of half to full pipe wall thickness, prior to grinding a conventional 60° included angle. For this a SAF Nertazip 540 plasma/arc-air gouger was used with copper coated carbon electrodes of 6 mm diameter.

It was found necessary to use an AC transformer for the root/hot pass of the full thickness SMAW/FCAW repair weld due to the considerable 'arc blow' observed when using DC in this situation. It was presumed that the grinding operation introduced considerable magnetism into the locality of the bevel. A Migatronic TIG Commander 400 AC/DC power source providing 295A at a 100% duty cycle of 10 minutes was used for both SMAW weld runs.

4.6 PIPE BEVEL PREPARATION EQUIPMENT

The WERC were loaned two CRC-Evans pipe facing machines for 30 and 36 in. OD pipe with the associated mains powered hydraulic pumping unit (Figure 4-5). These were initially set for the given pipe wall thickness by a CRC-Evans technician, with future modifications for wall thickness and bevel geometry undertaken by WERC staff. Serimer-Dasa prepared bevels utilising their own proprietary in-house equipment.

4.7 INTERNAL AND EXTERNAL PIPE WELDING EQUIPMENT

A six head internal pipe welding machine (IWM) for use with 36 in. OD pipe was also loaned by CRC-Evans (Figure 4-6). This was initially set for 16.3 mm wall thickness pipe and subsequently set for 19.05 mm WT. Half the pipe could be welded from 12 to 6 o'clock in one pass, using three heads welding simultaneously per half pipe. The machine was housed in a 6 m length of 19.05 mm WT, 36 in. OD pipe which provided easy alignment with 19.05 mm WT pup sections, and, after adjustment of the counterbalance points in the machine within the housing, provided alignment with the 16.3 mm WT. The 14.9 mm WT pups, however, proved extremely hard to align due to the considerable mismatch between housing and sections; for this reason it was decided to generate the internal bead by rotating the pipe and using a SAW column and boom holding a conventional GMAW torch (Figure 4-7). The IWM was set-up and operated by CRC-Evans technicians.

A CRC-Evans P100 welding bug and band system was used for all single wire and initial tandem wire welding trials (Figure 4-8). Due to the use of pulsed welding power supplies in both cases, torches with their associated 3 or 4 m power, wire transport and gas leads replaced the original CRC-Evans torch set-up (designed for remote welding power and gas only). The wire feed motor and reel holder assembly on the bug were also removed as these were superfluous to requirements. The travel motor gearbox was changed when required to suit the given process type. Operation of the bug involved manual adjustment of contact tip to workpiece distance (CTWD), groove tracking and travel speed, all via knurled adjustment wheels on the bug. Wire feed speed and arc on/ off were controlled from the power source. The single wire preheat variation trials used this bug, and with the controls located on the bug itself the operator was able to simultaneously place external thermocouples into the weldpool whilst maintaining the correct arc position within the narrow groove.

The same CRC-Evans bug type was also employed for the metal cored wire plate trials. A pipe band was cut and, after removal of the spacer bars, rolled to induce the flattest profile possible. Angle iron bars were subsequently used to support the band and maintain a flat running track. A plate clamping jig was also fabricated to hold the plates as flat as possible during welding (Figure 4-9).

Serimer-Dasa used their Saturnax 5 dual torch welding system and band in a similar fashion to that of the WERC (Figure 4-10). A remote pendant allows the welder to adjust similar parameters as mentioned above but from the best possible position; usually in front of the leading arc at all times. A given weld pass can be pre-programmed and, in conjunction with the power supply, delivers all of the required parameters. The bug shown in the photo has a fixed distance of 50 mm between the torches; the actual procedures which were developed for this work necessitated the use of varying torch spacing in order to obtain the required mechanical properties, but this will be discussed in detail later. All of Serimer-Dasa's welds used a copper backing system placed on the ID of the pipe, such that all welding passes proceeded from the outside of the pipe only. A major difference in this equipment compared with the CRC-Evans P100 and RMS MOW II bugs is the use of a lateral oscillation mechanism rather than a pendulum type. The former provides a more rigid set-up but does not allow the same degree of arc directionality into the sidewall at the oscillation extremes, resulting in the potentially increased chance of fusion defects occurring.

The tandem wire procedures initially used the CRC-Evans bug as mentioned above, but it was found necessary early on in the trials to increase the oscillation rate due to the high travel speeds required of the process (the oscillation motor of the CRC-Evans P100 bug allowed up to ~210bpm). The water-cooled version of the WERC-designed tandem torch (Figure 4-11) superseded the air-cooled version early on in the development trials due to the high peak current and weld lengths necessary. This torch is considerably heavier than the original CRC-Evans design, and coupled with the lack of rigidity in the torch fixing location on the bug, a new bug design was sought. RMS welding systems consequently lent their latest bug, MOW II, which was capable of holding two WERC tandem torches and allowing independent control of each torch head (Figure 4-12). Although the photo shows two tandem torches, the majority of the work reported utilised only a single tandem torch. In a similar fashion to the single wire welds, power source and wire feed drives for tandem wire welds were independent of the welding bug. Control of the bug utilised a pendant coupled with switching units for the power supplies. Pre-programming of a given weld pass was performed, with joint tracking and CTWD manually adjusted during the weld pass. Wire feed speed, arc length and droplet detachment/arc force corrections were the only parameters set on the power supply. The RMS bug was used for the process comparison trials whereby one or two tandem wire torches were fixed on the given oscillator head for single wire, dual torch, tandem torch or dual tandem tests. In order to maintain control over the welding whilst simultaneously allowing external thermocouple placement by the operator, the control pendant was fixed to the bug (Figure 4-13).

The WERC tandem wire torch provided complete electrical isolation between the individual contact tips, coupled with water cooling of the gas shroud. Two shroud lengths were manufactured; their screw-in arrangement allowed the gap between the shroud and pipe surface for each weld layer to be minimised thereby maximising gas shielding. The torch leads were a heavy duty type such that heat from the arcs could be conducted down them via the contact tips, but with the resultant disadvantage of added weight. The leads were supported on the bug, but a certain amount of flexibility was required due to the torch oscillation. The diameter of the original contact tips was 6mm at the thread end tapering to 3 mm over 75 mm; cooling was limited in this design so larger copper inserts were made allowing 'off-the-shelf' CuCrZr M6 contact tips to be inserted. Depending on the pipe wall thickness, it was sometimes necessary to machine the very end of the 'standard' contact tip to allow clearance within the groove for the hot pass and first fill pass (only pipes of maximum wall thickness 19.05mm were examined throughout the research). The angle between the contact tips was a nominal 12°, with the final separation of the arcs being a function of the CTWD and contact tip length; typically the wires were separated between 4 and 6 mm at the end of the given CTWD.

4.8 EXPERIMENTAL TECHNIQUES

The research undertaken for this project can be grouped into three major sections: ASME IX 5G procedure testing and qualification welds; thermocouple trials involving preheat and process variations; and metal cored wire chemistry variation trials.

4.8.1 *ASME IX 5G PROCEDURE TESTING AND QUALIFICATION WELDING*

4.8.1.1 WELDING PROCEDURE DEVELOPMENT FOR NARROW GAP WELDS

Narrow gap welding was performed in the ASME IX 5G position using either single or dual torch (Serimer-Dasa) or single and tandem torch (WERC) mechanised welding processes. Pipe sections were typically 1 m in length after welding. The joint preparations of the narrow gap type are as shown in Figure 4-14. Welding was performed from the outside of the pipe alone with the Serimer procedures, whereas the WERC utilised procedures featuring both internal and external weld deposition. A six-head CRC-Evans IWM or conventional GMAW power supply, with an AWS 5.18 ER70S-6 wire (0.9 mm C-Mn-Ti), was used to deposit the root run in the internal/external welds, whilst a copper backing bar was employed with the all-external procedures (the WERC version is shown in Figure 4-15). The same consumable was used throughout in the latter case, except for the root run of the Serimer welds (their standard procedure involved an ER70S-6 wire). The primary work undertaken at the WERC centred on the development of single wire pulsed waveforms using the Lincoln Powerwave 455 for 0.9 and 1.0mm diameter wires. A bug travel speed requirement of 450 to 500 mm/min for all passes provided a base line to work from, and an iterative process of narrow gap trials were used to determine a welding condition that provided adequate fusion characteristics around the circumference of the pipe. Pulse conditions used in narrow gap pipeline welding reported in the literature[129] again provided a base line, but due to the considerable development in power supply technology over the last decade it was necessary to modify the parameters. It was realised early on in the work that a reduced gap within the groove would be necessary to facilitate a flat profile between 4.30 and 6 o'clock. A typical offset value (the distance of the closed butt adjoining faces to the base of the major sidewall face) is 2.8 mm (i.e. 5.6 mm gap at the base of the groove). In a 19.05mm WT pipe with the root bevel dimensions indicated in the internal/external preparation of Figure 4-14, a theoretical cap gap width of 8.09mm would result. Dropping the offset to 2.3mm results in a cap gap width of 7.18mm, thereby reducing the required bridging distance, and helping the weld metal maintain the flattest possible profile, particularly in the outer fill passes.

Many waveform variants were examined, with the resulting synergic curves developed for the initial and later single wire weld procedure tests shown in Appendix A. The main criteria used to determine optimum fusion characteristics were external bead profile for each run, combined with macro section observation/dye penetrant testing, particularly at 3, 4, 5 and 6 o'clock.

The procedures adopted did not involve a bug travel speed change around the pipe circumference, except for the cap and penultimate run over the last 150-200 mm running into the 6 o'clock position. At this point a reduction in travel speed was necessary to prevent undercut, lack of fill or uneven profiles. A strip pass between 1.30 and 4.30 was also generally avoided, although the weld profile was considerably less 'reinforced' on the cap in this segment. A grinding wheel was usually run over the completed weld surface to remove the larger slag islands and any spatter, but cleaning to a fine degree was avoided except for the start and stop areas (run in/out sections were matched to the opposite side). As only one bug was used on a given pipe (two bugs on a single band are field practice), a maximum of two layers per side were completed before

welding the opposite side, allowing for tying-in of the various passes. All parameters are recorded in Appendix B, the current and voltage measurements being obtained using external meters.

The tandem procedures utilised two Fronius synchronised power sources as discussed above. Tandem wire narrow gap waveform development at the WERC was the subject of previous research[11,12], and the majority of tests utilised these pre-determined synergic curves. A modification was made to enhance transfer stability with the new digital power supplies; both initial and final waveforms for 1.0mm diameter wires are shown in Appendix A, alongside that developed for 0.9mm wire. Again, considerable effort was expended in obtaining the correct balance of travel speed and wire feed speed, particularly for the 4.30 to 6 o'clock sections.

Preheat and interpass levels of 100/130°C were maintained for all tests. The latest BS EN standard for the welding of ferritic steels (BS EN 1011-2[44]) was used to give guidance for the avoidance of hydrogen cracking (see Annex C3 of this standard) which was developed from experience with low alloy high strength steels. The weld metals and base materials fall within the scope of applicable alloy concentrations although, due to the high alloy contents of the weld metals, preheat calculations are based on the CET of the weld metal rather than the pipe (see Table 5-5, Table 5-6, and Table 5-13). Calculated values from the trial test weld metals fall within 50 to 80°C (assuming 2 mls diffusible H_2/100g WM, 19.05 mm WT pipe and a heat input of 0.4 kJ/mm). Therefore adopting 100°C preheat allows for an initial conservative approach alongside comparison with other procedure data. Retrospective preheat calculations from the procedure test welds confirm the previous statement (see Table 5-30). Preheat levels were checked at the 12, 3 and 6 o'clock positions prior to every pass, with welding only taking place at preheat levels between 100-130°C

4.8.1.2 CONSUMABLE SELECTION FOR NARROW GAP QUALIFICATION WELDS

Tensile and impact toughness measurements were taken from the trial welds and, in some cases, weld metal chemistry analyses and hardness traverses were also carried out. This process continued at the WERC and Serimer-Dasa until the required properties were attained with suitable consumables and welding processes (see Table 5-10 to Table 5-13). It should be noted that the alloys were chosen purely for their chemistry; no preference was given to a particular manufacturer, and chance dictated which manufacturer was selected for the given alloy when it was available from several manufacturers. It was decided through discussion with the relevant parties to concentrate on the use of two welding consumables; one which just overmatched the proposed weld metal minimum yield criterion, alongside one which would adequately overmatch this criterion. Serimer-Dasa chose Thyssen Union MoNi (1Ni 0.4Mo) and the WERC selected Oerlikon Carbofil HT (0.5Ni 0.5Mo 0.5Cr) as the wires which would just overmatch for dual torch and single torch respectively. Bohler X70-IG (1.3Ni 0.25Mo 0.25Cr) was used as the consumable that adequately overmatched for the dual torch welds and ESAB Spoolarc 120 (2.5Ni 0.5Mo 0.4Cr) was selected for single torch welds. At this point in the programme Serimer-Dasa had settled on using 100 mm torch spacing to attain the required tensile properties. All of these consumables gave good impact toughness levels (typically >100J at minus 30°C) from the trials. Complete pipe sections were then welded as per pre-production procedure testing (see Table 5-14

and Table 5-15) from which the various mechanical tests outlined below were obtained. On receipt of the 14.9 mm WT/36 in. OD pipe, a further series of procedures was undertaken with existing and new consumable types. Serimer-Dasa included Elga Elgamatic 135 (1.5Ni 0.3Mo 0.2Cr) and the WERC chose Oerlikon Carbofil NiMo-1 (0.9Ni 0.3Mo) as dual and single/tandem torch welds respectively. A programme of work conducted by Serimer-Dasa culminated in a torch spacing of 50 mm (typical of existing practice) using Elgamatic 135 and Thyssen Union X85 (1.8Ni 0.5Mo 0.3Cr). Both are relatively highly alloyed consumables (see Table 4-3) but are necessary due to the loss in strength via the closely following second heat cycle. All welding procedures are recorded in Appendix B.

4.8.1.3 PROCEDURE DEVELOPMENT AND CONSUMABLE SELECTION FOR TIE-IN AND REPAIR WELDS

The manual tie-in procedure used vertical-up low hydrogen AWS 5.5 E11018-M electrodes for the root and second pass as opposed to a more conventional vertical-down technique with cellulosic based electrodes, because the latter have a high hydrogen content. High strength low hydrogen vertical-down electrodes had been used in associated research work but were found not to have given overmatching properties, so it was therefore decided to examine high strength vertical-up electrodes. The advent of high strength low hydrogen rutile cored wires permit higher productivity compared with the SMAW equivalent for fill and cap passes. An ESAB wire OK 15.09 (2.7Ni 0.3Mo) was selected for the procedures and the manufacturer recommended keeping the heat input at or below 1.4 kJ/mm for this wire to avoid a reduction in strength. A typical API joint preparation was used (30° bevel, 2 mm root gap, 1.5 mm landing) with all welding proceeding in the upward direction.

The tie-in procedure all weld metal strength did not attain the $R_{p0.2}$ minimum of 810 MPa using semi-automatic FCAW and a conventional API 30° bevel. It was decided to investigate reduced bevel angles coupled with semi-automatic and mechanised deposition techniques in order to increase the weld metal strength levels. Another high strength rutile FCAW wire, Oerlikon Citoflux 110, was acquired and together with the ESAB wire, further tests as described later were conducted. A metal cored wire (Oerlikon Fluxofil M10S [C-Mn]) was also used for root run trials due to the reduced groove angles. The as-run welding parameters and joint preparations are recorded in Appendix B.

Repair procedures were undertaken to simulate typical defects that may be encountered in pipelay welds. A narrow gap single wire mechanised weld, which used Carbofil HT and an identical procedure to that described previously, had varying amounts of material removed to simulate defect excavation. Single/double pass repairs used a mechanically ground groove, whilst larger areas were first arc-air gouged and then mechanically ground. SMAW (Filarc 118) and GMAW (Carbofil HT) were used for internal root repairs (single and double pass procedures), with SMAW and FCAW (OK 15.09) used for single pass cap repairs. The root repairs were conducted in the overhead position as it is in this location the internal welding machine is most likely to experience problems in service. The cap repairs were performed over the 3 o'clock position as lack of fusion defects are most likely to occur here (where the weld metal can run ahead of the arc). A part-penetration FCAW repair was performed to simulate a defect on the fusion

boundary halfway through the pipe wall thickness, also at 3 o'clock position. A full penetration repair (essentially identical to the tie-in procedure) was conducted in the 6 to 4 o'clock position. Details of all joint preparations and important welding parameters are included in Appendix B.

4.8.2 THERMOCOUPLE TRIALS INVOLVING PREHEAT AND PROCESS VARIATIONS

The research methodology described in the following section was designed to examine the thermocycles within both the solidifying weld metal and the underlying weld beads, and subsequently to analyse the data generated with various mechanical properties from the deposited weld metal. Two major procedure variants were examined: the effect of preheat; and of process. The latter (as per the preheat trials) was restricted to PGMAW, but using deposition techniques involving single, dual, tandem and dual tandem torches.

The pipe material was 19.05mm WT X100 in all cases, although the preheat variants used one manufacturer and the process trials another, resulting in different pipe diameters. The root run was internally deposited in both cases (C-Mn-Ti), either by manual TIG (for the 30 in. OD pipe) or mechanised GMAW (36 in. OD), the latter employing the standard technique as per the procedure tests. The welding consumable for all externally deposited runs was 1.0mm Oerlikon Carbofil NiMo-1 (0.9Ni 0.3Mo), due to its conformance with the proposed mechanical property requirements outlined earlier (this will be discussed in a later section). A wire feed speed of 10.0m/min in combination with a constant travel speed was employed for all runs (hot pass to cap).This ensured that the arc energy was as consistent as practically possible for each of the two sets of experiments, alongside the deposition rate per layer being constant within each groove.

4.8.2.1 PREHEAT VARIANT TRIALS WELDING PROCEDURE

The preheat trials involved three variants: ambient (~20°C); 100°C; and 180°C. Heating was via propane torches on the external pipe surface; the relatively large flame area compared with the machined narrow gap ensured an even heat distribution for several centimetres either side of the joint line. The heating method was the same as that typically used in the field. Due to the nature of the experiments, internal thermocouples became permanently attached to a given layer in the weld sequence, allowing easy determination of the real pipe temperature and not that of a surface effect immediately after the flame was removed (see the ISO standard for weld preheating[325]). A single pipe of 1m length was divided into three sections, each for a particular preheat condition (i.e. 800 mm weld length for each test). The pipe was placed on rollers to allow internal drilling in the vertical position between each run, although the welding took place with the pipe fixed (i.e. ASME IX 5G). The actual welding started ~100 mm before 12 o'clock and finished between 3 and 4 o'clock. Preheat was applied before each run due to the long time delay between consecutive runs as a direct result of the drilling operations for thermocouple placement (described later). As the filling of the joint proceeded, the number of thermocouples in contact with the pipe increased, resulting in an increased likelihood of temperature consistency throughout the whole weldment area. Any variation due to non-uniform heating could easily be minimised by local application of heat, thereby ensuring that virtually all thermocouples were at least just

above the required preheat temperature. The Lincoln Powerwave 455 with the custom designed 1.0 mm wire waveform (final version) recorded in Appendix A was used for each preheat trial, with the welding procedures recorded in Appendix B.

4.8.2.2 PROCESS VARIANT TRIALS WELDING PROCEDURE

The process variant trials involved two pipe pups, such that half a pipe circumference was welded for each of four techniques: single wire, tandem wire, dual torch and dual tandem. Due to the necessity for a constant arc energy/deposition rate between the four welds to allow later data comparisons, it was considered necessary to rotate the pipe in combination with the relevant bug (counter) travel speed to maintain welding in the 12.30 to 1 o'clock position. This was a direct result of the chosen wire feed (10.0 m/min) and travel speed (550 mm/min single and dual torch, 1100 mm/min tandem and dual tandem) being impractible conditions for the outer fill runs in ASME IX 5G welding, or for all runs in the case of dual tandem welding. The latter process has been shown in (as yet unpublished) associated research to require significantly less wire deposition/heat input in the trailing torch due to the high temperature of the recently solidified leading torch weld metal. As soon as welding proceeds past 1 o'clock, the tendency for molten weld metal to run ahead of the arc increases significantly if the conditions allow. Thus in confining welding close to the horizontal position it was surmised that defect free welding should result, with the additional bonus of a constant deposition depth around the pipe circumference (the change in weldpool dynamics in a conventional fixed position pipeweld may require extra weld metal deposition in the 2 to 4 o'clock area (the strip pass) to prevent lack of fill in this location). The use of tandem wire welding in two of the process variants necessitated the application of synchronised power supplies; hence all welding was performed with the Fronius TPS 4000 sets for comparative purposes. The waveform used was the later 1.0mm wire version recorded in Appendix A, with the welding procedures recorded in Appendix B. Of particular importance in the dual torch and dual tandem procedures was the torch separation (88.5 mm and 85.0 mm with 13.5mm CTWD wire extension respectfully). This significantly influenced the cooling thermocycles as will be discussed later.

4.8.2.3 THERMOCOUPLE MATERIALS

The materials chosen to provide the thermoelectric voltage throughout the experiments were platinum (-ve limb) and platinum/13% rhodium (+ve limb) (R-type thermocouples). Standard specifications define the temperature of this thermopair to 1760°C, although the wire itself was manufactured and calibrated in accordance with BS EN 60584[326] which maximises the temperature in which a permissible variance (typically ±1.0°C) can occur to 1600°C. The necessity of high temperature thermopair stability was of prime importance as the limb ends would see temperatures at least that of molten steel (~1500°C), and possibly considerably higher if placed in the arc. It is known that higher temperatures can be tolerated by these thermocouples for limited time periods, but measurement accuracy above the previously quoted figures is reduced or voltage output is not even reported. Providing that temperature values were not required above these levels, the only concern was the stability of the thermopair through the very high temperature region. Hence the choice of R-type thermocouples over the more conventional K-type (NiCr/Ni) used in HAZ thermocycle studies (defined to

1370°C). Several experiments were performed in order to determine the optimum limb diameter; 0.5mm was chosen as the best compromise between welding arc survivability, ease of preparation of the thermocouple junction, rate of temperature rise and influence within the molten/cooling weldpool. The certificate of calibration for the wire batches used is shown in Appendix C; at the melting point of gold (1064.18°C) the difference between the specified and observed voltage was +1μV, resulting in a temperature difference of +0.1°C with an overall uncertainty value at this temperature for the wire suppliers experimental set-up of ±0.45°C.

The material chosen to insulate the limbs from each other between the compensating cables and the hot junction was sintered alumina, for the reasons given in section 2.6.3. Round tubes of 3.0mm diameter and twin bores of 0.8mm were the minimum size available for use with 0.5mm wire prior to insertion into predrilled holes. Externally placed thermocouples allowed the use of oval ceramic sheaths, with their correspondingly smaller ceramic volume reducing the temperature conduction should the sheath material penetrate the molten pool.

The compensating cables used were the appropriate Cu-based ones applicable for Pt-Pt13Rh; these were attached at one end to the individual wire limbs and at the other end into the junction box of the measurement module (+ve wire = orange, -ve wire = white). Male/female connectors suited to R type thermocouples were attached between the ceramic sheath and compensating cable, with the other end of the compensating cables individually located in the relevant screw terminal on the junction box.

4.8.2.4 THERMOCOUPLE CONSTRUCTION AND PLACEMENT

Several experiments were performed to determine the optimum method of thermocouple construction. It was concluded that the wires were best joined by autogenous TIG welding (limbs crimped together, the ends of which touch a Cu base plate to which the arc [8-12A] gradually approached the limbs). This produced the minimum 'balling' effect at the hot junction. Although very similar temperature results (within experimental scatter) were achieved with originally unjoined limbs placed in the molten pool (the solidified steel between the +ve and –ve terminals cancels out any voltage difference across it) it was decided to use joined limbs internally, prior to fusing them into the weldpool. This ensured a correct temperature was achieved before welding commenced, as well as ensuring contact between the thermocouple and hole base. A small extension of wire (1-2mm) from the end of the ceramic sheath served to reduce the dilution effect due to arc melting of the wires as it passed over them, as well as allowing the ceramic to closely fit the base of the drilled hole thereby allowing minimal weld metal to flow down the hole (which could significantly change the observed cooling rates). A drill size ~0.2mm larger than the ceramic sheath diameter minimised disturbance of the heat sink area whilst allowing the thermocouple to be firmly located at the base of the hole (see Figure 4-16). A capacitor discharge unit was used to spot weld the thermocouple hot junction points at the base of the drilled holes, or in the case of the root run on the exposed bead surface. The thermocouples were taped to the pipe surface (previously wire brushed to allow good adhesion) using heat resistant tape (useable up to 200°C or 300°C depending on the type); see Figure 4-16. The compensating cables were then attached, with sufficient length to allow pipe rotation whilst connected to the terminal block of the measurement modules.

Both internal and external thermocouples were used to gather thermocycle data from as many weld layers as possible throughout the course of joint completion. The internal thermocouples were drilled to specific depths depending on the process type being used. The apparently higher power of the tandem wire arc necessitated leaving more material between the base of the drilled hole and the weld metal surface (see Figure 4-16) to reduce the chances of the thermocouple being destroyed by the arc.

Whenever possible two thermocouples were used to capture the thermocycle for any given position; this often included a considerable distance between the individual monitoring points for the same type of thermocycle. At the time of the preheat trials only 8 channels were available for data capture, but by the time the process trials were conducted this had increased to 16 channels, enabling far more internal thermocouples to be left in-situ from the previous weld passes. The single wire and single torch tandem welds allowed internal and external thermocouples to be placed consecutively at the base and surface of each layer respectively to record the cooling cycles from the melt. The dual torch and dual tandem torch welds would only allow cooling curves from the melt to occur in the leading torch base and trailing torch surface due to the two layer deposition technique. Figure 4-17 shows the welding and thermocouple placement techniques. The deposition depth for all welds was recorded; this allowed accurate drilling to an intermediate depth between the lead and trial torches for the dual layer deposition, thereby improving the temperature profile data capturing capability throughout the joint. This would have been missed if only the original thermocouples collecting data from the molten phase were used. Figure 4-18 highlights the two approaches used to generate the various layer base thermocycles in the preheat and process trials. Examples of sections through drilled holes before and after thermocouple placement are shown in Figure 4-19.

External thermocouple placement involved harpooning the wires into the back of the molten pool, taking care to avoid the arc itself. There was typically a 5 to 8 mm molten tail behind the arc into which the thermocouples could be manually plunged; the steel would then solidify around the individual wires and the cooling cycle could be captured. Several experiments confirmed that the point of temperature measurement occurred at the last physical junction/path of least electrical resistance prior to the wires entering the ceramic sheath. In both base and surface layer temperature measurement this occured at the entry of the wires into the steel (see Figure 4-19 and Figure 4-20).

4.8.2.5 SYSTEM CALIBRATION

The ability of a given thermocouple to measure the correct temperature was checked using the solidification point of (commercially) pure aluminium, as this temperature is relatively close to the austenite to ferrite transformation temperatures envisaged for the weld metal under investigation. Commercially pure aluminium is produced from the reduction of Al_2O_3 in an electrolytic cell, can contain up to 0.5% impurities (wt %) and very seldom exceeds 99.79% purity[327]. Aluminium of 99.996% purity has a melting point of 660.4°C[328]. This freezing point has been used as a secondary reference point on the International Practical Temperature Scale of 1968 (IPTS68) to calibrate thermocouples[328]. Aluminium of 99.6% purity is reported to have a liquidus of 657°C and solidus of 646°C[327].

The commercially pure alloy used for the calibration was analysed as 99.68%Al, 0.32% Fe (wt%); calculated values for the liquidus are 659.5°C and the solidus 655°C based on an Al-Fe equilibrium diagram[330]. Several experiments with the finalised measurement system checking the solidification point of Al typically yielded a 3°C variance from the theoretical melting point (see Figure 4-21). The same thermocouple limb material batches were used throughout all experiments.

Although internally placed thermocouples were unchanged in length after their original placement in a given weld series, external thermocouples were continually shortened on extraction from the weldpool. Eventually a practical limit was reached and a new thermocouple was manufactured. It was realised that minor variances in measurement could be possible on production of each new thermopair, and for this reason the variance between thermocouples was checked by their mass insertion into a block of stainless steel heated to around 650°C. Nine drilled holes were evenly spaced and of the same depth throughout the block, such that the cooling rate of a thermocouple pushed to the base of any given hole should be equal (Figure 4-22). The results showed a banding of less than 5°C at any given point in time during air cooling of the stainless block, regardless of thermocouple length.

4.8.2.6 TEMPERATURE MEASUREMENT EQUIPMENT

Several types of equipment were examined to capture the thermoelectric voltage from the R-type thermocouples, the conclusion of which resulted in the purchase of several National Instrument modules allowing 16 channel temperature acquisition.

Two high accuracy isothermal terminal block modules (SCXI – 1328) allowed up to 8 thermocouple wire inputs each (i.e. 16 screw connections), for a total of 16 temperature measurement channels. Cold junction compensation was provided by a high-precision thermistor, with an aluminium isothermal plate minimising any temperature gradient across the screw terminals[331]. Accuracy of the cold-junction temperature sensing circuitry was stated as ±0.5°C between 15 and 35°C, with a repeatability of ±0.2°C in this range. Each terminal block slotted into a chassis unit (SCXI-1000), the latter of which performed the signal conditioning[332]. The chassis could accept up to four modules and was independently powered by the (AC) mains, with an integral cooling fan. The unit provided a low-noise environment for signal conditioning together with power and control circuitry for each module (see Figure 4-23 (a)).

The conditioned voltage signal was then fed into a data acquisition (DAQ) unit (PCI-MIO-16E1) which provided 12-bit analogue to digital conversion[333]. The DAQ was placed directly into an expansion slot of an industrial PC, in which National Instruments LabVIEW for Windows software had been pre-installed. The equipment is shown in Figure 4-23 (b). The software enabled the chassis unit to be configured for the relevant terminal block modules, alongside the operation and control of the DAQ. A standard temperature acquisition program from the National Instruments library was used as the basis for signal capture and storage to disk. A few modifications were made to enhance real-time viewing, sampling rate changes and data capture. An alternative program was developed involving the ability to incorporate considerable signal filtering if so desired. The programs allowed all thermocouple channels to be viewed, with actual data logging starting and finishing on the press of an on screen 'button'. The sampling rate was normally set at 400Hz for all channels to ensure a high resolution within the region of

austenite to ferrite transformation (envisaged as occurring over very short time periods due to the low arc energies); this consequently led to large data files (particularly when 10+ channels were being monitored). A proprietary data compression software package (Winrar) was therefore used to enable data to be transferred via floppy disc from the non-networked laboratory PC. The data itself was split into blocks of 1 second length, with header information dividing each block; a macro program was written in Excel (see Appendix E) to remove all headers and allow automatic division of the data to provide an (effectively) reduced sample rate e.g. picking out every tenth data point, and then automatically presenting the (reduced) data in a graphical format. The latter was useful for demonstrating the overall thermal cycle, when a sample rate of 20-40Hz was sufficient for display purposes.

Several methods for determining the cooling times, rates and transformation temperatures from the captured data were examined both in terms of methodology and data manipulation. It was decided that Matlab software exhibited excellent curve fitting capabilities and multiple differentiation of the resulting polynomial to enhance the transformation temperature start, maximum rate and finish. A program was written (see Appendix F) to display the original data in a graph format, nth order polynomial fit, 1^{st} and 2^{nd} order differentials. A 50^{th} order polynomial was usually used for curve fitting over a temperature range of 1000 to 300°C; the associated differentials could then be used to determine the time at which the required transformation point occurred as well as its rate, allowing the former to be fed back into the polynomial fit for the temperature determination.

4.8.2.7 THERMOCOUPLE SIGNAL NOISE REDUCTION

The preheat thermocycle experiments were conducted using the Lincoln Powerwave 455 STT; it was not found necessary to electrically ground the pipe in order to obtain very little scatter: easy observation occurred for the transformation points with the original data capture program (i.e. small signal filtering).

The process thermocycle trials involved the Fronius TPS 4000 power supplies, and even with just a single wire weld considerable scatter within the data precluded sensible observation of the cooling curves. A ground cable was consequently attached to the pipe; this linked directly to the building ground loop which ended at several Cu stakes driven into the ground. An auto-transformer was also used to power the data capture equipment; this did not completely isolate the equipment from the ring main (as per an uninterrupted power supply) but did provide a degree of mains stabilisation. All experiments (bar the dual tandem torch trials) consequently exhibited an acceptable level of data scatter. These experiments were conducted using a single or a pair of power supplies. The addition of another pair for the dual tandem weld increased the level of scatter, but it was decided at the time to use post signal acquisition processing to reduce data scatter, rather than introduce signal filtering at the capture stage.

4.8.3 METAL CORED WIRE CHEMISTRY VARIATION TRIALS

The numerous weld procedure tests conducted in the earlier research yielded several solid wire welding consumables eminently suitable for various PGMAW/GMAW process variations of mechanised narrow gap pipewelding. An attempt to correlate all of

the weld procedure data produced in the proceeding girth welding trials was made using the correlation package available in Microsoft's Excel data analysis toolpack. Unfortunately, very few correlations of individual elements against the numerous mechanical properties available could be distinguished. As a result it was decided to vary individual elements in small amounts relative to the 0.9Ni 0.3Mo consumable judged to be the optimum commercially available narrow gap single wire chemistry. Carbon, nickel, molybdenum and chromium are classical strength or toughness increasing elements, and for these reasons it was decided to examine their various changes within the joint configuration and cooling rates associated with the optimised mechanised narrow gap welding process. The resultant matrix of wires shown in Table 4-4 was drawn up from a general review available from the literature of the aforementioned elemental effects relative to their weight percentage within weld metals, coupled with the limited useful correlation data achieved from the girth welding trials. Two 7 kg reels of each alloy variant were supplied by a leading consumable manufacturer. The ability of the wires to be made on a very small batch basis was due to their metal cored construction. The internal powder fill allowed the various changes in alloy chemistry to be adjusted to suit, whilst the sheath material composition remained constant. A control sample was welded initially to determine the proximity of the base line composition to the target 0.9Ni 0.3Mo; slight adjustments were consequently made and the matrix of chemistries then manufactured.

Although a 1.0mm diameter metal cored wire could have been manufactured, discussions with consumable manufacturers led to the adoption of 1.2 mm wires throughout the matrix due to their similar characteristics to a 1.0 mm solid wire. A pulse waveform was developed from one within the databank of the Wavedesigner Pro software suitable for narrow gap welding (see Appendix A); due to the constant wire feed speed/arc energy requirement of the experiments only a condition involving a single wire feed speed was set. This was arrived at by converting the 1.0mm solid wire used at 10.0m/min to a 1.2mm metal cored wire equivalent. Deposition levels were calculated based on 100% transfer from the wire to the weld in both cases, resulting in a wire feed speed of 7.6 m/min for the metal cored wire. The actual WFS set resulted in 7.7 m/min due to optimum fusion/transfer characteristics and arc energy requirements from the waveform development work.

Each wire was deposited in a procedure as close as possible to that of a mechanised narrow gap pipeweld, even though welding was confined to the flat position using X100 plate material. The main difference was the incorporation of a backing bar, resulting in an added heat sink for the root/hot pass as compared to the pipe situation. Mechanical tests, however, were predominantly located at the plate mid-thickness. Root gap, bevel angle and plate flatness were carefully controlled prior to the cored wire welding. The bevels were initially bandsawn to a nominal 5° and then accurately machined. The backing bar was carefully clamped prior to tack welding, such that any potential gap between plate and backing bar due to plate bow was eliminated. A jig was manufactured to minimise plate distortion during welding (see Figure 4-9). To minimise the potential heat sink of the jig, only the packing shims and the restraining bolts were in contact with the test plates. Plate bow prior to welding could also be minimised by varying the torque on individual clamping bolts, such that a constant CTWD along the groove length could be maintained. Preheating of each run was provided by heating mats connected to a SMAW transformer, with temperature measurement monitored at the

plate ends and mid-joint length via a magnetically attached thermocouple. The welding procedures for each consumable variant are recorded in Appendix B.

In common with the majority of narrow gap welds produced throughout the research, the cap gap width was recorded alongside the remaining depth from pipe/plate surface to weld metal surface. This occurred after the internal root run for pipe welds, and after the attachment of a backing bar for the plate welds. The latter was recorded after every weld pass. On completion of welding, each plate was allowed to cool to room temperature prior to removal from the jig. Several plates using both cored and solid wires were employed for the sole purpose of testing the cooling rates of the weld metal for direct comparison with the pipe weld trials; external (harpoon) thermocouples were plunged at run mid-length for each deposited layer.

4.9 ELECTRICAL PARAMETER MEASUREMENT

The calculation of arc energy is an important parameter associated with most WPS and WPARs, and alongside the range of averaged current and voltage often forms one of the common essential variables in a given welding procedure. Its correlation with the associated mechanical properties of a welded joint is a well documented research area yielding valuable information regarding the likely properties to be achieved. Due to the nature of the predominant welding processes under examination (PGMAW and dip transfer GMAW) the transient waveforms of current and voltage exhibit considerable variation with repect to time. A stable waveform provides identical correlation between the theoretical average based on a perfectly repeatable waveform and the measured average value, but the introduction of any form of instability will diversify the two values. The statistical analysis of current and voltage waveforms is a research field in its own right, and it is not the intention to pusue this area in the current research. However the accurate representation of the averaged values, alongside the typical stable waveforms achieved was of interest. Several methods were used to record either the average values and/or the actual waveforms.

Initially, a WERC-developed monitoring system, Arcwatch, was used to capture the individual current and voltage waveforms from which an average value could be computed, alongside other statistical data. The shorter the data acquisition period, the higher the capture frequency possible, leading to a greater overall accuracy. However, the greater the number of channels desired (i.e. if multiple current and voltage readings from the various deposition techniques are employed for a given weld pass) the lower the number of capture 'windows' that can be generated for the same number of samples per 'window'. Hence a typical 5 kHz logging frequency for two channels with this equipment resulted in an acquisition time of only 9.83s. This is useful if a short weld run is to be studied with reasonable accuracy, but a typical pipeweld in, for instance 36 in. OD pipe would require approximately 3 minutes continuous logging for each half circumference. Another stumbling block for some of the weld procedures was the incapacity to log more than two current and voltage channels at any one time due to input limitations.

It was therefore decided to use hand held current and voltage meters to obtain average values over the entire length of a given weld run. This relied on the typical minimum and maximum values being visually noted throughout the weld run and subsequently recorded. In most cases the power supplies possessed their own current and voltage

display, which could be compared with that of the hand held meters as a cross check, but in general the latter were used as the recorded values. In these cases the specific waveforms and their stability were not regarded as being necessary to document.

Prior to the thermocycle and metal cored wire trials a Yokogawa DL750 oscilloscope was acquired to improve both the length, resolution and number of channels possible to record. Four current, four voltage and two thermocouple channels were initially added, with the potential for another six channels. A typical sample rate of 5 kHz allowed 100s logging, regardless of the the number of channels recorded. As per the Arcwatch system, calibrated LEM Hall effect current measurement probes and voltage leads were used. The oscilloscope itself was purchased with a calibration certificate. Waveforms could consequently be analysed easily, with a high level of accuracy of the measured values both in transient terms and as computed averages.

The attachment of voltage leads was performed in such a way as to minimise the voltage drop other than that across the arc. This involved placing one measurement point either as close as possible to the contact tip on the torch or on the wire feed unit, with the other measurement point usually at the work return connection of the power supply on the workpiece. The current clampmeters were usually positioned around the torch liner adjacent to the wire feed unit.

4.10 MISCELLANEOUS WELDING PROCEDURE DETAILS

The production of a welded joint involves a considerable number of variables, any one of which can alter the weldment properties to various degrees. In an attempt to highlight this, a checklist sequencing the variables involved in the production of a typical mechanised narrow gap weld conducted during the research is shown in Table 4-5. All of the actions were conducted prior to the start of a new weldment, whereas only those shown in bold were conducted prior to every pass. It should be noted that the synergic curve itself contains a high number of settings for each particular predetermined point, but once these are stored it usually requires only a single parameter, for instance wire feed speed, to be selected.

4.11 NDT AND MECHANICAL TESTING

Numerous mechanical specimens were extracted from both the pipe and plate welds. Prior to specimen extraction, all of the WERC pipe welds were radiographed using radioactive isotope sources (typically Iridium 192). These were full circumferential shots with D7 film quality, image quality according to BS EN 462-1[334] using a W10 image quality indicator (IQI) and 3 wire sensitivity, carried out to BS EN 1435[335] by an independent NDT inspection company (NDIS of Witney, Oxon.). The dual torch welds from Serimer-Dasa were X-rayed at their facility in Mitry-Mory, Paris, and evaluation performed to BS 4515, API 1104 or DNV with image quality according to BS EN 462-1 (W6). All defective areas were transferred from the film to the pipe, such that only 'clean' sections were taken for any destructive testing. During welding procedure development, the location of defective areas provided macro sections for quick determination of the specific defect type. Two example NDT reports are shown in Appendix D.

Wherever possible the dimensions and locations of the mechanical specimens were as specified in relevant industry standards, combinations of which were necessary to maximise the data:

- BS EN 288-9:1999[336] (Specification and approval of welding procedures for metallic materials – Part 9 : Welding procedure test for pipeline welding on land and offshore site butt welding of transmission pipelines), and
- BS 4515-1:2000[46] (Specification for welding of steel pipelines on land and offshore – Part 1 : Carbon and carbon manganese pipelines).

The two BS standards were used to specify requirements for testing, qualification, approval, essential variables and production welding criteria. The standards were also used to specify the type of impact specimens (2 mm sub-pipe ID, from the location between 11 and 1 o'clock) and the hardness traverse test/location details. Impact tests were performed on the weld metal centreline and fusion line at -20, -40, -60 and -80°C. These standards do not cover the type of pipe material being welded (X100 is group 4 of PD CR ISO 15608:2000 and above a yield strength of 500MPa) and as a consequence the hardness (and impact toughness) requirements specified are not applicable.

- The API standard for pipeline welding (API 1104, Welding of pipelines and related facilities[308]) specifies cross weld tensile, nick-break and side bend tests. One of each sample type was taken from the 2, 4, 8 and 10 o'clock positions when possible. The standard is currently relevant up to X80 grade pipes.
- The Canadian standard Z662-99[309] (Oil and gas pipeline systems) is very similar to API 1104 in terms of the destructive test requirements, and for the purposes of the current programme the API standard was used for conformance requirements.

Additional tests involved hardness traverses of the seam/girth weld interaction, macro sections from 12, 3 and 6 o'clock, all weld metal tensile tests and CTOD testing of weld metal and HAZ for which the relevant standards for the given test were used [320,337-339]. A diagram indicating the relative positions around the pipe from which samples were extracted is shown in Figure 4-25.

4.11.1 WELD METAL TENSILE TESTING

The all weld metal tensile tests originally used 4.0mm round bar specimens, but these were abandonded early in the work in favour of a rectangular (strip) tensile as shown in Figure 4-26. This specimen samples a greater depth of weld metal, thereby incorporating a more representative section of the microstructures present in a multi-pass joint. Specimen proportionality in terms of elongation value was maintained by the use of the standard gauge length (l_0) / original gauge length cross sectional area (S_0) relationship ($l_0 = 5.65(S_0)^{1/2}$). Strain rates of 0.006 strain/minute were employed at least until the proof stress (sometimes up to 2.5% strain) at which point the extensometer was removed, and crosshead control then employed at 0.2 strain/minute until fracture. The 0.2% proof strength, 0.5% tensile extension strength, UTS and elongation were recorded. The full penetration repair, tie–in, plate and thermocycle welds also allowed strip tensile specimens to be made. In the case of the tie-in tests, round bar specimens

were also performed for comparative purposes, allowing measurements of reduction in area.

4.11.2 HARDNESS TESTING

Two sections were taken from each narrow gap girth weld, one from the 3 o'clock position, the other from the girth/seam weld interaction. The latter was cut such that the polished face comprised the centre of the longitudinal seam weld on one side of the girth weld section, and pipe base material on the other side (provided that the seams were not in line either side of the girth weld). The tie-in weld was examined in the same fashion as for the narrow gap welds. The sections were ground to ensure parallel surfaces, polished to a 1 μm surface finish and etched in 2% Nital. Hardness traverses were then performed in accordance with BS 4515-1. The load allowed points to be placed 0.8 mm apart in the heat affected zone. Indentations were made 2 mm below the pipe ID and OD as shown in Figure 4-27.

The repair welds were tested in a similar fashion to the full girth welds, except that a single traverse was performed in the case of the cap and root repairs. The HAZ in these cases comprised either pipe base material or the original girth weld. The part penetration repair allowed a traverse 2 mm below the pipe OD as well as the pipe mid thickness, whereas the full penetration repair mimicked the tie-in survey (see Figure 4-28).

4.11.3 IMPACT TOUGHNESS TESTS

Impact toughness transition curves were created for most of the narrow gap and tie-in welds. Charpy tests were conducted at temperatures of -20, -40, -60 and -80°C. The test pieces were prepared from a location 2 mm sub-pipe ID (BS 4515-1) for both the weld centre-line and fusion-line. The partial and full penetration welds were impact tested at -20°C, the sampling location being shown in Figure 4-29.

4.11.4 CTOD TOUGHNESS TESTS

Standard B x 2B through pipe wall thickness CTOD tests to BS 7448-1/2[320] were conducted with the crack tip located either on the weld centreline or the fusion line. In the majority of cases the fusion line comprised 50% weld metal and 50% base material, but certain samples allowed the notch to be placed consistently within 0.25 mm of the fusion line into the HAZ. Three tests at each crack location were performed at -10°C for each weld. Specimens were typically extracted from the 4.30 to 5.30 and 6.30 to 7.30 positions around the pipe.

4.11.5 CROSS WELD TENSILE, NICK BREAK AND SIDE BEND TESTS

Wherever possible specimens were extracted close to the 45°, 135°, 225° and 315° positions around the pipe. Dimensions and acceptance criteria were according to API 1104[308]. A single side bend test was performed on the full and part penetration repairs, with the full penetration repair also having a cross weld tensile and nick break.

4.11.6 PLATE AND THERMOCYCLE WELD MECHANICAL TESTING

The plate tests involved hardness, all weld metal tensile and impact tests from the positions shown in Figure 4-30, with the thermocycle pipe weld mechanical specimens and thermocouple hole location sections extracted from the positions shown in Figure 4-31. Test procedures for the individual items were as above. Microhardness testing was performed on the thermocycle welds instead of the conventional pipeweld survey, using a 500g load with 15s load time on a vertical traverse just off the centreline of the weld metal. The indent size allowed a spacing between the centre of each point of 0.2mm, with traverses starting and ending within 1mm of the pipe OD and ID.

4.11.7 MECHANICAL TEST EQUIPMENT AND ITS CALIBRATION

The majority of tests were subcontracted to an independent testing company (Bodycote Materials Testing Ltd. of Daventry, Northants). This ensured traceability of calibration alongside the conformance with an independent accreditation service (UKAS). Parts of the research involved passing results to sponsor bodies who require quality assurance systems to be in place. Only specific testing machines at Cranfield are independently checked/calibrated on a rolling time basis, hence tensile, impact, bend, nick break and CTOD testing were all outsourced. At least one of each test type was witnessed for examination of the operating procedure and conformance with the relevant testing specification. Wherever possible electronic information generated throughout the test procedure was requested as a double check on the certificated result, alongside the possibility of further data analysis (e.g. the ASCII file of load vs extension/crosshead position for the tensile tests).

The majority of hardness testing was performed at Cranfield using either a Vickers-Armstrong pyramidal diamond indentor (typically 10 kg load) or a Matsuzawa Seiki Co. microhardness tester (typically 500 g load). The former was externally calibrated every 6 months, and the latter tested prior to each testing session with a certified steel hardness calibration block.

4.12 MICRO/MACROSTRUCTURAL EXAMINATION

Sections were obtained from all test welds. The sections were primarily from the 12 o'clock and seam/girth positions in the case of the pipewelds, although some sections from the 3 and 6 o'clock positions were also examined. High powered optical microscopy at magnifications up to 1000 times was used to examine the weld metals after polishing to a 1μm diamond surface finish and etching with Nital (nitric acid in methanol). A 2% acid solution was used for microstructral examination, whereas 10% was normally employed for photomacrographs. The microscope was a Nikon Eclipse ME600P, with a C-mount adaptor lens enabling a Nikon Coolpix 990 digital camera to capture the micro- and macrostructures (3.3M pixel resolution). Picture scaling was performed using a graduated microscope slide with 10μm divisions.

Quantification of the microstructural variants within selected deposited weld metals was attempted using the guidelines laid down by Abson, Duncan and Pargeter[173]. A Swift automatic point counter was connected to an electro-mechanical stage movement device, allowing assignment of up to ten phases and cumulative calculation to a preset

sample size. The sample size was set at 1000 points in response to the recommendations of Gladman and Woodhead[340] and Abson et al.[173] regarding the compromise between number of constituent (phase) types and the desired confidence interval/standard deviation. An optical magnification of 1000 times was used during all point counting due to the fine grain sizes in evidence. Incremental movement comprised of 0.1mm steps horizontally and 0.2mm vertically.

4.13 CHEMICAL ANALYSIS

All of the pipe and plate welds (bar some of the early procedure development trials) had chemical analysis performed on the weld metal by the chemistry laboratory of ESAB Group (UK) Ltd. In the case of the narrow gap welds a section (usually from the 3 o'clock position in the case of pipewelds) was cut longitudinally along the weld to allow an optical emission (OE) spectrometer to analyse the weld metal alone (spark diameter approximately 10 mm). Conventional i.e. 60° bevel joints allowed a transverse section to be sparked. The root pass was avoided in all cases as this may have given misleading chemical analysis results. The OE was calibrated at the start of each series of analysis tests using certified samples. The equipment operates by generating a spark in a similar fashion to that of an electric welding arc; the light emitted from the sample was analysed and the resulting wavelengths attributable to the type and subsequent percentage of the elements present. Two 'sparks' were conducted on every sample just after it had been linished to remove any surface contamination, the average of which became the certified result. Using this method the majority of elements required could be obtained with the desired accuracy (2 or 3 decimal places).

A further transverse section of the joint was cut to allow 5 x 4 x 4 mm sections of weld metal to provide samples for oxygen and nitrogen analysis. A Leco O_2 and N_2 analyser used a combination of infra-red detection (in the case of O_2) and thermal conductivity (N_2) to determine the sample levels. Three samples from each weld were placed in dilute hydrochloric acid, rinsed in methanol and stored in ether prior to anaylsis. Each individual sample was placed in a graphite crucible held between the two electrodes of the furnace. The sealed furnace was then flushed with helium to create an inert atmosphere devoid of nitrogen, and a high current (~1000A) subsequently applied. This generated temperatures in excess of 3000°C in the crucible, releasing both the free and combined oxygen and nitrogen to be carried through the system by the helium. The oxygen combines with the carbon of the crucible to form CO and CO_2; any CO was then fully converted to CO_2 using a Cu catalyst (at ~400°C) and the resulting CO_2 determined by an infra-red detector. An inbuilt calculation converted the CO_2 to O_2. All CO_2 was then scrubbed via a reaction with caustic soda, and the resulting nitrogen content determined by a thermal conductivity differential of the pure carrier gas and the nitrogen/carrier gas combination. All CO_2 must be removed prior to this due to the close thermal conductivites of N_2 and CO_2. Calibration via certified samples was again checked prior to each analysis session, with the average of the three weld metal samples recorded as the certified value.

Table 4-1: X100 Test material

Pipe Supplier Coding	Nominal Wall Thickness mm	Nominal Pipe Outside Diameter		Number of Pieces
		in.	mm	
A	19.05	30	762	12
A	19.05	Plate 1m x 2m		6
B15	14.9	36	914	12
B19	19.05	36	914	8
C	16.3	36	914	8
C	16.3	Plate : 1m x 2.8m		1

Pipe Storage

Mechanised oxy-acetylene cutting

Table 4-2: Electrode types used throughout the programme

Solid MIG Wires

Manufacturer	Wire Name	Diameter	Classification	Heat No.	Batch No.	Coil Size
Thyssen/CRC	K-Nova/ TS-6 (a)	0.9mm	AWS 5.18 ER70S-6	186 096		2.8Kg
Lincoln	SG2 Supramig (b)	1.0mm	AWS 5.18 ER70S-6	564D		
Thyssen	Union NiMo80 (~Union MoNi) (a)	1.0mm	AWS 5.28 ER90S-G	372116	47241	18Kg
Thyssen	Union MoNi (b)	1.0mm	AWS 5.28 ER90S-G	227309		
Oerlikon	Carbofil HT (a1)	1.0mm	AWS 5.28 ER100S-G		1004	15Kg
Oerlikon	Carbofil HT (a2)	1.0mm	AWS 5.28 ER100S-G		AJ2266	15Kg
Oerlikon	Carbofil NiMo-1 (a)	1.0mm	AWS 5.28 ER100S-G		14233	15Kg
Thyssen	Union NiMoCr (a)	1.0mm	AWS 5.28 ER100S-1	874658	46330	18Kg
Thyssen	Union NiMoCr (b)	1.0mm	AWS 5.28 ER100S-1	227206		
ESAB	OK 13.13 (b)	1.0mm	AWS 5.28 ER100S-G	23963		
Elga	Elgamatic 135 (b)	1.0mm	AWS 5.28 ER100S-G		024B1180	
ESAB	OK 13.29 (b)	1.0mm	AWS 5.28 ER110S-G		043113pv	
Bohler	X70-IG (a)	1.0mm	AWS 5.28 ER110S-G	58974	402945L	18Kg
Bohler	X70-IG (b)	1.0mm	AWS 5.28 ER110S-G	228554		
Thyssen	Union X85 (b)	1.0mm	AWS 5.28 ER110S-G			
ESAB	Spoolarc 120 (a1)	0.9mm	AWS 5.28 ER120S-1	120043	2402F25	15Kg
ESAB	Spoolarc 120 (a2)	0.9mm	AWS 5.28 ER120S-1	120049	2402F25	15Kg
Oerlikon	Carbofil 120 (a)	1.0mm	AWS 5.28 ER120S-G		227737	15Kg

SMAW Electrodes

Manufacturer	Wire Name	Diameter	Classification	Heat No.	Batch No.	Coil Size
Filarc	Filarc 118 (a)	2.5mm	AWS 5.5 E11018-M		5370063	
Filarc	Filarc 118 (a1)	3.2mm	AWS 5.5 E11018-M		4280233	
Filarc	Filarc 118 (a2)	3.2mm	AWS 5.5 E11018-M		7350743	
Oerlikon	Tenacito 80 (a)	2.5mm	AWS 5.5 E11018-G		000414	
Oerlikon	Tenacito 80 (a)	3.2mm	AWS 5.5 E11018-G		703249	

FCAW / MCAW Electrodes

Manufacturer	Wire Name	Diameter	Classification	Heat No.	Batch No.	Coil Size
ESAB	OK Tubrod 15.09 (a)	1.2mm	AWS 5.29 E111T1-GH4		0383049	5Kg
Oerlikon	Citoflux 110 (a)	1.2mm	AWS 5.29 E101T1-GH4		C1360-9085	16Kg
Oerlikon	Fluxofil M10S (a)	1.2mm	AWS 5.18 E70C-6C, E70C-6M		1D6343	16Kg

Where (a) = Cranfield electrode, (b) = Serimer-Dasa electrode

Table 4-3: Electrode chemistries

Solid Wires	Dia. (mm)	Batch N°	C	Mn	Si	S	P	Ni	Mo	Cr	Cu	Al	Nb	V	B	Ti	O_2 (ppm)	N_2 (ppm)	P_{CM}	CET	CE_{IIW}
K-Nova/ TS6	0.9	186 096	0.064	1.47	0.80	0.010	0.010	0.02	<0.005	0.03	0.12	<0.005	0.006	<0.005	<0.0005	0.06	30	46	0.17	0.22	0.33
SG2 Supramig	1.0	564D	0.1	1.5	0.8														Nominal		
Union MoNi (b)	1.0	227309	0.1	1.46	0.66	0.010	0.012	1.05	0.39		0.14			0.01					0.25	0.32	0.50
Union MoNi (a)	1.0	47241	0.099	1.55	0.63	0.016	0.01	1.07	0.41	0.03	0.09	0.008	0.005	0.007		0.07	30	106	0.25	0.33	0.52
Oerlikon Carbofil HT (a1)	1.0	1004	0.072	1.36	0.76	0.011	0.009	0.47	0.46	0.48	0.15	0.005	0.006	0.006	<0.0005	0.005	145	98	0.24	0.30	0.53
Oerlikon Carbofil HT (a2)	1.0	AJ2266	0.081	1.37	0.75	0.012	0.010	0.41	0.54	0.55	0.14								0.25	0.31	0.55
Oerlikon Carbofil NiMo-1 (a)	1.0	14233	0.087	1.62	0.63	0.008	0.009	0.91	0.31	0.03	0.10	<0.005	0.006	<0.005	<0.0005	0.070	79	68	0.23	0.31	0.49
Union NiMoCr (b)	1.0	227206	0.08	1.67	0.57	0.014	0.005	1.45	0.48	0.20									0.25	0.34	0.59
Union NiMoCr (a)	1.0	874658	0.074	1.46	0.58	0.014	0.009	1.38	0.52	0.18	0.12	0.012	0.005	0.007	<0.0005	0.06	28	82	0.24	0.32	0.56
OK 13.13 (b)	1.0	23963						0.50	0.25	0.55									Nominal		
Elgamatic 135 (b)	1.0	024B1180	0.1	1.6	0.55			1.35	0.3	0.35	0.1								0.26	0.35	0.59
OK 13.29 (b)	1.0	043113PV	0.1	1.6	0.50			1.25	0.25	0.3	0.1			0.08					Nominal		
X70-IG (a)	1.0	58974	0.081	1.45	0.59	0.016	0.008	1.32	0.25	0.26	0.08	0.005	0.005	0.1		0.05	37	56	0.24	0.30	0.54
X70-IG (b)	1.0	228554	0.09	1.57	0.62	0.012	0.007	1.36	0.23	0.29		0.006		0.09					0.25	0.32	0.56
Union X85 (b)	1.0	496086	0.08	1.68	0.68	0.012		1.77	0.54	0.32									0.27	0.36	0.65
ESAB Spoolarc 120 (a1)	0.9	120043	0.057	1.55	0.4	<0.005	0.007	2.28	0.50	0.28	0.08	0.012	0.006	0.006	0.0007	0.02	58	61	0.24	0.34	0.63
ESAB Spoolarc 120 (a2)	0.9	120049	0.079	1.51	0.36	0.006	0.005	2.28	0.51	0.27	0.02	0.008	<0.005	0.005	0.001	0.02	63	68	0.26	0.35	0.64
Flux/ metal cored electrodes	Dia. (mm)	Batch N°	C	Mn	Si	S	P	Ni	Mo	Cr	Cu	Al	Nb	V	B	Ti	O_2 (ppm)	N_2 (ppm)	P_{CM}	CET	CE_{IIW}
Filarc 118 (a)	2.5	5370063	0.06	1.65	0.44	0.006	0.015	2.14	0.39	0.01	0.04	<0.005	<0.005	0.01		0.02			0.22	0.32	0.56
Filarc 118 (a1)	3.2	4280233	0.057	1.62	0.4	0.008	0.013	1.95	0.39	0.02	0.04	<0.005	<0.005	0.01		0.014			0.21	0.31	0.54
Filarc 118 (a2)	3.2	7350743	0.047	1.56	0.3	0.007	0.015	2.14	0.44	0.02	0.04	<0.005	<0.005	0.01		0.01			0.20	0.30	0.55
Tenacito 80 (a)	2.5	000414	0.064	1.64	0.42	0.008	0.008	2.18	0.48	0.43									0.25	0.35	0.66
Tenacito 80 (a)	3.2	703249	0.045	1.60	0.33	0.006	0.007	2.19	0.46	0.37									0.22	0.32	0.62
OK 15.09 (a)	1.2	0383049	0.06	1.3	0.4			2.7	0.3										Nominal		
Citoflux 110 (a)	1.2	C1360-9085	0.1	1.3	0.35			2.0											Nominal		
Fluxofil M10S (a)	1.2	1D6343	0.06	1.6	0.5														Nominal		

Where $P_{cm} = C + Mn/20 + Mo/15 + Ni/60 + Cr/20 + V/10 + Cu/20 + Si/30 + 5B$ $CE_{IIW} = C + Mn/6 + (Cr + Mo + V)/5 + (Cu + Ni)/15$

$CET_{(BS\ EN\ 1011\text{-}2)} = C + (Mn+Mo)/10 + (Cr+Cu)/20 + Ni/40$

All results reported in wt% unless stated. Flux/ metal cored wire analyses as per manufacturer's batch tests

Table 4-4: Metal cored wire target analyses

Name	HB No.	Plate No.	C	Mn	Si	Ni	Mo	Cr
MC Control 1	B2803 3 0	MC1	0.080-0.90	1.65-1.75	0.50-0.60	0.85-0.95	0.25-0.35	0.00-0.05
MC Control 2	B2803 3 1	1	0.080-0.90	1.65-1.75	0.50-0.60	0.85-0.95	0.25-0.35	0.00-0.05
Ni low	B2803 3 2	2	0.080-0.90	1.65-1.75	0.50-0.60	0.0-0.1	0.25-0.35	0.00-0.05
Ni high	B2803 3 3	3	0.080-0.90	1.65-1.75	0.50-0.60	1.4-1.6	0.25-0.35	0.00-0.05
Mo low	B2803 3 4	4	0.080-0.90	1.65-1.75	0.50-0.60	0.85-0.95	0.15-0.20	0.00-0.05
Mo high	B2803 3 5	5	0.080-0.90	1.65-1.75	0.50-0.60	0.85-0.95	0.4-0.45	0.00-0.05
Cr medium	B2803 3 6	6	0.080-0.90	1.65-1.75	0.50-0.60	0.85-0.95	0.25-0.35	0.20-0.30
Cr high	B2803 3 7	7	0.080-0.90	1.65-1.75	0.50-0.60	0.85-0.95	0.25-0.35	0.45-0.55
C low	B2803 3 8	8	0.045-0.055	1.65-1.75	0.50-0.60	0.85-0.95	0.25-0.35	0.00-0.05
C high	B2803 3 9	9	0.115-0.125	1.65-1.75	0.50-0.60	0.85-0.95	0.25-0.35	0.00-0.05
C high, Mo low	B2803 3 10	10	0.115-0.125	1.65-1.76	0.50-0.61	0.85-0.96	0.0-0.10	0.00-0.05
C low, Mn low, Si low, Ni high, Mo low	B2803 3 11	11	0.065	1.50	0.3	1.45	0.15	0.00-0.05

Table 4-5: Welding procedure checklist for pipe and plate welds

Pipe geometry	**Bevel accuracy : typically 4 angles and 3 distances per pipe end** **Minimisation of high-low (preferably with pipe longitudinal seam welds out of line)**
Welding bug setup	Bug guiding band position Torch wire feed liner attachment/routing/condition
Torch setup	**Wire angle (lead and trail for tandem)** **Contact tip and shroud condition/anti spatter coating** **Gas shroud height above pipe surface** Wire separation at relevant CTWD (tandem torch) Torch separation (dual/dual tandem torches) **Wire centralisation in groove (cast and helix compensation)**
Power supply setup	Synergic curve selection **Wire feed speed** **Trim settings** Start/stop sequences Cable length compensation (inductance/resistance test) Torch cooling unit working Interface with bug control working correctly Work return attachment on pipe minimises voltage drop at this point
Welding parameters	**Travel speed** **Oscillation width** **Oscillation frequency** **CTWD** **Preheat/interpass** Gas flow rate **Start/stop grinding and interun cleaning**
Monitoring	**Current** **Voltage** **Time** **Distance** **Deposition depth** Cap gap width after internal root run

Items in bold are checked before or after every weld pass

Figure 4-1: Research programme flowsheet

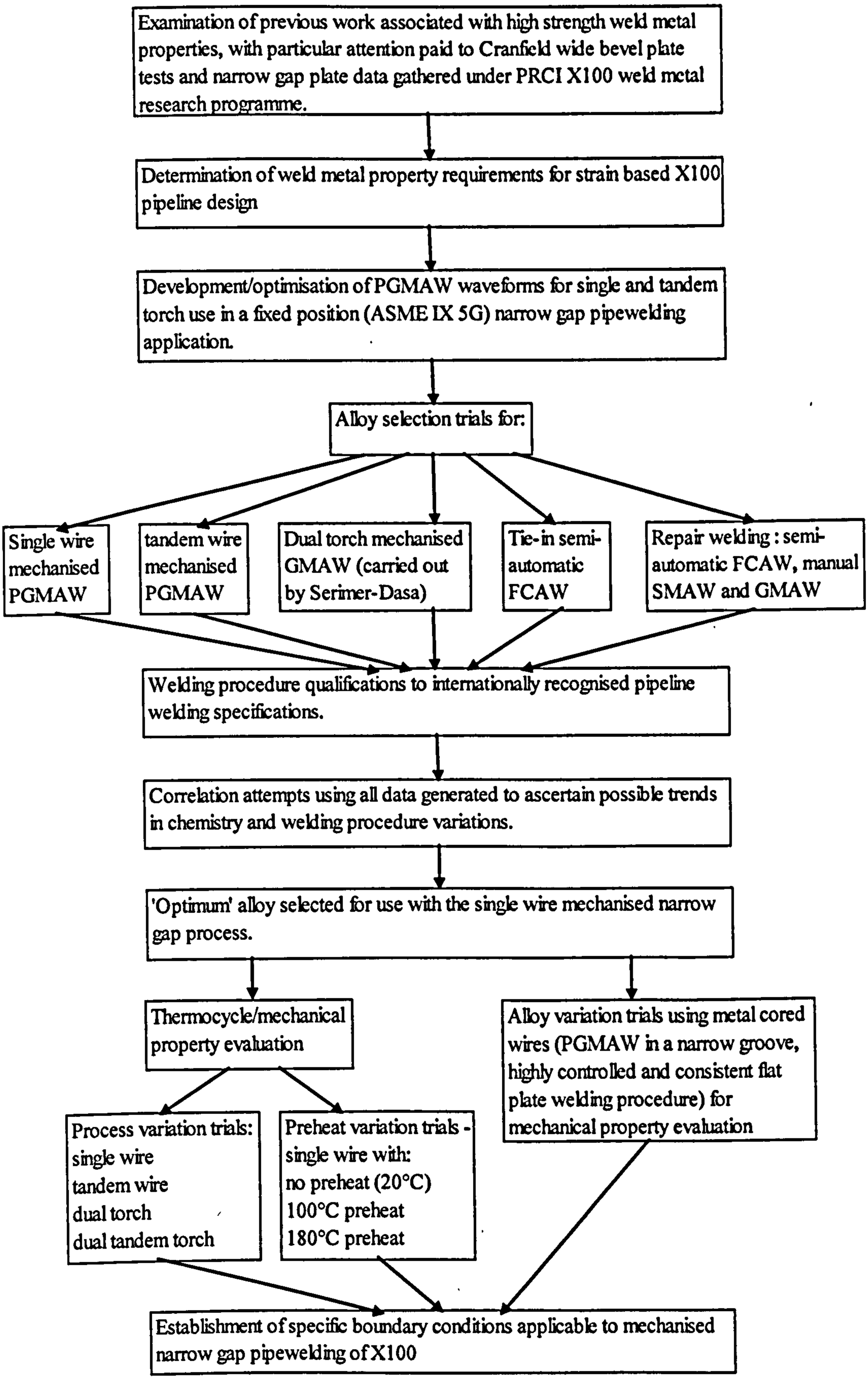

Figure 4-2: Narrow gap single wire welding power source (Lincoln 455 STT), Yokogawa Oscilloscope (DL 750) and Wavedesigner Pro® power source control software

a)

b)

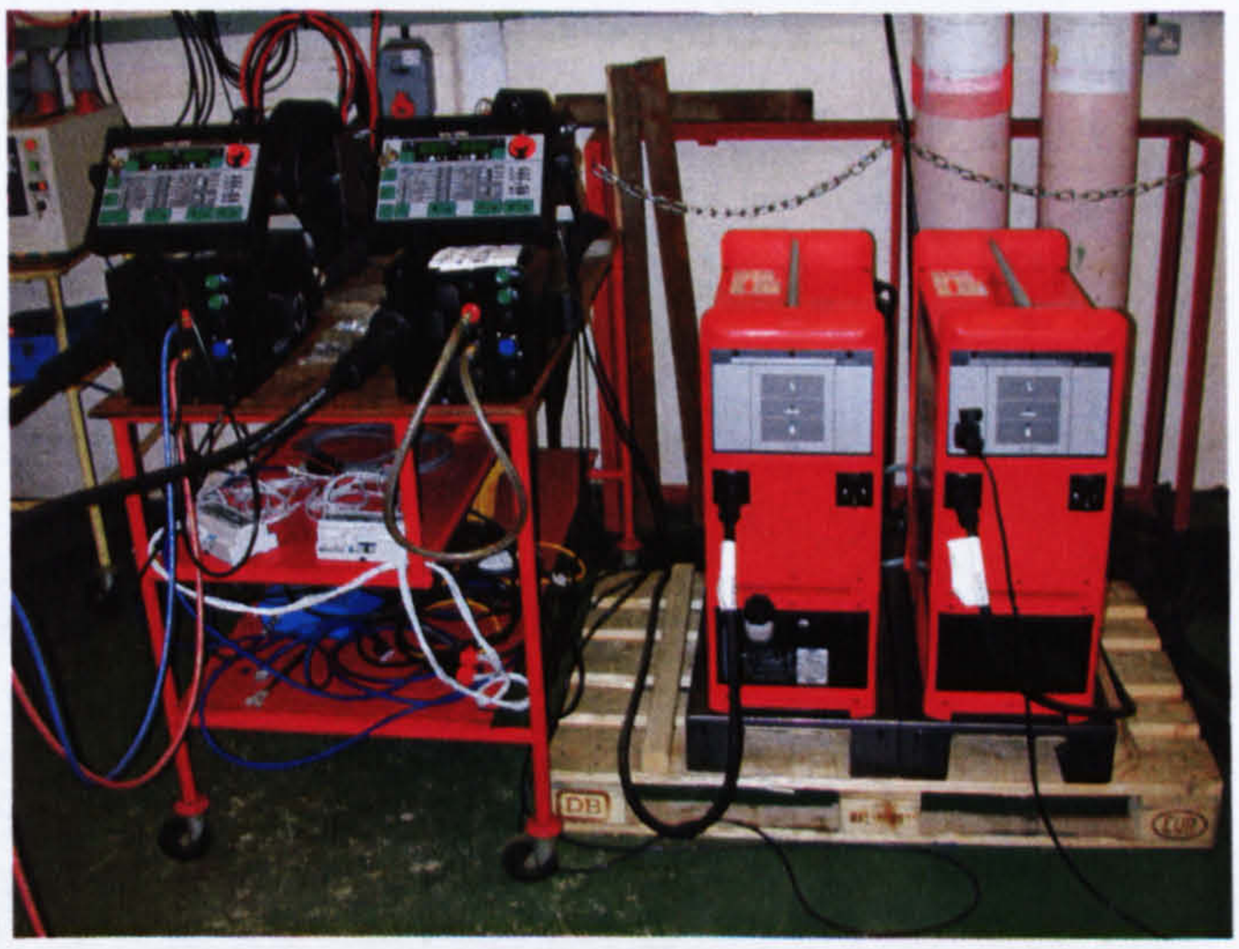

Figure 4-3: a) Initial and b) Later narrow gap synchronised tandem welding power sources (Fronius TransPuls Synergic)

Figure 4-4: Tie-in and repair welding power source (ESAB Aristo 2000)

Figure 4-5: CRC-Evans 36 in. pipe facing machine

Figure 4-6: CRC-Evans 36 in. internal pipewelding machine

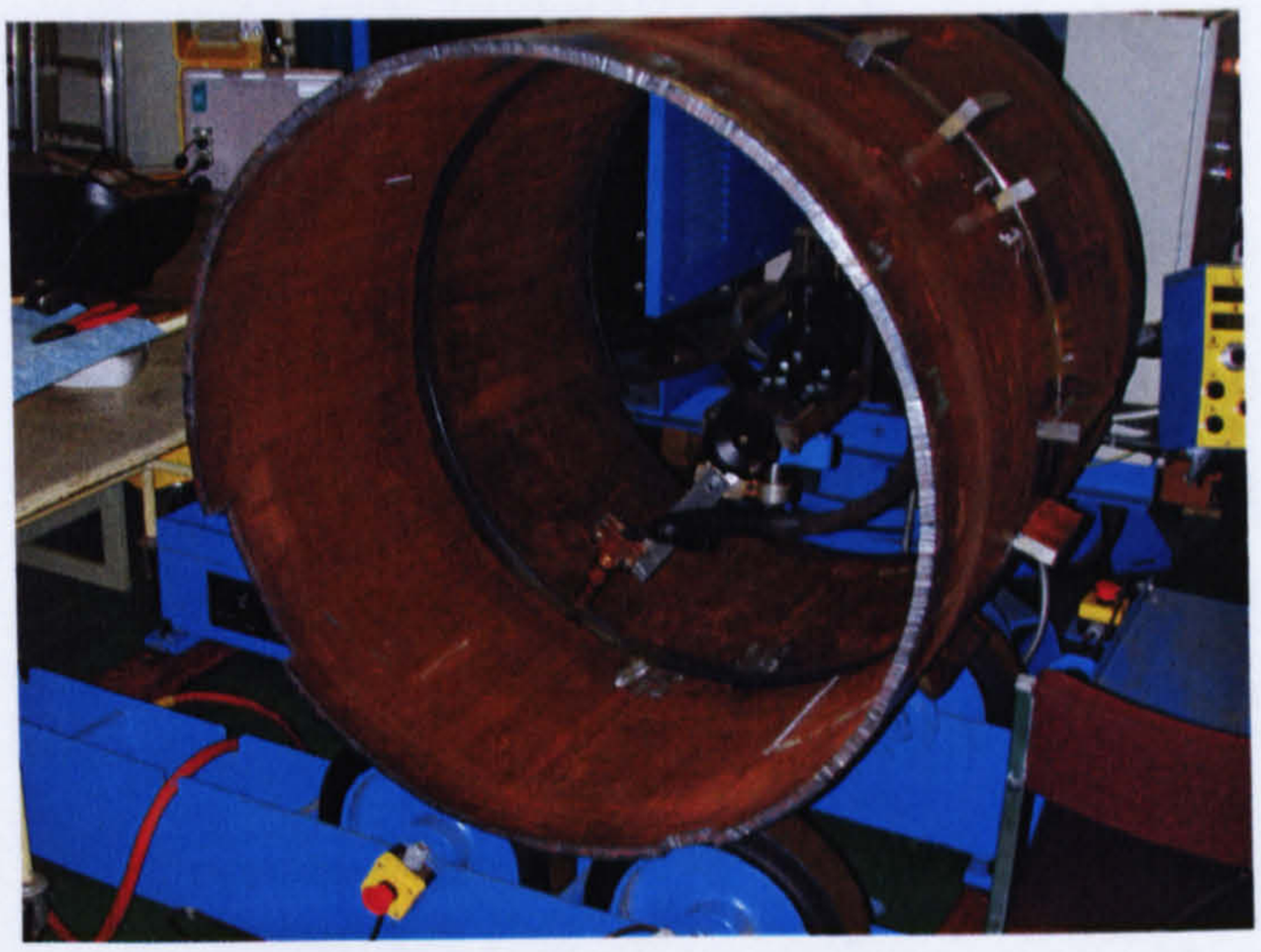

Figure 4-7: SAW column and boom setup for internal root welding

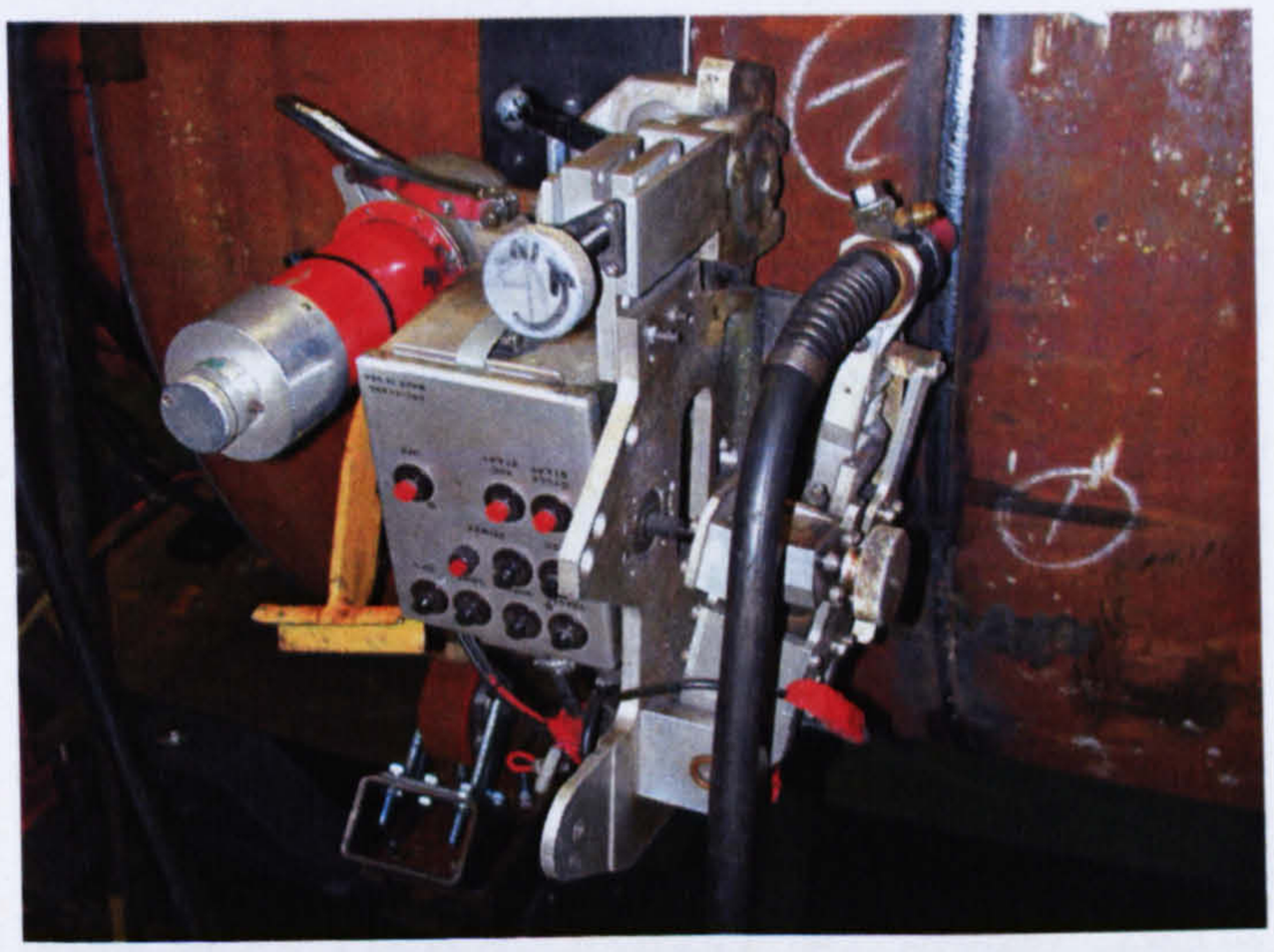

Figure 4-8: CRC-Evans P100 welding bug

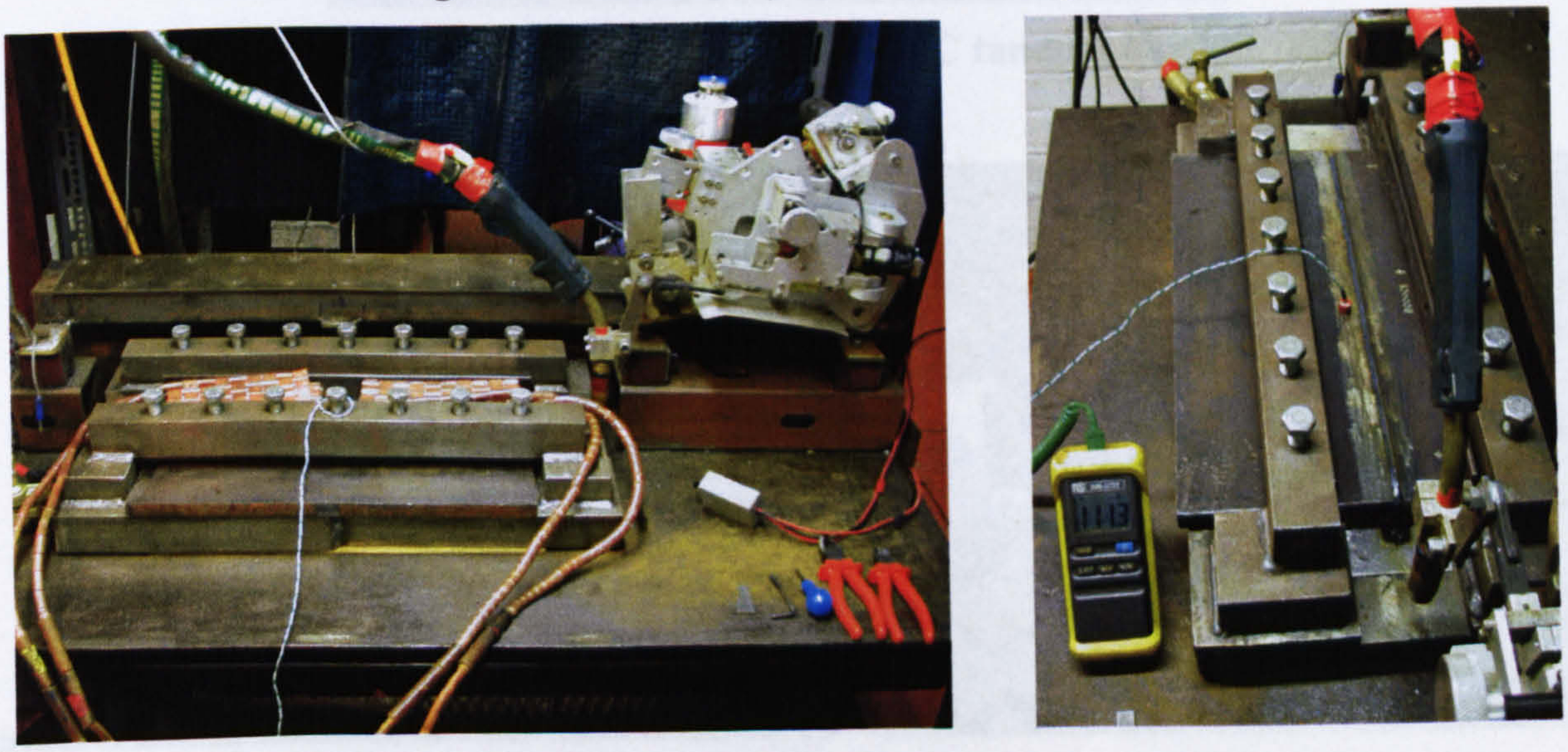

Figure 4-9: Equipment setup for flat plate welding

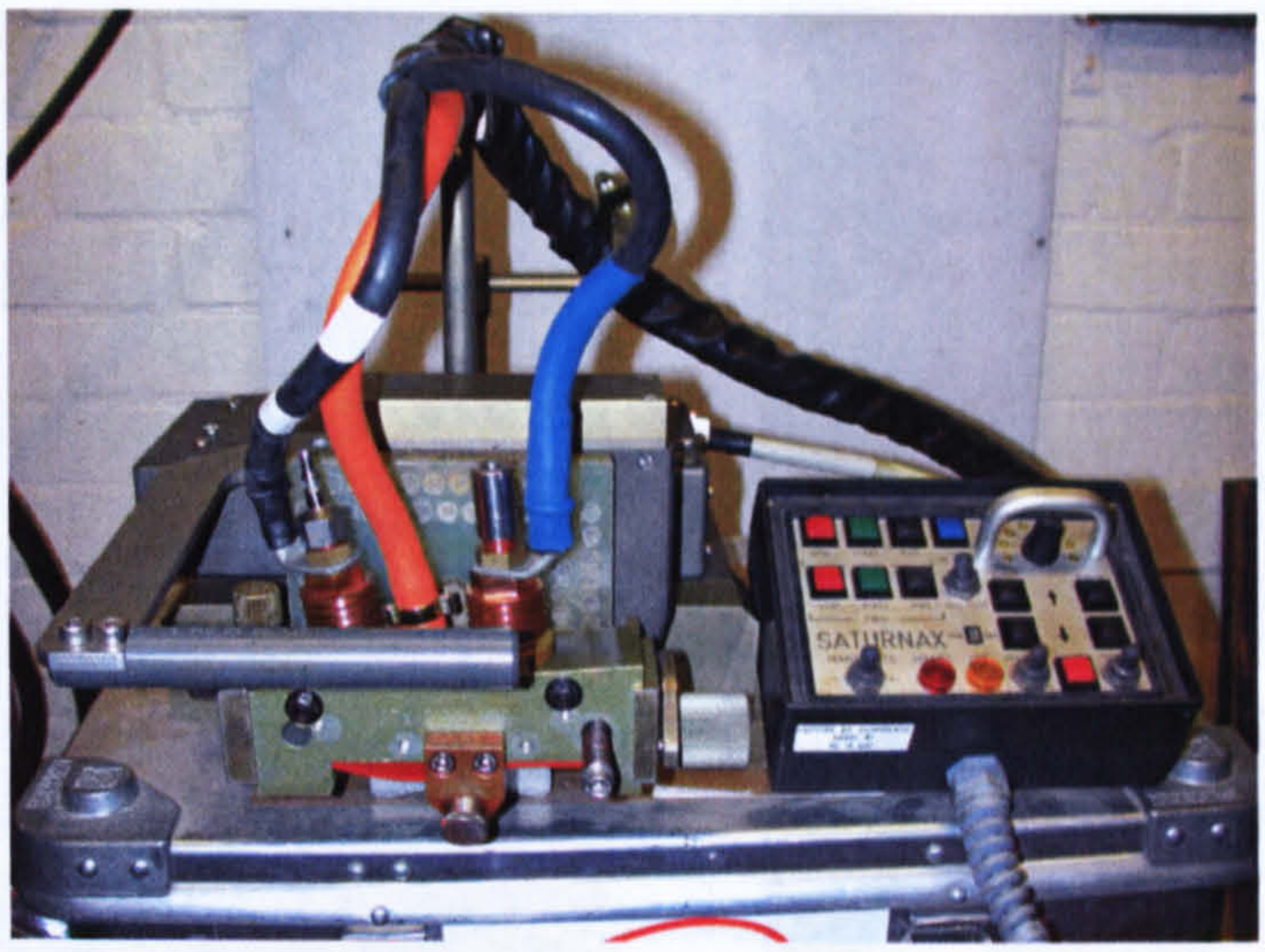

Figure 4-10: Serimer-Dasa's Saturnax 5 dual torch welding bug and controller

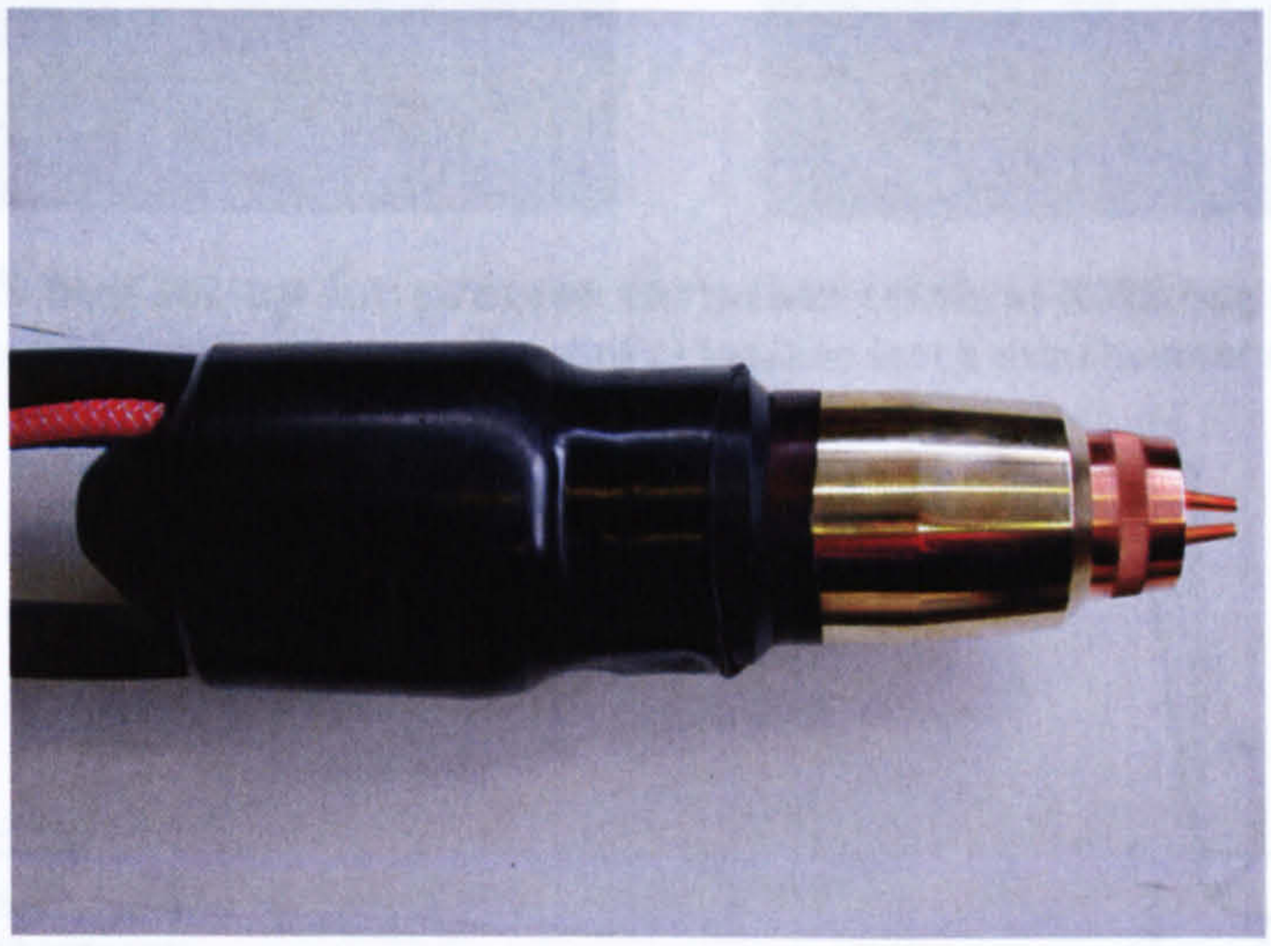

Figure 4-11: Water cooled WERC tandem torch

a)

b)

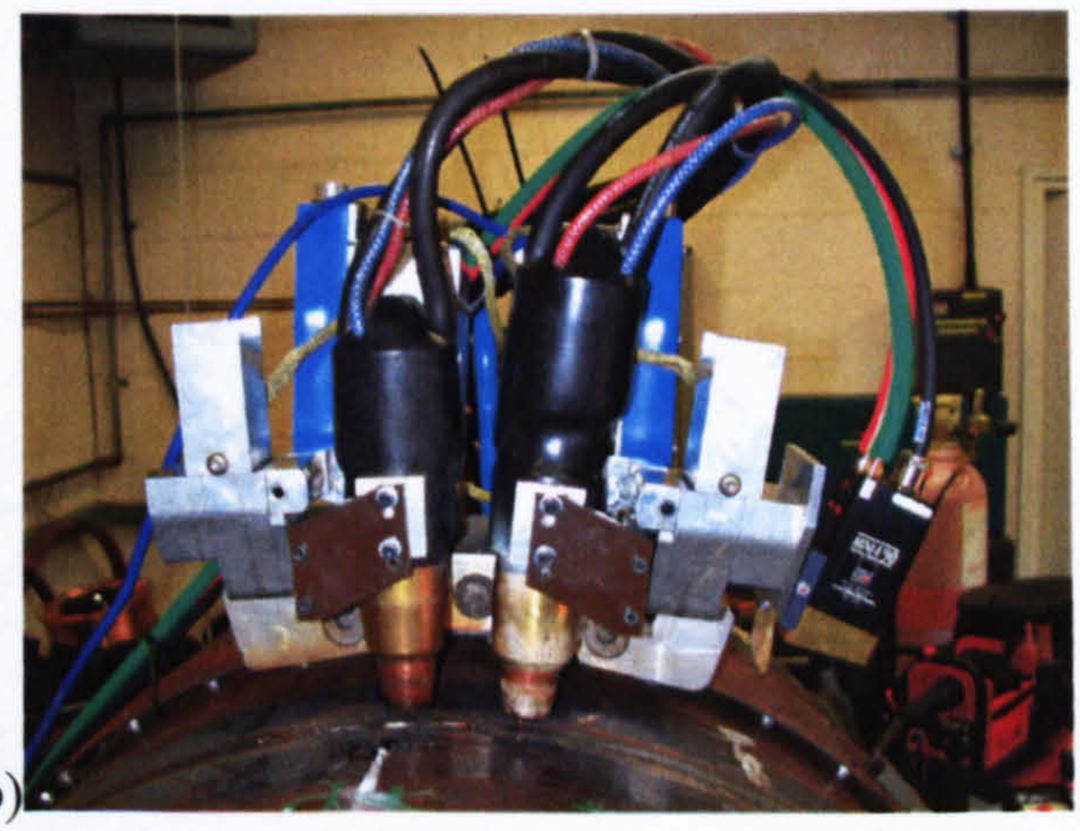

Figure 4-12: RMS MOW II welding system a) Control/switching boxes b) dual torch welding bug/ WERC tandem torches

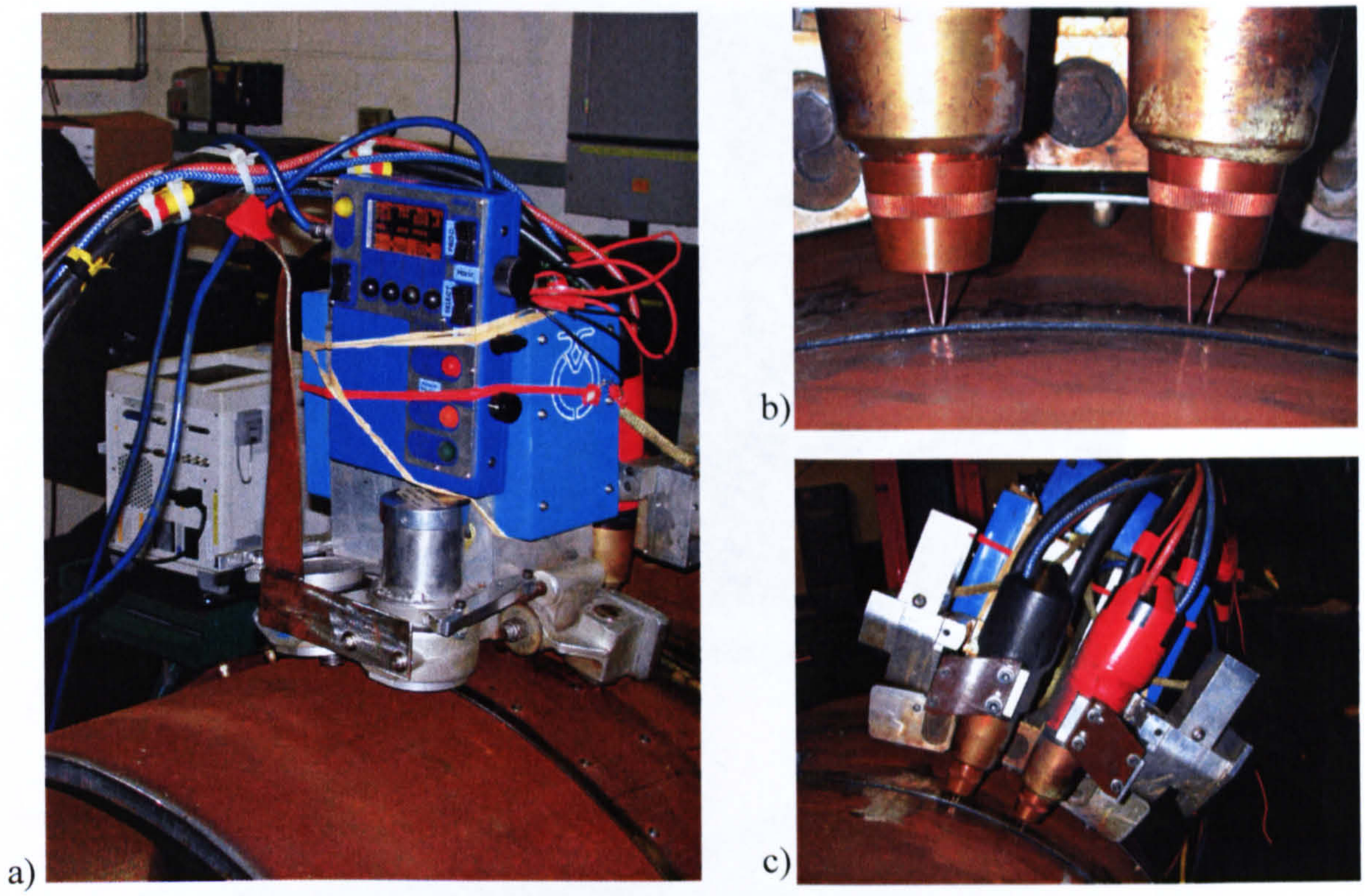

Figure 4-13: RMS bug set-up for process variation trials a) RMS bug with control pendant attached b) dual tandem torch setup c) tandem torch attachement on bug

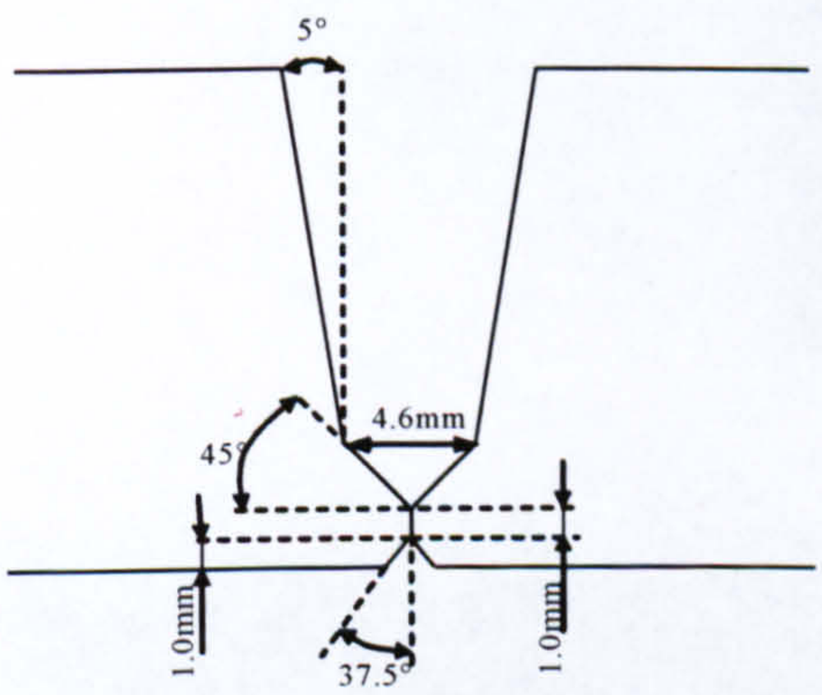

WERC : internal/external

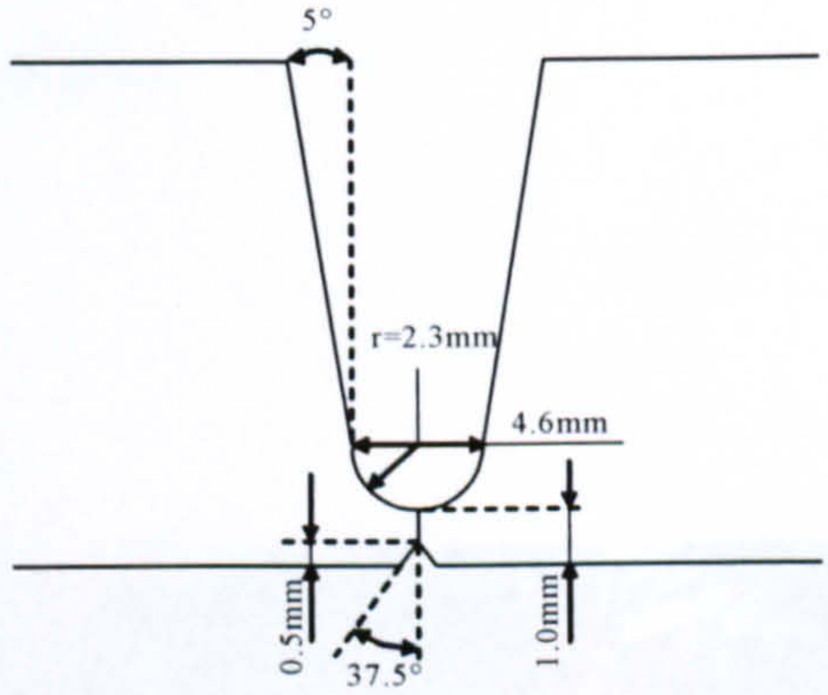

WERC : all external

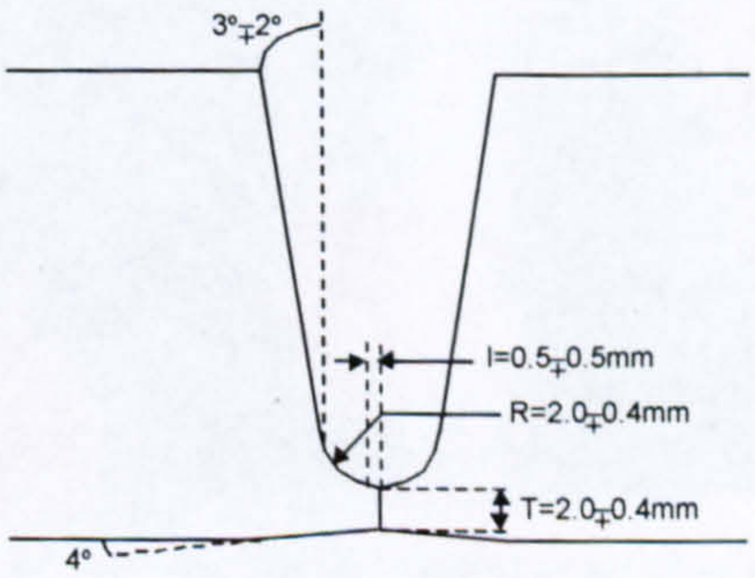

Serimer-Dasa : all external

Figure 4-14: Typical narrow gap weld preparations used throughout procedure development

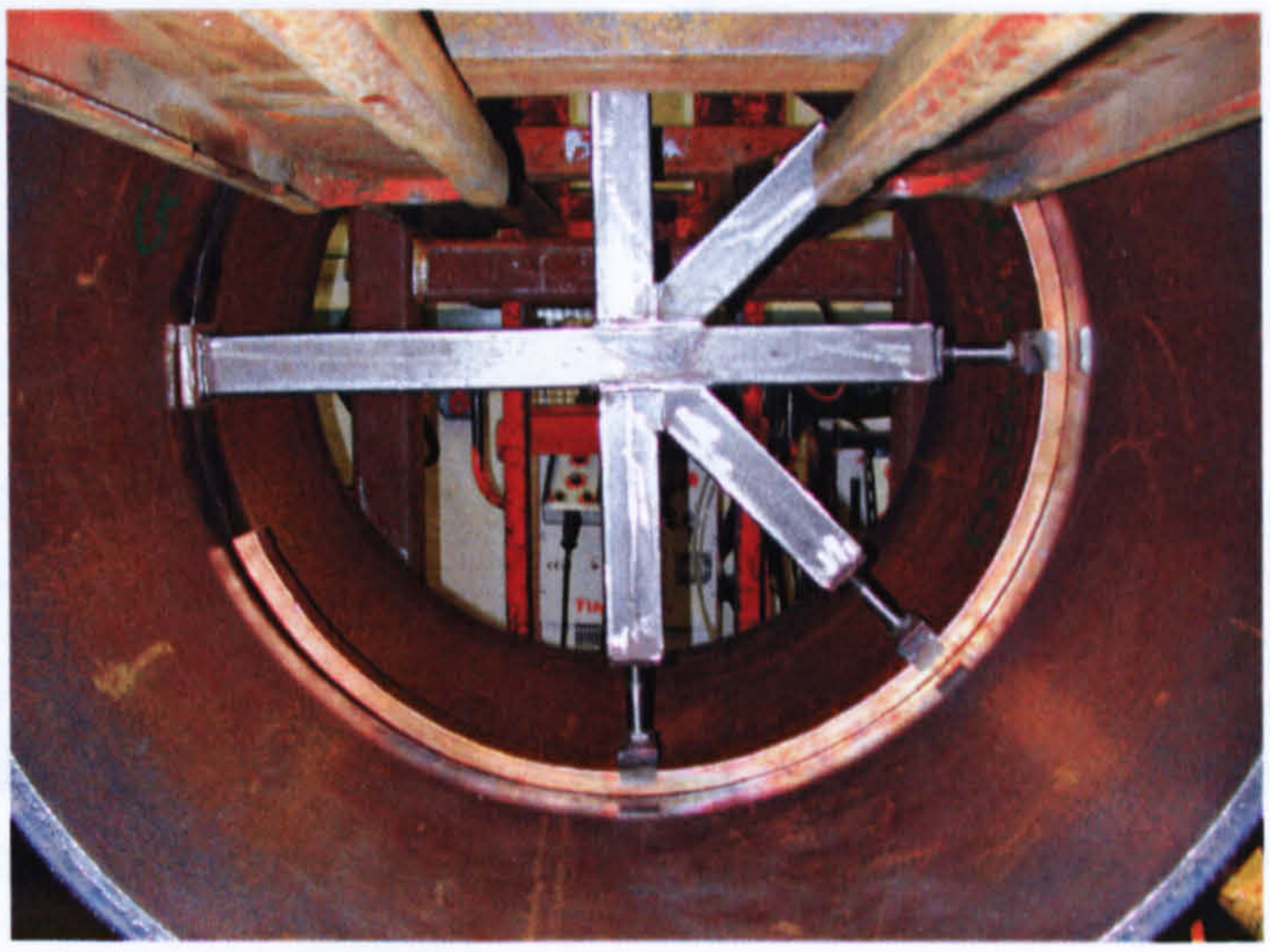

Figure 4-15: WERC copper backing system

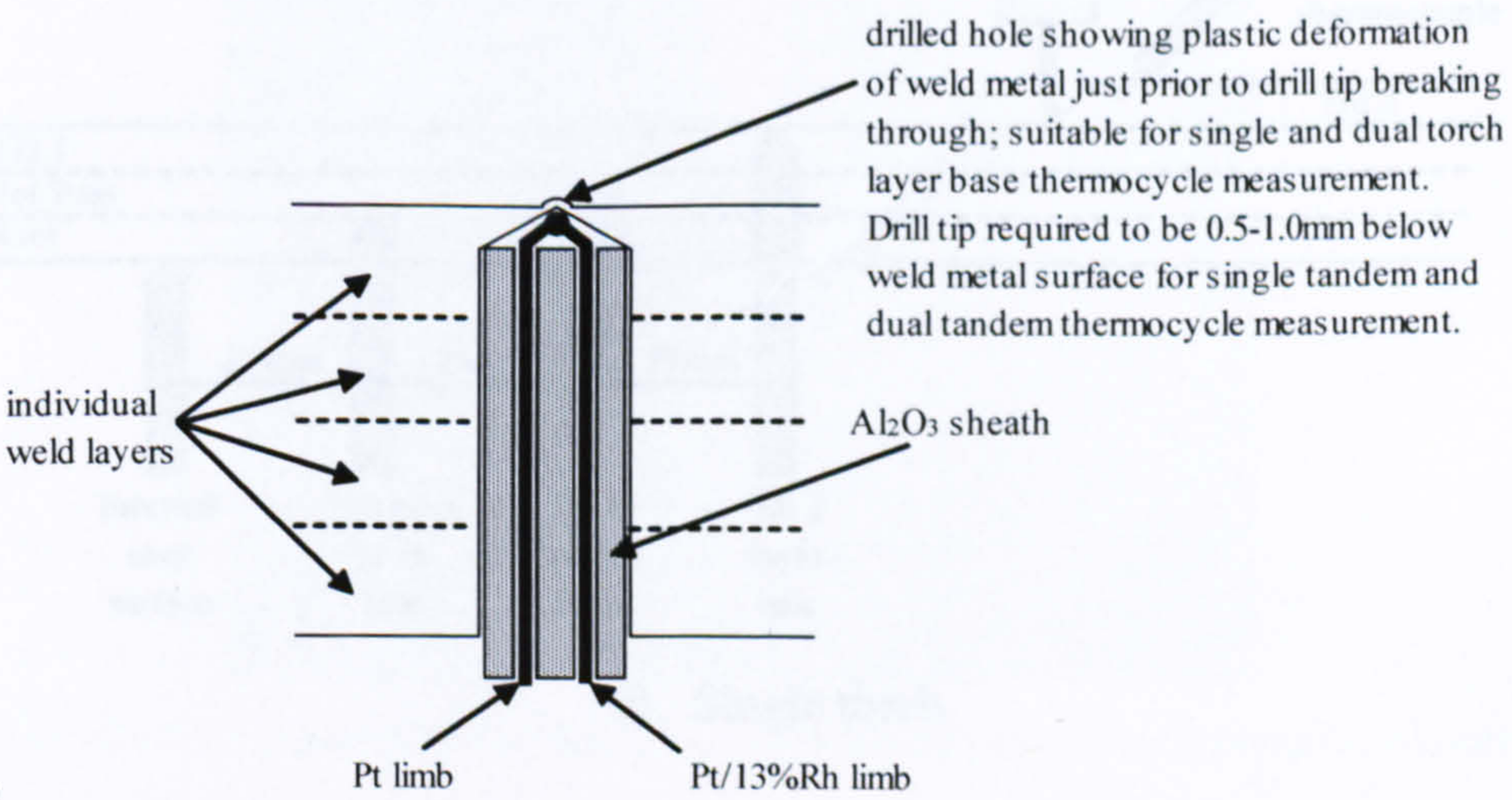

a)

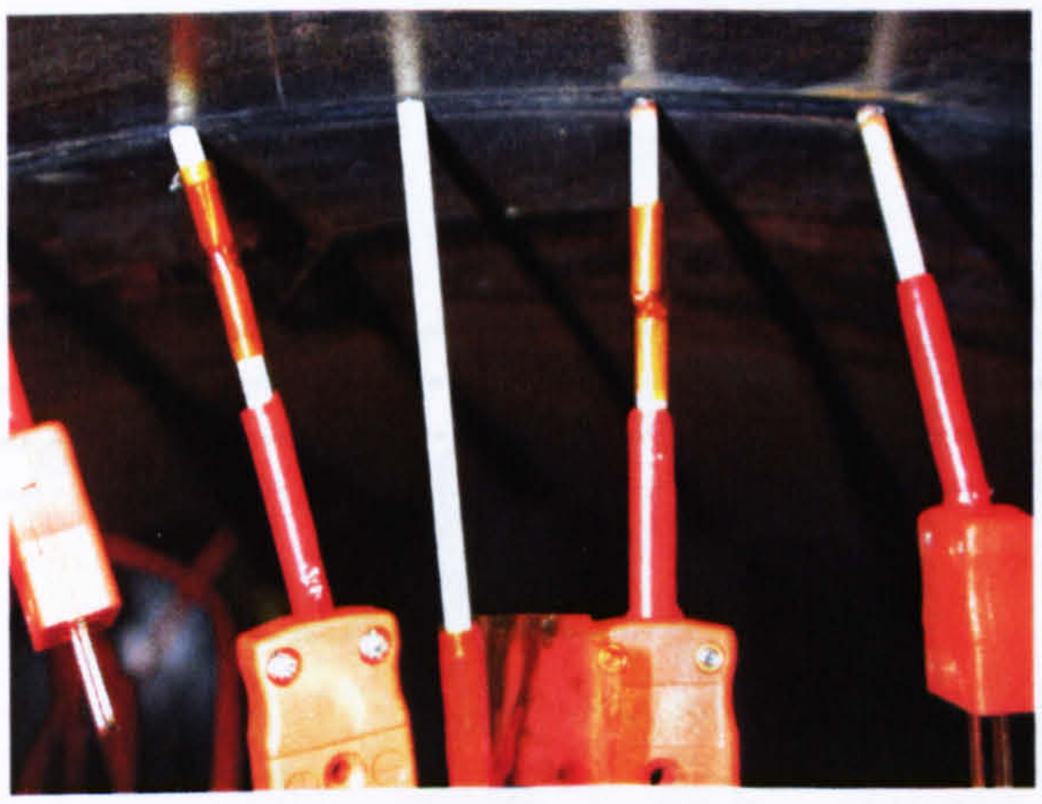

b)

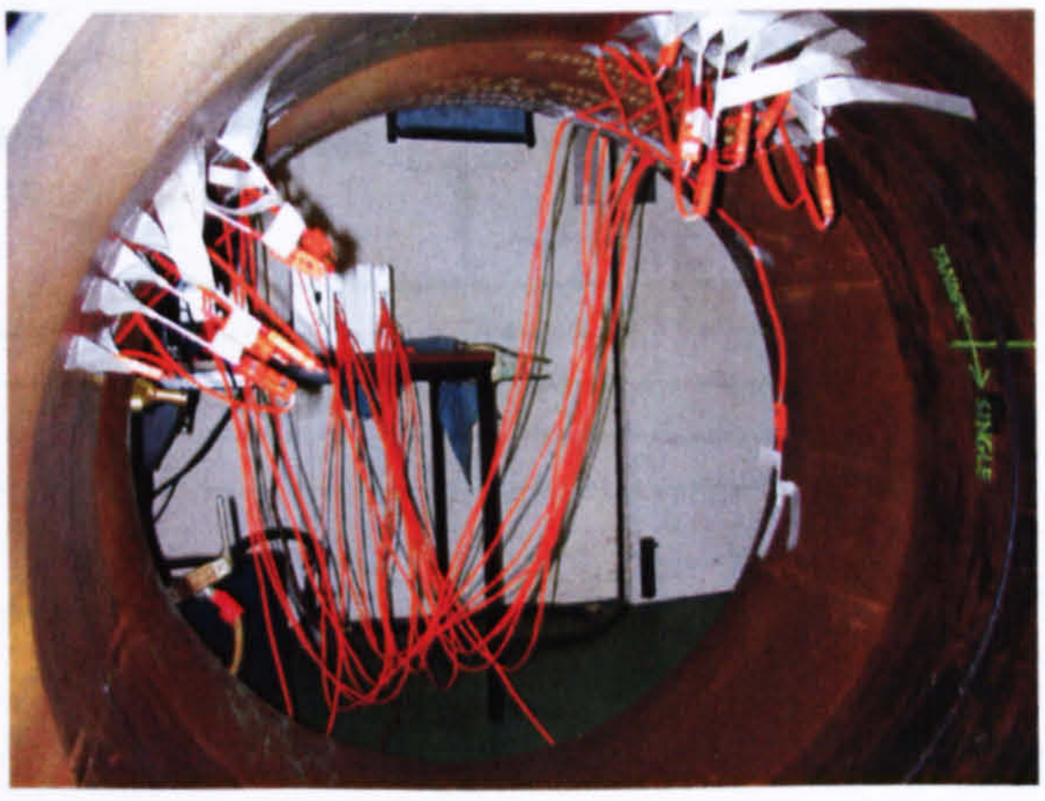

c)

Figure 4-16: Internal thermocouple placement a) correct thermocouple placement b) close up after welding and support tape removal c) final (cap) pass thermocycle monitoring set up

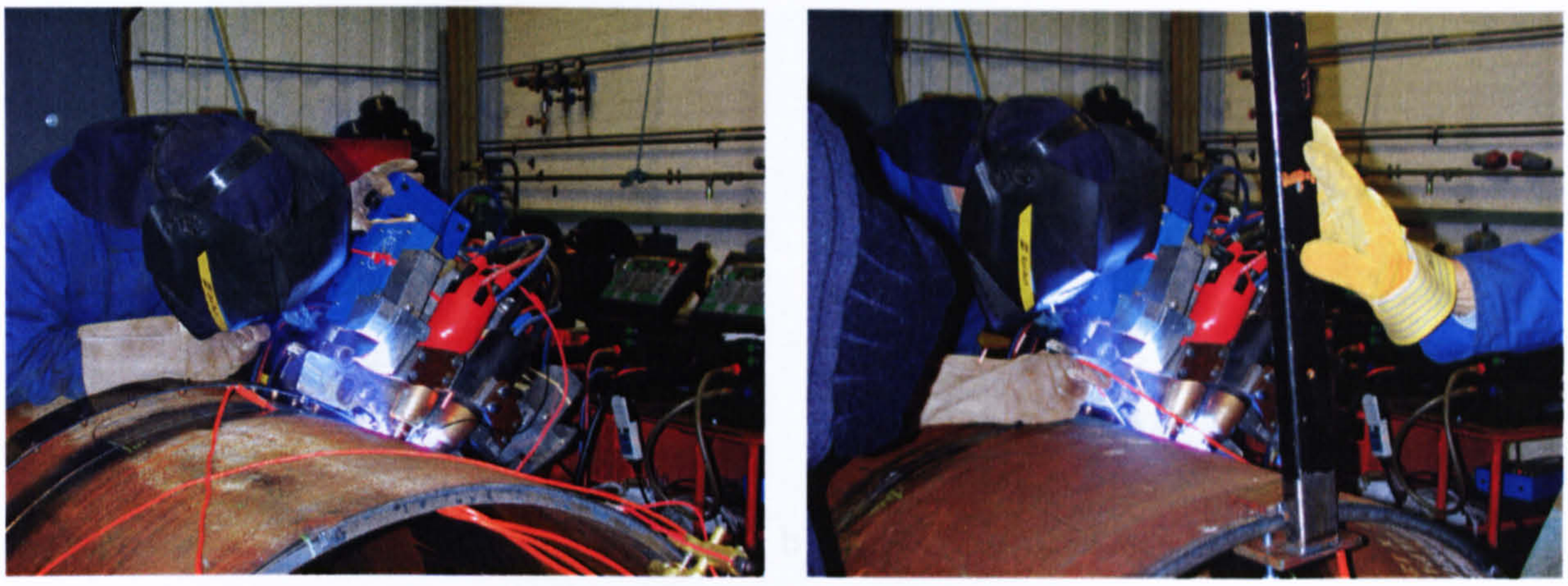

Figure 4-17: Welding and external thermocouple placement for process variation trials

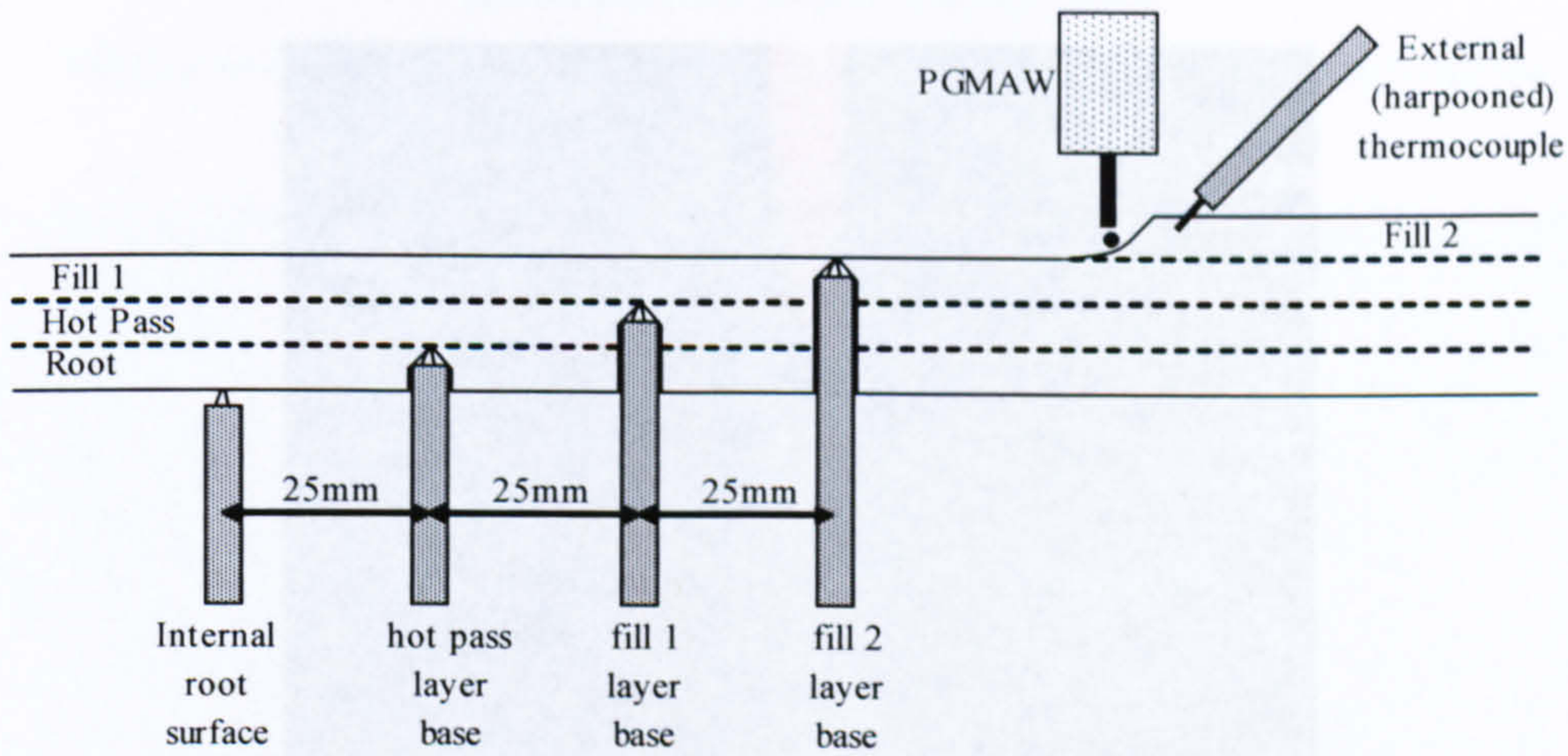

a) Single torch

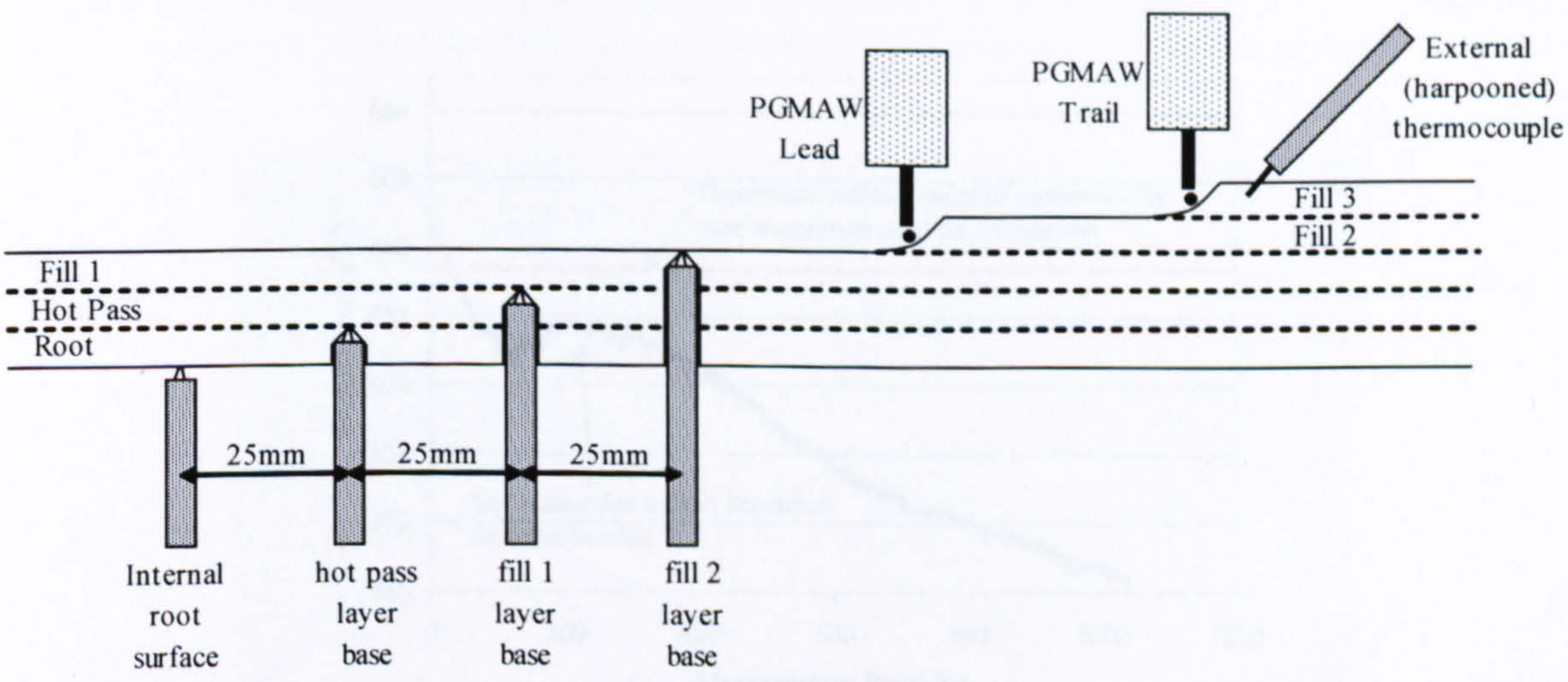

b) Dual torch

Figure 4-18: Typical thermocouple placement sequences

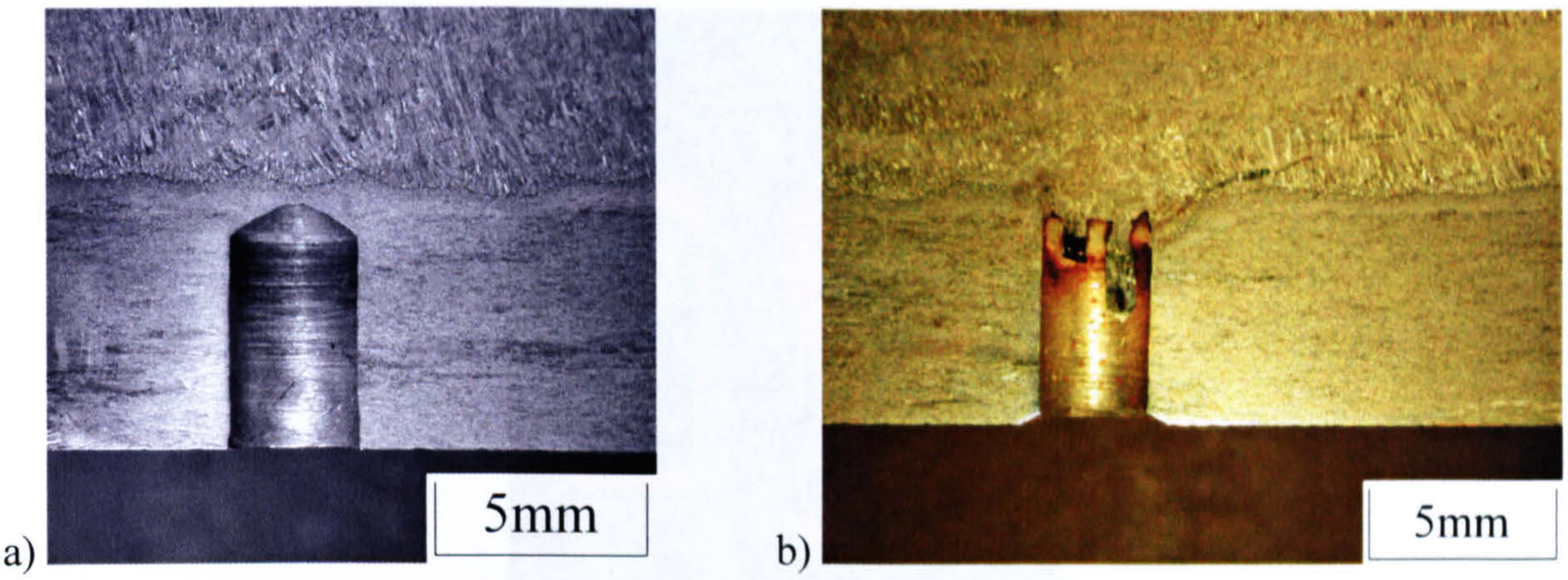

Figure 4-19: Internally placed thermocouple sections a) example of typical drilled hole b) thermocouple section after welding showing Pt limbs extending down hole

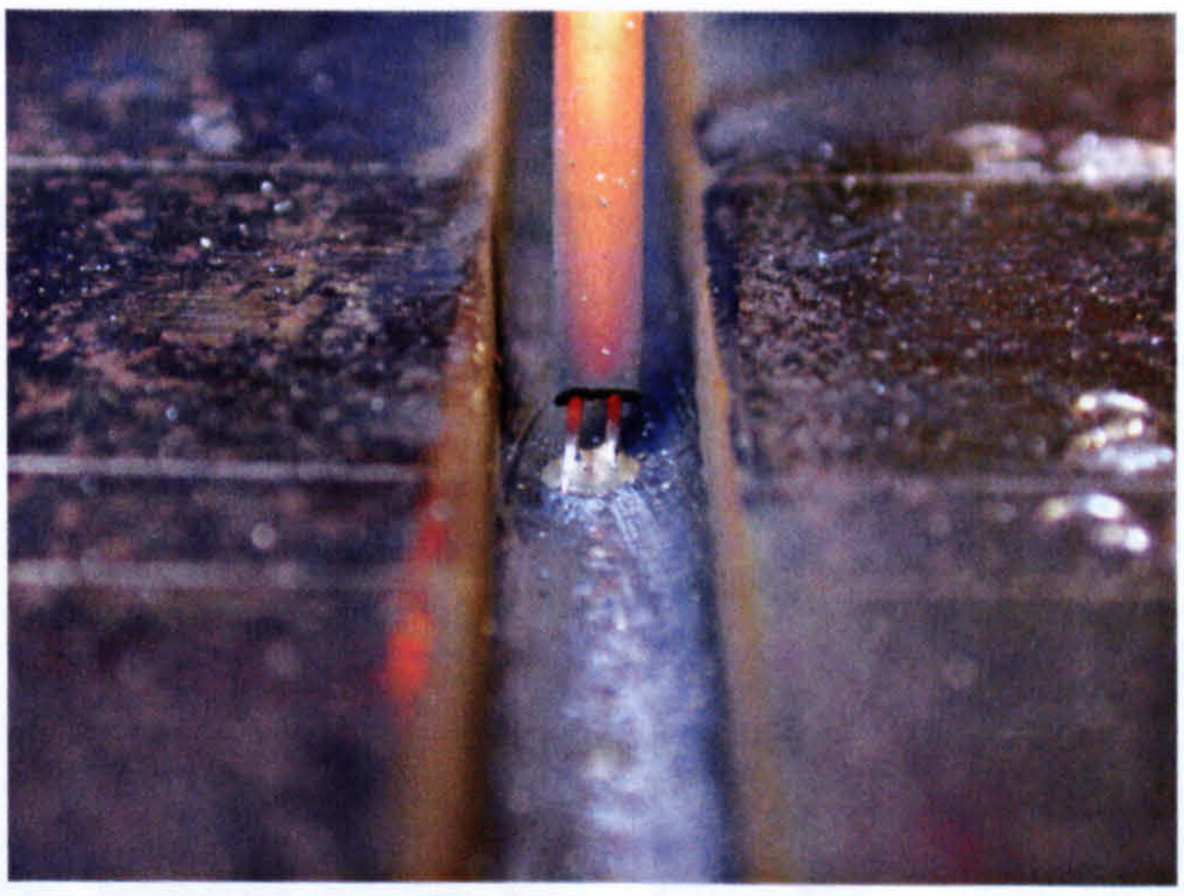

Figure 4-20: Typical external (layer surface) thermocouple placement

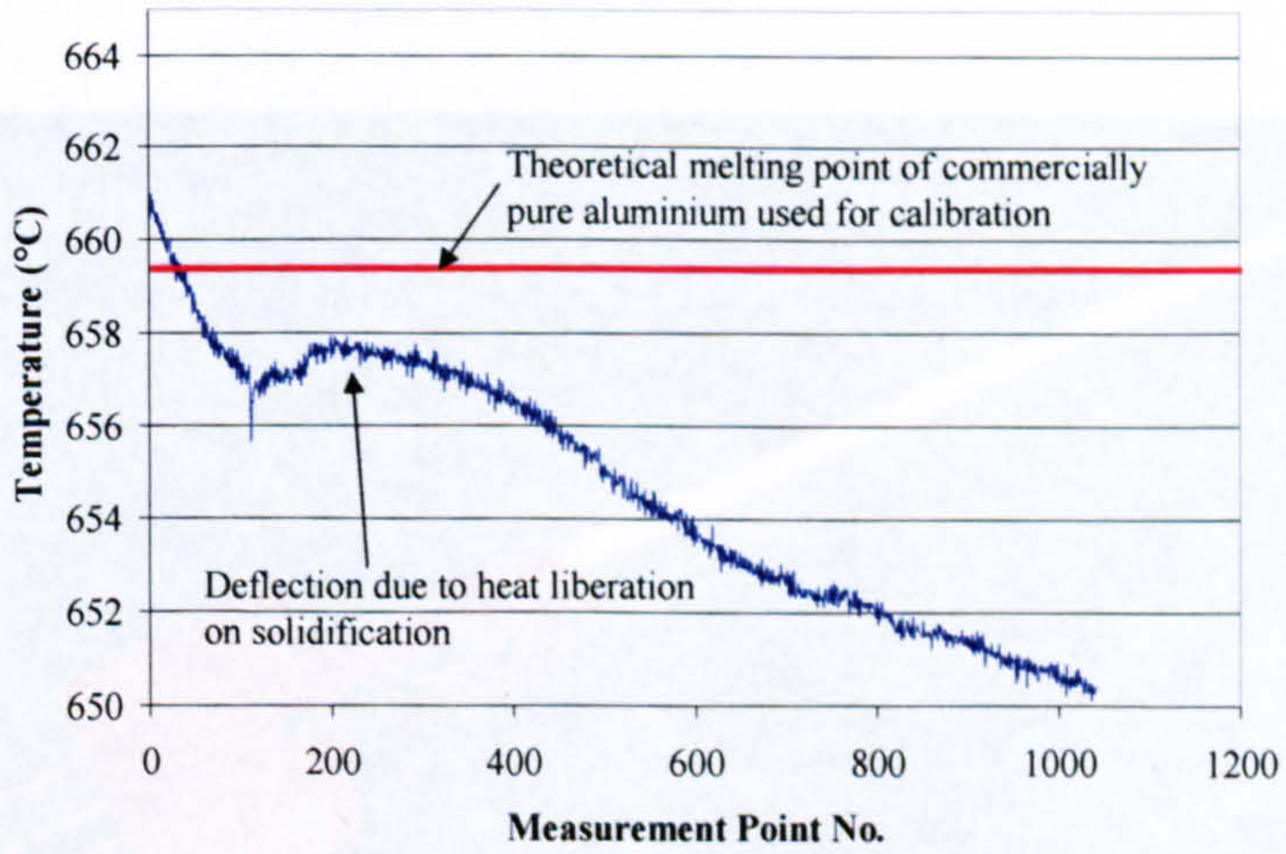

Figure 4-21: Typical thermocouple calibration curve using commercially pure aluminium solidification

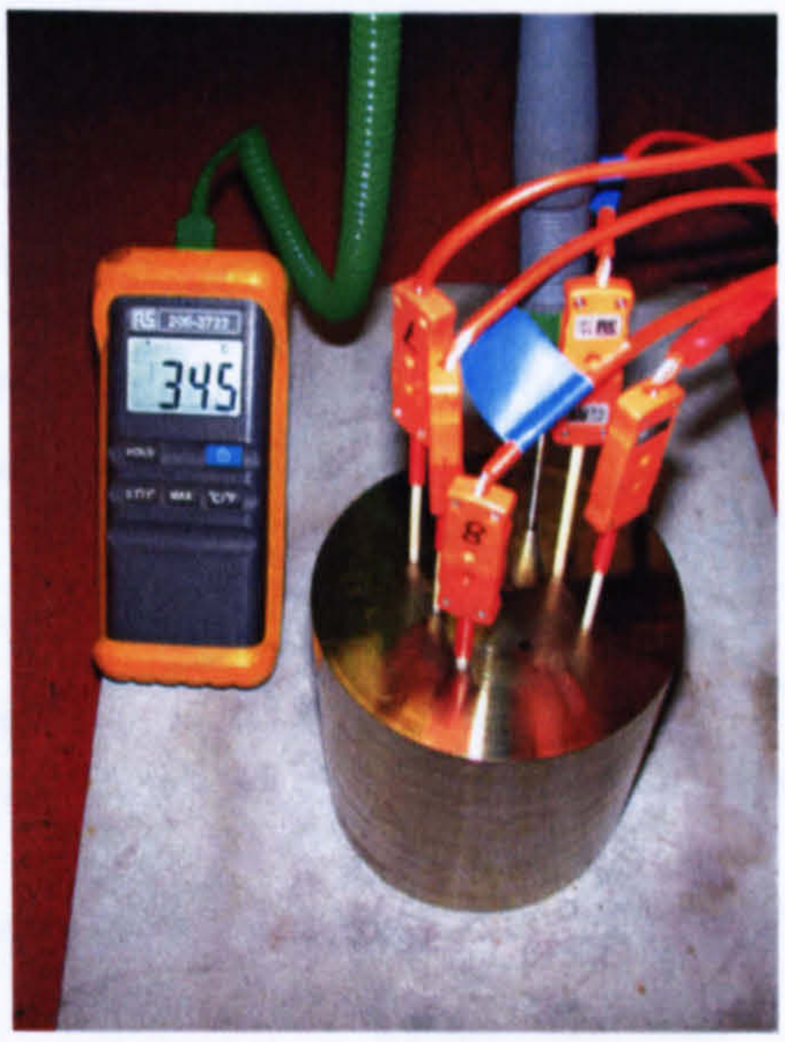

Figure 4-22: Testing of variance between individual thermocouples

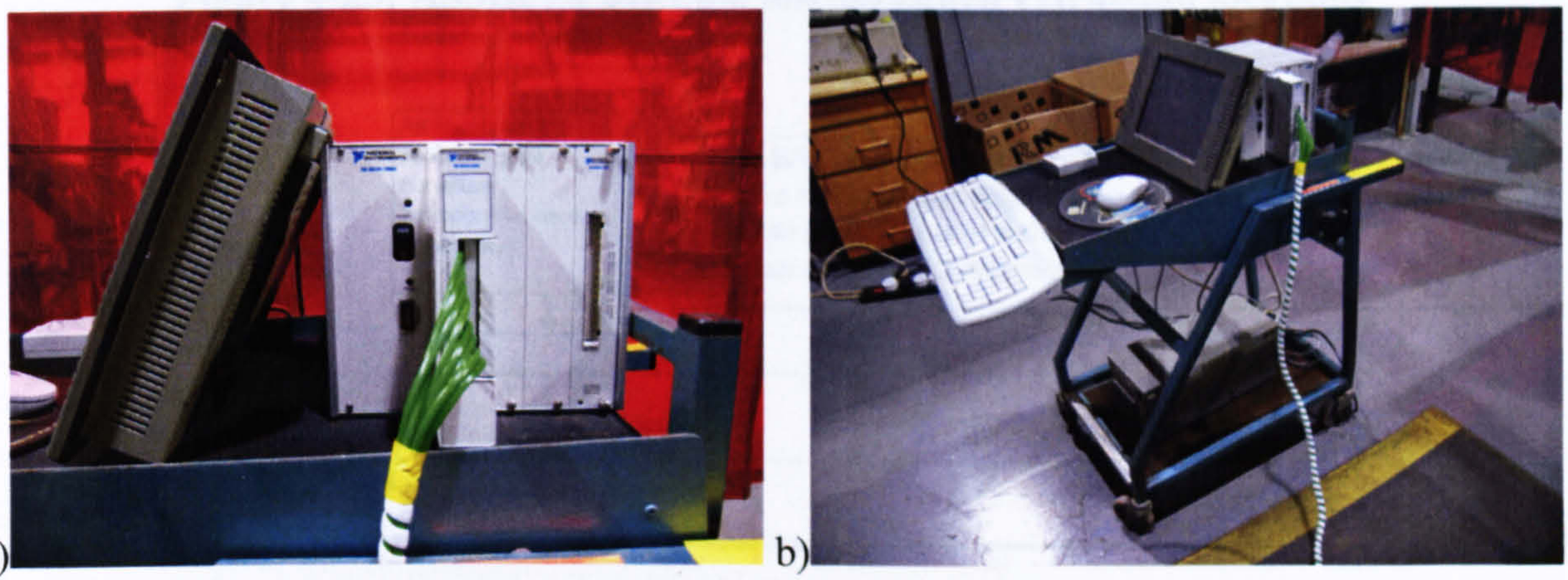

a) b)

Figure 4-23: Thermocycle data capture equipment a) SCXI chassis unit and thermocouple module b) total thermocycle capture equipment (industrial pc on lowest shelf)

Figure 4-24: Externally placed thermocouple

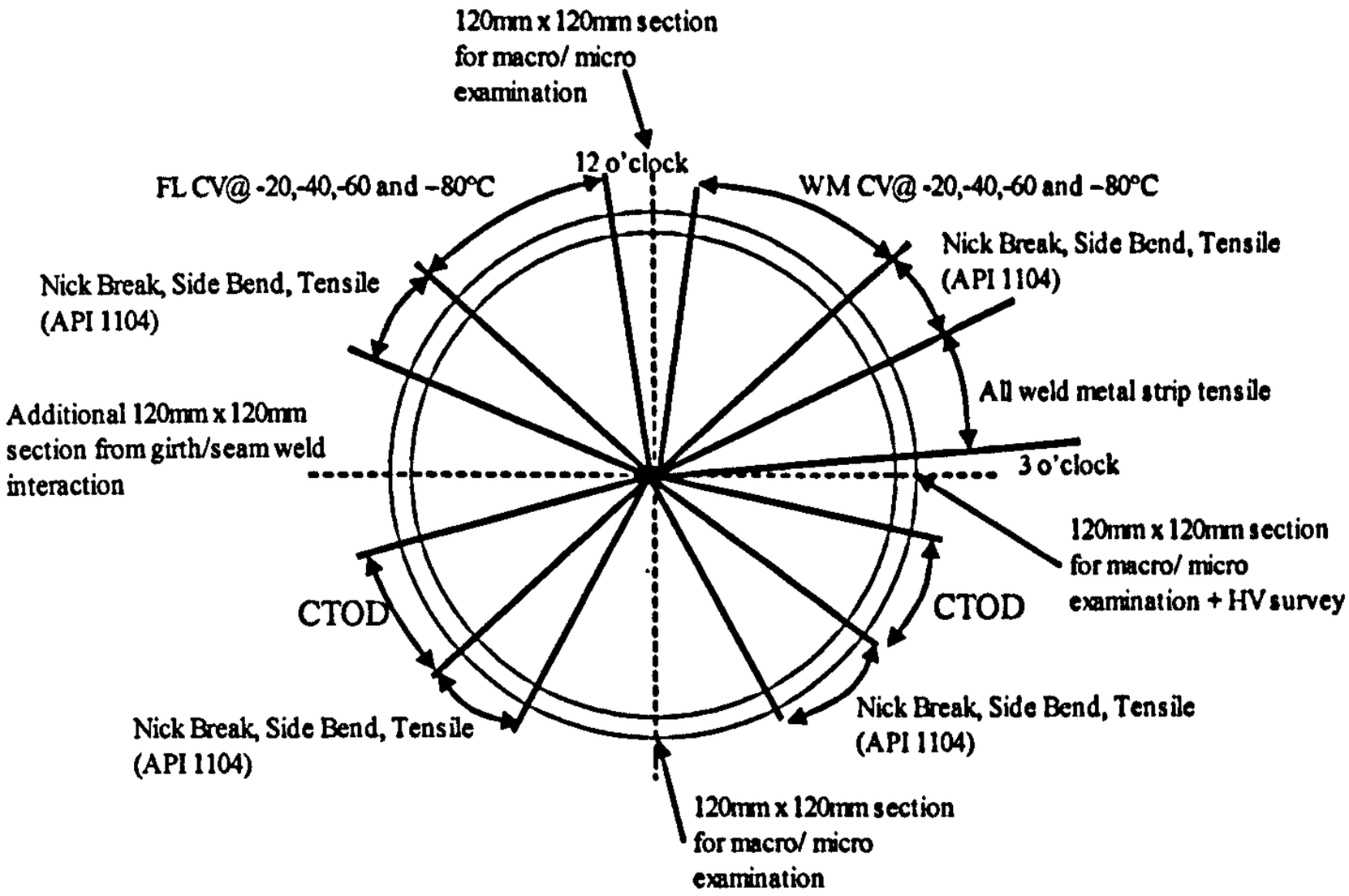

Figure 4-25: ASME IX 5G Pipe test specimen extraction locations

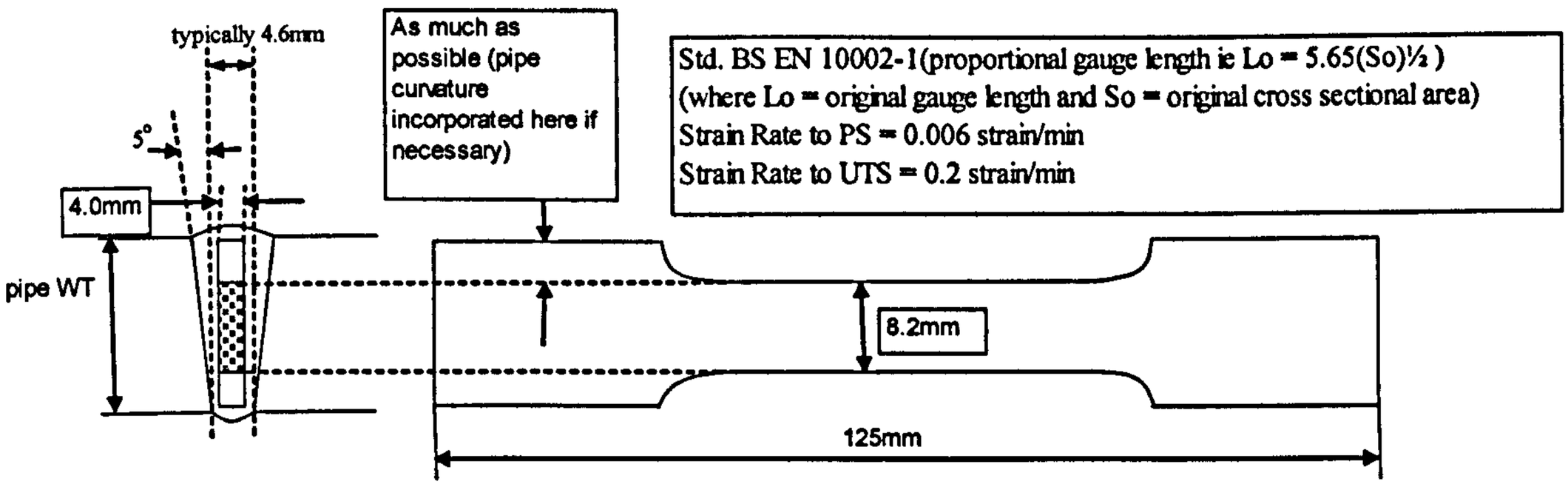

Figure 4-26: 5G Narrow gap all weld metal tensile dimensions/location

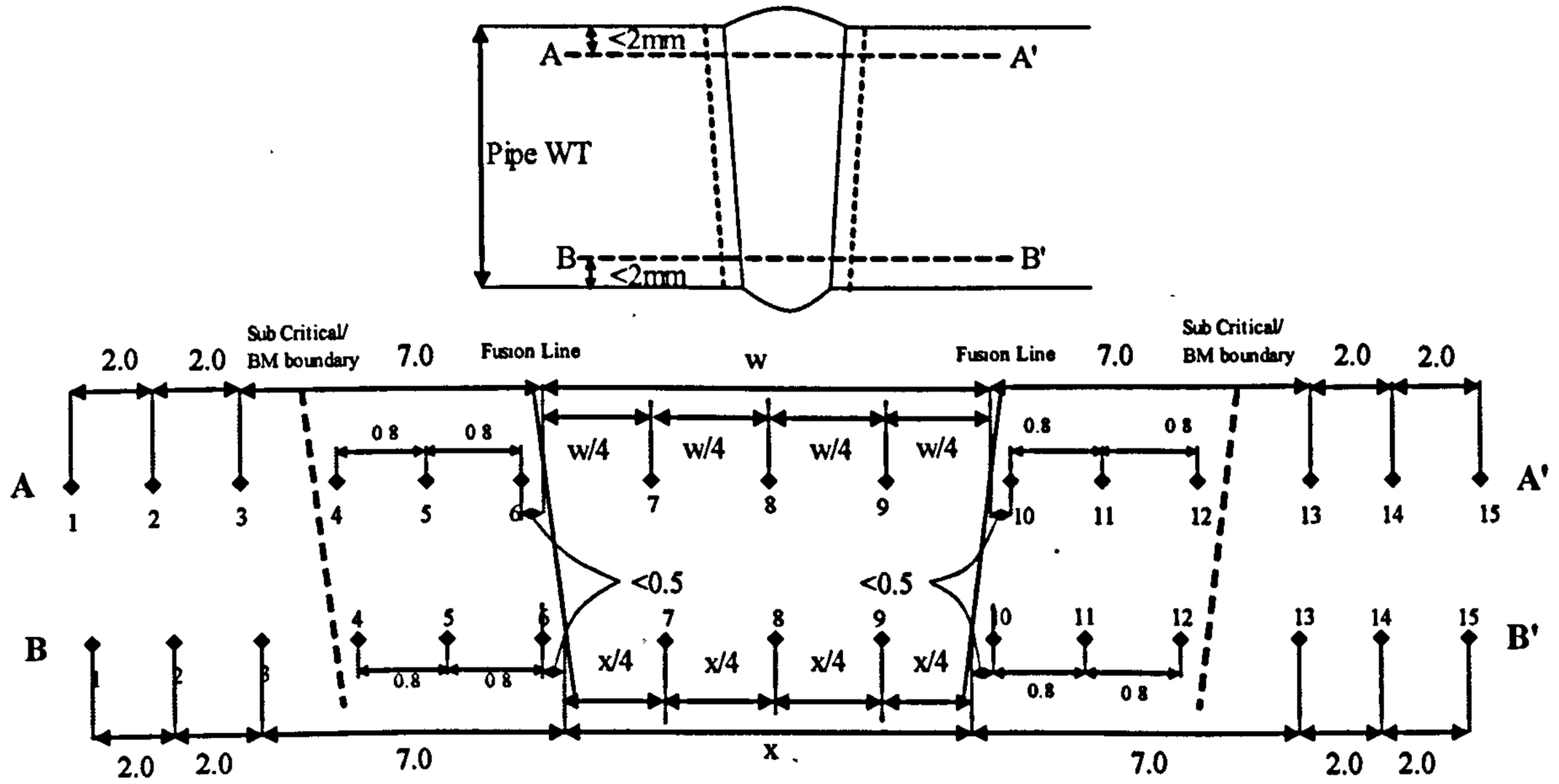

Figure 4-27: Narrow gap macro hardness indent location

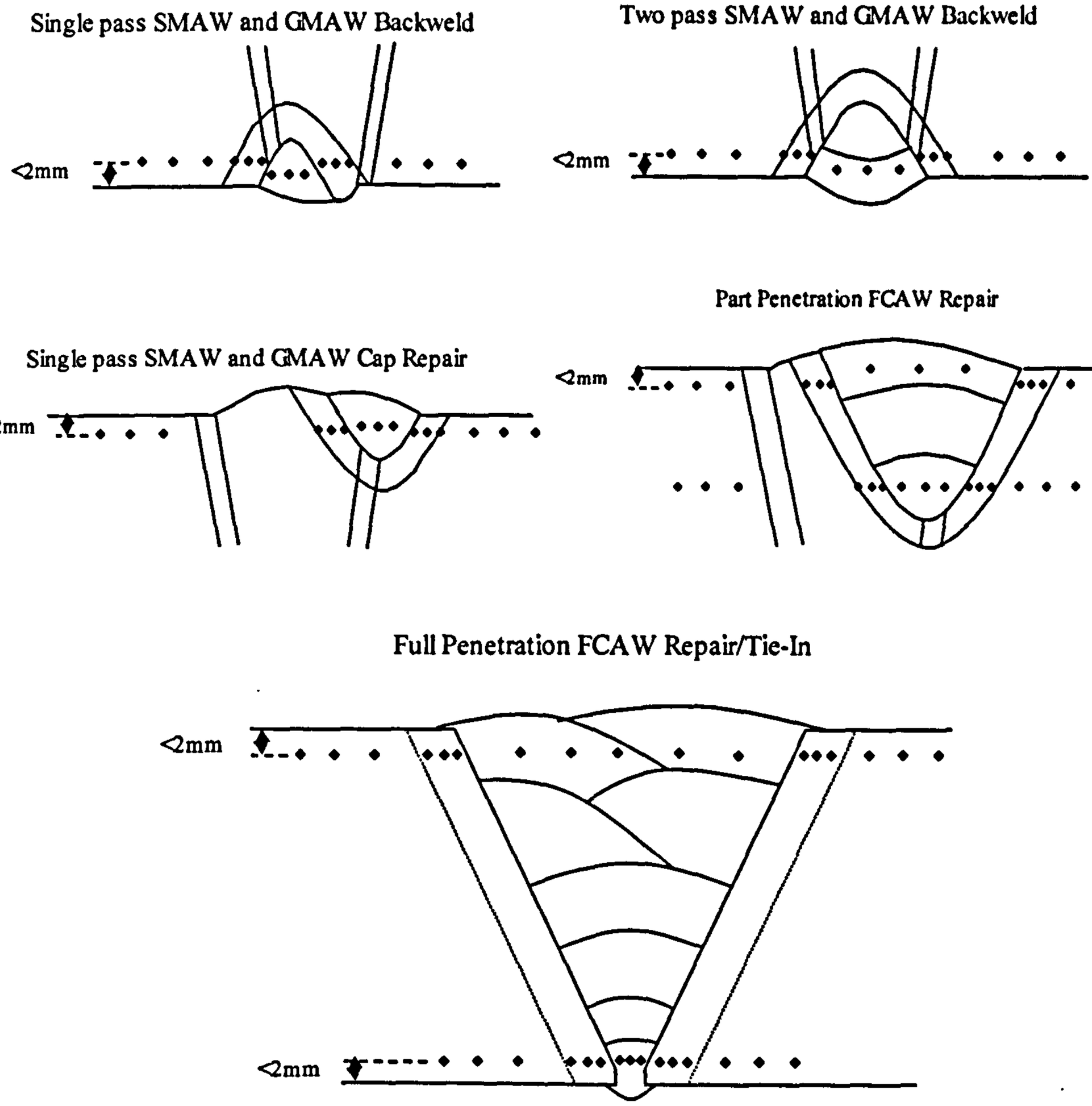

Figure 4-28: Repair weld hardness survey indent locations (HV10)

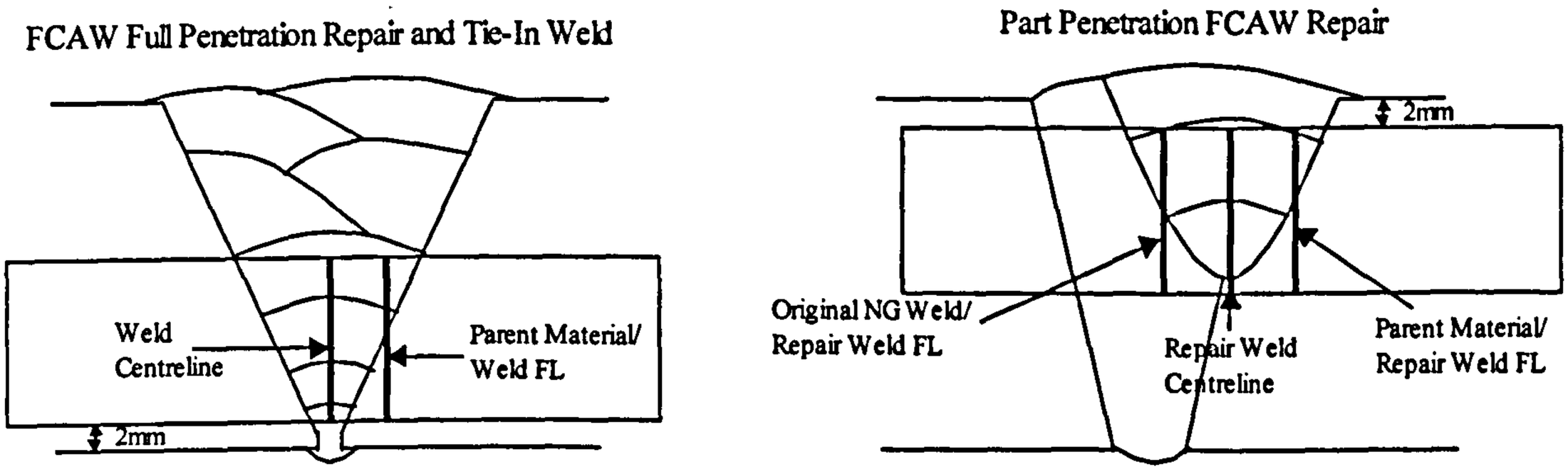

Figure 4-29: Impact toughness Cv sample location

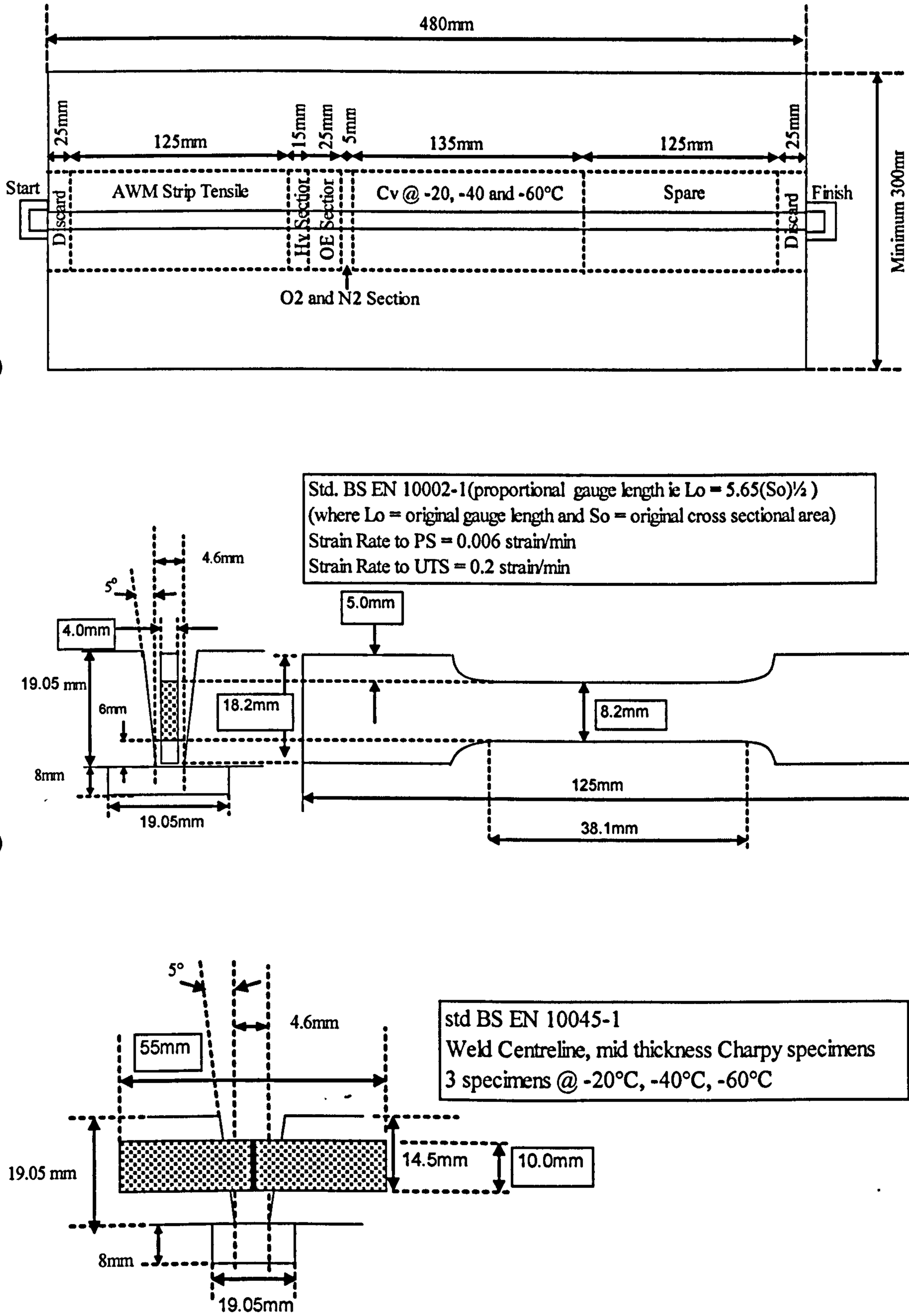

Figure 4-30: ASME IX 1G narrow gap plate mechanical test specimen locations (a) Plate cutting diagram b) all weld metal strip tensile c) impact specimen

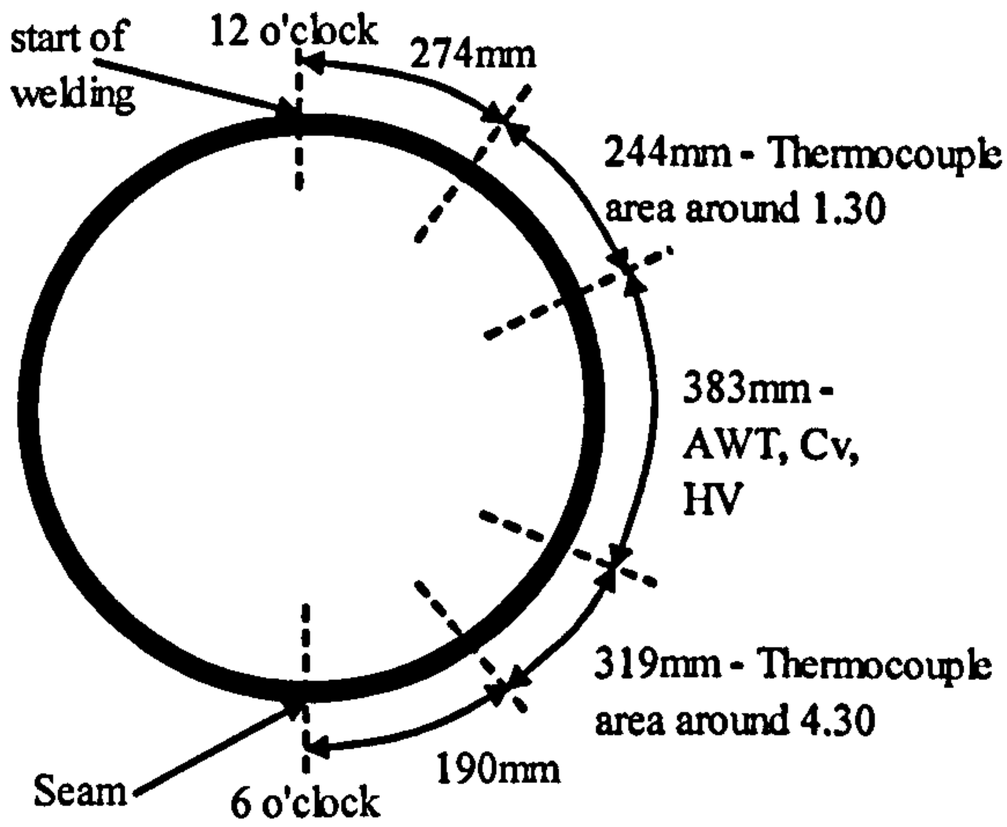

a) single torch

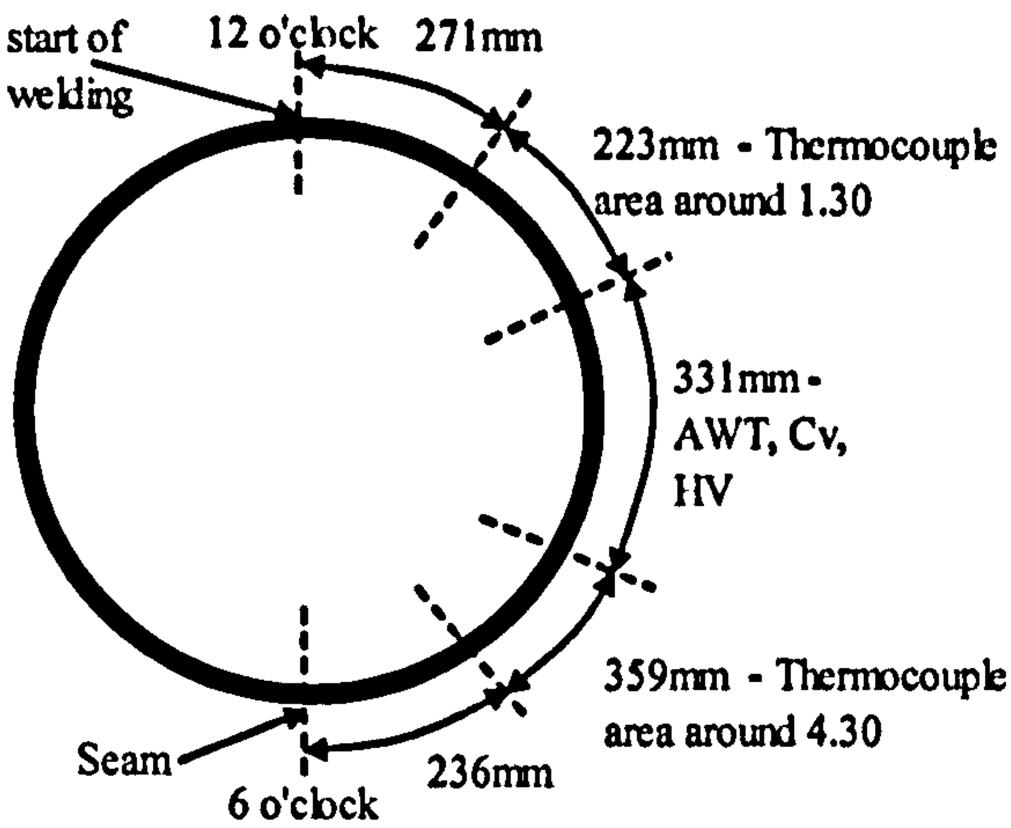

b) tandem torch

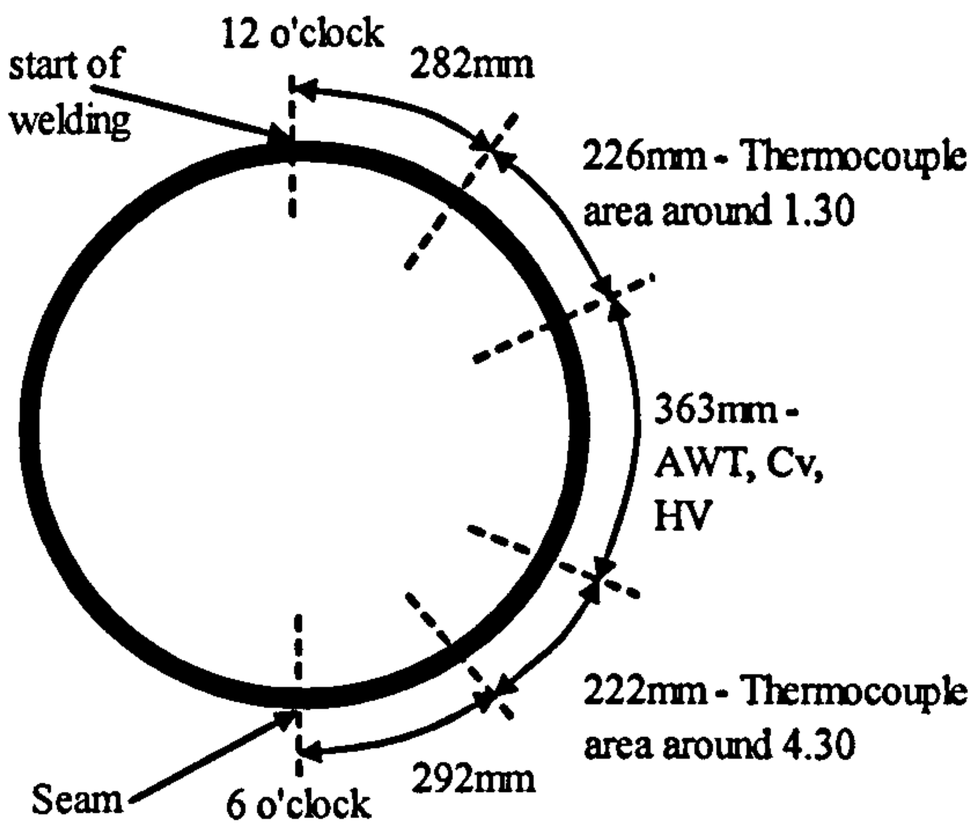

c) dual torch

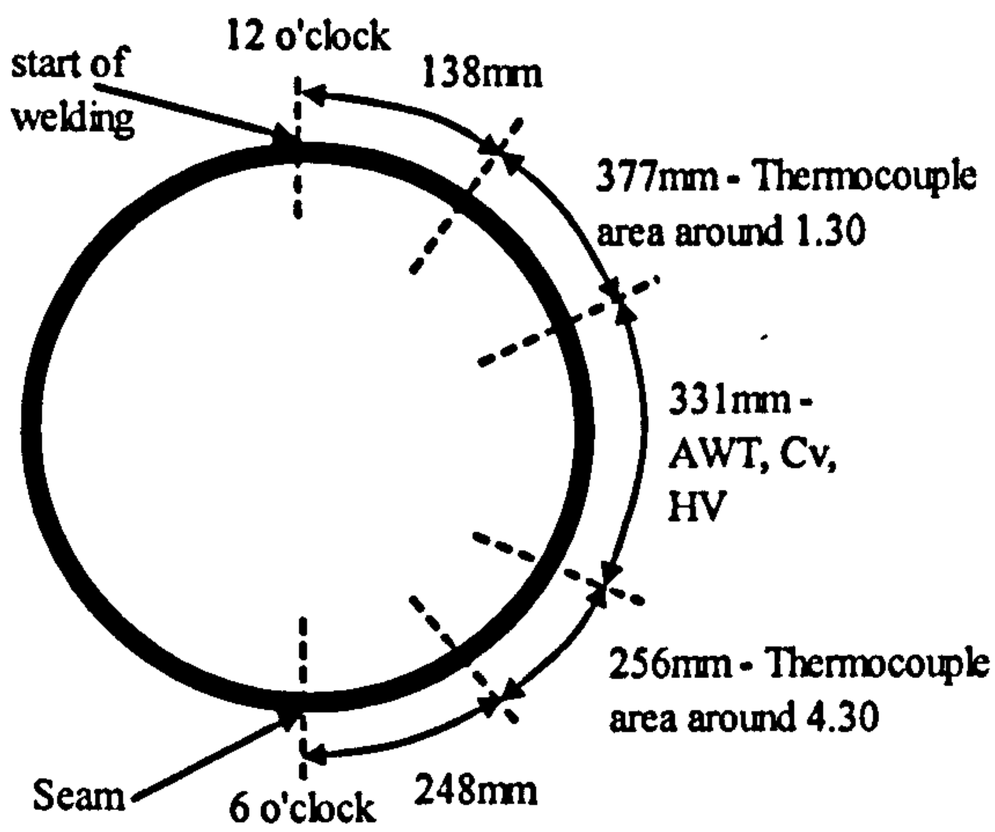

d) dual tandem torch

N.B. The above welds were conducted such that the pipe was rotated (simulating vertical down welding) allowing the welding head to be maintained at the ~1.30 position

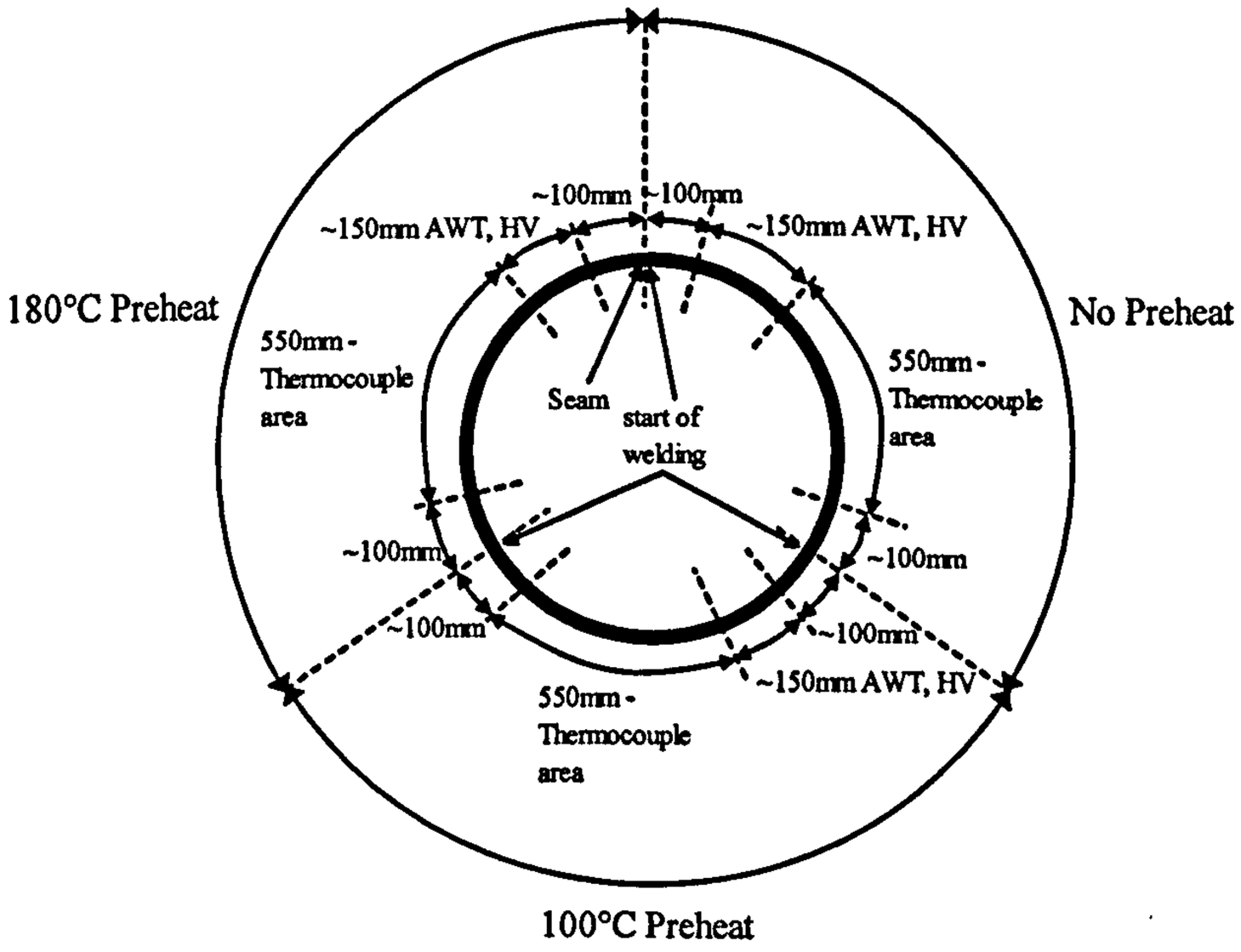

e) preheat variation trials

N.B. Welds conducted such that the start of welding was always at 12 o'clock. The pipe was fixed during welding with the bug travelling vertically down.

Bandsaw blade cut width = 1.45mm

Figure 4-31: Thermocycle pipe weld specimen extraction/thermocouple locations

5 RESULTS

In this chapter the results of the experimental programme will be presented under three major subject areas; (i) X100 girth welding procedure development, (ii) mechanised PGMAW narrow gap thermocycle experiments, and (iii) alloy variation trials for narrow gap high strength weld metal.

5.1 X100 GIRTH WELDING PROCEDURE DEVELOPMENT

5.1.1 X100 PIPE PROPERTIES

Table 5-1 to Table 5-6 show the mechanical and chemical properties for the four pipe materials investigated. Whenever possible the data generated in-house was compared to that provided by the individual manufacturer. Test locations refer to the pipe longitudinal seam weld being placed at 12 o'clock for comparative purposes. Yield ($R_{p0.2}$ and $R_{t0.5}$), ultimate tensile strength, elongation, reduction of area (for round bar tests) and yield to tensile ratios were recorded when possible for individual tests. The stress/strain graphs resulting from individual tests were also examined to confirm the reported data. Several strain to failure tests were also undertaken to observe the strain capacity of a given material in the longitudinal direction.

Standard hardness traverses of the various pipe seam welds are recorded in Table 5-7, with the base material microstructures shown in Figure 5-2 to Figure 5-5.

5.1.2 SINGLE WIRE NARROW GAP WELDS

Typical welding and joint profile photographs relevant to single wire mechanised welding are shown in Figure 5-7, with narrow gap pulsed arc high speed digital video images inside the timespan of peak and base currents shown in Figure 5-11.

Weld metal diffusible hydrogen contents were measured according to BS EN ISO 3690[322] for one of the high strength solid wires used during the mechanised welding trials (alongside the FCAW tie-in/repair consumable) to show the typical levels encountered; results are shown in Table 5-8.

The results of the initial fixed position experimental pipe trials are shown in Table 5-9, with the weld metal tensile, impact and chemistry tests shown in Table 5-10 to Table 5-13. Analysis of the results enabled the consumable selection to be narrowed down, resulting in two initial choices for the WERC single wire welds. A 0.5Ni 0.5Mo 0.5Cr wire of strength level just overmatching the proposed minimum ($R_{p0.2}$ 810MPa), and a 2.3Ni 0.5Mo 0.3Cr wire which considerably overmatched were then used to produce full procedure test welds as per standard pre-production girth welding. A 1.0Ni 0.4Mo wire was also used in a PGMAW single wire process by Serimer-Dasa, and on analysis of the WERC procedure test welds a further wire (0.9Ni 0.3Mo) was included for full procedure testing (see Table 5-14 and Table 5-15).

Tensile results from the single wire qualification procedures are shown in Table 5-18. Strip tensiles were used for all tensile measurements throughout the procedure qualification welds, due to the larger depth of weld deposit sampled (see section 4.11.1).

Hardness results are included within the same table; a simple cross weld traverse alongside a girth/seam weld metal interaction were tested for each full procedure test.

Impact and CTOD results are recorded in Table 5-25; Charpy impact testing covered the temperature range -20°C to -80°C in 20°C increments to enable potential transition curves to be produced, with all CTOD testing undertaken at -10°C.

Side bend, nick break and cross-weld tensile tests provided limited quantitative data, but are standard components of most pipeline welding qualification specifications. For this reason they are included in the current work, with results listed in Table 5-21.

Weld metal chemistry was determined primarily using optical emission spectroscopy on the weld centreline of a longitudinal section. Oxygen and nitrogen levels were obtained separately using a fusion method. Results for the single wire welds are displayed in Table 5-28. All residual elements were obtained to three decimal places in most cases. If an element (e.g. Boron) occurred at a level below the sensitivity of the measuring equipment, but has an impact on a calculation (e.g. P_{cm}), an assumed value just under that of the minimum measurable level was used.

Typical internal/external and all-external weld photo macrograph sections are shown in Figure 5-15. Weld metal microstructures at various magnifications are shown in Figure 5-32 for a variety of single wire consumables tested.

5.1.3 TANDEM WIRE NARROW GAP WELDS

The practices employed for the tandem wire welding followed a similar pattern to those of the single wire procedures, even though the welding bug, torch and power sources used were considerably different (Figure 5-8 (c)). All welding procedure details were recorded in a similar fashion (see Annexe B). Typical tandem joint profiles are shown in Figure 5-9.

Consumables were selected following initial pipewelding trials (see Table 5-9, Table 5-11 to Table 5-13) similar to those for the single wire welds. The initial chemistry chosen was the same as for the just overmatching single wire option (0.9Ni 0.3Mo). A slightly higher alloyed version (1.0Ni 0.4Mo) was then used as the wire to provide a higher degree of overmatch, and at the same time offer an insight into potential batch-to-batch variations and their effect on the tandem welding process (see Table 5-15).

Weld metal tensile and hardness (Table 5-18), side bend, nick break and cross weld tensiles (Table 5-22), impact and CTOD toughness (Table 5-26), and weld metal chemistry results (Table 5-29) were machined and tested as for the single wire welds.

Weld metal macrosections were again taken for microstructural analysis, photographs of cap microstructures being recorded in Figure 5-35.

5.1.4 DUAL TORCH NARROW GAP WELDS

As stated in the previous chapter, all dual torch trials and procedure test welds were undertaken by Serimer-Dasa (Paris), a pipeline welding equipment manufacturer. The welding set-up for the dual torch welds performed at Serimer-Dasa was typical of the practices undertaken at the WERC (Figure 5-10). Sections of all four pipe materials under investigation throughout this research were supplied by the WERC for welding

evaluation. The initial trial welds for consumable selection were tested in-house (see Table 5-9, Table 5-10, Table 5-12 and Table 5-13) until the correct balance of GMAW torch spacing and mechanical properties were attained in accordance to the proposed criteria (see section 2.9). Full girth welds were then made using two consumable chemistry variants (1.0Ni 0.4Mo and 1.3Ni 0.25Cr 0.25Mo) for each pipe material. A further series of welds were also manufactured using a reduced GMAW torch separation after further in-house testing, resulting in two further consumable chemistry variants (1.5Ni 0.3Mo 0.2Cr and 1.8Ni 0.5Mo 0.3Cr). Table 5-14 exhibits all the dual torch procedure welds completed. Each complete girth weld was returned to the WERC, with destructive testing subsequently undertaken as for the single and tandem wire weld procedures.

Weld metal tensile and hardness (Table 5-17), side bend, nick break and cross weld tensiles (Table 5-20), impact and CTOD toughness (Table 5-24), and weld metal chemistry results (Table 5-28) are exhibited in the relevant tables.

Weld metal macrosections were also taken for microstructural analysis, photographs of cap microstructures being recorded in Figure 5-33 from selected procedure welds.

5.1.5 TIE-IN WELD PROCEDURES

The tie-in weld was made using conditions as close as possible to that of field welding allowable in a laboratory environment (see Figure 5-12). High productivity FCAW was selected over conventional SMAW in a bid to improve the construction economics for this activity. Whilst the ecomomics were a major factor in deciding the choice of consumable, they did not constitute part of this reseach.

A 2.7Ni 0.3Mo rutile FCAW wire was used for the full girth weld testing, results of which are included in Table 5-19 (tensile and hardness), Table 5-23 (side bend, nick break and cross weld tensiles), Table 5-27 (impact and CTOD toughness) and Table 5-29 (weld metal chemistry). The weld metal microstructure is exhibited in Figure 5-36, with the weld metal cap pass surface profiles shown in Figure 5-13.

A further rutile FCAW wire (2.0Ni) was evaluated alongside the original wire using lower arc energies and reduced joint bevel angles (see Figure 5-23) in an attempt to promote the strength level. Results from these tests are shown in Table 5-31 and Table 5-32.

5.1.6 REPAIR WELD PROCEDURES

Welding of any pipeline needs to consider repair procedures for various defects encountered from the NDT process. The various repair procedures desribed in chapter 4 were assessed predominantly using hardness traverses due to the limited weld metal and HAZ areas created by the repair. The welding processes chosen were those typically available for either internal or external repairs, coupled with the most common position found for the given defect (see Figure 5-14). Photo macrographs of typical repair sections are shown in Figure 5-20 to Figure 5-22.

Results from the tests conducted are shown in Table 5-19 (hardness), Table 5-23 (side bend, nick break and cross weld tensile), Table 5-27 (impact toughness) and Table 5-29 (weld metal chemistry).

5.2 MECHANISED PGMAW NARROW GAP THERMOCYCLE EXPERIMENTS

The thermocycle experimental results are presented under the two main areas investigated: preheat; and process variation trials.

5.2.1 PREHEAT VARIATION TRIALS

Figure 5-49 to Figure 5-51 exhibit the thermocycles for all three preheat variants undertaken, each graph representing a particular weld pass. The time difference on the x-axis between individual thermocycles is artificial due to the varying positions of the individual thermocouples around the circumference of the pipe. The raw data has consequently been realigned to show the highest peak temperature (i.e. that arising from the layer being deposited) starting nearest the origin, with progressively decreasing peak temperatures (i.e. increasing distance of the deposited bead from the relevant thermocouple location below that of the deposited bead) placed at increasing start times from the origin. A nominal time separation between layers of 20-30 seconds has been used for easy identification. Colour coding for a particular layer is consistent between all graphs. In many instances two thermocycles per layer successfully recorded data, and in these cases the data are displaced a nominal 5 seconds apart to highlight their similarity of location within the weld deposition depth. A typical longitudinal section along the weld mid-thickness showing the proximity of the individual internal thermocouple locations is shown in Figure 5-26.

Examination of the cooling curves allowed several comparative measurements to be derived subsequently. Cooling times from 800°C to 500, 400 and 300°C (t_{85}, t_{84} and t_{83}) are shown in Table 5-33 to Table 5-35, and graphically in Figure 5-58.

The transformation start, finish and maximum rate temperatures were determined by differentiation of the polynomial fit to the original data as shown in Figure 5-61. The maximum rate of transformation and transformation finish times were easily determined from the 2nd order differential as the points at which the curve crosses 0 on the x-axis (i.e. inflection points on the 1st order differential curve). The start of transformation however was not easily distinguished, but was consistently taken as the first deviation point from the 1st order differential curve. The times at which these points occurred could then be translated to temperatures (see Figure 5-61(c)). Table 5-33 to Table 5-35 show the data obtained, and this is graphically represented in Figure 5-62 and Figure 5-63.

Cooling rates at a given temperature are another classical method of assessing the likely mechanical/microstructural characteristics of the resultant weld metal[44]. Figure 5-64 and Figure 5-65 show the cooling rates (°C/s) obtained at 800°C, 600°C and 400°C from the 1st order differential curves of the polynomial fit.

The tensile properties of the three preheat variant welds were obtained from the all-weld metal strip tensiles shown in Figure 4-26, and as such sampled material from the

deposited layers in the middle of the pipe wall thickness. Table 5-40 and Figure 5-28 show the results of the tensile tests.

In an attempt to correlate the tensile strengths with the microstructures observed for the preheat trial welds, the as-cast microstructural constituents from the cap beads were determined using standard point counting methods. Representative microstructures from the three variants are shown in Figure 5-38 and the resultant microstructural classification exhibited in Figure 5-31 (based on the microstructural classification shown in Figure 5-39).

As a result of the microstructural complexity throughout the complete joint and the uncertainty of correctly classifying the various constituents, a microhardness survey traversing the numerous weld metal layers was conducted to provide a more meaningful correlation with the tensile properties. The actual traverse was sited just off of the weld centreline to avoid any potential segregation effects. The 500g load allowed an indent spacing of 0.2mm centre to centre, with each traverse starting in the cap bead and ending in the root bead. Table 5-46 and Figure 5-70 show the individual traverses with the pipe OD, ID and weld metal interun fusion boundaries marked.

5.2.2 PROCESS VARIATION TRIALS

A similar set of experiments was conducted as per the preheat trials above, with the aim of examining the effects of four mechanised narrow gap PGMAW variants. Photo macrographs of the weld sections from the four process variants are shown in Figure 5-27.

Thermocycle data were gathered in a similar fashion as per the preheat trials, although due to the larger pipe diameter used (36 in.) thermocouples were placed in two groups beginning approximately 250mm after the start, and at a similar distance from the finish. This allowed approximately 350mm of unaffected weld metal in the middle of each weld run for mechanical specimen extraction (see Figure 4-31).

Thermocycle curves for each layer deposited are presented in Figure 5-52 to Figure 5-55 for the four process variants examined.

The t_{85}, t_{84} and t_{83} cooling times are shown in Table 5-36 to Table 5-39 and Figure 5-59. The transformation temperatures and cooling rates are also recorded in the same tables, and graphically in Figure 5-66/Figure 5-67 and Figure 5-68/Figure 5-69 respectively.

The tensile tests were conducted in the same manner as for the preheat trials, with results shown in Figure 5-29.

The increased weld length available from the process variant trials allowed three sets of Charpy impact specimens to be machined from the pipe mid thickness and notched weld centreline. Testing was performed at -20, -40 and -60°C with results shown in Table 5-41 and Figure 5-30.

5.3 ALLOY VARIATION TRIALS FOR NARROW GAP HIGH STRENGTH WELD METAL.

The results relevant to the various metal cored wires manufactured to examine specific changes in chemistry are presented in the following section.

5.3.1 WELD METAL CHEMISTRY

The weld metal chemistry results highlight the individual or multiple alloying elements examined in any given wire and are shown in Table 5-43. Nickel, molybdenum, chromium and carbon were specified to fall within the given stated ranges, and most of the time this was achieved. For the times the alloy levels fell outside of the desired range, the level by which they did so was minimal.

5.3.2 MECHANICAL AND THERMOCYCLE PROPERTY COMPARISON OF PLATE PROCEDURES

Tensile test data from the various welds are exhibited in Table 5-44 and Figure 5-79. Four samples were machined from the ultimate control sample (MC control 2) in order to determine the likely experimental scatter for any given wire composition test weld. Hardness results from a traverse down the weld centreline for the various chemistries are also included in this table. Charpy impact tests conducted at -20°C, -40°C and -60°C on the weld centreline (plate mid-thickness) are shown in Table 5-45, along with the various levels of scatter for the particular alloy and test temperature variant. The toughness levels are graphically displayed in Figure 5-80.

Cooling curves were obtained from both the metal cored and solid wire base line chemistry variants (0.9Ni 0.3Mo) for each layer deposited in order that a direct comparison between the two consumable types could be made, alongside thermocycle comparisons between the plate and pipewelding situations. The global cooling curves are shown in Figure 5-75, with the cooling times, rates and transformation temperatures shown in Table 5-47 and Figure 5-76 to Figure 5-78.

5.3.3 ALLOY VARIANT WELD METAL MICROSTRUCTURE RESULTS

Typical macro sections from the solid and metal cored plate welds are shown in Figure 5-72 alongside a high magnification comparison of the as-cast (cap pass) microstructures in Figure 5-73. A comparison between the prior austenite grain sizes of the two consumables is made in Figure 5-74.

The cap pass microstructures from all the alloy variants were studied at the highest available optical magnification (1000 times), and the photomicrographs shown in Figure 5-84 to Figure 5-88 record the various morphologies observed.

Table 5-1: Pipe A (19.05mm WT) X100 Mechanical Properties

Pipe A	Tensile dimen. (mm)	Cranfield Yield Bold = 0.2% Proof (MPa)	Supplier Yield Bold = 0.2% Proof (MPa)	Cranfield Yield 0.5% Total Extension. (MPa)	Supplier Yield 0.5% Total Extension (MPa)	Cranfield Ultimate Tensile Strength (MPa)	Supplier Ultimate Tensile Strength (MPa)	Cranfield Elong (%)	Supplier Elong (%)	Cranfield RoA (%)	Cranfield Y/T Yield = 0.2% PS T = UTS	Supplier Y/T Yield = 0.5% TE T = UTS
X100 Pipe – round bar transverse 1 o'clock	ϕ7.98	797	770*			819	808	15.3	17	79.6	0.97	0.95
X100 Pipe – round bar longitudinal 1 o'clock	ϕ7.98	751	721**			787	782	15	20	76.5	0.95	0.92
X100 Pipe – round bar longitudinal 1 o'clock	ϕ6.31	740[a]				798		37.6		75.2		0.93
X100 Pipe – strip transverse 1 o'clock	38x19	741	712	732		807	824	32.3	30		0.92	0.86
X100 Pipe – strip longitudinal 1 o'clock	38x19	752	717	733		806	798	32.9	34		0.93	0.90
X100 Pipe – round bar transverse 3 o'clock	ϕ7.98	792				809		14.8		77.3	0.98	
X100 Pipe – round bar longitudinal 3 o'clock	ϕ7.98	742				790		17.3		77.3	0.94	
X100 Pipe – strip transverse 3 o'clock	38x19	708		501[b]		797		32.7			0.89	
X100 Pipe – strip transverse 3 o'clock (repeat)	38x19.5	623		635		815		32.3			0.76	
X100 Pipe – strip longitudinal 3 o'clock	38x19	752		741		787		33.3			0.96	
X100 Plate – round bar transverse	ϕ7.98	651				834		18.8		76.1	0.78	
X100 Plate – round bar longitudinal	ϕ7.98	619				785		21.1		77.3	0.79	
X100 Plate – strip transverse	38x19	653		651		781		33.9			0.84	
X100 Plate – strip longitudinal	38x19	742		735		784		36.8			0.95	
X100 SAW Seam ID all weld tensile	ϕ6.35						838					
X100 SAW Seam OD all weld tensile	ϕ6.35						761					
X100 Pipe – strip transverse weld seam	38x19						822	fracture location : base metal. Weld bead reinforcement removed				
NB Longitudinal seam weld placed at 12 o'clock	* Supplier transverse round bar gauge diameter = 10mm ** Supplier longitudinal round bar gauge diameter = 12.7mm [a] Specimen used to generate strain to failure data: gauge length used for elongation = 12.5mm, extensometer length = 12mm, parallel portion = 14mm [b] Original Pipe 3 O'clock strip transverse test showed a much lower gradient on the load/extension curve, hence the low 0.2%PS/ 0.5%TE NB. All Cranfield tensile specimens to be considered proportional i.e. elongation calculated using gauge length = 5.65x(original cross sectional area)^½ (see BS EN 10 002-1)											

Table 5-2: Pipe B15 (14.9mm WT) X100 Mechanical Properties

		Cranfield	Supplier	Cranfield	Supplier	Cranfield	Supplier	Cranfield	Supplier	Cranfield	Cranfield	Supplier
Pipe B15	**Tensile dimen.** (mm)	**Yield** Bold = 0.2% Proof (MPa)	**Yield** Bold = 0.2% Proof (MPa)	**Yield** 0.5% Total Extension. (MPa)	**Yield** 0.5% Total Extension (MPa)	**Ultimate Tensile Strength** (MPa)	**Ultimate Tensile Strength** (MPa)	**Elong** (%)	**Elong** (%)	**RoA** (%)	**Y/T** Yield = 0.2% PS T = UTS	**Y/T** Yield = 0.5% TE T = UTS
X100 Pipe – round bar transverse 1 o'clock	ϕ7.98	**829**		854	*919	909	942	15.5	14.4	73.6	0.91	0.98
X100 Pipe – round bar longitudinal 1 o'clock	ϕ7.98	**658**		745	*689	862	920	16.5	19	72.3	0.76	0.75
X100 Pipe – strip transverse 1 o'clock	38.18x14.88	**692**		664		865		28			0.80	
X100 Pipe – strip longitudinal 1 o'clock	38.21x15.00	**671**		685		821		27			0.82	
X100 Pipe – round bar transverse 3 o'clock	ϕ7.98	**796**		823	*878	889	924	18	14.7	68.2	0.90	0.95
X100 Pipe – round bar longitudinal 3 o'clock	ϕ7.98	**676**		743	*687	851	889	17.5	16	72.3	0.79	0.77
X100 Pipe – strip transverse 3 o'clock	38.13x14.96	**676**		656		848		25			0.80	
X100 Pipe – strip longitudinal 3 o'clock	38.14x15.23	**712**		693		872		27.5			0.82	
X100 Pipe – strip transverse weld seam	38x14.9					863, 838 fracture location : from HAZ into base metal.						
NB Longitudinal seam weld placed at 12 o'clock	* Supplier transverse round bar gauge diameter = 6.35mm, position around pipe unknown NB. All Cranfield tensile specimens to be considered proportional i.e. elongation calculated using gauge length = 5.65x(original cross sectional area)^½ (BS EN 10 002-1)											

Table 5-3: Pipe B19 (19.05mm WT) X100 Mechanical Properties

Pipe B19	Tensile dimen. (mm)	Cranfield Yield Bold = 0.2% Proof (MPa)	Supplier Yield Bold = 0.2% Proof (MPa)	Cranfield Yield 0.5% Total Extension. (MPa)	Supplier Yield 0.5% Total Extension (MPa)	Cranfield Ultimate Tensile Strength (MPa)	Supplier Ultimate Tensile Strength (MPa)	Cranfield Elong (%)	Supplier Elong (%)	Cranfield RoA (%)	Cranfield Y/T Yield = 0.2% PS T = UTS	Supplier Y/T Yield = 0.5% TE T = UTS
X100 Pipe – round bar transverse 1 o'clock	ϕ8.00	671	792*			838	833	19.5	22.2	72.4	0.80	0.95
X100 Pipe – round bar longitudinal 1 o'clock RT	ϕ8.00	701				847		20.8		71.1	0.83	
X100 Pipe – round bar longitudinal 1 o'clock RT (Rpt.)	ϕ7.97	639				782		20.1		75.1	0.82	
X100 Pipe – round bar longitudinal 1 o'clock RT	ϕ6.33	675ª				795		38.4		73.3	0.85	
X100 Pipe – round bar longitudinal 1 o'clock 100°C	ϕ8.00	631				768		17.5		72	0.82	
X100 Pipe – round bar longitudinal 1 o'clock 100°C(Rpt.)	ϕ7.98	660				760		17		75.9	0.87	
X100 Pipe – round bar longitudinal 1 o'clock 150°C	ϕ7.92	640				769		17		69	0.83	
X100 Pipe – round bar longitudinal 1 o'clock 200°C	ϕ8.00	667				799		14		69.7	0.83	
X100 Pipe – strip transverse 1 o'clock	38x19	759		758	766	856	860	32.7	33.9		0.89	0.89
X100 Pipe – strip longitudinal 1 o'clock	38x19	733		723	774	837	849	34.4	33.2		0.88	0.91
X100 Pipe – round bar transverse 3 o'clock	ϕ7.90	772				869		18.5		73.7	0.89	
X100 Pipe – round bar longitudinal 3 o'clock	ϕ8.00	655				820		19.5		71.7	0.80	
X100 Pipe – strip transverse 3 o'clock	38x19	696		679		855		33.3			0.81	
X100 Pipe – strip longitudinal 3 o'clock	38x19	710		705		833		34.8			0.85	
X100 SAW Seam ID all weld tensile	ϕ6.25		829				891				0.93	
X100 SAW Seam centre all weld tensile	ϕ6.25		883				938				0.94	
X100 SAW Seam OD all weld tensile	ϕ6.25		824				894					
X100 Pipe – strip transverse weld seam	38x19						838	Fracture location : from HAZ into base metal				
NB Longitudinal seam weld placed at 12 o'clock	* Supplier transverse round bar gauge diameter = 8.9mm ª Specimen used to generate strain to failure data: gauge length used for elongation = 12.5mm, extensometer length = 12mm, parallel portion = 14mm NB. All Cranfield tensile specimens to be considered proportional i.e. elongation calculated using gauge length = 5.65x(original cross sectional area)^½ (BS EN 10 002-1)											

Table 5-4: Pipe C (16.3mm WT) X100 Mechanical Properties

Pipe C	Tensile dimen. (mm)	Cranfield Yield Bold = 0.2% Proof (MPa)	Supplier Yield Bold = 0.2% Proof (MPa)	Cranfield Yield 0.5% Total Extension. (MPa)	Supplier Yield 0.5% Total Extension (MPa)	Cranfield Ultimate Tensile Strength (MPa)	Supplier Ultimate Tensile Strength (MPa)	Cranfield Elong (%)	Supplier Elong (%)	Cranfield RoA (%)	Cranfield Y/T Yield = 0.2% PS T = UTS	Supplier Y/T Yield = 0.5% TE T = UTS
X100 Pipe – round bar transverse 1 o'clock	ϕ7.98	772				851		20.8		78.5	0.91	
X100 Pipe – round bar longitudinal 1 o'clock	ϕ7.98	628				824		21.1		73.6	0.76	
X100 Pipe – round bar longitudinal 1 o'clock	ϕ6.35	710[a]				855		41.8		69.8	0.83	
X100 Pipe – strip transverse 1 o'clock	38x16	705		481		858		30.9			0.82	
X100 Pipe – round bar transverse 3 o'clock	ϕ7.98	830				857		15.3		65.3	0.97	
X100 Pipe – round bar longitudinal 3 o'clock	ϕ7.98	652				824		21.1		74.2	0.79	
X100 Pipe – strip transverse 3 o'clock	38x16	675[#]		582		856.5		32.5			0.79	
X100 Plate – round bar transverse	ϕ7.98	613				861		19.0		66.8	0.71	
X100 Plate – round bar longitudinal	ϕ7.98	571				814		23.3		66.8	0.70	
X100 Plate – strip transverse	38x16	673		671		864		28.9			0.78	
NB Longitudinal seam weld placed at 12 o'clock	[#]Pipe 3 O'clock strip transverse load/ extension curve did not allow easy definition of the elastic tangent line for construction of the 0.2% PS line, hence value obtained somewhat dubious. [a] Specimen used to generate strain to failure data: gauge length used for elongation = 12.5mm, extensometer length = 12mm, parallel portion = 14mm NB. All Cranfield tensile specimens to be considered proportional i.e. elongation calculated using gauge length = 5.65x(original cross sectional area)^½ (BS EN 10 002-1)											

Table 5-5: X100 Pipe chemistry

	C wt%	Mn wt%	P wt%	S wt%	Si wt%	Cr wt%	Ni wt%	Mo wt%	Cu wt%	Al wt%	V wt%	Nb wt%	Ti wt%	O ppm	N ppm	B ppm	P_{CM}	CET BS EN 1011-2	CE_{IIW}
Pipe A (19.05mm WT) – Nominal 0.4Cr-0.5Ni-0.4Mo-0.5Cu-V-Nb-Ti (very low C)																			
X100 Pipe (Cranfield Analysis)	0.027	2.00	0.006	<0.005	0.20	0.43	0.48	0.43	0.46	0.005	0.07	0.05	0.015	66	54	<5	0.223	0.327	0.609
X100 Plate (Cranfield Analysis)	0.025	1.98	0.006	<0.005	0.20	0.42	0.48	0.43	0.46	0.006	0.07	0.05	0.015	38	50	<5	0.219	0.322	0.602
X100 Plate (Supplier Analysis)	0.027	1.95	0.005	0.0024	0.20	0.41	0.47	0.42	0.46	0.002	0.063	0.046	0.013		53	2	0.218	0.319	0.593
X100 Pipe Seam ID (Cranfield Analysis)	0.037	1.64	0.006	<0.005	0.22	0.56	1.10	0.58	0.33	0.013	0.05	0.03	0.010	212	71	<5	0.234	0.331	0.644
X100 Pipe Seam ID (Supplier Analysis)	0.048	1.64	0.006	0.0030	0.20	0.49	1.14	0.50	0.32	0.007	0.038	0.028	0.008		63	4	0.235	0.331	0.624
X100 Pipe Seam OD (Cranfield Analysis)	0.046	1.62	0.007	<0.005	0.20	0.50	1.09	0.51	0.31	0.012	0.04	0.03	0.010	230	63	<5	0.231	0.327	0.619
X100 Pipe Seam OD (Supplier Analysis)	0.043	1.66	0.006	0.0023	0.23	0.55	1.17	0.58	0.34	0.006	0.042	0.03	0.008		78	4	0.243	0.341	0.655

	C wt%	Mn wt%	P wt%	S wt%	Si wt%	Cr wt%	Ni wt%	Mo wt%	Cu wt%	Al wt%	V wt%	Nb wt%	Ti wt%	O ppm	N ppm	B ppm	P_{CM}	CET BS EN 1011-2	CE_{IIW}
Pipe B15 (14.9mm WT) - Nominal 0.5Ni-0.25Mo-0.3Cu-Al-Nb-Ti																			
X100 Pipe (Cranfield Analysis)	0.066	1.91	0.008	<0.005	0.10	0.02	0.54	0.27	0.30	0.02	0.006	0.03	0.013	16	24	<5	0.209	0.314	0.500
Base Metal Ladle (Supplier Analysis)	0.06	1.84	0.008	0.0017	0.09	0.02	0.55	0.26	0.3	0.023	<0.005	0.027	0.013		26	<5	0.200	0.300	0.479
X100 Pipe Seam ID (Cranfield Analysis)	0.068	1.88	0.009	<0.005	0.13	0.46	0.39	1.04	0.24	0.02	0.007	0.02	0.014	314	64	6	0.281	0.405	0.725
X100 Pipe Seam ID (Supplier Analysis)	0.07	1.88	0.009	0.003	0.17	0.47	0.38	0.96	0.23	0.011	0.01	0.025	0.015		69	<5	0.277	0.399	0.710
X100 Pipe Seam OD (Cranfield Analysis)	0.063	1.87	0.008	<0.005	0.16	0.34	1.75	0.6	0.26	0.017	0.007	0.019	0.016	358	47	7	0.265	0.384	0.698
X100 Pipe Seam OD (Supplier Analysis)	0.06	1.86	0.009	0.003	0.19	0.34	1.86	0.61	0.23	0.011	0.01	0.02	0.017		55	<5	0.262	0.382	0.699

Where Pcm = C + Mn/20 + Mo/15 + Ni/60 + Cr/20 + V/10 + Cu/20 + Si/30 + 5B

CET = C + (Mn+Mo)/10 + (Cr+Cu)/20 + Ni/40

CE_{IIW} = C + Mn/6 + (Cr +Mo+V)/5 + (Cu+Ni)/15

When elements are stated as < the given amount, calculations for carbon equivalents are based on the following assumptions: V = 0.002 and B = 0.0002

Table 5-6: X100 Pipe chemistry

	C wt%	Mn wt%	P wt%	S wt%	Si wt%	Cr wt%	Ni wt%	Mo wt%	Cu wt%	Al wt%	V wt%	Nb wt%	Ti wt%	O ppm	N ppm	B ppm	P_{CM}	CET BS EN 1011-2	CE_{IIW}
Pipe B19 (19.05mm WT) – Nominal 0.5Ni-0.25Mo-0.3Cu-Al-Nb-Ti																			
X100 Pipe (Cranfield Analysis)	0.066	1.88	0.008	<0.005	0.18	0.022	0.49	0.26	0.30	0.04	0.005	0.05	0.018	10	46	<5	0.209	0.308	0.489
X100 Pipe (Cranfield Analysis)	0.059	1.89	0.007	<0.005	0.18	0.022	0.50	0.26	0.30	0.04	0.005	0.06	0.018			<5	0.203	0.303	0.485
Base Metal Ladle (Supplier Analysis)	0.06	1.84	0.008	0.0011	0.18	0.03	0.50	0.25	0.31	0.036	-	0.05	0.018		55	1	0.201	0.299	0.477
X100 Pipe Seam ID (Cranfield Analysis)	0.059	1.99	0.008	<0.005	0.21	0.36	1.00	0.78	0.26	0.026	0.007	0.04	0.02	328	56	6	0.269	0.392	0.704
X100 Pipe Seam ID (Supplier Analysis)	0.06	1.88	0.008	0.003	0.22	0.37	1.03	0.76	0.26	0.015	-	0.033	0.02	279	61	11	0.266	0.381	0.685
X100 Pipe Seam OD (Cranfield Analysis)	0.053	1.91	0.007	<0.005	0.2	0.33	2.03	0.63	0.26	0.023	0.007	0.03	0.018	289	56	6	0.264	0.387	0.717
X100 Pipe Seam OD (Supplier Analysis)	0.06	1.78	0.008	0.003	0.21	0.34	2.04	0.6	0.24	0.012	-	0.027	0.018	335	60	9	0.264	0.378	0.697

	C wt%	Mn wt%	P wt%	S wt%	Si wt%	Cr wt%	Ni wt%	Mo wt%	Cu wt%	Al wt%	V wt%	Nb wt%	Ti wt%	O ppm	N ppm	B ppm	P_{CM}	CET BS EN 1011-2	CE_{IIW}
Pipe C (16.3mm WT) – Nominal 0.25Ni-0.3Mo-Al –Nb-Ti																			
X100 Pipe (Bodycote Analysis)	0.056	1.85	0.010	0.002	0.36	0.03	0.26	0.29	0.02	0.023	0.005	0.050	0.019	~20	~30	<10	0.188	0.279	0.448
X100 Pipe (Cranfield Analysis)	0.055	1.91	0.010	<0.005	0.37	0.03	0.24	0.28	0.01	0.023	0.005	0.05	0.02	17	32	<5	0.189	0.282	0.453
X100 Plate (Bodycote Analysis)	0.055	1.80	0.008	0.002	0.36	0.03	0.24	0.29	0.02	0.020	0.004	0.044	0.016	~30	~40	<10	0.184	0.273	0.437
X100 Plate (Cranfield Analysis)	0.052	1.90	0.009	<0.005	0.37	0.02	0.24	0.29	0.01	0.024	<0.005	0.05	0.02	24	39	<5	0.186	0.279	0.448
X100 Pipe Seam ID (Cranfield Analysis)	0.049	1.69	0.012	<0.005	0.38	0.04	0.17	0.34	0.01	0.023	0.006	0.03	0.03	296	50	30	0.190	0.259	0.420
X100 Pipe Seam OD (Cranfield Analysis)	0.05	1.64	0.012	<0.005	0.38	0.04	0.16	0.35	0.01	0.021	0.006	0.03	0.03	306	54	30	0.189	0.256	0.414

Where Pcm = C + Mn/20 + Mo/15 + Ni/60 + Cr/20 + V/10 + Cu/20 + Si/30 + 5B

CET = C + (Mn+Mo)/10 + (Cr+Cu)/20 + Ni/40

CE_{IIW} = C + Mn/6 + (Cr +Mo+V)/5 + (Cu+Ni)/15

When elements are stated as < the given amount, calculations for carbon equivalents are based on the following assumptions: V = 0.002 and B = 0.0002

Table 5-7: Pipe seam weld hardness traverses

Manufacturer	Location	Base Material HV10	Base Material HV10	Base Material HV10	HAZ HV10	HAZ HV10	HAZ HV10	Seam Weld HV10	Seam Weld HV10	Seam Weld HV10	HAZ HV10	HAZ HV10	HAZ HV10	Base Material HV10	Base Material HV10	Base Material HV10
19.05 mm WT,	2mm Sub OD	264	260	262	243	245	247	251	256	253	236	242	245	264	264	266
Pipe A	Pipe Mid Thickness	254	253	249	254	254	256	272	266	272	249	242	245	247	254	247
	2mm Sub ID	264	264	260	258	260	268	283	287	292	262	264	262	270	266	264
14.9 mm WT,	2mm Sub OD	262	262	251	225	219	235	264	270	268	232	228	224	258	266	281
Pipe B15	Pipe Mid Thickness	258	260	249	243	236	238	292	292	285	247	238	247	249	262	272
	2mm Sub ID	262	274	266	245	235	236	268	270	270	243	233	245	262	268	279
19.05mm WT,	2mm Sub OD	245	247	243	224	233	232	279	279	281	233	232	225	235	240	245
Pipe B19	Pipe Mid Thickness	243	243	276	232	232	243	297	294	297	238	230	247	240	240	236
	2mm Sub ID	287	287	245	245	247	249	281	283	287	258	249	253	274	264	276
16.3mm WT,	2mm Sub OD	260	258	251	236	238	240	254	245	249	240	243	240	247	253	258
Pipe C	Pipe Mid Thickness	254	258	249	256	262	276	274	264	266	254	243	253	253	253	240
	2mm Sub ID	285	281	272	274	287	298	276	272	281	287	285	279	251	253	224

Hardness indent locations as per EEMUA 166:1991 and BS ISO 3183-3:1999. Values determined from 10kg load

Summary of pipe seam weld hardness values

Manufacturer	BM Av.	BM Max.	HAZ Av.	HAZ Max.	WM Av.	WM Max.
A	260	270	252	268	270	292
B15	263	281	236	247	275	292
B19	254	287	239	258	286	297
C	256	285	261	298	265	281

Typical Indent locations

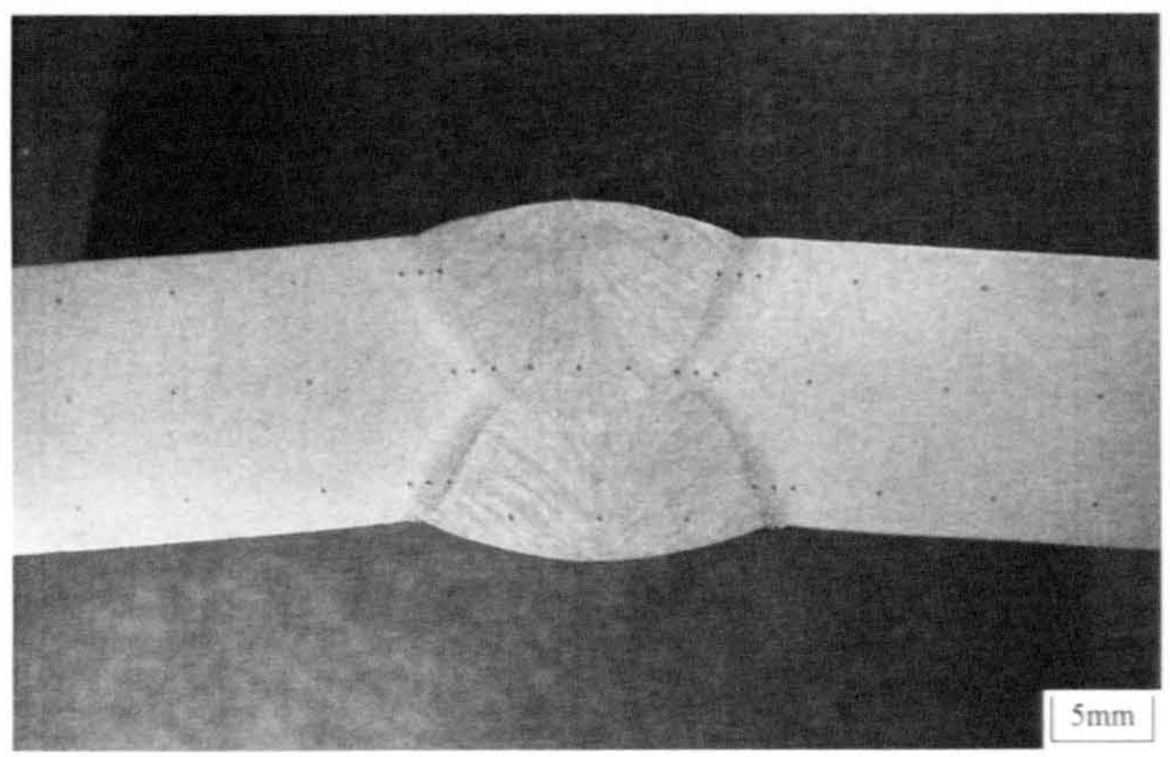

Table 5-8: Weld metal diffusible hydrogen measurements

Wire Brand Name	Wire type	Diameter (mm)	Current (A)	Voltage (V)	Travel Speed (mm/min)	Contact Tip to Workpiece Distance (mm)	Arc Energy (kJ/mm)	Shielding gas	Average diffusible hydrogen content ($ml H_2/100g$ weld metal)
Spoolarc 120	Solid	0.9	120	25.3	195	13	0.93	CO_2	1.60
OK 15.09	Rutile flux cored	1.2	200	27	330	20	0.98	78%Ar/20%CO_2/2%O_2	0.8
OK 15.09	Rutile flux cored	1.2	250	29	330	15	1.32	78%Ar/20%CO_2/2%O_2	2.1

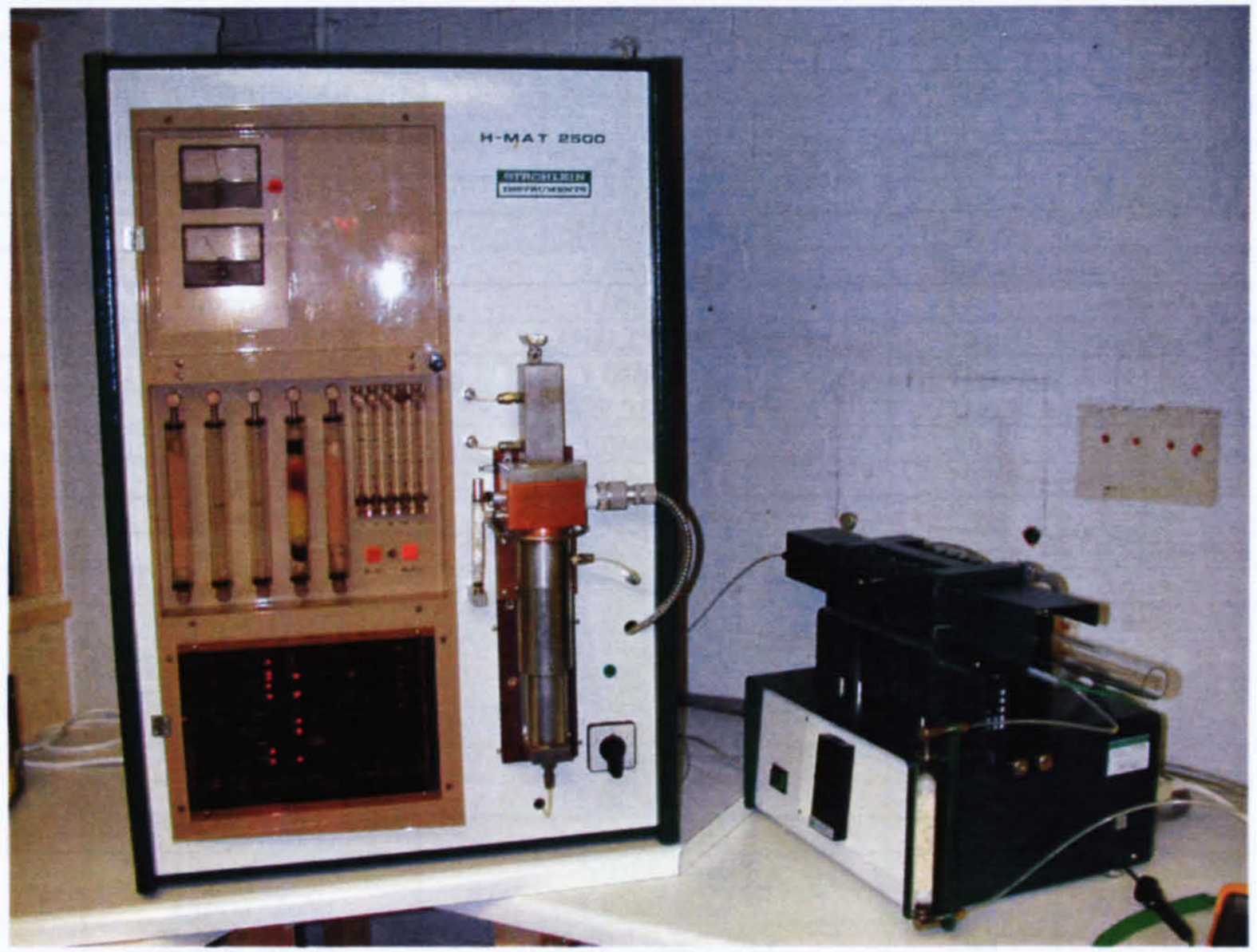

Diffusible hydrogen hot extraction equipment; Juwe Strohlein H Mat 2500

Table 5-9: X100 Pipe 5G Narrow Gap Trials - Tests Conducted

Weld N°	Bevel Angle & Width at Cap (mm)	Gas Type	Consumable	Nominal Wire Chemistry	Pulsed / Dip Transfer	Heat Input (kJ/mm)	Single / Dual / Tandem	Comments
Serimer-Dasa Welds								
7043a	3°30' (7.3-7.6)	50Ar/50CO_2	Union NiMoCr	1.5Ni 0.5Mo 0.2Cr	Dip	0.52 +/- 0.3	Dual	50mm spacing
7043MoNi	3°30' (7.3-7.6)	50Ar/50CO_2	Union MoNi	1.0Ni0.4Mo	Dip	0.52 +/- 0.3	Dual	50mm spacing
7044a	3°30' (6.9-7.1)	50Ar/50CO_2	Union NiMoCr	1.5Ni 0.5Mo 0.2Cr	Dip	0.52 +/- 0.3	Dual	50mm spacing
7044b	3°30' (6.9-7.1)	50Ar/50CO_2	Union MoNi	1.0Ni0.4Mo	Dip	0.52 +/- 0.3	Dual	50mm spacing
7049a	7.0-7.2	90Ar/10CO_2	Union NiMoCr	1.5Ni 0.5Mo 0.2Cr	Pulsed		Single	
7049b	7.0-7.2	90Ar/10CO_2	Union MoNi	1.0Ni0.4Mo	Pulsed		Single	
7089 13.13	4° (6.4-6.6)	50Ar/50CO_2	ESAB 13-13	0.5Ni0.25Mo0.5Cr	Dip	0.52 +/- 0.3	Dual	50mm spacing
7089b	4° (6.4-6.6)	50Ar/50CO_2	Union NiMoCr	1.5Ni 0.5Mo 0.2Cr	Dip	0.52 +/- 0.3	Dual	50mm spacing
7115 M	4° (6.6-7.0)	80Ar/20CO_2	Union NiMoCr	1.5Ni 0.5Mo 0.2Cr	Dip	0.52 +/- 0.3	Single	50mm spacing
7115 B1T	4° (6.6-7.0)	80Ar/20CO_2	Union NiMoCr	1.5Ni 0.5Mo 0.2Cr	Dip	0.52 +/- 0.3	Dual	
7116 13.29	4° (6.5-6.8)	80Ar/20CO_2	ESAB 13-29	1.5Ni0.25Mo0.25Cr	Dip	0.52 +/- 0.3	Dual	50mm spacing
7116 BT	4° (6.5-6.8)	80Ar/20CO_2	Bohler X70 IG	1.3Ni0.25Mo0.25Cr	Dip	0.52 +/- 0.3	Dual	50mm spacing
7138a	6.0-6.2	90Ar/10CO_2	Union NiMoCr	1.5Ni 0.5Mo 0.2Cr	Pulsed		Single	
7138b	6.0-6.2	90Ar/10CO_2	Union MoNi	1.0Ni0.4Mo	Pulsed		Single	
7151a	2° (6.1-6.35)	80Ar/20CO_2	Union MoNi	1.0Ni0.4Mo	Dip	0.49 +/- 0.3	Dual	X65 50mm spacing
7151b	2° (6.1-6.35)	80Ar/20CO_2	Bohler X70 IG	1.3Ni0.25Mo0.25Cr	Dip	0.49 +/- 0.3	Dual	X65 50mm spacing
7155a	2° (6.45-6.8)	80Ar/20CO_2	Union MoNi	1.0Ni0.4Mo	Dip	0.41 +/- 0.3	Dual	X65 - High speed procedure
7155b	2° (6.45-6.8)	80Ar/20CO_2	Bohler X70 IG	1.3Ni0.25Mo0.25Cr	Dip	0.41 +/- 0.3	Dual	X65 - High speed procedure
7162a	2° (6.3-6.6)	80Ar/20CO_2	Union MoNi	1.0Ni0.4Mo	Dip	0.41 +/- 0.3	Dual	X65 - High speed procedure -
7162b	2° (6.3-6.6)	80Ar/20CO_2	Bohler X70 IG	1.3Ni0.25Mo0.25Cr	Dip	0.41 +/- 0.3	Dual	100mm spaced torches
7164a	3°30' (7.3-7.5)	80Ar/20CO_2	Union MoNi	1.0Ni0.4Mo	Dip	0.52 +/- 0.3	Dual	X65
7164b	3°30' (7.3-7.5)	80Ar/20CO_2	Bohler X70 IG	1.3Ni0.25Mo0.25Cr	Dip	0.52 +/- 0.3	Dual	X65
7200b2	2° (6.1-6.35)	80Ar/20CO_2	Union MoNi (B2)	1.0Ni0.4Mo	Dip	0.41 +/- 0.3	Dual	X100 - High speed procedure
7200b1	2° (6.1-6.35)	80Ar/20CO_2	Union MoNi (B1)	1.0Ni0.4Mo	Dip	0.41 +/- 0.3	Dual	X100 - High speed procedure
7200a2	2° (6.1-6.35)	80Ar/20CO_2	Bohler X70 IG (A2)	1.3Ni0.25Mo0.25Cr	Dip	0.41 +/- 0.3	Dual	X100 - High speed procedure
7200a1	2° (6.1-6.35)	80Ar/20CO_2	Bohler X70 IG (A1)	1.3Ni0.25Mo0.25Cr	Dip	0.41 +/- 0.3	Dual	X100 - High speed procedure
7217a	2°(5.8-6.0)	80Ar/20CO_2	Union MoNi	1.0Ni0.4Mo	Dip	0.41 +/- 0.3	Dual	Root test (5mm dia.)
7217b	2°(5.8-6.0)	80Ar/20CO_2	Union MoNi	1.0Ni0.4Mo	Dip	0.41 +/- 0.3	Dual	Root test (5mm dia.)
7217c	2°(5.8-6.0)	80Ar/20CO_2	Union MoNi	1.0Ni0.4Mo	Dip	0.41 +/- 0.3	Dual	Cap test (5mm dia.)
7217d	2°(5.8-6.0)	80Ar/20CO_2	Union MoNi	1.0Ni0.4Mo	Dip	0.41 +/- 0.3	Dual	Cap test (5mm dia.)
7217e	2°(5.8-6.0)	80Ar/20CO_2	Union MoNi	1.0Ni0.4Mo	Dip	0.41 +/- 0.3	Dual	Strip tensile (4.5x8.0mm)
7217f	2°(5.8-6.0)	80Ar/20CO_2	Union MoNi	1.0Ni0.4Mo	Dip	0.41 +/- 0.3	Dual	Strip tensile (4.5x8.0mm)
7217g	2°(5.8-6.0)	80Ar/20CO_2	Bohler X70 IG	1.3Ni0.25Mo0.25Cr	Dip	0.41 +/- 0.3	Dual	Root test (5mm dia.)
7217h	2°(5.8-6.0)	80Ar/20CO_2	Bohler X70 IG	1.3Ni0.25Mo0.25Cr	Dip	0.41 +/- 0.3	Dual	Root test (failure close to grip end)
7217l	2°(5.8-6.0)	80Ar/20CO_2	Bohler X70 IG	1.3Ni0.25Mo0.25Cr	Dip	0.41 +/- 0.3	Dual	Cap (problem with test)(5mm dia.)
7217j	2°(5.8-6.0)	80Ar/20CO_2	Bohler X70 IG	1.3Ni0.25Mo0.25Cr	Dip	0.41 +/- 0.3	Dual	Cap Test (5mm dia.)
7217k	2°(5.8-6.0)	80Ar/20CO_2	Bohler X70 IG	1.3Ni0.25Mo0.25Cr	Dip	0.41 +/- 0.3	Dual	Strip tensile (4.5x8.0mm)(failure close to
7217l	2°(5.8-6.0)	80Ar/20CO_2	Bohler X70 IG	1.3Ni0.25Mo0.25Cr	Dip	0.41 +/- 0.3	Dual	Strip tensile (4.5x8.0mm)
7251a	2°(5.8-6.0)	80Ar/20CO_2	Union MoNi	1.0Ni0.4Mo	Dip	0.41 +/- 0.3	Dual	High Speed procedure, 100mm spacing
7251b	2°(5.8-6.0)	80Ar/20CO_2	Bohler X70 IG	1.3Ni0.25Mo0.25Cr	Dip	0.41 +/- 0.3	Dual	High Speed Procedure, 100mm spacing
7279a	2°(6.0-6.5)	80Ar/20CO_2	Union MoNi	1.0Ni0.4Mo	Dip	0.41 +/- 0.3	Single	High Speed Procedure -
7279b	2°(6.0-6.5)	80Ar/20CO_2	Bohler X70 IG	1.3Ni0.25Mo0.25Cr	Dip	0.41 +/- 0.2	Single	single torch

Table 5-9 (Cont.): X100 pipe 5G narrow gap trials - tests conducted

Weld N°	Bevel Angle(°) & Width at Cap (mm)	Gas Type	Consumable	Nominal Wire Chemistry	Pulsed / Dip Transfer	Heat Input (kJ/mm)	Single / Dual / Tandem	Comments
Serimer-Dasa Welds (Cont.)								
9077B	3, 6.2*	80Ar/20CO_2	Böhler X70-IG	1.3Ni0.25Mo0.25Cr	dip	0.25 - 0.50	Dual	50mm torch spacing
9077T	3, 6.2*	80Ar/20CO_2	Carbofil HT	0.5Ni0.5Mo0.5Cr	dip	0.25 - 0.50	Dual	50mm torch spacing
9086B	3, 6.2*	80Ar/20CO_2	Elgamatic 135	1.3Ni0.3Mo0.3Cr	dip	0.25 - 0.50	Dual	50mm torch spacing
9086T	3, 6.2*	80Ar/20CO_2	Union MoNi	1.0Ni0.4Mo	dip	0.25 - 0.50	Dual	50mm torch spacing
9551B	3, 6.4*	80Ar/20CO_2	Böhler X70-IG	1.3Ni0.25Mo0.25Cr	dip	0.25 - 0.50	Dual	50mm torch spacing
9551T	3, 6.4*	80Ar/20CO_2	RMS/T Raedelli		dip	0.25 - 0.50	Dual	50mm torch spacing
9555B	3, 6.0*	80Ar/20CO_2	Elgamatic 135	1.3Ni0.3Mo0.3Cr	dip	0.25 - 0.50	Dual	50mm torch spacing
9555T	3, 6.0*	80Ar/20CO_2	Union X85	1.8Ni0.5Mo0.3Cr	dip	0.25 - 0.50	Dual	50mm torch spacing
* bevel tolerance±0.5°, cap width tolerance ±0.5mm								
Cranfield Welds								
ML-B-1	5° (7.9-8.1)	82.5Ar/ 12.5CO_2/ 5He	Spoolarc 120	2.5Ni0.5Mo0.4Cr	Pulsed	0.29-0.68	Single	Lincoln Powerwave 455
ML-B-3	5° (7.9-8.1)	82.5Ar/ 12.5CO_2/ 5He	Union NiMoCr	1.5Ni 0.5Mo 0.2Cr	Pulsed	0.30-0.60	Tandem	Fronius Time Twin
ML-B-4	5° (7.9-8.1)	82.5Ar/ 12.5CO_2/ 5He	Union NiMoCr	1.5Ni 0.5Mo 0.2Cr	Pulsed	0.30-0.50	Tandem	Fronius Time Twin
ML-B-5	5° (7.9-8.1)	82.5Ar/ 12.5CO_2/ 5He	Bohler X70 IG	1.3Ni0.25Mo0.25Cr	Pulsed	0.30-0.57	Tandem	Fronius Time Twin
ML-B-6	5° (7.0-7.2)	82.5Ar/ 12.5CO_2/ 5He	Carbofil HT	0.5Ni0.5Mo0.5Cr	Pulsed	0.29-0.54	Single	Lincoln Powerwave 455
ML-B-11	5° (7.10-7.43)	82.5Ar/ 12.5CO_2/ 5He	Carbofil NiMo-1	1Ni0.3Mo	Pulsed	0.40-0.56	Tandem	Fronius Time Twin
ML-A-1	5° (6.3-6.6)	82.5Ar/ 12.5CO_2/ 5He	Carbofil HT	0.5Ni0.5Mo0.5Cr	Pulsed	0.47-0.69	Single	Lincoln Powerwave 455
ML-A-2	5° (6.3-6.6)	82.5Ar/ 12.5CO_2/ 5He	Spoolarc 120	2.5Ni0.5Mo0.4Cr	Pulsed	0.30-0.69	Single	Lincoln Powerwave 455
ML-A-3	5°(6.7-7.0)	82.5Ar/ 12.5CO_2/ 5He	Spoolarc 120	2.5Ni0.5Mo0.4Cr	Pulsed	0.45-0.68	Single	Lincoln Powerwave 455
ML-A-4	5°(6.35-6.8)	82.5Ar/ 12.5CO_2/ 5He	Carbofil HT	0.5Ni0.5Mo0.5Cr	Pulsed	0.40-0.49	Single	Lincoln Powerwave 455
ML-B15-5	5°(6.23-6.45)	82.5Ar/ 12.5CO_2/ 5He	Spoolarc 120	2.5Ni0.5Mo0.4Cr	Pulsed	0.31-0.60	Tandem	Fronius Time Twin
ML-B15-6 Sd A	5°(6.11-6.33)	82.5Ar/ 12.5CO_2/ 5He	Carbofil 120	1.85Ni0.55Mo0.2Cr	Pulsed	0.30-0.57	Tandem	Fronius Time Twin
ML-B15-6 Sd B	5°(6.11-6.27)	82.5Ar/ 12.5CO_2/ 5He	Spoolarc 120	2.5Ni0.5Mo0.4Cr	Pulsed	0.30-0.54	Tandem	Fronius Time Twin
ML-B15-10	5°(7.29-7.52)	82.5Ar/ 12.5CO_2/ 5He	Carbofil NiMo-1	1Ni0.3Mo	Pulsed	0.34-0.53	Tandem	Fronius Time Twin
ML-B15-12	5°(6.58-6.69)	82.5Ar/ 12.5CO_2/ 5He	Carbofil NiMo-1	1Ni0.3Mo	Pulsed	0.30-0.53	Tandem	Fronius Time Twin (Ib = 55A)
ML-B15-13	5°(6.30-6.51)	82.5Ar/ 12.5CO_2/ 5He	Carbofil NiMo-1	1Ni0.3Mo	Pulsed	0.30-0.51	Tandem	Fronius Time Twin (Ib = 60A)

Table 5-10: X100 Pipe 5G narrow gap trials – tensile and hardness results (Serimer-Dasa welds)

		All Weld Metal Round Bar Tensile					All Weld Metal Strip Tensile					WM Hardness	
Weld N°	**Consumable**	**$R_{p0.2}$ (MPa)**	**$R_{t0.5}$ (MPa)**	**R_m (MPa)**	**Yield/ Tensile Ratio**	**A (%)**	**$R_{p0.2}$ (MPa)**	**$R_{t0.5}$ (MPa)**	**R_m (MPa)**	**Yield/ Tensile Ratio**	**A (%)**	**HV2.5 Av.**	**HV2.5 Max.**
7043a	NiMoCr	715		772	0.93	22							
7043b	MoNi	740		812	0.91	16	707	707	766	0.92	26.2	252	258
7044a	NiMoCr	717		794	0.90	22							
7044b	MoNi	726		786	0.92	23							
7049a	NiMoCr	889		936	0.95	15							
7049b	MoNi	846		884	0.96	19							
7089a	ESAB 13-13	697		779	0.89	23	697	697	767	0.91	23.5	247	266
7089b	NiMoCr	693		778	0.89	21							
7115M	NiMoCr	840		881	0.95	11	894	880	927	0.96	10.6	285	301
7115B1T	NiMoCr	725		796	0.91	10	756	732	831	0.91	13.9	266	274
7116	ESAB 13-29	702		786	0.89	18	718	716	788	0.91	23.1	267	283
7116BT	Bohler X70 IG	771		831	0.93	12	726	721	792	0.92	13.3	262	270
7138a	NiMoCr	964		1039	0.93	11							
7138b	MoNi	960		1004	0.96	16							
7151a	MoNi	757		816	0.93	15							
7151b	Bohler X70 IG	753		818	0.92	20							
7155a	MoNi	807		849	0.95	11							
7155b	Bohler X70 IG	819		868	0.94	19							
7162a	MoNi	889		931	0.95	17							
7162b	Bohler X70 IG	860		904	0.95	12							
7164a	MoNi	743		793	0.94	20							
7164b	Bohler X70 IG	763		815	0.94	19							
7200b2	MoNi (B2)	781		852	0.92	17	725		889	0.82	19		
7200b1	MoNi (B1)	998		1076	0.93	18	747		860	0.87	21		
7200a2	Bohler X70 IG	811		873	0.93	10	758		877	0.86	19		
7200a1	Bohler X70 IG	813		866	0.94	10	732		863	0.85	18		
7217a	MoNi	778		873	0.89	15							
7217b	MoNi	775		876	0.88	20							
7217c	MoNi	785		893	0.88	16							
7217d	MoNi	783		889	0.88	18							
7217e	MoNi						783		859		15		
7217f	MoNi						777		864		19		
7217g	Bohler X70 IG	807		886	0.91	15							
7217h	Bohler X70 IG	815		889	0.92	13							
7217i	Bohler X70 IG			911		12							
7217j	Bohler X70 IG	832		915	0.91	13							
7217k	Bohler X70 IG						811		883		13		
7217l	Bohler X70 IG						811		875		17		
7251a	MoNi						830		891		19		
							828		916		20		
7251b	Bohler X70 IG						905		957		17		
							941		941		12		
7279a	MoNi	978		1012	0.97	13							
7279b	Bohler X70 IG	972		994	0.98	14							

Table 5-11: X100 pipe 5G narrow gap trials – tensile and hardness results (Serimer-Dasa and WERC welds)

		All Weld Metal Round Bar Tensile					All Weld Metal Strip Tensile					WM Hardness	
Weld N°	**Consumable**	**$R_{p0.2}$ (MPa)**	**$R_{t0.5}$ (MPa)**	**R_m (MPa)**	**Yield/ Tensile Ratio**	**A (%)**	**$R_{p0.2}$ (MPa)**	**$R_{t0.5}$ (MPa)**	**R_m (MPa)**	**Yield/ Tensile Ratio**	**A (%)**	**HV10 Av.**	**HV10 Max.**
Serimer-Dasa Welds													
9077B	Böhler X70-IG	950/985		995/1015	0.95/0.97	14/12							
9077T	Carbofil HT	754		804	0.94	21							
9086B	Elgamatic 135	854/860		916/910	0.93/0.95	17/18							
9086T	Union MoNi	820/815		896/897	0.92/0.91	1							
9551B	Böhler X70-IG	888/863		940/920	0.94/0.94	11.7/19.4							
9551T	RMS/T Raedelli	764/800		834/854	0.92/0.94	17/18.4							
9555B	Elgamatic 135	876/920		945/964	0.93/0.95	8.7/14.6							
9555T	Union X85	895/958		1032/1039	0.87/0.92	8.6/13							
Cranfield Welds													
ML-B-1	Spoolarc 120	875		913	0.96	12	874	842	906	0.96	17.6	307	322
ML-B-3	Union NiMoCr						1002	938	1025	0.98	8.6	329	360
ML-B-4	Union NiMoCr	X-rayed; not suitable for mechanical testing										287	294
ML-B-5	Bohler X70 IG						924	733	957	0.97	9.2	319	339
ML-B-6	Carbofil HT						843	842	887	0.95	17.9	272	294
ML-B-11	Oerlikon NiMo-1						870	836	931	0.93	17	302	325
ML-A-1	Carbofil HT						815	771	860	0.95	13	296	306
ML-A-2	Spoolarc 120						936	871	998	0.94	14.6	325	342
ML-A-3	Spoolarc 120						971	927	1017	0.95	15.1	331	345
ML-A-4	Carbofil HT						853	834	900	0.95	9.9	296	311
ML-B-11	Carbofil NiMo-1						870	836	931	0.93	17		
ML-B15-5	Spoolarc 120						931	804	965	0.96	16		
ML-B15-6 Sd A	Carbofil 120						1147		1171	0.98	11		
ML-B15-10	Carbofil NiMo-1						804	721	847	0.95	19.5		
ML-B15-12	Carbofil NiMo-1						875	879	921	0.95	16.5		

Table 5-12: X100 pipe 5G narrow gap trials – toughness results

		Impact Toughness			CTOD	
Weld N°	**Consumable**	**WM Cv -30°C (J)**	**FL Cv -40°C (J)**	**FL +2 Cv -40°C (J)**	**CTOD -10°C Weld Metal (mm)**	**CTOD -10°C HAZ (mm)**
Serimer-Dasa Welds						
7043a	NiMoCr	55 - 62 - 70				
7043b	MoNi	88 - 98 - 99				
7115M	NiMoCr	85 -125 - 131				
7115B1T	NiMoCr	109 - 145 - 181				
7116	ESAB 13-29	78 - 94 - 99				
7116B	Bohler X70 IG	86 - 98 - 100				
7151a	MoNi	137 - 197 - 220				
7151b	Bohler X70 IG	247 - 239 - 241				
7155a	MoNi	220 - 266 - 271				
7155b	Bohler X70 IG	154 - 225 - 176				
7162a	MoNi	192 - 276 - 279				
7162b	Bohler X70 IG	154 - 252 - 176				
7164a	MoNi	179 - 186 - 204				
7164b	Bohler X70 IG	117 - 125 - 145				
7279a	MoNi	216-203-204				
7279b	Bohler X70 IG	195-207-80				
Cranfield Welds						
ML-B-1	Spoolarc 120	182-192-194				
ML-B-6	Carbofil HT	116 - 104 – 98 (-40°C)	122 - 152 - 138	216 - 170 - 216	0.21, 0.14, 0.18	0.22, 0.24
ML-B15-5	Spoolarc 120	184 - 214 – 200 (-40°C)				
ML-B15-6 Sd A	Carbofil 120	74 - 62 – 76 (-40°C)				
ML-B15-10	Carbofil NiMo-1	128 - 198 – 220 (-40°C)				
ML-B15-12	Carbofil NiMo-1	176 - 212 – 195 (-40°C)				

Table 5-13: X100 pipe 5G narrow gap trials – weld metal chemistry results

		Weld Metal Chemical Composition (wt %)																			
Weld N°	**Consumable**	**C**	**Mn**	**P**	**S**	**Si**	**Cr**	**Ni**	**Mo**	**Cu**	**Al**	**V**	**Nb**	**Ti**	**B**	**O**	**N**	**CE_{IIW}**	**CET**	**P_{cm}**	**PH Temp (°C)**
Serimer Welds																					
7043b	MoNi	0.085	1.34	0.007	0.007	0.50	0.04	1.01	0.39	0.17	0.006	0.005	0.010	0.04	<0.0005	0.0460	0.0072	0.474	0.294	0.225	50
7089a	ESAB 13-13	0.097	1.33	0.013	0.006	0.59	0.48	0.48	0.21	0.12	0.007	<0.005	0.011	0.006	0.0011	0.0573	0.0060	0.497	0.293	0.241	40
7115a	NiMoCr (single)	0.081	1.57	0.006	0.013	0.50	0.18	1.32	0.48	0.09	0.006	0.006	0.010	0.03	<0.0005	0.0324	0.0046	0.570	0.333	0.246	68
7115b	NiMoCr (dual)	0.079	1.56	0.006	0.012	0.45	0.17	1.30	0.47	0.10	0.006	0.006	0.010	0.02	<0.0005	0.0354	0.0054	0.562	0.328	0.241	65
7116a	ESAB 13-29	0.084	1.50	0.012	0.007	0.44	0.24	1.11	0.26	0.10	0.008	0.060	0.008	0.005	0.0009	0.0422	0.0073	0.527	0.305	0.237	48
7116b	Bohler X70-IG	0.068	1.46	0.006	0.011	0.55	0.26	1.22	0.24	0.13	0.005	0.090	0.008	0.03	0.011	0.0337	0.0073	0.519	0.288	0.230	36
Cranfield Welds																					
ML-B-1	Spoolarc 120	0.055	1.49	0.007	<0.005	0.31	0.26	2.12	0.5	0.1	0.01	0.006	0.01	0.014	0.0011	0.0374	0.0076	0.605	0.325	0.233	73
ML-B-3	Union NiMoCr	0.069	1.52	0.009	0.013	0.56	0.17	1.31	0.51	0.13	0.01	0.007	0.008	0.04	<0.0005	0.0312	0.0099	0.556	0.320	0.237	69
ML-B-5	Bohler X70-IG	0.079	1.46	0.008	0.014	0.56	0.24	1.26	0.24	0.09	0.006	0.10	0.006	0.04	<0.0005	0.0299	0.0065	0.528	0.297	0.236	52
ML-B-6	Carbofil HT	0.067	1.36	0.008	0.010	0.6	0.41	0.48	0.44	0.17	0.006	0.005	0.011	0.006	<0.0005	0.0352	0.0085	0.508	0.288	0.224	46
ML-B-11	Oerlikon NiMo-1	0.082	1.65	0.01	0.009	0.58	0.03	0.87	0.3	0.11	0.005	0.006	0.006	0.04	<0.0005	0.0428	0.0078	0.490	0.306	0.228	59
ML-B15-10	Oerlikon NiMo-1	0.078	1.65	0.009	0.008	0.56	0.03	0.86	0.30	0.12	<0.005	0.006	0.005	0.04	<0.0005	0.0314	0.0069	0.486	0.302	0.224	46

$CE_{IIW} = C + Mn/6 + (Cr+Mo+V)/5 + (Ni + Cu)/15$

$CET_{(BS\ EN\ 1011\text{-}2)} = C + (Mn+Mo)/10 + (Cr+Cu)/20 + Ni/40$

$P_{cm} = C + Si/30 + (Mn+Cu+Cr)/20 + Ni/60 + Mo/15 + V/10 + 5B$

When elements are stated as < the given amount, calculations for carbon equivalents are based on the following assumptions: V = 0.004 and B = 0.0004

Preheat calculated according to BS EN 1011-2:2001 Method B. Pipe wall thickness of 19.05mm, weld metal diffusible H2 of 2ml/100g and heat input of 0.4kJ/mm used.

Table 5-14: X100 narrow gap pipe 5G procedure tests – tests conducted (Serimer-Dasa)

Weld N°	Consumable	Nominal Wire Chemistry	Bevel Angle & Width at Cap (mm)	X100 Pipe OD x WT	Gas Type	Electrode dia. (mm)	Pulsed / Dip	Heat Input (kJ/mm)	Single / Dual / Tandem	Backing System/ Root Run Location	Comments
7544	Bohler X70-IG (Supramig Root)	1.3Ni0.25Mo0.25Cr	2°(±0.5°) 6.1 (±0.5)	Pipe A 30" - 19mm	80%Ar/ 20%CO_2	1.0	Dip	0.25-0.51	Dual	Internal Copper/ external root/fill/cap	100mm torch spacing
7549	Bohler X70-IG (Supramig Root)	1.3Ni0.25Mo0.25Cr	2°(±0.5°) 6.1 (±0.5)	Pipe B19 36" - 19mm	80%Ar/ 20%CO_2	1.0	Dip	0.25-0.51	Dual	Internal Copper/ external root/fill/cap	100mm torch spacing
7624	Bohler X70-IG (Supramig Root)	1.3Ni0.25Mo0.25Cr	2°(±0.5°) 6.1 (±0.5)	Pipe C 36" - 16mm	80%Ar/ 20%CO_2	1.0	Dip	0.25-0.51	Dual	Internal Copper/ external root/fill/cap	100mm torch spacing
7632	Thyssen MoNi (Supramig Root)	1.0Ni0.4Mo	2°(±0.5°) 6.1 (±0.5)	Pipe A 30" - 19mm	80%Ar/ 20%CO_2	1.0	Dip	0.25-0.51	Dual	Internal Copper/ external root/fill/cap	100mm torch spacing
7546	Thyssen MoNi (Supramig Root)	1.0Ni0.4Mo	2°(±0.5°) 6.1 (±0.5)	Pipe B19 36" - 19mm	80%Ar/ 20%CO_2	1.0	Dip	0.25-0.51	Dual	Internal Copper/ external root/fill/cap	100mm torch spacing
7548	Thyssen MoNi (Supramig Root)	1.0Ni0.4Mo	2°(±0.5°) 6.1 (±0.5)	Pipe C 36" - 16mm	80%Ar/ 20%CO_2	1.0	Dip	0.25-0.51	Dual	Internal Copper/ external root/fill/cap	100mm torch spacing
7691	Thyssen MoNi (Supramig Root)	1.0Ni0.4Mo	2°(±0.5°) 6.1 (±0.5)	Pipe A 30" - 19mm	90%Ar/10%CO_2 80%Ar/20%CO2 (Root)	1.0	Pulsed	0.27-0.99	Single	Internal Copper/ external root/fill/cap	
7625	Thyssen MoNi (Supramig Root)	1.0Ni0.4Mo	2°(±0.5°) 6.1 (±0.5)	Pipe B19 36" - 19mm	90%Ar/10%CO_2 80%Ar/20%CO2 (Root)	1.0	Pulsed	0.27-1.00	Single	Internal Copper/ external root/fill/cap	
8868	Elga Elgamatic 135 (Supramig Root)	1.5Ni0.3Mo0.2Cr	3° (±0.5), 6.2 (±0.5)	Pipe B15 36" - 14.9mm	80%Ar/20%CO_2	1.0	Dip	0.25 - 0.5	Dual	Internal Copper/ external root	100mm torch spacing
8876	Thyssen MoNi (Supramig Root)	1.0Ni0.4Mo	3° (±0.5), 6.2 (±0.5)	Pipe B15 36" - 14.9mm	80%Ar/20%CO_2	1.0	Dip	0.25 - 0.5	Dual	Internal Copper/ external root	100mm torch spacing
9692B	Elga Elgamatic 135 (Supramig Root)	1.5Ni0.3Mo0.2Cr	2°(±0.5°), 6.0 - 6.4	Pipe B15 36" - 14.9mm	80%Ar/20%CO_2	1.0	Dip	0.25 - 0.5	Dual	Internal Copper/ external root	50mm torch spacing
9692T	Thyssen Union X85 (Supramig Root)	1.8Ni0.5Mo0.3Cr	2°(±0.5°), 6.0 - 6.4	Pipe B15 36" - 14.9mm	80%Ar/20%CO_2	1.0	Dip	0.25 - 0.5	Dual	Internal Copper/ external root	50mm torch spacing
9726B	Elga Elgamatic 135 (Supramig Root)	1.5Ni0.3Mo0.2Cr	2°(±0.5°), 6.0 - 6.4	Pipe B15 36" - 14.9mm	50%Ar/50%CO_2	1.0	Dip	0.25 - 0.5	Dual	Internal Copper/ external root	50mm torch spacing faster travel speed
9726T	Thyssen Union X85 (Supramig Root)	1.8Ni0.5Mo0.3Cr	2°(±0.5°), 6.0 - 6.4	Pipe B15 36" - 14.9mm	50%Ar/50%CO_2	1.0	Dip	0.25 - 0.5	Dual	Internal Copper/ external root	50mm torch spacing faster travel speed

Table 5-15: X100 narrow gap pipe 5G procedure tests – tests conducted (WERC)

Weld N°	Consumable	Nominal Wire Chemistry	Bevel Angle & Width at Cap (mm)	X100 Pipe OD x WT	Gas Type	Electrode dia. (mm)	Pulsed / Dip	Heat Input (kJ/mm)	Single / Dual / Tandem	Backing System/ Root Run Location	Comments
ML-A-3	Spoolarc 120	2.5Ni0.5Mo0.4Cr	5°(6.7-7.0)	Pipe A 30" - 19mm	82.5%Ar/12.5% CO_2/5%He	0.9	Pulsed	0.45-0.68	Single	Internal Copper/ external root	Lincoln Powerwave 455 custom waveform
ML-A-4	Carbofil HT	0.5Ni0.5Mo0.5Cr	5°(6.35-6.8)	Pipe A 30" - 19mm	82.5%Ar/12.5% CO_2/5%He	1.0	Pulsed	0.40-0.49	Single	Internal Copper/ external root	Lincoln Powerwave 455 custom waveform
ML-A-5	Carbofil HT	0.5Ni0.5Mo0.5Cr	5°(6.25-6.90)	Pipe A 30" - 19mm	82.5%Ar/12.5% CO_2/5%He	1.0	Pulsed	0.45-0.57	Single	Internal Copper/ external root	Lincoln Powerwave 455 custom waveform
ML-B-7	Carbofil HT (K-Nova Root)	0.5Ni0.5Mo0.5Cr	5°(6.53-6.90)	Pipe B19 36" - 19mm	82.5%Ar/12.5% CO_2/5%He 78%Ar/20%CO2/2%O_2 (Root)	1.0	Pulsed	0.30-0.59	Single	Internal Root/ external fill and cap	Lincoln Powerwave 455 custom waveform
ML-B-8 (For Repair Procedures)	Carbofil HT (K-Nova Root)	0.5Ni0.5Mo0.5Cr	5°(6.42-6.85)	Pipe B19 36" - 19mm	82.5%Ar/12.5% CO_2/5%He 78%Ar/20%CO2/2%O_2 (Root)	1.0	Pulsed	0.30-0.59	Single	Internal Root/ external fill and cap	Lincoln Powerwave 455 custom waveform
ML-B-10	Spoolarc 120 (K-Nova Root)	2.5Ni0.5Mo0.4Cr	5°(6.12-6.73)	Pipe B19 36" - 19mm	82.5%Ar/12.5% CO_2/5%He 78%Ar/20%CO2/2%O_2 (Root)	0.9	Pulsed	0.30-0.69	Single	Internal Root/ external fill and cap	Lincoln Powerwave 455 custom waveform
ML-B15-1	Spoolarc 120 (K-Nova Root)	2.5Ni0.5Mo0.4Cr	5°(6.09-6.40)	Pipe B15 36" – 14.9mm	82.5%Ar/12.5% CO_2/5%He 78%Ar/20%CO2/2%O_2 (Root)	0.9	Pulsed	0.30-0.60	Single	Internal Root/ external fill and cap	Lincoln Powerwave 455 custom waveform
ML-B15-3	Carbofil NiMo-1 (K-Nova Root)	1Ni0.3Mo	5°(5.74-6.12)	Pipe B15 36" – 14.9mm	82.5%Ar/12.5% CO_2/5%He 78%Ar/20%CO2/2%O_2 (Root)	1.0	Pulsed	0.3-0.53	Single	Internal Root/ external fill and cap	Lincoln Powerwave 455 custom waveform
ML-B-12	Carbofil NiMo-1 (K-Nova Root)	1Ni0.3Mo	5°(6.07-6.44)	Pipe B19 36" - 19mm	82.5%Ar/12.5% CO_2/5%He 78%Ar/20%CO2/2%O_2 (Root)	1.0	Pulsed	0.30 - 0.46	Tandem	Internal Root/ external fill and cap	Fronius Time Twin custom waveform
ML-B15-16	Carbofil NiMo-1 (K-Nova Root)	1Ni0.3Mo	5°(6.80-7.06)	Pipe B15 36" – 14.9mm	82.5%Ar/12.5% CO_2/5%He 78%Ar/20%CO2/2%O_2 (Root)	1.0	Pulsed	0.33-0.50	Tandem	Internal Root/ external fill and cap	Fronius Time Twin custom waveform
ML-B15-17	Union MoNi (K-Nova Root)	1Ni0.4Mo	5°(6.73-6.94)	Pipe B15 36" – 14.9mm	82.5%Ar/12.5% CO_2/5%He 78%Ar/20%CO2/2%O_2 (Root)	1.0	Pulsed	0.35 - 0.53	Tandem	Internal Root/ external fill and cap	Fronius Time Twin custom waveform
ML-B15-18	Union MoNi (K-Nova Root)	1Ni0.4Mo	5°(6.71-7.03)	Pipe B15 36" – 14.9mm	82.5%Ar/12.5% CO_2/5%He 78%Ar/20%CO2/2%O_2 (Root)	1.0	Pulsed	0.32 - 0.50	Tandem	Internal Root/ external fill and cap	Digital Fronius Time Twin custom waveform

Table 5-16: X100 tie-in and repair welds pipe 5G procedure tests – tests conducted (WERC)

Weld N°	Consumable	Nominal Wire Chemistry	Bevel Angle & Width at Cap (mm)	X100 Pipe OD x WT	Gas Type	Electrode dia. (mm)	Pulsed / Dip	Heat Input (kJ/mm)	Single / Dual / Tandem	Backing System/ Root Run Location	Comments
ML-B-8R BW SMAW Single Pass Backweld	Filarc 118	2.0Ni0.4Mo	2-3mm depth 3-5mm cap width	Pipe B19 36" - 19mm	N/A	2.5	Globular	0.76-0.83			Repair Position 0° Overhead
ML-B-8R BW GMAW Single Pass Backweld	Carbofil HT	0.5Ni0.5Mo0.5Cr	3-4mm depth 4-5mm cap width	Pipe B19 36" - 19mm	78%Ar/20%CO_2/ 2%O_2	1.0	Dip	0.55-0.58	Single		Repair Position 0° Overhead
ML-B-8R MPBW SMAW 2 Pass Backweld	Filarc 118	2.0Ni0.4Mo	4-5mm depth 7-8mm cap width	Pipe B19 36" - 19mm	N/A	2.5/3.2	Globular	0.91-1.47			Repair Position 0° Overhead
ML-B-8R MPBW GMAW 2 Pass Backweld	Carbofil HT	0.5Ni0.5Mo0.5Cr	4-5mm depth 8-10mm cap width	Pipe B19 36" - 19mm	78%Ar/20%CO_2/ 2%O_2	1.0	Dip	0.46-0.72	Single		Repair Position 0° Overhead
ML-B-8R CR SMAW Single Pass Cap Repair	Filarc 118	2.0Ni0.4Mo	3-4mm depth 4-5mm cap width	Pipe B19 36" - 19mm	N/A	2.5	Globular	0.82-0.87			Repair Position 90° Vertical Up
ML-B-8R CR FCAW Single Pass Cap Repair	OK 15.09	2.7Ni0.3Mo	5-7mm depth 8-10mm cap width	Pipe B19 36" - 19mm	78%Ar/20%CO_2/ 2%O_2	1.2	Spray	1.56-1.62	Single		Repair Position 90° Vertical Up
ML-B-8R PP Part Penetration Repair	OK 15.09	2.7Ni0.3Mo	25-30° bevel 1/2 pipe WT	Pipe B19 36" - 19mm	78%Ar/20%CO_2/ 2%O_2	1.2	Spray	0.97-1.61	Single		Repair Position 90° Vertical Up
ML-B-8R FP Full Penetration Repair	Filarc 118 OK 15.09	2.0Ni0.4Mo 2.7Ni0.3Mo	25-30° bevel full pipe WT	Pipe B19 36" - 19mm	N/A 78%Ar/20%CO_2/ 2%O_2	2.5/3.2 1.2	Globular Spray	1.32-2.16 1.11-1.89	Single		Repair Position 180° to 120° Vertical Up
ML-B-9 Tie-In	Filarc 118 (Root+HP) OK 15.09(Fill+Cap)	2.0Ni0.4Mo 2.7Ni0.3Mo	30°(21.8-22.3) Root Gap 1.8-2.2	Pipe B19 36" - 19mm	78%Ar/20%CO_2/ 2%O_2	2.5/3.2 1.2	Globular Spray	1.03-1.92 0.82-1.82	Single	All welding external	ESAB Aristo 2000 LUD 450W
Tie-In Strength Development Trials											
OT1	Tenacito 80 (R+HP) Citoflux 110(F+C)	2.2Ni0.5Mo0.4Cr 2Ni	25°	RQT701 Plate 25mm	80Ar/ 20CO_2	2.5/3.2 1.2mm	Globular Spray	1.52-2.10 1.04-1.31	Single	3G Up, 100°C PH 120°C max IP	Semi-automatic Oerlikon Citoarc M408
OT2	Tenacito 80 (R+HP) Citoflux 110(F+C)	2.2Ni0.5Mo0.4Cr 2Ni	25°	RQT701 Plate 25mm	80Ar/ 20CO_2	2.5/3.2 1.2mm	Globular Spray	1.52-2.10 0.89-1.44	Single	4G, 100°C PH 118°C max IP	Semi-automatic Oerlikon Citoarc M408
OT3	Fluxofil M10S(R) Citoflux110(HP+F+C	0.06C1.6Mn0.5Si 2Ni	15°	X100 Plate 19.05mm	80Ar/ 20CO_2 80Ar/ 20CO_2	1.2mm 1.2mm	Spray Spray	1.01 1.02-1.35	Single	3G Up, 100°C PH 118°C max IP	Semi-automatic Oerlikon Citoarc M408
OT4A	Tenacito 80 (R+HP) Citoflux 110(F+C)	2.2Ni0.5Mo0.4Cr 2Ni	22.5°	X100 Plate 19.05mm	80Ar/ 20CO_2	2.5/3.2 1.2mm	Globular Spray	1.52-2.10 1.04-1.32	Single	3G Up, 100°C PH 118°C max IP	Semi-automatic Oerlikon Citoarc M408
OT4B	Tenacito 80 (R) Citoflux110(HP+F+C	2.2Ni0.5Mo0.4Cr 2Ni	22.5°	X100 Plate 19.05mm	80Ar/ 20CO_2	2.5/3.2 1.2mm	Globular Spray	1.52-1.74 1.04-1.32	Single	3G Up, 100°C PH 118°C max IP	Semi-automatic Oerlikon Citoarc M408
TIC110	Fluxofil M10S(R) Citoflux110(HP+F+C	0.06C1.6Mn0.5Si 2Ni	15°	Pipe B15 36" –14.9mm	78Ar/ 20CO_2/2O_2 78Ar/ 20CO_2/2O_2	1.2mm 1.2mm	Spray Spray	1.0-1.3 1.02-1.45	Single	5G Up, 100°C PH 120°C max IP	Semi-automatic ESAB Aristo 2000
TI1509	Fluxofil M10S(R) OK 15.09(HP+F+C)	0.06C1.6Mn0.5Si 2.7Ni0.3Mo	15°	Pipe B15 36" –14.9mm	78Ar/ 20CO_2/2O_2 78Ar/ 20CO_2/2O_2	1.2mm 1.2mm	Spray Spray	1.0-1.3 1.08-1.43	Single	5G Up, 100°C PH 120°C max IP	Semi-automatic ESAB Aristo 2000
1509MNG1	Fluxofil M10S(R) OK 15.09(HP+F+C)	0.06C1.6Mn0.5Si 2.7Ni0.3Mo	15°	Pipe B15 36" –14.9mm	78Ar/ 20CO_2/2O_2 78Ar/ 20CO_2/2O_2	1.2mm 1.2mm	Spray Spray	0.55 1.05-1.16	Single	5G Up, 20°PH 40°C max IP	Mechanised ESAB Aristo 2000
1509MNG2	Fluxofil M10S(R) OK 15.09(HP+F+C)	0.06C1.6Mn0.5Si 2.7Ni0.3Mo	15°	Pipe B15 36" –14.9mm	78Ar/ 20CO_2/2O_2 78Ar/ 20CO_2/2O_2	1.2mm 1.2mm	Spray Spray	0.33 1.10-1.14	Single	5G Up, 20°PH 40°C max IP	Mechanised ESAB Aristo 2000

Table 5-17: X100 pipe 5G procedure tests – dual torch tensile and hardness results

		All Weld Metal Strip Tensile (90°Position)					Hardness Surveys (2mm sub Root)							Hardness Surveys (2mm sub Cap)					
Weld N°	X100 Pipe OD x WT	$R_{p0.2}$ (MPa)	$R_{t0.5}$ (MPa)	R_m (MPa)	0.2Proof/ Tensile Ratio	A (%)	Hardness Traverse Location	Weld Metal Average HV10	Weld Metal Max HV10	HAZ Average HV10	HAZ Max HV10	Base Material Average HV10	Base Material Max HV10	Weld Metal Average HV10	Weld Metal Max HV10	HAZ Average HV10	HAZ Max HV10	Base Material Average HV10	Base Material Max HV10
7544 Bohler X70-IG (Supramig Root)	Pipe A 30" - 19mm	841	840	887	0.95	16.8	3 o'clock	286	292	274	287	288	294	298	299	261	270	285	289
							Seam	267	272	292	306	279	283	318	322	307	325	255	262
7549 Bohler X70-IG (Supramig Root)	Pipe B19 36" - 19mm	847	845	878	0.96	18.5	3 o'clock	269	279	256	260	286	297	304	312	287	317	286	294
							Seam	268	279	299	312	283	285	290	297	347	363	281	287
7624 Bohler X70-IG (Supramig Root)	Pipe C 36" - 16mm	884	883	929	0.95	16.0	3 o'clock	268	274	263	270	285	299	319	322	264	274	290	292
							Seam	305	314	294	302	296	299	316	319	312	330	258	262
7632 Thyssen MoNi (Supramig Root)	Pipe A 30" - 19mm	835	836	881	0.95	19	3 o'clock	273	285	264	274	286	294	318	319	269	274	294	300
							Seam	284	292	301	306	288	290	311	311	295	309	261	262
7546 Thyssen MoNi (Supramig Root)	Pipe B19 36" - 19mm	856	862	898	0.95	17.7	3 o'clock	264	270	253	262	282	289	303	304	255	262	303	336
							Seam	276	283	294	297	282	285	291	292	333	342	276	279
7548 Thyssen MoNi (Supramig Root)	Pipe C 36" - 16mm	817	816	862	0.95	17.2	3 o'clock	299	304	270	281	293	299	306	315	275	281	301	306
							Seam	274	279	254	270	281	287	289	297	261	270	236	238
8868 Elga Elgamatic 135 (Supramig Root)	Pipe B15 36" - 14.9mm	793		840	0.94	17	3 o'clock	256	260	257	268	310	314	299	302	263	270	298	309
							Seam	262	270	298	301	311	314	297	299	337	339	293	297
8876 Thyssen MoNi (Supramig Root)	Pipe B15 36" - 14.9mm	836		874	0.96	19	3 o'clock	247	255	257	268	319	348	303	304	269	283	293	302
							Seam	280	281	286	291	300	304	282	285	335	336	297	299
9692B Elga Elgamatic 135 (Supramig Root)	Pipe B15 36" - 14.9mm	800	717	870	0.92	16.5	3 o'clock	266	268	260	272	288	291	333	342	281	306	289	304
							Seam	276	285	318	336	305	309	319	319	356	360	293	297
9692T Thyssen Union X85 (Supramig Root)	Pipe B15 36" - 14.9mm	860	823	949	0.91	12.5	3 o'clock	254	256	261	274	298	306	344	373	275	299	303	311
							Seam	314	325	305	325	288	293	367	394	347	360	287	292
9726B Elga Elgamatic 135 (Supramig Root)	Pipe B15 36" - 14.9mm	776	769	845	0.92	15.5	3 o'clock	281	292	260	264	295	302	305	314	258	266	286	287
							Seam	281	283	305	311	305	309	315	318	348	351	292	299
9726T Thyssen Union X85 (Supramig Root)	Pipe B15 36" - 14.9mm	825	800	904	0.91	18.5	3 o'clock	287	311	267	279	309	322	345	357	281	317	292	297
							Seam	302	306	310	314	293	294	345	357	360	363	287	290

NB For seam hardness traverses, base material = longitudinal seam weld metal

Table 5-18: X100 pipe 5G procedure tests – single and tandem torch tensile and hardness results

		All Weld Metal Strip Tensile (90°Position)					Hardness Surveys (2mm sub Root)							Hardness Surveys (2mm sub Cap)					
Weld N°	**X100 Pipe OD x WT**	**$R_{p0.2}$ (MPa)**	**$R_{t0.5}$ (MPa)**	**R_m (MPa)**	**0.2Yield/ Tensile Ratio**	**A (%)**	**Hardness Traverse Location**	**Weld Metal Average HV10**	**Weld Metal Max HV10**	**HAZ Average HV10**	**HAZ Max HV10**	**Base Material Average HV10**	**Base Material Max HV10**	**Weld Metal Average HV10**	**Weld Metal Max HV10**	**HAZ Average HV10**	**HAZ Max HV10**	**Base Material Average HV10**	**Base Material Max HV10**
Single Wire																			
7691 Thyssen MoNi	Pipe A	886	719	964	0.92	17.5	3 o'clock	281	287	266	279	279	290	342	345	261	279	275	281
(Supramig Root)	30" - 19mm						Seam	287	302	294	302	276	279	347	351	298	317	251	253
7625 Thyssen MoNi	Pipe B19	911	882	982	0.93	16	3 o'clock	281	294	260	290	297	317	319	325	263	271	291	294
(Supramig Root)	36" - 19mm						Seam	289	293	322	325	279	281	320	330	365	370	282	282
ML-A-3	Pipe A	971	927	1017	0.95	15.1	3 o'clock	304	312	269	272	277	281	337	339	269	274	280	285
Spoolarc 120	30" - 19mm						Seam	333	339	325	339	296	302	375	380	290	333	252	254
ML-A-4	Pipe A	853	834	900	0.95	9.9	3 o'clock	287	297	271	304	285	289	296	302	270	279	280	285
Carbofil HT	30" - 19mm						Seam	284	287	296	302	284	285	297	309	282	304	253	258
ML-A-5	Pipe A	807	809	865	0.93	19.5	3 o'clock	264	292	269	274	281	292	267	270	264	281	268	281
Carbofil HT	30" - 19mm						Seam	282	285	296	304	293	297	294	297	304	319	252	260
ML-B-7	Pipe B19	791	792	833	0.95	14.9	3 o'clock	268	274	267	287	295	304	303	309	261	274	272	276
Carbofil HT/ TS6 root	36" - 19mm						Seam	268	268	331	348	287	294	315	319	303	351	290	297
ML-B-10	Pipe B19	883	855	934	0.95	16.0	3 o'clock	271	272	276	302	318	345	349	351	306	332	299	311
Spoolarc 120/ TS6 Root	36" - 19mm						Seam	268	274	338	348	311	314	338	339	363	366	299	302
ML-B15-1	Pipe B15	844	854	951	0.89	16	3 o'clock	238	242	265	292	288	304	364	366	304	345	275	281
Spoolarc 120/ TS6 Root	36" – 14.9mm						Seam	232	245	314	327	292	294	370	370	347	383	289	297
ML-B15-3	Pipe B15	841	838	888	0.95	20.5	3 o'clock	216	222	257	285	297	314	302	306	268	285	280	285
Carbofil NiMo-1/ TS6Root	36" – 14.9mm						Seam	251	258	306	322	282	287	300	306	322	347	286	287
Tandem Wire																			
ML-B-12	Pipe B19	967	962	1004	0.96	14.5	3 o'clock	256	260	270	294	291	294	336	342	280	319	284	290
Carbofil NiMo-1/ TS6Root	36" - 19mm						Seam	362	363	313	376	271	297	320	336	327	373	267	292
ML-B15-16	Pipe B15	902	901	943	0.96	11.5	3 o'clock	240	245	270	294	291	294	319	322	273	319	282	290
Carbofil NiMo-1/ TS6Root	36" – 14.9mm						Seam	259	266	325	345	291	294	323	325	358	360	283	292
ML-B15-17	Pipe B15	942	800	977	0.96	12.5	3 o'clock	255	264	274	292	285	287	376	380	299	322	284	297
Thyssen MoNi/ TS6 Root	36" – 14.9mm						Seam	274	276	326	348	291	294	375	380	333	383	283	285
ML-B15-18	Pipe B15	876	793	926	0.95	18.5	3 o'clock	311	314	270	297	310	322	355	360	283	297	293	309
Thyssen MoNi/ TS6 Root	36" – 14.9mm						Seam	305	309	320	339	285	287	361	366	308	342	275	276

NB For seam hardness traverses, base material = longitudinal seam weld metal

Table 5-19: X100 Pipe 5G Procedure Tests – Tie-In and Repair Tensile and Hardness Results

		All Weld Metal Strip Tensile (90°Position)					Hardness Surveys (2mm sub Root)							Hardness Surveys (2mm sub Cap)					
Weld N°	**X100 Pipe OD x WT**	**$R_{p0.2}$ (MPa)**	**$R_{t0.5}$ (MPa)**	**R_m (MPa)**	**0.2Yield/ Tensile Ratio**	**A (%)**	**Hardness Traverse Location**	**Weld Metal Average HV10**	**Weld Metal Max HV10**	**HAZ Average HV10**	**HAZ Max HV10**	**Base Material Average HV10**	**Base Material Max HV10**	**Weld Metal Average HV10**	**Weld Metal Max HV10**	**HAZ Average HV10**	**HAZ Max HV10**	**Base Material Average HV10**	**Base Material Max HV10**
ML-B-8R BW SMAW Single Pass Backweld	Pipe B19 36" - 19mm						12 o'clck	305	306	262	317	273	279						
ML-B-8R BW GMAW Single Pass Backweld	Pipe B19 36" - 19mm						12 o'clck	273	283	259	294	288	297						
ML-B-8R MPBW SMAW 2 Pass Backweld	Pipe B19 36" - 19mm						12 o'clck							305	317	255	272	278	294
ML-B-8R MPBW GMAW 2 Pass Backweld	Pipe B19 36" - 19mm						12 o'clck							274	276	271	292	298	312
ML-B-8R CR SMAW Single Pass Cap Repair	Pipe B19 36" - 19mm						3 o'clock							378	387	290	330	279	289
ML-B-8R CR FCAW Single Pass Cap Repair	Pipe B19 36" - 19mm						3 o'clock							293	302	253	272	273	283
ML-B-8R PP Part Penetration Repair	Pipe B19 36" - 19mm						3 o'clock	259	260	245	292	257	270	311	319	252	266	281	287
ML-B-8R FP Full Penetration Repair	Pipe B19 36" - 19mm	724	725	816	0.89	19.1	5 o'clock	231	238	245	306	264	283	317	339	255	274	264	276
ML-B-9 (Tie-In)	Strip tensile	737	733	800	0.92	18.2	3 o'clock	233	235	228	243	276	304	281	304	259	272	271	283
Filarc 118 Root/HP, OK 15.09 Fill/ Cap	Round bar36" x 19mm	746	731	831	0.90	16.0	Seam	238	249	295	304	275	279	266	285	291	302	276	279

NB For seam hardness traverses, base material = longitudinal seam weld metal

Table 5-20: X100 Pipe 5G Procedure Tests – Dual Torch Cross Weld Tensile/ Nick Breaks and Side Bend Results

		Cross Weld Tensiles (API 1104)								Nick Break (API 1104)				Side Bend (API 1104)			
Weld N°	X100 Pipe OD x WT	R_m (MPa) 45°	Fracture Location	R_m (MPa) 135°	Fracture Location	R_m (MPa) 225°	Fracture Location	R_m (MPa) 315°	Fracture Location	45°	135°	225°	315°	45°	135°	225°	315°
7544 Bohler X70-IG (Supramig Root)	30" x 19mm (Pipe A)	798	PM	777	PM	783	PM	778	PM	Acceptable	Acceptable	Acceptable	Acceptable	Acceptable	Acceptable	Acceptable	Acceptable
7549 Bohler X70-IG (Supramig Root)	36" x 19mm (Pipe B19)	796	WM	791	WM	798	PM	801	WM	Acceptable	Acceptable	Acceptable	Acceptable	Acceptable	Acceptable	Acceptable	Acceptable
7624 Bohler X70-IG (Supramig Root)	36" x 16mm (Pipe C)	786	PM	773	PM	783	PM	783	PM	Acceptable	Acceptable	Acceptable	Acceptable	Acceptable	Acceptable	Acceptable	Acceptable
7632 Thyssen MoNi (Supramig Root)	30" x 19mm (Pipe A)	797	PM	791	PM	797	PM	805	PM	Acceptable	Acceptable	Acceptable	Acceptable	Acceptable	Acceptable	Acceptable	Acceptable
7546 Thyssen MoNi (Supramig Root)	36" x 19mm (Pipe B19)	809	PM	772	PM	805	PM	782	PM	Acceptable	Acceptable	Acceptable	Acceptable	Acceptable	Acceptable	Acceptable	Acceptable
7548 Thyssen MoNi (Supramig Root)	36" x 16mm (Pipe C)	780	WM	765	PM	770	WM	783	WM	Acceptable	Acceptable	Acceptable	Acceptable	Acceptable	Acceptable	Acceptable	Acceptable
8868 Elga Elgamatic 135 (Supramig Root)	36" x 14.9mm (Pipe B15)	848	HAZ	NB Only enough material for a single test of each type						Acceptable				Acceptable			
8876 Thyssen MoNi (Supramig Root)	36" x 14.9mm (Pipe B15)	785	PM	842	HAZ	835	HAZ	818	HAZ	Acceptable	Acceptable	Acceptable	Acceptable	Acceptable	Acceptable	Acceptable	Acceptable
9692B Elga Elgamatic 135 (Supramig Root)	36" x 14.9mm (Pipe B15)	814	PM	835	PM		No Material Available		No Material Available	Acceptable	Acceptable	No Material Available	No Material Available	Unacceptable - fractured at 90°; defect at weld centreline	Acceptable	No Material Available	No Material Available
9692T Thyssen Union X85 (Supramig Root)	36" x 14.9mm (Pipe B15)	834	PM	852	PM		No Material Available		No Material Available	Acceptable	Acceptable	No Material Available	No Material Available	Acceptable	Acceptable	No Material Available	No Material Available
9726B Elga Elgamatic 135 (Supramig Root)	36" x 14.9mm (Pipe B15)	831	PM	845 Root defect noted at toe	WM		No Material Available		No Material Available	Acceptable	Acceptable	No Material Available	No Material Available	Acceptable	Acceptable	No Material Available	No Material Available
9726T Thyssen Union X85 (Supramig Root)	36" x 14.9mm (Pipe B15)	851	PM	835	PM		No Material Available		No Material Available	Acceptable	Acceptable	No Material Available	No Material Available	Acceptable	Acceptable	No Material Available	No Material Available

Table 5-21: X100 Pipe 5G Procedure Tests – Single Wire Cross Weld Tensile/ Nick Breaks and Side Bend Results

Weld N°	X100 Pipe OD x WT	Cross Weld Tensiles (API 1104)								Nick Break (API 1104)				Side Bend (API 1104)			
		R_m (MPa) 45°	Fracture Location	R_m (MPa) 135°	Fracture Location	R_m (MPa) 225°	Fracture Location	R_m (MPa) 315°	Fracture Location	45°	135°	225°	315°	45°	135°	225°	315°
Single Wire Welds																	
7691 Thyssen MoNi (Supramig Root)	30" x 19mm (Pipe A)	711	PM	796	PM	797	PM	788	PM	Acceptable	Acceptable	Acceptable	Acceptable	Acceptable	Acceptable	Acceptable Minor surface tear 1.5mm	Acceptable Minor surface tear 1.5mm
7625 Thyssen MoNi (Supramig Root)	36" x 19mm (Pipe B19)	815	PM	814	PM	809	PM	811	PM	Acceptable	Acceptable	Acceptable	Acceptable	Acceptable	Acceptable	Acceptable	Acceptable
ML-A-5 Carbofil HT	30" x 19mm (Pipe A)	783	WM	803	PM	803	WM	803	PM	Unacceptable 2 elongated gas pores 18mm long	Acceptable	Unacceptable elongated gas pore 10mm long	Unacceptable 3.5mm dia. Inclusion	Unacceptable fracture of bend at 90°	Acceptable	Unacceptable 4mm tear emanating from root	Acceptable
ML-B-7 Carbofil HT/ TS6 root	36" x 19mm (Pipe B19)	806	WM	801	PM	805	PM	812	PM	Unacceptable 12mm long gas void	Acceptable	Acceptable	Acceptable	Acceptable	Unacceptable 8.5mm tear emanating from root	Acceptable	Acceptable
ML-B15-1 Spoolarc 120/ TS6 root	36" x 14.9mm (Pipe B15)	840	PM	865	PM	849	PM	852	PM	Acceptable	Acceptable	Acceptable	Acceptable	Acceptable	Acceptable	Acceptable	Acceptable
ML-B15-3 Carbofil NiMo-1/ TS6 root	36" x 14.9mm (Pipe B15)	839	PM NB repeat	849	WM	856	HAZ	844	HAZ	Acceptable	Acceptable	Acceptable	Acceptable	Acceptable	Acceptable NB Repeat	Acceptable	Acceptable

Table 5-22: X100 Pipe 5G Procedure Tests – Tandem Wire Cross Weld Tensile/ Nick Breaks and Side Bend Results

		Cross Weld Tensiles (API 1104)								Nick Break (API 1104)				Side Bend (API 1104)			
Weld N°	X100 Pipe OD x WT	R_m (MPa) 45°	Fracture Location	R_m (MPa) 135°	Fracture Location	R_m (MPa) 225°	Fracture Location	R_m (MPa) 315°	Fracture Location	45°	135°	225°	315°	45°	135°	225°	315°
Tandem Wire Welds																	
ML-B-12 Carbofil NiMo-1/ TS6Root	36" x 19mm (Pipe B19)	830	PM	811	PM	801	PM	805	PM	Acceptable	Acceptable	Acceptable	Acceptable	Acceptable	Acceptable	Acceptable	Unaccept. Fractured at <180°
ML-B15-16 Carbofil NiMo-1/ TS6Root	36" x 14.9mm (Pipe B15)	765	WM Lack of inter-run fusion defects noted	817	PM	822	PM NB repeat	847	HAZ	Unacceptable Lack of inter-run fusion defects noted	Acceptable	Acceptable NB Repeat test	Acceptable	Unacceptable Fracture of specimen - lack of inter-run fusion defects noted	Acceptable	Acceptable NB repeat test	Acceptable
ML-B15-17 Thyssen MoNi/ TS6 Root	36" x 14.9mm	831	WM Lack of inter-run fusion defects noted	823	PM	907	PM	822	WM Lack of inter-run fusion defects noted	Unacceptable Lack of inter-run fusion defects noted	Acceptable	Acceptable	Unacceptable Lack of inter-run fusion defects noted (1.5mm gas void)	Unacceptable Fracture of specimen - lack of inter-run fusion defects noted	Acceptable	Acceptable	Unaccept. Fracture of specimen - lack of inter-run fusion defects noted
ML-B15-18 Thyssen MoNi/ TS6 Root	36" x 14.9mm	842	PM	847	PM	829	PM	844	PM	Unacceptable Lack of inter-run fusion defects noted	Unacceptable Lack of inter-run fusion defects noted	Acceptable	Acceptable	Unacceptable tearing of specimen - lack of inter-run fusion defects noted	Unacceptable tearing of specimen - lack of inter-run fusion defects noted	Acceptable	Unacceptable tearing of specimen - lack of inter-run fusion defects noted

Table 5-23: X100 Pipe 5G Procedure Tests – Tie-In and Repair Cross Weld Tensile/ Nick Breaks and Side Bend Results

		Cross Weld Tensiles (API 1104)								Nick Break (API 1104)				Side Bend (API 1104)			
Weld N°	X100 Pipe OD x WT	R_m (MPa) 45°	Fracture Location	R_m (MPa) 135°	Fracture Location	R_m (MPa) 225°	Fracture Location	R_m (MPa) 315°	Fracture Location	45°	135°	225°	315°	45°	135°	225°	315°
Tie-In and Repair Welds																	
ML-B-8R PP Part Penetration Repair 15.09	36"x19mm (Pipe B19)													Single Test (90°) Unacceptable fracture along fusion boundary; lack of fusion defect noted at root position			
ML-B-8R FP Full Penetration Repair 15.09	36"x19mm (Pipe B19)	792 (165°)	PM								Acceptable (170°)			Single Test (160°) Unacceptable fracture along fusion boundary			
ML-B-9 Tie-In; Filarc 118/ OK 15.09	36"x19mm (Pipe B19)	770	PM	772	PM	782	PM	772	PM	Acceptable	Acceptable	Acceptable	Acceptable	Acceptable	Acceptable	Acceptable	Acceptable

Table 5-24: X100 Pipe 5G Procedure Tests – Dual Torch Toughness Results

Weld N°	X100 Pipe OD x WT	Impact Toughness (EN 288-9:1999)																						CTOD					
		Cv -20°C (J) Weld Metal Root			Cv -20°C (J) Fusion Line Root			Cv -40°C (J) Weld Metal Root			Cv -40°C (J) Fusion Line Root			Cv -60°C (J) Weld Metal Root			Cv -60°C (J) Fusion Line Root			Cv -80°C (J) Weld Metal Root			Cv -80°C (J) Fusion Line Root			CTOD -10°C Weld Metal (mm)			CTOD -10°C HAZ (mm)		
7544 Bohler X70-IG (Supramig Root)	30"x19mm (Pipe A)	174	170	168	218	232	78	177	144	104	220	228	104	152	168	106	18	80	56	106	108	96	34	100	26	0.20	0.18	0.16	0.37	0.40	0.28
			Av.			Av.			Av.			Av.			Av.			Av.			Av.			Av.		Valid	Valid	Valid	Valid	Valid	Valid
			171			**176**			**142**			**184**			**142**			**51**			**103**			**53**		M	M	M	M	M	U
7549 Bohler X70-IG (Supramig Root)	36"x19mm (Pipe B19)	190	148	190	232	228	222	178	188	146	106	228	222	172	168	178	80	240	62	108	88	188	28	36	22	0.22	0.33	0.30	0.16	0.17	0.34
			Av.			Av.			Av.			Av.			Av.			Av.			Av.			Av.		Valid	Valid	Valid	Valid	Valid	Valid
			176			**227**			**171**			**185**			**173**			**127**			**128**			**29**		M	M	M	U	U	M
7624 Bohler X70-IG (Supramig Root)	36"x16mm (Pipe C)	156	224	190	94	40	44	120	82	60	54	40	18	62	72	46	48	22	34	40	44	30	22	12	10	0.14	0.17	0.21	0.023	0.10	0.050
			Av.			Av.			Av.			Av.			Av.			Av.			Av.			Av.		Valid	Valid	Valid	Valid	Valid	Valid
			190			**59**			**87**			**37**			**60**			**35**			**38**			**15**		M	M	M	C	C	C
7632 Thyssen MoNi (Supramig Root)	30"x19mm (Pipe A)	188	158	158	208	190	244	236	122	146	228	180	172	162	208	220	68	64	152	166	206	102	40	72	42	0.26	0.15	0.31	0.11	0.38	0.20
			Av.			Av.			Av.			Av.			Av.			Av.			Av.			Av.		Valid	Valid	Valid	Valid	Valid	Valid
			168			**214**			**168**			**193**			**197**			**95**			**158**			**51**		M	M	M	C	M	M
7546 Thyssen MoNi (Supramig Root)	36"x19mm (Pipe B19)	114	186	172	216	230	230	130	172	188	84	72	224	126	150	130	66	232	68	148	160	88	30	36	42	0.17	0.26	0.19	0.42	0.22	0.24
			Av.			Av.			Av.			Av.			Av.			Av.			Av.			Av.		Valid	Invalid	Valid	Valid	Valid	Valid
			157			**225**			**163**			**127**			**135**			**122**			**132**			**36**		M	10.2.2c M	M	U	U	M
7548 Thyssen MoNi (Supramig Root)	36"x16mm (Pipe C)	180	190	184	94	120	72	170	202	200	22	32	32	176	124	106	30	34	48	220	132	130	20	20	26	0.36	0.28	0.37	0.38	0.37	0.11
			Av.			Av.			Av.			Av.			Av.			Av.			Av.			Av.		Valid	Valid	Valid	Valid	Valid	Valid
			185			**95**			**191**			**29**			**135**			**37**			**161**			**22**		M	M	M	U	U	U
8868 Elga Elgamatic 135 (Supramig Root)	36"x 14.9mm (Pipe B15)	150	140	148	166	220	206	148	128	142	232	118	80	92	110	126	84	84	118	60	72	64	104	38	108	0.20	0.20	0.16	0.41	0.34	0.44
			Av.			Av.			Av.			Av.			Av.			Av.			Av.			Av.		Valid	Valid	Valid	Valid	Valid	Valid
			146			**197**			**139**			**143**			**109**			**95**			**65**			**83**		M	M	M	M	M	M
8876 Thyssen MoNi (Supramig Root)	36"x 14.9mm (Pipe B15)	172	186	194	132	106	198	186	162	184	128	160	224	154	142	138	56	132	34	58	78	72	62	56	64	0.17	0.20	0.19	0.41	0.36	0.32
			Av.			Av.			Av.			Av.			Av.			Av.			Av.			Av.		Valid	Valid	Valid	Valid	Valid	Valid
			184			**145**			**177**			**171**			**145**			**74**			**69**			**61**		M	M	M	M	M	M
9692B Elga Elgamatic 135 (Supramig Root)	36"x 14.9mm (Pipe B15)	Material not available			Material not available			138	152	110	48	36	42	116	90	86	18	24	26	60	56	54	24	20	16						
									Av.			Av.			Av.			Av.			Av.			Av.		Not Tested			Not Tested		
									133			**42**			**97**			**23**			**57**			**20**							
9692T Thyssen Union X85 (Supramig Root)	36"x 14.9mm (Pipe B15)	Material not available			Material not available			168	200	170	38	50	46	136	152	112	26	38	22	200	84	112	32	40	46	0.24	0.15	0.15	0.19	0.27	0.34
									Av.			Av.			Av.			Av.			Av.			Av.		Valid	Valid	Valid	Valid	Valid	Valid
									179			**45**			**133**			**29**			**132**			**39**		M	M	M	M	U	M
9726B Elga Elgamatic 135 (Supramig Root)	36"x 14.9mm (Pipe B15)	Material not available			Material not available			80	82	82	38	86	48	66	70	68	54	40	34	58	40	38	32	46	24				0.19mm sample above		
									Av.			Av.			Av.			Av.			Av.			Av.		Not Tested			yielded prior to test		
									81			**57**			**68**			**43**			**45**			**34**					giving low result		
9726T Thyssen Union X85 (Supramig Root)	36"x 14.9mm (Pipe B15)	Material not available			Material not available			146	100	206	84	230	236	134	126	84	38	52	56	54	64	44	20	28	32						
									Av.			Av.			Av.			Av.			Av.			Av.		Not Tested			Not Tested		
									151			**183**			**115**			**49**			**54**			**27**							

Table 5-25: X100 Pipe 5G Procedure Tests – Single Wire Toughness Results

		Impact Toughness (EN 288-9:1999)																						CTOD					
Weld N°	**X100 Pipe OD x WT**	**Cv -20°C (J) Weld Metal Root**			**Cv -20°C (J) Fusion Line Root**			**Cv -40°C (J) Weld Metal Root**			**Cv -40°C (J) Fusion Line Root**			**Cv -60°C (J) Weld Metal Root**			**Cv -60°C (J) Fusion Line Root**			**Cv -80°C (J) Weld Metal Root**			**Cv -80°C (J) Fusion Line Root**			**CTOD -10°C Weld Metal (mm)**			**CTOD -10°C HAZ (mm)**		
7691 Thyssen MoNi (Supramig Root)	30"x19mm (Pipe A)	240	176	186	236	210	224	114	182	172	38	112	248	124	110	102	54	20	54	84	74	58	40	70	34	0.12	0.15	0.19	0.20	0.40	0.22
			Av.			Av.			Av.			Av.			Av.			Av.			Av.			Av.		Invalid	Valid	Valid	Valid	Valid	Valid
			201			**223**			**156**			**133**			**112**			**43**			**72**			**48**		M*	C	M	C	M	C
7625 Thyssen MoNi (Supramig Root)	36"x19mm (Pipe B19)	218	204	222	228	240	176	186	184	203	38	122	37	231	208	72	36	116	46	149	66	62	26	34	21	0.23	0.23	0.25	0.38	0.39	0.33
			Av.			Av.			Av.			Av.			Av.			Av.			Av.			Av.		Valid	Valid	Valid	Valid	Valid	Valid
			215			**215**			**191**			**66**			**170**			**66**			**92**			**27**		M	M	M	M	M	M
ML-A-3 Spoolarc 120	30"x19mm (Pipe A)							Mid T WM			Mid T FL			Mid T FL+2												0.096	0.16	0.12	0.18	0.095	0.21
								220	190	226	42	64	36	194	70	126										Valid	Valid	Valid	Valid	Valid	Valid
								Av.@ -40°C		**212**	Av.@ -40°C		**47**	Av.@ -40°C		**130**										C	M	C	M	C	M
ML-A-4 Carbofil HT	30"x19mm (Pipe A)							Mid T WM			Mid T FL			Mid T FL+2												0.16	0.082	0.23	0.22	0.14	0.14
								144	100	148	256	56	240	242	180	234										Valid	Valid	Valid	Valid	Valid	Valid
								Av.@ -40°C		**131**	Av.@ -40°C		**184**	Av.@ -40°C		**219**										M	C	U	U	M	U
ML-A-5 Carbofil HT	30"x19mm (Pipe A)	110	156	62	240	34	240	108	102	104	22	54	20	70	68	120	235	214	50	58	52	24	20	24	34	0.16	0.15	0.17	0.23	0.27	0.21
			Av.			Av.			Av.			Av.			Av.			Av.			Av.			Av.		Valid	Valid	Valid	Valid	Valid	Valid
			109			**171**			**105**			**32**			**86**			**166**			**45**			**26**		M	M	U	U	U	U
ML-B-7 Carbofil HT/ TS6 root	36"x19mm (Pipe B19)	90	80	110	242	182	56	52	58	56	130	128	148	62	66	46	170	88	70	35	42	40	28	58	26	0.13	0.15	0.23	0.40	0.30	0.45
			Av.			Av.			Av.			Av.			Av.			Av.			Av.			Av.		Valid	Valid	Valid	Valid	Valid	Valid
			93			**160**			**55**			**135**			**58**			**109**			**39**			**37**		M	M	M	U	U	U
ML-B-10 Spoolarc 120/ TS6 Root	36"x19mm (Pipe B19)							Mid T WM			Mid T FL			Mid T FL +2												0.20	0.26	0.31	0.43	0.36	0.34
								174	216	163	50	216	64	192	261	234										Valid	Valid	Valid	Valid	Valid	Valid
								Av.@ -40°C		**184**	Av.@ -40°C		**110**	Av.@ -40°C		**229**										M	M	M	M	M	M
ML-B15-1 Spoolarc 120/ TS6 Root	36"x14.9 (Pipe B15)	172	164	204	238	114	122	202	200	166	128	132	92	176	176	190	140	190	33	100	110	124	100	32	82	0.13	0.17	0.14	0.36	0.12	0.34
			Av.			Av.			Av.			Av.			Av.			Av.			Av.			Av.		Valid	Valid	Valid	Valid	Valid	Valid
			180			**158**			**189**			**117**			**181**			**121**			**111**			**71**		M	M	M	C	C	M
ML-B15-3 Carbofil NiMo-1/ TS6 Root	36"x14.9 (Pipe B15)	222	224	232	226	150	114	184	186	194	252	110	130	194	208	208	226	222	40	114	220	162	82	36	104	0.27	0.24	0.25	0.25	0.42	0.38
			Av.			Av.			Av.			Av.			Av.			Av.			Av.			Av.		Valid	Valid	Valid	Valid	Valid	Valid
			226			**163**			**188**			**164**			**203**			**163**			**165**			**74**		M	M	M	M	M	M

CTOD Classification C = critical CTOD at the onset of brittle crack extension or pop-in when Δa is less than 0.2mm
M = value of CTOD at the first attainment of a maximum force plateau for fully plastic behaviour
U = critical CTOD at the onset of brittle crack extension or pop-in when the event is preceded by Δa equal to or greater than 0.2mm

*CTOD Invalidity classified in accordance with BS 7448-1:1991 Section 10.2.2 (C) : before carrying out the fracture test the difference between the two surface crack length measurements was greater than 15% of the average of these two measurements; the procedure requires that the difference is less than this amount.

Table 5-26: X100 Pipe 5G Procedure Tests – Tandem Wire Toughness Results

Weld N°	X100 Pipe OD x WT	Impact Toughness (EN 288-9:1999)																						CTOD					
		Cv -20°C (J) Weld Metal Root			Cv -20°C (J) Fusion Line Root			Cv -40°C (J) Weld Metal Root			Cv -40°C (J) Fusion Line Root			Cv -60°C (J) Weld Metal Root			Cv -60°C (J) Fusion Line Root			Cv -80°C (J) Weld Metal Root			Cv -80°C (J) Fusion Line Root			CTOD -10°C Weld Metal (mm)			CTOD -10°C HAZ (mm)		
ML-B-12 Carbofil NiMo-1/ TS6 root	36"x19mm	90	80	110	242	182	56	52	58	56	130	128	148	62	66	46	170	88	70	35	42	40	28	58	26	0.13	0.15	0.23	0.40	0.30	0.45
			Av.			Av.			Av.			Av.			Av.			Av.			Av.			Av.		Valid	Valid	Valid	Valid	Valid	Valid
			93			**160**			**55**			**135**			**58**			**109**			**39**			**37**		M	M	M	U	U	U
ML-B15-16 Carbofil NiMo-1/ TS6 Root	36"x14.9 (Pipe B15)	176	188	204	260	244	212	200	188	184	230	232	70	164	172	184	96	100	84	70	88	124	42	42	38	0.23	0.18	0.24	0.36	0.42	0.34
			Av.			Av.			Av.			Av.			Av.			Av.			Av.			Av.		Valid	Valid	Valid	Valid	Valid	Valid
			189			**239**			**191**			**177**			**173**			**93**			**94**			**41**		M	M	M	M	M	M
ML-B15-17 Thyssen MoNi/ TS6 Root	36" x 14.9 (Pipe B15)	220	158	180	220	212	226	178	208	188	214	186	210	194	176	136	98	48	52	62	46	76	46	38	50						
			Av.			Av.			Av.			Av.			Av.			Av.			Av.			Av.		Not Tested			Not Tested		
			186			**219**			**191**			**203**			**169**			**66**			**61**			**45**							
ML-B15-18 Thyssen MoNi/ TS6 Root CTOD Classification	36"x14.9 (Pipe B15)																									0.15	0.14	0.15			
																										Valid	Valid	Valid			
																										M	M	M			

Table 5-27; X100 Pipe 5G Procedure Tests – Tie-In and Repair Toughness Results

Weld N°	X100 Pipe OD x WT	Impact Toughness (EN 288-9:1999)																						CTOD					
		Cv -20°C (J) Weld Metal Root			Cv -20°C (J) Fusion Line Root			Cv -40°C (J) Weld Metal Root			Cv -40°C (J) Fusion Line Root			Cv -60°C (J) Weld Metal Root			Cv -60°C (J) Fusion Line Root			Cv -80°C (J) Weld Metal Root			Cv -80°C (J) Fusion Line Root			CTOD -10°C Weld Metal (mm)			CTOD -10°C HAZ (mm)		
ML-B-8R PP Part Penetration Repair OK 15.09	36" x 19mm	Repair WM C/L			Orig./ Repair Weld FL			Repair Weld/Base FL																							
		74	74	74	76	66	68	114	118	94																					
		Av. @-20°C **74**			Av. @-20°C **70**			Av. @-20°C **109**																							
ML-B-8R FP Full Penetration Repair Filarc 118/ OK 15.09	36" x 19mm	82	80	78	98	136	168																								
			Av.			Av.																									
			80			**134**																									
ML-B-9 Tie-In Filarc 118/ OK 15.09	36" x 19mm	80	106	102	188	140	134	72	66	76	104	118	154	44	52	50	88	64	64	20	38	20	48	36	52	0.14	0.11	0.12	0.26	0.18	0.16
			Av.			Av.			Av.			Av.			Av.			Av.			Av.			Av.		Valid	Valid	Valid	Valid	Valid	Valid
			96			**154**			**71**			**125**			**49**			**72**			**26**			**45**		M	M	M	M	M	U

CTOD Classification C = critical CTOD at the onset of brittle crack extension or pop-in when Δa is less than 0.2mm
M = value of CTOD at the first attainment of a maximum force plateau for fully plastic behaviour
U = critical CTOD at the onset of brittle crack extension or pop-in when the event is preceded by Δa equal to or greater than 0.2mm

Table 5-28: X100 Pipe 5G Procedure Tests – Weld Metal Chemistry

		Weld Metal Chemical Composition (wt %)																		
Weld N°	**X100 Pipe OD x WT**	**C**	**Mn**	**P**	**S**	**Si**	**Cr**	**Ni**	**Mo**	**Cu**	**Al**	**V**	**Nb**	**Ti**	**B**	**O**	**N**	**CE_{IIW}**	**CET**	**P_{cm}**
Dual Torch Welds																				
7544 Bohler X70-IG	30" x 19mm	0.064	1.50	0.006	0.010	0.51	0.31	1.21	0.26	0.19	<0.005	0.090	0.008	0.04	<0.0005	0.0368	0.0102	0.539	0.295	0.230
7549 Bohler X70-IG	36" x 19mm	0.077	1.50	0.009	0.010	0.49	0.24	1.20	0.25	0.13	0.005	0.080	0.009	0.03	<0.0005	0.0382	0.0131	0.530	0.301	0.234
7624 Bohler X70-IG	36" x 16.3mm	0.071	1.53	0.006	0.011	0.56	0.26	1.16	0.24	0.10	<0.005	0.080	0.009	0.04	<0.0005	0.0408	0.0165	0.526	0.295	0.230
7632 Thyssen MoNi	30" x 19mm	0.083	1.39	0.007	0.008	0.56	0.10	1.00	0.40	0.17	<0.005	0.013	0.008	0.04	<0.0005	0.0297	0.0162	0.495	0.301	0.231
7546 Thyssen MoNi	36" x 19mm	0.080	1.46	0.006	0.006	0.50	0.04	0.94	0.39	0.19	0.009	0.006	0.013	0.04	<0.0005	0.0335	0.0085	0.486	0.300	0.225
7548 Thyssen MoNi	36" x 16.3mm	0.088	1.43	0.007	0.007	0.56	0.05	0.99	0.40	0.14	0.006	0.005	0.008	0.03	<0.0005	0.0360	0.0113	0.493	0.305	0.233
8868 Elga Elgamatic 135	36" x 14.9mm	0.062	1.49	0.010	0.010	0.51	0.30	1.28	0.22	0.20	<0.005	0.070	<0.005	0.005	<0.0005	0.0450	0.0086	0.527	0.290	0.224
8876 Thyssen MoNi	36" x 14.9mm	0.093	1.39	0.007	0.008	0.58	0.05	0.99	0.38	0.15	0.005	0.005	0.005	0.040	<0.0005	0.0317	0.0086	0.488	0.305	0.236
9692B Elga Elgamatic 135	36" x 14.9mm	0.076	1.47	0.008	0.011	0.46	0.27	1.25	0.23	0.19	<0.005	0.090	<0.005	<0.005	<0.0005	0.0332	0.0068	0.535	0.300	0.235
9692T Thyssen Union X85	36" x 14.9mm	0.081	1.52	0.011	0.010	0.59	0.26	1.51	0.50	0.13	<0.005	0.006	0.007	0.040	<0.0005	0.0283	0.0052	0.597	0.340	0.257
9726B Elga Elgamatic 135	36" x 14.9mm	0.083	1.45	0.008	0.011	0.43	0.25	1.20	0.23	0.20	<0.005	0.080	0.006	0.005	<0.0005	0.0494	0.0072	0.530	0.304	0.238
9726T Thyssen Union X85	36" x 14.9mm	0.079	1.50	0.010	0.009	0.53	0.25	1.43	0.48	0.14	<0.005	0.006	0.008	0.030	<0.0005	0.0395	0.0060	0.581	0.332	0.250
Single Wire Welds																				
7691 Thyssen MoNi	30" x 19mm	0.090	1.39	0.007	0.008	0.61	0.07	1.04	0.40	0.16	<0.005	0.008	0.005	0.040	<0.0005	0.0238	0.0094	0.497	0.307	0.238
7625 Thyssen MoNi	36" x 19mm	0.094	1.40	0.007	0.008	0.59	0.05	1.02	0.39	0.15	0.007	0.004	0.005	0.040	<0.0005	0.0216	0.0074	0.494	0.309	0.239
ML-A-3 Spoolarc 120	30" x 19mm	0.065	1.59	0.005	0.006	0.28	0.30	1.98	0.52	0.10	0.008	0.014	0.011	0.015	0.0010	0.0303	0.0066	0.635	0.346	0.248
ML-A-4 Carbofil HT	30" x 19mm	0.06	1.40	0.008	0.010	0.62	0.48	0.48	0.47	0.18	0.008	0.010	0.008	0.005	<0.0005	0.0349	0.0091	0.529	0.292	0.226
ML-A-5 Carbofil HT	30" x 19mm	0.063	1.40	0.008	0.010	0.62	0.48	0.47	0.48	0.18	<0.005	0.009	0.080	0.005	<0.0005	0.0341	0.0092	0.533	0.296	0.229
ML-B-7 Carbofil HT	36" x 19mm	0.067	1.38	0.008	0.010	0.61	0.45	0.47	0.46	0.17	0.005	0.005	0.008	0.005	<0.0005	0.0406	0.0091	0.523	0.294	0.228
ML-B-10 Spoolarc 120	36" x 19mm	0.066	1.45	0.005	0.006	0.28	0.23	2.03	0.48	0.06	0.009	0.005	0.010	0.014	0.0009	0.0326	0.0068	0.590	0.324	0.233
ML-B15-1 Spoolarc 120	36" x 14.9mm	0.070	1.54	0.006	0.007	0.30	0.25	2.12	0.50	0.05	0.008	<0.005	0.008	0.015	0.0012	0.0311	0.0064	0.622	0.342	0.247
ML-B15-3 Carbofil NiMo-1	36" x 14.9mm	0.085	1.71	0.010	0.008	0.54	0.03	0.87	0.30	0.13	<0.005	0.005	0.008	0.004	0.0005	0.0258	0.0062	0.504	0.316	0.234

$CE_{IIW} = C + Mn/6 + (Cr+Mo+V)/5 + (Ni + Cu)/15$

$CET = C + (Mn+Mo)/10 + (Cr+Cu)/20 + Ni/40$

$P_{cm} = C + Si/30 + (Mn+Cu+Cr)/20 + Ni/60 + Mo/15 + V/10 + 5B$

When elements are stated as < the given amount, calculations for carbon equivalents are based on the following assumptions: V = 0.004 and B = 0.0004

Table 5-29: X100 pipe 5G procedure tests – weld metal chemistry

		Weld Metal Chemical Composition (wt %)																		
Weld N°	**X100 Pipe OD x WT**	**C**	**Mn**	**P**	**S**	**Si**	**Cr**	**Ni**	**Mo**	**Cu**	**Al**	**V**	**Nb**	**Ti**	**B**	**O**	**N**	**CE_{IIW}**	**CET**	**P_{cm}**
Tandem Wire Welds																				
ML-B-12 Carbofil NiMo-1	36" x 19mm	0.080	1.66	0.010	0.008	0.56	0.03	0.85	0.30	0.12	0.007	0.006	0.010	0.050	<0.0005	0.0234	0.0076	0.489	0.305	0.244
ML-B15-16 Carbofil NiMo-1	36" x 14.9mm	0.079	1.66	0.009	0.008	0.56	0.03	0.85	0.30	0.12	0.005	0.004	0.006	0.040	<0.0005	0.0296	0.0075	0.487	0.304	0.243
ML-B15-17 Thyssen MoNi	36" x 14.9mm	0.090	1.47	0.009	0.014	0.53	0.03	0.95	0.37	0.13	0.006	0.006	0.007	0.040	<0.0005	0.0213	0.0100	0.488	0.306	0.250
ML-B15-18 Thyssen MoNi	36" x 14.9mm	0.100	1.50	0.009	0.015	0.57	0.03	0.98	0.38	0.12	0.005	0.006	0.005	0.040	<0.0005	0.0299	0.0112	0.507	0.320	0.264
Repair and Tie-In Welds																				
ML-B-8R FP OK 15.09	36" x 19mm	0.061	1.27	0.012	0.010	0.39	0.03	2.64	0.31	0.02	<0.005	0.030	0.020	0.070	0.0060	0.0531	0.0027	0.524	0.288	0.238
ML-B-9 OK 15.09	36" x 19mm	0.054	1.24	0.012	0.009	0.36	0.03	2.56	0.31	0.02	<0.005	0.020	0.020	0.050	0.0050	0.0629	0.0030	0.505	0.276	0.221

$CE_{IIW} = C + Mn/6 + (Cr+Mo+V)/5 + (Ni + Cu)/15$

$CET = C + (Mn+Mo)/10 + (Cr+Cu)/20 + Ni/40$

$P_{cm} = C + Si/30 + (Mn+Cu+Cr)/20 + Ni/60 + Mo/15 + V/10 + 5B$

When elements are stated as < the given amount, calculations for carbon equivalents are based on the following assumptions: V = 0.004 and B = 0.0004

Table 5-30: Calculated pipe preheat temperatures

Weld No.	**Pipe OD x WT**	**Preheat Temperature (°C)**	**Weld No.**	**Pipe OD x WT**	**Preheat Temperature (°C)**
7544 Bohler X70-IG	30 in.x 19 mm	51	7691 Thyssen MoNi	30 in. x 19 mm	59
7549 Bohler X70-IG	36 in. x 19 mm	55	7625 Thyssen MoNi	36 in. x 19 mm	61
7624 Bohler X70-IG	36 in. x 16.3 mm	41	ML-A-3 Spoolarc 120	30 in. x 19 mm	87
7632 Thyssen MoNi	30 in. x 19 mm	55	ML-A-4 Carbofil HT	30 in. x 19 mm	49
7546 Thyssen MoNi	36 in. x 19 mm	55	ML-A-5 Carbofil HT	30 in. x 19 mm	52
7548 Thyssen MoNi	36 in. x 16.3 mm	49	ML-B-7 Carbofil HT	36 in. x 19 mm	50
8868 Elga Elgamatic 135	36 in. x 14.9 mm	32	ML-B-10 Spoolarc 120	36 in. x 19 mm	72
8876 Thyssen MoNi	36 in. x 14.9 mm	43	ML-B15-1 Spoolarc 120	36 in. x 14.9 mm	70
9692B Elga Elgamatic 135	36 in. x 14.9 mm	40	ML-B15-3 Carbofil NiMo-1	36 in. x 14.9 mm	51
9692T Thyssen Union X85	36 in. x 14.9 mm	68	ML-B-12 Carbofil NiMo-1	36 in. x 19 mm	58
9726B Elga Elgamatic 135	36 in. x 14.9 mm	42	ML-B15-16 Carbofil NiMo-1	36 in. x 14.9 mm	42
9726T Thyssen Union X85	36 in. x 14.9 mm	63	ML-B15-17 Thyssen MoNi	36 in. x 14.9 mm	44
ML-B-8R FP OK 15.09	36 in x 19 mm	46	ML-B15-18 Thyssen MoNi	36 in. x 14.9 mm	54
ML-B-9 OK 15.09	36 in x 19 mm	37			

NB Preheat calculation based on relevant pipe wall thickness, a heat input of 0.4kJ/mm (0.8 arc efficiency factor) and diffusible weld metal hydrogen content of 2ml H_2/ 100g wm in conjunction with the CET (BS EN 1011-2) of the weld metal

Table 5-31: Tie-In Trials for Improved Rutile FCAW Wire Tensile Properties – Mechanical Results

Weld No.	Groove angle	Welding Position/ Parent Metal	Heat input (kJ/mm)	Preheat (°C)	max interpass (°C)	$R_{p0.2}$ (MPa)	$R_{t0.5}$ (MPa)	R_m (MPa)	A (%) z (%)	WM Cv @ -40°C (J)	WM HV10 Average
OT1	50°	3G Up/ RQT 701	1.04-1.31	100	120	752	752	807	11.7	50,39,54	273
OT2	50°	4G/ RQT 701	0.89-1.44	100	118	762	773	814	11.5	58,55,60	276
OT3	30°	3G Up/ X100	1.01-1.35	100	118	465	475	770	17.3	78,74,63	255
OT4A	45°	3G Up/ X100	1.04-1.32	100	118	716	740	796	17.2	Not tested	Not tested
OT4B	45°	3G Up/ X100	1.04-1.32	100	118	477	480	759	16.2	Not tested	265
TIC110	30°	5G (6 to 3o'c)/ X100	1.02-1.45	100	120	590[#]	588	754	18.0 (61.1)	58,42,46	248
TIC110	30°	5G (6 to 3o'c)/ X100	1.02-1.45	100	120	601	586	744	20		
TI1509	30°	5G (6 to 3o'c)/ X100	1.08-1.43	100	120	637[#]	625	809	17 (61.6)	78,76,60	251
TI1509	30°	5G (6 to 3o'c)/ X100	1.08-1.43	100	120	634	639	748	23		
1509MNG1	30°	5G (2.30 to 12o'c)/X100	1.05-1.16	20	40	745	737	807	14.5	72,70,68	265
1509MNG2	30°	5G (6.0 to 4.30)/ X100	1.10-1.14	20	40	683	671	790	18		290

NB the only difference between OT4A and OT4B was the root and HP procedure : OT4A had a single run of MMA for the root, then FCW HP, fill and cap; OT4B had a root and HP with MMA, then FCW fill and cap. The tensile test should have given the same result within experimental scatter (say 10-20MPa), due to the position the specimen was extracted.
All tensile specimens (except [#]) ~ 8.2 x 4mm. Location should ensure only FCW weld metal tested
Tensile specimen [#] = 5mm round bar (mid thickness to cap region)
Weld metal HV taken from a traverse down the weld centreline; at least 8 points were measured

Table 5-32: Tie-In Trials for Improved Rutile FCAW Wire Tensile Properties – Weld Metal Chemistry Results

	Weld Metal Chemical Composition (wt %)																		
Weld N°	C	Mn	P	S	Si	Cr	Ni	Mo	Cu	Al	V	Nb	Ti	B	O	N	CE_{IIW}	CET	P_{cm}
RQT701	0.088	0.57	0.009	0.007	0.22	2.20	0.03	1.05	<0.01	0.012	0.012	<0.005	<0.005	<0.0005	0.0018	0.0044	0.838	0.361	0.316
X100	0.025	1.98	0.006	<0.005	0.20	0.42	0.48	0.43	0.46	0.006	0.07	0.05	0.015	<0.0005	0.0038	0.0050	0.602	0.322	0.228
OT1	0.098	1.31	0.010	0.010	0.38	0.12	2.18	0.06	0.01	<0.005	0.020	0.015	0.06	0.004	0.0518	0.0055	0.502	0.296	0.245
OT2	As per OT1																		
OT3	0.10	1.31	0.009	0.009	0.32	0.08	2.00	0.07	0.08	<0.005	0.030	0.02	0.05	0.003	0.0557	0.0056	0.493	0.296	0.240
OT4A	0.083	1.34	0.009	0.008	0.32	0.10	1.94	0.09	0.09	<0.005	0.030	0.019	0.04	0.003	0.0486	0.0081	0.486	0.284	0.227
OT4B	As per OT4A																		
ML-B-9 (OK 15.09)	0.054	1.24	0.012	0.009	0.36	0.03	2.56	0.31	0.02	<0.005	0.020	0.020	0.050	0.0050	0.0629	0.0030	0.505	0.276	0.197

Table 5-33: Single wire PGMAW preheat variation trials – no preheat thermocycle data

	Cooling time from 800°C to 500, 400 or 300°C (s)								
Run	t85 (data 1)	t85 (data 2)	t85 (av.)	t84 (data 1)	t84 (data 2)	t84 (av.)	t83 (data 1)	t83 (data 2)	t83 (av.)
Hot Pass Internal	3.488	3.362	**3.43**	5.975	5.737	**5.86**	9.25	9.012	**9.13**
Fill 1 Internal	2.363	2.425	**2.39**	4.538	4.7	**4.62**	7.913	8.063	**7.99**
Fill 2 Internal	2.408	2.288	**2.35**	4.67	4.15	**4.41**	8.358	7.138	**7.75**
Fill 3 Internal	2.62		**2.62**	4.385		**4.39**	7.285		**7.29**
Fill 4 Internal	2.688	2.827	**2.76**	4.963	5.027	**5.00**	8.1	8.047	**8.07**
Cap Internal	3.312		**3.31**	5.592		**5.59**	8.675		**8.68**
Hot Pass External	2.888		**2.89**	5.38		**5.38**	8.788		**8.79**
Fill 1 External	1.76		**1.76**	3.45		**3.45**	6.575		**6.58**
Fill 2 External	1.75		**1.75**	3.238		**3.24**	5.725		**5.73**
Fill 3 External	1.988		**1.99**	3.5		**3.50**	5.775		**5.78**
Fill 4 External	2.888		**2.89**	4.7		**4.70**	7.463		**7.46**
Cap External	3.537	3.525	**3.53**	5.55	5.425	**5.49**	8.4	8.2	**8.30**

Run	Transformation start temperature (data 1)	Transformation start temperature (data 2)	**Transformation start Temperature (Av.)**	Maximum rate of transformation temperature (data 1)	Maximum rate of transformation temperature (data 2)	**Maximum rate of transformation temperature (Av.)**	Transformation finish temperature (data 1)	Transformation finish temperature (data 2)	**Transformation finish temperature (Av.)**
Hot Pass Internal	514	522	**518**	495	496	**496**	445	448	**447**
Fill 1 Internal	496	489	**493**	463	463	**463**	424	423	**424**
Fill 2 Internal	455	464	**460**	423		**423**	395		**395**
Fill 3 Internal									
Fill 4 Internal	500	480	**490**	463	444	**454**	423	412	**418**
Cap Internal	514		**514**	494		**494**	439		**439**
Hot Pass External	497		**497**	471		**471**	433		**433**
Fill 1 External	509		**509**	472		**472**	433		**433**
Fill 2 External	534		**534**	475		**475**	449		**449**
Fill 3 External	512		**512**	491		**491**	433		**433**
Fill 4 External	534		**534**	510		**510**	452		**452**
Cap External	533		**533**	516		**516**	456		**456**

Table 5-33(Cont.): Single wire PGMAW preheat variation trials – no preheat thermocycle data

Run	Cooling rate at 800°C (°C/s) (data 1)	Cooling rate at 800°C (°C/s) (data 2)	**Cooling rate at 800°C (°C/s) (av.)**	Cooling rate at 600°C (°C/s) (data 1)	Cooling rate at 600°C (°C/s) (data 2)	**Cooling rate at 600°C (°C/s) (av.)**	Cooling rate at 400°C (°C/s) (data 1)	Cooling rate at 400°C (°C/s) (data 2)	**Cooling rate at 400°C (°C/s) (av.)**
Hot Pass Internal	148	160	**154**	83	86	**85**	36	36	**36**
Fill 1 Internal	203	220	**212**	122	114	**118**	43	41	**42**
Fill 2 Internal	213	184	**199**	110	122	**116**	36	44	**40**
Fill 3 Internal				116		**116**	43		**43**
Fill 4 Internal	142	122	**132**	109	104	**107**	42	42	**42**
Cap Internal	151		**151**	89		**89**	42		**42**
Hot Pass External	192		**192**	94		**94**	36		**36**
Fill 1 External	329		**329**	164		**164**	52		**52**
Fill 2 External	321		**321**	167		**167**	57		**57**
Fill 3 External	292		**292**	149		**149**	64		**64**
Fill 4 External	207		**207**	107		**107**	44		**44**
Cap External	169		**169**	97		**97**	42		**42**

Table 5-34: Single wire PGMAW preheat variation trials – 100°C preheat thermocycle data

	Cooling time from 800°C to 500, 400 or 300°C (s)								
Run	t85 (data 1)	t85 (data 2)	**t85 (av.)**	t84 (data 1)	t84 (data 2)	**t84 (av.)**	t83 (data 1)	t83 (data 2)	**t83 (av.)**
Hot Pass Internal	5.6125		**5.61**	9.2625		**9.26**	16.9		**16.90**
Fill 1 Internal	3.275	3.555	**3.42**	6.503	6.875	**6.69**	12.403	13	**12.70**
Fill 2 Internal	2.762	2.775	**2.77**	5.25	5.712	**5.48**	12.637	12.35	**12.49**
Fill 3 Internal	2.475	2.438	**2.46**	5.017	4.988	**5.00**	9.975	9.975	**9.98**
Fill 4 Internal	3.325	3.542	**3.43**	6.55	6.85	**6.70**	12.36	12.862	**12.61**
Cap Internal	4.45		**4.45**	7.638		**7.64**	13.925		**13.93**
Hot Pass External	4.125		**4.13**	8.675		**8.68**	17.425		**17.43**
Fill 1 External	2.215	2.425	**2.32**	5.125	5.15	**5.14**	10.913	11.588	**11.25**
Fill 2 External	2.26		**2.26**	4.577		**4.58**	10.385		**10.39**
Fill 3 External	2.39		**2.39**	4.907		**4.91**	9.052		**9.05**
Fill 4 External	3.695		**3.70**	6.107		**6.11**	11.387		**11.39**
Cap External	4.62		**4.62**	7.12		**7.12**	12.57		**12.57**

Table 5-34(Cont.): Single wire PGMAW preheat variation trials – 100°C preheat thermocycle data

Run	Transformation start temperature (data 1)	Transformation start temperature (data 2)	Transformation start Temperature (Av.)	Maximum rate of transformation temperature (data 1)	Maximum rate of transformation temperature (data 2)	Maximum rate of transformation temperature (Av.)	Transformation finish temperature (data 1)	Transformation finish temperature (data 2)	Transformation finish temperature (Av.)
Hot Pass Internal	528		528	516		516	469		469
Fill 1 Internal	502	509	506	484	483	484	443	445	444
Fill 2 Internal		497	497		455	455		430	430
Fill 3 Internal	460	475	468	429	430	430	408	414	411
Fill 4 Internal	507	497	502	479	472	476	440	432	436
Cap Internal	524		524	505		505	460		460
Hot Pass External	504		504	490		490	460		460
Fill 1 External	511	498	505	481	474	478	444	433	439
Fill 2 External	508		508	486		486	438		438
Fill 3 External	488		488	463		463	424		424
Fill 4 External	536		536	517		517	461		461
Cap External	537		537	525		525	472		472

Run	Cooling rate at 800°C (°C/s) (data 1)	Cooling rate at 800°C (°C/s) (data 2)	Cooling rate at 800°C (°C/s) (av.)	Cooling rate at 600°C (°C/s) (data 1)	Cooling rate at 600°C (°C/s) (data 2)	Cooling rate at 600°C (°C/s) (av.)	Cooling rate at 400°C (°C/s) (data 1)	Cooling rate at 400°C (°C/s) (data 2)	Cooling rate at 400°C (°C/s) (av.)
Hot Pass Internal	121		121		57	57	21		21
Fill 1 Internal	175	176	176	80	86	83	26	25	26
Fill 2 Internal		164	164	105		105		28	28
Fill 3 Internal	182	188	185	115	115	115	31	34	33
Fill 4 Internal	145	133	139	80	88	84	28	28	28
Cap Internal	131		131		69	69	27		27
Hot Pass External	161		161	65		65	19		19
Fill 1 External	273	295	284	117	133	125	29	31	30
Fill 2 External	282		282	129		129	37		37
Fill 3 External	244		244	114		114	37		37
Fill 4 External	184		184	88		88	31		31
Cap External	148		148	76		76	29		29

Table 5-35: Single wire PGMAW preheat variation trials – 180°C preheat thermocycle data

	Cooling time from 800°C to 500, 400 or 300°C (s)								
Run	t85 (data 1)	t85 (data 2)	t85 (av.)	t84 (data 1)	t84 (data 2)	t84 (av.)	t83 (data 1)	t83 (data 2)	t83 (av.)
Hot Pass Internal	9.125	9.088	9.11	16.65	16.613	16.63	53.7	52.063	52.88
Fill 1 Internal	5.55		5.55	10.875		10.88	28.892		28.89
Fill 2 Internal	4.225	4.325	4.28	9.955	9.7	9.83	29.038	29.262	29.15
Fill 3 Internal	3.675		3.68	8.463		8.46	25.313		25.31
Fill 4 Internal	4.262		4.26	8.725		8.73	21.937		21.94
Cap Internal	5.558	5.563	5.56	9.82	9.55	9.69	23.333	21.875	22.60
Hot Pass External	8.325		8.33	16.625		16.63	63.4		63.40
Fill 1 External	4.288		4.29	9.313		9.31	30.563		30.56
Fill 2 External	4		4.00	8.125		8.13	25.355		25.36
Fill 3 External	3.8		3.80	8.175		8.18	24.063		24.06
Fill 4 External	4.33		4.33	7.875		7.88	19.575		19.58
Cap External	5.73		5.73	9.363		9.36	20.563		20.56

Run	Transformation start temperature (data 1)	Transformation start temperature (data 2)	Transformation start Temperature (Av.)	Maximum rate of transformation temperature (data 1)	Maximum rate of transformation temperature (data 2)	Maximum rate of transformation temperature (Av.)	Transformation finish temperature (data 1)	Transformation finish temperature (data 2)	Transformation finish temperature (Av.)
Hot Pass Internal	541	534	538	532	525	529	496	490	493
Fill 1 Internal	547		547	513		513	478		478
Fill 2 Internal	507	531	519	486	496	491	456	464	460
Fill 3 Internal	517		517	476		476	448		448
Fill 4 Internal	523		523	491		491	454		454
Cap Internal	532	533	533	514	515	515	469	467	468
Hot Pass External	528		528	517		517	488		488
Fill 1 External	529		529	508		508	470		470
Fill 2 External									
Fill 3 External	523		523	483		483	454		454
Fill 4 External	527		527	507		507	457		457
Cap External	552		552	530		530	476		476

Table 5-35(Cont.): Single wire PGMAW preheat variation trials – 180°C preheat thermocycle data

Run	Cooling rate at 800°C (°C/s) (data 1)	Cooling rate at 800°C (°C/s) (data 2)	Cooling rate at 800°C (°C/s) (av.)	Cooling rate at 600°C (°C/s) (data 1)	Cooling rate at 600°C (°C/s) (data 2)	Cooling rate at 600°C (°C/s) (av.)	Cooling rate at 400°C (°C/s) (data 1)	Cooling rate at 400°C (°C/s) (data 2)	Cooling rate at 400°C (°C/s) (av.)
Hot Pass Internal	86	89	88	36	37	37	8	8	8
Fill 1 Internal	137		137	55		55	13		13
Fill 2 Internal	141	143	142	70	74	72	13	12	13
Fill 3 Internal	128		128	83		83	15		15
Fill 4 Internal	136		136	71		71	18		18
Cap Internal	126	122	124	60	59	60	17	18	18
Hot Pass External	101		101	40		40	8		8
Fill 1 External	225		225	83		83	13		13
Fill 2 External	206		206	79		79	15		15
Fill 3 External	188		188	76		76	16		16
Fill 4 External	178		178	77		77	20		20
Cap External	128		128	59		59	19		19

Table 5-36: Process variation trials – single wire thermocycle data

	Cooling time from 800°C to 500, 400 or 300°C (s)								
Run	t85 (data 1)	t85 (data 2)	t85 (av.)	t84 (data 1)	t84 (data 2)	t84 (av.)	t83 (data 1)	t83 (data 2)	t83 (av.)
Hot Pass Internal									
Fill 1 Internal	2.938		2.94	4.155		4.16	12.355		12.36
Fill 2 Internal	2.113		2.11	4.455		4.46	9.863		9.86
Fill 3 Internal	1.975	1.837	1.91	4.062	3.845	3.95	8.15	7.557	7.85
Fill 4 Internal	1.97	2.04	2.01	4.03	4.23	4.13	7.9	8.122	8.01
Fill 5 Internal	2.288		2.29	4.7		4.70	8.7		8.70
Cap Internal	2.917	3.235	3.08	5.525	5.91	5.72	9.787	10.06	9.92
Hot Pass External									
Fill 1 External	2.645	2.313	2.48	5.02	4.525	4.77	11.1	9.688	10.39
Fill 2 External	1.767	1.82	1.79	3.705	3.545	3.63	8.68	7.637	8.16
Fill 3 External	1.9	1.75	1.83	3.525	3.66	3.59	7.025	7.297	7.16
Fill 4 External		2.125	2.13		3.925	3.93		7.125	7.13
Fill 5 External	2.238	2.517	2.38	4.338	4.272	4.31	7.813	7.655	7.73
Cap External	3.3	3.125	3.21	5.2	5.012	5.11	9.125	8.675	8.90

Table 5-36(Cont.): Process variation trials – single wire thermocycle data

Run	Transformation start temperature (data 1)	Transformation start temperature (data 2)	**Transformation start Temperature (Av.)**	Maximum rate of transformation temperature (data 1)	Maximum rate of transformation temperature (data 2)	**Maximum rate of transformation temperature (Av.)**	Transformation finish temperature (data 1)	Transformation finish temperature (data 2)	**Transformation finish temperature (Av.)**
Hot Pass Internal									
Fill 1 Internal	509		**509**	485		**485**	448		**448**
Fill 2 Internal	495		**495**	464		**464**	431		**431**
Fill 3 Internal	479	472	**476**	449	441	**445**	419	406	**413**
Fill 4 Internal	482	471	**477**	447	444	**446**	416	408	**412**
Fill 5 Internal	492		**492**	465		**465**	428		**428**
Cap Internal	500	479	**490**	473	455	**464**	423	415	**419**
Hot Pass External									
Fill 1 External	529	522	**526**	506	500	**503**	458	452	**455**
Fill 2 External	505	512	**509**	482	488	**485**	437	442	**440**
Fill 3 External	517	500	**509**	493	472	**483**	447	434	**441**
Fill 4 External		519	**519**		491	**491**		443	**443**
Fill 5 External		533	**533**		510	**510**		452	**452**
Cap External	545	541	**543**	530	518	**524**	478	459	**469**

Run	Cooling rate at 800°C (°C/s) (data 1)	Cooling rate at 800°C (°C/s) (data 2)	**Cooling rate at 800°C (°C/s) (av.)**	Cooling rate at 600°C (°C/s) (data 1)	Cooling rate at 600°C (°C/s) (data 2)	**Cooling rate at 600°C (°C/s) (av.)**	Cooling rate at 400°C (°C/s) (data 1)	Cooling rate at 400°C (°C/s) (data 2)	**Cooling rate at 400°C (°C/s) (av.)**
Hot Pass Internal									
Fill 1 Internal	227		**227**		95	**95**		26	**26**
Fill 2 Internal	237		**237**		136	**136**		36	**36**
Fill 3 Internal	233	232	**233**	155	143	**149**	45	42	**44**
Fill 4 Internal	232		**232**	139	141	**140**	42	43	**43**
Fill 5 Internal	214		**214**		121	**121**		36	**36**
Cap Internal				90	97	**94**	37	40	**39**
Hot Pass External									
Fill 1 External	296	294	**295**	133	126	**130**	34	30	**32**
Fill 2 External	335	343	**339**	167	166	**167**	47	43	**45**
Fill 3 External	340	313	**327**	164	160	**162**	44	49	**47**
Fill 4 External	281		**281**	141		**141**	47		**47**
Fill 5 External	270		**270**	129		**129**	43		**43**
Cap External	213	188	**201**	111	102	**107**	37	38	**38**

Table 5-37: Process variation trials – tandem wire thermocycle data

	Cooling time from 800°C to 500, 400 or 300°C (s)								
Run	t85 (data 1)	t85 (data 2)	t85 (av.)	t84 (data 1)	t84 (data 2)	t84 (av.)	t83 (data 1)	t83 (data 2)	t83 (av.)
Hot Pass Internal	5.1		5.10	8.092		8.09	13.012		13.01
Fill 1 Internal									
Fill 2 Internal	1.932	1.85	1.89	4.27	3.937	4.10	9.095	8.567	8.83
Fill 3 Internal	2.096	1.85	1.97	4.209	3.837	4.02	8.509	7.675	8.09
Fill 4 Internal	1.955	1.937	1.95	3.963	4.01	3.99	7.563	7.87	7.72
Fill 5 Internal	2.313		2.31	4.5		4.50	8.05		8.05
Cap Internal	3.28	2.838	3.06	5.338	5	5.17	9.138	8.588	8.86
Hot Pass External	3.93	3.895	3.91	6.705	8.092	7.40	12.205	11.295	11.75
Fill 1 External	2.562		2.56	4.85		4.85	10.325		10.33
Fill 2 External	1.95	1.782	1.87	3.513	3.409	3.46	7.45	7.209	7.33
Fill 3 External	1.825	2.009	1.92	3.45	3.734	3.59	6.767	7.571	7.17
Fill 4 External	2.17	2.142	2.16	3.923	3.655	3.79	7.345	6.667	7.01
Fill 5 External		2.832	2.83		4.482	4.48		8.112	8.11
Cap External	3.155	3.738	3.45	4.863	5.663	5.26	8.388	10.15	9.27

Run	Transformation start temperature (data 1)	Transformation start temperature (data 2)	Transformation start Temperature (Av.)	Maximum rate of transformation temperature (data 1)	Maximum rate of transformation temperature (data 2)	Maximum rate of transformation temperature (Av.)	Transformation finish temperature (data 1)	Transformation finish temperature (data 2)	Transformation finish temperature (Av.)
Hot Pass Internal	513		513	500		500	456		456
Fill 1 Internal									
Fill 2 Internal	465	483	474	441	447	444	408	419	414
Fill 3 Internal	464	474	469	426	442	434	406	407	407
Fill 4 Internal	480	483	482	453	450	452	415	414	415
Fill 5 Internal	520		520	484		484	434		434
Cap Internal	534	518	526	512	498	505	454	441	448
Hot Pass External	547	551	549	516	528	522	470	476	473
Fill 1 External	546		546	512		512	469		469
Fill 2 External	529	514	522	502	486	494	449	443	446
Fill 3 External	518	522	520	493	497	495	441	446	444
Fill 4 External	531	538	535	502	510	506	449	452	451
Fill 5 External		545	545		520	520		457	457
Cap External	550	555	553	527	536	532	461	472	467

Table 5-37(Cont.): Process variation trials – tandem wire thermocycle data

Run	Cooling rate at 800°C (°C/s) (data 1)	Cooling rate at 800°C (°C/s) (data 2)	Cooling rate at 800°C (°C/s) (av.)	Cooling rate at 600°C (°C/s) (data 1)	Cooling rate at 600°C (°C/s) (data 2)	Cooling rate at 600°C (°C/s) (av.)	Cooling rate at 400°C (°C/s) (data 1)	Cooling rate at 400°C (°C/s) (data 2)	Cooling rate at 400°C (°C/s) (av.)
Hot Pass Internal	105		105	58		58	30		30
Fill 1 Internal									
Fill 2 Internal	225	225	225	148	159	154	38	42	40
Fill 3 Internal	230	239	235	132	157	145	37	45	41
Fill 4 Internal	222	258	240	147	144	146	47	44	46
Fill 5 Internal	231		231	130		130	44		44
Cap Internal	193	210	202	102	112	107	40	43	42
Hot Pass External	205	206	206	73	77	75	29	31	30
Fill 1 External	297		297	121		121	31		31
Fill 2 External	313	334	324	167	171	169	49	51	50
Fill 3 External	342	312	327	169	158	164	53	45	49
Fill 4 External	286	288	287	144	144	144	35	53	44
Fill 5 External	226	245	236	120	122	121		45	45
Cap External	222	185	204	111	88	100	43	36	40

Table 5-38: Process variation trials – dual torch thermocycle data

	Cooling time from 800°C to 500, 400 or 300°C (s)								
Run	t85 (data 1)	t85 (data 2)	t85 (av.)	t84 (data 1)	t84 (data 2)	t84 (av.)	t83 (data 1)	t83 (data 2)	t83 (av.)
Hot Pass Internal	4.62	4.665	4.64	Reheated before lower temp. reached			Reheated before lower temp. reached		
Fill 1 Internal									
Fill 2 Internal	2.187	2.292	2.24	4.5	4.512	4.51	Reheated before lower temp. reached		
Fill 3 Internal									
Fill 4 Internal	2.417	2.348	2.38	4.637	4.545	4.59	Reheated before lower temp. reached		
Fill 5 Internal									
Fill 6 Internal	3.125		3.13	5.812		5.81	Reheated before lower temp. reached		
Cap Internal									
Hot Pass External									
Fill 1 External	5.817	6.355	6.09	11.367	12.642	12.00	27.797	29.642	28.72
Fill 2 External									
Fill 3 External	4.32	4.531	4.43	8.52	8.769	8.64	23.082	24.381	23.73
Fill 4 External									
Fill 5 External	5.088	5.255	5.17	9.313	9.375	9.34	22.58	21.813	22.20
Fill 6 Internal									
Cap External	6.317	6.81	6.56	10.375	10.66	10.52	21.887	21.585	21.74

NB internal thermocycles show initial cooling from molten state of lead torch, external thermocycles show cooling from molten state of trail torch (incorporating preheating effect of lead torch)

Table 5-38(Cont.): Process variation trials – dual torch thermocycle data

Run	Transformation start temperature (data 1)	Transformation start temperature (data 2)	**Transformation start Temperature (Av.)**	Maximum rate of transformation temperature (data 1)	Maximum rate of transformation temperature (data 2)	**Maximum rate of transformation temperature (Av.)**	Transformation finish temperature (data 1)	Transformation finish temperature (data 2)	**Transformation finish temperature (Av.)**
Initial cooling									
Hot Pass Internal	556	553	**555**	508	541	**525**	470	482	**476**
Fill 1 Internal									
Fill 2 Internal	481	480	**481**	467	448	**458**	442		**442**
Fill 3 Internal									
Fill 4 Internal	457	469	**463**	446	451	**449**	417	409	**413**
Fill 5 Internal									
Fill 6 Internal	500		**500**	491		**491**	Deviation from cooling curve not detectable		
Cap Internal									
Secondary cooling									
Hot Pass Internal	544	566	**555**	528	540	**534**	Deviation from cooling curve not detectable		
Fill 1 Internal									
Fill 2 Internal	486	502	**494**	448	461	**455**	Deviation from cooling curve not detectable		
Fill 3 Internal									
Fill 4 Internal	477	485	**481**	436	452	**444**	Deviation from cooling curve not detectable		
Fill 5 Internal									
Fill 6 Internal	526		**526**	512		**512**	470		**470**
Cap Internal									
Initial cooling									
Hot Pass External									
Fill 1 External	573	582	**578**	520	528	**524**	499	494	**497**
Fill 2 External									
Fill 3 External	535	557	**546**	514	535	**525**	477	496	**487**
Fill 4 External									
Fill 5 External	532	534	**533**	519	518	**519**	468	475	**472**
Fill 6 Internal									
Cap External	551	560	**556**	544	553	**549**	503	494	**499**

Blanks in table are due to thermocouples not being present in the particular layer.

NB Internal thermocycles show initial and secondary cooling from molten state of lead torch, external thermocycles show cooling from molten state of trail torch (incorporating preheating effect of lead torch)

Table 5-38(Cont.): Process variation trials – dual torch thermocycle data

Run	Cooling rate at 800°C (°C/s) (data 1)	Cooling rate at 800°C (°C/s) (data 2)	**Cooling rate at 800°C (°C/s) (av.)**	Cooling rate at 600°C (°C/s) (data 1)	Cooling rate at 600°C (°C/s) (data 2)	**Cooling rate at 600°C (°C/s) (av.)**	Cooling rate at 400°C (°C/s) (data 1)	Cooling rate at 400°C (°C/s) (data 2)	**Cooling rate at 400°C (°C/s) (av.)**
Initial cooling									
Hot Pass Internal	121	140	**131**	60	63	**62**	Reheated before temperature. reached		
Fill 1 Internal									
Fill 2 Internal	200	201	**201**	134	125	**130**	38	38	**38**
Fill 3 Internal									
Fill 4 Internal	180	190	**185**	124	122	**123**	42	41	**42**
Fill 5 Internal									
Fill 6 Internal	163		**163**	94		**94**	Reheated before temperature. reached		
Cap Internal									
Secondary cooling									
Hot Pass Internal	Higher temperature not attained after reheating			31	32	**32**	12	12	**12**
Fill 1 Internal									
Fill 2 Internal	Higher temperature not attained after reheating			Higher temperature not attained after reheating			12	11	**12**
Fill 3 Internal									
Fill 4 Internal	Higher temperature not attained after reheating			Higher temperature not attained after reheating			13	14	**14**
Fill 5 Internal									
Fill 6 Internal	83		**83**	50		**50**	16		**16**
Cap Internal									
Initial cooling									
Hot Pass External									
Fill 1 External	177	157	**167**	55	47	**51**	12	11	**12**
Fill 2 External									
Fill 3 External	191	185	**188**	76	72	**74**	16	13	**15**
Fill 4 External									
Fill 5 External	158	146	**152**	63	57	**60**	17	17	**17**
Fill 6 Internal									
Cap External	116	108	**112**	53	48	**51**	18	18	**18**

Blanks in table are due to thermocouples not being present in the particular layer.

NB Internal thermocycles show initial and secondary cooling from molten state of lead torch, external thermocycles show cooling from molten state of trail torch (incorporating preheating effect of lead torch)

Table 5-39: Process variation trials – dual tandem torch thermocycle data

	Cooling time from 800°C to 500, 400 or 300°C (s) – initial cooling from molten state								
Run	t85 (data 1)	t85 (data 2)	t85 (av.)	t84 (data 1)	t84 (data 2)	t84 (av.)	t83 (data 1)	t83 (data 2)	t83 (av.)
Initial cooling									
Hot Pass Internal	Reheated before temperature reached			Reheated before temperature reached			Reheated before temperature reached		
Fill 1 Internal									
Fill 2 Internal	Data not acquired			Data not acquired			Data not acquired		
Fill 3 Internal									
Fill 4 Internal	2.013	2.485	**2.25**	Reheated before temperature reached			Reheated before temperature reached		
Fill 5 Internal									
Fill 6 Internal	Reheated before temperature reached			Reheated before temperature reached			Reheated before temperature reached		
Cap Internal									
Secondary cooling									
Hot Pass Internal	10.712		**10.71**	17.667		**17.67**	36.187		**36.19**
Fill 1 Internal									
Fill 2 Internal	Data not acquired			Data not acquired			Data not acquired		
Fill 3 Internal									
Fill 4 Internal	7.65		**7.65**	16.2		**16.20**	40.375		**40.38**
Fill 5 Internal									
Fill 6 Internal	7.725		**7.73**	13.675		**13.68**	32.475		**32.48**
Cap Internal									
Initial cooling									
Hot Pass External									
Fill 1 External									
Fill 2 External									
Fill 3 External	3.975		**3.98**	7.163		**7.16**	18.638		**18.64**
Fill 4 External									
Fill 5 External	6.438		**6.44**	14.263		**14.26**	38.963		**38.96**
Fill 6 Internal									
Cap External	7.395		**7.40**	12.245		**12.25**	29.245		**29.25**

Blanks in table are due to thermocouples not being present in the particular layer.

NB Internal thermocycles show initial and secondary cooling from molten state of lead torch, external thermocycles show cooling from molten state of trail torch (incorporating preheating effect of lead torch)

Table 5-39(Cont.): Process variation trials – dual tandem torch thermocycle data

Run	Transformation start temperature (data 1)	Transformation start temperature (data 2)	**Transformation start Temperature (Av.)**	Maximum rate of transformation temperature (data 1)	Maximum rate of transformation temperature (data 2)	**Maximum rate of transformation temperature (Av.)**	Transformation finish temperature (data 1)	Transformation finish temperature (data 2)	**Transformation finish temperature (Av.)**
Secondary cooling									
Hot Pass Internal	570		**570**	527		**527**	490		**490**
Fill 1 Internal									
Fill 2 Internal	Data not acquired			Data not acquired			Data not acquired		
Fill 3 Internal									
Fill 4 Internal	531	511	**521**	Deviation from cooling curve not detectable			Deviation from cooling curve not detectable		
Fill 5 Internal									
Fill 6 Internal	549		**549**	540		**540**	505		**505**
Cap Internal									
Initial cooling									
Hot Pass External									
Fill 1 External	Data not acquired			Data not acquired			Data not acquired		
Fill 2 External									
Fill 3 External	544		**544**	529		**529**	484		**484**
Fill 4 External									
Fill 5 External	538		**538**	525		**525**			
Fill 6 Internal									
Cap External	564		**564**	556		**556**	507		**507**

Internal thermocouple initial cooling data from molten state did not allow transformation temperatures to be determined either due to the reheating occurring before transformation or the close proximity of the reheating effect to the likely transformation temperature masking any transformation determination.

Blanks in table are due to thermocouples not being present in the particular layer.

NB Internal thermocycles show secondary cooling from molten state of lead torch, external thermocycles show cooling from molten state of trail torch (incorporating preheating effect of lead torch)

Table 5-39(Cont.): Process variation trials – dual tandem torch thermocycle data

Run	Cooling rate at 800°C (°C/s) (data 1)	Cooling rate at 800°C (°C/s) (data 2)	**Cooling rate at 800°C (°C/s) (av.)**	Cooling rate at 600°C (°C/s) (data 1)	Cooling rate at 600°C (°C/s) (data 2)	**Cooling rate at 600°C (°C/s) (av.)**	Cooling rate at 400°C (°C/s) (data 1)	Cooling rate at 400°C (°C/s) (data 2)	**Cooling rate at 400°C (°C/s) (av.)**
Initial cooling									
Hot Pass Internal	134		**134**	Reheated before temperature reached			Reheated before temperature reached		
Fill 1 Internal									
Fill 2 Internal	Data not acquired			Data not acquired			Data not acquired		
Fill 3 Internal									
Fill 4 Internal	206	192	**199**	118		**118**	Reheated before temperature reached		
Fill 5 Internal									
Fill 6 Internal	166		**166**	Reheated before temperature reached			Reheated before temperature reached		
Cap Internal									
Secondary cooling									
Hot Pass Internal	Turning point i.e. rate not applicable			28		**28**	10		**10**
Fill 1 Internal									
Fill 2 Internal	Data not acquired			Data not acquired			Data not acquired		
Fill 3 Internal									
Fill 4 Internal	not defined	N/A		44	39	**42**	8	9	**9**
Fill 5 Internal									
Fill 6 Internal	85		**85**	41		**41**	12		**12**
Cap Internal									
Initial cooling									
Hot Pass External									
Fill 1 External	Data not acquired			Data not acquired			Data not acquired		
Fill 2 External									
Fill 3 External	211		**211**	87		**87**	20		**20**
Fill 4 External									
Fill 5 External	118		**118**	51		**51**	9		**9**
Fill 6 Internal									
Cap External	102		**102**	42		**42**	14		**14**

Blanks in table are due to thermocouples not being present in the particular layer.

NB Internal thermocycles show initial and secondary cooling from molten state of lead torch, external thermocycles show cooling from molten state of trail torch (incorporating preheating effect of lead torch)

Table 5-40: Mechanical data from preheat variation trials

						All Weld Metal Strip Tensile (45° Position)				
Weld N°	**Consumable**	**X100 Pipe OD x WT**	**Arc Energy (kJ/mm)**	**Cap Gap Width (mm)**	**Preheat (°C)**	**Rp0.2 (MPa)**	**Rt0.5 (MPa)**	**Rm (MPa)**	**Yield/ Tensile Ratio**	**A (%) [z(%)]**
Thermocycle RT	NiMo-1 (ER 70S-2 TIG root)	30" x 19mm (Pipe A)	0.50 - 0.57	6.03 – 6.54	20	935	879	1000	0.94	15.5
Thermocycle 100 Test 1	NiMo-1 (ER 70S-2 TIG root)	30" x 19mm (Pipe A)	0.50 - 0.57	6.20 – 6.47	100	900	874	950	0.95	16
Thermocycle 100 Test 2	NiMo-1 (ER 70S-2 TIG root)	30" x 19mm (Pipe A)	0.50 - 0.57	6.20 – 6.47	100	903	830	958	0.94	14.5
Thermocycle 180	NiMo-1 (ER 70S-2 TIG root)	30" x 19mm (Pipe A)	0.49 - 0.59	6.55 – 6.82	180	842	844	890	0.95	28.5

Table 5-41: Mechanical data from process variation trials

						All Weld Metal Strip Tensile (90° Position)				
Process Type	**Consumable**	**X100 Pipe OD x WT**	**Arc Energy (kJ/mm)**	**Cap Gap Width (mm)**	**Preheat (°C)**	**Rp0.2 (MPa)**	**Rt0.5 (MPa)**	**Rm (MPa)**	**Yield/ Tensile Ratio**	**A (%) [z(%)]**
Single Wire	NiMo-1 fill and cap (ER70S-6 root)	36" x 19mm (Pipe B19)	0.42-0.48	7.05 - 7.37	100-120	959	885	994	0.96	18.5
Tandem Wire	NiMo-1 fill and cap (ER70S-6 root)	36" x 19mm (Pipe B19)	0.44-0.46	7.02 - 7.45	100-120	957	895	993	0.96	17
Dual Torch	NiMo-1 fill and cap (ER70S-6 root)	36" x 19mm (Pipe B19)	0.41-0.47	6.92 - 7.28	100-120	851	845	898	0.95	20.5
Dual Tandem	NiMo-1 fill and cap (ER70S-6 root)	36" x 19mm (Pipe B19)	0.45-0.50	7.01 - 7.14	100-120	806	785	857	0.94	20

	Charpy Impact Toughness (J)											
Process Type	WM CL Cv @ -20°C	WM CL Cv @ -20°C	WM CL Cv @ -20°C	**WM CL Cv Av.@ -20°C**	WM CL Cv @ -40°C	WM CL Cv @ -40°C	WM CL Cv @ -40°C	**WM CL Cv Av.@ -40°C**	WM CL Cv @ -60°C	WM CL Cv @ -60°C	WM CL Cv @ -60°C	**WM CL Cv Av. @ -60°C**
Single Wire	164	158	220	**181**	180	252	198	**210**	96	100	124	**107**
Tandem Wire	156	122	182	**153**	100	94	102	**99**	82	70	78	**77**
Dual Torch	178	230	166	**191**	152	196	216	**188**	120	120	124	**121**
Dual Tandem	168	150		**159**	168	126	174	**156**	72	84	38	**65**

Table 5-42: Weld metal chemistry from preheat and process variant trials

		Weld Metal Chemical Composition (wt %) (82.5%Ar, 12.5%CO_2,5%He shielding gas)																		
Weld N°	**X100 Pipe OD x WT**	**C**	**Mn**	**P**	**S**	**Si**	**Cr**	**Ni**	**Mo**	**Cu**	**Al**	**V**	**Nb**	**Ti**	**B**	**O**	**N**	**CE_{IIW}**	**CET**	**P_{cm}**
Preheat Weld																				
100°C Preheat Trial	30" x 19mm	0.080	1.64	0.009	0.008	0.56	0.07	0.85	0.32	0.14	<0.005	0.013	0.008	0.05	<0.0005	0.0196	0.0076	0.500	0.308	0.229
Process Weld																				
Single Wire	36" x 19mm	0.081	1.64	0.010	0.008	0.56	0.03	0.86	0.30	0.11	<0.005	0.006	0.007	0.04	<0.0005	0.0236	0.0073	0.486	0.304	0.225

Table 5-43: Metal core wire alloy variation trials – weld metal chemistry

			Weld Metal Chemical Composition (wt %) (82.5%Ar, 12.5%CO_2,5%He shielding gas)																		
Weld N°	**HB No.**	**Plate No.**	**C**	**Mn**	**Si**	**Ni**	**Mo**	**Cr**	**P**	**S**	**Cu**	**Nb**	**V**	**Al**	**Ti**	**B**	**O**	**N**	**CE_{IIW}**	**CET**	**P_{cm}**
MC Control 1 (target)			**0.080-0.90**	**1.65-1.75**	**0.50-0.60**	**0.85-0.95**	**0.25-0.35**	**0.00-0.05**	Above elements to be at minimum possible levels												
MC Cntrl 1 (actual)		MCT1	0.094	1.66	0.51	0.77	0.30	0.07	0.013	0.009	0.06	0.007	0.009	0.029	0.016	<0.0005	0.0537	0.0043	0.502	0.316	0.236
MC Cntrl 2 (HB check)	B2803 3 1	1	0.084	1.63	0.52	0.94	0.30	0.04	0.011	0.011											
MC Cntrl 2 (actual)			0.094	1.72	0.5	0.78	0.30	0.08	0.010	0.009	0.09	0.008	0.013	0.02	0.03	<0.0005	0.0473	0.0075	0.517	0.324	0.241
Ni low (target)	B2803 3 2	2	0.080-0.90	1.65-1.75	0.50-0.60	**0.0-0.1**	0.25-0.35	0.00-0.05													
Ni low (HB check)			0.083	1.59	0.5	**0.01**	0.28	0.02	0.011	0.012											
Ni low (actual)			0.091	1.67	0.48	**0.08**	0.29	0.08	0.010	0.009	0.09	0.008	0.012	0.02	0.02	<0.0005	0.0514	0.0069	0.457	0.298	0.223
Ni high (target)	B2803 3 3	3	0.080-0.90	1.65-1.75	0.50-0.60	**1.4-1.6**	0.25-0.35	0.00-0.05													
Ni high (HB check)			0.081	1.61	0.51	**1.66**	0.29	0.03	0.012	0.011											
Ni high (actual)			0.09	1.77	0.52	**1.28**	0.31	0.09	0.010	0.009	0.10	0.009	0.014	0.02	0.02	<0.0005	0.0462	0.0072	0.560	0.340	0.251
Mo low (target)	B2803 3 4	4	0.080-0.90	1.65-1.75	0.50-0.60	0.85-0.95	**0.15-0.20**	0.00-0.05													
Mo low (HB check)			0.082	1.64	0.52	0.91	**0.17**	0.04	0.011	0.012											
Mo low (actual)			0.098	1.74	0.51	0.81	**0.19**	0.08	0.010	0.009	0.09	0.008	0.012	0.02	0.02	<0.0005	0.0448	0.0077	0.504	0.320	0.240
Mo high (target)	B2803 3 5	5	0.080-0.90	1.65-1.75	0.50-0.60	0.85-0.95	**0.4-0.45**	0.00-0.05													
Mo high (HB check)			0.081	1.71	0.57	0.98	**0.45**	0.02	0.011	0.012											
Mo high (actual)			0.094	1.71	0.51	0.82	**0.42**	0.08	0.010	0.009	0.09	0.008	0.012	0.02	0.02	<0.0005	0.0459	0.0074	0.542	0.336	0.250
Cr medium (target)	B2803 3 6	6	0.080-0.90	1.65-1.75	0.50-0.60	0.85-0.95	0.25-0.35	**0.20-0.30**													
Cr med. (HB check)			0.085	1.70	0.57	1	0.29	**0.28**	0.012	0.012											
Cr medium (actual)			0.089	1.75	0.53	0.88	0.32	**0.32**	0.009	0.009	0.10	0.009	0.013	0.02	0.03	<0.0005	0.0437	0.0083	0.577	0.339	0.254
Cr high (target)	B2803 3 7	7	0.080-0.90	1.65-1.75	0.50-0.60	0.85-0.95	0.25-0.35	**0.45-0.55**													
Cr high (HB check)			0.083	1.70	0.53	1.01	0.31	**0.52**	0.012	0.012											
Cr high (actual)			0.088	1.71	0.51	0.84	0.32	**0.53**	0.009	0.009	0.10	0.010	0.014	0.02	0.03	<0.0005	0.0474	0.0093	0.608	0.344	0.261
C low (target)	B2803 3 8	8	**0.045-0.055**	1.65-1.75	0.50-0.60	0.85-0.95	0.25-0.35	0.00-0.05													
C low (HB check)			**0.038**	1.61	0.5	0.92	0.28	0.03	0.010	0.011											
C low (actual)			**0.057**	1.70	0.51	0.83	0.29	0.08	0.009	0.009	0.10	0.009	0.012	0.02	0.02	<0.0005	0.056	0.0089	0.479	0.286	0.204
C high (target)	B2803 3 9	9	**0.115-0.125**	1.65-1.75	0.50-0.60	0.85-0.95	0.25-0.35	0.00-0.05													
C high (HB check)			**0.112**	1.65	0.53	0.93	0.29	0.02	0.012	0.012											
C high (actual)			**0.12**	1.71	0.52	0.81	0.31	0.08	0.010	0.009	0.09	0.008	0.011	0.02	0.02	<0.0005	0.0443	0.0083	0.545	0.351	0.269
C high, Mo low (target)	B2803 310	10	**0.115-0.125**	1.65-1.76	0.50-0.61	0.85-0.96	**0.0-0.10**	0.00-0.05													
C high, Mo low (HB chk)			**0.11**	1.59	0.52	0.94	**0.03**	0.02	0.011	0.012											
C high, Mo low (actual)			**0.11**	1.69	0.5	0.8	**0.09**	0.08	0.010	0.009	0.10	0.008	0.012	0.019	0.02	<0.0005	0.0443	0.0076	0.488	0.317	0.243
JB Composition .(target)			**0.065**	**1.50**	**0.3**	**1.45**	**0.15**														
JB Comp. (HB check)	B2803 311	11	**0.05**	**1.55**	**0.25**	**1.6**	**0.16**	0.02	0.011	0.013											
JB Comp. (actual)			**0.067**	**1.72**	**0.28**	**1.32**	**0.20**	0.08	0.009	0.009	0.10	0.010	0.014	0.018	0.04	<0.0005	0.0545	0.0077	0.507	0.301	0.210
Carbofil NiMo-1 Pipe		ML-B15-3	0.085	1.71	0.54	0.87	0.30	0.03	0.010	0.008	0.13	0.008	0.005	<0.005	0.040	0.0005	0.0258	0.0062	0.504	0.316	0.234
Carbofil NiMo-1 Plate		12	0.076	1.62	0.53	0.85	0.32	0.08	0.009	0.008	0.14	0.009	0.014	<0.005	0.040	<0.0005	0.0210	0.0088	0.495	0.302	0.225

N.B. for calculation purposes when B level stated as <0.005, 0.004 used in equation

HB check = Hobart factory check analysis

Table 5-44: Metal cored wire alloy variation trials – tensile strength and hardness results

			All Weld Metal Strip Tensile								Weld metal hardness (vertical traverse on weld centreline - 15 indents)		
Weld N°	**HB No.**	**Plate No.**	**Specimen original gauge area dimensions (mm)**	**$R_{p0.2}$ (MPa)**	**Change in $R_{p0.2}$ wrt MC Control 2 average**	**$R_{t0.5}$ (MPa)**	**R_m (MPa)**	**Change in R_m wrt MC Control 2 average**	**$R_{p0.2}$ /R_m**	**A (%)**	**Weld Metal Average HV10**	**Weld Metal Max HV10**	**Standard Deviation of WM HV10 values**
MC Control 1	B2802 2 2		4.03 x 8.10	848		757	893		0.95	12.5	285	304	10.81
MC Control 2 test 1	B2803 3 1	1	4.03 x 8.25	876	Average	764	906	Average	0.97	16.5	287	309	10.74
MC Control 2 test 2	B2803 3 1	1	4.02 x 8.20	868	**868**	873	913	**918**	0.95	21			
MC Control 2 test 3	B2803 3 1	1a	4.00 x 8.22	865	Std. Dev.	746	926	Std. Dev.	0.93	18			
MC Control 2 test 4	B2803 3 1	1a	4.00 x 8.17	863	4.95	856	926	8.61	0.93	16.5			
Ni low	B2803 3 2	2	4.04 x 8.19	793	-75	808	841	-77	0.94	18	270	289	9.92
Ni high	B2803 3 3	3	4.04 x 8.05	958	90	790	997	79	0.96	14.5	321	351	13.92
Mo low	B2803 3 4	4	4.01 x 8.07	885	17	865	932	14	0.95	16.5	308	325	11.24
Mo high	B2803 3 5	5	4.01 x 8.29	908	40	859	955	37	0.95	17	310	339	15.07
Cr medium	B2803 3 6	6	3.99 x 8.14	933	65	838	991	73	0.94	17	320	342	15.52
Cr high	B2803 3 7	7	4.02 x 8.10	1009	141	785	1043	125	0.97	14.5	333	354	13.74
C low	B2803 3 8	8	4.03 x 8.14	822	-46	793	857	-61	0.96	18.5	280	294	11.52
C high	B2803 3 9	9	4.07 x 8.14	944	76	925	1002	84	0.94	18	322	348	19.20
C high, Mo low	B2803 3 10	10	4.01 x 8.27	913	45	800	955	37	0.96	15.5	310	348	16.94
Ni high,C low, Mo low	B2803 3 11	11	4.01 x 8.20	846	-22	843	879	-39	0.96	14	285	306	13.68
Carbofil NiMo-1 (pipe)	ML-B15-1		4.04 x 8.23	841		838	888		0.95	20.5			
Carbofil NiMo-1 (plate)	14233	12	4.03 x 8.17	909	41	825	942	24	0.96	20	293	312	10.14

NB Standard deviation calculated using biased (n) method i.e. STDEVP =((nΣx^2-(Σx)^2)/n^2)^½)

Table 5-45: Metal cored wire alloy variation trials - impact toughness results

	Charpy Impact Toughness (J)											
Process Type	WM CL Cv @ -20°C	WM CL Cv @ -20°C	WM CL Cv @ -20°C	**WM CL Cv Av.@ -20°C**	WM CL Cv @ -40°C	WM CL Cv @ -40°C	WM CL Cv @ -40°C	**WM CL Cv Av.@ -40°C**	WM CL Cv @ -60°C	WM CL Cv @ -60°C	WM CL Cv @ -60°C	**WM CL Cv Av. @ -60°C**
MC Control 1					84	72	64	**73**				
MC Control 2	82	84	74	**80**	70	58	60	**63**	50	56	44	**50**
Ni low	76	82	80	**79**	70	66	64	**67**	52	44	54	**50**
Ni high	58	64	58	**60**	50	52	44	**49**	42	36	30	**36**
Mo low	78	72	72	**74**	48	60	62	**57**	50	46	46	**47**
Mo high	62	70	68	**67**	48	48	60	**52**	38	50	44	**44**
Cr medium	68	64	66	**66**	60	52	46	**53**	36	46	30	**37**
Cr high	54	66	62	**61**	46	44	38	**43**	30	38	30	**33**
C low	72	64	68	**68**	52	56	54	**54**	40	38	44	**41**
C high	64	74	64	**67**	58	62	54	**58**	32	40	46	**39**
C high, Mo low	68	66	64	**66**	62	68	62	**64**	50	52	50	**51**
Carbofil NiMo-1 (pipe)	164	158	220	**181**	180	252	198	**210**	96	100	124	**107**
Carbofil NiMo-1 (plate)	210	176	180	**189**	108	120	128	**119**	80	90	52	**74**

Process Type	Absorbed Energy Scatter @ -20°C (J)	Absorbed Energy Scatter @ -40°C (J)	Absorbed Energy Scatter @ -60°C (J)
MC Control 1		21	
MC Control 2	11	13	13
Ni low	7	7	11
Ni high	7	9	13
Mo low	7	15	5
Mo high	9	13	13
Cr medium	5	15	17
Cr high	13	9	9
C low	9	5	7
C high	11	9	15
C high, Mo low	5	7	3
Carbofil NiMo-1 (pipe)	63	73	29
Carbofil NiMo-1 (plate)	35	21	39

Table 5-46: Weld metal microhardness surveys

Distance from Cap OD (mm)	Process Variation HV0.5				Preheat variation HV0.5		
	Single TC	Tandem TC	Dual TC	Dual Tandem TC	RT TC	100°C TC	180°C TC
-0.5					365		
-0.3					336		
-0.1					334	324	
0.1					335	317	294
0.3					353	311	305
0.5			265		355	315	292
0.7			266	278	335	311	294
0.9			270	270	342	328	293
1.1			267	277	326	304	293
1.3			256	265	335	322	289
1.5	316	299	264	276	335	315	303
1.7	311	298	268	271	335	329	289
1.9	315	298	266	271	342	320	295
2.1	311	302	262	267	340	317	286
2.3	318	305	267	273	328	320	294
2.5	312	295	284	274	328	317	295
2.7	323	298	272	264	330	317	294
2.9	328	300	277	277	326	308	292
3.1	329	297	271	267	280	330	297
3.3	331	291	278	273	294	319	292
3.5	312	282	265	277	308	328	298
3.7	324	303	262	280	294	310	295
3.9	320	297	257	274	295	285	303
4.1	297	307	262	279	297	304	279
4.3	313	296	266	278	311	317	276
4.5	308	294	266	266	324	299	283
4.7	311	295	265	269	312	292	299
4.9	304	301	258	279	339	296	280
5.1	315	298	271	287	330	303	283
5.3	311	296	266	274	326	304	279
5.5	315	310	267	283	340	311	283
5.7	310	301	273	280	323	319	282
5.9	319	295	276	275	303	299	287
6.1	319	312	276	270	317	326	272
6.3	298	319	263	272	312	302	287
6.5	318	319	277	262	326	313	289
6.7	308	331	274	263	348	319	300
6.9	318	333	266	258	346	319	295
7.1	320	344	263	267	367	315	277
7.3	329	339	279	273	356	300	283
7.5	339	339	299	272	374	308	275
7.7	334	333	305	279	393	336	279
7.9	344	343	286	279	370	346	282
8.1	342	343	271	271	353	347	282
8.3	292	297	283	274	351	331	296
8.5	307	310	280	273	342	325	291
8.7	315	308	268	275	309	335	291
8.9	311	320	269	281	323	336	303
9.1	324	328	283	276	333	287	295
9.3	344	333	277	270	329	302	300
9.5	350	336	281	267	364	297	301
9.7	355	330	281	277	355	299	299
9.9	338	325	299	285	362	299	284
10.1	336	350	285	285	374	317	294
10.3	333	338	281	283	374	320	275
10.5	281	333	284	282	374	333	280
10.7	299	331	288	293	378	335	284
10.9	297	294	281	284	370	329	287

Table 5-46(Cont.): Weld metal microhardness surveys

Distance from Cap OD (mm)	Process Variation HV0.5				Preheat variation HV0.5		
	Single TC	Tandem TC	Dual TC	Dual Tandem TC	RT TC	100°C TC	180°C TC
11.1	302	305	287	284	375	339	300
11.5	323	312	302	296	340	344	305
11.7	329	328	300	299	336	343	301
11.9	331	336	300	281	326	343	312
12.1	320	334	280	287	305	316	287
12.3	326	317	280	298	293	312	291
12.5	310	334	281	297	295	313	291
12.7	307	310	286	281	304	288	293
12.9	310	333	295	283	329	294	279
13.1	275	281	288	280	338	301	279
13.3	302	310	279	280	331	307	283
13.5	284	301	268	284	350	307	281
13.7	283	303	271	280	353	323	279
13.9	295	308	274	282	347	326	292
14.1	302	311	276	278	358	326	286
14.3	305	324	278	279	339	342	296
14.5	311	322	276	283	318	344	300
14.7	315	313	266	271	319	350	289
14.9	296	324	278	279	310	347	298
15.1	287	323	272	294	307	335	288
15.3	294	325	277	281	307	299	309
15.5	287	291	270	283	280	304	268
15.7	263	291	267	281	303	307	281
15.9	276	286	272	273	289	297	287
16.1	278	293	266	269	289	269	301
16.3	280	296	278	270	297	289	270
16.5	282	288	270	273	313	283	274
16.7	291	295	262	266	316	268	275
16.9	288	305	286	275	323	287	270
17.1	296	312	285	280	315	296	280
17.3	295	311	252	277	320	301	276
17.5	270	302	235	221	298	289	269
17.7	262	312	224	226	324	283	270
17.9	238	292	230	223	329	299	266
18.1	234	252	229	220	316	299	272
18.3	243	259	227	231	315	283	280
18.5	249	254	237	244	326	283	285
18.7	231	244	219	226		288	280
18.9	237	234	214	222		279	
19.1	226	237	218	216			
19.3	231	240	216	215			
19.5			208	221			
19.7				213			
Average	**303**	**307**	**269**	**271**	**331**	**313**	**288**

Vertical traverse through pipe wall thickness, beginning in cap weld metal. Negative numbers signify distance above pipe OD surface

Table 5-47: Plate trial thermocycle data for solid wire (SW) and metal cored (MC) base-line alloy composition (0.9Ni 0.3Mo)

	Cooling times from 800°C to 500, 400 or 300°C (s)					
Weld Pass	SW t_{85}	MC t_{85}	SW t_{84}	MC t_{84}	SW t_{83}	MC t_{83}
Fill 1 (root)	2.14	2.51	4.23	4.71	9.23	10.68
Fill 2	2.08	2.24	4.28	4.22	8.50	8.28
Fill 3	2.28	2.64	4.19	4.13	7.85	8.03
Fill 4	2.56	2.66	4.64	4.44	8.98	8.59
Fill 5	3.03	3.18	5.21	5.32	9.55	10.21
Fill 6	3.16	4.05	5.68	6.30	10.12	11.50
Fill 7(cap)	4.07	4.38	6.41	6.64	11.08	11.52

	Transition temperatures (°C)					
Weld Pass	SW transition start temperature	MC transition start temperature	SW maximum rate of transition temperature	MC maximum rate of transition temperature	SW transition finish temperature	MC transition finish temperature
Fill 1 (root)	513	523	486	491	439	446
Fill 2	476	516	445	476	411	430
Fill 3	521	537	452	501	442	450
Fill 4	524	554	499	514	449	455
Fill 5	528	551	507	517	453	458
Fill 6	518	566	495	542	443	481
Fill 7(cap)	534	562	519	543	462	480

	Cooling rates (°C/s)					
Weld Pass	SW cooling rate at 800°C (°C/s)	MC cooling rate at 800°C (°C/s)	SW cooling rate at 600°C (°C/s)	MC cooling rate at 600°C (°C/s)	SW cooling rate at 400°C (°C/s)	MC cooling rate at 400°C (°C/s)
Fill 1 (root)	284	258	139	117	41	36
Fill 2	273	264	130	127	42	47
Fill 3	265	242	129	127	44	48
Fill 4	242	238	117	112	37	45
Fill 5	225	220	107	100	35	37
Fill 6	195	178	94	77	33	34
Fill 7(cap)	161	152	88	70	34	34

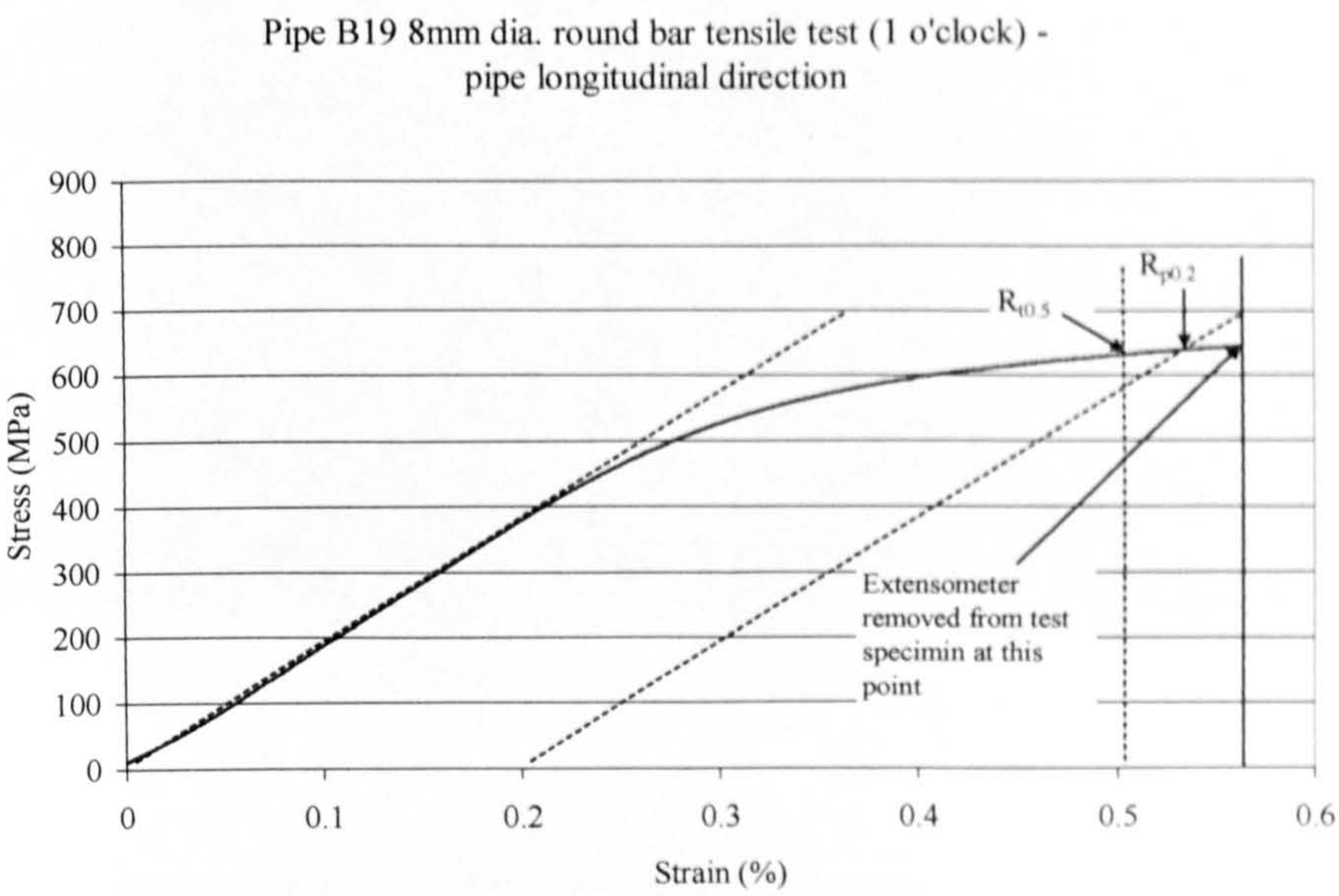

(a) Stress/strain curve showing close matching of $R_{p0.2}$ and $R_{t0.5}$

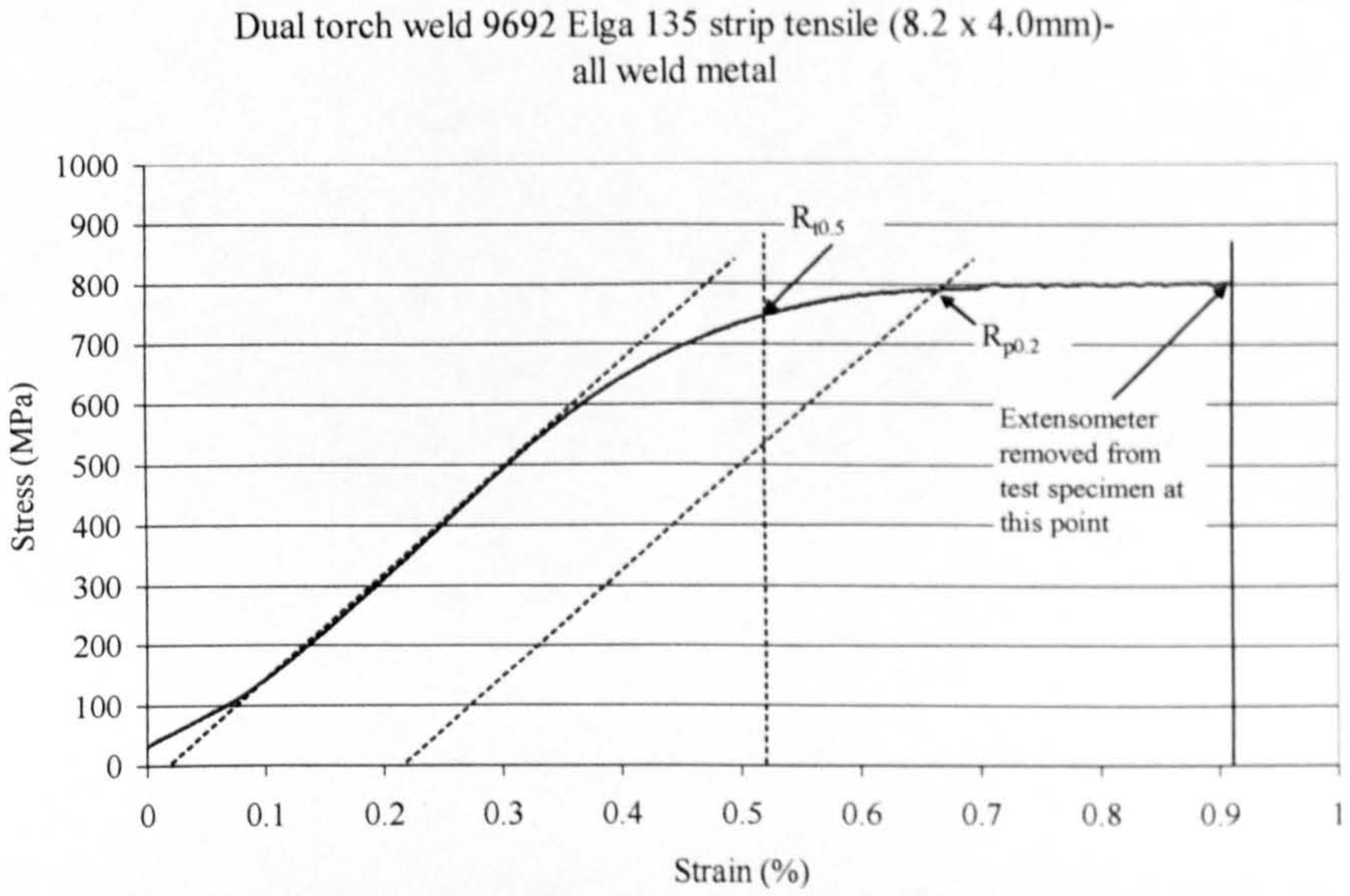

(b) Stress/strain curve showing ~50MPa discrepancy between $R_{p0.2}$ and $R_{t0.5}$

Figure 5-1: Example stress-strain curves

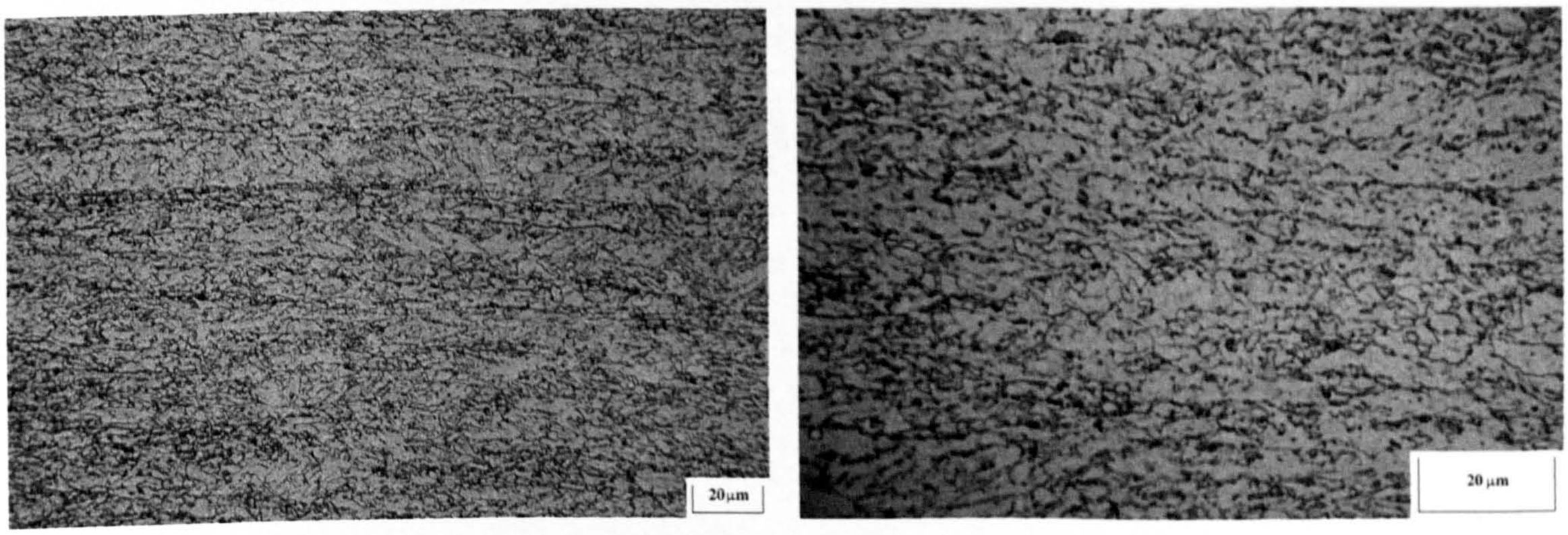

Figure 5-2: Pipe A Base Material Microstructure (1/3 thickness from outer surface)

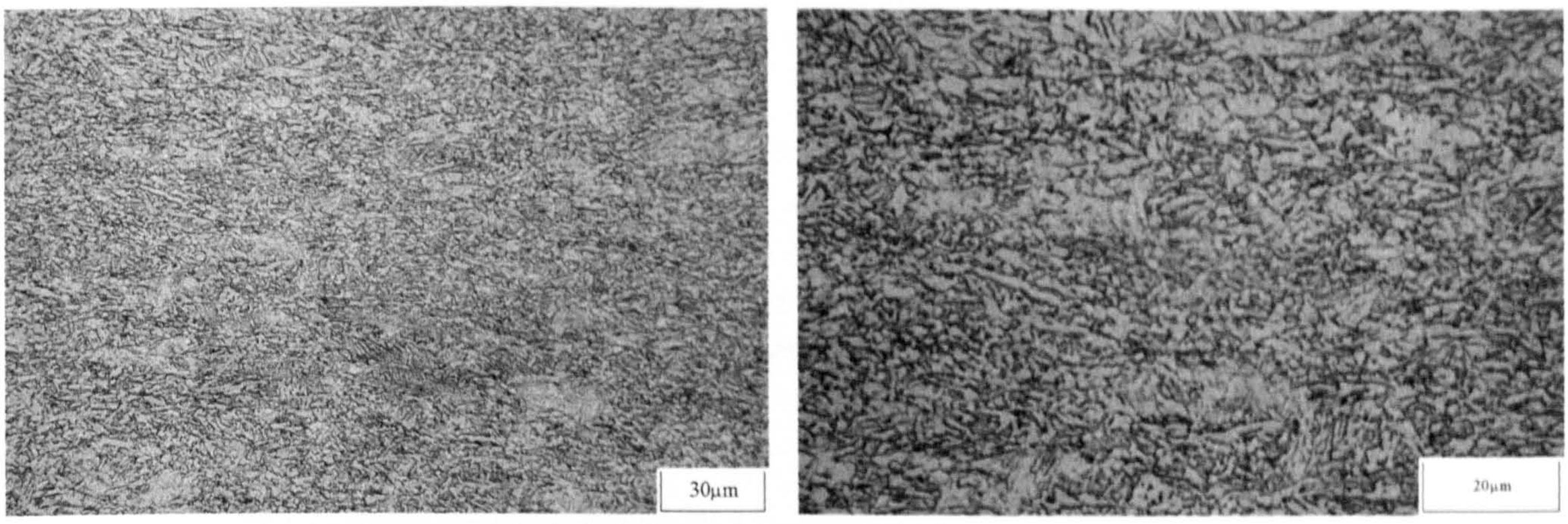

Figure 5-3: Pipe B15 Base Material Microstructure (1/3 thickness from outer surface)

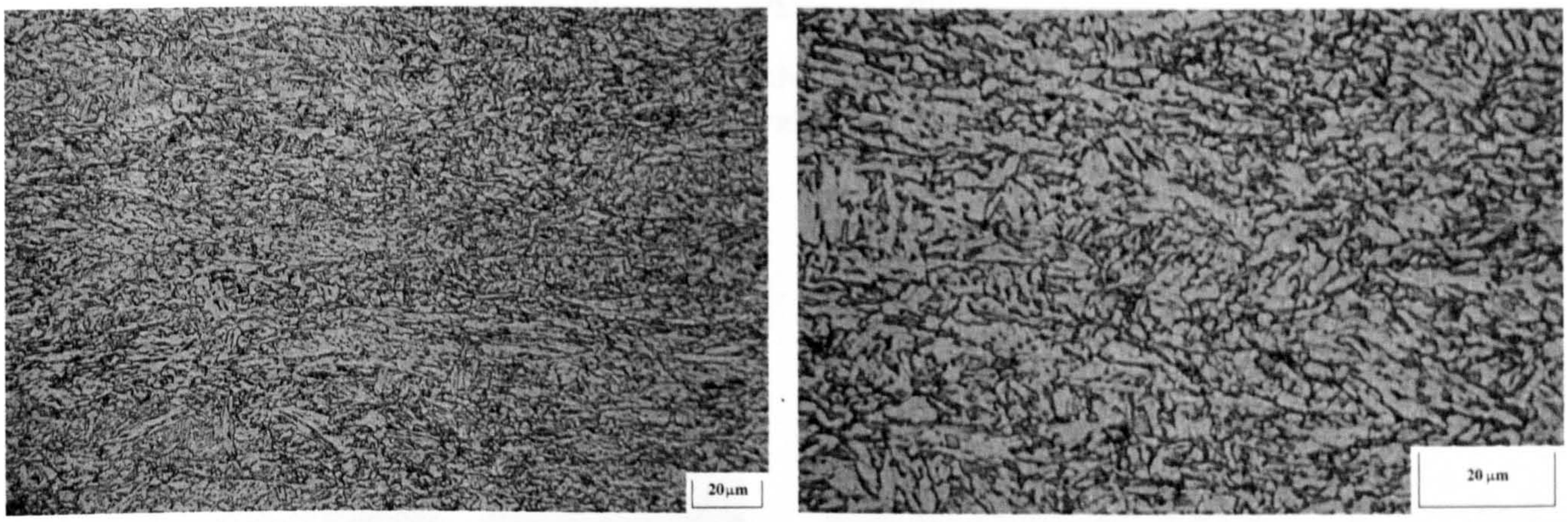

Figure 5-4: Pipe B19 Base Material Microstructure (1/3 thickness from outer surface)

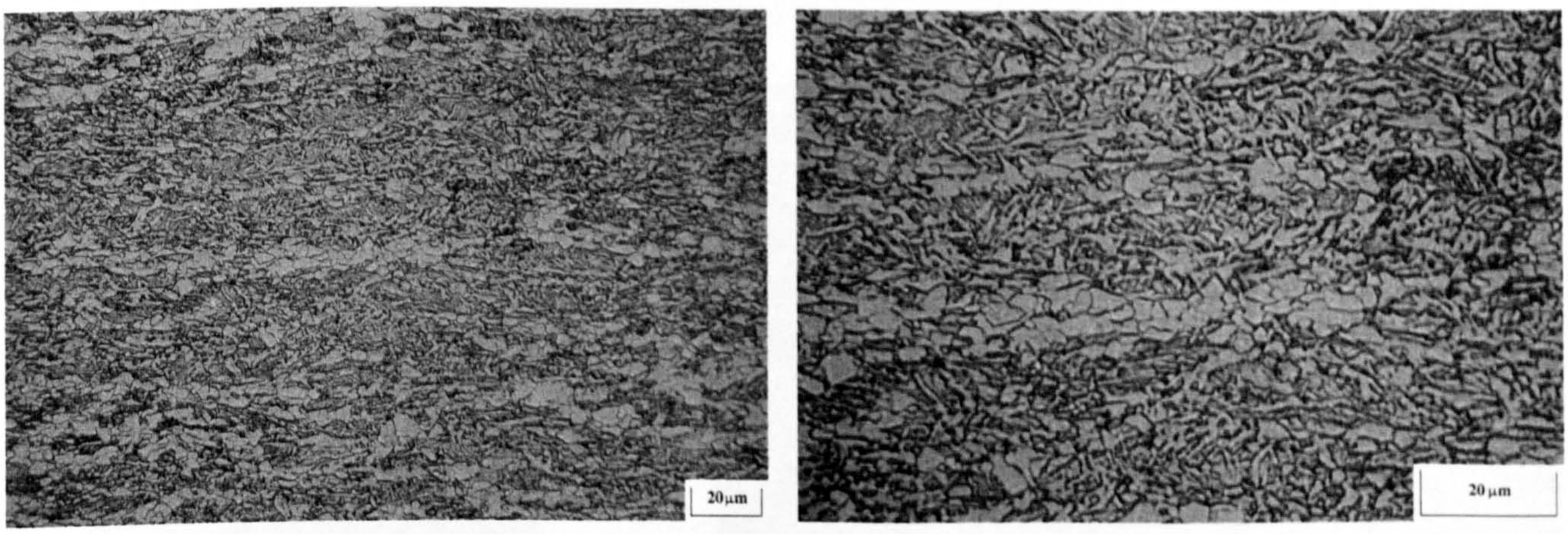

Figure 5-5: Pipe C Base Material Microstructure (1/3 thickness from outer surface)

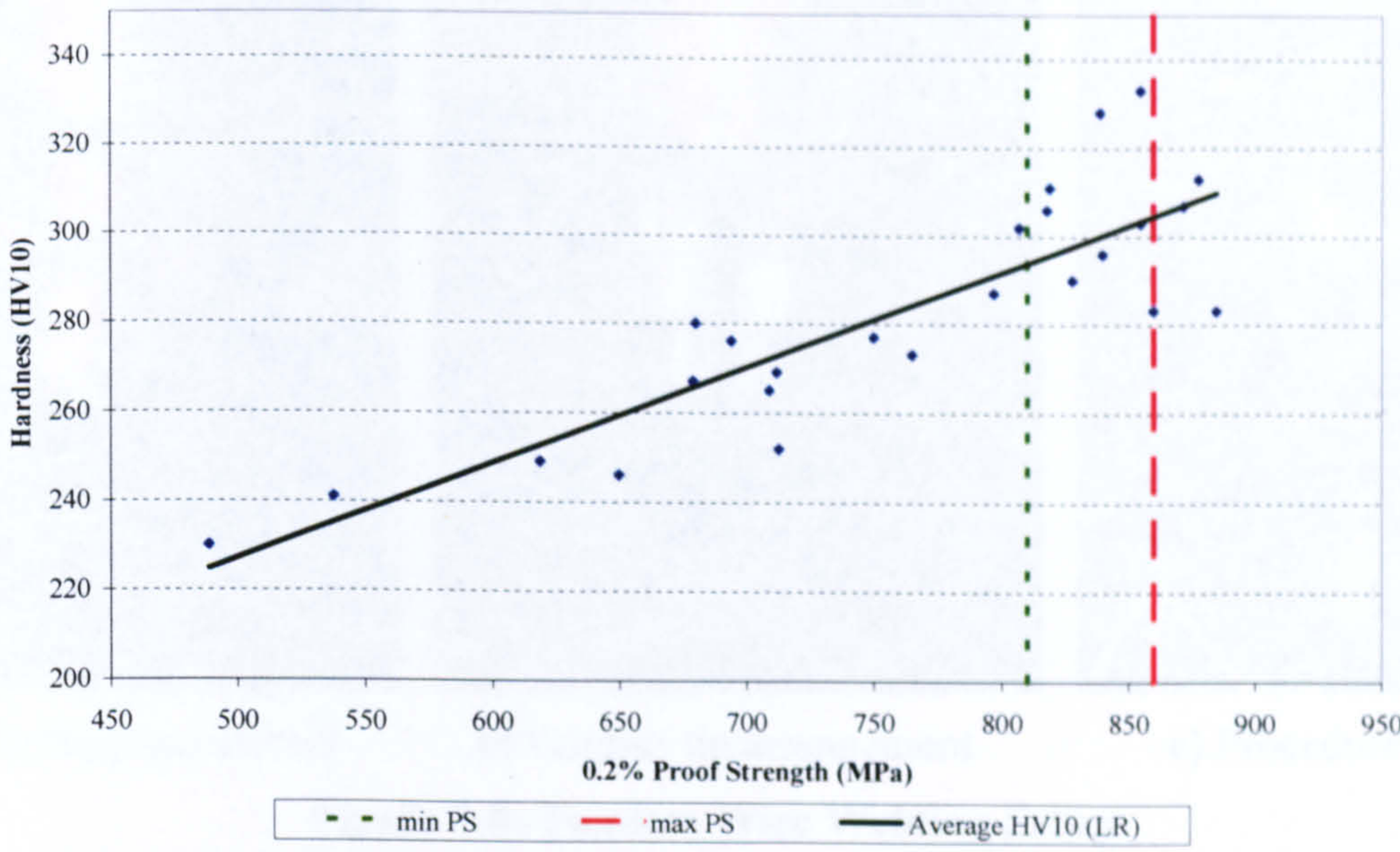

Figure 5-6: Regression Analysis of 60° Bevel Joints (As Cast Weld Metal) for Hardness/$R_{p0.2}$ Correlation

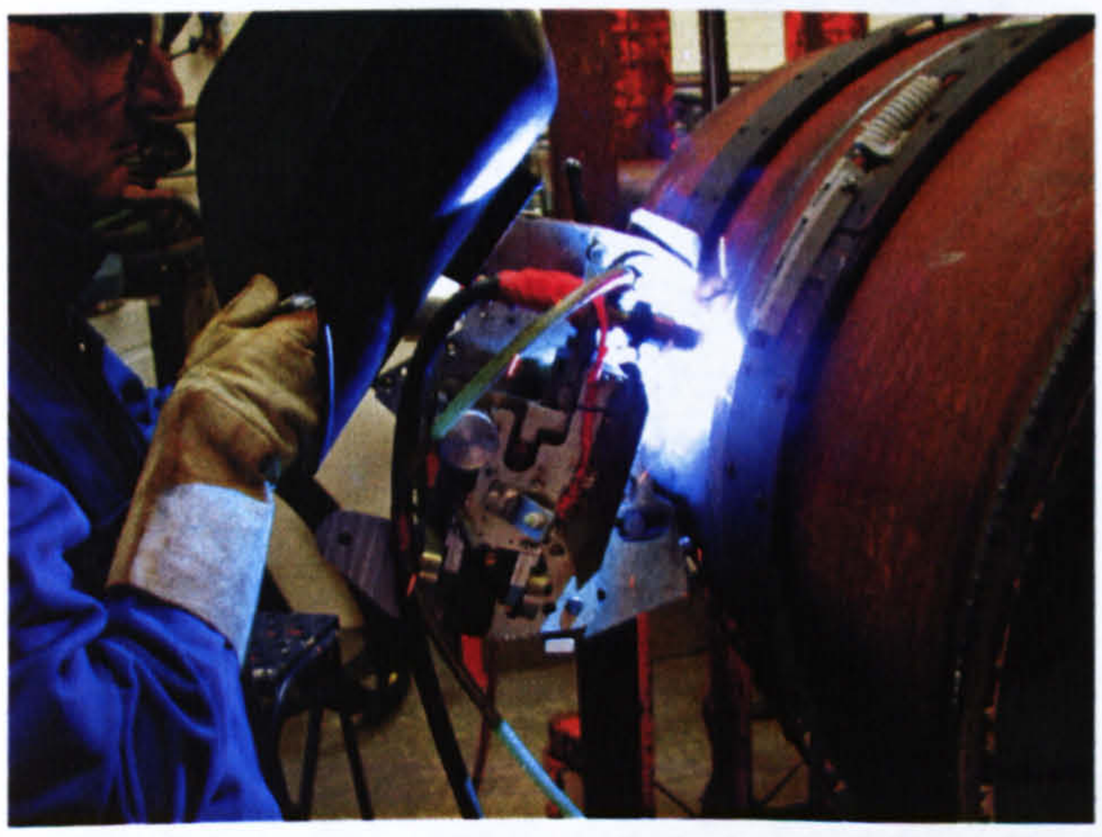

a) ASME IX 5G welding

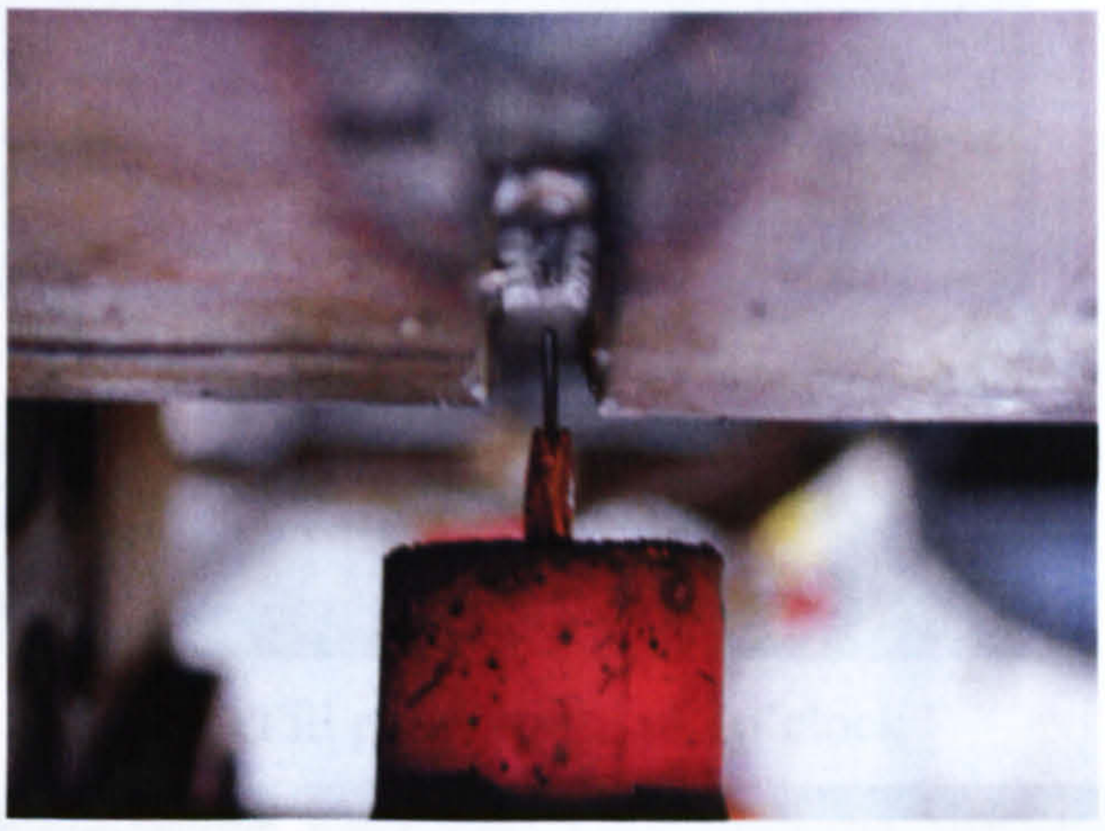

b) Typical bead profile at 6 o'clock

c) Typical single wire cap profile

d) Welded pipe section

Figure 5-7: Single Wire Weld Procedure Generation

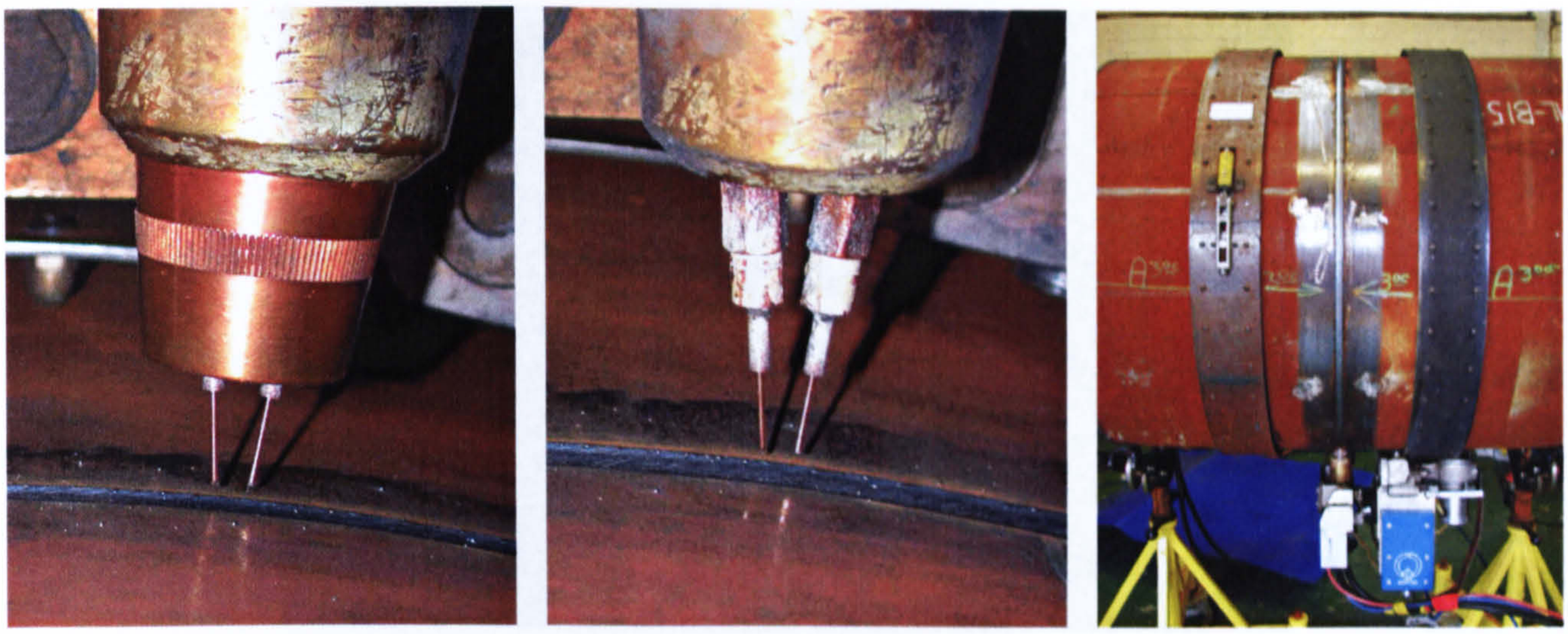

a) Torch with long gas shroud b) Contact tip arrangement c) Procedure set-up

Figure 5-8: Tandem Wire Welding Setup

a) Bevel geometry prior to internal root b) Fill pass profile at 6 o'clock

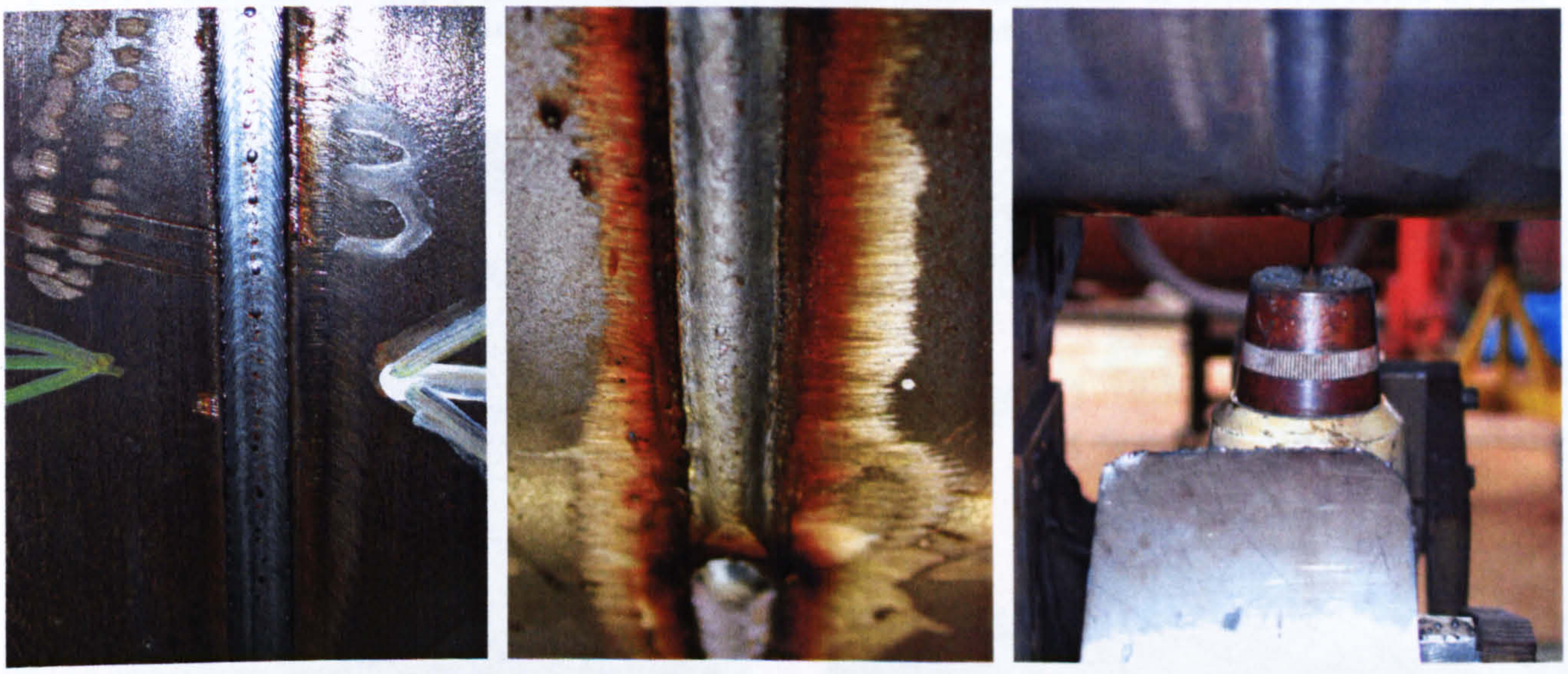

c) 3 0'c tandem cap profile d) 6 o'c tandem cap profile e) 6 o'c tandem cap profile

Figure 5-9: Tandem Wire Joint Profiles

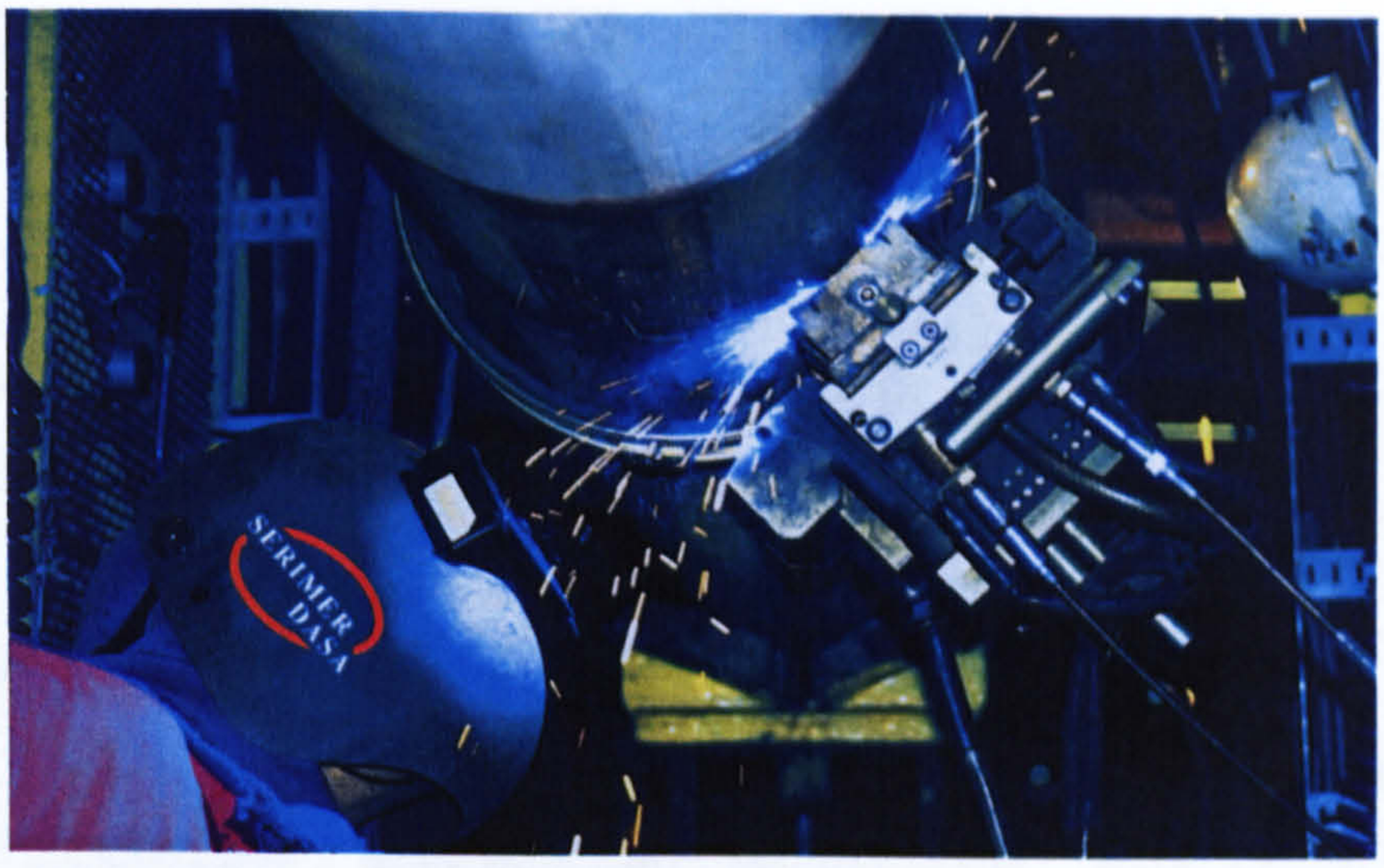

Figure 5-10: Dual torch welding (picture courtesy of Serimer-Dasa)

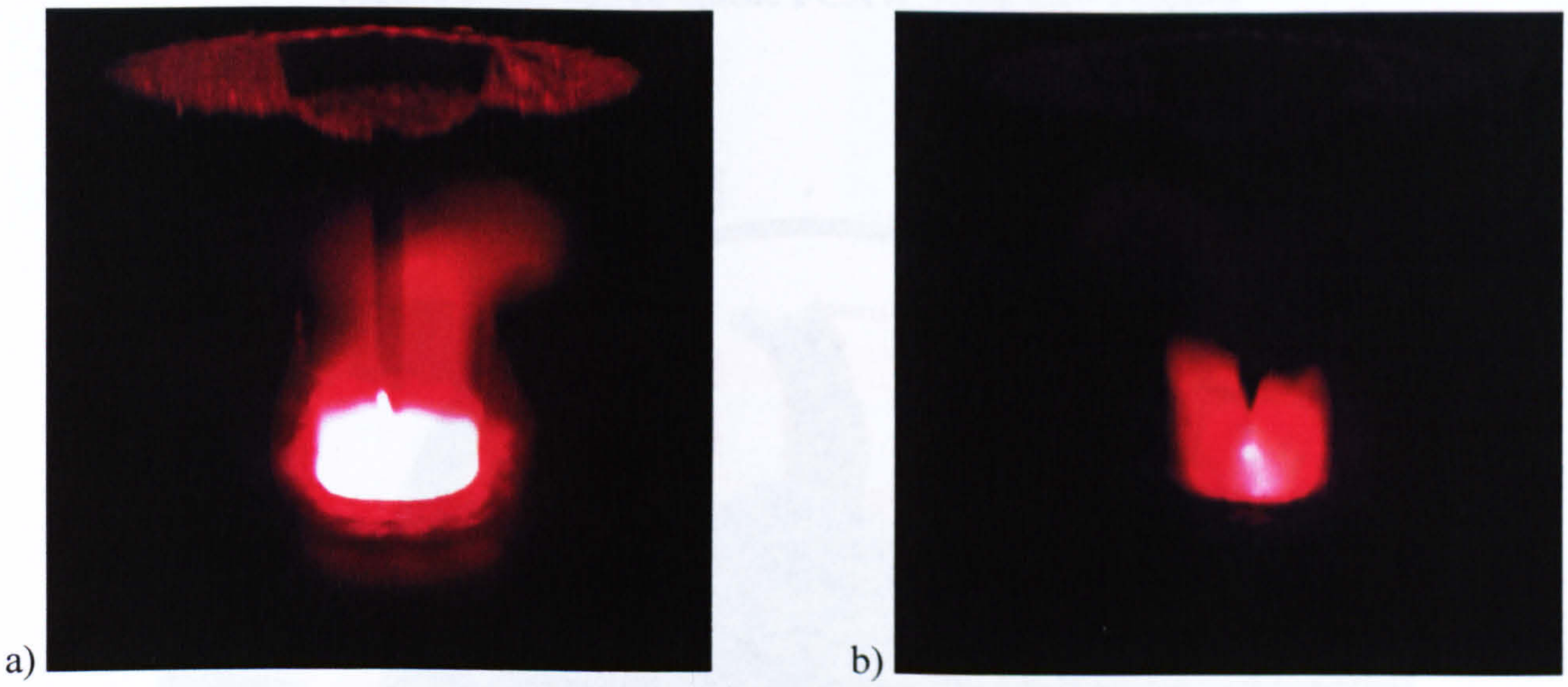

a) b)

Figure 5-11: Narrow gap pulsed welding – mid pipe wall thickness of 19.05mm X100 a) peak current pulse b) base current arc maintenance

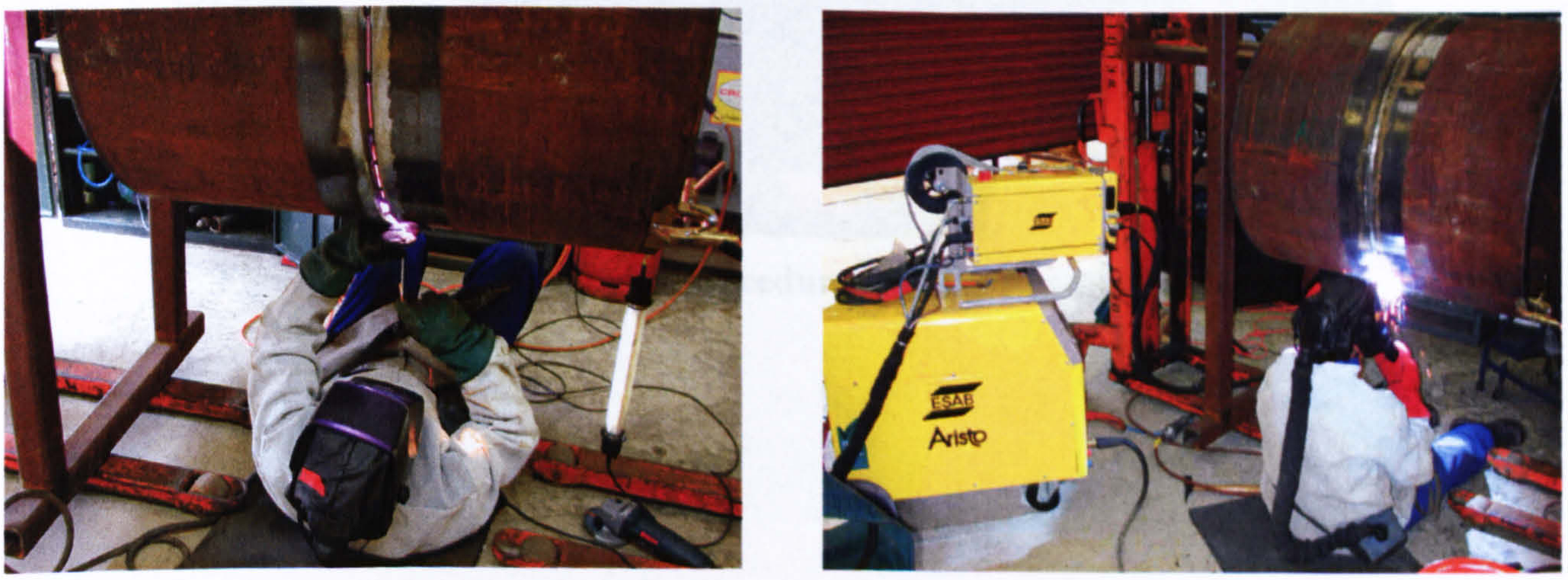

a) SMAW root welding b) FCAW fill and cap welding

Figure 5-12: Tie-in procedure welding

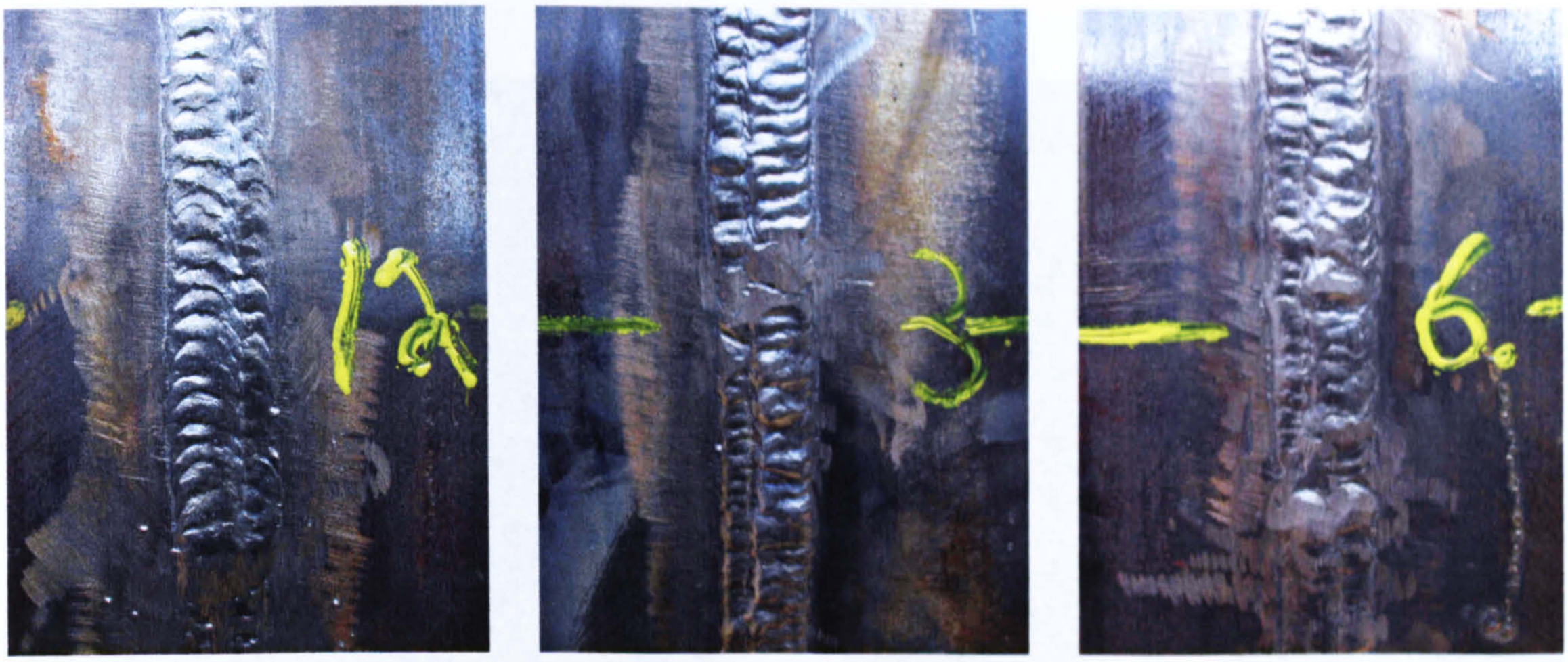

a) 12 o'clock b) 3 o'clock c) 6 o'clock

Figure 5-13: Tie-In Rutile FCAW Wire Cap Profiles

Figure 5-14: Typical repair procedure welding (internal root repair)

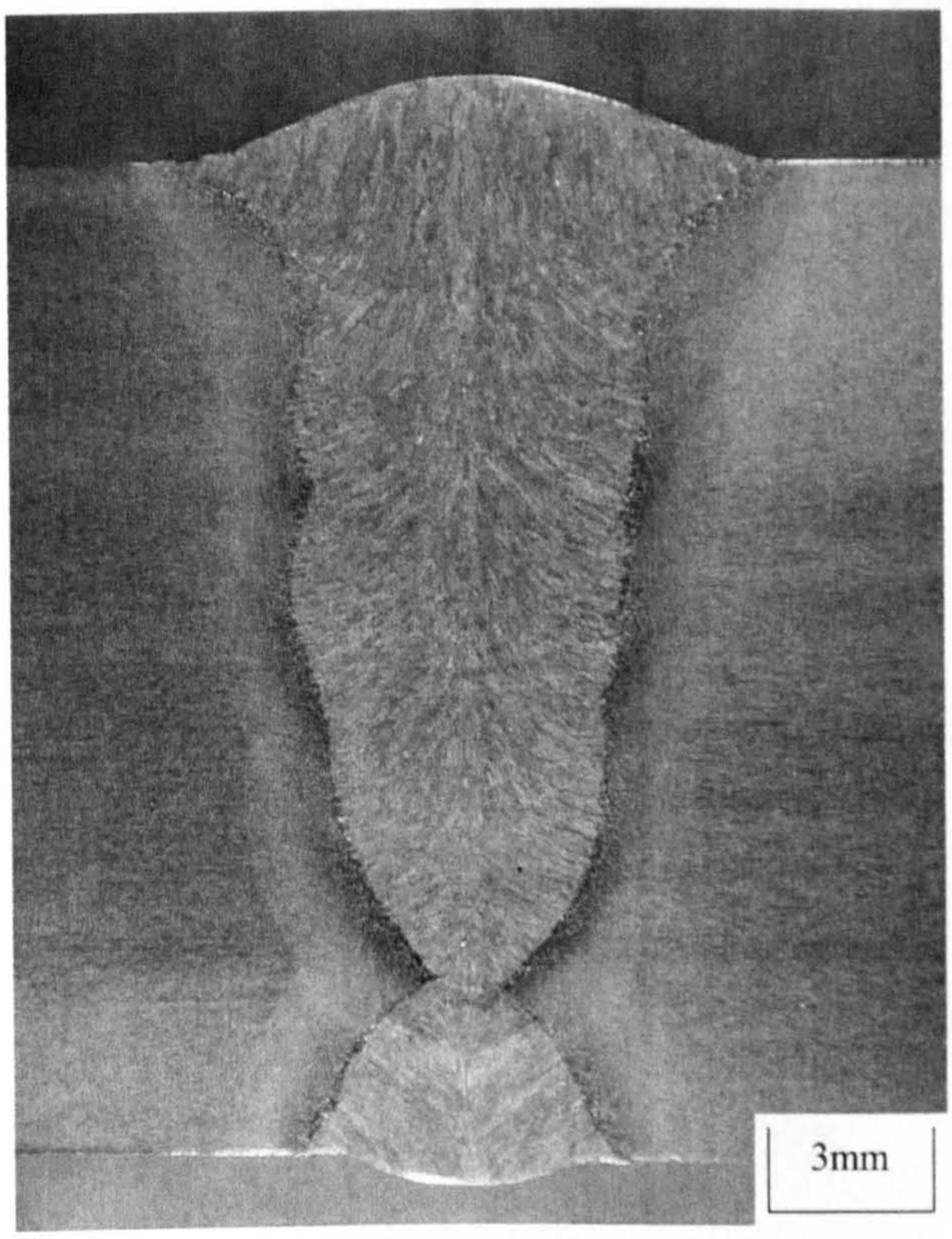

Carbofil HT, Pulsed, Pipe B19
(internal/external procedure)

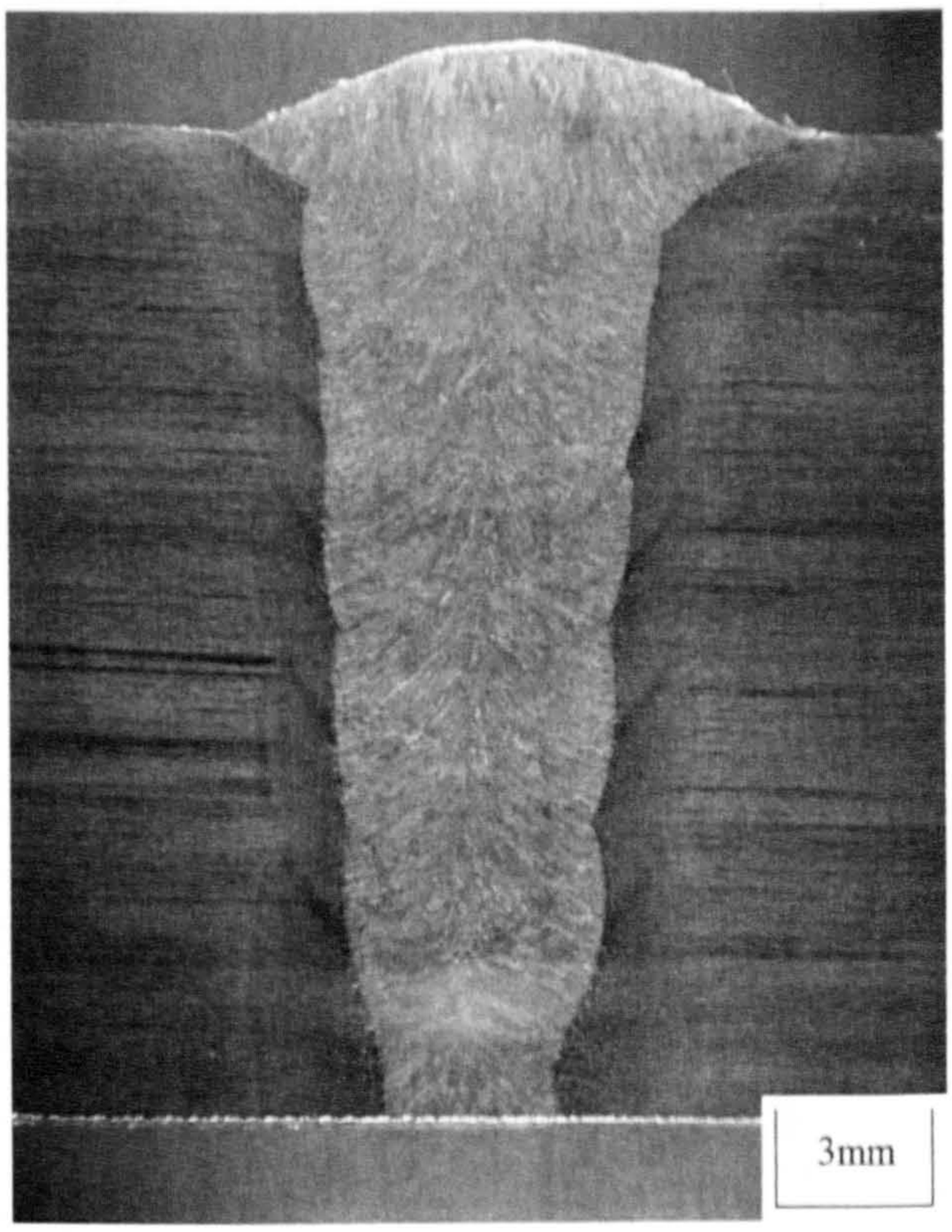

Carbofil HT, Pulsed, Pipe A
(all external procedure)

Figure 5-15: Typical single torch macro sections

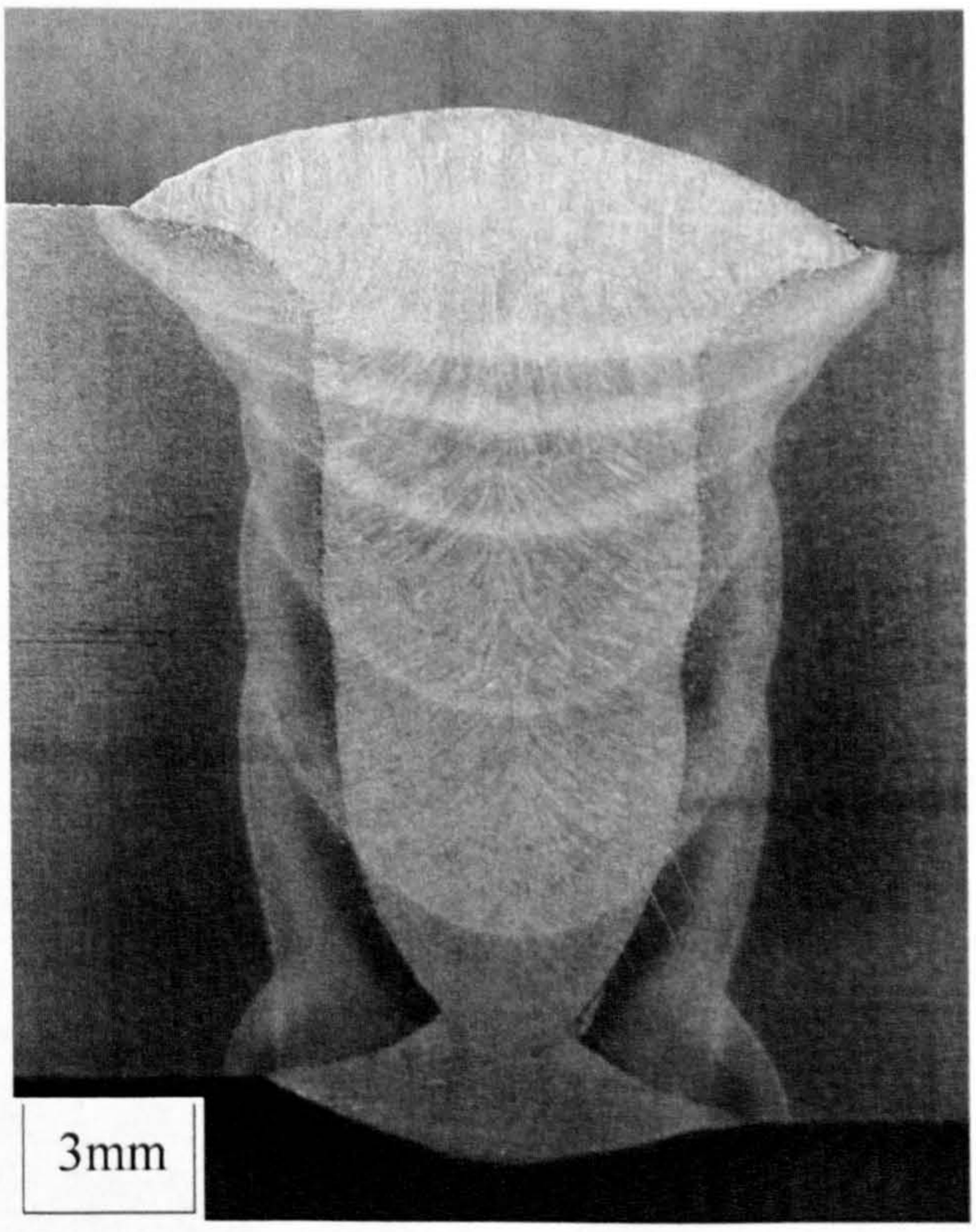

Carbofil NiMo-1, Pulsed, Pipe B15

Figure 5-16: Typical tandem wire weld macro section

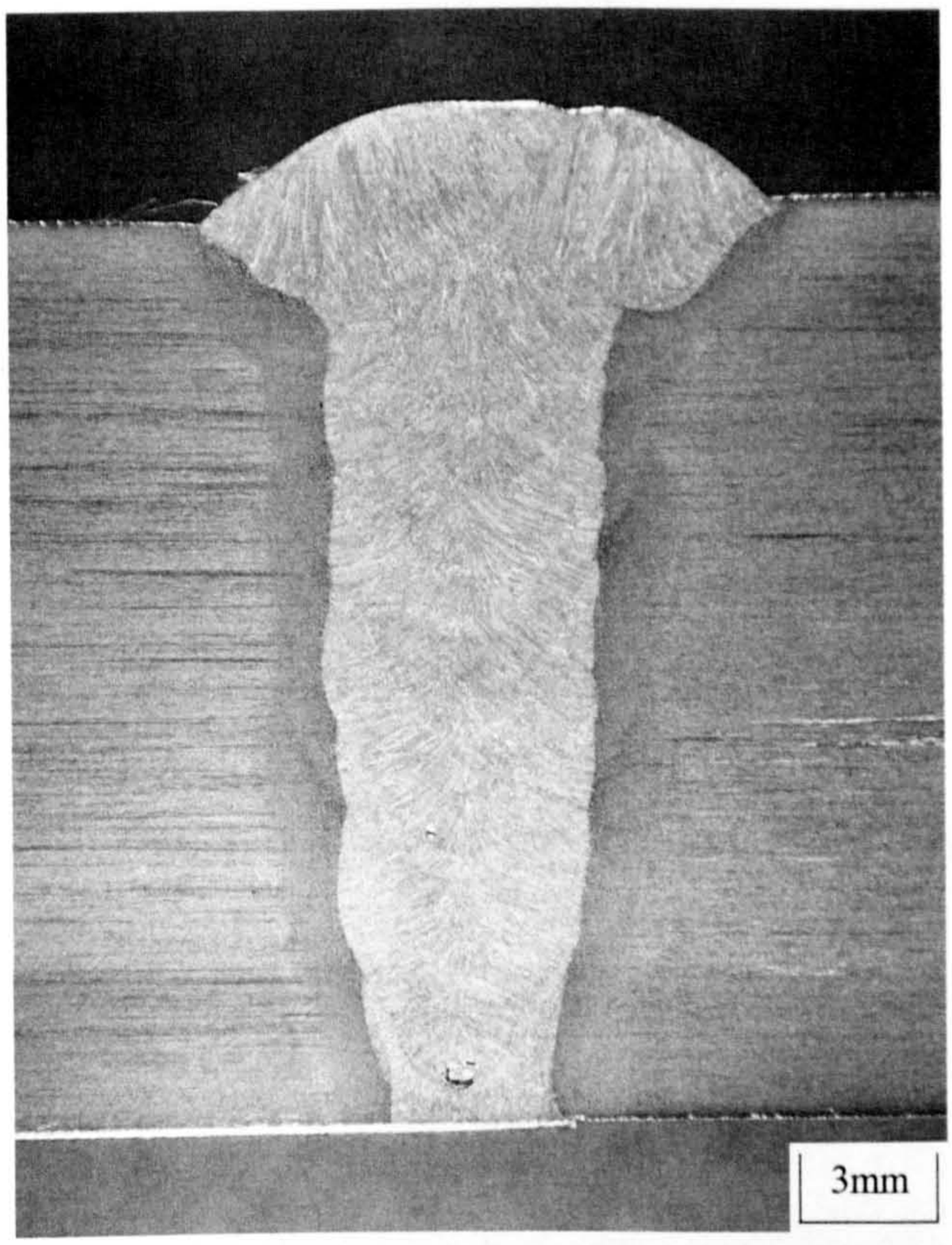

Weld 7544 (Bohler X70-IG, Dip Trans)

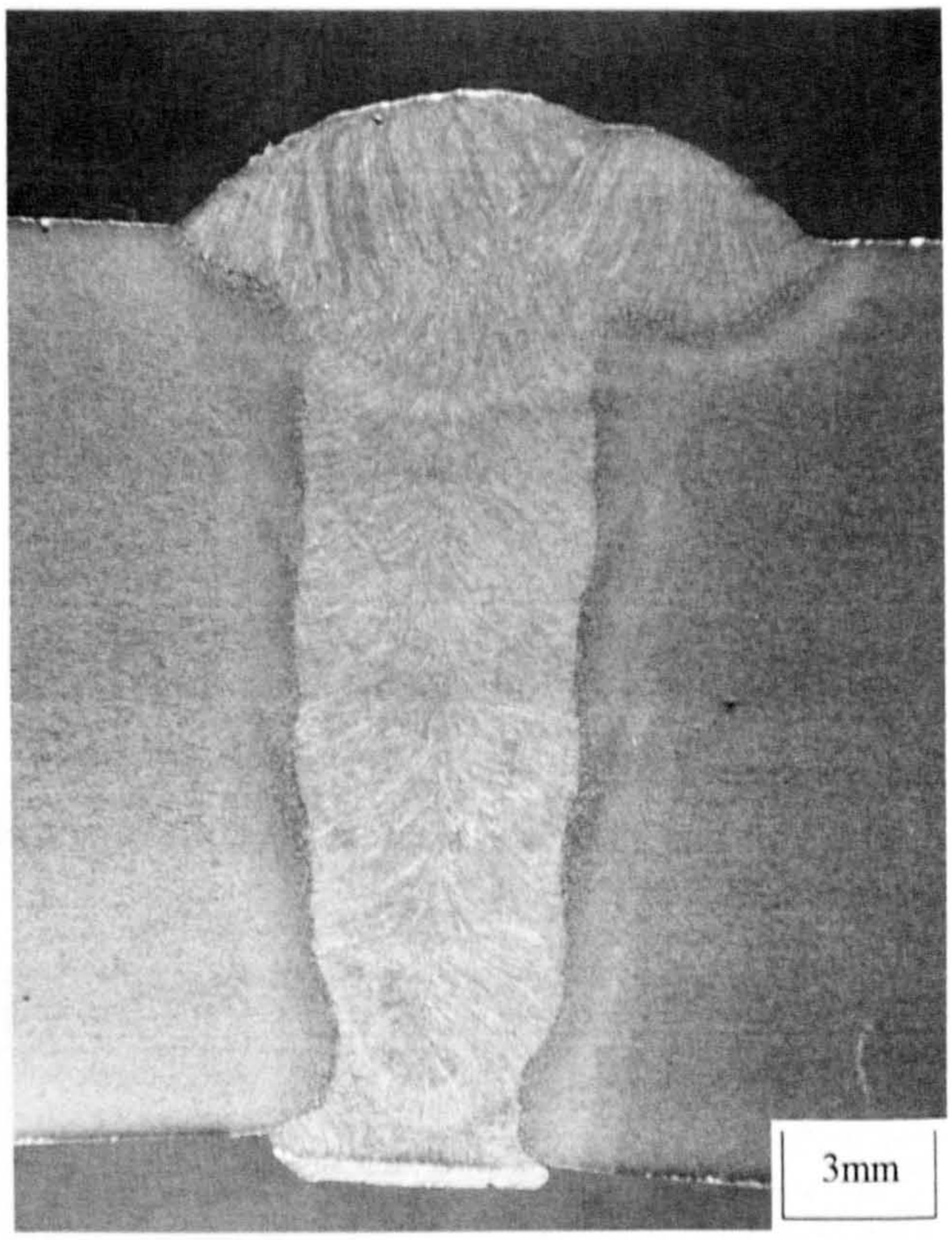

Weld 7549 (Bohler X70-IG, Dip Trans)

Figure 5-17: Typical dual torch macro sections

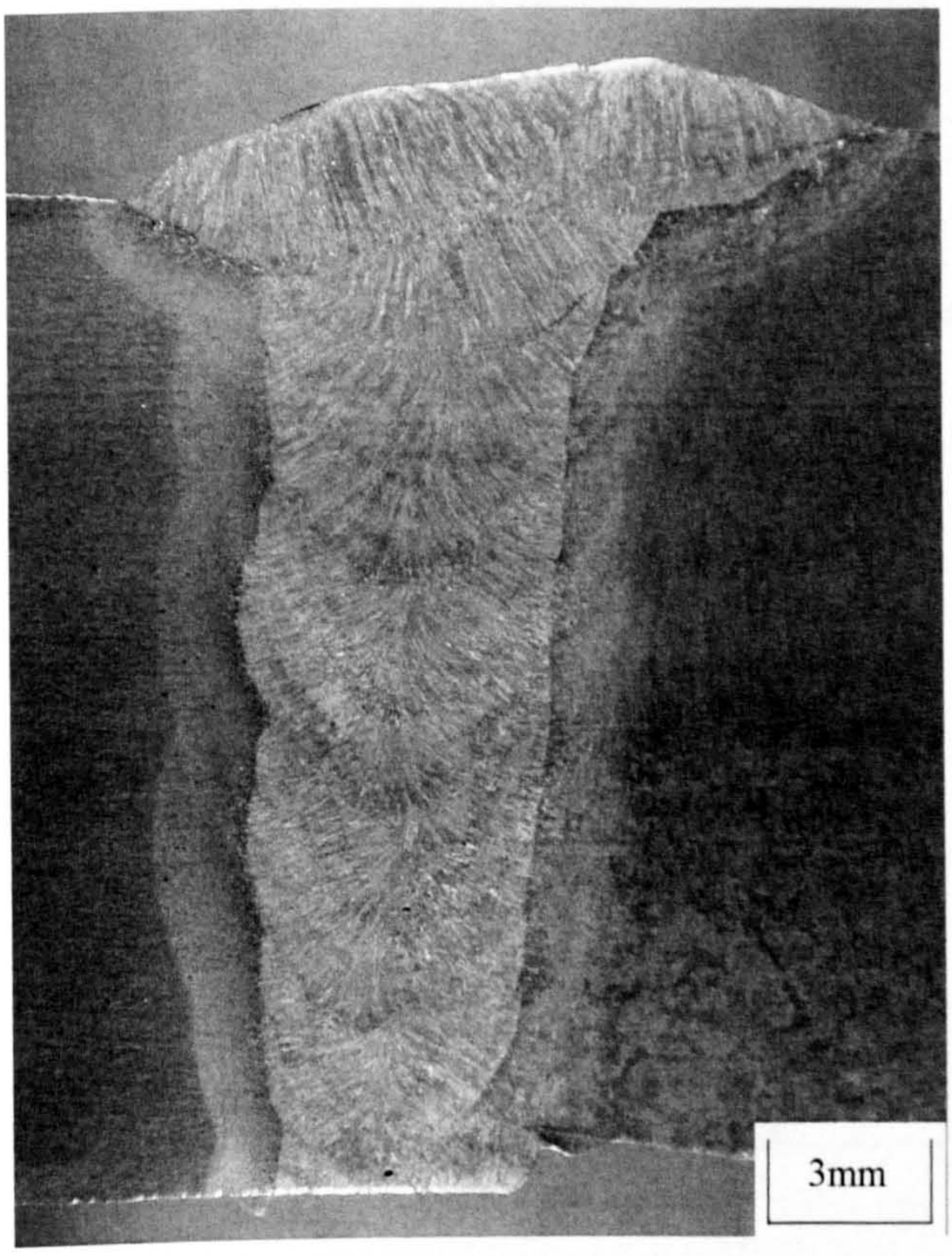

Weld 7546 (Thyssen MoNi, Dip Trans)

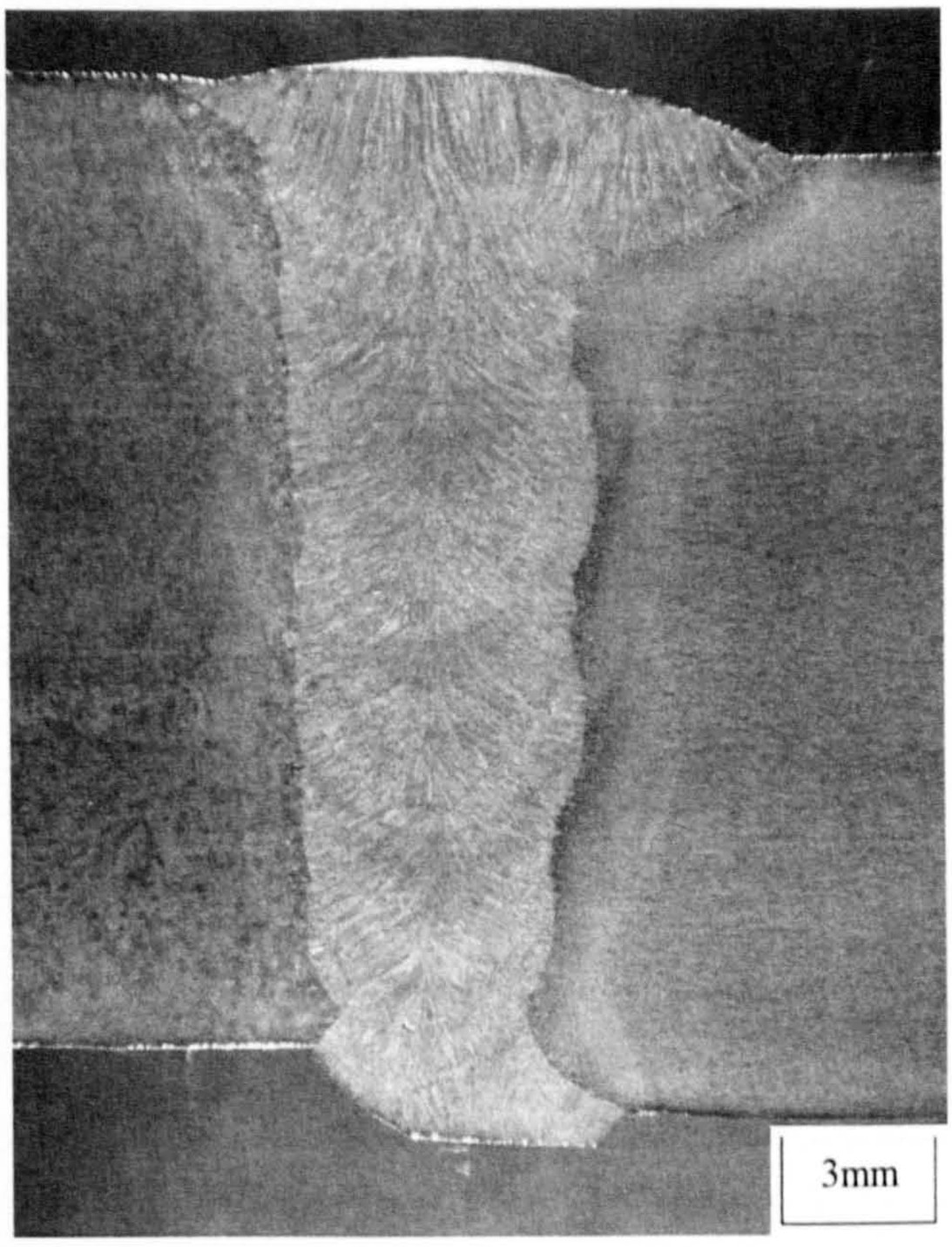

Weld 7549 (Bohler X70-IG, Dip Trans)

Figure 5-18; Typical dual torch girth/seam macro sections

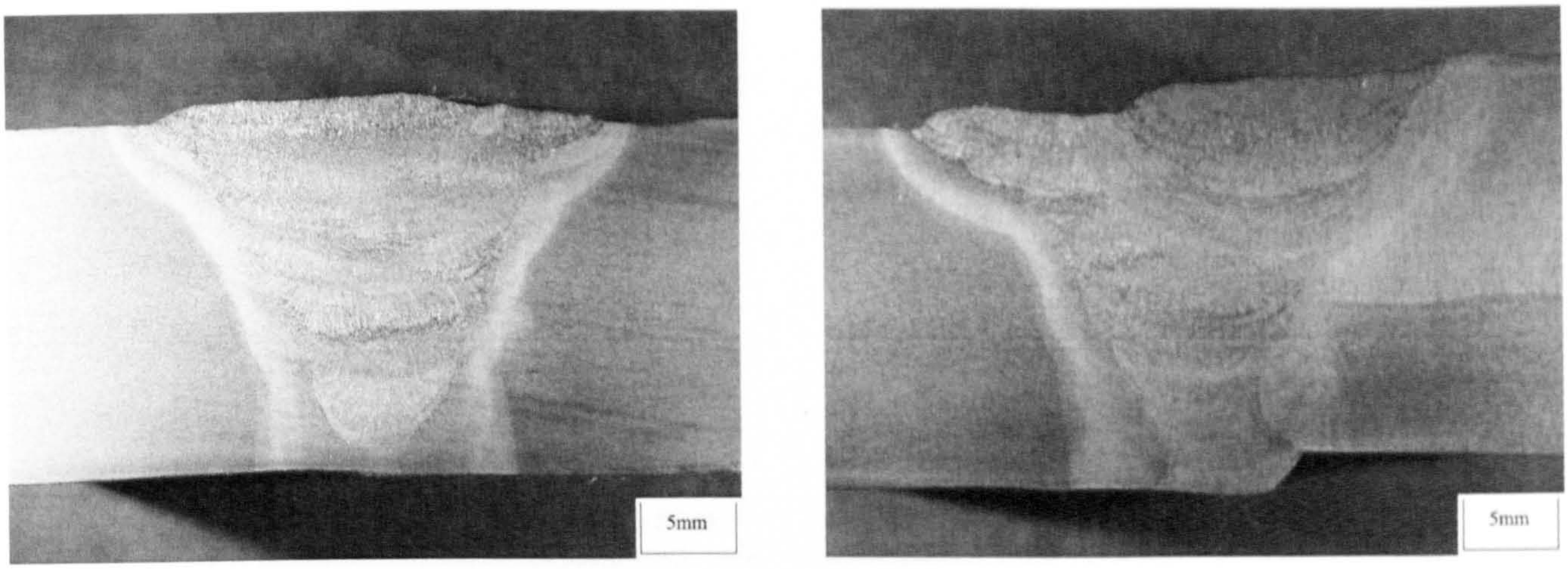

12 o'clock Girth/ Seam Weld

Figure 5-19: Tie-in (OK 15.09, 80%Ar/20%CO2) macro sections

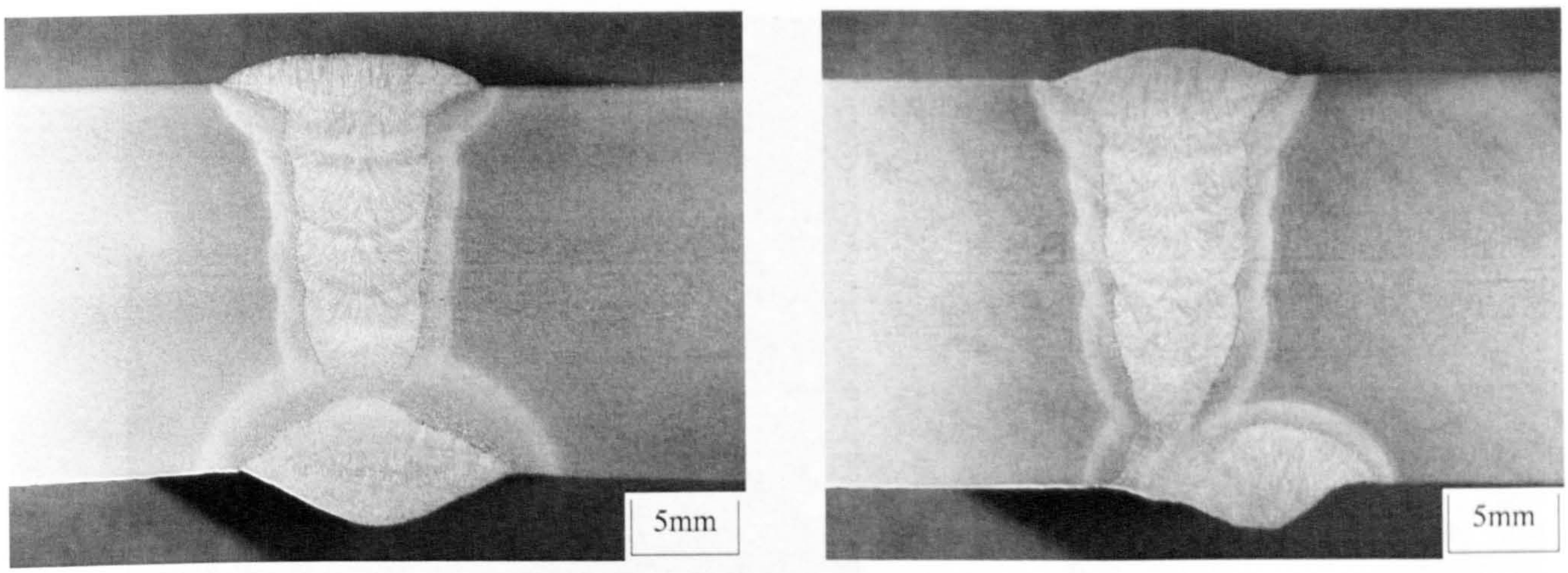

Two Pass SMAW Backweld Repair Single Pass GMAW Backweld Repair

Figure 5-20: Backweld repair macro sections

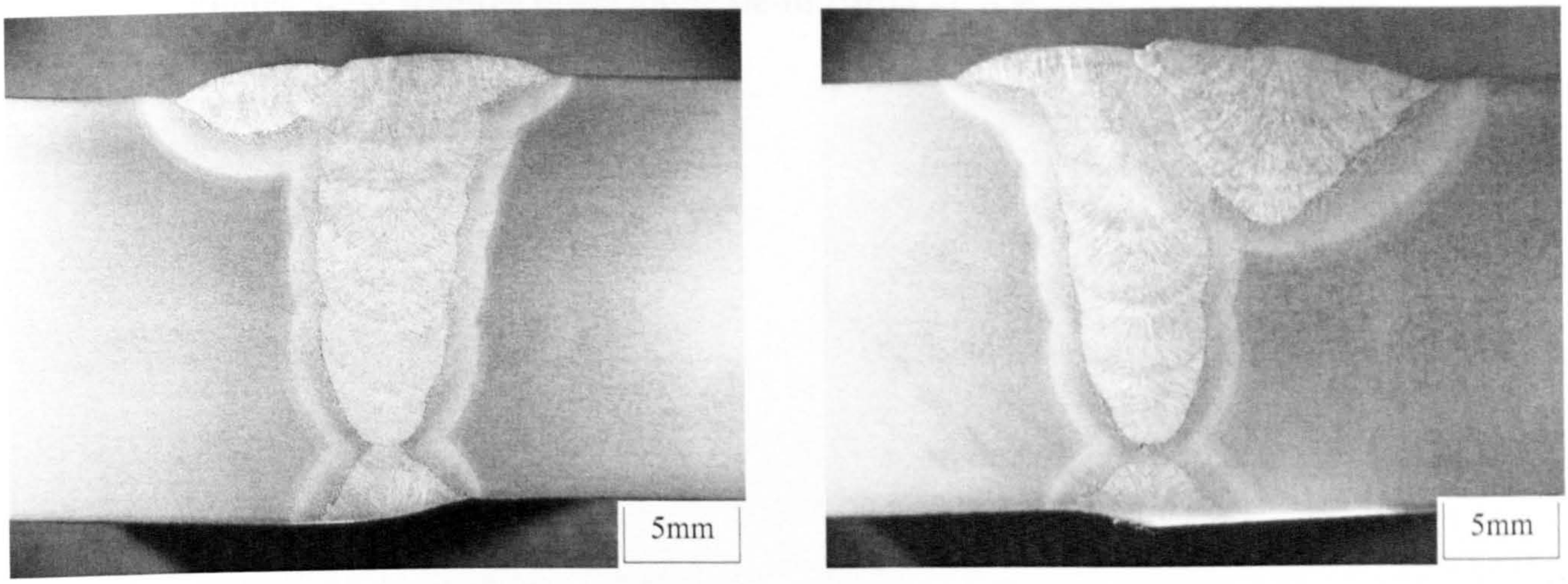

Single Pass SMAW Repair Single Pass FCAW Repair

Figure 5-21: Cap repair macro sections

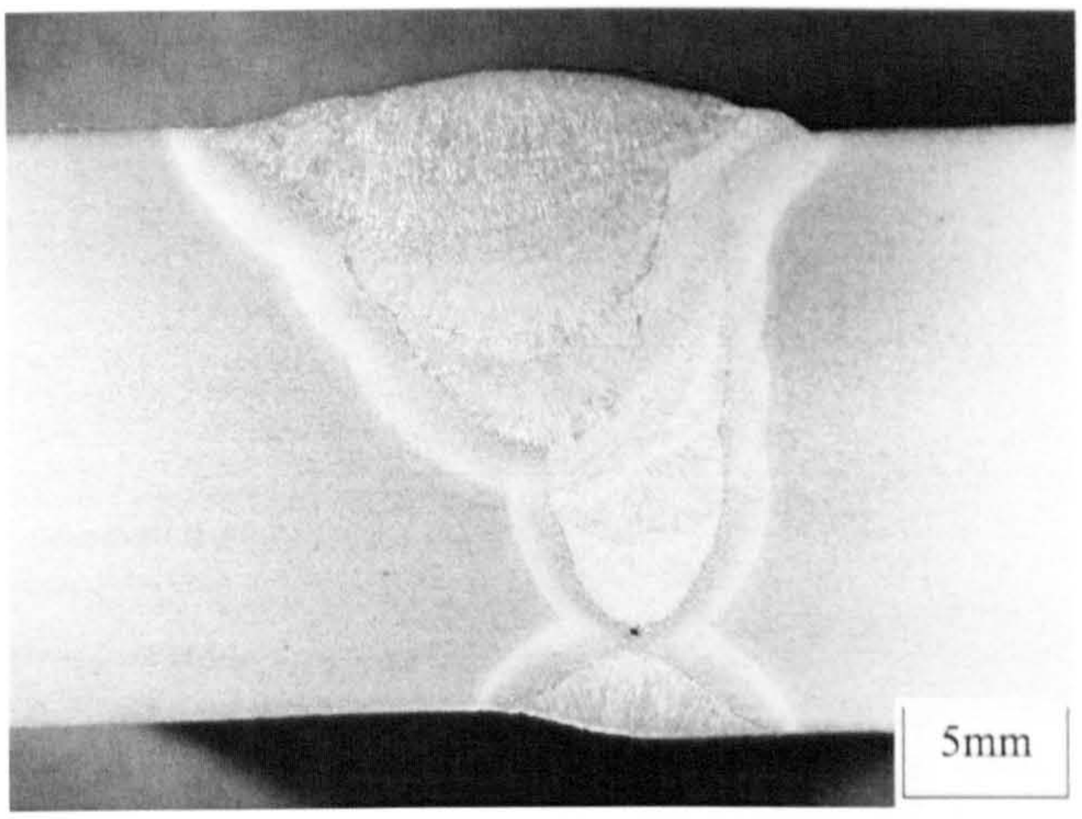

Part Penetration FCAW Repair

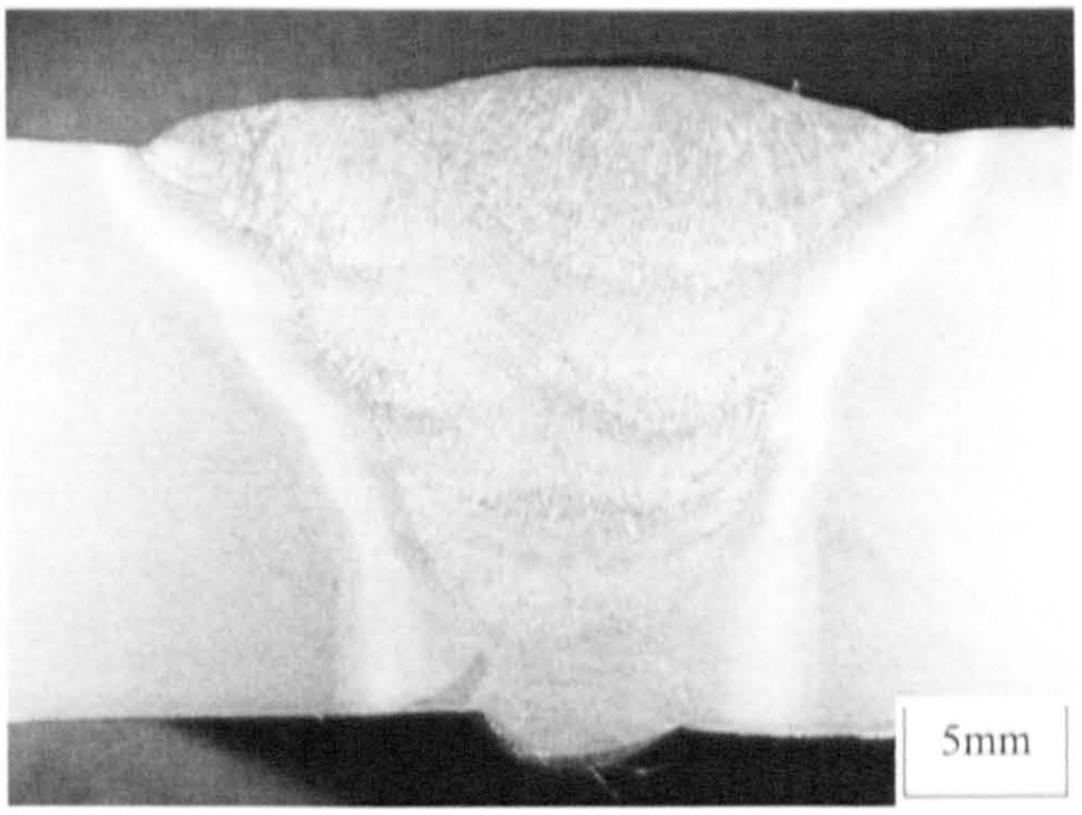

Full Penetration SMAW/FCAW Repair

Figure 5-22: Multi-pass repair macro sections

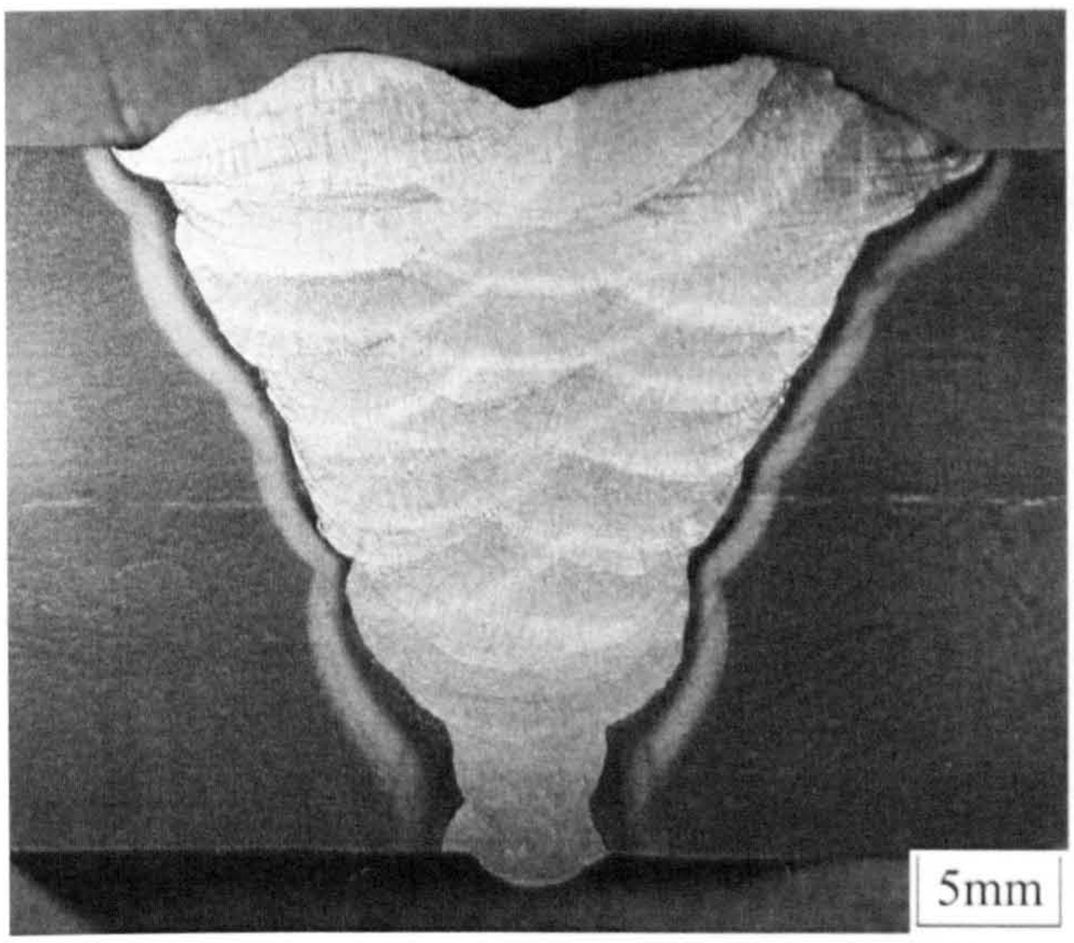

a) 50° included angle

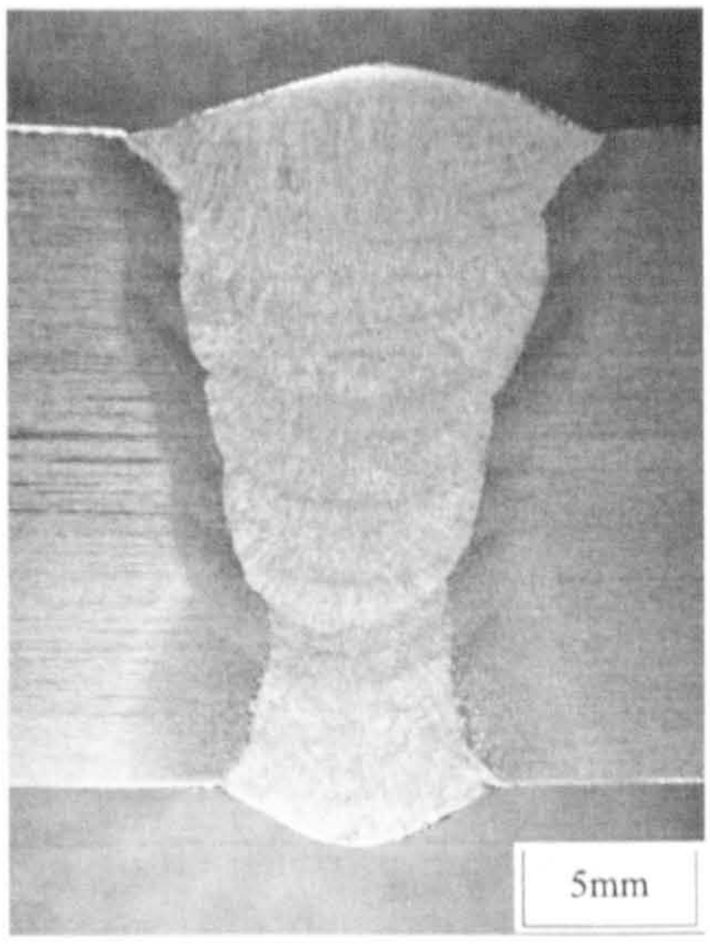

b) 30° included angle

Figure 5-23: Reduce bevel angle tie-in rutile FCAW trial macro sections

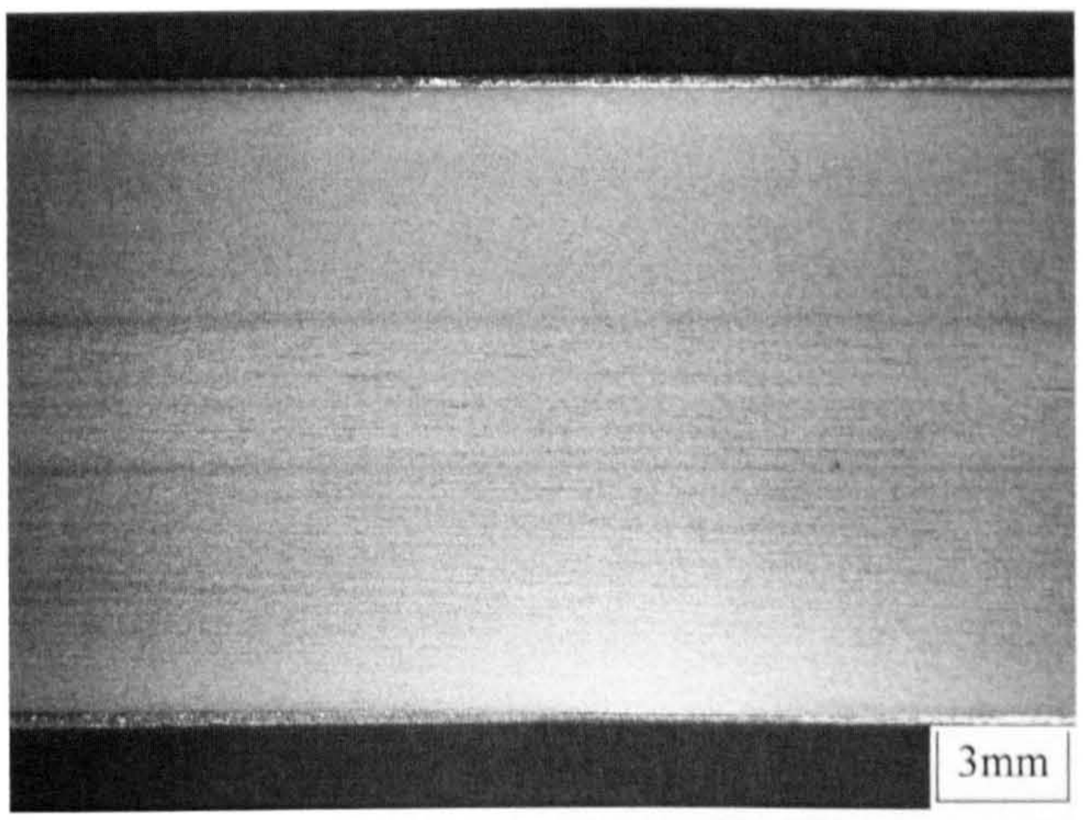

a) Pipe section without segregation

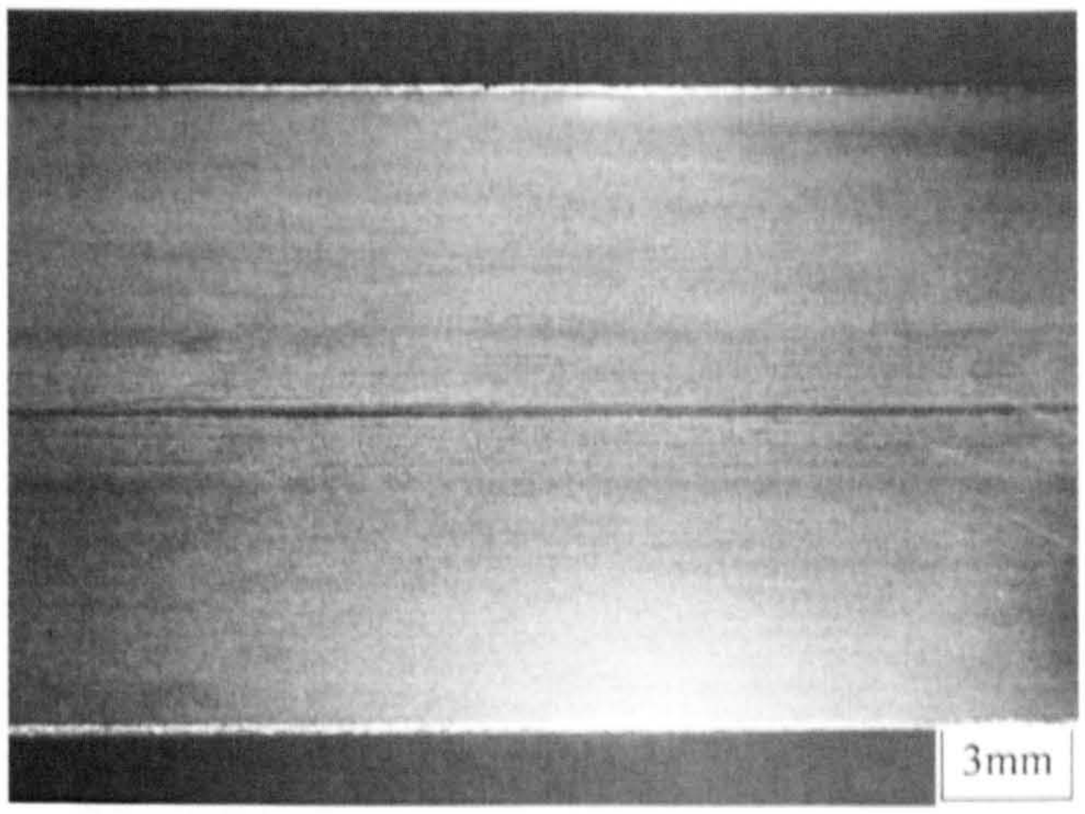

b) Same pipe material, but with segregation

Figure 5-24: Centreline segregation (pipe B15)

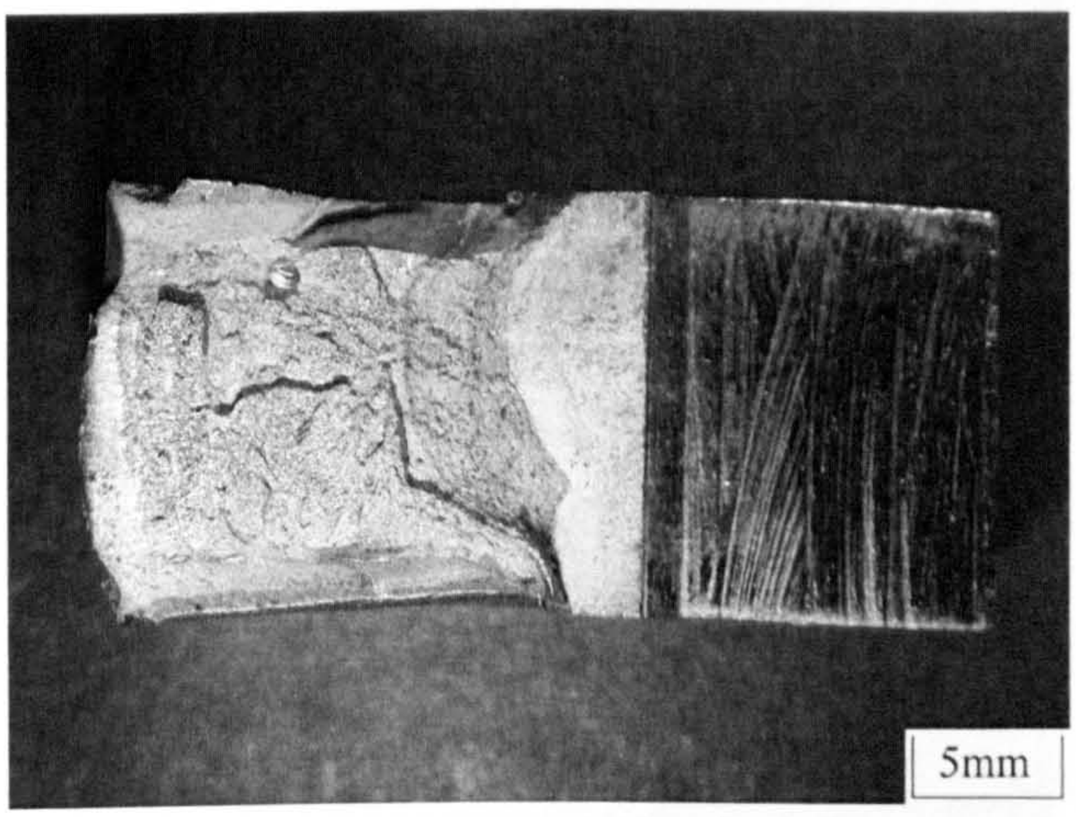

a) Weld metal centreline CTOD fracture face

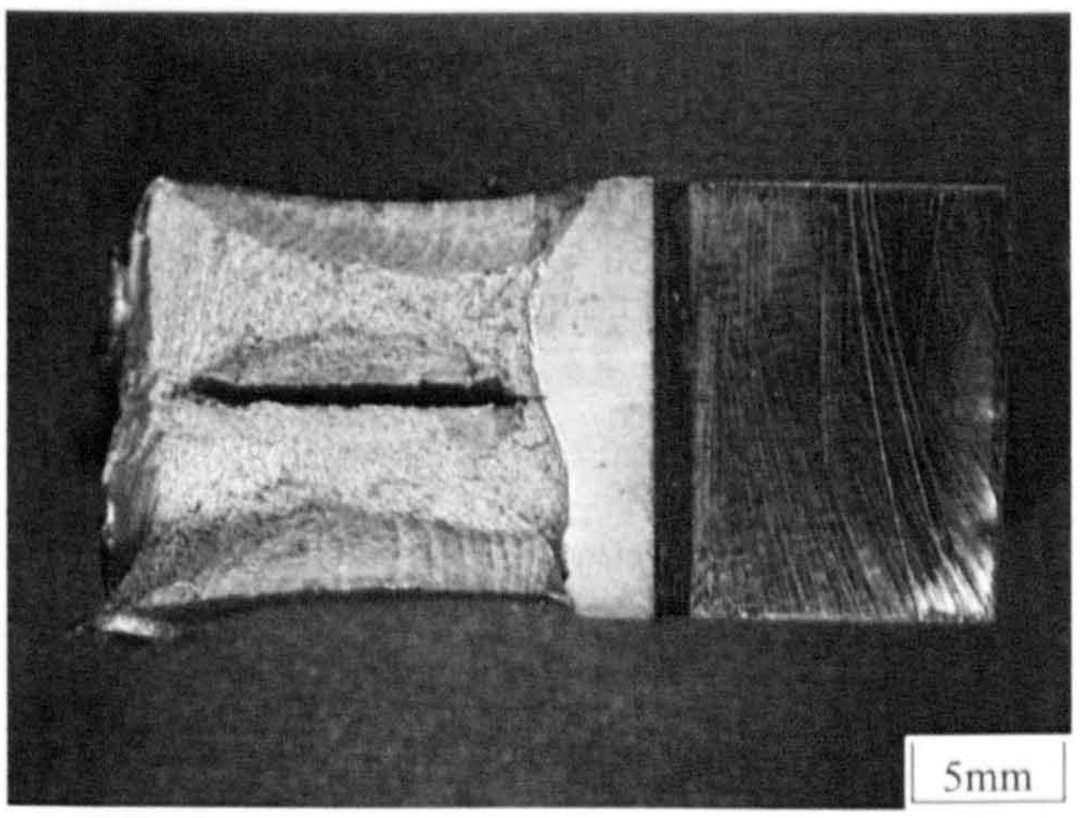

b) Fusion Line CTOD fracture face showing effects of segregation after testing

Figure 5-25: Post test CTOD sections (pipe B15)

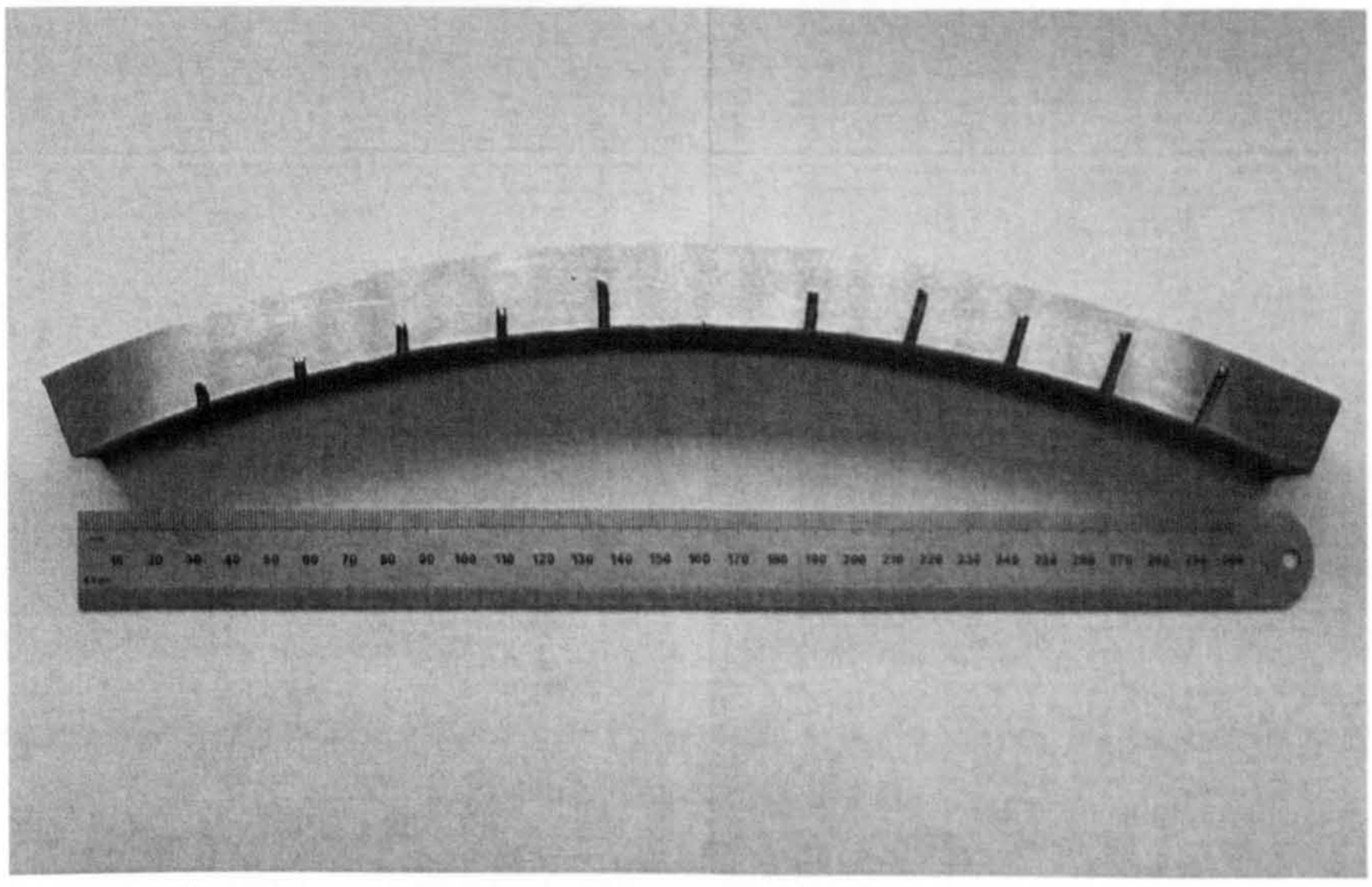

Figure 5-26: Typical weld longitudinal section showing drilled holes for thermocouple placement

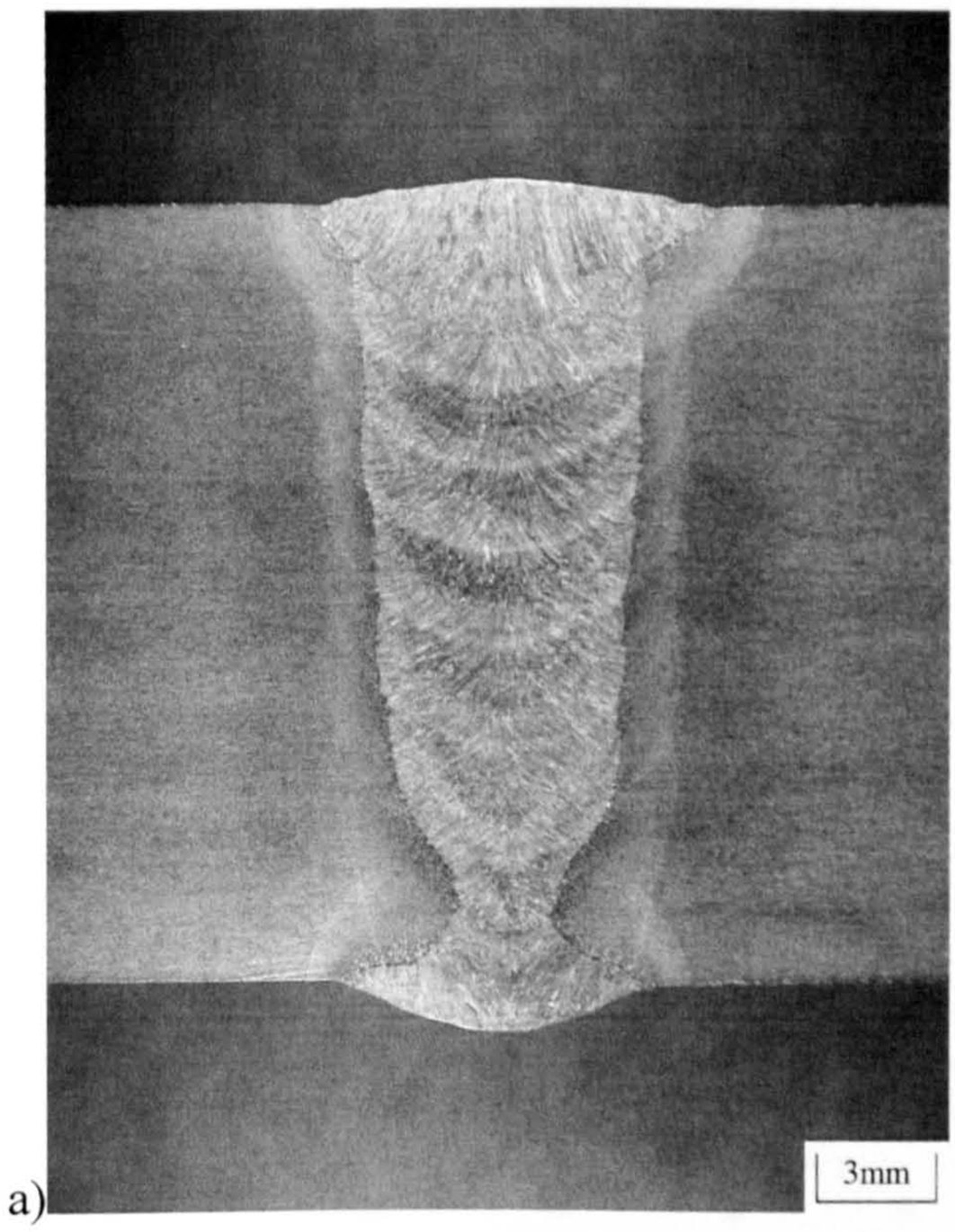

a)

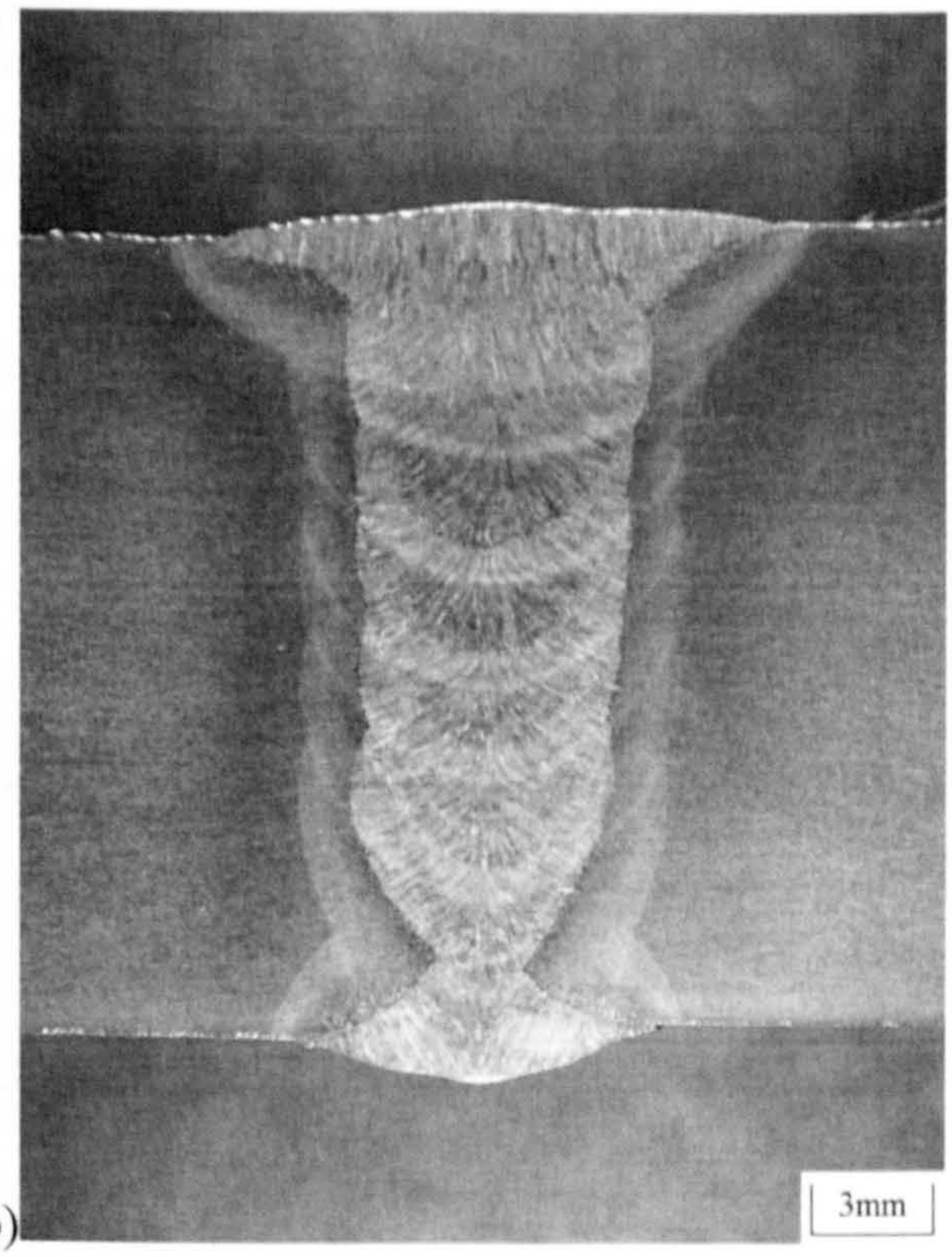

b)

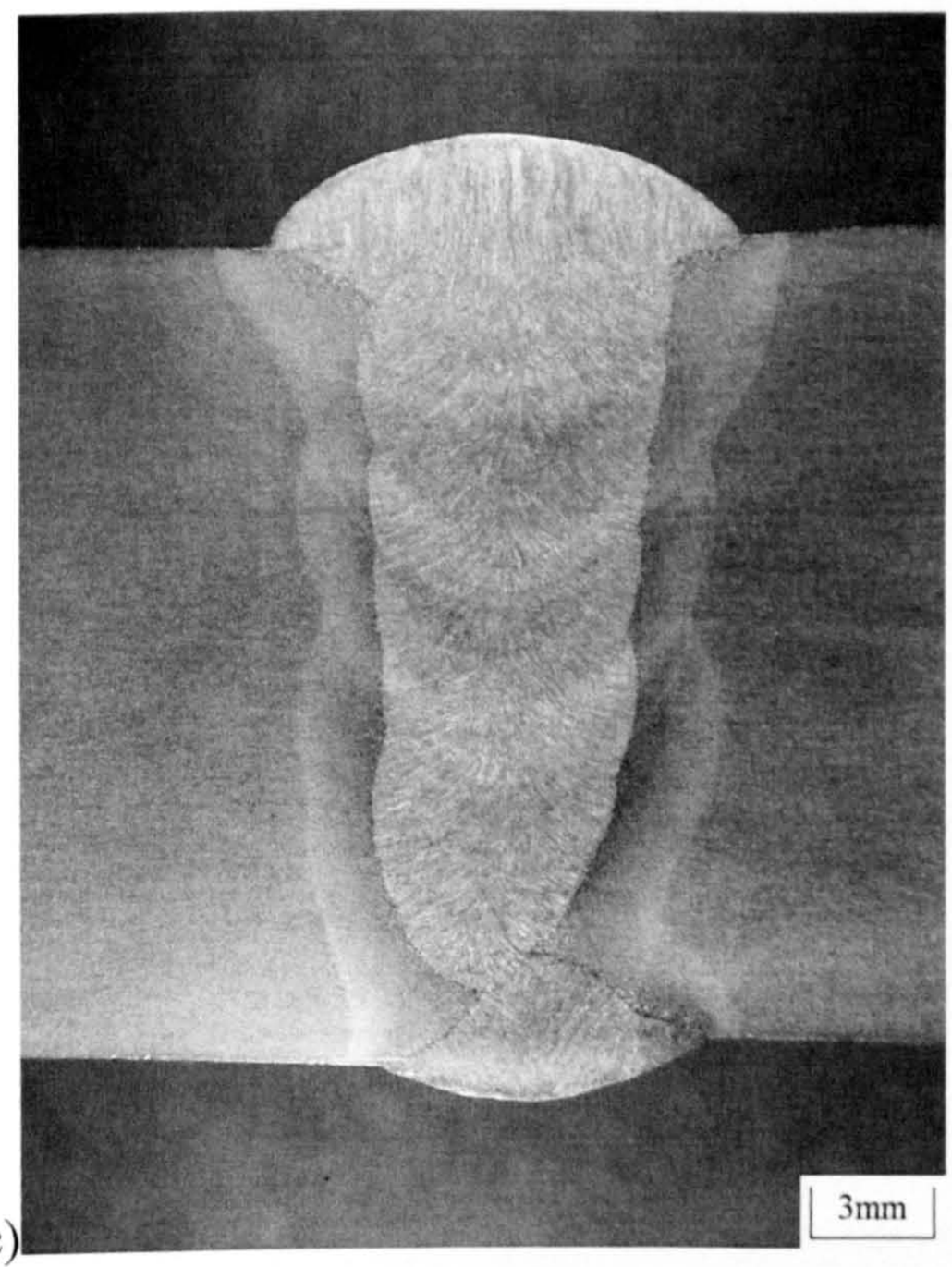

c)

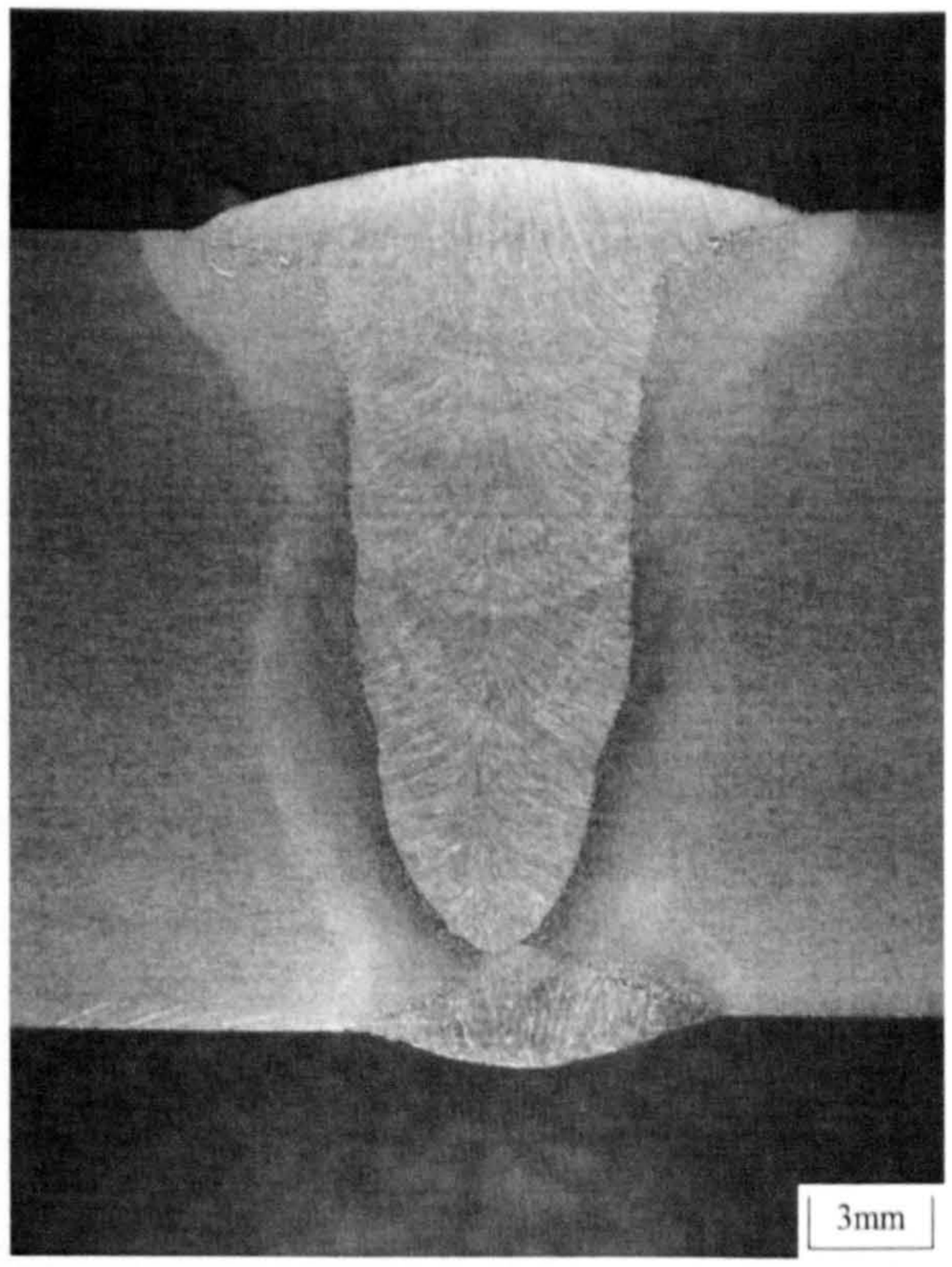

d)

Figure 5-27: Process variant weld macro sections a) single wire, b) tandem wire, c) dual torch, d) dual tandem torch

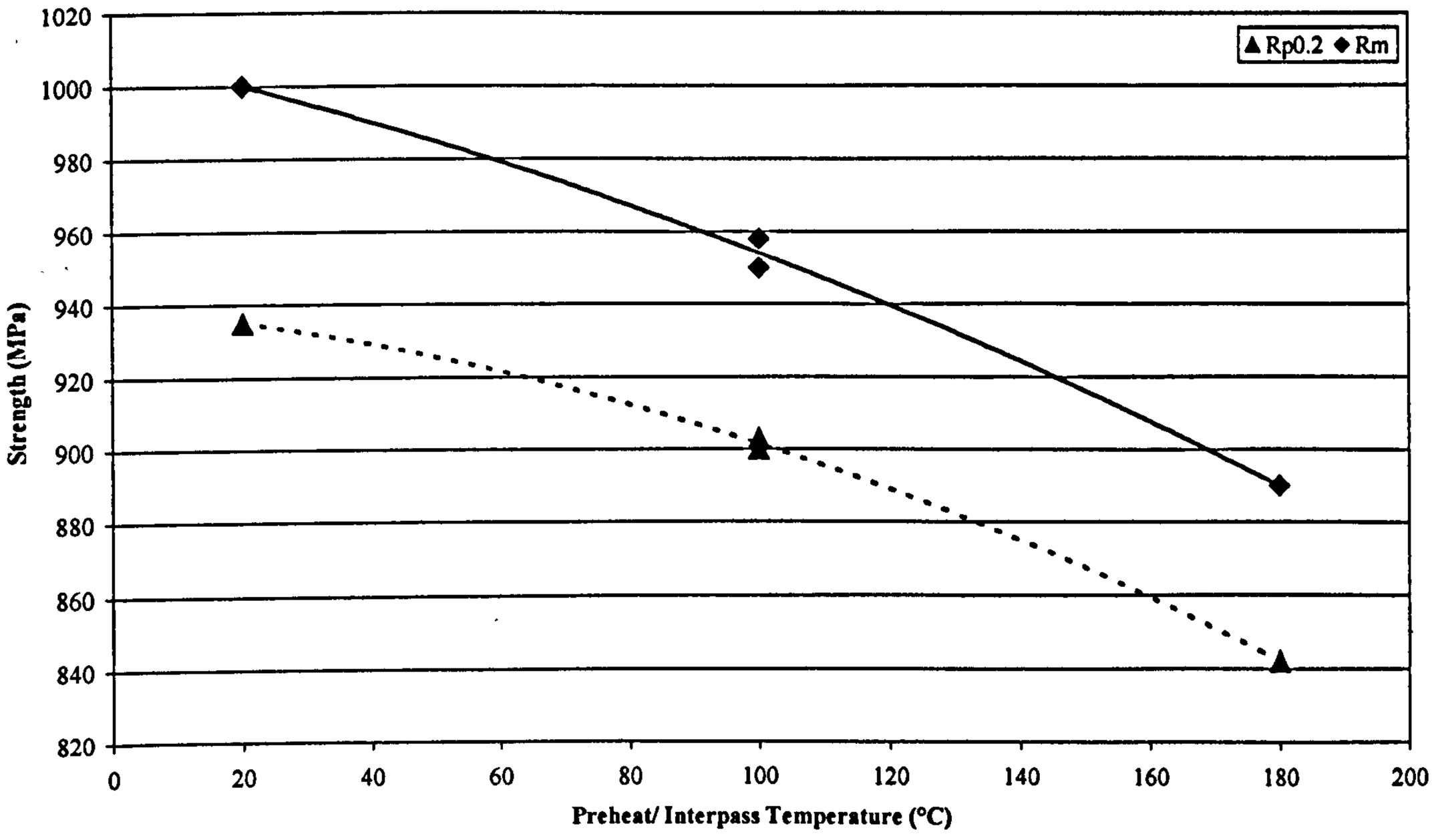

Figure 5-28: Effect of preheat/interpass variation on strength measurement

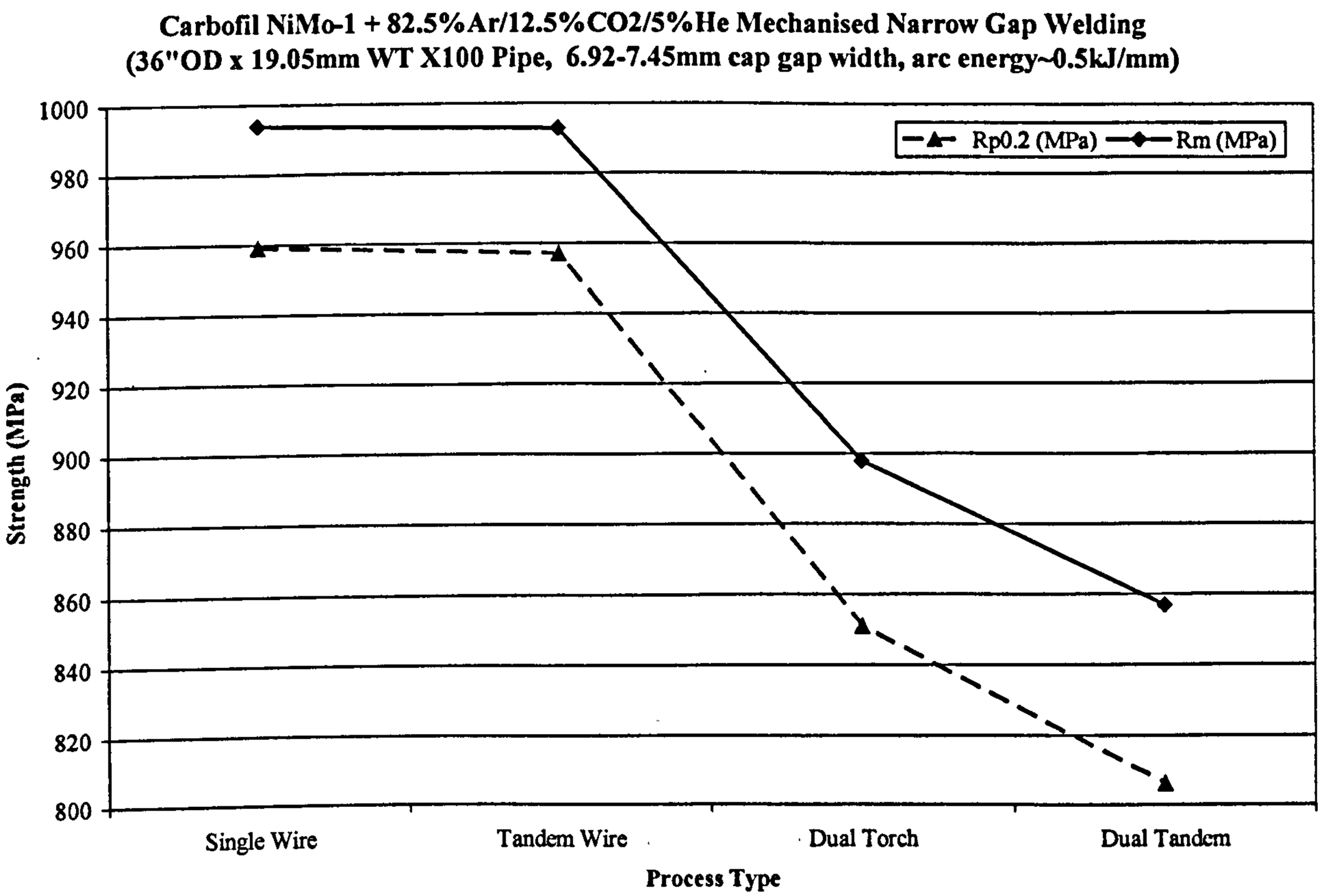

Figure 5-29: Effect of process variation on strength measurement

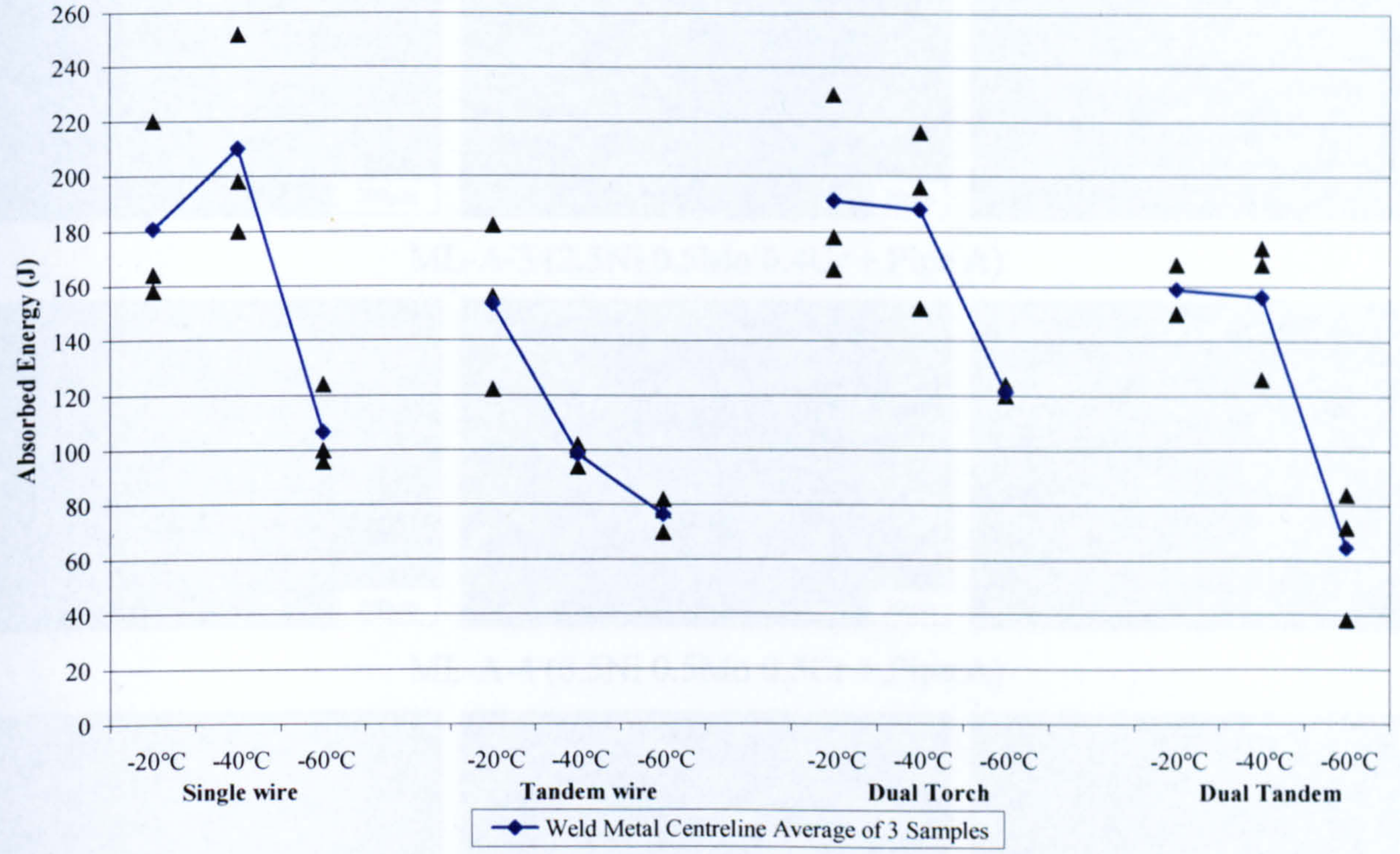

Figure 5-30: Effect of process variation on impact toughness

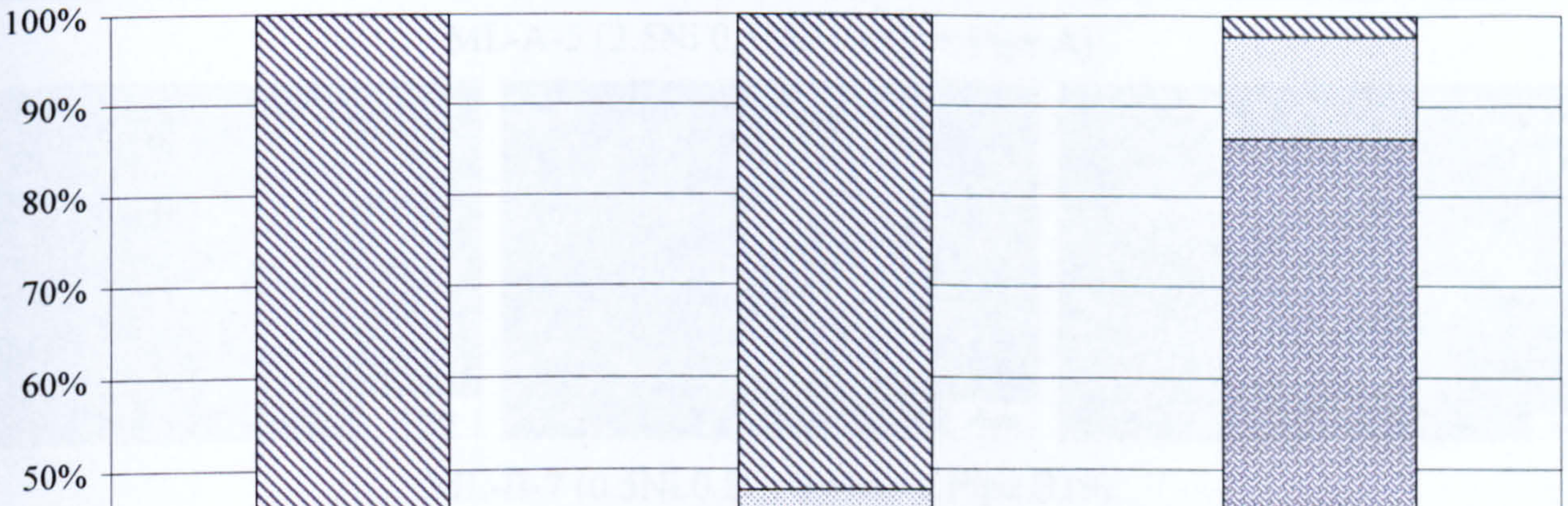

Figure 5-31: Microstructural characterisation of preheat variant trials using cap bead only (1000 points sampled per variant)

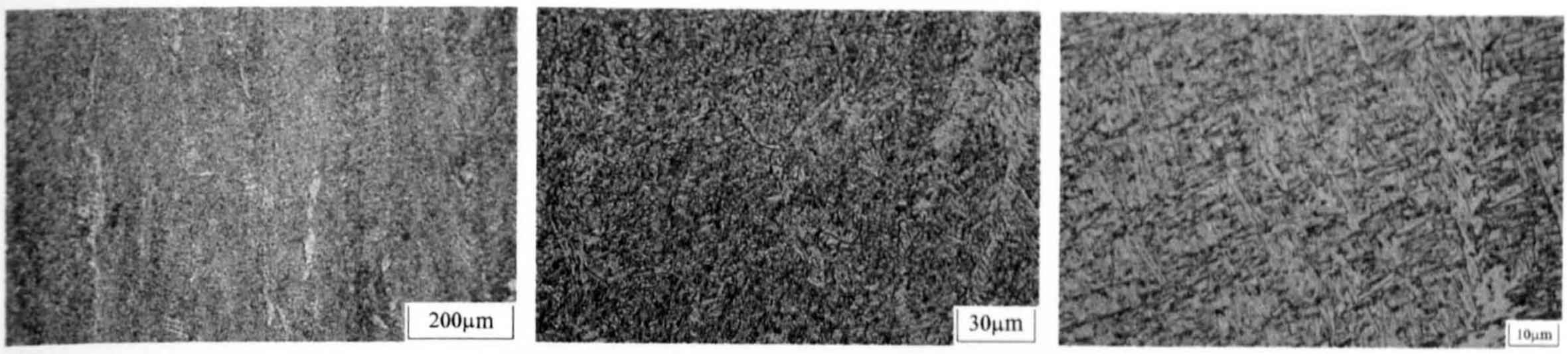

ML-A-3 (2.5Ni 0.5Mo 0.4Cr + Pipe A)

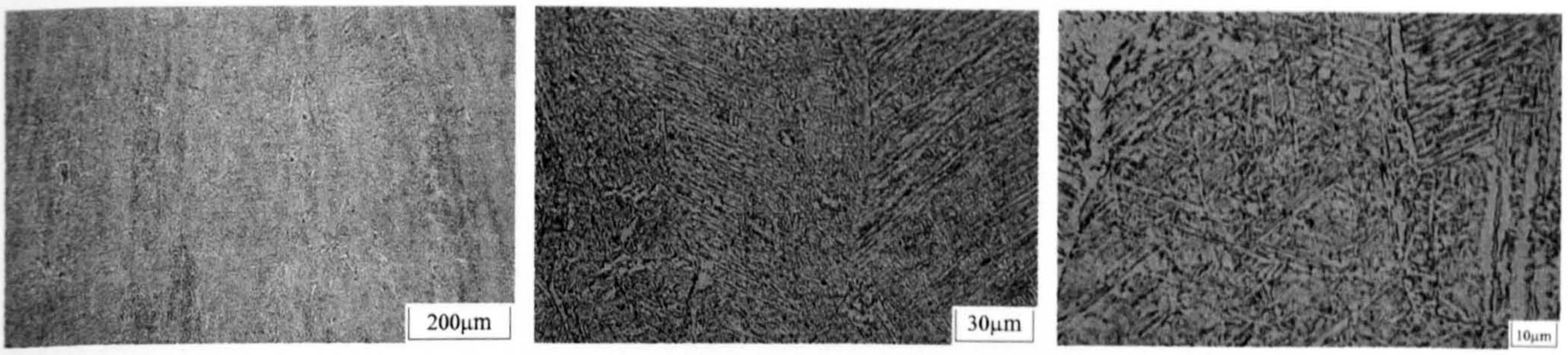

ML-A-4 (0.5Ni 0.5Mo 0.5Cr + Pipe A)

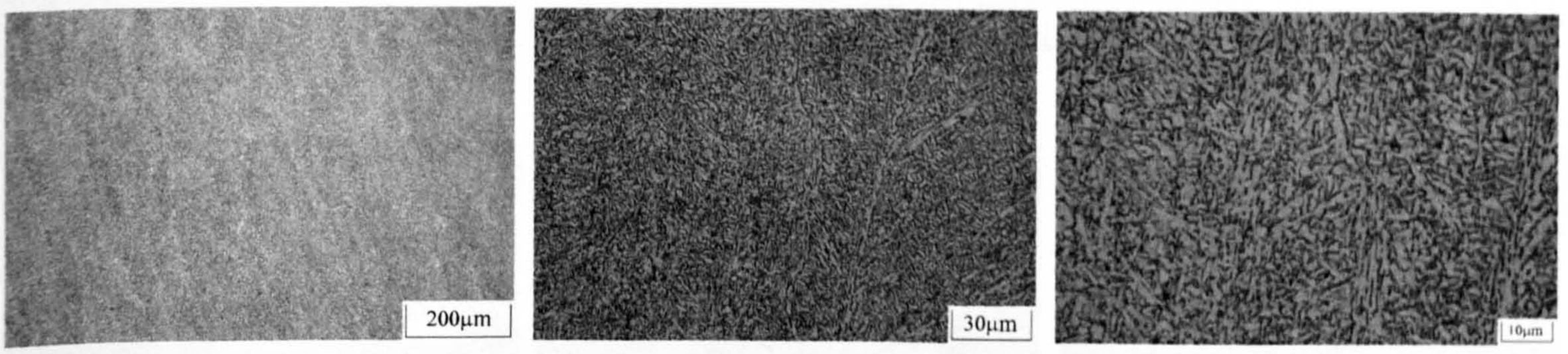

ML-A-5 (2.5Ni 0.5Mo 0.4Cr + Pipe A)

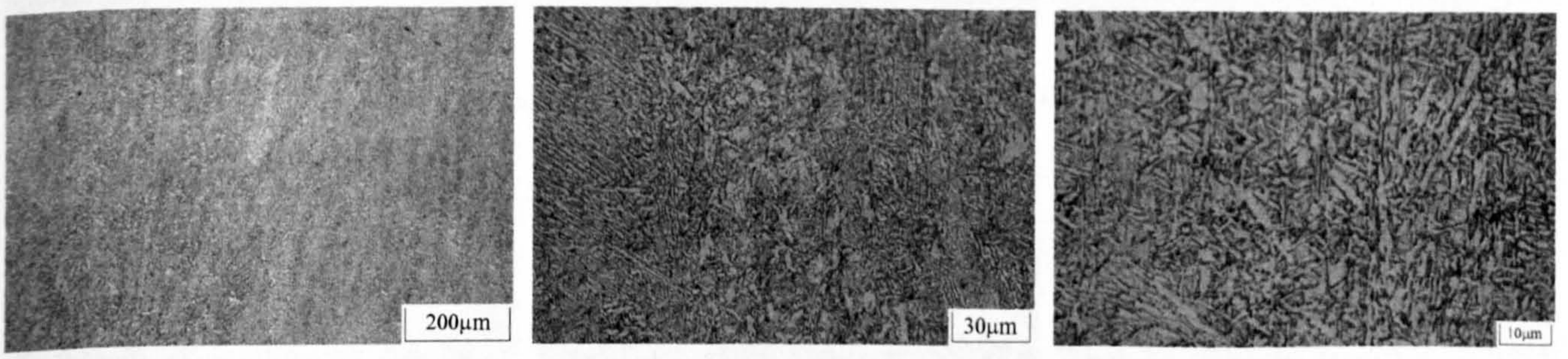

ML-B-7 (0.5Ni 0.5Cr 0.5Mo + Pipe B19)

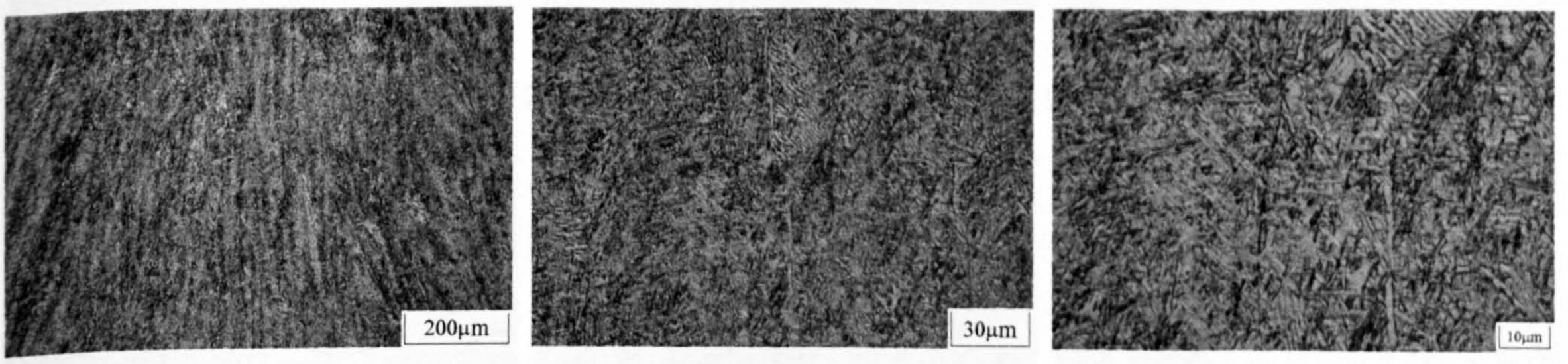

ML-B15-1 (2.5Ni 0.5Mo 0.4Cr + Pipe B15)

Figure 5-32: Single wire cap pass weld metal microstructures

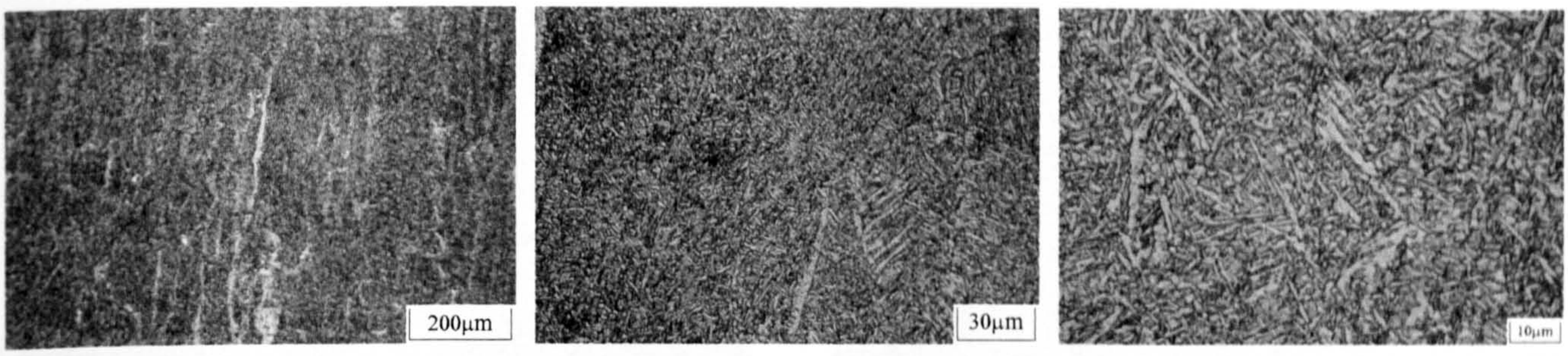

ML-B15-3 (0.9Ni 0.3Mo + Pipe B15)

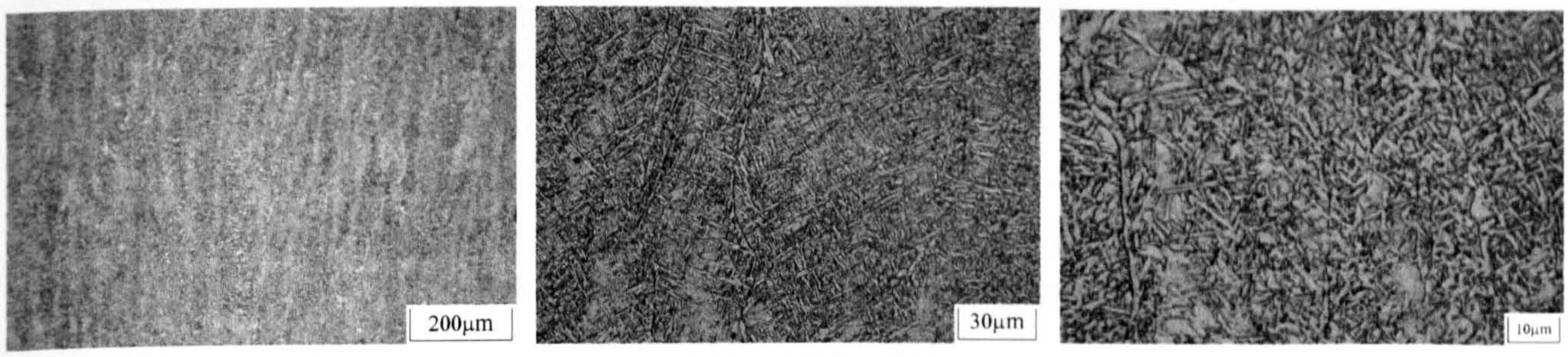

7625 (1.0Ni 0.4Mo + Pipe B19)

Figure 5-32 (Cont.): Single wire cap pass weld metal microstructures

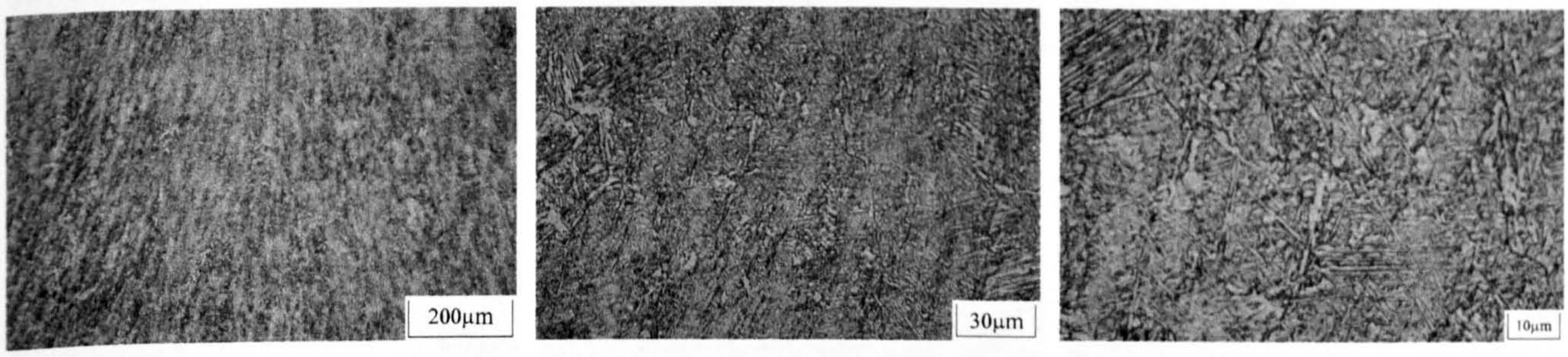

ML-B-12 (0.9Ni 0.3Mo + Pipe B19)

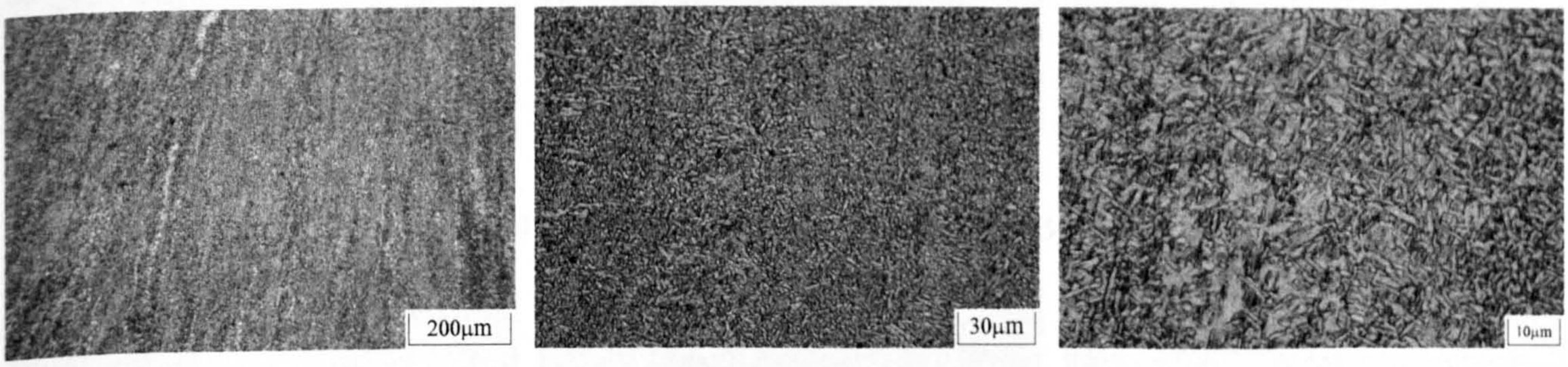

ML-B15-16 (0.9Ni 0.3Mo + Pipe B15)

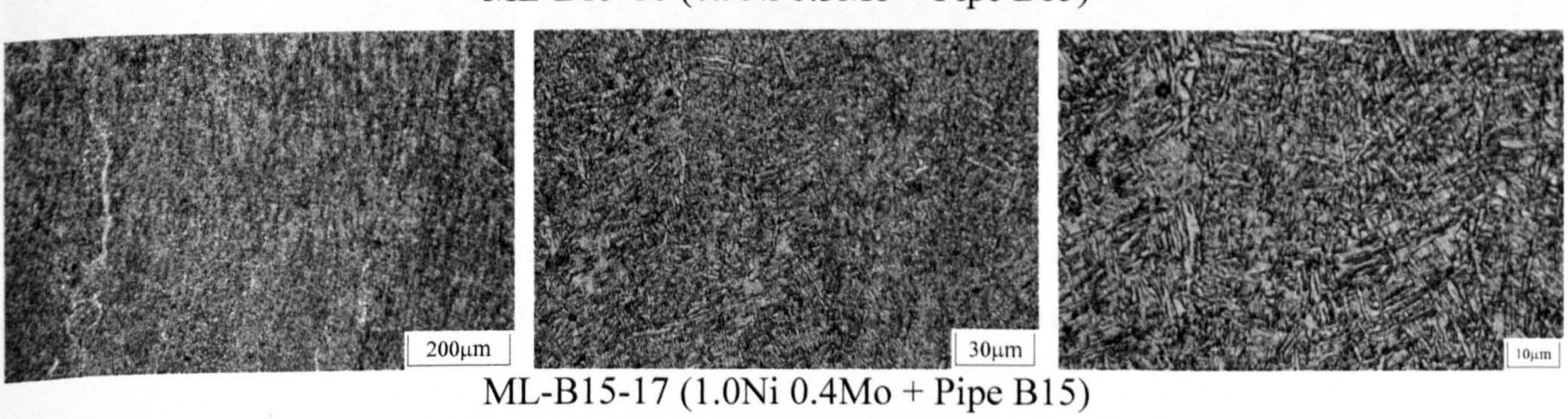

ML-B15-17 (1.0Ni 0.4Mo + Pipe B15)

Figure 5-33: Tandem wire cap pass weld metal microstructures

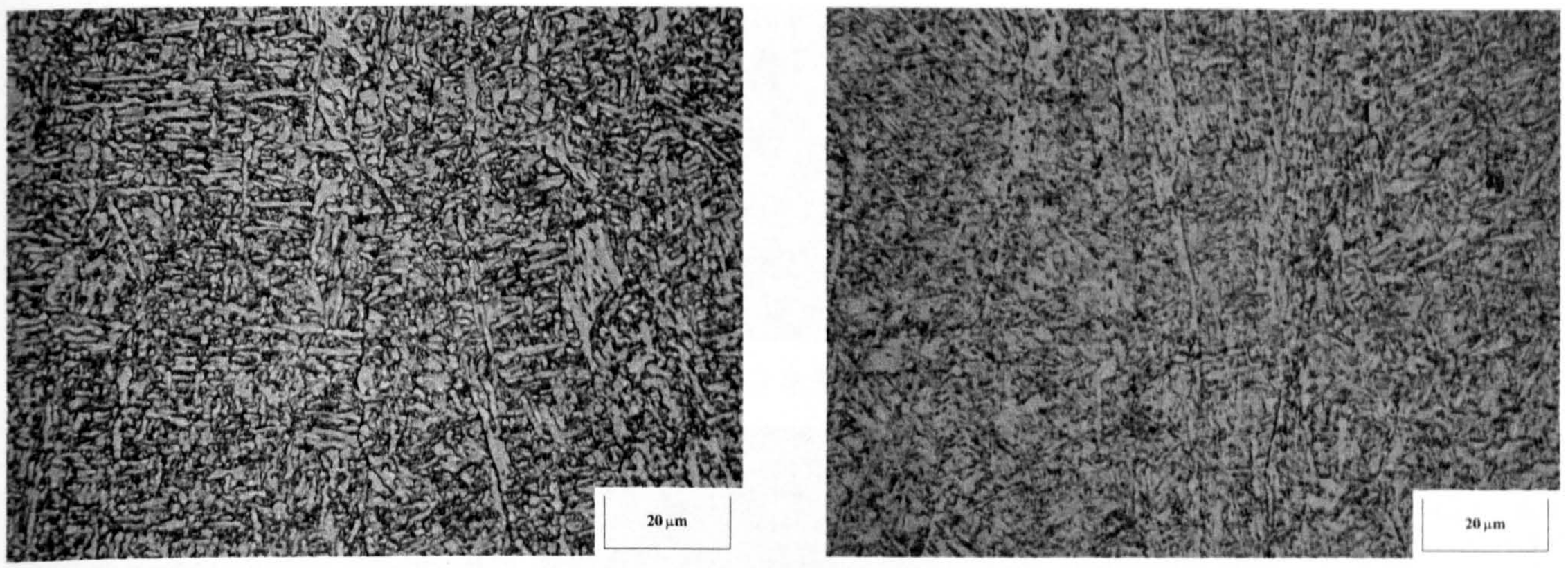

a) dual torch (50mm spacing) b) single torch

Figure 5-34: Weld 7115 – 1.5Ni 0.5Mo 0.2Cr (Thyssen Union NiMoCr), dip transfer, 80Ar/20CO2, cap pass microstructures.

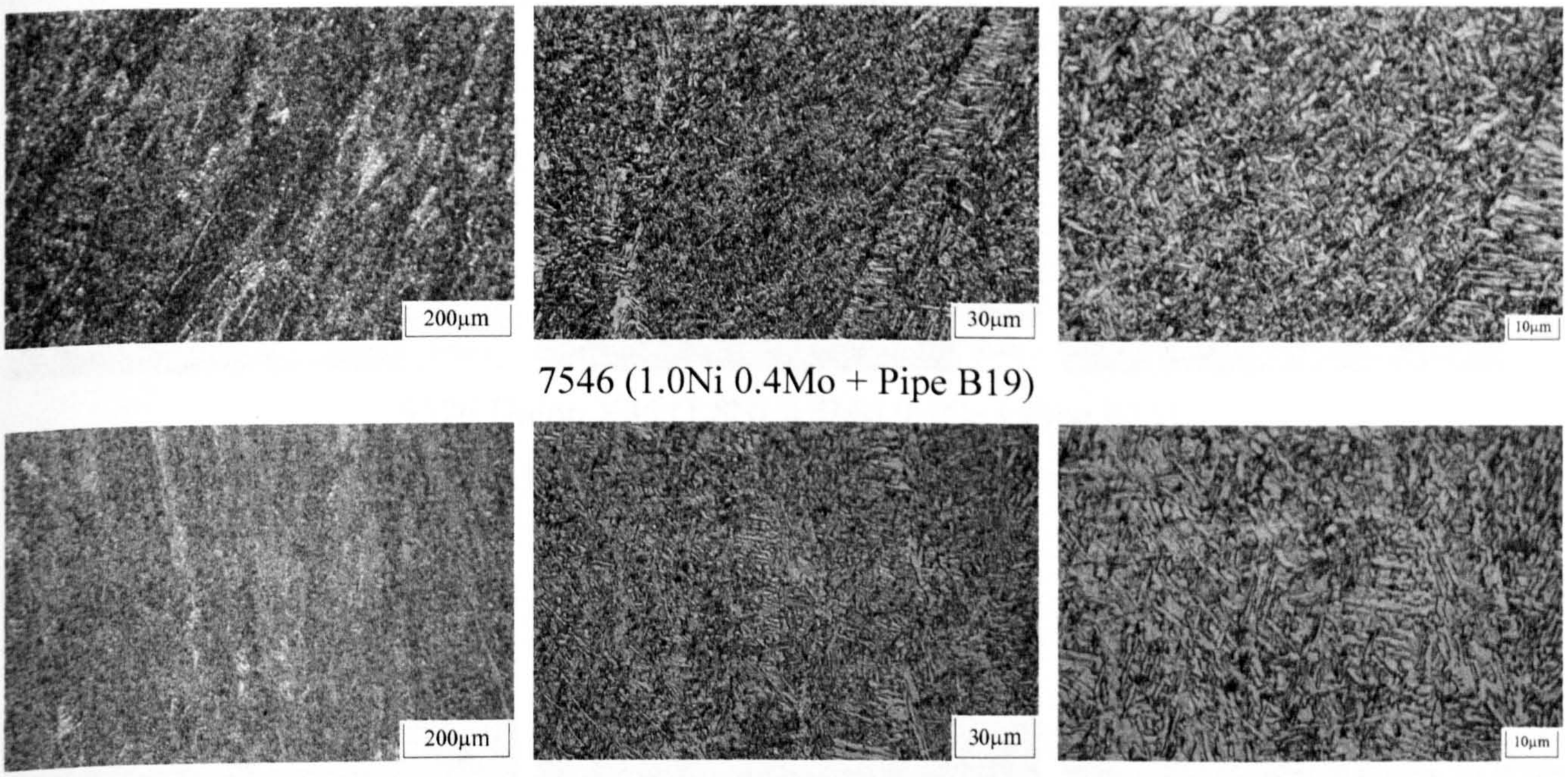

9692 Elgamatic 135 (1.5Ni 0.3Mo 0.2Cr + Pipe B15)

Figure 5-35: Dual torch cap pass weld metal microstructures

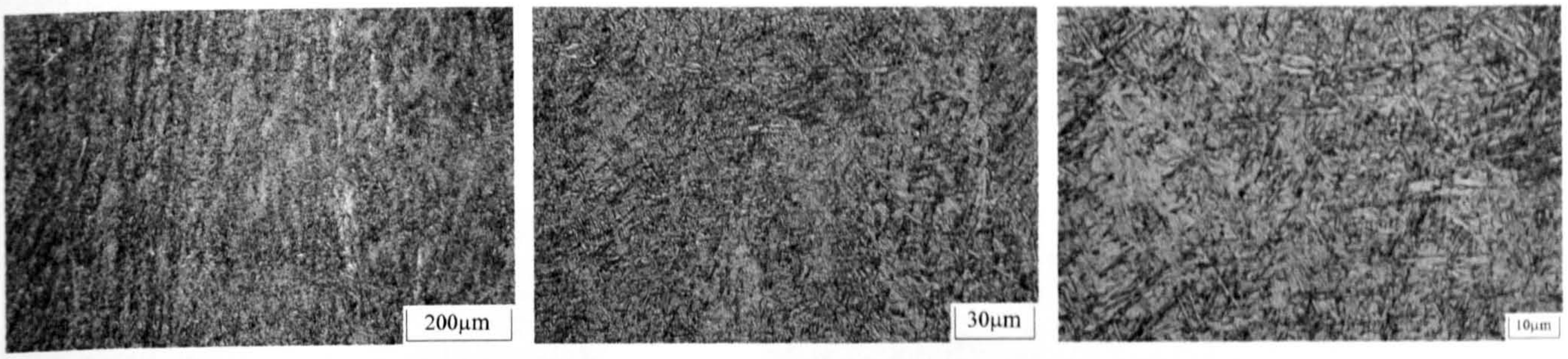

9692 Union X85 (1.8Ni 0.5Mo 0.3Cr + Pipe B15)

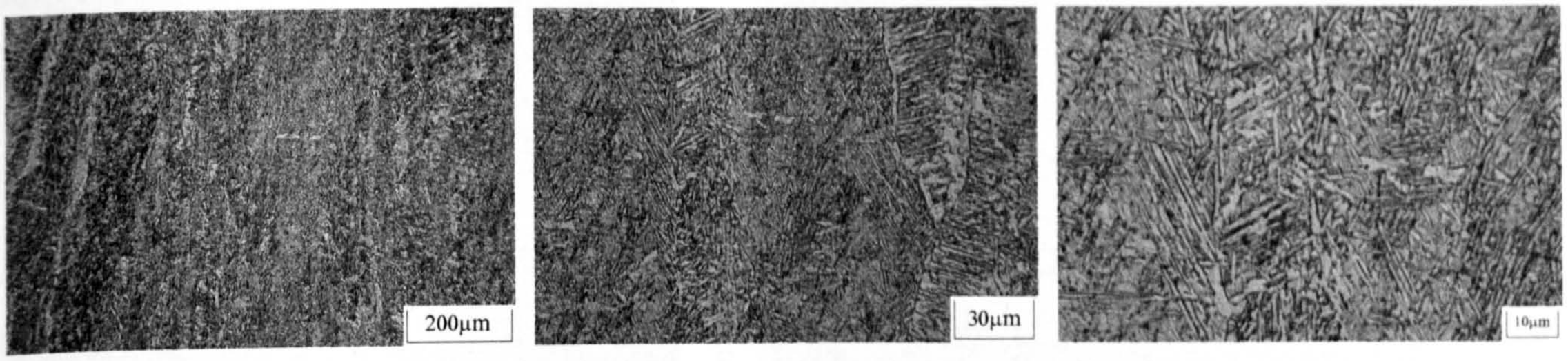

9726 Elgamatic 135 (1.5Ni 0.3Mo 0.2Cr + Pipe B15)

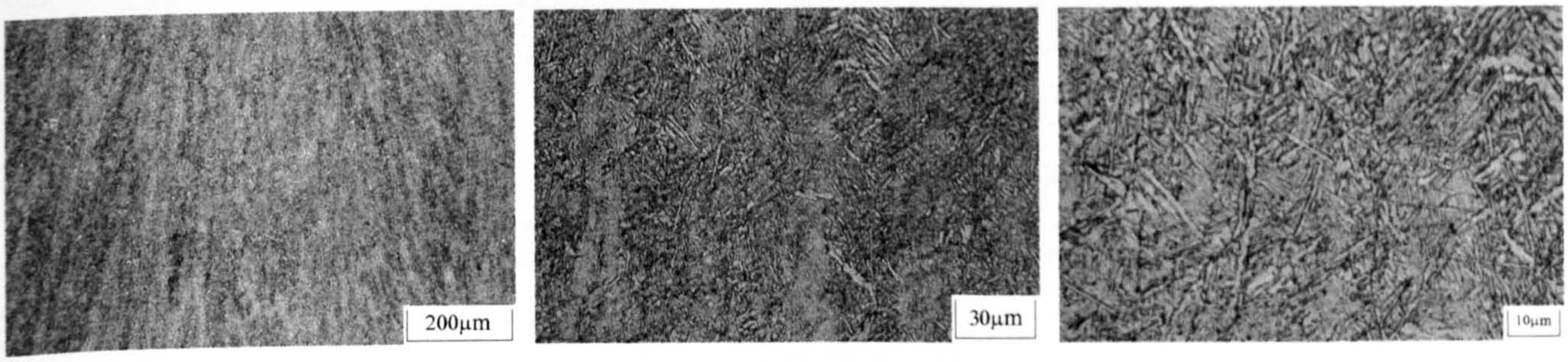

9726 Union X85 (1.8Ni 0.5Mo 0.3Cr + Pipe B15)

Figure 5-35(Cont.): Dual torch cap pass weld metal microstructures

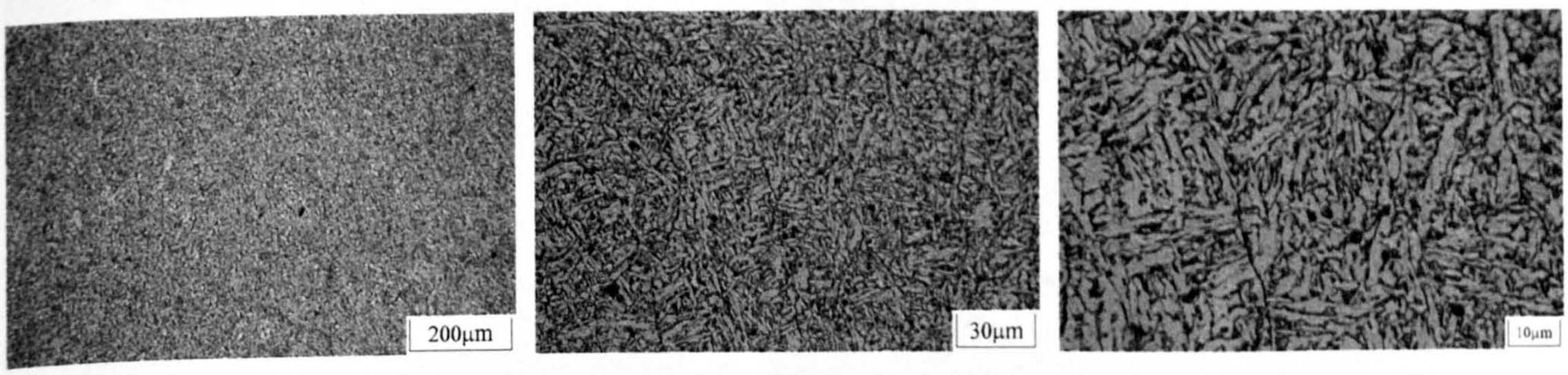

ML-B-9 (2.7Ni 0.3Mo + Pipe B19)

Figure 5-36: Tie-in cap pass weld metal microstructures

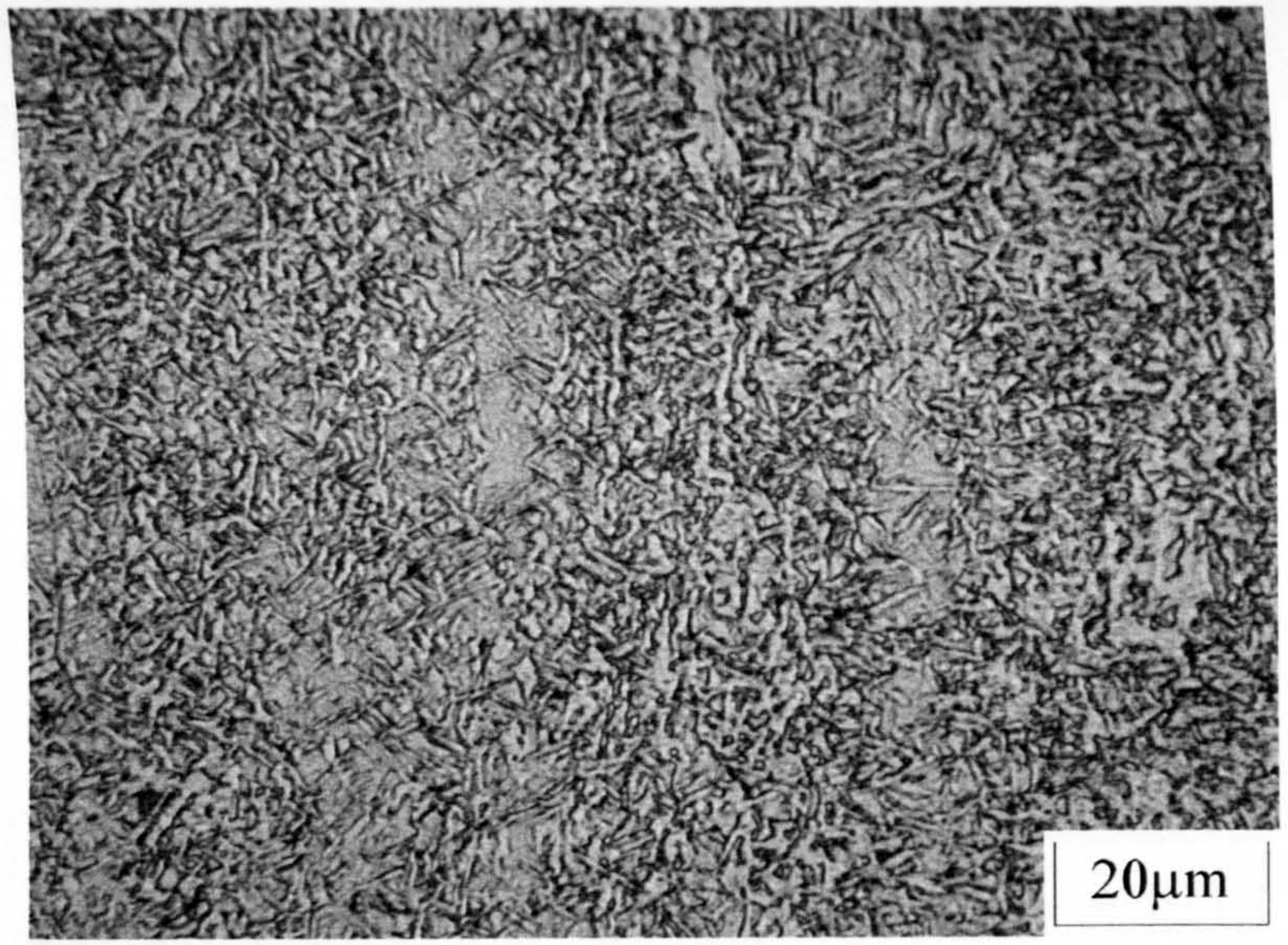

a) Single wire cap

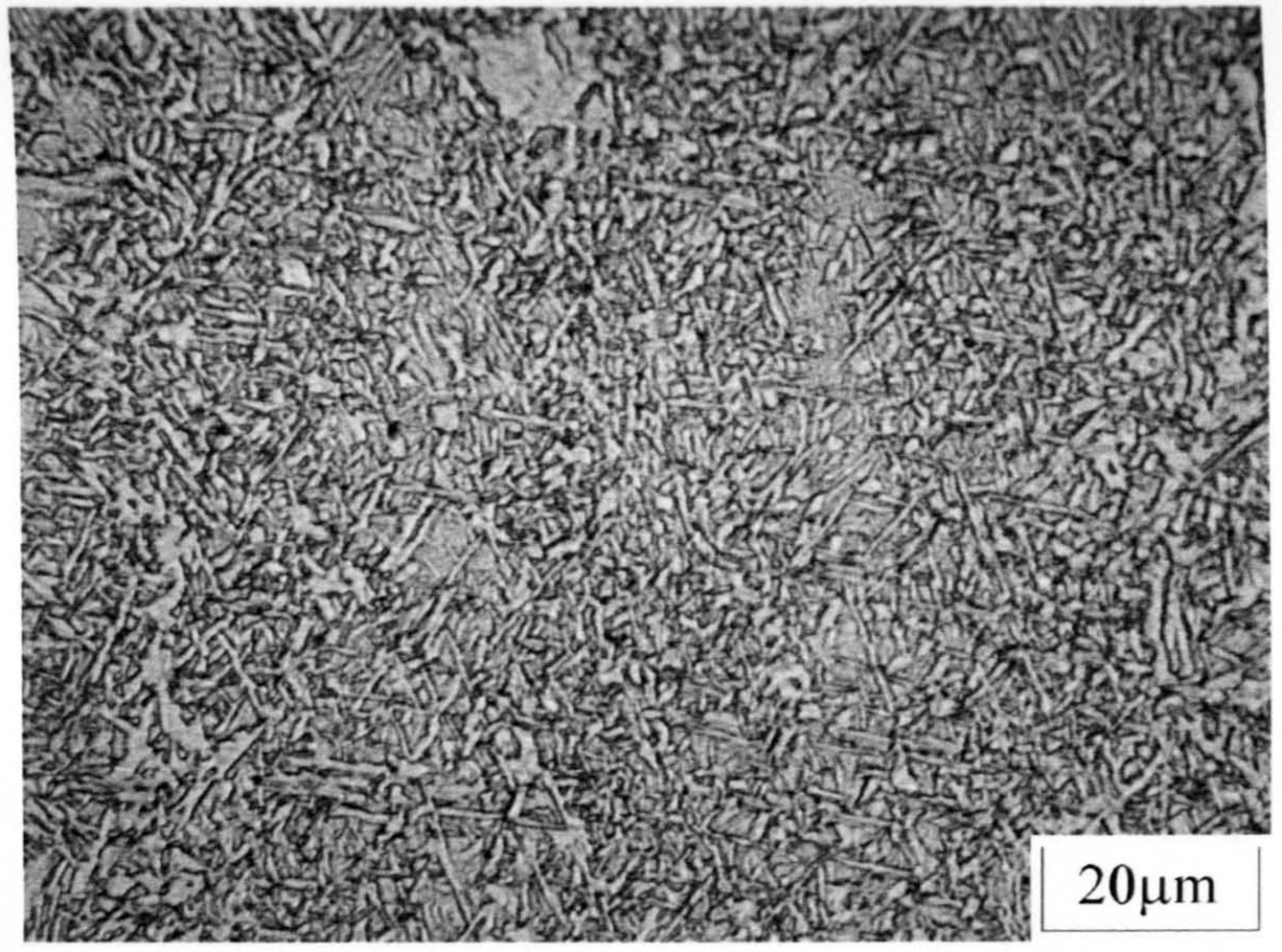

b) Tandem wire cap

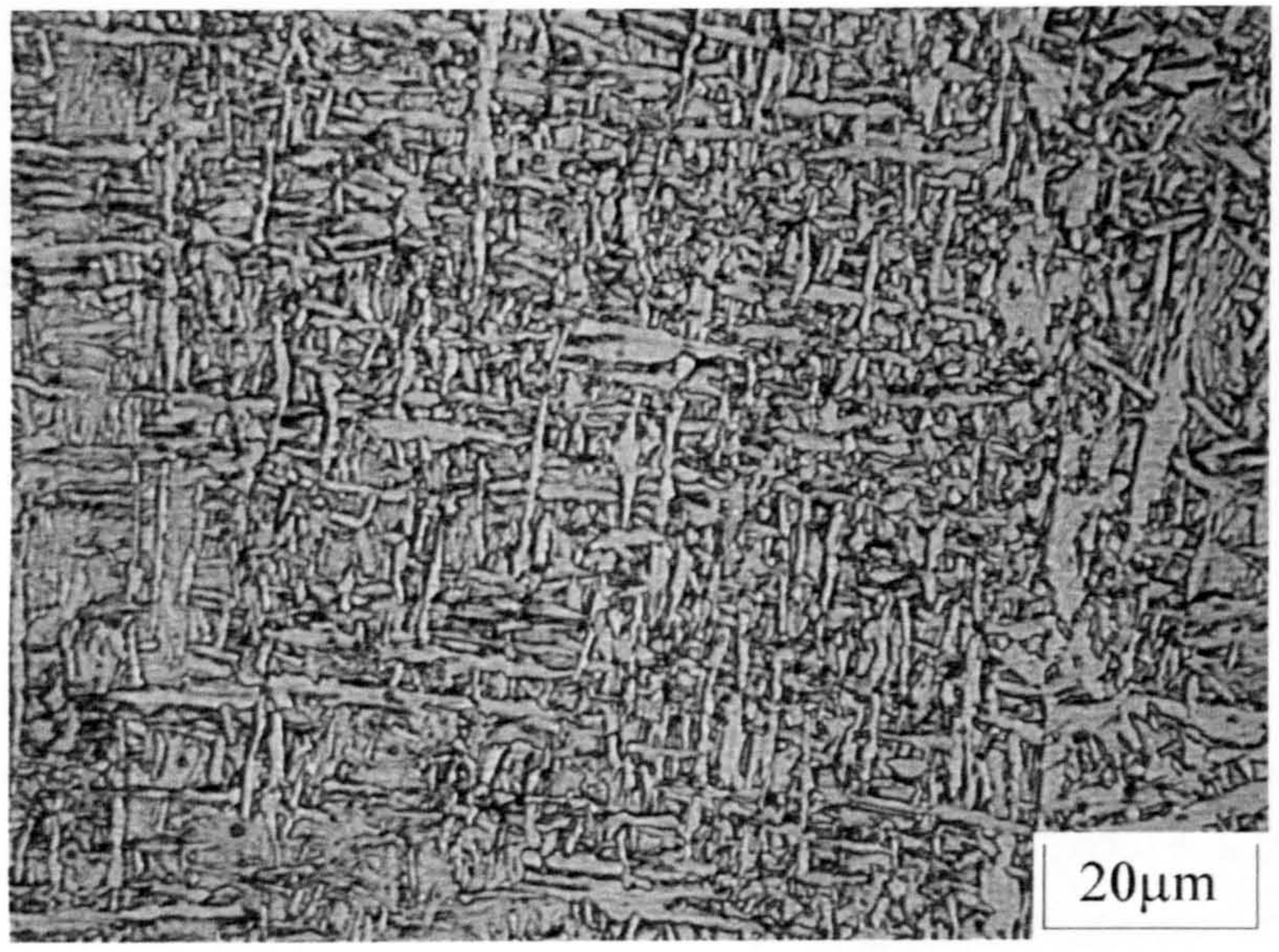

c) dual torch cap

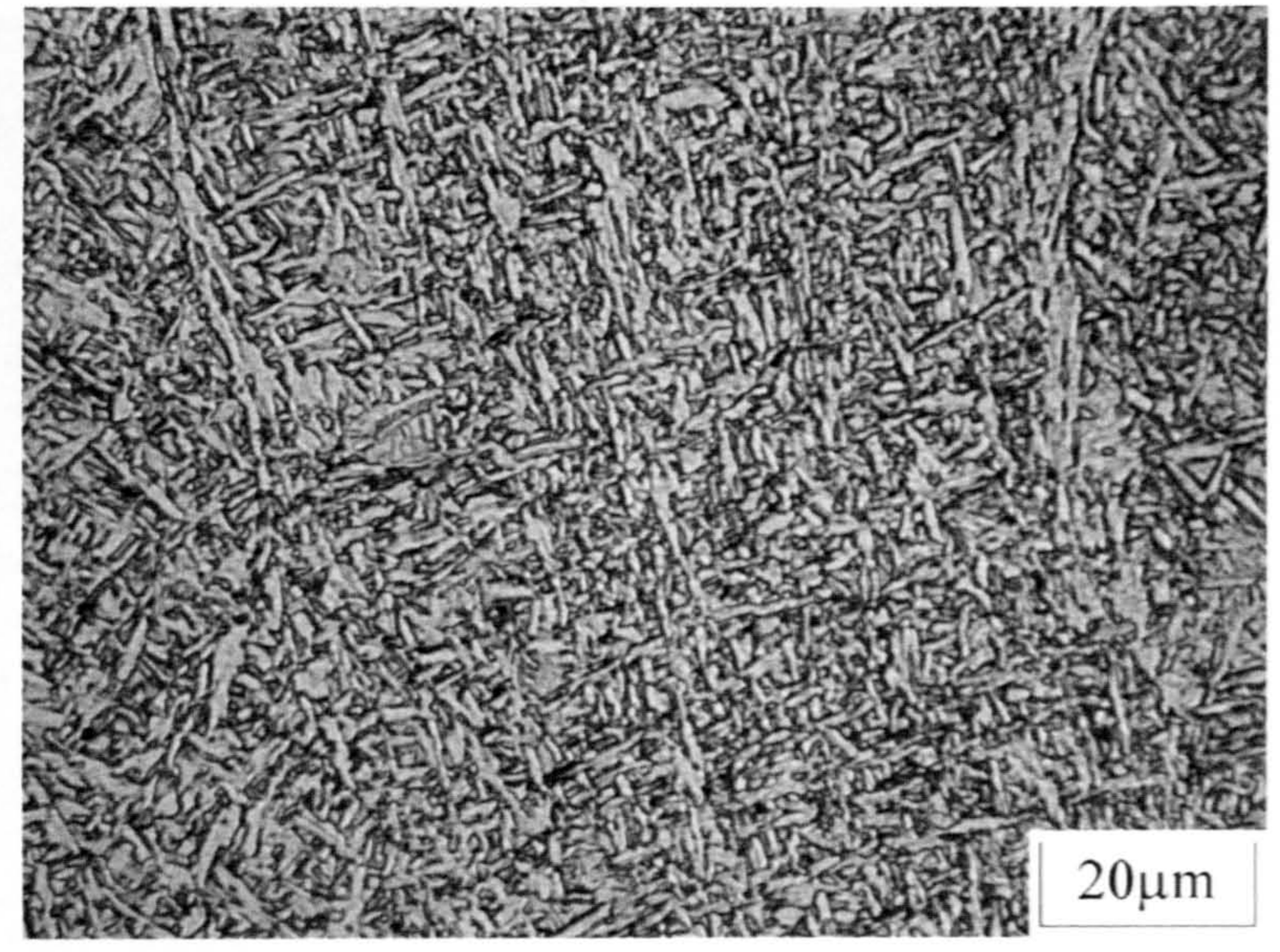

d) dual tandem cap

Figure 5-37: Process variation trials - typical cap pass microstructures

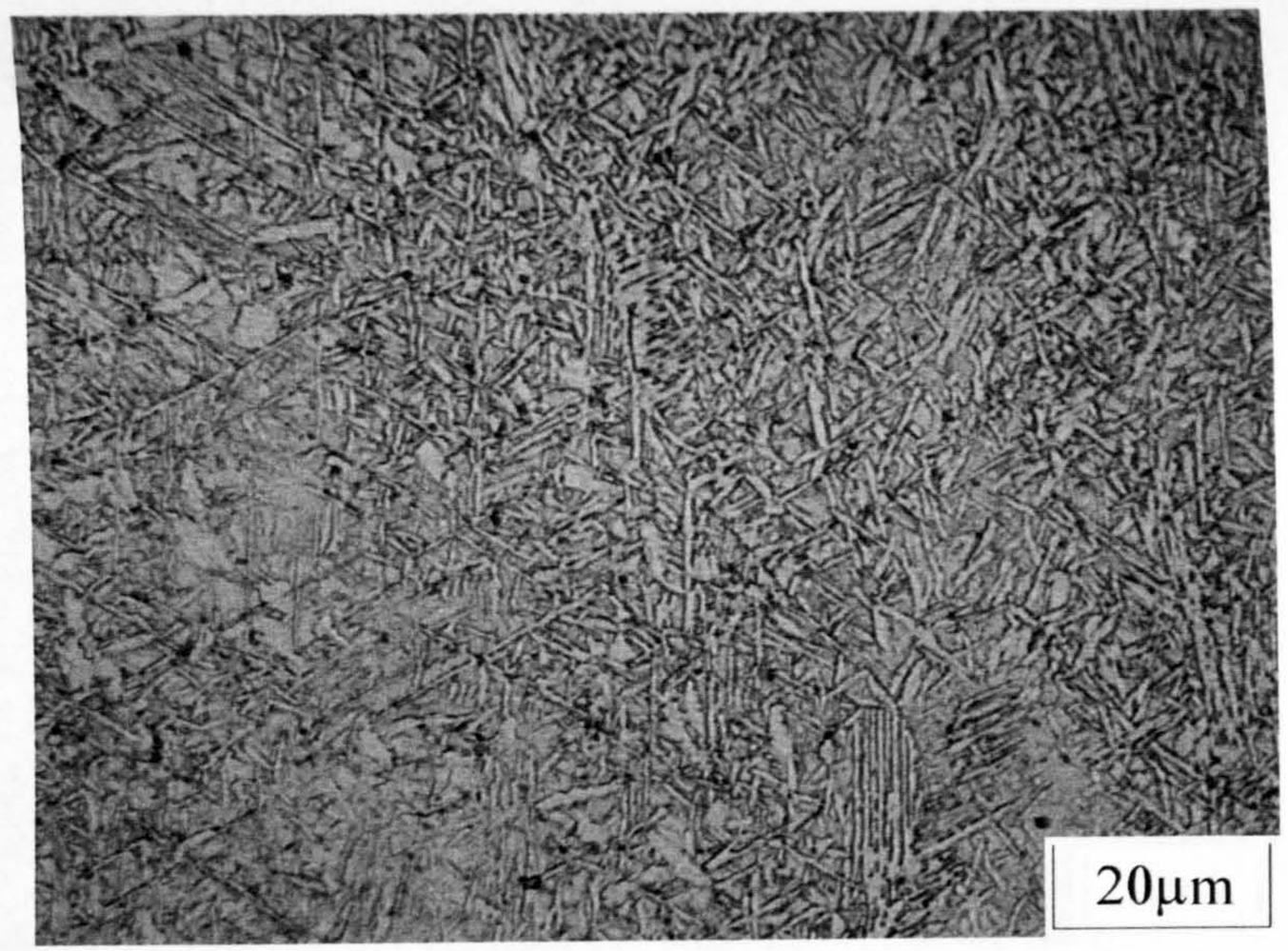

a) no preheat

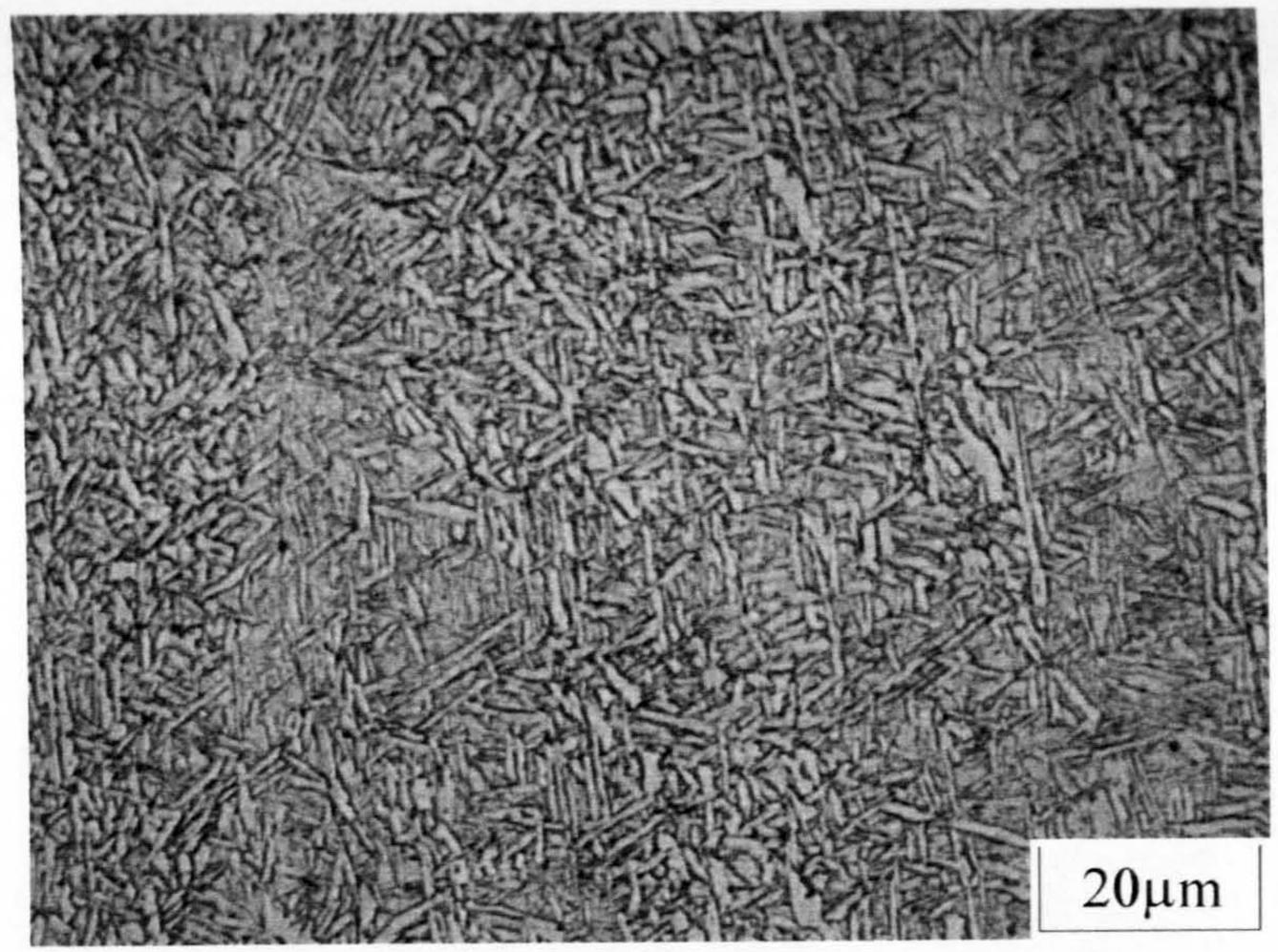

b) 100°C preheat

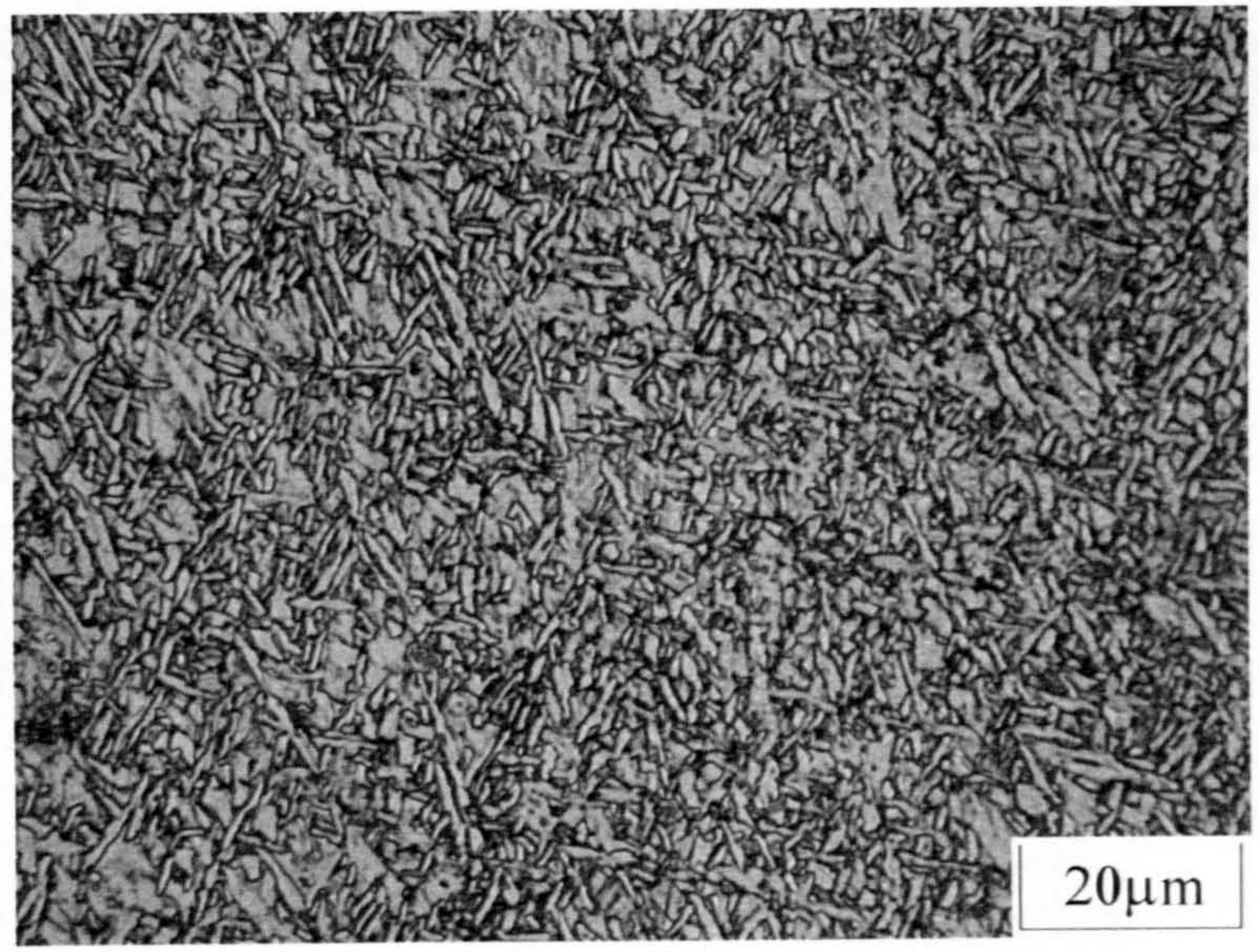

c) 180°C preheat

Figure 5-38: Preheat variation trials - typical cap pass microstructure

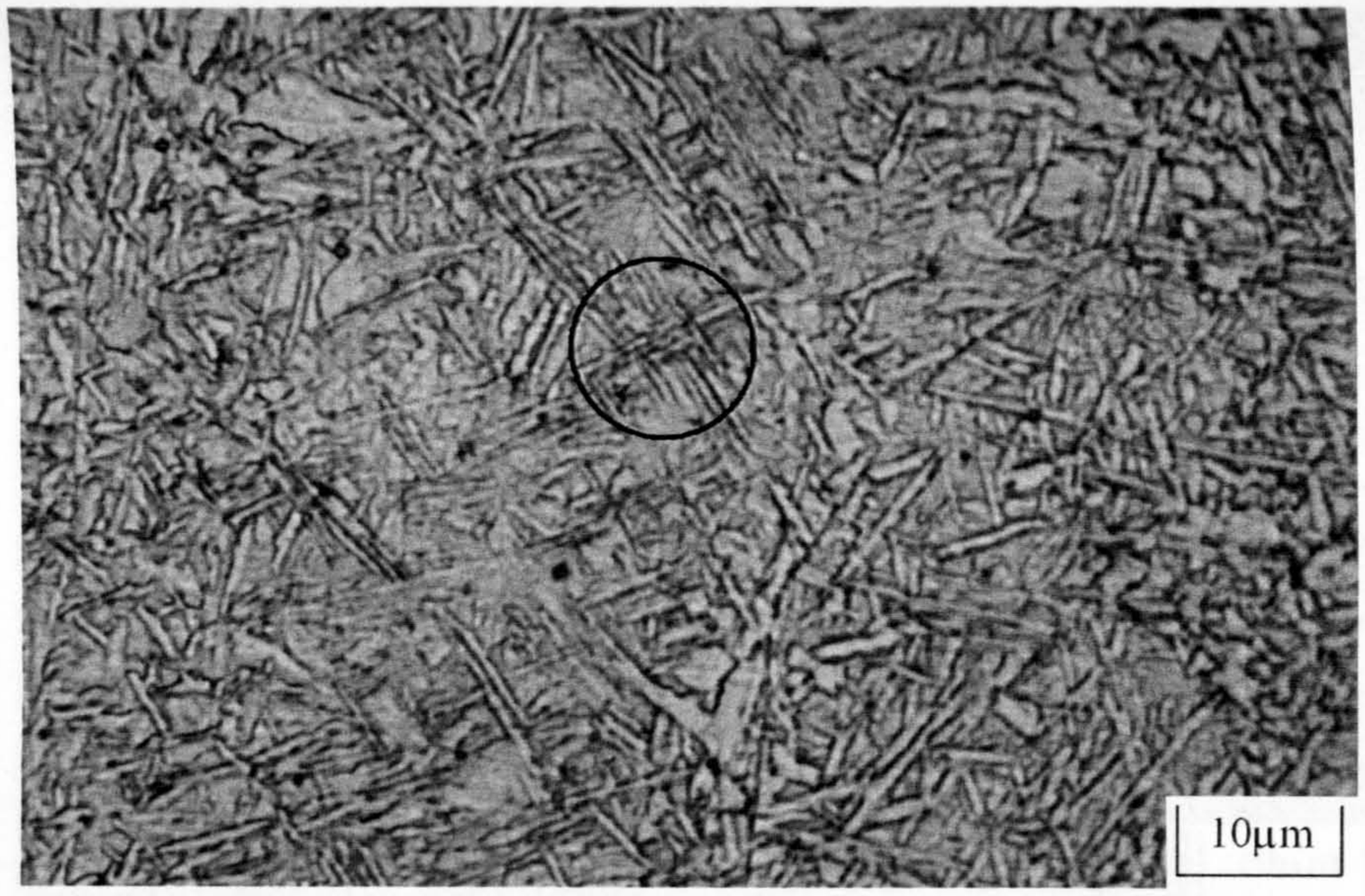

a) Martensite

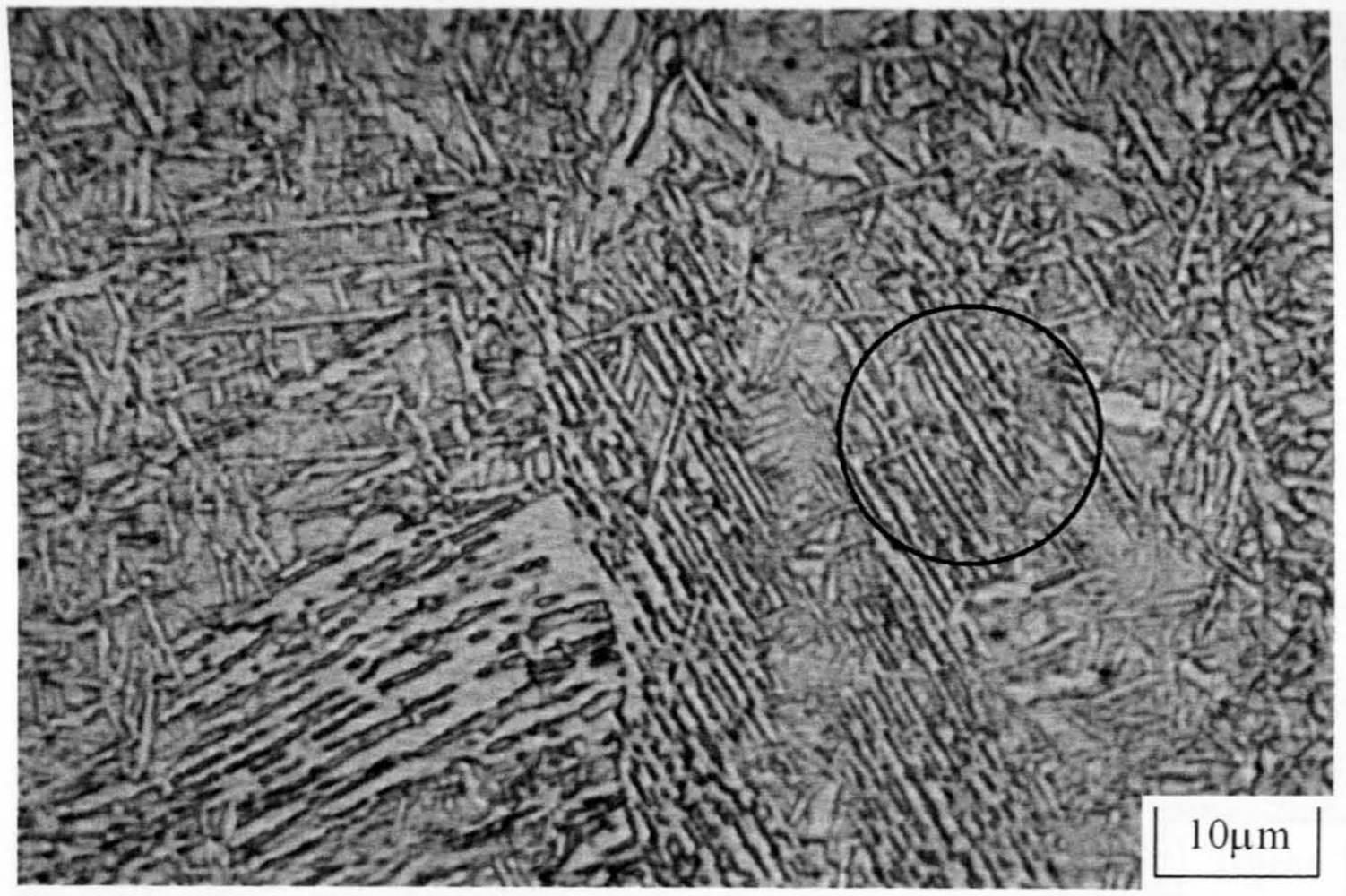

b) Ferrite with aligned second phase (FS(B) – Bainite)

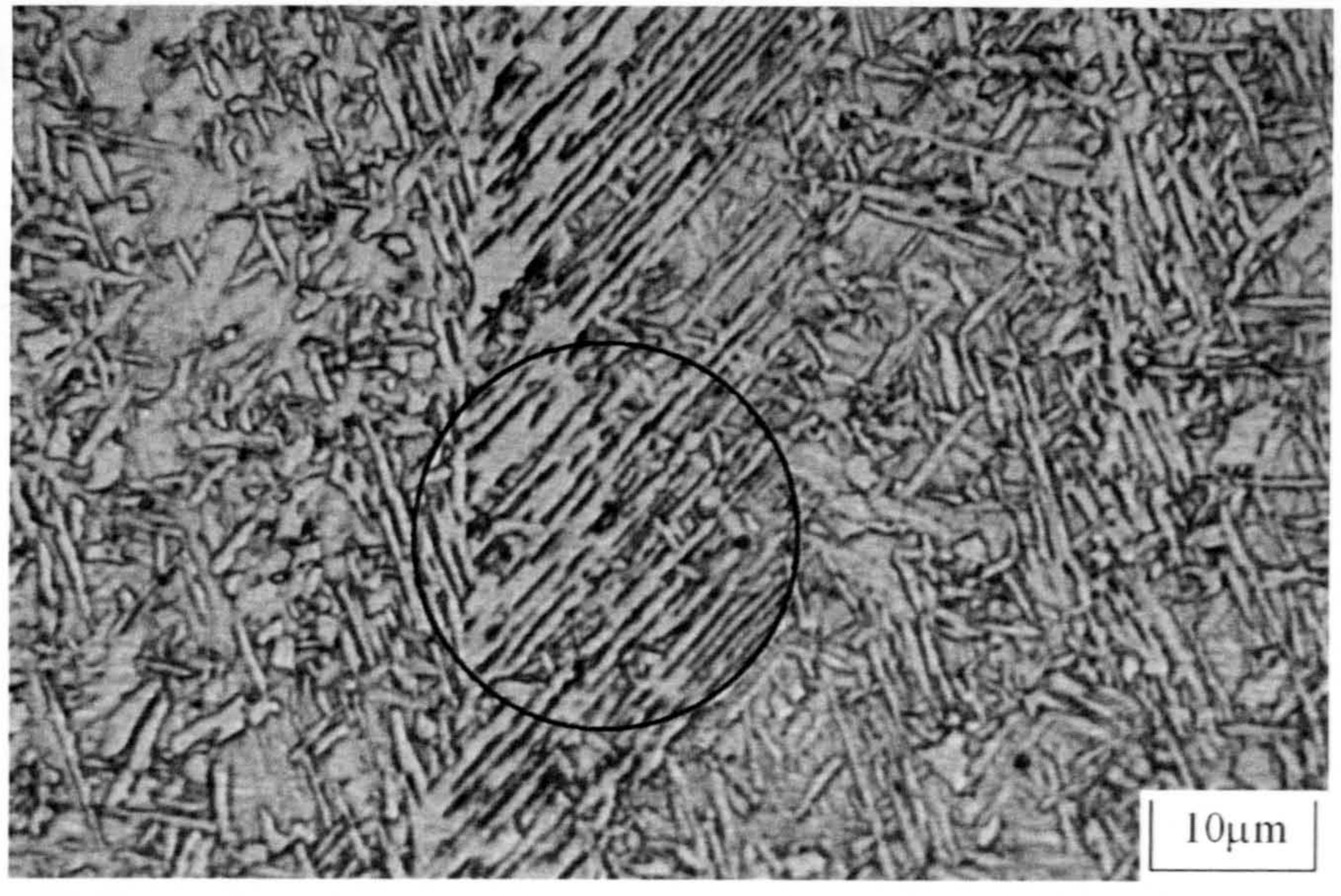

c) Ferrite with aligned second phase (FS(SP) –Side plate/Widmanstätten ferrite)

Figure 5-39: Typical microstructural constituents observed in process and preheat variation trials

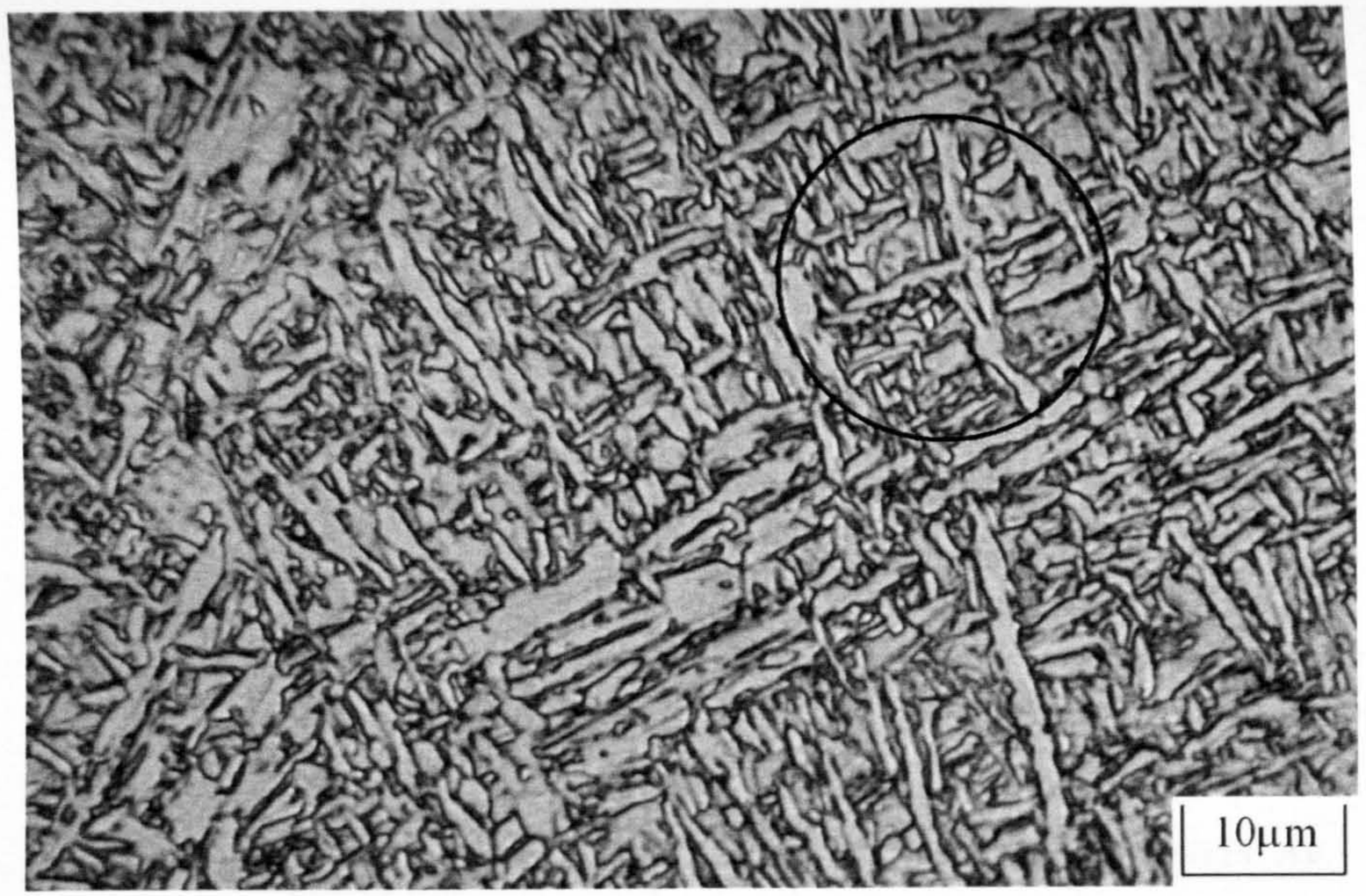

d) Acicular ferrite (AF)

e) Intragranular polygonal ferrite (PF(I))

Figure 5-39(Cont.): Typical microstructural constituents observed in process and preheat variation trials

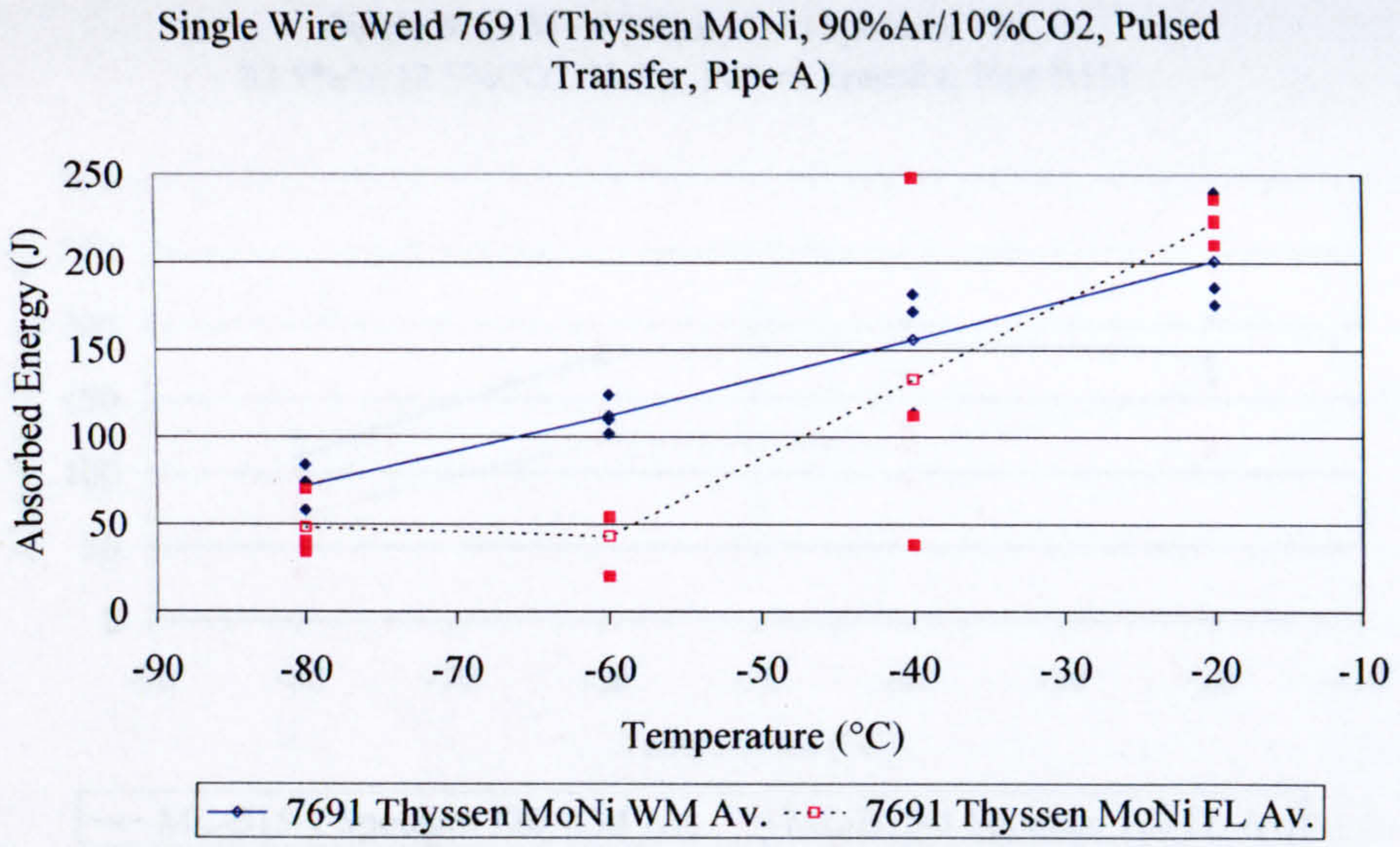

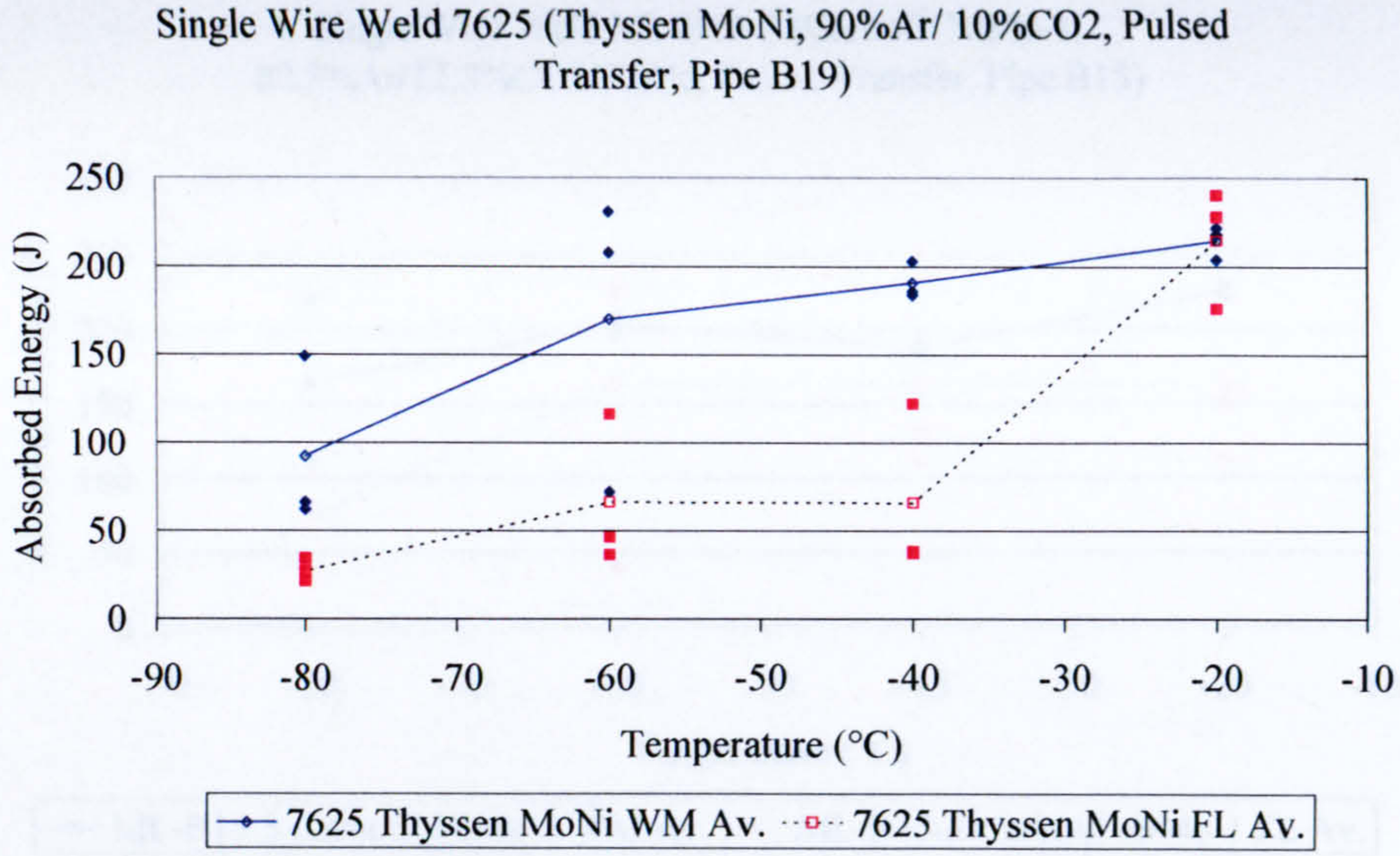

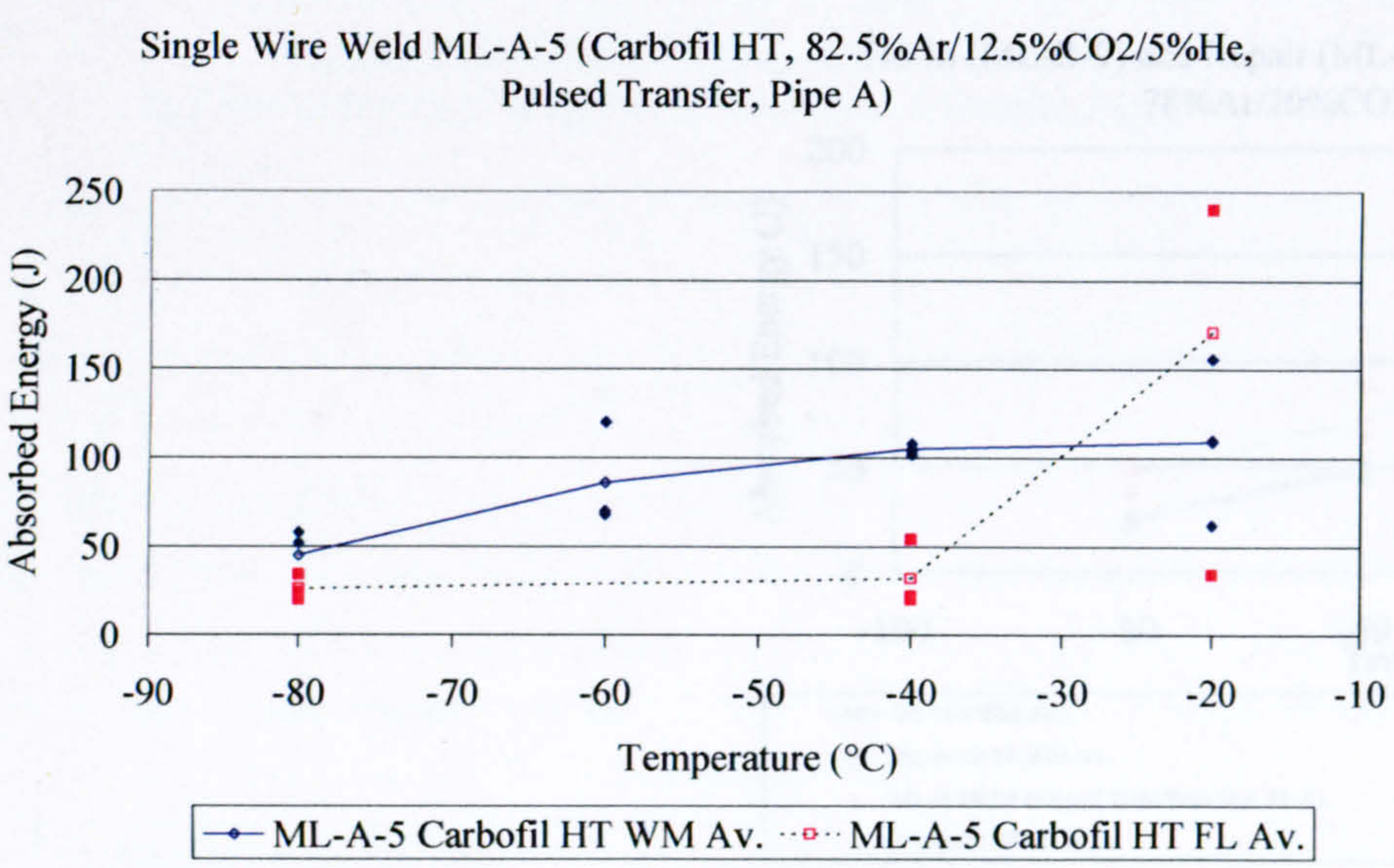

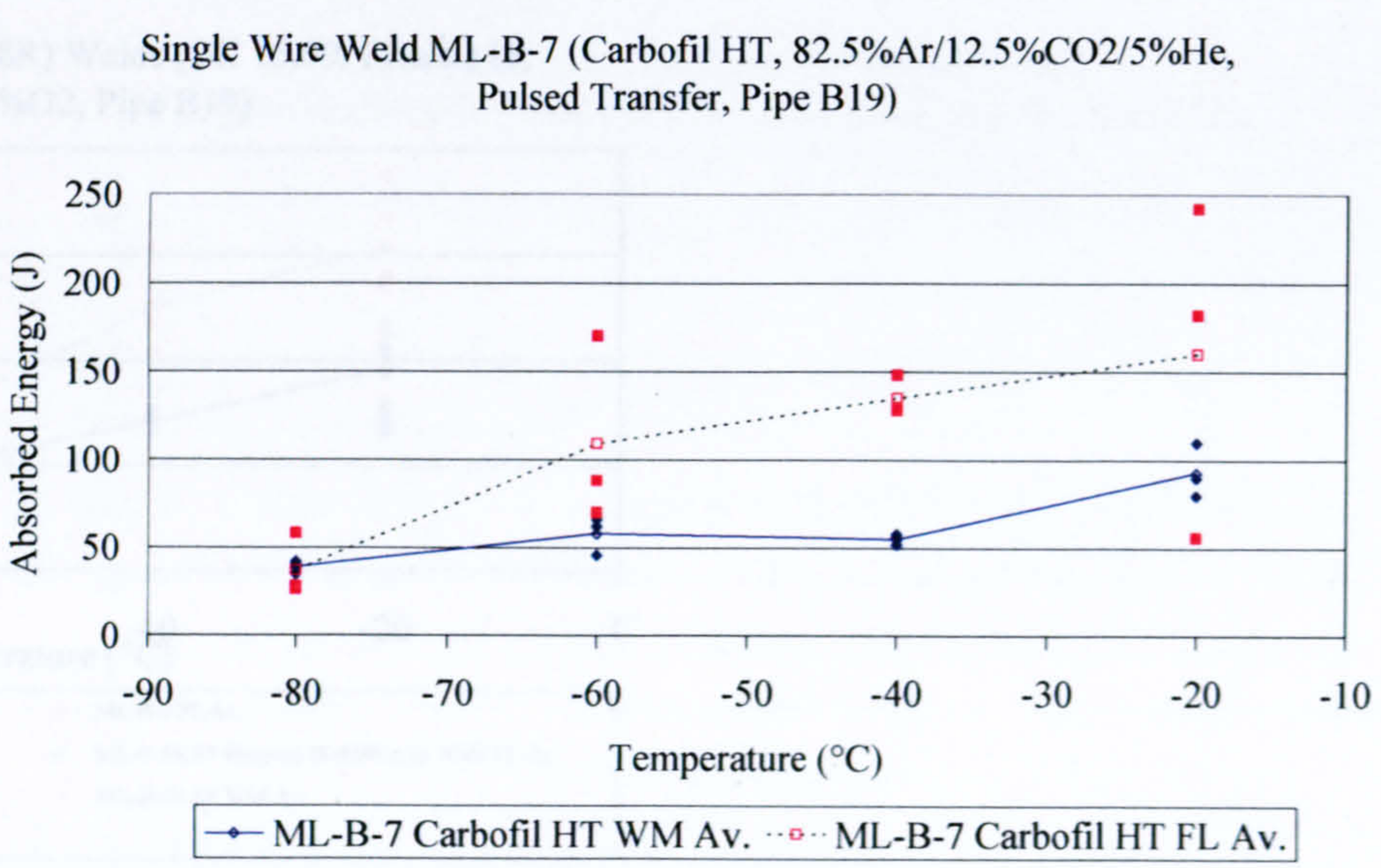

Figure 5-40: Single Wire Narrow Gap Weld Impact Transition Curves

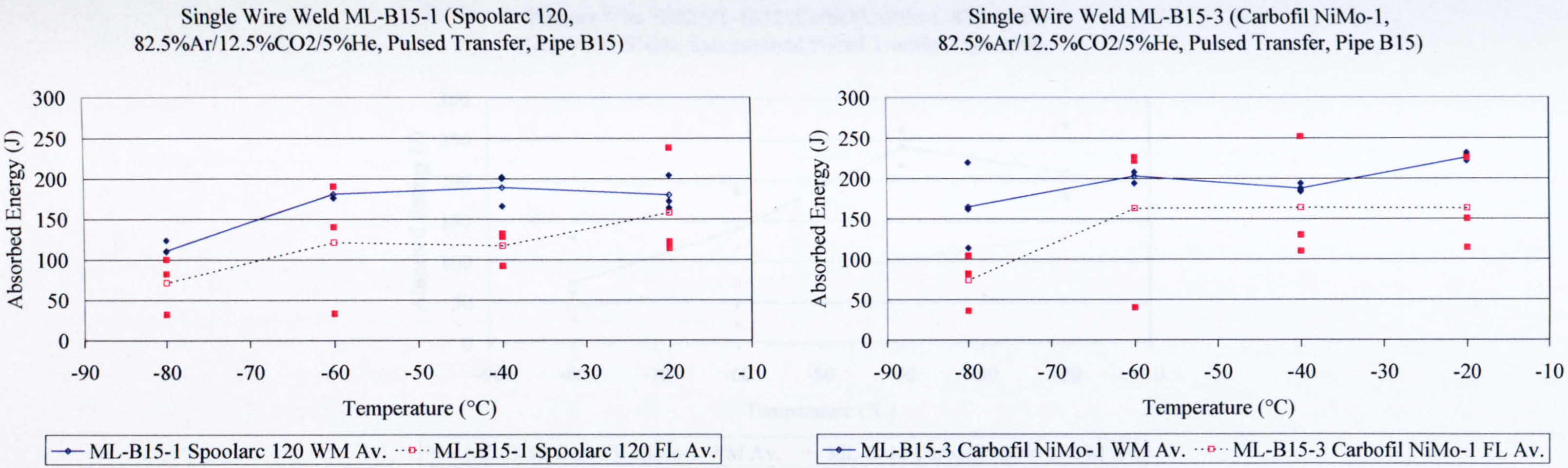

Figure 5-41: Single Wire Narrow Gap Weld Impact Transition Curves

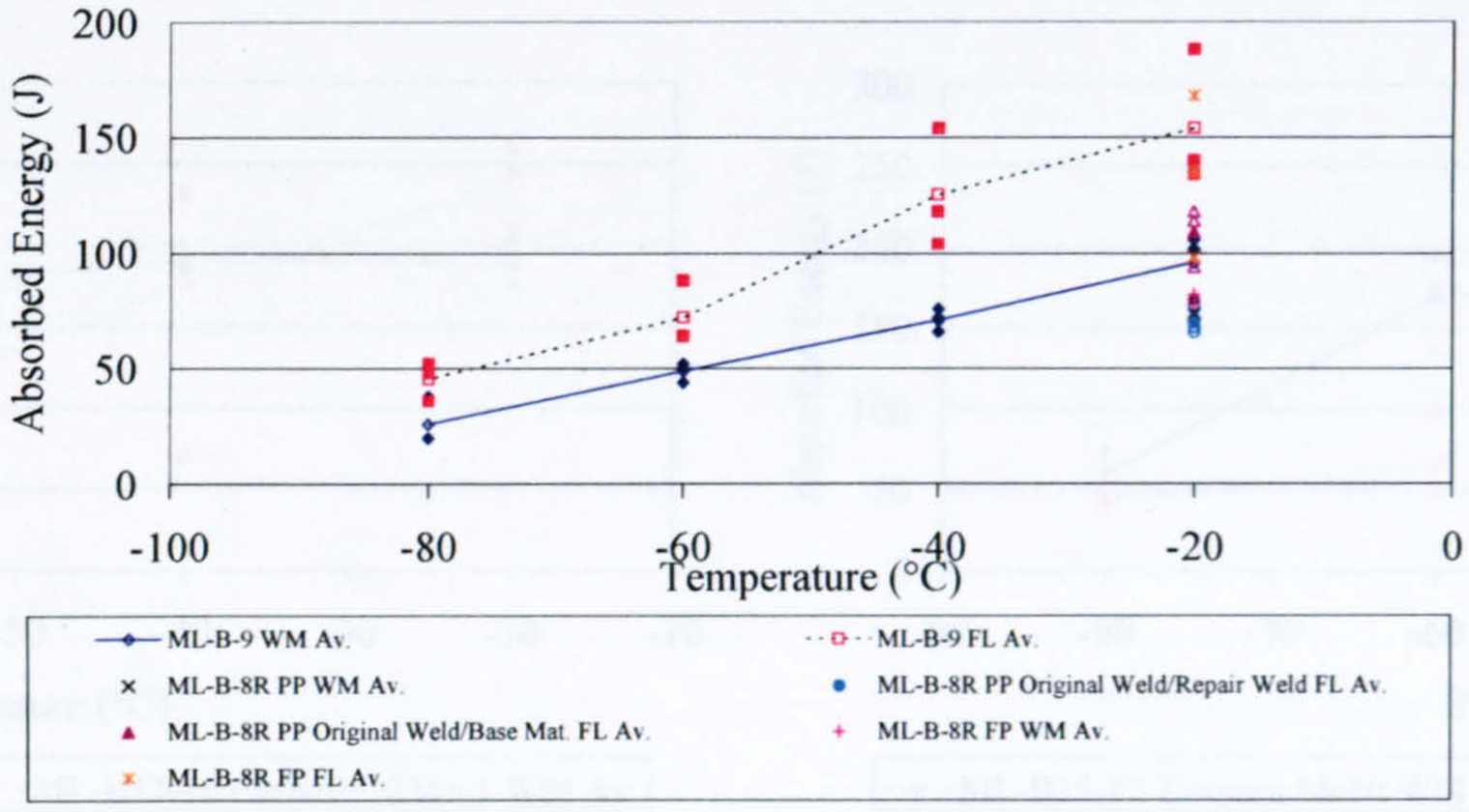

Figure 5-42: Tie-In and Repair Weld Impact Transition Curve

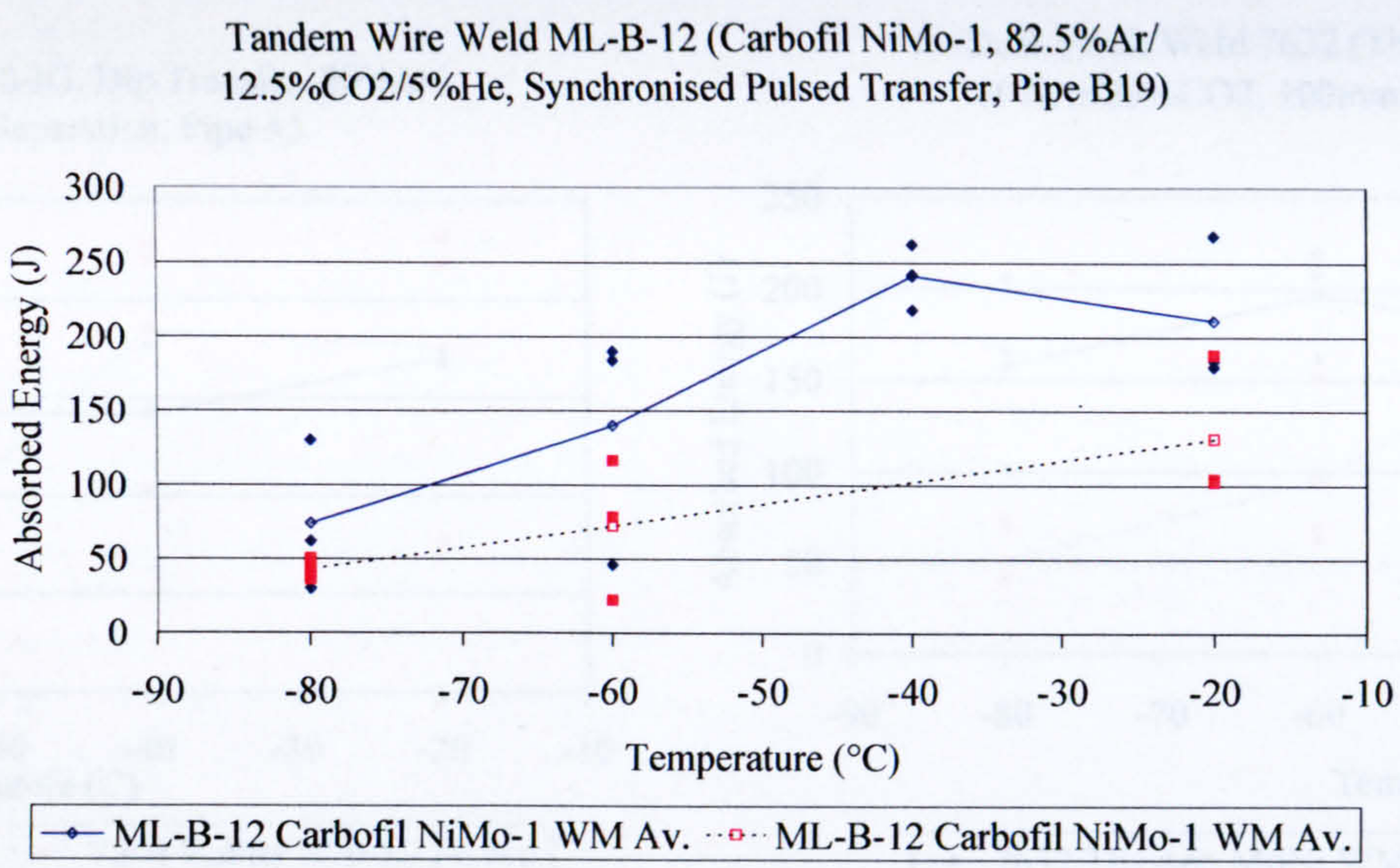

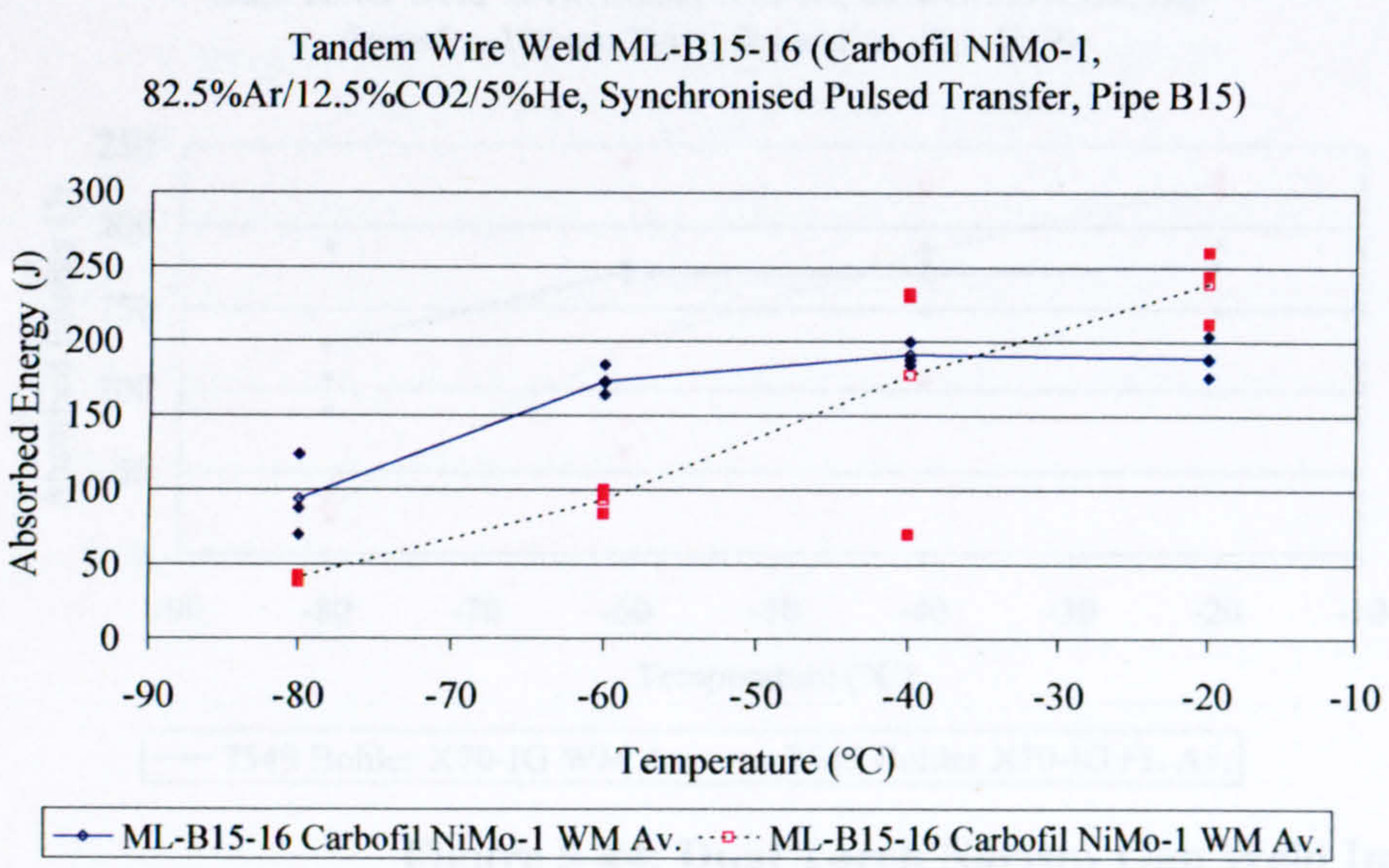

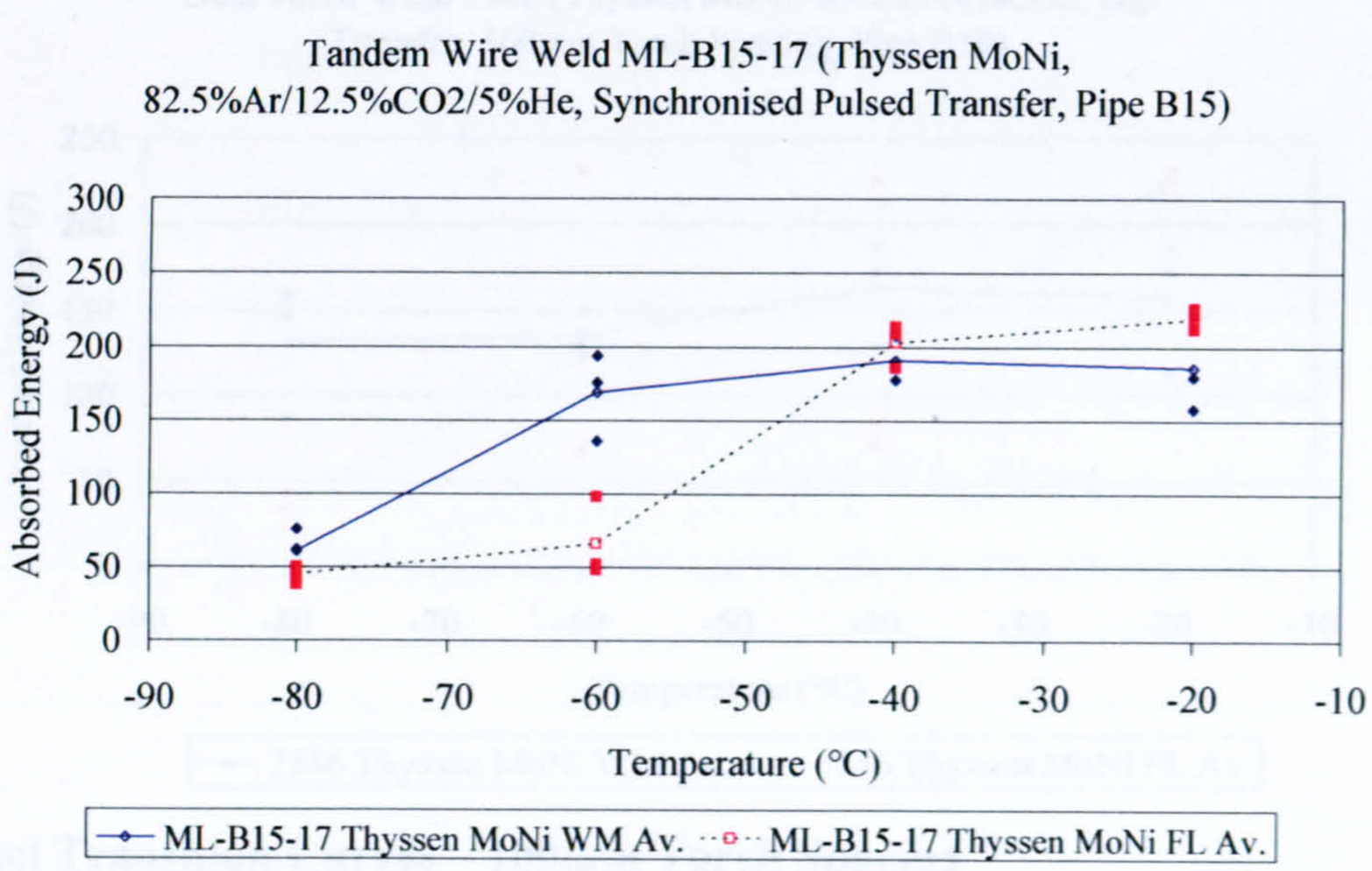

Figure 5-43: Tandem Wire Narrow Gap Weld Impact Transition Curves

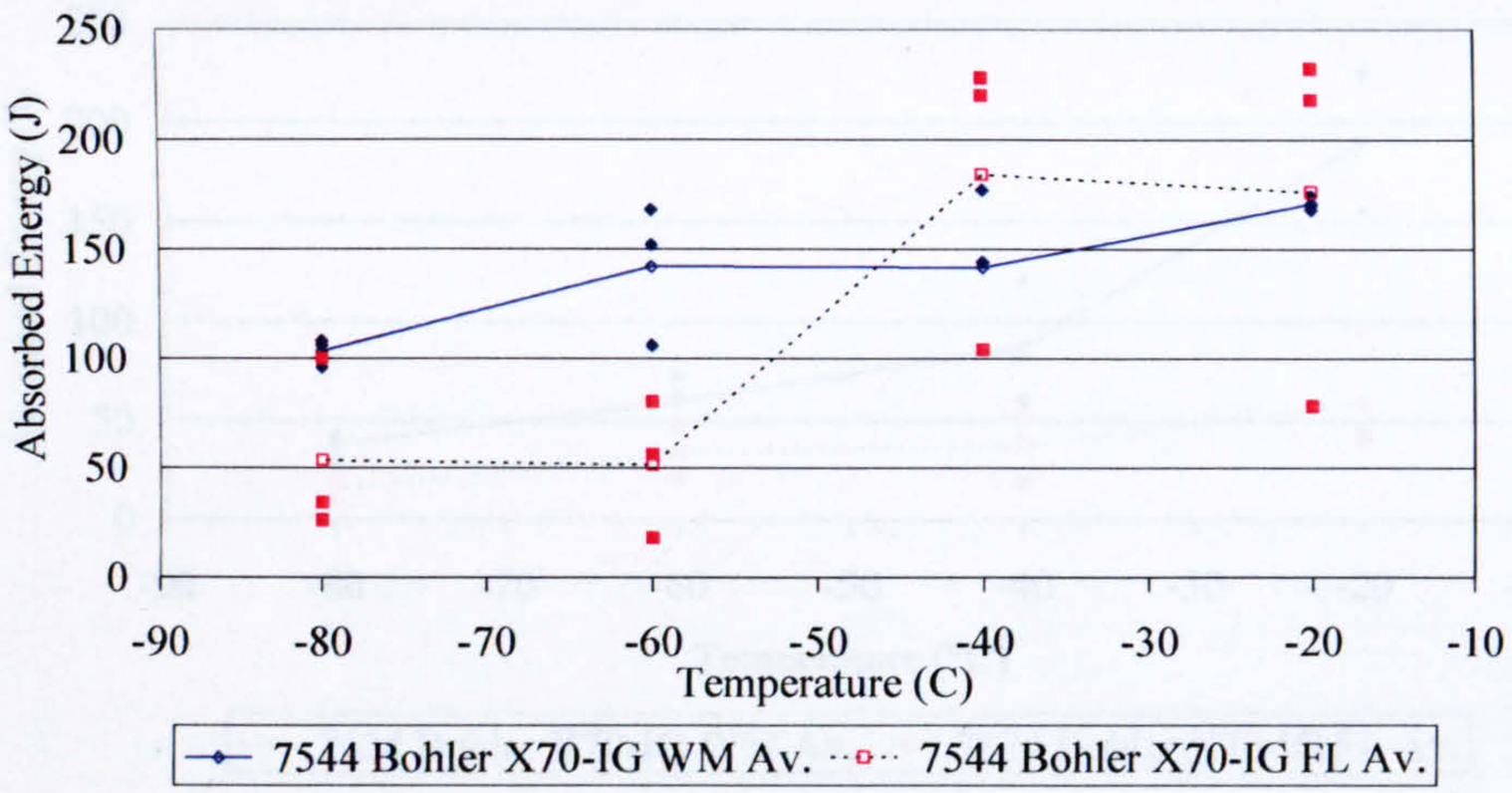

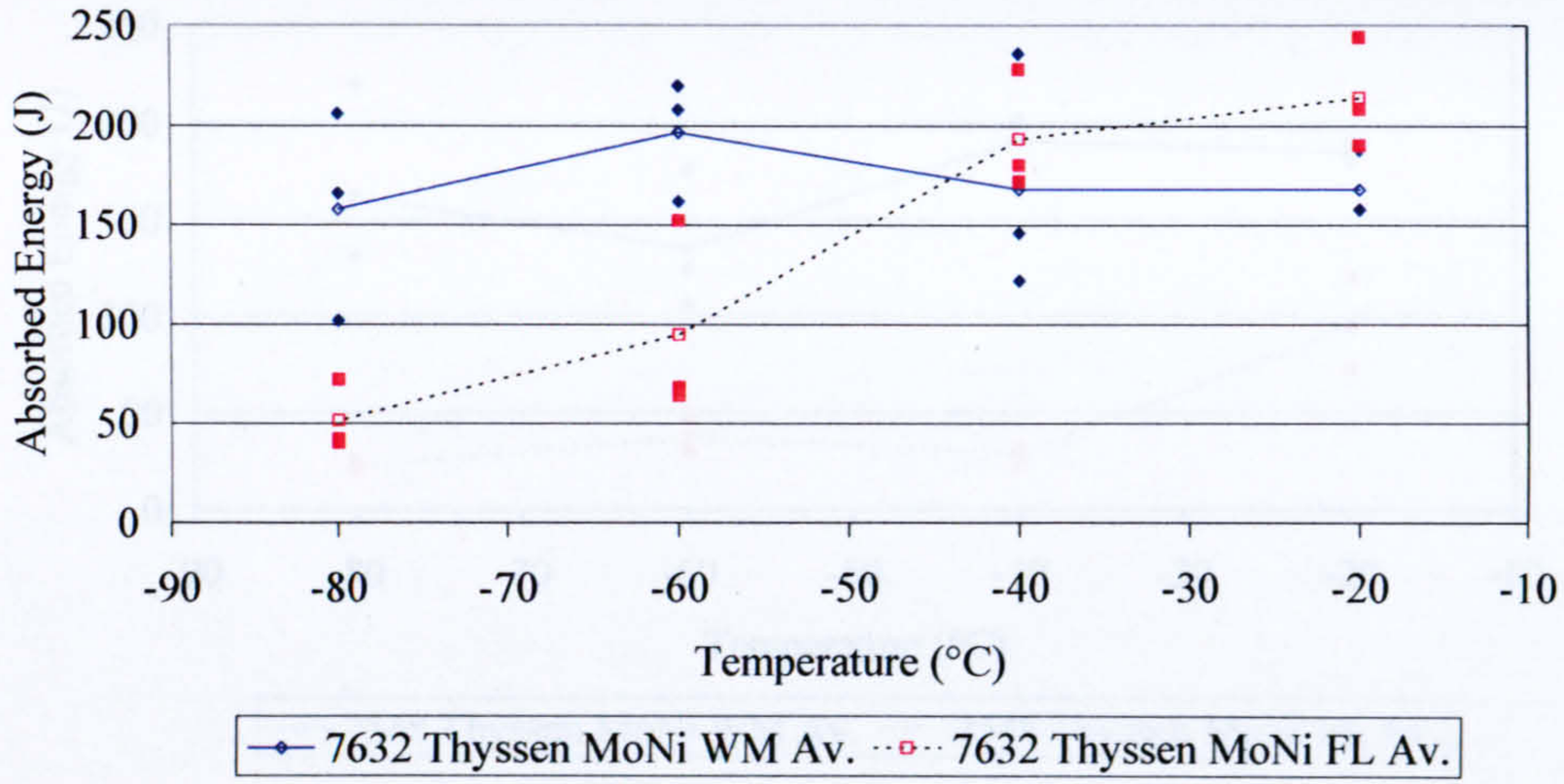

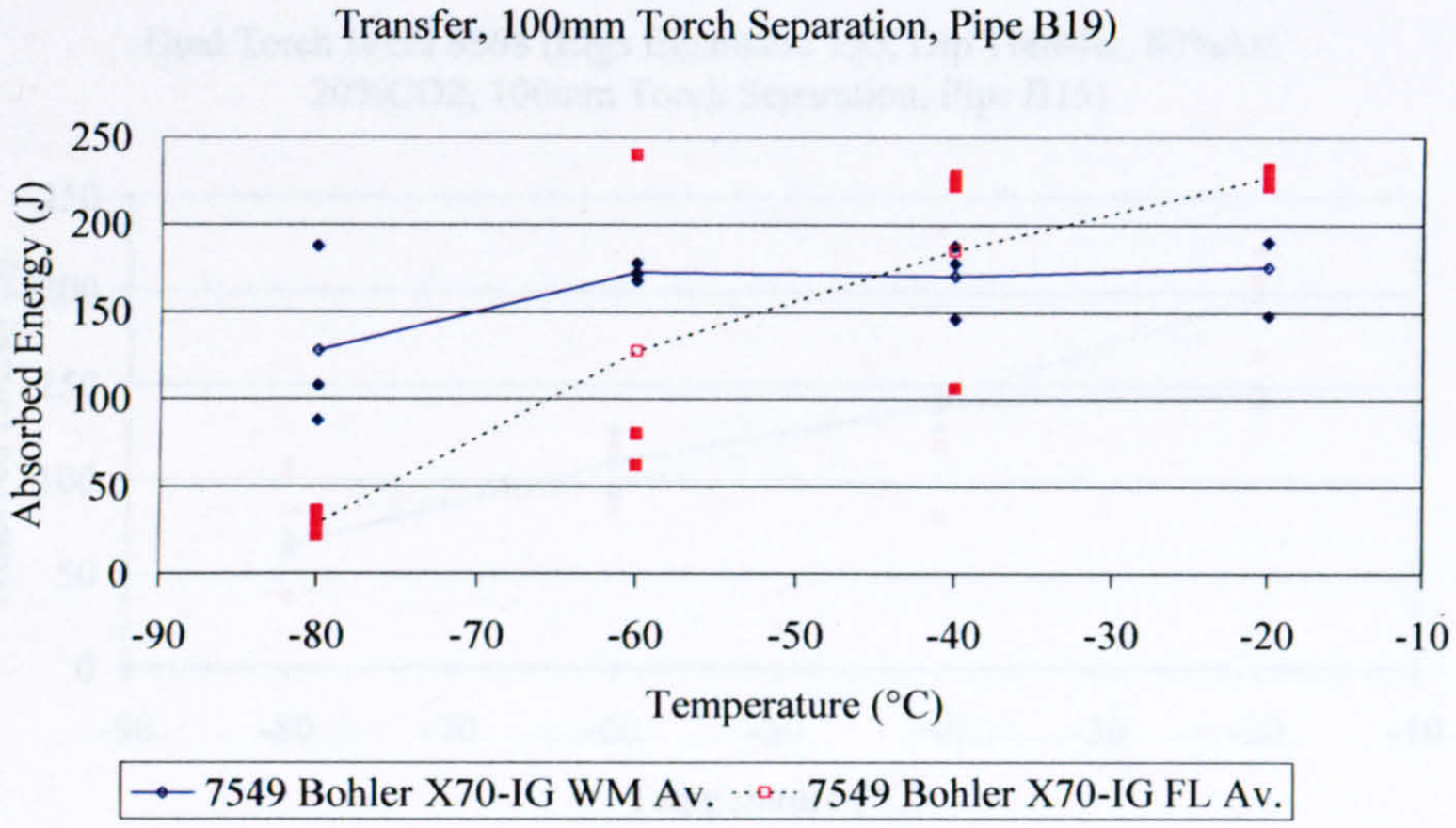

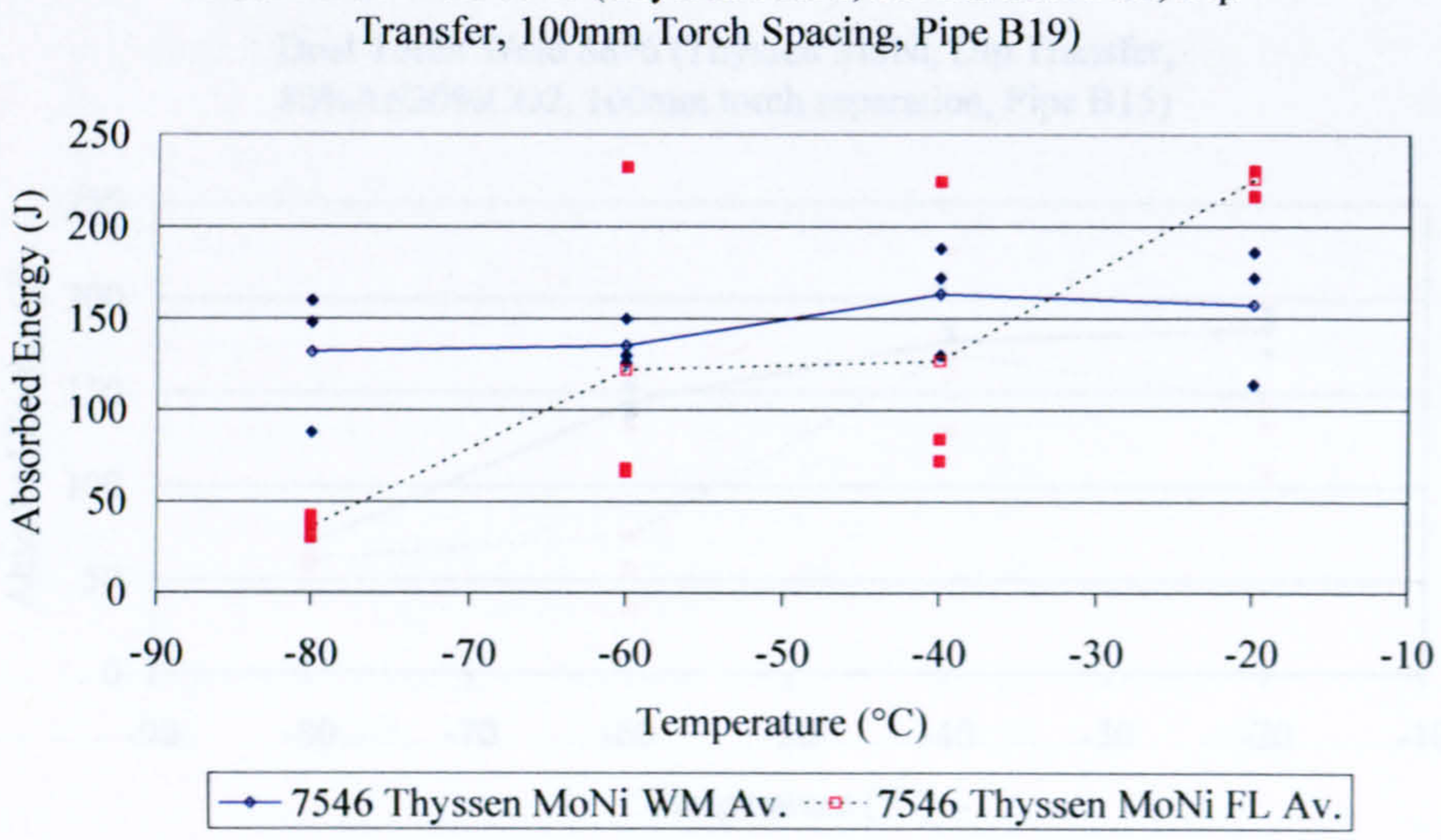

Figure 5-44: Dual Torch Narrow Gap Weld Impact Transition Curves – 100mm Torch Spacing

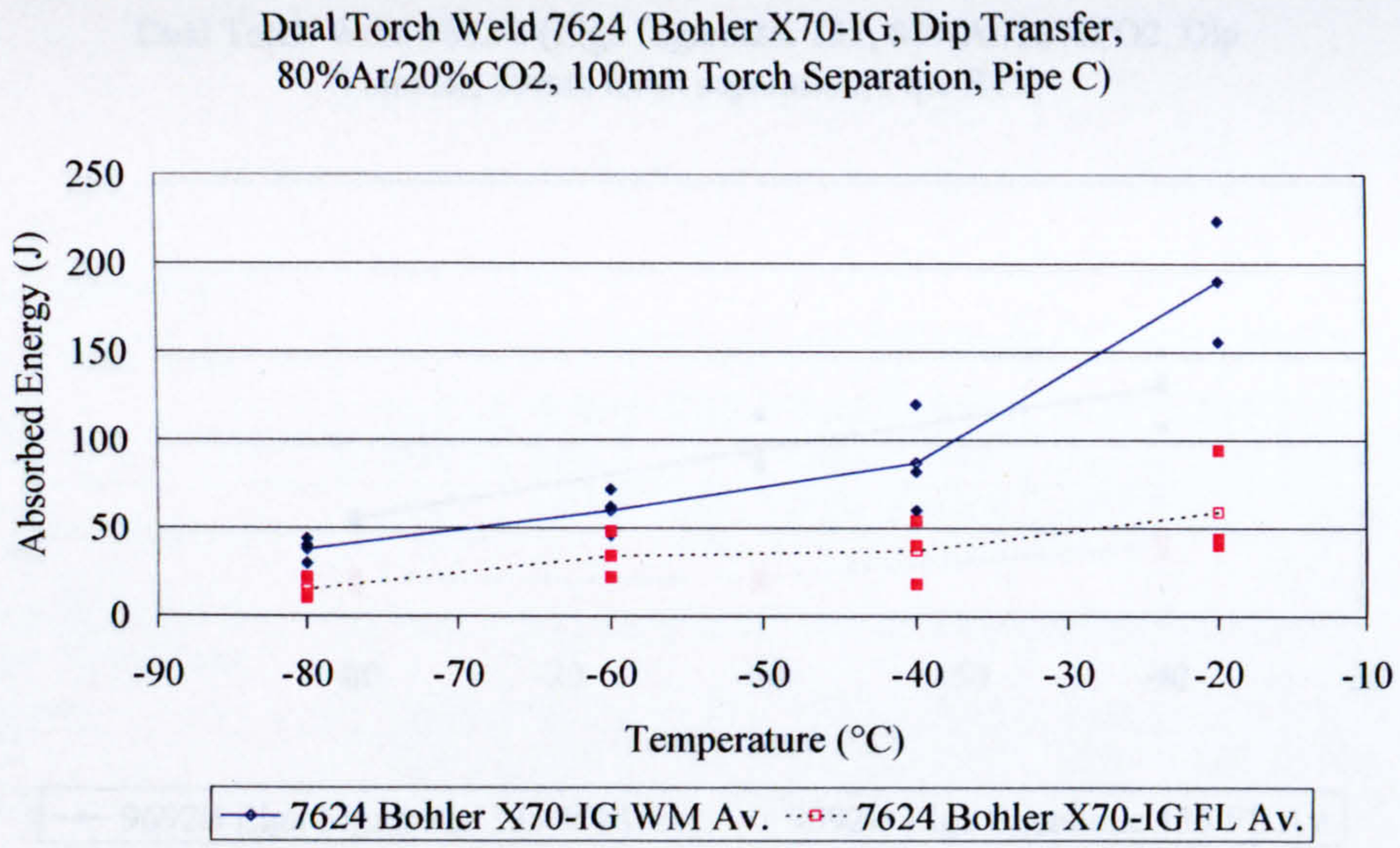

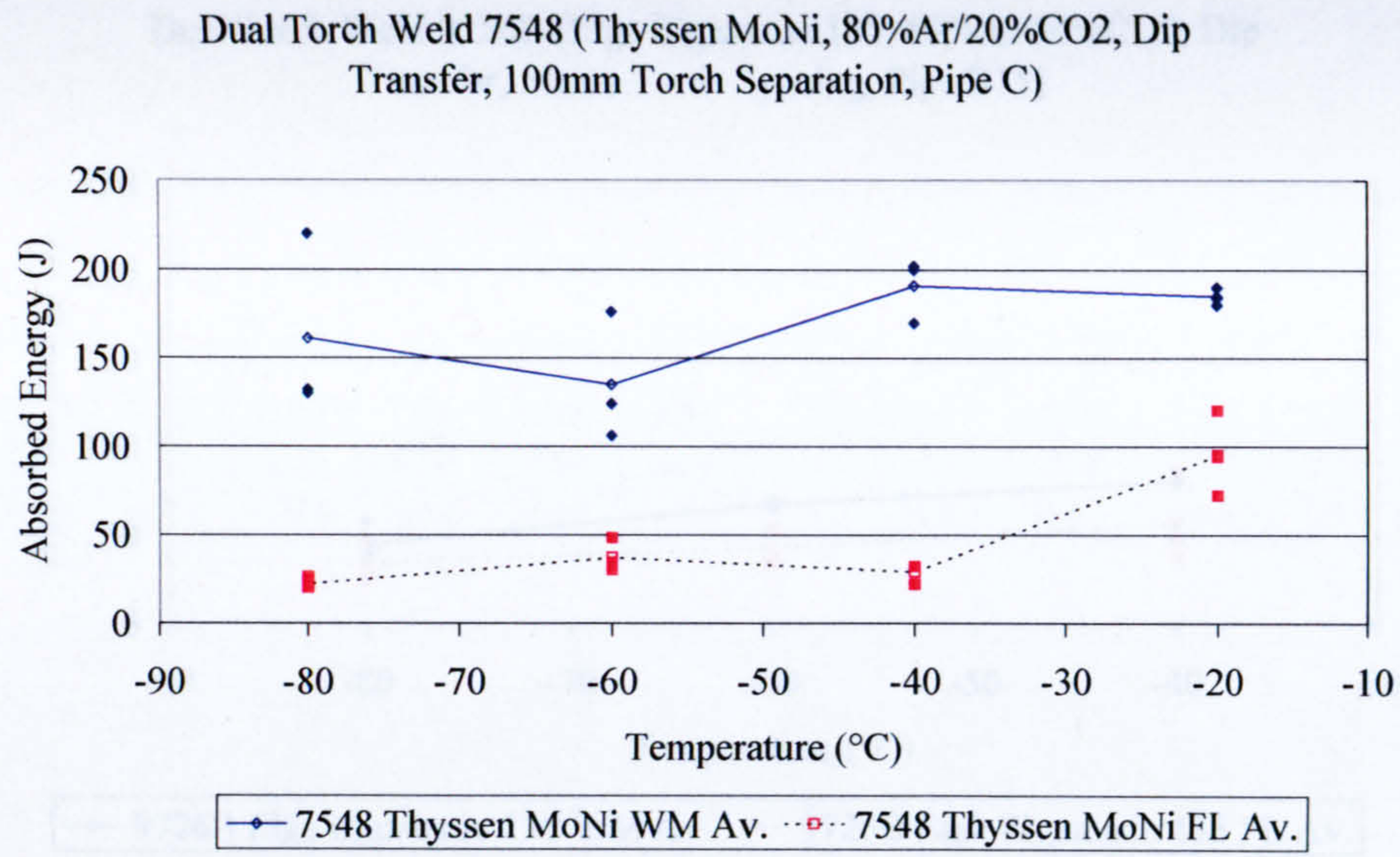

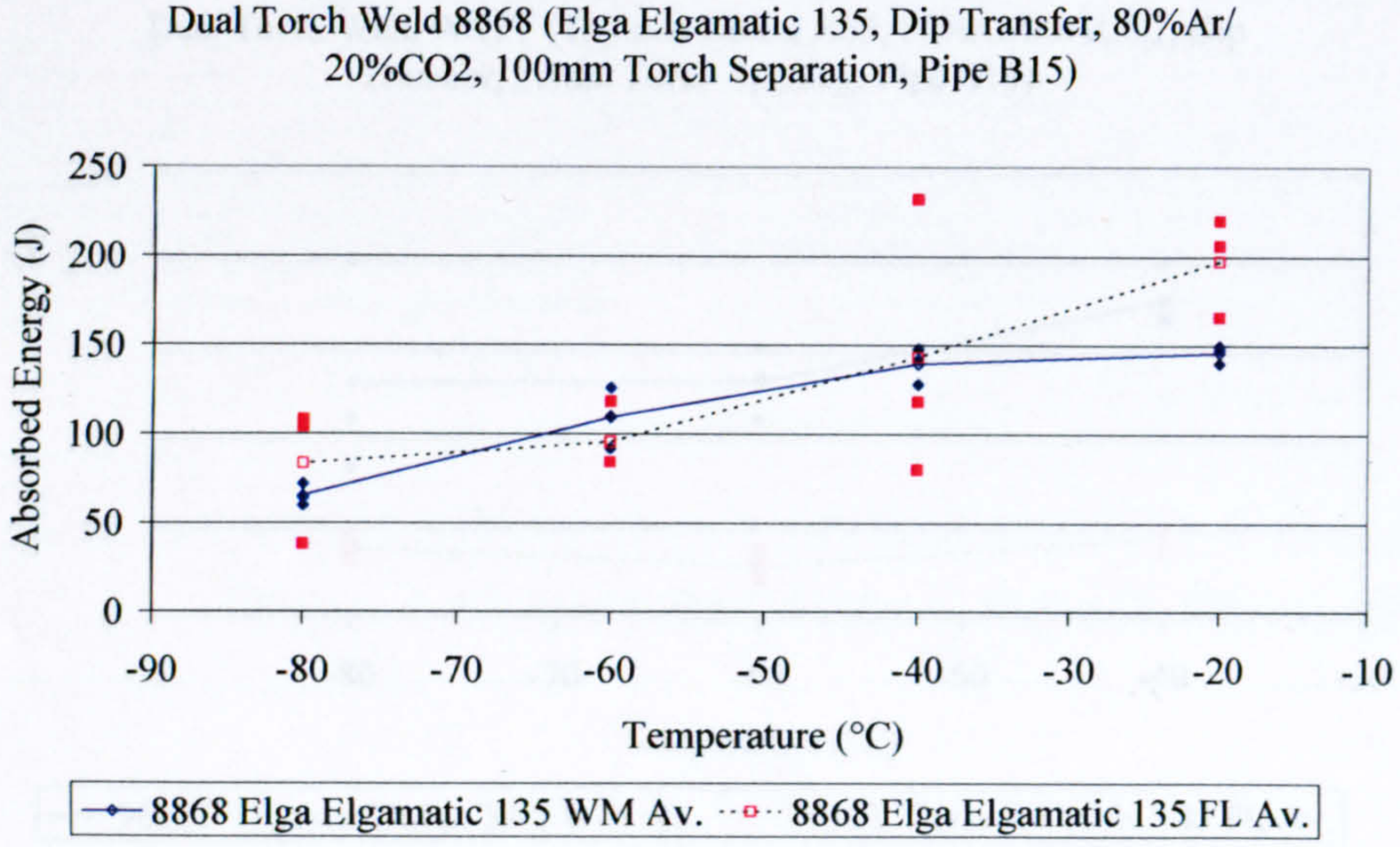

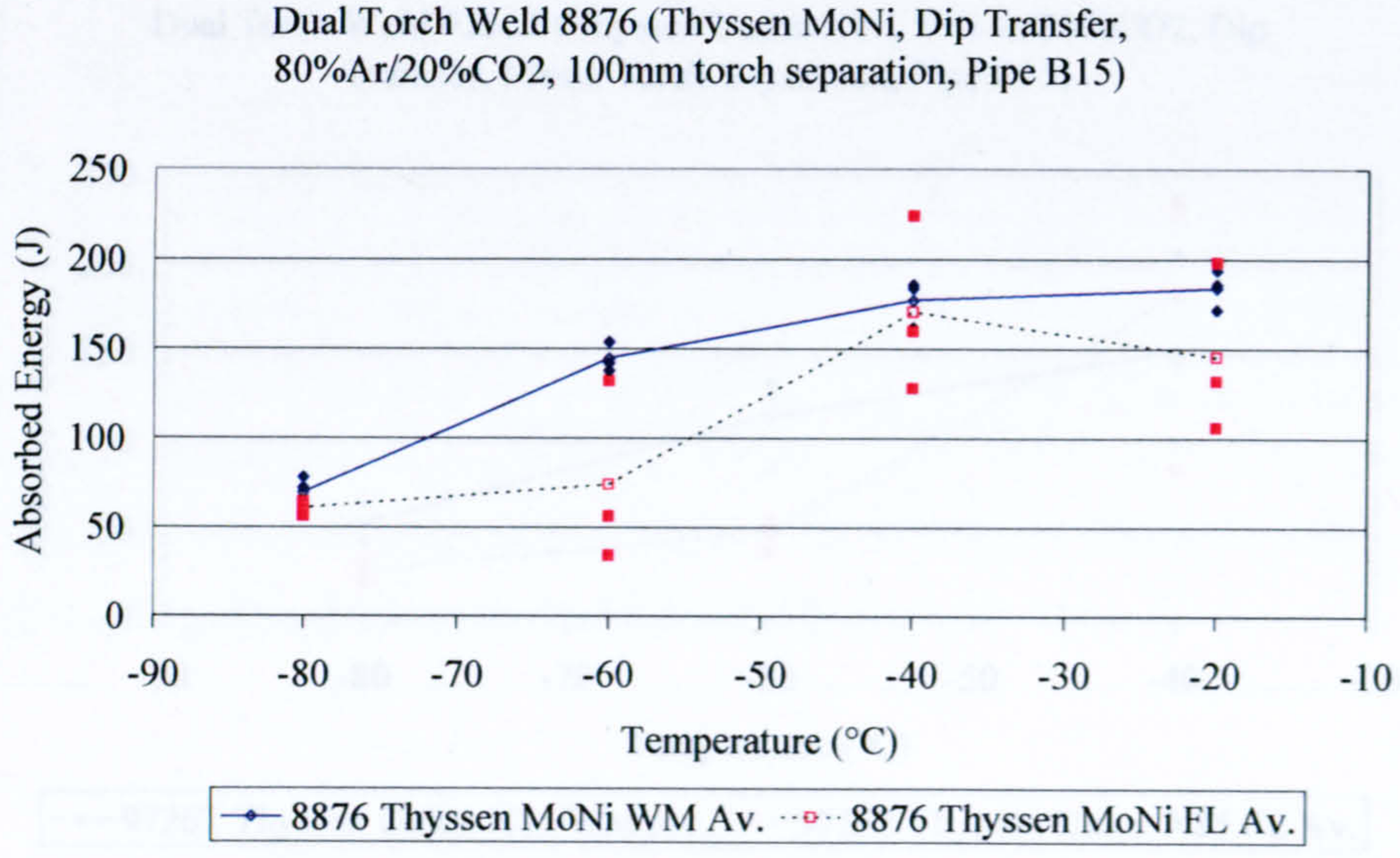

Figure 5-45: Dual Torch Narrow Gap Weld Impact Transition Curves – 100mm Torch Spacing

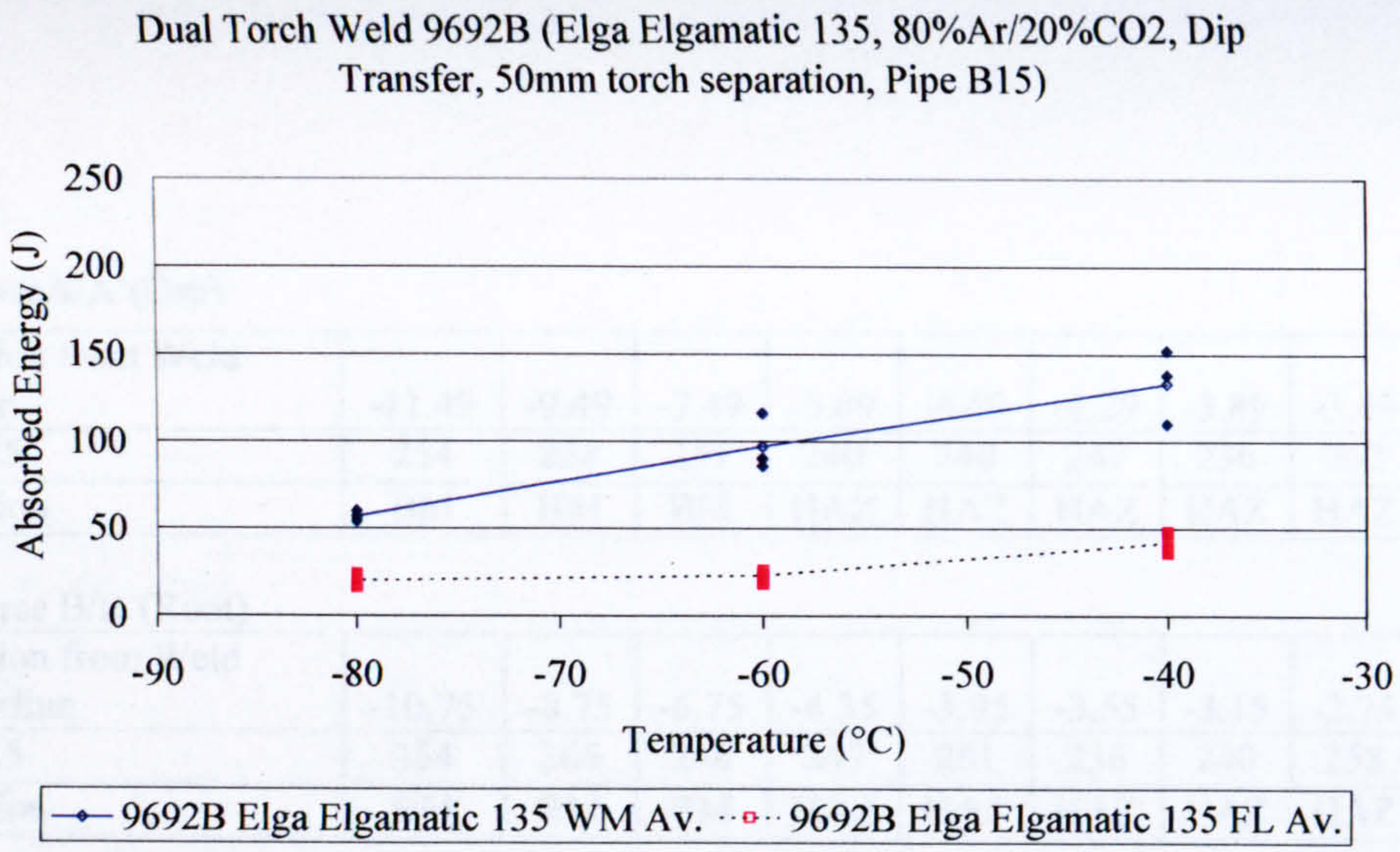

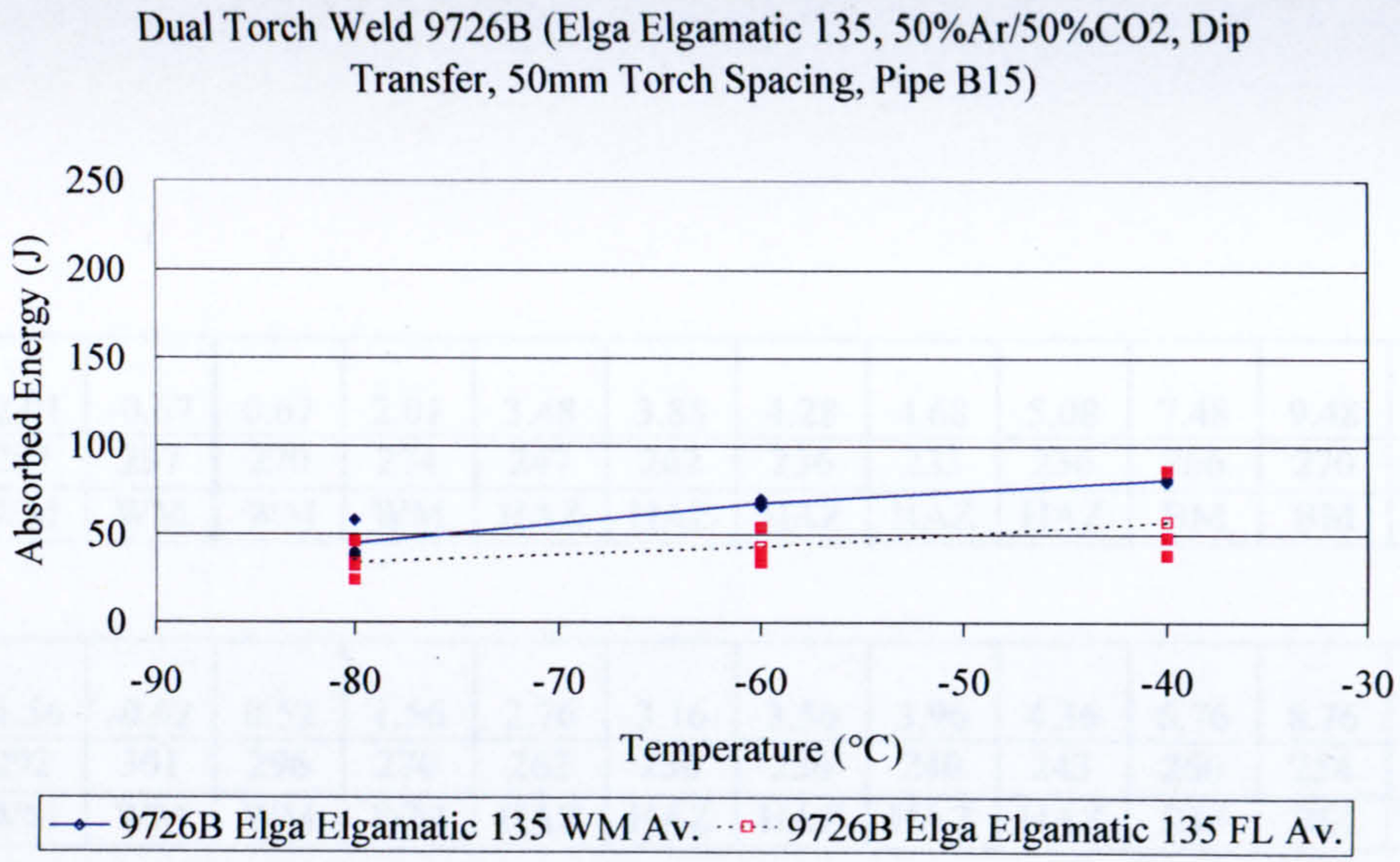

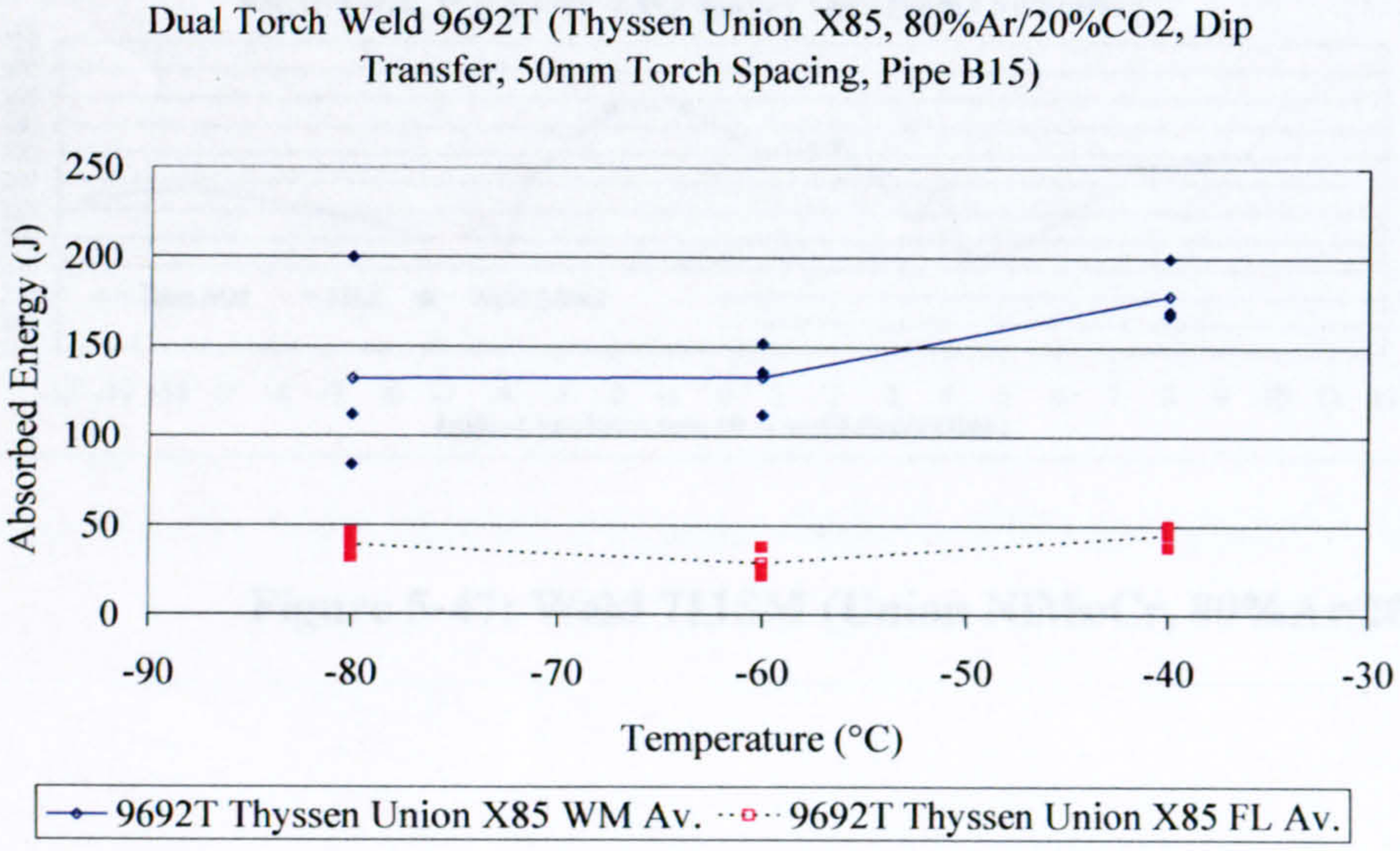

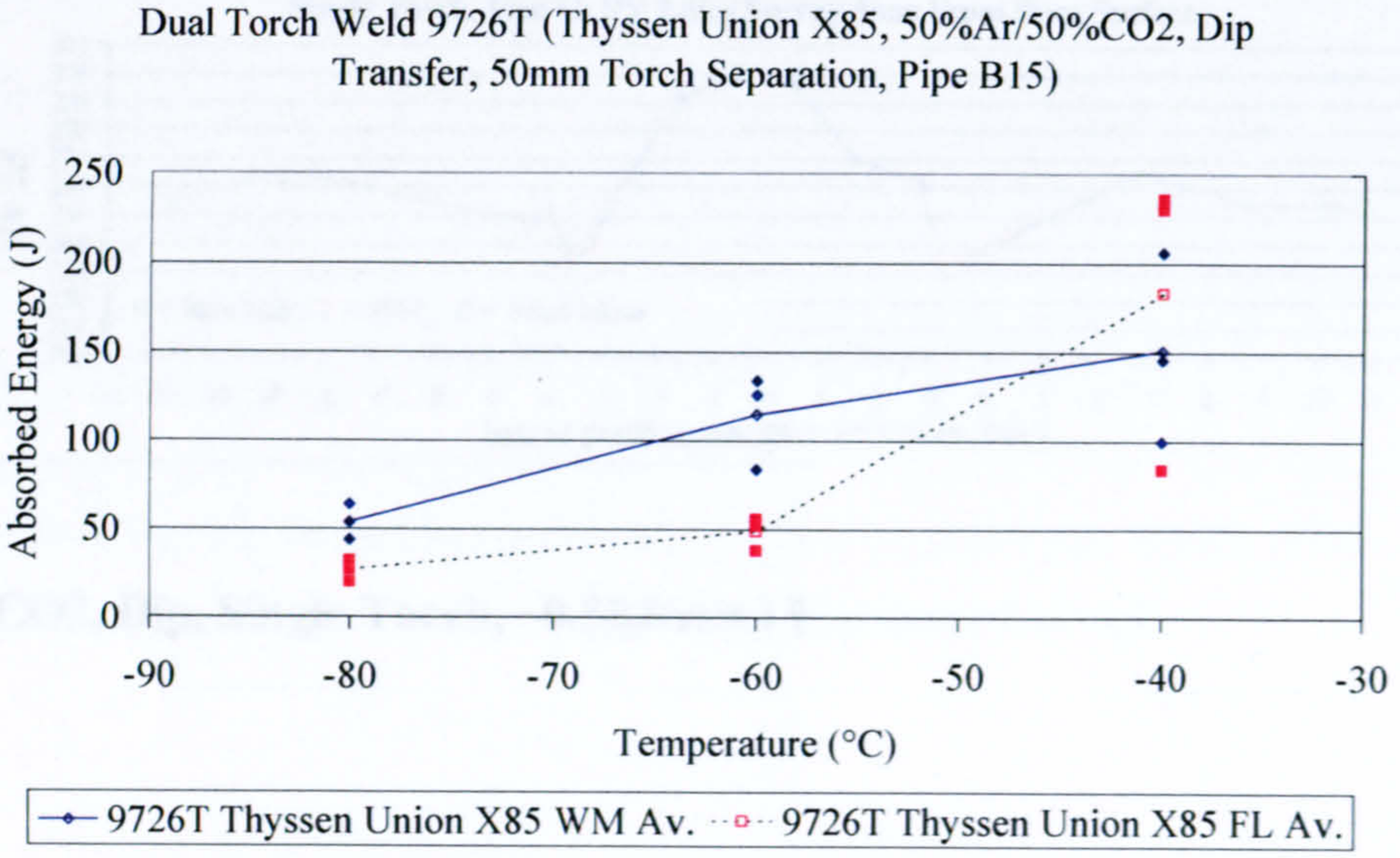

Figure 5-46: Dual Torch Narrow Gap Weld Impact Transition Curves – 50mm Torch Spacing

TraverseA/A'(Cap)

Location from Weld Center	-11.49	-9.49	-7.49	-5.09	-4.69	-4.29	-3.89	-3.49	-2.01	-0.67	0.67	2.01	3.48	3.88	4.28	4.68	5.08	7.48	9.48	11.48
HV 2.5	254	258	251	240	240	247	236	262	287	287	270	274	247	262	236	233	236	266	270	270
Location	BM	BM	BM	HAZ	HAZ	HAZ	HAZ	HAZ	WM	WM	WM	WM	HAZ	HAZ	HAZ	HAZ	HAZ	BM	BM	BM

Traverse B/B'(Root)

Location from Weld Centerline	-10.75	-8.75	-6.75	-4.35	-3.95	-3.55	-3.15	-2.75	-1.56	-0.52	0.52	1.56	2.76	3.16	3.56	3.96	4.36	6.76	8.76	10.76
HV 2.5	254	266	258	247	251	236	240	258	292	301	296	270	262	236	236	240	243	266	254	254
Location	BM	BM	BM	HAZ	HAZ	HAZ	HAZ	HAZ	WM	WM	WM	WM	HAZ	HAZ	HAZ	HAZ	HAZ	BM	BM	BM

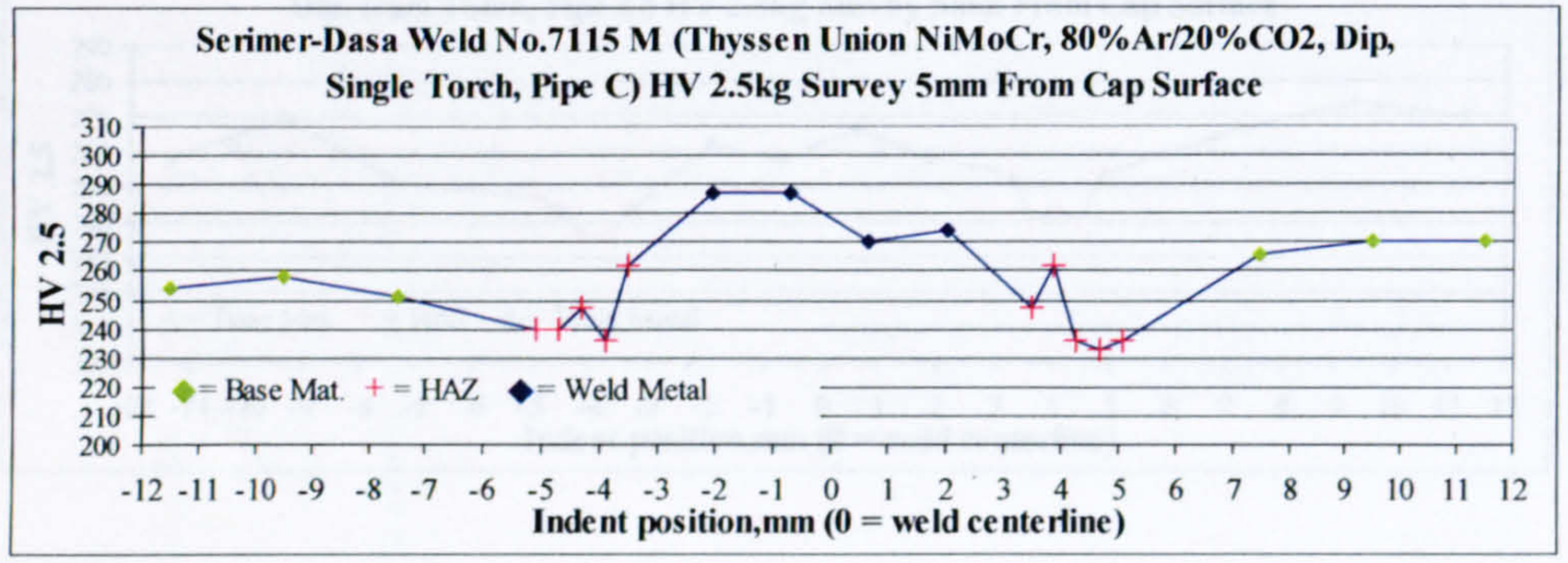

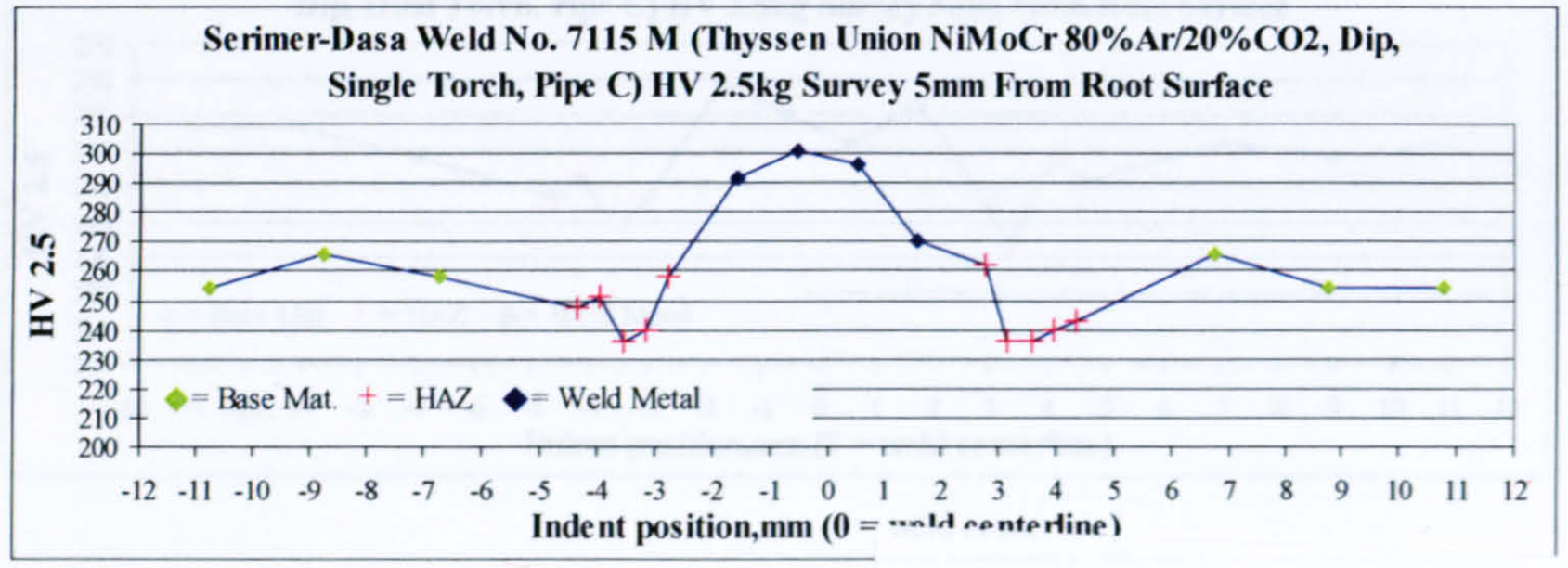

Figure 5-47: Weld 7115M (Union NiMoCr, 80%Ar/20%CO2, Dip, Single Torch, ~0.5kJ/mm) H

TraverseA/A'(Cap)

Location from Weld Center	-11.30	-9.30	-7.30	-4.90	-4.50	-4.10	-3.70	-3.30	-1.86	-0.62	0.62	1.86	3.27	3.67	4.07	4.47	4.87	7.27	9.27	11.27
HV 2.5	258	270	251	247	243	236	236	243	262	258	266	258	254	240	243	240	254	266	274	270
Location	BM	BM	BM	HAZ	HAZ	HAZ	HAZ	HAZ	WM	WM	WM	WM	HAZ	HAZ	HAZ	HAZ	HAZ	BM	BM	BM

Traverse B/B' (root)

Location from Weld Centerline	-11.00	-9.00	-7.00	-4.60	-4.20	-3.80	-3.40	-3.00	-1.72	-0.57	0.57	1.72	3.00	3.40	3.80	4.20	4.60	7.00	9.00	11.00
HV 2.5	266	266	258	247	254	243	240	247	279	270	262	274	243	233	251	258	251	262	258	262
Location	BM	BM	BM	HAZ	HAZ	HAZ	HAZ	HAZ	WM	WM	WM	WM	HAZ	HAZ	HAZ	HAZ	HAZ	BM	BM	BM

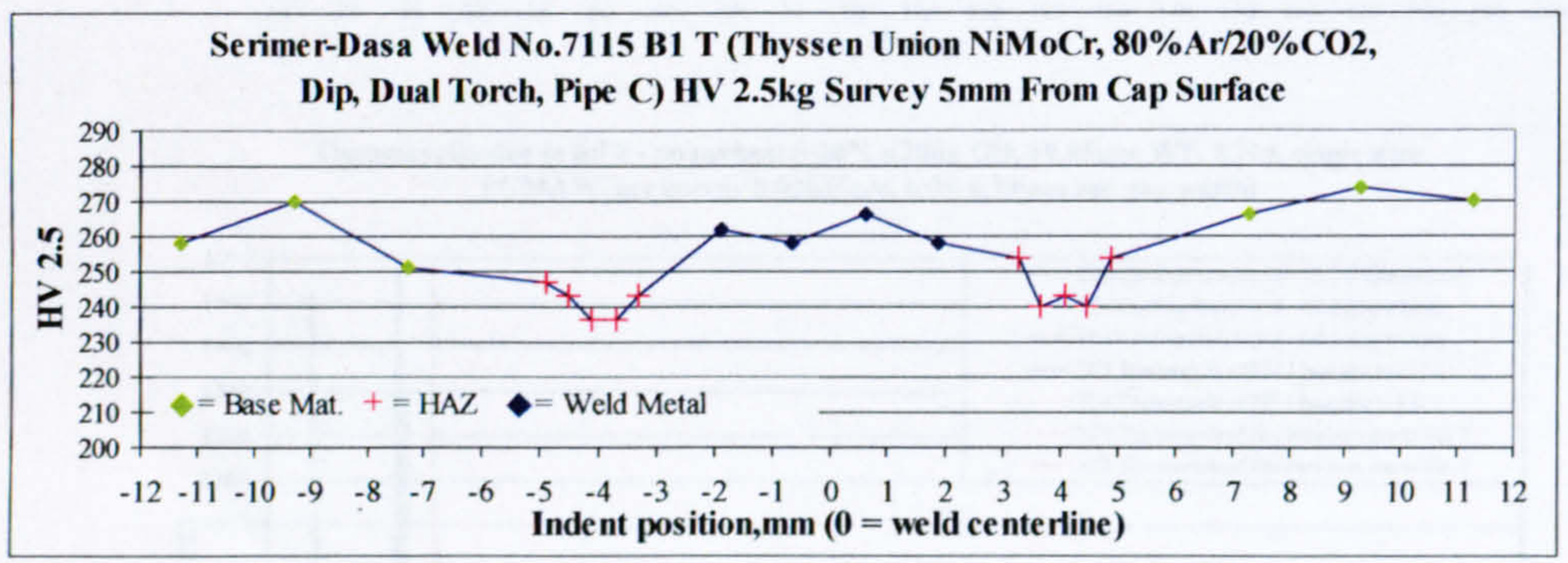

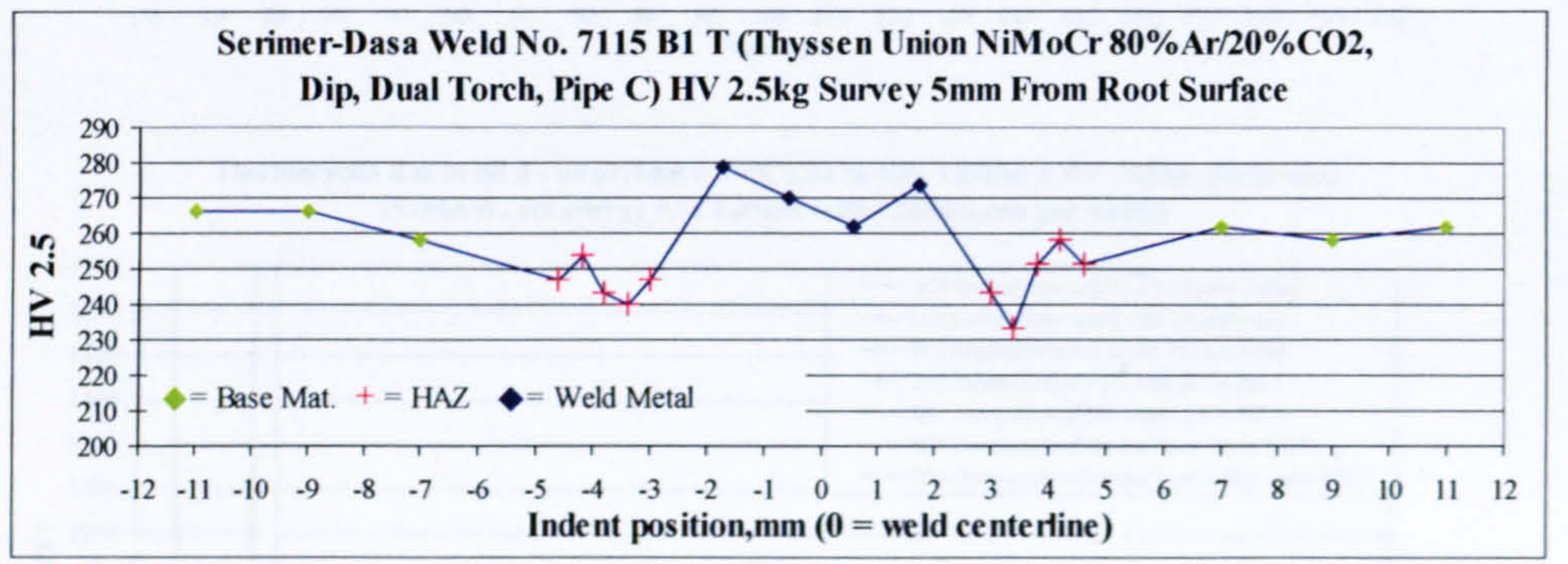

Figure 5-48: Weld 7115B1 T (Union NiMoCr, 80%Ar/20%CO2, Dip, Dual Torch, ~0.5kJ/mm, 50mm Torch Spacing) Hardness Survey

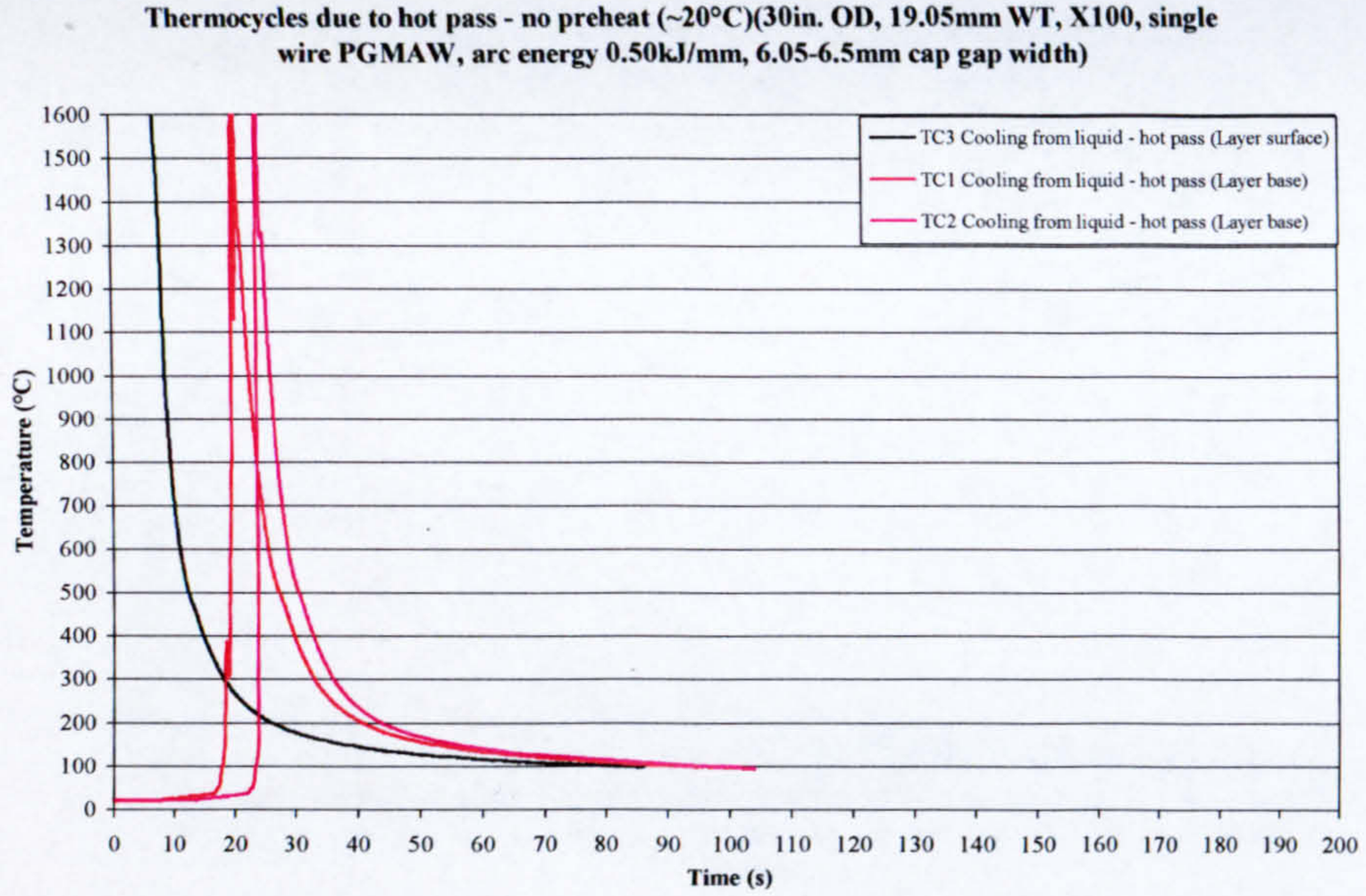

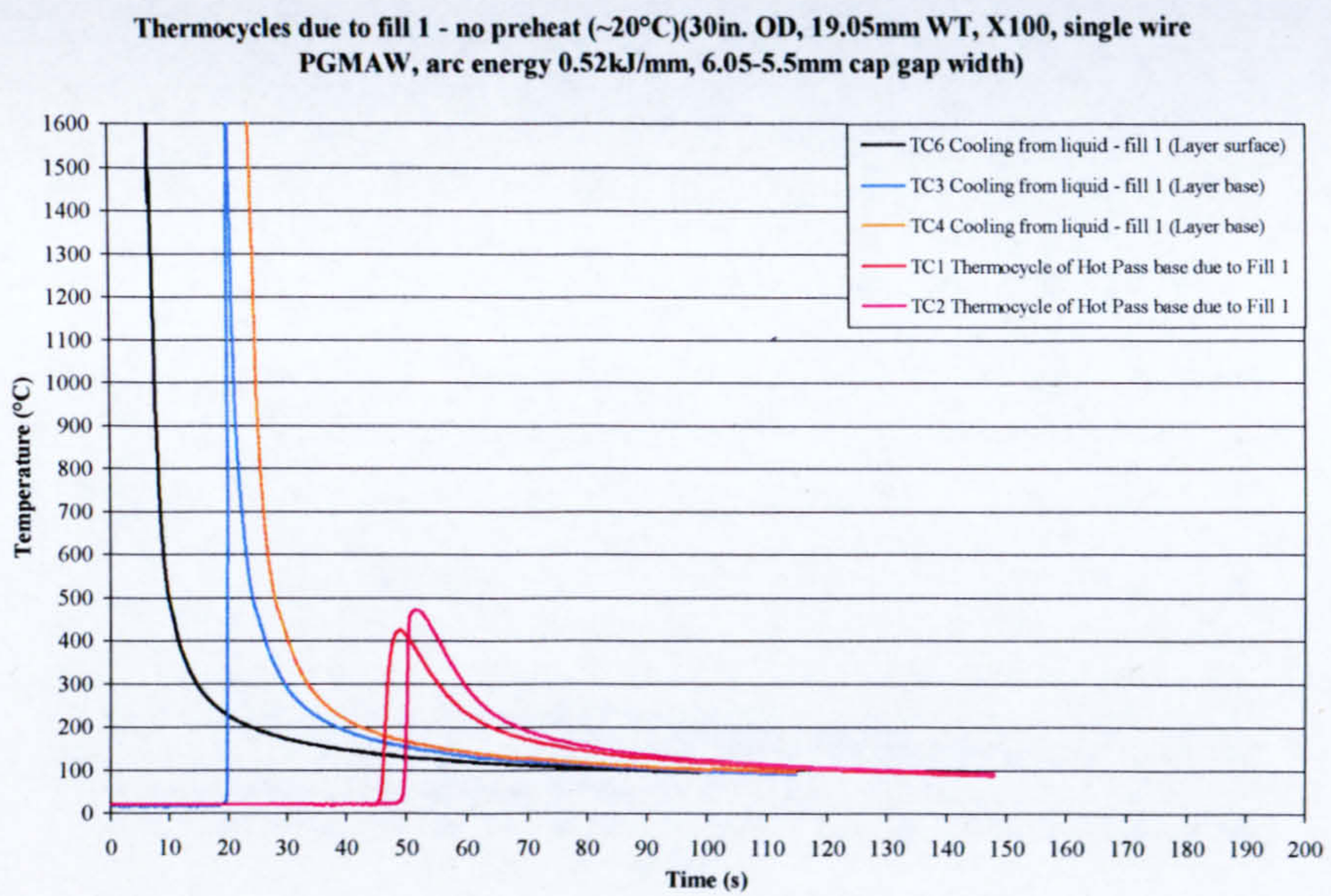

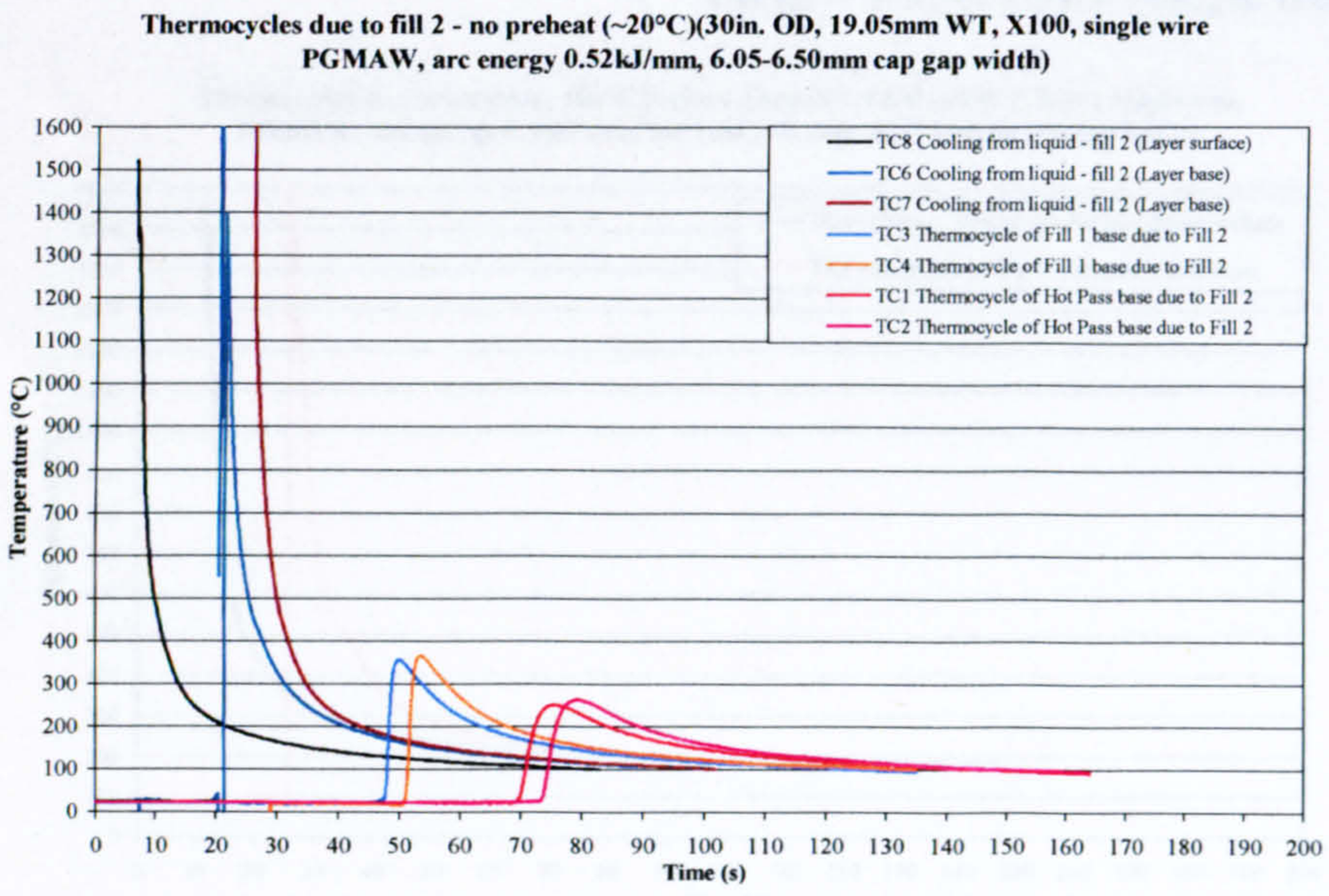

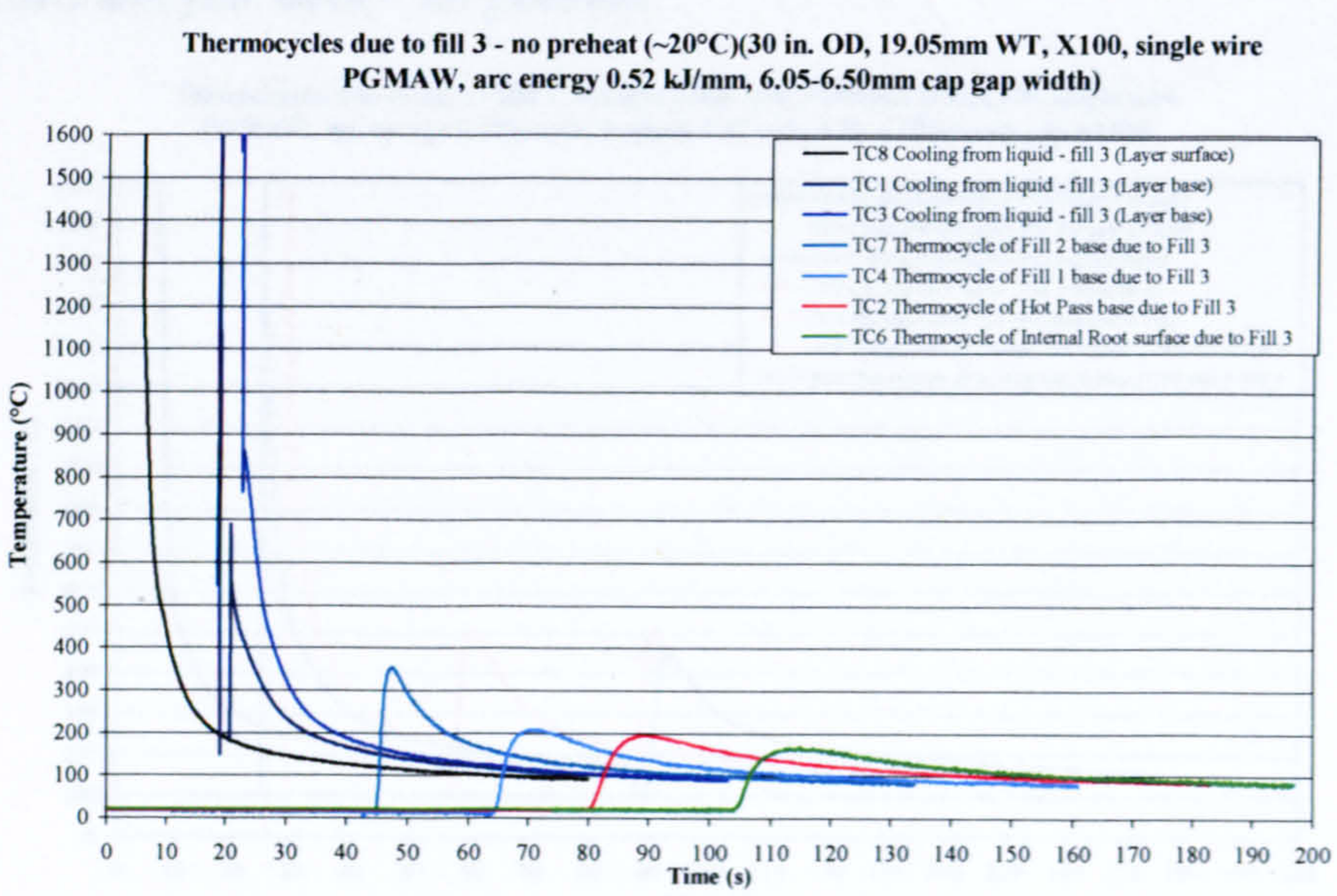

Figure 5-49: Single wire thermocycle data – no preheat

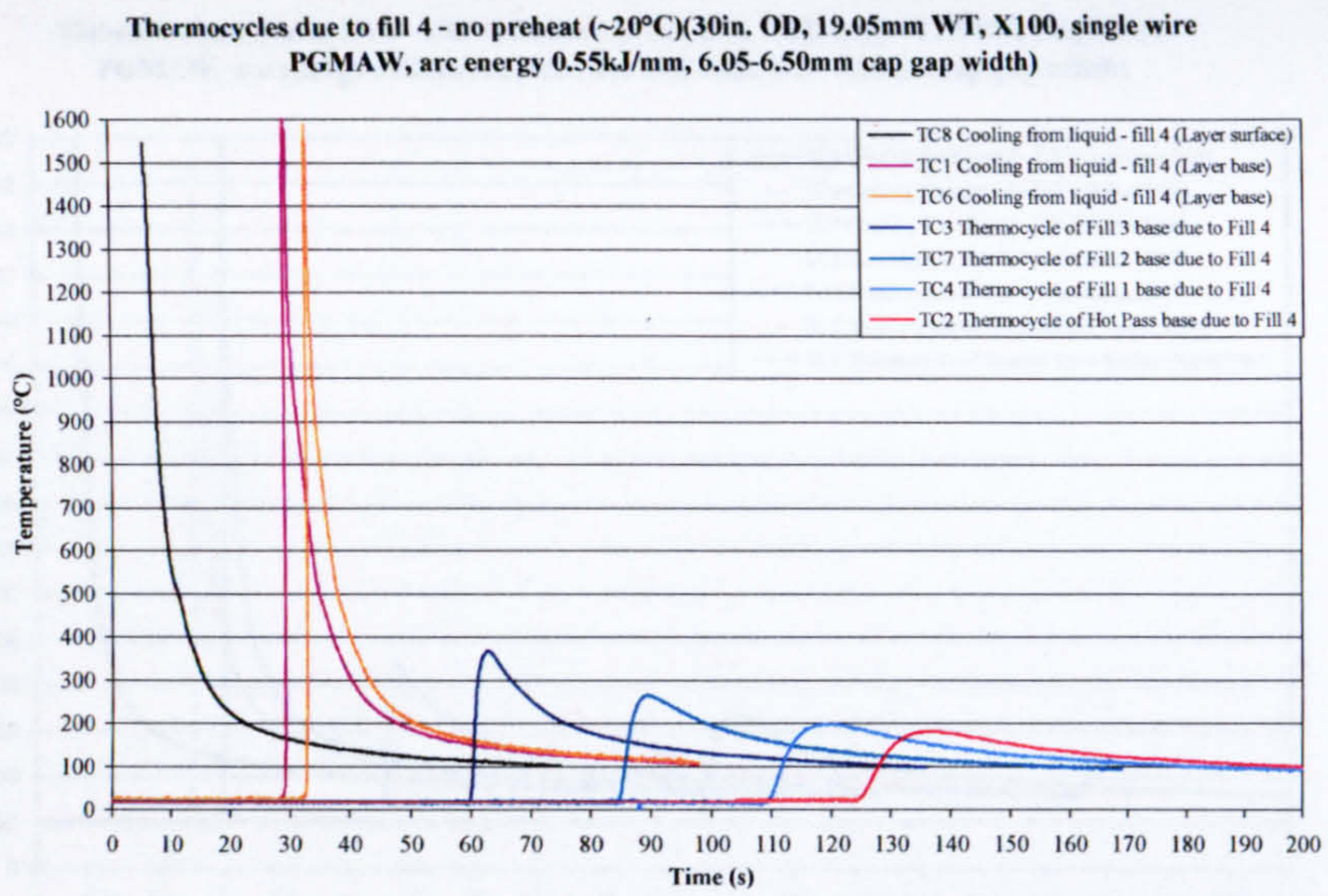

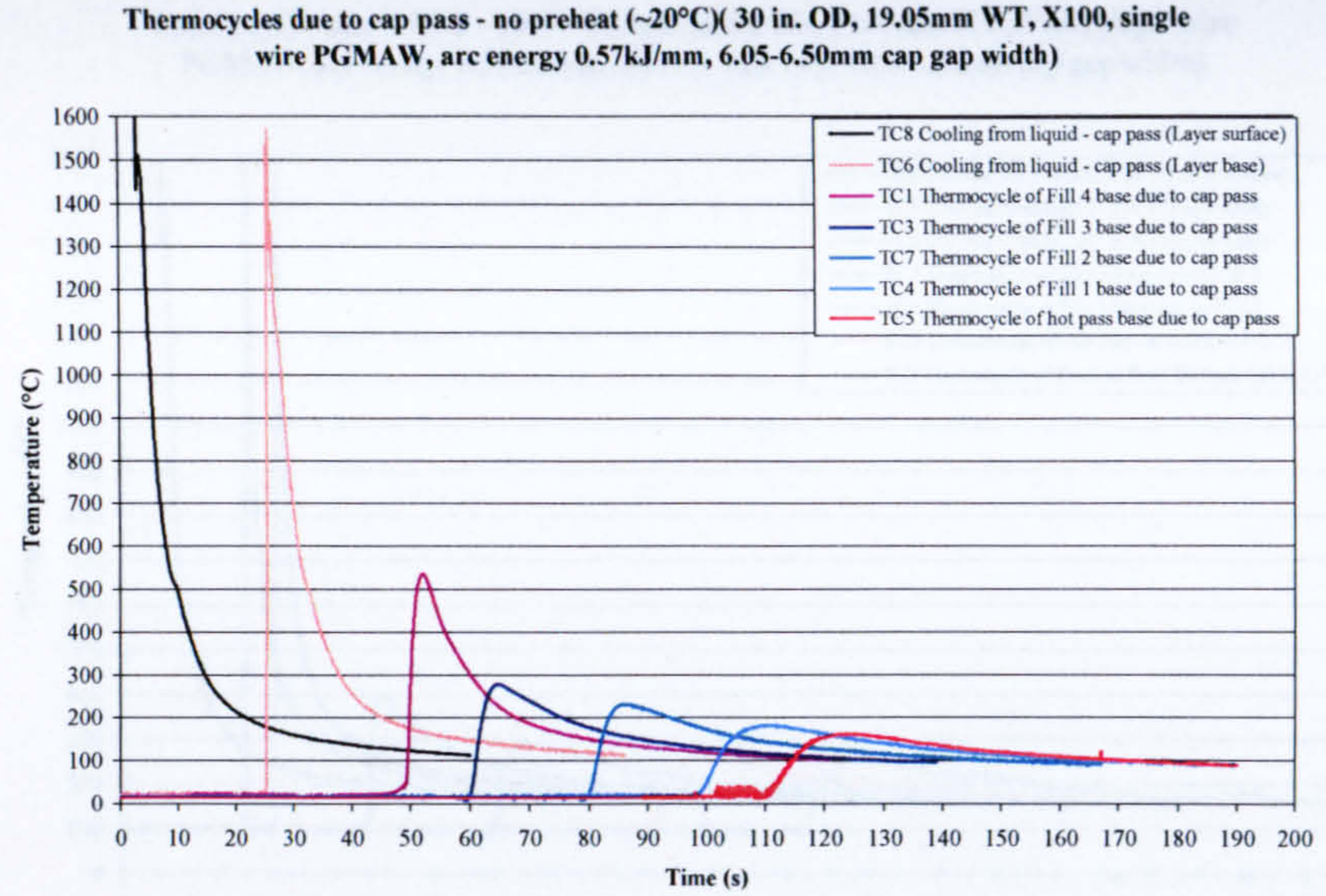

Figure 5-49(Cont.): Single wire thermocycle data – no preheat

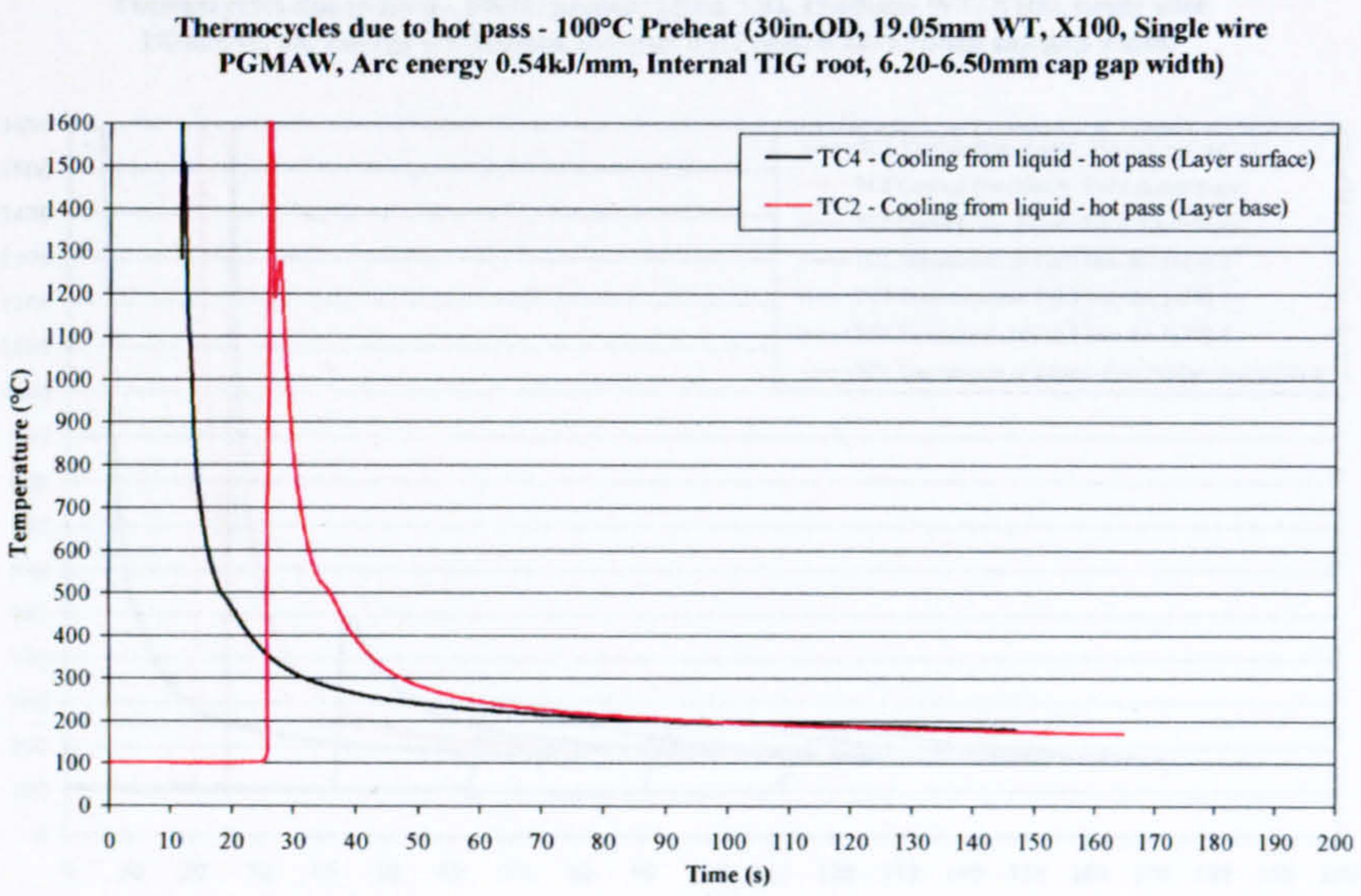

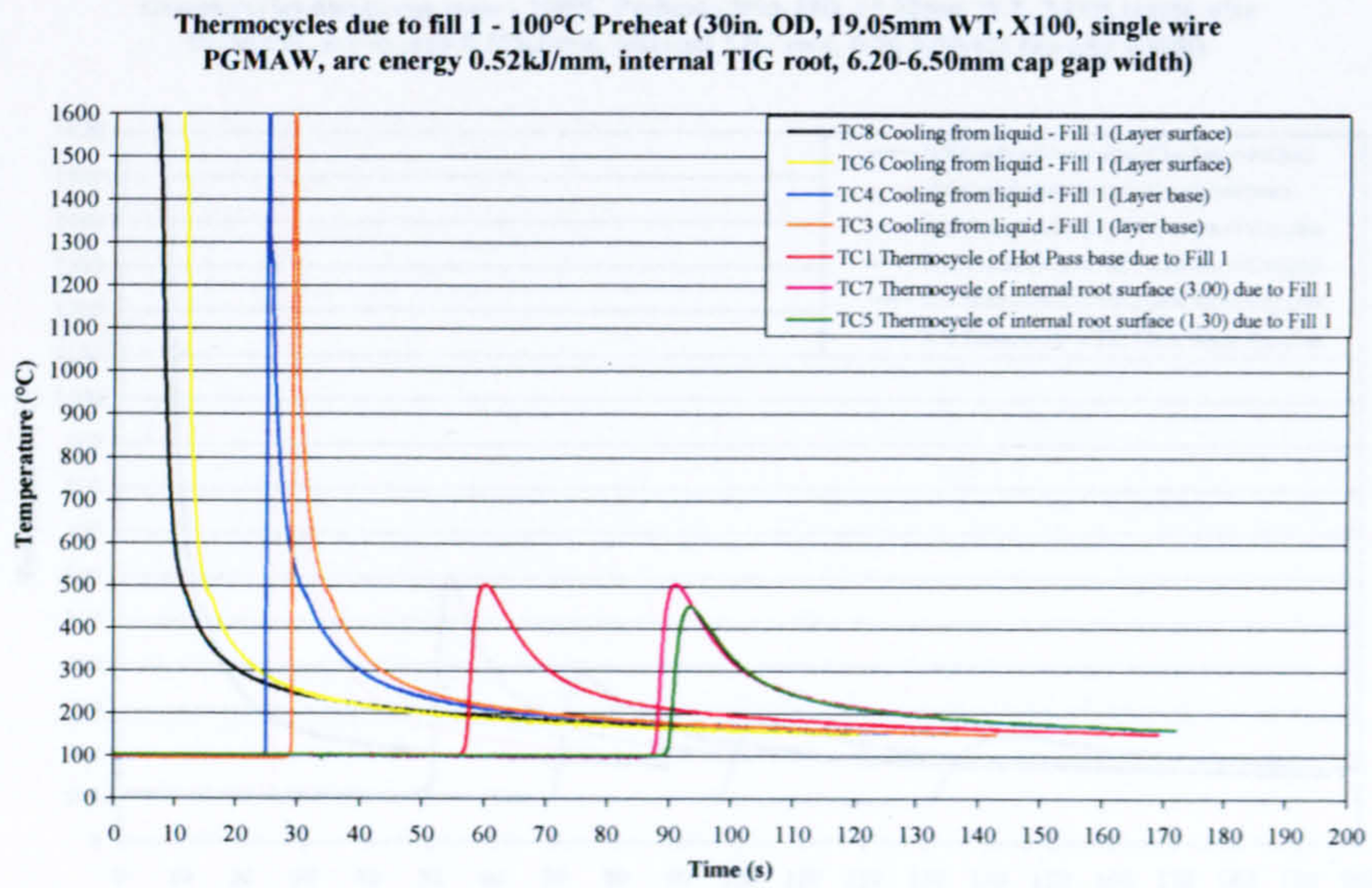

Figure 5-50: Single wire thermocycle data – 100°C preheat

Thermocouples due to fill 2 - 100°C Preheat (30in. OD, 19.05mm WT, X100, single wire PGMAW, arc energy 0.52kJ/mm, internal TIG root, 6.20-6.50mm cap gap width)

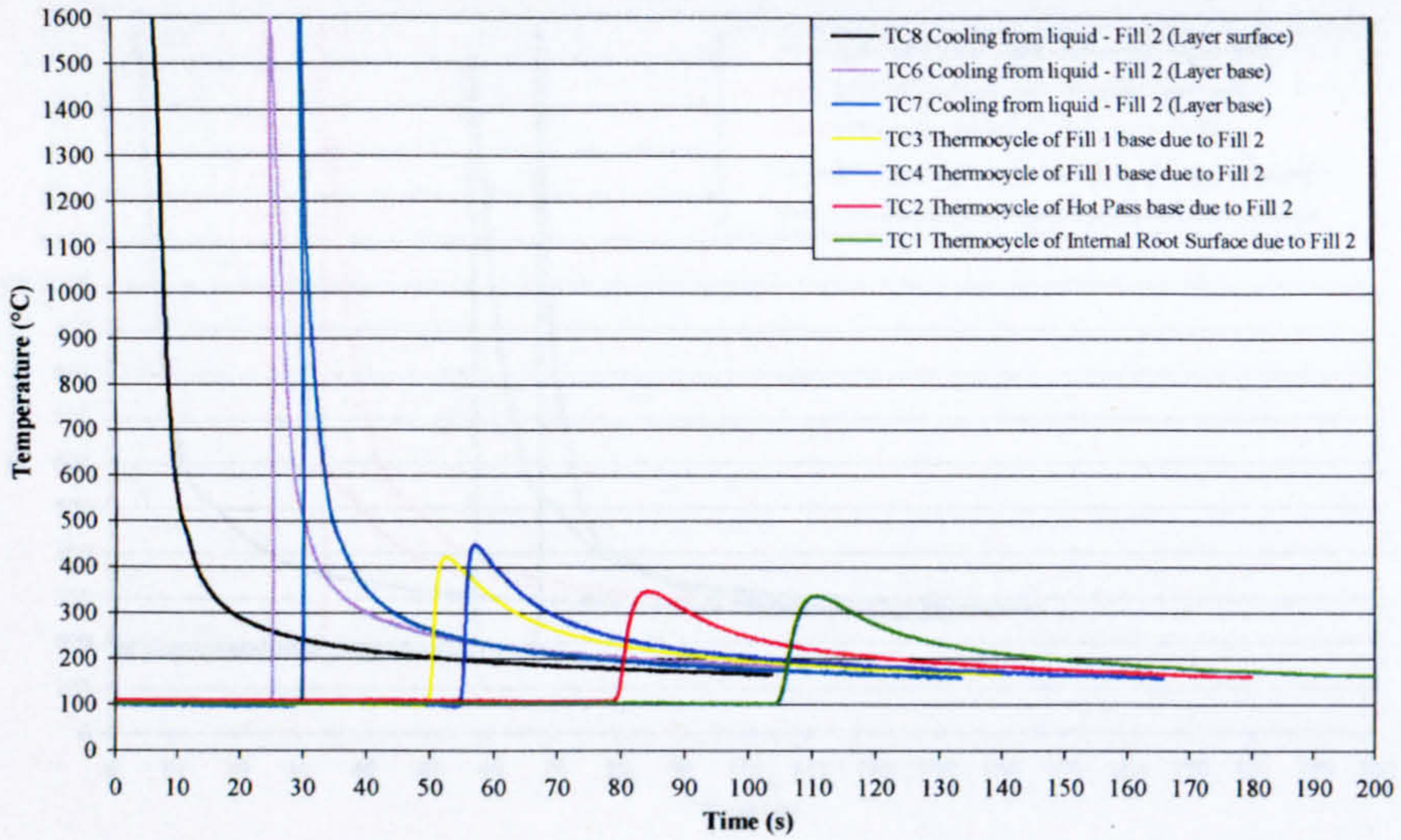

Thermocycles due to fill 3 - 100°C Preheat (30in. OD, 19.05mm WT, X100, single wire PGMAW, arc energy 0.52kJ/mm, internal TIG root, 6.20-6.50mm cap gap width)

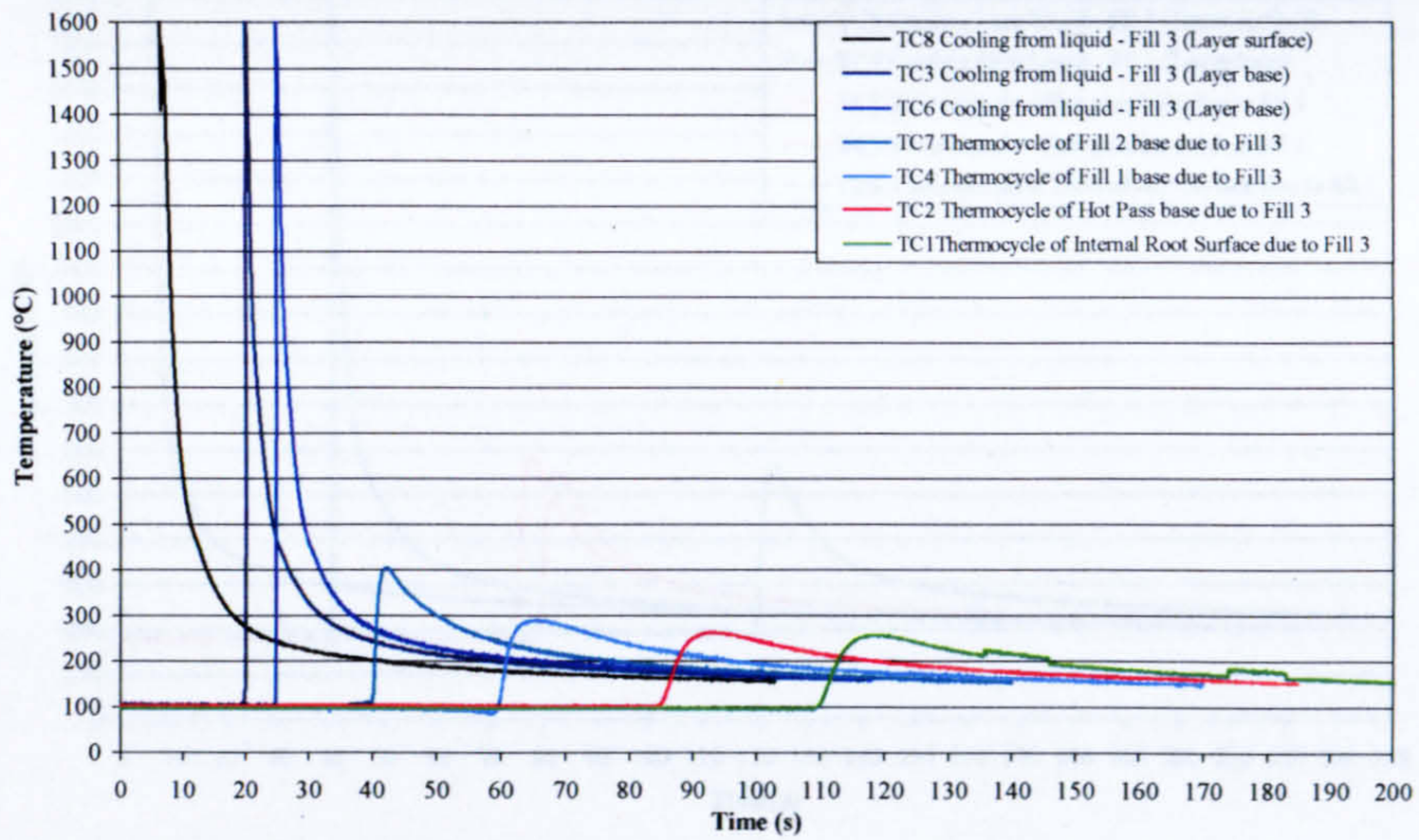

Thermocycles due to fill 4 - 100°C preheat (30in. OD, 19.05mm WT, X100, single wire PGMAW, arc energy 0.55kJ/mm, internal TIG root, 6.20-6.50mm cap gap width)

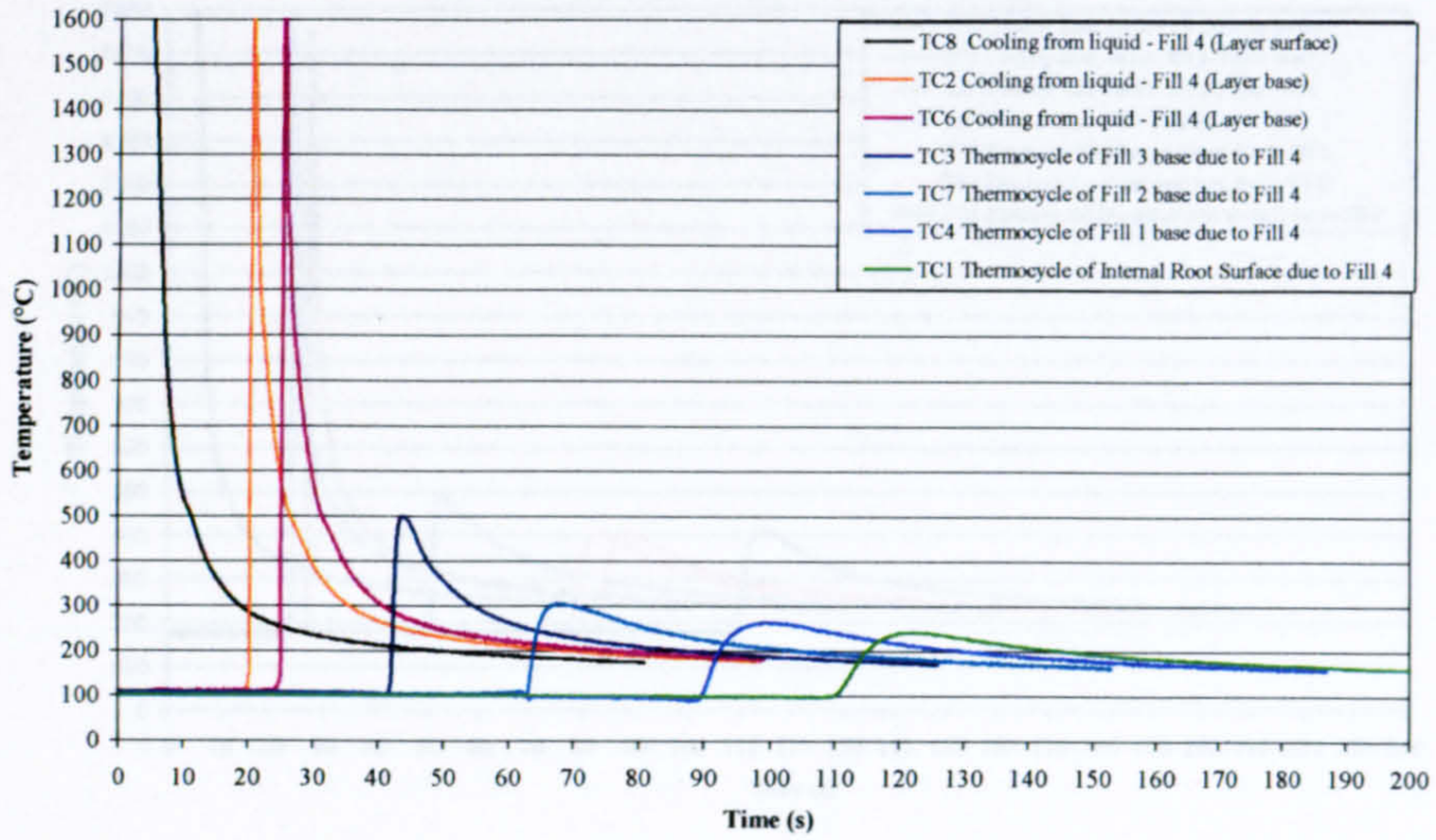

Thermocycles due to cap pass - 100°C Preheat (30in. OD, 19.05mm WT, X100, single wire PGMAW, arc energy 0.57kJ/mm, internal TIG root, 6.20-6.50mm cap gap width)

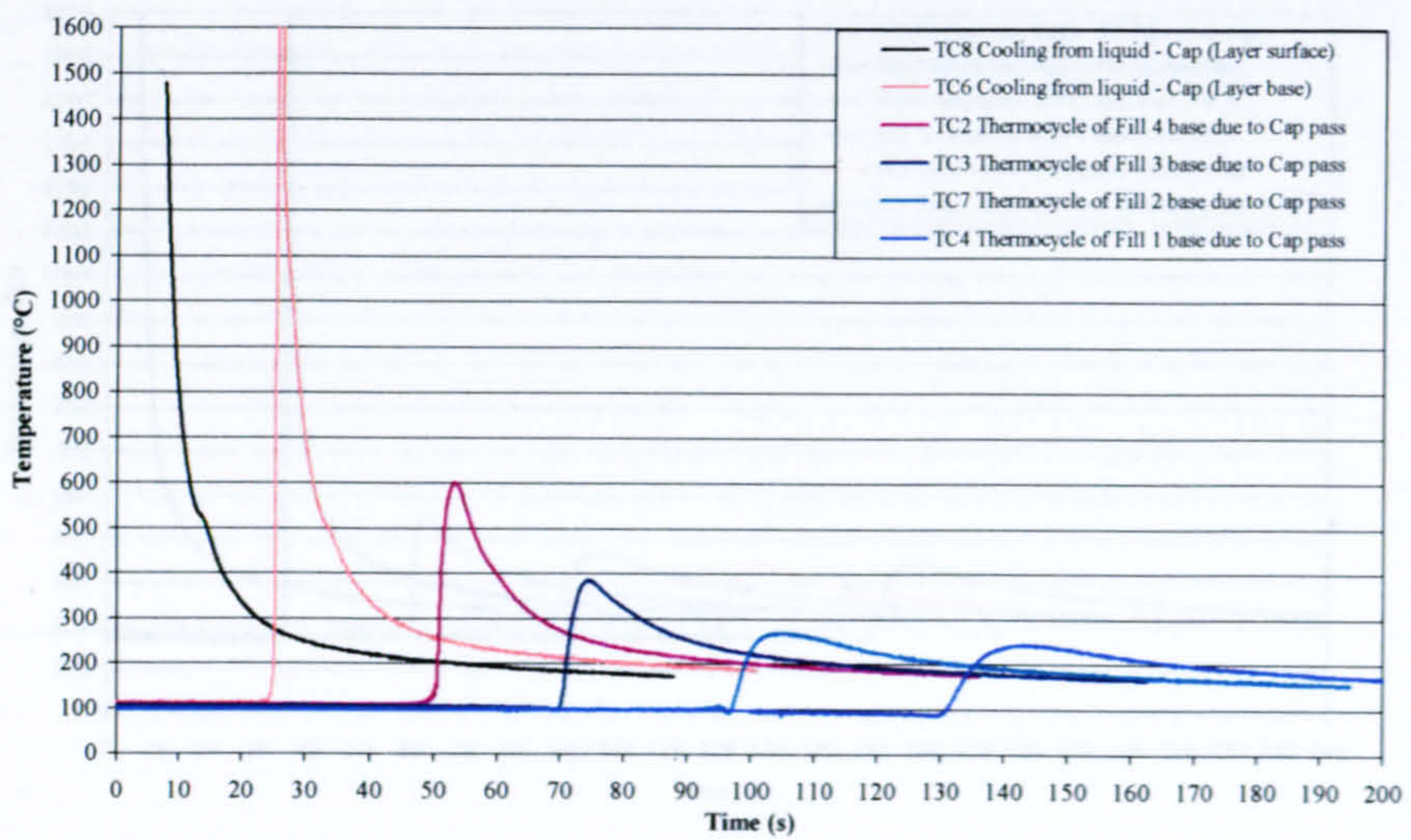

Figure 5-50(Cont.): Single wire thermocycle data – 100°C preheat

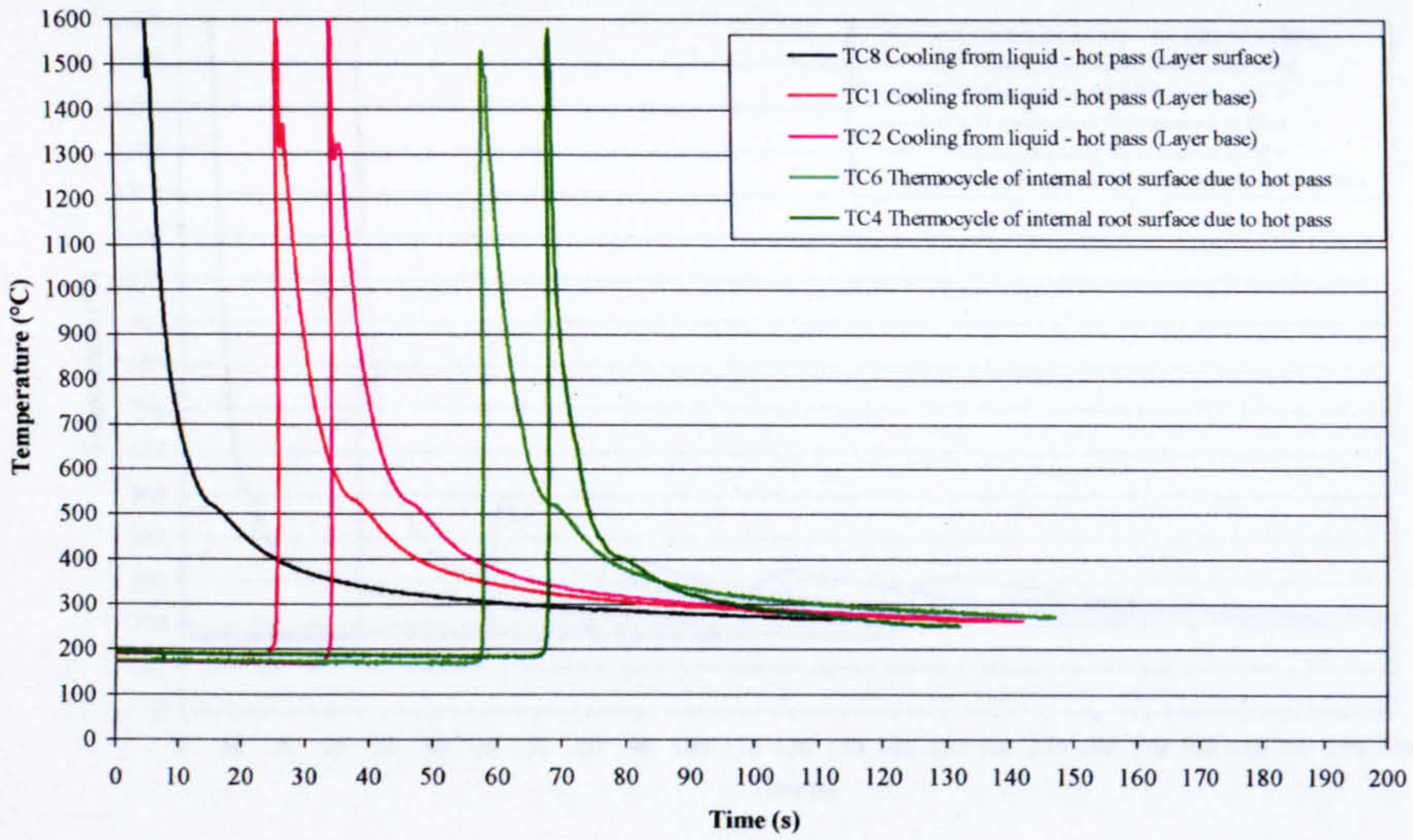

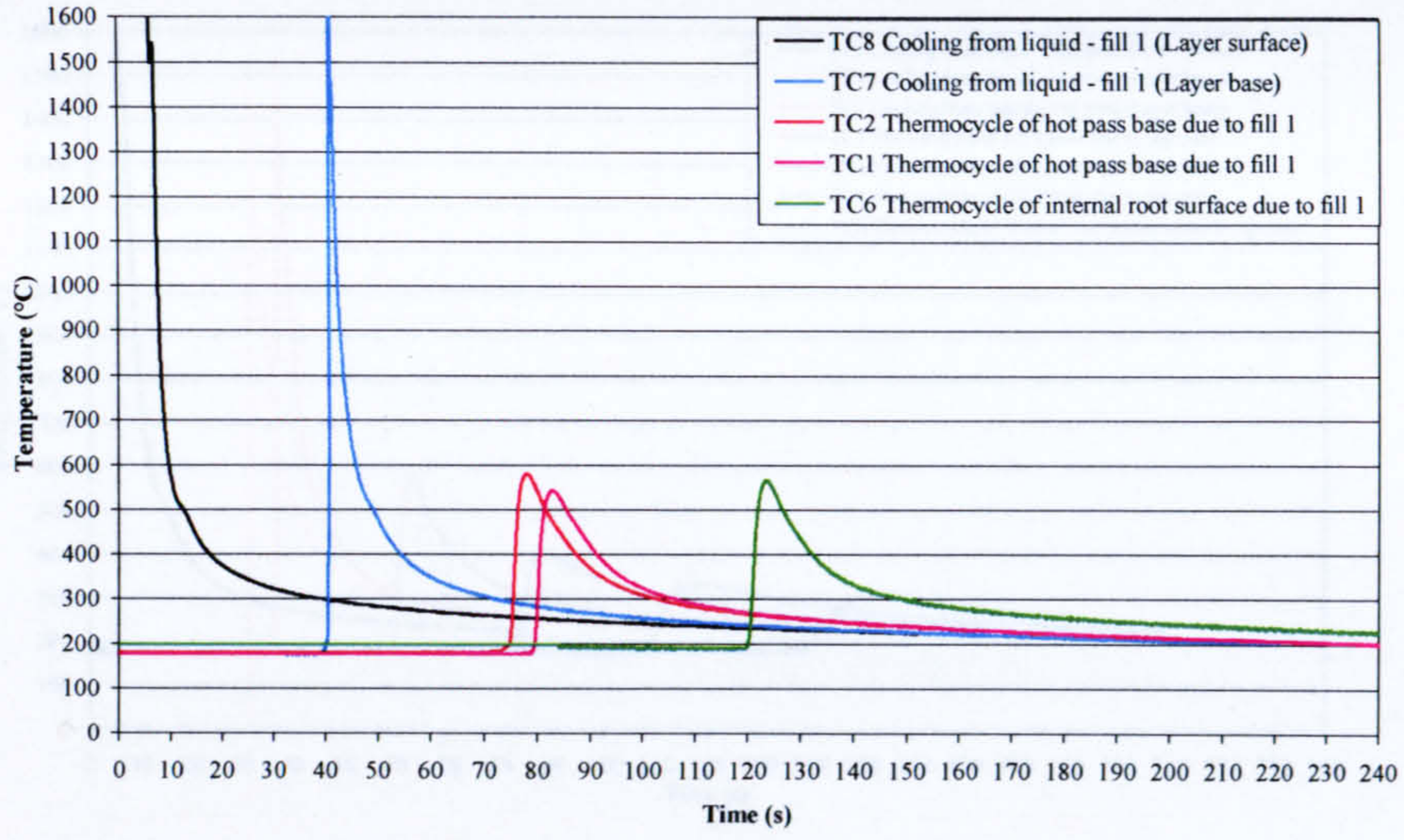

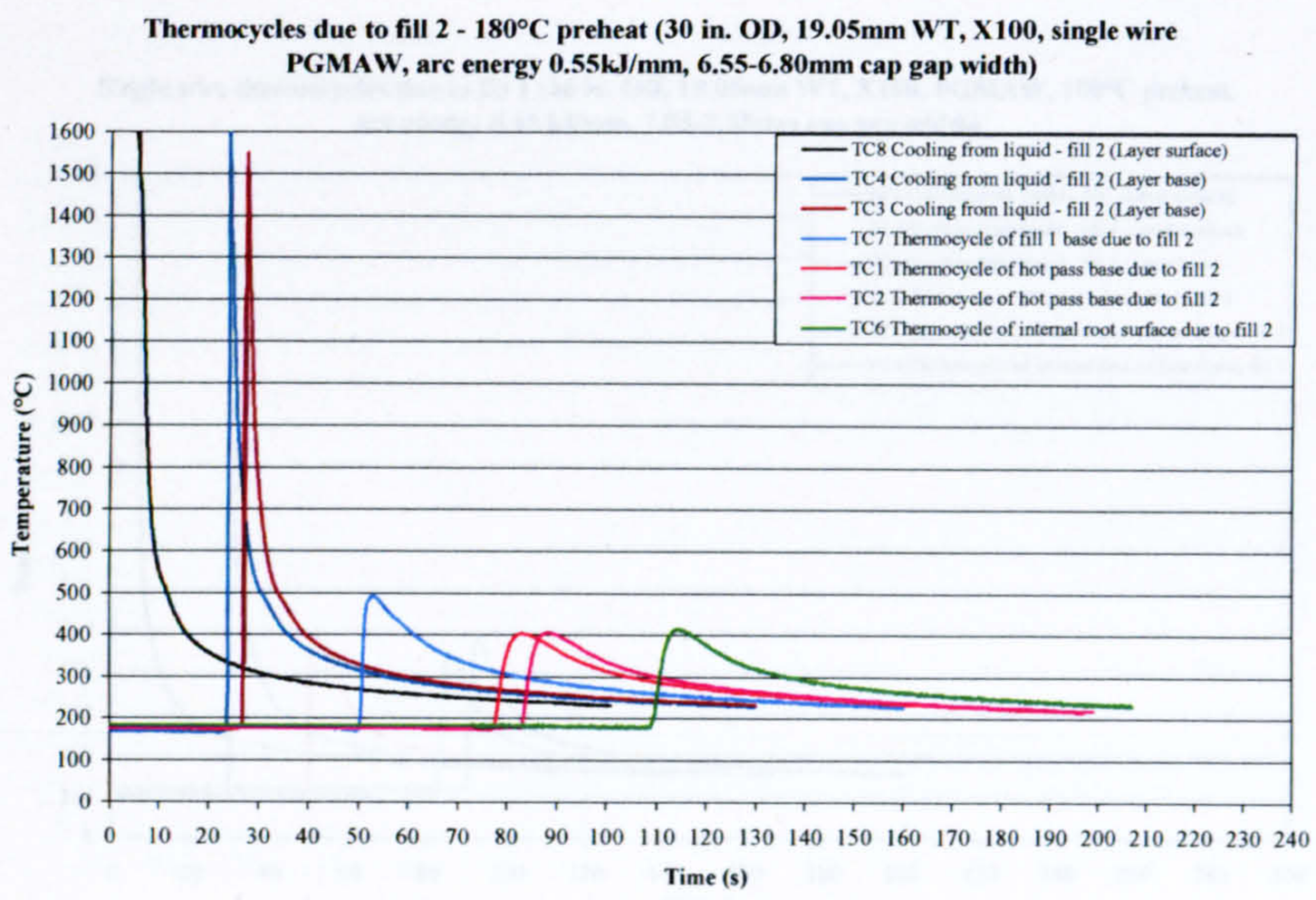

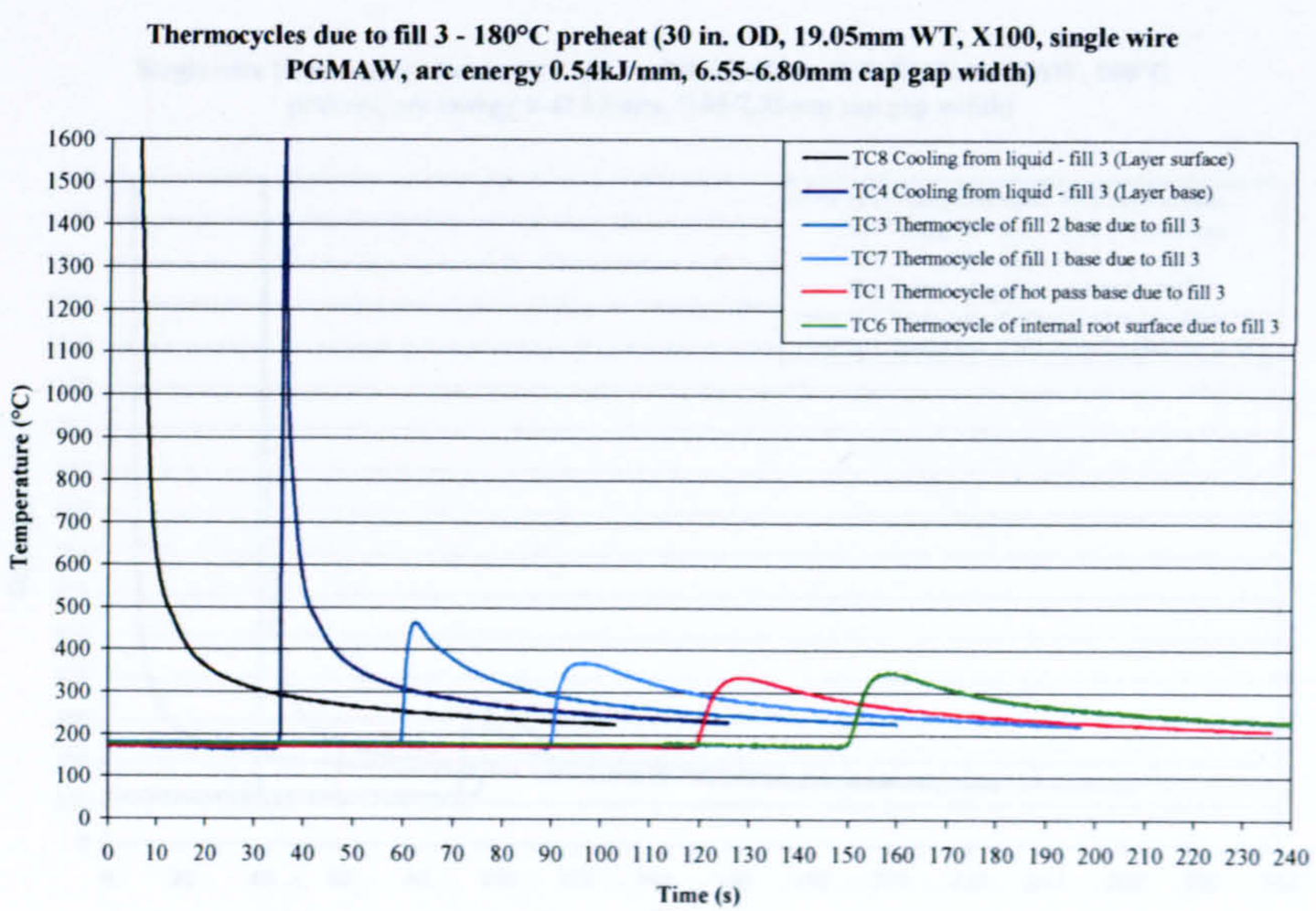

Figure 5-51: Single wire thermocycle data – 180°C preheat

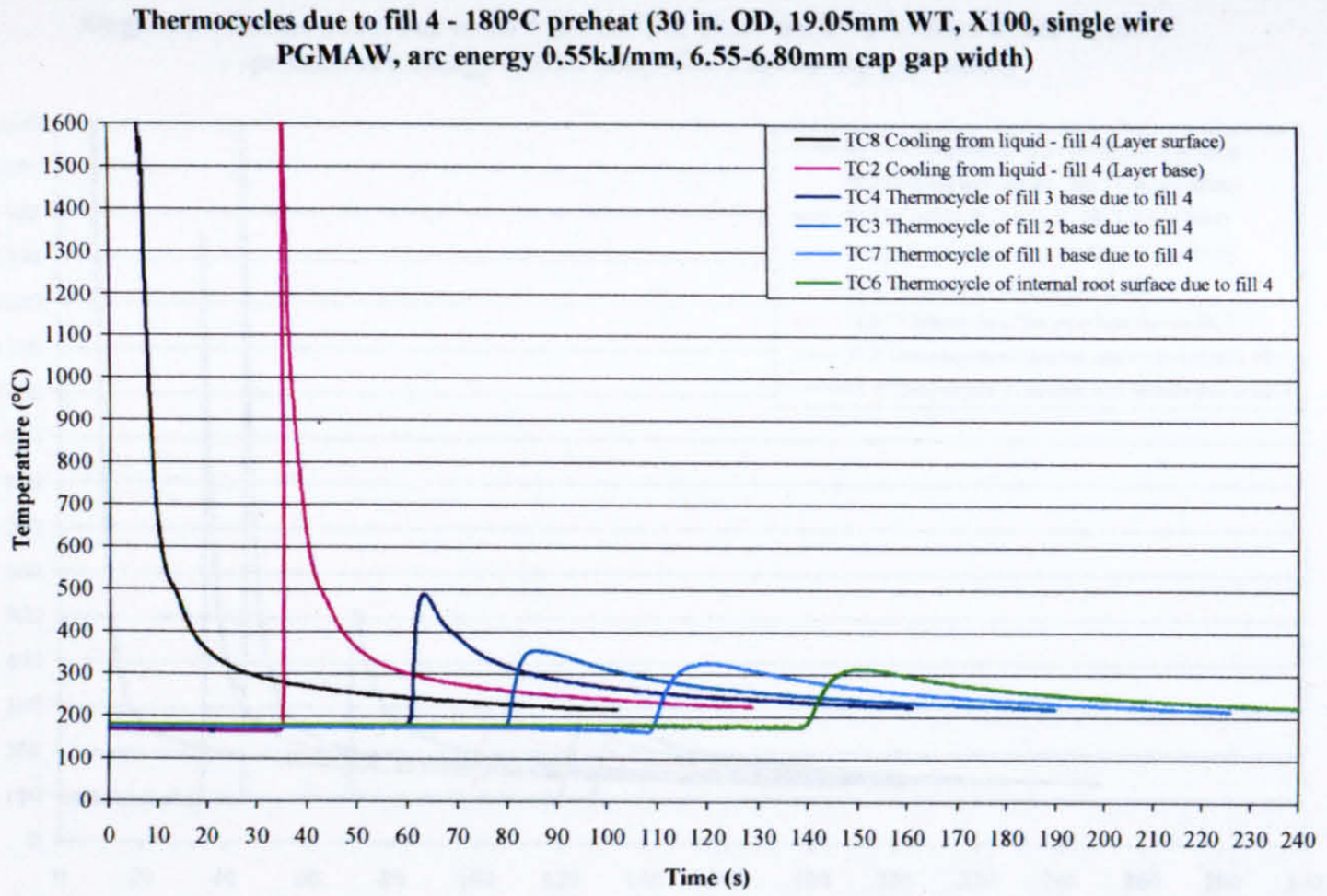

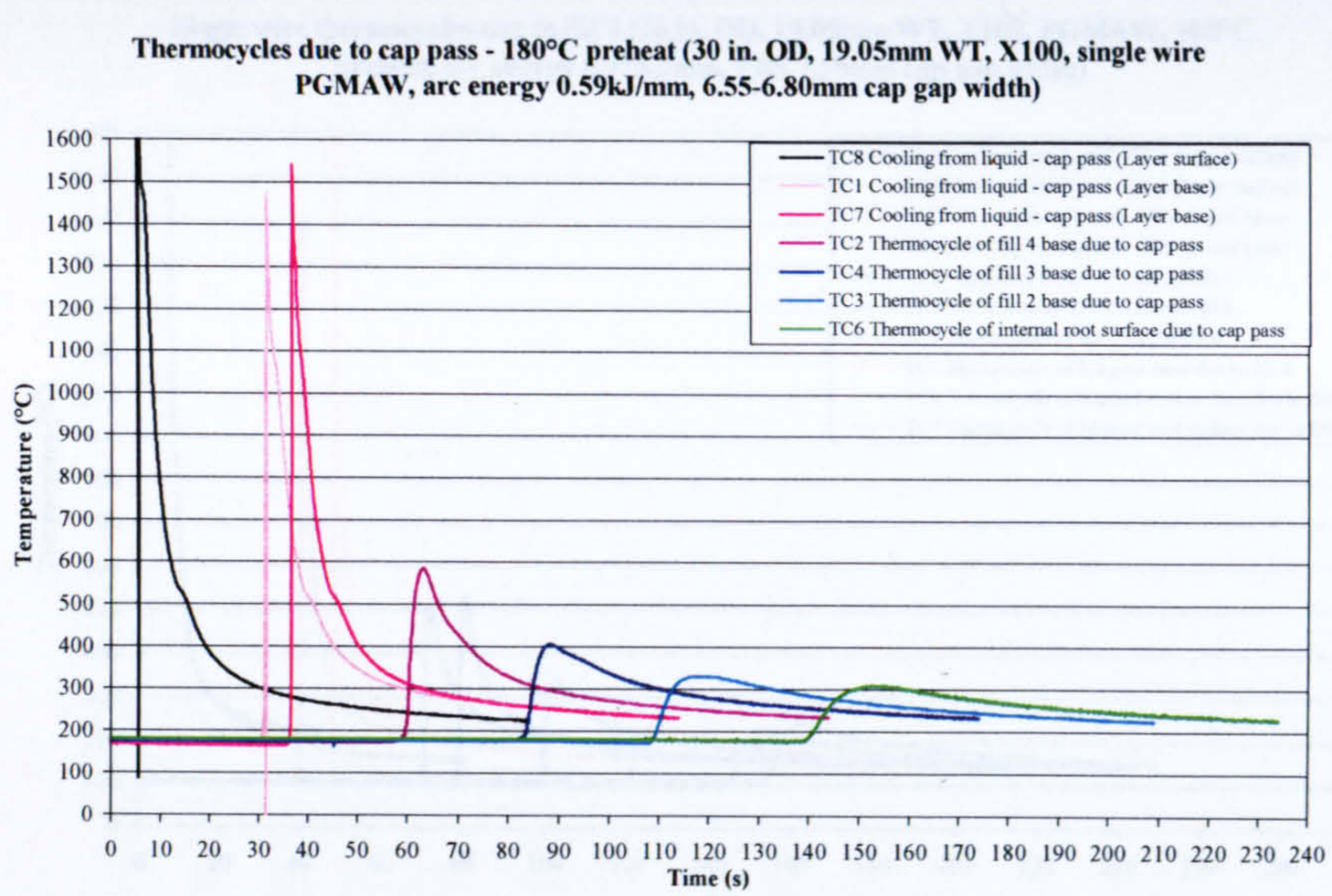

Figure 5-51(Cont.): Single wire thermocycle data – 180°C preheat

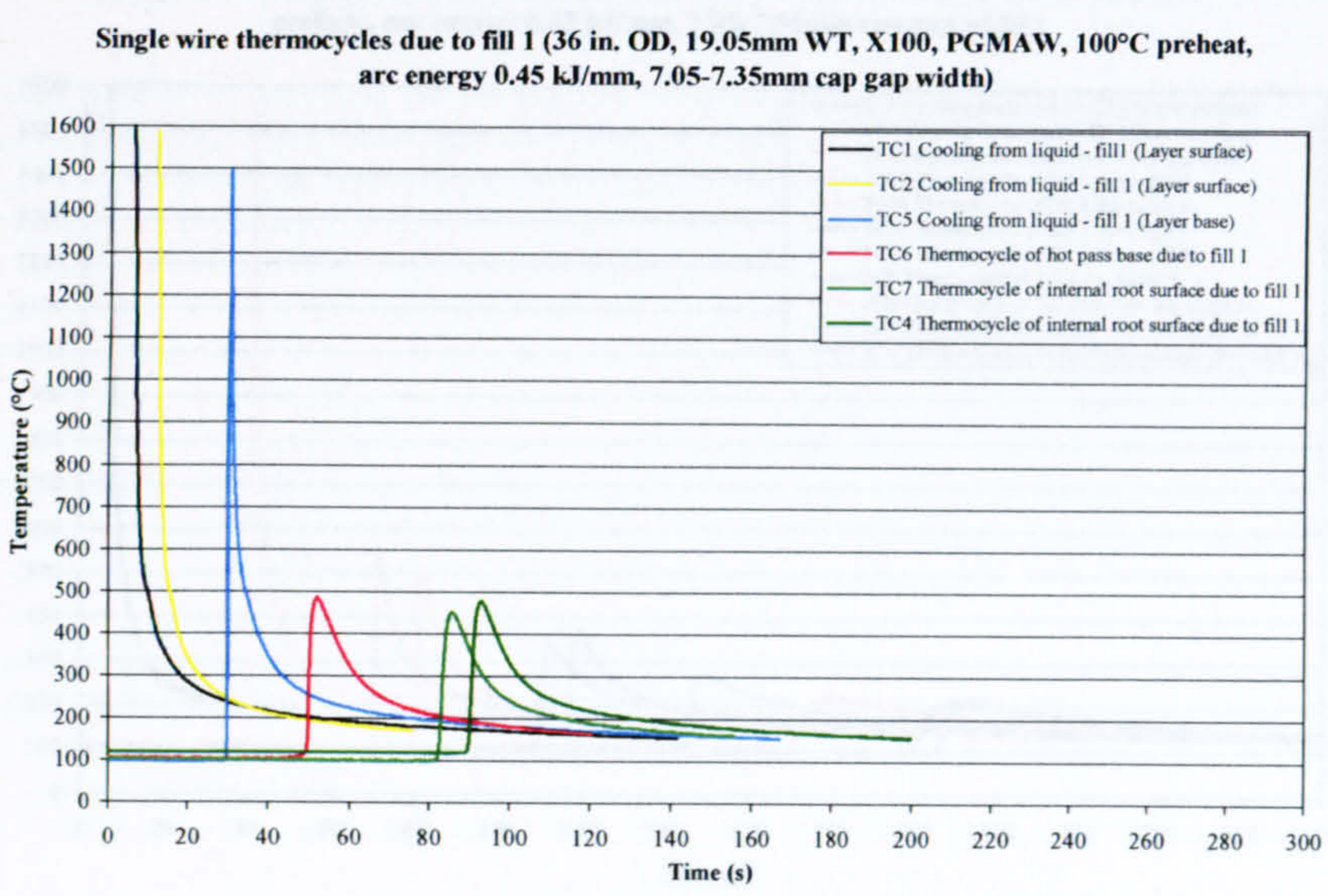

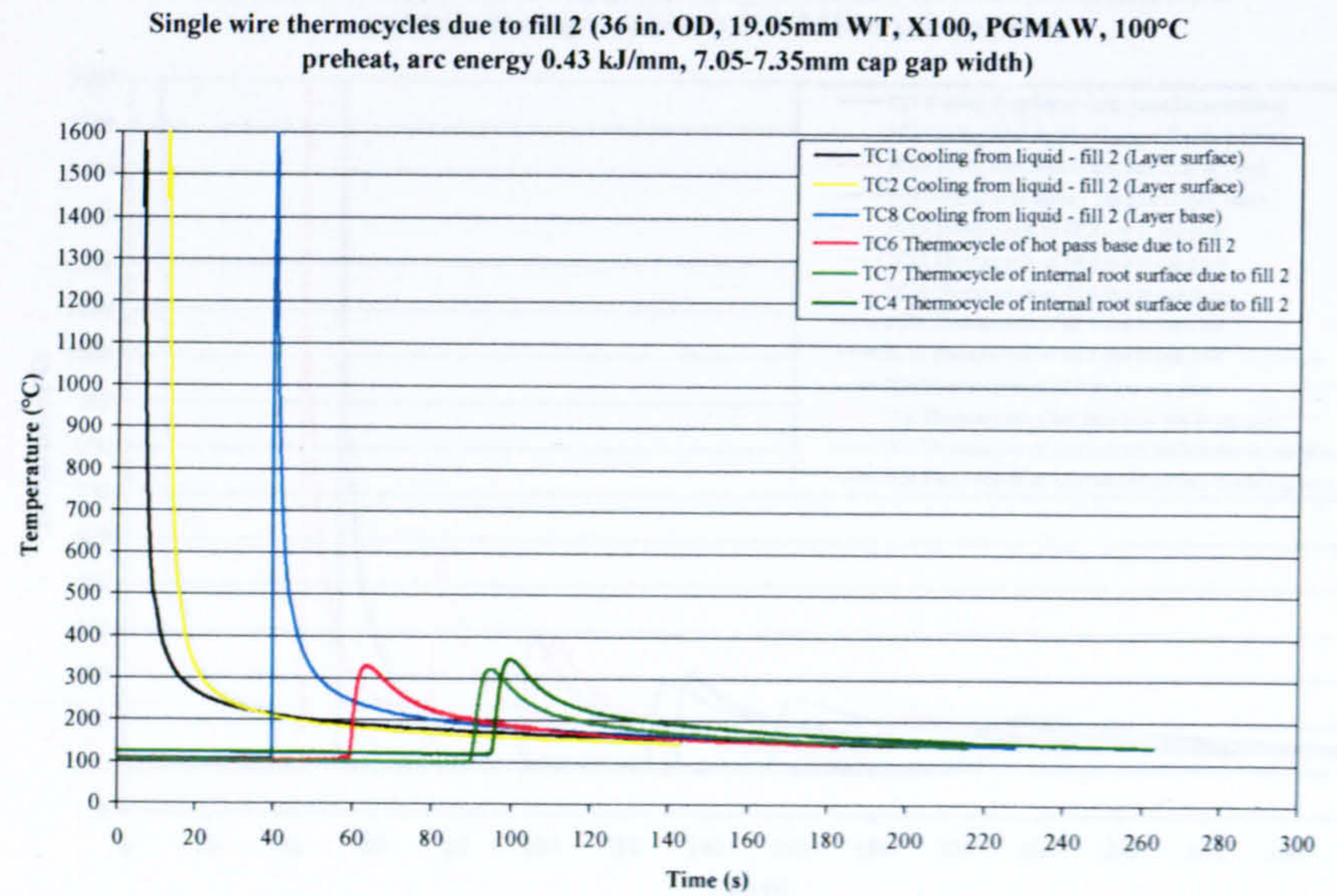

Figure 5-52: Process variation trials - single wire thermocycle data

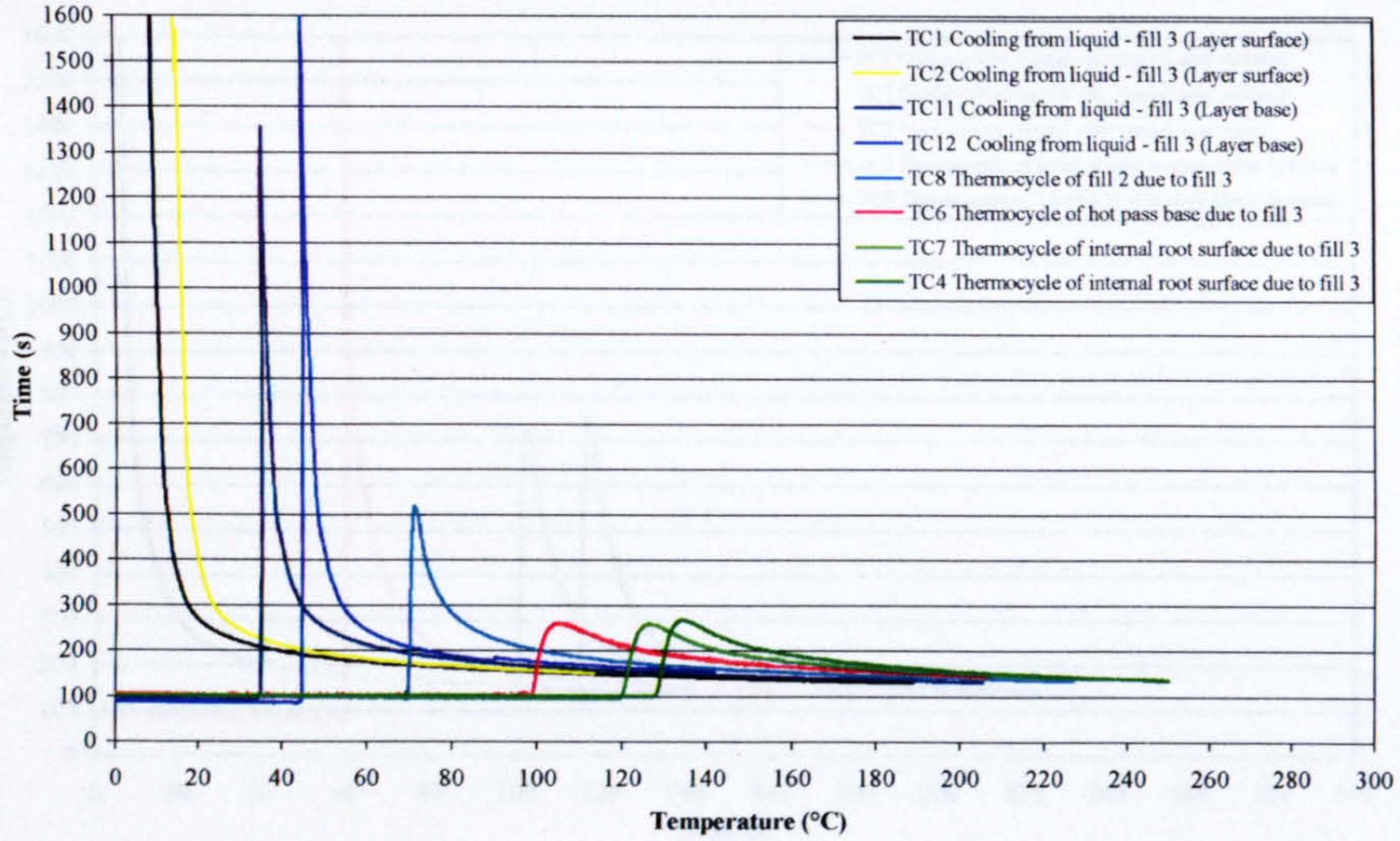

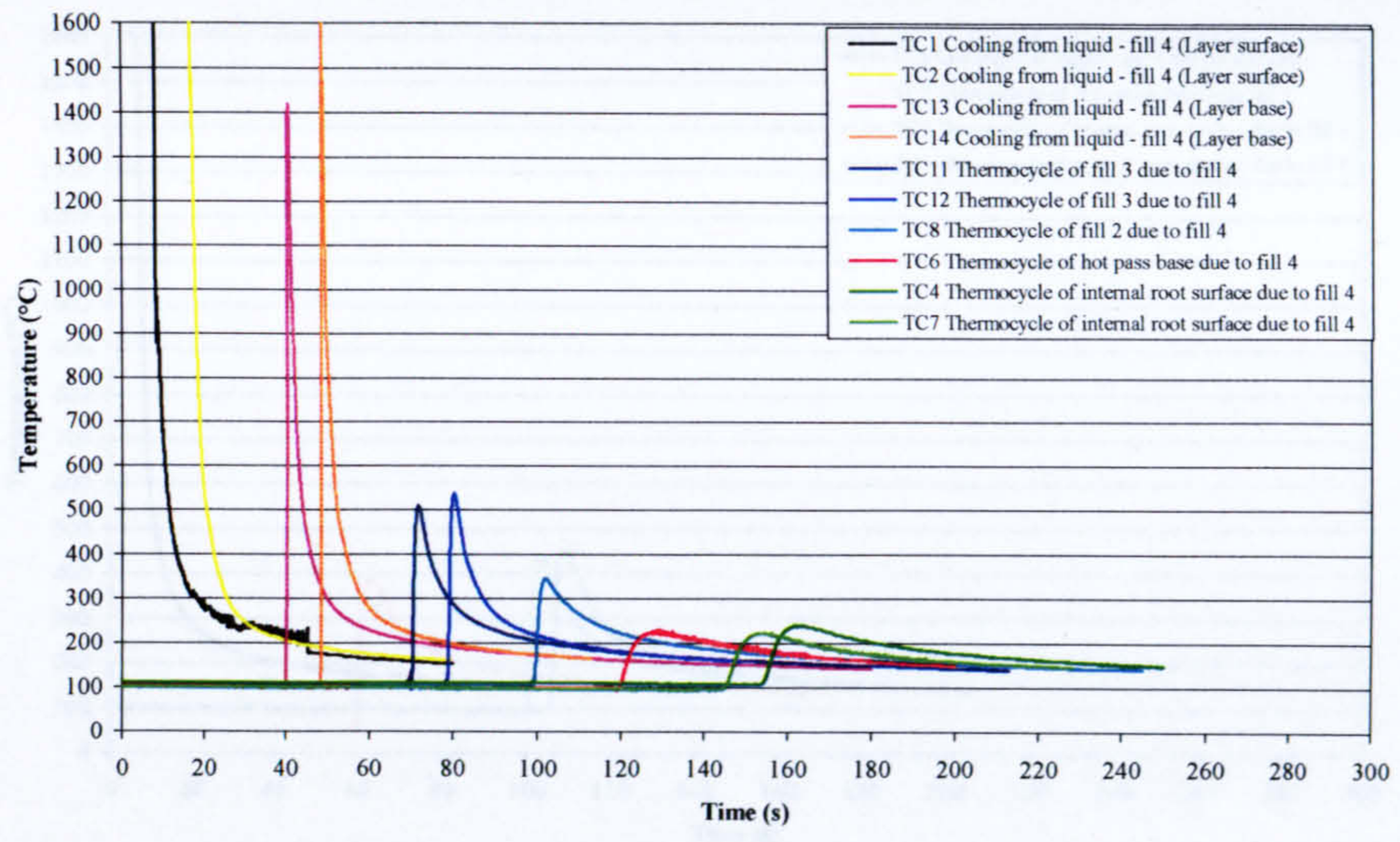

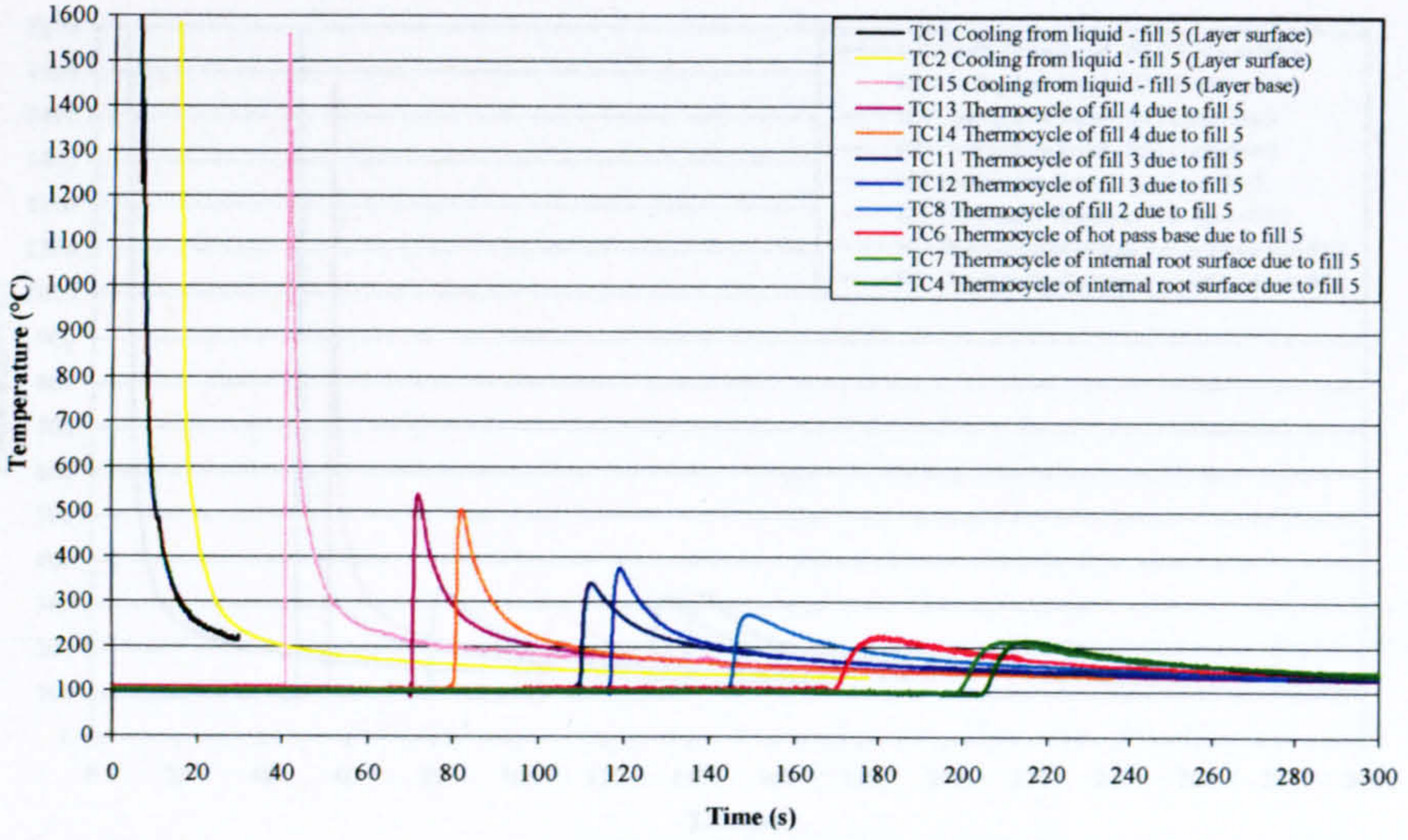

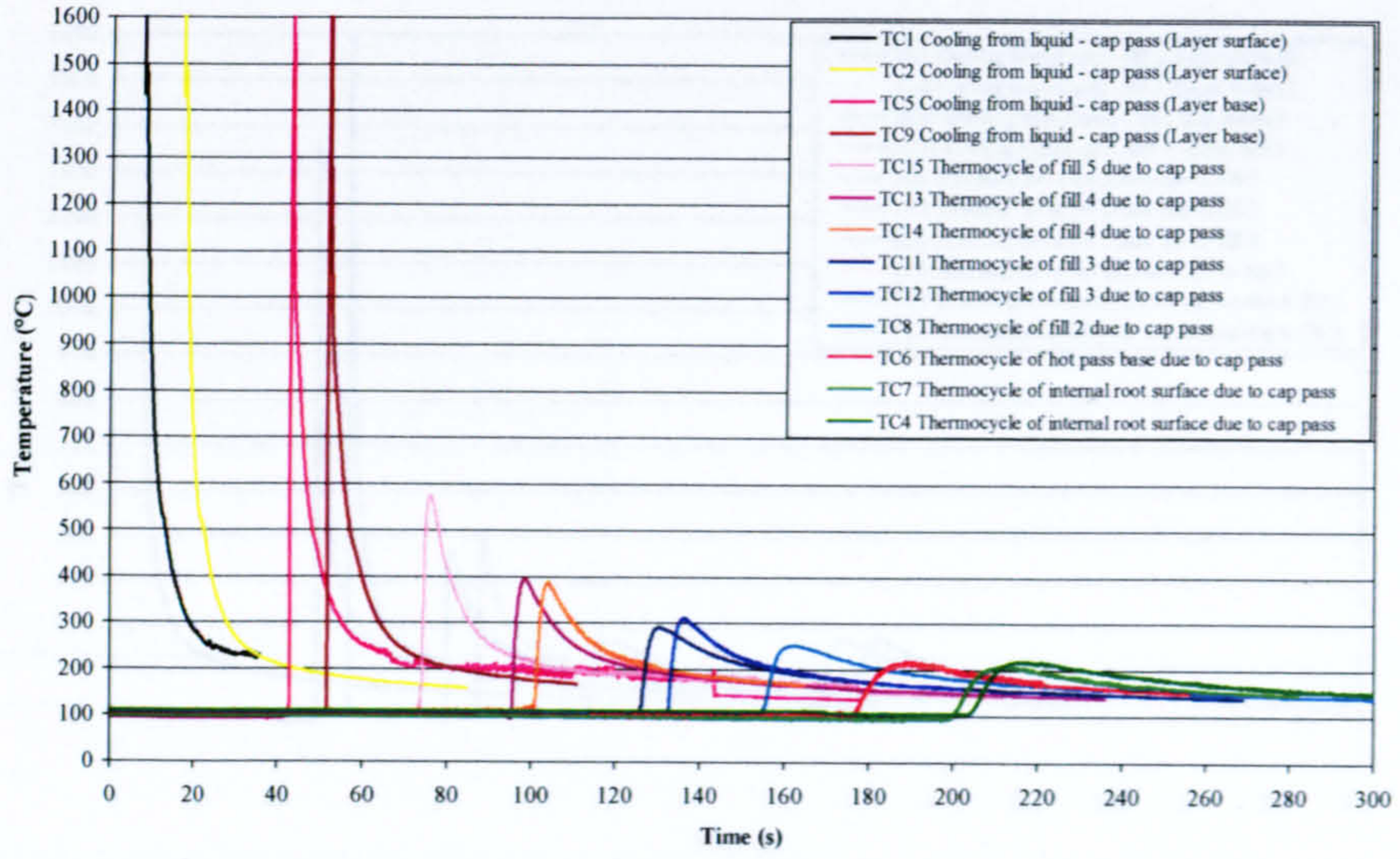

Figure 5-52 (Cont.): Process variation trials - single wire thermocycle data

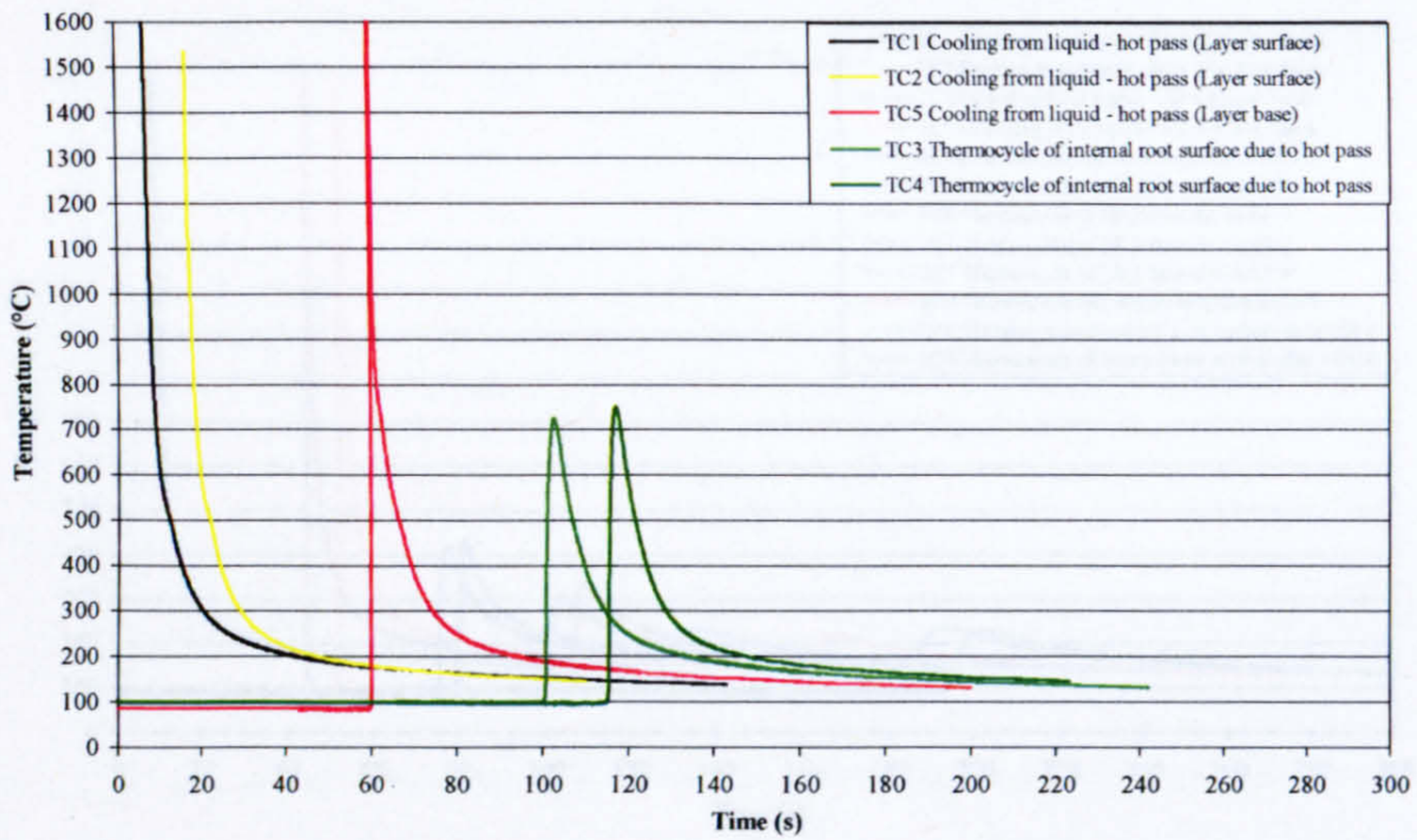

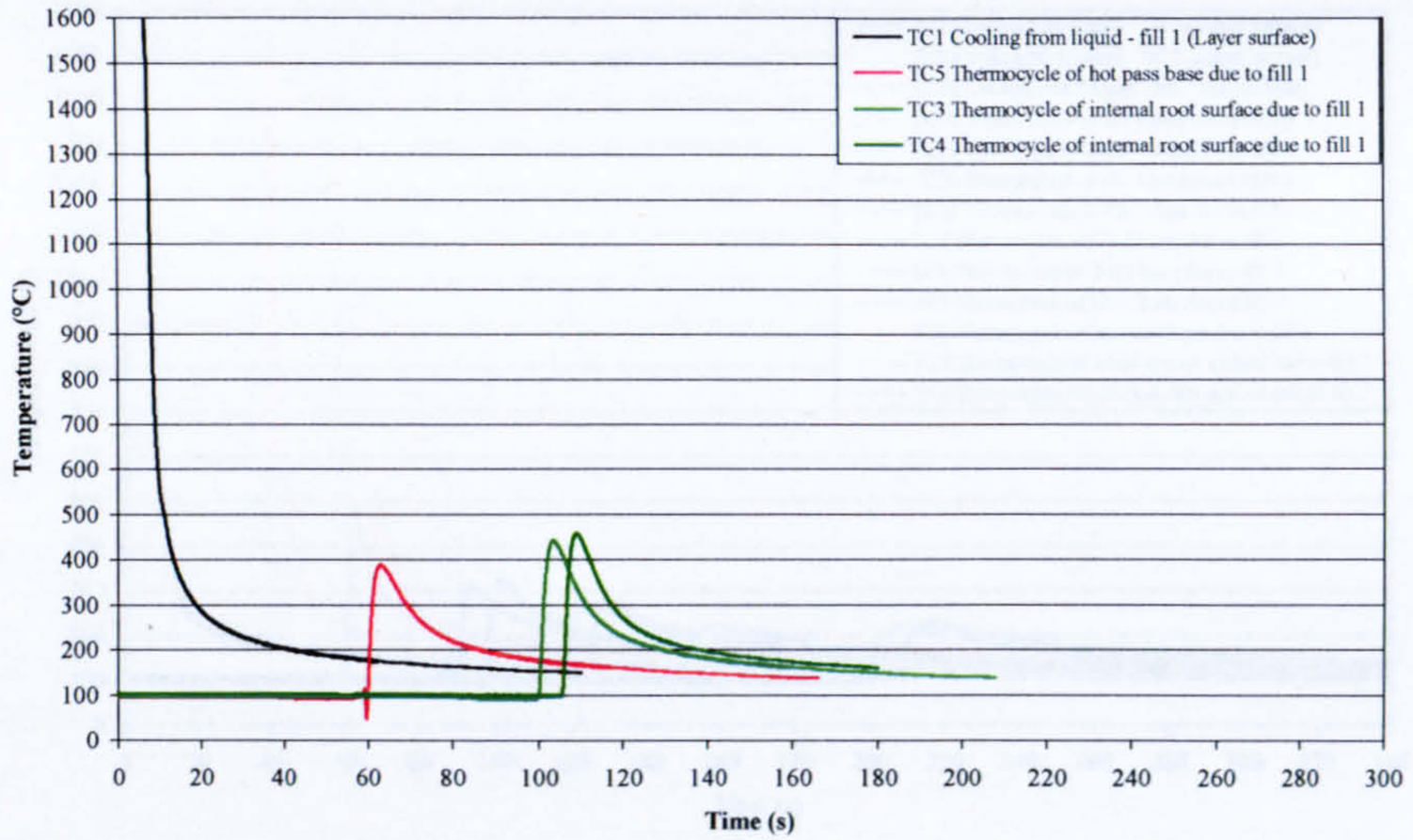

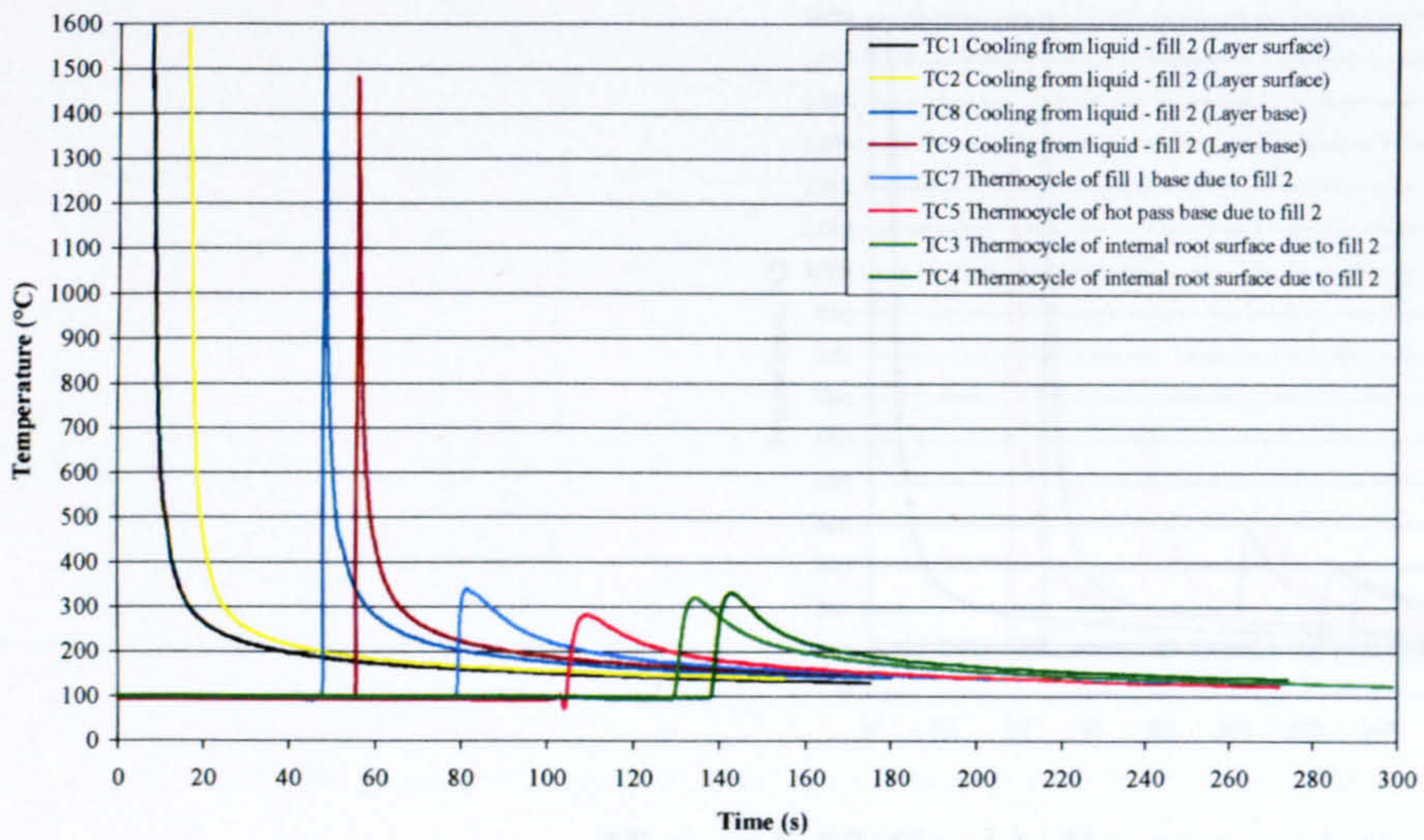

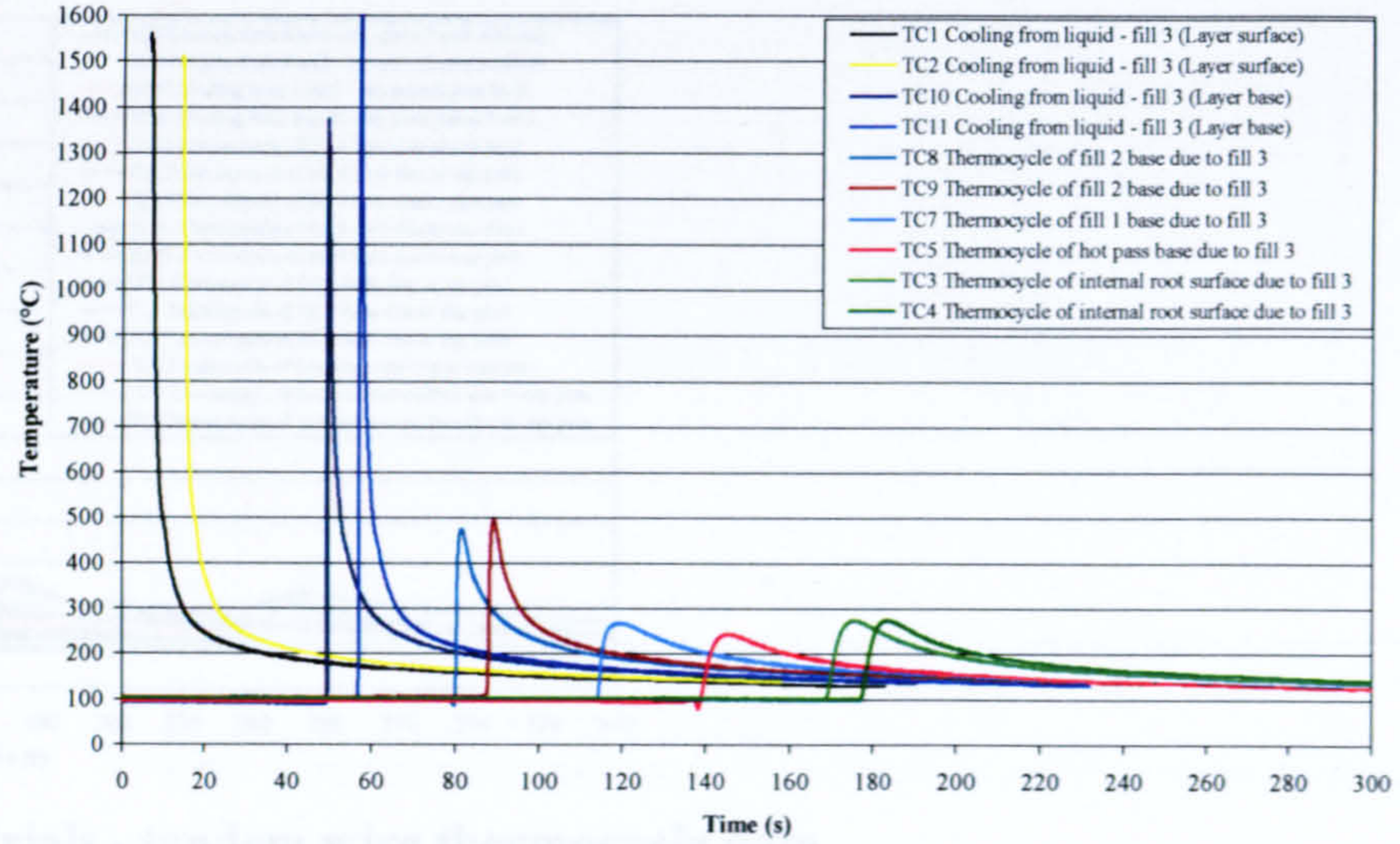

Figure 5-53: Process variation trials - tandem wire thermocycle data

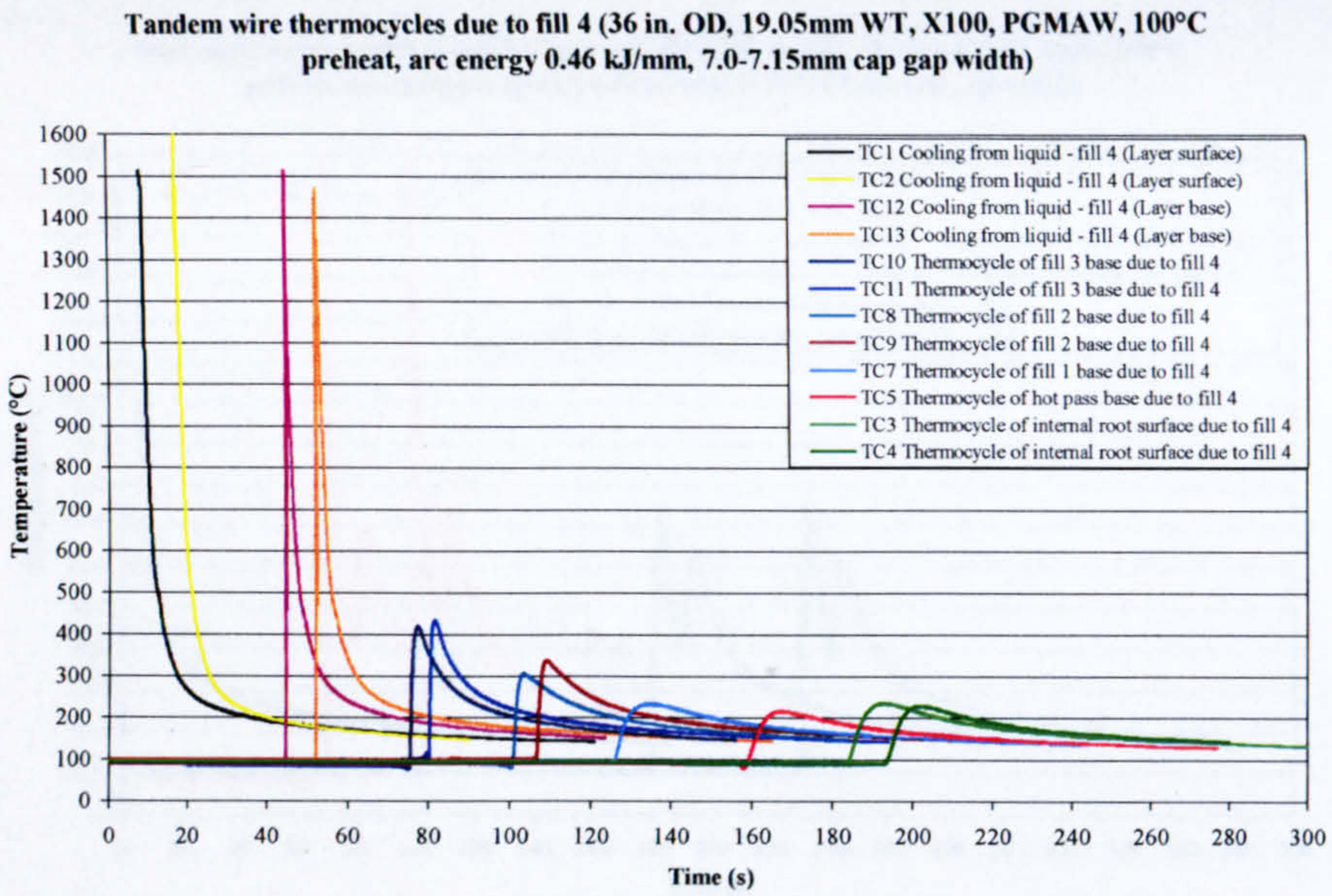

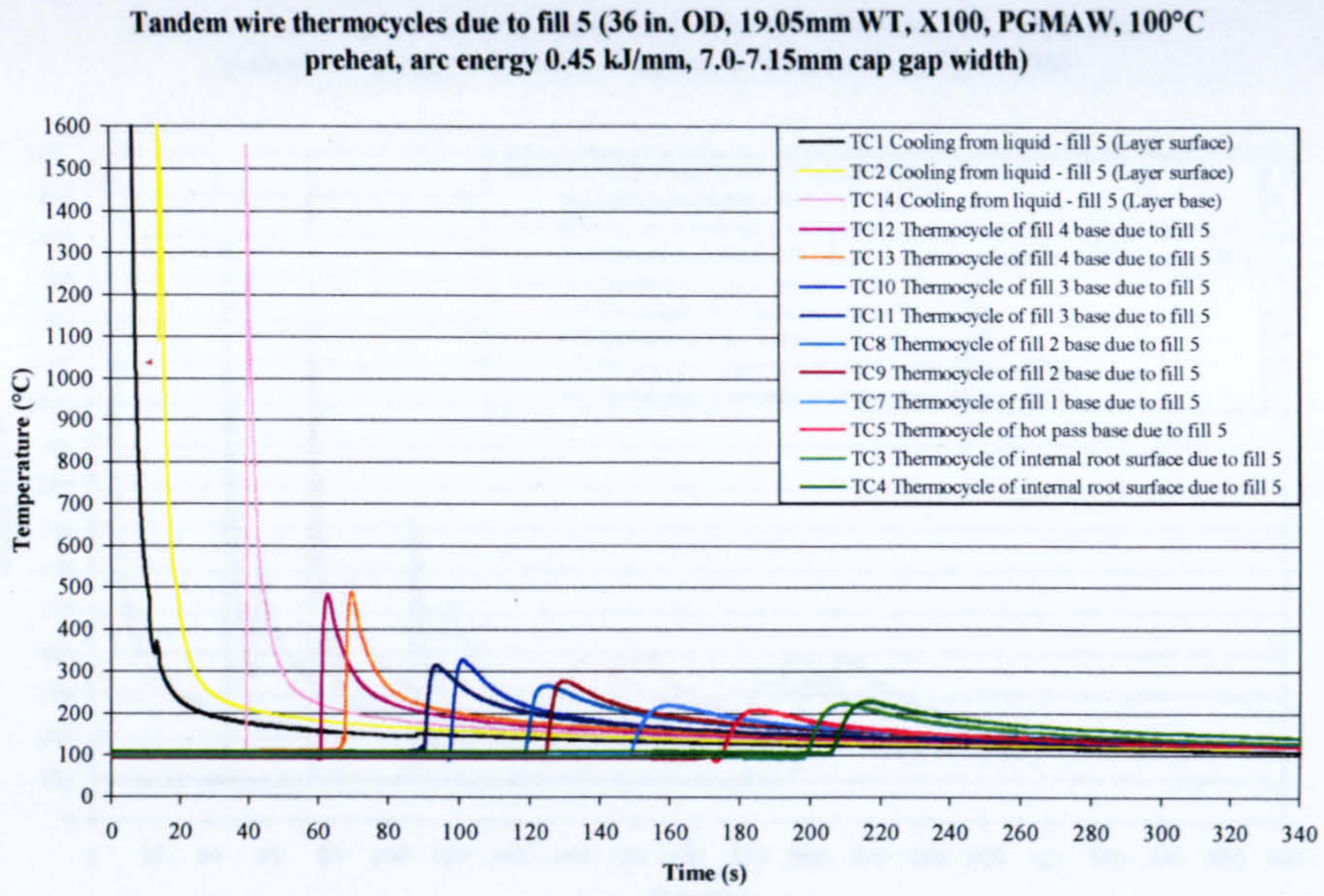

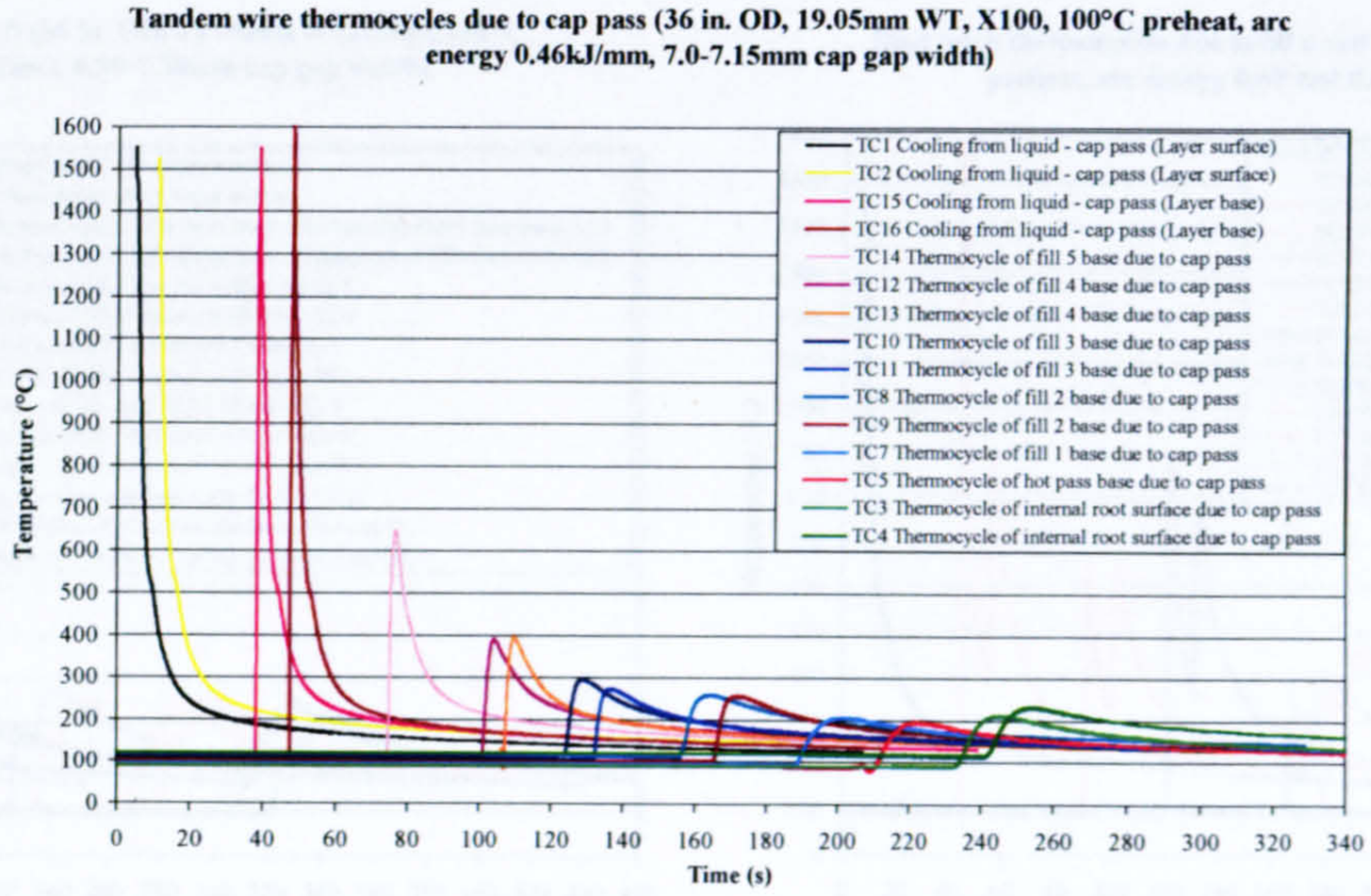

Figure 5-53(Cont.): Process variation trials - tandem wire thermocycle data

Dual torch thermocycles due to hot pass and fill 1 (36 in. OD, 19.05mm WT, X100, 100°C preheat, arc energy 0.42 and 0.42 kJ/mm, 6.90-7.30mm cap gap width)

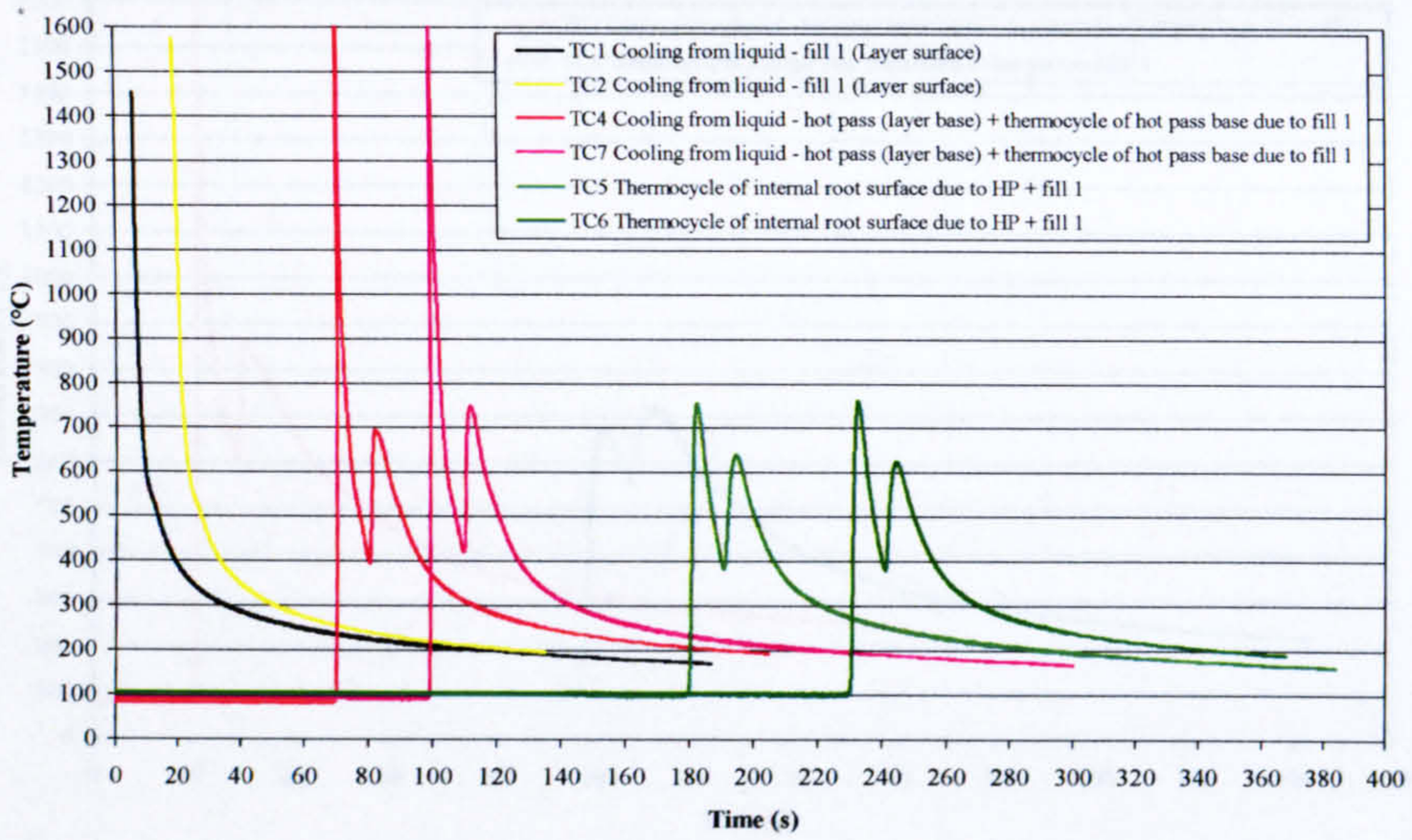

Dual torch thermocycles due to fill 2 and fill 3 (36 in. OD, 19.05mm WT, X100, 100°C preheat, arc energy 0.43 and 0.41 kJ/mm, 6.90-7.30mm cap gap width)

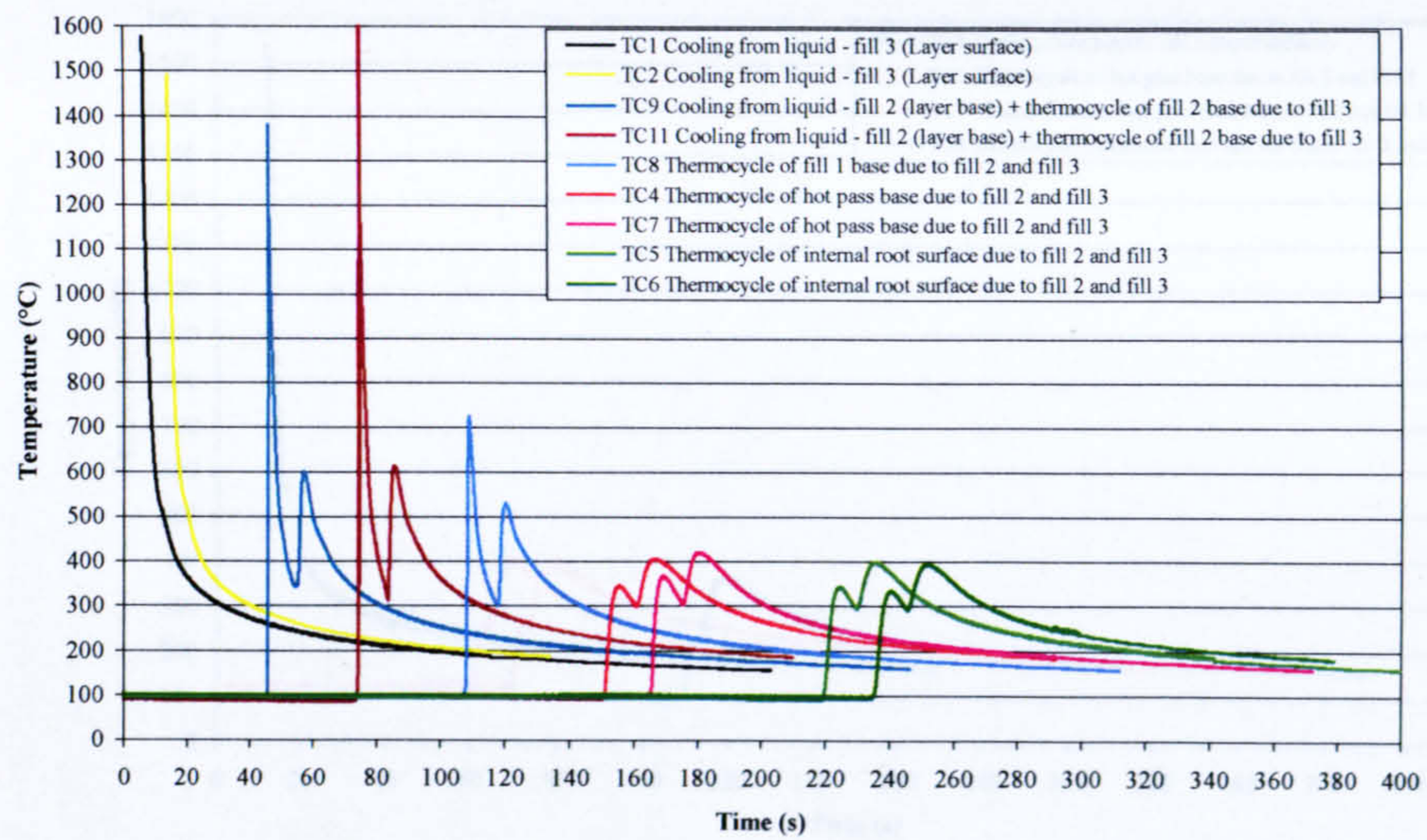

Dual torch thermocycles due to fill 4 and fill 5 (36 in. OD, 19.05mm WT, X100, 100°C preheat, arc energy 0.44 and 0.43 kJ/mm, 6.90-7.30mm cap gap width)

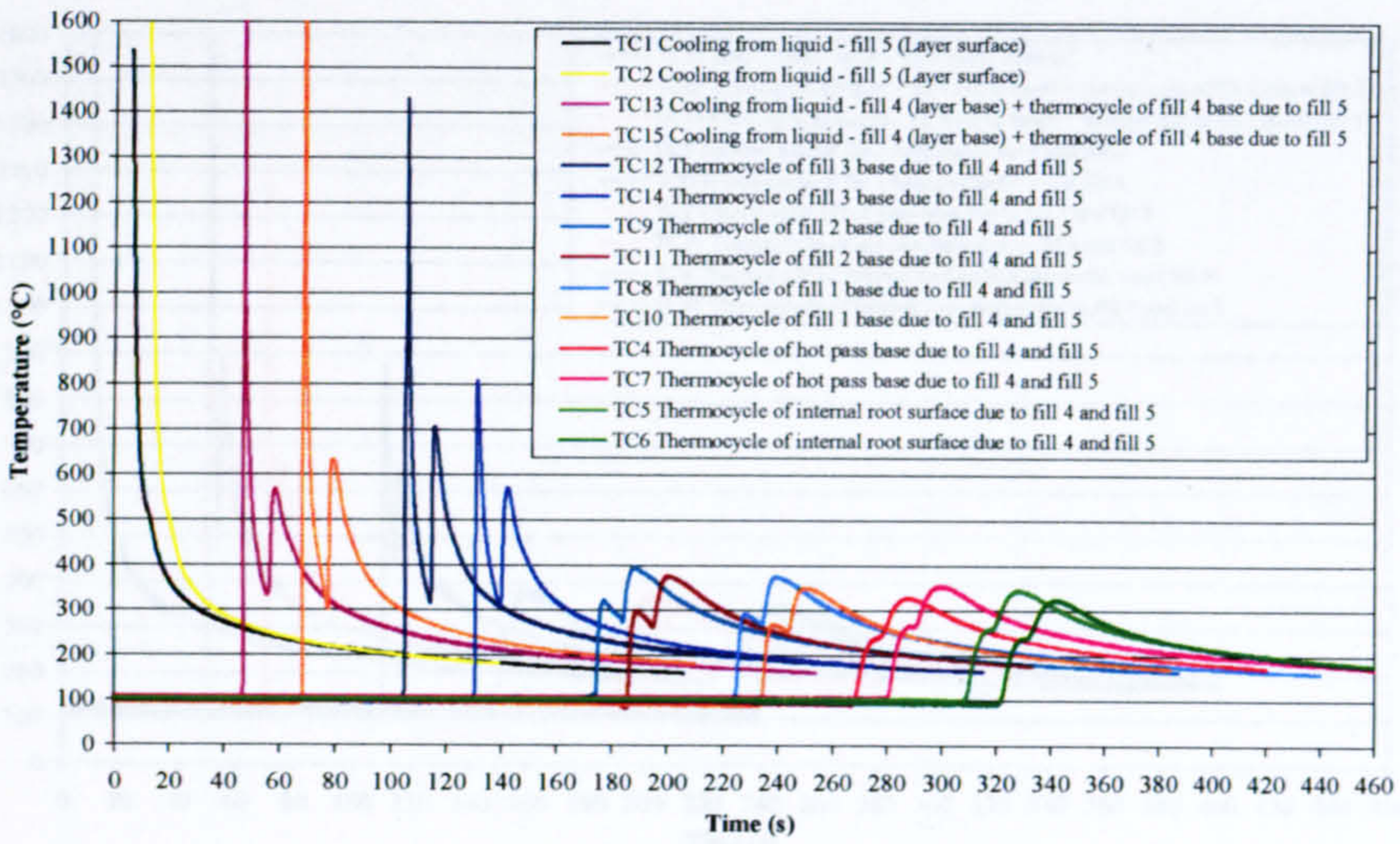

Dual torch thermocycles due to fill 6 and cap pass (36 in. OD, 19.05mm WT, X100, 100°C preheat, arc energy 0.47 and 0.45 kJ/mm, 6.90-7.30mm cap gap width)

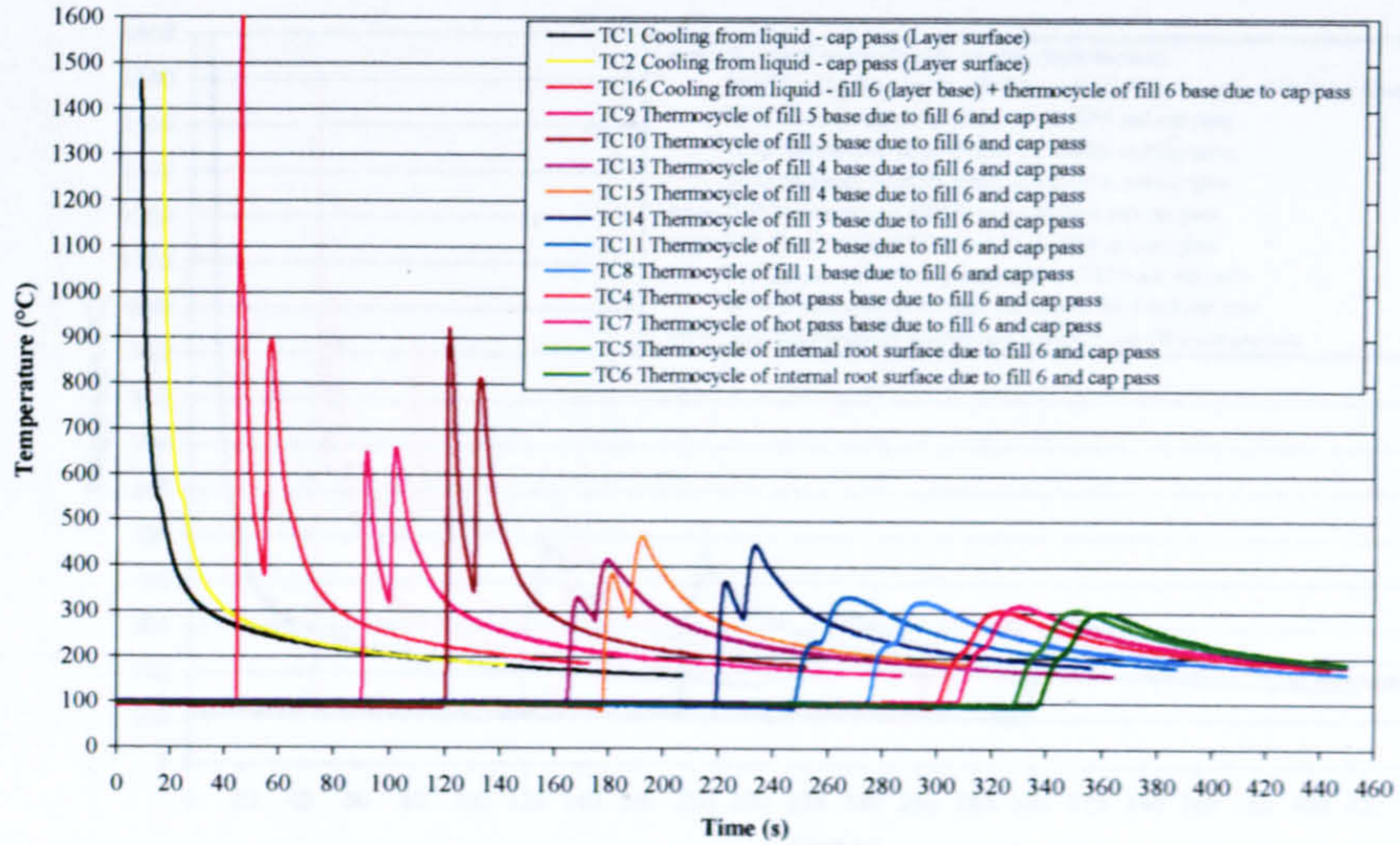

Figure 5-54: Process variation trials – dual torch thermocycle data

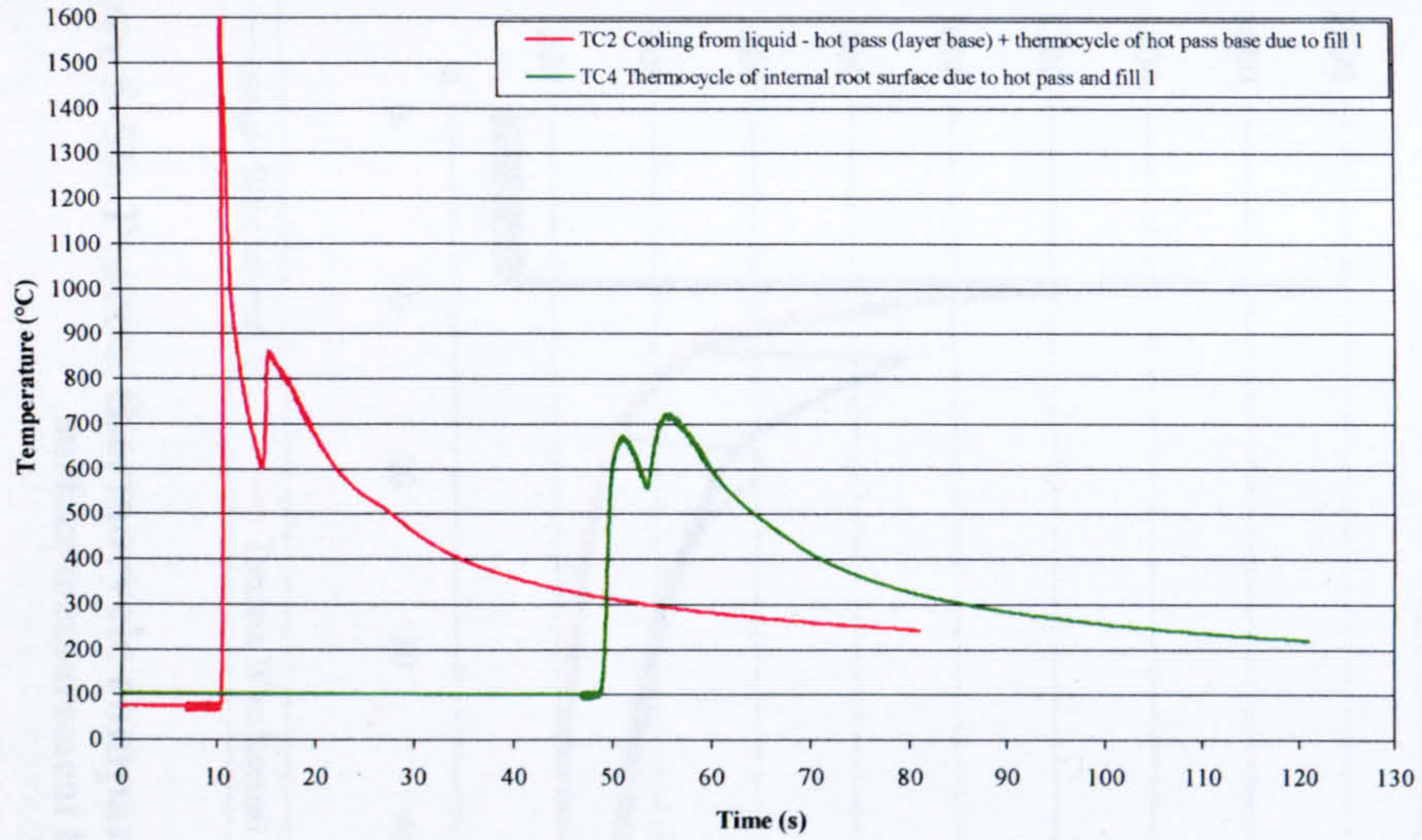

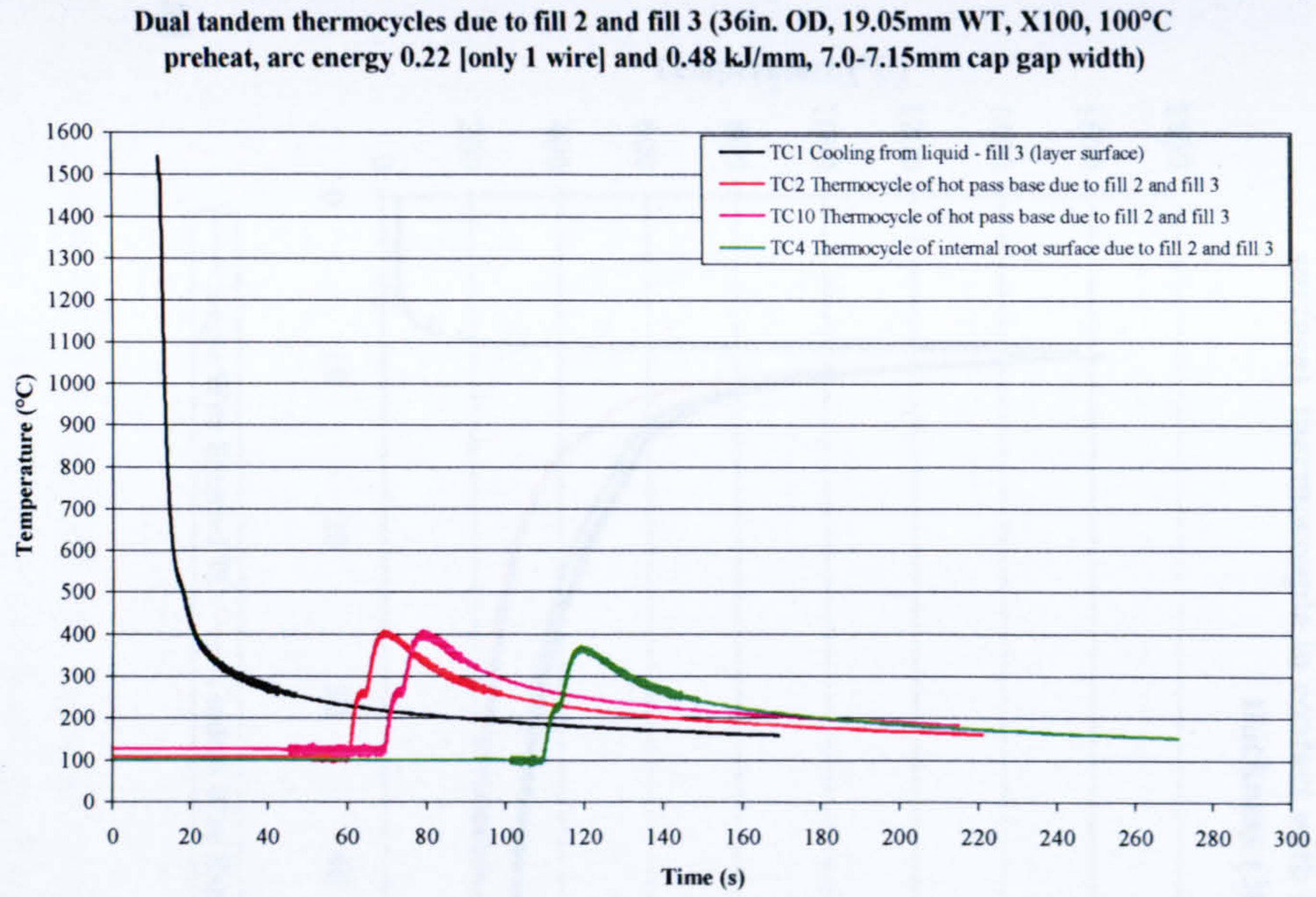

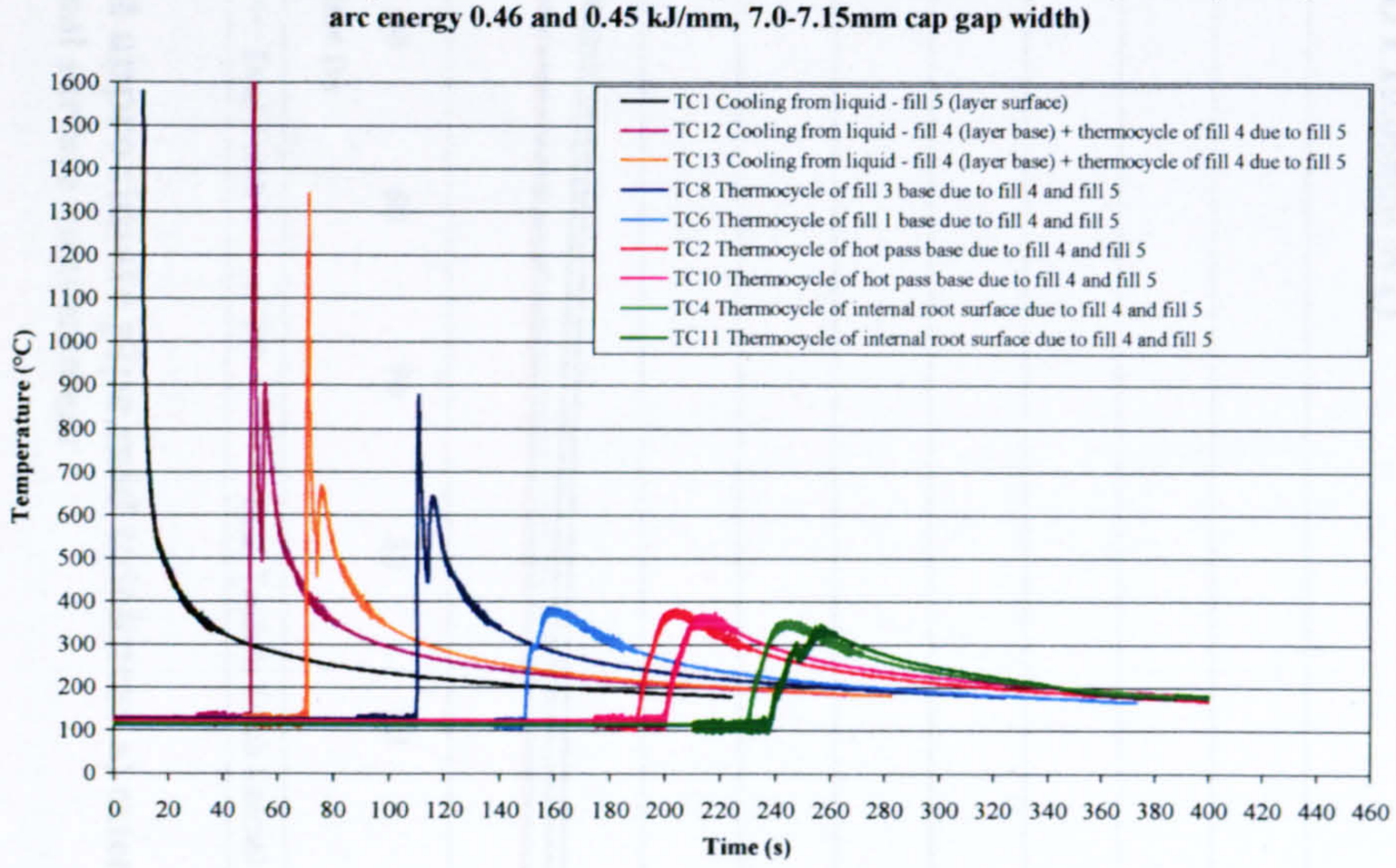

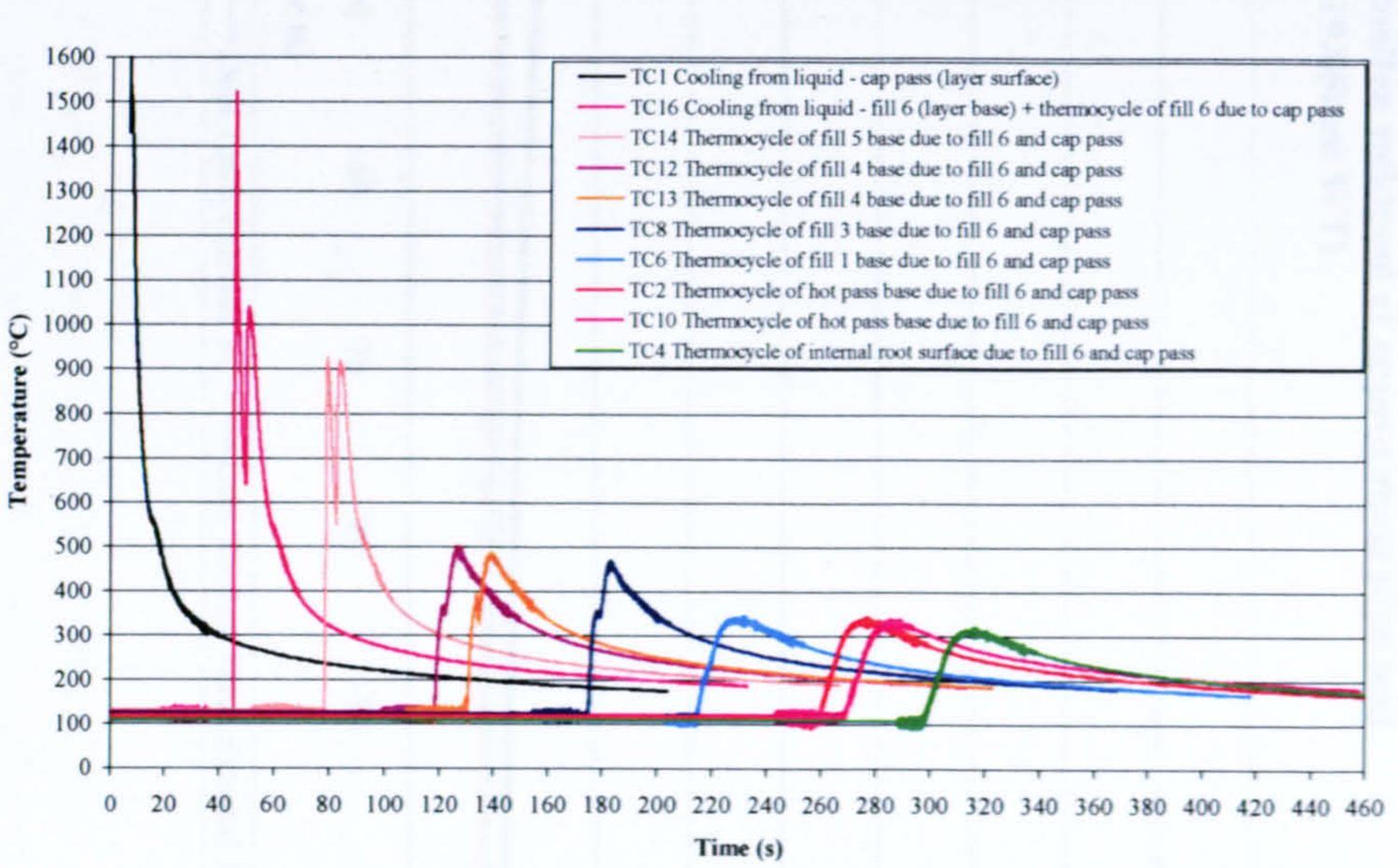

Figure 5-55: Process variation trials – dual tandem torch thermocycle data

Cooling curves for narrow gap PGMAW pipewelding process variants - externally placed (layer surface) thermocouple in contact with initially molten weldpool at approximate pipe mid thickness (36"OD x 19.05mm WT)

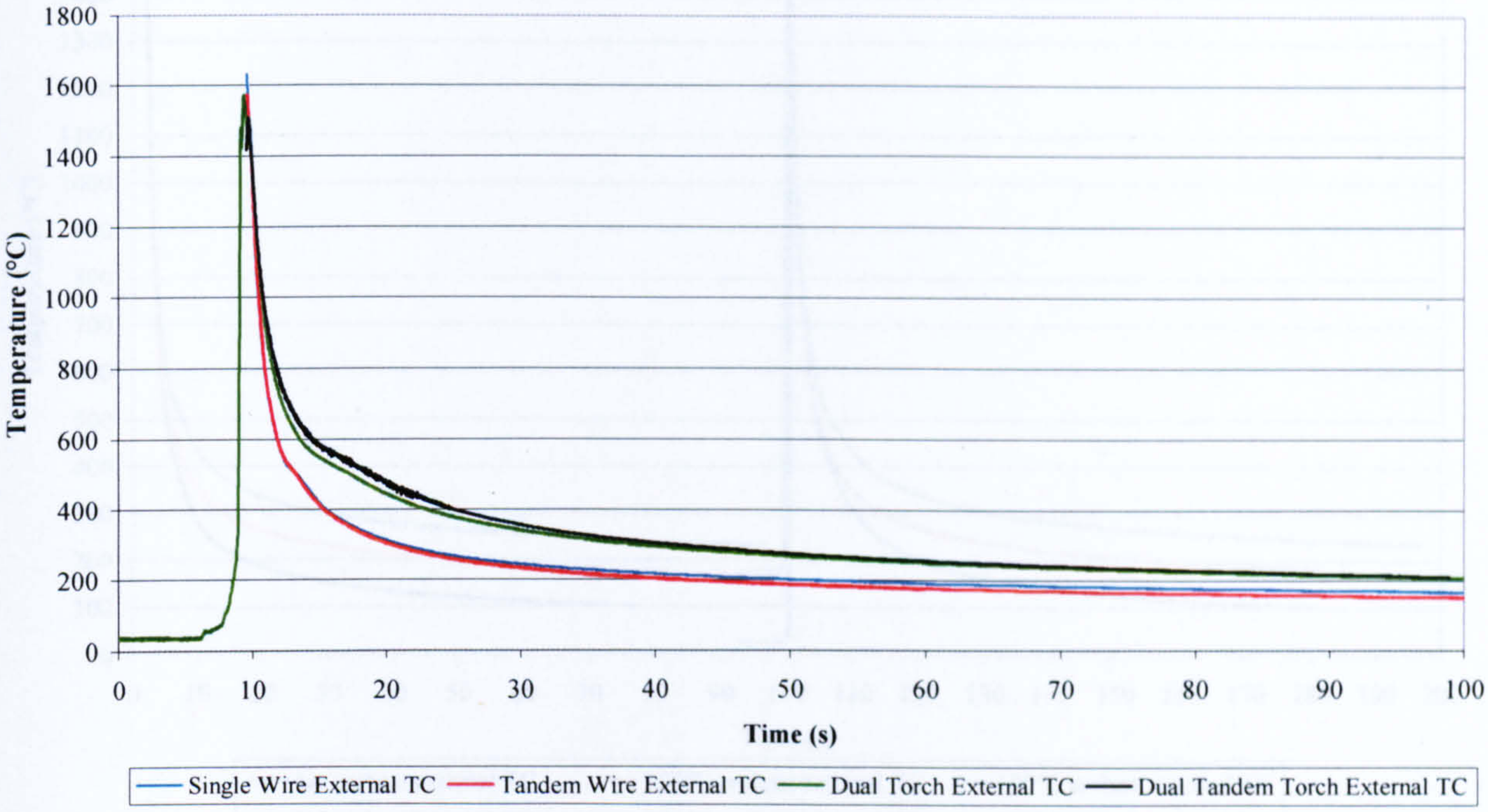

a)

Cooling curves for narrow gap PGMAW pipewelding process variants - internally placed (layer base) thermocouple in contact with initially molten weldpool at approximate pipe mid thickness (36" OD x 19.05mm WT)

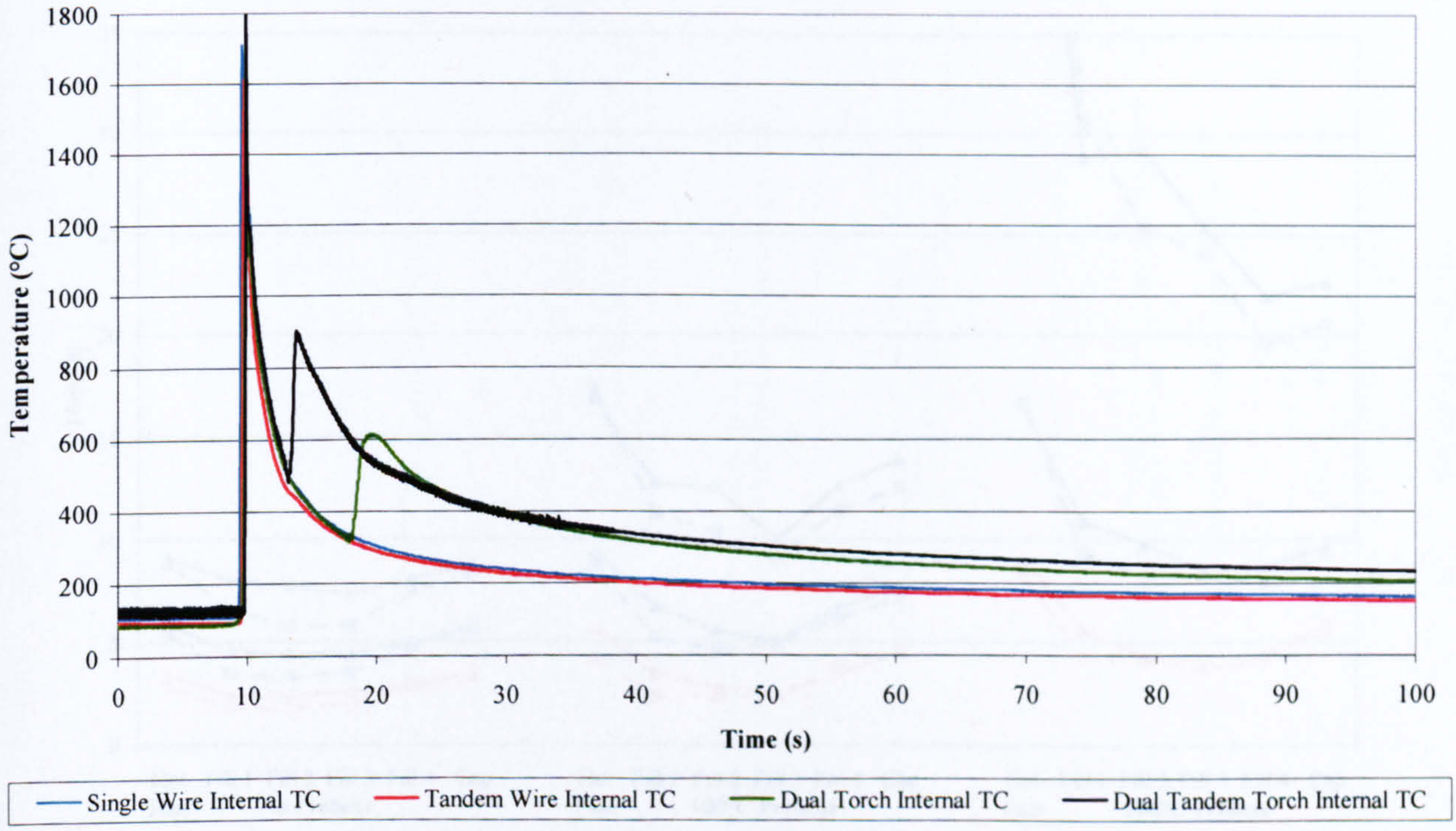

b)

Figure 5-56: Process thermocycle comparison at approximate pipe mid thickness a) external surface measurement b) internal surface measurement

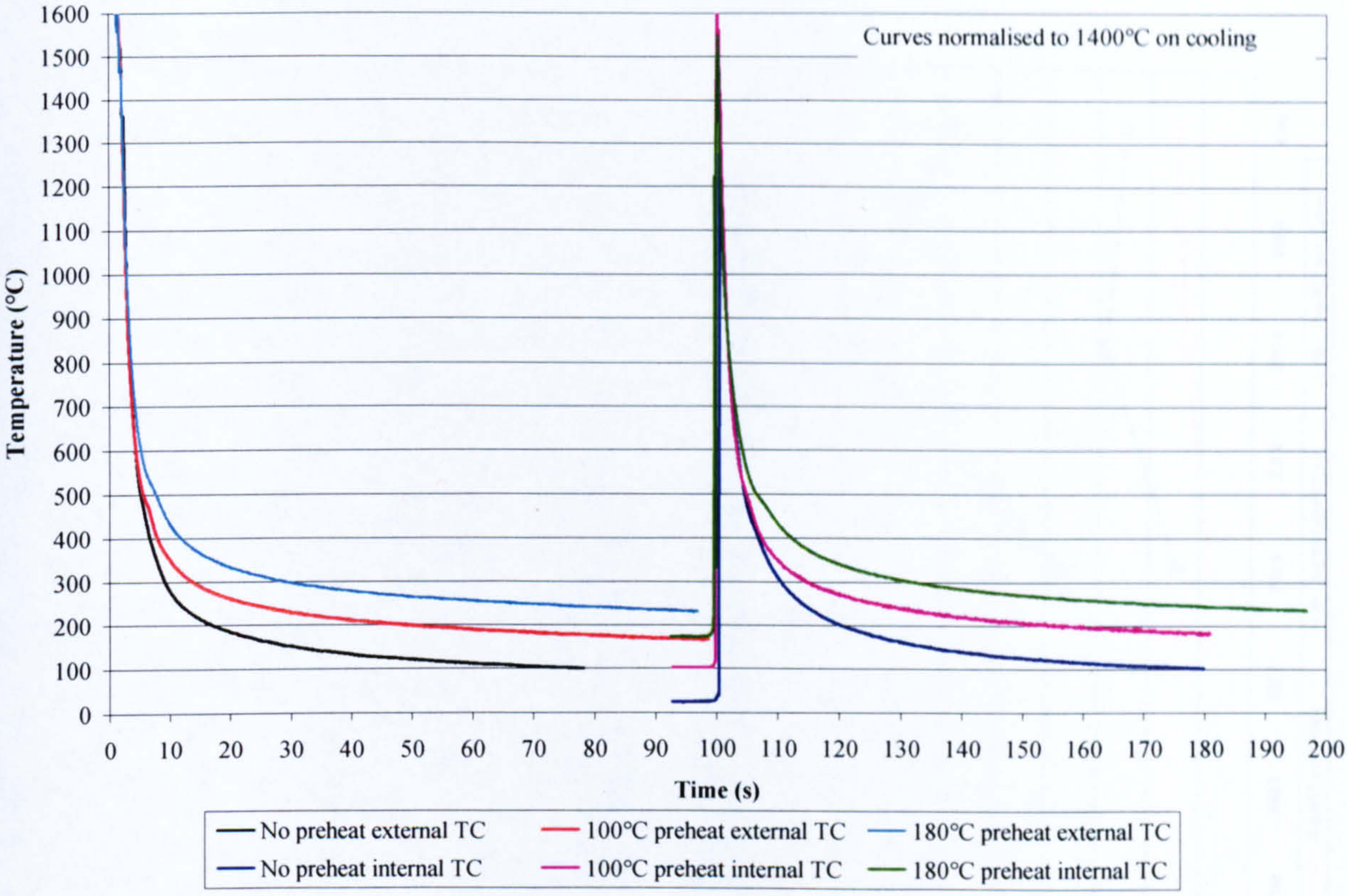

Figure 5-57: Cooling curves for narrow gap PGMAW pipewelding preheat variants – externally placed (layer surface) and internally placed (layer base) thermocouples at approximate pipe mid thickness (30 in. OD x 19.05mm WT)

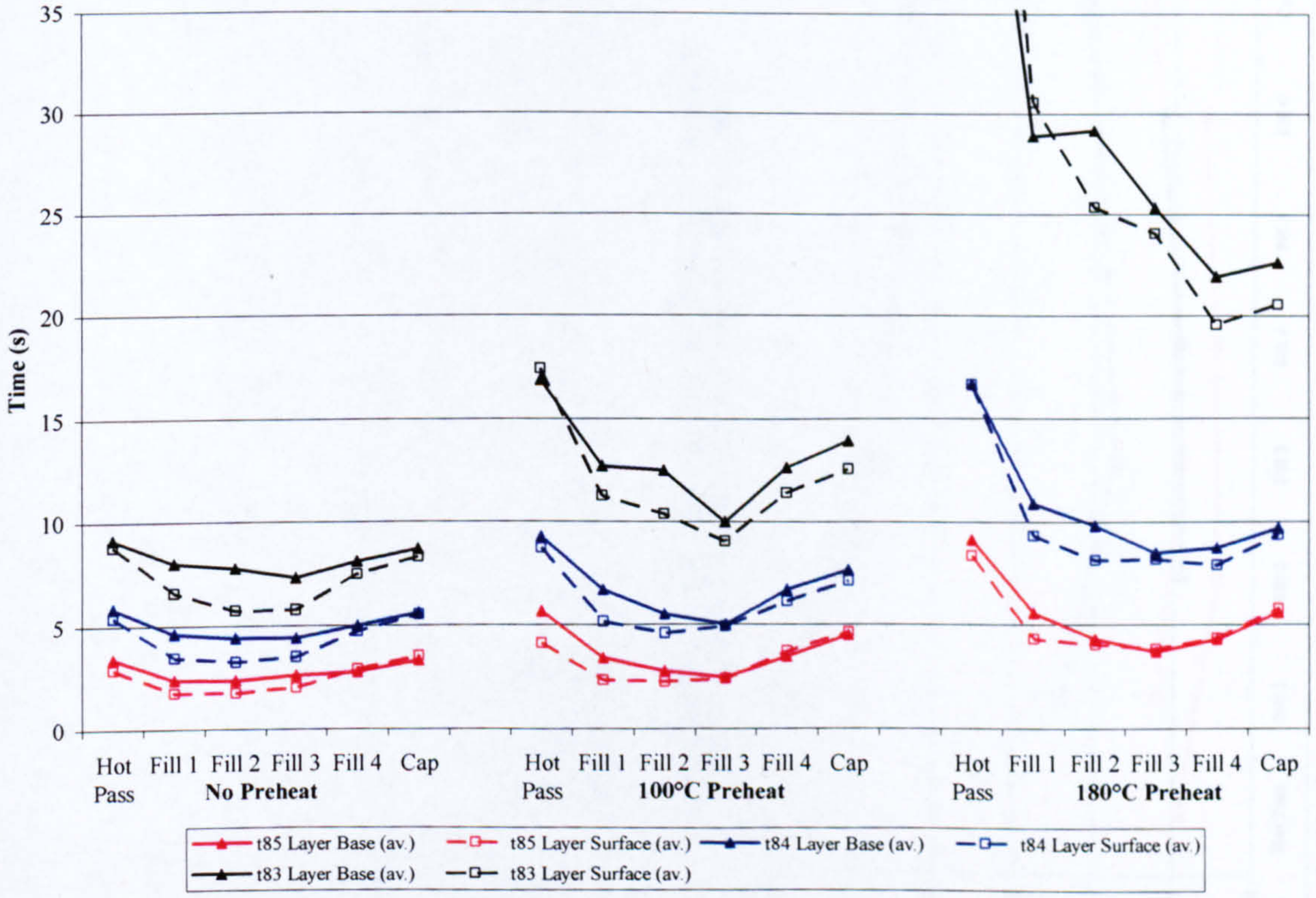

Figure 5-58: Preheat variation comparison – cooling times from liquid state (30 in. OD, 19.05mm WT, X100, single wire PGMAW, arc energy 0.48-0.59 kJ/mm, 6.05-6.85mm cap gap width)

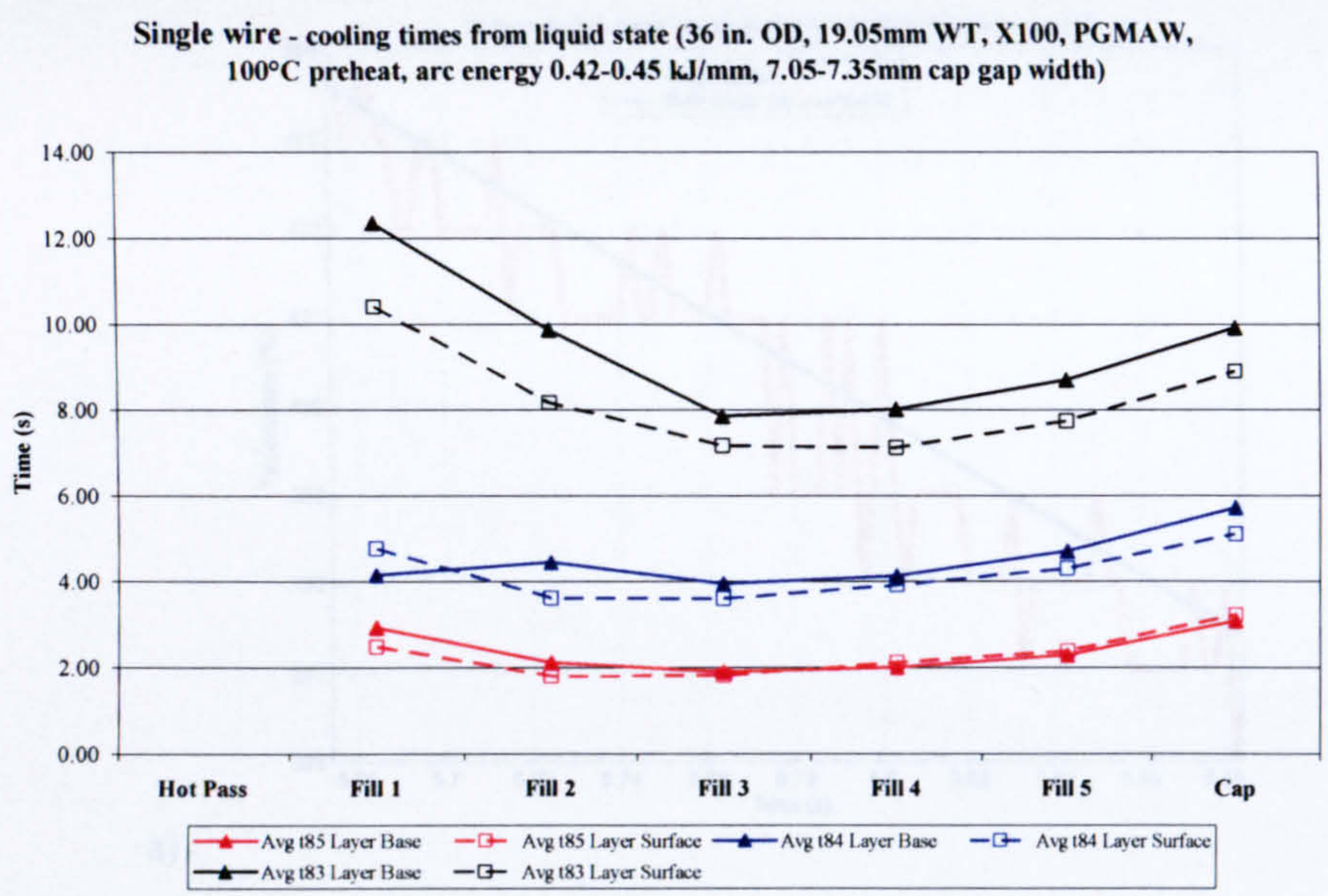

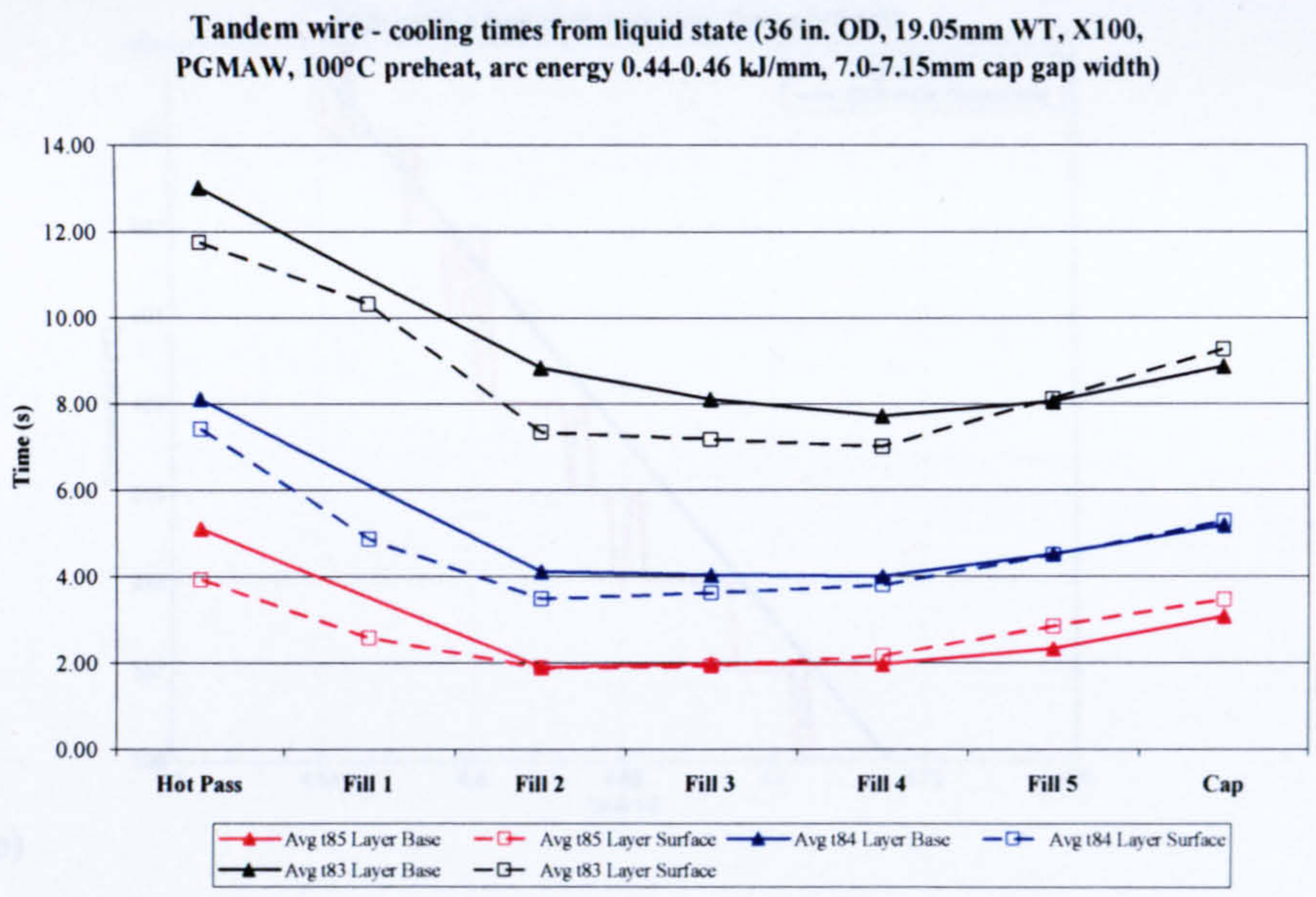

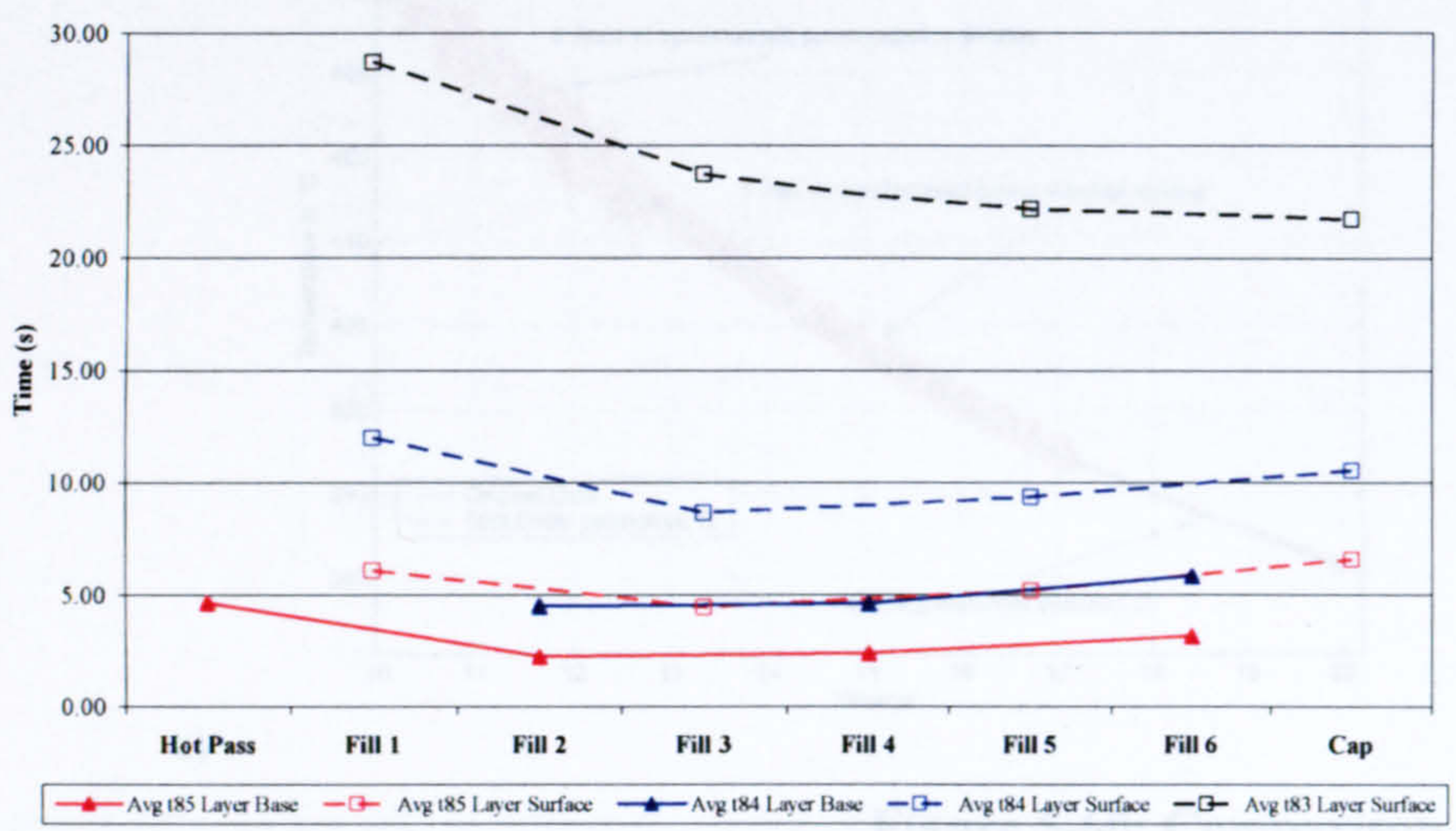

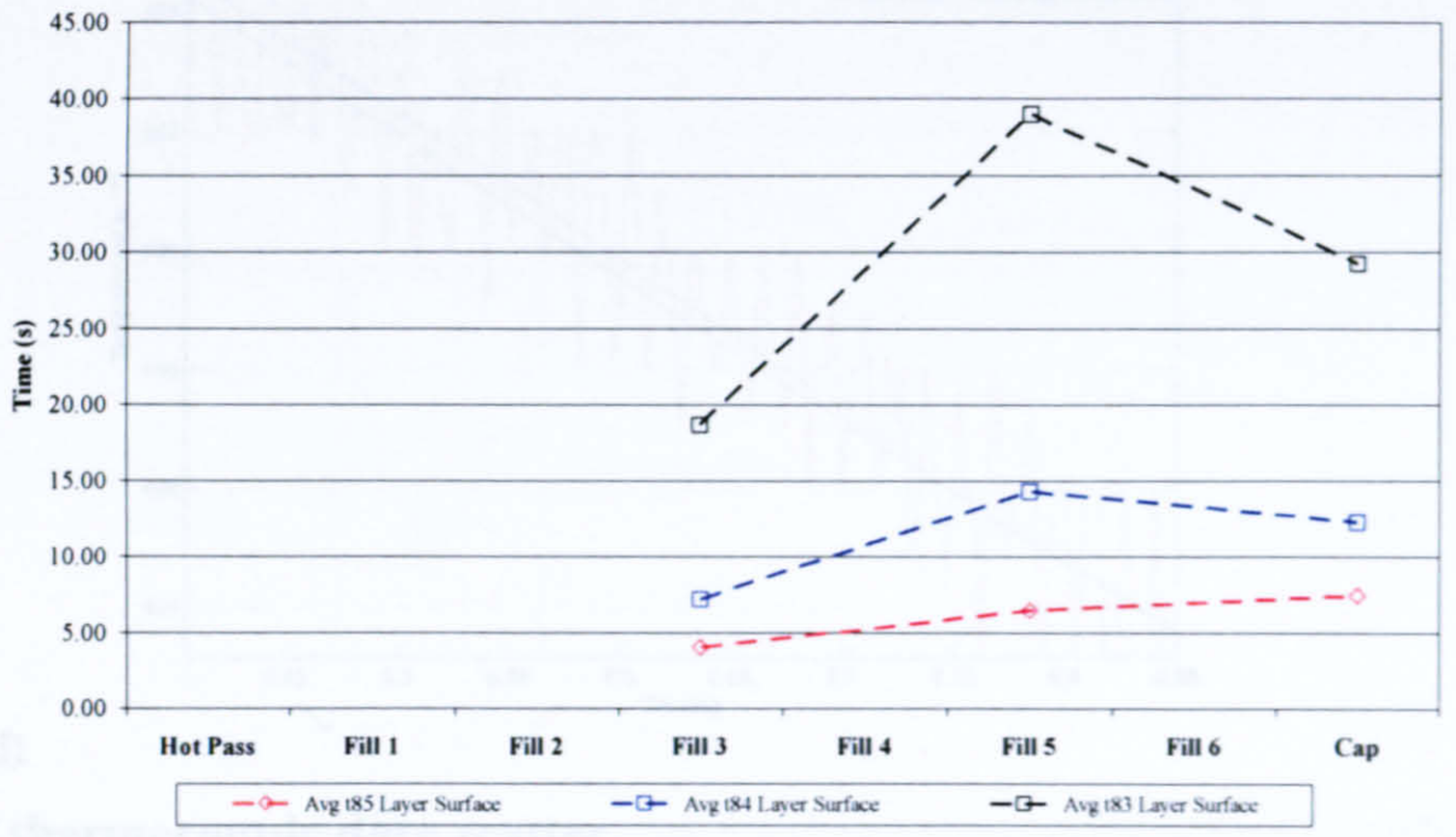

Figure 5-59: Process variation t_{85}, t_{84} and t_{83} cooling time comparison

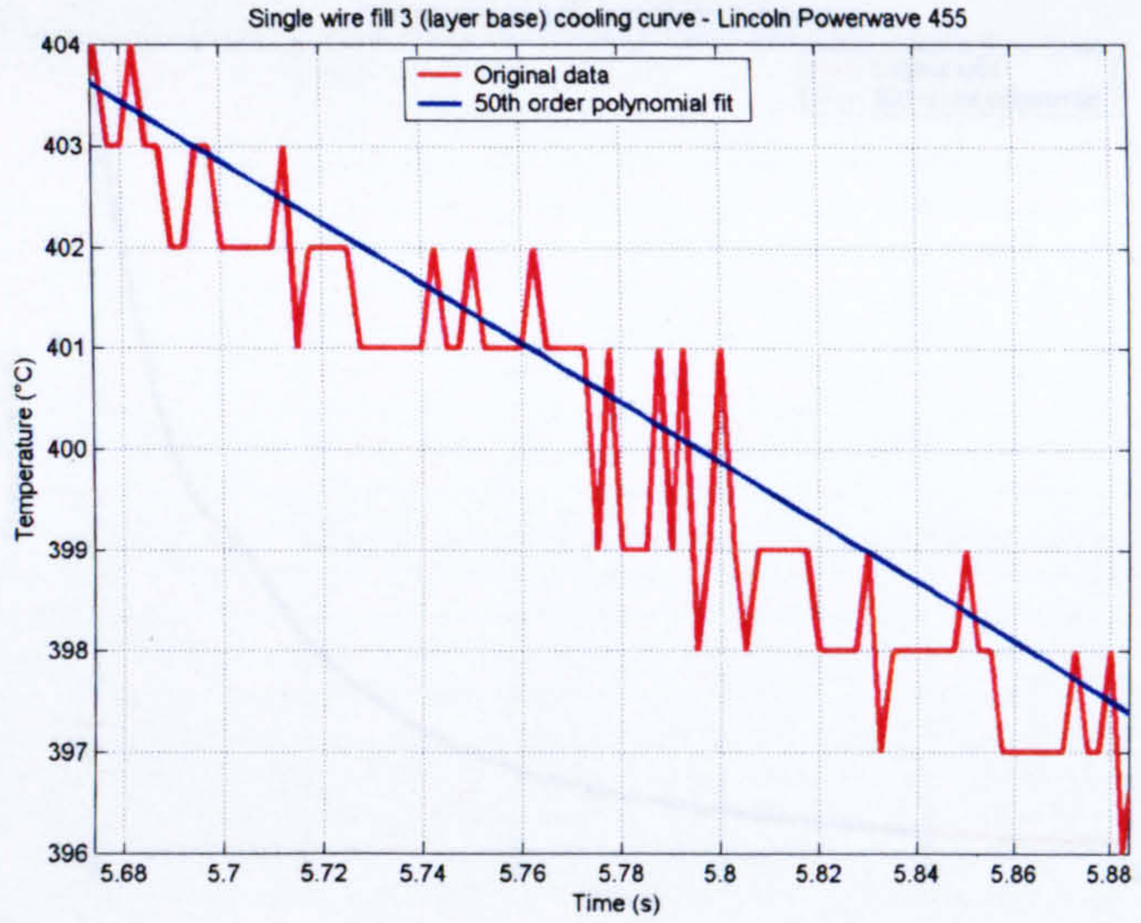

a)

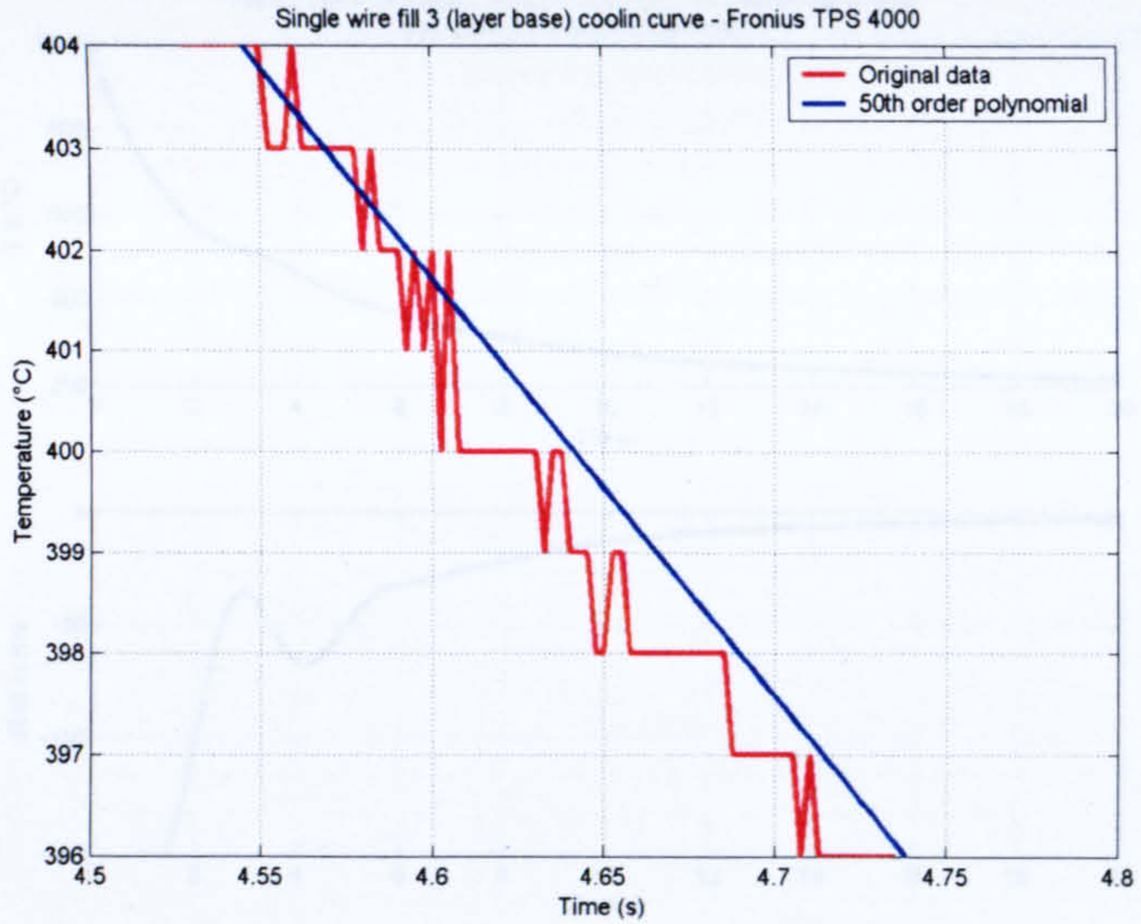

b)

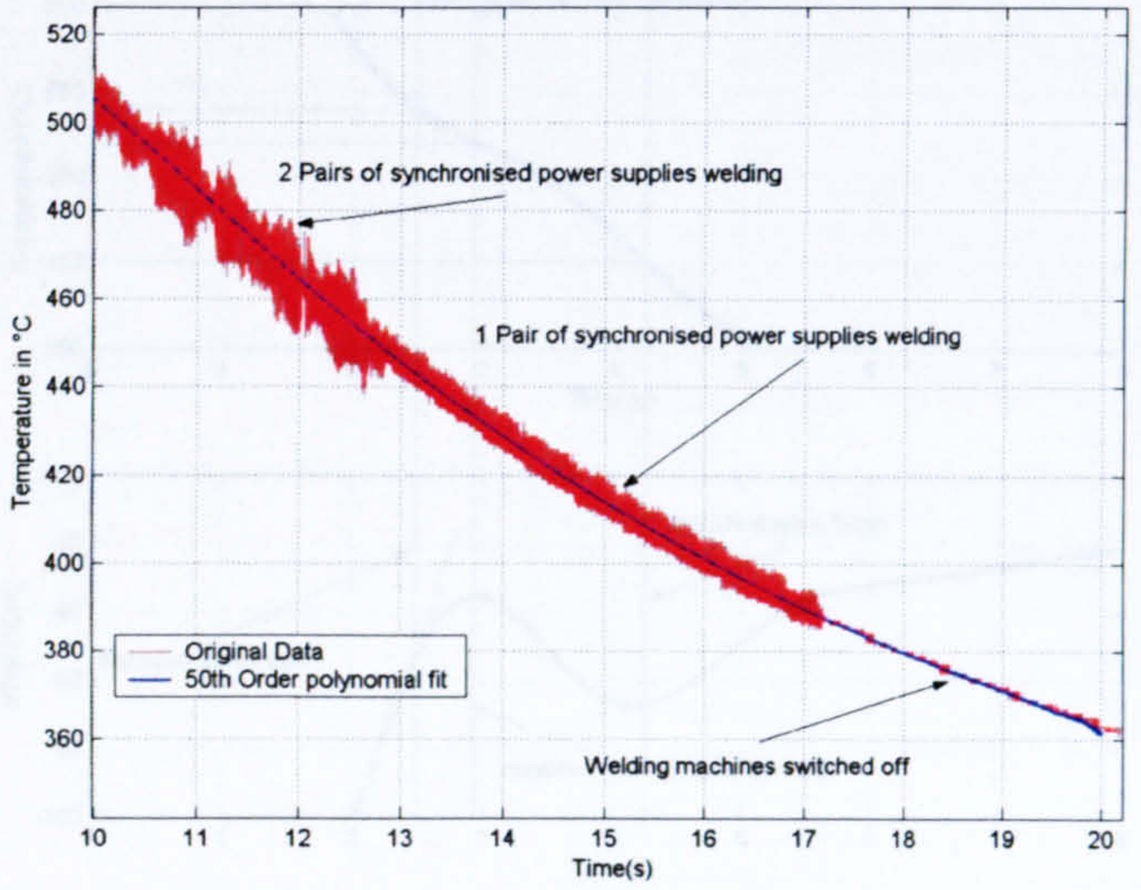

c)

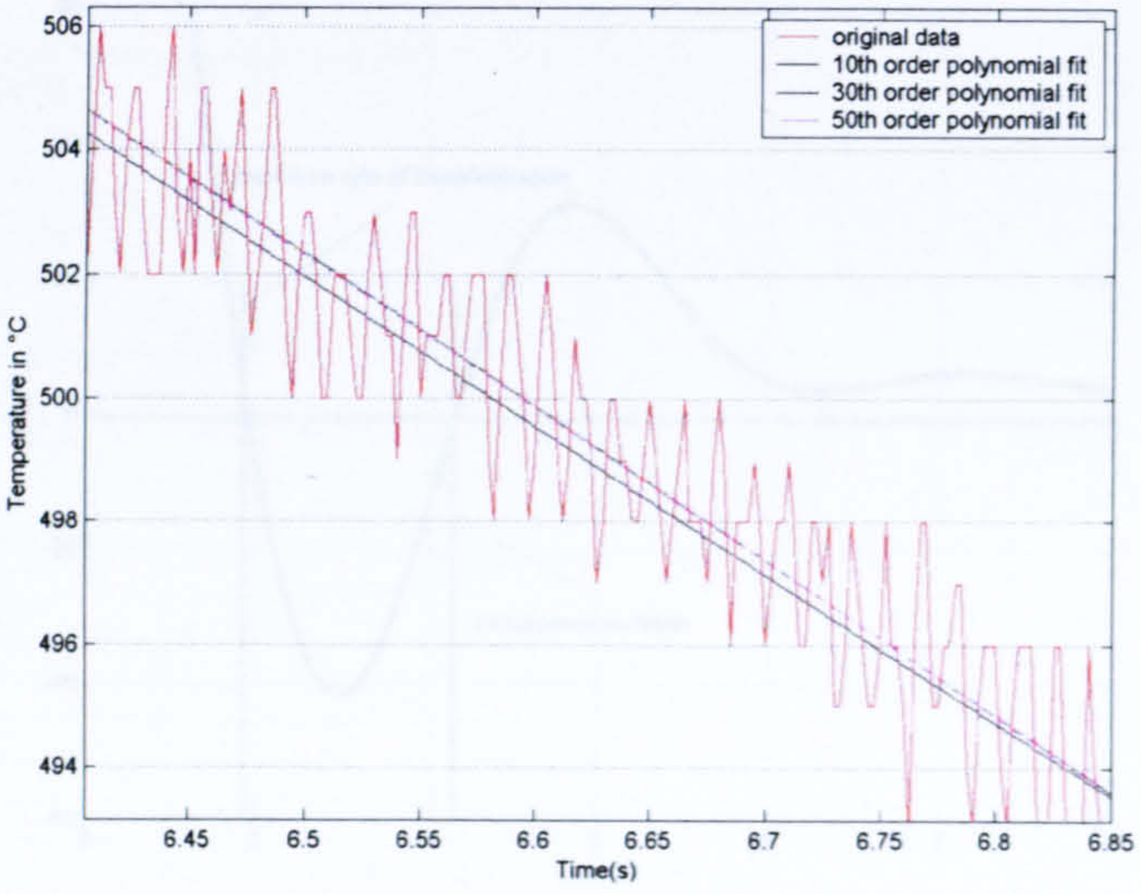

d)

Figure 5-60: Comparison of thermocouple data scatter

a) Lincoln Powerwave 455 data scatter – single wire b) Fronius TPS 4000 data scatter – single wire c) Fronius TPS 4000 data scatter – 4, 2 and no power supplies welding d) Polynomial order comparison for curve fitting of original data

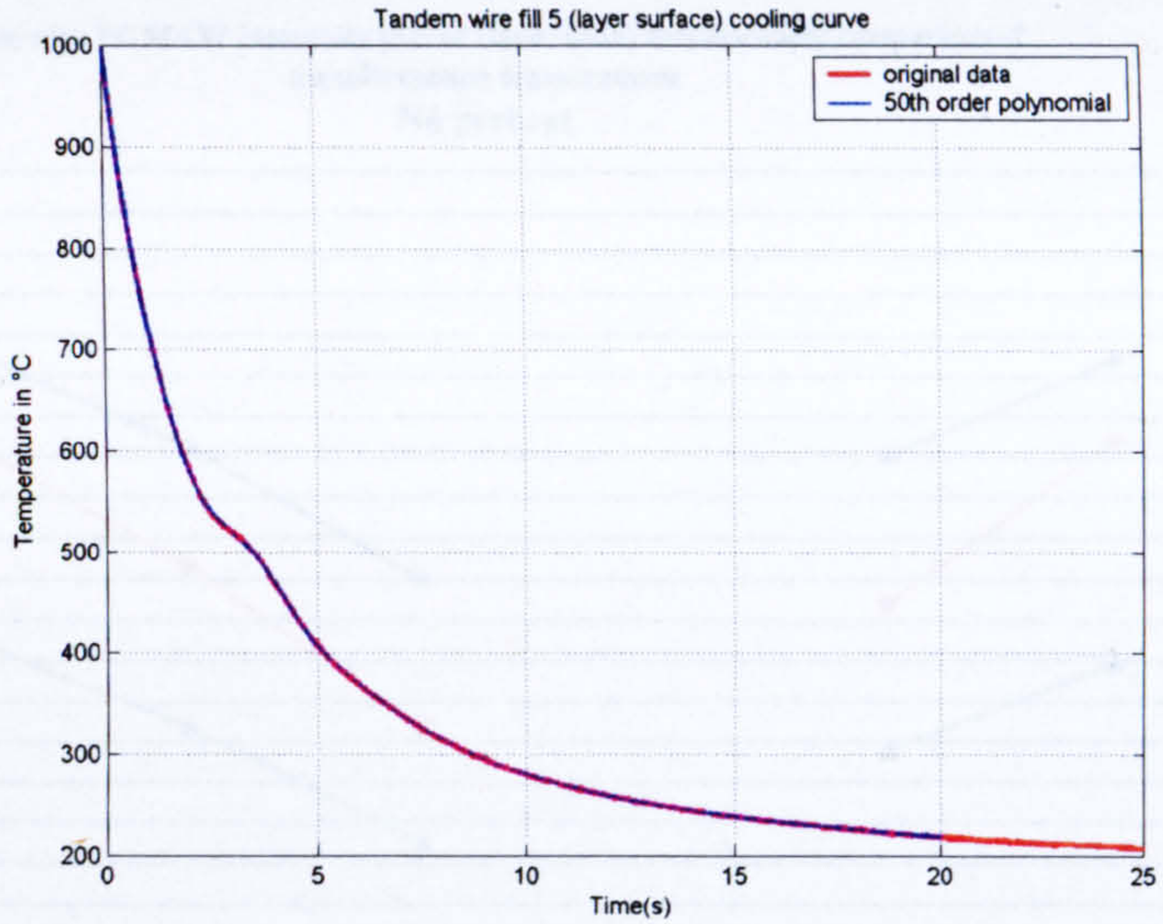

a)

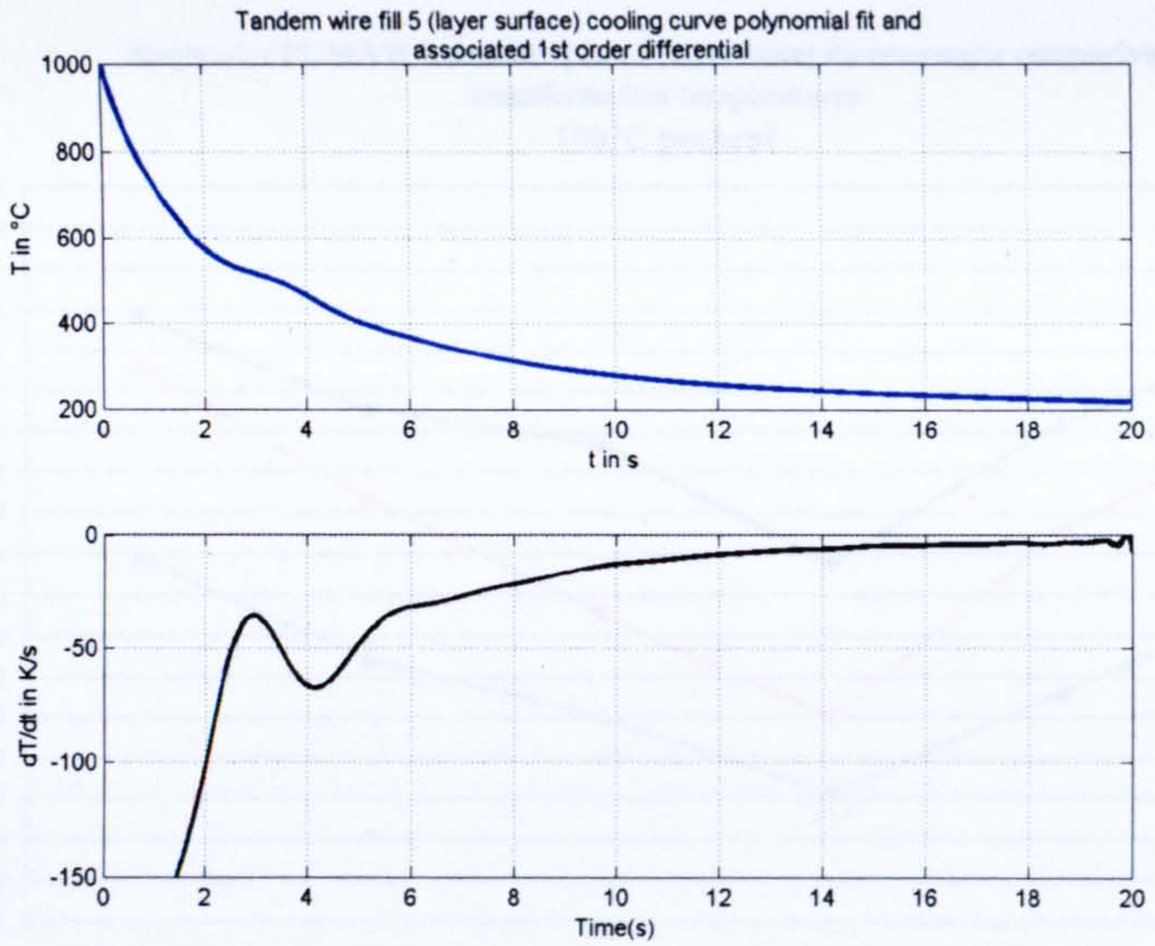

b)

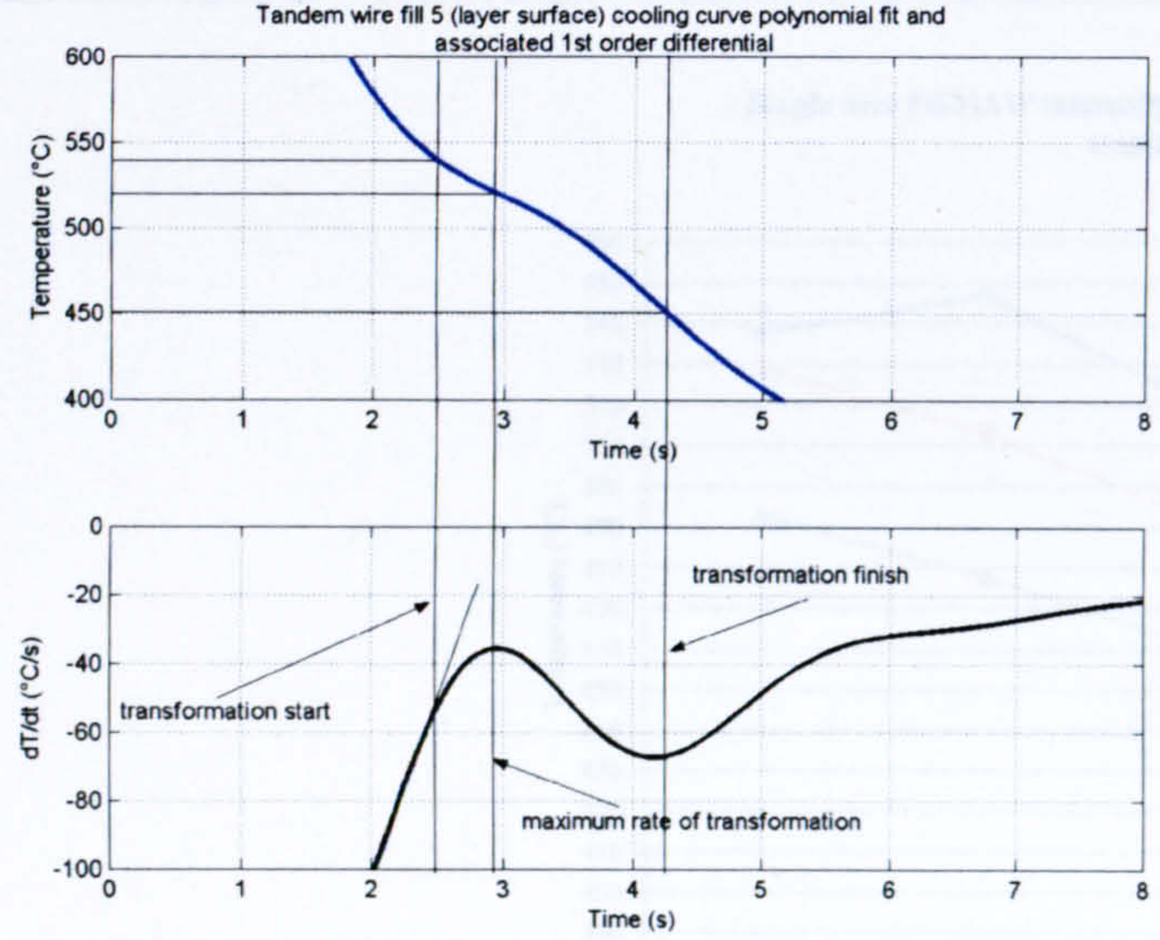

c)

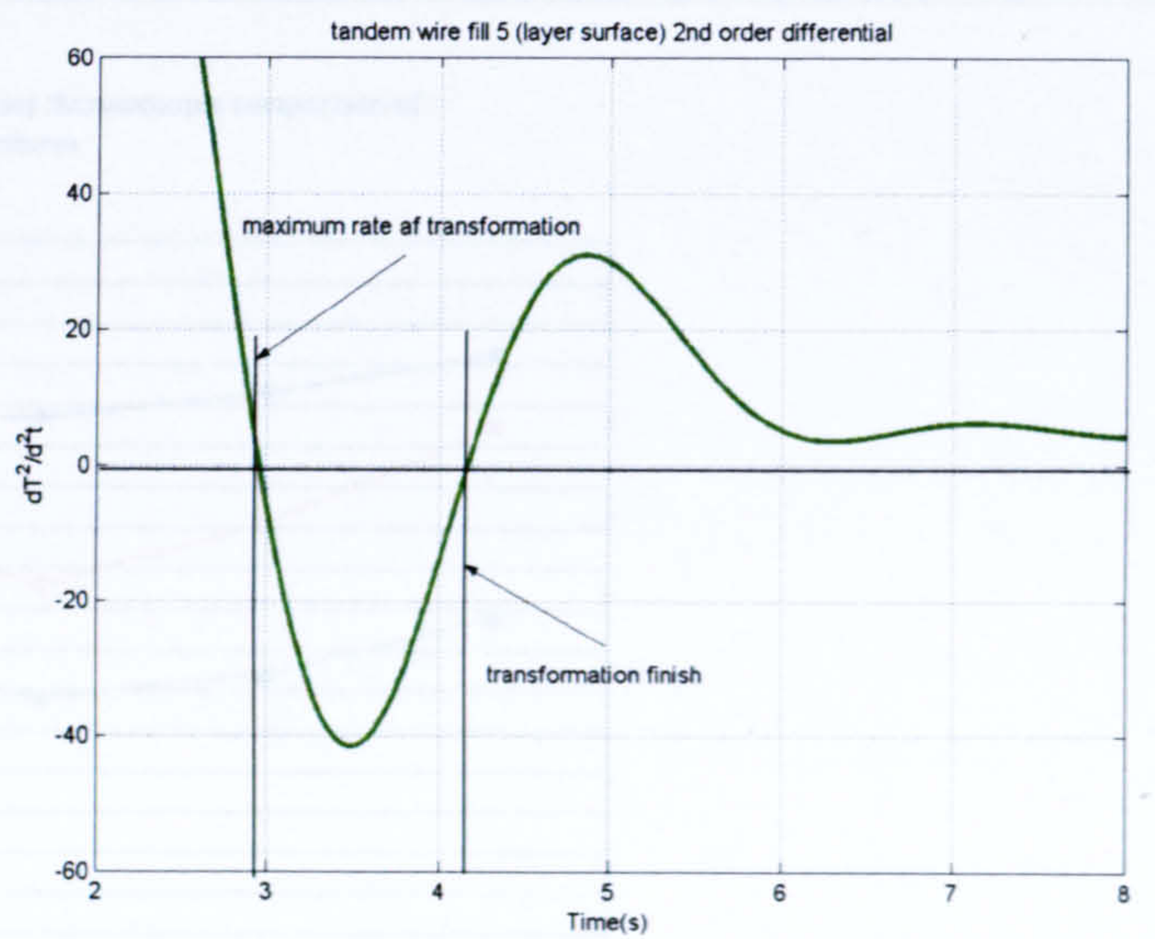

d)

Figure 5-61: Example method for determination of transformation temperatures, cooling times and cooling rates via MATLAB software

a) original data with polynomial fit superimposed b) Polynomial fit (top) and associated 1st order differential (bottom) c) enlargement of inflection point to determine transformation start temperature d) 2nd order differential to determine transformation finish and maximum rate temperatures

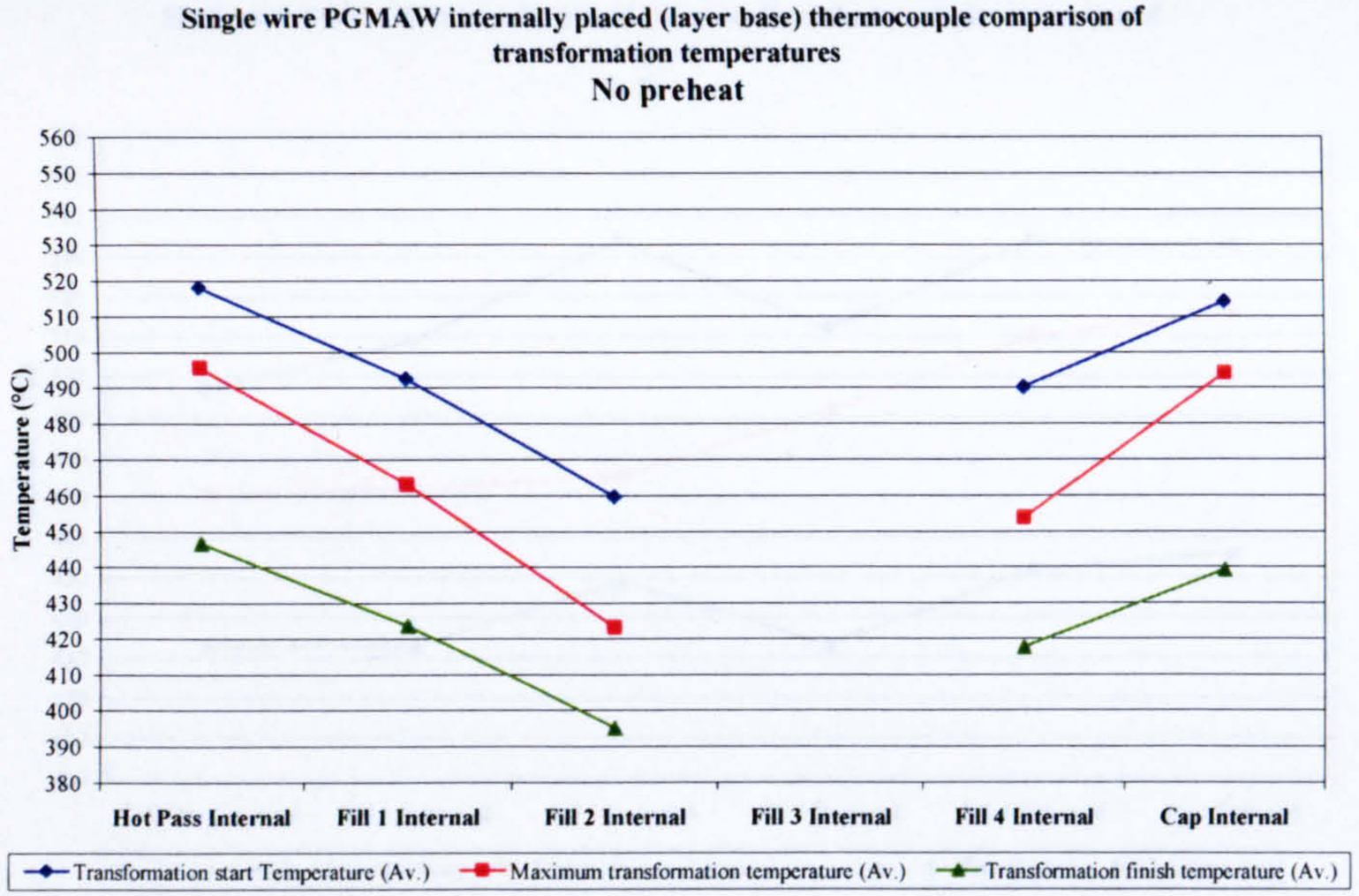

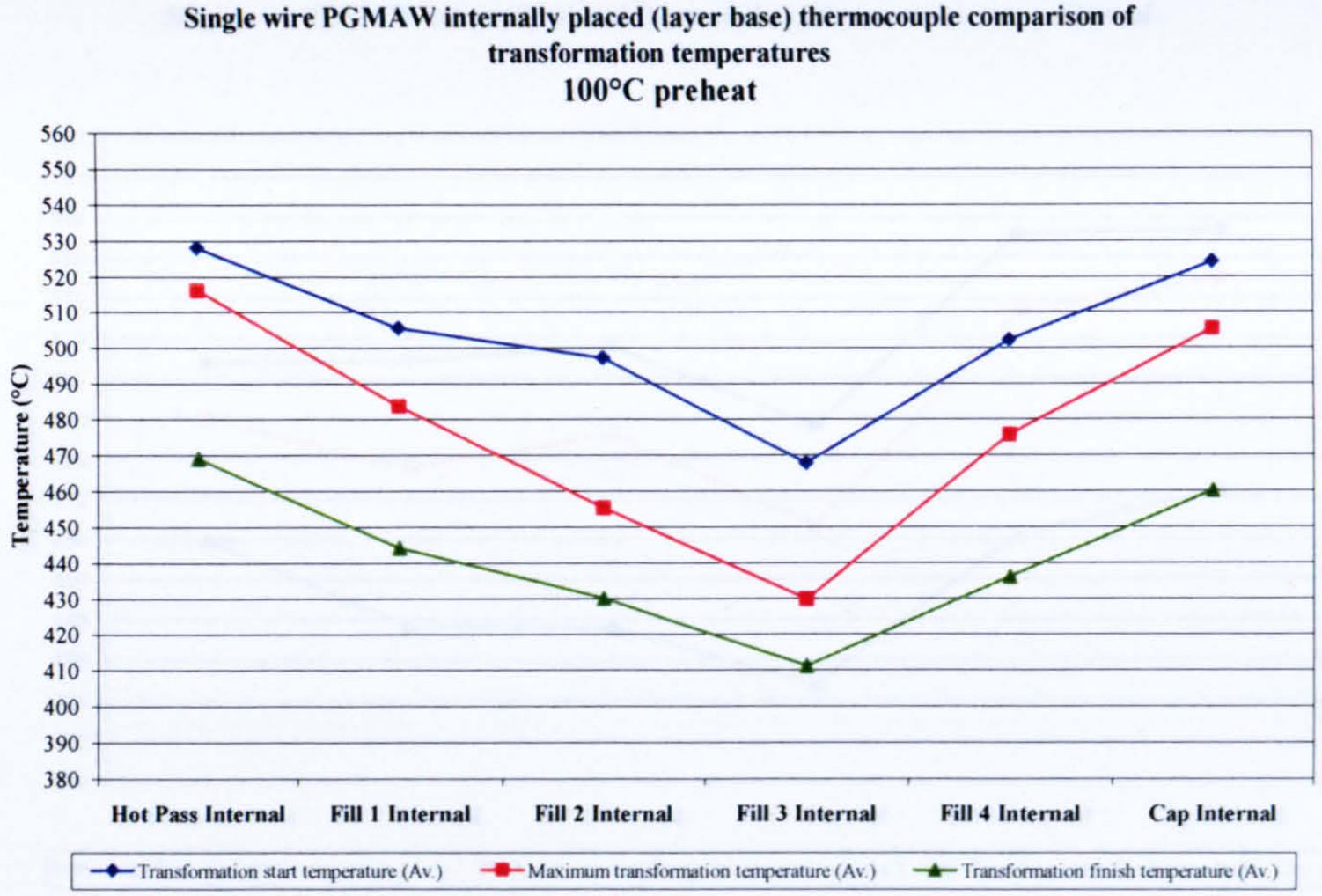

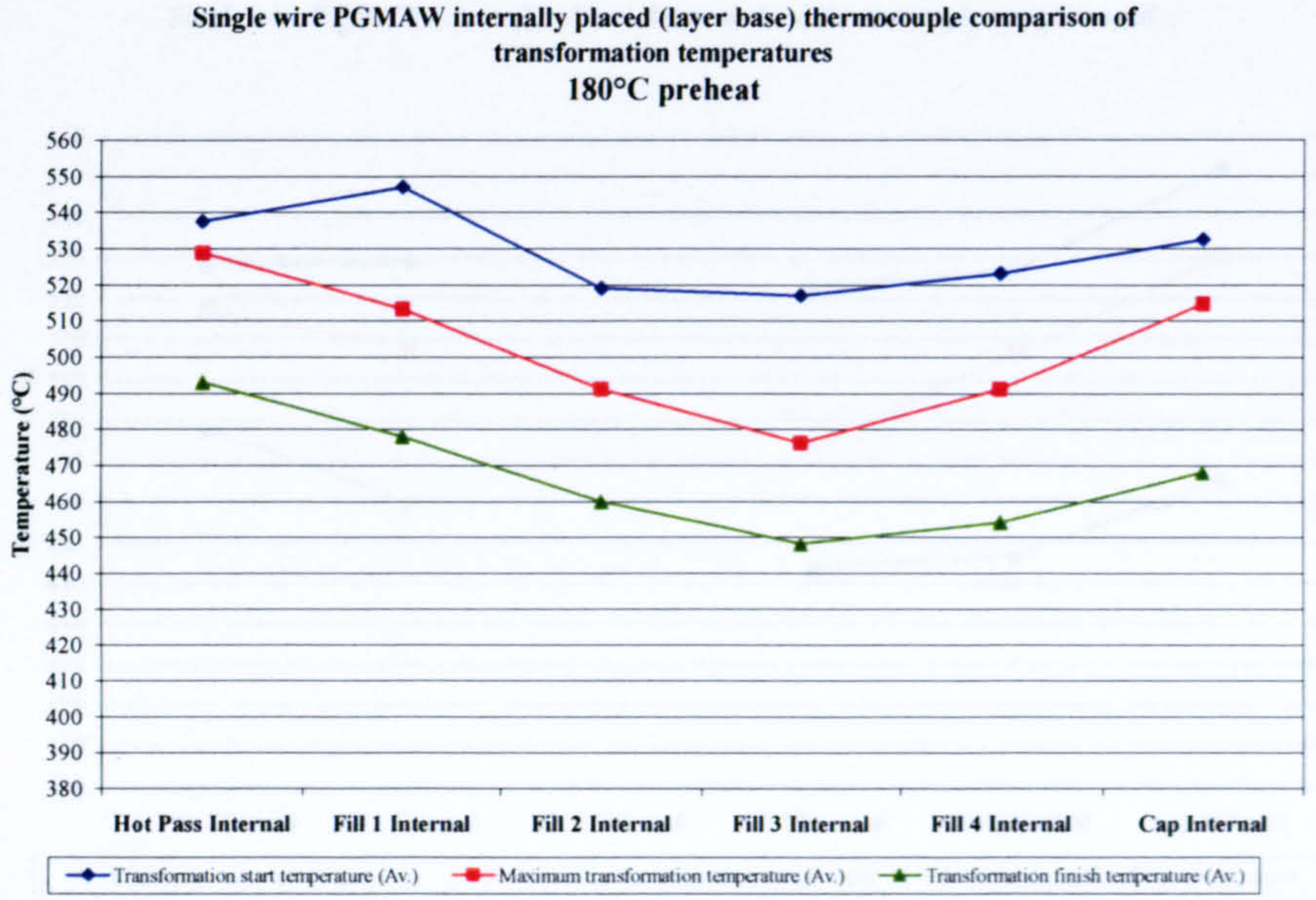

Figure 5-62: Effect of preheat on transformation temperatures through pipe wall thickness – internal (layer base) thermocouples

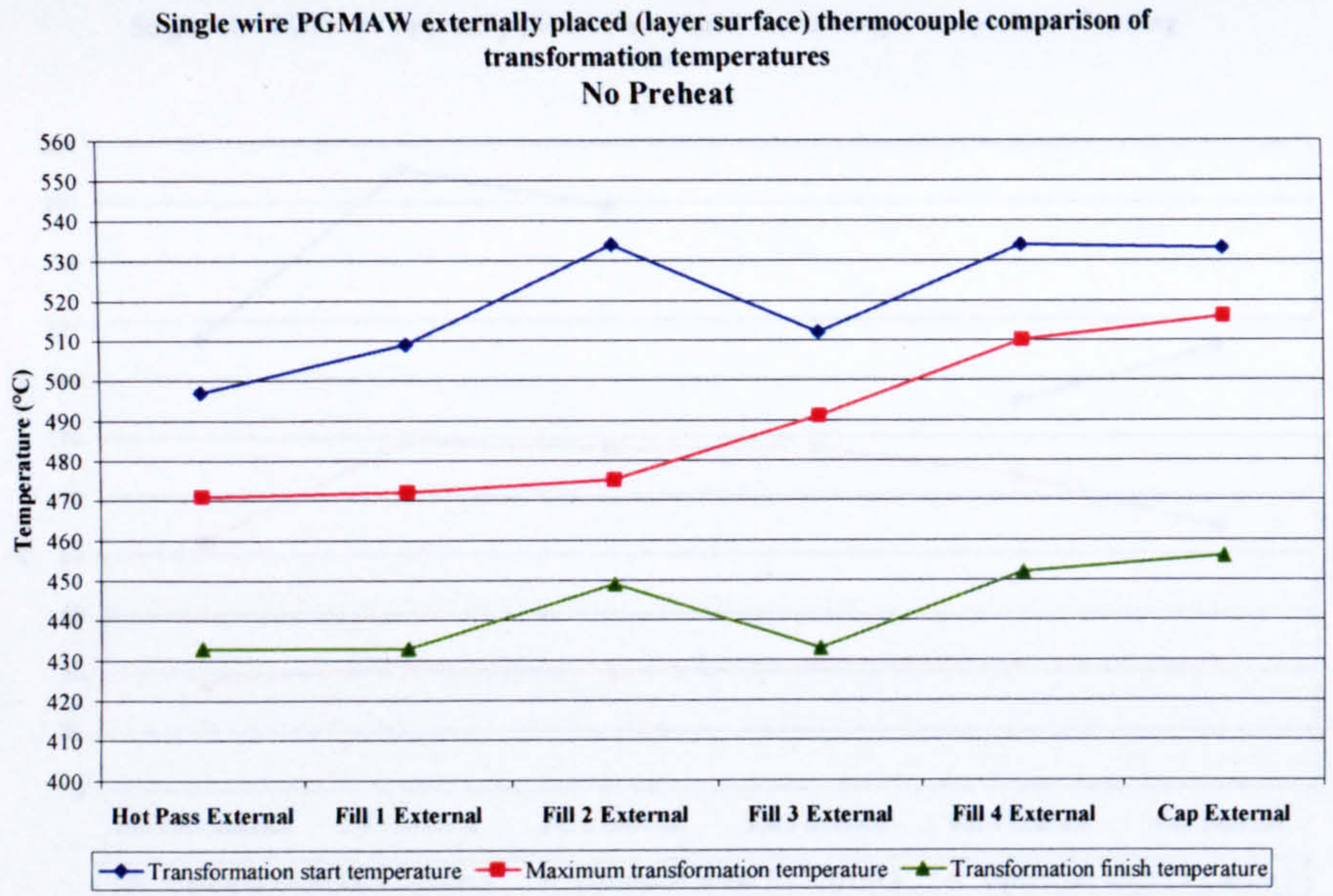

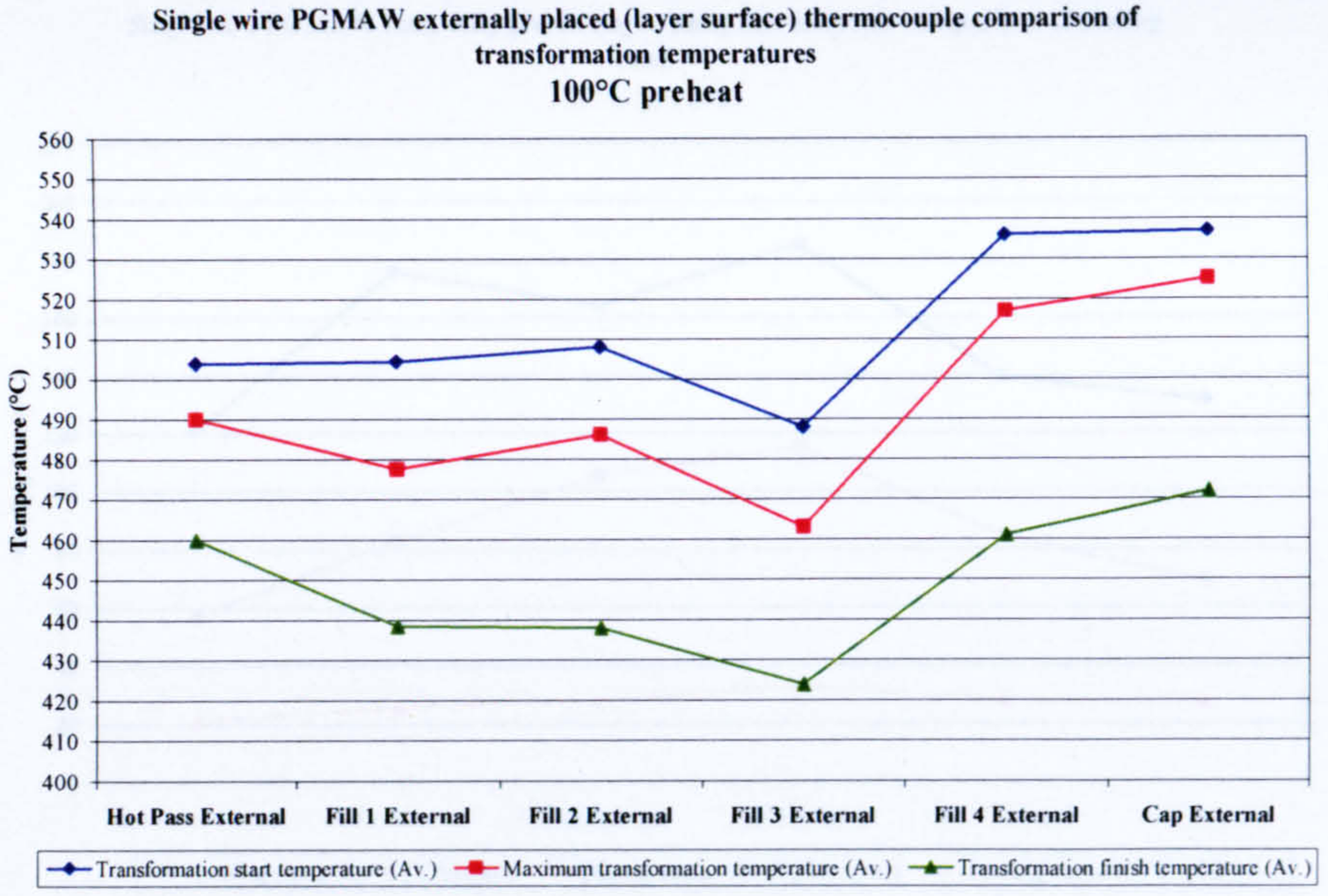

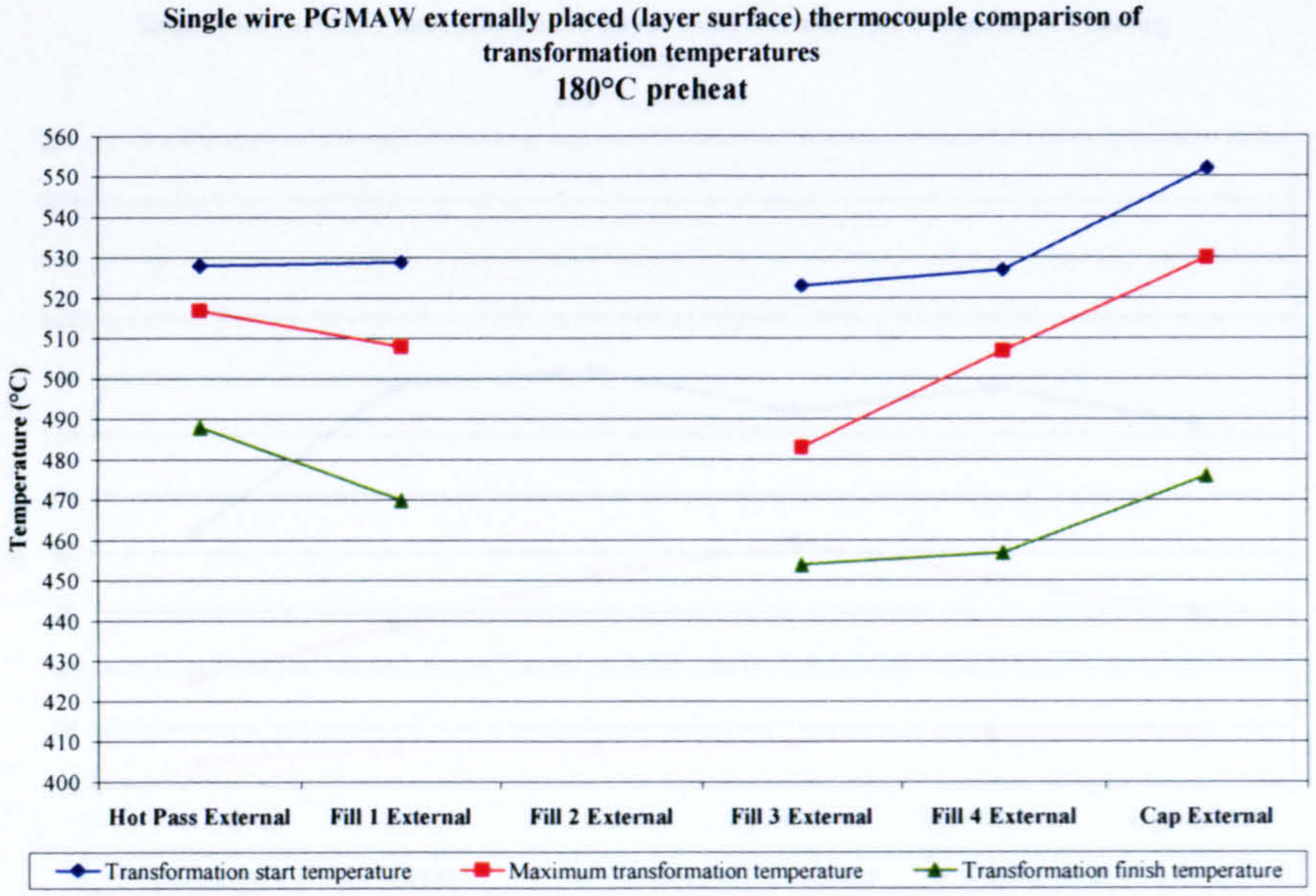

Figure 5-63: Effect of preheat on transformation temperatures through pipe wall thickness – external (layer surface) thermocouples

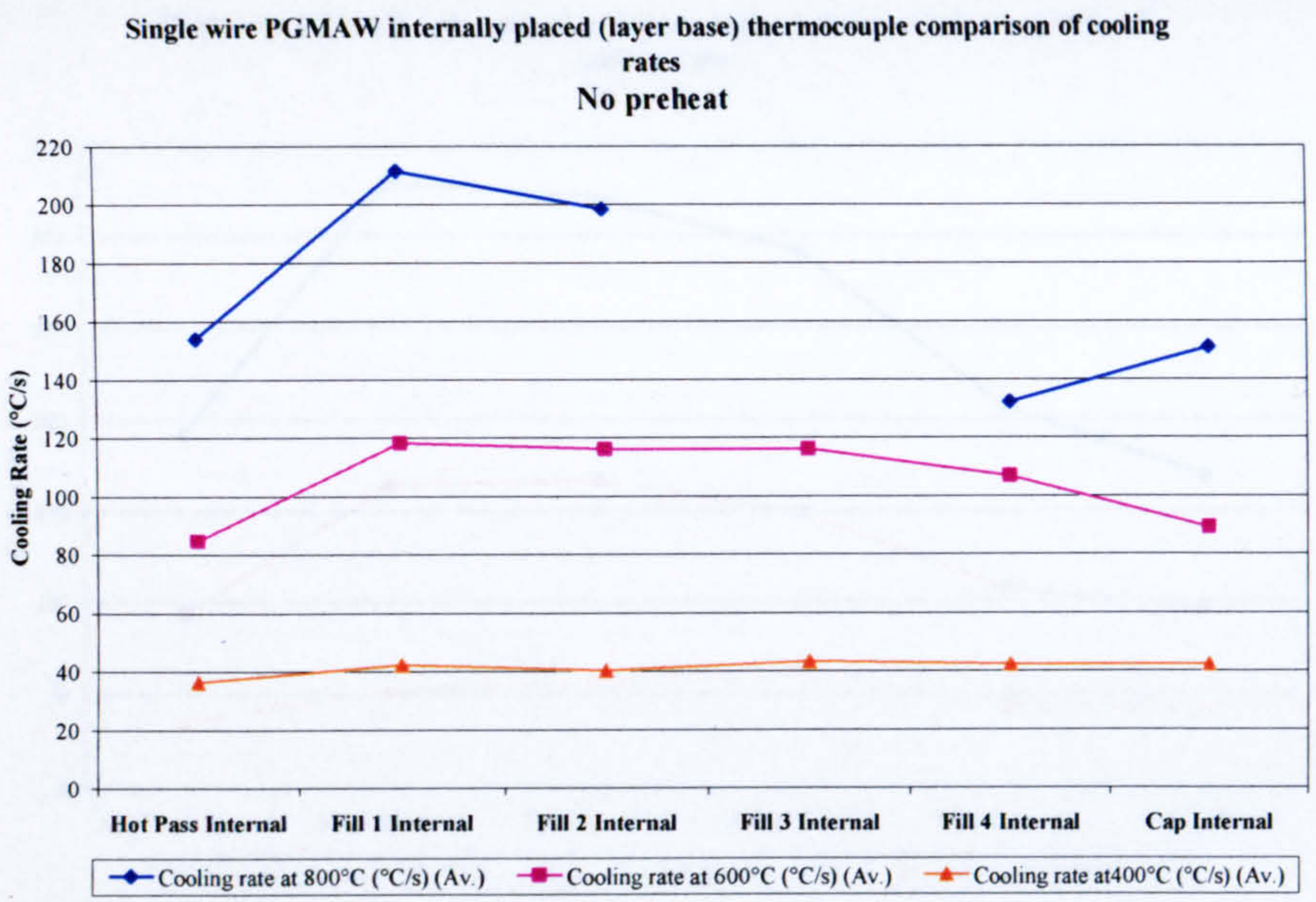

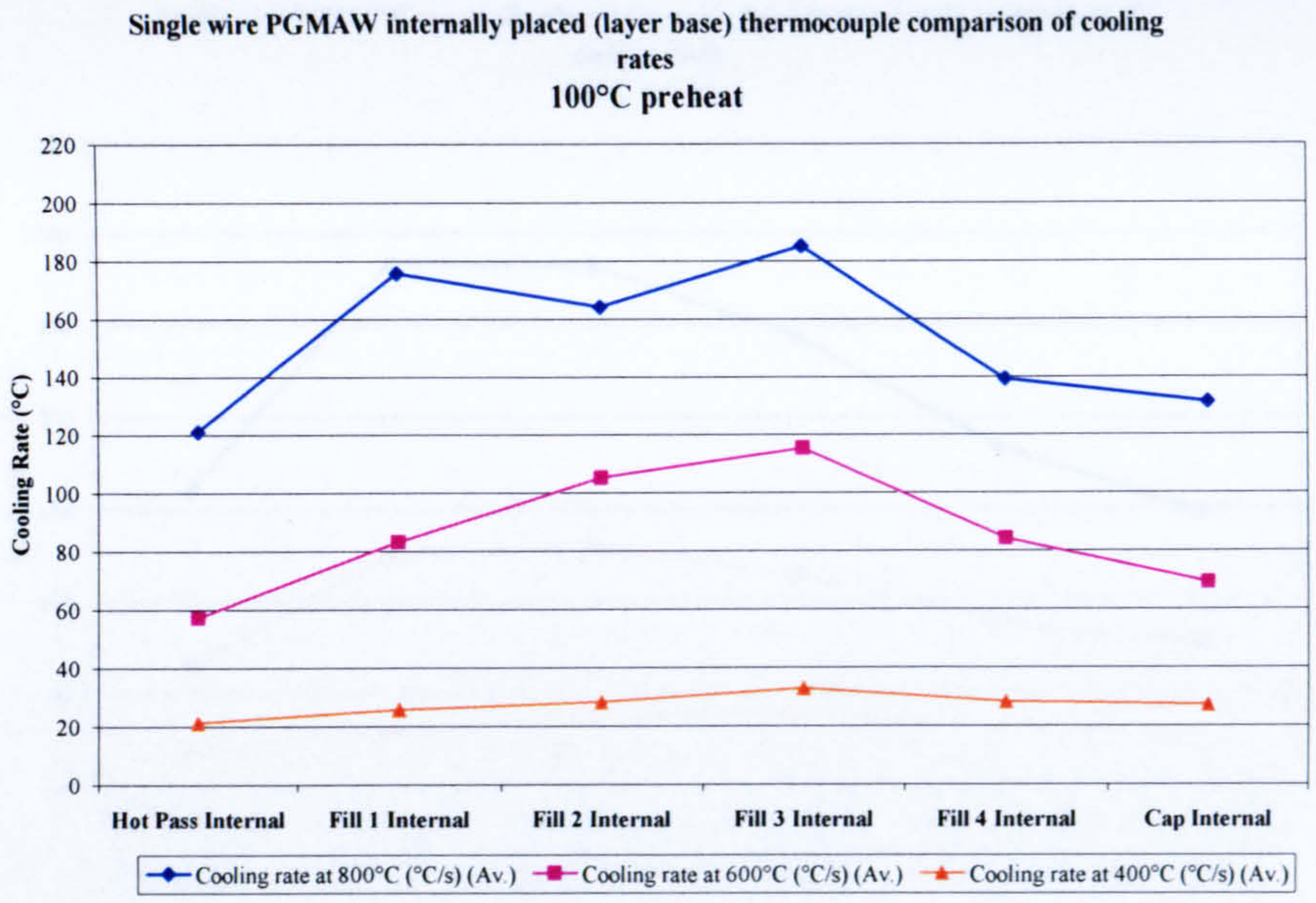

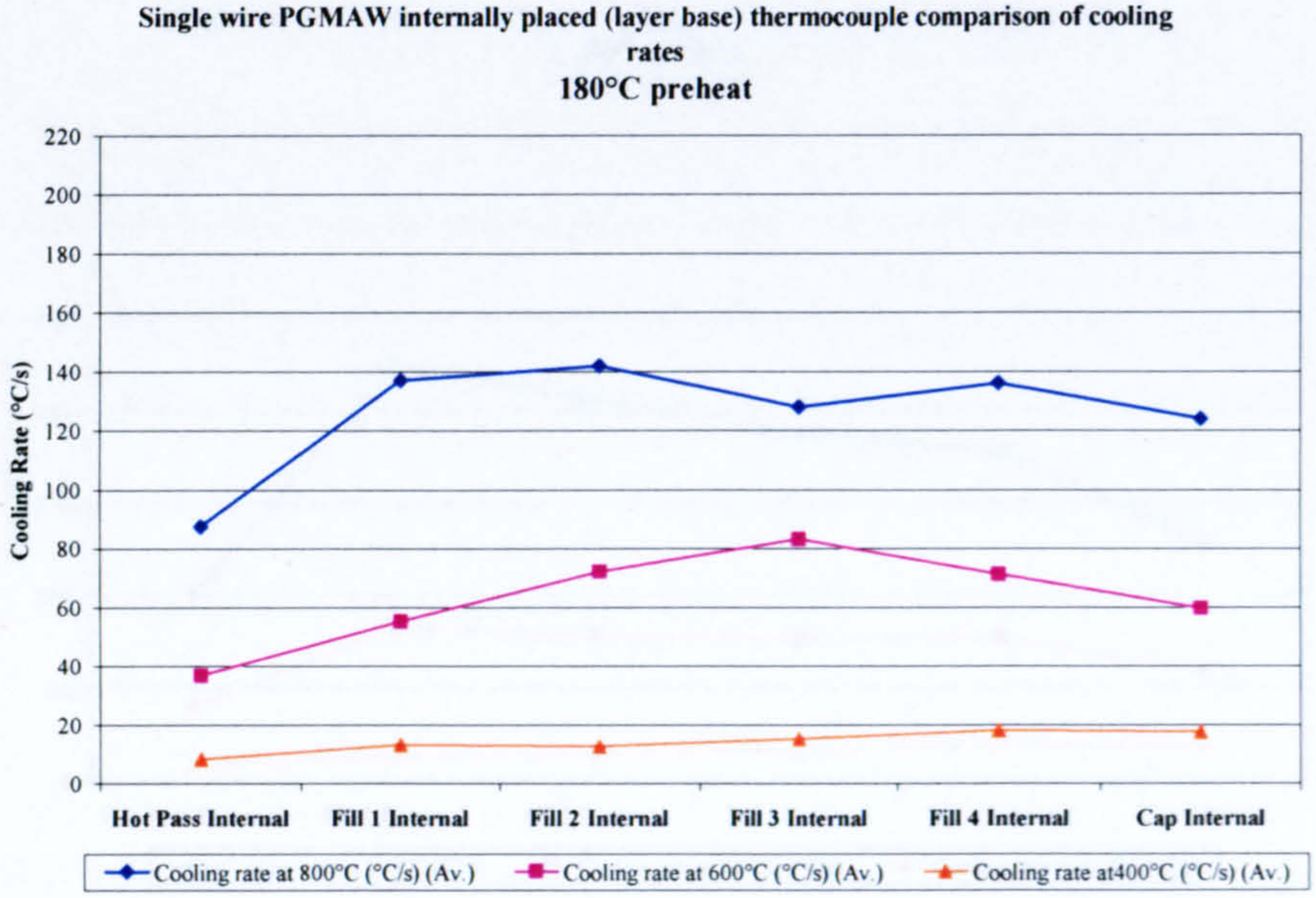

Figure 5-64: Effect of preheat on cooling rate through pipe wall thickness – internal (layer base) thermocouples

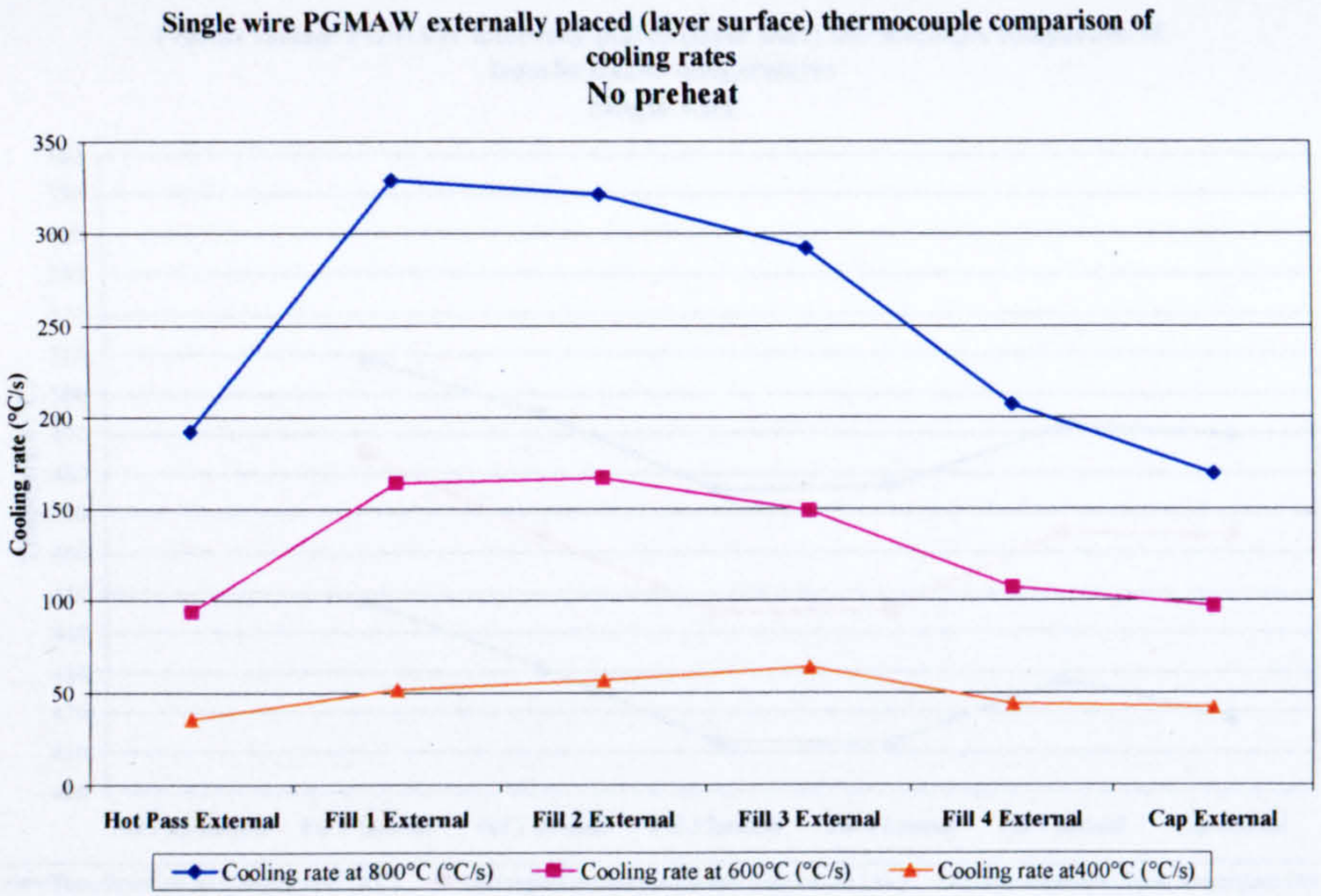

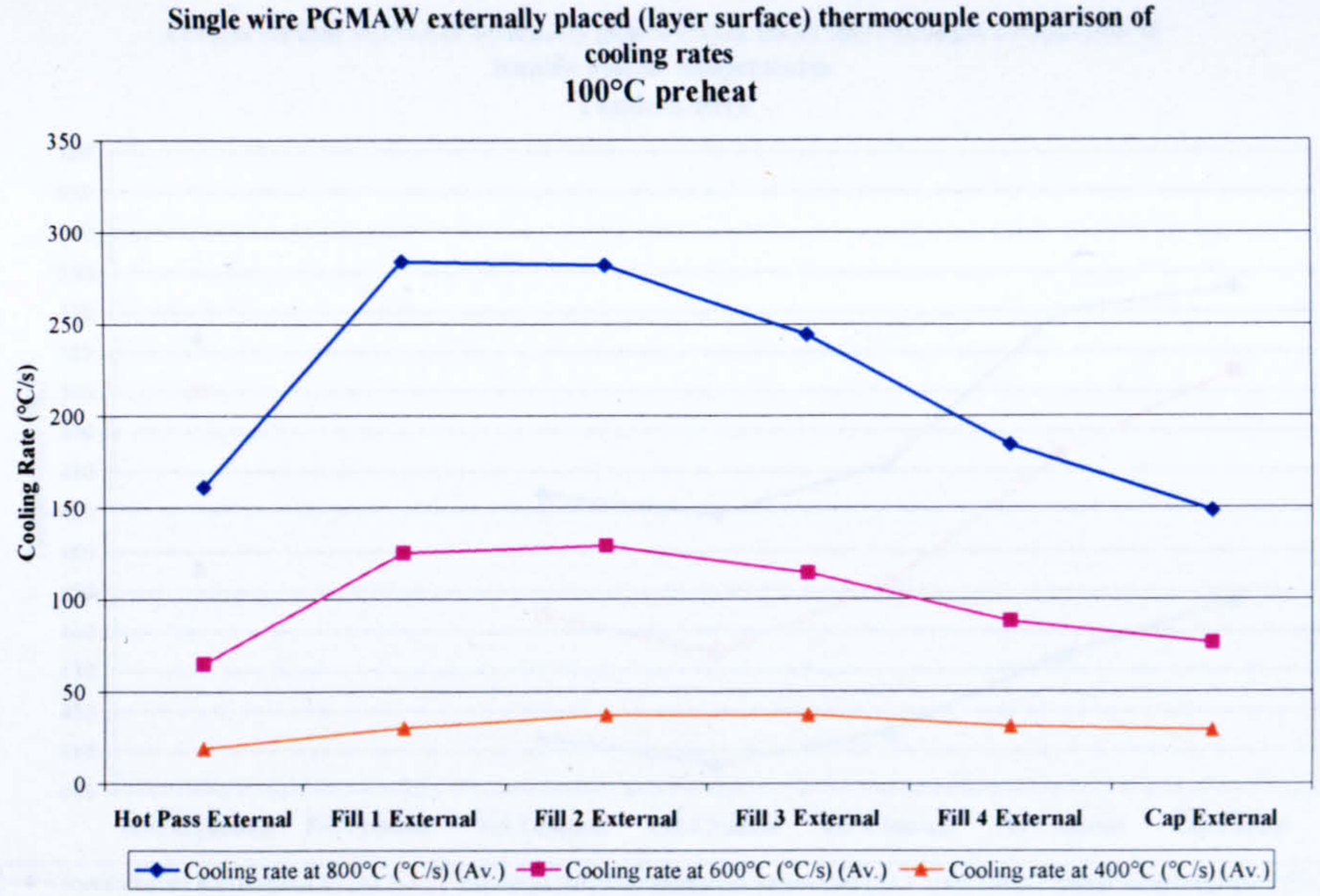

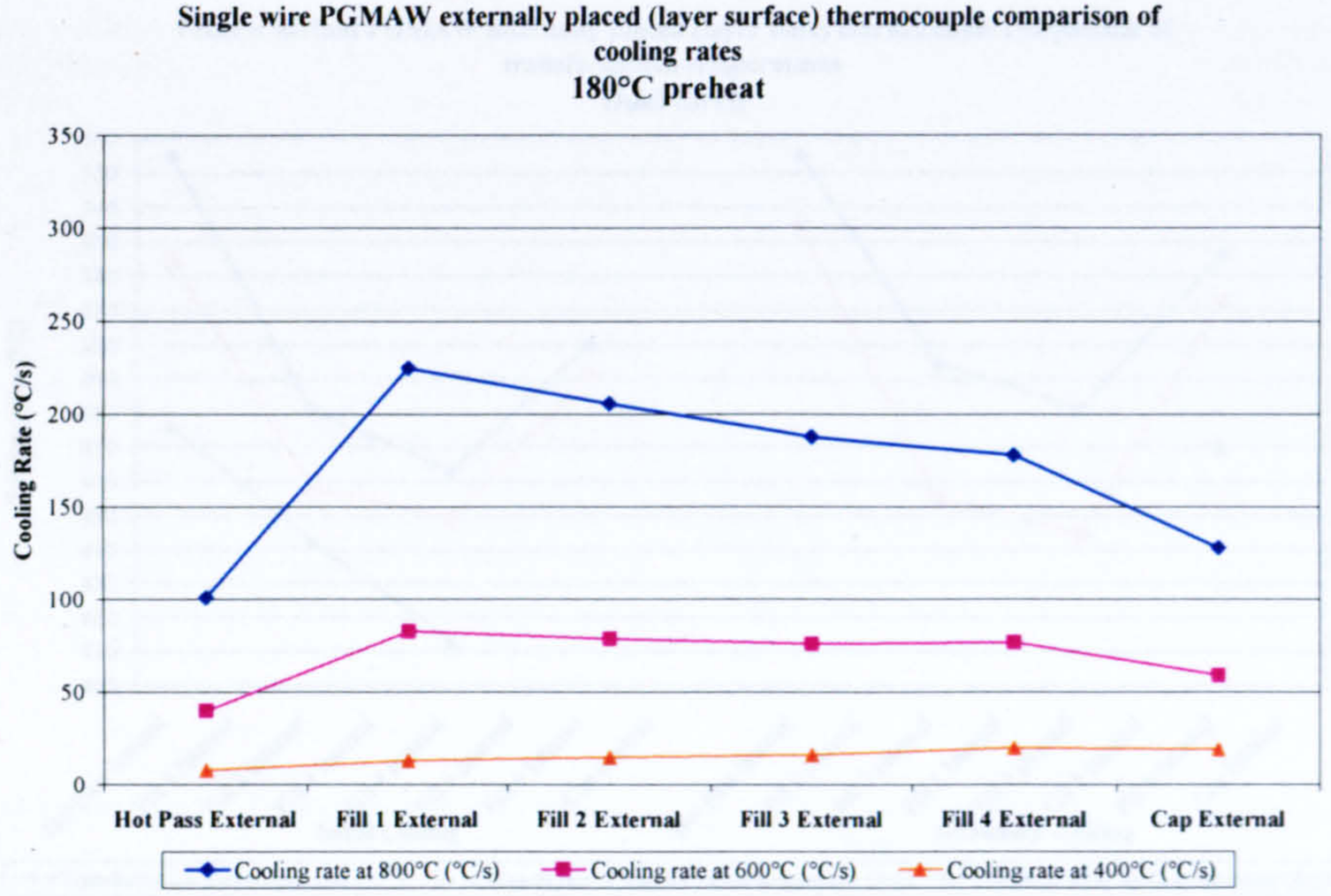

Figure 5-65: Effect of preheat on cooling rate through pipe wall thickness – external (layer surface) thermocouples

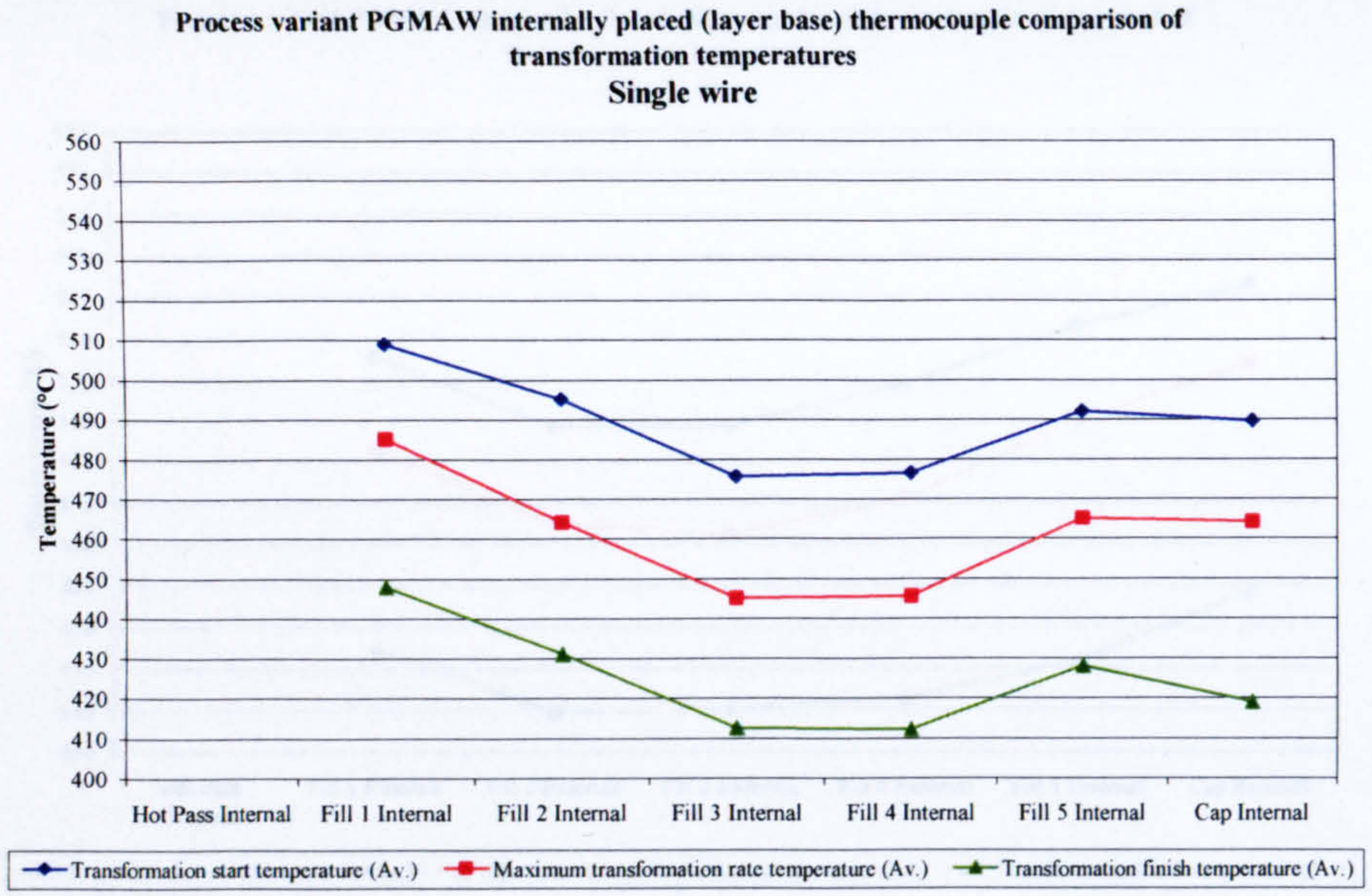

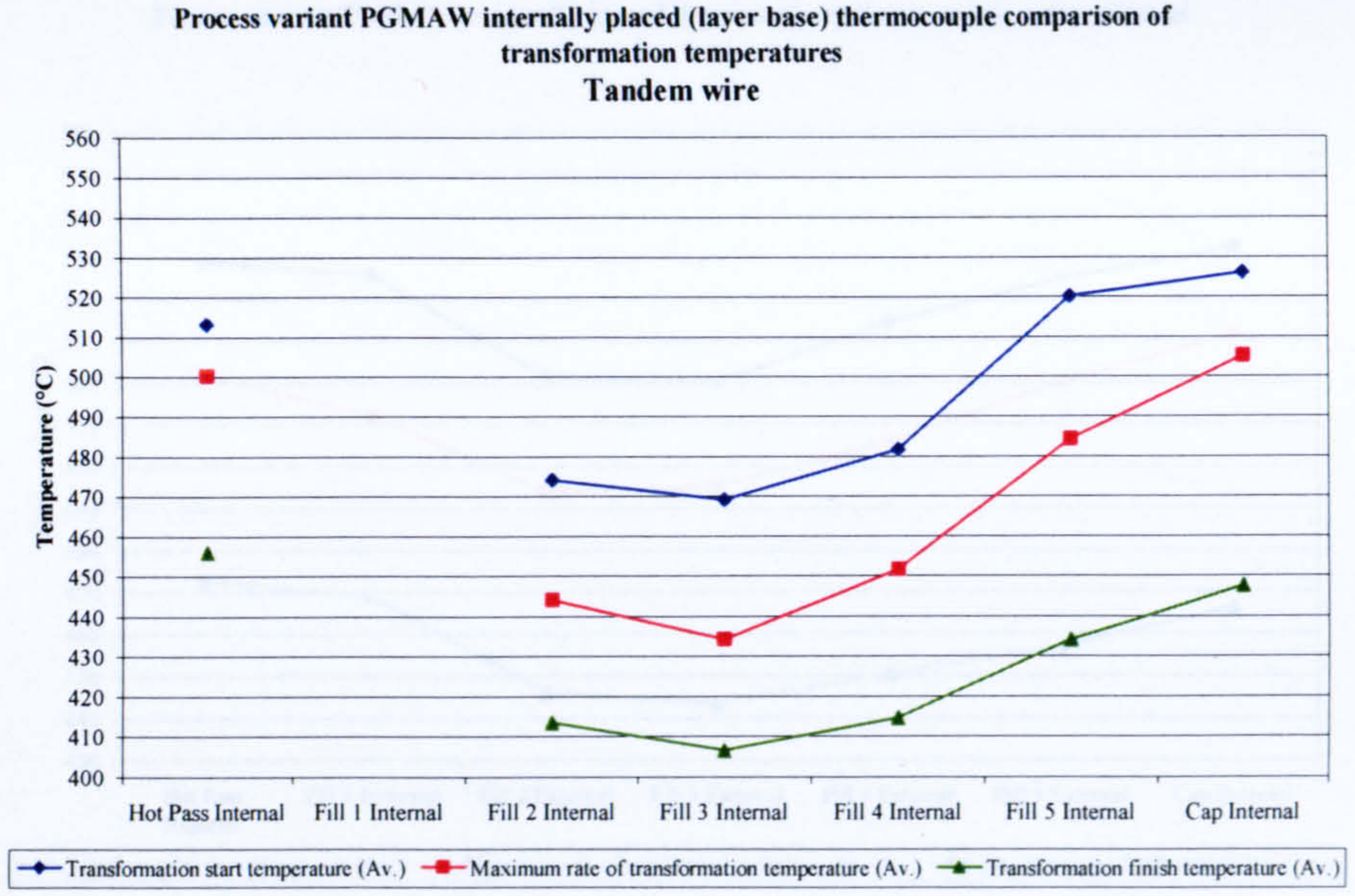

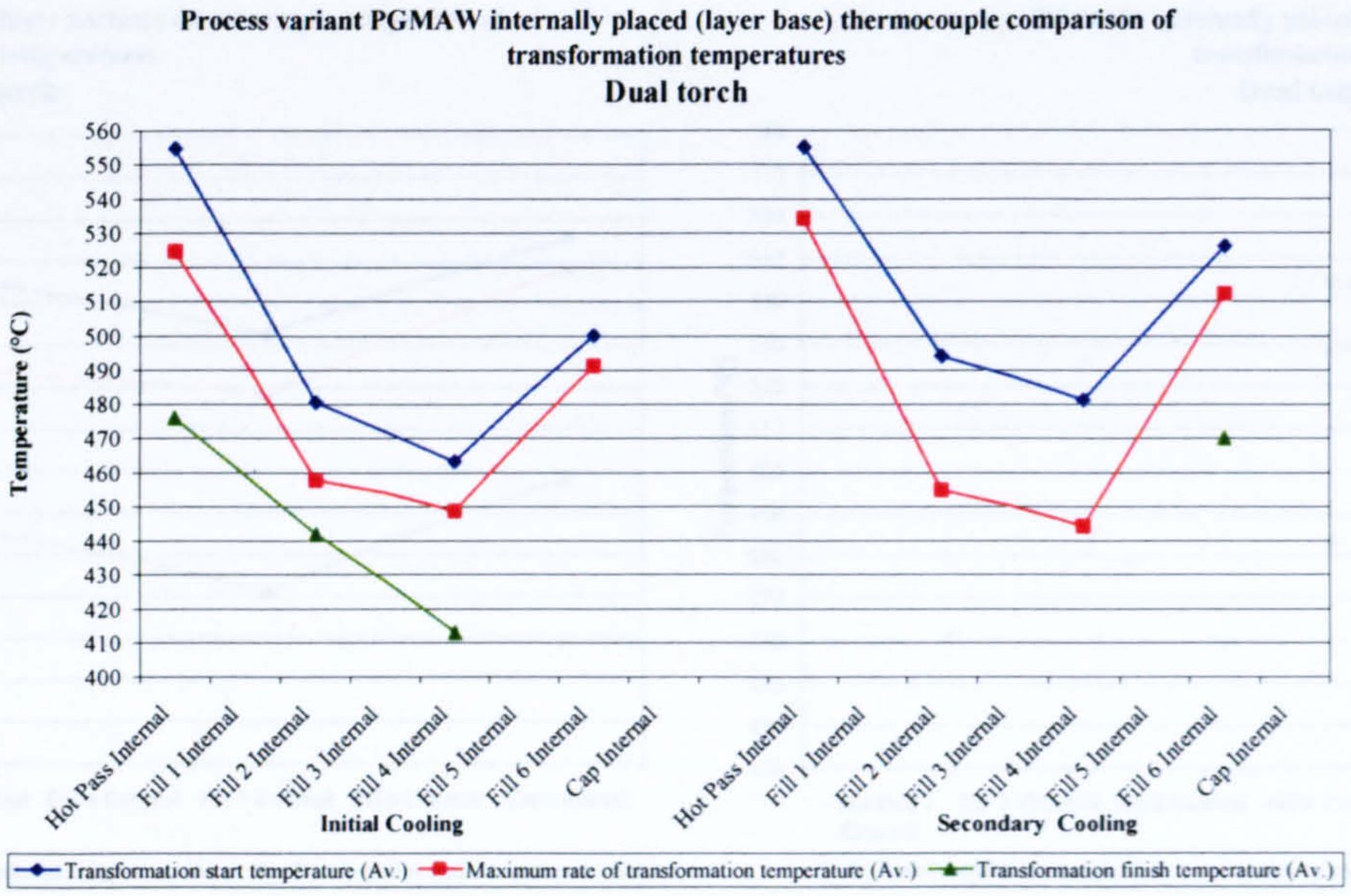

Figure 5-66: Effect of process on transformation temperatures through pipe wall thickness – internal (layer base) thermocouples

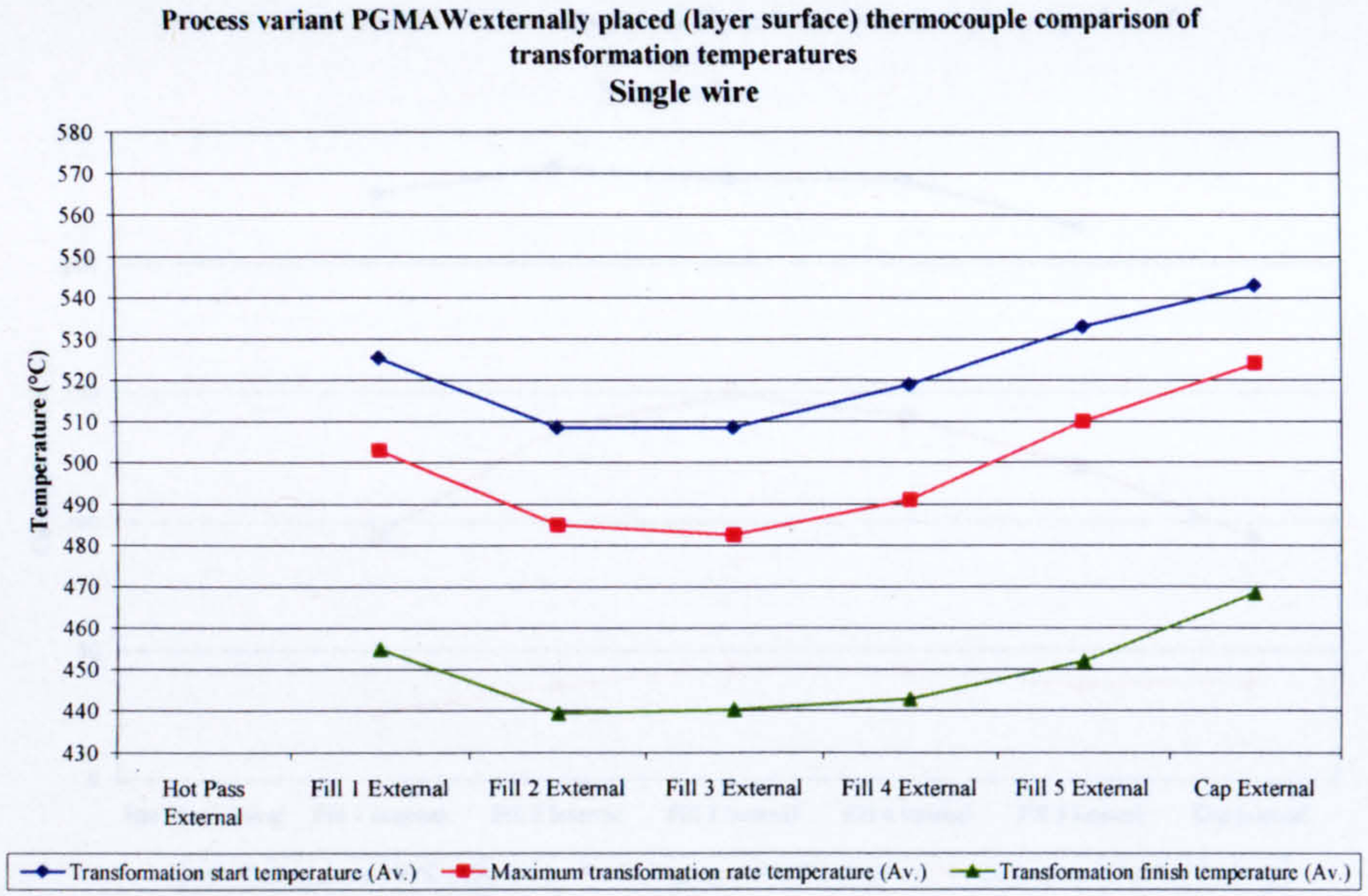

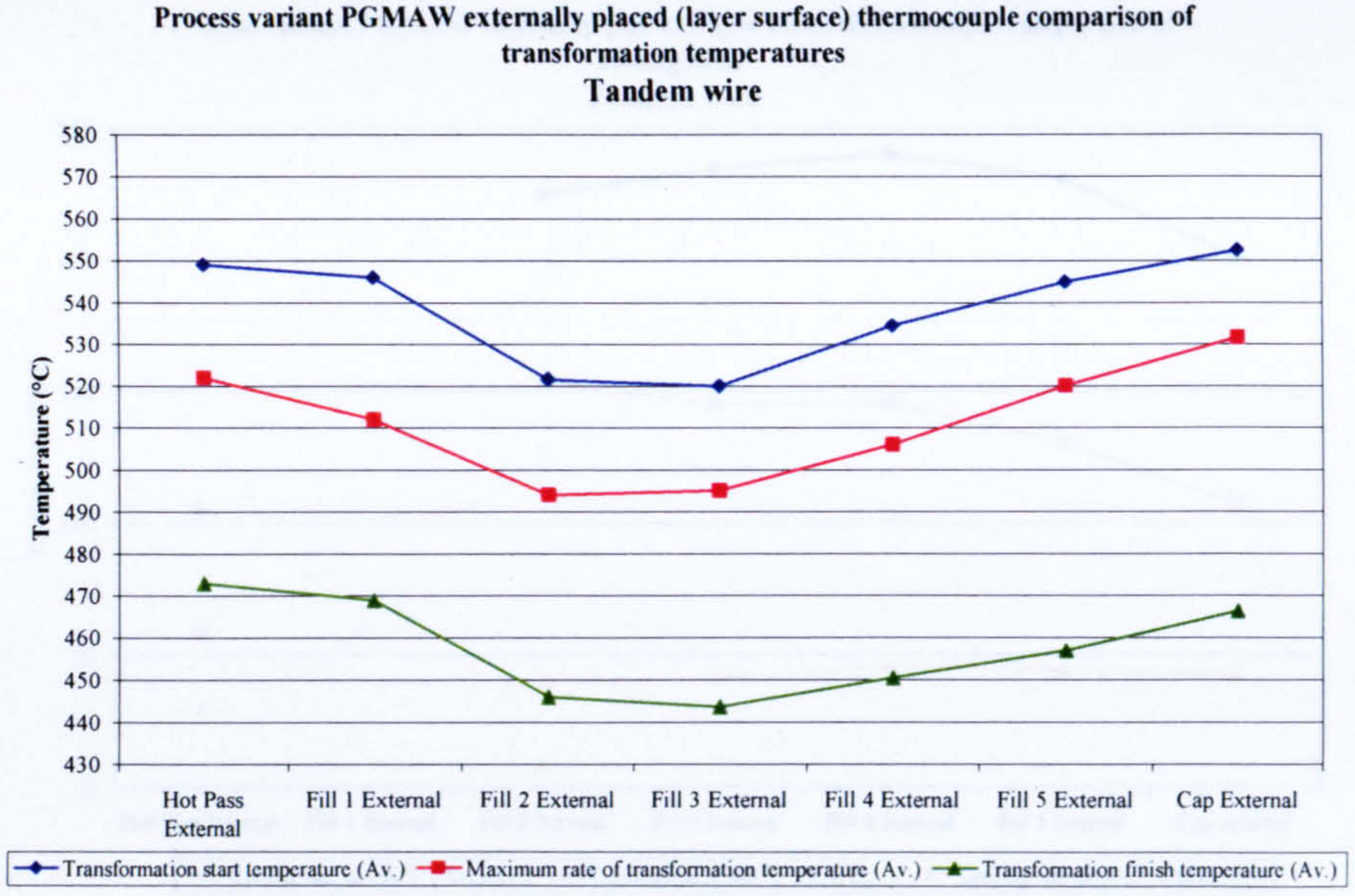

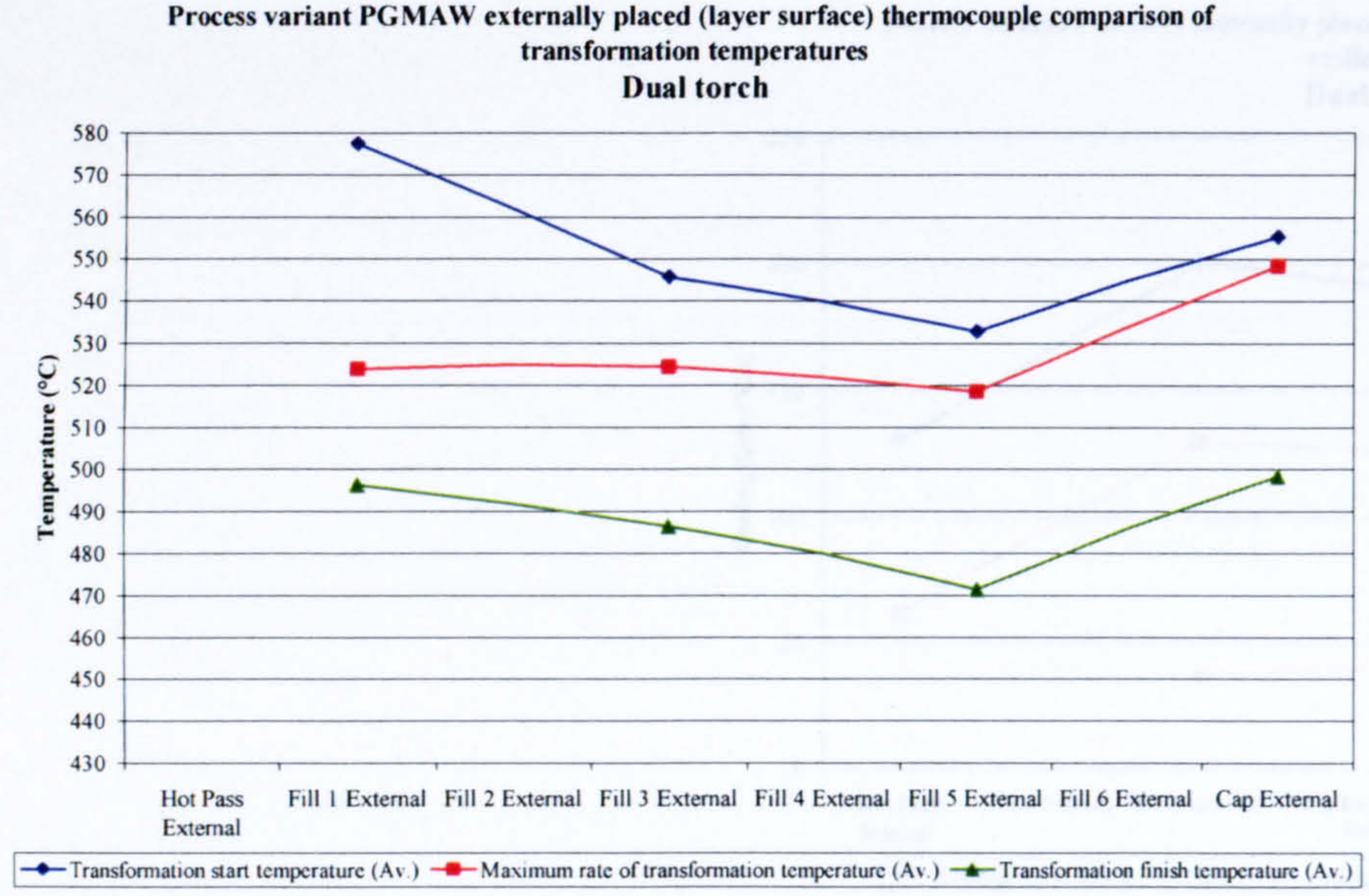

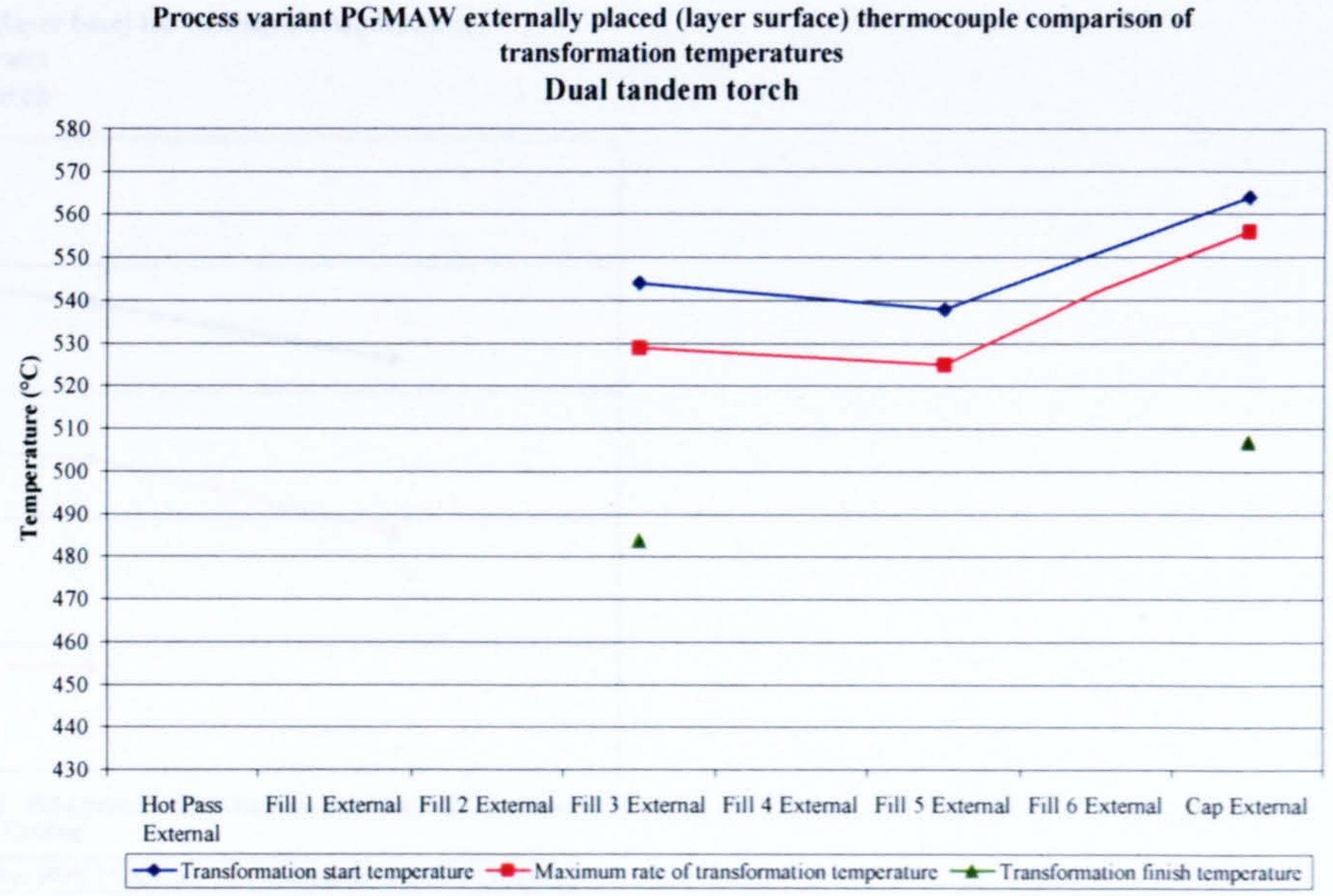

Figure 5-67: Effect of process on transformation temperatures through pipe wall thickness – external (layer surface) thermocouples

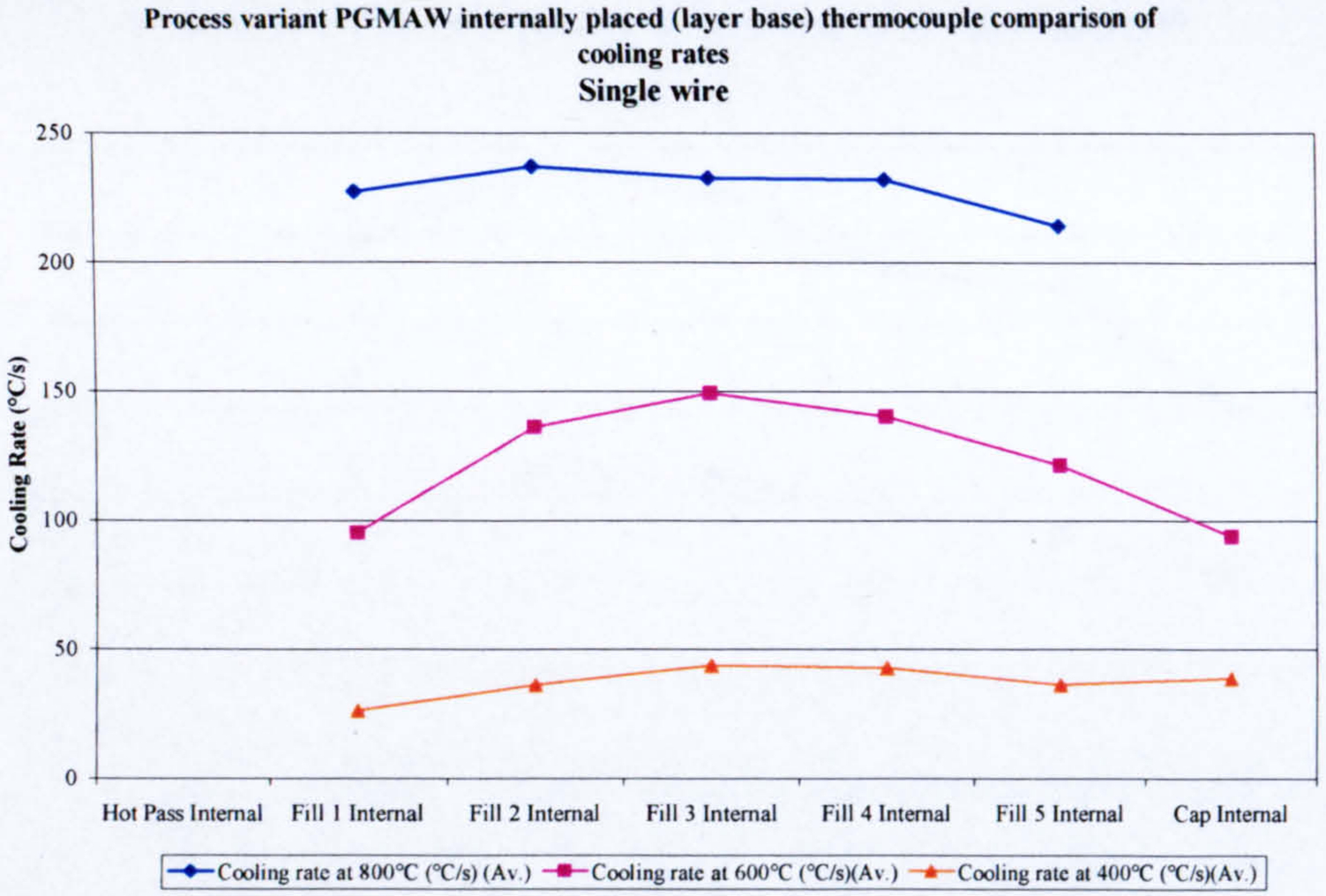

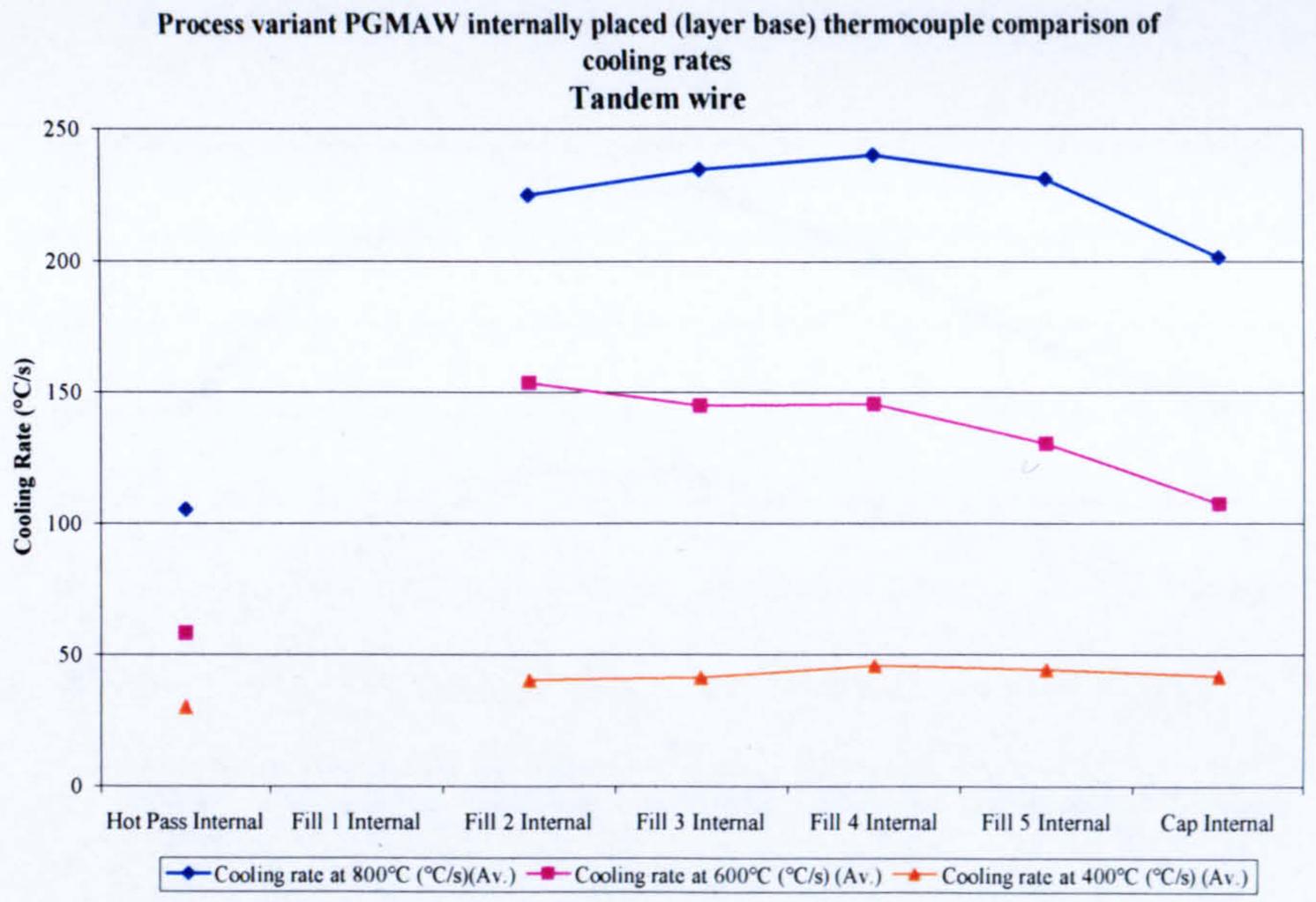

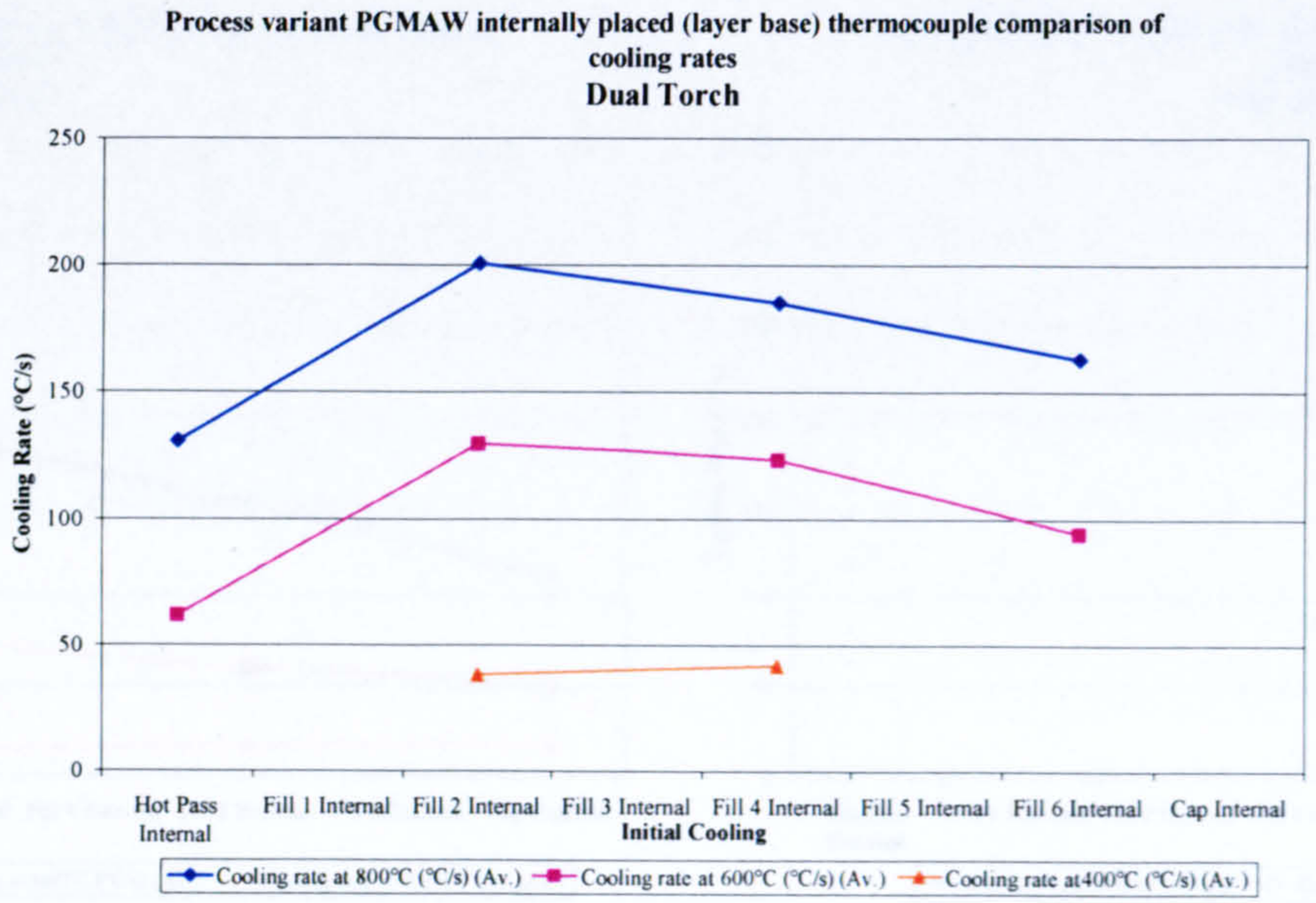

Figure 5-68: Effect of process on cooling rate through pipe wall thickness – internal (layer base) thermocouples

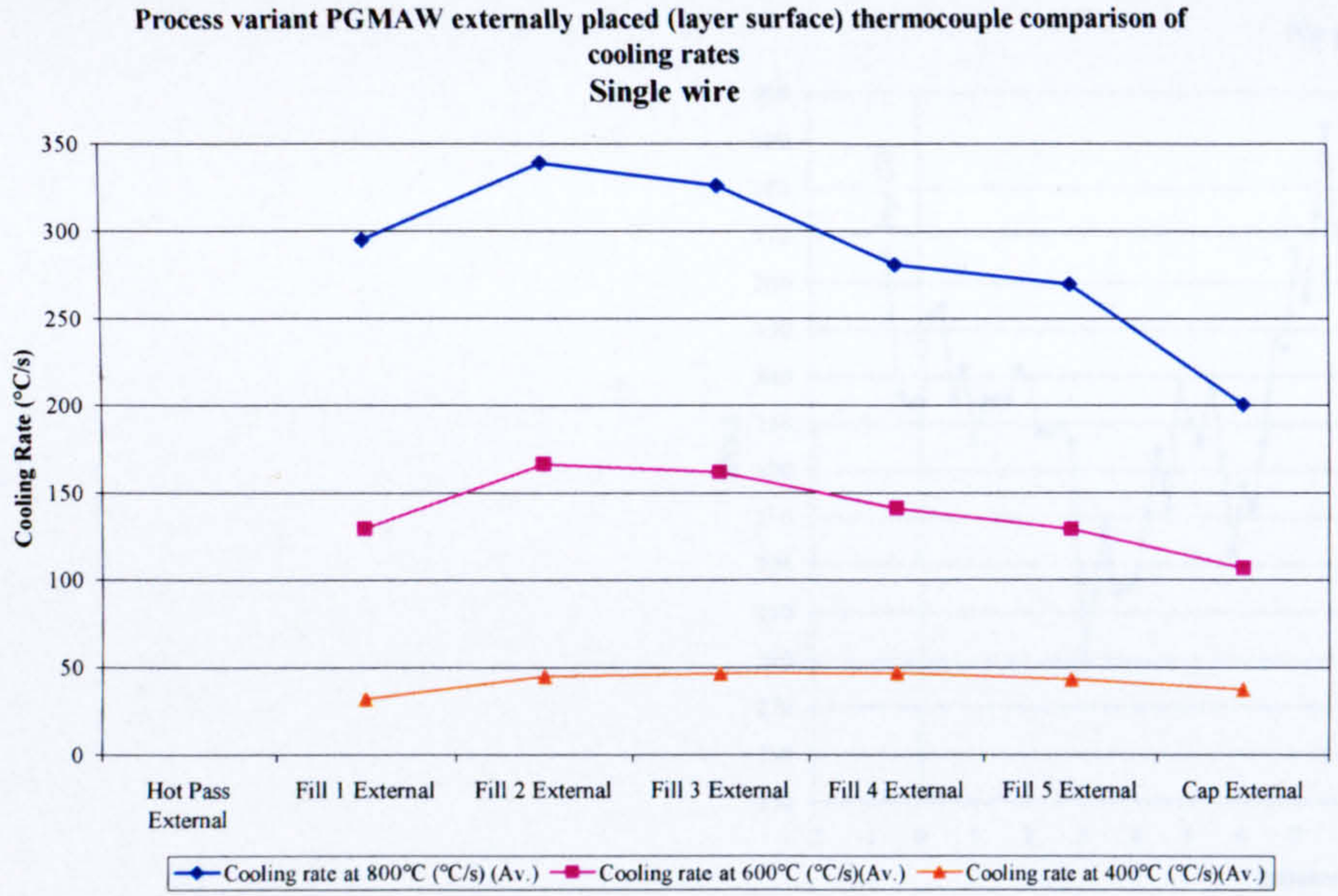

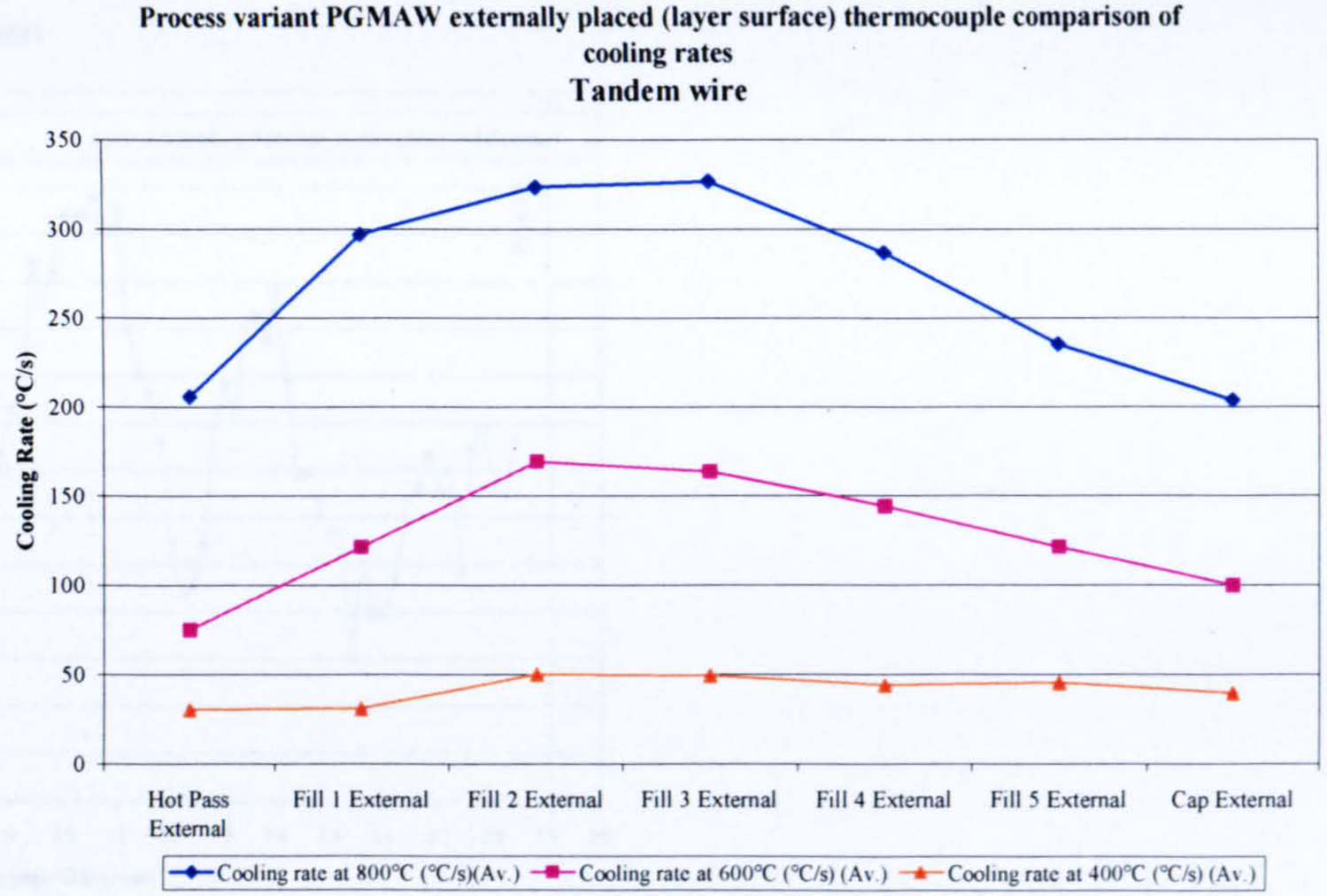

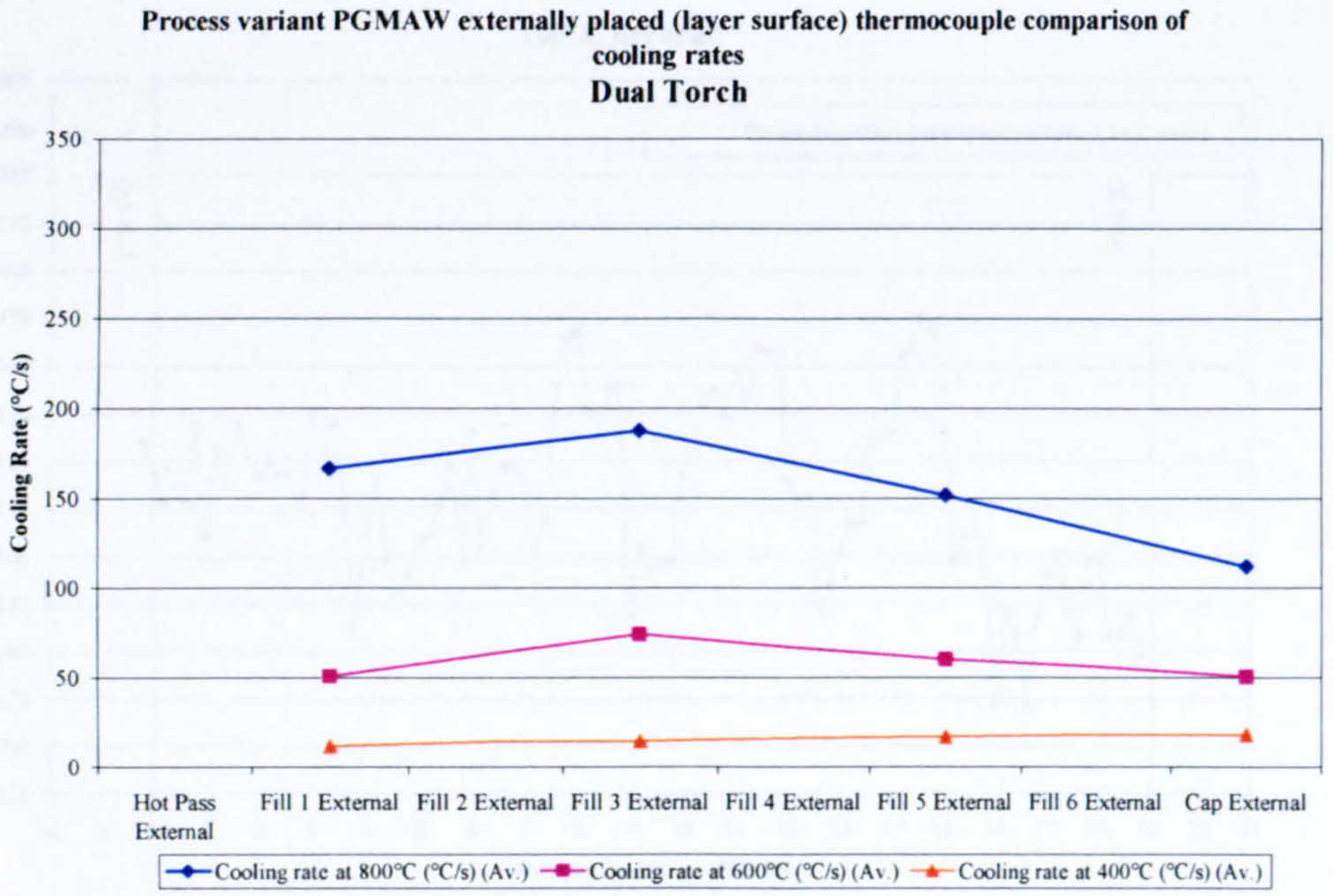

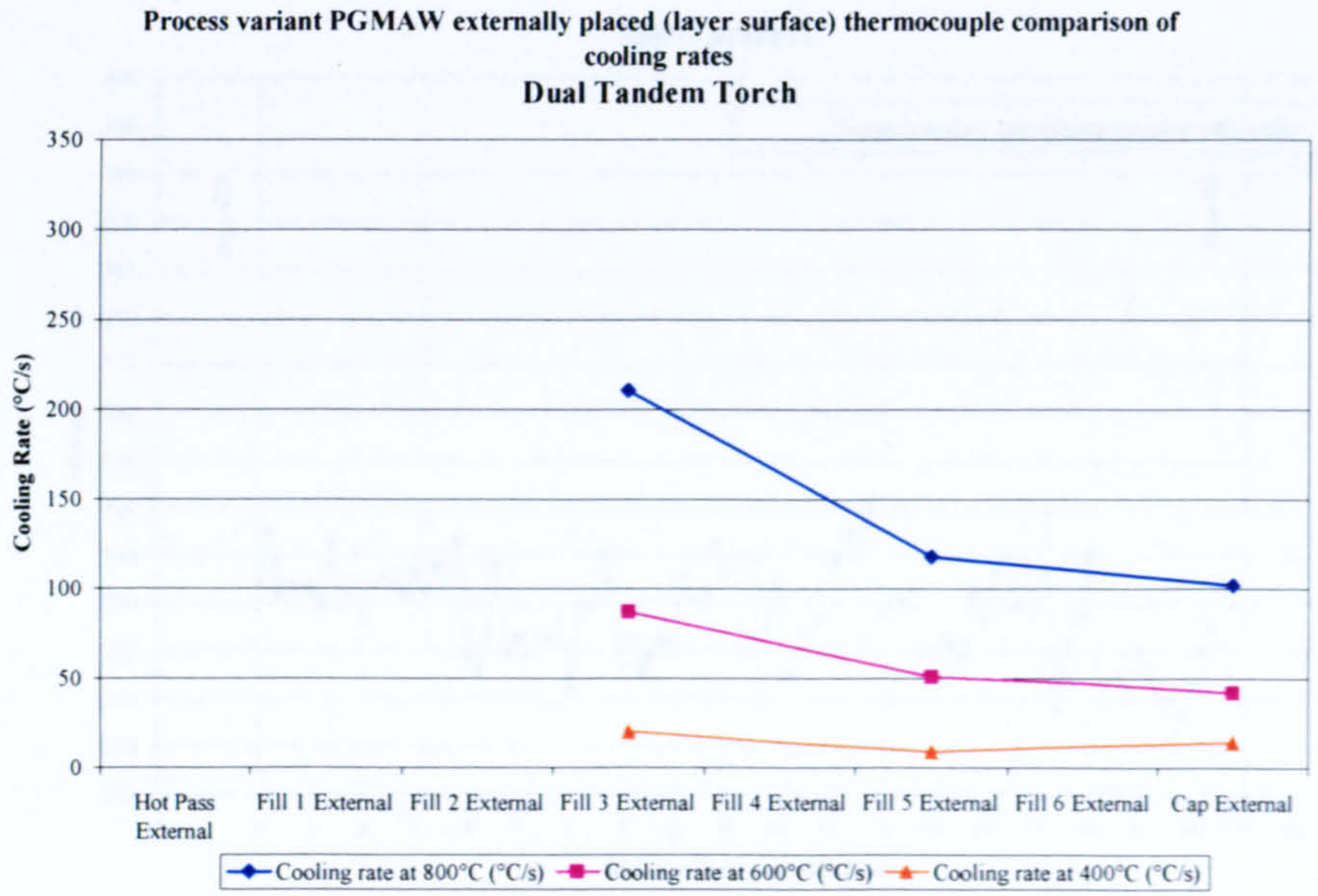

Figure 5-69: Effect of process on cooling rate through pipe wall thickness – external (layer surface) thermocouples

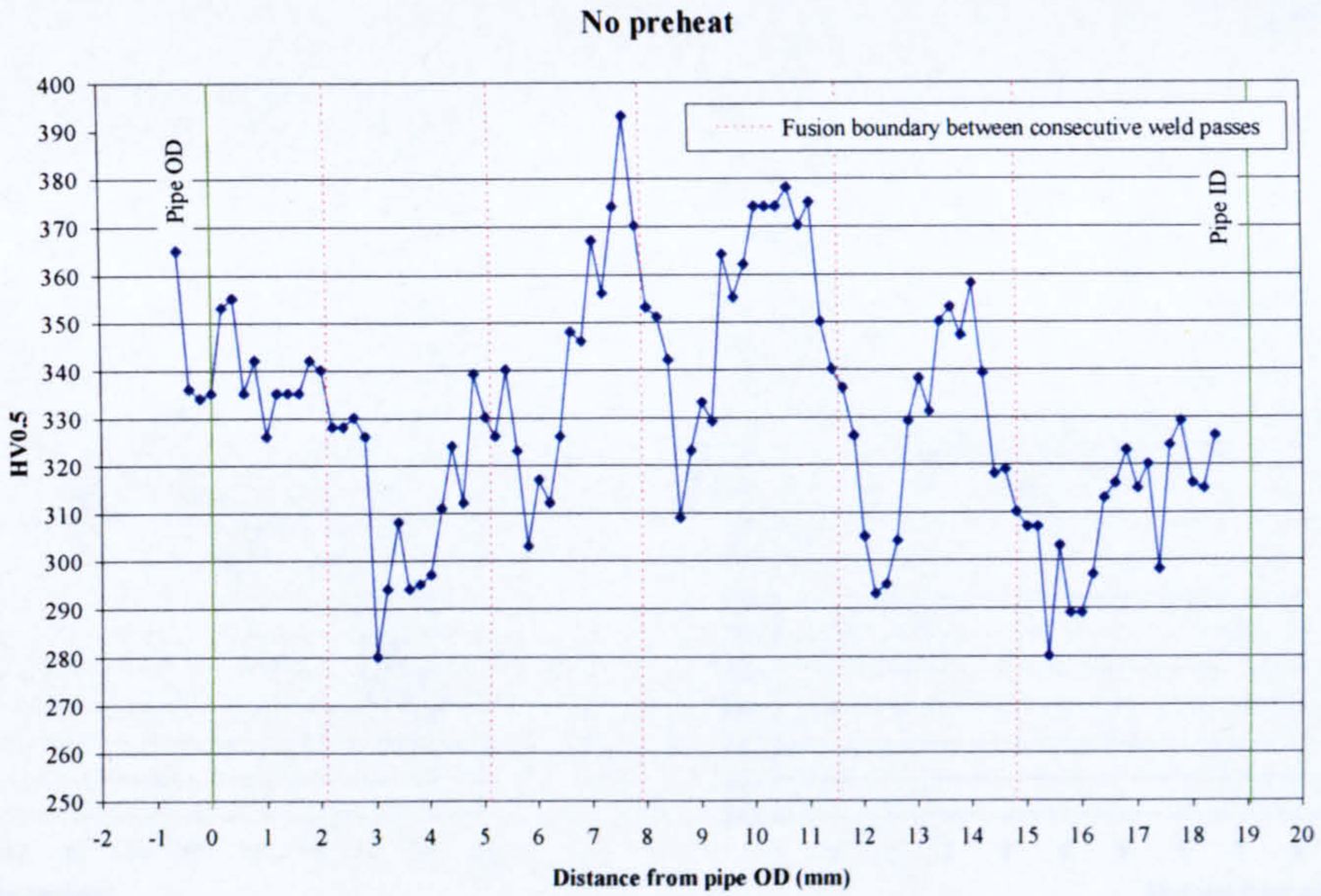

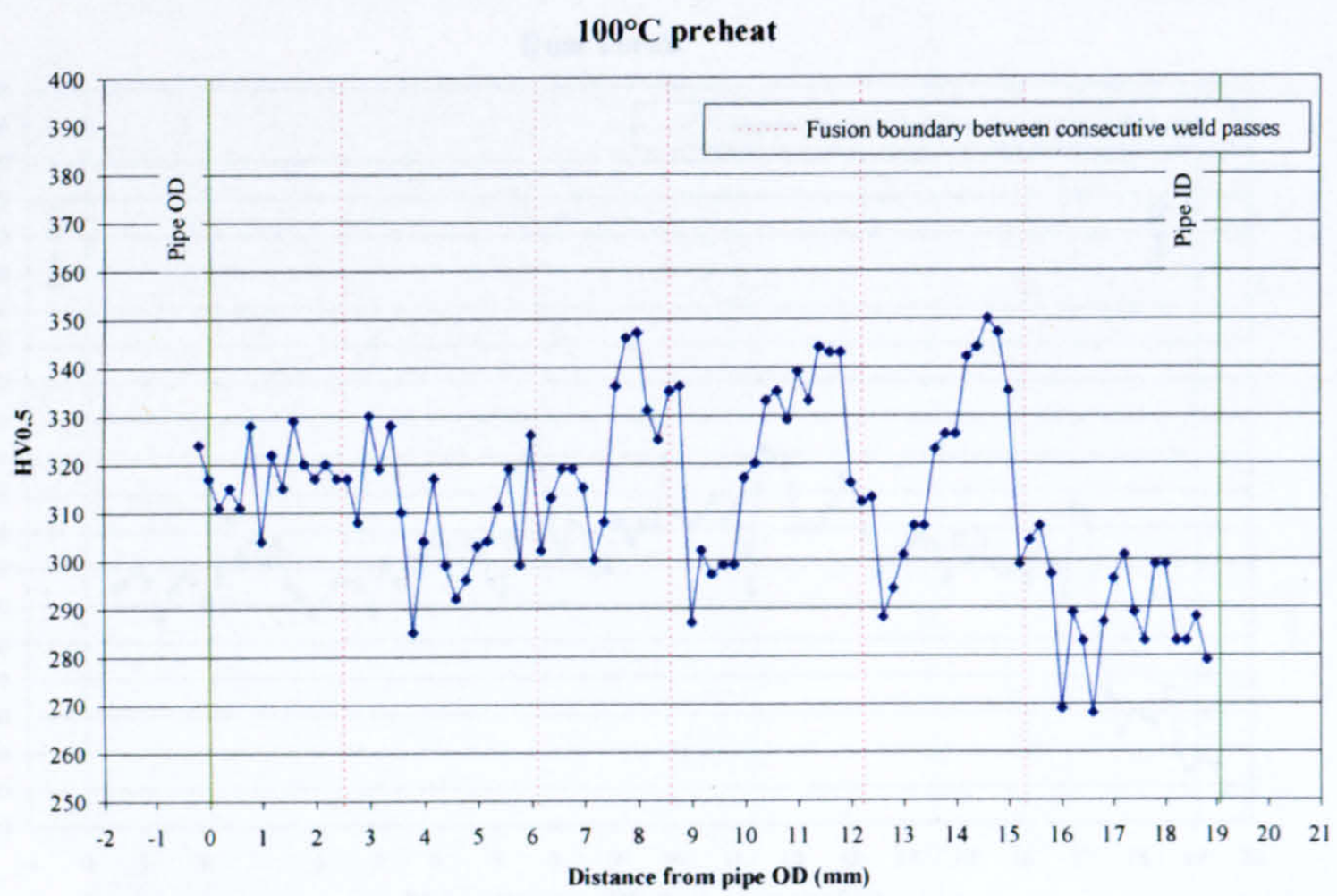

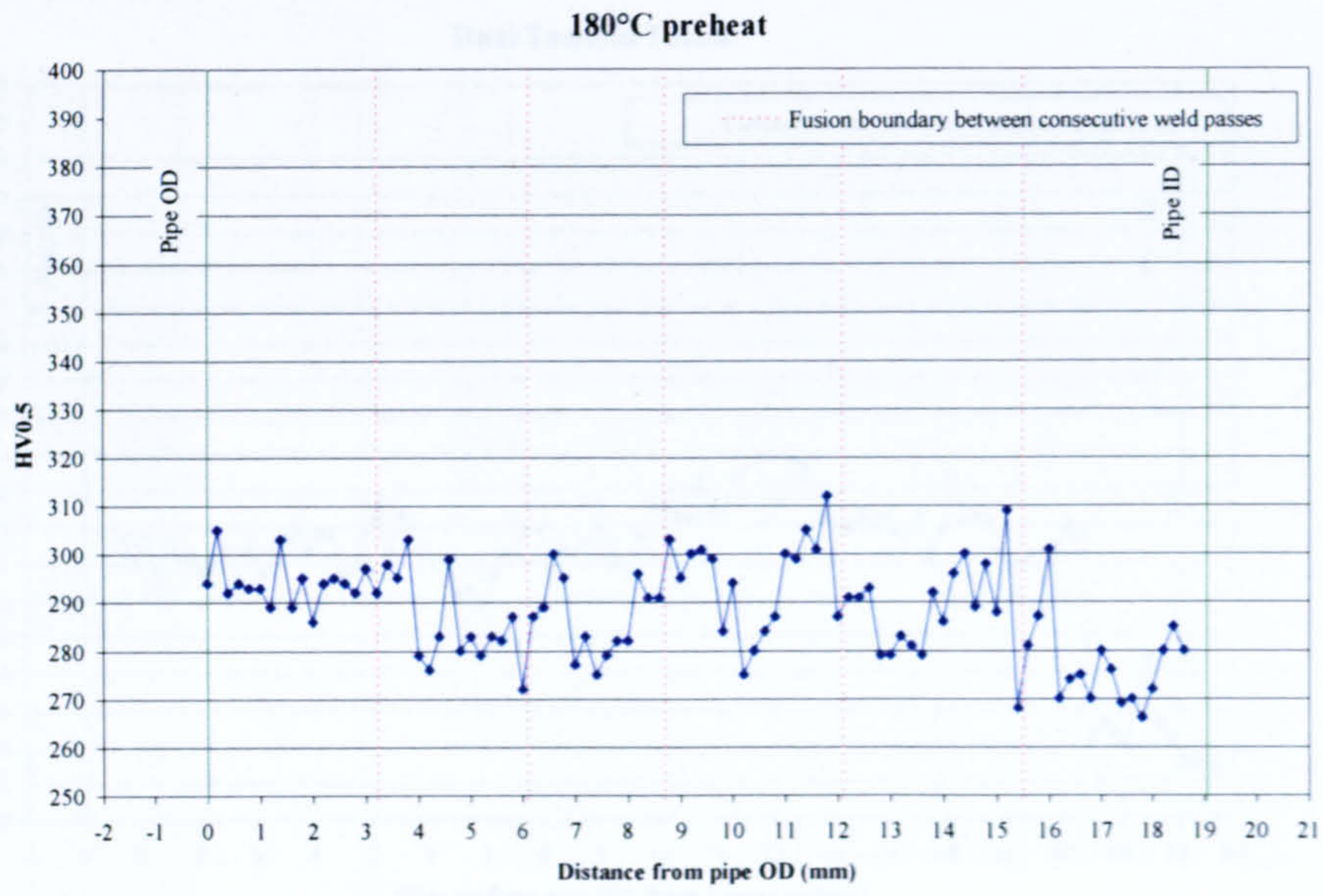

Figure 5-70: Preheat variation weld metal microhardness surveys

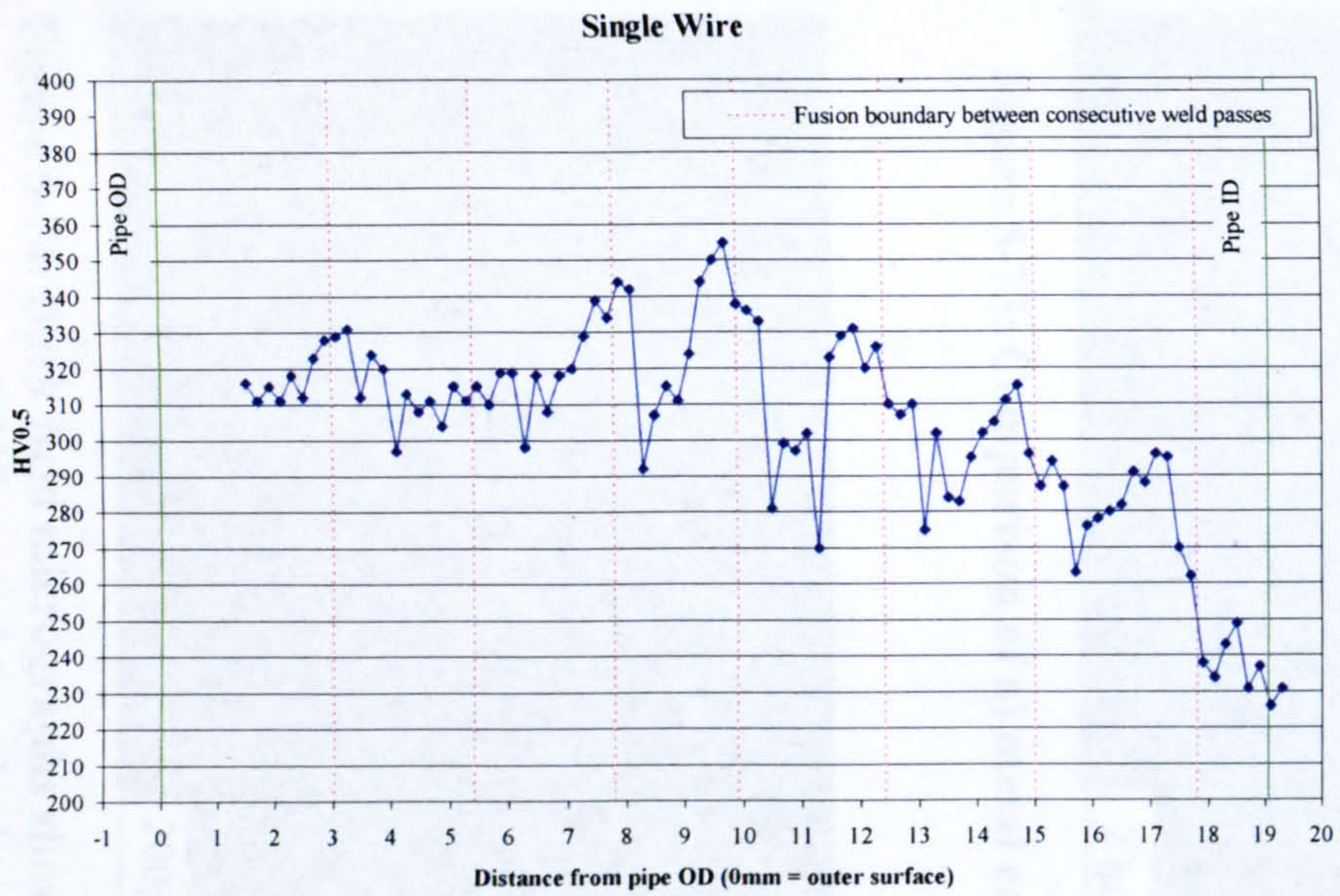

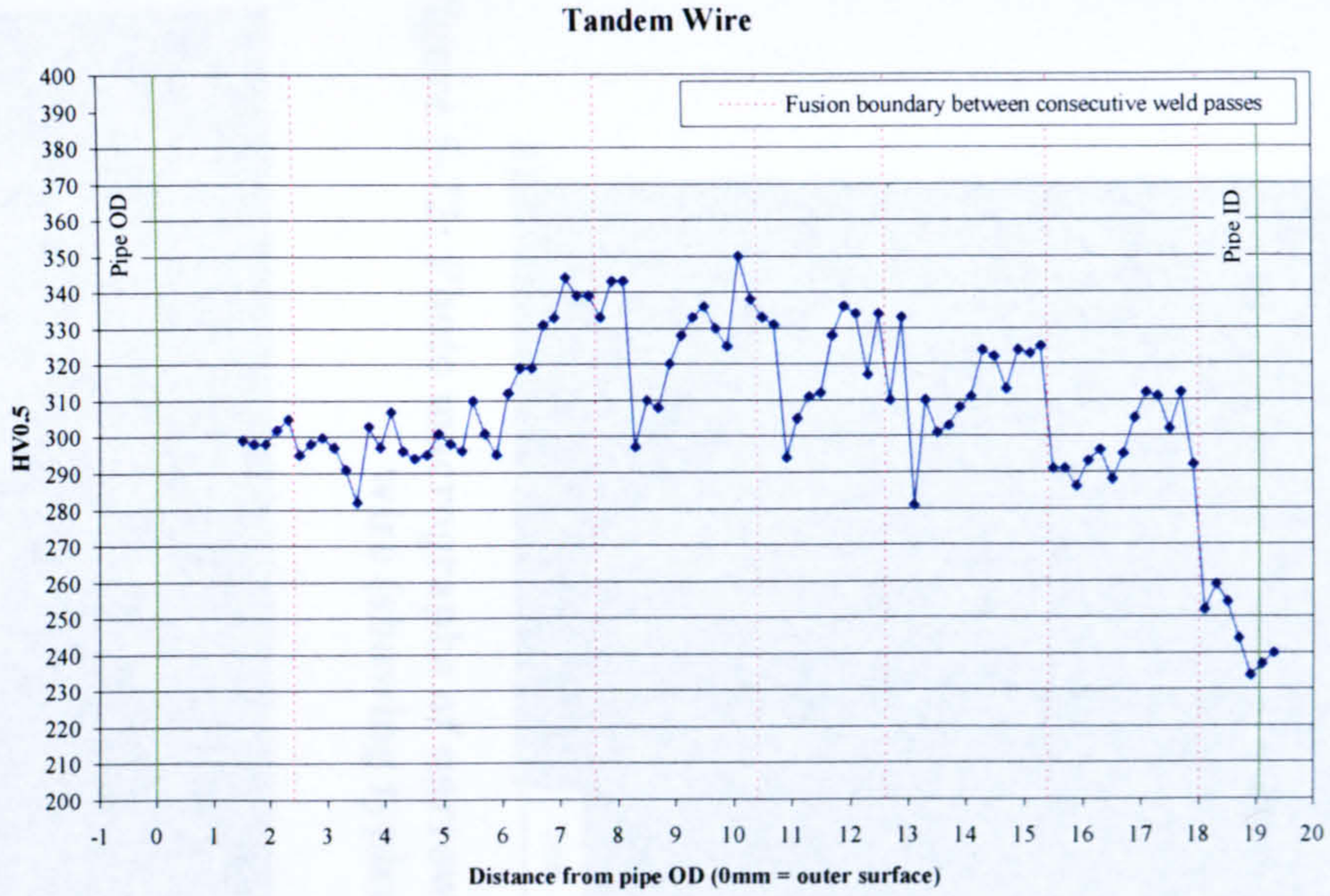

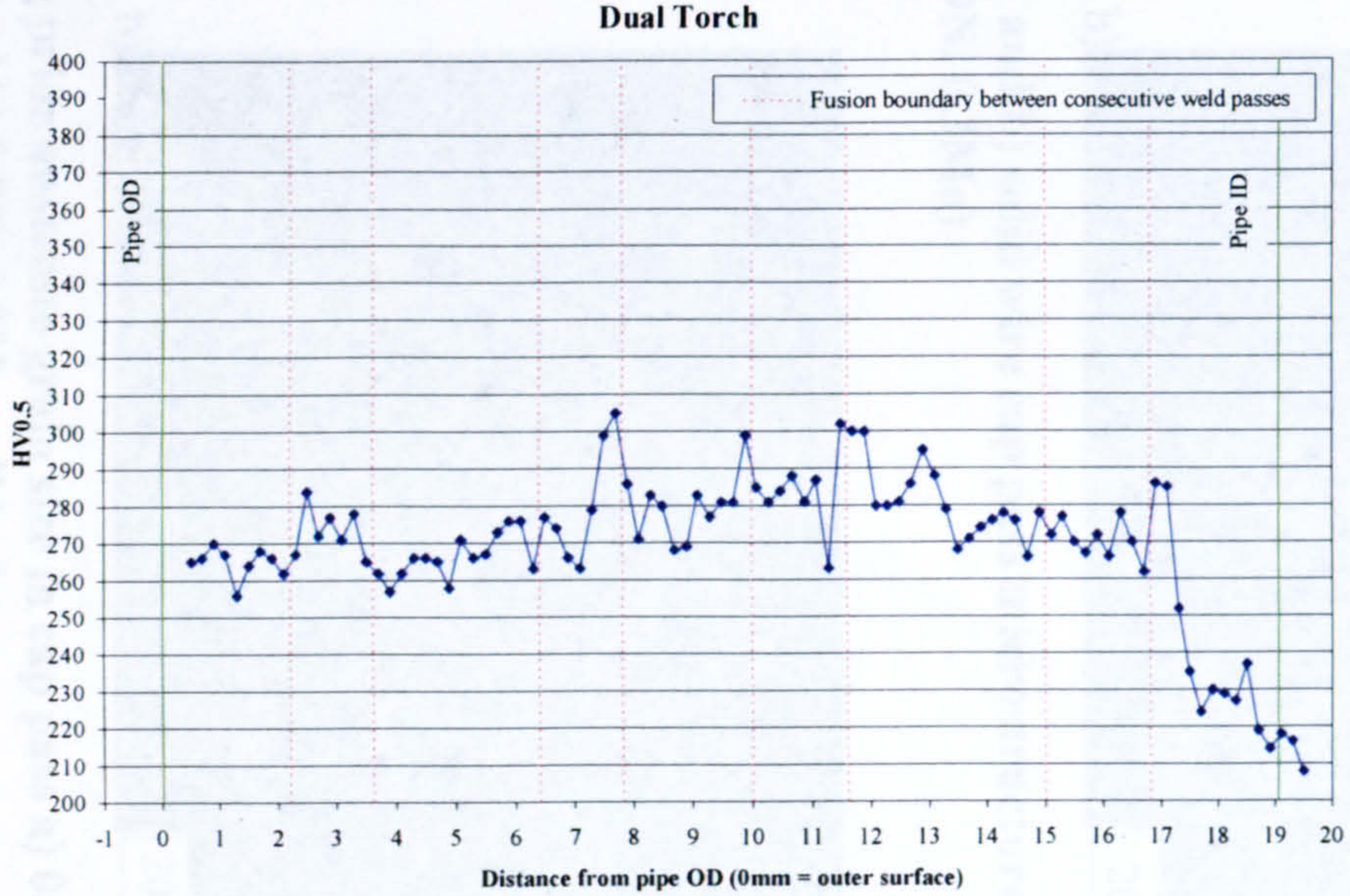

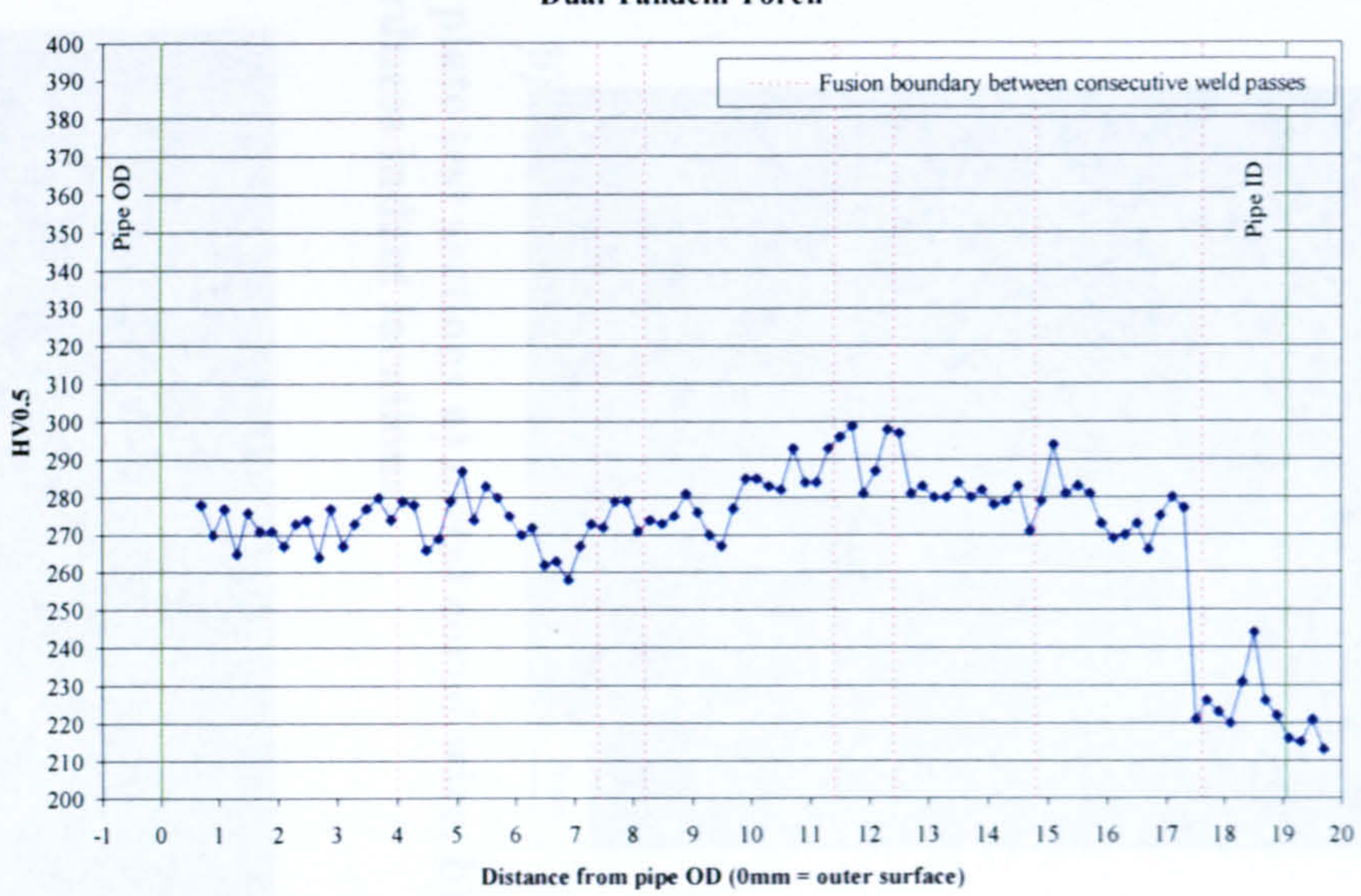

Figure 5-71: Process variation weld metal microhardness surveys

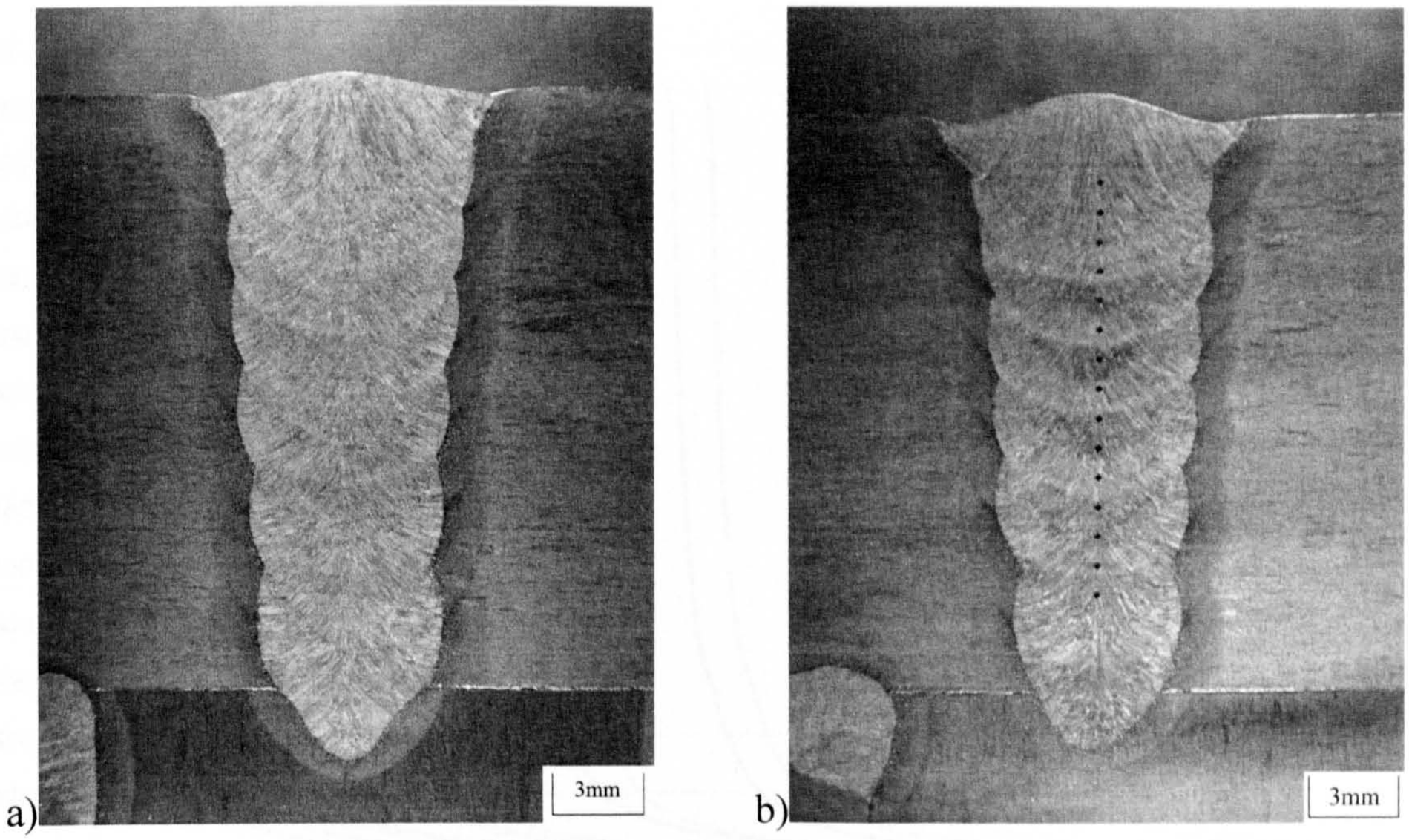

Figure 5-72: Photo macrographs of narrow gap plate test sections a) metal cored wire, b) solid wire (showing typical hardness indent locations)

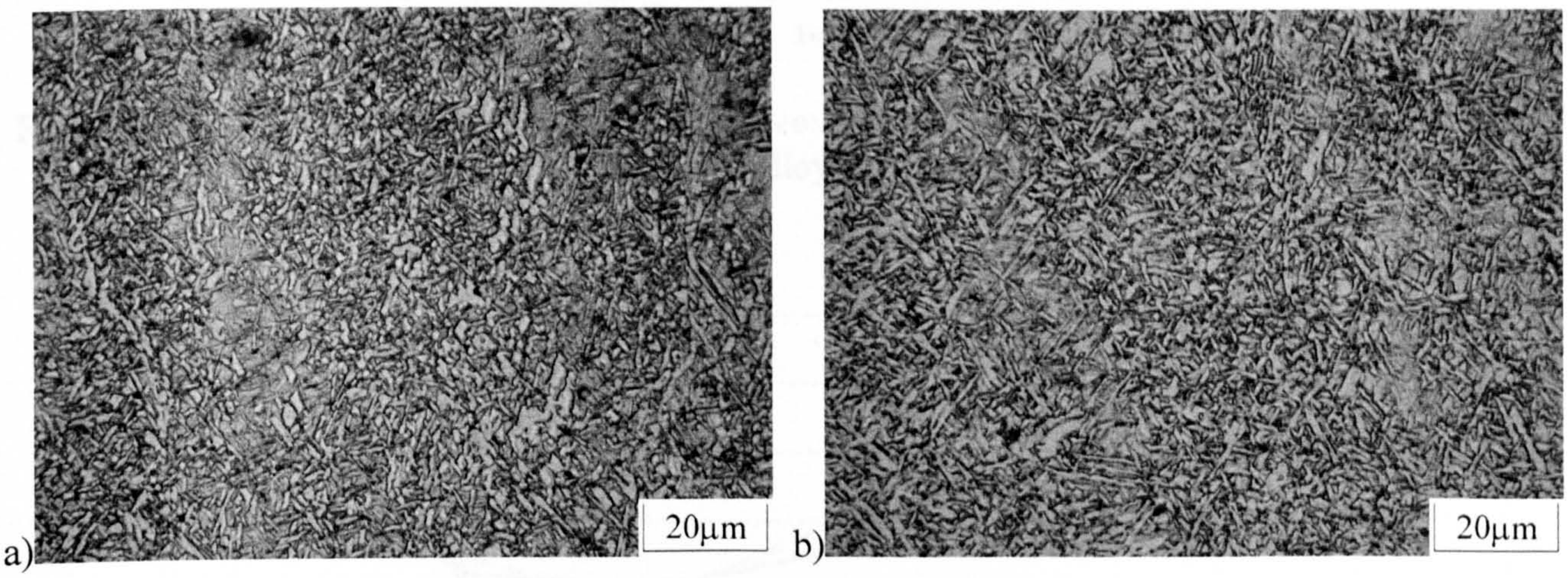

Figure 5-73: Comparison of a) metal cored and b) solid wire cap pass microstructures (0.9Ni 0.3Mo)

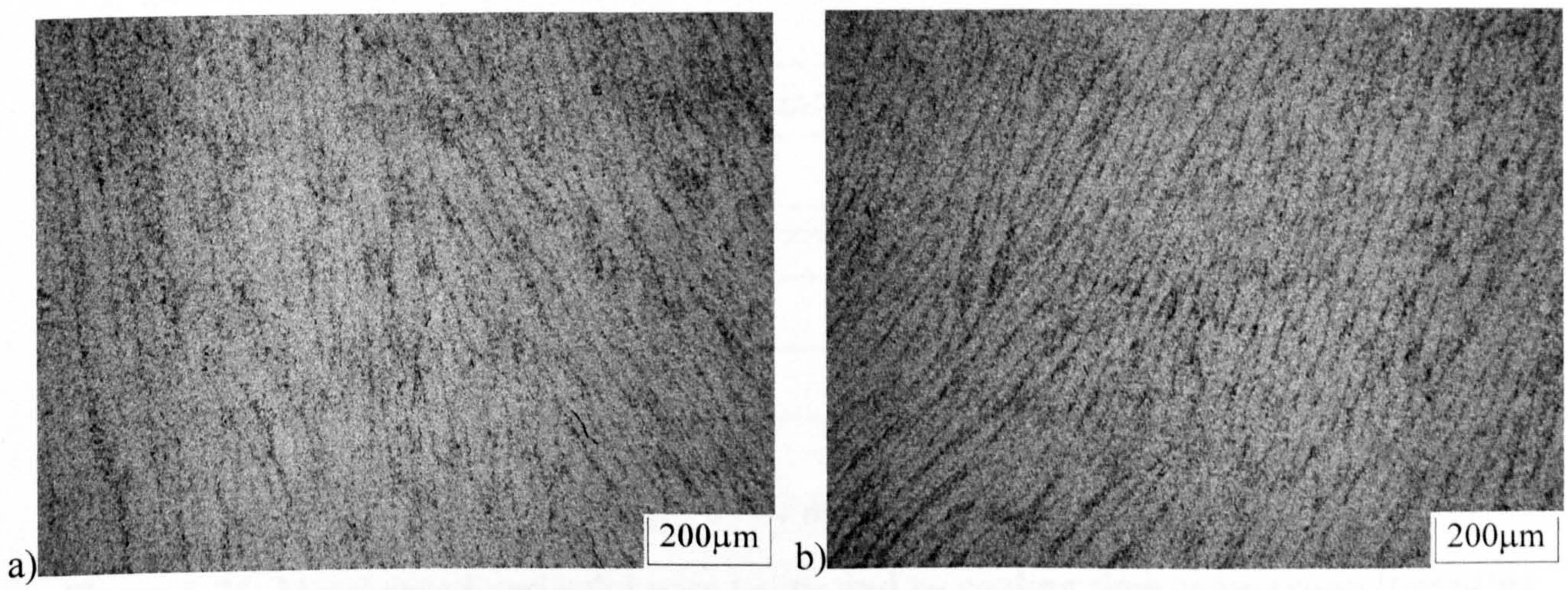

Figure 5-74: Dark field micrographs showing prior austenite grain size in cap pass a) 0.9Ni 0.3Mo metal cored wire control b) 0.9Ni 0.3Mo solid wire

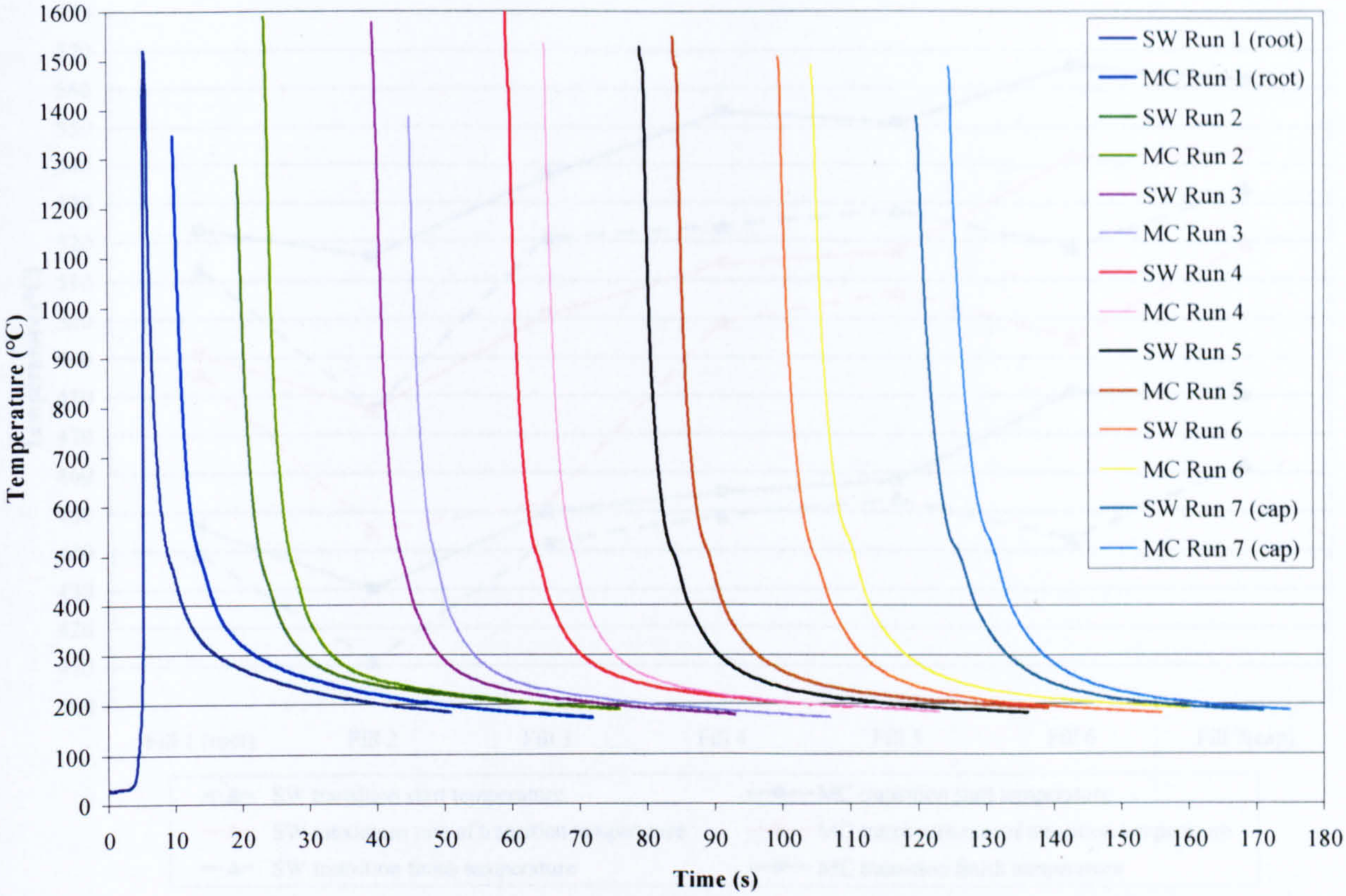

Figure 5-75: Externally plunged thermocycle comparison per layer for metal cored (MC) and solid wire (SW) base-line alloy (0.9Ni 0.3Mo) plate trials

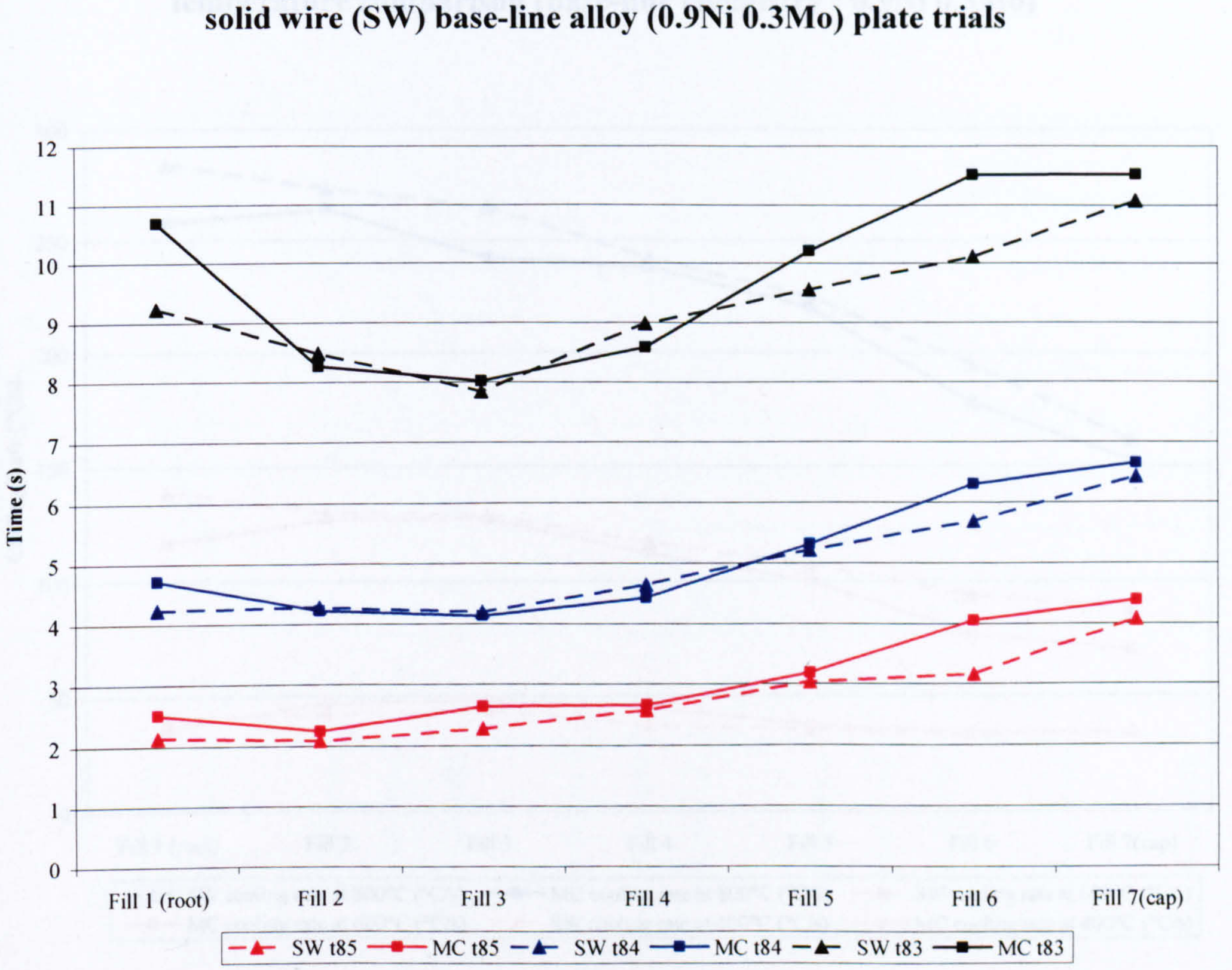

Figure 5-76: Metal cored and solid wire t_{85}, t_{84} and t_{83} cooling time comparison (base-line chemistry : 0.9Ni 0.3Mo)

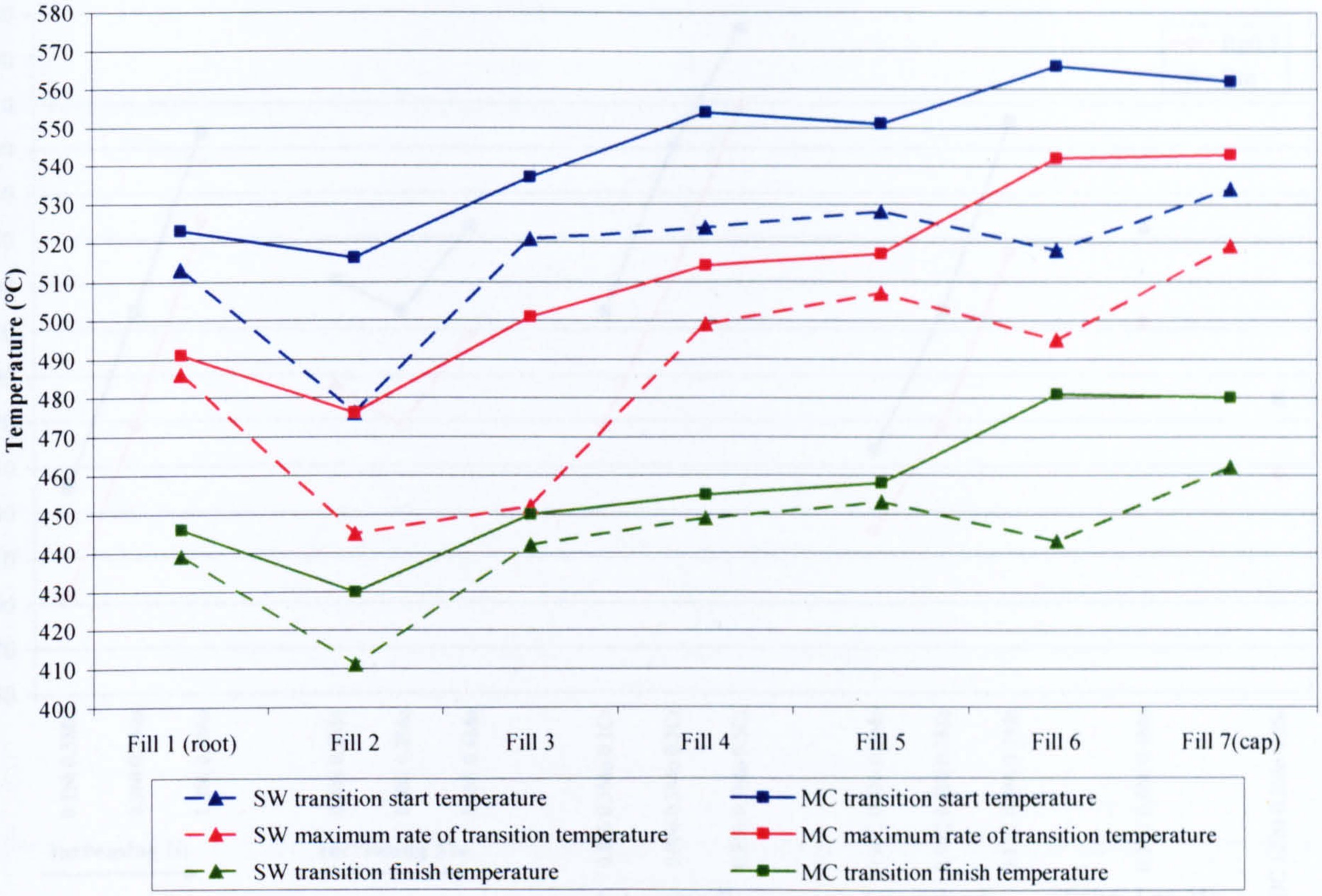

Figure 5-77: Metal cored and solid wire transition start, finish and maximum rate temperature comparison (base-line chemistry : 0.9Ni 0.3Mo)

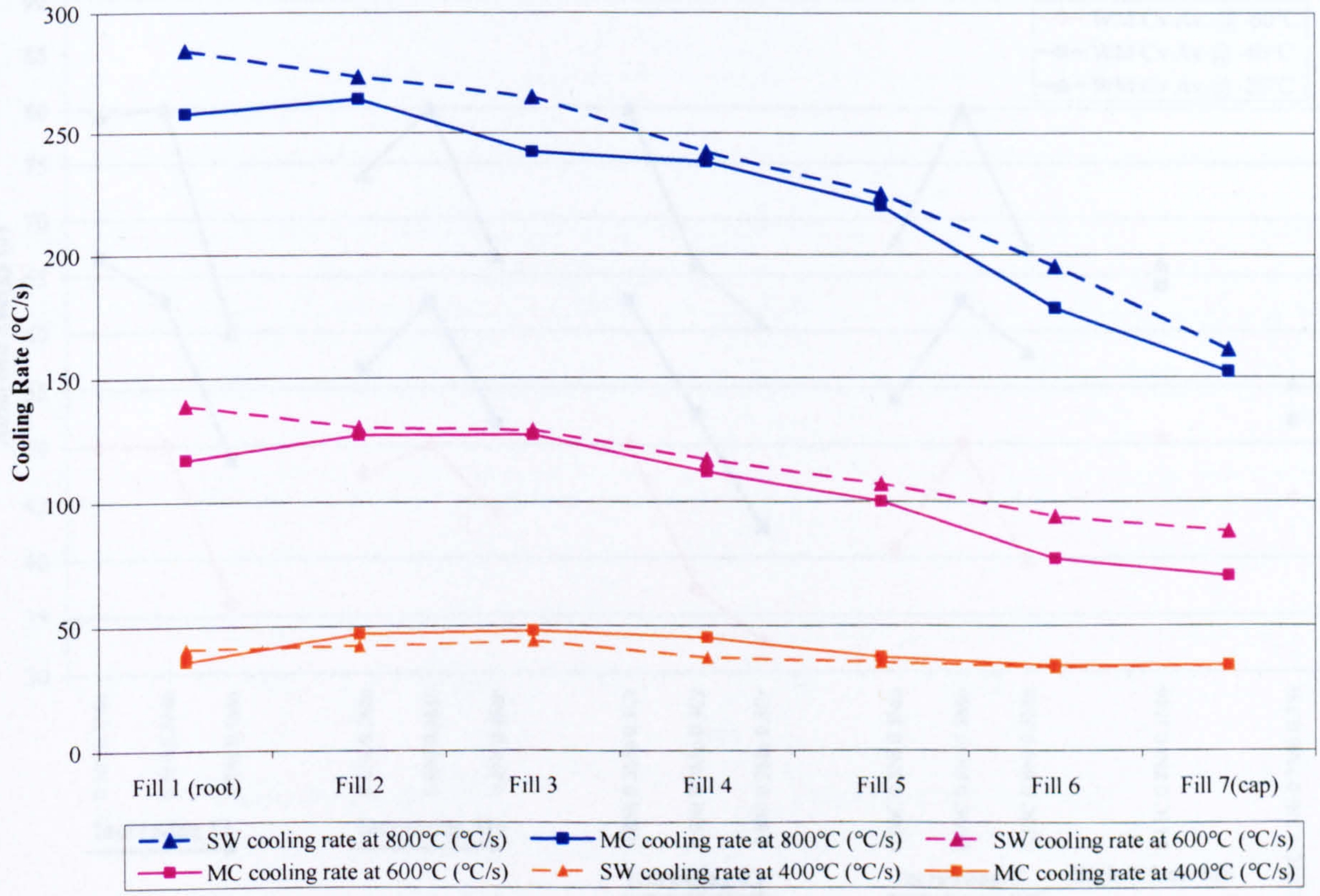

Figure 5-78: Metal cored and solid wire cooling rate comparison (base-line chemistry : 0.9Ni 0.3Mo)

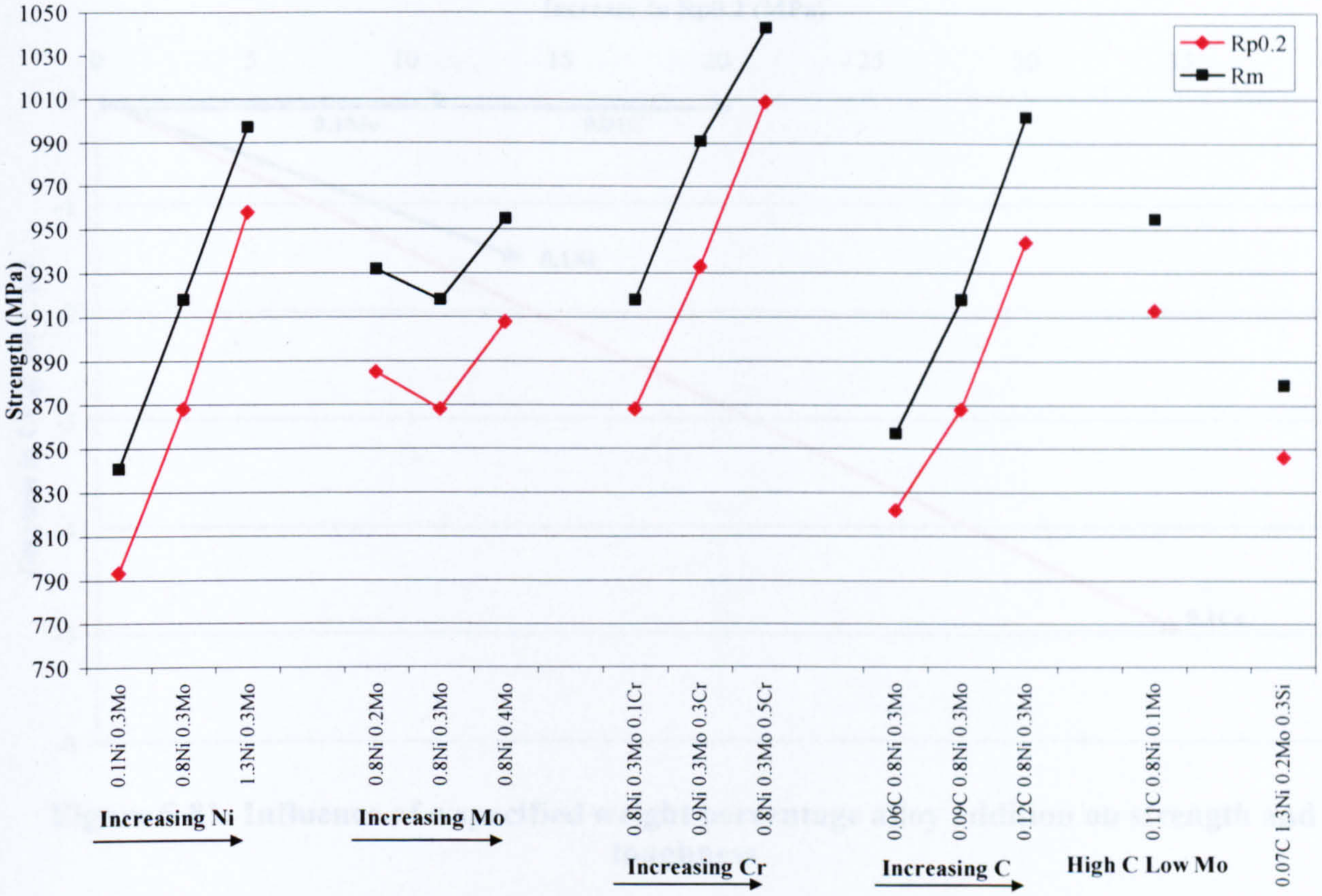

Figure 5-79: Metal cored wire alloy effects on strength

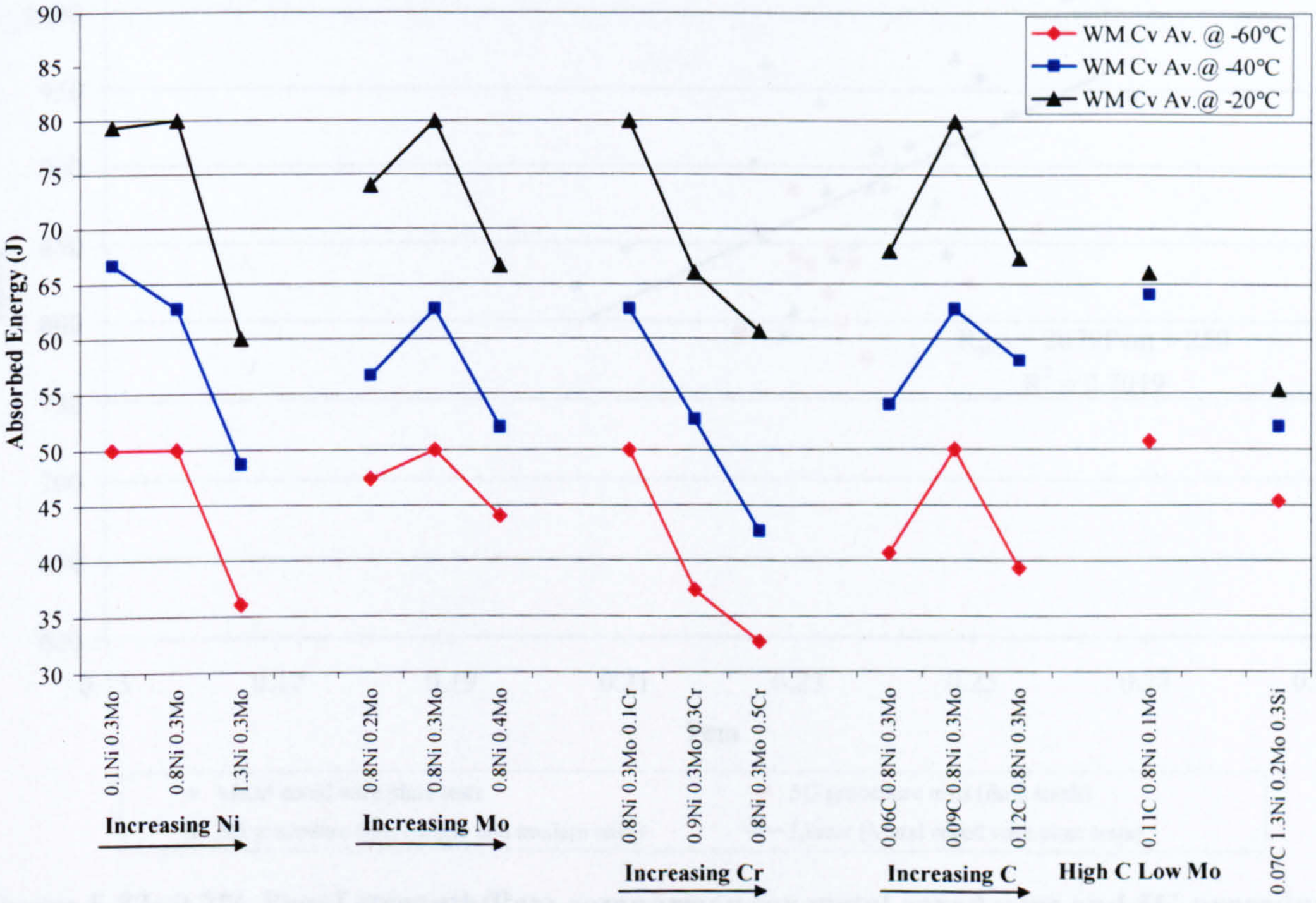

Figure 5-80: Metal cored wire alloy effects on impact toughness

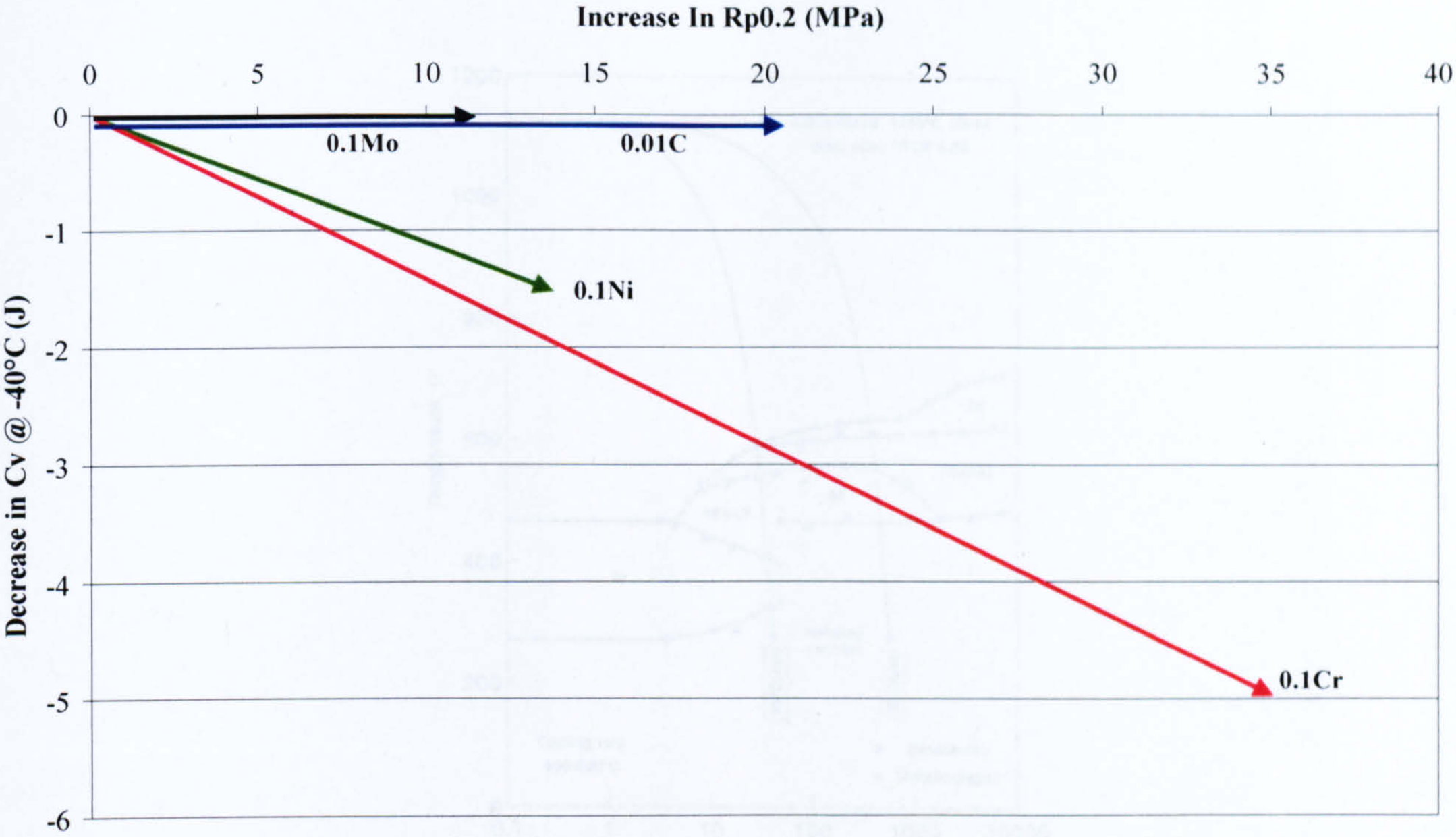

Figure 5-81: Influence of a specified weight percentage alloy addition on strength and toughness

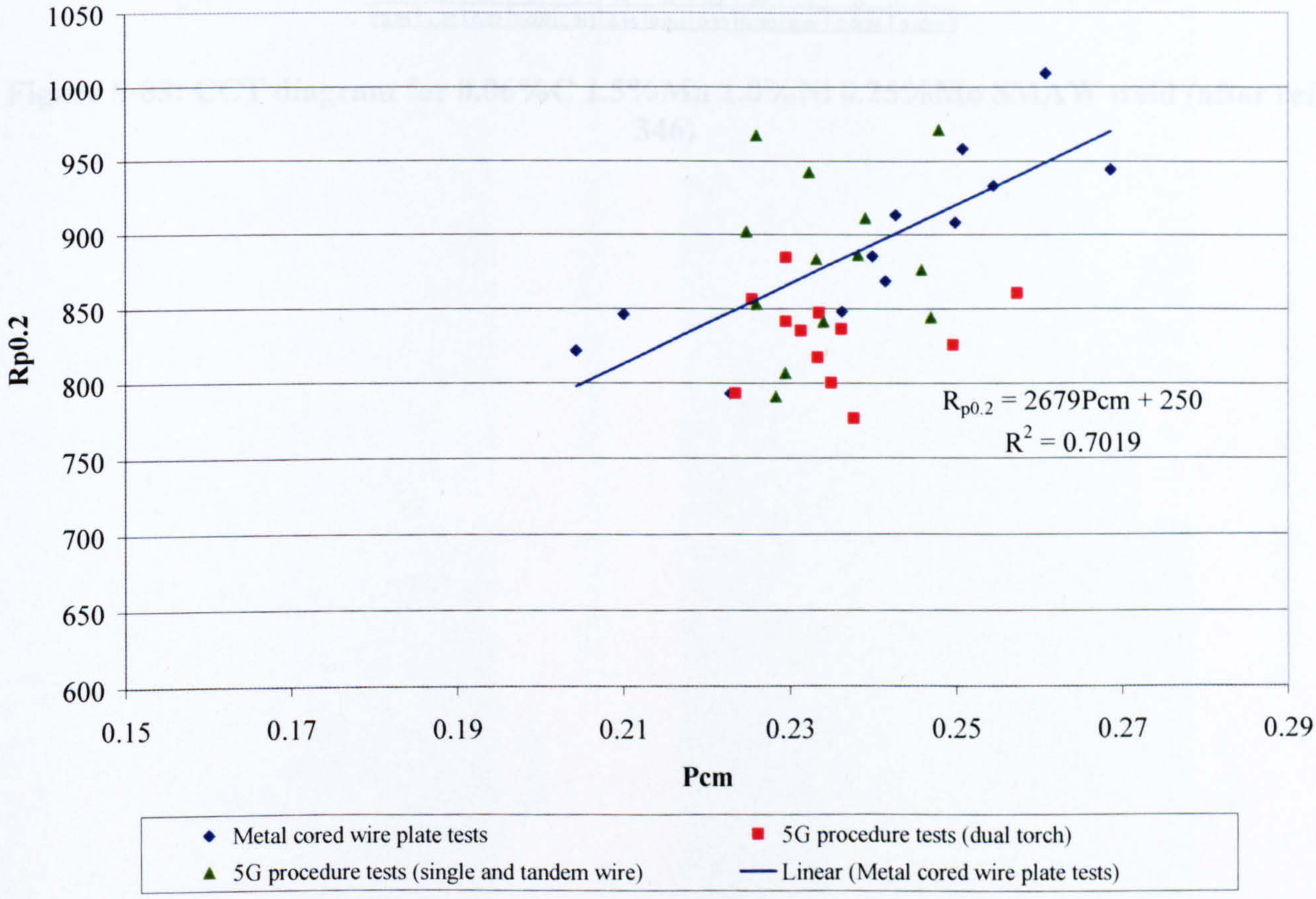

Figure 5-82: 0.2% Proof strength/Pcm comparison for metal cored wire and 5G procedure tests

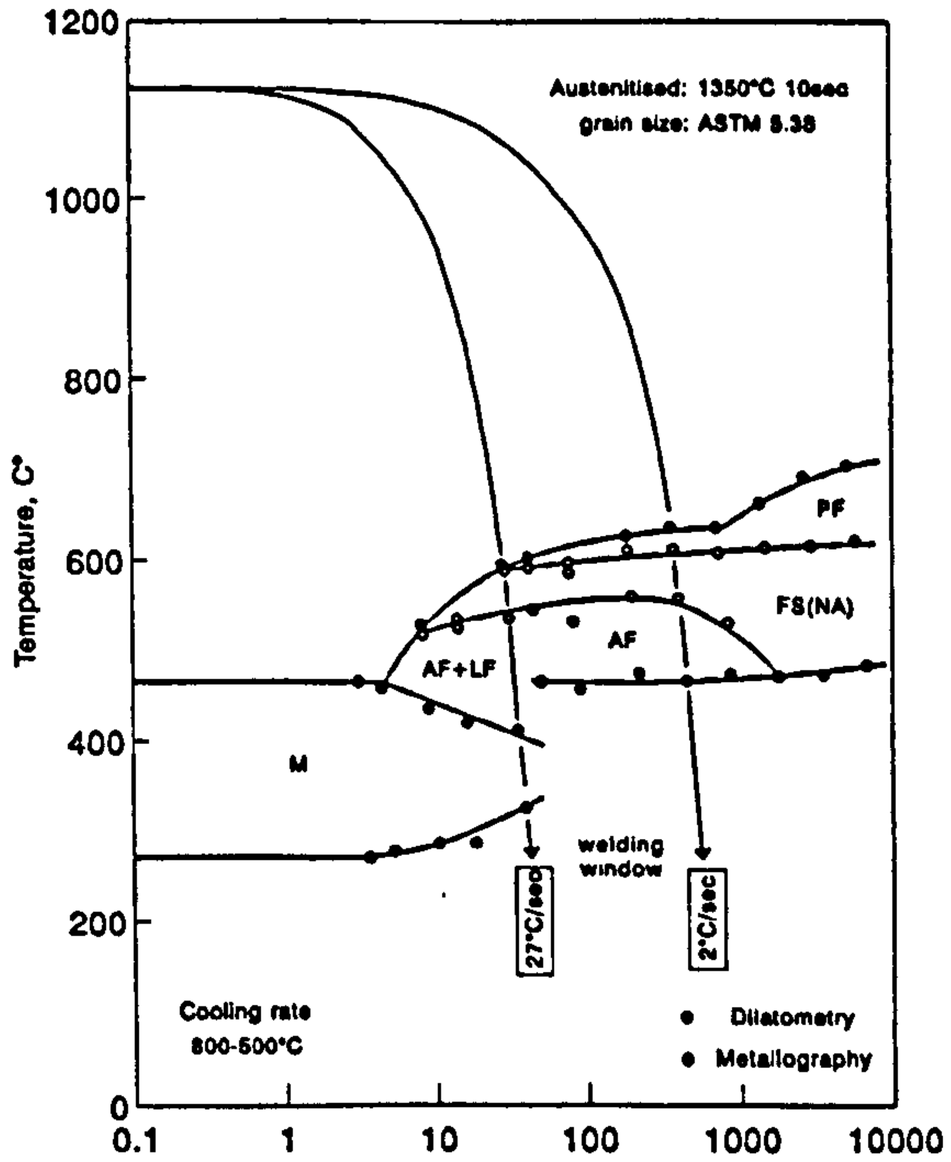

Chemical composition of the weld metal (wt%)

C	Mn	Si	S	P	Ni	Ti	Mo	Al	Cu	N	O
0.06	1.50	0.37	0.009	0.015	0.96	0.018	0.23	0.003	0.06	0.0054	0.0205

Figure 5-83: CCT diagram for 0.06%C 1.5%Mn 1.0%Ni 0.25%Mo SMAW weld (after ref. 346)

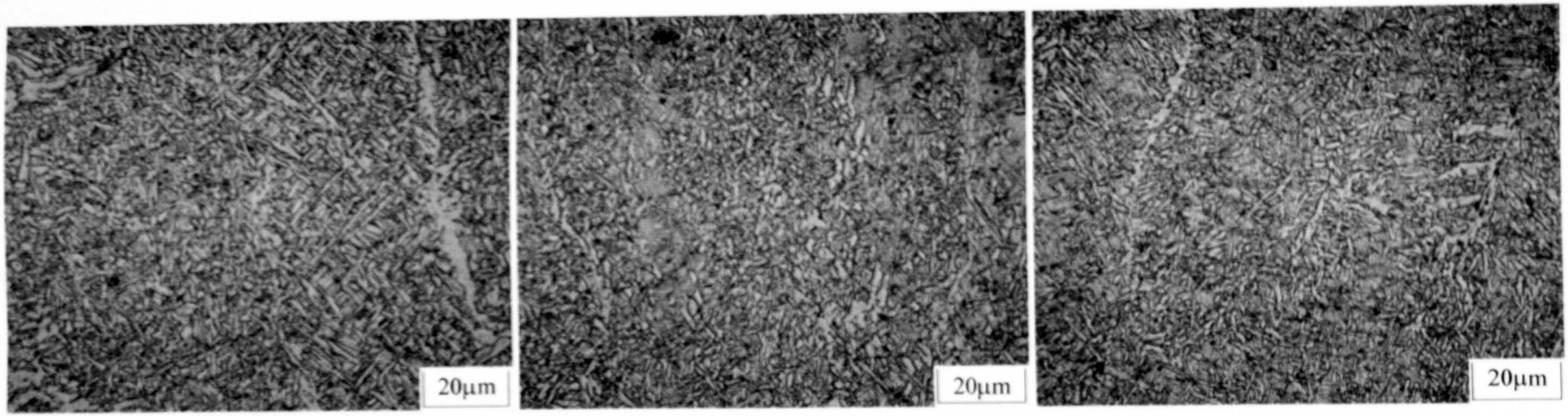

0.1 Ni 0.8 Ni 1.3 Ni

Figure 5-84: Metal cored wire cap pass microstructures – effect of increasing nickel

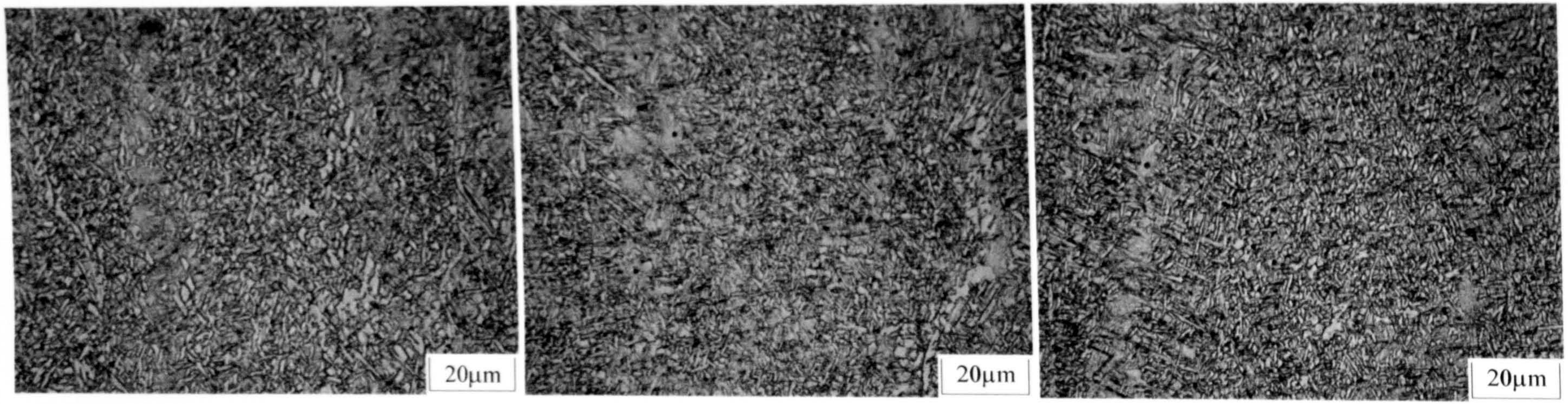

0.1 Cr 0.3 Cr 0.5 Cr

Figure 5-85: Metal cored wire cap pass microstructures – effect of increasing chromium

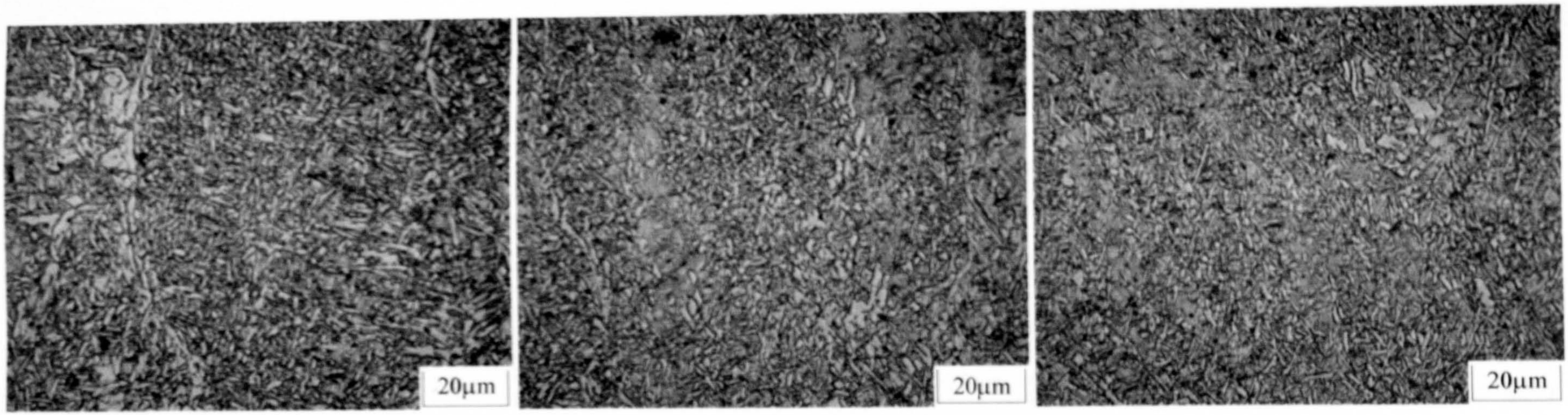

0.2 Mo 0.3 Mo 0.4 Mo

Figure 5-86: Metal cored wire cap pass microstructures – effect of increasing molybdenum

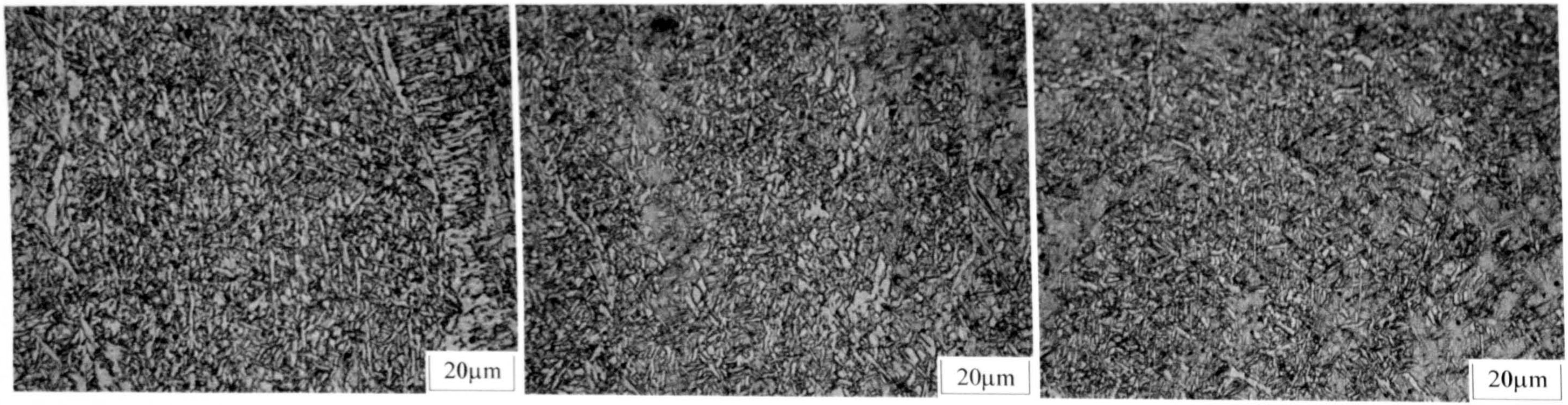

0.06 C 0.09 C 0.12 C

Figure 5-87: Metal cored wire cap pass microstructures – effect of increasing carbon

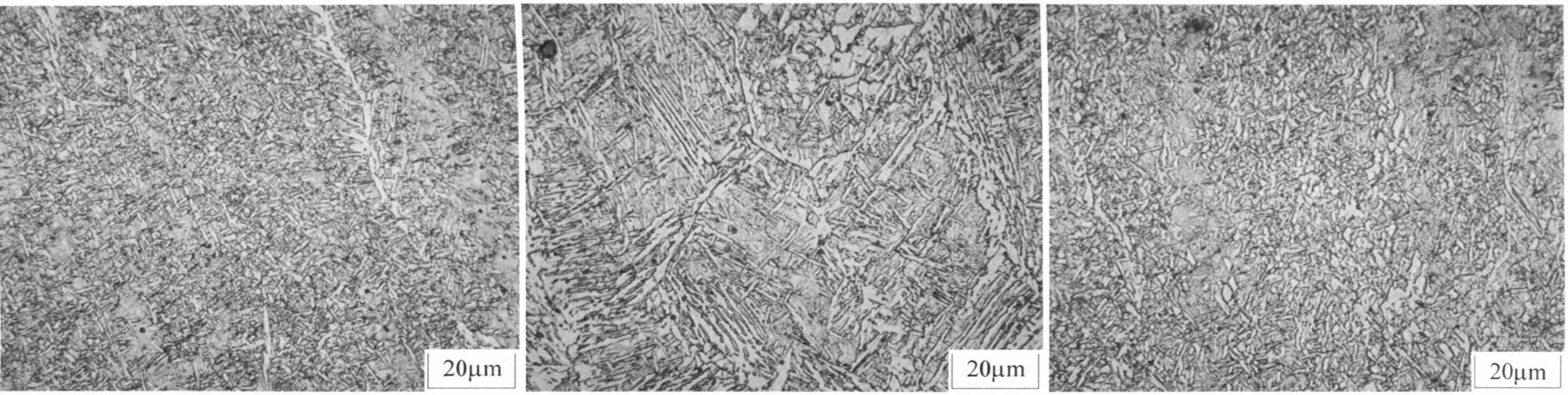

a) 0.11C 1.7Mn 0.5Si 0.8Ni 0.1Mo

b) 0.07C 1.7Mn 0.3Si 1.3Ni 0.2Mo

c) 0.09C 1.7Mn 0.5Si 0.8Ni 0.3Mo

Figure 5-88: Metal cored wire cap pass microstructures – multiple alloy variant effects a) high C lowMo b) low C, low Si, low Mo, high Ni c) control composition

6 DISCUSSION

The following chapter will incorporate a discussion of the results generated within this research alongside their comparison to other published data. A final section will combine the various subject areas to discuss the results in their totality. Particular importance will be placed on the feasibility and practical working tolerance constraints derived from analysis of the data for welded construction of X100 linepipe.

6.1 GIRTH WELDING

The primary tasks in the steps towards successful girth weld development centred on the establishment of the base material properties. X100 strength pipe had been acquired from several linepipe manufacturers, and before welding consumables could be selected knowledge of the spread of yield and tensile strengths was required.

The selection of welding consumables, initially for mechanised GMAW, could then begin alongside the development and/or application of suitable PGMAW waveforms with the two power source variants considered for single and tandem wire welding. Reference to earlier work performed at Cranfield, alongside other published work in the area relevant to high strength steel welding, was undertaken, with early welding consumable selection and narrow gap trials based on the various researchers' findings. Problems associated with this approach are discussed in the relevant section.

Numerous narrow gap tests were consequently conducted to obtain the optimum balance of properties with comparison to the proposed criteria outlined in section 2.9. From these results two consumable types were selected for each welding process variant to provide strength levels which in the first case just overmatch the target criteria, and in the second case provide a considerable overmatch to the same criteria. Full procedure qualification testing was then performed using a combination of the various standards highlighted in section 4.11.

The procedures described above were then repeated for the tie-in and repair welds, with a single consumable type for each process variant tested (FCAW, GMAW and SMAW) relevant to a specific repair situation.

The results of the various tests conducted are consequently discussed in their relevant section.

6.1.1 X100 PIPE PROPERTIES

The 'X100' materials received from the various manufacturers gave a good indication of the likely variances in design philosophy possible at this strength level. The alloying levels used are intricately involved with the TMCP route employed, which explains the considerable variation in base material chemistry. Due to the commercial sensitivity of the TMCP processing route used by a given pipe manufacturer, and the relative irrelevance this would have on the current research investigations, this information was neither given nor sought from the manufacturers. The forming of pipe from plate coupled with the cold expansion is one of the several factors of the production process, all of which have a significant effect on the resultant pipe properties. Longitudinal strength of the pipe was frequently lower than its transverse (or hoop) equivalent (Table

5-1 to Table 5-4), with some $R_{p0.2}$ values dipping below the 690 MPa design minimum. Although design considerations are usually concerned with the hoop stress of transmission pipelines, the longitudinal stress (and strain) may be equally important in regions where the pipeline could undergo flexing due to unstable ground conditions such as frost heave or thaw settlement[297,302,304]. In these areas it is becoming increasingly common to use strain-based design[304], with particular emphasis for the material placed on its ability to attain high uniform elongation levels in order to resist the onset of buckling. Post buckling behaviour is another important material consideration determining the ability of the pipeline to maintain its integrity/avoid catastrophic failure. Particular attention has also been paid to the material characteristics under catastrophic failure, with several small- and full-scale burst tests completed on X100 pipe to date[37,302]. The results of these tests have shown it is unlikely that toughness levels will be achieved to avoid the occurrence of propagating ductile fractures in regions of low temperature use (e.g. Alaska), such that crack arrestors will be an integral component of the pipeline design. Whilst these material characteristics are not the subject of the current research, the effects girth welds have on the holistic pipeline properties should not be underestimated, and tests incorporating both parent and weld material are essential in defining the boundaries for a limit state design.

The increase in strength from plate to pipe is clearly illustrated by manufacturers A and C where the two materials were available, and this phenomenon can be attributed to the Bauschinger effect[299,300]. It should be stated that the relatively few in-house tensile tests conducted on the base materials investigated do not provide a definitive guide on chemistry/property relationships for the X100 pipes received; the manufacturers will undoubtedly have significantly more information about their respective pipes. What is of interest is the often considerable difference between round bar and full thickness strip tensiles; the latter frequently giving a lower result. The standard API 5L[20]/CSA Z245[21]/ISO 3183[296] method of tensile testing pipe usually involves a flattened strip tensile taken from the transverse (hoop) direction, with options available for round bar testing or longitudinal tensile testing (round or flat). Transverse tensile testing of X100 strength pipe has highlighted a discrepancy between the conventional strip and round bar tensile[7,304], with the former resulting in an underestimate of the value as determined by the ring expansion method (deemed to be a true representation of the hoop proof stress). Hence the round bar test has been adopted within several internal company specifications[304,341] as the required transverse tensile measurement.

API 5L specifies a yield value arising from the $R_{t0.5}$, whereas in general engineering design the $R_{p0.2}$ is a more conventional measurement. The weld metal yield strength values when discussed in the following sections will refer, unless stated, to the $R_{p0.2}$ i.e. effectively non-dependant on the material modulus when the change from elastic to fully plastic does not occur over too large a range (see Figure 5-1(a)). If the moduli do not change between the various pipe steels or weld metals, as would be expected with the alloys investigated, the $R_{t0.5}$ values are likely to be closely associated with the $R_{p0.2}$, but, as observed on some stress-strain curves, this is not always the case, resulting in considerable discrepancy between the two values (see Figure 5-1(b)). API 5CT[351] attempts to correlate the $R_{p0.2}$ with an associated R_t value for the higher yield strength steels (>90ksi), but the work has been based on traditional Q and T steels. A better understanding of the comparison of yield measurements for the latest generation TMCP

steels at X90+ strength levels is therefore required for specification purposes, both for parent and weld metals.

Yield to tensile (Y/T) ratios are typically 0.80 to 0.95, the latter normally associated with round bar transverse tensiles. Some results are even above 0.95, again highlighting the need for careful consideration in specification writing. The high Y/T ratios are in agreement with other test data[7,8], and are recognised to be the direct result of the high yield values.

The classical Dearden/O'Neill carbon equivalent (CE_{IIW}) formulation[35] resulted in rather high values for some of the pipes (Table 5-5 and Table 5-6), which would normally be associated with the necessity for special precautions or very high preheat requirements for welding. A more realistic guide to material weldability of these steels is provided by the Ito/Bessyo P_{cm}[36] or EN1011-2 CET[44] formulae when carbon levels are below 0.1%. The preheat levels needed for practical welding have not proved to be onerous as shown in Table 5-30 (based on the weld metal, due to the higher CET value of this chemistry compared to the base material). The steels examined typically included nickel, molybdenum, chromium and copper alongside carbon, manganese and silicon as the major alloying elements to provide strength. Microalloying additions of aluminium, vanadium, niobium and titanium provide grain refinement and de-oxidation to various extents in the quest for optimum microstructural development leading to high levels of toughness. These elements also help with the control of grain growth and limit the production of deleterious microstructures in the HAZ[1,3,5,10,54,59,63]. Carbon is controlled at low levels, presumably with the aim of lowering preheat temperatures due to the strong effect this element has on the material hardenability. Phosphorus, sulphur, oxygen, nitrogen, and with the steels of this research boron, are all considered as trace elements, being kept at the lowest levels possible to avoid deleterious effects.

The seam weld metal chemistry philosophy is also different between the manufacturers. Pipes A, B15 and B19 have considerably different compositions from that of the base material, whereas pipe C is nominally the same (except for O_2 and N_2 as would be expected). Pipes B15 and B19 even use different alloy levels for the inside and outside passes, undoubtedly in the pursuit of improved toughness levels given the different cooling cycle/chemistry interaction. Seam weld strength and toughness measurements were not an aspect of the current programme, and again reference should be made to the manufacturers' data. The case of the girth weld/seam weld interaction however was investigated, and will be discussed later under the various weld metal hardness test sections.

The pipe seam weld hardess traverses (Table 5-7) exhibited relatively low levels of hardness in the weld metal, HAZ and base material. All results were below 300 HV10, with the HAZ's typically giving the lowest average values and highest scatter. This phenomenon is typical within a region experiencing a high temperature gradient alongside the associated variable reheating effects of a high strength, very fine grained TMCP steel.

The base material microstructures (Figure 5-2 to Figure 5-5) go some way towards explaining the greater disparity of longitudinal versus transverse proof strengths exhibited by pipe C in comparison with pipes A, B15 and B19. Pipe C exhibited a rather less homogeneous microstructure compared to the other pipes, incorporating a significant 'banding' structure in the longitudinal plane. The pipe microstructures are all

extremely fine, with the bainite sheafs/martensite present alongside the retained austenite/ferrite in the three materials at the limit of optical resolution. This is consistent with other published data on microstructural characteristion of various X100 linepipe steels[3-10].

6.1.2 SINGLE WIRE NARROW GAP WELDS

Consumable selection was based initially on research carried out at Cranfield, in-which a conventional wide bevel joint design, heat input of 0.8 kJ/mm and preheat/interpass of 100/150°C were used in a downhand ASME IX 1G plate situation[154-156]. Numerous consumables were evaluated together with various gas mixtures and transfer modes, providing an overview of strength, toughness and process stability. This allowed a ranking of potential candidate consumables for an X100 strength match. At this point a guaranteed weld metal yield strength overmatching requirement had not been proposed. At the start of the current experimental programme of narrow gap welding, the proposed mechanical properties highlighted in section 2.9 were taken into account. The typical classification tests performed by the manufacturers on the wires (similar to the wide bevel tests conducted at Cranfield) allow a ranking of the mechanical properties, but cannot be used in terms of required property generation for the proposed target values. This was highlighted in associated research just prior to the start of the current programme[157]. The significantly different strength levels obtained in a narrow gap weld in combination with the lower welding arc energy of the various GMAW/PGMAW process combinations required considerable effort to be expended on obtaining the required strength. Most of the published work on high strength steel consumable development uses arc energy values of 1.0 kJ/mm or greater[215-217,252,283,284], in combination with standard (wide) bevel joint geometries. The degree of strength increase obtainable from the low arc energies and narrow bevel geometry providing an enhanced cooling rate is a known phenomenon for the standard C-Mn wires used for pipe up to X80 strength levels[145,150]. What was not understood, however, was the strength increase likely to be attained from a similar welding situation, but with the higher alloying required to generate the proposed mechanical properties for X100. The variation of possible alloy combinations in generating the strength levels at high cooling rates adds a further degree of complexity, the effects of which are discussed in the following sections.

Work began on the single wire mechanised welds using 'standard' CRC-Evans narrow gap joint geometry and bug travel speeds of 450-500 mm/min. Having generated reasonable weld profiles and weld metal transfer characteristics for the majority of the pipe circumference, the 'problem area' of 5 to 6 o'clock (where the weld profile tends towards convex in the outer fill layers) was considerably mitigated through a reduction in overall bevel width, coupled with the correct torch oscillation width for the given weld pass. Mechanisation of the welding process should not be confused with automation; a considerable degree of operator involvement is required with the equipment used, and together they determine the completed weld integrity. The wire 'cast' (natural diameter that wire forms on unreeling) can change as the bug moves around the pipe due to the remote wire feeder and 3-4 m wire liner used during the research. This can result in arc and metal transfer variation, with resultant potential lack of fusion and other defects. The pipes themselves are never perfectly round, and although the band holding the bug is designed to follow the pipe contour, out-of-

roundness, such as that encompassing the seam weld, produces variations in the contact tip to workpiece distance (CTWD). Gravitational effects also cause the equipment to 'sag' in the inclined/overhead positions. Depending on the severity of CTWD variation the welding arc will lose its stability alongside gaining a tendency to conduct preferentially to one of the sidewalls. This effect can be reduced by incorporating feedback mechanisms such as arc length control within the overall pulse waveform. In the case of the WERC waveforms however, waveform adaption was not used. It was preferred always to have a known and consistent powersource output based on a given CTWD, resulting in an approximate 3 mm arc length. Hence manual control of CTWD was quite critical in maintaining this arc length and the process stability.

The initial wire selected from the early trials incorporated alloying levels of 0.5Ni 0.5Mo 0.5Cr (Oerlikon Carbofil HT), producing weld metal yield strengths which overmatched the pipe SMYS by at least 100 MPa, but did not always reach the 810 MPa minimum proof strength criteria proposed (Table 5-18). A welding wire judged to be the next highest available in terms of strength was a 2.3Ni 0.5Mo 0.3Cr wire (ESAB Spoolarc 120). However, welds made with this consumable gave proof strengths of between 844 and 971 MPa, potentially overshooting the proposed minimum by more than 160 MPa. The single-wire welds made by Serimer-Dasa using a 1.0Ni 0.4Mo wire (Thyssen MoNi) also overshot, giving proof strengths of 911 and 886 MPa. These higher strength welds however gave relatively good weld metal toughness results, with impact levels of at least 50J at –60°C and 0.12 mm CTOD at –10°C (average, although very few individual results were below these values – see Table 5-25). In an attempt to 'stabilise' the proof strength to the 810-860 MPa desired range a further consumable was investigated using the (now standard) reduced bevel offset (Figure 2-27) in combination with the lessons learnt from the 1.0Ni 0.4Mo wire. This resulted in the use of a 0.9Ni 0.3Mo wire (Oerlikon Carbofil NiMo-1). Results using this alloy from single wire welds with a normal bevel width resulting from an offset of 2.3 mm gave $R_{p0.2}$ values of around 840 MPa, but if the groove width was reduced (as per weld ML-B-12) a considerable increase in strength ($R_{p0.2}$ 967MPa in this case) is possible for the same welding arc energy/cooling rate. This highlights the sensitivity of the joint geometry on weld metal properties. Elongation values were typically between 15% and 20% (proportional test pieces were used), with yield to tensile ratios of typically 0.90 to 0.95. These latter two parameters were typical of all the weld metal tensile tests conducted throughout the research, and compare well with published values for weld metal at these strength levels[150,152,154-157].

The impact transition curves (Figure 5-40 and Figure 5-41) tend to show a maintenance of toughness levels within the weld metal as compared with the fusion line on decreasing test temperature, although scatter at a given temperature can be very high for the fusion line results. This scatter may be explained by the narrow heat affected zones typical of mechanised narrow gap pipewelds; visibly affected widths are 1 – 1.5mm, resulting in a sharp change of the microstructural characteristics across this width. Notch location consequently requires highly accurate positioning within this region, such that the difference of the notch root being exactly on the fusion line compared with 0.25mm into the HAZ or weld metal could account for the scatter in observed values. This level of notch positioning may be impractical for routine test laboratories. Levels in both cases are however nearly always above 50J at -40°C. Weld metal CTOD levels are conversely nearly always lower than their counterpart fusion line result (Table

5-25), with most tests classified as δm values (value of CTOD at the first attainment of a maximum force plateau for fully plastic behaviour). The reason for this apparent reversal of toughness value between the two test types for the same weldment location is not clear. It should be stated though that whilst the fusion line impact toughness values are lower than their counterpart weld metal tests, the values do not represent 'brittle' material. The same is true of the weld metal CTOD values. The two major differences between an impact test and a CTOD test are the speed at which the test is conducted (much higher for the impact test) and the initial flaw geometry (higher stress concentration for the initial CTOD crack). The weld metal and HAZ both contain mixed microstructures with their associated (local area) material toughness values. It is postulated that the 'sharp' intial CTOD crack within the HAZ is less likely to 'find' areas of poor toughness compared with the 'blunt' Cv impact test notch for which the initial area/volume loaded is much greater. The latter effect within the Cv test may allow the crack to initiate in a low toughness area, from which propagation is much easier due to the high stress intensity factor at the crack tip from this point onwards.

Cross weld tensiles from all procedures typically failed in the parent material, for which only one UTS value was below 780 MPa (Table 5-21). Nick break and side bend results were generally acceptable. It should be stated that whilst a 100% acceptance criterion is required of procedure tests, the prime concern during this research was the generation of acceptable mechanical properties; the 'welder tests' of nick breaks, side bends and cross-weld tensiles taking a second place. With the continued development of equipment and operator familiarity during the course of the work, an associated improvement in total joint quality was realised as proved by the later welds.

Weld metal chemistry results highlight the different alloying levels used (Table 5-28). Oxygen levels were typically 200 – 400 ppm, with nitrogen less than 100 ppm, which, together with the general alloying, were conducive to the overall high toughness levels observed and in good agreement with the extensive literature surrounding this area of weld metal metallurgy[158-165,174-183,185-208]. It should be noted that the chosen shielding gas plays an important part in the resultant weld metal chemistry and mechanical properties, and is an integral component of the welding procedure. The trimix gas used for most of the narrow gap welds throughout this research was a direct result of using the findings from an extensive research programme carried out in the late 1980's[152]. The helium increases the heat input and consequently improves the fusion capability of the process, and the reduced CO_2 content (compared with the conventional 80%Ar/20%CO_2) lowers the weld metal oxygen content thereby improving the toughness.

Joint hardness traverses are observed to follow a consistent pattern as witnessed in the pipe longitudinal seam weld traverses. The HAZ is nearly always softer than the unaffected base material by 10-20 HV10, due to a net softening effect of the weld thermal cycle on these TMCP steels. The microstructural development during manufacture of the steel is destroyed to greater or lesser extents within the HAZ, depending on the heat input of the welding process. As a result of this, the weld metal typically shows the highest hardness (Table 5-18) due to the absence of post solidification processing coupled with the alloy levels required to generate the high strength levels when compared to the base metal properties. The strong correlation of strength and hardness is shown in Figure 5-6, the data having been compiled from numerous GMAW and PGMAW wide bevel flat plate tests[157,342]. Weld metal levels

are thus likely to be between 280 and 350 HV10 in order to generate the required $R_{p0.2}$ of 810MPa; this is clearly demonstrated in the tensile and hardness data of Table 5-17 and Table 5-18. Weld metal root hardnesses were always lower than their cap equivalent due to the effect of subsequent tempering and the very low-alloyed root welding consumable used in some cases. Nearly all results from the cap and root areas were below 350 HV10; those that crept above this level were solely in the weld metal cap of the high alloy welds. The girth/seam weld metal intersection, however, exhibited a different pattern for the hardness levels of girth/seam HAZ's. Pipes B15 and B19 were consistently at or above 350HV10 for the cap traverses, complementing the high CE_{IIW} values of their seam weld metals in comparison to the two other pipe variants. Some of the girth weld metals in all the pipe materials tested also exceeded this value, invariably due to dilution effects further increasing the total alloy content.

A macro section from each procedure weld was used to produce a series of micrographs created from the use of x10, x50 and x100 lenses (coupled with a converter lens to the camera of ~x10) to show the prior austenite grain size as well as the fine microstructural detail (Figure 5-32). All micrographs were from the weld cap (i.e. as-cast) pass to allow direct comparisons. The higher alloyed consumable (2.5Ni 0.5Mo 0.4Cr) exhibited high aspect ratio constituents of a martensitic nature when compared against the lower alloyed consumables (0.5Ni 0.5Mo 0.5Cr or 0.9Ni 0.3Mo/ 1Ni 0.4Mo). In the latter a greater proportion of bainitic and acicular ferrite components were present. The small grain size (both prior austenite grain boundaries and final microstructure) are evidence of the low heat inputs and fast cooling rates that are characteristic of the welding process, in conjunction with the high rate of intergranular nucleation.

A high strength solid wire diffusible hydrogen measurement undertaken early on in the research programme exhibited a value well below the maximum 4 or 5 mls diffusible hydrogen/100g deposited weld metal associated with the most stringent classification test categories currently specified (see Table 5-8). A parallel research programme conducted with a large number of the solid welding wires employed throughout this research, using arc energies associated with mechanised narrow gap procedures under highly restrained conditions, confirmed the solid wire value generated[323]. It proved extremely hard to produce HICC, even with preheat/interpass levels below 40°C, and this was confirmed in the present research by the absence of any form of cold cracking in the numerous weld metal sections examined.

6.1.3 TANDEM WIRE NARROW GAP WELDS

The development of tandem wire equipment and procedures for pipeline girth welding has been evolving at the WERC for several years[11,12,13,324]. The initial synchronised power supplies used for these trials (Fronius TPS 450) have also evolved to totally digitized, microprocessor-controlled inverter power sources. An interactive power source manager is coupled with a digital signal processor, and together they control and regulate the entire welding process[343]. However, as stated in chapter 4, the majority of experiments carried out utilised the original equipment design. The synergic curves were those developed by Walker[12] for the TPS 450, with slight modifications made (predominantly using background current ramping) for the TPS 4000 (see Appendix A). As for the single wire Lincoln Electric Powerwave waveforms, adaptation of the welding process was disabled, resulting in a consistent powersource current waveform

output. Again, maintenance of the correct CTWD was vital in ensuring a stable metal transfer of the correct (approximately 3 mm) arc length.

Torch design has evolved from simple air-cooled devices derived from existing mechanised pipe torches to the integral water-cooled tandem torch design currently used (Figure 4-11). The main disadvantage of the torch and its associated liners is the overall weight imposed on the bug torch holding and oscillation system. The torch is required to oscillate at up to 500 beats per minute at the high travel speeds without transferring extra vibration and potential tracking problems to the bug itself. The issue of wire cast is extremely important bearing in mind the close proximity of the two wires (Figure 5-8); providing the cast is similar between the two wires, any offset required can be countered with the initial torch alignment. The narrow contact tips shown in the previous figure are necessary for the initial weld passes due to access/oscillation requirements deeper in the weld groove; these are replaced with conventional tips as soon as possible to aid heat dissipation.

The main issue involved with the development of sound welds centred on the avoidance of porosity and lack of fusion defects, usually brought about by inconsistent wire feeding at the tips as a consequence of spatter and/or tip contraction. This in turn was usually a result of an unstable arc length caused by CTWD variation or wire feeding problems. In this respect the welding process improved an order of magnitude with ostensibly the same waveform design, but using the latest generation power supplies coupled with improved contact tip design. There is still scope for development of the system, but the research to date has shown that acceptable welds can be produced to standard NDT code requirements. Welding between the 4.30 and 6 o'clock positions requires careful set-up to avoid inconsistent and convex profiles in the outer fill passes, usually involving a precise balance of travel speed, oscillation width and wire feed speed/pulsing parameters coupled with accurate wire positioning within the joint. A move towards higher overall bug travel speeds resulted in the prevention of 'roll-over' and consequent lack of fusion defects in the 2 to 4 o'clock positions. Care is however required to avoid centreline (hot) cracking due to depth to width ratios in the early passes coupled with a high travel speed. In common with typical pipeline spreads, improvement of practice came with the number of welds performed. The torch shroud needed to be placed within 15 mm of the pipe surface for all passes to prevent porosity; each power supply/torch liner had its own gas supply to reduce pressure drop effects. The torch gas flow rate was also essential in providing stable transfer and porosity free welds. Maintenance of the equipment proved vital in ensuring free and consistent wire feeding; liners and contact tips were renewed if there was the slightest concern they may have been causing a hindrance. The complexity of the system coupled with the high travel speeds used lends itself to a high degree of automation in order to maximise joint completion times. Manual tracking in two axis coupled with travel speed adjustment requires considerable skill for conventional single wire mechanised pipewelding; the skill level is multiplied when moving to higher speed systems in order to generate the same degree of weld quality. For this reason it is essential that automatic joint tracking systems are incorporated within the bug, as well as some degree of feedback control regarding the arc stability. Although these factors were realised early in the research, timescales did not allow the useful incorporation of proprietary (laser) or in-house (arc voltage control) developed tracking systems, such that careful attention to equipment set-up was the only option available for weldment completion.

As per the single wire welds, any defective areas resulting from the NDT reports were avoided for mechanical test piece extraction. Macro sections were taken from initial test welds that showed promising radiography results. In some cases lateral inter-run lack of fusion defects were observed, particularly in the area around the 3 o'clock position, even though the radiograph appeared 'clear'. This was attributed to the circumferential radiography direction not discerning any change in material density. A different technique is required to pick out these defects such as ultrasonic testing. Higher quality radiography (X-ray rather than Gamma) possibly coupled with improved film quality (D4 instead of D7) may also improve defect detection.

The chosen consumable chemistries again employed a 'just overmatching' and 'considerable overmatching' philosophy. The 0.9Ni 0.3Mo wire (Oerlikon Carbofil NiMo-1) was judged from the trials to meet the 810 to 860 MPa proof stress requirement (Table 5-11), but actually gave results in excess of 900 MPa (Table 5-18). This was attributed to a reduced bevel width, especially in the case of the Pipe B19 weld (ML-B-12). For the same arc energy, preheat and joint geometry the cooling rates for single and tandem pipewelding processes using the same consumable are identical, resulting in very similar tensile properties (see later section on process variant thermocycles and Figure 5-29). This reinforces the necessity of close control over bevel geometry for correct property maintenance. The alternative higher strength consumable chosen was the 1.0Ni 0.4Mo wire (Thyssen Union MoNi), which gave similar results to the 0.9Ni 0.3Mo wire and considerably overmatched the 810-860 MPa requirement. The two welds made with this consumable were produced under similar conditions except for the power supplies (old then new generation Fronius TPS). The 60 MPa spread in $R_{p0.2}$ gives an indication of the potential spread in values between procedures. The elongation values were rather low, with yield to tensile ratios 0.95 or 0.96, as would be expected with the high strengths obtained.

Toughness values however were still very acceptable (Table 5-26), again giving over 50J at -60°C for both weld metal and fusion line. The impact transition curves (Figure 5-43) follow a similar pattern to those of the single wire test welds; weld metal toughness decreases at a slower rate than that of the fusion line. Scatter within the fusion line results was observed to be confined to a particular temperature tested (either -40 or -60°C) as is normal in a transition region. CTOD values were comparable with single wire tests, with results predominantly classified as δm. Some of the results highlighted an interesting effect with regards to the base steel. Considerable segregation at the centreline of one of the pipe materials (Figure 5-24) manifested itself as an open tear in the fractured CTOD specimen (Figure 5-25) within some of the fusion line tests (the figure shows that the weld metal tests were unaffected as would be expected). This phenomenon has been observed before in fracture toughness tests[344], and providing any pop-in shown on the load/clip gauge displacement graph is small, with the event being traced to the material split and not a brittle failure of the HAZ, the result is acceptable.

Cross weld tensile results (Table 5-22) again gave UTS values over 800 MPa when failures were in the parent metal/HAZ. The few results that failed in the weld metal mostly gave UTS values in excess of 800 MPa. Nick break and side bend tests were just over 50% successful; those that failed were mainly due to lack of inter-run fusion defects. The same philosophy as per the single wire welds was taken with respect to

these results; metallurgically the properties are sound, but refinement in actual welding practice is required for optimum testing performance.

Weld metal chemistries (Table 5-29) were identical to their single wire counterpart, as would be expected for the similar joint profiles and dilution effects.

Hardness traverses (Table 5-18) for the pure girth/pipe base material were similar to those of the single wire welds. The HAZ is nearly always softer than the unaffected base material, with the bulk weld metal (i.e. not that used in the root) exhibiting the highest hardness levels. In the case of the higher alloyed consumable (1.0Ni 0.4Mo) the cap weld metal hardness results are consistently above 350 HV10, whereas the 0.9Ni 0.3Mo wire fell in the 300-350 HV10 range. This highlights the important role minor changes in chemistry can have on certain mechanical property values, especially when these are close to potential limits. The girth/seam weld interaction indicated high hardness levels in the HAZ of the seam weld metal for both pipe materials tested (B15 and B19) as per the single wire welds. The cap hardness levels in these cases frequently exceeded 350 HV10. High weld metal cap hardness was again shown in the higher alloyed consumable (1.0Ni 0.4Mo).

A typical photo macrograph is shown in Figure 5-16 highlighting the similarities between the single and tandem macro sections. Weld metal microstructures taken in a similar fashion to those of the single wire welds are shown in Figure 5-33. Comparison with the single wire alloy equivalents show very similar microstructures, which is not surprising considering the similar arc energies involved in the weld deposition.

6.1.4 DUAL TORCH NARROW GAP WELDS

Torch spacing plays a vital part in the mechanical properties generated in the weld metal (and the HAZ) due to the considerably different heating and cooling effects associated with an additional weldpool closely following the lead torch deposition. The Saturnax dual torch welding bug used for the initial trials employed a 50 mm spacing between the two torches (Table 5-9) and the majority of consumables tested did not achieve the 810 MPa minimum $R_{p0.2}$ (Table 5-10). An early test using the same consumable and arc energy in a single and then dual torch procedure on each half of the same pipe highlighted the dramatic change in properties brought about by the different weld metal cooling cycles. The single wire gave an $R_{p0.2}$ of 894 MPa whereas the dual torch (50 mm spacing) gave 756 MPa, respectively overshooting and undershooting the desired range. Observation of the two cap pass weld metal microstructures alone (Figure 5-34) explains the large discrepancy in tensile results; the finer grain size of the single torch weld no doubt providing the key. The hardness levels obtained from these two joints using a lower load (HV2.5) than normally performed with procedure tests (HV10), allowed a closer examination of the HAZ of the particular pipe steel used (Pipe C). The HAZ softening effect is clearly seen in both cases (Figure 5-47 and Figure 5-48), and although the minimum hardness levels achieved in both welds are similar, the overall softening is somewhat enhanced in the case of the dual torch weld. This can be explained with reference to the thermocycle measurements discussed in a later section. A typical single wire weld bead cooling time (layer surface) from 800°C to 500°C in the middle of a 19.05 mm pipe narrow gap joint, using a preheat of 100°C and arc energy of 0.5 kJ/mm is 1.8s (see Table 5-36). The equivalent cooling time for the second torch bead (85 mm behind the first torch) of a dual torch weld is typically 4.4s (see Table

5-38) i.e. greater than twice the time. The loss in strength due to this effect is clearly reflected in the tensile properties. Interestingly, the reduction in toughness from single to dual torch is relatively minimal (Table 5-41).

It was consequently decided to increase the torch spacing to 100 mm, which allowed greater cooling of the first weld bead prior to the second bead being deposited. Transformation start temperatures are typically around 450°C to 550°C for the alloy levels investigated in the current programme (see Table 5-36 to Table 5-39); therefore if the second torch arrives prior to the first weld bead transformation, the increased austenization and cooling time will generate considerably different microstructures with an associated shift in mechanical properties. Although the actual cooling cycles from the Serimer-Dasa procedures were not monitored, comparative tests conducted within this research have shown that a torch spacing of 85 mm and arc energy of 0.5 kJ/mm at a bug travel speed of 550 mm/min allow the underside of the first bead (i.e. the full bead depth) to transform prior to the arrival of the second bead (Figure 5-54). At higher travel speeds or reduced torch separation a point will arise at which transformation of the first bead full depth will not occur. In the current example this would be at a travel speed of approximately 1100 mm/min or a torch separation of approximately 40 mm. The combination of preheating, welding parameters, bug travel speed and torch spacing are consequently extremely important in the generation of the desired mechanical properties. The previous statement would hold true for a range of welding processes and conditions, but the narrow gap and alloyed weld metal relevant to the current work further exacerbate any potential property variation for the high strength requirements of X100.

The dual torch procedures with 100 mm torch separation gave tensile results falling virtually in the centre of the desired range from two quite differently alloyed consumables; 1.0Ni 0.4Mo (Thyssen MoNi) and 1.3Ni 0.25Mo 0.35Cr (Bohler X70-IG) (Table 5-17). The use of all the pipe material variants highlighted the consistency of the consumable chemistry/process combination for the tensile properties, regardless of pipe chemistry. A further alloy fully procedure tested, 1.5Ni 0.3Mo 0.2Cr (Elga Elgamatic 135), gave a result just under the proposed minimum $R_{p0.2}$, but this could be considered an anomaly due to previous trials attaining the required strengths. Yield to tensile ratios were high at 0.94 to 0.96, but perhaps surprisingly elongation values remained (relatively) high at 16 to 19%.

Toughness results were very good in all cases (Table 5-24 and Figure 5-44 to Figure 5-46), with weld metal average values always in excess of 50J at -60°C (often in excess of 100J at this temperature). The fusion line results highlighted a potential variance between the different pipe manufacturers; pipe C exhibited much lower impact toughness than pipes A, B15 and B19 at all temperatures tested (the latter three gave similar results). The impact transition curves again exhibited the maintenance of weld metal toughness over that of the fusion line with decreasing temperature (the weld metal average is typically greater than that of the fusion line at -40°C and below). CTOD properties followed those of the single and tandem tests; weld metal values were typically 0.16 to 0.26 mm and fusion line 0.25 to 0.40 mm. Most results were classified as δm.

Hardness results for the 100 mm separation (Table 5-17) were consistently below 350 HV10 for both average and maximum values. In only one case a maximum value in the

seam/girth cap HAZ exceeded 350 HV10. Comparison between the various pipes did not highlight any major differences between them, and a common trend of higher values (between 300 to 350 HV10) existed for the untempered cap seam/girth HAZ.

On the basis of the encouraging results achieved with a 100 mm torch spacing, it was decided to improve the practical welding aspect by reducing the torch spacing to the standard 50 mm. This allows greater consistency between the two torches for the CTWD and joint tracking. Bearing in mind the previous discussion and prior trials conducted with 50 mm spacing, a further test programme was conducted using various consumable chemistries (Table 5-9 and Table 5-11). The results indicated two potential wires; 1.8Ni 0.5Mo 0.3Cr (Thyssen Union X85) as highly overmatching and 1.3Ni 0.3Mo 0.3Cr (Elga Elgamatic 135) as just overmatching. Each consumable was also tested with two different gas mixtures; an 80% Ar/20% CO_2 mix with a 'conventional' bug travel speed, and a 50% Ar/50% CO_2 mix with a higher bug travel speed to compensate for the loss in strength assumed likely to occur with the increased CO_2 content (Table 5-14). All procedures were conducted in the same pipe material (pipe B15). Tensile results (Table 5-17) indicated that the 1.3Ni 0.3Mo 0.3Cr wire was not strong enough with either gas mix, whereas the 1.8Ni 0.5Mo 0.3Cr wire fell in the desired range with both gas mixes. In both cases the 80% Ar/20% CO_2 gave a higher tensile value, even though the arc energy was higher than for the 50% Ar/50% CO_2 mix. These results further the case for weld metal chemistry and joint geometry playing a decisive role in mechanical property generation, as opposed to minor changes in arc energy. Elongation values for the four welds were, on average, lower than for the 100 mm separation tests but are still at reasonable levels for the strength achieved (12.5 – 18.5%). Conversely the yield to tensile ratios were also lower than the 100 mm separation tests, with some of the lowest values achieved in all weld metal tests (0.91 to 0.92). This may be due to the lower cooling rates achieved with this pipe (the lowest wall thickness variant) in comparison with the other pipes, in combination with the particular cooling cycles involved.

Toughness results of the 50 mm torch separation again gave weld metal impact levels greater than 50J at -60°C (Table 5-24), but the fusion line results were typically much lower than those from their 100 mm separation counterparts in the same pipe material. This provides an indication of the base material sensitivity to considerable changes in heating/cooling cycles. The impact transition curves (Figure 5-46) show a marginal improvement in toughness levels using the less 'active' gas mix of 80% Ar/20% CO_2, with the resultant weld metal chemistries promoting this outcome in the higher recovery of Mn, Si and lower O_2. Due to the timing within the programme and the funds available, it was decided to test only the best of the 50 mm torch separation procedures for CTOD, with the result that the 1.8Ni 0.5Mo 0.3Cr (Thyssen Union X85) with 80% Ar/20% CO_2 joint was examined. Results from both the weld metal and fusion line were comparable to the 100 mm separation trials.

Average hardness levels (excluding seam/girth interactions) were below 350 HV10 in all cases (Table 5-17). The cap HAZ levels were slightly higher on average for the 50 mm separation compared to the same steel with 100 mm separation, which goes some way in explaining the lower toughness levels encountered. Considering the small (typically <2 mm) HAZ and consequent high rate of metallurgical changes possible, coupled with the relatively large indent spacing in this zone (0.8 mm apart), the HV indent value just adjacent to the fusion line provides the real key to any fusion line

property comparison. The maximum HV value stated in the tables usually occurs at this point. Seam/girth weld metal intersections show slightly higher cap HAZ values than the 100 mm separation equivalent, with average and maximum results typically between 350 and 360 HV10 for the steel examined (pipe B15).

The cross weld tensile results (Table 5-20) for both 50 and 100 mm torch separations nearly always failed in the parent material at UTS levels mostly greater than 780 MPa. In some cases the weld metal failure strengths were higher than parent material failures in the same pipe, highlighting the need for careful consideration of results. Nick break and side bend results were usually acceptable.

Weld metal chemistry results (Table 5-28) exhibit very similar alloy levels for the same wire used within a variety of different parent materials. A further comparison with the different processes used (e.g. Thyssen MoNi for single, tandem and dual torch) again shows no major effect of process change; small differences are discernable most probably due to shielding gas changes or batch-to-batch wire variation. This highlights the similarity in dilution effects between the three narrow gap processes examined.

Photo macrographs of typical dual torch weld sections are shown in Figure 5-17 and Figure 5-18; the typical mismatch often associated with the longitudinal seam weld is clearly shown in the latter. Microstructures of the cap (as-cast) weld metals are shown in Figure 5-35. The 100 mm separated torches do not exhibit very different microstructures from the 50 mm separated torches, which would be expected due to the similar mechanical properties attained. The alloying levels employed to generate the strengths in either case however are considerably different to account for the different cooling rates.

6.1.5 TIE-IN WELD PROCEDURES

Tie-in welding is an integral part of any pipeline construction that is required for river/road/rail crossings, branch connections, pipe diameter reductions etc., and therefore forms an important component of any suite of procedure welds obligatory to a construction project. For reasons outlined in Chapter 4, a rutile FCAW wire was selected for use in these welds to improve the productivity; a semi-automatic process has the advantage of continuous wire feeding. The same considerations of care in terms of heat input and welding practice are still required, and in this respect are no different to that of a fully SMAW procedure (particularly at the strength levels required). Rutile FCAW wires provide excellent positional weldability due to the slag system employed, coupled with a smooth arc characteristic.

The tie-in weld was made using conditions as close to those of real field welding practice allowable in a laboratory environment (see Figure 5-12). As per the mechanised narrow gap welds, adequate shielding gas cover is of prime importance in the field and should not be underestimated.

When the original procedure qualification test was conducted, relatively few high strength rutile FCAW wires were commercially available. A consumable guaranteeing a minimum $R_{p0.2}$ of 810 MPa via its AWS or BS EN etc. classification could not be found, but preliminary discussions with the manufacturers highlighted the improved strength levels potentially attainable with restricted arc energy. A conventional 60° joint was used for ease of root accessibility coupled with it being standard field practice.

The selected rutile FCAW consumable (2.7Ni/0.3Mo; ESAB Tubrod OK 15.09) did not overmatch the pipe SMYS by 120 MPa and results of 730-740 MPa $R_{p0.2}$ were typically obtained (Table 5-19). Weld metal toughness levels (Table 5-27 and Figure 5-42) were lower than for mechanised narrow gap welds, typically giving 70J at -40°C, but this is a direct consequence of the much higher oxygen levels found (Table 5-29). The oxygen is necessary in order to provide the smooth transfer characteristics associated with rutile based consumables, with the latter slag system providing the fast freezing required to support the weld metal in position (see Figure 5-13). CTOD levels were similar to those obtained from the mechanised welds, with the same trend in terms of the weld metal and fusion line discrepancy. The higher arc energies of 1.2-1.6 kJ/mm used in comparison to the mechanised welds did not however result in any great change with fusion line impact toughness levels. Hardness values (Table 5-19) in the HAZ followed a similar pattern to those of the mechanised welds, with all results well below 350 HV10. The cross weld tensiles (Table 5-23) all failed in the parent metal at UTS levels of 770-780 MPa, with side bend and nick breaks all acceptable. The cap pass microstructure is shown in Figure 5-36. The much larger grain size, compared with the narrow gap welds, indicates the greater arc energy and slower cooling rates apparent with this process. Although the as-cast microstructure is highly homogenous, it does not show any great evidence of bainitic constituents which consequently accounts for the lower strength levels observed.

In an attempt to improve the strength of the rutile consumable, the philosophy of a narrower gap increasing the strength as per the mechanised welds was utilised in conjunction with lower arc energies. A further rutile FCAW wire was acquired (2Ni composition; Oerlikon Citoflux 110) and a matrix of tests conducted (Table 5-31). Bevel geometries as low as 15° were used in conjunction with manual and mechanised torch positioning (Figure 5-23). A mechanised vertical up open root pass was developed with a metal cored wire due to the limited access available within the groove (extremely tight for a manual operator to prevent the contact tip touching the groove sidewalls). Whether this would be achievable for site fit-up is an important consideration given the small tolerances required of the procedure. The external clamps normally used to align the pipes also inhibit the easy transference of conventional mechanised technology due to the horizontal bridging of the joint area in numerous locations around the pipe. Pipe preheat/interpass levels were even reduced to between 20°C and 40°C in a further attempt to boost the strength levels. As the results show (Table 5-31 and Table 5-32), it would appear no major gains in strength are achievable with the rutile FCAW wires under investigation, and that the standard 30° bevel/semi- automatic procedure still gives the best result.

The question of overmatching for tie-ins requires careful consideration. If pipe yield strengths fall below 730 MPa it is likely that the weld metal $R_{p0.2}$ strength should overmatch, but this would involve pipe selection at tie-in junctions. Whether an absolute guarantee of overmatch is a precondition for construction should be a question for the design engineers; strain based design places the emphasis on the longitudinal strength of the pipe, for which the yield values are by default lower than their hoop counterparts, resulting in a possible lower girth weld yield criteria for guaranteed overmatching. Given respective Gaussian distributions for pipe and joint strengths, the envelope of over/undermatching will be somewhat defined[276].

6.1.6 *REPAIR WELD PROCEDURES*

The repair welds were predominantly assessed using hardness testing (Table 5-19); results were nearly always below 350 HV10; only those from the SMAW cap repair were above this value due to the low heat input and high alloy content. In this instance a lower alloyed consumable would be required to reduce hardness levels. It should also be noted that none of the repairs undertaken were considered for in-service situations where cooling rates are likely to be considerably different. The full penetration repair allowed a cross weld tensile, nick break and side bend test (Table 5-23), of which only the latter did not match the tie-in results. The part penetration repair allowed a side bend test; the failure was thought to be due to a root defect in the original mechanised weld still being present (this was not part of the repaired area). The impact tests conducted on the part penetration and full penetration welds (Table 5-27) all exhibited absorbed energy values of at least 70J at -20°C.

6.2 MECHANISED PGMAW NARROW GAP THERMOCYCLE CONSIDERATIONS

The numerous tests conducted up to this point highlighted the sensitivity of the joint geometry, alloying and particular process type used in determining the properties, with the result that thermal cycle measurement was deemed a useful tool in the prediction of mechanical properties via knowledge of the microstructural development. The successful qualification of a number of commercially available welding consumables allowed a suitable chemistry and joint preparation to be selected for the examination of the weld metal cooling cycles and their relationship to the resultant joint mechanical properties. Very little published data could be found with regard to narrow gap pipewelding using the low arc energies associated with mechanised GMAW, especially not with the wire chemistries and process variants suitable for high productivity welding of X100 linepipe. It was therefore hypothesised that experiments using both preheat and process variations would shed some light on this situation in order to examine the tolerance box for selected welding procedures.

6.2.1 *PREHEAT VARIATION TRIALS*

A technique to guarantee multiple thermocycle measurement from an initially molten weld pool using a single drilled hole thermocouple was successfully developed. The temperature measurements obtained from each deposited layer provided a comparison of internal and external thermocycles generated from the molten state, as well as the temperature profile of each underlying layer due to the deposition of the consecutive layers above. Disturbance of the heat flow surrounding the internally placed thermocouples was minimal (see Figure 4-19), attributed to the drilled holes being normal to the fusion line and as small as practically possible in diameter[221,230]. The high cooling rates associated with the mechanised GMAW processes used in pipeline construction require a high degree of sensitivity of the thermocycle measurement equipment in order to reliably capture the small cooling curve inflections generated through the transformation process. The relatively recent availability of high frequency/high resolution data capture equipment with multiple channel inputs at an affordable cost enabled greater accuracy than had previously been possible with in-situ

weld temperature measurement. Araujo[224] noted this effect in the inadequacy of his equipment to accurately record in-situ measurement, and consequently recommended the use of higher specification equipment. The ability of the data to be recorded digitally allowed easy manipulation of the numerous files generated throughout the research, especially in terms of inflection point analysis.

Figure 5-49 to Figure 5-51 exhibit the thermocycles for all three preheat variants undertaken, each graph representing a particular weld run. The 30 in. pipe chosen for the preheat variation trials used a manually deposited internal TIG run, and as such did not contain the same consistency of penetration/internal reinforcement as a mechanised internal root. The main effect of this was to change the depth of hole required at any given position within the pipe circumference to reach the required layer surface, but as the depth of deposition changed around the pipe due to the fixed position of welding (i.e. gravity affected the deposition depth) this effect was potentially only noticed for the variation in temperature measurement on the internal root surface. A typical longitudinal section along the weld mid thickness showing the proximity of the individual internal thermocouple locations is shown in Figure 5-26.

Weld metal cooling times from 800°C to 500°C (t_{85}) are a well established means of gaining an understanding of the weld metal mechanical properties, particularly strength and hardness. In the case of the preheat trials transformation start and finish temperatures were typically between 400°C and 550°C, rather than a more conventional 550°C to 700°C experienced with conventional manual welding processes and chemistries together with a 60° included angle joint geometry. For this reason it was decided to gather cooling times from 800°C to 500 (t_{85}), 400 (t_{84}) and 300°C (t_{83}), such that the latter two temperatures would ensure the inclusion of the transformation event. The cooling times are shown in Table 5-33 to Table 5-35, and graphically in Figure 5-58. These were obtained from the 50th order polynomial fit of the raw data using Matlab software; the original data contained a degree of scatter due to digitisation and electromagnetic interference, but as shown in Figure 5-60(a), this was usually below 3°C, but for ease of obtaining times at 800, 500, 400 and 300°C the polynomial was used. The order chosen was determined by examination of the raw data in conjunction with the polynomial fit for a selection of orders (see Figure 5-60(d)); a 50th order fit appeared to give a good compromise between over- and underfitting for the large range of curves examined. It was found that considerable data above and below the transformation event should be incorporated into the cooling curve fitted length, as this enabled spurious data at the start and finish of the subsequent differential curves to be ignored, leaving 'true' data around the transformation event of interest. Hence the use of curve fitting between 1000°C and 300°C.

It is evident that cooling times decrease as the overall deposited depth increases, until the pipe mid wall thickness (Fill 2/3) is reached, at which point the cooling times increase. This can be explained in terms of the heat conduction path; heat is most efficiently extracted from the cooling weld bead when the surface area of the deposited bead in contact with the surrounding material and the distance of the bead to the pipe surface are both maximised, hence the first (hot pass) and last (cap) beads cool at a slower rate in comparison to the inner beads. The peak temperatures attained from the individual thermocycles for a given weld pass follow a similar pattern in that higher peak temperatures are reached at the inner and outer surfaces of the pipe. It should be noted though that the deposition depth (i.e. layer thickness) decreases from the inner to

outer surface due to the increasing gap width, resulting in the layer base thermocouples (excluding the one monitoring the cooling from liquid) becoming increasingly closer to the fusion line of the deposited layer. Although this effect masks a direct comparison of peak temperatures for the individual underlying layers, a degree of correlation can be expected with that of the molten bead cooling times. As would be expected, both the cooling times and peak temperatures of the underlying layers increase as the preheat level escalates due to the reduced driving force for heat extraction.

The question of heat flow within a given welding situation was initially examined by Rosenthal[233,350]. Equating the thin (2 dimensional) and thick (3 dimensional) plate heat flow solutions to his equation allows a boundary condition to be derived for the critical plate thickness for the change from one regime to the other[177]:

$$d' = \left\{ \frac{q}{2\rho c v} \times \left(\frac{1}{773 - T_o} + \frac{1}{1073 - T_o} \right) \right\}^{\frac{1}{2}}$$

where d' = boundary condition thickness between thin and thick plates (m)

q/v = arc energy (Jm^{-1})

ρc = volume thermal capacity ($Jm^{-3}K^{-1}$) = 4.5×10^6 for carbon steel

T_o = preheat temperature (K)

Using an arc energy of 5×10^5 J/m (0.5kJ/mm) and preheat of 373K (100°C) results in a d' of 14.8mm. All of the tests conducted within this research involved pipe wall thicknesses greater than this amount, and whilst a bead on plate weld would be considered as resulting in three dimensional heat flow the absence of material bulk below the first few runs in the groove considerably reduces the available heat sink. This has the effect of introducing a two dimensional heat flow regime for the early runs. Increasing the preheat to 180°C results in a d' of 16.2mm, but the same effect in terms of reduced heat sink promotes two dimensional heat flow for the majority of weld passes.

A common feature between the temperature measurements of the molten beads is the ability of the externally plunged thermocouple (i.e. layer surface) to exhibit faster cooling times over the t_{85}, t_{84} and t_{83} ranges than the internal (i.e. layer base) equivalent (see Figure 5-58). This effect is not immediately apparent if the global cooling curves for the three preheat variants are observed for a given layer (see Figure 5-57), but close examination of the cooling times shows a consistent trend. This may be due to the less intrusive surface thermocouple, where ideally only the limb material enters the weldpool. The layer base thermocouples invariably result in the molten pool 'sitting' on the Al_2O_3 thermocouple insulation sheath, which may reduce the cooling rate due to heat build up on and around the ceramic (which is a poor conductor of heat at temperatures below 1000°C).

The transformation temperatures determined via differentiation of the original cooling curves are shown in Table 5-33 to Table 5-35, and graphically in Figure 5-62 and Figure 5-63. A similar pattern to that of the cooling times was observed for the transformation temperatures, especially for the layer base thermocouples. Transformation temperatures close to the inner and outer surfaces were very similar for all preheat variants using data from the layer base thermocouples, but a considerable increase of the observed

transformation temperatures occured with increasing preheat temperature for the inner layers. Overall lower transformation temperatures were observed for the layer surface thermocouples in comparison to their layer base counterparts, tying in with the shorter cooling times observed for the former. The maximum rate of transformation occured between 430°C and 530°C, depending on the preheat level and particular weld layer, although the temperature range from start to finish of transformation was relatively constant at 60°C to 80°C.

Figure 5-64 and Figure 5-65 show the cooling rates (°C/s) obtained at 800°C, 600°C and 400°C from the 1st order differential curves of the polynomial fit. In theory the graphs should exhibit the inverse effect for the transformation temperature or cooling time curves. This trend was certainly observed, although the maximum rates of cooling have been displaced to layers lower in the fill sequence than the transformation temperatures/cooling times would suggest. The ability to distinguish the thermocycle differences associated with the various preheat levels, particularly at 800°C and 600°C, was also much clearer from these measurements. For example, at 600°C the external thermocouples record typical cooling rates of between 100-160°C/s for no preheat, 60-130°C/s for 100°C preheat and 40-80°C/s for 180°C preheat.

Table 5-40 and Figure 5-28 show the results of the tensile tests; the high strength values obtained in comparison to other tests using the same consumable and arc energy were a direct result of the reduced gap width employed (6.0-6.5mm cap gap width) and the consequent high cooling rates achieved. The strength attained from the 180°C preheat weld still met the proposed weld metal criteria ($R_{p0.2}$ 810MPa min.) and was equivalent to the value obtained from a standard (7.0-7.5mm cap gap width) bevel configuration using 100°C preheat. Elongation values exhibited levels in excess of 14% with consistent yield to tensile ratios of 0.94-0.95. A consistency check was performed with the testing of another tensile specimen from the 100°C preheat weld; the spread of $R_{p0.2}$ results (3 MPa) was well within likely experimental scatter.

Representative microstructures from the three preheat variants are shown in Figure 5-38; the increase in grain size was clearly evident as the cooling rate decreased with increasing preheat. The major microstructural constituents were classified using optical microscopy as shown in Figure 5-39, and although the classification is relevant in comparative terms for the variants examined, the true distinction of the lower transformation temperature products (martensite, upper and lower bainite) is only really possible using TEM[(294)]. The resultant microstructural classification exhibited in Figure 5-31 however provides a useful insight into property variation between the trials. As would be expected the lowest preheat variant contains a high proportion of 'martensite', whereas the highest preheat mainly comprises acicular ferrite. An important consideration however is the reheating effect of each pass on the previous ones. Classifying the microstructure within these areas is usually limited to refined and unrefined weld metal due to the complexity of microstructural variation, although it is from these areas that most mechanical specimens are taken i.e. from the bulk of the weld metal thickness.

In response to the uncertainty of microstructural classification, it was decided to undertake microhardness traverses encompassing the various weld layers to compare with the tensile and impact properties. Figure 5-70 shows the individual microhardness traverses undertaken with the various preheat welds; the pipe OD, ID and weld metal

interun fusion boundaries marked. The degree of hardness variation is observed to increase with decreasing preheat temperature, alongside the average hardness level increasing (see Table 5-46). This implies that the as cast microstructure type predominant in the lower preheat variants (i.e. lath ferrite/martensite) is far more susceptible to tempering effects than the higher preheat variant microstructures, resulting in the observed scatter of the former. The relative position of the tensile test gauge area within the various weld metal layers therefore plays a more significant role at lower preheat temperatures, and reinforces the notion of acquiring the maximum weld metal depth for obtaining realistic through thickness weld metal properties. The high individual hardness levels (>340 HV0.5) experienced with the 100°C and no preheat conditions show that local areas of low transformation temperature products exist, even with each previous layer reheated to at least 300°C. This effect would probably be masked by the use of a conventional higher load hardness test (e.g. HV10) sampling a greater area/volume, but the occurrence of high hardness areas should be borne in mind with respect to potential crack initiation from defects and inclusions.

6.2.2 PROCESS VARIATION TRIALS

The four narrow gap mechanised welding systems currently in existence or in the later stages of development were used to generate thermocycle and mechanical data in the most comparable fashion possible. The pipe wall thickness remained the same as for the preheat trials, along with the wire feed speed (10 m/min for all passes). The arc energy per torch (weldpool) however, was reduced slightly on account of the higher travel speed required of the dual torch/dual tandem torch process variants to avoid 'roll-over' and lack of fusion defects due to the chosen wire feed speed. The chance of defects occurring were minimised by maintaining the welding head(s) at the 12.30-1.30 position using counter-rotation of the pipe to that of the bug travel. As a result, deposition depths per layer were constant along the weld length, allowing good correlation of thermocouples measuring the same thermocycle at different locations around the pipe circumference. Deposition rates and arc energy per torch were identical for all layers and processes, and in conjunction with the same joint geometry for the two pipe pups used in the experiments a high degree of comparison could be achieved between the various processes. Photo macrographs of the four process variant weld sections are shown in Figure 5-27. It was immediately apparent from the macrographs the similarity existing between the single and tandem processes, with a similar comparison existing for the dual torch and dual tandem torch processes. Macroscopically this was to be expected due to the general similarity of the heating/reheating cycles between the two groups. The overall similarity in weld metal deposition/dilution between the four processes provides for easy integration/acceptance of the new processes (tandem and dual tandem) in terms of regulatory approval and conformance with the existing codes and standards.

An important difference between the preheat and process variant trials was the change in power supply due to the synchronisation requirement of the tandem welding process. When a single Fronius power supply was used, the degree of scatter observed in the thermocycle traces was very similar to that of the Lincoln (see Figure 5-60 (b)), but as soon as the tandem torches were in operation the degree of electromagnetic interference increased significantly (see Figure 5-60 (c)), even though considerable earthing of the thermocouple data capture equipment was employed. The polynomial fitting of the raw

data however provided curve smoothing and consequently allowed easy extraction of comparative data (Figure 5-60 (a,b,d)).

Thermocycle curves for each layer deposited are presented in Figure 5-52 to Figure 5-55 for the four process variants examined. It was immediately apparent that the minimum temperatures experienced by each underlying layer were somewhat higher than for the equivalent preheat trial, but this could be explained by the reduced deposition depth per layer caused by the higher travel speed and wider joint width (an extra layer was consequently deposited in the single and tandem torch trials). The single wire thermocycles exhibited a minimum reheating temperature for each underlying layer to that just deposited of at least 500°C (NB thermocycle of fill 1 due to fill 2 was not recorded). This compared with a minimum temperature of 400°C for the preheat trial equivalent.

The tandem wire thermocycles, whilst exhibiting virtually identical arc energies to that of the single wire weld during deposition, showed an increased minimum reheat temperature of at least 600°C for the inner (internal root) and penultimate (fill 5) passes. Whilst there was a small (<2mm) change in reinforcement of the internal root run around the pipe circumference between the two trials, the temperature increase was still thought to be a real effect of the process rather than an artefact of the experiment (NB TC5; hot pass base thermocycle is somewhat dubious given the higher temperatures attained by the internal root surface thermocouples TC3 and TC4). The inner passes experienced minimum reheat temperatures similar to those of the single wire weld. As for the single wire thermocycles, the tandem thermocycles showed that all underlying layers were reheated to at least 200°C. The higher temperatures experienced by the underlying weld bead at the inner and outer pipe surfaces may be due to an increased heat input effect of the tandem wire process over that of the single wire, which is more apparent at these locations due to the reduced heat sink effect of the surrounding material. Both the tandem and dual tandem internal thermocouple placement also required positioning at a greater depth below the surface to be welded in order that the thermocouple would survive the passage of the arc and still obtain the cooling curve from the molten steel temperature. This again reinforced the theory that a greater heat input was achieved with these processes.

Both the dual torch and dual tandem internally measured thermocycles recorded the reheating effect of the second torch as it passed over the layer deposited by the first torch. In both process cases an extra layer was incorporated in the procedures such that every weld pass resulted in deposition from both torches (the single and tandem procedures contained an odd number of passes). This resulted in rather more reinforcement than would be required/allowed in the field, but was justified in terms of academic interest. Due to the two layer deposition for each bug pass, it was not possible to record the first layer externally measured thermocycle or second layer internally measured thermocycle from the molten state. Subsequent passes for the latter thermocycles were recorded by drilling to the calculated fusion line using the deposition depth data recorded from each pass. Consequently the thermal history at the base of each layer could be gathered from the subsequent passes above (Figure 5-54 and Figure 5-55). The reheating effect of the second torch increased the maximum temperature observed at the base of each layer two deposition depths below the surface of the first torch. The internally recorded layers above this point exhibited a higher temperature due to the heating effect of the first torch; this can be explained in terms of the relative

proximity of the thermocouple in relation to the heat source in conjunction with the thermal capacity and distribution within the surrounding metal. This effect was apparent in both the tandem and dual tandem trials.

The first layer of each dual torch pass (for the particular arc energy and torch separation examined) initially cooled to between 300°C and 400°C, and from the data exhibited in Table 5-38 and Figure 5-66 (initial cooling) it can be seen that transformation will have completed prior to any retransformation occurring due to the second torch reheating effect. Reheating above the retransformation temperature occurs for the whole depth of the first torch bead as evidenced by the secondary cooling curve deflection from the standard exponential decay. The second torch t_{85} etc. cooling times are also significantly increased (see Figure 5-59) due to the preheating effect of the first torch (in the dual torch case examined this will be at least 300°C for all secondary layers). The increased time spent within the γ and α region of the transformation diagram for the given alloy increases the resultant grain size (see Figure 5-37), with a concomitant decrease in strength level (see Figure 5-29).

The cooling curve situation exhibited by the dual tandem trial was similar in global terms to that of the dual torch, the main difference being the shorter time period of a given point between the passing of the first and second torches. This effect produced a preheat level for the second tandem torch bead of at least 500°C, which in turn resulted in the first torch bead being untransformed for its whole depth prior to being reheated by the second torch. As a consequence the cumulative time spent above the Ar_1 is the greatest of all the process variants, and although the cap pass grain size (see Figure 5-37) does not appear to be significantly different to the dual torch trial, the resultant mechanical properties showed a significant change (discussed later).

The t_{85}, t_{84} and t_{83} cooling times (Table 5-36 to Table 5-39 and Figure 5-59) exhibited similar characteristics to those generated from the preheat trials i.e. the fastest times occured in the middle of the pipe wall thickness. The single and tandem wire variants were very similar and exhibited a comparable effect to that of the preheat trials; the layer surface cooling times were faster than their layer base equivalent. Due to the reheating effect of the second torch for both the dual and dual tandem torch trials complete data for all the cooling times were not acquired, but it was clearly demonstrated that the significant preheating effect of the first torch pass increased the cooling times to levels at least twice that of the single or tandem wire equivalent.

The transformation temperatures (Figure 5-66 and Figure 5-67) followed a similar pattern to that of the cooling times for the various processes. The single and tandem temperatures illustrated very similar data from the layer surface measurements (~10°C increase for all tandem transformation temperatures), but a divergence in the layer base measurements with the outer runs was discernable, possibly due to a higher heat input effect of the tandem process. Both the dual torch and dual tandem torch exhibited overall higher transformation temperatures for the layer surface measurements, as would be expected from the increased preheat level/decreased transformation driving force. The dual torch layer base cooling curves allowed a comparison of initial and secondary (post-reheat) cooling; the initial cooling transformation temperatures should have followed a similar pattern to that of the single wire weld, but transformation start temperatures were observed to be 10°C to 20°C lower than the latter (for the runs in the middle of the pipe wall thickness). A possible explanation is the level of uncertainty

created by the differential curves when the area of interest is close to the extremities of the data set (see explanation in Chapter 4 for curve fitting over the transformation event). The secondary cooling curves however displayed a similar pattern, but with the transformation start temperatures displaced to slightly higher levels.

The cooling rates again illustrated very similar results for both the single and tandem wire trials, with the difference observed between the layer base and layer surface measurements from the rate data even more evident than with the cooling time data (see Figure 5-68 and Figure 5-69). The dual torch and dual tandem torch data from the layer surface measurements were again comparable with each other (particularly at 600°C and 400°C). The initial cooling of the dual torch layer base measurements followed a similar pattern to the single and tandem torch welds across the various layers recorded, but the overall rates were displaced to lower levels. This may again be due to the reason highlighted in the previous paragraph in terms of the level of uncertainty.

The tensile tests (conducted in the same manner as for the preheat trials) confirmed the cooling time/rate and transformation temperature similarities and discrepancies between the various processes. The single and tandem wire results (Figure 5-29) were identical within experimental scatter, with a considerable reduction in strength observed for the dual torch and dual tandem tests. The latter showed the lowest overall strength as would be expected from the process maintaining the greatest time for each layer at temperatures above Ar_1. The similarities between the cap microstructures for the single and tandem, and between the dual torch and dual tandem torch variants (Figure 5-37) did not warrant a point counting exercise, but as for the preheat trials a microhardness survey was considered to provide useful quantitative data for correlation with the tensile tests. Results are shown in Figure 5-71; a similar effect was observed as for the preheat trials – the slower the cooling rate/greater the time above A_{r1} the less scatter within the results and the lower the overall hardness levels. Although the average hardness levels between the single and tandem, and between the dual torch and dual tandem torch welds were identical within experimental scatter, a clear reduction in scatter was observed from single to tandem to dual torch to dual tandem. This phenomenon can again be attributed to a change in the overall percentage of lower transformation temperature products coupled with differing levels of refinement/reheating due to the particular thermocycles in evidence for the given process.

Charpy impact testing of the weld metal was performed at -20, -40 and -60°C from the pipe mid-thickness, with results shown in Table 5-41 and Figure 5-30. The overall impact toughness levels exhibited at least 60J average at -60°C for all processes. The single wire results at -20°C and -40°C should be considered as upper shelf values; the apparent reversal in average values can be attributed to scatter within the upper shelf banding. The comparative reduction in toughness exhibited by the tandem weld in comparison with the single wire weld is surprising considering the similarity of all other data gathered. Higher nitrogen levels within weld metal are known to reduce impact toughness results[258-260]; the tandem wire process used in the trials may require improved gas shielding to cope with the larger weld pool/greater travel speeds/potentially more turbulent weldpool and metal transfer in use. Unfortunately chemical analysis data for all of the individual preheat and process trials were not available (a selection are shown in Table 5-42), so it was not possible to confirm/deny any effect due to chemical variance between the processes. The small sample size at each temperature is another possible cause of variance, but scatter levels are minimal at

-60°C whilst maintaining an overall trend for each variant, thereby promoting the observed mean values in being representative of a true mean value. The dual torch absorbed energy values mimic those of the single wire, whilst the tandem and dual tandem results are both displaced to (similar) lower values at each temperature. The difference between the dual torch and dual tandem torch values reflects the reduction in strength between the two variants. The slightly larger mean grain size expected within the dual tandem microstructure, due to the greater time above the Ar_1 temperature, may explain the slightly lower toughness levels experienced at -20°C and -40°C. A trend of lower toughness exhibited by the tandem processes over the single wire per torch variants however may partially be explained by the nitrogen argument highlighted above.

6.3 ALLOY DEVELOPMENT FOR NARROW GAP HIGH STRENGTH WELD METAL

The commercially available GMAW consumables investigated in the earlier experiments involved significant steps in alloy chemistry in order to initially examine the tolerance box for a single wire process or allow a significant change of an essential variable e.g. torch separation, and still maintain the proposed target values. The development of GMAW consumables to meet the simultaneous demands of increased yield strength, high toughness and low hardness at the most economic price possible is an extremely complex challenge. The consumable manufacturers need to cover a considerable range of strength and toughness levels, and for economic purposes need to achieve this with the minimum number of consumable chemistry variants. The basic grouping of consumables relevant to a particular strength level are usually achieved via their classification to an applicable standard e.g. AWS 5.28 or BS EN 440, but the chemical ranges allowed within a given group usually require significant 'tightening' in order to produce consistent mechanical properties from the resultant weld metal classification test. Batch-to-batch chemical variation of present day consumables from reputable manufacturers is very low (typically $< \pm 5\%$ for major alloying elements). As a result, the minor alloying changes that were thought to be of significance for a chosen base-line chemistry (e.g. ±20-50%) at the fast cooling rates/times in evidence with the mechanised narrow gap processes could not be obtained as a commercial product from a single manufacturer (the latter point is significant in terms of maintaining the same level of trace elements). From this standpoint it was decided to examine specific weld metal chemistry variants for use in a narrow gap situation, the results of which are discussed in the following sections.

6.3.1 WELD METAL CHEMISTRY

In common with the preheat and process thermocycle measurements, the base-line chemistry chosen was 0.9Ni 0.3Mo due to this composition's fulfilment of the narrow gap single wire proposed weld metal properties. An initial batch of the metal cored consumable (MC control 1) was welded to check chemistry and strength levels (see Table 5-43 and Table 5-44); the results indicated a slight decrease in C and increase in Ni were necessary to reach the desired ranges. The revised control (MC control 2) used as the basis for all other alloy variants improved the carbon and nickel levels, but these still tended to respectively slightly undershoot and overshoot the target values. The

variation between the major alloying elements (when desired to be kept constant across the various compositions) however was small; 0.01 wt.% for C, 0.1 wt. % for Mn, 0.05 wt% for Si, 0.1 wt. % for Ni, and 0.03 wt. % for Mo. This amounted to a percentage change on the total concentration of each elemental group average of no more than 12%; considering elements were varied when required to do so by at least ±20% of their control value (often significantly more), the observed scatter in the 'unchanged' elements was judged to be at a low enough value so as not to affect the deliberate elemental change being studied. It should also be borne in mind that increasing or decreasing a given element affects the recovery of associated elements, such that normal consumable development requires several attempts (using the envisaged welding conditions) to attain the correct consumable chemistry balance. This luxury was not available at the time of the research, hence a degree of scatter for the 'unchanged' elements in a given trial was expected, but these fell within the small levels highlighted above.

The main aim of the control sample was to mimic the chemistry of the Oerlikon Carbofil NiMo-1 solid wire. This was achieved to reasonably close levels, although the carbon content of the metal cored wire was consistently higher (typically 0.005 – 0.01 wt %) than the solid counterpart throughout the series. The trace element levels were all very similar except copper and oxygen. A copper coating on the solid wire is normal practice to aid contact/feedability and reduce potential for rusting, but due to the manufacturing process of the cored versions (seamed) this process could not be applied. The change in level though between solid and cored was judged to be of no significance. The other major change was that of oxygen; the levels in the metal cored wires were typically twice that of the solid wire. This is a direct result of the powdered constituents (high surface area ≡ high oxide content), and although powerful deoxidants such as magnesium, titanium, aluminium and zirconium can be added, this is generally not performed due to the associated loss in physical weldability (smooth arc and fine droplet transfer) epitomised by metal cored wires. This has a significant effect on toughness which will be discussed in the next section.

The alloy changes desired of the carbon, nickel, molybdenum and chromium levels fell either within or very close to the (tight) target ranges desired (see Table 5-43).

6.3.2 BASE-LINE CHEMISTRY COMPARISON OF SOLID AND METAL CORED WIRE PLATE PROCEDURES

A comparison of the metal cored wire with that of the solid wire chemical equivalent exhibited a decrease of approximately 40MPa for the $R_{p0.2}$ values of the metal cored wire (see Table 5-44). This was surprising given the very close similarity in alloying and weld procedure. Carbon, one of the most effective strengthening elements per weight percentage, was even slightly lower in the solid wire. A comparison of microstructures (see Figure 5-73) though revealed a slightly higher aspect ratio (more 'bainitic') structure in the solid wire compared to the metal cored equivalent. This is only apparent at the high magnification required to study the microstructures; the low magnification used to see the prior austenite grain size revealed little difference between the two (see Figure 5-74). The layer surface thermocycles were recorded for both the solid and metal cored chemical equivalents in the same fashion as per the earlier preheat and process trials, as a further check on potential differences between the consumable

types (see Table 5-47). Although the global cooling curves between the solid and metal cored wires appear very similar for each layer deposited (see Figure 5-75), closer examination of the transformation temperatures (Figure 5-77) and cooling rates (Figure 5-78) explain the observed microstructural and strength differences. The solid wire exhibited both higher cooling rates (at 800 and 600°C) and lower transformation temperatures than the cored wire, confirming the production of a more 'bainitic' microstructure for the former. The cooling times from 800°C to 400°C and 300°C (Figure 5-76) though did not substantiate this effect due to the similarity of the data. This is thought due to the major differences in alloy development for these chemistries and cooling rates occurring at temperatures greater than 400°C, hence the similarity of all data below this temperature. The major differences between the solid and cored wire plate weld equivalents were the wire diameter, welding waveform and resultant weld metal oxygen content. The former two features may result in a different heat input even though the calculated arc energies were extremely close, whilst the latter is known to affect microstructural development through the nucleation and growth effects due to oxide inclusions. The effects of increasing oxygen levels within weld metals are well documented in terms of toughness decreases (above ~200ppm O_2)[164,174,177,180,181,188-193], but a similar effect on strength and hardness observed between the two consumable types may be due to this as well, either alone or in combination with a variation in energy transfer efficiency (heat input). Any change in the weldpool shape/fusion boundary surface area due to the latter may also have an effect on microstructural development due to the size and number of precipitates. The desorption of oxygen resulting in inclusion precipitation has been proposed to occur at the greatest rate in the boundary layer at the rear of the weldpool and in the subsequently solidified weld metal[147], thereby influencing the final microstructural development.

The same type of effect for the plate weld thermocycles as for the pipe welds were observed regarding the change in cooling time, cooling rate and transformation temperature graphs for the given layer deposited, although the presence of a backing bar increased the heat sink for at least the first weld pass. This had the effect of reducing the overall concavity or convexity of the above mentioned graphs in comparison to the pipe welds. The cooling times and transformation temperatures were lower, and the cooling rates higher in the single wire thermocycle pipe weld compared to the solid wire plate weld, but it was noted that the arc energies of the former were somewhat less due to the higher travel speed employed (0.44 kJ/mm average vs. 0.52 kJ/mm average). Although the greatest care in experimental set-up and procedure was taken with the plate welds in order to mimic the pipe welding situation, it was likely that the exact same (high) degree of heat sink for the runs in the middle of the material thickness (where the majority of mechanical properties were obtained) would not be achieved in the plate welds. This was most probably due to the combination of backing bar and restraining jig, and although it was desired to equate the results of the plate tests to the pipe situation without a factor being required, the resultant change in strength and hardness for the equivalent chemistry, preheat and arc energy (weld ML-B15-1) was still less than 5% (much smaller than nearly all of the observed changes due to the alloy variation series).

6.3.3 EFFECT OF WELD METAL CHEMISTRY ON MECHANICAL PROPERTIES

All-weld metal tensile, hardness and impact toughness measurements for the alloy variant plate trials are recorded in Table 5-44 and Table 5-45. An idea of the variability

of tensile strength measurements for the series was attained from the metal cored control weld chemistry; four identical tests were undertaken from two plate welds, giving an $R_{p0.2}$ spread of 13 MPa (average value 868MPa, standard deviation 4.95) and an R_m spread of 20 MPa (average value 916 MPa, standard deviation 8.61). The tight banding of this group with respect to the alloy variation trials justify the latter's change in observed strength levels from those of the control chemistry as being a true effect, and not one clouded in issues of value uncertainty for the chemical changes investigated.

Strength levels were observed to change in a classically increasing fashion for all addition increases, except with the molybdenum variants (see Figure 5-79). The latter showed a slightly higher strength for the lowest addition compared to the control (mid-level of Mo). It is thought that for this element the percentage change between the variants was not enough to observe a trend.

Trends due to alloying effects on impact toughness levels (Figure 5-80) were not easy to determine, predominantly due to the small (typically less than 20J) difference over the individual elemental ranges examined. The small sample size for each variant and temperature tested coupled with the inherent scatter due to the nature of the test also reduced the chances of trend determination. Observation of the scatter levels highlighted an average absorbed energy range at all temperatures tested for the metal cored wire series (bar the initial control test) of 10J (see Table 5-45), hence the difficulty in determining any trends when the range over the alloy change was of a similar amount (as for Mo and C). The increasing level of chromium is the only alloy series to demonstrate the expected decrease in toughness due to the increase in hardenability. Increasing Ni levels in steel are normally associated with improvements in toughness, but the highest addition (1.3Ni) exhibits a significant drop in toughness, most likely due to the (overriding) increase in hardenability observed through the strength and hardness change for this series. This highlights the judicious balance of elements required when improvements in e.g. strength are desired so as not to deteriorate other properties e.g. toughness at a similar rate. The elemental balancing effect was demonstrated with the alloy variant chosen to increase the carbon and concurrently decrease the molybdenum level (0.11C 0.8Ni 0.1Mo) compared with the control chemistry (0.09C 0.8Ni 0.3Mo). A slight increase in strength and hardness was observed without any loss in toughness (at -40°C and -60°C).

In order to determine the effectiveness of a given alloy by its weight percent addition on strength and toughness, the vector diagram shown in Figure 5-81 was compiled from the data generated through the various individual alloy increments. It is clearly apparent that carbon exhibits the greatest effect on strength with the added bonus of no apparent change in impact toughness. Chromium, whilst significantly increasing strength, promotes a concomitant reduction in toughness, with nickel following suit to a lesser extent. As discussed earlier, the effect of molybdenum within this series did not allow conclusions to be drawn, most likely due to the alloy content variation being too small. It should also be noted that the vector diagram results are only applicable within the ranges examined for the relevant alloy series studied.

6.3.4 *EFFECT OF WELD METAL CHEMISTRY ON MICROSTRUCTURE*

The cap pass microstructures from all the alloy variants were studied at the highest available optical magnification (1000 times), and the photomicrographs shown in Figure 5-84 to Figure 5-88 record the various morphologies observed. Whilst point counting can provide a more general explanation of any trends experienced, it was decided not to pursue quantification of the microstructure via this method after an initial examination of the alloy variants exhibited a reasonably high degree of similarity. The same arguments put forward for the girth weld and process trials, in terms of applicability of point counting results to the actual mechanical properties generated, were relevant for the plate welds. The area from which most of the mechanical data was extracted incorporated considerable reheating of the as cast weld, such that the microstructures recorded in the various figures (as-cast weld metal) form only a percentage of the total sampled within an impact , hardness or tensile specimen. Accurate description of these microstructures using optical methods is also extremely difficult due to the close similarity of the lower transformation temperature products and fine grained nature of the bulk morphology[294,295].

Whilst the photomicrographs only exhibited a small area of that available to study in the cap pass (due to the high magnification required vs. the available recordable area), the following observations were based on a written record of a larger cap pass area taken during sample examination. General trends in microstructure were observed with most of the individual alloy series which compared well with published data on microstructure/mechanical property relationships[174-179etc.]. Increasing levels of carbon, nickel and chromium all exhibited a reduction in grain size, explaining the increase in observed strength values. This was most prevalent with nickel, which also explained the largest strength increase observed for the alloy ranges studied. A reduction in primary (grain boundary) ferrite with increasing nickel was also apparent (Figure 5-84), and in combination with the decreasing grain size, an increase in impact toughness may have been expected had the addition of more 'bainitic/martensitic' components of the microstructure not occurred in a parallel fashion. The molybdenum series of welds (Figure 5-86) exhibited the smallest change in microstructure; a slight decrease in grain boundary and side plate ferrite coupled with a minor reduction in overall grain size was evident with increasing Mo content. This confirmed the minor change in mechanical properties experienced for the series. The highest chromium addition (0.5 wt. %) corresponded with the finest grain size of all the alloy variants (see Figure 5-85), and coupled with the high aspect ratio constituents (martensite/bainite) explained the highest strength/hardness levels and lowest impact toughness recorded across all variants. Raising the carbon levels exhibited the smallest increase in high aspect ratio constituents, although the overall grain size decreased (see Figure 5-87) thereby explaining the increase in strength without an obvious loss of toughness. The high carbon, low molybdenum alloy exhibited a slightly smaller grain size but without an increase in high aspect ratio constituents (see Figure 5-88(a)), resulting in the observed strength increase and toughness maintenance compared to the control chemistry. The low carbon, low silicon, low molybdenum, high nickel alloy exhibited the greatest change in microstructural appearance of all the alloys investigated (see Figure 5-88(b)). Although the microstructure contained a large proportion of very high aspect ratio constituents in combination with coarse primary ferrite and an overall larger grain size

than the control chemistry, the reduction in both strength and toughness was less than might be expected with this morphology.

6.4 EFFECTS OF WELD METAL CHEMISTRY AND WELDING PROCEDURE IN GENERATING GIRTH WELD PROPERTIES SUITABLE FOR X100 LINEPIPE

The following section combines the data analysis of the various experiments undertaken within the research and discusses their implications. Special attention has been paid with respect to their practical implementation for the girth welding of X100 linepipe.

'X100' strength linepipe has evolved independently within several leading high quality pipeline manufacturers, all of whom have their own philosophy on the optimum chemistry and production route. The last fifteen years in particular have seen significant developments in property achievement[1,3-10], predominantly brought about by interest in the product from several gas owner/operator companies. The standardisation of pipe at this strength level is presently under-way, with several of the leading standardisation bodies (e.g. API and ISO) currently employing working groups on the subject. Whilst considerable effort has been expended in the pipe material properties and longitudinal seam welding capability, very little in terms of girth welding research results have been published to date. This is most probably a direct result of the manufacturing companies' reluctance to provide pre-production pipes to 'outside' institutions capable of conducting the investigations, until such time that the internal company confidence level in the product had been achieved. This point in time coincided with the current research programme for several linepipe manufacturers.

Considerable girth welding research has, however, been conducted on X80 strength linepipe, which is widely commercially available and in common use by certain owner/operator companies[276,277,279,281 etc.], providing a base line for the X100 weld metal research presented here. The girth weld metal metallurgy for pipe strengths up to X80 is well documented, and a microstructure consisting predominantly of acicular ferrite generates the required strength with high levels of toughness. This is achieved through a careful balance of alloying and de-oxidising elements, in combination with the low heat inputs and high degree of refinement associated with mechanised GMAW. As the linepipe strength increases, the weld metal strength needs to increase at a similar rate. This is mainly achieved through an increase in the volume percentage of lower transformation temperature products such as bainite and martensite. These in turn are generated predominantly through increased levels of substitutional solid solution strengthening elements such as chromium, molybdenum, nickel and manganese, all of which have been examined to various extents in the current research. It has also been demonstrated by the girth welding experiments and procedure tests conducted within this research that the standard welding and bevel preparation equipment currently used for pipeline field construction is suitable for X100. During the course of the programme, information resulting from the research fed directly into the welding procedures used for the world's first 'X100' construction project, successfully completed in Canada, September 2002[304].

Minor changes in welding procedure for X100 grade steel can result in quite significant changes in mechanical properties. This is amply illustrated between two similar single

wire welds from the research; the 100°C preheat variant that gave an $R_{p0.2}$ value of 900MPa (19.05mm WT) and weld ML-B15-3 which gave an $R_{p0.2}$ of 841MPa (14.9mm WT). The observed reduction in strength can be attributed to an increase in joint gap width (for the same height within the joint, measured from the pipe ID) in combination with the pipe wall thickness decrease. This effect is a direct result of weld metal cooling rate changes, exhibiting an effect similar to that observed in the preheat/process variation trials. A comparison of mechanical properties from the single wire 100°C preheat and process variant trials allowed a direct comparison of thermocycle and mechanical data. Considerably different strength levels were exhibited between the two procedures (see Table 5-40 and Table 5-41), the only differences between them being travel speed and joint gap width. The welding waveform shape used between the trials was different, but the power (average amps x average volts) was virtually identical. The travel speed was higher in the process variant trial (550mm/min vs. 480mm/min), and the joint gap width larger (7.20mm vs. 6.35mm). Whilst an increase in gap width would be expected to decrease the cooling rate due to the improved heat sink available to the deposited bead (thereby decreasing the strength), the increase in travel speed proved to be a stronger effect and resulted in a considerable increase in strength over that of the preheat variant ($R_{p0.2}$ of 959MPa vs. $R_{p0.2}$ 900MPa). The increased cooling rate and decreased cooling time data of the process variant trial supported the observed mechanical property (see Table 5-34 and Table 5-36) and microstructural differences (see Figure 5-37 and Figure 5-38) between the two welds, with the higher strength weld metal of the process variant trial exhibiting a finer grain size.

The changes in procedure described above are likely to be found in typical current mechanised field welding practice. This highlights the need for closer control over welding procedure parameters than would perhaps be necessary for strength levels lower than X100 linepipe construction in order to avoid significant change of the joint metallurgical properties. Comparison with the mechanised GMAW procedures from a recent X80 pipeline construction[348] exhibited a considerable increase in the range of travel speed and consequent heat input compared with both the laboratory procedures developed in this research and those used on the X100 'loop' constructed in Canada, September 2002[349]. The alloy levels used in the X80 construction were of a very similar composition to that of the optimum (guaranteed just overmatching) single/tandem composition (0.9Ni/0.3Mo) concluded from this research for use with X100. The proof strength required of the weld metal for X80 is considerably less than for X100, yet the WPAR from the X80 construction exhibited $R_{p0.2}$ values of 690MPa, compared with the typical values (5G procedures) obtained in this research of 810-860 MPa. It was decided that this was a direct result of the standard bevel configuration and travel speeds used by the contractor, compared with the narrower bevel and higher travel speeds developed during this research (see following section) promoting increased strength from the latter. In Canada, X80 construction often uses only 50°C preheat coupled with a C-Mn-Ti alloyed weld metal, usually with GMAW and CO_2 shielding (for the fill passes)[145,150]; weld metal $R_{p0.2}$ strengths between 610-670MPa are typical[276]. These strength levels provide a correlation with those achieved in this research with respect to the relative alloying/strength balance.

The cooling rates calculated from the various thermocycles, in conjunction with the resulting microstructural and mechanical properties explain the observance of the low transformation temperatures exhibited. Comparison of the cooling rates and

transformation temperatures with CCT data of Zhang[346] for a very similar weld metal chemistry confirmed the various data gathered from the thermocycle welds (see Figure 5-83). At cooling times from 800°C to 500°C of less than 10 seconds Zhang reported microstructures consisting of acicular ferrite, lath ferrite (bainite) and lath martensite or just lath martensite. Hardness levels reported for these structures were at least 350 HV10, with an Ms temperature of 470°C and acicular ferrite/lath ferrite start temperature of 515°C (the latter at a t_{85} of ~10s). This compares well with the initial cooling data from the preheat and process variant trials. The microstructures of the cap passes for the single, tandem and low preheat welds were mainly lath ferrite/martensite and acicular ferrite (see Figure 5-37 and Figure 5-38), with associated transformation start temperatures typically ranging from 490°C to 550°C. Cooling times of the cap passes (t_{85}) were typically 3 seconds for 100°C preheat. As mentioned earlier, a notable reduction in t_{85} times and transformation temperatures was observed for weld layers in the middle of the pipe wall thickness due to the increased efficiency of heat extraction, potentially leading to a higher percentage of lower transformation temperature products (lath ferrite/martensite). The final microstructures in these regions have the added complication of reheating effects modifying the original as-cast microstructure to varying degrees, such that the transformation data gathered is not an absolute indication of the resultant properties, but can at least provide a good indication. The microhardness profiles (Figure 5-70 and Figure 5-71), which by association represent the final weld metal through pipe wall local microstructural and strength effects, however back up the observed thermocycle data mechanical property variations between the various preheat and process variations. A hardness peak is generally observed in the mid pipe wall for the single, tandem and low preheat variants, whereas a much flatter profile is observed for the slow cooling rate variants (dual, dual tandem and high preheat variant). The former variants are much more likely to contain martensite/lower bainite in the mid pipe wall, and although areas immediately below the fusion line of each bead are considerably tempered, high hardness levels are still prevalent here as a result of the original solidification structure.

The process variation trials highlight the sensitivity of the particular welding process (single, dual etc.) in determining the resultant weld mechanical properties when all other parameters are effectively equal. The dual and dual tandem torch separation/bug travel speed is highly critical with respect to the weld metal cooling rates and maximum reheat temperatures observed, the effect of which is magnified due to the narrow gap joint preparations in comparison to conventional wide bevel angles. The alloying levels used to generate the required properties are therefore crucial with respect to a given equipment set-up, as shown with the dual torch procedure qualification welds using 50mm and 100mm torch separations. The alloy transformation temperatures also play an important role in terms of the minimum torch separation possible if retransformation is to occur, the latter consequently reducing grain growth effects and promoting increased strength from a given alloying level.

The preheat levels examined using the same weld metal chemistry and procedure are close to a linear relationship between strength and temperature (Figure 5-28) over the range studied (20°C-180°C). This compares well with the relative percentages of the various microstructural constituents (Figure 5-31) which generate the associated mechanical properties. As mentioned earlier, the distinction between lower baintite and self tempered martensite in low carbon alloy steels is very hard to achieve using optical

microscopy[294,347]. To achieve a true classification of the microstructures present TEM should be employed, particularly when carbon levels are below 0.1%[294]. Unfortunately time did not allow this equipment to be used in the present study. The maintenance of correct preheat and interpass levels within traditional single wire mechanised welding is usually self-controlled due to the consistent time periods between each weld pass and subsequent shack movement. The original preheat temperature is set high enough to allow for a reduction between each weld station to take place, such that the final cap pass station is still above the specified minimum preheat. As an example, an X80 pipeline construction initial preheat could be 150°C, with a minimum of 80°C[348]. The same philosophy could be employed with X100, albeit with a likely tightening of the permissible range. The development of equipment capable of easily depositing multiple weld layers in several circumferential passes at a given station can potentially change the preheat situation depending on the given pipe diameter being welded. Welding production speeds are a critical aspect of any pipeline construction; if the welding bug has returned to the start position and the pipe is still at e.g. 200°C, the resultant tensile properties will be significantly different to those attained if the pipe was at 100°C. The dual and dual tandem torch process variant thermocycle welds exhibited temperatures in excess of 200°C after 90 seconds (see Figure 5-56), a 36 in. half pipe diameter only takes 66 seconds travelling at 1.3m/min (typical dual tandem fill pass condition[324]). Taking into account the time required for repositioning the bug, tip cleaning and layer program adjustment (say 1 minute), the preheat level will not be much below 200°C as observed from the cooling curves. The consumable chemistry must therefore be tailored to suit the envisaged construction conditions.

It is generally recognised good practice to use the minimum alloying levels possible to generate the required mechanical properties. Apart from the obvious reduction in cost, lower alloying levels normally reduce the propensity for classical weld metal defects such as hot and cold cracking. Until the advent of welding powersources capable of generating waveforms tailored to suit very specific wire compositions and welding situations (joint geometry/position etc.), higher alloying was often detrimental to stable and consistent droplet transfer. Disadvantages of lower alloying can be the large range of mechanical properties possible with various cooling rates (see Figure 2-59), which could be an issue when welding procedure control is not adequately maintained, but for mechanised welding within a highly repeatable joint configuration this potential scatter is minimised to a very low level. Hence the ability to use low alloying to best effect in a narrow gap mechanised welding situation. The alloying variants examined within this research provide an insight into the chemical composition limits allowed for a specific arc energy and preheat typical of X100 mechanised linepipe construction. Assuming the required strength and hardness properties are those specified in Section 2.9, linear extrapolation of the metal cored wire data (see Figure 5-79, Table 5-43 and Table 5-44) allowed the following individual alloy variations to be determined based around a nominal composition of 0.09C/0.8Ni/0.3Mo:

1/ Nickel : 0.25% to 0.62%

2/ Molybdenum : 0% to 0.042%

3/ Chromium : 0% to 0.065%

4/ Carbon : 0.054% to 0.080%

A comparison of weld metal $R_{p0.2}$ and Pcm values between the metal cored wire and 5G procedure tests confirms the global relationship of strength and composition (see Figure 5-82). The higher degree of scatter within the results of the 5G procedure tests is a direct reflection on the reduced ability to maintain constant conditions with respect to deposition depth, arc energy and joint geometry relative to the flat plate tests. The overall lower $R_{p0.2}$ values achieved for a given Pcm value with the dual torch procedures confirms the increased alloying levels required with this process if maintenance of the proposed strength properties is to be achieved.

The toughness data from the various metal cored trials do not allow for direct comparison with the proposed levels of Section 2.9 due to the higher oxygen content shifting all toughness values to lower levels. A general trend can however be observed, with increasing alloying above that of the nominal 0.09C/0.8Ni/0.3Mo tending to reduce the impact toughness level (see Figure 5-80).

7 CONCLUSIONS

- The aim of this research was to develop a greater understanding of the factors influencing the properties of X100 girth welds made under field conditions, and to provide guidance on the specification of mechanical properties and the selection of consumables and processes that could be used for the field-welding of X100 linepipe. Target mechanical properties have been established to suit field welding under strain-based design conditions. Full pipe girth welds have been produced using a number of different consumables, several welding processes and several different sources of pipe supply. The target mechanical properties were achieved through appropriate combination of consumables, process and welding parameters. This research has led to a greater understanding of the field welding of X100 linepipe and has allowed pipeline operators to proceed with the first installation of TMCP X100 linepipe in a gas transmission pipeline.

- A major objective of the work was to produce girth welds having a yield strength of at least 810 MPa (117 ksi) to ensure that welds overmatched the parent metal, while simultaneously achieving high toughness in the weld metal and heat affected zones alongside controlling the joint hardness. Extensive mechanical testing proved that this objective was met.

- The experimental mechanised GMAW procedures developed during the welding trials of this programme have shown that, subject to careful selection of welding consumable and fairly precise control of welding process variables and parameters, there are no major problems in obtaining weld metal strength levels of at least 120 MPa above the 690 MPa SMYS of the parent pipe. This objective has been achieved in welds made using all three mechanised process variants examined: single wire; tandem wire; and dual torch. The desired target properties of strength and toughness were achieved with a variety of consumables of different composition.

- The nature of the mechanised narrow gap GMAW process for welding large diameter pipelines imposes considerable constraints on the physical welding process if sound weldments with the required combination of properties are to be obtained. This demands a high degree of control over the welding parameters and thereby limits the procedural variations possible.

- Weld bevel geometry should be considered as an essential variable in the context of the specified welding procedure. It has been found that variation of bevel or other weld preparation details, for a given weld metal chemistry and welding procedure, can result in markedly different weld metal properties. In the case of dual torch welds, the torch spacing is a critical parameter in determining the correct consumable/property balance.

- The selection of the welding consumable for X100 requires particular care. The solid GMAW wires are invariably of the low alloy type. It was found that the same wire could give weld metal of very different properties when used with different variants of the mechanised GMAW process. This implies that, when contractors for future X100 pipelines are qualifying welding procedures, it will be essential to qualify particular welding wire/process/welding parameter combinations in each case. A particular wire, which may give satisfactory results with, for example single

torch PGMAW, may not perform to the same level with dual torch or dual tandem arc applications or vice versa.

- Single and tandem wire mechanised PGMAW narrow gap welds gave very similar strength measurements for the same chemistry, arc energy and joint geometry.
- The development of a technique to obtain multiple thermocycle measurements from an initially molten weld pool using a single drilled hole thermocouple was successfully completed.
- The individual weld metal layer cooling curves were shown to exhibit consistent trends in terms of cooling times, rates and transformation temperatures with respect to the weld layer position within the narrow gap bevel for a constant arc energy and bevel geometry. Faster cooling rates/times and lower transformation temperatures occurred in the middle of the pipe wall thickness compared to the outer surfaces.
- The 0.9Ni 0.3Mo alloy examined for preheat and interpass variation with narrow gap mechanised PGMAW showed an almost linear relationship of increasing strength with decreasing preheat/interpass between 20°C and 180°C. The spread of yield properties within this temperature range was greater than the proposed weld metal yield range, highlighting the necessity for close control over the welding procedure.
- Carbon has been shown to provide the greatest increase in strength in a narrow gap welding geometry compared with nickel, molybdenum and chromium for the same weight percentage addition. Carbon also exhibited the added benefit of no impact toughness deterioration within the range examined.
- The mechanised GMAW field welding technique increasingly uses pulsed waveform power sources. The power supplies used to generate the various pulsed waveform procedures are a critical element for stable weld metal transfer in a narrow groove; the waveforms developed are specific to the given power supply and any transference to another equipment manufacturer will undoubtedly require tuning of the process.
- The weld metal yield strength generated from the tie-in experimental programme succeeded in overmatching the 690 MPa SMYS of the parent pipe, but with much less margin than was attained by the narrow gap mechanised welds. The rutile FCAW wires used, although giving excellent weldability and field handling performance, combined with reasonable toughness, do not currently have the metallurgical ability to reach the higher strengths desired.
- Repair procedures in X100 were developed successfully and should present no problems for field use, providing that careful attention is paid to heat input/cooling rate and consumable selection.
- The X100 pipeline steels examined during the course of this programme have generally exhibited no obvious problems of high hardness or poor toughness in the HAZ of the base material. A small amount of HAZ softening was noted in the majority of the welds. The actual toughness criteria required for both weld metal and pipe material need to be thoroughly evaluated for each specific application. The effects of the welding process, in terms of both HAZ and weld metal toughness, also need to be taken into account.

- The girth/longitudinal seam weld interaction in some of the X100 steels is an item requiring special attention, as in this zone, the HAZ resulting from the girth weld which is created in weld metal of the longitudinal seam weld metal can sometimes exceed 350 HV10.

8 RECOMMENDATIONS FOR FURTHER WORK

- The tandem and dual tandem processes discussed within the current programme are capable of welding travel speeds in the region of 1.0-1.3 m/min. These are over double the normal single/dual torch travel speeds (excluding the hot pass), and in combination with torch oscillation, manual operator tracking of the process requires a high degree of dexterity. It is consequently important for field implementation of the processes, which are likely to encompass a wide range of welder skill levels, that robust automatic joint tracking systems are developed. These should incorporate both horizontal and vertical torch placement suitable for a narrow gap weld bevel, preferably in combination with feedback control mechanisms for stable metal transfer.

- The thermocouple placement below the surface of the welded layer in the tandem/dual tandem thermocycle experiments required increasing in comparison to the single/dual torch processes (for the same arc energy per weldpool) in order that the thermocouple would survive the passage of the arc over it. This phenomenon indicated a greater penetration of the tandem/dual tandem processes, even though the bead shape and degree of dilution appeared similar to that of the single/dual torch processes. It is therefore hypothesised that for a constant arc energy between the processes, the actual heat input may vary between the two groups. Experiments examining this, using techniques such as liquid nitrogen calorimetry, should allow a better understanding of the potential differences between the processes, alongside the determination of relevant heat input factors.

- The dual tandem torch welding process was in its infancy during the course of this research. The process requires considerable procedural development to ensure its successful qualification and transference to a field welding situation.

- Transformation temperatures determined throughout the research would benefit from dilatometric comparison using the thermocycle profiles generated in the current work.

- The fine grained high strength microstructures generated with the various mechanised welding processes during this research are at the limit of optical microscopy resolution. Distinction between the various forms of bainite and low carbon martensite requires TEM for a definitive answer in terms of their classification for microstructure/property relationships.

- It is recommended that attempts are made to develop and qualify a FCAW tie-in weld with a basic flux-cored tubular wire to improve the strength levels, whilst maintaining the higher productivity levels of the semi-automatic process. The high strength of welds made from these wires however comes at a price of weldability, and considerable effort will need to be expended in this direction for field use.

References

1 Tamehiro H. and Chino H. (1991). The progress in pipeline material properties, 29th April 1991, Laboratory Soete, University of Ghent

2 Chaudhari V. et al. (1995). German gas pipeline first to use new generation linepipe, *Oil and Gas Journal*, **93** (Jan 2), 40-47

3 Takeuchi, I. (1998). Advanced linepipe production technologies. *Steel Today and Tomorrow* (Japan), **144** (Oct – Dec), 5-8

4 Wang Y. et al. (2002). The research and development of high-strength line pipe in China, in: *Proceedings of Pipe Dreamer's Conference, Application and Evaluation of High-Grade Linepipes in Hostile Environments*, Yokohama, Japan, 7-8 November 2002, 53-84

5 Terada Y. et al (1997). Development of API X100 UOE line pipe, *Nippon Steel Technical Report*, Jan 1997, No. 72

6 Tamehiro H. et al. (1990). High-toughness age-hardenable copper-bearing steel for large-diameter line pipe, in: *Proceedings of the 8th International Conference on Offshore Mechanics and Arctic Engineering (OMAE)*, The Hague, March 1989. American Society of Mechanical Engineers, **5**, 339-346

7 Hillenbrand H.G. et al. (1995). Manufacturability of linepipe in grades up to X100 from TM processed plate, in: *Proceedings of the Conference of Pipeline Technology*, Ostend, Belgium, September 11-14, 1995, **II**, 273-286

8 Takeuchi I. et al (2002).The prospect of high-grade steel pipe for gas pipelines, in: *Proceedings of Pipe Dreamer's Conference, Application and Evaluation of High-Grade Linepipes in Hostile Environments*, Yokohama, Japan, 7-8 November 2002, 185-202

9 Terada Y. et al. (2003) X100 Linepipe with excellent HAZ toughness and deformability, in: *Proceedings of the 22nd International Conference on Offshore Mechanics and Arctic Engineering (OMAE03)*, Cancun, Mexico, 8-13 June 2003

10 Okatsu M. et al. (1997) Metallurgical and mechanical features of X100 linepipe steel, in: *Proceedings of the 16th International Conference on Offshore Mechanics and Arctic Engineering (OMAE97)*, **III** - Materials Engineering, 119-124

11 Michie K. (1998). Twin-wire GMAW of pipeline girth welds, *MSc Thesis*, Cranfield University, Cranfield, Bedfordshire, UK

12 Walker A.P. (2000). Twin-wire welding of X80 linepipe, *MSc Thesis*, Cranfield University, Cranfield, Bedfordshire, UK

13 Michie K, Blackman S.A. and Ogunbiyi T.E.B (1999), Twin-Wire GMAW : Process Characterisitics and Applications, *Welding Journal*, 31-34, May 1999

14 BP Statistical Review of World Energy. (2003), A consistent and objective series of historical energy market data, *Citing Internet resources* (WWW document). http://www.bp.com/centres/energy/index.asp (accessed 11th June 2003), 10th June 2003

15 Anon., *Pipeline*, January 2000, 22

16 International Energy Outlook (2003). DOE/EIA-0484(2003), Energy Information Administration, Office of Integrated Analysis and Forecasting, U.S. Department of Energy, May 2003

17 Hopkins, P. (2002). The challenges for frontier linepipe projects, in *Pipe Dreamer's Conference, Application and Evaluation of High-Grade Linepipes in Hostile Environments*, Yokohama, Japan, 7-8 November 2002, 3-32

18 Hopkins P. (2000). Time to change?, *Pipes and Pipelines International*, October 2000

19 King G. et al. (2002). Superhigh pressure dense phase artic pipelines increase reliability and reduce costs, in: *Proceedings of International Pipeline Conference (IPC '02)*, Calgary, Alberta, Canada, 29 September – 3 October 2002

20 API 5L (2000) Specification for Linepipe, *American Petroleum Institute*, 42nd Ed, January 2000

21 CSA Z245.1 – 02 (2002). Steel Pipe, *Canadian Standards Association*, September 2002

22 Blackman S.A. (2003). An economic assessment of mechanised welding of high strength linepipe for the Australian pipeline industry, *Pipes and Pipelines International*, 48, No.2, March-April 2003, 27-37

23 Fairchild D.P. et al. (2002). High strength steels – beyond X80, in: Proceedings of Pipe Dreamer's Conference, Application and Evaluation of High-Grade Linepipes in Hostile Environments, Yokohama, Japan, 7-8 November 2002, 307 – 321

24 Pipelines: All you wanted to know..... (1994). *The Pipeline Industries Guild*, ISBN 095172862X, 4

25 Pulici M. and Cavicchi M. (2003). Bluestream gas pipeline – The deepest gas trunkline completed, in : *Proceedings of the 14th Biennial Joint Technical Meeting on Pipeline Research*, Berlin, May 19-23, 2003

26 NACE TM0177-96 (1996). Standard test method – laboratory testing of metals for resistance to specific forms of environmental cracking in H_2S environments

27 NACE TM0284-96 (1996). Standard test method – evaluation of pipeline steels and pressure vessels for resistance to hydrogen-induced cracking

28 Dittrich S. (1992). Welding of high yield strength X80 – state of the art 1991, *Welding in the World*, 30, 33-36

29 Gray J.M. and Pontremoli M. (1988). Metallurgical options for API grade X70 and X80 linepipe, in: *Proceedings of the Conference on Microalloyed HSLA Steels*, Chicago, USA, 24-30 Sept 1988, 171-199

30 Asahia H., Fujii H.and Sato N. (1995). Heavy wall X80 seamless linepipe, in: *Proceedings of the 2nd International Conference on Pipeline Technology*, Ostende, Belgium, 11-14th September 1995,2, 253-261,

31 Hall O.E. (1951). The deformation and ageing of mild steel : III discussion of results. *Proceedings of the Physical Society*, B64, 747-755

32 Cracknell A. and Petch N.J. (1955). Frictional forces on dislocation arrays at the lower yield point in iron. *Acta Metallurgica*, 3, 186-189

33 Cottrell A.H. (1958). Theory of brittle fracture in steel and similar metals, *Transactions of the Metallurgical Society of A.I.M.E*, 212, 192-203

34 Petch N.J. (1958). The ductile brittle transition in the fracture of a-iron. *Philosophical Magazine*, 3, 1089-1097

35 Dearden J. and O'Neill H. (1940). A guide to the selection and welding of low alloy structural steels, *Institute of Welding Transactions*, October 1940, 203-214

36 Ito Y. and Bessyo K. (1968). Weldability formula of high strength steels. *IIW doc IX-576-68*

37 Demofonti G. et al (2002). Fracture behaviour of X100 gas pipeline by full-scale tests, in: *Proceedings of Pipe Dreamer's Conference, Application and Evaluation of High-Grade Linepipes in Hostile Environments*, Yokohama, Japan, 7-8 November 2002, 245–261

38 Amano K. et al (1986). in: *Proceedings of 7th Symposium on Linepipe Research*, Pipeline Research Committee of the American Gas Association (AGA), Houston, USA, 8.1

39 Sugie, E. et al (1988). Propagating shear fracture in natural gas transmission pipelines, *ASTM STP945*, 237-246

40 Maxey W. (1974). Fracture initiation, propagation and arrest, in: *Proceedings of 5th Symposium on Linepipe Research*, Pipeline Research Committee of the American Gas Association (AGA), Houston, USA

41 Eiber R.J. Bubenik T.A. (1993). Fracture control plan methodology, in: *Proceedings of 8th Symposium on Linepipe Research*, Pipeline Research Committee of the American Gas Association (AGA), Houston, USA

42 Yurioka N. (1990). Carbon equivalents for hardenability and cold cracking susceptibility of steels, in: *Proceedings of Select Conference on Hardenability of Steels*, Derby, UK, 17 May 1990, 41-50

43 Guide to weldability and metallurgy of welding of steels processed by thermomechanical rolling or by accelerated cooling (1994). *Welding in the World*, 33, No.1, 34-65

44 BS EN 1011, Welding – Recommendations for welding of metallic materials, Part 1 (1998): General guidance for arc welding and Part 2 (2001): Arc welding of ferritic steels.

45 CR ISO 15608. (2000). Welding – guidelines for a metallic material grouping system (ISO/TR 15608:2000)

46 BS 4515-1:2000. Specification for welding of steel pipelines on land and offshore – part 1: carbon and carbon manganese steel pipelines

47 Ouchi, C. (1983) 90th, 91st Nishiyama Memorial Lecture, Iron and Steel Institute of Japan, 93

48 Yurioka N., Ohshita S. and Tamehiro H. (1981). Study on carbon equivalents to assess cold cracking tendency and hardness in steel welding in connection with the development of low-carbon bainitic line-pipe steel, in: *Proceedings of the Specialist Symposium of Pipeline Welding in the 80's*, Melbourne, 19-20 March 1981, Paper 1c

49 Tamehiro H. and Yoshino T. (1989). High strength sour service linepipe for offshore use, in: *Proceedings of the 8th International Conference of Offshore Mechanics and Arctic Engineering*, American Society of Mechanical Engineers, The Hague, Netherlands, March 1989, **V**, 339-346

50 NACE Material Requirement MR-01-75

51 Ume K. et al. (1985). Initiation and propagation morphology of sulphide stress corrosion cracking at welds on linepipe steels, in: *Proceedings of Corrosion '85*, Boston USA, Paper No. 240, Publ. National Association of Corrosion Engineers (NACE), Houston, Texas

52 Umemoto M. and DeArdo A.J. (1984). 'HSLA steels', in: *Proceedings of the International Conference*, Wollongong, Australia, 20-21 Aug. 1984

53 Heistakamp F. and Hulka K. (1984). Low carbon Mn-Ni-Nb steel, part 2: weldability, *Metals Technology*, **11**, No.12, 545-549

54 Gladman T., Dulieu D. and McIvor I.D. (1975). Structure-property relationships in high strength microalloyed steels, in: *Proceedings of Microalloying 75*, Washington D.C., USA, 1-3 October 1975, 32-55

55 Sage A.M. (1981). Effect of rolling schedules on structure and properties of 0.45% vanadium weldable steel for X70 pipelines, *Metals Technology*, **8**, No.3. March 1981, 94-102

56 Nakasugi H. et al. (1980). Properties of high strength titanium bearing steel for large diameter pipeline, in: *Proceedings of the International Conference on Pipeline and Energy Plant Piping: Design and Technology*, Calgary, Canada, 10-13 Nov. 1980, 51-67

57 Cuddy L.J. (1981). Microstructures developed during thermomechanical treatment of HSLA steels, *Metallurgical Transactions A*, **12A**, no. 7, 1313-1320

58 Matsubara H. et al. (1979). Tetsu-to-Hagane, *Journal of the Iron and Steel Institute of Japan*, **65**, 1644

59 Pickering F.B. (1967). Transformation and hardenability in steels, *Climax Molybdenum Company Symposium*, Ann Arbor, 192

60 Smith E., Coldren A.P. and Cryderman R.L. (1972). Mn-Mo-Nb acicular ferrite steels with high strength and toughness, *Towards Improved Ductility and Toughness*, Publ. Climax Molybdenum Development Company (Japan) Ltd., 119-142

61 Gondoh H et al., (1979). Development of acicular-ferrite steel for Arctic-grade line pipe, *Nippon Steel Technical Report*, **14**, Dec.1979, 55-65

62 Loberg B. et al. (1984). The role of alloy composition on the stability of nitrides in Ti-microalloyed steels during weld thermal cycles, *Metallurgical Transactions A*, **15A**, 33-41

63 Tamehiro H. et al. (1985). Thermo-mechanically controlled-rolled low nickel-niobium steel plate for cryogenic service pipelines, in: *Proceedings of the 7th International Conference on the Strength of Metals and Alloys (ICSMA 7)*, Montreal, Canada, 12-16 August 1985, **2**, 1043-1048

64 Tamehiro H. and Terada Y. (1994). Metallurgical design of X100 line pipe, *Nippon Steel Corporation Internal Report*, August 1994

65 Tanaka T. (1978). Bulletin of the Japan Institute of Metals, 1978, **17**, 104

66 Nishioka K. (2000). Market requirements of thermomechanically processed steel for the twenty first century, *Steel World*, **5**, No.1, p.62, publ. IOM Communications

67 Irvine K.J. and Pickering F.B. (1963). The impact properties of low carbon bainitic steels, *Journal of the Iron and Steel Institute*, **201**, 518

68 Hillenbrand H-G. and Kalwa C. (2003). Production and service behaviour of high-strength large-diameter pipe, in: *Proceedings of Pipe Dreamer's Conference, Application and Evaluation of High-Grade Linepipes in Hostile Environments*, Yokohama, Japan, 7-8 November 2002, 203-215

69 Mitchell P.S. (1995). The effects of Vanadium on the parent plate and weldment properties of accelerated cooled API 5L X100 Steels, in: *Proceedings of the Conference of Pipeline Technology*, Ostend, Belgium, September 11-14, 1995, **II**, 239-251

70 Sunami H., Nagkazawa M. and Sekizawa M. (1992). The manufacture of large diameter welded pipe, in: *Proceedings of the Conference of Manufacture, Fabrication and Operation of Pipelines*, Glasgow, UK, 30 September 1992

71 Civallero M.A., Parrini C. and Pizzimenti N. (1975). Production of large-diameter high-strength low-alloy pipe in Italy, *Proceedings of Micro Alloying 75*, Washington, 1-3 October, 1975, 451-468

72 Streisselberger A., Bauer J., Bergman B. and Schultz W. (1992). Correlation of pipe to plate properties – model calculations and application in the design of X80 linepipe steels, in: *Proceedings of the International Conference on Pipeline Reliability*, Calgary, Canada, 2-5 June 1992, 3, 1-13

73 Hillenbrand H.-G., Norris C. and Hafner F. (2003). The Gulfstream project – meeting the pipe supply challenge, in: *Proceedings of the 14th Biennial Joint Technical Meeting on Pipeline Research*, EPRG/PRCI/APIA, Berlin, Germany, 19-23 May 2003, 2-1 – 2-15

74 Blackman S.A. (2003). Internal communication, WERC, Cranfield University, Cranfield, Bedfordshire

75 Kennedy J.L. (1993). In book: *Oil and gas pipeline fundamentals*, 2nd Edition, Publ. Penwell Publishing, Tulsa, Oklahoma, USA

76 Houldcroft P.T. and John R. (1988). In book: *Welding and cutting*, 1st Edition, Publ. Woodhead-Faulkner, Cambridge, UK, 3

77 Breeze H. and Chetcuti J. (1970). Experiences with CO2 welding of pipelines , in: *Proceedings of the Pipe Welding Conference*, TWI, Abington, UK, 10-13 November 1969, Paper 28, 192-197

78 Foote W.J. (1986). Welding C-Mn steels with the pulsed current MIG welding process, *PhD Thesis*, Cranfield University, Cranfield, UK

79 Needham J.C. (1962). Control of transfer in aluminium consumable electrode welding, in: *Proceedings of the Physics of the Welding Arc Symposium*, The Welding Institute, London, 114-122

80 Boughton P. (1967). Two years of pulsed arc welding, *Welding and Metal Fabrication*, 85, No. 10, 410-420

81 Needham J.C. and Carter A.W. (1965). Material transfer characteristics with pulse current, *British Welding Journal*, 12, No. 5, May 1965, 229-241

82 Watkins P.V.C. (1975). The transistor controlled DC welding power source, *Welding Institute Research Report*, 35/10/75, October 1975

83 Allum C.J. (1983). MIG welding – time for reassessment, *Metal Construction*, June 1983, 347-353

84 Quintino L. (1986). Fusion characteristics in P-GMAW of mild steel, *PhD Thesis*, Cranfield University, Cranfield, Bedfordshire

85 Allum C.J. and Quintino L. (1984). Control of fusion characteristics in pulsed current GMAW, Part 1 – Fusion Characteristics, *I.I.W. Doc 212-582-84*

86 Smati Z. (1985). Automatic pulse MIG welding, *Metal Construction*, 18, No.1, January 1986, 38R-44R

87 Lincoln Electric Company (1999)., *Wave Designer Software Operating Manual*, IM649, May 1999

88 Lesnewich A. (1958). Control of melting rate and metal transfer in gas shielded metal arc welding, *Welding Journal*, 37, No. 8, August 1958, 343s-353s

89 Lancaster J.F. (1979). Metal transfer in fusion welding, in: *Proceedings of the Conference on Arc Physics and Weld Pool Behaviour*, The Welding Institute, Cambridge, UK, 135-146

90 Allum C.J. (1985). Metal transfer as a varicose instability, *Journal of Physics D Applied Physics*, 18, 1431-1468

91 Norrish J and Richardson I.M. (1988). Metal transfer mechanisms (in arc welding), *Welding and Metal Fabrication*, 56, No. 1, Jan.-Feb. 1988, 17-22

92 Harwig D. (2003). Arc behaviour and metal transfer of the VP-GMAW Process, *PhD Thesis*, Cranfield University, Cranfield, Bedfordshire, May 2003

93 Classification of metal transfer of arc welding processes (1976), *IIW Doc. XII-636-76*

94 Linnert G.E. (1994).in Book: *Welding Metallurgy*, 4th Edition, publ. AWS, 493

95 Norrish J. (1992). Advanced Welding Processes, IOP Publishing Ltd, Bristol, UK

96 Hirata Y. (2003). Pulsed arc welding, *Welding International*, 17, No.2, 98-115

97 Norrish J. et al (2001). A new approach to controlled short circuit transfer in GMAW, in: *Proceedings of Recent Developments and Future Trends in Welding Technology*, Cranfield University, Cranfield, UK, 3-4 September 2001

98 Ma J. (1982). Metal transfer in MIG welding, *PhD Thesis*, Cranfield University, Cranfield, UK

99 Brown K.W. (1978). Switched-arc MIG welding, in: *Proceedings of the Conference on Advances in welding Processes*, The Welding Institute, Abingdon, Cambs

100 Lassaline E., Zajaczkowski B. and North T.H. (1989). Narrow groove twin-wire GMAW of high-strength steel, *Welding Journal*, **68**, No.9, Sept. 1989, 53-58

101 Yasuda K., Hinata T., Jimma T. and Onzawa T. (1989). High speed single sided welding of thin [stainless steel] sheet by multi-electrode arc welding, *Welding International*, **3**, No.1, Jan 1989, 37-41

102 Hackl H. (1998). Faster welding with two wire electrodes: MIG welding of aluminium materials, in : *Proceedings of the Conference on Exploiting Advances in Arc Welding Technology*, The Welding Institute, Abington, Cambridge, UK, 30-31 March 1998.

103 Van Mourick T.(2001). Welds apart, *World Pipelines*, Autumn 2001, 99-100

104 Reed P. (1961). Automatic welding hits the pipeline right of way, *Oil and Gas Journal*, Jan 30th 1961

105 Sugitani Y et al. (2000). Automatic pipeline GMA welding technology for high efficiency and intellectualization, in: C*onference Proceedings of the IIW, Commission XII*, Florence, Italy, 10-12 July, 2000. IIW Doc XII-1641-00

106 Cotton H.C. (1977). Automatic welding of transmission pipelines, in: *Proceedings of the 9th Annual Convention of the Pipeline Construction Association*, Acapulco, Mexico, Oct. 1975

107 Bove O. and Rinaldi F. (1988). Semi-automatic welding processes and the mechanised 'PASSO' process, *Welding International*, **2**, No.2, 1988, 160-167

108 Hansen E. and Poirier N. (1995). Offshore welding technology applied to a major onshore pipeline construction project : Maghreb to Europe 48" gasline in Morocco, in: *Proceeding of the Conference on Pipeline Tecgnology*, Ostende, Belgium, Sept 11-14, 1995, **III**, 119-137

109 Blackman S.A. and Dorling D.V. (1999). Capabilities and limitations of mechanised GMAW systems for transmission pipelines, in: *Proceedings of the 1st International Conference on Weld Metal Hydrogen Cracking in Pipeline Girth Welds*, Wollongong, Australia, March 1999, 19-1 – 19-19

110 Widgery D. (1994). Tubular wire welding, publ. *Abington Publishing*, Cambridge, England

111 Matsuda F. et al (1980). Arc characteristics and metal transfer for flux cored electrode in GMA welding, *Transactions of the Japanese Welding Research Institute*, **9**, No. 1, 39-46

112 Filarc flux and metal-cored welding wires product catalogue (1993), publ. The Esab Group, Utrecht, The Netherlands, 1993/1994 Edition

113 Houldcroft P.T. (1989). In book: *Submerged-Arc Welding*, 2nd Edition, Publ. Abington Publishing, Cambridge, UK

114 Tuliana S.S., Boniszewski T. and Eaton N.F. (1969). Notch toughness of commercial submerged-arc weld metal, *Welding and Metal Fabrication*, **37**, No. 8, 327 – 339

115 ESAB submerged arc welding consumable catalogue. (1997). Publ. The Esab Group, Gothenburg, Sweden

116 BS EN 499 (1995). Welding consumables – covered electrodes for metal arc welding of non-alloy and fine grain steels – classification

117 Rothwell A.B., Dorling D.V. and Glover A.G. (1990). Welding metallurgy and process development research for the gas pipeline industry, in: *Proceedings of Advanced Joining Technologies, IIW Congress on Joining Research*, Montreal, Canada, 20-21 July, 1990, 175-192

118 Latvis S.D. and Valentini, Jr. T.N. (2000). Technology trends – overcoming issues with welding high strength pipe, in: *Proceedings of the Conference on Gas Metal Arc Welding for the 21st Century*, publ. AWS, Orlando, Florida, 6-8 Dec 2000, 239-246

119 Perteneder E., Konigshofer H. and Mlekusch J. (1995). Characteristic profiles of modern filler metals for on-site pipeline welding, in: *Proceedings of the Conference on Pipeline Technology*, Ostend, Belgium, 11-14 Sept 1995, **I**, 117-128

120 Stalker A.W. (1971). Root bead welding of pipes and pipelines in the fixed horizontal position by CO_2 welding, Report R/RB/PE5/71, March 1971

121 Meister R.P. and Martin D.C. (1966). Narrow gap welding process, *British Welding Journal*, **13**, **252**

122 General review of narrow gap welding (NGW) – the state of the art in Japan (1986). Technical Commission on Welding Processes, The Japan Welding Society, Ed. Matsuda F., Tokyo, Japan, 13-33

123 Lucas W. (1983). Trends in MIG welding process developments, in book: *Exploiting MIG Welding Developments*, publ. TWI, Cambridge, UK, 1-8

124 Baxter C.F.G. (1979). Narrow gap MIG welding – a review of the literature, *Welding Institute Research Report 104/1979*

125 Hutt G.A. (1984). Narrow gap welding, *Metal Construction*, **16**, No.6, June 1984, 335-361

126 Gilroy-Scott A., Huntley B. and Gross B. (2001). Welding challenges constructing the Alliance pipeline, *Australasian Welding Journal*, **46**, First Quarter 2001

127 Belchuk G.A. and Titov N.Y. (1970). Effects of automatic welding conditions with a narrow gap on weld shape, *Automatic Welding*, **23**, No. 12, December 1970, 49-52

128 Kurokawa T. et al. (1966). The narrow gap MIG welding process for thick steel plates, *Mitsubishi Technical Review*, **3**, No.3, 47-57

129 Dorling D. et al. (1986). Pulsed gas metal arc welding of thick section steels for low temperature applications, *Canmet/ Nova Report*, DSS file No. 14SQ.23440-4-9065

130 Nomura H., Sugitani Y and Kobayashi Y. (1986). Narrow gap welding process with high speed rotating arc, *Narrow Gap Welding (NGW) – The State-of-the-Art in Japan*, Technical Commission on Welding Processes, The Japan Welding Society, Ed. Matsuda F., Tokyo, Japan, 74-80

131 Druhen-Charnaux M.-A. (2000). Solidification cracking tendency of X100 weld metals, MSc Thesis, Cranfield University, Cranfield, Bedfordshire, UK, September 2000

132 Hutt G.A. (1984). A review of recent developments in mechanised high efficiency gas shielded arc welding processes for steel, *Welding Institute research Report 235/1984*, April 1984

133 Barabash Z.N., Bubenko V.A. and Shono S.A. (1973). Some technological aspects of narrow gap welding, *Welding Production*, **20**, No.9, Sept 1973, 34-36

134 Cazes R. and Ducrot A. (1974). Narrow Gap Welding, *in: Proceedings of the International Conference on Advances in Welding Processes*, Harrogate, 7-9 May, 1974, publ. TWI, Abington, Cambridge, UK, Paper No. 17, 129-136

135 Matsunawa A. and Nishiguchi K. (1980). Arc behaviour, plate melting and pressure balance of the molten pool in narrow grooves, *in: Proceedings of the Conference on Arc Physics and Weldpool Behaviour*, London, England, 8-10 May 1979, publ. TWI, Cambridge, UK, 301-310

136 Baxter C.F.G. (1980). Mechanised electrode weaving for vertical MIG welding, *TWI Research Report 129/1980*, November 1980

137 Baxter CF.G. (1983). Welding linepipe steel by pulsed MIG, *TWI Research Bulletin*, September 1983.

138 Lucas W., Street J.A. and Watkins P.V.C. (1975). Solid wire AC MIG-welding, *Welding Institute Members Report P65/75*, January 1975

139 Lucas W. and Needham J.C. (1975). Why not AC MIG-welding? *Welding Institute Research Bulletin*, March 1975

140 Matumoto J. et al. (1980). Some characteristics of the electrode melting phenomena in narrow-gap MIG-arc welding, *Transactions of the Japanese Welding Society*, **11**, No.1, April 1980, 3-8

141 Nakajima M. (1974). Development and application of narrow gap arc welding processes in Japan, *IIW Doc. XII-584-74*, April 1974

142 Smith A.A. and Dye S.A. (1963). Significance of wire diameter in the CO_2 welding of pipe, *British Welding Journal*, Spring Meeting, May 1963, 258-265

143 AWS/SFA 5.18-01 (2001). Specification for carbon steel filler metals for gas shielded arc welding, publ. ASME/AWS, Florida, USA

144 AWS/SFA 5.28-96 (1996). Specification for low alloy steel electrodes for gas shielded metal arc welding, publ. ASME/AWS, Florida, USA

145 Dorling D.V., Loyer A., Russell A.N. and Thompson T.S. (1992). Gas metal arc welding used on mainline 80 ksi pipeline in Canada, *Welding Journal*, May 1992, 55-61

146 Amin M. (1983). Pulse current parameters for arc stability and controlled metal transfer, *Metal Construction*, **15**, No. 5, May 1983, 272-278

147 Lancaster J.F. (1999). In book: *The Metallurgy of Welding*, 6th Edition, publ. Abington publishing, Cambridge, UK

148 BS EN 439 : 1994 (1994). Welding consumables – shielding gases for arc welding and cutting

149 Quintino L. and Pires I. (1996). Influence of shielding gas composition on features of the GMAW process, *IIW Doc. XII-1427-96*

150 Laing B.S., Dittrich S. and Dorling D.V. (1995). Mechanized field welding of large diameter X-80 Pipelines, *in: Proceedings of the Conference on Pipeline Technology*, Ostend, Belgium, 11-14 September 1995, I, 505-512

151 Crawford M. (2002). Welding at Matching Green, *World Pipelines*, **2**, Sept/Oct 2002

152 Thompson T.S., Rothwell A.B. and Dorling D.V. (1988). The influence of shielding gas composition on pulsed gas metal arc welding of arctic and offshore structures and pipelines, *Nova/Canmet Report*, DSS File No. 03SQ.23440-6-9113

153 Church J. (1990). Welding characteristics of a new welding process – TIME process, *IIW Doc XII-1099-90*

154 Brun G. (1996) Welding of X80 and X100 high strength pipeline steels, *MSc. Thesis*, Cranfield University, Cranfield, Bedfordshire, UK

155 Miranda A.B. (1997) The effects of shielding gas and transfer mode on the weldability of X100 pipeline steels, *MPhil. Thesis*, Cranfield University, Cranfield, Bedfordshire, UK

156 Caizley D.L. (1999). The welding of high strength steel for transmission pipelines, *MSc Thesis*, Cranfield University, Cranfield, Bedfordshire, UK

157 PRCI Report No. PR-171-9906, Girth welding of X100 pipe, to be published

158 Grong O. and Kluken A.O.(1992). Microstructure and properties of steel weld metals, in book: *Ferrous Alloy Weldments*, publ. Trans Tech Publications Ltd., Brookfield, USA, 21-46

159 Farrar R.A. and Harrison P.L. (1987). Acicular ferrite in carbon-manganese weld metals : an overview, *Journal of Materials Science*, **22**, No.11, November 1987, 3812-3820

160 Ricks R.A., Howell P.R. and Barrite G.S. (1982). The nature of acicular ferrite in HSLA steel weld deposits, *Journal of Materials Science*, **17**, 732-740

161 Yang J.R. and Bhadeshia H.K.D.H, (1986). Thermodynamics of the Acicular Ferrite Transformation in Alloy Steel Weld Deposits, in: *Proceedings of the Conference on Advances in Welding Science and Technology*, Ohio, USA, Publ. ASM, 187-191,

162 Mills A.R., Thewlis G. and Whiteman J.A. (1987). Nature of inclusions in steel weld metals and their influence on formation of acicular ferrite, *Materials Science and Technology*, **3**, 1051

163 Devillers L., Kaplan D., Marandet B., Ribes A. and Riboud P.V. (1983). The effect of low level concentrations of some elements on the toughness of submerged arc welded C-Mn steel welds, in: *Proceedings of the Conference on Residual, Impurity and Microalloying Elements on Weldability and Weld Properties*, TWI, Cambridge, UK, November 1983

164 Abson D.J. (1987). Non-metallic inclusions in ferritic steel weld metals – a review, *IIW Doc. IX-1486-87*,

165 Frost R.H., Olsen D.L. and Liu S. (1992). Influence of solidification on inclusion formation in welds, in: *Proceedings of the International Conference on Trends in Welding Science and Technology*, Gatlinburg, USA

166 Hansen M. and Anderko K. (1958). In book: *Constitution of binary alloys*, publ. McGraw-Hill, New York, USA, 353

167 Dubé C.A., Aaronson H.I and Mehl R.F. (1958) The formation of proeutectoid ferrite in carbon steels, *Revue de Metallurgie Memoires*, **55**, 201-210

168 Davey T.G. and Widgery D.J. (1976). A technique for the characterisation of weld metal microstructures, *IIW Doc. II-A-389-76*

169 Abson D.J. and Dolby R.E. (1980). A scheme for the quantitative description of ferritic weld metal microstructures, *Welding Institute Research Bulletin, April 1980, 100* and *IIW Doc. IXJ-29-80*

170 Committee of welding metallurgy of japan welding society, Chairman : Kikuta Y (1983), Classification of microstructures in low-C alloy steel weld metal and terminology, *IIW Doc IX-1282-83*

171 Pargeter R.J. (1983). Quantification of weld metal microstructure, *IIW Doc IXJ-78-83*

172 Dolby R.E. (1986). Guidelines for the classification of ferritic steel weld metal microstructural constituents using the light microscope, *Welding in the World*, **24**, No. 7/8, 144-148

173 Abson D.J., Duncan A. and Pargeter R.J. (1991). Guide to the light microscope examination of ferritic steel weld metal, *Welding in the World*, **29**, No. 7/8, 160-176

174 Bhadeshia H.K.D.H and Svensson L.-E. (1993). Modelling the evolution of microstructure in steel weld metal, in book: *Mathematical modelling of weld phenomena*, Ed. Cerjak H. and Easterling K.E., Publ. The Institute of Materials, London, UK, 109-180

175 Grong O. and Matlock D.K. (1986). Microstructural development in mild and low-alloy steel weld metals, *International Metals Reviews*, **31**, No.1, 27-48

176 Dadian M. (1986). The contribution of welding to the understanding of metallurgical phenomena, in book: *Advances in the Science and Technology of Welding*, publ. ASM Int., Ohio, USA, 101-117

177 Easterling K.E., in book: *Introduction to the Physical Metallurgy of Welding*, 2nd Edition, Publ. Butterworth-Heinemann Ltd., 1992

178 Cottrell A. (1985). In book: *An Introduction to Metallurgy*, 2nd Edition, publ. Edward Arnold, London, UK

179 Devletian J.H., Singh D. and Wood, W.E. (1995). Welding of HSLA-100 steel using ultra low carbon bainitic weld metal to eliminate preheating, in: *Proceedings of the 4th International Conference on Trends in Welding Research*, Gatlinburg, Tennessee, USA, 5-8th June 1995, 341-345

180 Farrar R.A., Zhang Z., Bannister S.R. and Barrite G.S. (1993) The effect of the prior austenite grain size on the transformation behaviour of C-Mn-Ni weld metal, *Journal of Material Science*, **28**, No.5, March 1993, 1385-1390

181 Zang Z. and Farrar R.A. (1996). The role of inclusions in formation of acicular ferrite in low alloy weld metals, *Materials Science and Technology*, **12**, March 1996, 237-260

182 Bhadhesia, H.K.D.H. (2001). In book: *Bainite in Steels*, 2nd Edition, Publ. IOM Communications Ltd., London, UK

183 Evans G.M. and Bailey N. (1997). In book: *Metallurgy of Basic Weld Metal*, publ. Woodhead Publishing Ltd., Cambridge, UK

184 Davenport E.S. and Bain E.C. (1930). Transformation of austenite at constant subcritical temperature, *Transactions of the Metallurgical Society of AIME*, **90**, 117-154

185 Honeycombe R.W.K. and Bhadeshia H.K.D.H. (1995). In book: *Steels – Microstructure and Properties*, 2nd Edition, Publ. Edward Arnold, London, UK

186 Chang L.C. and Bhadeshia H.K.D.H. (1995). Metallographic observations of bainite transformation mechanism, *Materials Science and Technology*, **11**, No.2, February 1995, 105-108

187 Sing S.B. and Bhadeshia H.K.D.H. (1998). Estimation of bainite plate thickness in low-alloy steels, *Materials Science and Engineering A*, **245**, No.1, 30th April 1998, 72-79

188 Farrar R.A. (1976). The role of inclusions in the ductile fracture of weld metals. *Welding and Metal fabrication*, **44**, No.8, 578 – 581

189 Ito Y. & Nakanski M. (1976). Study on Charpy impact properties of weld metal with submerged arc welding. *Sumitomo Search*, **15**, 42 – 62

190 Liu S. & Olson DL. (1986). The role of inclusions in controlling HSLA steel weld microstructures. *Welding Journal.*, **65**, No.6, 139s – 149s

191 Tweed J.H. & Knott J.F. (1983). Effect of reheating on microstructure and toughness of C-Mn weld metal. *Metal Science*, **17**, No.2, February 1983, 45 – 54

192 Gloor K, Christensen N, Maehle G and Simonson T. (1966). Non-metallic inclusions in weld metals, *Welding in the World*, **4**, No.2, 70 – 85

193 Widgery D.J. (1978). New ideas on submerged arc welding, in: *Proceedings of the International Conference on Trends in Steels and Consumables for Welding.*, publ. The Welding Institute, Cambridge, UK, 217 – 229

194 Franklin A.G. (1969). Comparison between a quantitative microscope and chemical methods for assessment of non-metallic inclusions. *Journal of the Iron & Steel Institute*, **207**, No.1, 181 – 186

195 Evans G.M. (1986). The effect of sulphur and phosphorus on the microstructure and properties of C-Mn all-weld deposits. *Oerlikon Schweissmitteilungen*, **44**, No.111, 25–35

196 Mori N., Homma H., Okita S. and Wakabayashi M. (1981). Mechanism of notch toughness improvement in Ti-B bearing weld metals. *IIW Doc IX-1196-81*

197 Dowling J.M., Corbett J.M. and Kerr H.W. (1985). Effects of inclusion compositions and size distribution on the microstructure and properties of submerged arc welds, in: *Proceedings of the Conference on Inclusions and Residuals in Steels; Effects on Fabrication and Service Behaviour*, Ottowa, Canada, publ. CANMET-CSIRA, 469 – 486

198 Barritte G.S. & Edmonds D.V. (1982). The microstructure and toughness of HSLA steel weld metal, in: *Proceedings of the Conference on Advances in the Physical Metallurgy of Steel*, Liverpool, 21-24 September 1981, publ. The Metals Society, London, 126 – 135

199 Saggase ME, Bhatti AR, Hawkins DN and Whiteman JA. (1984). Factors influencing inclusion chemistry and microstructure in submerged arc welds, in: *Proceedings of the Conference on The Effects of Residual, Impurity and Microalloying Elements on Weldability and Weld Properties*. London, 15-17th November 1983, publ. The Welding Institute, Cambridge, UK, 15-1 to 15-11

200 Akselsen O.M. and Rørvik G. (1990). Tensile Properties of heat affected zone of medium strength low carbon, C-Mn and 2.25%Cr-1%Mo steels, *Materials Science and Technology*, **6**, No.4, April 1990, 383-389

201 Svensson L-E. (1994). In book: *Control of microstructures and properties in steel arc welds*, publ. CRC Press, Florida, USA

202 Barnes A.M. (1989). The effect of intercritical thermal cycles on HAZ microstructure and toughness in C-Mn-Al-Nb steel, *Welding Institute Research Report 402*, TWI, Cambridge, UK

203 Olson D.L. and North H. (1992). In Book: Ferrous Alloy Weldments, 1st Edition, publ. Transtech Publications Ltd.

204 Fairchild D.P. (1987). Local Brittle Zones in Structural Welds, in: *Proceedings of the Conference on Welding Metallurgy of Structural Steels*, Denver, Colorado, USA, 22-26 February 1987, Publ. The Metallurgical Society/AIME, 308-318

205 Irvine K.J., Pickering F.B., Heselwood W.C. and Atkins M., *Journal of the Iron and Steel Institute*, **195**, 54-67, 1957

206 Farrar R.A.and Zhang Z.Y. (1991). Microstructural Development of C-Mn-Ni Weld Metals and the Influence of Nickel and Manganese, In: *Proceedings of the International Conference for Joining of Materials*, JOM-6, JOM-Institute, Helsingor, Denmark, 397-404

207 DeLoach Jr J.J. (1990). Microstructural features controlling ductile-to-brittle transition behaviour in high-strength martensitic steel weld metals, *United States Navy Ship Materials Engineering Department Report DTRC-SME-89/79*, October 1990

208 Blackburn J.M. (1995). Factors affecting impact toughness of low carbon bainitic weld metal, in: *Proceedings of the 4th International Conference on Trends in Welding Research*, Gatlinburg, Tennessee, 5-8th June 1995, 651-656

209 Akselsen O.M. and Simonsen T. (1987). Techniques for examining transformation behaviour in weld metal and HAZ – a state of the art review, *Welding in the World*, **25**, No.1/2, 26-34

210 Van Bohmen S.M., Sietsma J., Hermans M.J. and Richardson I.M. (2003). Kinetics of the martensitic transformation in low-alloy steel studied by means of acoustic emission, *Acta Materialia*, **51**, No.14, 4183-4196

211 Nippes E.F. and Savage W.F. (1949). Development of a specimen simulating weld heat-affected zones, *Welding Journal*, **28**, 534s-545s

212 Garner J. (1998). The influence of microalloying elements on the heat affected zone properties of linepipe steels, *MSc Thesis*, Cranfield University, Cranfield, Bedfordshire, UK

213 Phillips R.H. (1968). Improved techniques for determining transformation temperatures during simulated welding conditions, *British Welding Journal*, **15**, No.11, November 1968, 547-552

214 Dolby R.E. and Widgery D.J. (1971). The simulation of HAZ microstructures, *Welding Research International*, **1**, No.3, 1-15

215 Johnson M.Q., Edwards G.R. and Evans G.M. (1995). The effect of thermal cycles on high strength steel SMA weld metal microstructures and properties, in: *Proceedings of the 4th International Conference on Trends in Welding Research*, Gatlinburg, Tennessee, USA, 5-8 June 1995, 547-552

216 Blackburn J.M., Vassilaros M., Brandemarte A., Fox A. and Franke G. (1996). The effects of thermal cycling on ULCB weld metal, in Book: *Welding and Weld Automation in Shipbuilding*, publ. The Minerals, Metals and Materials Society, Warrendale, Pennsylvania, USA

217 Lord M. and Bhadeshia H.K.D.H. (1999). Scatter in high strength steel weld properties due to interpass temperature, in: *Proceedings of the 5th International Conference on Trends in Welding Research*, Gatlinburg, Tennessee, USA, 1-5 June 1998, publ. ASM International, 870-875

218 Berkhout C.F. (1972). A comparison of the microstructures in the simulated and weld HAZ, in: *Proceedings of the Conference on Weld Thermal Simulators for Research and Problem Solving*, London, 27 April 1972, publ. TWI, Cambridge, UK, 21-24

219 Granjon H. and Gaillard R. (1967). In-situ analysis of weld thermal cycles, *Mémoires Scientifiques Revue Métallurgic*, **64**, No.4, 335-343

220 Peddar C. (1973). Harpoon thermocouples, *Welding Institute Research Bulletin*, **14**, No.11

221 Barlow J.A. (1982). Measurement of thermal cycles in submerged arc welding, *Welding Institute Research Bulletin*, **23**, No.1, 5-8

222 Rodrigues P.E.L.B. (1978). The relationship between the welding conditions, thermal cycles, microstructure and toughness of weld metal in C-Mn steels, *PhD Thesis*, Cranfield University, Cranfield, Bedfordshire, UK

223 Tecco D.G. (1985). Thermal cycles and HAZ characteristics of single pass welds in HSLA steels, *PhD Thesis*, Cranfield University, Cranfield, Bedfordshire, UK

224 Araujo C.L.D. (1990). A study of coarse grain heat affected zone of accelerated cooled structural steels, *PhD Thesis*, Cranfield University, Cranfield, Bedfordshire, UK

225 Wei X.C., Giedt W.H. and Wei S.R. (1984). Weld zone surface temperature variation during stationary GTA (TIG) welding, in: *Proceedings of the International Conference of Quality and Reliability in Welding*, Hangzhou, China, 6-8 September 1984, **4**, Paper D31

226 Wong J. et al. (1997). In-situ phase mapping and transformation study in fusion welds, *Journal of Materials Science*, **32**, No.6, 1493-1500

227 Granjon H. (1969). The implant method for studying the weldability of high strength steel, *Metal Construction and British Welding Journal*, **1**, No.11, November 1969, 509-515

228 Phillips R.H. (1983). In situ determination of transformation temperatures in the weld heat affected zone, *Welding Journal*, **62**, No.1, January 1983,12s-18s

229 Apps R.L. and Coward M.D. (1967). Measurement of weld thermal cycles in the heat affected zone of mild steel, Cranfield College of Aeronautics, Department of Materials Report, September 1967

230 Khono R. and Jones S.B. (1978). An initial study of arc energy and thermal cycles in the submerged arc welding of steel, *Welding Institute Research Report 81/1978/PE*, December 1978, 1-20

231 Weber D. and Nau M. (1991). In book: *Electrical temperature measurement*, publ. M.K.Juchheim, Fulda, Germany

232 BS 1041-4: 1992. Temperature measurement – Part 4: Guide to the selection and use of thermocouples

233 Rosenthal D. and Schmerber R. (1938). Thermal study of arc welding – experimental verification of theoretical formulae, *Welding Journal*, **17**, April 1938, 2-8

234 Christensen N. and Simonsen T. (1981) Transformation behaviour of weld metal, *Scandinavian Journal of Metallurgy*, **10**, No.4, 147-156

235 Evans G.M. (1982). Factors affecting the microstructure and properties of C-Mn all-weld metal deposits; carbon, *Oerlikon Shweissmitteilungen*, **40**, No.99, 17-31

236 Surian E. (1991). Influence of carbon on the mechanical properties and microstructure of weld metal from high strength SMA electrodes, *Welding Journal*, **70**, No.6, 133s-140s

237 Evans G.M. (1977). Effect of manganese on the microstructure and properties of all-weld-metal deposits, *IIW Doc II-A-432-77*

238 Evans G.M. (1986). Factors affecting the microstructure and properties of C-Mn all-weld metal deposits; silicon, *Oerlikon Shweissmitteilungen*, **44**, No.110, 19-33

239 Widgery D.J. (1976). Deoxidation practice and toughness of mild steel weld metal, *Welding Journal*, **55**, March 1976, 57s-68s

240 Harrison P.L. and Farrar R.A. (1987). Microstructural development and toughness of C-Mn and C-Mn-Ni weld metals; Part 1 – microstructural development, *Metal Construction*, **19**, No.7, July 1987, 392R-399R and Part 2 – Toughness, **19**, No.8, August 1987, 447R-450R

241 Taylor D.S. and Evans G.M. (1983). Development of MMA electrodes for offshore fabrication, *Metal Construction*, **15**, No.8, August 1983, 438-443

242 Evans G.M. and Bailey N. (1997). In book: *Metallurgy of basic weld metal*, publ. Woodhead publishing Ltd., Cambridge, UK

243 Jorge J.C.F., Souza L.F.G. and Rebello J.M.A. (2001). The effect of chromium on the microstructure/toughness relationship of C-Mn weld metal deposits, *Materials Characterisation*, **47**, 195-205

244 Raiter V. and Gonzalez J.C. (1989). Influence of molybdenum on the microstructure and properties of C-Mn all-weld-metal deposits with different manganese contents, *Canadian Metallurgical Quarterly*, **28**, No.2, April/June 1989, 179-185

245 Es-Souni M., Beaven P.A. and Evans G.M. (1990). Microstructure and mechanical properties of Cu-bearing MMA C-Mn weld metal, *Oerlikon Shweissmitteilungen*, **48**, No.123, June 1990, 15-31

246 Evans G.M. (1991). The effect of titanium on the Microstructure and properties of C-Mn all-weld –metal deposits, *Oerlikon Shweissmitteilungen*, **49**, No.125, 22-33

247 Murray A.M. (1997). Examination of SAW and FCAW high strength steels for offshore structural fabrications, *PhD Thesis*, Cranfield University, Cranfield, Bedfordshire, UK

248 Johnson M.Q., Evans G.M. and Edwards G.R. (1995). The influence of titanium additions and interpass temperature on the microstructures and mechanical properties of high strength SMA weld metals, *ISIJ International*, **35**, No.10, October 1995, 1222-1231

249 Evans G.M. (1990). The effect of aluminium on the microstructure and properties of C-Mn all-weld –metal deposits, *Oerlikon Shweissmitteilungen*, **48**, No.124, 15-31

250 Brownlee J.K., Matlock D.K. and Edwards G.R. (1986). Effects of aluminium and titanium on the microstructure and properties of microalloyed steel weld metal, in: *Proceedings of the Conference on Advances in Welding Science and Technology*, Gatlinburg, Tennessee, USA, 18-22 May 1986, publ. ASM International, 245-250

251 Thewlis G. (1990).Transformation kinetics of ferrous weld metals, *Materials Science and Technology*, **10**, No.2, February 1994, 110-125

252 Fiore S. (1996). The development of welding electrodes for producing low carbon bainitic ferrite weld deposits, in Book: *Welding and Weld Automation in Shipbuilding*, publ. The Minerals, Metals and Materials Society, 135-150

253 Evans G.M. (1991). The effect of niobium in Mn containing MMA deposits, *Oerlikon Shweissmitteilungen*, **49**, No.127, 24-39

254 Evans G.M. (1991). The effect of vanadium in Mn containing MMA deposits, *Oerlikon Shweissmitteilungen*, **49**, No.126, 18-33

255 Levine E. and Hill D. (1978). Structure and Properties of HSLA weld metal containing Cb or V, in: *Proceedings of the International Conference on Welding of HSLA (Microalloyed) Structural Steels*, Rome, Italy, 9-12 November 1976, publ. ASM, 402-427

256 Mori N. et al (1982). Characteristics of mechanical properties of Ti-B bearing weld metals, *IIW Doc. II-980-82* and *IIW Doc. IX-1229-82*

257 Kluken A.O. and Grong O. (1993). Temper embrittlement in steel weld metals containing titanium and boron, in: *Proceedings of the 3rd International Conference on Trends in Welding Research*, Gatlinburg, Tennessee, USA, 1-5 June 1992, Publ. ASM International, 569-574

258 Jenkins N. and Stevens S.M. (1977). Nitrogen in ferrous welding, *Welding Institute Research Bulletin*, January 1977, 3-6

259 Blake P.D. (1979). Oxygen and nitrogen in weld metal, *Welding Research International*, **9**, No.1, 23-56

260 Kocak M. et al. (1994). Influence of titanium and nitrogen on the fracture properties of weld metals, in: *Proceedings of the Conference of Offshore Mechanics and Artic Engineering*, 1994 OMAE, **III** – Materials Engineering, 277-289

261 Evans GM. (1986). The effect of silicon on the microstructure and properties of C-Mn all-weld metal deposit. Metal Construction, **18**, No.7, 438R – 444R

262 Cochrane R.C.(1983). Weld metal microstructures – a state of the art review, *Welding in the World*, **21**, No.1/2, 16-24

263 Potapov N.N (1993) Oxygen effect on low alloy steel weld metal, *Welding Journal*, **72**, No.8, August 1993, 367s-370s

264 Ito Y., Effects of oxygen on low carbon steel weld metal, *Metal Construction*, **14**, Sept. 1982, 472-478,

265 Schuman O., Powell G. and French I. (1994) Control of microstructure in GMAW and FCAW, *Australian Welding Research CRC No. 1*, Nov 1994

266 Surian E.S., Trotte J.L. and Boniszewski T. (1992). Effect of oxygen content on Charpy V-notch toughness in 3%Ni steel SMA weld metal, *Welding Journal*, July 1992, 263s-268s

267 McRobie D.E. and Knott J.F. (1989). Effects of strain and strain ageing on fracture toughness of C-Mn weld metal, *IIW Doc. IIA-772-89*

268 Evans G.M. (1986). The effects of sulphur and phosphorous on the microstructure and properties of C-Mn all-weld metal deposits, *Oerlikon Shweissmitteilungen*, **44**, No.111, 22-35

269 Pickering F.B. (1975). High-strength, low alloy steels – a decade of progress, in: *Proceedings of Microalloying 75*, Washington D.C., USA, 1-3 October 1975, 9-30

270 Bailey N. (1994). In book: *Weldability of ferritic steels*, publ. Woodhead Publishing Ltd., Cambridge, UK

271 Oriani R.A. and Josephic P.H. (1974). Equilibrium aspects of H-induced cracking of steels, *Acta Metallurgica*, **22**, No.9, September 1974, 1065-1074

272 Wang W. et al. (1996). The use of martensite start temperature for hydrogen control, in book: *Welding and Weld Automation in Shipbuilding*, publ. The Minerals, Metals and Materials Society, 17-31

273 Liu S. (2002). Critical concerns of welding high strength steel pipelines: X80 and beyond, in proceedings of *Pipe Dreamer's Conference, Application and Evaluation of High-Grade Linepipes in Hostile Environments*, Yokohama, Japan, 7-8 November 2002, 91-108

274 Self J.A., Matlock D.K. and Olson D.L. (1984). An evaluation of austenitic Fe-Mn-Ni weld metal for dissimilar metal welding, *Welding Journal Research Supplement*, **63**, No.9, September 1984, 282s-288s

275 Wildash C. (1999). Microstructural factors affecting hydrogen induced cold cracking in high strength steel weld metal, *PhD Thesis*, University of Leeds, UK

276 Glover A.G., Horsley D.J. and Dorling D.V. (1999). High-strength steel becomes standard on Alberta gas system, *Oil and Gas Journal*, January 4th 1999

277 Barbaro F.J et al. (1996). Weldability of X80 linepipe, in : *Proceedings of the IIW Asian Pacific Welding Conference* (58th NZIW and 43rd WTIA Congress), Auckland, New Zealand, 4-9 Feb 1996, publ. New Zealand Welding Committee, Manukau City, New Zealand, **3**, 1437-1456

278 Dallam C., Narayanan B. and Quintana M. (2003). Alloying effects on properties of welds made with high strength cellulosic electrodes, in: *Proceedings of the 6th International Conference on Trends in Welding Research*, 15-19 April 2002, Pine Mountain, Georgia, publ. ASM International, 517-522

279 Widgery D.J. (2003). From laboratory to field, *World Pipelines*, **3**, No.5, June 2003, 45-47

280 Nassau L. van et al. (1995). Pipe line welding with the Innershield process, in : *Proceedings of the Conference on Pipeline Technology*, Ostende, Belgium, September 11-14 1995, publ. Elsevier Science B.V., Amsterdam, The Netherlands, **1**, 129-138

281 Price J.C. (1995). Applying the latest technology to optimise production and cost in the construction of pipelines using X80 and X100 steels, in : *Proceedings of the Conference on Pipeline Technology*, Ostende, Belgium, September 11-14 1995, publ. Elsevier Science B.V., Amsterdam, The Netherlands, **1**, 287-295

282 Glover A.G. et al. (1977). The influence of cooling rate and composition on weld metal microstructures in a C/Mn and HSLA steel, *Welding Journal Research Suppliment*, **56**, No.9, September 1977, 267s-273s

283 DeLoach Jr. J.J. et al. (1993). Current welding consumables research in the U.S. navy, *Naval Surface Warfare Centre Report CARDIVNSWC-SSM-61-93/09*, Bethesda, Maryland, USA, March 1993

284 DeLoach Jr. J.J. et al. (1999). The right welding wire could help the U.S. navy save millions, *Welding Journal*, **78**, No.6, June 1999, 55-58

285 Vassilaros M.G. and Czyryca E.J. (1993). The development of high strength, cooling rate insensitive ultra low carbon steel weld metals, *Key Engineering Materials*, **84-85**, 587-601

286 Green R.S. et al. (1993). Filler wire development for GMA welding of HSLA-100 steel, in: *Proceedings of the 3rd International Conference on the Trends in Welding Research*, Gatlinburg, Tennessee, USA, 1-5 June 1992, publ. ASM International, 359-364

287 Johnson M.Q. et al. (1993). Consumable development for advanced high strength steels, in: *Proceedings of the 3rd International Conference on the Trends in Welding Research*, Gatlinburg, Tennessee, USA, 1-5 June 1992, publ. ASM International, 353-358

288 US Patent No. 5,523,540, June 4 1996 : Alloy Rods High Strength Wire

289 European Patent 0 448 791 B1, November 29 1990 : Lincoln Electric High Strength Wire

290 Widgery D.J. (1997). Weld metals for X120 pipe, *Esab Internal Technical Report TR 815*, 27th February 1997

291 Widgery D.J. (1997). High strength weld metals: Lincoln Patent EP 0448 791 B1, *Esab Internal Technical Report TR 807*, 7th January 1997

292 Nakano T. et al. (2002). State-of-the-art GMAW wires for pipeline construction in Japan, in: *Pipe Dreamer's Conference, Application and Evaluation of High-Grade Linepipes in Hostile Environments*, Yokohama, Japan, 7-8 November 2002, 823-839

293 Barsanti L., Bruschi R. and Donati E. (2002). From X80 to X100: know-how reached by the ENI group on high strength steel, in: *Pipe Dreamer's Conference, Application and Evaluation of High-Grade Linepipes in Hostile Environments*, Yokohama, Japan, 7-8 November 2002, 231-244

294 Fonda R.W. and Spanos G. (2000). Microstructural evolution in ultra-low-carbon steel weldments – part I: controlled thermal cycling and continuous cooling transformation diagram of the weld metal, *Metallurgical and Materials Transactions A*, **31A**, September 2000, 2145-2153

295 Fairchild D. et al. (2003). Girth welding development for X120 linepipe, in: *Proceedings of the 13th International Offshore and Polar Engineering Conference*, Honolulu, Hawaii, USA, 25-30 May 2003, 26-35

296 BS ISO 3183-3:1999. Petroleum and natural gas industries – steel pipe for pipelines – technical delivery conditions – part 3: pipes of requirement class 3

297 Denys R., Lefevre A. and De Baets P. (2002). A rational approach to weld and pipe material requirements for a strain-based pipeline design, in: *Pipe Dreamer's Conference, Application and Evaluation of High-Grade Linepipes in Hostile Environments*, Yokohama, Japan, 7-8 November 2002, 121-157

298 DNV-OS-F101 (2003). Submarine Pipeline Systems, *Det Norsk Veritas Offshore Standard*

299 Cottrell A.H. (1985). In book: *An Introduction to metallurgy*, 2nd Edition, publ. Edward Arnold Ltd., London, UK

300 Civallero M.A., Parrini C. and Pizzimenti N.(1977). Production of Large-Diameter High-Strength Low-Alloy Pipe in Italy, in: *Proceedings of Micro Alloying 75*, Washington, October 1-3 1975, 451-468

301 Streisselberger A., Bauer J., Bergman B. and Schultz W. (1992). Correlation of Pipe to Plate Properties – Model Calculations and Application in the Design of X80 Linepipe Steels, in: *Proceedings of the International Conference on Pipeline Reliability*, Calgary, Canada, 3, 1-13, 2nd-5th June 1992

302 Edwards A. (2003). Control of propagating fractures in high strength steel pipelines, in: *Proceedings of the 14th Biennial Joint Technical Meeting on Pipeline Research*, EPRG/PRCI/APIA, Berlin, Germany, 19-23 May 2003, 10-1 – 10-11

303 Dawson J. and Pistone V. (1998). Probabilistic evaluation of the safety embodied in the EPRG recommendations for shear fracture arrest toughness, publ. 3R International

304 Glover A., Horsley D. and Dorling D.V. (2003). Application and installation of grade 690 (X100) linepipe, in: *Proceedings of the 14th Biennial Joint Technical Meeting on Pipeline Research*, EPRG/PRCI/APIA, Berlin, Germany, 19-23 May 2003, 7-1 – 7-14

305 Jones B.L. and Johnson D.L. (1981). Metallurgical design of major pipelines, in: *Proceedings of the Conference on Steels for Linepipe and Pipeline Fittings*, London, 21-22 Oct 1981, Publ. The Metals Society, 14-21

306 Komizo F. (1988) Weldability of large diameter grade X80 and X100 line pipe, *IIW Doc. IX-1520-88*

307 EEMUA Publication 166 (1992). Specification for line pikpe for offshore pipelines, publ. *The Engineering Equipment and Materials Users Association*, London, UK

308 API 1104 (1999). Welding of pipelines and related facilities, 19th Edition, September 1999, publ. *American Petroleum Institute*

309 CSA Z662-99 (1999). Oil and gas pipeline systems, publ. *Canadian Standards Association*

310 Tørstad E.H. and Bratfos H.A. (2002). Materials and fabrication requirements for pipelines according to DNV OS-F101, in: *Pipe Dreamer's Conference, Application and Evaluation of High-Grade Linepipes in Hostile Environments*, Yokohama, Japan, 7-8 November 2002, 109-119

311 Lian B., Denys R. and Van de Walle L. (1986) An experimental assessment on the effect of weld metal overmatching in pipeline girth welds, in: *Proceedings of the 3rd International Conference on the Welding and Performance of Pipelines*, London, 18-21 November 1986, **1**, 101-112

312 Hudson M.G., Blackman S.A., Hammond J. and Dorling D.V. (2002). The girth welding of X100 pipeline steels, in : *Proceedings of the International Pipeline Conference, IPC 02*, Calgary, Alberta, Canada, 29th September – 3rd October 2002.

313 Hammond J., Blackman S.A. and Hudson M.G. (2002). Challenges of welding X100 linepipe, in: *Pipe Dreamer's Conference, Application and Evaluation of High-Grade Linepipes in Hostile Environments*, Yokohama, Japan, 7-8 November 2002, 931-955

314 Crawford M. (2002). Welding at Matching Green, *World Pipelines*, September/October 2002

315 Sooi T.K. et al. (1995). Stress-strain properties of high performance steel and the implications for civil-structure design, in: *Proceedings of the Conference on High Performance Structural Steels*, Cleveland, Ohio, USA,30th October -1st November 1995, publ. ASM International, 35-43

316 Denys R.M., A study of the effect of yield point elongation and strain hardening rate on the fracture behaviour of welded low carbon steel, in: *Proceedings of the Seventh International Conference on Offshore Mechanics and Arctic Engineering*, Houston, Texas, 7-12 February 1988, **3**, 405-413

317 BS EN 12732:2000. Gas supply systems – welding steel pipework – functional requirements

318 R-SF-260 (1996). Statoil Pipeline Welding Specification, *Doc No. DXXX-S-000-R-SF-260*, Reissued 10.01.96

319 BS 7910:1999. Guide on methods for assessing the acceptability of flaws in metallic structures

320 BS 7448. Fracture mechanics toughness tests – Part 1 (1991)*: method for determination of KIc, critical CTOD and critical J values of metallic materials, and Part 2 (1997): method for determination of KIc, critical CTOD and critical J values of welds in metallic materials. * Part 1 now partly superseded by BS EN 12737

321 Millwood N., Sanderson N. and Hammond J. (2001). Design and construction in ultra-high strength linepipe, *Pipes and Pipelines International*, March-April 2001, 17-22

322 BS EN ISO 3690:2001, Welding and allied processes – Determination of hydrogen content in ferritic steel arc weld metal

323 Barbosa P.M.R. (2002), Development of a test geometry for evaluating the hydrogen cracking susceptibility of high strength GMA welding consumables, *MPhil Thesis*, Cranfield University, Cranfield, Bedfordshire, Sept. 2002

324 Blackman S.A. and Dorling D.V. (2002), High-speed tandem GMAW for pipeline welding, in : *Proceedings of the International Pipeline Conference, IPC 02*, Calgary, Alberta, Canada, 29th September – 3rd October 2002.

325 EN ISO 13916:1996. Welding – Guidance on the measurement of preheating temperature, interpass temperature and preheat maintenance temperature

326 BS EN 60584 Part 1 (1996) Thermocouples. Reference tables, Part 2 (1993) Thermocouple tolerances

327 Aluminium and Aluminium Alloys (1994), Publ. *ASM International*, Ohio, USA,p 641

328 Stingele A. (1968). Melting point and phase diagram determination with a new precision high-temperature microscope technique, in: *Proceedings of Thermodynamics of Nuclear Materials*, 9-24

329 Furukawa G.T.(1974), *J. Res. Natl. Bur. Stand.*, **78A**, No. 4, p 477-495

330 Mondolfo L. F (1976)., in book: *Aluminium Alloys, Structures and Properties*, Publ. Butterworths, London

331 SCXI-1328 High-accuracy isothermal terminal block installation guide (2001), publ. *National Instruments*, January 2001

332 SCXI Chassis user manual (2002), publ. *National Instruments*, December 2002

333 PCI-MIO E Series DAQ user manual (1997), publ. *National Instruments*, January 1997

334 BS EN 462-1:1994. Non-destructive testing – Image quality of radiographs – Part 1 – Image quality indicators (wire type) – determination of image quality value

335 BS EN 1435:1997. Non-destructive examination of welds – Radiographic examination of welded joints

336 BS EN 288-9:1999. Specification and approval of welding procedures for metallic materials – Part 9 : Welding procedure test for pipeline welding on land and offshore site butt welding of transmission pipelines

337 BS EN 10002-1:2001. Tensile testing of metallic materials. Part 1 : Methos of test at ambient temperature

338 BS EN 10045-1 : 1990. Charpy impact test on metallic materials. Part 1 : Test method (V- and U- notches)

339 BS EN 1043. Destructive tests on welds in metallic materials – Hardness test. Part 1 (1996) : Hardness test on arc welded joints. Part 2 (1997) : Micro hardness testing on welded joints.

340 Gladman T. and Woodhead J.H. (1960). The accuracy of point counting in metallographic investigations, *Journal of the Iron and Steel Institute*, February 1960, 189-193

341 BP Exploration Operating Company Ltd (2002). Specification for the manufacture of longitudinal seam submerged arc welded grade high strength steel (X80-X100) linepipe for gas pipelines – Supplementary requirements to API 5L (42nd edition)

342 Hudson M.G.(2000), Data analysis of Caizley D.L. MSc Thesis and associated experiments

343 Fronius TransPuls Synergic 2700/ 4000/ 5000 power source operating instructions and spare parts list, Part No. 42.0410.0882, 20/03/2002

344 Wiesner C.S. and Pisarski H.G.(1996). The significance of pop-ins during initiation fracture toughness tests, *3R International*, **35**, 10/11, 638 – 643

345 Widgery D.J. (2004) to be published in the *International Pipeline Technology Conference*, Bruge, 2004

346 Zhang Z. and Farrar R.A. (1995). An atlas of continuous cooling transformation (CCT) diagrams applicable to low carbon low alloy weld metals, publ. *The Institute of Materials*, London, **57**

347 Habraken L.J and Economopoulos M. (1967). Bainitic microstructures in low carbon alloy steels and their mechanical properties, in: *Proceedings of the conference on Transformation and Hardenability in Steels*, publ. Climax Molybdenum Co., 69-108

348 Murphy Pipelines (2002). Weld procedures (WPS and WPAR) for the Cambridge to Matching Green gas transmission extension, June 2002

349 Transcanada Pipelines Ltd. (2002). Weld procedure for Saratoga X100 loop, September 2002

350 Rosenthal D. (1935). Theoretical study of heat flow during arc welding, *National science conference*, Comptes Rendus, Bruxelles, **2**, 1277

351 API 5CT (2001). Specification for casings and tubings, seventh edition, October 1st 2001

Appendix A - WERC Single and Tandem Synergic Curve Waveforms

Table 1: Original 0.9mm Diameter Wire Waveform for Lincoln Electric Powerwave 455 STT

Wave Designer Pro - Template Pulse - 0.9mm Spoolarc 120 Trimix P2.swf

WireFeed meter / min	6	7	8	9	10	11	12	13	14	15	16
Ramp_Up_Rate	290	290	290	290	290	290	290	290	290	290	290
Tailout_Time	0.1	0.1	0.1	0.1	0.1	0.1	0.1	0.1	0.1	0.1	0.1
Peak_Amps	450	450	450	450	450	450	450	450	450	450	450
Stepoff_Amps	35	37	40	43	45	48	50	53	56	58	60
Backgrd_Amps	35	37	40	43	45	48	50	53	56	58	60
Peak_Time_ms	0.8	0.8	0.8	0.8	0.8	0.8	0.8	0.8	0.8	0.8	0.8
Backgrd_Time	8	7.2	6.4	5.6	4.8	4	3.1	2.7	2.3	1.8	1.3
Frequency	97.1	105.3	114.9	126.6	140.8	158.7	185.2	200	217.4	243.9	277.8
Tailout_Speed	0.4	0.4	0.4	0.4	0.4	0.4	0.4	0.4	0.4	0.4	0.4
Ramp_Overshoot_%	-2	-2	-1	0	0	1	1	2	3	3	4
Peak_Voltage	39.41	39.41	39.41	39.41	39.41	39.41	39.41	39.41	39.41	39.41	39.41
Adaptive_Type	Custom	Custom	Custom	Custom	Custom	Custom	Custom	Custom	Custom	Custom	Custom
Inductance	2	2	2	2	2	2	2	2	2	2	2
Short_Detect_Volt	1.93	1.93	1.93	1.93	1.93	1.93	1.93	1.93	1.93	1.93	1.93
Pinch_Current_Rise_Rate	200	200	200	200	200	200	200	200	200	200	200
Arc_Restablish_Volt	5	5	5	5	5	5	5	5	5	5	5
End_Amp	550	550	550	550	550	550	550	550	550	550	550
End_Time	2.5	2.5	2.5	2.5	2.5	2.5	2.5	2.5	2.5	2.5	2.5
Open_Circuit_Volt	40	40	40	40	40	40	40	40	40	40	40
Strike_Peak_Time	2	2	2	2	2	2	2	2	2	2	2
Strike_Peak_Amps	450	450	450	450	450	450	450	450	450	450	450
Start_Volt	21	21	21	21	21	21	21	21	21	21	21
Start_Time	35	35	35	35	35	35	35	35	35	35	35
Start_Amps	100	100	100	100	100	100	100	100	100	100	100
Adapt_PeakAmp_SF	0.02	0.02	0.02	0.02	0.02	0.02	0.02	0.02	0.02	0.02	0.02
Adapt_PeakTime_SF	0.1	0.1	0.1	0.1	0.1	0.1	0.1	0.1	0.1	0.1	0.1
Adapt_StepOff_SF	0.1	0.1	0.1	0.1	0.1	0.1	0.1	0.1	0.1	0.1	0.1
Adapt_BkgdAmp_SF	0.1	0.1	0.1	0.1	0.1	0.1	0.1	0.1	0.1	0.1	0.1
Adapt_Freq_SF	-0.1	-0.1	-0.1	-0.1	-0.1	-0.1	-0.1	-0.1	-0.1	-0.1	-0.1

Weld Process	Pulse GMAW
Wire Type	Steel
Wire Size	0.9mm
Process Name	0.9mm Spoolarc 120 Trimix P2
Procedure	ASME IX 5G Single Wire
Gas	Trimix

Table 2: Final 0.9mm Diameter Wire Waveform for Lincoln Electric Powerwave 455 STT

Wave Designer Pro - Template Pulse - 0.9mm Spoolarc 120 Trimix SAV 3.swf

WireFeed meter / min	6	7	8	9	10	11	12	13	14	15	16
Ramp_Up_Rate	290	290	290	290	290	290	290	290	287	284	281
Tailout_Time	0.1	0.1	0.1	0.1	0.1	0.1	0.1	0.1	0.1	0.1	0
Peak_Amps	401	408	415	422	429	436	443	450	457	464	471
Stepoff_Amps	14	18	22	26	30	34	38	42	45	45	45
Backgrd_Amps	14	18	22	26	30	34	38	42	45	45	45
Peak_Time_ms	0.8	0.8	0.8	0.8	0.8	0.8	0.8	0.8	0.8	0.8	0.8
Backgrd_Time	3.9	3.7	3.5	3.3	3.1	2.9	2.7	2.2	2	1.7	1.5
Frequency	163.9	166.7	172.4	178.6	185.2	192.3	200	222.2	232.6	250	270.3
Tailout_Speed	0.4	0.4	0.4	0.4	0.4	0.4	0.4	0.4	0.4	0.4	0.4
Ramp_Overshoot_%	-2	4	3	2	2	1	0	0	-2	-5	-7
Peak_Voltage	39.38	39.38	39.38	39.38	39.38	39.38	39.38	39.38	39.38	39.38	39.38
Adaptive_Type	Custom	Custom	Custom	Custom	Custom	Custom	Custom	Custom	Custom	Custom	Custom
Inductance	2	2	2	2	2	2	2	2	2	2	2
Short_Detect_Volt	1.9	1.9	1.9	1.9	1.9	1.9	1.9	1.9	1.9	1.9	1.9
Pinch_Current_Rise_Rate	200	200	200	200	200	200	200	200	200	200	200
Arc_Restablish_Volt	5	5	5	5	5	5	5	5	5	5	5
End_Amp	550	550	550	550	550	550	550	550	550	550	550
End_Time	2.5	2.5	2.5	2.5	2.5	2.5	2.5	2.5	2.5	2.5	2.5
Open_Circuit_Volt	40	40	40	40	40	40	40	40	40	40	40
Strike_Peak_Time	2	2	2	2	2	2	2	2	2	2	2
Strike_Peak_Amps	450	450	450	450	450	450	450	450	450	450	450
Start_Volt	21	21	21	21	21	21	21	21	21	21	21
Start_Time	35	35	35	35	35	35	35	35	35	35	35
Start_Amps	100	100	100	100	100	100	100	100	100	100	100
Adapt_PeakAmp_SF	0.02	0.02	0.02	0.02	0.02	0.02	0.02	0.02	0.02	0.02	0.02
Adapt_PeakTime_SF	0.1	0.1	0.1	0.1	0.1	0.1	0.1	0.1	0.1	0.1	0.1
Adapt_StepOff_SF	0.1	0.1	0.1	0.1	0.1	0.1	0.1	0.1	0.1	0.1	0.1
Adapt_BkgdAmp_SF	0.1	0.1	0.1	0.1	0.1	0.1	0.1	0.1	0.1	0.1	0.1
Adapt_Freq_SF	-0.1	-0.1	-0.1	-0.1	-0.1	-0.1	-0.1	-0.1	-0.1	-0.1	-0.1

Weld Process	Pulse GMAW
Wire Type	Steel
Wire Size	0.9mm
Process Name	0.9mm Spoolarc 120 Trimix SAV3
Procedure	ASME IX 5G Single Wire
Gas	Trimix

Table 3: Original 1.0mm Diameter Wire Waveform for Lincoln Electric Powerwave 455 STT

Wave Designer Pro - Template Pulse - 1.0mm Carbofil HT Trimix P1.swf

WireFeed meter / min	6	7	8	9	10	11	12	13	14	15
Ramp_Up_Rate	290	290	290	290	290	290	290	290	290	290
Tailout_Time	0.1	0.1	0.1	0.1	0.1	0.1	0.1	0.1	0.1	0.1
Peak_Amps	450	450	450	450	450	450	450	450	450	450
Stepoff_Amps	30	35	40	45	50	55	60	65	70	75
Backgrd_Amps	30	35	40	45	50	55	60	65	70	75
Peak_Time_ms	0.8	0.8	0.8	0.8	0.8	0.8	0.8	0.8	0.8	0.8
Backgrd_Time	6.4	5.6	4.7	3.9	3	2.3	1.8	1.5	1.2	0.9
Frequency	109.9	122	138.9	158.7	188.7	217.4	243.9	263.2	285.7	312.5
Tailout_Speed	0.4	0.4	0.4	0.4	0.4	0.4	0.4	0.4	0.4	0.4
Ramp_Overshoot_%	22	17	12	7	1	2	3	5	6	7
Peak_Voltage	39.38	39.38	39.38	39.38	39.38	39.38	39.38	39.38	39.38	39.38
Adaptive_Type	Custom	Custom	Custom	Custom	Custom	Custom	Custom	Custom	Custom	Custom
Inductance	2	2	2	2	2	2	2	2	2	2
Short_Detect_Volt	1.88	1.88	1.88	1.88	1.88	1.88	1.88	1.88	1.88	1.88
Pinch_Current_Rise_Rat	200	200	200	200	200	200	200	200	200	200
Arc_Restablish_Volt	5	5	5	5	5	5	5	5	5	5
End_Amp	550	550	550	550	550	550	550	550	550	550
End_Time	2.5	2.5	2.5	2.5	2.5	2.5	2.5	2.5	2.5	2.5
Open_Circuit_Volt	45	45	45	45	45	45	45	45	45	45
Strike_Peak_Time	2.5	2.5	2.5	2.5	2.5	2.5	2.5	2.5	2.5	2.5
Strike_Peak_Amps	550	550	550	550	550	550	550	550	550	550
Start_Volt	21	21	21	21	21	21	21	21	21	21
Start_Time	35	35	35	35	35	35	35	35	35	35
Start_Amps	200	200	200	200	200	200	200	200	200	200
Adapt_PeakAmp_SF	0.02	0.02	0.02	0.02	0.02	0.02	0.02	0.02	0.02	0.02
Adapt_PeakTime_SF	0.1	0.1	0.1	0.1	0.1	0.1	0.1	0.1	0.1	0.1
Adapt_StepOff_SF	0.1	0.1	0.1	0.1	0.1	0.1	0.1	0.1	0.1	0.1
Adapt_BkgdAmp_SF	0.1	0.1	0.1	0.1	0.1	0.1	0.1	0.1	0.1	0.1
Adapt_Freq_SF	-0.1	-0.1	-0.1	-0.1	-0.1	-0.1	-0.1	-0.1	-0.1	-0.1

Weld Process	Pulse GMAW
Wire Type	Steel
Wire Size	1.0mm
Process Name	1.0mm Carbofil HT Trimix P1
Procedure	ASME IX 5G - Single Wire
Gas	Trimix

Table 4: Final 1.0mm Diameter Wire Waveform for Lincoln Electric Powerwave 455 STT

Wave Designer Pro - Template Pulse - 1.0mm NiMo-1 Trimix sav.swf

WireFeed meter / min	6	7	8	9	10	11	12	13	14	15
Ramp_Up_Rate	273	280	287	294	300	314	328	342	356	370
Tailout_Time	0.1	0.1	0.1	0.1	0.1	0.1	0.1	0.1	0.1	0.1
Peak_Amps	485	485	485	485	485	485	485	485	485	485
Stepoff_Amps	18	24	30	36	41	44	47	50	53	56
Backgrd_Amps	18	24	30	36	41	44	47	50	53	56
Peak_Time_ms	0.8	0.8	0.8	0.8	0.8	0.8	0.7	0.7	0.7	0.7
Backgrd_Time	4.8	4.4	3.9	3.5	3.1	2.8	2.6	2.3	2	1.7
Frequency	135.1	144.9	156.3	169.5	181.8	196.1	212.8	232.6	250	277.8
Tailout_Speed	0.4	0.4	0.4	0.4	0.4	0.4	0.4	0.4	0.4	0.4
Ramp_Overshoot_%	3	2	0	-2	1	0	-2	-5	-1	-5
Peak_Voltage	39.38	39.38	39.38	39.38	39.38	39.38	39.38	39.38	39.38	39.38
Adaptive_Type	Custom	Custom	Custom	Custom	Custom	Custom	Custom	Custom	Custom	Custom
Inductance	2	2	2	2	2	2	2	2	2	2
Short_Detect_Volt	1.88	1.88	1.88	1.88	1.88	1.88	1.88	1.88	1.88	1.88
Pinch_Current_Rise_Rate	200	200	200	200	200	200	200	200	200	200
Arc_Restablish_Volt	5	5	5	5	5	5	5	5	5	5
End_Amp	550	550	550	550	550	550	550	550	550	550
End_Time	2.5	2.5	2.5	2.5	2.5	2.5	2.5	2.5	2.5	2.5
Open_Circuit_Volt	45	45	45	45	45	45	45	45	45	45
Strike_Peak_Time	2.5	2.5	2.5	2.5	2.5	2.5	2.5	2.5	2.5	2.5
Strike_Peak_Amps	550	550	550	550	550	550	550	550	550	550
Start_Volt	21	21	21	21	21	21	21	21	21	21
Start_Time	35	35	35	35	35	35	35	35	35	35
Start_Amps	200	200	200	200	200	200	200	200	200	200
Adapt_PeakAmp_SF	0.02	0.02	0.02	0.02	0.02	0.02	0.02	0.02	0.02	0.02
Adapt_PeakTime_SF	0.1	0.1	0.1	0.1	0.1	0.1	0.1	0.1	0.1	0.1
Adapt_StepOff_SF	0.1	0.1	0.1	0.1	0.1	0.1	0.1	0.1	0.1	0.1
Adapt_BkgdAmp_SF	0.1	0.1	0.1	0.1	0.1	0.1	0.1	0.1	0.1	0.1
Adapt_Freq_SF	-0.1	-0.1	-0.1	-0.1	-0.1	-0.1	-0.1	-0.1	-0.1	-0.1

Weld Process	Pulse GMAW
Wire Type	Steel
Wire Size	1.0mm
Process Name	1.0mm NiMo-1 Trimix SAV
Procedure	ASME IX 5G - Single Wire
Gas	Trimix

Table 5: 0.9mm Diameter Wire Waveform for Fronius Time Twin TPS 450

0.9mm Spoolarc 120

Synergic Point Number	1	2	3	4	5	6	7	8
WireFeed meter / min	9	10	11	12	13	14	15	16
U-Comm	16	16	16	16	16	16	16	16
Peak Time (tp) ms	1.5	1.5	1.5	1.5	1.5	1.5	1.5	1.5
Frequency (f) Hz	178	185	192	200	222	232	250	260
Background Amps (IG) A	26	30	34	50	55	60	65	65
Peak Amps (IP) A	422	430	437	444	451	465	465	465
Trigger Current (IT) A	100	100	100	100	100	100	100	100
Backgrd Time ms	4.1	3.8	3.7	3.5	3	2.8	2.5	2.3
Operating Mode	PulsPRG	PulsPRG	PulsPRG	PulsPRG	PulsPRG	PulsPRG	PulsPRG	PulsPRG
MAT mm	14.9	14.9	14.9	14.9	14.9	14.9	14.9	14.9
Burnback (s)	0.15	0.15	0.15	0.15	0.15	0.15	0.15	0.17
Pulsdelay	0	0	0	0	0	0	0	0
Delay Mode	Auto	Auto	Auto	Auto	Auto	Auto	Auto	Auto
+/- IP	0	0	0	0	0	0	0	0
+/- f	0	0	0	0	0	0	0	0
+/- IG	0	0	0	0	0	0	0	0
Ramp Up Rate (Iup) A/ms	300	300	300	300	300	300	300	300
Ramp Down Rate (Idown) A/ms	500	500	500	500	500	500	500	500
Ignition Current (A)	400	400	400	400	400	400	400	400
Ignition Increment (%)	60	60	60	60	60	60	60	60
Ignition Time (s)	0.1	0.1	0.1	0.1	0.1	0.1	0.1	0.1
CODE	CAEAC4E2	CAEAC4E2	CAEAC4E2	CAEAC4E2	CAEAC4E2	CAEAC4E2	CAEAC4E2	CAEAC4E2

Weld Process	Pulse GMAW
Wire Type	LAHS Steel
Wire Size	0.9mm
Process Name	0.9mm Spoolarc 120
Procedure	ASME IX 5G - Tandem Wire
Gas	Trimix

Table 6: Original 1.0mm Diameter Wire Waveform for Fronius Time Twin TPS 450

TCP 475

Synergic Point Number	1	2	3	4	5	6	7	8
WireFeed meter / min	6	8	10	12	14	16	18	20
U-Comm	16	16	16	16	16	16	18	20
Peak Time (tp) ms	1.8	1.8	1.8	1.8	1.8	1.8	1.8	1.8
Frequency (f) Hz	90	125	170	190	225	270	290	300
Background Amps (IG) A	60	60	60	60	60	60	100	150
Peak Amps (IP) A	475	475	475	475	475	475	525	600
Trigger Current (IT) A	100	100	100	100	100	100	100	100
Backgrd Time ms	9.3	6.2	4.1	3.5	2.6	1.9	1.6	1.5
Operating Mode	PulsPRG	PulsPRG	PulsPRG	PulsPRG	PulsPRG	PulsPRG	PulsPRG	PulsPRG
MAT mm	19	19	19	19	19	19	19	19
Burnback s	0.16	0.16	0.16	0.16	0.16	0.16	0.16	0.16
Pulsdelay	0	0	0	0	0	0	0	0
Delay Mode	Auto	Auto	Auto	Auto	Auto	Auto	Auto	Auto
+/- IP	0	0	0	0	0	0	0	0
+/- f	0	0	0	0	0	0	0	0
+/- IG	0	0	0	0	0	0	0	0
Ramp Up Rate (Iup) A/ms	300	300	300	300	300	300	300	300
Ramp Down Rate (Idown) A/ms	500	500	500	500	500	500	500	500
Ignition Current (A)	400	400	400	400	400	400	400	400
Ignition Increment (%)	60	60	60	60	60	60	60	60
Ignition Time (s)	0.1	0.1	0.1	0.1	0.1	0.1	0.1	0.1
CODE	CAEAC4E2	CAEAC4E2	CAEAC4E2	CAEAC4E2	CAEAC4E2	CAEAC4E2	CAEAC4E2	CAEAC4E2

Weld Process	Pulse GMAW
Wire Type	LAHS Steel
Wire Size	1.0mm
Process Name	TCP 475
Procedure	ASME IX 5G - Tandem Wire
Gas	Trimix

Table 7: Final 1.0mm Diameter Wire Waveform for Fronius Time Twin TPS 450 and TPS 4000 (Digital)

Fronius TPS4000 Digital Synergic Curve for 1.0mm wire based on Cranfield TCP475
(databank file name at Fronius = Puls 0622)
Located by selecting 0.9mm diameter wire and SP1 on pendant of TPS4000
Trimix Gas

WireFeed m/min	6	8	10	12	14	16	18	20
Mat lim (mm)	10.0	10.0	10.0	10.0	10.0	10.0	10.0	10.0
Mat (mm)	3.0	4.0	6.0	8.0	10.0	10.9	15.0	20.0
U r (V)	18.50	19.50	21.00	21.50	23.00	25.00	27.00	29.00
I r (A)	115.0	145.0	180.0	205.0	225.0	250.0	285.0	325.0
vD (m/min)	**6.00**	**8.00**	**10.00**	**12.00**	**14.00**	**16.00**	**18.00**	**20.00**
U pstart (V)	19.60	20.80	22.00	23.20	24.40	25.43	26.29	27.14
U pinit (V)	0.00	0.00	0.00	0.00	0.00	0.00	0.00	0.00
I sigon (A)	3.0	3.0	3.0	3.0	3.0	3.0	3.0	3.0
I b (A)	**45.0**	**47.0**	**51.0**	**55.0**	**58.0**	**58.0**	**61.0**	**65.0**
d pup (A/ms)	300.0	300.0	300.0	300.0	300.0	300.0	300.0	300.0
tau pup (ms)	0.20	0.20	0.20	0.20	0.20	0.20	0.20	0.20
I p1 (A)	**475.0**	**475.0**	**475.0**	**475.0**	**475.0**	**475.0**	**525.0**	**600.0**
t p1 (ms)	**1.80**	**1.80**	**1.80**	**1.80**	**1.80**	**1.80**	**1.80**	**1.80**
d pdo (A/ms)	500.0	500.0	500.0	500.0	500.0	500.0	500.0	500.0
I p2 (A)	100.0	100.0	100.0	100.0	100.0	100.0	100.0	100.0
t p2 (ms)	3.30	3.30	3.30	3.30	3.30	3.30	3.30	3.30
f puls (Hz)	**90.0**	**125.0**	**170.0**	**190.0**	**225.0**	**270.0**	**290.0**	**300.0**
U set (V)	**21.00**	**21.00**	**22.00**	**23.00**	**23.50**	**24.50**	**27.00**	**29.00**
F Ib pureg pi (%)	0.00	0.00	0.00	0.00	0.00	0.00	0.00	0.00
F Ip1 pureg pi (%	10.00	10.00	10.00	10.00	10.00	10.00	10.00	10.00
F f pureg pi (%)	0.00	0.00	0.00	0.00	0.00	0.00	0.00	0.00
F f pureg p (%)	0.00	0.00	0.00	0.00	0.00	0.00	0.00	0.00
I p1min (A)	280.0	280.0	280.0	280.0	280.0	280.0	280.0	280.0
F Uact int (%)	0.00	0.00	0.00	0.00	0.00	0.00	0.00	0.00
F pbal pureg (%)	50.00	50.00	50.00	50.00	50.00	50.00	50.00	50.00
F dIdU pureg (%)	0.00	0.00	0.00	0.00	0.00	0.00	0.00	0.00
F Ib alcorr (%)	5.00	5.00	5.00	5.00	5.00	5.00	5.00	5.00
F Ip1 alcorr (%)	5.00	5.00	5.00	5.00	5.00	5.00	5.00	5.00
F f alcorr (%)	0.00	0.00	0.00	0.00	0.00	0.00	0.00	0.00

Inductance (l) and Resistance (r) Measurements For WERC TPS 4000 Power Sources
25m Power and Work Return Cables

Original	l	r
Master	31	12.5
Slave	32	16

Pendant control settings: Arc length correction = 12
Droplet detachment/ arc force correction = 0

Table 8: 1.2mm metal cored wire waveform for Lincoln Electric Powerwave 455 STT

Wave Designer Pro - 1.2 Metal Core Pulse trimix 7.7 227hz 515IP.swf

WireFeed meter / min	7.7
Ramp_Up_Rate	400
Tailout_Time	0
Peak_Amps	515
Stepoff_Amps	80
Backgrd_Amps	50
Peak_Time_ms	0.8
Backgrd_Time	2.4
Frequency	227.3
Tailout_Speed	0.4
Ramp_Overshoot_%	3
Peak_Voltage	33
Adaptive_Type	Sandia
Inductance	2
Short_Detect_Volt	5
Pinch_Current_Rise_Rate	55
Arc_Restablish_Volt	15
End_Amp	550
End_Time	2.5
Open_Circuit_Volt	48
Strike_Peak_Time	2.5
Strike_Peak_Amps	550
Start_Volt	20
Start_Time	35
Start_Amps	190
Adapt_PeakAmp_SF	0
Adapt_PeakTime_SF	0
Adapt_StepOff_SF	0.3
Adapt_BkgdAmp_SF	0.3
Adapt_Freq_SF	-0.45

Weld Process	Pulse GMAW
Wire Type	Metal Core
Wire Size	0.045"
Process Name	MC Pulse
Procedure	1.2 Metal Core Pulse trimix 7.7 227hz 515IP.swf
Gas	Trimix

Appendix B - Welding Procedure Record Sheets

Single Wire Pulsed Narrow Gap Weld Procedure ML-A-3 – Spoolarc 120 + Pipe A

Cranfield UNIVERSITY

As-run Parameter Record

Weld No.: ML-A-3

Date: 12/04/2001

Description:

30" X100 Single Wire Test Weld

Welders Name/Position:

Vince DiCarlo

Material Grade:	X100
Heat Number:	*
Diameter:	30"
Thickness:	19.05mm
Welding Position:	5G
Preparation Method:	PFM
Alignment Method:	Manual
Alignment Removed:	N/A
Preheat Method:	Propane torch
Backing System	N/A
Cleaning Method:	Grinding

Joint Preparation:

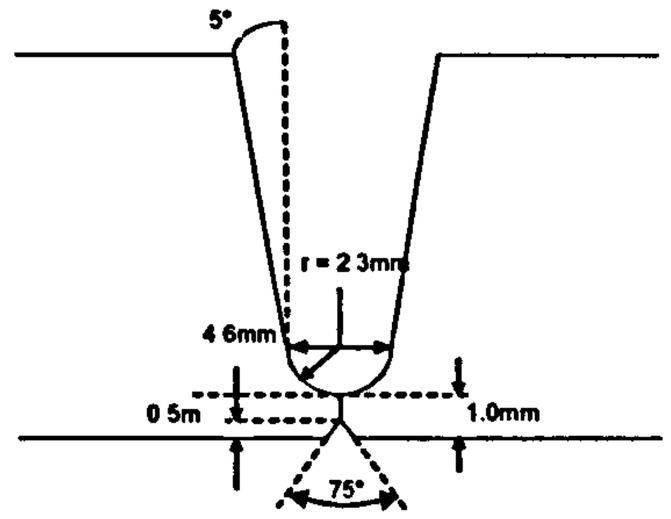

Run Sequence:

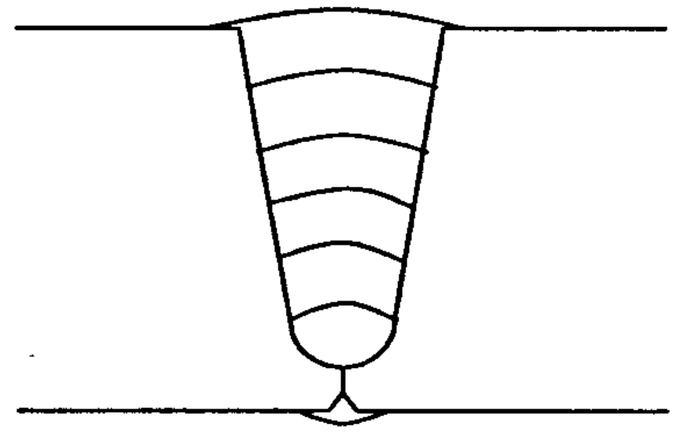

Pass	Process	Polarity	Electrode Brand	Batch	Size mm	Shielding Gas Type	Flow L/min	Temp @ Start °C	Side A WFS m/min	Amps I	Volts V	Side B WFS m/min	Amps I	Volts V	Osc mm	Travel Speed mm/min	Arc Energy kJ/min
Root	PGMAW	DC+ve	Spoolarc 120	120043	0 9	82.5Ar/12 5CO2/5He	30	110-120	13.50	190-195	17.5-19 0	13.00	180-185	19-21	-	450	0.45-0.52
Hot Pass	PGMAW	DC+ve	Spoolarc 120	120043	0.9	82.5Ar/12.5CO2/5He	30	100-105	13 00	180-185	20-22	12.50	175-180	22-24	1.5	450	0.48-0.58
Fill 1	PGMAW	DC+ve	Spoolarc 120	120043	0.9	82.5Ar/12 5CO2/5He	30	105-115	13.50	190-195	20-23	13.50	190-195	20-24	3	450	0.51-0.62
Fill2	PGMAW	DC+ve	Spoolarc 120	120043	0.9	82.5Ar/12.5CO2/5He	30	105-115	13.50	190-195	19-21	13.50	190-195	20-22	4	450	0.48-0.57
Fill3	PGMAW	DC+ve	Spoolarc 120	120043	0 9	82.5Ar/12.5CO2/5He	30	100-105	13.50	190-195	21-23	13.50	190-195	18-21	4	450	0 46-0 60
Cap	PGMAW	DC+ve	Spoolarc 120	120043	0.9	82.5Ar/12 5CO2/5He	30	95-100	13.50	190-195	25-26.5	13.50	190-195	24-26	6	450	0 61-0 68

Additional Comments:

Copper backing ring (40mm wide, 20mm deep) expanded to fit internal diameter
External passes Lincoln Powerwave 455 with pulse waveform (0.9mm Spoolarc 120 Trimix P2.swf)
Contact Tip to workpiece distance = 13mm (14-15mm for CAP)
Torch head angle 6-7° pushing
Gap at OD: 6.35 - 6.75mm
Cap oscillation side A 5.0mm; not enough

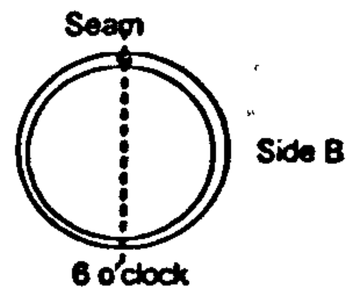

*Not stated in the interests of manufacturer confidentiality

Single Wire Pulsed Narrow Gap Procedure ML-A-4 – Carbofil HT + Pipe A

Cranfield UNIVERSITY

As-run Parameter Record

Weld No.: **ML-A-4**

Date: 17+18/ 04/01

Description:

30" X100 Single Wire Test Weld

Welders Name/Position:

Vince DiCarlo

Material Grade:	X100
Heat Number:	*
Diameter:	30"
Thickness:	19.05mm
Welding Position:	5G
Preparation Method:	PFM
Alignment Method:	Manual
Alignment Removed:	N/A
Preheat Method:	Propane torch
Backing System	N/A
Cleaning Method:	Grinding

Joint Preparation:

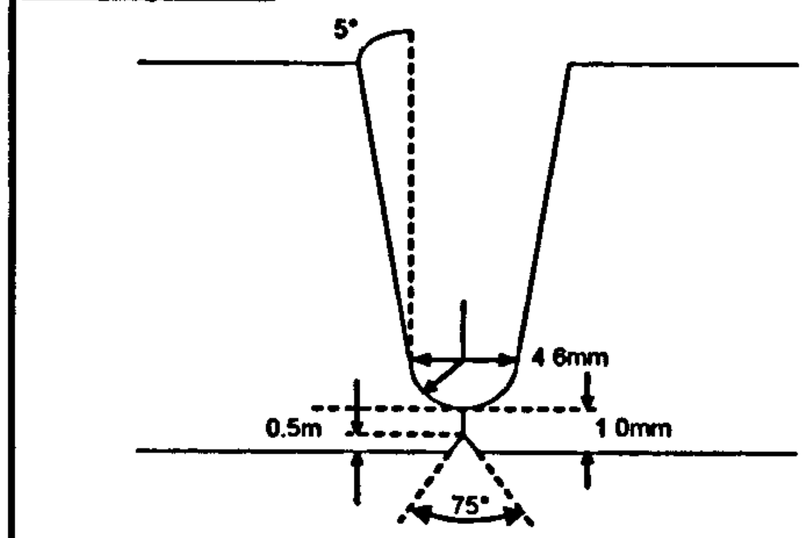

Run Sequence:

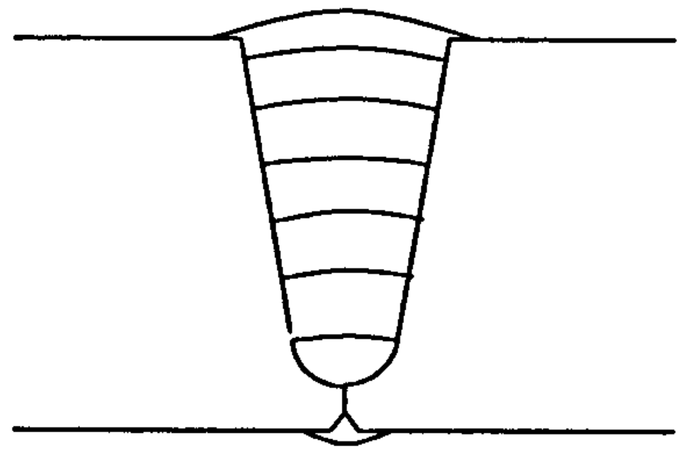

Pass	Process	Polarity	Electrode Brand	Batch	Size mm	Shielding Gas Type	Flow L/min	Temp @ Start °C	Side A WFS m/min	Amps I	Volts V	Side B WFS m/min	Amps I	Volts V	Osc mm	Travel Speed mm/min	Arc Energy kJ/min
Root	PGMAW	DC+ve	Carbofil HT	1004	1.0	82.5Ar/12.5CO2/5He	30	100-110	10.00	173-177	21-23	10 00	173-177	21-23	-	520	0 42-0.47
Hot Pass	PGMAW	DC+ve	Carbofil HT	1004	1.0	82.5Ar/12 5CO2/5He	30	100-105	10.10	175-180	21-23	10.10	175-180	21-23	1.5	520	0.42-0.48
Fill 1	PGMAW	DC+ve	Carbofil HT	1004	1.0	82.5Ar/12 5CO2/5He	30	100-110	10 00	173-177	21-23	10.00	172-176	21-23	2	520	0.42-0 47
Fill2	PGMAW	DC+ve	Carbofil HT	1004	1.0	82.5Ar/12.5CO2/5He	30	105-115	10.00	173-177	21-23	10.00	173-177	22-24	3	520	0.42-0 49
Fill3	PGMAW	DC+ve	Carbofil HT	1004	1 0	82.5Ar/12.5CO2/5He	30	105-115	10.00	173-177	21-24	10.00	173-177	21-23	4.0/3 5	520	0.42-0 49
Fill 4	PGMAW	DC+ve	Carbofil HT	1004	1 0	82.5Ar/12.5CO2/5He	30	100-110	10.00	173-177	21-24	10.00	173-177	20-23	4	520	0 40-0 49
Cap	PGMAW	DC+ve	Carbofil HT	1004	1.0	82.5Ar/12.5CO2/5He	30	105-115	8 00	145-150	24-26	8.00	145-150	24-26	6	520	0.40-0.45

Additional Comments:

Copper backing ring (40mm wide, 20mm deep) expanded to fit internal diameter
External passes Lincoln Powerwave 455 with pulse waveform (1.0mm Carbofil HT Trimix P1.swf)
Contact Tip to workpiece distance = 13mm (12mm for root, 14-15mm for CAP)
Torch head angle 6-7° pushing
Gap at OD: 6.7 - 7.0mm
Cap oscillation shoud be 7mm

*Not stated in the interests of manufacturer confidentiality

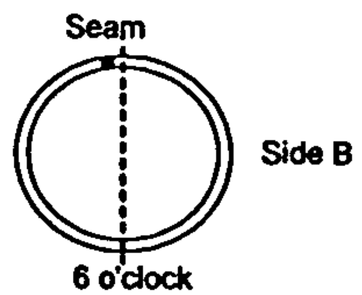

Single Wire Pulsed Narrow Gap Procedure ML-A-5 – Carbofil HT + Pipe A

Cranfield UNIVERSITY

As-run Parameter Record

Weld No.: **ML-A-5**

Date: 20/04/2001

Description:

30" X100 Single Wire Test Weld

Welders Name/Position:

Vince DiCarlo

Material Grade:	X100
Heat Number:	*
Diameter:	30"
Thickness:	19.05mm
Welding Position:	5G
Preparation Method:	PFM
Alignment Method:	Manual
Alignment Removed:	N/A
Preheat Method:	Propane torch
Backing System	N/A
Cleaning Method:	Grinding/ Wire Brush

Joint Preparation:

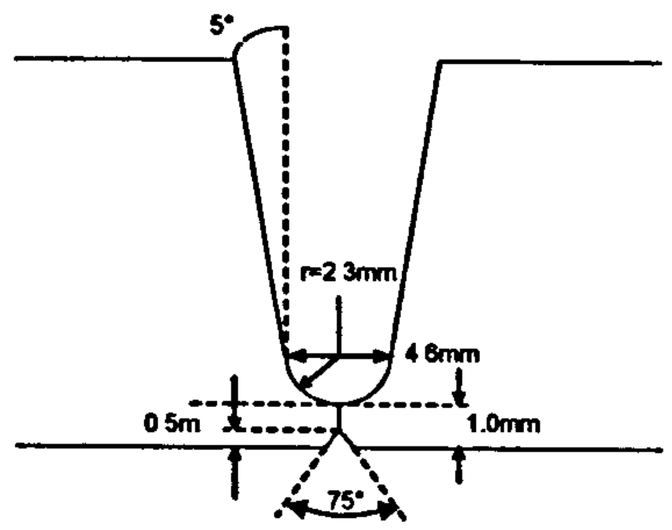

Run Sequence:

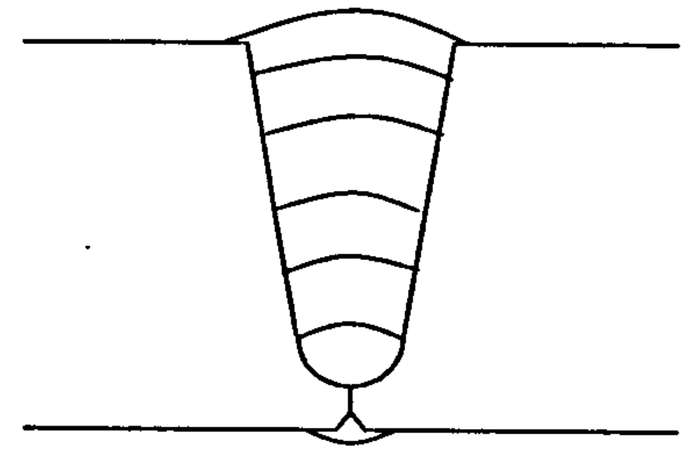

Pass	Process	Polarity	Electrode Brand	Batch	Size mm	Shielding Gas Type	Flow L/min	Temp @ Start °C	Side A WFS m/min	Amps I	Volts V	Side B WFS m/min	Amps I	Volts V	Osc mm	Travel Speed mm/min	Arc Energy kJ/min
Root	PGMAW	DC+ve	Carbofil HT	1004	1.0	82.5Ar/12.5CO2/5He	30	100-110	10.00	180-190	20-23	10 00	180-186	20-23	-	480-450	0.45-0.57
Hot Pass	PGMAW	DC+ve	Carbofil HT	1004	1 0	82.5Ar/12.5CO2/5He	30	105-115	10.00	182-186	21-23	10 00	182-186	21-23	1.5	450	0 51-0.57
Fill 1	PGMAW	DC+ve	Carbofil HT	1004	1.0	82.5Ar/12.5CO2/5He	30	110-120	10 00	182-185	21.5-23	10 00	182-186	21.5-23	2	450	0.52-0.57
Fill2	PGMAW	DC+ve	Carbofil HT	1004	1.0	82.5Ar/12 5CO2/5He	30	110-115	10 00	181-185	21-23	10.00	182-186	21.5-23	2.8	450	0 51-0.57
Fill3	PGMAW	DC+ve	Carbofil HT	1004	1.0	82.5Ar/12 5CO2/5He	30	100-115	10.00	182-186	22-24	10 00	182-186	22-24	3.5	455	0.53-0.59
Cap	PGMAW	DC+ve	Carbofil HT	1004	1.0	82.5Ar/12.5CO2/5He	30	100-110	8 00	152-156	24-26	10 00	152-156	24-25 5	6.5	460	0 48-0.52

Additional Comments:

Copper backing ring (40mm wide, 20mm deep) expanded to fit internal diameter
External passes Lincoln Powerwave 455 with pulse waveform (1.0mm Carbofil HT Trimix P1.swf)
Contact Tip to workpiece distance = 13mm (12mm for root, 14-15mm for CAP)
Torch head angle 6-7° pushing
Gap at OD: 6.25 - 6.9mm
Cap weave set ~1.5mm in from bevel edge (bevel edges still visible 5.30-6.00 for cap run)
*Not stated in the interests of manufacturer confidentiality

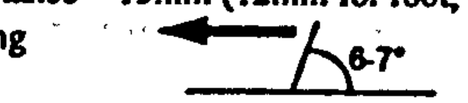

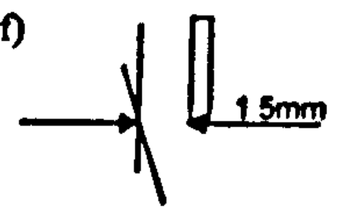

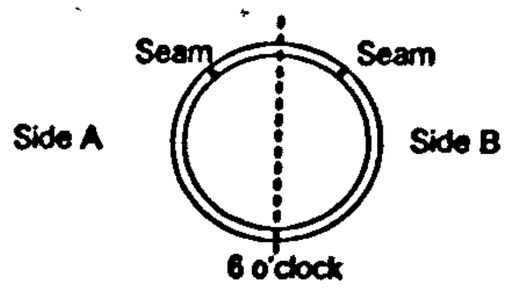

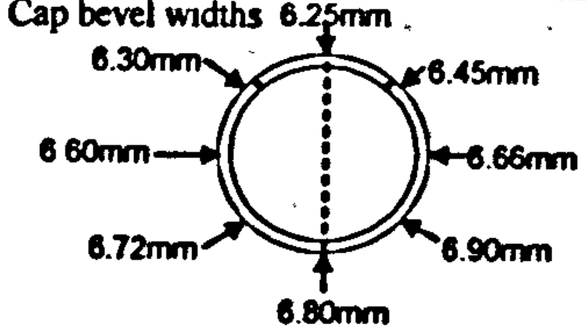

Single Wire Pulsed Narrow Gap Procedure ML-B-7 – Carbofil HT + Pipe B19

Cranfield UNIVERSITY

As-run Parameter Record

Weld No.: **ML-B-7**

Date: 24 and 25/04/01

Description:

36" X100 Single Wire Weld

Welders Name/Position:

Vince DiCarlo

Material Grade:	X100
Heat Number:	*
Diameter:	36"
Thickness:	19.05mm
Welding Position:	5G
Preparation Method:	PFM
Alignment Method:	IWM
Alignment Removed:	After Root Run
Preheat Method:	Propane torch
Backing System	N/A
Cleaning Method:	Grinding/ Wire Brush

Joint Preparation:

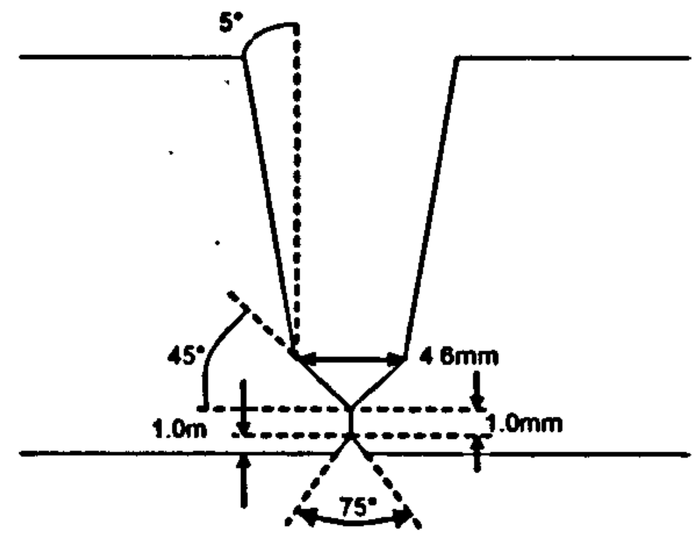

Run Sequence:

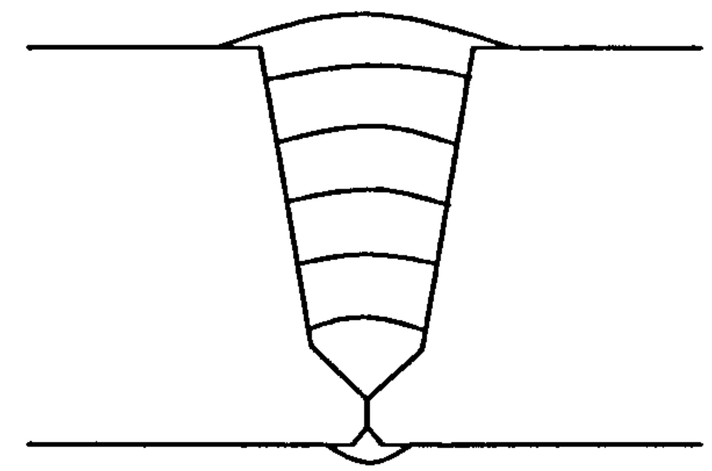

Pass	Process	Polarity	Electrode Brand	Batch	Size mm	Shielding Gas Type	Flow L/min	Temp @ Start °C	Side A WFS m/min	Amps I	Volts V	Side B WFS m/min	Amps I	Volts V	Osc mm	Travel Speed mm/min	Arc Energy kJ/min
Int. root	GMAW	DC+ve	TS-6	135346	0.9	78Ar/20CO_2/2O_2	35	100	9.65	176-180	20.5	-	-	-	-	710	0.30-0.31
Hot Pass	PGMAW	DC+ve	Carbofil HT	1004	1.0	82.5Ar/12.5CO_2/5He	30	100-110	10.00	175-183	20-23	10.00	175-183	20-23	-	500/460	0.42-0.55
Fill 1	PGMAW	DC+ve	Carbofil HT	1004	1.0	82.5Ar/12.5CO_2/5He	30	100-110	10.00	174-180	21-23	10.00	174-180	21-23	1.5	460/450	0.48-0.55
Fill2	PGMAW	DC+ve	Carbofil HT	1004	1.0	82.5Ar/12.5CO_2/5He	30	105-115	10.00	174-178	21-23	10.00	174-180	21-23	2	480/460	0.46-0.54
Fill3	PGMAW	DC+ve	Carbofil HT	1004	1.0	82.5Ar/12.5CO_2/5He	30	100-110	10.00	174-178	22-24	10.00	174-178	22-24	3	460	0.50-0.56
Strip	PGMAW	DC+ve	Carbofil HT	1004	1.0	82.5Ar/12.5CO_2/5He	30	105-115	10.00	174-178	22-24	10.00	174-180	23-25	3.0/3.5	500/460	0.46-0.59
Cap	PGMAW	DC+ve	Carbofil HT	1004	1.0	82.5Ar/12.5CO_2/5He	30	100-110	8.00	144-147	23-25	8.00	144-147	23-25.5	6.5	500	0.40-0.45
	Strip: Side A; 1.30-4.00, Side B; 1.00-4.30																

Additional Comments:

Root 6 Head IWM with Lincoln DC400 Power Supply

External passes Lincoln Powerwave 455 with pulse waveform (1.0mm Carbofil HT Trimix P1.swf)

Contact Tip to workpiece distance = 13mm (12mm for root, 14-15mm for CAP)

Torch head angle 6-7° pushing

Gap at OD: 6.53 - 6.90mm

Weave set ~1.5mm in from bevel edge (run prior to cap concave; bevel edge allready fused)

*Not stated in the interests of manufacturer confidentiality

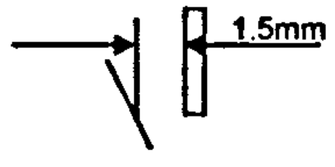

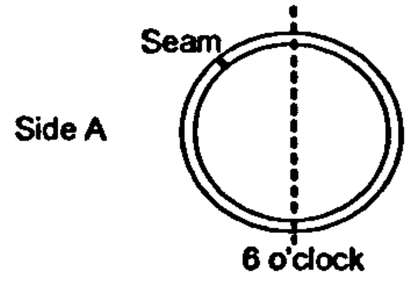

Cap bevel widths

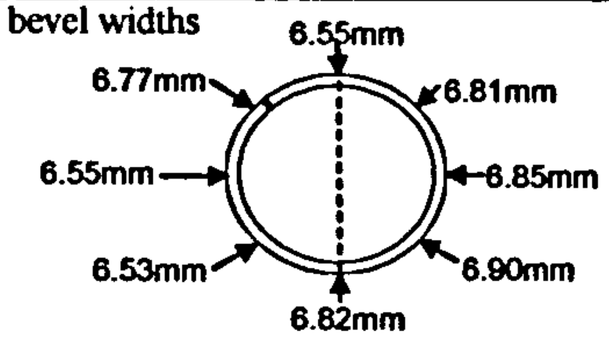

Single Wire Pulsed Narrow Gap Procedure ML-B-8 – Carbofil HT + Pipe B19 (For Repair Welds)

Cranfield UNIVERSITY

As-run Parameter Record

Weld No.: **ML-B-8**

Date: 27/04/2001

Description:

36" X100 Single Wire Weld

Welders Name/Position:

John Savill

Material Grade:	X100
Heat Number:	*
Diameter:	36"
Thickness:	19.05mm
Welding Position:	5G
Preparation Method:	PFM
Alignment Method:	IWM
Alignment Removed:	After Root Run
Preheat Method:	Propane torch
Backing System	N/A
Cleaning Method:	Grinding/ Wire Brush

Joint Preparation:

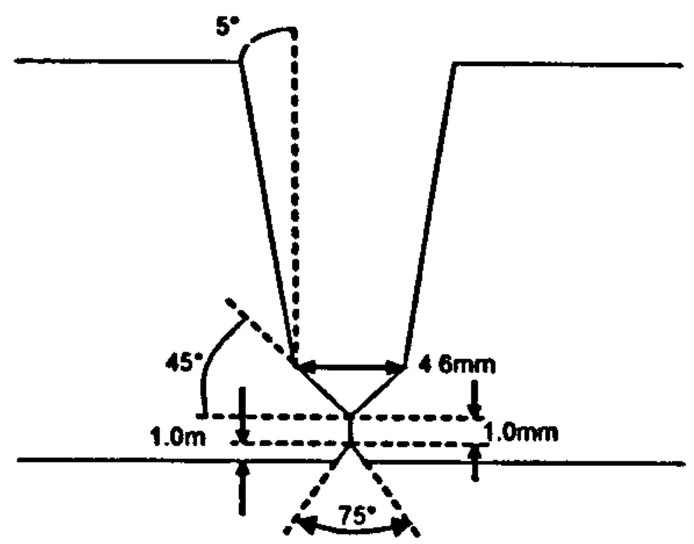

Run Sequence:

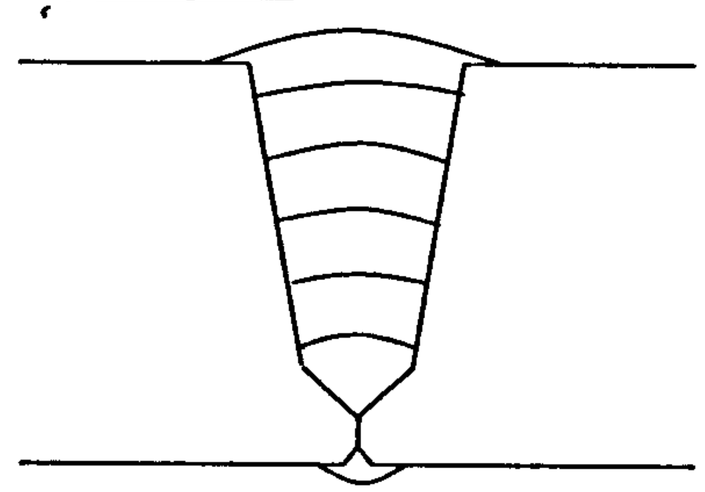

Pass	Process	Polarity	Electrode Brand	Batch	Size mm	Shielding Gas Type	Flow L/min	Temp @ Start °C	Side A WFS m/min	Amps I	Volts V	Side B WFS m/min	Amps I	Volts V	Osc mm	Travel Speed mm/min	Arc Energy kJ/min
Int. root	GMAW	DC+ve	TS-6	135346	0.9	78Ar/20CO_2/2O_2	35	100	9.65	176-180	20.5	-	-	-	-	710	0.30-0.31
Hot Pass	PGMAW	DC+ve	Carbofil HT	1004	1.0	82.5Ar/12.5CO_2/5He	30	105-115	10.00	175-180	20-23	10.00	174-178	21-23	-	480	0.44-0.52
Fill 1	PGMAW	DC+ve	Carbofil HT	1004	1.0	82.5Ar/12.5CO_2/5He	30	100-105	10.00	173-177	21-23	10.00	174-178	21-23	2	480	0.45-0.51
Fill2	PGMAW	DC+ve	Carbofil HT	1004	1.0	82.5Ar/12.5CO_2/5He	30	105-115	10.00	174-178	22-24	10.00	174-178	22-24	3	470	0.49-0.55
Fill3	PGMAW	DC+ve	Carbofil HT	1004	1.0	82.5Ar/12.5CO_2/5He	30	100-110	10.00	174-178	22-25	10.00	174-178	22-24.5	3.5	480	0.48-0.56
Strip	PGMAW	DC+ve	Carbofil HT	1004	1.0	82.5Ar/12.5CO_2/5He	30	100-105	10.00	174-178	23-25.5	10.00	174-178	23-25	3.5	460	0.52-0.59
Cap	PGMAW	DC+ve	Carbofil HT	1004	1.0	82.5Ar/12.5CO_2/5He	30	105-115	8.50	150-155	24-26	8.65	153-156	24-26	6.5	460	0.47-0.53
	Strip: Side A; 1.30-4 00, Side B; 1.00-4.30																

Additional Comments:

Root 6 Head IWM with Lincoln DC400 Power Supply
External passes Lincoln Powerwave 455 with pulse waveform (1.0mm Carbofil HT Trimix P1.swf)
Contact Tip to workpiece distance = 13mm (12mm for root, 14-15mm for CAP)
Torch head angle 6-7° pushing

Gap at OD: 6.42 - 6.85mm
Weave set ~1.5mm in from bevel edge
*Not stated in the interests of manufacturer confidentiality

Pipe mismatch; cap surface

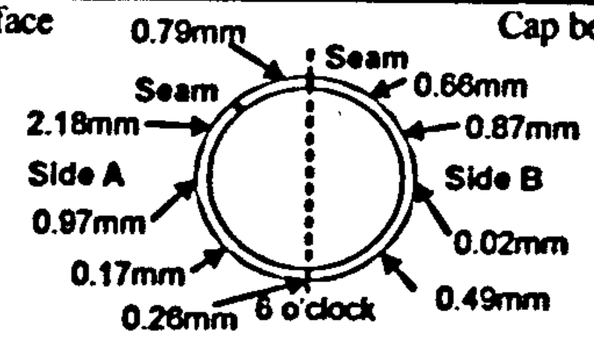

Cap bevel widths

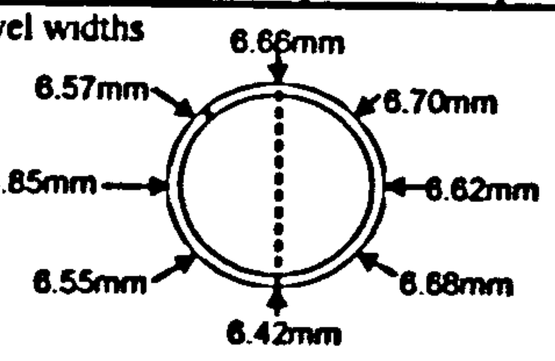

Pipe Thickness
A 18.98-19.28
B 19.28-19.34

Single Wire Pulsed Narrow Gap Procedure 7691 (Thyssen MoNi + Pipe A)

Pass No.	Process	Electrode			Shielding Gas		Temp .at start (°C)	Contact Tip to workpiece distance (mm)	Wire Feed Speed (m/min)	Amps (A)	Voltage (V)	Oscillation (mm)	Travel Speed (mm/min)	Arc Energy (kJ/mm)
		Polarity	Brand	Wire dia.(mm)	Type	Flow (l/min)								
1	GMAW	DC+ve	Supramig	1.0	80Ar/ 20CO_2	30	100	11-14	11-14	250-270	24-26	0-1	1100-1400	0.27-0.40
Fill	PGMAW	DC+ve	MoNi	1.0	90Ar/ 10CO_2	30	110-140	9-12	9-12	210-240	24-26	1-3	400-600	0.43-0.86
Cap	PGMAW	DC+ve	MoNi	1.0	90Ar/ 10CO_2	30	150	9-12	7-9	160-190	24-26	2-4	300-500	0.46-1.00
Comments: Pulsed Transfer, Welding Position 5G, Power Supply Miller Invision 456P + 564M Controller														

Single Wire Pulsed Narrow Gap Procedure 7625 (Thyssen MoNi + Pipe B19)

Pass No.	Process	Electrode			Shielding Gas		Temp .at start (°C)	Contact Tip to workpiece distance (mm)	Wire Feed Speed (m/min)	Amps (A)	Voltage (V)	Oscillation (mm)	Travel Speed (mm/min)	Arc Energy (kJ/mm)
		Polarity	Brand	Wire dia.(mm)	Type	Flow (l/min)								
1	GMAW	DC+ve	Supramig	1.0	80Ar/ 20CO_2	30	100	11-14	11-14	250-270	24-26	0-1	1100-1400	0.27-0.40
Fill	PGMAW	DC+ve	MoNi	1.0	90Ar/ 10CO_2	30	110-140	9-12	9-12	210-240	24-26	1-3	400-600	0.43-0.86
Cap	PGMAW	DC+ve	MoNi	1.0	90Ar/ 10CO_2	30	150	9-12	7-9	160-190	24-26	2-4	300-500	0.46-1.00
Comments: Pulsed Transfer, Welding Position 5G, Power Supply Miller Invision 456P + 564M Controller														

Single Wire Pulsed Narrow Gap Procedure ML-B15-1 – Spoolarc 120 + Pipe B15

Cranfield UNIVERSITY

As-run Parameter Record

Weld No.: ML-B15-1

Date: 23/10/2001

Description:

X100 Single Wire Weld

Welders Name/Position:

Vince DiCarlo

Material Grade:	X100
Heat Number:	*
Diameter:	36"
Thickness:	14.90mm
Welding Position:	ASME IX 5G
Preparation Method:	PFM
Alignment Method:	IWM
Alignment Removed:	After Root Run
Preheat Method:	Propane
Backing System	N/A
Cleaning Method:	Grind/ Wire Brush

Joint Preparation:

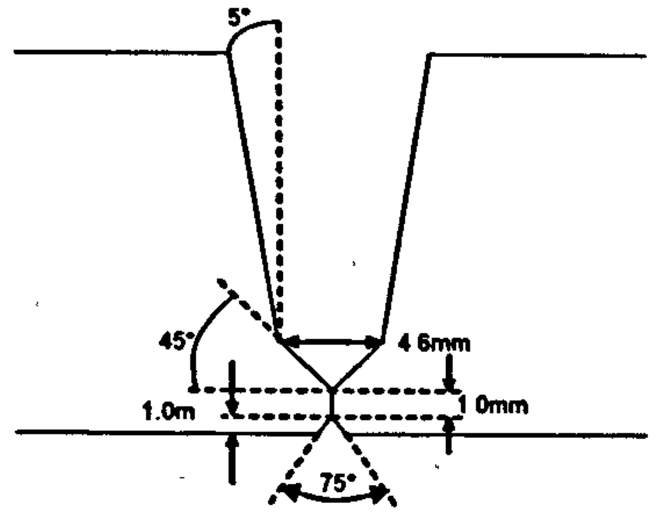

Run Sequence:

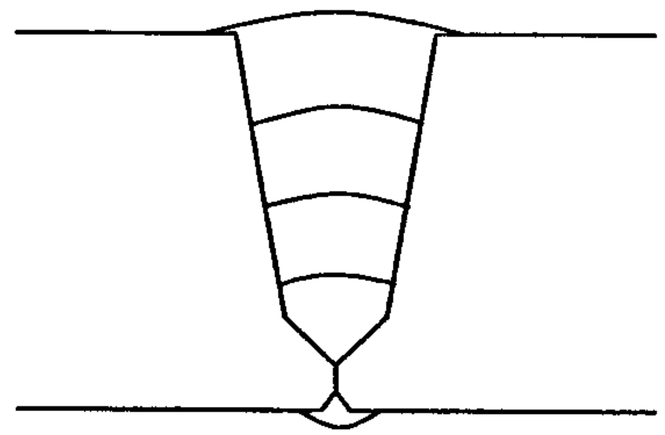

Pass	Process	Polarity	Electrode Brand	Batch	Size mm	Shielding Gas Type	Flow L/min	Temp @ Start °C	Side A WFS m/min	Amps I	Volts V	Side B WFS m/min	Amps I	Volts V	Osc mm	Travel Speed mm/min	Arc Energy kJ/min
Int. root	GMAW	DC+ve	TS-6	135346	0.9	78Ar/20CO_2/2O_2	35	100	9.65	176-180	20.5	9.65	176-180	20.5	-	710	0.30-0.31
1	PGMAW	DC+ve	Spoolarc 120	120049	0.9	82 5%Ar/ 12 5%CO2/ 5%He	25	100-120	12 50	178-182	19-21	12.50	178-182	20-22	-	460	0 44-0.52
2	PGMAW	DC+ve	Spoolarc 120	120049	0.9	82 5%Ar/ 12 5%CO2/ 5%He	25	100-120	12.50	178-182	21-23	12.50	178-182	22-24	1 5	460	0.49-0.57
3	PGMAW	DC+ve	Spoolarc 120	120049	0.9	82 5%Ar/ 12 5%CO2/ 5%He	25	100-120	12.50	178-182	22-24	12.50	178-182	22-24	2 65	450/440	0.52-0 60
Cap	PGMAW	DC+ve	Spoolarc 120	120049	0 9	82 5%Ar/ 12 5%CO2/ 5%He	25	100-120	11.00	160-165	23-25	12.50	155-160	23-25	6.5	450/440	0 47-0 56

Additional Comments:

Root 6 Head IWM with Lincoln DC400 Power Supply
External passes Lincoln Powerwave 455 with pulse waveform (0.9mm Spoolarc 120 Trimix SAV3.swf)
Contact Tip to workpiece distance = 12.5mm (14 mm for CAP)
Torch head angle 6-7° pushing
Gap at OD: 6.09 - 6.40mm

X-Ray markings;

12 o'clock	64
3 o'clock	137 Side A
6 o'clock	208
9 o'clock	281 Side B

*Not stated in the interests of manufacturer confidentiality

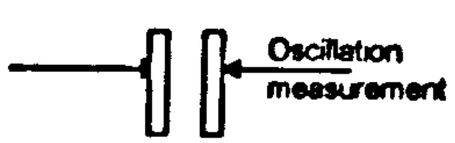

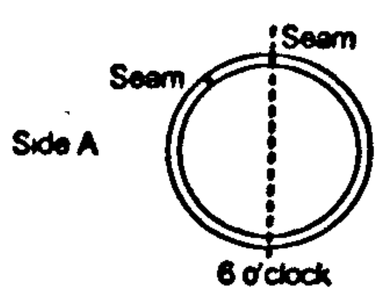

Cap Widths

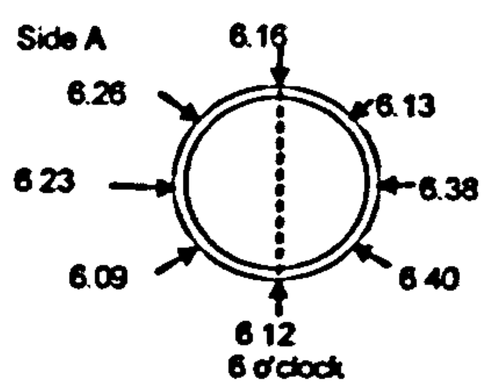

Depth to bevel base (add 0.75mm to values)

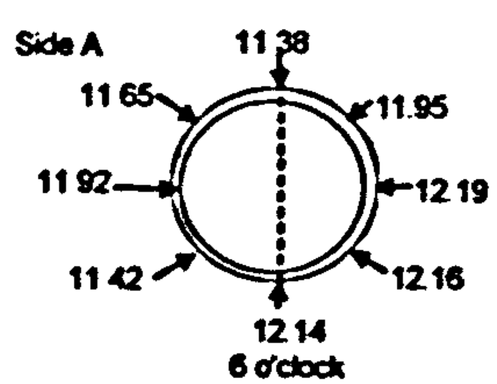

Single Wire Pulsed Narrow Gap Procedure ML-B15-3 – Carbofil NiMo-1 + Pipe B15

Cranfield UNIVERSITY — **As-run Parameter Record**

Weld No.: ML-B15-3

Date: 03/01/2002

Description:

X100 Single Wire Weld

Welders Name/Position:

John Savill
Vince DiCarlo

Material Grade:	X100
Heat Number:	*
Diameter:	36"
Thickness:	14.9mm
Welding Position:	ASME IX 5G
Preparation Method:	PFM
Alignment Method:	IWM
Alignment Removed:	After Root Run
Preheat Method:	Propane
Backing System	N/A
Cleaning Method	Grind/ wire Brush

Joint Preparation:

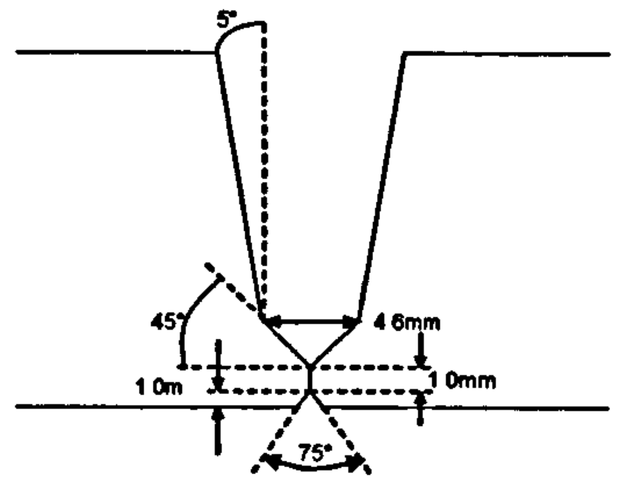

Run Sequence:

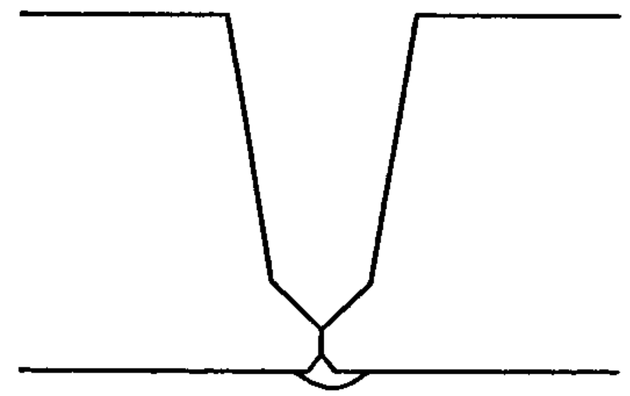

Pass	Process	Polarity	Electrode Brand	Batch	Size mm	Shielding Gas Type	Flow L/min	Temp @ Start °C	Side A WFS m/min	Amps I	Volts V	Side B WFS m/min	Amps I	Volts V	Osc. Freq beats per min	Osc Width mm	CTWD mm	Travel Speed mm/min	Arc Energy kJ/mm
Int. root	GMAW	DC+ve	TS-6	135346	0.9	78Ar/20CO_2/2O_2	35	100	9.65	176-180	20.5	9.65	176-180	20.5	-	-	10	710	0.30-0.31
1	PGMAW	DC+ve	Carbofil NiMo-1	14233	1 0	82 5%Ar/12 5%CO2/5%He	25	100	10 00	175-180	23-24	10.00	175-180	23-24	211	1.5	15	490	0 49-0.53
2	PGMAW	DC+ve	Carbofil NiMo-1	14233	1 0	82 5%Ar/12 5%CO2/5%He	25	100	10 00	175-180	23-24	10 00	175-180	23-24	211	2	15	490	0.49-0 53
3	PGMAW	DC+ve	Carbofil NiMo-1	14233	1 0	82 5%Ar/12 5%CO2/5%He	25	100	10 00	175-180	23-24	10.00	175-180	23-24	211	3.5	15	490	0.49-0.53
4	PGMAW	DC+ve	Carbofil NiMo-1	14233	1.0	82 5%Ar/12 5%CO2/5%He	25	100	8 50	157-162	22-24	8 50	157-162	22-24	211	4.5	15	490	0 42-0 48
Cap	PGMAW	DC+ve	Carbofil NiMo-1	14233	1 0	82 5%Ar/12 5%CO2/5%He	25	100	8.50	157-162	22-24	8 50	157-162	22-24	211	6.5	15	490	0 42-0 48

Additional Comments:

Root 6 Head IWM with Lincoln DC400 Power Supply
External passes Lincoln Powerwave 455 with pulse waveform: NiMo-1 Trimix Sav.swf
Torch head angle 6-7° pushing
Gap at OD: 5.74 - 6.12mm
Pass 3 should have 3.0mm oscillation
beats per minute = no. of complete cycles per minute (ie left-right-left)
*Not stated in the interests of manufacturer confidentiality

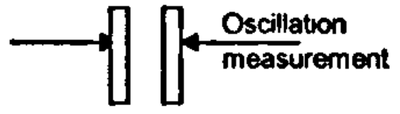

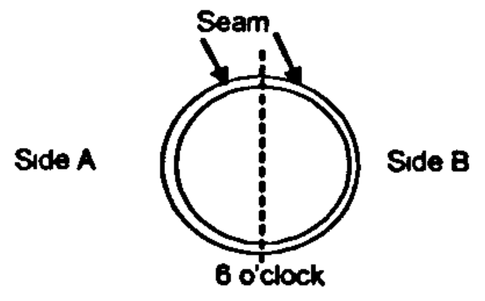

Cap Widths

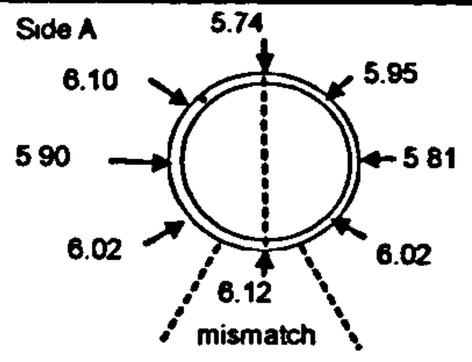

Dual Torch Dip Transfer Narrow Gap Welding Procedures – 100mm Torch Spacing

Weld No. 7544 – Bohler X70-IG+ Pipe A, Weld No. 7549 - Bohler X70-IG+ Pipe B19, Weld No. 7624 – Bohler X70-IG + Pipe C

Pass No.	Process	Electrode			Shielding Gas			Contact Tip to workpiece distance (mm)	Torch 1			Torch 2					
		Polarity	Brand	Wire dia. (mm)	Type	Flow (l/min)	Temp .at start (°C)		Wire Feed Speed (m/min)	Amps (A)	Voltage (V)	Wire Feed Speed (m/min)	Amps (A)	Voltage (V)	Oscillation (mm)	Travel Speed (mm/min)	Arc Energy (kJ/mm)
1+ 2	GMAW	DC+ve	Supramig X70-IG	1.0 1.0	80Ar/ 20CO_2	24-28	100	12-15 13-17	12-15	260-280	24-26	12-14	230-250	25-27	0-1	1100-1400	0.25-0.40
Fills	GMAW	DC+ve	X70-IG	1.0	80Ar/ 20CO_2	24-28	110-130	13-17	12-14	230-250	25-27	11-13	220-240	25-27	1-3	800-1000	0.33-0.51
Cap	GMAW	DC+ve	X70-IG	1.0	80Ar/ 20CO_2	24-28	130	13-17	9-10	210-230	23-25	9-10	210-230	23-25	1-3	800-1000	0.29-0.43
Comments Dip Transfer, Welding Position 5G, Power Supply Kemppi PS 3500, Torch spacing 100mm, Cap run torches offset																	

Dual Torch Dip Transfer Narrow Gap Welding Procedures – 100mm Torch Spacing

Weld No. 7632 – Thyssen MoNi + Pipe A, 7546 – Thyssen MoNi + Pipe B19, 7548 – Thyssen MoNi + Pipe C

Pass No.	Process	Electrode			Shielding Gas			Contact Tip to workpiece distance (mm)	Torch 1			Torch 2					
		Polarity	Brand	Wire dia. (mm)	Type	Flow (l/min)	Temp .at start (°C)		Wire Feed Speed (m/min)	Amps (A)	Voltage (V)	Wire Feed Speed (m/min)	Amps (A)	Voltage (V)	Oscillation (mm)	Travel Speed (mm/min)	Arc Energy (kJ/mm)
1+ 2	GMAW	DC+ve	Supramig MoNi	1.0 1.0	80Ar/ 20CO_2	24-28	100	12-15 13-17	12-15	260-280	24-26	12-14	230-250	25-27	0-1	1100-1400	0.25-0.40
Fills	GMAW	DC+ve	MoNi	1.0	80Ar/ 20CO_2	24-28	110-130	13-17	12-14	230-250	25-27	11-13	220-240	25-27	1-3	800-1000	0.33-0.51
Cap	GMAW	DC+ve	MoNi	1.0	80Ar/ 20CO_2	24-28	130	13-17	9-10	210-230	23-25	9-10	210-230	23-25	1-3	800-1000	0.29-0.43
Comments Dip Transfer, Welding Position 5G, Power Supply Kemppi PS 3500, Torch spacing 100mm, Cap run torches offset																	

Dual Torch Dip Transfer Narrow Gap Welding Procedures – 100mm Torch Spacing

Weld No. 8868 – Elgamatic 135 + Pipe B15

Pass No.	Process	Electrode			Shielding Gas			Contact Tip to workpiece distance (mm)	Torch 1			Torch 2			Oscillation (mm)	Travel Speed (mm/min)	Arc Energy (kJ/mm)
		Polarity	Brand	Wire dia. (mm)	Type	Flow (l/min)	Temp .at start (°C)		Wire Feed Speed (m/min)	Amps (A)	Voltage (V)	Wire Feed Speed (m/min)	Amps (A)	Voltage (V)			
1+ 2	GMAW	DC+ve	Supramig Elgamatic 135	1.0 1.0	80Ar/ 20CO_2	24-28	100	12-15 13-17	12-15	260-280	24-26	12-14	230-250	25-27	0-1	1100-1400	0.25-0.40
Fills	GMAW	DC+ve	Elgamatic 135	1.0	80Ar/ 20CO_2	24-28	110-130	13-17	12-14	230-250	25-27	11-13	220-240	25-27	1-3	800-1000	0.33-0.51
Cap	GMAW	DC+ve	Elgamatic 135	1.0	80Ar/ 20CO_2	24-28	130	13-17	9-10	210-230	23-25	9-10	210-230	23-25	1-3	800-1000	0.29-0.43
Comments Dip Transfer, Welding Position 5G, Power Supply Kemppi PS 3500, Torch spacing 100mm, Cap run torches offset																	

Weld No. 8876 – Thyssen MoNi + Pipe B15

Pass No.	Process	Electrode			Shielding Gas			Contact Tip to workpiece distance (mm)	Torch 1			Torch 2			Oscillation (mm)	Travel Speed (mm/min)	Arc Energy (kJ/mm)
		Polarity	Brand	Wire dia. (mm)	Type	Flow (l/min)	Temp .at start (°C)		Wire Feed Speed (m/min)	Amps (A)	Voltage (V)	Wire Feed Speed (m/min)	Amps (A)	Voltage (V)			
1+ 2	GMAW	DC+ve	Supramig MoNi	1.0 1.0	80Ar/ 20CO_2	24-28	100	12-15 13-17	12-15	260-280	24-26	12-14	230-250	25-27	0-1	1100-1400	0.25-0.40
Fills	GMAW	DC+ve	MoNi	1.0	80Ar/ 20CO_2	24-28	110-130	13-17	12-14	230-250	25-27	11-13	220-240	25-27	1-3	800-1000	0.33-0.51
Cap	GMAW	DC+ve	MoNi	1.0	80Ar/ 20CO_2	24-28	130	13-17	9-10	210-230	23-25	9-10	210-230	23-25	1-3	800-1000	0.29-0.43
Comments Dip Transfer, Welding Position 5G, Power Supply Kemppi PS 3500, Torch spacing 100mm, Cap run torches offset																	

Dual Torch Dip Transfer Narrow Gap Welding Procedures – 50mm Torch Spacing

Weld No. 9692B – Elgamatic 135 + Pipe B15, 9692T – Thyssen Union X85 + Pipe B15

Pass No.	Process	Electrode			Shielding Gas			Contact Tip to workpiece distance (mm)	Torch 1			Torch 2			Oscillation (mm)	Travel Speed (mm/min)	Arc Energy (kJ/mm)
		Polarity	Brand	Wire dia. (mm)	Type	Flow (l/min)	Temp .at start (°C)		Wire Feed Speed (m/min)	Amps (A)	Voltage (V)	Wire Feed Speed (m/min)	Amps (A)	Voltage (V)			
1+ 2	GMAW	DC+ve	Supramig Elgamatic 135/ Union X85	1.0 1.0	80Ar/ 20CO_2	24-28	100	12-15 13-17	12-15	260-280	24-26	12-14	230-250	25-27	0-1	1100-1400	0.25-0.40
Fills	GMAW	DC+ve	Elgamatic 135/ Union X85	1.0	80Ar/ 20CO_2	24-28	110-130	13-17	12-14	230-250	25-27	11-13	220-240	25-27	1-3	800-1000	0.33-0.51
Cap	GMAW	DC+ve	Elgamatic 135/ Union X85	1.0	80Ar/ 20CO_2	24-28	130	13-17	9-10	210-230	23-25	9-10	210-230	23-25	1-3	800-1000	0.29-0.43
Comments Dip Transfer, Welding Position 5G, Power Supply Kemppi PS 3500, Torch spacing 50mm, Cap run torches offset																	

352

Weld No. 9726B Elga Elgamatic 135 + Pipe B15, Weld No. 9726T Thyssen Union X85 + Pipe B15

Pass No.	Process	Electrode			Shielding Gas			Contact Tip to workpiece distance (mm)	Torch 1			Torch 2			Oscillation (mm)	Travel Speed (mm/min)	Arc Energy (kJ/mm)
		Polarity	Brand	Wire dia. (mm)	Type	Flow (l/min)	Temp .at start (°C)		Wire Feed Speed (m/min)	Amps (A)	Voltage (V)	Wire Feed Speed (m/min)	Amps (A)	Voltage (V)			
1+ 2	GMAW	DC+ve	Supramig Elgamatic 135/ Union X85	1.0 1.0	50Ar/ 50CO_2	24-28	100	12-15 13-17	12-15	260-280	24-26	12-14	230-250	25-27	0-1	1100-1400	0.25-0.40
Fills	GMAW	DC+ve	Elgamatic 135/ Union X85	1.0	50Ar/ 50CO_2	24-28	110-130	13-17	12-14	230-250	25-27	11-13	220-240	25-27	1-3	800-1000	0.33-0.51
Cap	GMAW	DC+ve	Elgamatic 135/ Union X85	1.0	50Ar/ 50CO_2	24-28	130	13-17	9-10	210-230	23-25	9-10	210-230	23-25	1-3	800-1000	0.29-0.43
Comments Dip Transfer, Welding Position 5G, Power Supply Kemppi PS 3500, Torch spacing 50mm, Cap run torches offset																	

Tandem Wire Synchronised Pulsed Transfer Narrow Gap Welding Procedure ML-B-12

Cranfield UNIVERSITY

As-run Parameter Record

Weld No.: ML-B-12

Date: 29/07/2002

Description:

X100 Tandem Weld

Welders Name/Position:

J Savill

Material Grade:	X100
Heat Number.	•
Diameter:	36"
Thickness	19.05mm
Welding Position:	ASME IX 5G
Preparation Method	PFM
Alignment Method	Manually tacked (external) prior to internal root
Alignment Removed.	After Root Run
Preheat Method.	Propane
Backing System	N/A
Cleaning Method	Grind/ wire Brush

Joint Preparation:

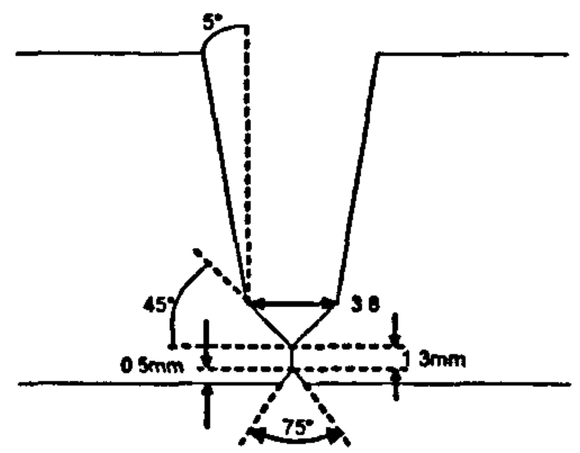

Run Sequence:

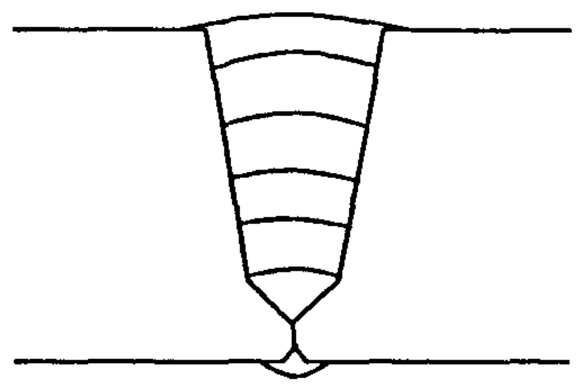

Pass	Process	Polarity	Electrode Brand	Batch	Size mm	Shielding Gas Type	Flow L/min	Temp @ Start °C	Lead WFS m/min	Lead Amps I	Lead Volts V	Trial WFS m/min	Trial Amps I	Trial Volts V	Osc. Freq beats per min	Osc mm	CTWD mm	Travel Speed mm/min	Arc Energy kJ/min
Int root	GMAW	DC+ve	TS-6	135346	0 9	78Ar/20CO_2/2O_2	35	100	9 65	176-180	20 5	9 65	176-180	20 5	-	-	10	710	0 30-0 31
1	PGMAW	DC+ve	Carbofil NiMo-1	14233	1 0	82 5%Ar/12 5%CO2/5%He	30	100-105	13 50	220-225	17-19	13 50	220-225	17-19	600	1 60 (35)	~13 5	1295	0 35-0 40
2	PGMAW	DC+ve	Carbofil NiMo-1	14233	1 0	82 5%Ar/12 5%CO2/5%He	30	105-110	13 50	220-230	18-20	13 50	220-230	18-20	600	2 75 (70)	~13 5	1295	0 37-0 43
3	PGMAW	DC+ve	Carbofil NiMo-1	14233	1 0	82 5%Ar/12 5%CO2/5%He	30	100-110	13 50	220-230	18-20	13 50	220-230	18-20	600	2 75 (70)	~13 5	1295	0 37-0 43
4 Sd A	PGMAW	DC+ve	Carbofil NiMo-1	14233	1 0	82 5%Ar/12 5%CO2/5%He	30	105-115	11 70	195-200	18-21	11.70	195-200	18-21	600	3 50 (95)	~13 5	1295	0 32-0 39
4 Sd B	PGMAW	DC+ve	Carbofil NiMo-1	14233	1 0	82 5%Ar/12 5%CO2/5%He	30	100-110	10 00	180-190	17-20	10 00	180-190	17-20	600	3 35 (90)	~13 5	1092	0 34-0 42
5	PGMAW	DC+ve	Carbofil NiMo-1	14233	1 0	82 5%Ar/12 5%CO2/5%He	30	110-120	10 00	180-190	18-21	10 00	180-190	18-21	600	4 05 (115)	~13 5	1194	0 33-0 40
Cap Sd A	PGMAW	DC+ve	Carbofil NiMo-1	14233	1 0	82 5%Ar/12 5%CO2/5%He	30	115-120	10 00	180-190	19-22	10 00	180-190	19-22	600	4 05 (95)	~13 5	1092	0 38-0 46
Cap Sd B	PGMAW	DC+ve	Carbofil NiMo-1	14233	1 0	82 5%Ar/12 5%CO2/5%He	30	110-120	10 00	180-190	19-22	10 00	180-190	19-22	600	7 0 (220)	~13 5	1092	0 38-0 46
															Values in brackets are RMS setting				

Additional Comments.

Internal Root used ESAB Arist 2000 and rotated pipe (effectively vertical down welding)
External passes Fronius Time Twin syncronised power sources (waveform as per ML-B15-16)
Torch head angle 6-7° pushing
Gap at OD. 6 07 - 6.44
beats per minute = no of complete cycles per minute (ie left-right-left)
*Not stated in the interests of manufacturer confidentiality
Run 1 Sd A : Centreline crack from 2 00 to 5 30. V good profile @ 6 00
Run 1 Sd B : Cracking as per Sd A RMS osc width value = 20, made no difference to cracking
Run 2 Sd A Intermittent (1-2cm long) centreline cracking from 3 00 to 6.00 Sl ridge in centre of bead @ 6 00
Run 2 Sd B : Centreline cracking 4 00 to 5.00
Run 3 Sd A : Original RMS osc width value used = 95. Stopped @ 4.30 due to increased S/O causing lack of fill, Osc value reduced to 70.
Run 4 Sd A : Possibility of cold lapping due to weldpool ahead of arc. Stopped at 5 00 due to only one side of joint being correctly fused (wires not central). Restarted for 5.00 to 6.00. Possible cold lapping @ 5.00 - 6 00
Run 4 Sd B : Reduced wire and travel wrt Sd A : consistent @ 6 00
Run 5 Sd A : Fell out @ 3.00 Restarted @ 1194mm/min TS; OK to 6 00. Possible cold lapping @ 2 00 - 4 00
Cap Sd A : Increased TS from 2 30 - 4.00 to avoid rollover. Slowed TS from 1092 to 991mm/min for last 200mm to reduce undercut, but this was evident for last 150mm
Cap Sd B : Rotated torch through 90° so that each wire contacted the parent material side by side Increased TS from 2 30 - 4 00 to avoid rollover Slowed TS for last 50mm but undercut still present for last 150mm

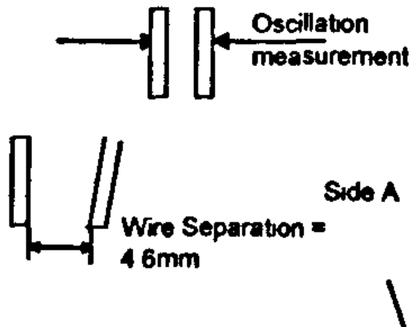

Cap Widths

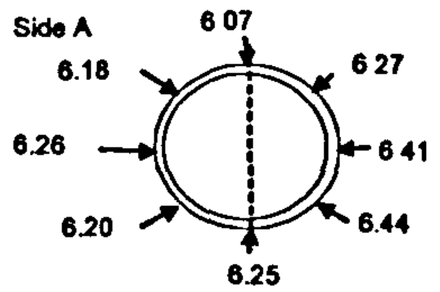

Remaining Depth to Pipe OD (mm)

After Pass No	12	3 (Sd A)	3 (Sd B)	6
0	15.98	15 84	16 13	15 82
1	11.23	11 84	12.28	11.34
2	7.9	8 85	9.14	8 09
3	5 67	5.78	6 28	5
4	2.93	3 54	3.83	3.59
5	flush	1.94	1.63	(2.50)
				NB ground back

Murex tips with machined end used for Runs 1 and 2 (~4mm longer than ESAB tips)

Less severe undercut cf Side A

Tandem Wire Synchronised Pulsed Transfer Narrow Gap Welding Procedure ML-B15-16

Cranfield UNIVERSITY

As-run Parameter Record

Weld No.: ML-B15-16

Date: 10/07/2002

Description:

X100 Tandem Test Weld

Welders Name/Position:

J Savill

Material Grade:	X100
Heat Number:	*
Diameter:	36"
Thickness:	14 9mm
Welding Position:	ASME IX 5G
Preparation Method:	PFM
Alignment Method:	Manually tacked (external) prior to internal root
Alignment Removed:	After Root Run
Preheat Method:	Propane
Backing System	N/A
Cleaning Method	Grind/ wire Brush

Joint Preparation:

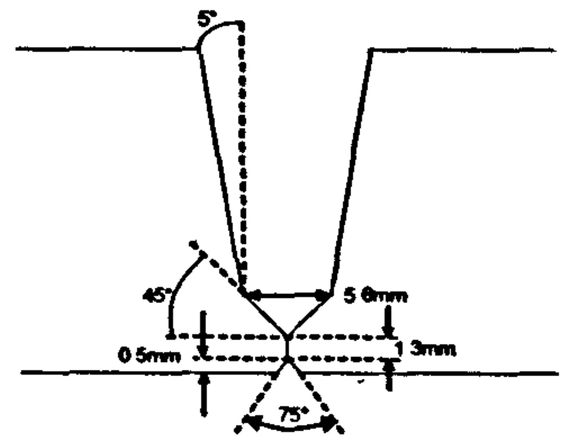

Run Sequence:

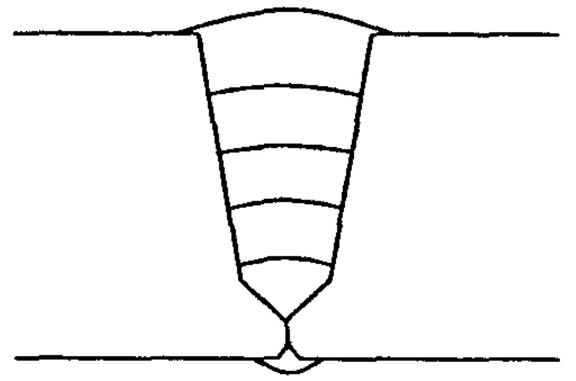

Pass	Process	Polarity	Electrode Brand	Batch	Size mm	Shielding Gas Type	Flow L/min	Temp @ Start °C	Lead WFS m/min	Amps I	Volts V	Trial WFS m/min	Amps I	Volts V	Osc. Freq beats per min	Osc mm	CTWD mm	Travel Speed mm/min	Arc Energy kJ/min
Int root	GMAW	DC+ve	TS-6	135346	0 9	78Ar/20CO_2/2O_2	20	100	9 70	190-195	20 7-21 0	-	-	-	-	-	10	710	0 33-0.35
1	PGMAW	DC+ve	Carbofil NiMo-1	14233	1 0	82 5%Ar/12 5%CO2/5%He	30	105-120	13 50	220-225	17-19	13 50	220-225	17-19	450	2 75 (70)	~13 5	1295	0 35-0 40
2	PGMAW	DC+ve	Carbofil NiMo-1	14233	1 0	82 5%Ar/12 5%CO2/5%He	30	105-115	13 50	220-225	18-22	13 50	220-225	18-22	450	3 60 (100)	~13 5	1295	0 37-0 46
3	PGMAW	DC+ve	Carbofil NiMo-1	14233	1 0	82 5%Ar/12 5%CO2/5%He	30	100-115	11 70	194-198	18-22	11 70	194-198	18-22	450	4 20 (120)	~13 5	1295	0 32-0 40
4	PGMAW	DC+ve	Carbofil NiMo-1	14233	1 0	82 5%Ar/12 5%CO2/5%He	30	105-115	10 50	182-188	19-22	10 50	182-188	19-22	450	4 80 (140)	~13 5	1092	0 38-0 45
Cap	PGMAW	DC+ve	Carbofil NiMo-1	14233	1 0	82 5%Ar/12 5%CO2/5%He	30	105-120	10 00	178-182	23-25	10 00	178-182	23-25	450	7 50 (240)	~15 5	1092	0 45-0 50
															Values in brackets are RMS setting				

Additional Comments:

Internal Root used ESAB Arist 2000 and rotated pipe (effectively vertical down welding)
External passes Fronius Time Twin syncronised power sources
*Not stated in the interests of manufacturer confidentiality
Gap at OD: 6 80 - 7.06
beats per minute = no. of complete cycles per minute (ie left-right-left)
Run 1 Side A : Used 2.75mm osc (RMS value = 70)
Run 3 Side A : Used 12 0m/min WFS to increase deposition sl. A few areas of LSWF @ 5.30 to 6 00
Run 4 Side B : Initially used 11.0 m/min WFS but weld fell out at 2 30; used 10 5m/min for 2.30 - 6 00 ; OK until 5 o'clock but then not enough fill on one side
Run 4 Side A : Fell out at 3 o'clk. Restarted ; OK to 6 o'clk. Wire cast causing LSWF @ 5.30 to 6 00

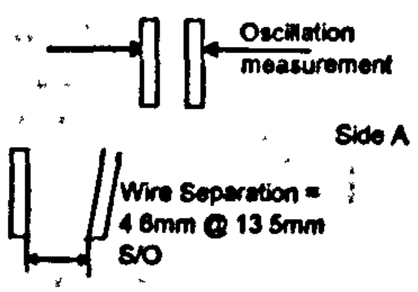

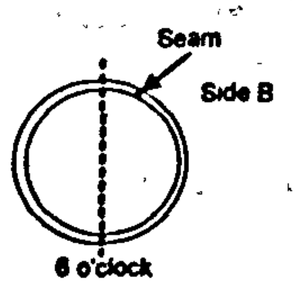

Cap Widths

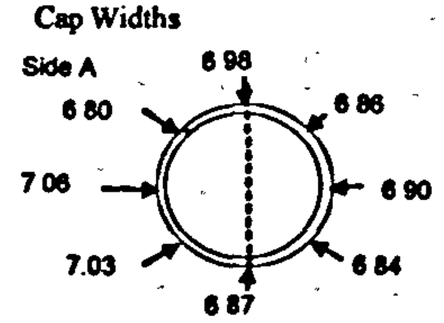

Depth from pipe OD to weld surface (mm)

After Pass No	12	3 (sd A)	3(sd B)	6
0	12.02	11.95	12.12	11.59
1	8.76	9.32	9.35	8 69
2	6 32	6.98	6 83	5.35
3	4.32	4.5	4.28	3 46
4	1.87	1.44	1.71	
5				

WFS	Ip (A)	Ib (A)	tp (ms)	freq (Hz)
6	475	33	1 8	90
8	475	33	1 8	125
10	475	41	1 8	170
12	475	49	1 8	190
14	475	57	1 8	225
16	475	57	1 8	270

NB Contact tip = ESAB M6 1 0mm CuCrZr

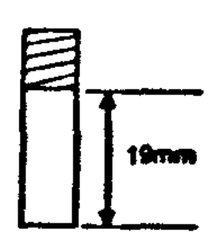

Tandem Wire Synchronised Pulsed Transfer Narrow Gap Welding Procedure ML-B15-17

Cranfield UNIVERSITY

As-run Parameter Record

Weld No.: ML-B15-17

Date: 07/08/2002

Description:

X100 Tandem Weld

Welders Name/Position:

J Savill

Material Grade:	X100
Heat Number:	*
Diameter:	36"
Thickness:	14 9mm
Welding Position:	ASME IX 5G
Preparation Method	PFM
Alignment Method	Manually tacked (external) prior to internal root
Alignment Removed	After Root Run
Preheat Method	Propane
Backing System	N/A
Cleaning Method	Grind/ wire Brush

Joint Preparation:

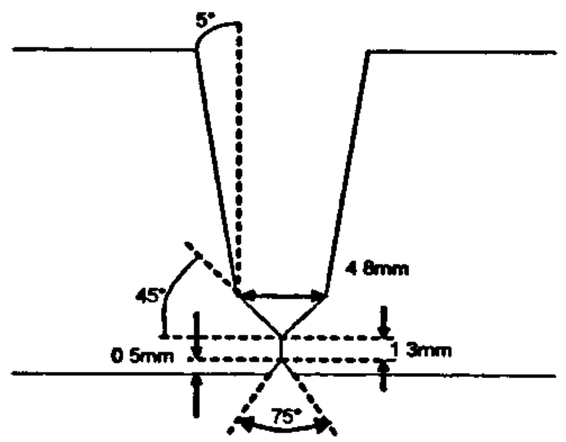

Run Sequence.

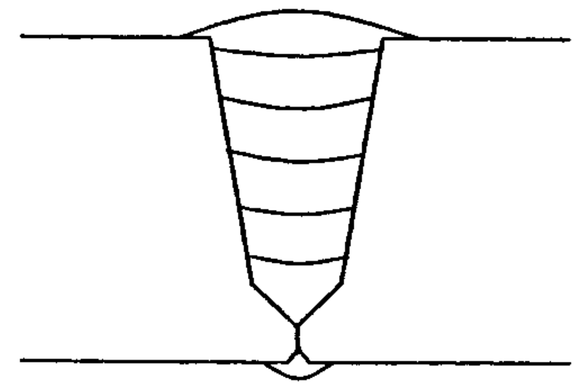

Pass	Process	Polarity	Electrode Brand	Batch	Size mm	Shielding Gas Type	Flow L/min	Temp @ Start °C	Lead WFS m/min	Amps I	Volts V	Trial WFS m/min	Amps I	Volts V	Osc Freq beats per min	Osc mm	CTWD mm	Travel Speed mm/min	Arc Energy kJ/mm
Int root	GMAW	DC+ve	TS-6	135346	0 9	78Ar/20CO_2/2O_2	25	100-110	9 70	200-205	20 8-21 3	-	-	-	-	-	10	710	0 35-0 37
1	PGMAW	DC+ve	Thyssen MoNi	372116	1 0	82 5%Ar/12 5%CO2/5%He	30	105-125	13 50	220-230	17 5-19 5	13 50	220-230	17 5-19 5	600	2 2 (50)	~13 5	1295 (51")	0 36-0 42
2	PGMAW	DC+ve	Thyssen MoNi	372116	1 0	82 5%Ar/12 5%CO2/5%He	30	100-120	13.50	215-225	18-21	13 50	215-225	18-21	600	2 85 (75)	~13 5	1295 (51")	0 36-0 44
3	PGMAW	DC+ve	Thyssen MoNi	372116	1 0	82 5%Ar/12 5%CO2/5%He	30	105-120	10 00	175-185	20-23	10 00	175-185	20-23	600	3 60 (100)	~13 5	1194 (47")	0 36-0 43
4	PGMAW	DC+ve	Thyssen MoNi	372116	1 0	82 5%Ar/12 5%CO2/5%He	30	105-120	10 00	175-185	21-24	10 00	175-185	21-24	600	3 95 (115)	~13.5	1194 (47")	0 37-0 45
5 Side A	PGMAW	DC+ve	Thyssen MoNi	372116	1 0	82 5%Ar/12 5%CO2/5%He	30	100-110	10 00	175-185	24-26	10 00	175-185	24-26	600/250	6 9 (220)	~13 5	1092-1194	0 42-0 53
5 Side B	PGMAW	DC+ve	Thyssen MoNi	372116	1 0	82 5%Ar/12 5%CO2/5%He	30	100-120	9 50	166-172	24-26	9 50	166-172	24-26	600	4 25 (125)	~13 5	1143-1245	0 39-0 47
Cap Sd A	PGMAW	DC+ve	Thyssen MoNi	372116	1 0	82 5%Ar/12 5%CO2/5%He	30	100-110	9 00	157-163	24-26	9 00	157-163	24-26	600	7 0 (225)	~14 5	1092-1194	0 38-0 47
Cap Sd B	PGMAW	DC+ve	Thyssen MoNi	372116	1 0	82 5%Ar/12 5%CO2/5%He	30	100-110	9 00	157-163	24-26	9 00	157-163	24-26	600	5 9 (185)	~14 5	1143-1295	0 35-0 44

Additional Comments:

Internal Root used ESAB Arist 2000 and rotated pipe (effectively vertical down welding)
External passes Fronius Time Twin syncronised power sources (modified waveform TCP475)
*Not stated in the interests of manufacturer confidentiality
Gap at OD. 6 73 - 6.94
beats per minute = no. of complete cycles per minute (ie left-right-left)
Run 1A ; V. good @ 6 o'clock (ran past for 3")
Run 2A; 100 RMS osc Value. Wire hunting @ 4 30 to 6o'c. Last 1" to 6 o'c lack of fill (too much osc ?)
Run 1B, As per run 1A
Run 2B, RMS osc. Value reduced to 75 Reduced Ip to 460 then incr. to 465 (4.30-6 0) Problems with wire feeding (catching within reel). Stopped at 1 and 4 o'c. OK @ 6o'c
Run 3B, Stable to 6 o'c Lack of fill at crossover point (~5 o'c)
Run 4B; Crossover problem at same point as run 3B. Lack of fill at 12 and 6 o'c. Repaired crossover with same condition but 43"/min TS
Run 3A; OK but wire feeding problems within reel (Master PS)
Run 4A, Good. Crossover problem as per 4B. Better at 6 o'c. Groove sidewall still present @ 5 30 -6 o'c
Run 5A; Rollover at 2 to 4 o'c. Tried various combinations of osc width and BPM. Too much wire.
Cap Sd A; Started at 43"/min, increased to 47" min for 2-5 o'c, slowed to 43"/min for 5 - 6 o'c. Rollover immenent but not quite
Run 5B, started at 47"/min, increased to 49"/min from 2 to 4 o'c, then slowed to 45"/min for 5-6o'c. 2 rollovers at 2 30 and 30'c Weld flush with pipe surface.
Cap SdB, Started at 51"/min slowed to 47"/min from 5 to 5 45, then 45"/min for last 2"

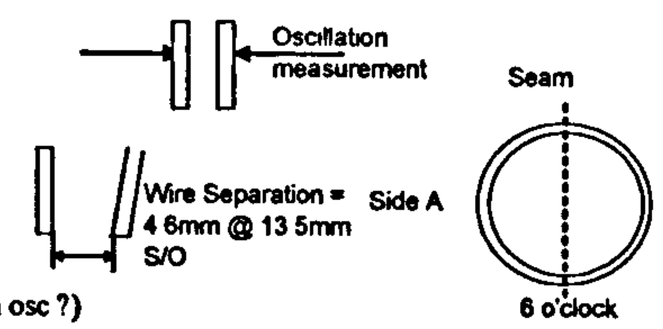

Cap Widths

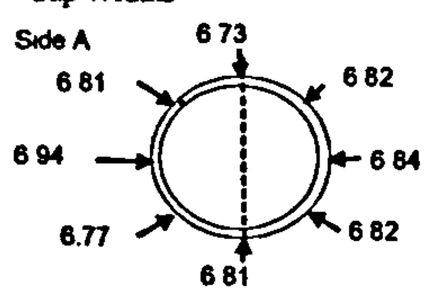

After Pass No	Remaining Depth to Pipe OD (mm) 12	3 (Sd A)	3 (Sd B)	6
0	11.54	11.38	11.63	11.45
1	8.45	9.27	9 26	8.03
2	6.11	7.03	6 92	5.42
3	3.32	4.77	4.31	3 02
4	1.19	2	1.81	1.63 (Sd B)
5				

WFS(m/min	Ip (A)	Ib (A)	tp (ms)	freq (Hz)
6	465	50	1.8	90
8	465	50	1.8	125
10	465	50	1.8	170
12	465	50	1.8	190
14	465	57	1 8	225
16	465	57	1.8	270

Tandem Wire Synchronised Pulsed Transfer Narrow Gap Welding Procedure ML-B15-18

Cranfield UNIVERSITY

As-run Parameter Record

Weld No.: ML-B15-18

Date: 12/09/2002

Description:

X100 Tandem Weld

Welders Name/Position:

J.Savill

Material Grade:	X100
Heat Number:	*
Diameter:	36"
Thickness:	14.9mm
Welding Position:	ASME IX 5G
Preparation Method:	PFM
Alignment Method:	Manually tacked (external) prior to internal root
Alignment Removed:	After Root Run
Preheat Method:	Propane
Backing System	N/A
Cleaning Method:	Grind/ wire Brush

Joint Preparation:

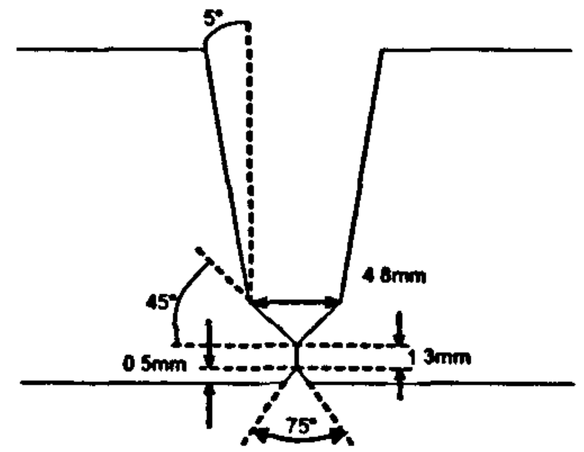

Run Sequence:

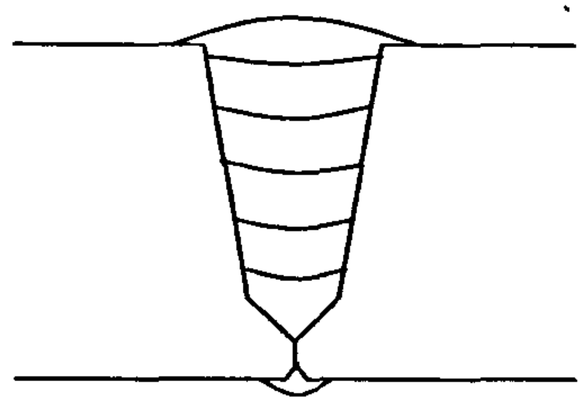

Pass	Process	Polarity	Electrode Brand	Batch	Size mm	Shielding Gas Type	Flow L/min	Temp @ Start °C	Lead WFS m/min	Lead Amps I	Lead Volts V	Trial WFS m/min	Trial Amps I	Trial Volts V	Osc. Freq beats per min.	Osc mm	CTWD mm	Travel Speed mm/min	Arc Energy kJ/min
Int. root	GMAW	DC+ve	TS-6	135346	0.9	78Ar/20CO_2/2O_2	20	110-115	9.70	195-200	21.3-21.5	-	-	-	-	-	10	710	0.35-0.36
1	PGMAW	DC+ve	Thyssen MoNi	372116	1 0	82 5%Ar/12 5%CO2/5%He	25	110-120	13.50	230-240	20-22 5	110-120	13.50	230-240	20-22 5	1.5 (25)	13.5	1295 (51")	0.43-0 50
2	PGMAW	DC+ve	Thyssen MoNi	372116	1 0	82 5%Ar/12 5%CO2/5%He	25	110-120	13.50	235-245	19-22	110-120	13 50	235-245	19-22	2 9 (75)	13.5	1295 (51")	0 41-0 50
3	PGMAW	DC+ve	Thyssen MoNi	372116	1.0	82 5%Ar/12 5%CO2/5%He	25	105-120	10 80	195-205	19-21	105-120	10 80	195-205	19-21	3 6 (100)	13.5	1295 (51")	0 34-0 42
4	PGMAW	DC+ve	Thyssen MoNi	372116	1.0	82 5%Ar/12 5%CO2/5%He	25	100-115	10 80	195-205	21-22	100-115	10 80	195-205	21-22	4 1 (120)	13.5	1295 (51")	0.38-0 42
5	PGMAW	DC+ve	Thyssen MoNi	372116	1 0	82 5%Ar/12 5%CO2/5%He	25	100-110	9 00	163-167	21.5-23	100-110	9 00	163-167	21.5-23	4 1 (120)	13 5	1295 (51")	0.32-0 36
CAP	PGMAW	DC+ve	Thyssen MoNi	372116	1 0	82 5%Ar/12 5%CO2/5%He	25	100-110	9 00	163-167	22.5-24	100-110	9.00	163-167	22.5-24	6 2 (195)	14-15	1295 (51")	0.34-0.37

Additional Comments:

Internal Root used ESAB Arist 2000 and rotated pipe (effectively vertical down welding)
External passes Digital Fronius Time Twin syncronised power sources (modified waveform TCP475)
Gap at OD: 6.71 - 7.03
beats per minute = no. of complete cycles per minute (ie left-right-left)
*Not stated in the interests of manufacturer confidentiality

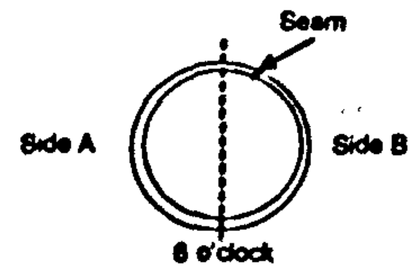

Cap Widths

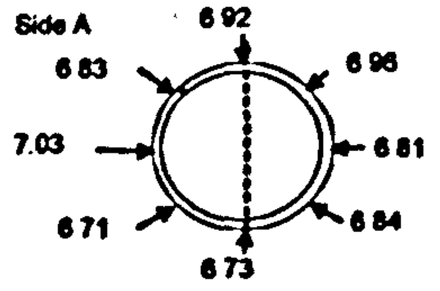

Remaining Depth to Pipe OD (mm)

After Pass No	12	3 (Sd A)	3 (Sd B)	6
0	12.02	12.12	11.72	12.3
1			9.3	
2	5 89	6.95	6.77	5.87
3	3.84	4.59	4.1	4 03
4	1.59	3.41	2.55	
5				

Run 1A; 0.9mm contact tips used accidently; wire snatching from 4.30 to 6.00
Run 2A; 1.0mm CuCr Zr tips; still snatching from 4.30 to 6 00 - contact tips too hot? Lack of side fill at 5 to 6, but flat profile
Run 3A; Stopped at 3 o'c to cool torch. Better running stability from 3 to 6. Some lack of side fill at 5 and 5.45 to 6
Run 4B; WM fell ahead of arc at 2.30; stopped and restarted. Fell ahead again at 3.30. Wire snatching on lead - tried 1.2mm contact tip - better
Run 4A; Same as 4B - WM fell out at 2.30 and 3. Slowed TS to 1194 (47") from 5 to 6; OK
Run 5B; TS 47"/min - too slow. For run 5A incr TS to 51"/min; better. Reduced TS to 43"/min from 4.30 to 6
CAP; 51"/min TS for majority, reduced TS to 43"/min from 5 to 6

Repair Procedure for 6 o'c (conducted at 3 o'c) : fill 1 10 0m/min WFS, 47"/min, 25osc
fill 2 and fill 3 as per fill 1, fill 4 9 0m/min WFS, 47"/min, 100 osc
Cap 9 0m/min WFS, 47"/min, 140 osc

Manual/ Semi Automatic Tie-In Procedure

Cranfield UNIVERSITY

As-run Parameter Record

Weld No.: ML-B-9

Date: 19-21/06/01

Description:

X100 Tie-In Weld

Welders Name/Position:

Vince DiCarlo

Material Grade:	X100
Heat Number:	*
Diameter:	36"
Thickness:	19mm
Welding Position:	ASME IX 5G
Preparation Method:	PFM
Alignment Method:	Manual
Alignment Removed:	N/A
Preheat Method:	Propane Torch
Backing System	N/A
Cleaning Method:	Wire Brush/ Grind

Joint Preparation:

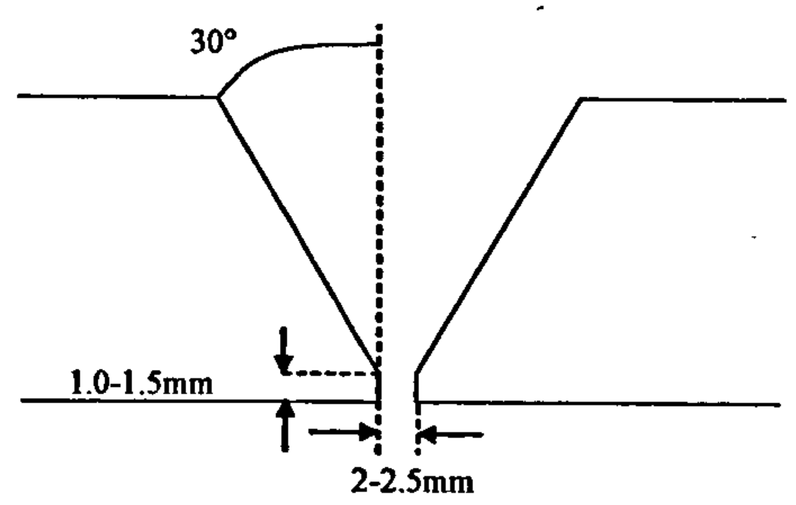

Run Sequence:

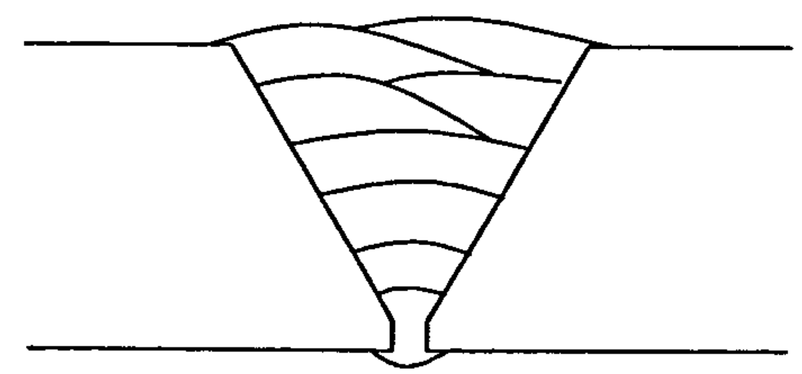

Pass	Process	Polarity	Electrode Brand	Batch	Size mm	Shielding Gas Type	Flow L/min	Temp @ Start °C	WFS m/min	Amps I	Volts V	WFS m/min	Amps I	Volts V	Osc mm	Travel Speed mm/min	Arc Energy kJ/min
Root	SMAW	DC-ve	Filarc 118	5370063	2.5	N/A	N/A	100-120	N/A	76-88	17.7-20.0					65-90	1.03-1.54
Hot Pass	SMAW	DC+ve	Filarc 118	see comments	3.2	N/A	N/A	100-120	N/A	93-118	19.4-20.8					62-130	1.10-1.92
Fill 1	FCAW	DC+ve	Esab 15.09	0383049	1 2	78Ar/20CO2/2O2	20	100-120	9 00	192-197	26 4-26 6					225-267	1 19-1.6
Fill 2	FCAW	DC+ve	Esab 15.09	0383049	1.2	78Ar/20CO2/2O2	20	100-120	9 00	190-206	26.2-26.6					200-250	0.82-1.79
Fill 3	FCAW	DC+ve	Esab 15.09	0383049	1.2	78Ar/20CO2/2O2	20	100-120	9 00	194-209	26.1-26 6					228-333	0 96-1 41
Fill 4	FCAW	DC+ve	Esab 15 09	0383049	1 2	78Ar/20CO2/2O2	20	100-120	9.00	195-205	26 0-26.6					188-330	0 98-1.56
Cap 1	FCAW	DC+ve	Esab 15 09	0383049	1.2	78Ar/20CO2/2O2	20	100-120	9.00	189-197	26.3-26.6					203-312	1.03-1 60
Cap 2	FCAW	DC+ve	Esab 15.09	0383049	1.2	78Ar/20CO2/2O2	20	100-120	9 00	181-198	26.0-26 6					171-332	0.98-1.82

Additional Comments:

*Not stated in the interests of manufacturer confidentiality

Wire stick out : 20-25mm

Joint had 8 restraining bars welded and equally spaced around circumference to maintain the root gap

Vertical Up Welding

Equipment = ESAB ARISTO 2000, using rutile FCW program

Arc Time

Root	32'5"
Hot Pass	48'19"
Fill 1	13'18"
Fill 2	15'11"
Fill 3	10'52"
Fill 4	12'3"
Cap1	13'35'
Cap2	16'19"

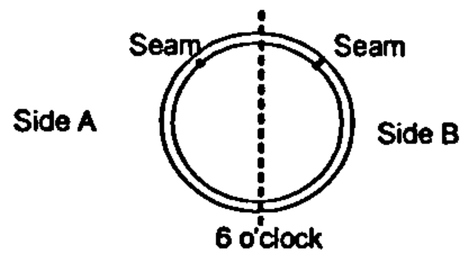

Cap widths

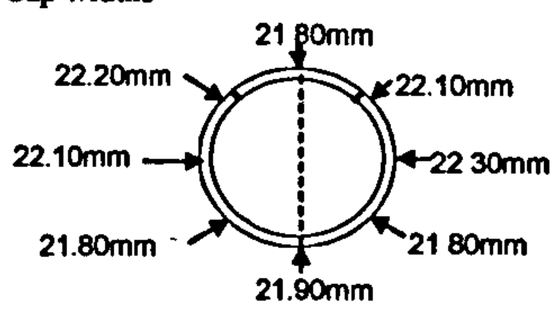

Root gaps

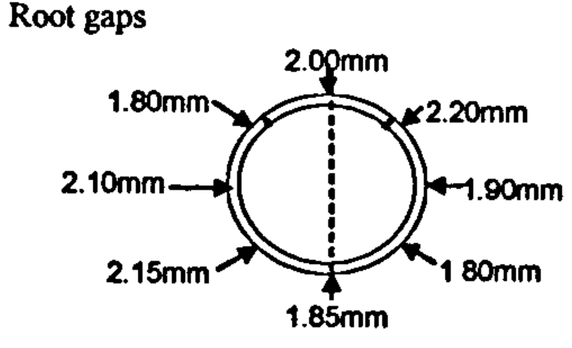

SMAW 3.2mm electrode batch no.s = 7350743 and 4280233

Filarc 118 = AWS 5 5 E11018M

ESAB OK Tubrod 15.09 = AWS 5.29 E111T1-G H4

SMAW Single Pass Backweld Repair Procedure

Cranfield UNIVERSITY

As-run Parameter Record

Weld No.: **ML-B-8-BW SMAW**

Date: 26/06/2001

Description:

36" X100 Repair Procedure:
Single Pass Backweld Repair

Welders Name/Position:

Vince DiCarlo

Material Grade:	X100
Heat Number:	*
Diameter:	36"
Thickness:	19.05mm
Welding Position:	5G
Preparation Method:	Grinding
Alignment Method:	N/A
Alignment Removed:	N/A
Preheat Method:	Propane torch
Backing System	N/A
Cleaning Method:	Grinding/ Wire Brush

Joint Preparation:

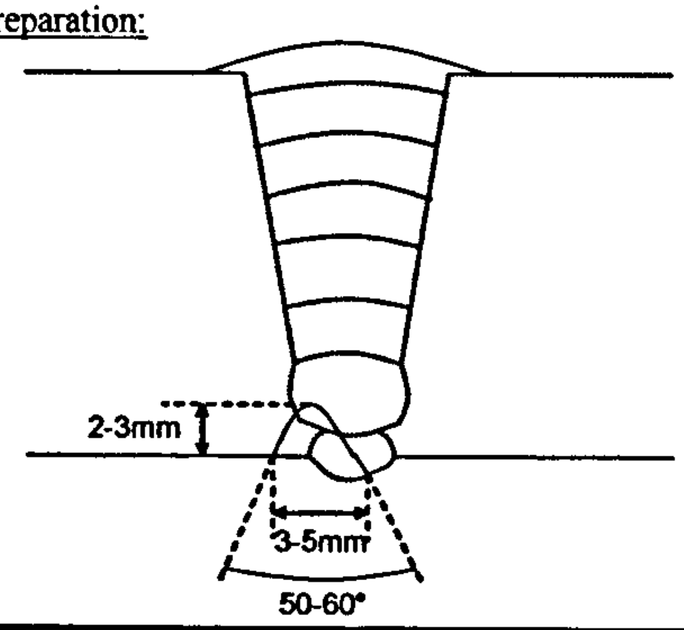

Run Sequence:

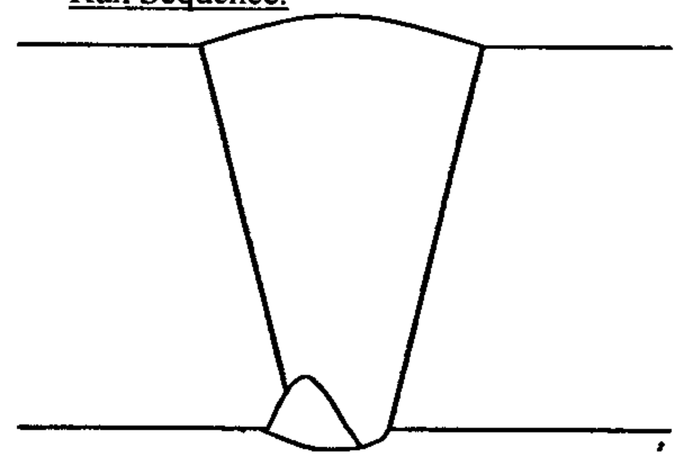

Pass	Process	Polarity	Electrode Brand	Batch	Size mm	Shielding Gas Type	Flow L/min	Temp @ Start °C	Side A WFS m/min	Amps I	Volts V	Side B WFS m/min	Amps I	Volts V	Osc mm	Travel Speed mm/min	Arc Energy kJ/min
1	SMAW	DC+ve	Filarc 118	5370063	2.5	N/A	N/A	105	N/A	75-80	23.2-23.7					137	0.76-0.83

Additional Comments:

Original Weld ML-B-8 : Mechanised single wire narrow gap girth weld: Oerlikon Carbofil HT, 82.5%Ar/12.5% CO2/ 5%He, Pulsed transfer
SMAW Electrodes; Filarc 118 AWS 5.5 E11018-M
Repair length = 110mm
Position of repair = Overhead Internal
* Not stated in the interest of manufacturer confidentiality

Require: Hardness
Macro

GMAW Single Pass Backweld Repair Procedure

Cranfield UNIVERSITY

As-run Parameter Record

Weld No.: **ML-B-8-BW GMAW**

Date: 26/06/2001

Description:

36" X100 Repair Procedure:
Single Pass Backweld Repair

Welders Name/Position:

Vince DiCarlo

Material Grade:	X100
Heat Number:	*
Diameter:	36"
Thickness:	19.05mm
Welding Position:	5G
Preparation Method:	Grinding
Alignment Method:	N/A
Alignment Removed:	N/A
Preheat Method:	Propane torch
Backing System	N/A
Cleaning Method:	Grinding/ Wire Brush

Joint Preparation:

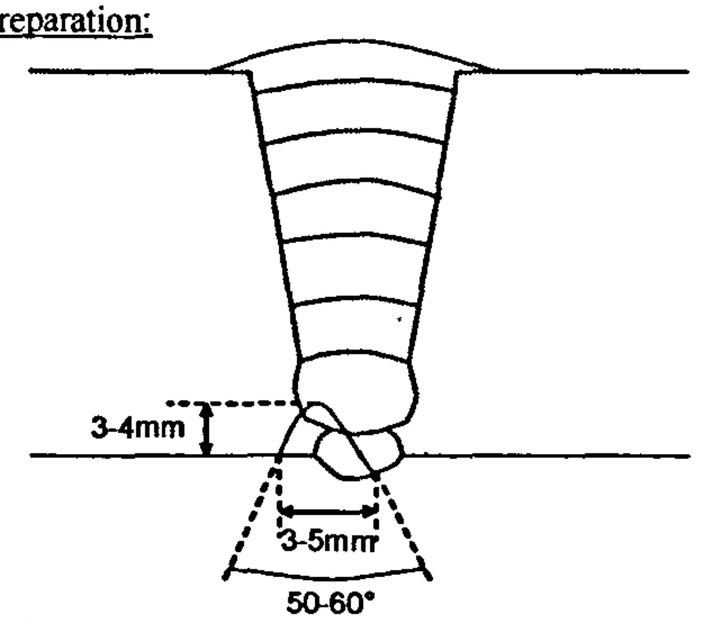

Run Sequence:

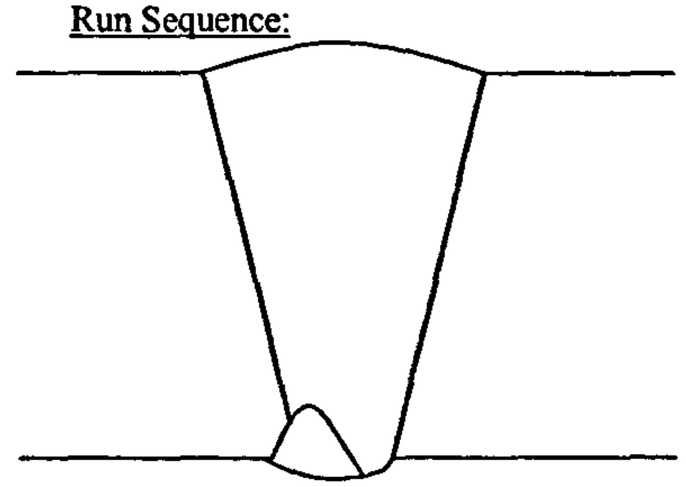

Pass	Process	Polarity	Electrode Brand	Batch	Size mm	Shielding Gas Type	Flow L/min	Temp @ Start °C	Side A WFS m/min	Amps I	Volts V	Side B WFS m/min	Amps I	Volts V	Osc mm	Travel Speed mm/min	Arc Energy kJ/min
1	GMAW	DC+ve	Carbofil HT	1004	1 0	78Ar/20CO2/2O2	20	115	8.50	190-195	20.8-21.2					431	0 55-0.58

Additional Comments:

Original Weld ML-B-8 : Mechanised single wire narrow gap girth weld: Oerlikon Carbofil HT, 82.5%Ar/12.5% CO2/ 5%He, Pulsed transfer
GMAW electrode : Oerlikon Carbofil HT AWS 5.28 ER100S-G
Repair length = 110mm
Position of repair = Overhead Internal
Contact tip to workpiece distance = 12-14mm
* Not stated in the interest of manufacturer confidentiality

Require: Hardness
Macro

Two Pass SMAW Backweld Repair Procedure

Cranfield UNIVERSITY

As-run Parameter Record

Weld No.: **ML-B-8-BWMP SMAW**

Date: 26/06/2001

Description:

36" X100 Repair Procedure:
Multi-Pass Backweld Repair

Welders Name/Position:

Vince DiCarlo

Material Grade:	X100
Heat Number:	*
Diameter:	36"
Thickness:	19.05mm
Welding Position:	5G
Preparation Method:	Grinding
Alignment Method:	N/A
Alignment Removed:	N/A
Preheat Method:	Propane torch
Backing System	N/A
Cleaning Method:	Grinding/ Wire Brush

Joint Preparation:

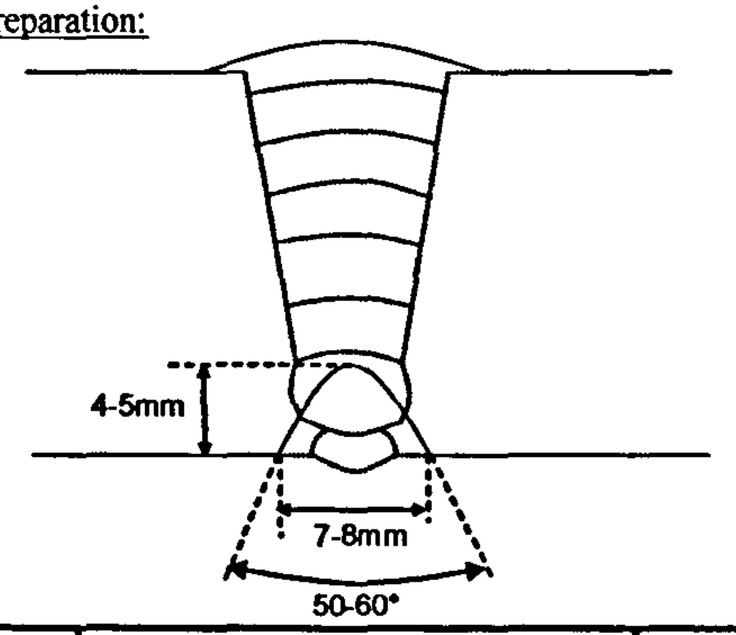

Run Sequence:

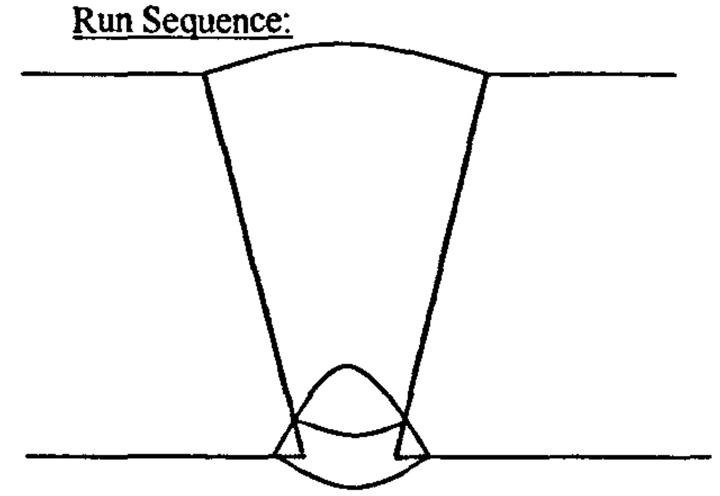

Pass	Process	Electrode Polarity	Electrode Brand	Electrode Batch	Electrode Size mm	Shielding Gas Type	Shielding Gas Flow L/min	Temp @ Start °C	Side A WFS m/min	Side A Amps I	Side A Volts V	Side B WFS m/min	Side B Amps I	Side B Volts V	Osc mm	Travel Speed mm/min	Arc Energy kJ/min
1	SMAW	DC+ve	Filarc 118	5370063	2.5	N/A	N/A	110	N/A	75-80	23.3-23.7					115	0.91-0.99
2	SMAW	DC+ve	Filarc 118	4280233	3.2	N/A	N/A	115	N/A	98-102	22.2-22.6					94	1.38-1.47

Additional Comments:

Original Weld ML-B-8 : Mechanised single wire narrow gap girth weld: Oerlikon Carbofil HT, 82.5%Ar/12.5% CO2/ 5%He, Pulsed transfer
SMAW Electrodes; Filarc 118 AWS 5.5 E11018-M
Repair length = 100mm
Position of repair = Overhead Internal
* Not stated in the interest of manufacturer confidentiality

Require: Hardness
Macro

Two Pass GMAW Backweld Repair Procedure

Cranfield UNIVERSITY

As-run Parameter Record

Weld No.: **ML-B-8-BWMP GMAW**

Date: 26/06/2001

Description:

36" X100 Repair Procedure:
Multi-Pass Backweld Repair

Welders Name/Position:

Vince DiCarlo

Material Grade:	X100
Heat Number:	*
Diameter:	36"
Thickness:	19.05mm
Welding Position:	5G
Preparation Method:	Grinding
Alignment Method:	N/A
Alignment Removed:	N/A
Preheat Method:	Propane torch
Backing System	N/A
Cleaning Method:	Grinding/ Wire Brush

Joint Preparation:

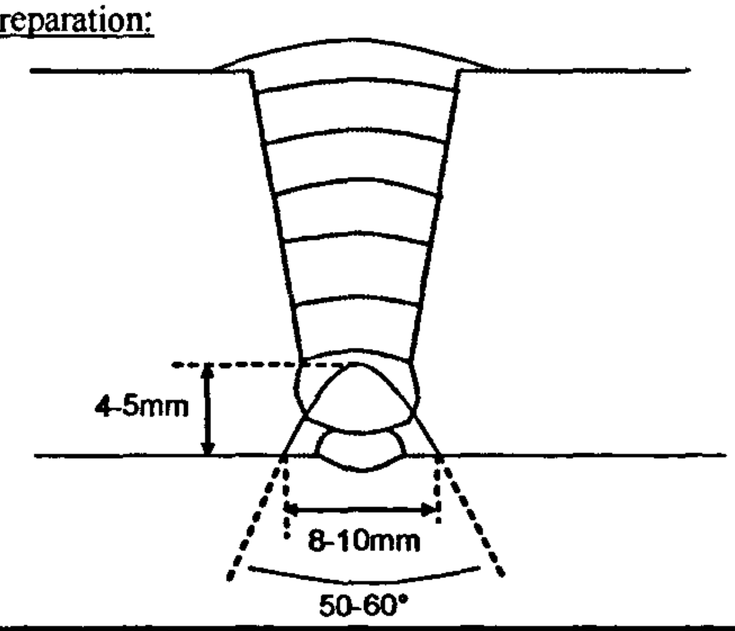

Run Sequence:

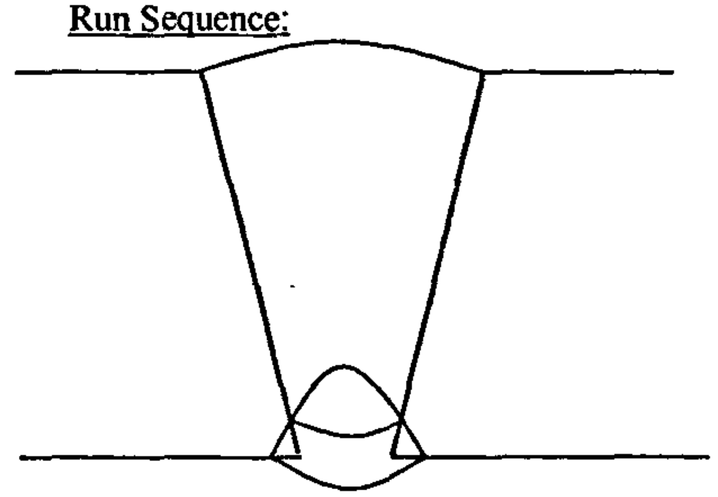

Pass	Process	Polarity	Electrode Brand	Batch	Size mm	Shielding Gas Type	Flow L/min	Temp @ Start °C	Side A WFS m/min	Amps I	Volts V	Side B WFS m/min	Amps I	Volts V	Osc mm	Travel Speed mm/min	Arc Energy kJ/min
1	GMAW	DC+ve	Carbofil HT	1004	1.0	78Ar/20CO2/2O2	20	105	9 00	204-210	21.2-21.7					560	0.46-0.49
2	GMAW	DC+ve	Carbofil HT	1004	1.0	78Ar/20CO2/2O2	20	110	8.50	182-188	20.8-21.2					330	0.69-0.72

Additional Comments:

Original Weld ML-B-8 : Mechanised single wire narrow gap girth weld: Oerlikon Carbofil HT, 82.5%Ar/12.5% CO2/ 5%He, Pulsed transfer
GMAW electrode : Oerlikon Carbofil HT AWS 5.28 ER100S-G
Repair length = 170mm
Position of repair = Overhead Internal
Contact tip to workpiece distance = 12-14mm
* Not stated in the interest of manufacturer confidentiality

Require: Hardness
Macro

FCAW Single Pass Cap Repair Procedure

Cranfield UNIVERSITY

As-run Parameter Record

Weld No.: **ML-B-8-CR FCAW**

Date: 26/06/2001

Description:

36" X100 Repair Procedure:
Cap Repair

Welders Name/Position:

Vince DiCarlo

Material Grade:	X100
Heat Number:	*
Diameter:	36"
Thickness:	19.05mm
Welding Position:	5G
Preparation Method:	Grinding
Alignment Method:	N/A
Alignment Removed:	N/A
Preheat Method:	Propane torch
Backing System	N/A
Cleaning Method:	Grinding/ Wire Brush

Joint Preparation:

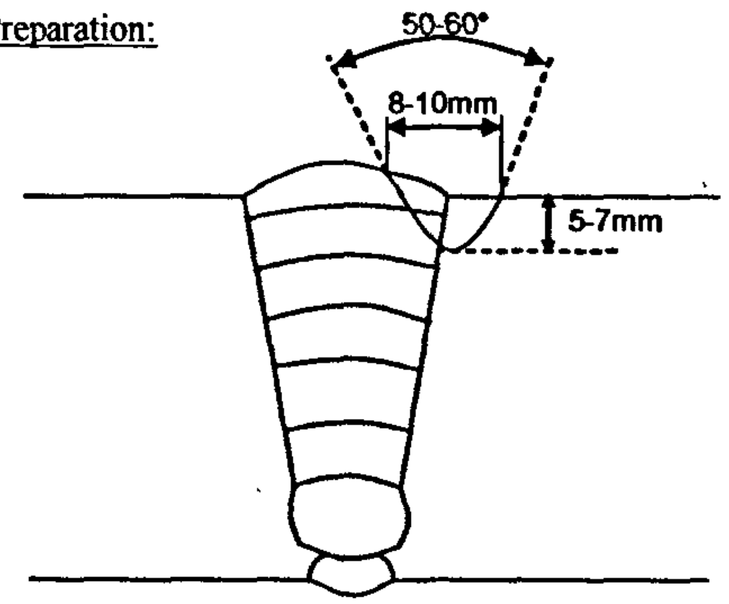

Run Sequence:

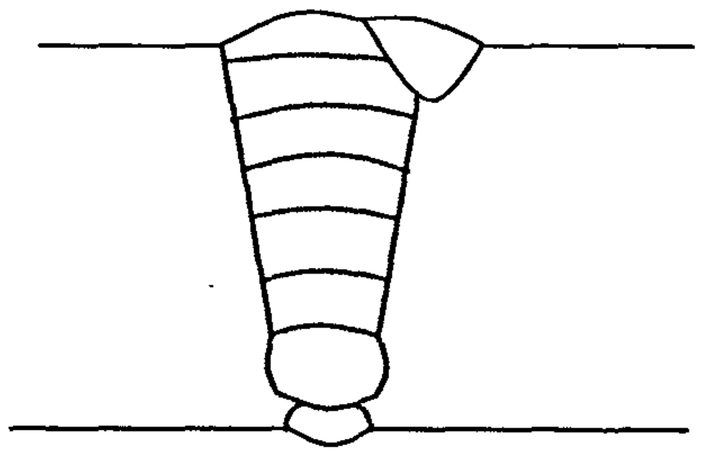

Pass	Process	Polarity	Electrode Brand	Batch	Size mm	Shielding Gas Type	Flow L/min	Temp @ Start °C	Side A WFS m/min	Amps I	Volts V	Side B WFS m/min	Amps I	Volts V	Osc mm	Travel Speed mm/min	Arc Energy kJ/min
1	FCAW	DC+ve	OK 15.09	0383049	1.2	78Ar/20CO2/2O2	20	110	9.00	198-202	25 3-25.7					192	1.56-1.62

Additional Comments:

Original Weld ML-B-8 : Mechanised single wire narrow gap girth weld: Oerlikon Carbofil HT, 82.5%Ar/12.5% CO2/ 5%He, Pulsed transfer
FCAW electrode : ESAB OK Tubrod 15.09 AWS 5.29 E111T1-G H4
Contact tip to workpiece distane = 20mm
Position of repair = 3 0'clock external, Vertical Up Welding
Repair length =100mm
Contact tip to workpiece distance = 20-23mm

Require : Hardness
Macro

* Not stated in the interest of manufacturer confidentiality

SMAW Single Pass Cap Repair Procedure

Cranfield UNIVERSITY

As-run Parameter Record

Weld No.: **ML-B-8-CR SMAW**

Date: 26/06/2001

Description:

36" X100 Repair Procedure:
Cap Repair

Welders Name/Position:

Vince DiCarlo

Material Grade:	X100
Heat Number:	*
Diameter:	36"
Thickness:	19.05mm
Welding Position:	5G
Preparation Method:	Grinding
Alignment Method:	N/A
Alignment Removed:	N/A
Preheat Method:	Propane torch
Backing System	N/A
Cleaning Method:	Grinding/ Wire Brush

Joint Preparation:

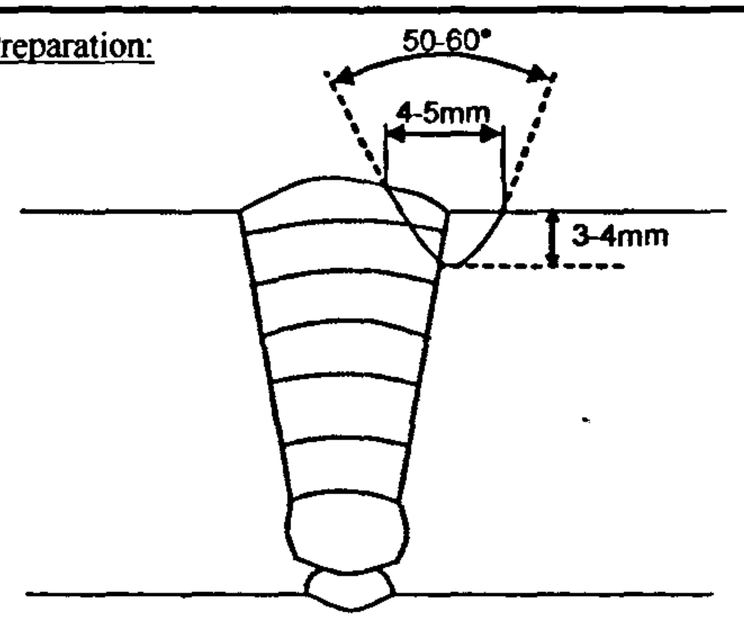

Run Sequence:

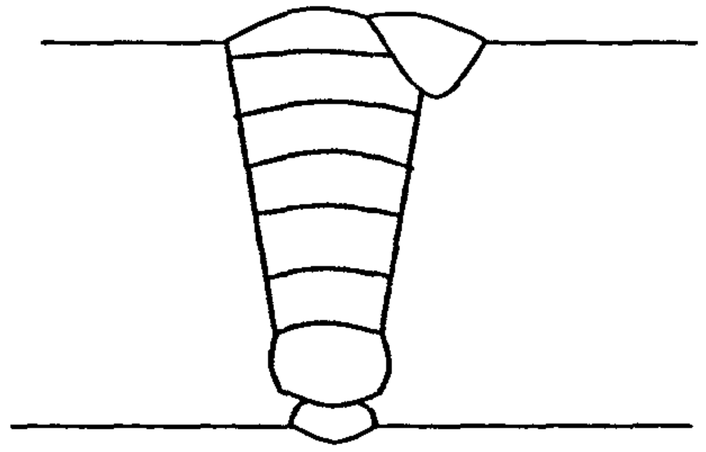

Pass	Process	Polarity	Electrode Brand	Batch	Size mm	Shielding Gas Type	Flow L/min	Temp @ Start °C	Side A WFS m/min	Amps I	Volts V	Side B WFS m/min	Amps I	Volts V	Osc mm	Travel Speed mm/min	Arc Energy kJ/min
1	SMAW	DC+ve	Filarc 118		2 5	N/A	N/A	105	N/A	72-75	24.8-25.2					130	0.82-0 87

Additional Comments:

Original Weld ML-B-8 : Mechanised single wire narrow gap girth weld: Oerlikon Carbofil HT, 82.5%Ar/12.5% CO2/ 5%He, Pulsed transfer
SMAW Electrodes; Filarc 118 AWS 5.5 E11018-M
Repair length =150mm
Position of repair = 3 0'clock external, Vertical Up Welding
* Not stated in the interest of manufacturer confidentiality

Require : Hardness
Macro

FCAW Partial Penetration Repair Procedure

Cranfield UNIVERSITY

As-run Parameter Record

Weld No.: **ML-B-8-PP**

Date: 26/06/2001

Description:

36" X100 Repair Procedure:
Part-Pen Repair

Welders Name/Position:

Vince DiCarlo

Material Grade:	X100
Heat Number:	*
Diameter:	36"
Thickness:	19.05mm
Welding Position:	5G
Preparation Method:	Arc-Air Gouge/Grinding
Alignment Method:	N/A
Alignment Removed:	N/A
Preheat Method:	Propane torch
Backing System	N/A
Cleaning Method:	Grinding/ Wire Brush

Joint Preparation:

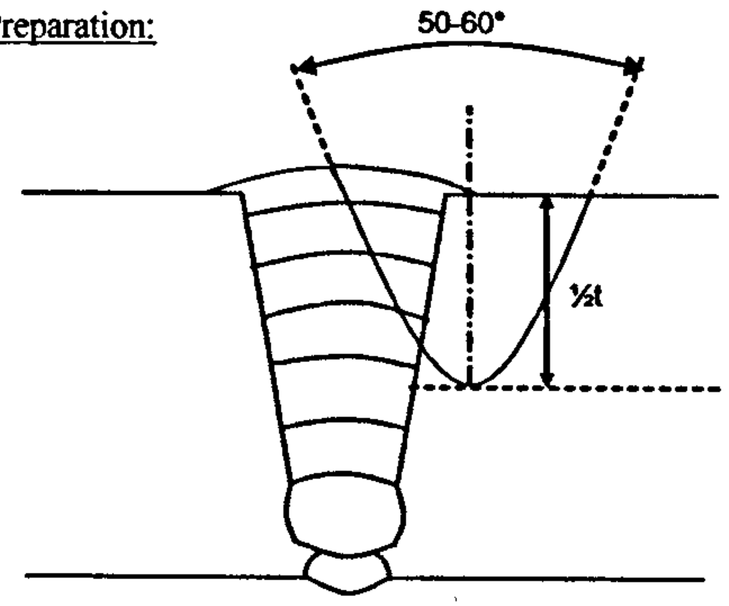

Run Sequence:

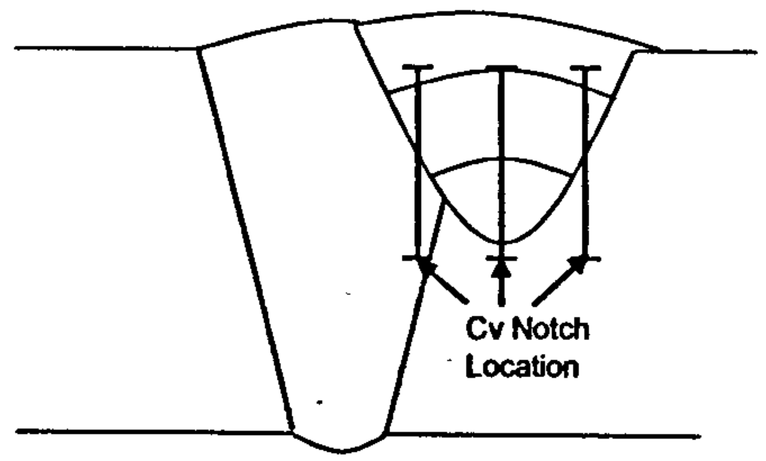

Pass	Process	Polarity	Electrode Brand	Batch	Size mm	Shielding Gas Type	Flow L/min	Temp @ Start °C	Side A WFS m/min	Amps I	Volts V	Side B WFS m/min	Amps I	Volts V	Osc mm	Travel Speed mm/min	Arc Energy kJ/min
1	FCAW	DC+ve	OK 15.09	0383049	1.2	78Ar/20CO2/2O2	20	120	9 00	195-201	25.3-25.6					306	0.97-1.00
2	FCAW	DC+ve	OK 15.09	0383049	1.2	78Ar/20CO2/2O2	20	100	9 00	195-201	25.3-25.6					192	1.54-1.61
3	FCAW	DC+ve	OK 15 09	0383049	1.2	78Ar/20CO2/2O2	20	115	9 00	195-201	25.3-25 6					210	1.41-1 47

Additional Comments:

Original Weld ML-B-8 : Mechanised single wire narrow gap girth weld: Oerlikon Carbofil HT, 82.5%Ar/12.5% CO2/ 5%He, Pulsed transfer
FCAW electrode : ESAB OK Tubrod 15.09 AWS 5.29 E111T1-G H4
Repair length =350mm (not including ramp up/down areas)
Position of repair = 3 0'clock external, Vertical Up Welding
Preheat applied prior to arc air gouging, at least 1.5mm removed post gouging via grinding
Groove centered on cap toe
Contact tip to workpiece distance = 20-23mm
* Not stated in the interest of manufacturer confidentiality

Require : Original WM/ Repair WM Cv @ -20°C
Repair WM CL Cv @ -20°C
Repair WM/ Base Mat Cv @ -20°C
1 x Side Bend (API 1104)
Hardness
Macro

SMAW/ FCAW Full Penetration Repair Weld Procedure

Cranfield UNIVERSITY

As-run Parameter Record

Weld No.: **ML-B-8-FP**

Date: 27/06/2001

Description:

36" X100 Repair Procedure:
Full Pen Repair

Welders Name/Position:

Vince DiCarlo

Material Grade:	X100
Heat Number:	*
Diameter:	36"
Thickness:	19.05mm
Welding Position:	5G
Preparation Method:	Arc Air/ Grinding
Alignment Method:	N/A
Alignment Removed:	N/A
Preheat Method:	Propane torch
Backing System	N/A
Cleaning Method:	Grinding/ Wire Brush

Joint Preparation:

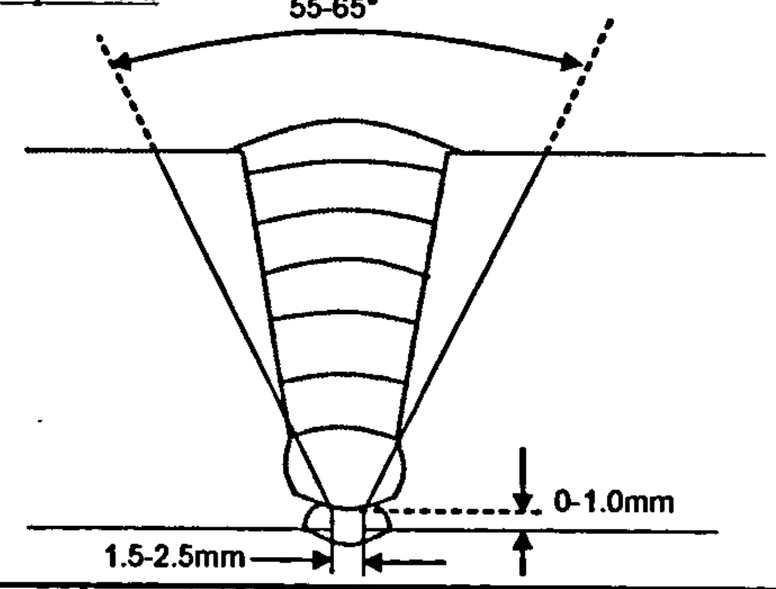

Run Sequence:

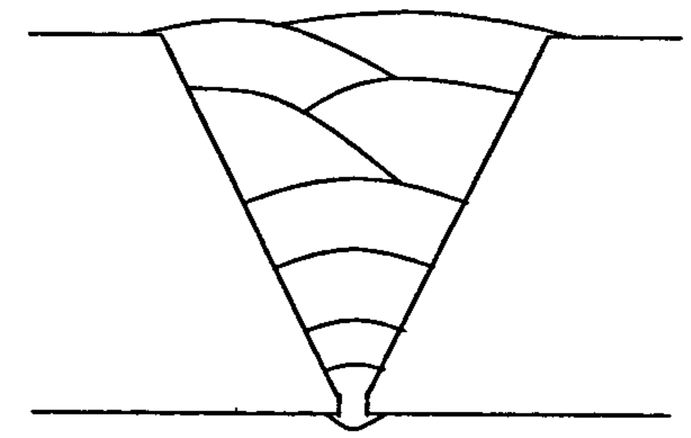

Pass	Process	Polarity	Electrode Brand	Batch	Size mm	Shielding Gas Type	Flow L/min	Temp @ Start °C	Side A WFS m/min	Amps I	Volts V	Side B WFS m/min	Amps I	Volts V	Osc mm	Travel Speed mm/min	Arc Energy kJ/min
Root	SMAW	AC	Filarc 118	5370063	2.5	N/A	N/A	100-120	N/A	60-85	22-24					60	1.32-2 04
Hot Pass	SMAW	AC	Filarc 118	see comments	3.2	N/A	N/A	100-120	N/A	98-105	22-24					70	1.85-2.16
Fill 1	FCAW	DC+ve	Esab 15.09	0383049	1.2	78Ar/20CO2/2O2	20	100-120	9.00	188-194	25.2-25.5					255	1 11-1.16
Fill 2	FCAW	DC+ve	Esab 15.09	0383049	1.2	78Ar/20CO2/2O2	20	100-120	9 00	195-201	25.1-25 4					226	1.30-1 36
Fill 3	FCAW	DC+ve	Esab 15.09	0383049	1.2	78Ar/20CO2/2O2	20	100-120	9.00	194-199	25.3-25.4					238	1.24-1 27
Fill 4	FCAW	DC+ve	Esab 15.09	0383049	1.2	78Ar/20CO2/2O2	20	100-120	9 00	189-201	25.2-25 5					200	1.43-1 54
Cap 1	FCAW	DC+ve	Esab 15 09	0383049	1.2	78Ar/20CO2/2O2	20	100-120	9 00	191-199	25.1-25.4					204	1.41-1.49
Cap 2	FCAW	DC+ve	Esab 15 09	0383049	1.2	78Ar/20CO2/2O2	20	100-120	9.00	184-199	25.2-25.5					161	1.73-1 89

Additional Comments:

Original Weld ML-B-8 : Mechanised single wire narrow gap girth weld: Oerlikon Carbofil HT, 82.5%Ar/12.5% CO2/ 5%He, Pulsed transfer
SMAW Electrodes; Filarc 118 AWS 5.5 E11018-M SMAW 3.2mm electrode batch no.s = 7350743 and 4280233
FCAW electrode : ESAB OK Tubrod 15.09 AWS 5.29 E111T1-G H4
Preheat to 100°C prior to arc-air. Arc-air to within 3mm of ID; grind to create a wafer thin layer of material left at root; open up with hacksaw/ thin grinding disk as required
Repair length =450mm (excluding ramp up/down)
Position of repair = Start at 6 0'clock external, Vertical Up Welding

NB AC used for SMAW due to extreme arc blow using DC+/-ve

* Not stated in the interest of manufacturer confidentiality

Require : WM + FL Cv @ -20°C 2mm sub ID
AWM Strip Tensile
Cross Weld Tensile (API 1104)
Nick Break (API 1104)
Side Bend (API 1104)
Hardness
Macro

Thermocycle weld procedure : no preheat

Cranfield UNIVERSITY

As-run Parameter Record

Preheat Variation

Weld No.: Thermo Cycle RT

Date: 8/9/10 Oct 2002

Description:

X100 Thermocouple Trials on Pipe

Welders Name/Position:

MGH

Material Grade:	X100
Heat Number:	026401-0004-1
Diameter:	30"
Thickness:	19.05mm
Welding Position:	ASME IX 5G
Preparation Method:	PFM
Alignment Method:	Manually clamped and tacked
Alignment Removed:	After Root Run
Preheat Method:	Propane
Backing System	N/A
Cleaning Method:	Grind/ wire Brush

Joint Preparation:

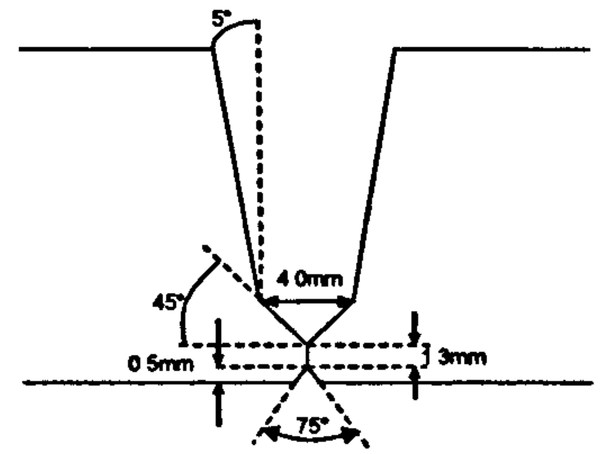

Run Sequence:

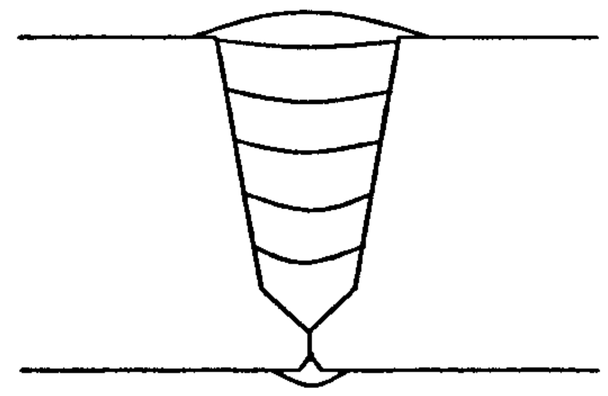

Pass	Process	Polarity	Electrode Brand	Batch	Size mm	Shielding Gas Type	Flow L/min	Temp @ Start °C	Arcscope WFS m/min	Arcscope Amps I	Arcscope Volts V	Yokogawa WFS m/min	Yokogawa Amps I	Yokogawa Volts V	Osc. Freq beats per min.	Osc mm	CTWD mm	Travel Speed mm/min	Arc Energy kJ/min
Int. root	TIG	DC-ve	ER70S-2		2.4	Ar	15	100							-	-			
1	PGMAW	DC+ve	Carbofil NiMo-1	14233	1.0	82 5%Ar/12 5%CO2/5%He	25	19 8	10 00	178	24	-	190	21	210	1.5	13.5	480	0 50
2	PGMAW	DC+ve	Carbofil NiMo-1	14233	1.0	82 5%Ar/12 5%CO2/5%He	25	20.3	10.00	177	23 8	-	190	22	210	1.5	13.5	480	0.52
3	PGMAW	DC+ve	Carbofil NiMo-1	14233	1.0	82 5%Ar/12 5%CO2/5%He	25	20 8	10.00	177	24.2	-	190	22	210	2	13.5	480	0.52
4	PGMAW	DC+ve	Carbofil NiMo-1	14233	1.0	82 5%Ar/12 5%CO2/5%He	25	18	10 00	179	24	-	190	22	210	2.5	13 5	480	0.52
5	PGMAW	DC+ve	Carbofil NiMo-1	14233	1.0	82 5%Ar/12 5%CO2/5%He	25	20.4	10 00	177	24	-	190	23	210	3	13.5	480	0.55
Cap	PGMAW	DC+ve	Carbofil NiMo-1	14233	1 0	82 5%Ar/12 5%CO2/5%He	25	18	10 00	177	26.7	-	190	24	210	6 75	14	480	0 57
Cap 2	PGMAW	DC+ve	Carbofil NiMo-1	14233	1 0	82 5%Ar/12 5%CO2/5%He	25	18	10 00	171	24 5		190	24	210	6.75	14	480	0 57

Additional Comments:

Internal Root manual TIG
External passes Lincoln 455 STT Powerwave with Carbofil NiMo-1 Trimix Pulsed sav.swf
Current and voltage averages recorded from Wavedesigner Arcscope and Yokogawa oscilloscope
Torch head angle 6-7° pushing
Welding from100mm before 12o'c to just past 3 o'c (~800mm total)
Gap at OD: 6.03 - 6.54
beats per minute = no. of complete cycles per minute (ie left-right-left)
Welding 5G down
Internal thermocouples placed at 25mm intervals, beginning at 12 o'clock
Internal Thermocouple placement:
Drilled Hole just about to break surface

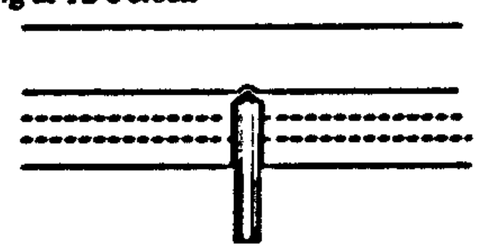

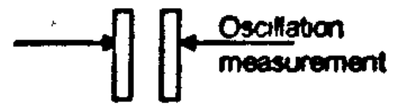

Cap Gap Widths

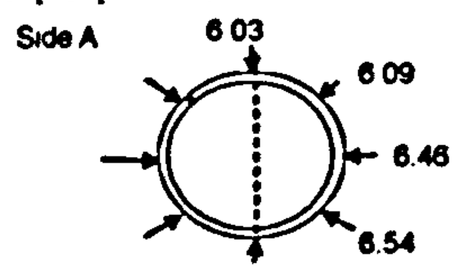

Remaining Depth to Pipe OD (mm)

After Pass No	12	1 30	3	6
0	18.06		17.62	
1	12.53	12.94	12.99	
2	8.78	9.64	9.5	
3	5.51	5.88	7.54	
4	2.58	2.92	3.94	
5	+0.56	0.4	1.68	
Cap	+2.01	+1.38	+0.94	

Thermocycle weld procedure : 100°C preheat

Cranfield UNIVERSITY

As-run Parameter Record

Preheat Variation

Weld No.: Thermo Cycle 100

Date: 14/15/16/17 Oct 2002

Description:

X100 Thermocouple Trials on Pipe

Welders Name/Position:

MGH

Material Grade:	X100
Heat Number:	026401-0004-1
Diameter:	30"
Thickness:	19.05mm
Welding Position:	ASME IX 5G
Preparation Method:	PFM
Alignment Method:	Manually clamped and tacked
Alignment Removed:	After Root Run
Preheat Method:	Propane
Backing System	N/A
Cleaning Method:	Grind/ wire Brush

Joint Preparation:

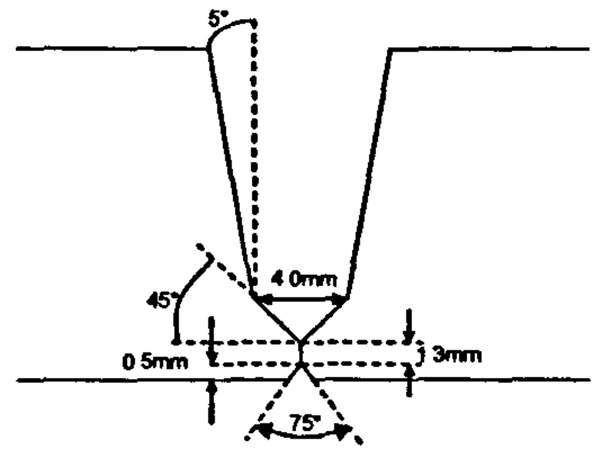

Run Sequence:

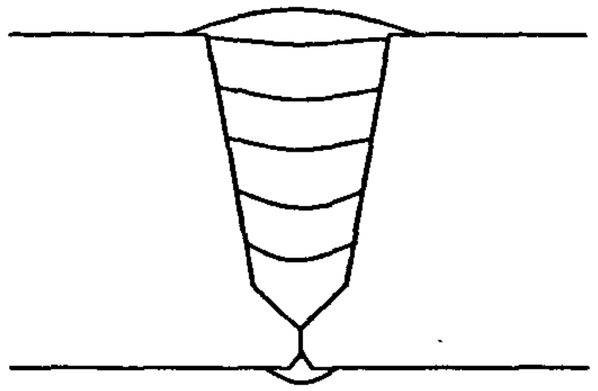

Pass	Process	Polarity	Electrode Brand	Batch	Size mm	Shielding Gas Type	Flow L/min	Temp @ Start °C	Arcsope WFS m/min	Arcsope Amps I	Arcsope Volts V	Yokogawa WFS m/min	Yokogawa Amps I	Yokogawa Volts V	Osc. Freq beats per min.	Osc mm	CTWD mm	Travel Speed mm/min	Arc Energy kJ/min
Int root	TIG	DC-ve	ER70S-2		2.4	Ar	15	100							-	-			
1	PGMAW	DC+ve	Carbofil NiMo-1	14233	1.0	82 5%Ar/12 5%CO2/5%He	25	100-120	10.00	177	22.7	-	190	21	210	1.5	13.5	480	0.50
2	PGMAW	DC+ve	Carbofil NiMo-1	14233	1.0	82 5%Ar/12 5%CO2/5%He	25	100-120	10.00	176	24.4	-	190	22	210	1.5	13 5	480	0.52
3	PGMAW	DC+ve	Carbofil NiMo-1	14233	1.0	82 5%Ar/12 5%CO2/5%He	25	100-120	10 00	177	24	-	190	22	210	2	13.5	480	0 52
4	PGMAW	DC+ve	Carbofil NiMo-1	14233	1.0	82 5%Ar/12 5%CO2/5%He	25	100-120	10.00	177	24 3	-	190	22	210	2.5	13.5	480	0.52
5	PGMAW	DC+ve	Carbofil NiMo-1	14233	1.0	82 5%Ar/12 5%CO2/5%He	25	100-120	10.00	177	24 1	-	190	23	210	3	13 5	480	0.55
Cap	PGMAW	DC+ve	Carbofil NiMo-1	14233	1.0	82 5%Ar/12 5%CO2/5%He	25	100-120	10 00	173	26.1	-	190	24	210	6.75	14	480	0.57

Additional Comments:

Internal Root manual TIG
External passes Lincoln 455 STT Powerwave with Carbofil NiMo-1 Trimix Pulsed sav.swf
Current and voltage averages recorded from Wavedesigner Arcscope and Yokogawa oscilloscope
Torch head angle 6-7° pushing
Welding from100mm before 12o'c to just past 3 o'c (~800mm total)
Gap at OD: 6.20-6.47
beats per minute = no. of complete cycles per minute (ie left-right-left)
Welding 5G down
Internal thermocouples placed at 25mm intervals, beginning at 12 o'clock
Internal Thermocouple placement:
Drilled Hole just about to break surface

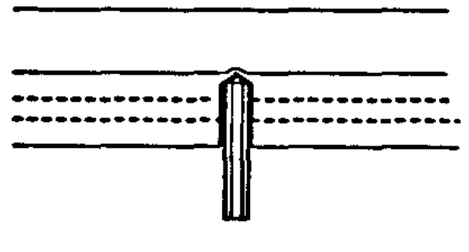

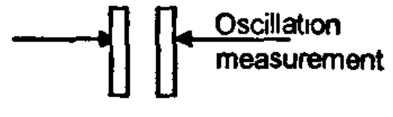

Cap Gap Widths

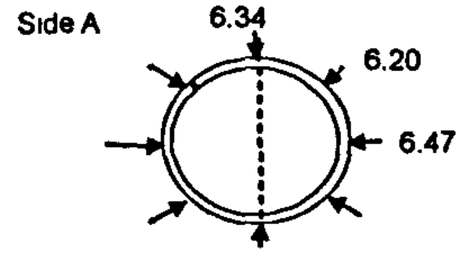

Remaining Depth to Pipe OD (mm)

After Pass No.	12	1.3	3	6
0	17.49	17.71	18.37	
1	12.8	13.04	13.28	
2	9	9.29	9.47	
3				
4	2.9	3.56	3.97	
5	+0.18	0.33	1.05	
Cap	+2.21	+1.05	+1.39	

Thermocycle weld procedure : 180°C preheat

Cranfield UNIVERSITY

As-run Parameter Record

Preheat Variation

Weld No.: Thermo Cycle 180

Date: 28th Oct 2002

Description:

X100 Thermocouple Trials on Pipe

Welders Name/Position:

MGH

Material Grade:	X100
Heat Number:	026401-0004-1
Diameter:	30"
Thickness:	19.05mm
Welding Position:	ASME IX 5G
Preparation Method:	PFM
Alignment Method:	Manually clamped and tacked
Alignment Removed:	After Root Run
Preheat Method:	Propane
Backing System	N/A
Cleaning Method:	Grind/ wire Brush

Joint Preparation:

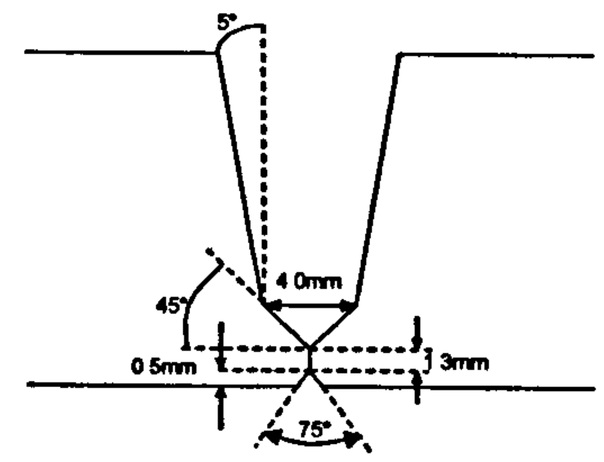

Run Sequence:

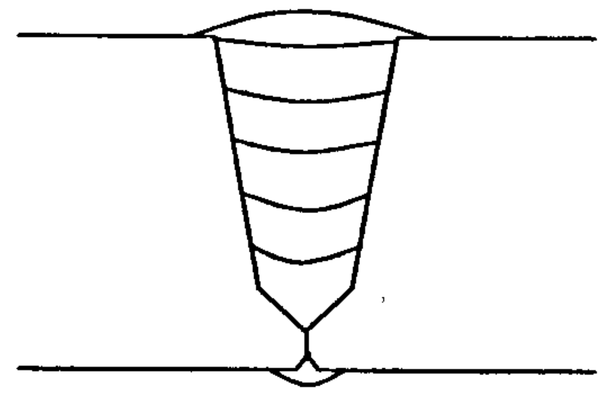

Pass	Process	Polarity	Electrode Brand	Batch	Size mm	Shielding Gas Type	Flow L/min	Temp @ Start °C	Arcscope WFS m/min	Arcscope Amps I	Arcscope Volts V	Yokogawa WFS m/min	Yokogawa Amps I	Yokogawa Volts V	Osc. Freq beats per min.	Osc mm	CTWD mm	Travel Speed mm/min	Arc Energy kJ/min
Int. root	TIG	DC-ve	ER70S-2		2.4	Ar	15	100							-	-			
1	PGMAW	DC+ve	Carbofil NiMo-1	14233	1.0	82 5%Ar/12 5%CO2/5%He	25	170-200	10.00				189	24.1	210	1.6	13.5	475	0 56
2	PGMAW	DC+ve	Carbofil NiMo-1	14233	1.0	82 5%Ar/12 5%CO2/5%He	25	180-200	10.00				190	20 2	210	2	13 5	475	0.49
3	PGMAW	DC+ve	Carbofil NiMo-1	14233	1 0	82 5%Ar/12 5%CO2/5%He	25	180-190	10.00				193	22 6	210	2.5	13.5	475	0.55
4	PGMAW	DC+ve	Carbofil NiMo-1	14233	1.0	82 5%Ar/12 5%CO2/5%He	25	185-200	10.00		20 8		192	22.6	210	3	13.5	475	0.55
5	PGMAW	DC+ve	Carbofil NiMo-1	14233	1.0	82 5%Ar/12 5%CO2/5%He	25	175-185	10 00		19		191	22.8	210	3 5	13.5	475	0 55
Cap	PGMAW	DC+ve	Carbofil NiMo-1	14233	1.0	82 5%Ar/12 5%CO2/5%He	25	180-195	10 00		25.1		190	24.7	210	6	14	475	0.59

Additional Comments:

Internal Root manual TIG
External passes Lincoln 455 STT Powerwave with Carbofil NiMo-1 Trimix Pulsed sav.swf
Current and voltage averages recorded from Yokogawa Oscilloscope and Wavedesigner Arcscope
Torch head angle 6-7° pushing
Welding from 100mm before 12o'c to 3 o'c (~700mm total)
Gap at OD: 6.55 - 6.82
beats per minute = no. of complete cycles per minute (ie left-right-left)
Welding 5G down
Internal thermocouples placed at 25mm intervals, beginning at 12 o'clock
Internal Thermocouple placement:
Drilled Hole just about to break surface

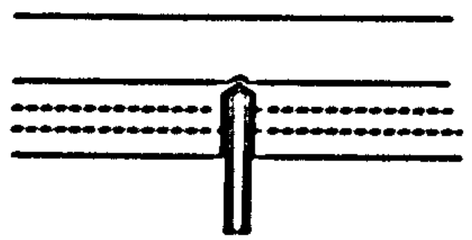

Cap Gap Widths

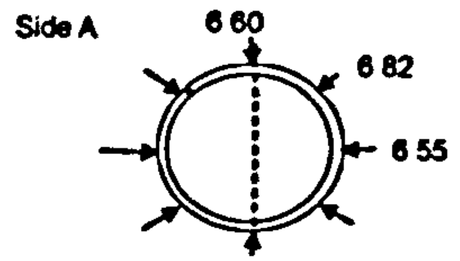

Remaining Depth to Pipe OD (mm)

After Pass No	12	1 3	3	6
0	18.05	17.54	17.95	
1	12.88	13.46	12.65	
2	9.6	9.74	9.27	
3	6.35	6.63	5.71	
4	3.53	3 81	2.94	
5	0.76	1.11	+0.13	
Cap	+2.24	+1.12	+2.13	

Thermocycle weld procedure : process variant trials – single wire

Cranfield UNIVERSITY

As-run Parameter Record

Weld No.: Single Wire Thermo Cycle

Date: 10/12/02 - 13/12/02

Description:

X100 Thermocouple Trials on Pipe

Welders Name/Position:

MGH

Material Grade:	X100
Heat Number:	KYYU 1352, Heat 9B23017, Pipe No. 2
Diameter:	36"
Thickness:	19.05mm
Welding Position:	ASME IX 5G
Preparation Method:	PFM
Alignment Method:	Manually clamped and tacked
Alignment Removed:	After Root Run
Preheat Method:	Propane
Backing System	N/A
Cleaning Method:	Grind/ wire Brush

Joint Preparation:

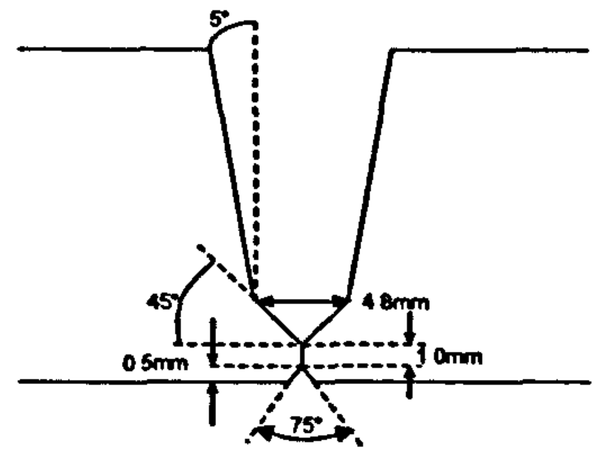

Run Sequence:

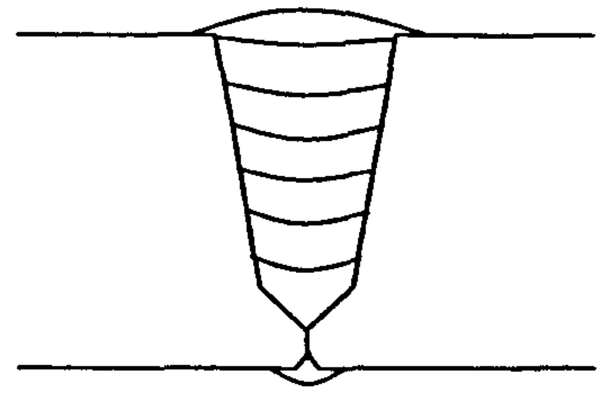

Pass	Process	Polarity	Electrode Brand	Batch	Size mm	Shielding Gas Type	Flow L/min	Temp @ Start °C	Lead WFS m/min	Fronius Amps I	Volts V	Trial WFS m/min	Yokogawa Amps I	Volts V	Osc. Freq beats per min	Osc mm	CTWD mm	Travel Speed mm/min	Arc Energy kJ/min
Int root	GMAW	DC+ve	TS-6	135346	0.9	78Ar/20CO_2/2O_2	35	100	9 70	195	20.8	-	-	-	-	-	10	710	0.34
1	PGMAW	DC+ve	Carbofil NiMo-1	14233	1.0	82 5%Ar/12 5%CO2/5%He	25	100-120	10 00	186	20.9	-	186	22.5	210	1.8	14	558	0.45
2	PGMAW	DC+ve	Carbofil NiMo-1	14233	1.0	82 5%Ar/12 5%CO2/5%He	25	100-120	10 00	187	21 9	-	187	22.5	210	2.5	14	558	0 45
3	PGMAW	DC+ve	Carbofil NiMo-1	14233	1.0	82 5%Ar/12 5%CO2/5%He	25	100-120	10.00	188	21.6	-	191	21	210	3	14	558	0.43
4	PGMAW	DC+ve	Carbofil NiMo-1	14233	1.0	82 5%Ar/12 5%CO2/5%He	25	100-120	10.00	N/A	N/A	-	190	20.9	210	3.75	14	558	0 43
5	PGMAW	DC+ve	Carbofil NiMo-1	14233	1 0	82 5%Ar/12 5%CO2/5%He	25	100-120	10.00	187	21.4	-	192	20.3	210	4	14	558	0 42
6	PGMAW	DC+ve	Carbofil NiMo-1	14233	1 0	82 5%Ar/12 5%CO2/5%He	25	100-120	10.00	186	21.6	-	193	20.4	210	4.25	14	565	0 42
Cap	PGMAW	DC+ve	Carbofil NiMo-1	14233	1.0	82 5%Ar/12 5%CO2/5%He	25	100-120	10.00	182	23.5	-	191	N/A	210	5 25	15	565	0.48

Additional Comments:

Internal Root used ESAB Arist 2000 and rotated pipe (effectively vertical down welding)
External passes Fronius TPS4000 Digital with Puls 0622 synergic curve (1.0mm Carbofil NiMo-1 Trimix Pulsed located with 0.9mm and SP1 buttons on pendant)
Current and voltage averages recorded from Fronius (end of run display) and Yokogawa oscilloscope
Torch head angle 6-7° pushing
Half of pipe welded, pipe rotated such that bug kept between 12.30 and 1.30
Gap at OD: 7.05 - 7.38
beats per minute = no. of complete cycles per minute (ie left-right-left)
Bug direction: downwards

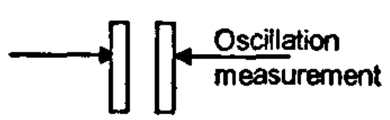

Internal thermocouples placed at 25mm intervals, each pass comprising a thermocouple in the 1.30 and 4.30 position (relative to start position)
Internal Thermocouple placement:
Drilled Hole just about to break surface

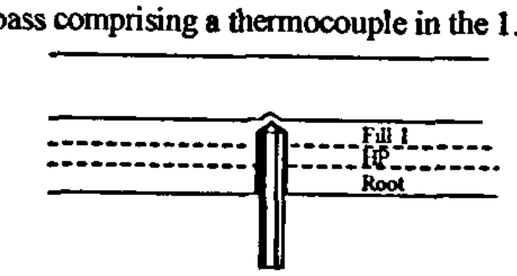

Remaining Depth to Pipe OD (mm)

After Pass No	12	1.30	3	4.3
0	16.52	16.09	15.94	16.00
1	N/A	13.10	12.85	12.87
2	10.62	10.66	10.25	10.49
3	8.33	8.29	7.94	8.09
4	5.97	6.00	5.45	5.39
5	3.79	3.78	3.36	3.48
6	1.65	1.79	1.13	1.38

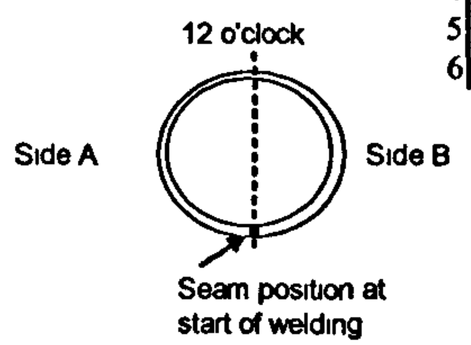

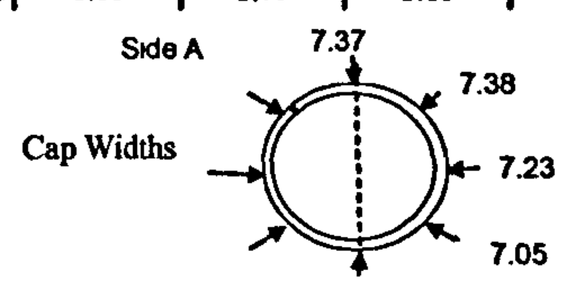

Thermocycle weld procedure : process variant trials – tandem wire

Cranfield UNIVERSITY

As-run Parameter Record

Weld No.: Tandem Wire Thermo Cycle

Date: 17/12/02 - 19/12/02

Description:

X100 Thermocouple Trials on Pipe

Welders Name/Position:

MGH

Material Grade:	X100
Heat Number:	KYYU 1352, Heat 9B23017, Pipe No. 2
Diameter:	36"
Thickness:	19.05mm
Welding Position:	ASME IX 5G
Preparation Method:	PFM
Alignment Method:	Manually clamped and tacked
Alignment Removed:	After Root Run
Preheat Method:	Propane
Backing System	N/A
Cleaning Method	Grind/ wire Brush

Joint Preparation:

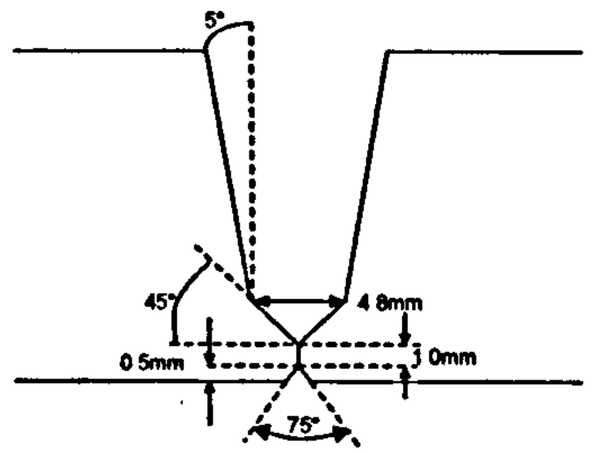

Run Sequence:

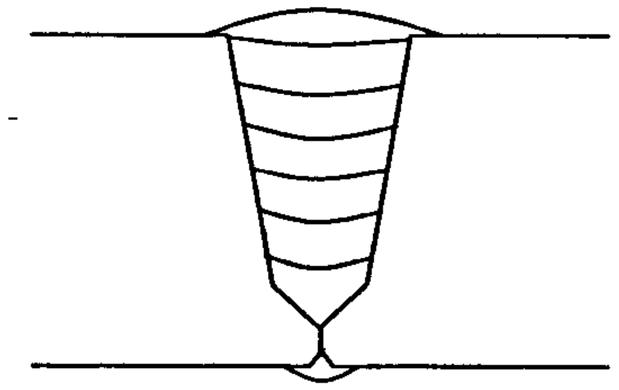

Pass	Process	Polarity	Electrode Brand	Batch	Size mm	Shielding Gas Type	Flow L/min	Temp @ Start °C	Lead WFS m/min	Yokogawa Amps I	Volts V	Trial WFS m/min	Yokogawa Amps I	Volts V	Osc. Freq beats per min.	Osc mm	CTWD mm	Travel Speed mm/min	Arc Energy kJ/min
Int. root	GMAW	DC+ve	TS-6	135346	0.9	78Ar/20CO_2/2O_2	35	100	9.70	195	20.8	-	-	-	-	-	10	710	0.34
1	PGMAW	DC+ve	Carbofil NiMo-1	14233	1.0	82 5%Ar/12 5%CO2/5%He	25	100-120	10 00	193	20 8	10.00	188	21.3	435	2.2 (50)	13.5	1081	0.44
2	PGMAW	DC+ve	Carbofil NiMo-1	14233	1 0	82 5%Ar/12 5%CO2/5%He	25	100-120	10.00	186	22	10 00	194	20 6	435	2.9 (75)	13 5	1081	0.45
3	PGMAW	DC+ve	Carbofil NiMo-1	14233	1.0	82 5%Ar/12 5%CO2/5%He	25	100-120	10.00	192	21.4	10 00	184	N/A	435	3 6 (100)	13.5	1081	0.45
4	PGMAW	DC+ve	Carbofil NiMo-1	14233	1.0	82 5%Ar/12 5%CO2/5%He	25	100-120	10.00	195	20.6	10.00	188	N/A	435	4.1 (120)	13.5	1081	0.45
5	PGMAW	DC+ve	Carbofil NiMo-1	14233	1 0	82 5%Ar/12 5%CO2/5%He	25	100-120	10.00	186	21 8	10 00	192	21.7	435	4.7 (140)	13.5	1081	0 46
6	PGMAW	DC+ve	Carbofil NiMo-1	14233	1.0	82 5%Ar/12 5%CO2/5%He	25	100-120	10.00	186	21 8	10.00	195	20.7	435	5.2 (160)	13.5	1081	0.45
Cap	PGMAW	DC+ve	Carbofil NiMo-1	14233	1.0	82 5%Ar/12 5%CO2/5%He	25	100-120	10.00	182	22 8	10.00	191	21.9	435	5.5 (170)	13 5	1081	0 46
															RMS values shown in brackets				

Additional Comments:

Internal Root used ESAB Arist 2000 and rotated pipe (effectively vertical down welding)
External passes Fronius TPS4000 Digital with Puls 0622 synergic curve (1.0mm Carbofil NiMo-1 Trimix Pulsed located with 0.9mm and SP1 buttons on pendant)
Current and voltage averages recorded from Fronius (end of run display) and Yokogawa oscilloscope
Torch head angle 6-7° pushing
Half of pipe welded; pipe rotated such that bug kept between 12.30 and 1.30
Gap at OD: 7.02 - 7.45
beats per minute = no. of complete cycles per minute (ie left-right-left)
Bug direction: downwards
Internal thermocouples placed at 25mm intervals; each pass comprising a thermocouple in the 1.30 and 4.30 position (relative to start position)
Internal Thermocouple placement:
Drilled Hole 0.5-1.0mm below run surface

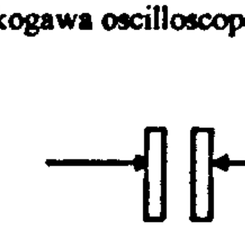

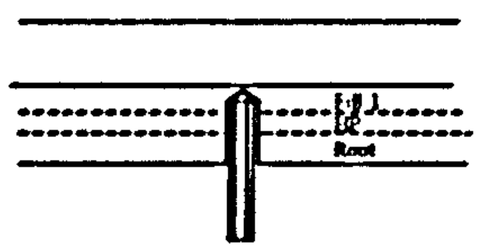

Remaining Depth to Pipe OD (mm)

After Pass No	12	1.30	3	4 3
0	16.29	16.30	16.06	16.55
1	13.13	13.08	13.08	13.10
2	10.28	10.57	10.43	10.59
3	7.70	7.85	8.07	8.20
4	5.84	5.65	5.57	5.96
5	3.01	3.46	3.28	4.02
6	0.69	0.93	1.01	1.60

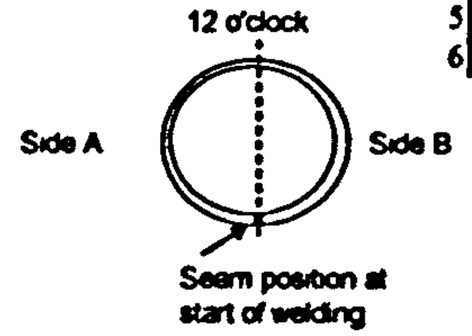

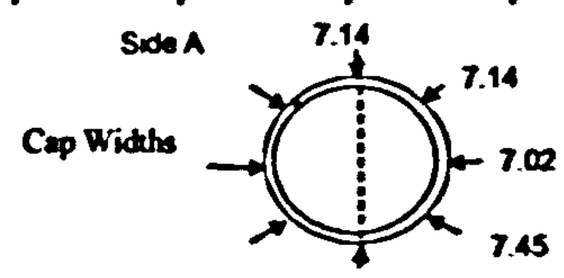

Thermocycle weld procedure : process variant trials – dual torch

Cranfield UNIVERSITY

As-run Parameter Record

Weld No.: Dual Torch Thermo Cycle

Date: 17/01/03 - 20/01/03

Description:

X100 Thermocouple Trials on Pipe

Welders Name/Position:

MGH

Material Grade:	X100
Heat Number:	KYYU 1352, Heat 9B23017, Pipe No. 2
Diameter:	36"
Thickness:	19.05mm
Welding Position:	ASME IX 5G
Preparation Method:	PFM
Alignment Method.	Manually clamped and tacked
Alignment Removed:	After Root Run
Preheat Method.	Propane
Backing System	N/A
Cleaning Method	Grind/ wire Brush

Joint Preparation:

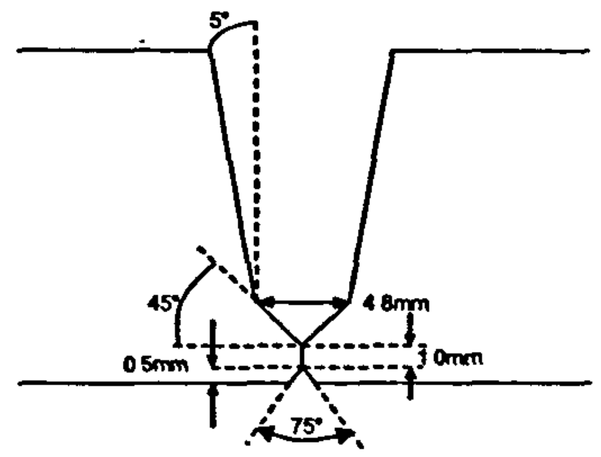

Run Sequence:

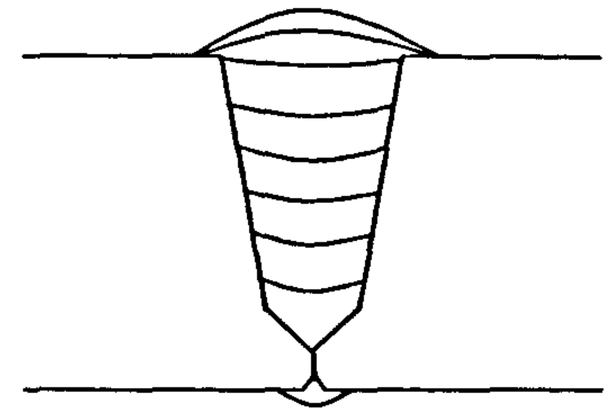

Pass	Process	Polarity	Electrode Brand	Batch	Size mm	Shielding Gas Type	Flow L/min	Temp @ Start °C	Yokogawa WFS m/min	Yokogawa Amps I	Yokogawa Volts V	Fronius WFS m/min	Fronius Amps I	Fronius Volts V	Osc. Freq beats per min.	Osc mm	CTWD mm	Travel Speed mm/min	Arc Energy kJ/min
Int. root	GMAW	DC+ve	TS-6	135346	0.9	78Ar/20CO_2/2O_2	25	100-110	9 70	186	20.8	-	-	-	-	-	10	710	0.33
1 (lead)	PGMAW	DC+ve	Carbofil NiMo-1	14233	1.0	82 5%Ar/12 5%CO2/5%He	23	100-120	10 00	201	19 5		-	-	215	2 1 (45)	14	558	0.42
2 (trail)	PGMAW	DC+ve	Carbofil NiMo-1	14233	1 0	82 5%Ar/12 5%CO2/5%He	23	100-120	10.00	198	19.7		-	-	215	2.9 (75)	16	558	0.42
3 (lead)	PGMAW	DC+ve	Carbofil NiMo-1	14233	1.0	82 5%Ar/12 5%CO2/5%He	23	100-120	10 00	196	20.4		-	-	215	3.6 (100)	14	558	0 43
4 (trail)	PGMAW	DC+ve	Carbofil NiMo-1	14233	1 0	82 5%Ar/12 5%CO2/5%He	23	100-120	10.00	200	18.9		-	-	215	4.3 (125)	16	558	0.41
5 (lead)	PGMAW	DC+ve	Carbofil NiMo-1	14233	1.0	82 5%Ar/12 5%CO2/5%He	23	100-120	10.00	194	21.1	192	20.6		215	4 8 (145)	14	558	0.44
6 (trail)	PGMAW	DC+ve	Carbofil NiMo-1	14233	1.0	82 5%Ar/12 5%CO2/5%He	23	100-120	10 00	193	20 8	189	20.8		215	5 1 (155)	16	558	0 43
7 (lead)	PGMAW	DC+ve	Carbofil NiMo-1	14233	1.0	82 5%Ar/12 5%CO2/5%He	23	100-120	10.00	194	22.3	191	21.5		215	5.4 (165)	14	558	0.47
Cap (trail)	PGMAW	DC+ve	Carbofil NiMo-1	14233	1.0	82 5%Ar/12 5%CO2/5%He	23	100-120	10.00	193	21 8	190	21		215	6.5 (200)	16	558	0.45
															RMS values shown in brackets				

Additional Comments:

Internal Root used ESAB Arist 2000 and rotated pipe (effectively vertical down welding)
External passes Fronius TPS4000 Digital with Puls 0622 synergic curve (1.0mm Carbofil NiMo-1 Trimix Pulsed located with 0.9mm and SP1 buttons on pendant)
Current and voltage averages recorded from Fronius (end of run display) and Yokogawa oscilloscope
Torch head angle 6-7° pushing on each torch
Wire separation = 88.5mm
Half of pipe welded; pipe rotated such that bug kept between 12.30 and 1.30
Gap at OD: 6.92 - 7.28
beats per minute = no. of complete cycles per minute (ie left-right-left)
Bug direction: downwards
Internal thermocouples placed at 25mm intervals; each pass comprising a thermocouple in the ~1.30 and ~4.30 position (relative to start position)
Internal Thermocouple placement:
Drilled Hole just about to break surface

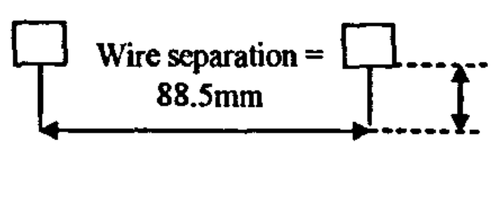

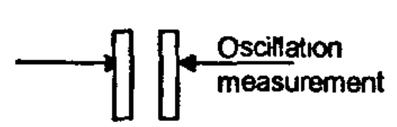

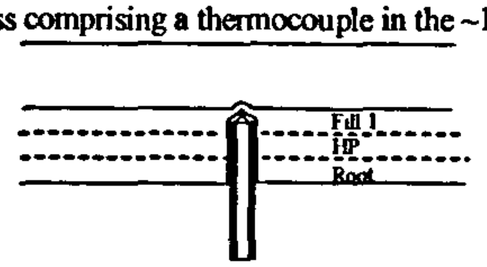

Remaining Depth to Pipe OD (mm)

After Pass No	12	1.30	3	4.3
0	16.03	16.07	16.55	16.14
1	-	-	-	-
2	10.48	10.26	10.31	10.41
3	-	-	-	-
4	5.32	5.32	5.07	5.61
5	-	-	-	-
6	0.71	1.16	0.72	1.26

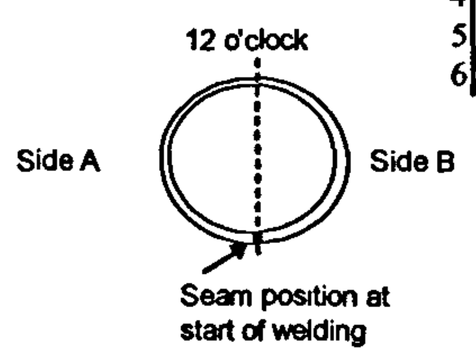

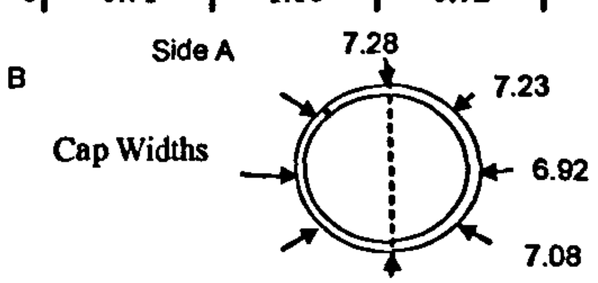

Thermocycle weld procedure : process variant trials – dual tandem torch

Cranfield UNIVERSITY

As-run Parameter Record

Weld No.: Dual Tandem Thermo Cycle

Date:

Description:

X100 Thermocouple Trials on Pipe

Welders Name/Position:

MGH

Material Grade:	X100
Heat Number:	KYYU 1352, Heat 9B23017,
Diameter:	36"
Thickness:	19.05mm
Welding Position:	ASME IX 5G
Preparation Method:	PFM
Alignment Method:	Manually clamped and tacked
Alignment Removed:	After Root Run
Preheat Method:	Propane
Backing System	N/A
Cleaning Method	Grind/ wire Brush

Joint Preparation:

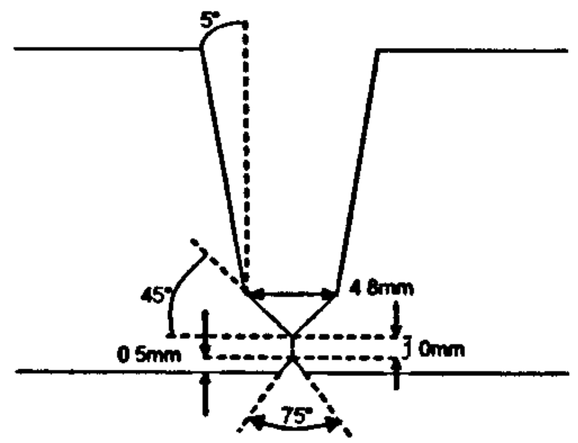

Run Sequence:

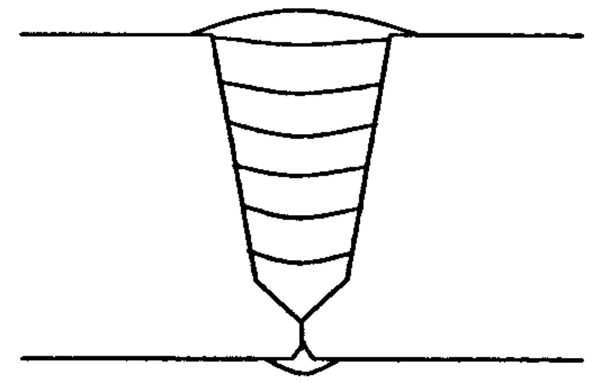

Pass	Process	Polarity	Electrode Brand	Batch	Size mm	Shielding Gas Type	Flow L/min	Temp @ Start °C	Lead Wire WFS m/min	Yokogawa Amps I	Yokogawa Volts V	Trail Wire WFS m/min	Yokogawa Amps I	Yokogawa Volts V	Osc. Freq beats per min.	Osc mm	CTWD mm	Travel Speed mm/min	Arc Energy kJ/min
Int. root	GMAW	DC+ve	TS-6	135346	0.9	78Ar/20CO_2/2O_2	35	100	9.70	186	20 8	-	-	-	-	-	10	710	0.33
1(Lead Torch)	PGMAW	DC+ve	Carbofil NiMo-1	14233	1.0	82 5%Ar/12 5%CO2/5%He	23	100-105	10.00	192	24.9	10 00	193	21 9	430	(40)	15	1092	0 50
2(Trail Torch)	PGMAW	DC+ve	Carbofil NiMo-1	14233	1.0	82 5%Ar/12 5%CO2/5%He	23	100-105	10.00	195	23.3	10.00	192	22 4	430	(65)	16	1092	0.49
3(Lead Torch)	PGMAW	DC+ve	Carbofil NiMo-1	14233	1.0	82 5%Ar/12 5%CO2/5%He	23	100-110	10 00	191	20.9	10 00	-	-	430	(85)	15	1092	0.22
4(Trail Torch)	PGMAW	DC+ve	Carbofil NiMo-1	14233	1.0	82 5%Ar/12 5%CO2/5%He	23	100-110	10.00	196	22 5	10.00	192	22 6	430	(100)	16	1092	0 48
5(Lead Torch)	PGMAW	DC+ve	Carbofil NiMo-1	14233	1.0	82 5%Ar/12 5%CO2/5%He	23	105-115	10 00	194	22.3	10 00	189	21.9	430	(120)	15	1092	0 46
6(Trail Torch)	PGMAW	DC+ve	Carbofil NiMo-1	14233	1.0	82 5%Ar/12 5%CO2/5%He	23	105-115	10.00	211	19.3	10 00	203	19.8	430	(145)	16	1092	0 45
7(Lead Torch)	PGMAW	DC+ve	Carbofil NiMo-1	14233	1.0	82 5%Ar/12 5%CO2/5%He	23	105-115	10.00	196	21.4	10 00	192	20 9	430	(155)	15	1092	0.45
Cap(Trail Torch)	PGMAW	DC+ve	Carbofil NiMo-1	14233	1 0	82 5%Ar/12 5%CO2/5%He	23	105-115	10 00	197	23.5	10.00	188	23 5	430	(170)	16	1092	0 50
															RMS values shown in brackets				

Additional Comments:

Internal Root manual TIG
External passes Fronius TPS4000 Digital with Puls 0622 synergic curve (1.0mm Carbofil NiMo-1 Trimix Pulsed located with 0.9mm and SP1 buttons on pendant)
Current and voltage averages recorded from Fronius (end of run display) and Yokogawa oscilloscope
Torch head angle 6-7° pushing on each torch
Wire separation =
Half of pipe welded, pipe rotated such that bug kept between 12.30 and 1.30
Gap at OD:
beats per minute = no. of complete cycles per minute (ie left-right-left)
Bug direction: downwards
Internal thermocouples placed at 25mm intervals; each pass comprising a thermocouple in the 1.30 and 4.30 position (relative to start position)
Internal Thermocouple placement:
Drilled Hole 0.5-1.0mm below run surface
Layer 3 - only 1 wire

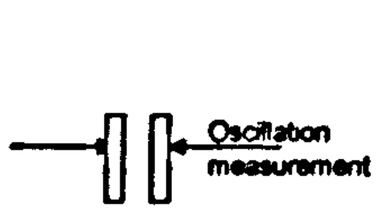

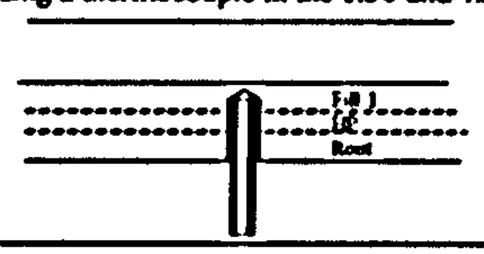

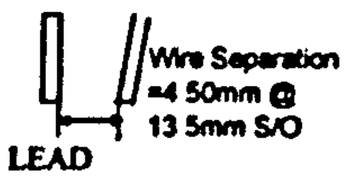

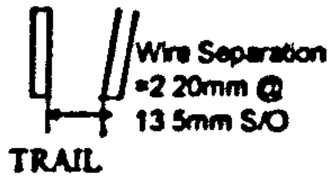

Remaining Depth to Pipe OD (mm)

After Pass No	12	1 00	2	3
0		16.07	16.01	16.35
1				
2		10.31	10.47	10.54
3				
4		6.51	6.42	6.69
5				
6		1.49	1.50	2.07

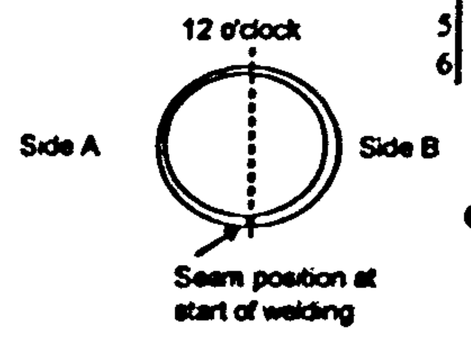

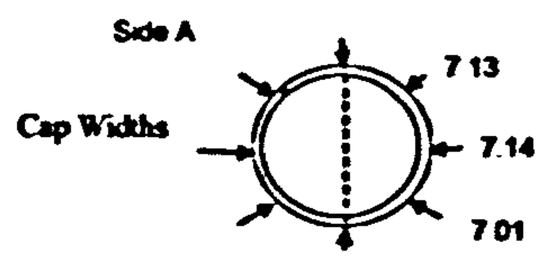

Metal cored wire alloy variation trials – Metal cored control test 1

Cranfield UNIVERSITY

As-run Parameter Record

Weld No.: MC Control Variant 1

Date: 08/11/2002

Description:

X100 Metal Cored Wire Plate Tests - Control Wire 1 0.9Ni 0 3Mo

Welders Name/Position:

MGH

Material Grade:	X100
Heat Number:	1-9887-01-040
Diameter:	N/A
Thickness:	19.05mm
Welding Position:	ASME IX 1G
Preparation Method:	Bandsawn bevel
Alignment Method:	Manually clamped and tacked
Alignment Removed:	N/A
Preheat Method:	Electric Resistance Mats
Backing System	X100 bar
Cleaning Method:	Scriber/ wire Brush

Joint Preparation:

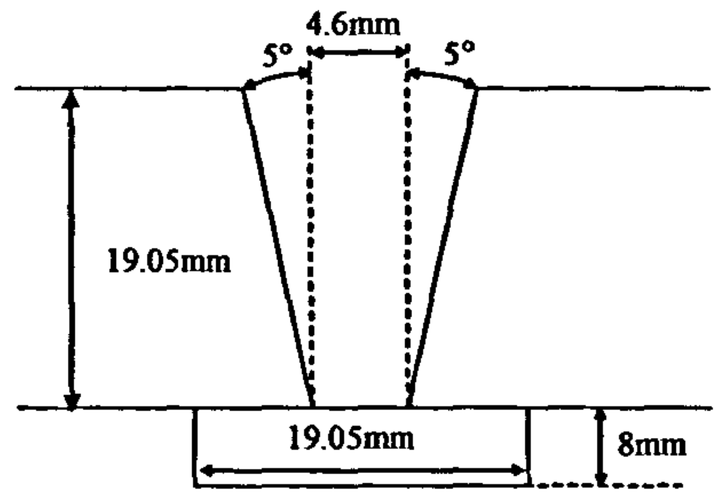

Run Sequence:

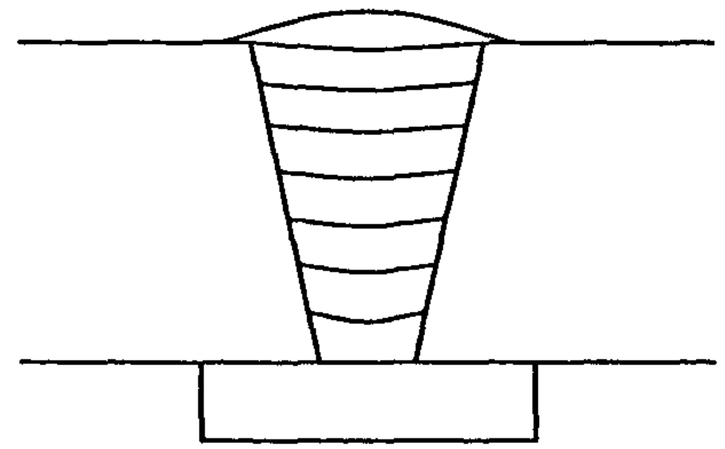

Pass	Process	Polarity	Electrode Brand	Batch	Size mm	Shielding Gas Type	Flow L/min	Temp @ Start °C	Lead WFS m/min	Arcscope Amps I	Arcscope Volts V	Trial WFS m/min	Trial Amps I	DVM Volts V	Osc. Freq beats per min.	Osc mm	CTWD mm	Travel Speed mm/min	Arc Energy kJ/min
1	PGMAW	DC+ve	MC Control 1		1.2	82 5%Ar/12 5%CO_2/5%He	20	105	7.70	204-206	23-24			18.0-18.5	210	2	13.5	474	0.46-0.48
2	PGMAW	DC+ve	MC Control 1		1.2	82 5%Ar/12 5%CO_2/5%He	20	100	7.70	204-205	24-27			18-19	210	2.5	13.5	474	0.46-0.49
3	PGMAW	DC+ve	MC Control 1		1.2	82 5%Ar/12 5%CO_2/5%He	20	100	7.70	204-205	24-25			18-19	210	3	13.5	474	0.46-0.49
4	PGMAW	DC+ve	MC Control 1		1.2	82 5%Ar/12 5%CO_2/5%He	20	108	7.70	208-214	21-22			18-20	210	3.7	13.5	474	0.47-0 54
5	PGMAW	DC+ve	MC Control 1		1.2	82 5%Ar/12 5%CO_2/5%He	20	105	7.70	204-212	22-23			18-21	210	4.3	13 5	474	0.46-0.56
6	PGMAW	DC+ve	MC Control 1		1.2	82 5%Ar/12 5%CO_2/5%He	20	107	7.70	205-210	20-22			18-21	210	4.7	13.5	474	0.47-0.56
7	PGMAW	DC+ve	MC Control 1		1.2	82 5%Ar/12 5%CO_2/5%He	20	110	7.70	203-208	23-26			19-22	210	5	13.5	474	0.49-0 58
Cap	PGMAW	DC+ve	MC Control 1		1.2	82 5%Ar/12 5%CO_2/5%He	20	100	7.70	204-210	21-25			20-23	210	6.7	13.5	474	0.52-0 61

Additional Comments:

Torch head angle 5-7° pushing
Lincoln Powerwave 455 STT with custom waveform: 1.2 metal core pulse trimix 7.7 222hz 515IP.swf
beats per minute = no. of complete cycles per minute (ie left-right-left)

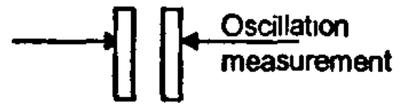

Welding bug : CRC P200

Plates cut on bandsaw (2 cuts for plate length); gap width not constant due to this (variation ±0.75mm), hence weld depth at a given point not constant
Plates fully restrained

	Remaining Depth to Pipe OD (mm)			
After Pass No	start	mid	end	Av. deposition
0	19.51	19.52	19.77	
1	16.37	16.03	16.77	3.21
2	13.37	12.42	13.34	3.35
3	10.48	9.41	10.56	2.89
4	7.78	6.61	8.02	2.68
5	5.63	3.91	5.47	2.47
6	3.36	1.05	2.88	2.57
7	0.86	+1.17	0.36	2.41
Cap				

Metal cored wire alloy variation trials – Metal cored control test 2

Cranfield UNIVERSITY

As-run Parameter Record

Weld No.: MC Control variant 2 B2803 3 1

Date: 05/03/2003

Description:

X100 Metal Cored Wire Plate Tests - Control No.2 0.9Ni 0.3Mo

Welders Name/Position:

MGH

Material Grade:	X100
Heat Number:	1-9887-01-040
Diameter:	N/A
Thickness:	19.05mm
Welding Position:	ASME IX 1G
Preparation Method:	Machined bevel
Alignment Method:	Manually clamped and tacked
Alignment Removed:	N/A
Preheat Method:	Electric Resistance Mats
Backing System	X100 bar
Cleaning Method	Scriber/ wire Brush

Joint Preparation:

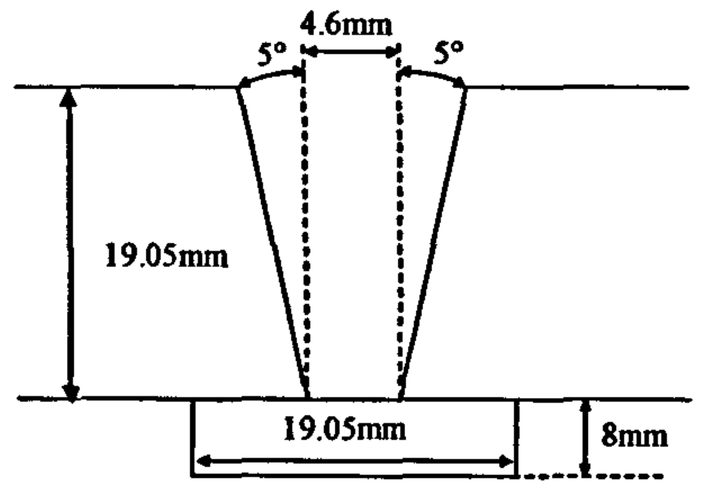

Run Sequence:

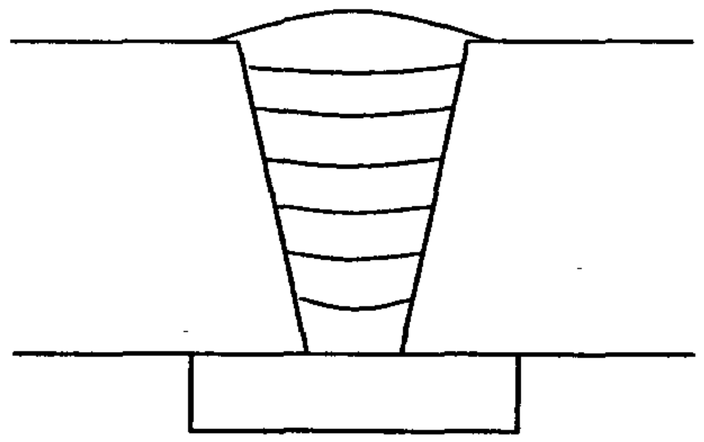

Pass	Process	Polarity	Electrode Brand	Batch	Size mm	Shielding Gas Type	Flow L/min	Temp @ Start °C	Yokogawa WFS m/min	Yokogawa Amps I	Yokogawa Volts V	Arcscope WFS m/min	Arcscope Amps I	Arcscope Volts V	Osc. Freq beats per min	Osc mm	CTWD mm	Travel Speed mm/min	Arc Energy kJ/min
1	PGMAW	DC+ve	MC Control 2	B2803 3 1	1.2	82.5%Ar/12.5%CO_2/5%He	23	100-110	7.70	210	21.3		207	27	210	2.2	13.5	499	0.54
2	PGMAW	DC+ve	MC Control 2	B2803 3 1	1.2	82.5%Ar/12.5%CO_2/5%He	23	100-110	7.70	210	20.8		205	26.3	210	2.6	13.5	507	0.52
3	PGMAW	DC+ve	MC Control 2	B2803 3 1	1.2	82.5%Ar/12.5%CO_2/5%He	23	100-110	7.70	210	22.4		207	26.4	210	3.2	13.5	505	0.56
4	PGMAW	DC+ve	MC Control 2	B2803 3 1	1.2	82.5%Ar/12.5%CO_2/5%He	23	100-110	7.70	210	22.2		207	27.1	210	3.6	13.5	507	0.55
5	PGMAW	DC+ve	MC Control 2	B2803 3 1	1.2	82.5%Ar/12.5%CO_2/5%He	23	100-110	7.70	210	22.7		204	27.3	210	4.2	13.5	504	0.57
6	PGMAW	DC+ve	MC Control 2	B2803 3 1	1.2	82.5%Ar/12.5%CO_2/5%He	23	100-110	7.70	211	21.4		208	27.5	210	4.5	13.5	507	0.53
Cap	PGMAW	DC+ve	MC Control 2	B2803 3 1	1.2	82.5%Ar/12.5%CO_2/5%He	23	100-110	7.70	211	20.8		207	28.1	210	5	13.5	493	0.53
																	Average	503	0.54

Additional Comments:

Torch head angle 5-7° pushing
Lincoln Powerwave 455 STT with custom waveform: 1.2 metal core pulse trimix 7.7 227hz 515IP.swf
beats per minute = no. of complete cycles per minute (ie left-right-left)

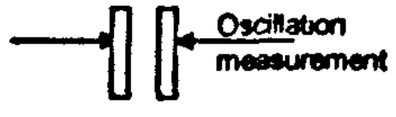

Welding bug : CRC P200

Plates cut on bandsaw then machined to give a 5° bevel.
Plates fully restrained

Cap width

start	mid	end
7.31	7.36	7.4

Remaining Depth to Plate surface (mm)

After Pass No	start	mid	end	Av. Deposition depth
0	19.55	19.7	19.61	
1	15.96	16.16	16.25	3.50
2	12.69	12.8	12.76	3.37
3	9.85	9.82	9.9	2.89
4	7.25	7.09	7.35	2.63
5	4.86	4.65	4.95	2.41
6	2.29	1.97	2.45	2.58
Cap				

Metal cored wire alloy variation trials – Low Ni (0Ni 0.3Mo)

Cranfield UNIVERSITY

As-run Parameter Record

Weld No.: MC Low Ni B2803 3 2

Date: 12/02/03 - 13/02/03

Description:

X100 Metal Cored Wire Plate Tests - Low Ni 0Ni0 3Mo

Welders Name/Position:

MGH

Material Grade:	X100
Heat Number:	1-9887-01-040
Diameter:	N/A
Thickness:	19.05mm
Welding Position:	ASME IX 1G
Preparation Method.	Machined bevel
Alignment Method:	Manually clamped and tacked
Alignment Removed:	N/A
Preheat Method.	Electric Resistance Mats
Backing System	X100 bar
Cleaning Method	Scriber/ wire Brush

Joint Preparation:

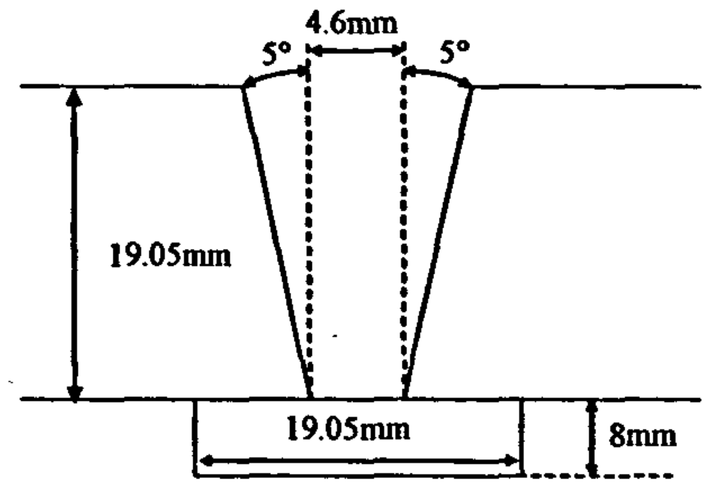

Run Sequence:

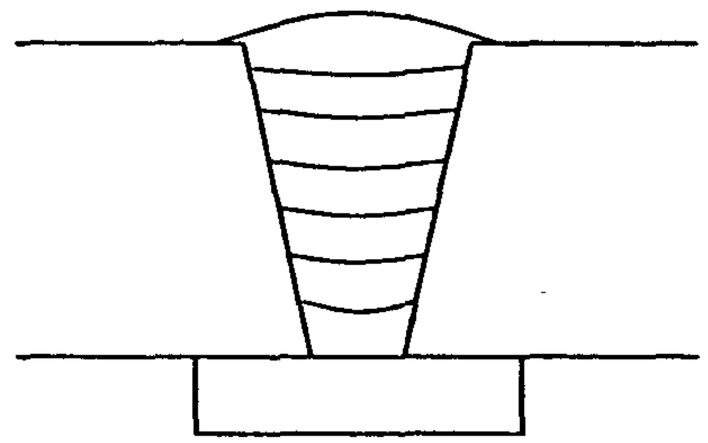

Pass	Process	Polarity	Electrode Brand	Batch	Size mm	Shielding Gas Type	Flow L/min	Temp @ Start °C	Yokogawa WFS m/min	Yokogawa Amps I	Yokogawa Volts V	Arcscope WFS m/min	Arcscope Amps I	Arcscope Volts V	Osc. Freq beats per min.	Osc mm	CTWD mm	Travel Speed mm/min	Arc Energy kJ/mm
1	PGMAW	DC+ve	MC Control 2	B2803 3 2	1.2	82 5%Ar/12 5%CO_2/5%He	23	100-110	7 70	214	18.5		207	23 4	210	2.2	13.5	467	0 51
2	PGMAW	DC+ve	MC Control 2	B2803 3 2	1.2	82 5%Ar/12 5%CO_2/5%He	23	100-110	7.70	210	20.1		201	25.1	210	2.7	13.5	467	0.54
3	PGMAW	DC+ve	MC Control 2	B2803 3 2	1 2	82 5%Ar/12 5%CO_2/5%He	23	100-110	7.70	209	20.7		202	26.5	210	3.2	13.5	461	0.56
4	PGMAW	DC+ve	MC Control 2	B2803 3 2	1.2	82 5%Ar/12 5%CO_2/5%He	23	100-110	7.70	208	19.5		207	26.5	210	3.7	13.5	465	0 52
5	PGMAW	DC+ve	MC Control 2	B2803 3 2	1.2	82 5%Ar/12 5%CO_2/5%He	23	100-110	7.70	209	21 2		207	27.4	210	4.2	13.5	467	0.57
6	PGMAW	DC+ve	MC Control 2	B2803 3 2	1.2	82 5%Ar/12 5%CO_2/5%He	23	100-110	7.70	209	22 1		202	27.3	210	4 2	13 5	472	0.59
Cap	PGMAW	DC+ve	MC Control 2	B2803 3 2	1.2	82 5%Ar/12 5%CO_2/5%He	23	100-110	7.70	210	20.7		207	28.4	210	6	13.5	472	0.55
																	Average	467	0.55

Additional Comments:

Torch head angle 5-7° pushing
Lincoln Powerwave 455 STT with custom waveform: 1.2 metal core pulse trimix 7.7 227hz 515IP.swf
beats per minute = no. of complete cycles per minute (ie left-right-left)

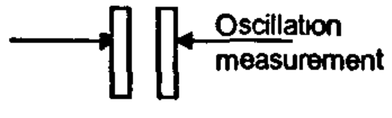

Welding bug : CRC P200

Plates cut on bandsaw then machined to give a 5° bevel.
Plates fully restrained

Cap width

start	mid	end
7.26	7.48	7.28

Remaining Depth to Plate surface (mm)

After Pass No	start	mid	end	Av. Deposition depth
0	19.81	19.85	19.65	
1	15.73	15.85	15.79	3.98
2	12.31	12.18	12.11	3.59
3	8.64	8.84	8.74	3.46
4	5.78	5.89	5.71	2.95
5	3.28	3.04	2.89	2.72
6	0.1	0.17	0.03	2.97
Cap				

Metal cored wire alloy variation trials – High Ni (1.6Ni 0.3Mo)

Cranfield UNIVERSITY

As-run Parameter Record

Weld No.: MC High Ni B2803 3 3

Date: 14/02/03 - 18/02/03

Description:

X100 Metal Cored Wire Plate Tests - High Ni 1 6Ni 0 3Mo

Welders Name/Position:

MGH

Material Grade:	X100
Heat Number:	1-9887-01-040
Diameter:	N/A
Thickness:	19.05mm
Welding Position:	ASME IX 1G
Preparation Method:	Machined bevel
Alignment Method:	Manually clamped and tacked
Alignment Removed:	N/A
Preheat Method:	Electric Resistance Mats
Backing System	X100 bar
Cleaning Method	Scriber/ wire Brush

Joint Preparation:

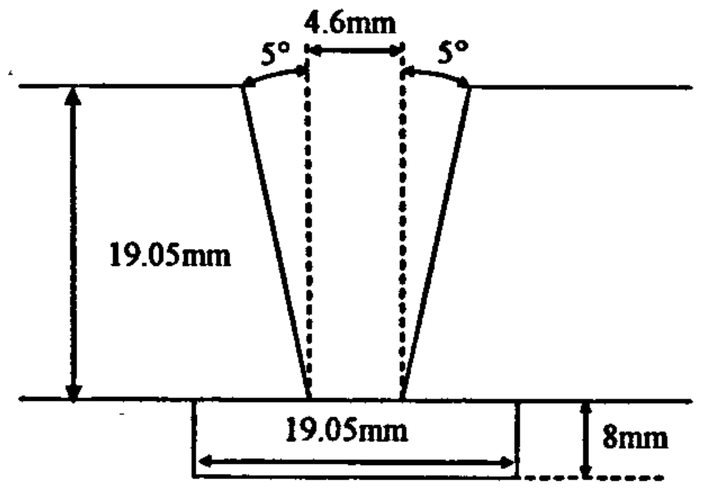

Run Sequence:

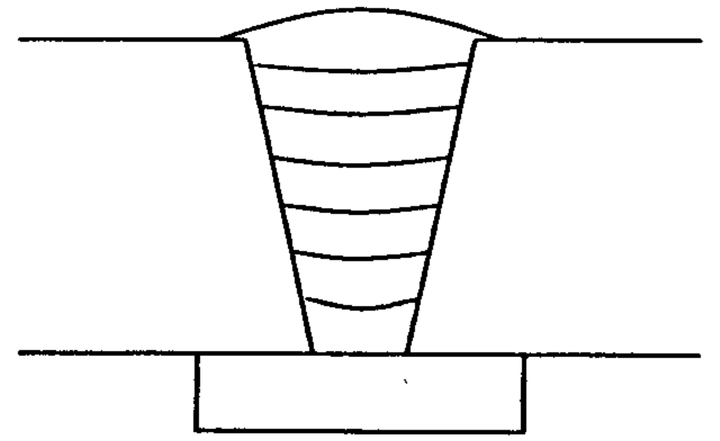

Pass	Process	Polarity	Electrode Brand	Batch	Size mm	Shielding Gas Type	Flow L/min	Temp @ Start ℃	Yokogawa WFS m/min	Yokogawa Amps I	Yokogawa Volts V	Arcscope WFS m/min	Arcscope Amps I	Arcscope Volts V	Osc. Freq beats per min.	Osc mm	CTWD mm	Travel Speed mm/min	Arc Energy kJ/min
1	PGMAW	DC+ve	MC High Ni	B2803 3 3	1.2	82 5%Ar/12 5%CO_2/5%He	23	100-110	7.70	213	18 7		211	22 4	210	2.2	13.5	538	0.44
2	PGMAW	DC+ve	MC High Ni	B2803 3 3	1.2	82 5%Ar/12 5%CO_2/5%He	23	100-110	7.70	213	19.1		207	26.1	210	2 6	13.5	533	0 46
3	PGMAW	DC+ve	MC High Ni	B2803 3 3	1.2	82 5%Ar/12 5%CO_2/5%He	23	100-110	7.70	209	19.7		204	25 6	210	3.1	13.5	474	0 52
4	PGMAW	DC+ve	MC High Ni	B2803 3 3	1.2	82 5%Ar/12 5%CO_2/5%He	23	100-110	7.70	210	19.4		208	25	210	3.7	13.5	503	0.49
5	PGMAW	DC+ve	MC High Ni	B2803 3 3	1.2	82 5%Ar/12 5%CO_2/5%He	23	100-110	7.70	210	20.3		207	26	210	4	13.5	497	0 51
6	PGMAW	DC+ve	MC High Ni	B2803 3 3	1.2	82 5%Ar/12 5%CO_2/5%He	23	100-110	7.70	211	21.4		208	27.2	210	4.3	13.5	503	0.54
Cap	PGMAW	DC+ve	MC High Ni	B2803 3 3	1.2	82 5%Ar/12 5%CO_2/5%He	23	100-110	7.70	211	21.4		207	28 1	210	5	13.5	502	0.54
																	Average	507	0.50

Additional Comments:

Torch head angle 5-7° pushing
Lincoln Powerwave 455 STT with custom waveform: 1.2 metal core pulse trimix 7.7 227hz 515IP.swf
beats per minute = no. of complete cycles per minute (ie left-right-left)

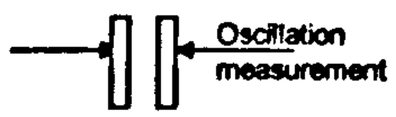

Welding bug : CRC P200

Plates cut on bandsaw then machined to give a 5° bevel.
Plates fully restrained

Cap width

start	mid	end
7.22	7.36	7.24

Remaining Depth to Plate surface (mm)

After Pass No	start	mid	end	Av. Deposition depth
0	19.44	19.52	19.46	
1	16.09	16.16	16.19	3.33
2	12.97	12.99	13.1	3.13
3	9.85	9.58	9.87	3.25
4	6.91	6.78	7.05	2.85
5	4.33	4.01	4.43	2.66
6	1.7	1.75	1.97	2.45
Cap				

Metal cored wire alloy variation trials – Low Mo (0.9Ni 0.15Mo)

Cranfield UNIVERSITY

As-run Parameter Record

Weld No.: MC Low Mo B2803 3 4

Date: 19/02/03-21/02/03

Description:

X100 Metal Cored Wire Plate Tests - Low Mo 1.0Ni 0.17Mo

Welders Name/Position

MGH

Material Grade:	X100
Heat Number:	1-9887-01-040
Diameter:	N/A
Thickness:	19.05mm
Welding Position:	ASME IX 1G
Preparation Method:	Machined bevel
Alignment Method.	Manually clamped and tacked
Alignment Removed:	N/A
Preheat Method.	Electric Resistance Mats
Backing System	X100 bar
Cleaning Method	Scriber/ wire Brush

Joint Preparation:

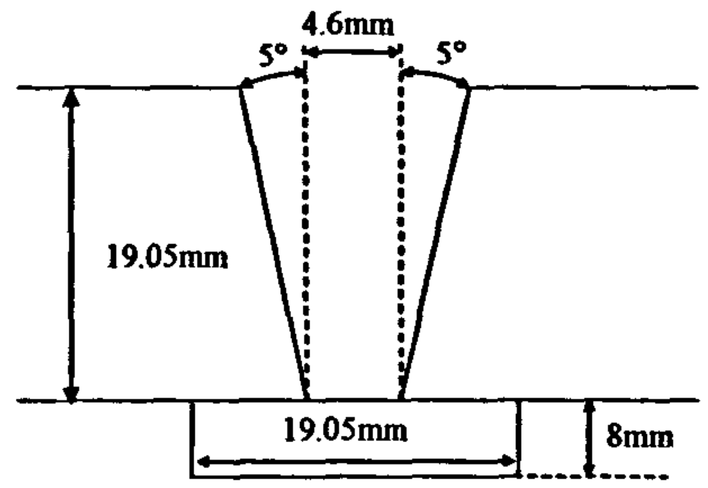

Run Sequence:

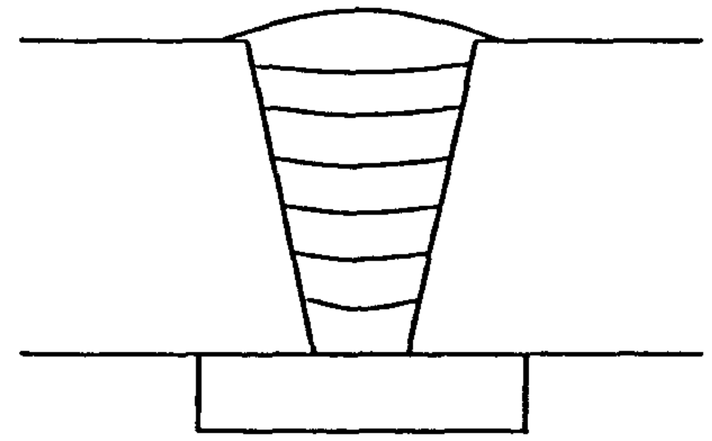

Pass	Process	Polarity	Electrode Brand	Batch	Size mm	Shielding Gas Type	Flow L/min	Temp @ Start °C	Yokogawa WFS m/min	Yokogawa Amps I	Yokogawa Volts V	Arcscope WFS m/min	Arcscope Amps I	Arcscope Volts V	Osc. Freq beats per min.	Osc mm	CTWD mm	Travel Speed mm/min	Arc Energy kJ/min
1	PGMAW	DC+ve	MC Low Mo	B2803 3 4	1.2	82 5%Ar/12 5%CO_2/5%He	23	100-110	7.70	211	20.6		207	26.9	210	2.2	13 5	502	0.52
2	PGMAW	DC+ve	MC Low Mo	B2803 3 4	1 2	82 5%Ar/12 5%CO_2/5%He	23	100-110	7.70	211	20.7		203	26.8	210	2.5	13.5	502	0 52
3	PGMAW	DC+ve	MC Low Mo	B2803 3 4	1.2	82 5%Ar/12 5%CO_2/5%He	23	100-110	7.70	212	21.2		207	26.5	210	3	13 5	504	0.54
4	PGMAW	DC+ve	MC Low Mo	B2803 3 4	1.2	82 5%Ar/12 5%CO_2/5%He	23	100-110	7.70	211	21.6		207	26.3	210	3 6	13.5	503	0.54
5	PGMAW	DC+ve	MC Low Mo	B2803 3 4	1.2	82 5%Ar/12 5%CO_2/5%He	23	100-110	7.70	212	20.3		207	26.5	210	4.1	13.5	502	0.51
6	PGMAW	DC+ve	MC Low Mo	B2803 3 4	1.2	82 5%Ar/12 5%CO_2/5%He	23	100-110	7.70	212	21.4		207	27.7	210	4.6	13.5	505	0.54
Cap	PGMAW	DC+ve	MC Low Mo	B2803 3 4	1.2	82 5%Ar/12 5%CO_2/5%He	23	100-110	7.70	211	23.3		208	29 6	210	5	13.5	487	0 61
																	Average	501	0.54

Additional Comments:

Torch head angle 5-7° pushing
Lincoln Powerwave 455 STT with custom waveform: 1.2 metal core pulse trimix 7.7 227hz 515IP.swf
beats per minute = no. of complete cycles per minute (ie left-right-left)

Welding bug : CRC P200

Plates cut on bandsaw then machined to give a 5° bevel.
Plates fully restrained

Cap width

start	mid	end
7.52	7.63	7.62

Remaining Depth to Plate surface (mm)

After Pass No.	start	mid	end	Av. Deposition depth
0	19.61	19.55	19.43	
1	15.96	16.37	16.33	3.31
2	12.71	13.03	13.02	3.30
3	10	10.03	10.13	2.87
4	7.25	7.43	7.56	2.64
5	4.84	4.93	5.11	2.45
6	2.41	2.4	2.84	2.41
Cap				

Metal cored wire alloy variation trials – High Mo (0.9Ni 0.45Mo)

Cranfield UNIVERSITY

As-run Parameter Record

Weld No.: MC High Mo B2803 3 5

Date: 19/02/2003

Description:

X100 Metal Cored Wire Plate Tests - High Mo 1.0Ni 0.45Mo

Welders Name/Position:

MGH

Material Grade:	X100
Heat Number:	1-9887-01-040
Diameter:	N/A
Thickness:	19.05mm
Welding Position:	ASME IX 1G
Preparation Method:	Machined bevel
Alignment Method:	Manually clamped and tacked
Alignment Removed:	N/A
Preheat Method:	Electric Resistance Mats
Backing System	X100 bar
Cleaning Method:	Scriber/ wire Brush

Joint Preparation:

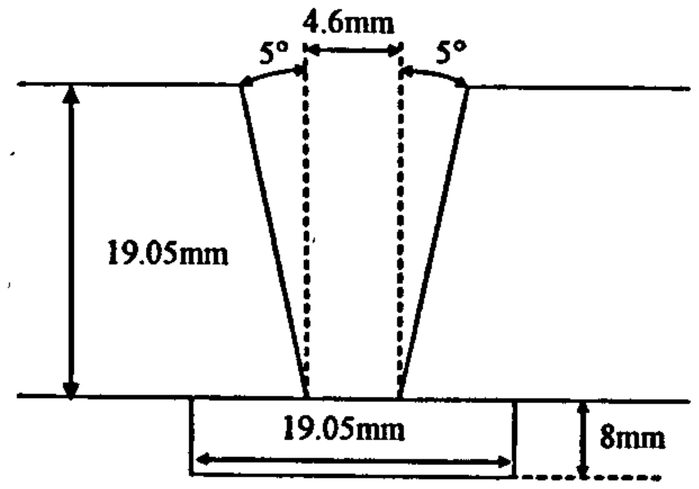

Run Sequence:

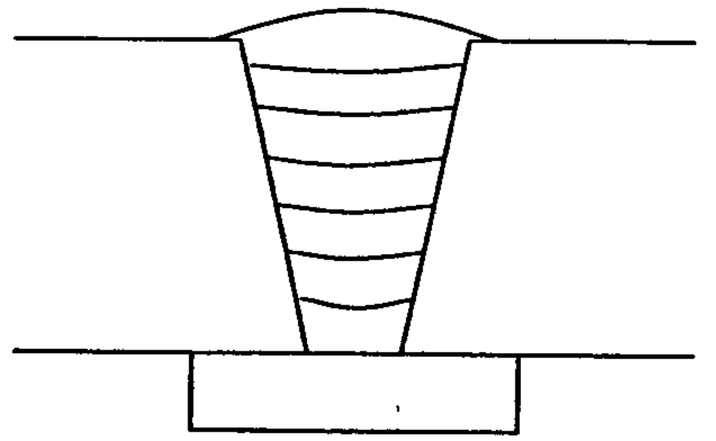

Pass	Process	Polarity	Electrode Brand	Batch	Size mm	Shielding Gas Type	Flow L/min	Temp @ Start ℃	Yokogawa WFS m/min	Yokogawa Amps I	Yokogawa Volts V	Arcscope WFS m/min	Arcscope Amps I	Arcscope Volts V	Osc. Freq beats per min.	Osc mm	CTWD mm	Travel Speed mm/min	Arc Energy kJ/min
1	PGMAW	DC+ve	MC High Mo	B2803 3 5	1.2	82 5%Ar/12 5%CO_2/5%He	23	100-105	7.70	211	20 1		207	23.8	210	2.2	13.5	498	0.51
2	PGMAW	DC+ve	MC High Mo	B2803 3 5	1.2	82 5%Ar/12 5%CO_2/5%He	23	100-110	7.70	211	20.6		208	26 9	210	2 6	13.5	498	0.52
3	PGMAW	DC+ve	MC High Mo	B2803 3 5	1.2	82 5%Ar/12 5%CO_2/5%He	23	100-110	7.70	211	21.6		200	26 4	210	3.1	13.5	503	0.54
4	PGMAW	DC+ve	MC High Mo	B2803 3 5	1.2	82 5%Ar/12 5%CO_2/5%He	23	100-110	7.70	211	20.5		207	26.5	210	3.6	13.5	503	0.52
5	PGMAW	DC+ve	MC High Mo	B2803 3 5	1.2	82 5%Ar/12 5%CO_2/5%He	23	100-110	7.70	211	21 4		208	27	210	4.15	13.5	504	0 54
6	PGMAW	DC+ve	MC High Mo	B2803 3 5	1.2	82 5%Ar/12 5%CO_2/5%He	23	100-110	7.70	211	21.2		207	27.8	210	4 6	13.5	500	0.54
Cap	PGMAW	DC+ve	MC High Mo	B2803 3 5	1.2	82 5%Ar/12 5%CO_2/5%He	23	100-110	7.70	211	22.1		208	28 5	210	5	13.5	478	0.59
																	Average	498	0 54

Additional Comments:

Torch head angle 5-7° pushing
Lincoln Powerwave 455 STT with custom waveform: 1.2 metal core pulse trimix 7.7 227hz 515IP.swf
beats per minute = no. of complete cycles per minute (ie left-right-left)

Welding bug : CRC P200

Plates cut on bandsaw then machined to give a 5° bevel.
Plates fully restrained

All Current and Voltage waveforms recorded on Yokogawa Oscilloscope

Cap width

start	mid	end
7.32	7.48	7.59

Remaining Depth to Plate surface (mm)

After Pass No	start	mid	end	Av. Deposition depth
0	19.52	19.74	19.61	
1	15.89	16.2	16.13	3.55
2	12.79	13.04	13.04	3.12
3	10.16	10.12	9.79	2.93
4	7.45	7.33	7.04	2.75
5	4.61	4.7	5.3	2.40
6	2.21	2.38	3.03	2.33
Cap				

Metal cored wire alloy variation trials – Medium Cr (0.9Ni 0.3Mo 0.3Cr)

Cranfield UNIVERSITY

As-run Parameter Record

Weld No.: MC Medium Cr B2803 3 6

Date: 25/02/2003

Description:

X100 Metal Cored Wire Plate Tests - Medium Cr 0.9Ni 0 3Mo 0 3Cr

Welders Name/Position:

MGH

Material Grade:	X100
Heat Number:	1-9887-01-040
Diameter:	N/A
Thickness:	19.05mm
Welding Position:	ASME IX 1G
Preparation Method:	Machined bevel
Alignment Method.	Manually clamped and tacked
Alignment Removed:	N/A
Preheat Method.	Electric Resistance Mats
Backing System	X100 bar
Cleaning Method	Scriber/ wire Brush

Joint Preparation:

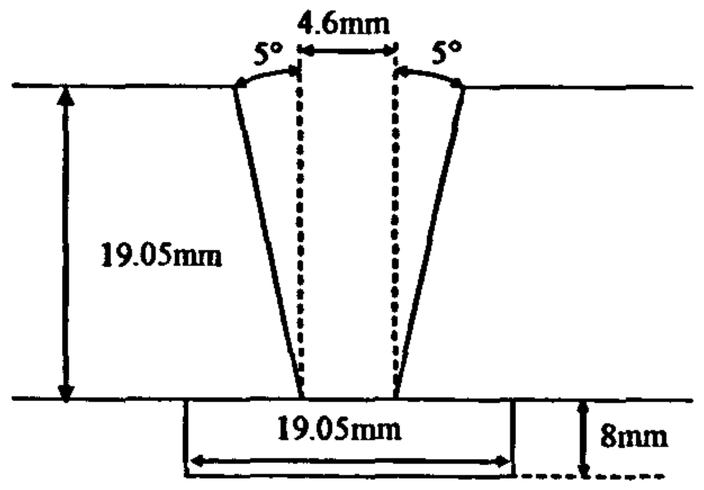

Run Sequence:

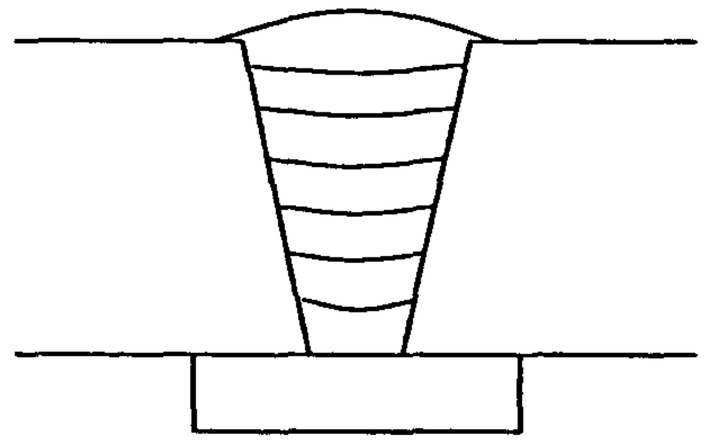

Pass	Process	Polarity	Electrode Brand	Batch	Size mm	Shielding Gas Type	Flow L/min	Temp @ Start °C	Yokogawa WFS m/min	Yokogawa Amps I	Yokogawa Volts V	Arcscope WFS m/min	Arcscope Amps I	Arcscope Volts V	Osc. Freq beats per min.	Osc mm	CTWD mm	Travel Speed mm/min	Arc Energy kJ/min
1	PGMAW	DC+ve	MC Medium Cr	B2803 3 6	1.2	82 5%Ar/12 5%CO_2/5%He	23	100-110	7 70	211	20.2		208	25.8	210	2.2	13.5	496	0.52
2	PGMAW	DC+ve	MC Medium Cr	B2803 3 6	1.2	82 5%Ar/12 5%CO_2/5%He	23	100-110	7.70	211	20.5		204	26 6	210	2.6	13.5	502	0.52
3	PGMAW	DC+ve	MC Medium Cr	B2803 3 6	1.2	82 5%Ar/12 5%CO_2/5%He	23	100-110	7.70	211	22.3		205	26.6	210	3.2	13.5	503	0.56
4	PGMAW	DC+ve	MC Medium Cr	B2803 3 6	1.2	82 5%Ar/12 5%CO_2/5%He	23	100-110	7.70	211	22.4		207	27.2	210	3.6	13 5	503	0.56
5	PGMAW	DC+ve	MC Medium Cr	B2803 3 6	1.2	82 5%Ar/12 5%CO_2/5%He	23	100-110	7.70	211	22.8		200	26.9	210	4.2	13.5	503	0.57
6	PGMAW	DC+ve	MC Medium Cr	B2803 3 6	1 2	82 5%Ar/12 5%CO_2/5%He	23	100-110	7.70	211	23.2		207	28.9	210	4.5	13.5	503	0.58
Cap	PGMAW	DC+ve	MC Medium Cr	B2803 3 6	1.2	82 5%Ar/12 5%CO_2/5%He	23	100-110	7.70	211	22.7		207	29.1	210	5	13.5	476	0 60
																	Average	498	0.56

Additional Comments:

Torch head angle 5-7° pushing
Lincoln Powerwave 455 STT with custom waveform: 1.2 metal core pulse trimix 7.7 227hz 515IP.swf
beats per minute = no. of complete cycles per minute (ie left-right-left)

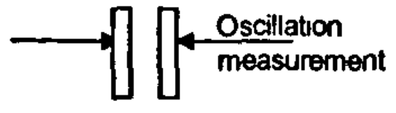

Welding bug : CRC P200

Plates cut on bandsaw then machined to give a 5° bevel.
Plates fully restrained

Cap width

start	mid	end
7.28	7.39	7.26

Remaining Depth to Plate surface (mm)

After Pass No	start	mid	end	Av. Deposition depth
0	19.55	19.63	19.57	
1	16.06	16.08	15.93	3.56
2	12.83	12 8	12.85	3.20
3	9.78	9.84	9.88	2.99
4	7.17	7.06	7.24	2.68
5	4.67	4.5	4.92	2.46
6	2.3	2.29	2.36	2.38
Cap				

Metal cored wire alloy variation trials – High Cr (0.9Ni 0.3Mo 0.5Cr)

Cranfield UNIVERSITY

As-run Parameter Record

Weld No.: MC High Cr B2803 3 7

Date: 26/02/2003

Description:

X100 Metal Cored Wire Plate Tests - High Cr 0 9Ni 0 3Mo 0 5Cr

Welders Name/Position:

MGH

Material Grade:	X100
Heat Number:	1-9887-01-040
Diameter.	N/A
Thickness:	19.05mm
Welding Position:	ASME IX 1G
Preparation Method:	Machined bevel
Alignment Method.	Manually clamped and tacked
Alignment Removed:	N/A
Preheat Method.	Electric Resistance Mats
Backing System	X100 bar
Cleaning Method:	Scriber/ wire Brush

Joint Preparation:

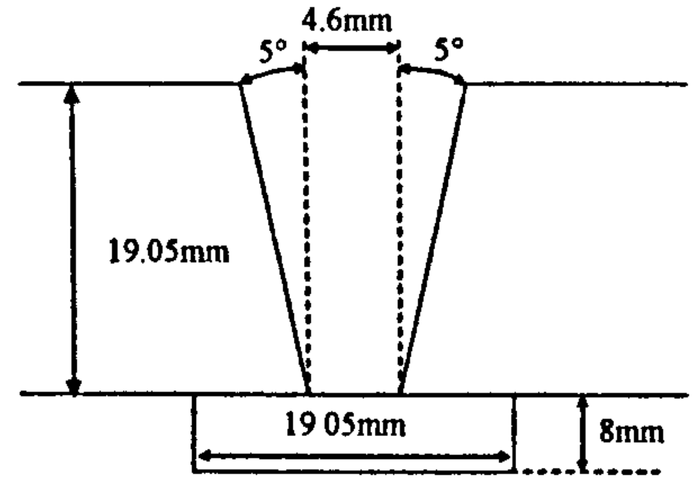

Run Sequence:

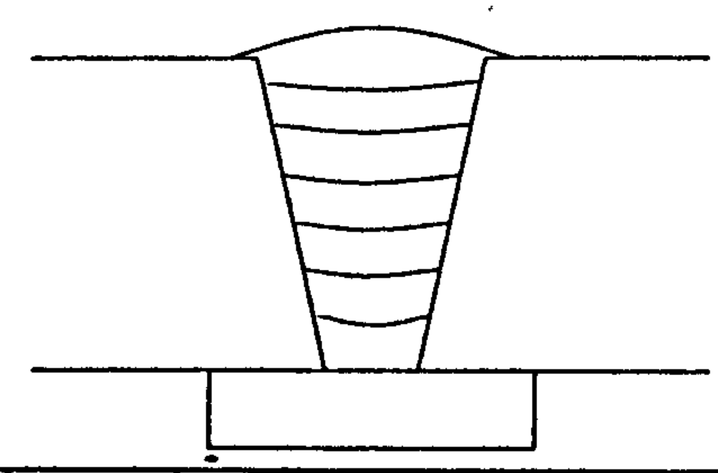

Pass	Process	Polarity	Electrode Brand	Batch	Size mm	Shielding Gas Type	Flow L/min	Temp @ Start °C	Yokogawa WFS m/min	Yokogawa Amps I	Yokogawa Volts V	Arcscope WFS m/min	Arcscope Amps I	Arcscope Volts V	Osc. Freq beats per min.	Osc mm	CTWD mm	Travel Speed mm/min	Arc Energy kJ/min
1	PGMAW	DC+ve	MC High Cr	B2803 3 7	1.2	82 5%Ar/12 5%CO_2/5%He	23	100-110	7.70	210	20 6		207	26.3	210	2.2	13.5	510	0.51
2	PGMAW	DC+ve	MC High Cr	B2803 3 7	1 2	82 5%Ar/12 5%CO_2/5%He	23	100-110	7.70	211	22 5		208	28 8	210	2 6	13 5	498	0 57
3	PGMAW	DC+ve	MC High Cr	B2803 3 7	1 2	82 5%Ar/12 5%CO_2/5%He	23	100-110	7.70	211	21 9		207	26 9	210	3 15	13 5	502	0 55
4	PGMAW	DC+ve	MC High Cr	B2803 3 7	1.2	82 5%Ar/12 5%CO_2/5%He	23	100-110	7.70	211	22 2		208	26.7	210	3 6	13.5	504	0 56
5	PGMAW	DC+ve	MC High Cr	B2803 3 7	1.2	82 5%Ar/12 5%CO_2/5%He	23	100-110	7.70	211	23		207	27.5	210	4 1	13 5	500	0 58
6	PGMAW	DC+ve	MC High Cr	B2803 3 7	1 2	82 5%Ar/12 5%CO_2/5%He	23	100-110	7.70	211	23 3		207	27 9	210	4 55	13.5	507	0 58
Cap	PGMAW	DC+ve	MC High Cr	B2803 3 7	1 2	82 5%Ar/12 5%CO_2/5%He	23	100-110	7.70	212	24 2		207	29 7	210	5	13.5	491	0 63
																	Average	502	0 57

Additional Comments:

Torch head angle 5-7° pushing
Lincoln Powerwave 455 STT with custom waveform: 1.2 metal core pulse trimix 7.7 227hz 5151P swf
beats per minute = no. of complete cycles per minute (ie left-right-left)

Welding bug : CRC P200

Plates cut on bandsaw then machined to give a 5° bevel.
Plates fully restrained

Cap width

start	mid	end
7.32	7.51	7.42

Remaining Depth to Plate surface (mm)

After Pass No	start	mid	end	Av. Deposition depth
0	19.66	19.53	19.51	
1	16.02	16.15	16.04	3.50
2	12.78	12.72	12.8	3.30
3	9.53	9.72	9.94	3 04
4	7.18	6 98	6.94	2.70
5	4.51	4.34	4.59	2.55
6	1.94	1.71	1.95	2 61
Cap				

Metal cored wire alloy variation trials – Low C (0.9Ni 0.3Mo 0.04C)

Cranfield UNIVERSITY

As-run Parameter Record

Weld No.: MC Low C B2803 3 8

Date:

Description:

X100 Metal Cored Wire Plate - Tests - Low C
1 0Ni 0 3Mo 0 04C

Welders Name/Position:

MGH

Material Grade:	X100
Heat Number:	1-9887-01-040
Diameter.	N/A
Thickness:	19.05mm
Welding Position:	ASME IX 1G
Preparation Method:	Machined bevel
Alignment Method:	Manually clamped and tacked
Alignment Removed	N/A
Preheat Method	Electric Resistance Mats
Backing System	X100 bar
Cleaning Method	Scriber/ wire Brush

Joint Preparation:

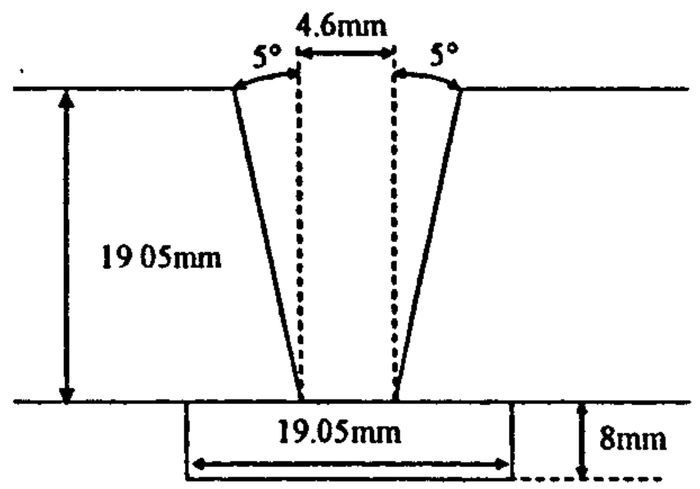

Run Sequence:

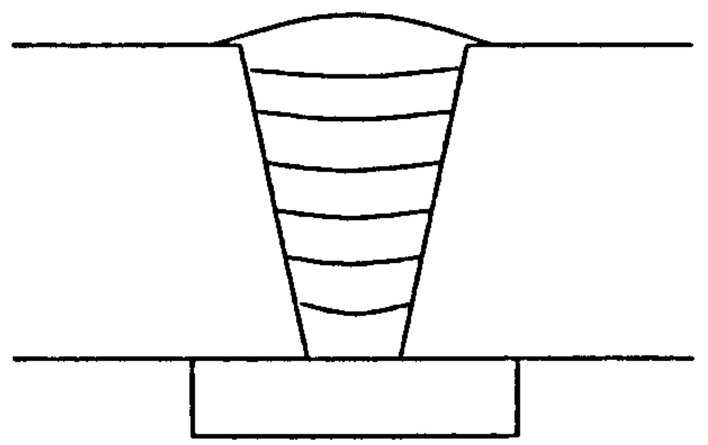

Pass	Process	Polarity	Electrode Brand	Batch	Size mm	Shielding Gas Type	Flow L/min	Temp @ Start °C	Yokogawa WFS m/min	Yokogawa Amps I	Yokogawa Volts V	Arcscope WFS m/min	Arcscope Amps I	Arcscope Volts V	Osc. Freq beats per min	Osc mm	CTWD mm	Travel Speed mm/min	Arc Energy kJ/min
1	PGMAW	DC+ve	MC Control 2	B2803 3 8	1 2	82 5%Ar/12 5%CO_2/5%He	23	100-110	7 70	211	19.7		206	26 2	210	2.2	13 5	509	0 49
2	PGMAW	DC+ve	MC Control 2	B2803 3 8	1 2	82 5%Ar/12 5%CO_2/5%He	23	100-110	7 70	210	21.4		207	26 3	210	2 6	13.5	505	0 53
3	PGMAW	DC+ve	MC Control 2	B2803 3 8	1 2	82 5%Ar/12 5%CO_2/5%He	23	100-110	7 70	211	22 8		208	27.8	210	3 2	13 5	499	0 58
4	PGMAW	DC+ve	MC Control 2	B2803 3 8	1 2	82 5%Ar/12 5%CO_2/5%He	23	100-110	7 70	210	21 7		207	27.3	210	3 6	13 5	501	0 55
5	PGMAW	DC+ve	MC Control 2	B2803 3 8	1 2	82 5%Ar/12 5%CO_2/5%He	23	100-110	7 70	211	22 3		208	27.4	210	4 2	13 5	501	0 56
6	PGMAW	DC+ve	MC Control 2	B2803 3 8	1 2	82 5%Ar/12 5%CO_2/5%He	23	100-110	7 70	211	23 5		207	29	210	4 6	13 5	508	0.59
Cap	PGMAW	DC+ve	MC Control 2	B2803 3 8	1 2	82 5%Ar/12 5%CO_2/5%He	23	100-110	7 70	211	23 9		207	29.6	210	5	13 5	495	0 61
																	Average	503	0 56

Additional Comments.

Torch head angle 5-7° pushing
Lincoln Powerwave 455 STT with custom waveform: 1.2 metal core pulse trimix 7.7 227hz 515IP.swf
beats per minute = no. of complete cycles per minute (ie left-right-left)

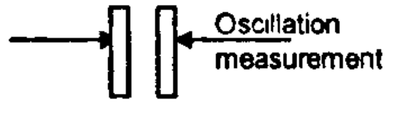

Welding bug : CRC P200

Plates cut on bandsaw then machined to give a 5° bevel
Plates fully restrained

Cap width

start	mid	end
7.47	7.54	7.41

Remaining Depth to Plate surface (mm)

After Pass No	start	mid	end	Av Deposition depth
0	19.75	19.69	19.54	
1	16.31	16.29	16.03	3.45
2	13.01	12.88	12.72	3.34
3	10.01	9.91	9.77	2.97
4	7.28	7.17	7.11	2.71
5	4.84	4.6	4.51	2.54
6	2.37	2.23	2.18	2.39
Cap				

Metal cored wire alloy variation trials – High C (0.9Ni 0.3Mo 0.11C)

Cranfield UNIVERSITY

As-run Parameter Record

Weld No.: MC High C B2803 3 9

Date: 28/02/03

Description:

X100 Metal Cored Wire Plate
Tests - High C
1.0Ni 0.3Mo 0 11C

Welders Name/Position:

MGH

Material Grade:	X100
Heat Number:	1-9887-01-040
Diameter:	N/A
Thickness:	19.05mm
Welding Position:	ASME IX 1G
Preparation Method:	Machined bevel
Alignment Method:	Manually clamped and tacked
Alignment Removed:	N/A
Preheat Method:	Electric Resistance Mats
Backing System	X100 bar
Cleaning Method:	Scriber/ wire Brush

Joint Preparation:

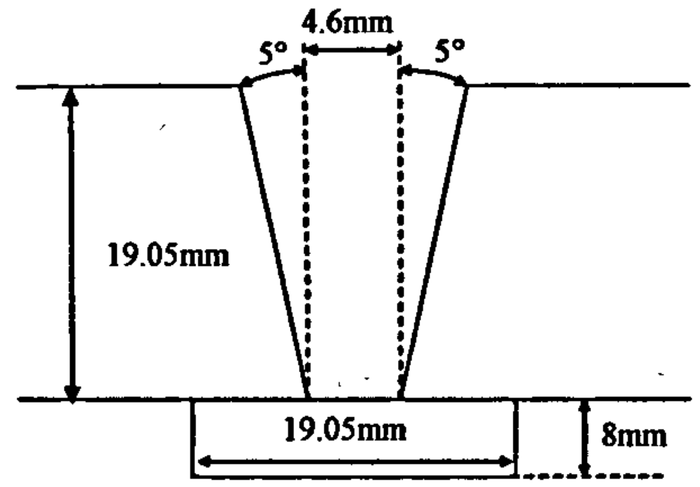

Run Sequence:

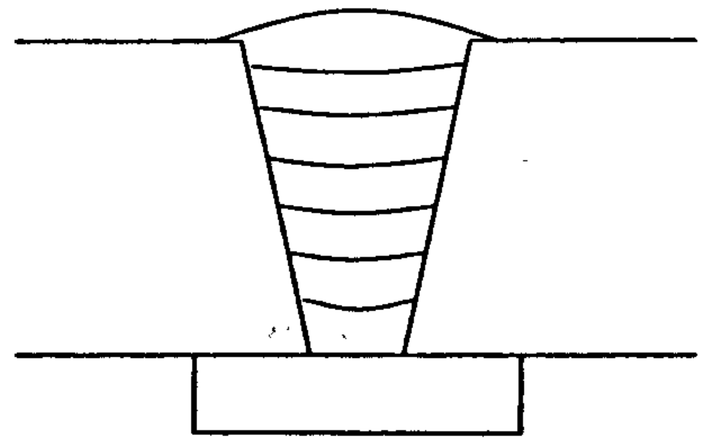

Pass	Process	Polarity	Electrode Brand	Batch	Size mm	Shielding Gas Type	Flow L/min	Temp @ Start °C	Yokogawa WFS m/min	Yokogawa Amps I	Yokogawa Volts V	Arcscope WFS m/min	Arcscope Amps I	Arcscope Volts V	Osc. Freq beats per min.	Osc mm	CTWD mm	Travel Speed mm/min	Arc Energy kJ/min
1	PGMAW	DC+ve	MC High C	B2803 3 9	1.2	82 5%Ar/12 5%CO_2/5%He	23	100-110	7.70	211	19 8		208	24 6	210	2.2	13.5	504	0.50
2	PGMAW	DC+ve	MC High C	B2803 3 9	1.2	82 5%Ar/12 5%CO_2/5%He	23	100-110	7.70	211	20.6		204	29 5	210	2 6	13 5	480	0 54
3	PGMAW	DC+ve	MC High C	B2803 3 9	1.2	82 5%Ar/12 5%CO_2/5%He	23	100-110	7.70	210	22 1		-	-	210	3 2	13 5	480	0.58
4	PGMAW	DC+ve	MC High C	B2803 3 9	1.2	82 5%Ar/12 5%CO_2/5%He	23	100-110	7.70	211	21 6		203	27.2	210	3 6	13.5	487	0 56
5	PGMAW	DC+ve	MC High C	B2803 3 9	1.2	82 5%Ar/12 5%CO_2/5%He	23	100-110	7.70	210	21.5		207	27 1	210	4.2	13 5	497	0 55
6	PGMAW	DC+ve	MC High C	B2803 3 9	1.2	82 5%Ar/12 5%CO_2/5%He	23	100-110	7.70	211	21.2		207	27 4	210	4 6	13.5	507	0 53
Cap	PGMAW	DC+ve	MC High C	B2803 3 9	1.2	82 5%Ar/12 5%CO_2/5%He	23	100-110	7.70	211	22.7		203	28 2	210	5	13.5	505	0 57
																	Average	494	0 55

Additional Comments:

Torch head angle 5-7° pushing
Lincoln Powerwave 455 STT with custom waveform: 1.2 metal core pulse trimix 7.7 227hz 515IP.swf
beats per minute = no. of complete cycles per minute (ie left-right-left)

Welding bug : CRC P200

Plates cut on bandsaw then machined to give a 5° bevel.
Plates fully restrained

Cap width

start	mid	end
7.39	7.50	7.38

Remaining Depth to Plate surface (mm)

After Pass No	start	mid	end	Av. Deposition depth
0	19 62	19.64	19.53	
1	16.07	16.13	16.09	3.50
2	12.63	12.66	12.87	3.38
3	9.54	9.55	9 84	3.08
4	6.67	6.83	7.28	2.72
5	4.2	4.31	4 63	2.55
6	1.74	1.81	2.34	2.42
Cap				

Metal cored wire alloy variation trials – High C Low Mo (0.9Ni 0.03Mo 0.11C)

Cranfield UNIVERSITY

As-run Parameter Record

Weld No.: MC High C Low Mo B2803 3 10

Date: 03/03/03 - 04/03/03

Description:

X100 Metal Cored Wire Plate
Tests - High C Low Mo
1.0Ni 0.03Mo 0 11C

Welders Name/Position:

MGH

Material Grade:	X100
Heat Number:	1-9887-01-040
Diameter:	N/A
Thickness:	19.05mm
Welding Position:	ASME IX 1G
Preparation Method:	Machined bevel
Alignment Method:	Manually clamped and tacked
Alignment Removed:	N/A
Preheat Method:	Electric Resistance Mats
Backing System	X100 bar
Cleaning Method:	Scriber/ wire Brush

Joint Preparation:

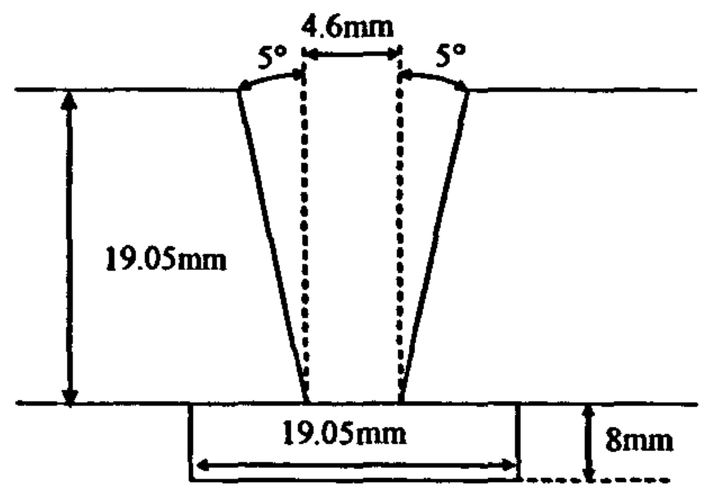

Run Sequence:

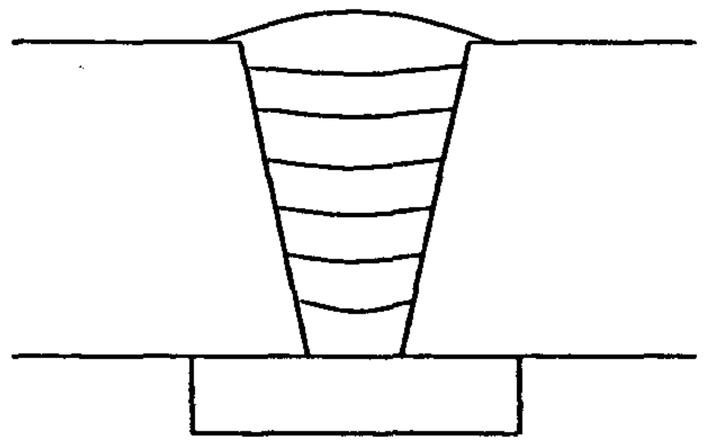

Pass	Process	Polarity	Electrode Brand	Batch	Size mm	Shielding Gas Type	Flow L/min	Temp @ Start °C	Yokogawa WFS m/min	Yokogawa Amps I	Yokogawa Volts V	Arcscope WFS m/min	Arcscope Amps I	Arcscope Volts V	Osc. Freq beats per min	Osc mm	CTWD mm	Travel Speed mm/min	Arc Energy kJ/min
1	PGMAW	DC+ve	MC High C Low Mo	B2803 3 10	1.2	82 5%Ar/12 5%CO_2/5%He	23	100-110	7.70	211	20.4		208	24.6	210	2.2	13.5	505	0 51
2	PGMAW	DC+ve	MC High C Low Mo	B2803 3 10	1.2	82 5%Ar/12 5%CO_2/5%He	23	100-110	7 70	214	18 9		208	26.3	210	2 6	13.5	504	0 48
3	PGMAW	DC+ve	MC High C Low Mo	B2803 3 10	1.2	82 5%Ar/12 5%CO_2/5%He	23	100-110	7.70	211	19.5		207	26.8	210	3.2	13.5	501	0.49
4	PGMAW	DC+ve	MC High C Low Mo	B2803 3 10	1.2	82 5%Ar/12 5%CO_2/5%He	23	100-110	7.70	211	21		203	26.3	210	3.6	13 5	504	0.53
5	PGMAW	DC+ve	MC High C Low Mo	B2803 3 10	1.2	82 5%Ar/12 5%CO_2/5%He	23	100-110	7.70	211	21.7		207	27.2	210	4 2	13.5	506	0.54
6	PGMAW	DC+ve	MC High C Low Mo	B2803 3 10	1.2	82 5%Ar/12 5%CO_2/5%He	23	100-110	7.70	211	23 3		207	28.5	210	4.6	13.5	510	0.58
Cap	PGMAW	DC+ve	MC High C Low Mo	B2803 3 10	1.2	82 5%Ar/12 5%CO_2/5%He	23	100-105	7.70	211	22 1		208	28.9	210	5.2	13.5	501	0.56
																	Average	504	0.53

Additional Comments:

Torch head angle 5-7° pushing
Lincoln Powerwave 455 STT with custom waveform: 1.2 metal core pulse trimix 7.7 227hz 515IP.swf
beats per minute = no. of complete cycles per minute (ie left-right-left)

Welding bug : CRC P200

Plates cut on bandsaw then machined to give a 5° bevel.
Plates fully restrained

Cap width

start	mid	end
7.40	7.50	7.38

Remaining Depth to Plate surface (mm)

After Pass No	start	mid	end	Av. Deposition depth
0	19.74	19.56	19.63	
1	16.04	16.05	16.28	3.52
2	12.69	12.8	12.94	3.31
3	9.95	9.95	10.12	2.80
4	7.34	7.22	7.42	2.68
5	5.03	4.8	4.95	2.40
6	2.66	2.55	2.72	2.28
Cap				

Metal cored wire alloy variation trials – High Ni Low Mo Low C(1.6Ni 0.15Mo 0.05C)

Cranfield UNIVERSITY

As-run Parameter Record

Weld No.: MC High Ni Low Mo Low C - JB comp B2803 3 11

Date: 04/03/02

Description:
X100 Metal Cored Wire Plate
Joe Bundy Composition
High Ni Low Mo Low C
1 6Ni 0.15Mo 0 05C

Welders Name/Position:
MGH

Material Grade:	X100
Heat Number:	1-9887-01-040
Diameter:	N/A
Thickness:	19.05mm
Welding Position:	ASME IX 1G
Preparation Method:	Machined bevel
Alignment Method:	Manually clamped and tacked
Alignment Removed:	N/A
Preheat Method:	Electric Resistance Mats
Backing System	X100 bar
Cleaning Method	Scriber/ wire Brush

Joint Preparation:

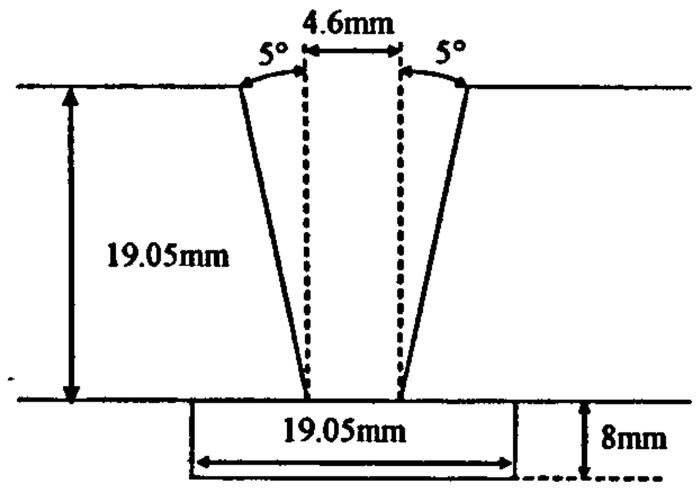

Run Sequence:

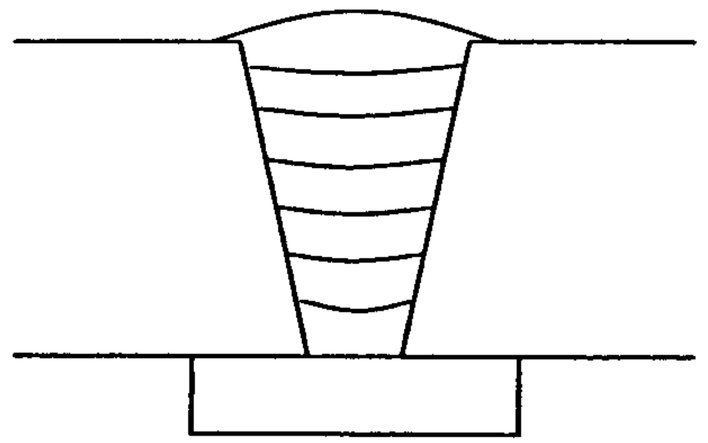

Pass	Process	Polarity	Electrode Brand	Batch	Size mm	Shielding Gas Type	Flow L/min	Temp @ Start ℃	Yokogawa WFS m/min	Yokogawa Amps I	Yokogawa Volts V	Arcscope WFS m/min	Arcscope Amps I	Arcscope Volts V	Osc. Freq beats per min.	Osc mm	CTWD mm	Travel Speed mm/min	Arc Energy kJ/min
1	PGMAW	DC+ve	MC JB comp	B2803 3 11	1.2	82 5%Ar/12 5%CO_2/5%He	23	100-110	7.70	211	20.3		208	22.1	210	2.2	13.5	496	0 52
2	PGMAW	DC+ve	MC JB comp	B2803 3 11	1.2	82 5%Ar/12 5%CO_2/5%He	23	100-110	7.70	210	21.8		210	26.5	210	2 6	13.5	508	0.54
3	PGMAW	DC+ve	MC JB comp	B2803 3 11	1.2	82 5%Ar/12 5%CO_2/5%He	23	100-110	7.70	210	22.7		203	26.3	210	3.2	13 5	500	0 57
4	PGMAW	DC+ve	MC JB comp	B2803 3 11	1.2	82 5%Ar/12 5%CO_2/5%He	23	100-110	7.70	210	21 1		207	25.7	210	3 6	13.5	507	0 52
5	PGMAW	DC+ve	MC JB comp	B2803 3 11	1.2	82 5%Ar/12 5%CO_2/5%He	23	100-110	7.70	211	21.2		208	25 6	210	4 2	13.5	506	0.53
6	PGMAW	DC+ve	MC JB comp	B2803 3 11	1.2	82 5%Ar/12 5%CO_2/5%He	23	100-110	7.70	210	21 8		206	28 6	210	4 6	13.5	502	0 55
Cap	PGMAW	DC+ve	MC JB comp	B2803 3 11	1.2	82 5%Ar/12 5%CO_2/5%He	23	100-110	7.70	211	22.9		-	-	210	5	13.5	488	0.59
																	Average	501	0.55

Additional Comments:

Torch head angle 5-7° pushing
Lincoln Powerwave 455 STT with custom waveform: 1.2 metal core pulse trimix 7.7 227hz 515IP.swf
beats per minute = no. of complete cycles per minute (ie left-right-left)

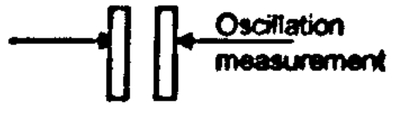

Welding bug : CRC P200

Plates cut on bandsaw then machined to give a 5° bevel.
Plates fully restrained

Cap width

start	mid	end
7.38	7.36	7.24

Remaining Depth to Plate surface (mm)

After Pass No	start	mid	end	Av. Deposition depth
0	19.59	19.77	19.64	
1	16.44	16.18	16.1	3.43
2	13.02	12.94	12.77	3.33
3	9 82	9.85	9.74	3.11
4	7.15	7.32	7.33	2.54
5	4.52	4.73	4 69	2.62
6	2.2	2.53	2.47	2.25
Cap				

Metal cored wire alloy variation trials –Solid wire control test (0.9Ni 0.3Mo)

Cranfield UNIVERSITY

As-run Parameter Record

Weld No.: Carbofil NiMo-1 Control Plate 12

Date: 07/03/2003

Description:

X100 Metal Cored Wire Plate
Carbofil NiMo-1
0.9Ni 0.3Mo

Welders Name/Position:

MGH

Material Grade:	X100
Heat Number:	1-9887-01-040
Diameter:	N/A
Thickness:	19.05mm
Welding Position:	ASME IX 1G
Preparation Method.	Machined bevel
Alignment Method:	Manually clamped and tacked
Alignment Removed:	N/A
Preheat Method:	Electric Resistance Mats
Backing System	X100 bar
Cleaning Method	Scriber/ wire Brush

Joint Preparation:

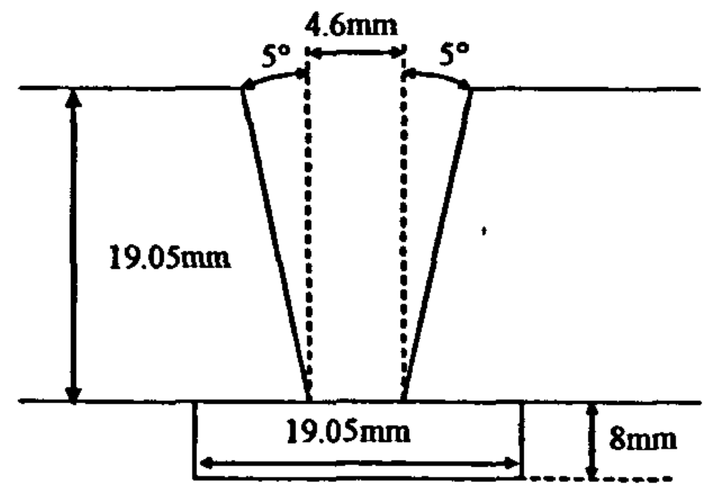

Run Sequence:

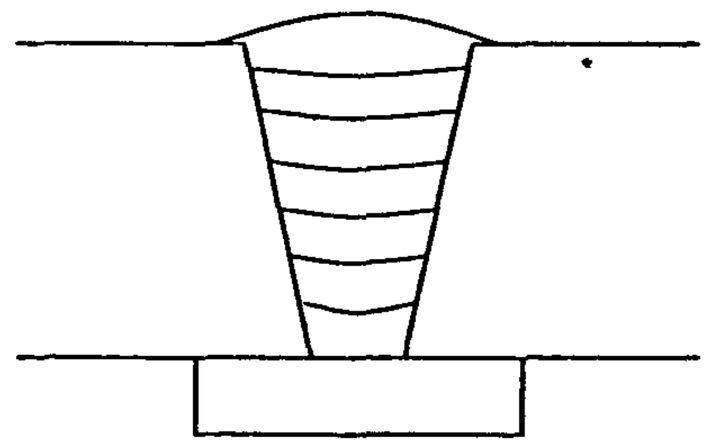

Pass	Process	Polarity	Electrode Brand	Batch	Size mm	Shielding Gas Type	Flow L/min	Temp @ Start °C	Yokogawa WFS m/min	Yokogawa Amps I	Yokogawa Volts V	Arcscope WFS m/min	Arcscope Amps I	Arcscope Volts V	Osc. Freq beats per min.	Osc mm	CTWD mm	Travel Speed mm/min	Arc Energy kJ/min
1	PGMAW	DC+ve	Carbofil NiMo-1	14233	1.0	82 5%Ar/12 5%CO_2/5%He	23	100-110	10 00	180	20.6		171	24.2	210	2.25	13.5	478	0.47
2	PGMAW	DC+ve	Carbofil NiMo-1	14233	1 0	82 5%Ar/12 5%CO_2/5%He	23	100-110	10.00	180	22.7		174	28.7	210	2.5	14	491	0.50
3	PGMAW	DC+ve	Carbofil NiMo-1	14233	1.0	82 5%Ar/12 5%CO_2/5%He	23	100-110	10.00	180	23 6		177	26 8	210	2.7	14.5	496	0.51
4	PGMAW	DC+ve	Carbofil NiMo-1	14233	1.0	82 5%Ar/12 5%CO_2/5%He	23	100-110	10 00	180	23.6		177	27.3	210	3	14	491	0 52
5	PGMAW	DC+ve	Carbofil NiMo-1	14233	1.0	82 5%Ar/12 5%CO_2/5%He	23	100-110	10.00	180	24 3		177	28.3	210	3.2	14	495	0.53
6	PGMAW	DC+ve	Carbofil NiMo-1	14233	1.0	82 5%Ar/12 5%CO_2/5%He	23	100-110	10 00	180	24.4		178	27.7	210	3.5	14	495	0 53
Cap	PGMAW	DC+ve	Carbofil NiMo-1	14233	1.0	82 5%Ar/12 5%CO_2/5%He	23	100-110	10 00	180	24.9		178	31.3	210	5	14	492	0.55
																	Average	491	0.52

Additional Comments:

Torch head angle 5-7° pushing
Lincoln Powerwave 455 STT with custom waveform: 1.0mm NiMo-1 Trimix sav.swf
beats per minute = no. of complete cycles per minute (ie left-right-left)

Oscillation measurement

Welding bug : CRC P200

Plates cut on bandsaw then machined to give a 5° bevel.
Plates fully restrained

Cap width

start	mid	end
7.43	7.41	7.32

Remaining Depth to Plate surface (mm)

After Pass No.	start	mid	end	Av. Deposition depth
0	19.62	19.69	19.81	
1	15.93	15.98	16.18	3.68
2	12.63	12.62	12.82	3.34
3	9.85	9.5	9.83	2.96
4	7.09	6.73	7.3	2.69
5	4.47	4.22	4.75	2.56
6	2.25	1.97	2.28	2.31
Cap				

Appendix C - Thermocouple Wire Certificate of Calibration

ENGELHARD-CLAL

CERTIFICATE OF CALIBRATION

DATE OF ISSUE 17.05.02 :

CUSTOMER NAME CRANFIELD UNIVERSITY

CUSTOMER ADDRESS CRANFIELD CAMPUS
CRANFIELD
BEDFORD MK43 0AL

CUSTOMER ORDER NUMBER WUO 7330:

ENGELHARD-CLAL ORDER NUMBER : C124479-002 / 158949.001

DATE OF CALIBRATION : 17th January 2002

MATERIALS : Pt-13%Rh Positive leg. Batch No. W11121
: Pt Negative leg Batch No. W11120

WIRE DIAMETER : 0.5mm

TEST REPORT NUMBER : 21905

We certify that these thermo-elements when formed into a thermocouple and fully annealed will be in accordance with BS EN60584-1: 1996. The e.m.f produced will not deviate from the published table by an amount greater than the limits defined in BS EN60584-2: 1993, Class 1, at the reproducible fixed points 1064.18°C (freezing point of gold) and 1553.54°C (melting point of palladium).

The temperature/emf relationship of the thermocouple may be affected by slight work hardening and the wire should be re-annealed if it is required for precise work.

Fixed point	t90'°C	Emf (μV)		Difference between the specified & observed emf	
		Specified	Observed	μV	°C
Gold	1064.18	11363.7	11365	+1	+0.1
Palladium	1553.54	18201	18192	-9	-0.6

Uncertainty value at 1064.18°C: ± 0.45°C
Uncertainty value at 1553.54 °C: ± 2.4°C
Nominal room temperature: 20°C ±2°C
The reported expanded uncertainty is based on a standard uncertainty multiplied by a coverage factor K=2, providing a level of confidence of approximately 95%.

Approved Signatory: Name: JR Taylor Signature: pp.

This certificate provides traceability of measurement to recognised national standards, and to units of measurement realised at the National Physical Laboratory or other recognised national standards laboratories. This certificate may not be produced other than in full, except with the prior written approval of the issuing laboratory.

Engelhard-CLAL UK Ltd., Davis Road, Chessington, Surrey KT9 1TD
TEL: +44 (0) 20-8974-3000 FAX: +44 (0) 20-8974-3082

Appendix D - Example NDT Test Reports

SERIMER DASA

RADIOGRAPHIC INSPECTION REPORT

Affaire 062908011

Weld n° 8868

Welding procedure :

Process : **GMAW**

Diameter	:	36"
Thickness	:	15 mm
Amperage I	:	5 mA
Voltage U	:	260 KV
Time	:	01' 30"
Film focus distance	:	450 mm

Radiation source :	:	X Ray
Apparatus :	:	ICM C 3005
Film type :	:	STRUCTURIX D 5
Intensifying screen	:	Lead
IQI / Sensitivity :	:	EN 462.1 W.6
Film density :	:	2,8
Automatic processing	:	KODAK automatic

Acceptance Criteria - Specification : **DNV 2000**

Interval	Interpretation	Assessement
0 - 720	Lack of fusion from 5 to 12 length 7mm Scattered porosity Lack of fusion from 450 to 500 cumulated length 8mm Lack of fusion from 540 to 680 cumulated length 23mm	Accept
720 - 1440	Scattered porosity Lack of fusion at 1230 length 3mm	Accept
1440 - 2160	Lack of fusion from 1450 to 1465 cumulated length 6mm Scattered porosity Lack of fusion from 1670 to 1690 cumulated length 10mm	Accept
2160 - 0	Scattered porosity Lack of fusion from 2450 to 2470 cumulated length 12mm Lack of fusion from 2580 to 2625 cumulated length 16mm	Accept

	For SERIMER DASA	For the CONTRACTOR	For the CLIENT	For Third Party
Nom	S.GAVOIS			
Date	13 mars 2002			
Signed				

Doc Q 132 Rév. 2

NDIS NON-DESTRUCTIVE INSPECTION SERVICES LTD.

UNIT 18, CRAWLEY MILL INDUSTRIAL ESTATE, WITNEY, OXON. OX29 9TJ. TEL: (01993) 778522 & 702577 FAX: (01993) 708673

RADIOGRAPHY	TEST REPORT		Page 1 of 1
Customer Bodycote Material Testing 8-14 High March DAVENTRY Northants NN11 4HB	Order No T.B.A.	NDIS Job No 010673	Report No MTS/258/1001
	Date of Receipt 25/10/01	Date of Test 26/10/01	Description Weld sample
	Procedure No NDIS/GEN/2R	Joint Type Butt	Weld Process Not stated
Test Standard BS EN 1435:1997	Acceptance Standard Not stated	Outside Diameter 36 inch	Material Carbon Steel
Surface As welded	Access Ext/Int	Thickness 19mm	Film Identification See below

Source Type:	Ir 192	Serial No:	4661SB	Activity:	2.5 Ci	
Focal Spot:	2x1mm	Penetrameter:	10 Fe EN	Film Type:	Agfa D7	
DFL Ident:	Numeric	Screens:	Pb 0.125mm F/B	Filters:	None	

METHOD	kV	mA	Time	FFD	UG	Sensitivity	Beam Angle
	N/A	N/A	26mins	Panoramic	0.02mm	3 wires	As required

Additional Information
SWSI Technique carried out. Qty 1 panoramic shot taken of the weld for complete coverage. Datum position has been marked on the component.

Details of Test

Radiographic inspection of the welded sample as specified below was carried out in accordance with the above procedure. As no acceptance standard has been specified, all defects were considered relevant.

SAMPLE IDENT: D105488, MIF 11282, Re. ML-B15-1

SHOT AREA: 0-290-0

OBSERVATIONS: Spatter noted at 127-130 cms
Root undercut noted at 200 cms
Gas pores (largest 1.5mm) noted at 240, 243, and 260.

As no acceptance standard has been specified, the above radiographs are returned to Bodycote Materials Testing Ltd for interpretation and sentencing.

Tester PCN details: Andy Brown - R level 2 Cat XYInov (PCN No.205142)

NDIS LTD.

Name of Tester	Signature of Tester	Approved by	Date of Report	Company Stamp
A.Brown			30 October 2001	QUALITY INSPECTED

Our standard terms and conditions apply.

Appendix E – Thermocycle raw data selection and plotting macro in Microsoft Excel

Program : Raw2Graph

```
Dim bool_check_value(16) As Boolean

Private Sub CommandButton1_Click()

  TextBox1.Text = OpenTextFile()

End Sub

Private Sub CommandButton2_Click()
If tgl_allchannel = True Then
   With UserForm1
      .CheckBox1.Value = False
      .CheckBox2.Value = False
      .CheckBox3.Value = False
      .CheckBox4.Value = False
      .CheckBox5.Value = False
      .CheckBox6.Value = False
      .CheckBox7.Value = False
      .CheckBox8.Value = False
      .CheckBox9.Value = False
      .CheckBox10.Value = False
      .CheckBox11.Value = False
      .CheckBox12.Value = False
      .CheckBox13.Value = False
      .CheckBox14.Value = False
      .CheckBox15.Value = False
      .CheckBox16.Value = False
   End With
   CommandButton2.Caption = "Select all"
   tgl_allchannel = False
Else
   With UserForm1
```

```
.CheckBox1.Value = True
.CheckBox2.Value = True
.CheckBox3.Value = True
.CheckBox4.Value = True
.CheckBox5.Value = True
.CheckBox6.Value = True
.CheckBox7.Value = True
.CheckBox8.Value = True
    .CheckBox9.Value = True
    .CheckBox10.Value = True
    .CheckBox11.Value = True
    .CheckBox12.Value = True
    .CheckBox13.Value = True
    .CheckBox14.Value = True
    .CheckBox15.Value = True
    .CheckBox16.Value = True
End With
CommandButton2.Caption = "Select none"
    tgl_allchannel = True
End If
End Sub

Private Sub CommandButton3_Click()
    End
End Sub

Private Sub CommandButton4_Click()
Dim str_file_in, str_file_out As String
Dim str_line_read, str_line_write As String
Dim str_date, str_delta, str_range As String
Dim i, int_count, int_channels_used, int_divisor As Integer
Dim dbl_time As Double
Dim lg_reg_count As Long
```

```
' Start of new raw data file process

Call validate_checkbox
str_file_in = TextBox1.Text
str_file_out = file_free(str_file_in)
str_delta = "0.002500"
str_range = ""
lg_reg_count = 0
int_count = 0
int_divisor = 1
dbl_time = 0#

Open str_file_in For Input As #1
Open str_file_out For Output As #2

   str_line_write = "Time"
   For i = 1 To 16
   If bool_check_value(i) = True Then
      DoEvents
      str_line_write = str_line_write + Chr(9) + "TC" + Trim(Str(i))
      int_channels_used = int_channels_used + 1
   End If
Next i
Print #2, str_line_write

While Not EOF(1)
   DoEvents
   str_line_write = ""
   Line Input #1, str_line_read
   int_count = InStr(str_line_read, " ")
   If int_count > 0 Then
      str_date = Mid(str_line_read, 1, int_count - 1)
      If str_date = "delta" Then
         int_count = InStr(str_line_read, Chr(9)) + 1
```

```
            str_delta = Mid(str_line_read, int_count, InStr(int_count, str_line_read,
Chr(9)) - int_count)
        End If
        If (IsDate(str_date)) Then
           If int_divisor = Val(TextBox2.Value) Then
              str_line_write = CDbl(dbl_time)
              For i = 1 To 16
                 DoEvents
                 int_count = InStr(str_line_read, Chr(9)) + 1
                 str_line_read = Mid(str_line_read, int_count)
                 int_count = InStr(str_line_read, Chr(9))
                 If bool_check_value(i) = True Then
                    If int_count = 0 Then
                       str_line_write = str_line_write + Chr(9) + Mid(str_line_read, 1)
                    Else
                       str_line_write = str_line_write + Chr(9) + Mid(str_line_read, 1,
int_count - 1)
                    End If
                 End If
              Next i
              Print #2, str_line_write
              lg_reg_count = lg_reg_count + 1
              dbl_time = dbl_time + (CDbl(str_delta) * Val(TextBox2.Value))
              int_divisor = 1
           Else
              int_divisor = int_divisor + 1
           End If
        End If
        End If
     Wend
     Label7.Caption = Str(lg_reg_count) & " Records found"
Close #2
Close #1
' End of new raw data file process
```

```
' Start of excel importing process and graph construction

Workbooks.Open str_file_out
Sheets(1).Name = "Data"

str_range = "A1:" + Chr(65 + int_channels_used) + Trim(Str(lg_reg_count + 1))

Charts.Add
ActiveChart.ChartType = xlXYScatter
ActiveChart.SetSourceData Source:=Sheets("Data").Range(str_range),
PlotBy:=xlColumns
ActiveChart.Location xlLocationAsNewSheet, "Graph"
With ActiveChart
    .HasTitle = False
    .Axes(xlCategory, xlPrimary).HasTitle = False
    .Axes(xlValue, xlPrimary).HasTitle = False
End With
ActiveChart.Axes(xlValue).Select
With ActiveChart.Axes(xlValue)
    .MinimumScale = Val(TextBox4.Value)
    .MaximumScale = Val(TextBox3.Value)
    .MinorUnit = 1
    .MajorUnit = 100
    .Crosses = xlAutomatic
    .ReversePlotOrder = False
    .ScaleType = xlLinear
End With
ActiveChart.ChartArea.Select
ActiveWorkbook.SaveAs FileName:=str_file_out + ".xls", FileFormat:=xlNormal,
Password:="", WriteResPassword:="", _
    ReadOnlyRecommended:=False, CreateBackup:=False


' End of excel importing process and graph construction
```

```
End Sub

Sub validate_checkbox()
    bool_check_value(1) = CheckBox1.Value
    bool_check_value(2) = CheckBox2.Value
    bool_check_value(3) = CheckBox3.Value
    bool_check_value(4) = CheckBox4.Value
    bool_check_value(5) = CheckBox5.Value
    bool_check_value(6) = CheckBox6.Value
    bool_check_value(7) = CheckBox7.Value
    bool_check_value(8) = CheckBox8.Value
    bool_check_value(9) = CheckBox9.Value
    bool_check_value(10) = CheckBox10.Value
    bool_check_value(11) = CheckBox11.Value
    bool_check_value(12) = CheckBox12.Value
    bool_check_value(13) = CheckBox13.Value
    bool_check_value(14) = CheckBox14.Value
    bool_check_value(15) = CheckBox15.Value
    bool_check_value(16) = CheckBox16.Value
End Sub

Function file_free(str_file_in) As String
Dim str_file_out As String
Dim flag As Boolean
Dim i As Integer

flag = True
i = 1
str_file_out = ""
While flag
    str_file_out = Dir(str_file_in + "_" + Str(i))
    If str_file_out = "" Then
        str_file_out = Dir(str_file_in + "_" + Str(i) + ".xls")
        If str_file_out = "" Then
```

```
        flag = False
    Else
        str_file_out = ""
        i = i + 1
    End If
Else
    str_file_out = ""
    i = i + 1
    End If
    If i = 10000 Then
        MsgBox ("File size too large. Reduce the data length within the file. Thanks")
        End
    End If
Wend
file_free = str_file_in + "_" + Str(i)

End Function
```

User screen display for file and thermocouple channel selection, data divisor, and temperature limits on temperature/time graph:

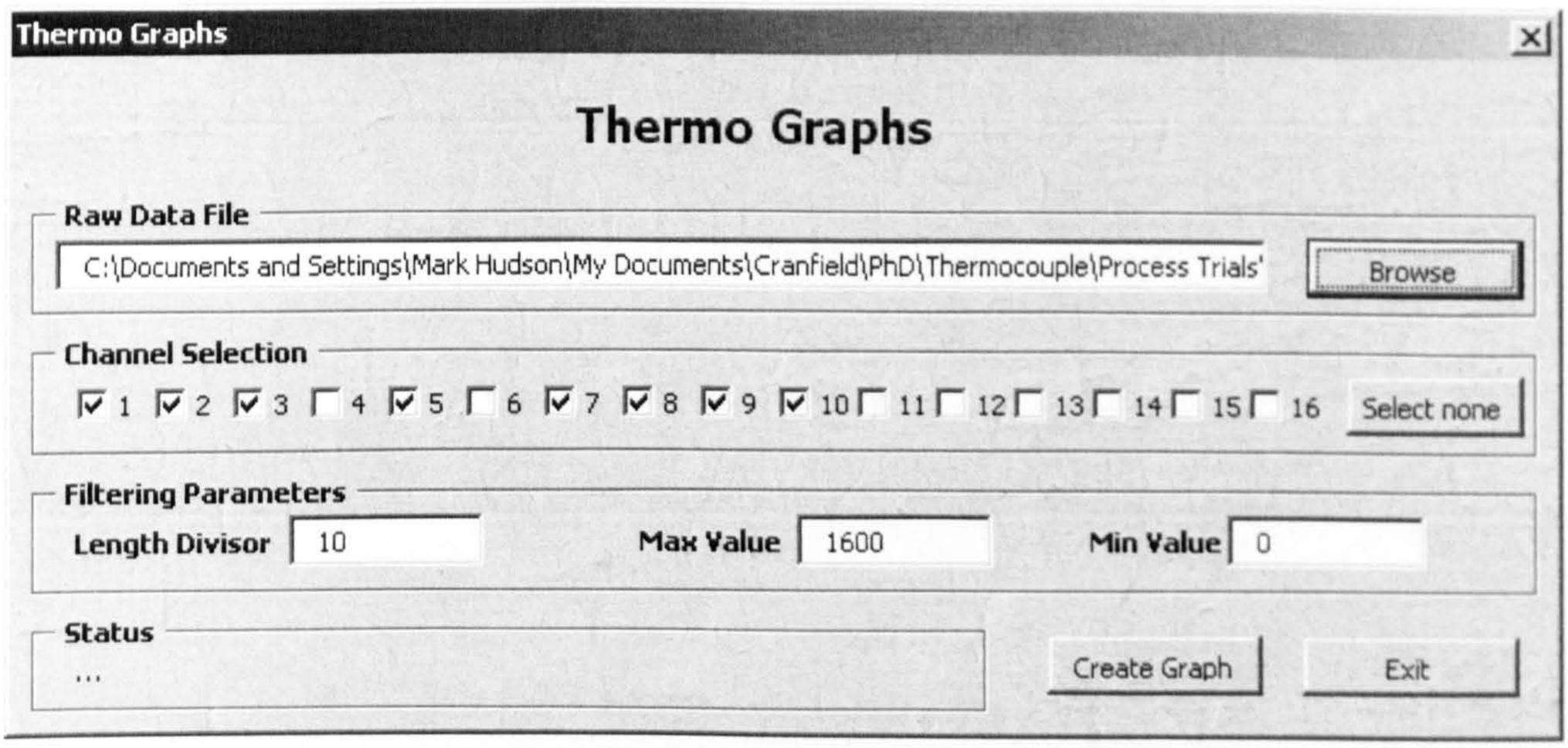

Appendix F – MATLAB thermocycle curve fitting/ differential program

Program: CCT_plot_MGH.m

```
clear all
close all
clc

A=[
```

Time/temperature data set : column 1 time (starting at 0), column 2 temperature

```
];

figure(11);
grid on;
plot(A(:,1),A(:,2),'r-');
hold on;
axis([0 140 0 1800]);
xlabel('Time (s)');
ylabel('Temperature (°C) ');

time0=input('Enter time0 : ');
timeend=input('Enter timeend : ');
time=linspace(time0,timeend,10000);

for LL=1:5

grau=input('Enter order: ');
[dummy,pos0]=min(abs(A(:,1)-time0));
[dummy,posend]=min(abs(A(:,1)-timeend));

coef=polyfit(A(pos0:posend,1),A(pos0:posend,2),grau);

save('savefile','coef','-ASCII');
plot_poly=polyval(coef,time);
```